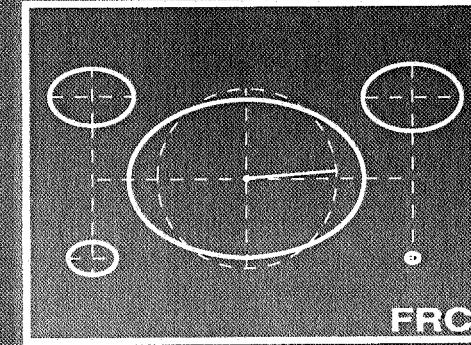
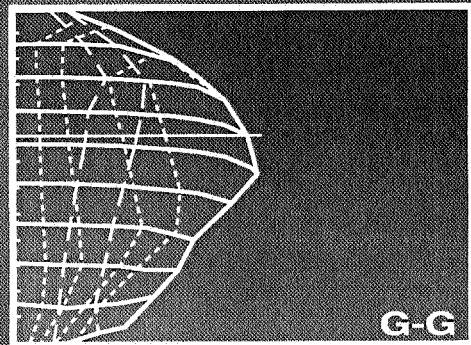
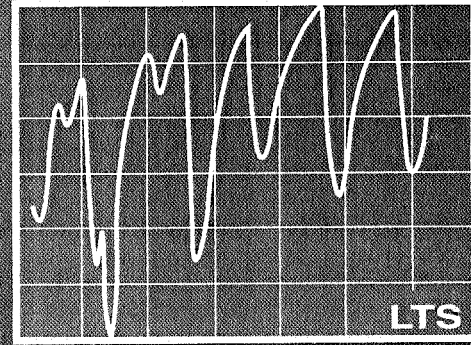
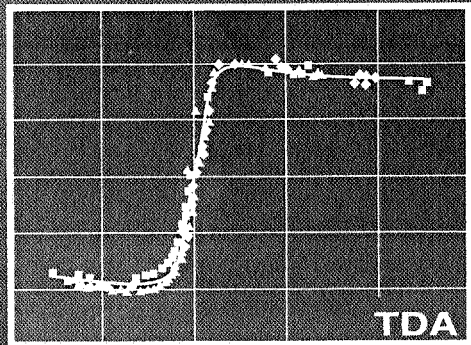
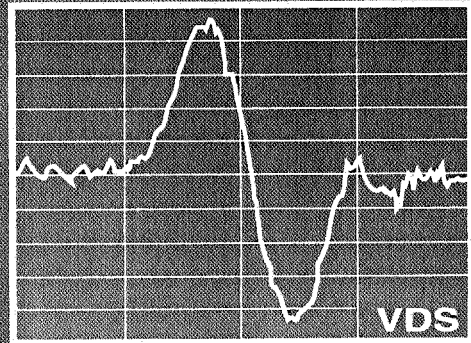
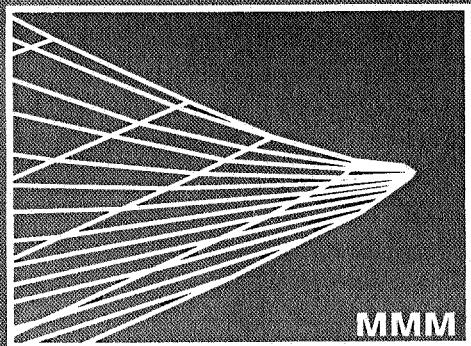


RACE CAR VEHICLE DYNAMICS



WILLIAM F. MILLIKEN AND DOUGLAS L. MILLIKEN

\$39.50

Race Car Vehicle Dynamics

William F. Milliken and Douglas L. Milliken

Written for the engineer as well as the race car enthusiast, *Race Car Vehicle Dynamics* is a comprehensive book on the fundamental concepts of vehicle dynamics and their application in a racing environment. Much of the information included is not available in any other vehicle dynamics text. Although the book's primary focus is the race car, the engineering fundamentals it details are also applicable to passenger car design and engineering.

Chapters include:

- 1 The Problem Imposed By Racing
- 2 Tire Behavior
- 3 Aerodynamic Fundamentals
- 4 Vehicle Axis Systems
- 5 Simplified Steady-State Stability and Control
- 6 Simplified Transient Stability and Control
- 7 Steady-State Pair Analysis
- 8 Force-Moment Analysis
- 9 "g-g" Diagram
- 10 Race Car Design
- 11 Testing and Development
- 12 Chassis Set-up
- 13 Historical Note on Vehicle Dynamics Development
- 14 Tire Data Treatment
- 15 Applied Aerodynamics
- 16 Ride and Roll Rates
- 17 Suspension Geometry
- 18 Wheel Loads
- 19 Steering Systems
- 20 Driving and Braking
- 21 Suspension Springs
- 22 Dampers
- 23 Compliances

The book is also well-illustrated with over 450 figures and tables.

About the authors

Bill and Doug Milliken have pioneered the transfer of aeronautical stability control technologies to the automobile. They have been involved in developing many original vehicle dynamics theories and principles, including the Moment Method, "g-g" Diagram, Pair Analysis, Lap Time Simulation, and Tire Data Normalization. As President and Vice President of Milliken Research Associates, Inc., respectively, they have collaborated on research programs for race teams, automobile, and tire companies for over 20 years. Bill has been involved in various aspects of racing and race car engineering since the 1940's and has over forty years of experience in automotive and aeronautical vehicle dynamics.

Key to Front Cover:

MMM = Milliken Moment Method
VDS = Vehicle Dynamics Simulation
TDA = Tire Data Assistant
LTS = Lap Time Simulation
G-G = Maneuvering Envelope
FRC = Friction "Circles"

ISBN 1-56091-526-3



9 781560 915263

List of Symbols

1DF	Single-degree-of-freedom system
2DF	Two-degree-of-freedom system
3DF	Three-degree-of-freedom system
4WD	Four-wheel drive
A	Area
A_x	Longitudinal acceleration ($g = a_x/g$)
A_y	Lateral acceleration ($g = a_y/g$)
AR	Aspect ratio (of a wing)
B.L.	Boundary layer (of a wing)
C	Damping constant or coefficient
C	Vehicle cornering stiffness
CF	Centrifugal force
CG	Vehicle center of gravity
C_α	Tire cornering stiffness
C_F, C_R	Cornering stiffness for bicycle model front and rear tires
C_γ	Tire inclination stiffness
C_ϕ	Tire camber stiffness
C_0	Control moment gain
C_X	Longitudinal force coefficient
C_Y	Lateral force coefficient
C_N	Yawing moment coefficient = N/W
C_L	Aerodynamic lift coefficient
C_D	Aerodynamic drag coefficient
C_S	Aerodynamic side force coefficient
C_{PM}, C_M	Aerodynamic pitching moment coefficient
C_{YM}	Aerodynamic yawing moment coefficient
C_{RM}	Aerodynamic rolling moment coefficient
C_p	Aerodynamic pressure coefficient
D	Aerodynamic drag or tire drag
D_F, D_R	Bundorf cornering compliance
DR	Damping ratio
D.T.	Dropped throttle
F	Force
F_B	Tire braking force
F_R	Tire net rolling resistance
F_T	Tire tractive force
F_x, F_y, F_z	Forces on the vehicle axes
F_x, F_y, F_z	Forces on the tire axes
FLT	Fraction load transfer
FT	Full throttle
FWD	Front-wheel drive
G	Overall steering ratio (δ_{SW}/δ)
G.W.	Gross (total) weight
H	Total head pressure, aerodynamic
	Height of total CG above roll axis
H_s	Height of sprung mass CG above roll axis
Hz	Hertz (cycles per second)
I	Moment of inertia
IC	Instant center (suspension linkage)
IR	Installation ratio (suspension spring)
I_Z	Moment of inertia about Z axis, commonly called polar moment of inertia
K	Stability factor
K', K_F, K_R	Spring constant (lb./in., lb./ft.)
KE	Axle roll stiffness or $K_{\phi F}, K_{\phi R}$
L	Kinetic energy
L	Aerodynamic lift
L.E.	Surface length (as in RN)
L.F.	Leading edge (of a wing)
LLTD	Lateral load transfer distribution
M	Lateral force
M_x	Moment
M_y	Tire overturning moment
M_z	Tire rolling resistance moment
N	Tire aligning torque
NRA	Yawing moment
NS	Neutral roll axis
NSP	Neutral steer
O	Neutral steer point
OS	Origin of axis system
P	Oversteer
PC	Point
P.E.	Path curvature
PM	Potential energy
R	P.E.
R_0	Aerodynamic pitching moment
R	Tire undeflected radius
R_e	Tire rolling radius, 0° slip angle
R_ℓ	Tire effective rolling radius (rev./mile)
R	Tire loaded radius
RC	Turn radius or resultant
RCH	Roll center location
RWD	Roll center height
RL	Rear-wheel drive
RM	Road load
RN	Aerodynamic rolling moment
S	Reynolds Number
S	Distance or aero side force
S	Distance or aero side force
SI	Spring rate
SLA	Stability index
SM	Short long arm suspension
SR, S	Static margin
T	Tire slip ratio
	Absolute temperature or torque

List of Symbols

T	Thrust
T_{in}	Wheel input drive torque
T.E.	Trailing edge (of a wing)
UG	Understeer gradient
UO	Understeer/oversteer
US	Understeer
V	Velocity, damper velocity
V_{Char}	Characteristic speed
V_{Crit}	Critical speed
V_t	Tangent speed
V_∞	Velocity of remote airstream
W	Weight (force)
W_F, W_R	Lateral load transfer
W_s	Weight of sprung mass
W_u	Weight of unsprung mass
WOT	Wide open throttle
X, Y, Z	SAE earth fixed axis system
X, Y, Z	Forces in vehicle axis system
YM	Aerodynamic yawing moment
a	Distance CG to front axle or track
a	Acceleration in ft./sec. ² units
b	Distance CG to rear axle or track
c	Circumference of circle or wing chord
cpm	Cycles per minute
d	Distance
f	Force or friction force
f	Function
ft.-lb.	Foot-pounds (Work)
fvsa	Front view swing arm (length)
g	Acceleration due to gravity, ft./sec. ² units
h	Height of vehicle CG
h	Roll center height, also z_{RF}, z_{RR}
h_e	Effective CG height, pair analysis
hp	Horsepower (550 ft.-lb./sec.)
k	Understeer gradient, also UG
k	Radius of gyration
k	Spring rate (lb./in.)
lb.-ft.	Pounds-foot (Torque)
ℓ	Length or wheelbase (a+b)
lbj	Lower ball joint location
lca	Lower control arm
m	Mass
mph	Miles per hour
p	Point
p	Aerodynamic static pressure
psi	Pounds per square inch, pressure
q	Aerodynamic dynamic pressure
r	Yaw rate or radius of circle
rms	root-mean-square average
rpm	Revolutions per minute
svsa	Side view swing arm (length)
t	Thickness (aerodynamic boundary layer)
t	Temperature or time
t	Track (tread width)
u	Velocity along x in xyz system
ubj	Upper ball joint location
uca	Upper control arm
v	Lateral velocity component in xyz system
x,y,z	SAE vehicle and tire axes systems
z_{RF}, z_{RR}	Front and rear roll center height
z_{WF}, z_{WR}	Unsprung CG heights
Δ	Small change in
Σ	The sum of
Ω	Angular velocity
α	Tire slip angle or aero angle-of-attack
α	Angular acceleration
β	Vehicle slip angle at CG
δ	Front wheel steer angle
δ_{Acker}	Ackermann steer angle at front wheel
δ_{SW}	Steering wheel steer angle
$\dot{\delta}_{SW}$	Rate of change of steering wheel angle
ϵ	Small distance
ϕ	Angle
ϕ	Camber angle or body roll angle
γ	Tire inclination angle
η	Coefficient or factor
μ	Coefficient of friction
μ	Coefficient of absolute air viscosity
ν	Kinematic air viscosity
π	3.14159...
θ	Angle
ρ	Air mass density
τ	Time constant
ω	Angular velocity
ω	Damped natural frequency
ω_n	Undamped natural frequency
ψ	Heading angle
ζ	Damping ratio
Subscripts:	
1 or F	Front axle location
2 or R	Rear axle location
LF, RF, LR, RR	Individual wheel positions
∞	Ambient conditions

Race Car Vehicle Dynamics

William F. Milliken

Douglas L. Milliken



Society of Automotive Engineers, Inc.
Warrendale, Pa.

Preface

Library of Congress Cataloging-in-Publication Data

Milliken, William F., 1911-

Race car vehicle dynamics / William F. Milliken, Douglas L.

Milliken.

p. cm.

Includes bibliographical references and index.

ISBN 1-56091-526-9

1. Automobiles, Racing--Dynamics. I. Milliken, Douglas L., 1954-. II. Title.

TL243.M55 1995

629.23'1--dc20

94-36941
CIP

Copyright © 1995 W.F. Milliken and D.L. Milliken
Society of Automotive Engineers, Inc.
400 Commonwealth Drive
Warrendale, PA 15096-0001 U.S.A.
Phone: (724)776-4841
Fax: (724)776-5760
E-mail: publications@sae.org
<http://www.sae.org>

ISBN1-56091-526-9

All rights reserved. Printed in the United States of America.
Fifth printing.

Permission to photocopy for internal or personal use, or the internal or personal use of specific clients, is granted by SAE for libraries and other users registered with the Copyright Clearance Center (CCC), provided that the base fee of \$.50 per page is paid directly to CCC, 222 Rosewood Dr., Danvers, MA 01923. Special requests should be addressed to the SAE Publications Group. 1-56091-526-9/95\$.50

SAE Order No. R-146

"He who follows another is always behind."

Anon.

The objective in motor racing is to *win* races—whether one views racing as a sport, a promotional, entertainment, or corporate R & D activity. Motor racing is enormously complex and intense at the higher levels of the sport and significantly so at any level. At the very heart of this activity is the problem of achieving a performance from the driver-vehicle entity which, in the particular race environment, exceeds the competition. This is the challenge. It is the dynamic behavior of the combination of high-tech machines and infinitely complex human beings that makes the sport so intriguing for participants and spectators alike.

As vitally important as the driver is, this book concentrates on the vehicle component. The vehicle can be modified and adjusted to enhance the performance of the driver-vehicle combination and facilitate driver control. This leads to the area of *vehicle dynamics*. Vehicle dynamics, as we use the term, is the branch of engineering which relates tire and aerodynamic forces to overall vehicle accelerations, velocities and motions, using Newton's Laws of Motion. It encompasses the behavior of the vehicle as affected by driveline, tires, aerodynamics and chassis characteristics. The subject is a complex one because of the large number of variables involved.

The purpose of this book is to make available to the racing community, and race engineers in particular, an understandable summary of vehicle dynamics technology as it has developed over the last 60 years. This technology provides a consistent way of looking at the vehicle part of handling problems. We have tried to follow a path between a "theoretical" textbook on vehicle dynamics (which could miss the unique needs of racers) and producing a "popular" book on handling (skipping over the engineering details). While much of the material is mathematical, the practical application of the theory is becoming available in computer programs. To intelligently select and use computer programs, it is necessary to know the assumptions they are based on, and it is vitally important in the use of these tools to be able to relate the various analytical concepts to physical hardware in the car. We recognize that some knowledge of engineering mechanics cannot be avoided but this is best left to a good college level physics text.

Much of the material in this book is new and is based on our long experience in handling research and its application to racing. Our early work was supported by the automobile manufacturers and we believe that this book will also prove useful to passenger car engineers. Although the focus in racing and road cars is different, the same engineering fundamentals apply.

The vehicle dynamics of cornering is of particular interest. The objective is to use the cornering forces of the four tires to achieve maximum lateral acceleration while balancing the contributions of the front and rear tires so the car neither runs wide (plow, "understeer") nor tightens (spin, "oversteer") the intended turn. Traditionally the process of "setting up" or "balancing out" the car involved trial and error. An experienced race driver can usually tell if a car is balanced or not in a particular situation and can, in words, describe the problem. Now, while the result (plow, drift, spin) seems simple enough, the actual physics is complex. This is where data from on-board instrumentation combined with the analytical techniques of vehicle dynamics can predict the effect of configuration changes.

It is our belief, and it permeates this book, that the great reservoir of vehicle dynamics knowledge resides in aircraft engineering. After all, the development of high-performance military aircraft under government sponsorship has enabled tremendous advances in the theory and application of vehicle dynamics. The senior author of this book has an aeronautical background and was among the earliest to utilize aircraft technology for the study of automobiles. The great distinction between the automotive and the aeronautical, which must always be borne in mind, is the tire forces.

A look at the contents will show that the book is roughly split in half—Part I treats fundamental concepts while Part II is devoted to specific problem areas. In Part I, we start with a brief look at our definition of the problem of racing and then move quickly to an in-depth look at the way tires and aerodynamics produce the forces which allow the car to maneuver. Next are a series of chapters that relate the forces (and moments) to the motion of a vehicle, starting with an elementary vehicle and progressing to a description of a very complete nonlinear representation, the MRA Moment Method. Worked examples are provided. The following three chapters attempt to relate the theory back to race car design and tuning.

The final chapter in Part I reviews the early history of automotive vehicle dynamics development. We hope that it will cast some light on how and why various analysis techniques and conventions have been established. The field is still young and its development falls within the lifetime of the senior author, a major participant.

The chapters in Part II give more detailed analysis of specific problem areas that a vehicle dynamicist is likely to come across, starting with a unique treatment of tire data. Next is a review of aerodynamics as applied to race cars; in recent years it is fair to say that aero improvements have had the biggest effect on overall race car performance. The remainder of the chapters deal with various aspects of chassis or "mechanical" setup.

We have tried to reference all the various books, technical papers and articles that we used; most of the references are in the Milliken Research Associates library, without which writing this book would have been nearly impossible.

Acknowledgments

The original draft of this book was funded on a contract from Chevrolet Engineering Raceshop. It was initially intended as a replacement for the Vehicle Dynamics chapter of *Chevrolet Power* (available at Chevrolet dealers), but as interest grew, numerous appendices were added until it assumed book size. The original draft was completed in 1990 and remained with General Motors until late 1992 when it was released by GM Motorsports Technology for publication. At that time the authors took complete responsibility for the contents of this book.

The authors wish to acknowledge the support of John Pierce, GM Motorsports. It would be hard to find a more helpful and understanding program sponsor representative. We also wish to thank Fred Seng, GM, who facilitated the steps toward publication.

Early in 1993, arrangements were completed for the publication of the book by the Society of Automotive Engineers (SAE). Since then the book has been completely reorganized including integration of the appendices into chapters, introduction of new material, and updating where necessary. SAE has put out an extraordinary effort in meeting a tight deadline and in producing a quality book replete with considerable mathematics. The authors wish to express their appreciation to all members of the SAE staff who contributed to this effort. We worked closely with Mark Mecklenborg, Peggy Holleran Greb, Terry Wilson, and Ann Moats. We also wish to thank Bob Richardson who produced the index. Together they came up with many worthwhile improvements in the book and made its publication a pleasant, cooperative adventure.

The line drawings (over 400) were done on computer by Rob Ramsey with help from his father Ross (also an outstanding graphics designer) and were transmitted to SAE on disk. Meeting weekly with Rob and Ross, of Ramsey Associates, has been part of the authors' lives for the last year. The results attest to the accuracy and consistency Rob has brought to this task—many thanks.

In addition to the principal authors, several chapters and sections were written by recognized experts in particular areas; these are identified by footnotes on the chapter title pages. Major parts were authored by: Terry Satchell, Penske Racing Inc.; Tony Best, Anthony Best Dynamics Ltd.; David Segal, MRA; Dr. Hugo Radt, MRA; and Fred Dell'Amico, MRA (deceased). The three MRA Associates also made detailed contributions to a number of chapters, performed many calculations and generally came to the rescue when an impasse was reached. The book owes a great deal to them.

The following individuals have proofread various parts of the book for technical content and/or supplied needed data:

- Dave Glemming, Al Gammon, and Jim Sprague, Goodyear Technical Center
- Peter Wright, Team Lotus
- Max Schenkel, GM Aero Laboratory
- Prof. Al George, Cornell University, Mechanical and Aerospace Engineering
- Dave Kennedy, Prototype Development
- Jeff Ryan, Penske Racing Shocks, Inc.
- Don Van Dis, Mike Raymond, and Dan Thomas, Chrysler Corporation
- Terry Laise, GM Motorsports Technology
- John Beal, MTS Systems Corporation
- Max Behensky, Software Consultant (formerly Atari Games Corp.)
- Al Mugel, Jaeckle, Fleichmann and Mugel

For the historical chapter, we are indebted to the following individuals for their reminiscence of pioneering vehicle dynamics developments in which they were involved: Len Segel, Joe Bidwell, Al Fonda, Ray McHenry, Doug Roland, Dennis Kunkel, and King Bird.

The authors give special thanks to Frank Winchell, Jim Hall, and Jim Musser who spent much effort in piecing together the events of the Chaparral / Chevrolet Engineering collaboration. We believe that this is the most authentic account of this important episode in racing history.

Before his death, René Dreyfus was helpful in clarifying the intuitive approach to classic race car design in the pre-Olley era.

The contributions of Roy Rice (Cornell Aeronautical Laboratory and Calspan) are spread throughout this book, notably in the chapters on Moment Method, "g-g" Diagram, and Simplified Stability and Control. His physical feel, analytical skill, and long association have had a strong influence on the authors' approach to handling. Unfortunately Roy died before we began this book.

Thanks to all of our many friends in the racing fraternity for their help and suggestions, notably Tony Rudd, Chuck Matthews, and Peter Gibbons.

We wish to express our appreciation to Barbara Milliken for help with the manuscript and great general support.

Bill Milliken and Doug Milliken

1995

Technical Contributors

- Anthony Best, MA CEng FIMechE, studied Mechanical Engineering at Cambridge University. He started his career at Rolls-Royce Motor Car Division on vehicle suspensions; moved to Avon Tyres and, in 1967, joined Moulton Developments working on fluid interconnected suspensions. He founded Anthony Best Dynamics, Ltd., where he is Managing Director, 1982. This company specializes in suspension system design and development and software for noise/vibration analysis, as well as noise/vibration testing for automotive firms and other companies.
- Fred Dell'Amico, studied at City College, NY, and later obtained a B.S. in Mechanical Engineering with graduate studies at State University of NY, Buffalo. He started his career at Curtiss-Wright, served a year at Wright-Patterson Landing Gear Lab., followed by 28 years at Cornell Aeronautical Laboratory (CAL)/Calspan, and then 10 years with Metro (subway) Construction, Buffalo. At CAL he worked with William Moog on development of the first electrohydraulic servo valve and its application to aircraft/missiles; later in Calspan Vehicle Research (Asst. Dept. Head) on a variety of vehicles and transportation systems. At that time he made important contributions to the Moment Method.
- Douglas Milliken grew up in the heady atmosphere of basic vehicle stability and control research at CAL/Calspan, first in the flight hangar and later with the ground vehicle activity. During the same period he attended numerous motor races including time in the pits and garage with the Formula One teams at Watkins Glen; he worked with a Trans-Am race team (2.5 liter). He received a B.S. from Massachusetts Institute of Technology in 1977 and joined MRA shortly thereafter. Projects at MRA include mechanical design and fabrication of prototypes and instrumentation. Test and development work includes planning, driving and data analysis with a wide range of vehicles including bicycles, motorcycles, production and race cars, and utility vehicles.
- William Milliken studied Mechanical Engineering at the University of Maine, and received a B.S. from Massachusetts Institute of Technology in Mathematics/Aeronautical Engineering, 1934; he also took private pilot training at the Boeing School. He was successively employed at MIT, Chance Vought, Vought-Sikorsky, Boeing Aircraft, Avion/Northrup, Curtiss-Wright, and CAL/Calspan until 1976—aircraft stability and control/flight tests, 20 years, automotive stability and control since. In 1976 he founded Milliken Research Associates, Inc. (MRA). Initial research was in flight dynamics, including pioneering work in stability augmentation and variable stability; also in automobile dynamics. He designed, built and crashed his own airplane, and competed in over 100 post-war road races and hill climbs.

- Dr. Hugo Radt received a B.S. in Mechanical Engineering from Worcester Polytechnic Institute, M.S. in Aeronautical Engineering from Massachusetts Institute of Technology, and Ph.D. in Physics from the State University of NY at Buffalo. He worked on automotive engineering at CAL/Calspan for 30 years, including the pioneering period in the 1950s when vehicle dynamic analyses were initiated in the United States. He was engaged in ballistic missile defense in the 1960s and '70s but returned to automotive and tire research in 1983 with MRA. He initiated the nondimensional approach to tire data analysis and continues to develop this theoretical/experimental technology.
- Terry Satchell, Michigan State University, B.S. in Mechanical Engineering. Career: 22 years at General Motors, majority at Pontiac in Chassis Department, later at C-P-C in Advanced Engineering Group. Had corporate responsibility for all rear suspensions and numerous advanced projects in front and rear suspensions and components at Pontiac. At C-P-C he was involved in suspension development for active ride and active rear steer. Designed suspension for GM Sunraycer and participated as driver in 1st Australian Solar Car Race. Consulting activity with IMSA and Indy car race teams. Currently employed at Penske Racing, Inc., as Race Engineer.
- David Segal received his B.S. in Mechanical Engineering from Rensselaer Polytechnic Institute in 1966 and studied Engineering Science at the University of Buffalo. He began his professional career at CAL/Calspan. He was involved with applying the (then) newly developed digital computer technology to the solution of complex engineering problems in the areas of vehicle dynamics, crash dynamics, and transportation systems. Subsequently he pioneered the use of personal computers for solving complex vehicle dynamics problems. He is currently an Associate of MRA and is involved with the development of engineering software for vehicle dynamics development and evaluation. He is specifically responsible for major advances in MRA Moment Method Technology.

Table of Contents

Part I

Chapter 1 The Problem Imposed by Racing	3
Chapter 2 Tire Behavior	13
2.1 Lateral Force	15
2.2 Aligning Torque and Pneumatic Trail	28
2.3 Longitudinal Force	32
2.4 Combined Operation	41
2.5 Camber Effects	46
2.6 Other Tire Effects	54
2.7 Friction Circle and Ellipse	57
2.8 SAE Tire Axis System	61
2.9 Discussion of Tire Forces	63
2.10 Discussion of Tire Moments	69
2.11 Torque About the Wheel Spin Axis	74
2.12 Goodyear Tire Data	75
Chapter 3 Aerodynamic Fundamentals	83
3.1 Properties of Air	84
3.2 Bernoulli's Equation	87
3.3 Discussion of Bernoulli's Equation	90
3.4 Pressure Distribution	95
3.5 Consideration of Real Flows	97
3.6 Aerodynamic Testing	101
3.7 Pressure Coefficient, C_p	107
3.8 SAE Aerodynamic Axis System	109
3.9 Aerodynamic Force/Moment Coefficients	110
Chapter 4 Vehicle Axis Systems	113
4.1 Two Types of Axis Systems	114
4.2 Vehicle Motions	117
4.3 Some Thoughts on Sign Conventions	119
4.4 Symbol Conventions in this Book	121
Chapter 5 Simplified Steady-State Stability and Control	123
5.1 Approach	124
5.2 The Elementary Automobile Defined	126
5.3 Steady-State Low-Speed Cornering Geometry	128

5.4 Steady-State Cornering of the Neutral Steer Car	129
5.5 Steady-State Cornering of the Understeer Car	135
5.6 Steady-State Cornering of the Oversteer Car	140
5.7 Equations of Motion	144
5.8 Physical Significance of the Derivatives	151
5.9 Steady-State Responses	153
5.10 Neutral Steer Responses	157
5.11 Understeer and Oversteer Responses	160
5.12 Significant Speeds	174
5.13 Static Stability and Control	191
5.14 Steady-State Path Curvature Stiffness	201
5.15 Steady-State Response Data	210
5.16 Steady-State Nonlinear Analysis	219
5.17 General Conclusions on Steady-State	224
 Chapter 6 Simplified Transient Stability and Control	231
6.1 Approach	232
6.2 The Spring-Mass-Damper System	233
6.3 Dynamic Stability—Two-Degree-of-Freedom Automobile	241
6.4 Single-Degree-of-Freedom Analysis	245
6.5 Two-Degree-of-Freedom Normalized Response Charts	249
6.6 Notes on Stability Derivative Concept	260
6.7 Transient Response Data	260
6.8 Early Analytical Approach	266
6.9 Advanced Vehicle Dynamics Models	272
 Chapter 7 Steady-State Pair Analysis	279
7.1 Pair Analysis Procedure	283
7.2 MRA Computer Program	287
7.3 Example Calculations	288
7.4 Lateral Load Transfer—Discussion	289
 Chapter 8 Force - Moment Analysis	293
8.1 Approach	294
8.2 Constrained Testing	294
8.3 Computer Program	297
8.4 Moment Method Results	301
8.5 Limit Behavior	313
8.6 N-A _Y , Race Car Example	319
8.7 C _N -A _Y , Sports Car Chassis Tuning Example	327
8.8 Lap Time Analysis	340
 Chapter 9 “g-g” Diagram	345
9.1 Conceptual Development	345
9.2 General Uses	348

9.3 Vehicle Capability	350
9.4 Race Car Applications	354
9.5 Historical Notes	359
 Chapter 10 Race Car Design	367
10.1 Constraints and Specification	368
10.2 A Design Process	369
 Chapter 11 Testing and Development	373
11.1 Driver-Vehicle Relationship	374
11.2 Desirable Vehicle Characteristics	375
11.3 Fundamentals of Testing	376
11.4 Track Test Program Planning	378
11.5 Test Methodology	378
11.6 Some General Notes on Development	381
11.7 Circular Skid Pad Testing	383
 Chapter 12 Chassis Set-Up	387
12.1 Set-up	388
12.2 Primary Set-up	391
12.3 Secondary Set-up	401
 Chapter 13 Historical Note on Vehicle Dynamics Development	413
 Part II	
 Chapter 14 Tire Data Treatment	473
14.1 Tire Data Nondimensionalization	474
14.2 Pure Slip Characteristics	475
14.3 Combined Slip Characteristics	480
14.4 Summary of Nondimensionalization of Tire Force/Moment Data	484
 Chapter 15 Applied Aerodynamics	489
15.1 Historical Note on Aerodynamic (Lift) Downforce	490
15.2 Spoilers and Dams	492
15.3 Wings (Airfoils)	496
15.4 Legislated Wings	511
15.5 Ground Effects	521
15.6 Ground Effects Without Skirts	528
15.7 Drag	536
15.8 Flow Control Devices	546
15.9 Internal Airflow	555
15.10 Flat Plate Aerodynamics	560

15.11 Miscellaneous	566
15.12 Aerodynamics and Balance	570
Chapter 16 Ride and Roll Rates	579
16.1 Definitions	580
16.2 First Example with More Complete Calculations	582
16.3 Installation Ratios	595
16.4 Finishing the First Example Case	600
16.5 Second Example with Simplified Calculations	601
Chapter 17 Suspension Geometry	607
17.1 Degrees of Freedom and Motion Path	608
17.2 Instant Center Defined	610
17.3 Independent Suspensions	612
17.4 Beam Type Axle Suspensions	621
17.5 Front Suspensions	624
17.6 Independent Rear Suspensions	636
17.7 Beam Axle Rear Suspensions	647
17.8 Twist Axle Rear Suspensions	661
Chapter 18 Wheel Loads	665
18.1 Assumptions Used in this Chapter	665
18.2 Center of Gravity Location	666
18.3 Chassis Stiffness	673
18.4 Lateral Load Transfer	678
18.5 Longitudinal Weight Transfer	684
18.6 The Effects of Banking	685
18.7 Other Terrain Effects	690
18.8 Aerodynamic Loads	694
18.9 Engine Torque Reaction	697
18.10 Asymmetrical Effects	700
18.11 Summary Example	704
Chapter 19 Steering Systems	709
19.1 Steering Geometry	709
19.2 Ackermann Steering Geometry	713
19.3 Steering Gears	716
19.4 Ride and Roll Steer	721
19.5 Alignment	726
Chapter 20 Driving and Braking	729
20.1 Merits of Front-, Rear-, and Four-Wheel Drive	729
20.2 Differentials	733
20.3 Brake Systems	749

Chapter 21 Suspension Springs	755
21.1 Torsion Springs	755
21.2 Coil Springs	762
21.3 Coil Springs in Series and Parallel	766
21.4 Coil Spring Calculations	770
21.5 Leaf Springs	771
21.6 Leaf Spring Installation Considerations	775
21.7 Fatigue	777
Chapter 22 Dampers (Shock Absorbers)	781
22.1 Approach	783
22.2 Technical Literature	783
22.3 Damping Fundamentals	786
22.4 Racing Application	810
22.5 Race Cars with Modest Aerodynamic Downforce	820
22.6 Race Cars with Aerodynamics Critically Affected by Ride Height and Pitch	823
Chapter 23 Compliances	833
References	841
Index	857

Figures

1.1	Circuit simulation results.....	4
1.2	Vector velocity representation of race car performance	5
1.3	Acceleration components	6
1.4	Vector acceleration representation of race car performance.....	9
1.5	"g-g" measurements on a Grand Prix car (Ref. 167)	10
2.1	Model tire	16
2.2	Mechanism of tire lateral force in elastic range	17
2.3	Walking analogy to tire "slip angle"	19
2.4	Gough's device for study of tire print characteristics	21
2.5	Tire print characteristics—lateral force (Ref. 33).....	23
2.6	Calspan Tire Research Facility, TIRF	24
2.7	Lateral force vs. slip angle for a racing tire.....	25
2.8	Lateral force vs. slip angle for several loads.....	26
2.9	Normalized lateral force vs. slip angle	27
2.10	Lateral force vs. load	29
2.11	Aligning torque vs. slip angle for several loads	30
2.12	Pneumatic and mechanical trail.....	31
2.13	Rim force due to pneumatic and mechanical trail.....	33
2.14	Tire print characteristics—driving (Ref. 33).....	34
2.15	Tire print characteristics—braking (Ref. 33)	36
2.16	Typical traction—slip ratio curve; slip angle = 0°	38
2.17	Typical braking—slip ratio curve; slip angle = 0°	38
2.18	Braking and traction forces vs. slip ratio and slip angle (Ref. 136)	42
2.19	Lateral force vs. slip ratio and slip angle.....	42
2.20	Effect of slip angle and slip ratio on lateral force	43
2.21	Effect of slip angle and slip ratio on traction/braking force	44
2.22	Resultant force vs. resultant slip velocity (Ref. 136)	45
2.23	Distortion in print of a tire at a camber angle	47
2.24	Camber thrust and camber roll-off at constant load	48
2.25	Peak side force vs. camber (Ref. 46).....	49
2.26	Peak lateral force vs. camber, P225/70R15 tire	49
2.27	Lateral force at zero camber	51
2.28	Lateral force at 5° camber, lean to right for LH front wheel	52
2.29	Lateral force at 10° camber, lean to right for LH front wheel	53
2.30	Load sensitivity for several camber angles	54
2.31	Friction circle diagram, right-hand turn	58
2.32	Slip ratio vs. slip angle for cornering example	61
2.33	SAE tire axis system (Ref. 1)	62
2.34	Components of the net rolling resistance, F_R	65

2.35	Tire resistance due to slip angle and input torque (Ref. 55)	66
2.36	Lateral force induced drag—cornering vehicle	67
2.37	Aligning torque	70
2.38	Tire overturning moment	70
2.39	Free-rolling tire	72
2.40	Rolling resistance torque	73
2.41	Rolling resistance moment as a function of load	74
2.42	Goodyear data—Eagle GT-S	76
2.43	Goodyear data—Short Track Stock	77
2.44	Goodyear data—Eagle ZR	78
2.45	Goodyear data—Indy Car road course rear	79
2.46	Goodyear data—F.1 front	80
3.1	Static pressure tube, for measuring p in free stream	91
3.2	Static pressure tap, for measuring p along a surface	91
3.3	Dynamic or “stop” pressure, “ q ”	92
3.4	Total pressure tap, to measure “ H ”	93
3.5	Weather vane, left, and Kiel tube, right, for measuring total pressure . .	94
3.6	Pitot-static tube airspeed indicator	95
3.7	Pressure distribution around a wing	96
3.8	Critical behavior of a hatchback automobile (Ref. 70)	98
3.9	Turbulent wake formation (Ref. 79)	99
3.10	Simple wind tunnel showing diffuser angle	100
3.11	Streamlines in the center cross-section of a VW Rabbit (Ref. 151) . .	100
3.12	Tufts on a wing (Ref. 119)	104
3.13	Tuft grid (Ref. 119)	105
3.14	Smoke tunnel and smoke photo (Ref. 119)	106
3.15	SAE Aerodynamic Axis System (Ref. 2)	109
4.1	Axis systems used in determination of the vehicle axis system (Ref. 111)	115
4.2	Vehicle axis system (Ref. 1)	116
4.3	Heading, sideslip, course, and steer angles (Ref. 1)	118
5.1	Generalized block diagram of driver-vehicle relationship	124
5.2	The “bicycle” model (two degrees of freedom)	127
5.3	The wheelbase angle or “Ackermann steering angle”	128
5.4	Ackermann, parallel, and reverse Ackermann steering	129
5.5	Turning with lateral forces	131
5.6	Research vehicle, constant radius test	132
5.7	Variation of slip angles with lateral acceleration (NS)	133
5.8	NS car on a tilted road	134
5.9	Turning with lateral forces, US car	136
5.10	Turning with lateral forces, US car, $\delta = \delta_{\text{Ackermann}}$ (for NS) . .	138
5.11	Constant radius test for US car	139

5.12	Turning with lateral forces, OS car	141
5.13	Turning with lateral forces, OS car, $\delta = \delta_{\text{Ackermann}}$ (for NS) . .	142
5.14	Steer behaviors on tilted road	143
5.15	Acceleration components in a transient	147
5.16	Velocities at rear tire	147
5.17	Velocities at front tire	148
5.18	The understeer/oversteer spring	152
5.19	Path curvature response (Ref. 92)	163
5.20	Yawing velocity response (Ref. 92)	163
5.21	Neutral steer point	166
5.22	Under/oversteer representation of vehicle stability (Olley) . . .	169
5.23	US speed relationships	178
5.24	Critical speed relationships	179
5.25	Ackermann term, constant throttle test	182
5.26	Slip angle difference term	182
5.27	Simple 2DF car, moment components	183
5.28	Yaw velocity response to control	184
5.29	Minimizing $f = 1/V + KV$	185
5.30	Tire lateral velocity and side force	186
5.31	Tire damper side force—2DF automobile	187
5.32	The damping-in-sideslip	188
5.33	Damping-in-yaw	189
5.34	Trim and stability	193
5.35	NS car directionally disturbed	195
5.36	US car directionally disturbed	196
5.37	Static stability curve for US car	196
5.38	OS car directionally disturbed	197
5.39	Static directional stability	198
5.40	Motions of cars following a disturbance in vehicle slip angle . .	199
5.41	Steering control moment	200
5.42	Static stability and control, US car, constant speed	201
5.43	Slip angles induced by path curvature, vehicle at $\beta = \delta = 0$. .	202
5.44	Yaw moment due to Ackermann steer angle	203
5.45	Path curvature stiffness and yaw damping	203
5.46	Static stability, control, and yaw damping	205
5.47	Stability plot: $C_N \cdot A_Y$ with constant V and constant δ	207
5.48	Stability plot: $C_N \cdot A_Y$; $\delta = 0$; neutral steer car	208
5.49	Stability plot: $C_N \cdot A_Y$; $\delta = 0$; understeer car	209
5.50	Stability plot: $C_N \cdot A_Y$; $\delta = 0$; oversteer car	210
5.51	Steady-state response tests	213
5.52	Steering sensitivity vs. speed	216
5.53	Steady-state steer test and “understeer” gradient	217
5.54	Steering sensitivity vs. lateral acceleration, steady-state test .	218
5.55	Path radius, R , vs. total input thrust, T	220

5.51	Steady-state response tests	213
5.52	Steering sensitivity vs. speed	216
5.53	Steady-state steer test and “understeer” gradient	217
5.54	Steering sensitivity vs. lateral acceleration, steady-state test	218
5.55	Path radius, R, vs. total input thrust, T	220
5.56	Plan view of vehicle showing responses and tire forces ($\delta = 8^\circ$)	222
5.57	Plot of vehicle responses vs. driving thrust	223
6.1	Spring-mass-damper system	234
6.2	Another SMD system	235
6.3	Effect of damping ratio on transient response of spring-mass-damper system	238
6.4	“Quarter-car” SMD system	239
6.5	Transient sideslip response to side force, F_y ($r = 0$)	247
6.6	Yawing motion definitions	248
6.7	Normalized responses, $\omega_n\tau = 0.5$	252
6.8	Normalized responses, $\omega_n\tau = 1.0$	252
6.9	Response time, underdamped case	253
6.10	Response time, overdamped case	253
6.11	Time to peak response	254
6.12	Percent overshoot	255
6.13	Rise time and peak response time (Ref. 9)	261
6.14	Transient response to ramp steer inputs, $V = 62$ mph	262
6.15	Yaw velocity / lateral acceleration rise times, from straight path, 62 mph	263
6.16	Yaw velocity / lateral acceleration rise times, from curved path, 62 mph	264
6.17	Typical free control data records	265
6.18	Effect of front- and rear-wheel driving thrust on steady turning at low speed	266
6.19	Effect of front- and rear-wheel driving thrust on step steer response	268
6.20	Neutralizing steering on “spin” recovery, rear-wheel driving thrust = 500 lb.	269
6.21	“Spin” recovery by simulated “driver” at low speed	270
6.22	“Spin” recovery by simulated “driver” at higher speed	271
6.23	VDS correlation—1	275
6.24	VDS correlation—2	276
7.1	Wheel pair on a single track	284
7.2	Ackermann steer, 0° camber, 0° toe	286
7.3	Axle pair analysis—1	290
7.4	Axle pair analysis—2	291
7.5	Reverse Ackermann steer, -15° camber, 1° toe-out/wheel	292

8.6	C_N-C_Y example, right-hand turn, RL power	304
8.7	Typical four quadrant MMM diagram	307
8.8	Lateral force vs. slip angle for a racing tire	314
8.9	Idealized cornering force curve	316
8.10	Cornering forces for the front and rear tracks	317
8.11	Force-moment envelopes	318
8.12	Chaparral, condition #1	321
8.13	Chaparral, condition #2	322
8.14	Chaparral, condition #3	323
8.15	Chaparral, condition #4	324
8.16	Chaparral, condition #5	325
8.17	Chaparral, condition #6	326
8.18	Sports car, baseline	328
8.19	Roll angle vs. A_Y	329
8.20	Steer angle response	330
8.21	Stability index	331
8.22	Trimmed sideslip angle response	331
8.23	Understeer gradient	332
8.24	GM steering sensitivity	332
8.25	Friction circles, baseline	333
8.26	Baseline, rescaled to show peak	334
8.27	MMM parameter study results	337
8.28	MMM study, near-limit friction circles	338
8.29	Formula 1 car performance envelope, c. 1971	342
8.30	Formula 1 performance profile on Watkins Glen fourth circuit	342
9.1	RWD, braking and D.T.	347
9.2	Maneuvering performance of different drivers	349
9.3	On-road maneuvering (typical driver)	349
9.4	Vehicle “g-g” estimates	351
9.5	“g-g” diagram, rear-wheel drive	352
9.6	“g-g” diagram, front-wheel drive	353
9.7	Adelaide, 1987, Senna	355
9.8	Silverstone, 1993, Herbert	356
9.9	Belle Isle, 1992, LTS calculations	357
9.10	Belle Isle, speed segregated (lower speeds)	358
9.11	Belle Isle, speed segregated (higher speed)	359
9.12	Silverstone, 1993, Herbert	360
9.13	Longitudinal force vs. side force and torque (Ref. 47)	361
9.14	Corvette “g-g” diagram, 1958	362
9.15	“g-g” diagrams from Isuzu, c.1970 (Ref. 108)	365
9.16	“g-g” diagrams from Isuzu, continued	366
11.1	Gain and offset for an accelerometer	380
11.2	Skid pad plot	384

13.1	Bill Milliken and Type 35 Bugatti.....	414
13.2	Maurice Olley	416
13.3	Leonard Segel	423
13.4	Air Force—CAL six component tire test rig	428
13.5	Dave Whitcomb	429
13.6	Cover of "The IME Papers"	430
13.7	Bob Schilling and Joe Bidwell	432
13.8	Frank Winchell, Jim Hall, Jim Musser. STV at Midland with front and rear wings, 1964. Bill Milliken, Frank Winchell, Hap Sharp, Jim Hall at Watkins Glen	440
13.9	Ray McHenry and the Spiral Jump	458
13.10	King Bird and TIRF	461
13.11	Roy Rice, Fred Dell'Amico, and Doug Roland	464
13.12	MTS Flat-Trac Roadway Simulator	466
13.13	Peter Wright and David Williams	467
13.14	CAL, February 5, 1954. Dr. W. Kamm, Bill Milliken, Bob Schilling, Ed Dye, Dave Whitcomb, W. Cyrus, Cliff Nuthall, Len Segel, Bill Close, Ernie DeFusco, Al Fonda	470
14.1	Normalized lateral force, 0° camber	477
14.2	Normalized self-aligning torque, 0° camber	477
14.3	Normalized camber thrust, 0° slip angle	478
14.4	Normalized longitudinal force, 0° slip angle	480
14.5	Normalized lateral force at 1800 lb. load	481
14.6	Normalized lateral force at -6° camber	482
14.7	Normalized resultant force vs. normalized slip variable	484
14.8	Lateral force vs. braking force, constant slip angles	485
14.9	Lateral vs. longitudinal force, constant slip angles	485
15.1	Rear spoiler on G.T. car (Ref. 143)	493
15.2	Rear spoiler G.T. car, effect of yaw angle (Ref. 143)	494
15.3	Effect of rear deck lip height on a notchback sedan (Ref. 140)	495
15.4	Front spoiler position—aerodynamics of Charger Daytona front end (Ref. 86)	497
15.5	Front and rear axle lift vs. speed and aerodynamic aids (Ref. 63)	498
15.6	Chaparral G.S. 2G with high-mounted, two-position wing	499
15.7	NACA 0008 airfoil data (Ref. 14)	500
15.8	Airfoil characteristics corrected to Chaparral wing aspect ratio (Ref. 14)	501
15.9	G.S. 2G total resistance from coastdown tests at Midland	503
15.10	Changes in wheel load due to wing drag	504
15.11	G.S. 2G full-scale pressure measurements, unpublished	504
15.12	G.S. 2G aerodynamic downforce	505
15.13	Acceleration, G.S. 2G WOT	506

15.14	Deceleration, G.S. 2G	507
15.15	Firestone 10.50 × 16, 10" rim, 30 psi	509
15.16	Firestone 6.00/13.50 × 15, 13" rim, 30 psi	510
15.17	Negative-lift wing integrated with the body shape	512
15.18	Multiple slotted airfoil (Ref. 165)	512
15.19	Effect of flaps and slats on airfoil lift characteristics (Ref. 61)	513
15.20	High-lift devices (Ref. 61)	514
15.21	Effective aspect ratio of wings as a function of end plate height ratio (Ref. 61)	514
15.22	Rear wing effect on vehicle lift and drag (Ref. 75)	516
15.23	Spanwise load distribution of the rear wing (Ref. 75)	517
15.24	Front wing data (Ref. 75)	518
15.25	Two-dimensional airfoil shapes and computed lift coefficients (Ref. 76)	519
15.26	Modeling of three-dimensional airfoil shapes (Ref. 76)	520
15.27	Historical development of negative lift (Ref. 168)	522
15.28	C_L vs. incidence, symmetrical nose, effect of ground (Ref. 155)	523
15.29	Lotus ground-effects wind tunnel results (Ref. 168)	524
15.30	Simple ground-effects vehicle	525
15.31	Lift, drag, and pitching moment near fixed ground board (Ref. 49)	529
15.32	Sketches of flow with lee side vortices (Ref. 49)	529
15.33	Body with wheels and rough underbody (Ref. 49)	530
15.34	Tests with and without moving belt (Ref. 49)	530
15.35	Venturi test configurations (Ref. 50)	531
15.36	Flow with vortex formation under venturi model (Ref. 50)	532
15.37	Static pressure distribution (Ref. 50)	533
15.38	View of the underbody channels (Ref. 77)	533
15.39	Vortices inside the underbody channels (Ref. 77)	534
15.40	Effect of rear wing (Ref. 77)	535
15.41	Effect of wings on underbody pressure distribution, CART car (Ref. 76)	536
15.42	March F.1 aero features (Ref. 160)	537
15.43	Penske PC-18	537
15.44	Types of airflow in boundary layer, two-dimensional flow	539
15.45	Induced drag, three-dimensional wing	540
15.46	Idealized flow field around a fastback car, schematic (Ref. 65)	540
15.47	VW basic aerodynamic flow body (Ref. 26)	542
15.48	Morelli basic body shape (Ref. 97)	542
15.49	Goldenrod land speed record car (Ref. 80)	543
15.50	Comparison of computed drag forces with experimental values (Ref. 75)	544
15.51	Probe IV body surface nomenclature (Ref. 137)	544
15.52	Fence on wing to prohibit spanwise flow	547
15.53	Guide vanes	548
15.54	Fence on McLaren CanAm car (side of nose)	548

15.55	Vortex structure on rear of a car (Ref. 63)	550
15.56	Trapped vortex produced by cusp on rear body top (see also Ref. 36)	550
15.57	Vortex generator	551
15.58	Use of diffuser and contractor in radiator air duct	552
15.59	Gurney Lip installed on slotted T.E. flap (Ref. 149)	553
15.60	Rao slot and L.E. cuff (Ref. 39)	554
15.61	Fillet at wing/fuselage juncture	554
15.62	Ideal ram air ducted radiator	557
15.63	Simple cooling system model (Ref. 106)	558
15.64	Efficient diffuser / plenum (Ref. 149)	559
15.65	NACA inlet duct (Ref. 23)	561
15.66	Large sideboards	562
15.67	Flat plate drag (Ref. 62)	562
15.68	Drag coefficients of rectangular flat plate (Ref. 62)	563
15.69	C_L and C_D for a flat plate, AR = 6 (Ref. 71)	563
15.70	Normal force coefficient of square or circular plates (Ref. 62)	564
15.71	Flat plate axes	564
15.72	Permissible grain diameter to maintain min. surface drag (Ref. 78) ..	566
15.73	Relative drag of protuberances and gaps (Ref. 78)	567
15.74	Wake patterns—isolated wheel (Ref. 34)	568
15.75	Pressure distributions beneath wheel (Ref. 34)	569
15.76	Pressure distributions around front and rear wheels (Ref. 153)	571
15.77	Tire load sensitivity	574
15.78	F_Y and CF vs. V	576
15.79	Velocity vs. path radius	577
16.1	Ride natural frequency vs. static wheel deflection	583
16.2	Installation ratio for a simple suspension	595
16.3	Installation ratio as a function of ride travel	597
17.1	Degrees of freedom and suspension motion definitions (Ref. 1)	608
17.2	Kinematics—all independent suspensions have five links	609
17.3	Kinematics—Independent wheel motion	610
17.4	Kinematics—axle suspensions have four links	611
17.5	Instant center concept	611
17.6	Kinematics—instant axis concept	613
17.7	Roll center construction	614
17.8	Jacking effect with a high roll center	615
17.9	Camber change	615
17.10	Scrub is a function of IC height	616
17.11	Wheel path on rough road with a large amount of scrub	616
17.12	Derivation of braking anti features with outboard brakes	617
17.13	Braking anti features with inboard brakes	618
17.14	Front-wheel-drive anti-lift (or pro-lift)	619

17.15	Rear anti-squat, (a) solid axle and (b) independent rear suspension ..	619
17.16	Lateral restraint devices	623
17.17	Front suspension packaging	625
17.18	SLA front view geometry	628
17.19	SLA side view geometry	629
17.20	SLA control arm inner-pivot-axis layout	631
17.21	Choice of instant axis determines the control arm planes	632
17.22	MacPherson strut layout	633
17.23	MacPherson strut spring location to minimize bending	635
17.24	Trailing arm rear suspension	637
17.25	Semi-trailing arm rear suspension	637
17.26	Swing axle rear suspension	638
17.27	Pre-84 Corvette rear suspension	639
17.28	Rear strut suspensions—I	641
17.29	Rear strut suspensions—II	642
17.30	SLA rear suspension—double A-arm and toe link	643
17.31	SLA suspensions—upper A-arm with three links	644
17.32	Thunderbird rear suspension—H-arm and camber link	645
17.33	SLA suspensions—five-link Mercedes type	646
17.34	SLA suspensions—five-link Corvette type	646
17.35	Basic four bar link axle suspension	648
17.36	Parallel lower arm four bar link	650
17.37	A-arm and links axle suspension	651
17.38	Three-link and track bar (Panhard bar)	653
17.39	Torque tube rear axle	655
17.40	“NASCAR” type rear axle	656
17.41	Torque arm rear axle suspension	657
17.42	Decoupled rear axle suspension	659
17.43	Mercedes W125 de Dion rear axle suspension (Ref. 29)	660
17.44	Hotchkiss rear axle (leaf springs)	662
17.45	Twist axle types	663
18.1	Horizontal location of total vehicle center of gravity	667
18.2	Vertical location of the center of gravity	669
18.3	Lateral and longitudinal sprung mass CG location	671
18.4	Sprung mass center of gravity height	673
18.5	Chassis assembly set up for torsional stiffness testing (Ref. 118) ..	674
18.6	Bending and torsional stiffness plotted along the length of the chassis (Ref. 118)	675
18.7	Stiffening up tubing joints in bending (Ref. 164)	677
18.8	Total lateral load transfer	678
18.9	Lateral load transfer geometry	681
18.10	Longitudinal weight transfer—driving	685
18.11	Banked RH turn, looking forward	686
18.12	Effect of grade	691

18.13	Effect of crests	693
18.14	Conventional live rear axle (rear view)	698
18.15	Offset CG car on banked RH turn	703
19.1	Kingpin geometry	710
19.2	Ackermann steering geometry	714
19.3	Ackermann geometry, with steering rack behind the axle line	714
19.4	Modified steer geometry—moving steering rack forward and backward	715
19.5	Steering ratio test	717
19.6	Ride steer equipment (Ref. 150)	722
19.7	Zero ride steer—generally most desirable	723
19.8	Linear ride steer—tie rod length correct, height incorrect	724
19.9	Nonlinear ride steer—tie rod length incorrect	725
20.1	Differential wheel speed, low-speed turning	735
20.2	Open differentials and lever analogy to differential gear action (Ref. 99)	736
20.3	Open differential characteristics	737
20.4	Planetary, unequal torque differential	738
20.5	Locked axle characteristic (spool)	739
20.6	Dana Trac-Loc® limited-slip differential	741
20.7	Dana Trac-Loc® characteristics	742
20.8	Salisbury axle (from ZF)	743
20.9	Torsen® all-gear limited-slip differential	744
20.10	Torsen II® all-gear limited-slip differential	745
20.11	Ferguson Formula viscous differential with planetary differential for 4WD center-box use	746
20.12	Ferguson Formula viscous differential characteristics	747
21.1	Basic geometry of a torsion spring	756
21.2	Maximum stress per unit applied torque, k , vs. bar area	758
21.3	Helical coil compression springs (Ref. 6)	762
21.4	Springs in series	766
21.5	Two springs in series, (a) no bottoming and (b) one bottoming	767
21.6	Springs in series—general case	768
21.7	Springs in parallel	769
21.8	Coil spring rate test	772
21.9	Leaf springs (Ref. 12)	773
21.10	Shackle angle effect on spring rate	775
21.11	Estimating fatigue life of steel leaf springs (preset / not shot peened) (Ref. 5)	778

22.1	Damped spring and mass system	787
22.2	Time histories showing different levels of damping ratio, $\zeta = 0.1$ to 1.2	789
22.3	Simple “one corner” ride model	790
22.4	Vertical accelerations on simple “one corner” ride model	790
22.5	“One corner” ride model including unsprung mass and tire spring	791
22.6	Vertical accelerations on “one corner” ride model of Figure 22.5	791
22.7	Transmissibility of unsprung mass	792
22.8	Ride model including seat flexibility	793
22.9	Passenger acceleration, including seat flexibility	793
22.10	Passenger acceleration vs. damping ratio, ζ	794
22.11	Figure 22.10, with wheel transmissibility	794
22.12	Conventional suspension pitch and bounce centers	795
22.13	Time history of Figure 22.12 (upper part)	796
22.14	Time history of Figure 22.12 (lower part)	796
22.15	Ride comparison in frequency domain	797
22.16	Ride model including damper end rubber isolators	798
22.17	Effects of damper relaxation spring, k_C (carpet plot)	799
22.18	Simple damper characteristics	800
22.19	Damper characteristic showing bump-rebound force ratio	800
22.20	Damper characteristic including orifice effects and “dry” friction	801
22.21	Bump and rebound both plotted in the first quadrant	802
22.22	Damper characteristic with high velocity roll-off	802
22.23	Damper constructions	804
22.24	Damper characteristic, force vs. deflection, classical measurement	805
22.25	Damper characteristic, single loop of the classical measurement	805
22.26	Damper characteristic, replotted against velocity	806
22.27	Effects of damper relaxation spring, 1000 lb./in.	807
22.28	Effects of damper relaxation spring, 500 lb./in.	808
22.29	Effects of damper relaxation spring, 250 lb./in.	809
22.30	DR vs. ride and road-holding performance, compact passenger car	812
22.31	Definitions of tire-ground contact and load fluctuation rates	812
22.32	Load fluctuation and body acceleration, smooth road	813
22.33	Load fluctuation and body acceleration, rough road	813
22.34	Loss of lateral force due to wheel load fluctuation	814
22.35	Steady-state cornering on smooth and good (average) road surface	815
22.36	Steady-state cornering with damper degradation	816
22.37	Steady-state cornering on uneven roadways	816
22.38	Transient maneuver with standard damper	818
22.39	Transient maneuver with twice standard damper	819
22.40	KONI “Graph A”	822
22.41	Transient response as a function of damping ratio, DR	827
22.42	Penske oval track dampers	830
22.43	Penske road course dampers	831

23.1	Lateral force application (Ref. 109)	837
23.2	Lateral force compliance test data (Ref. 109)	838

Tables

2.1	Goodyear Data, Tread Compound Durometer Readings	81
2.2	Calculated C_α for Five Race Tires	82
5.1	Terminology Used in Equations of Motion	145
5.2	The Derivatives (Simple Two-Degree-of-Freedom Automobile)	153
5.3	Response Parameters, Test Speed = 62 mph	214
5.4	Sports Car Response Parameters	214
5.5	Grand Prix Response Parameters	216
6.1	Comparison of Rectilinear and Rotational Dynamics	238
6.2	Inertia, Damping, and Spring Coefficients	241
6.3	US/OS Factor and Natural Frequency in Yaw	242
6.4	Total Cornering Factor	244
8.1	Model Data for $\beta = 0$, δ Varies	304
8.2	Model Data for $\delta = 0$, β Varies	305
8.3	Model Data for $\alpha = 0$, β Varies	306
8.4	Summary of MRA Moment Method Diagrams	310
8.5	Moment Method Run List	320
8.6	MRA Moment Method Parameter Study	336
11.1	Data and Data Reduction from Skid Pad Test	384
12.1	Principal Chassis Tuning Items	389
12.2	Additional Principal Chassis Tuning Items	390
12.3	Key to Primary Set-up Guide	392
12.4	Key to Secondary Set-up Guide	402
15.1	Weight, Dimension, and Wing Data, G.S. 2G	499
15.2	Flat Plate Drag by Two Different Methods	565
15.3	Rotating Wheel Drag (Ref. 34)	570
15.4	Wheel Aero Forces and Moments (Ref. 34)	570
16.1	Typical Roll Gradients, Based on Ref. 91	584
16.2	Effect of Installation Ratio with Different Spring Rates	597
16.3	Data for Simplified Example	601
16.4	Additional Data for Simplified Example—Roll Properties	603
16.5	Suggested Numbers for Simplified Method	605
18.1	Wheel Load Summary	708

21.1 Operating Stress Levels—Round Torsion Bars (Ref. 7)	760
21.2 Recommended Maximum Stress Levels for Coil Springs	764
21.3 Maximum (Uncorrected) Stress Levels for Coil Springs	765
22.1 Indy Oval Track Car—Baseline Configuration	825
22.2 Non-Aerodynamic Version of Indy Oval Track Car	826
22.3 Indy Oval Track Car Damping Ratios	826

Part I

The Problem Imposed by Racing

“Driving a car as fast as possible (in a race) is all about maintaining the highest possible acceleration level in the appropriate direction.”

Peter G. Wright
Technical Director
Team Lotus



The overall technical objective in racing is the achievement of a vehicle configuration, acceptable within the practical interpretation of the rules, which can traverse a given course in a minimum time (or at the highest average speed) when operated manually by a driver utilizing techniques within his/her capabilities. Suitable performance margins must be available for dealing with traffic, environmental factors such as wind and surface conditions, driver fatigue and emergencies.

In its simplest terms a race circuit may be thought of as a number of segments, each composed of a corner, a straight, and a corner. Figure 1.1 is a plot of speed versus path distance of eight such segments.¹ At point A, for example, the vehicle has reached the apex of a turn and is about to begin accelerating down the straight; at point B heavy braking is initiated and the speed falls off in preparation for corner C. The curvature of the plot in

¹ This plot was generated by MRA's Lap Time Simulation (LTS) program using a reasonably complete four-wheel representation of the car.

the vicinity of the corners is due to braking and accelerating during cornering. The fall-off in acceleration at the higher speeds on the straights is the result of increase in aerodynamic drag and use of higher transmission gear ratios.

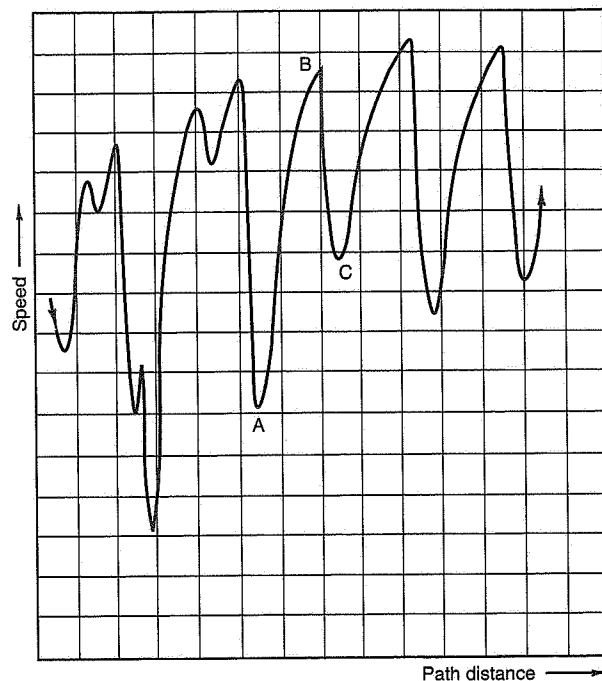


Figure 1.1 Circuit simulation results.

An important principle of circuit racing, which may be observed in Figure 1.1, is that the velocity should never be constant unless held arbitrarily for reasons of endurance, traffic, or safety, or limited by the maximum speed of the vehicle. One should increase speed at a maximum rate (accelerate) out of each turn and continue to the point where, with maximum braking (deceleration) the speed can just be brought down to the maximum speed for the next corner. Ideally braking should be continued toward the apex of the turn and acceleration initiated shortly thereafter.

In engineering terms, velocity is a “vector”² quantity because it possesses both a magnitude (speed) and a direction. It may be represented by an arrow whose length, to some

² In this text, the vector quantities are velocity, acceleration, and force.

arbitrary scale, corresponds to the speed and whose direction is given by the arrow’s orientation, i.e., the direction that it is pointing. Using velocity vectors, the performance of a race car on a segment of a circuit may be presented graphically as shown in Figure 1.2. The vector directions³ are along (tangent to) the path of the center of gravity (CG) of the vehicle and the length of each vector is proportional to the speed at that point. Figure 1.2 indicates that the vector velocity variations are the result of changes in both speed and direction.

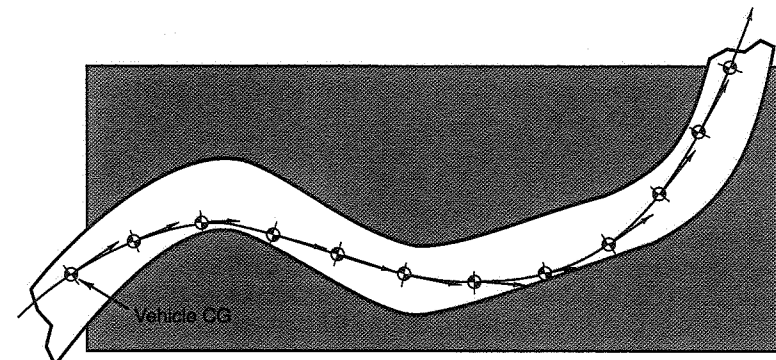


Figure 1.2 Vector velocity representation of race car performance.

For a number of reasons that will become apparent, **race car requirements are best expressed in terms of acceleration**. This might be anticipated because, as we have noted, the vector velocity is constantly changing in racing and acceleration is, by definition, the change in vector velocity with time.

To the layman, acceleration is the rate of change of speed with time on a straight path, as when one “accelerates away” from a stop light. This is a length change of the velocity vector. The layman is also aware of straight line braking as a negative acceleration, i.e., deceleration. The race driver is conscious of an additional form of acceleration, namely *cornering acceleration*. This acceleration is associated with the change in direction of the velocity vector with time. For purposes of clarifying these acceleration components consider the following:

Figure 1.3(a) is a vector velocity diagram. The velocity vector V_1 is shown at Point A on a corner and V_2 at Point B, a small distance, S , further along.

³ These directions should not be confused with the heading (attitude) of the vehicle which is another matter. This heading angle is β —the angle between the centerline of the vehicle and the path, measured at the center of gravity of the vehicle.

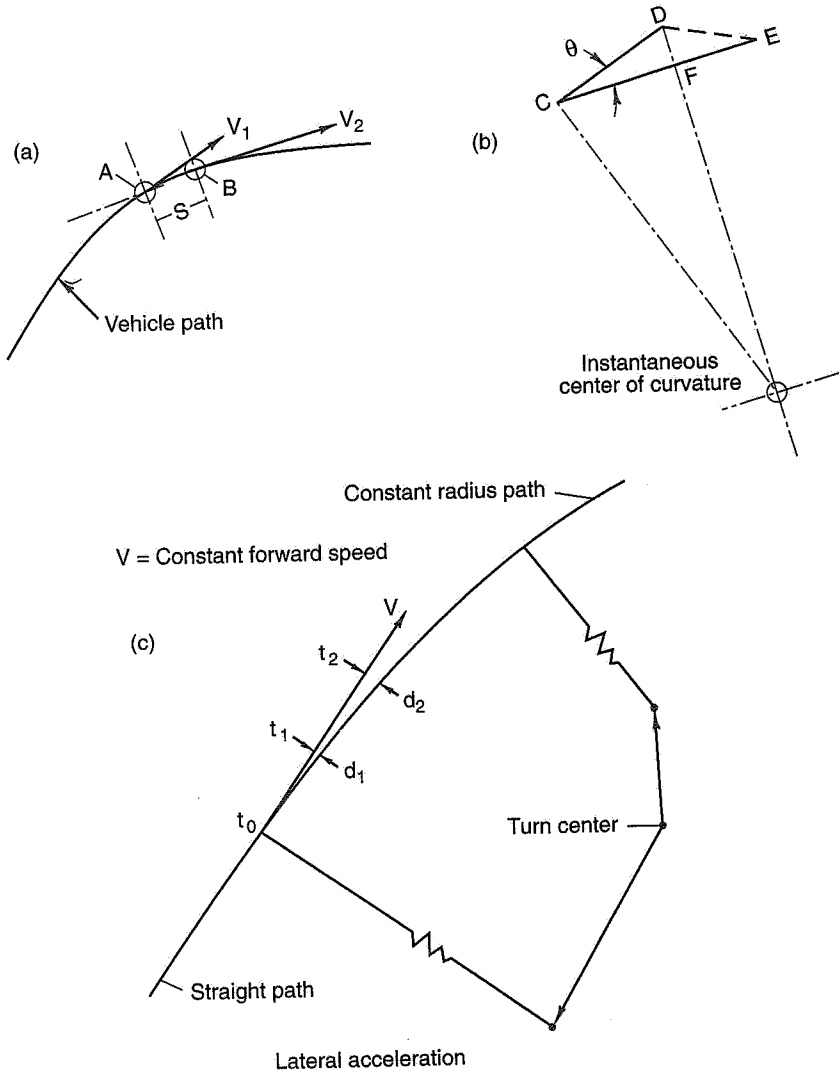


Figure 1.3 Acceleration components.

In the situation shown, the vehicle is changing in both speed and direction. The time to travel from A to B is t .

Figure 1.3(b) is a distance diagram. If the vehicle, now starting at Point C, had continued at the same velocity represented by vector V_1 (that is, if there had been no acceleration or velocity change) it would have reached Point D in the time, t , whereas in actual fact it reached Point E (CD being parallel to V_1 and CE being parallel to V_2). Thus, during the time, t , the vehicle must have experienced a speed change in an inward direction (toward the center of curvature) of DF/t . This rotates the vector V_1 through an angle θ . During the same time a speed change must have occurred in the FE direction, of FE/t . These are called the *normal* (or centripetal) and *tangential* components of the acceleration; to the driver they are the *lateral* (sideways) and *longitudinal* (fore and aft) accelerations experienced in rotating and lengthening the velocity vector from V_1 to V_2 in the time, t . The total acceleration vector (acceleration, like velocity, having magnitude and direction) is DE/t , which lies along the dotted line in the figure. The point to be emphasized is that to maintain a curved path on the ground the vehicle must be moving sideways as well as forward, and lateral acceleration is merely the change in lateral speed with time to achieve this.

Lateral acceleration seems to be a more difficult concept to think about than acceleration in a straight line, although it is perfectly apparent to the driver. As a consequence of longitudinal acceleration, one is pressed backward against the seat when the vehicle increases velocity in a forward direction, and hangs on the harness during braking when the forward velocity is decreasing; one is pulled sideways when the lateral velocity changes toward the center of a turn. Since an understanding of lateral acceleration is so important in racing, consider the process whereby a vehicle follows a curved path of constant radius:

In Figure 1.3(c) (another distance diagram) a vehicle enters a turn at the point t_0 (also taken as time zero). At this point the vehicle has a velocity V , shown by the velocity vector originating at t_0 . Assume that the turn is taken at a constant forward speed. A short time, say 1 second, after the vehicle has entered the turn it will have reached point t_1 and, in 2 seconds, point t_2 . The question is: What does it take in the way of lateral velocity for the vehicle to stay on this curved path? At t_1 the vehicle must have moved laterally a distance, d_1 . To do this required a lateral velocity of $d_1/1$ sec. At t_2 the vehicle must have moved laterally a distance, d_2 , which from observation is about three times the lateral distance required at t_1 . The lateral velocity to move d_2 is $d_2/2$ sec. which is greater than the lateral velocity required to stay on the path at t_1 by a factor of about $(d_2/2 \text{ sec.}) / (d_1/1 \text{ sec.}) = (d_2/d_1) \times (1/2) = (3/1) \times (1/2) = 1.5$.

Thus the lateral velocity is increasing with time. An increase in velocity with time is an acceleration, in this case a lateral acceleration.

Physically, the above occurs because the curved path is continually sweeping away from the instantaneous forward velocity, in a nonlinear manner.

The lateral acceleration is given by the relation V^2/R where V is the speed along the path in ft./sec. and R is the instantaneous radius of the path in feet. The acceleration is then in ft./sec.² units. The longitudinal acceleration is $\Delta V/\Delta t$, where ΔV is the speed change occurring in the small time Δt ; ΔV is in ft./sec. units and Δt is in sec. It is common to express these acceleration components in terms of the acceleration experienced by a falling body in the earth's gravitational field. In each second of free fall a body picks up an additional velocity of 32.2 ft./sec. (assuming no air resistance). Thus the gravitational acceleration is 32.2 ft./sec.² (or 32.2 ft./sec. each sec.) and this is called 1g of acceleration. Lateral acceleration then becomes V^2/gR and longitudinal acceleration, $\Delta V/g\Delta t$, both in "g" units. For example, 2g acceleration means the velocity is changing at the rate of 64.4 ft./sec. each second.

A convenient (approximate) relation for lateral acceleration is

$$V^2 \text{ (mph)} / 15 \times \text{Radius (in feet)}, \text{ in "g" units}$$

If V is 80 mph and R is 500 ft., the lateral acceleration is

$$(80)^2/(15)(500) = 0.85g$$

Returning now to race car circuit performance, Figure 1.2 may be redrawn in terms of the acceleration components and the resultant accelerations, as in Figure 1.4. The resultant accelerations are obtained by the parallelogram law of vector addition sketched at the bottom of the figure. Note the negative (braking/deceleration) and positive (acceleration) directions of the resultant vector components.

The rotation and length changes of the resultant acceleration vector, as the vehicle progresses along a circuit, has led to the concept of the "g-g" diagram. By recording the outputs of longitudinal and lateral accelerometers (instruments that measure acceleration) in the vehicle, a plot can be made of driver/vehicle performance. Figures 1.5(a), (b), and (c) present actual data points obtained from such measurements by three different world-class drivers in the same 1977 Grand Prix car on the Paul Ricard circuit. These data points indicate the levels and combinations of longitudinal and lateral acceleration that each driver used in negotiating the same portion of the circuit at racing speeds; in effect they are the end points of the acceleration vector as it rotated and changed length. An examination of these figures will show that these drivers spent most of the time at acceleration limits while utilizing somewhat different driving techniques, such as placing more emphasis on braking, cornering or combined cornering/longitudinal acceleration. However, the drivers were ultimately limited by the maneuvering acceleration capability of the vehicle. All of the data points for the three drivers are encompassed in Figure 1.5(d). Since we know that these drivers were capable of reaching the vehicle's

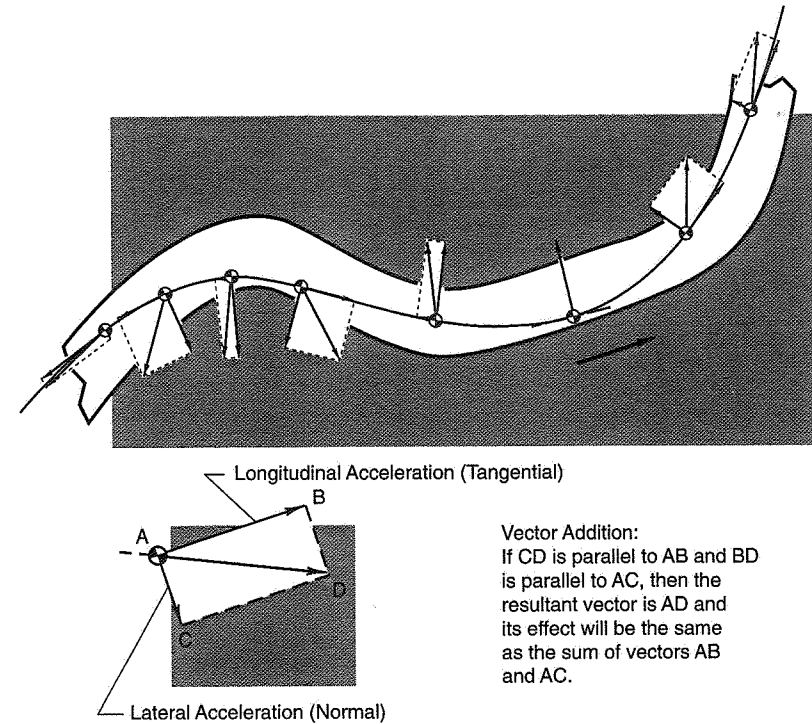


Figure 1.4 Vector acceleration representation of race car performance.

limit, a boundary (shown as a solid line) can be drawn around these points as the probable maneuvering acceleration capability of the vehicle if ideally driven, i.e., the maximum potential of the vehicle.

The problem imposed by racing may now be summarized as one of spending as much time as possible as close as possible to the potential vehicle "g-g" boundary.⁴ It follows that the basic design requirements of a race car (and qualitatively the same for any performance car) are:

⁴ The potential vehicle "g-g" diagram boundary is always changing. The forward acceleration side of the diagram depends on engine characteristics, gearing and, at low speeds, traction. The turning and braking sides of the diagram depend primarily on the tire-road friction coefficient (or "grip") which is affected by road surface, banking, grade, speed, and many complex (and interrelated) tire and aerodynamic effects.

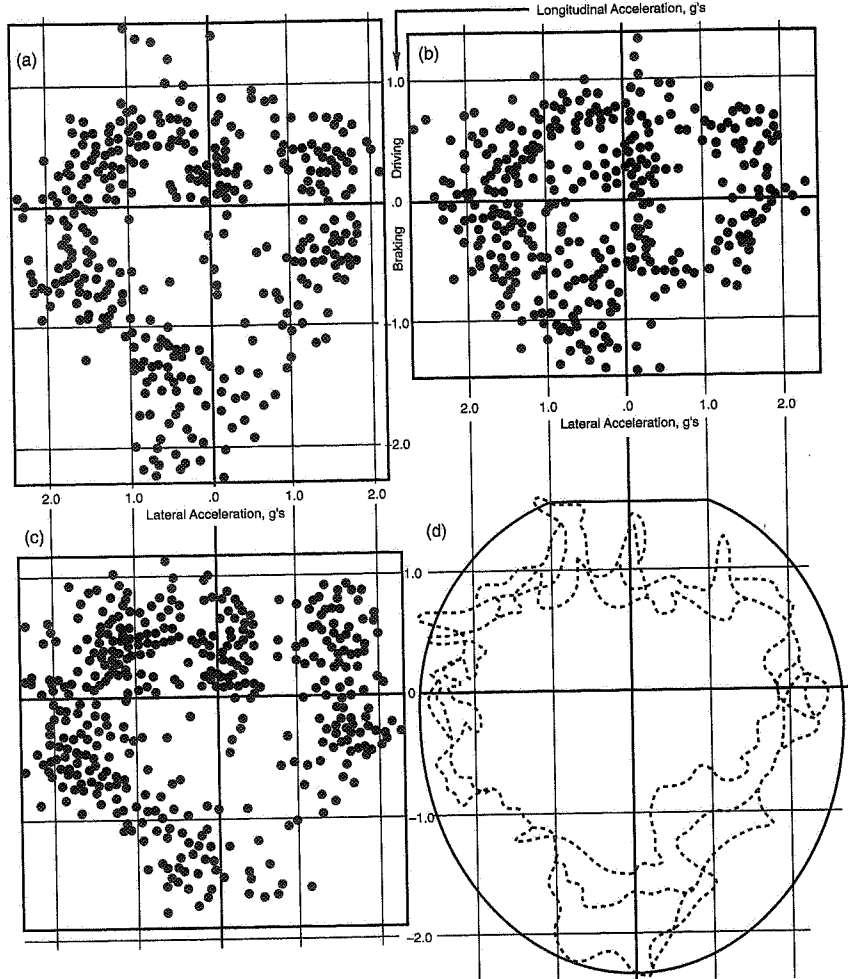


Figure 1.5 "g-g" measurements on a Grand Prix car (Ref. 167).

- The provision of the largest vehicle "g-g" maneuvering areas throughout the range of operating conditions.
- The provision of vehicle control and stability characteristics that enable a skilled driver to operate at or near these acceleration limits.

Historically, every major innovation in race car design has resulted in extensions of these "g-g" acceleration boundaries and an exploitation of them through improved control or driving technique. A dramatic example is that of aerodynamic downforce.

Subsequent chapters in this book deal with the basic technologies underlying vehicle design as affected by these requirements.

Tire Behavior

"No living thing but a snail has as good a shoe as a motor car."

"With the introduction of Independent Front Suspension... in this country and with the first tire tests on smooth drums, by Goodyear in 1931 (by Cap Evans)..., the real study of the steering and handling of cars began."

Maurice Olley, 1961



Introduction

The forces for accelerating the race car in the horizontal plane originate principally at the tires; an understanding of tire behavior is one key to the achievement of the largest "g-g" diagram. Furthermore, tires are the primary source of the forces and torques which provide the control and stability (or "handling") of the vehicle.⁵ This chapter is a review of tire mechanics—the behavior of tires in producing forces and torques.

Dr. Hugo Radt, MRA, reviewed this chapter and contributed to the material on slip ratio. Fred Dell'Amico wrote the material on the tire axis system and individual tire force and moment components. Goodyear made available the engineering tire data shown at the end of the chapter.

⁵ "Handling" commonly refers to the directional stability and controllability of a vehicle. In technical circles, it generally refers to the behavior of the driver-vehicle combination in maneuvering tasks. Further discussion of these terms will be found in Chapter 5.

The forces and torques (or moments) developed by the pneumatic tire affect the vehicle in a variety of ways. Obviously, the tires support the vehicle weight, and any other vertical forces developed such as aerodynamic or the result of road banking. The interactions between the tires and the road supply the tractive, braking and cornering forces for maneuvering (as plotted on the “g-g” diagram). The tires also supply the forces used for controlling and stabilizing the vehicle and for resisting external disturbances from road and wind. For these beneficial effects the tire demands a price in rolling resistance and induced forces in the drag direction. The tire generates steering torques which give rise to centering effects in the steering system and related torques felt at the steering wheel by the driver. These effects are all in addition to enveloping the small scale roughness of the road and providing the basic “grip” to the road which makes all these other effects possible.

The tire is too complex to tackle as a whole; one must isolate and explain its characteristics separately. We will start with the generation of *lateral force* which is of primary interest in cornering and then move to the generation of *aligning torque* (or *pneumatic trail*) and *tractive/braking force*. Next is a discussion of the effects of *camber*. Tires are sensitive to *pressure*, *temperature*, and *speed*, which are discussed next. Finally, the above is gathered together in the concept of the *tire friction circle* (or *ellipse*) which is related to the whole vehicle “g-g” diagram. Tire design (selection of tire dimensions, rubber compounds, cord angles, cord types, etc.) is beyond the scope of this book and remains the province of the tire designer.

Tires are tested to determine their force and moment producing capabilities under different operating conditions. These tests can be carried out in the laboratory and/or on the road, depending on the equipment available. For any given tire operating condition (snapshot), there is one resultant vector that represents the force between the tire and the road. This vector changes length, point of origin and angle as tire operating conditions change. For convenience, the single resultant vector is broken down into six components for measurement and analysis purposes. The last several sections of this chapter describe the tire axis system in which test results are given and present some sample race car tire data.

The Print and Tire “Grip”

The area of the tread of a tire that is in contact with the ground at any given moment is called the *print* or *footprint*. The rubber elements in the print are either “stuck” to the road or are sliding across the road.

- The rubber is stuck to the road by a variety of mechanisms including mechanical “gearing” to the texture of the pavement and molecular adhesion to the surface. These mechanisms are not totally understood.

- When the local coefficient of friction is reached, part (or all) of the rubber in the print slides across the road. The force generated depends on the sliding velocity, the local load, rubber and surface characteristics, etc. The sliding process is not fully understood either.

For the race car designer and driver it is necessary to recognize the extent to which the tire is stuck or sliding and the associated forces that are developed in the print; luckily it is not necessary to understand the sticking or sliding mechanisms. The acceleration performance of the vehicle at any given instant is limited by the tire print forces.

The tire as a whole can develop motions relative to the ground without gross sliding of the print. This is possible because the carcass and tread distort, and new rubber constantly enters the print as the tire rotates. Elastic forces are developed in the tire structure which are reacted (is equal and opposite to) the forces in the tire print.⁶

The other source of forces/moment on the vehicle is aerodynamic. Of the aerodynamic components, the downforce (or negative lift in SAE J1594, Vehicle Aerodynamics Terminology [Ref. 2]) has had the largest effect on race car performance. This force acts through the tires, changing the effective load on them. The lateral and longitudinal tire forces which determine the “g-g” diagram are functions of the total tire load.

2.1 Lateral Force

In SAE J670, Vehicle Dynamics Terminology (Ref. 1), a lateral tire force originates at the “center” of the tire contact with the road,⁷ lies in the horizontal road plane and is perpendicular to the direction in which the wheel is headed if no inclination or camber exists (the distinction between camber and inclination is discussed later in this chapter). The term side force is frequently used as interchangeable with lateral force, but is better reserved for situations involving the complete vehicle.

A vehicle turns because of the applied lateral tire forces. In the next several sections all wheels are assumed vertical. As mentioned earlier the forces are limited by conditions in the print.

We begin with a series of demonstrations with a model tire; the model tire simulates the behavior of the centerline of a real tire. The same effects are described next for real tires. Finally, some additional effects that real tires have which are important for racing are described.

⁶ Or, if you prefer, the reaction in the tire structure of the forces that are developed in the print, in accordance with Newton’s third law.

⁷ More strictly speaking, the origin of the SAE Tire Axis System is at the intersection of the wheel center plane with the ground plane and at a point directly below the center of the upright wheel.

The Model Tire

The model tire described here was first used by Chevrolet R&D as an instructional tool in the 1960s (see Refs. 35 and 57). This tire is made by sandwiching a sheet of hard rubber between two metal disks as shown in Figure 2.1. To keep things simple, the only item that is varied over a set of these tires is the diameter of the metal disks; the rubber composition, thickness and diameter of the rubber are kept constant.

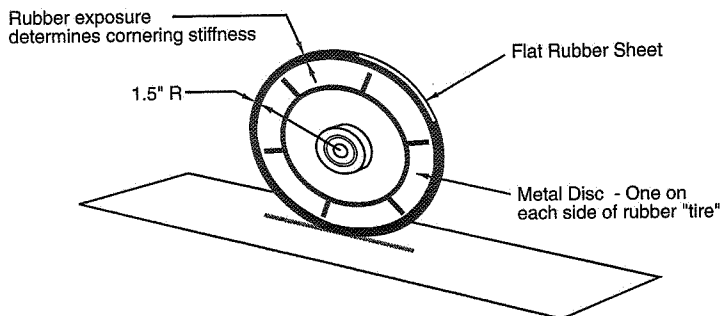


Figure 2.1 Model tire.

First Experiment - Static Lateral Stiffness and Sliding

If the model tire is pressed lightly on a table with a constant vertical force, it is easy to see that when it is pushed sideways (by a small lateral force) the rubber deflects and the wheel moves a small amount laterally (see the bottom of Figure 2.2). If the force is increased a little, the deflection increases a little. If the force is increased still more, the tire begins to slide laterally along the surface. What happened? First the tire acted like a spring, the sidewalls bent elastically, and the lateral distortion increased roughly in proportion to the lateral force. After the tire began sliding, lateral force remained approximately constant.

If a different tire is used, say one with smaller-diameter metal disks (more rubber "sidewall"), the experiment has a similar outcome but the lateral displacement for a given lateral force is greater.

The lateral stiffness (tire standing still) is given as a lateral spring rate, say, in pounds per inch of deflection. The force required to slide the tire is a function of the friction coefficient, μ , which is defined as the ratio of two forces, the lateral force divided by the vertical force (the load on the tire). This is approximately constant over a range of loads for the model tire.

Most tire operation involves a mix of *elastic distortion* and *sliding friction*.

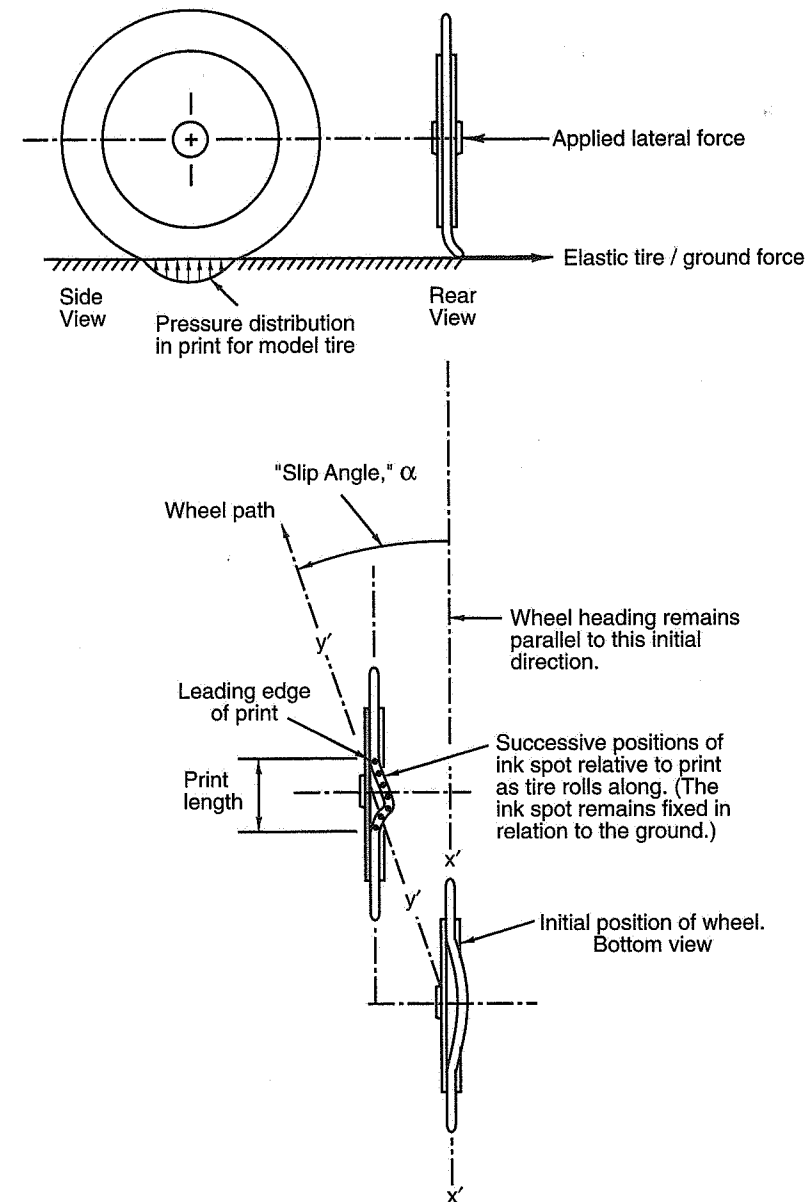


Figure 2.2 Mechanism of tire lateral force in elastic range.

Second Experiment - Rolling at Small Slip Angles

If the model tire is deflected (or bent) laterally and then rolled along, it moves in a direction at an angle to the wheel plane or heading; while somewhat of a misnomer, this angle is called the *slip angle*. The relationship between lateral force and slip angle can be illustrated with the model tire by placing a series of ink spots on the surface of the tire and rolling it along under a steady lateral force. Since the model tire behaves like the center plane of a real tire, it will give an idea of how real tires produce lateral force.

As shown in Figure 2.2 (rear view), the application of a lateral force gives rise to a lateral deflection of the tire in the vicinity of the print (the applied lateral force should be small enough to avoid sliding or exceeding the friction limit). As the wheel is rolled forward without steering (that is, as its plane remains parallel to its heading—see top view Figure 2.2) it will be observed that the path of the wheel is at an angle, α , to the wheel plane. This occurs for the following reason: each point (indicated by the ink spots) of the undeflected tread enters the print at the leading edge where it becomes fixed to the road. As the tire rolls along, these points move aft relative to the print and also move sideways relative to the wheel because of the lateral deflection in the print. (It is convenient to think of points moving through the print, while in reality, each ink spot in the print is stuck to the road as the tire rolls along.)

cop enter

The lateral distortion pattern of the model tire in the print area and the successive positions of an ink spot relative to the print are shown in the upper of the two top views of Figure 2.2. As a spot moves aft in the print, its lateral deflection relative to the wheel plane increases until it approaches the trailing edge of the print. Here the local vertical force, as shown in the side view of the tire in Figure 2.2, decreases and the frictional force (which can be calculated using the coefficient of friction, μ , above) can no longer maintain the lateral distortion. At this point in the print the tread moves rapidly back to the undeflected position (in the center plane of the wheel) and shortly thereafter leaves the print.

High Slip Angles

If the lateral force is increased, the slip angle will increase, the tire will be distorted further, and the onset of sliding at the rear of the print will move forward. The process is progressive. When the tire has enough applied lateral force that most of the print is sliding, it is said to have "broken away" and the lateral force is determined by the coefficient of friction.

Slip Angle Clarified

It is important to understand that there is no sliding in the print except near the trailing edge, where the vertical forces are low. The ability of the tire to travel out of its

plane without appreciable slippage is the result of laying down successive prints, each laterally displaced because of the sideways tire distortion. It is equivalent to heading in a given direction but walking at an angle to that direction by displacing each foot laterally as it is put on the ground (Figure 2.3). The tire behaves as if it had an infinite number of feet around its periphery.

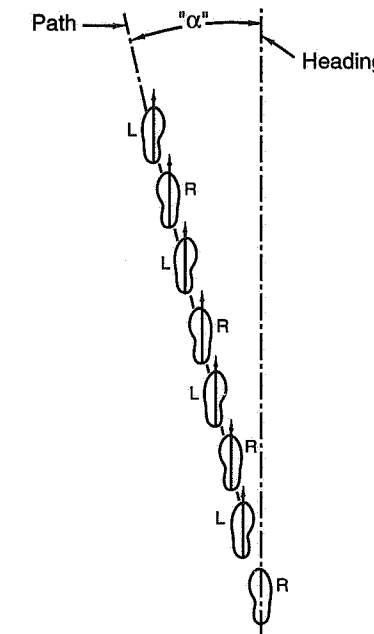


Figure 2.3 Walking analogy to tire "slip angle."

From the above description of what happens in the tire print it should be apparent that "slip" angle is somewhat of a misnomer; in the elastic range of tire operation, very little slipping occurs. Nonetheless, slip angle is the traditional term for this angle and will be used here.

Relationship Between Lateral Force and Slip Angle

The lateral (or cornering) force may be thought of as the result of slip angle, or the slip angle as the result of lateral force. Some examples:

- If the front wheels of a vehicle are steered, a slip angle is created which gives rise to a lateral force, this lateral force then turns (or yaws) the vehicle.
- On tire test machines it is common to set the tire at a series of slip angles and measure the resulting lateral force at each angle.
- When a lateral wind gust strikes a vehicle, the wind force must be reacted by lateral tire forces due to changes in tire slip angles.
- When cornering ("centrifugal force") or on a banked road (gravitational force component), the lateral force is reacted by changes in tire slip angles and resultant tire forces.

One's point of view must be adapted to the situation.

The tire steady-state lateral force comes from the elastic distortion of the tire. From the standpoint of the tire, the road is pulling the print sideways in the triangular pattern shown in Figure 2.2. If the applied force were increased one would expect the distortion in the print and the slip angle to increase approximately proportionately, provided that the print was not distorted so much that sliding occurred in a large area of the print.

Gough Testing Machine

Early measurements made on real tires confirm the behavior of the model tire. Figure 2.4 shows a device (Ref. 52) developed by Eric Gough (pronounced Goff) in the early 1950s, for measuring both the lateral distortion and associated stress distribution in the print. Gough was a member of the Dunlop Research Centre in England and a pioneer researcher in tire behavior. Although these measurements of print behavior have been made many times since using more modern instrumentation techniques, we have chosen to present Gough's simple mechanical apparatus.

The tire/wheel/axle assembly of Figure 2.4 is supported to ground by a structure not shown in the figure. The axial force on the axle, perpendicular to the wheel plane, is measured by a "capsule." This force reacts (is equal and opposite to) the tire lateral force, i.e., the force applied by the roadway to the tire. The tire rests on a plank assembly simulating a roadway, which can be moved slowly along on the support wheels to give relative motion between the axle and the "ground." A vertical pin at "a" engages in a groove in the tread (tires with simple circumferential grooves were used) and its lateral motion is recorded by the pointer at "b." If the tire is set at a slip angle, the pin will track the lateral distortion as the tire rolls relative to the platform. A narrow, flat, lateral bar, "c," supported on stiff leaf springs at its ends, enables the force or stress in lateral "slices" of the print to be recorded as the tire rolls past. The slight movement of the leaf spring is linked to a recording pointer with a mechanical amplification ratio of some 18 to 1. A final measurement is the longitudinal position of the pin and bar in the print.

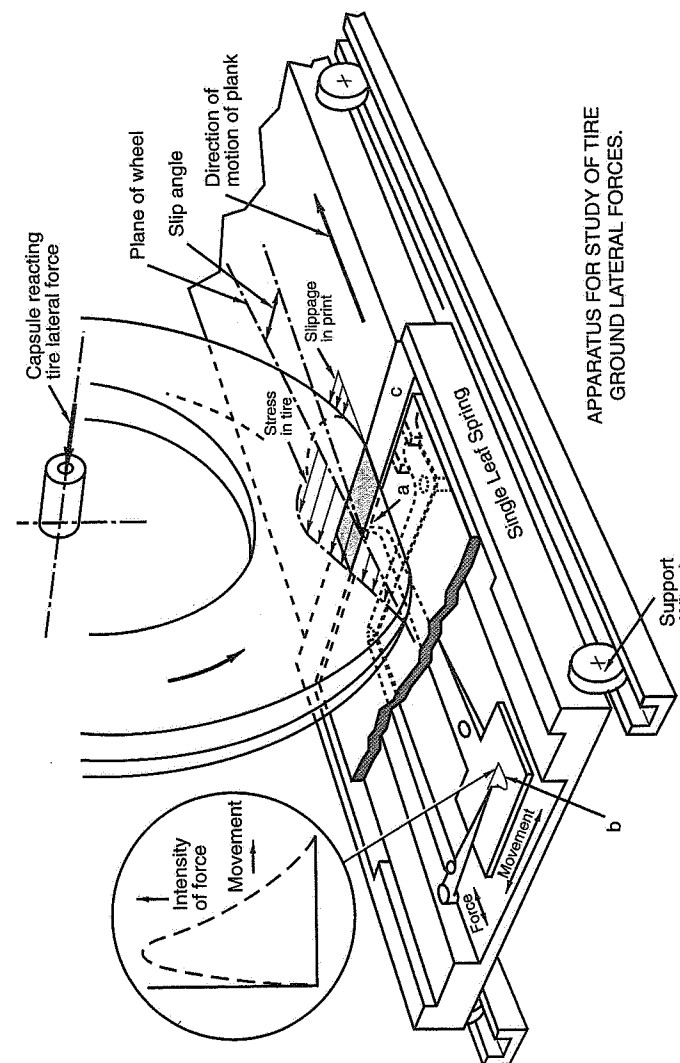


Figure 2.4 Gough's device for study of tire print characteristics.

It was found that the force computed from the area under a curve of lateral force (stress) distribution along the print and perpendicular to the wheel plane equaled the lateral force measured at the axle. Thus the lateral tire force was the result of the print distortion plus any frictional sliding forces in the aft portion of the print.

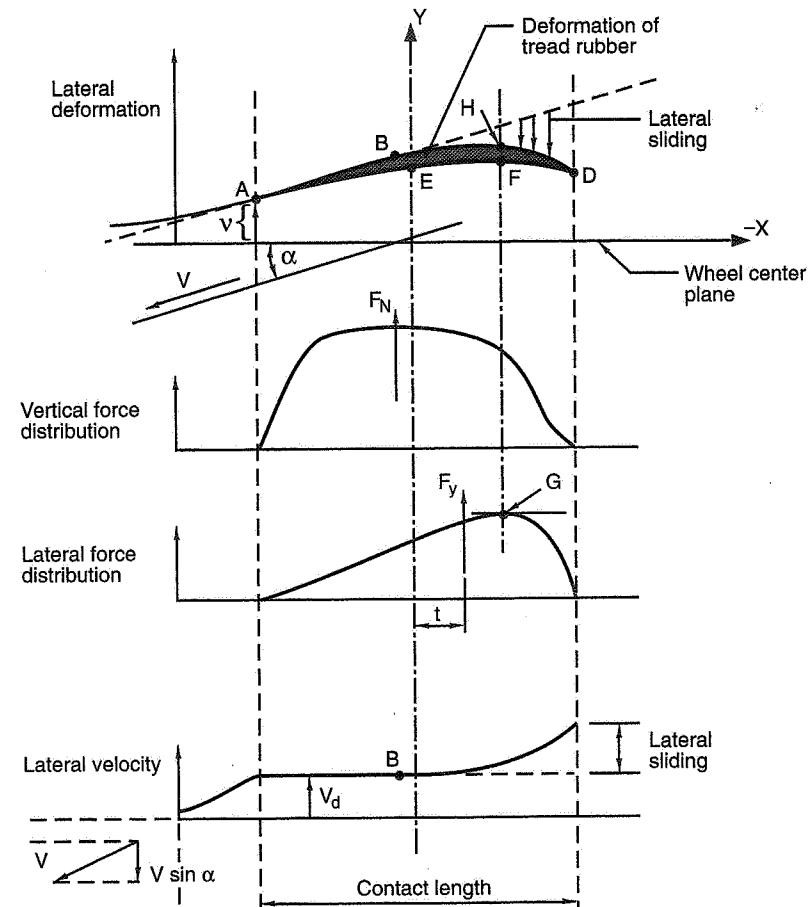
Figure 2.5 illustrates some data taken from a Gough-type device at a fairly high slip angle, approximately 15° . Point A is the leading edge of the print where the lateral deflection is v in the steady-state rolling situation. The carcass of the tire has some bending stiffness and hence deflection has propagated ahead of the footprint. As point A moves aft in the print with an increasing vertical force, complete adhesion prevails and the point moves along line A—B which is parallel to the velocity vector, V . The lateral velocity, $V_d = V \sin \alpha$ (α = slip angle) is constant. At point B, the lateral stress in the carcass and tread (the tread is shown cross-hatched) exceeds the local friction coefficient times the local load and lateral sliding starts. The sliding continues to point D where the element leaves the print and lifts off the road. The tread and the carcass can be viewed as two lateral springs in series. Although they have different spring constants, they are both exposed to the same lateral force. In this simple model, their maximum deflections would occur at the same time and at the peak of the lateral force curve. Thus, points H, F, and G occur at about the same place along the print length.

The following observations on Gough's tests can be made:

- The centroid of the lateral force is aft of the center of the print. The distance aft is called the *pneumatic trail* (t in Figure 2.5c). The pneumatic trail times the lateral force is the *tire aligning torque*. These are discussed further in this chapter.
- Lateral slippage of rubber across the road occurs in the back of the print. The amount of lateral movement depends on the sliding velocity and the slip angle.
- Glass plates flush with the road surface are used for observing the print at speed; observations can be made with high-speed cameras from below. The photos generally confirm the findings of the slow-speed Gough machine in terms of the character of tire distortion.
- Tire lateral force characteristics in the elastic range (small slip angles) are a function of lateral displacements in the print associated with the rolling process and are largely independent of speed. Low-speed tire testers (1-2 mph) are adequate for measuring tire characteristics in the elastic regime.

Measurement of Tire Lateral Force Data

Tire force and moment data are measured by constrained test. Laboratory and on-road test machines are used. In the laboratory, the road surface may be either a drum (external or internal) or flat steel belt with various surface treatments, or it may be an actual road surface. Figure 2.6 shows TIRF, the first large, flat belt, high-speed tire tester, which is



Distribution of forces and lateral velocity over the contact length.

Figure 2.5 Tire print characteristics—lateral force (Ref. 33).

still in service and is frequently used to test race tires. Tire forces and moments are measured by a special hub generally referred to as a "balance." Modern six-component balances are based on wind tunnel technology (wind tunnel testing is another example of constrained testing). There are many problems connected with the accurate measurement of tire data, for example:

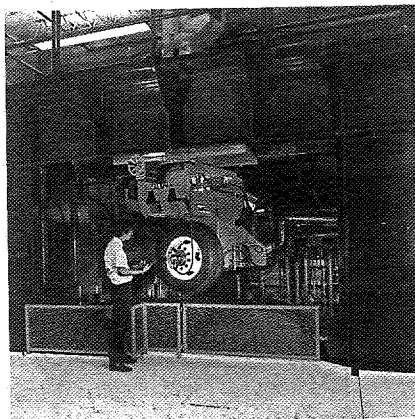


Figure 2.6 Calspan Tire Research Facility, TIRF.

- Tire wear and use of multiple tire samples (to obtain data on one tire design)
- Lack of control of tire temperature (both tread and carcass)
- Accurate control of test conditions, including load, longitudinal slip ratio (tractive force), etc.
- Test machine limitations in ranges of load, power, speed, slip/camber angles, etc.
- Treatment of measured test data and data reduction

One of the major problems in vehicle dynamics is obtaining enough reliable data on tire designs of interest. Because of the number of independent variables, raw tire data is seldom complete. In those cases where complete data is available, it is voluminous—inch-thick reports are typical. The user then has the problem of converting the raw data to a useful format. In this book, tire data is presented in graphic form for different variables.

Turning now to the complete slip angle range of tire operation, Figure 2.7 is a plot of lateral force versus slip angle for a typical racing tire. This data was taken on Calspan's Tire Research Facility on a flat, dry, simulated road. The tire is free-rolling and the curve is for a single load. The *elastic*, *transitional*, and *frictional* ranges of tire operation are labeled (see Figure 2.33 for SAE sign conventions).

The peak of the curve may remain at a constant value or fall off slowly as indicated. In dry conditions, race tires generally reach their peak lateral force at slip angles in the vicinity of 3° - 7° . On a wet surface the peak will in general be lower, and the fall-off in lateral force after the peak will be more rapid.

P215/60 R15 Goodyear Eagle GT-S (shaved for racing) 31 psi.

For a given load, in this case 1800 lb.

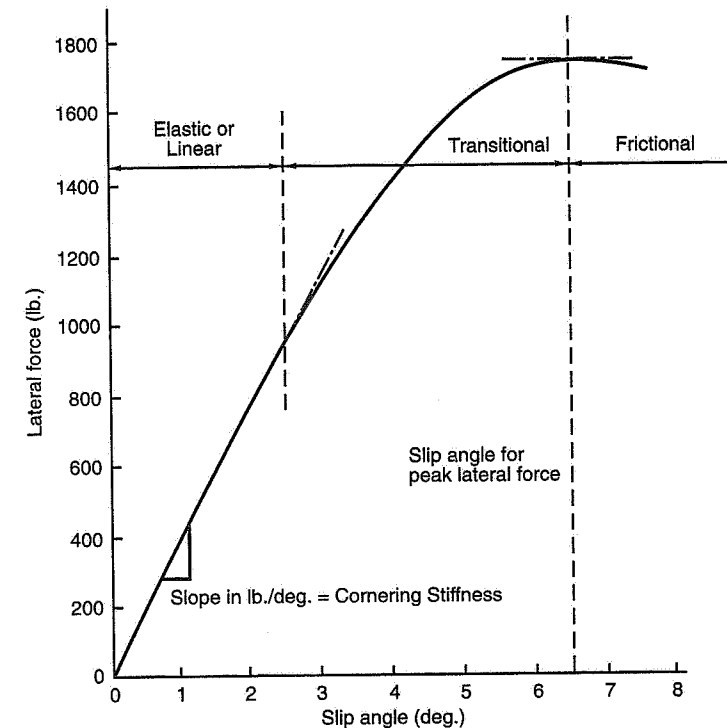


Figure 2.7 Lateral force vs. slip angle for a racing tire.

When a particular tire is tested at a series of loads, the lateral force curves appear as in Figure 2.8. It will be noted that as the load increases, the peak lateral force occurs at a somewhat higher slip angle. Also, the cornering stiffness (slope in the elastic range) increases.

The trend of the peaks (dotted curve) is predictable from nondimensional tire theory (see Chapter 14).

Tire Load Sensitivity

At and beyond the peak most of the print is sliding and the lateral force is the result of friction between the tire and the road surface. As noted earlier, physics utilizes the

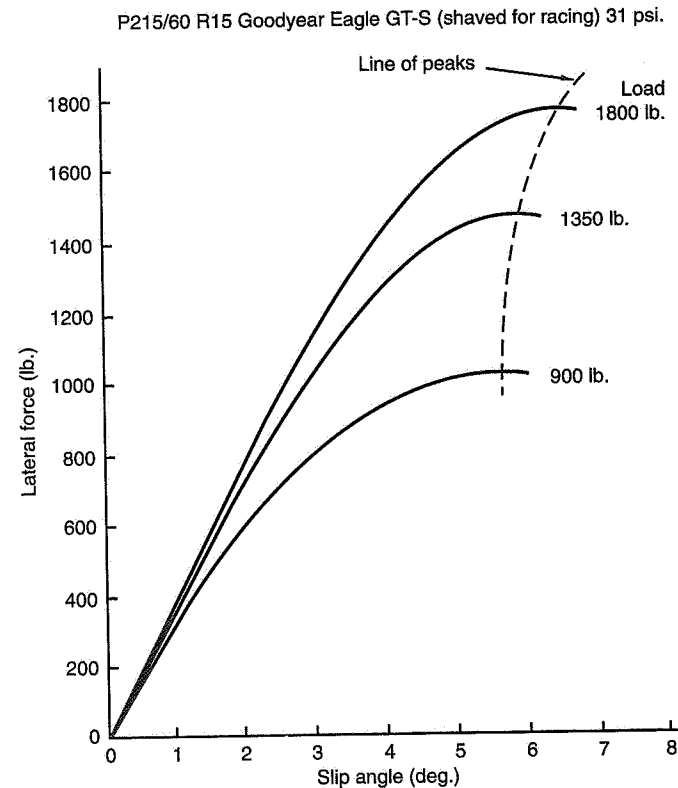


Figure 2.8 Lateral force vs. slip angle for several loads.

concept of a friction coefficient defined as

$$\mu = \frac{\text{Frictional force between two bodies}}{\text{Normal force between two bodies}}$$

This suggests normalizing (also referred to as nondimensionalizing) the lateral force vs. slip angle curve by dividing by the load to give a dimensionless measure of the amount of lateral force obtained in relation to the load:

$$\frac{\text{Lateral force}}{\text{Load on tire}} = \text{Lateral Force Coefficient}, \frac{F_y}{F_z}$$

and curves such as those of Figure 2.8 can be replotted as in Figure 2.9.

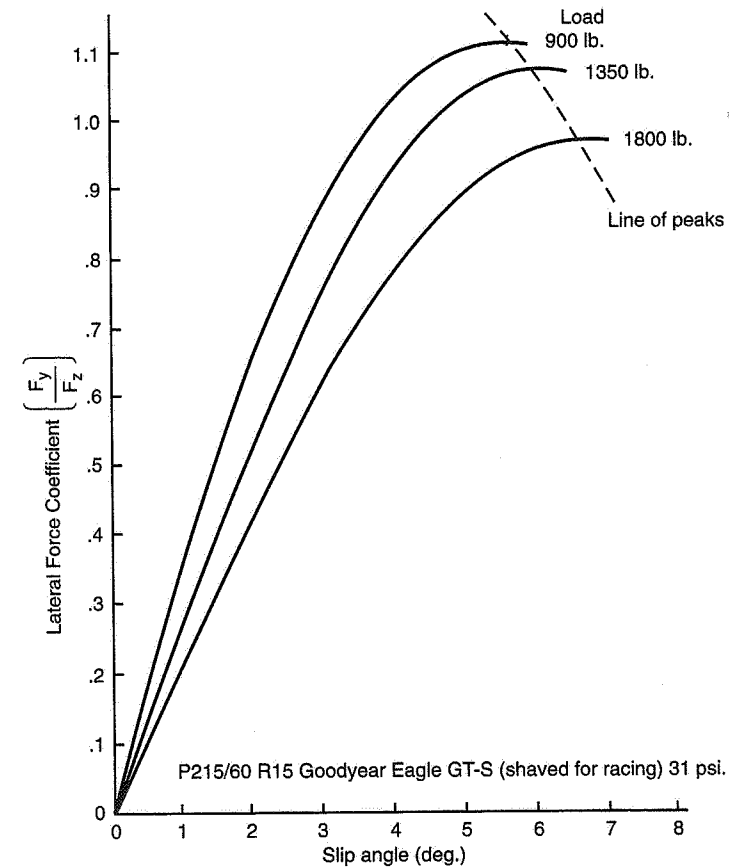


Figure 2.9 Normalized lateral force vs. slip angle.

It will be noted that the peaks of all of the load curves are brought more closely together when plotted in this fashion. If they all reached exactly the same value, the peak lateral force for any load would be simply (lateral force coefficient) \times (load on tire).

Actually, the peak lateral force coefficient (or lateral friction coefficient) is normally higher for the lighter loads or, conversely, falls off as the load increases. This effect is called the *tire load sensitivity*. Both the magnitude of the lateral friction coefficient and its variation with load (load sensitivity) are important in racing. The lateral friction coefficient is approximately independent of speed but can be increased by "stickier" rubber compounds and by insuring appropriate operating temperatures. For a current Grand Prix tire the coefficient may run as high as 1.8 at light load.

The tire load sensitivity has a major effect on the balance (plow/spin) of a race car operating near the limit. As the tire vertical loads change due to cornering, accelerating, or braking, the tire performance is constantly changing. A description of how the loads on the wheels affect the overall stability of the vehicle is given in Chapter 5. Chapter 18 includes techniques for estimating the actual wheel loads.

The transitional zone of tire operation varies with tire design parameters. It can be fairly gradual, extending over a sizable slip angle range or it can be more abrupt. Some tires have smooth, gentle breakaway characteristics giving plenty of warning while other tires "let go" suddenly. So many tire design factors are involved that it is difficult to cite generalities. However, tires that reach higher coefficients may let go faster as more of the print has been utilized for elastic distortion. For example, radial tires have a belt that inhibits sliding in the print. Radials have the reputation of more sudden transition and higher peaks. Many of the older bias-ply tires reached their peak very gradually with lots of warning. One would also expect that breakaway would be a more gradual affair with longer narrower print shapes. The tread depth and pattern can also be influential.

Before leaving the subject of lateral force, it is important to note its variation with load for a given slip angle. Figure 2.10 is typical of modern radial tires. All the curves are nonlinear—the lateral force falls off at higher loads. This type of presentation is particularly useful for the analysis of a pair of wheels on a single "axle" with lateral load transfer. This will be discussed further in Chapter 7.

2.2 Aligning Torque and Pneumatic Trail

Aligning torque (or moment), M_Z in SAE J670, describes a tire's tendency to steer about a vertical axis through the "center" of the print (the origin of the tire axis system). At low and medium slip angles the tire tends to align its heading with its path. This is a stabilizing effect analogous to a weather vane aligning with the wind direction. In other words, tires like to point the way they are going. For the present discussion the wheel is assumed to have zero camber (upright wheel).

The aligning torque comes from the shape of the print, as described in a previous section. Figure 2.2 shows that the shape of the distortion in the print is roughly triangular and is not symmetric about the fore-aft center of the print. The elastic distortion in the print increases from front to back and this gives an uneven distribution of lateral force along the length of the print. This uneven distribution gives rise to aligning torque. The aligning torque is typically measured in pounds-feet, at a given operating condition of slip angle and load.

Pneumatic trail is a different way of looking at this asymmetry in the print, shown in Figure 2.12. The pneumatic trail is the distance from the fore-aft center of the print to the center of action of the lateral force. The tire aligning torque is the lateral force times the pneumatic trail, or, pneumatic trail equals aligning torque divided by the lateral force.

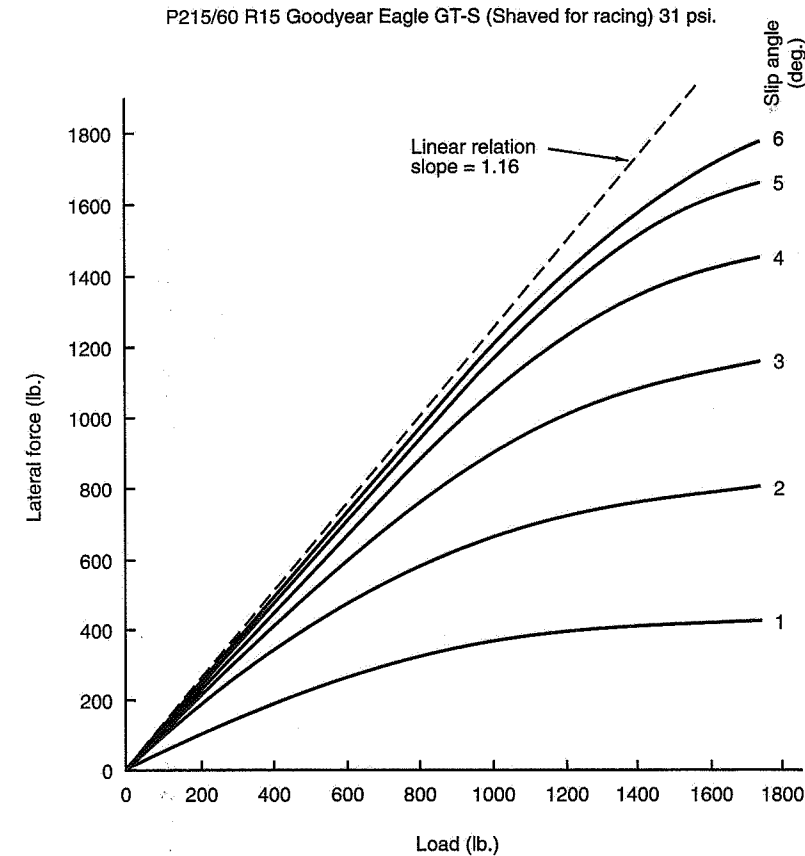


Figure 2.10 Lateral force vs. load.

Linear Range - Low Slip Angles

From Figure 2.2, the higher stresses in the aft part of the print work to reduce the slip angle. This is true in the linear range of tire performance. In fact, the center of tire lateral force can be found by measuring the contribution of each part of the print to the torque around the center of the print, in the same way that center of gravity is estimated (in Chapter 18).

Nonlinear Range - High Slip Angles

At high slip angles, the rear of the print is sliding laterally along the ground. This reduces the amount of stabilizing aligning torque. At breakaway (the friction limit) the aligning torque is reduced to near zero, and in many cases actually reverses sign. This means that when the tire is sliding, it no longer has any tendency to line up with its path (and may actually try to increase its slip angle). Some tire data for aligning torque is shown in Figure 2.11.

Mechanical Trail, Pneumatic Trail and Steering Torques

Trail, in its simplest sense, is illustrated by a swiveling caster. The tire print trails behind its steering pivot. Automotive steering systems are designed the same way, the caster angle gives a *mechanical trail*, as shown in Figure 2.12. Another way to obtain mechanical trail is to move the kingpin forward of the wheel center; this kingpin offset is shown in Figure 19.1. In practice, both methods are used to obtain mechanical trail.

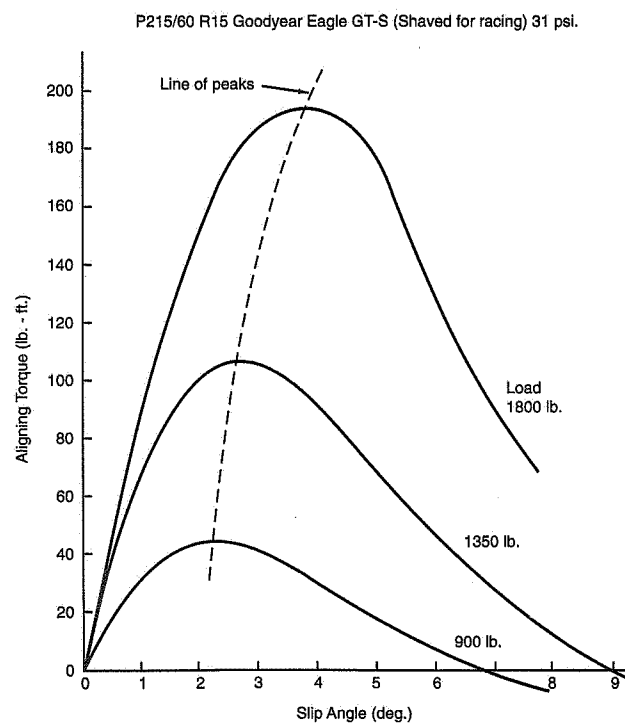


Figure 2.11 Aligning torque vs. slip angle for several loads.

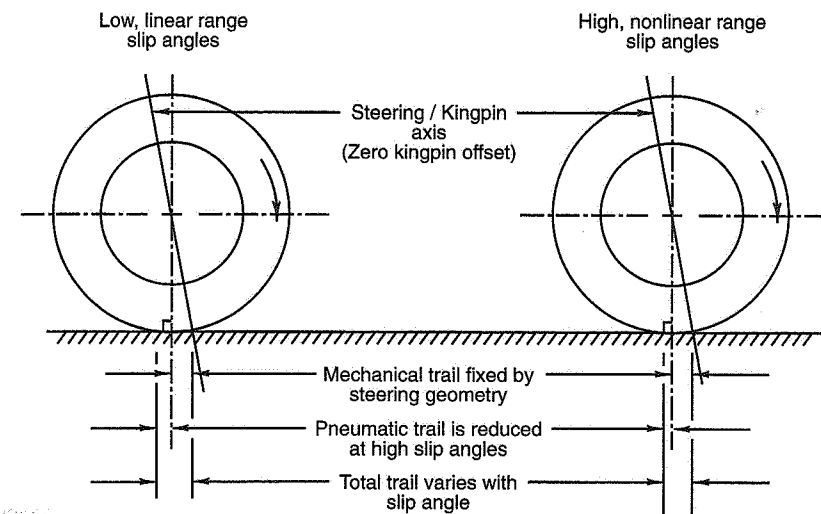


Figure 2.12 Pneumatic and mechanical trail.

If all the tire lateral force at the print was concentrated directly below the axle, the steering torque would be given by the mechanical trail times the lateral force. The aligning torque can also be thought of as a "trail" effect, hence the term *pneumatic trail* as noted above. The pneumatic trail is always present; it changes with tire operating conditions. The sum of the mechanical trail plus the pneumatic trail times the lateral force gives the *steer torque* about the kingpin (assuming that any other torques cancel out when left and right wheel effects are added).

When the mechanical trail is small, the tire aligning torque (pneumatic trail) will dominate the steering torque. An extreme case was in older cars where there was no mechanical trail at all. In this case, the steering self-centering was reduced as the front tires neared their limit, tending to reduce the radius of turn. (This can be seen in Figure 2.11: at high slip angles the aligning torque approaches zero and can become negative.)

At the other extreme, some modern cars have so much mechanical trail and/or power boost that the effect of the aligning torque is minimized. This gives a linear relationship between lateral force and kingpin torque, with no information from the aligning torque reaching the driver. Maximum warning of breakaway would occur if all of the steering torque came from the pneumatic trail (or tire aligning torque). Thus the pronounced fall-off in aligning torque shown in Figure 2.11, which occurs before the lateral force peak, would tell the driver that the limit was being reached. A balance between the two gives

the skilled driver some warning that the front wheels are nearing the limit, while maintaining reasonable steering torques.

Pneumatic Trail and Skid Warning

The following numerical example illustrates the significance of pneumatic trail (tire aligning torque) in warning the driver of impending breakaway. It is based on the tire data shown in Figures 2.8 and 2.11. This tire size would be used on a large front-engined sports car or performance street car of some 3500 lb. gross weight with 1800 lb. on the front wheels. Consider that this vehicle is set up with a front anti-roll bar to lift the inside front wheel on approach to max lateral. Since the inside wheel is "dancing" along the road producing negligible lateral force and aligning torque, the calculation can be performed for the outside front wheel only, now carrying the full 1800 lb. Maximum lateral force for this tire occurs at $\alpha = 6.5^\circ$ (Figure 2.8) at a maximum lateral acceleration of the vehicle of about 0.97g.

We are interested in estimating the steering wheel rim force due to pneumatic and mechanical trail over a small range of slip angle and lateral acceleration prior to breakaway. We have chosen to use slip angles of 5.5° to 6.5° corresponding to 0.94 to 0.97g. The calculation is performed for mechanical trail offsets of the kingpin of 0.0", 1.25", and 2.49" which correspond respectively to 0°, 6°, and 12° of caster angle on a front tire radius of 12". For this example, offset is used to avoid other components of torque which arise with caster angle and which are not relevant to the present example. Finally, the calculation assumes no steering boost, a steering system with low friction and a steering wheel radius of 7".

The results given in Figure 2.13 show that a reduction of steering wheel rim force of nearly 30% occurs during the last 1° of slip angle before breakaway when all of the rim force comes from pneumatic trail. This should constitute a substantial warning to the driver of impending breakaway. When mechanical trail is added, the percent reduction is substantially diluted. The two dashed curves show that rim force due to mechanical trail alone actually increases slightly due to the increase in tire lateral force as maximum lateral is approached.

With any level of mechanical trail, the calculated rim forces in this example are high and power steering would normally be used.

2.3 Longitudinal Force

In order to accelerate or brake a vehicle, longitudinal forces must be developed between the tires and the ground, in the tire footprints. No change in speed (acceleration) can take place without an applied force acting on the vehicle mass in accordance with Newton's second law. The mechanism in the tire for developing longitudinal forces bears some

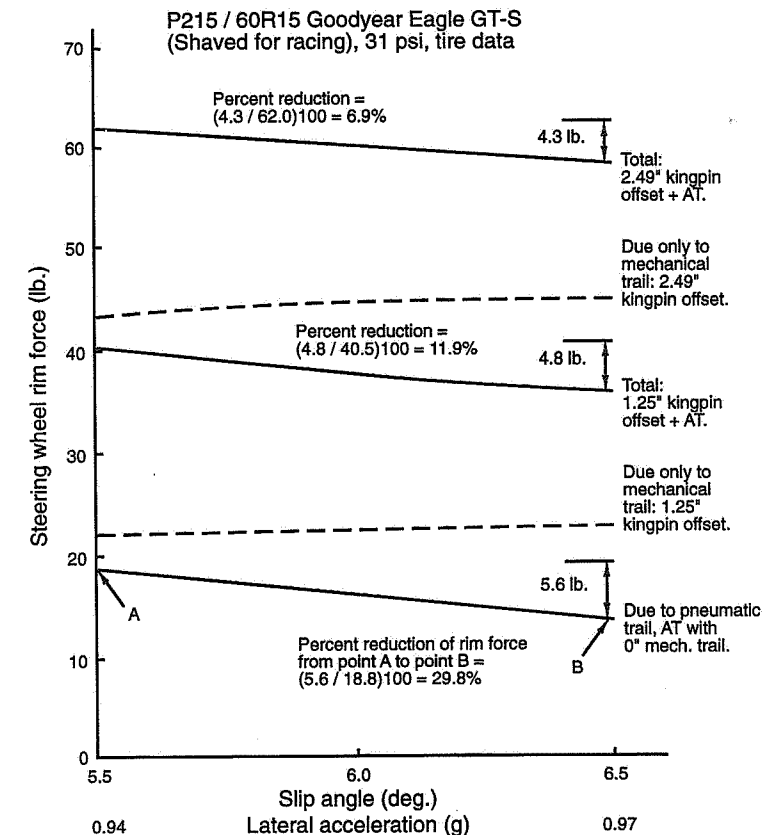


Figure 2.13 Rim force due to pneumatic and mechanical trail.

relationship to that for lateral forces inasmuch as there is an elastic distortion region (in this case longitudinal stretching) and a sliding or frictional region. Let us look at the acceleration situation first, where the tire is experiencing a driving torque at zero slip angle.

Tractive Force

In Figure 2.14 the axle of the wheel is fixed and horizontal and the platform representing the road is moved relative to it. This way of obtaining the relative motion between tire and "road" is convenient and typical in indoor tire testers. The situation shown corresponds in real life to the tire rolling forward to the left of the figure under the action of the applied driving torque, M_T .

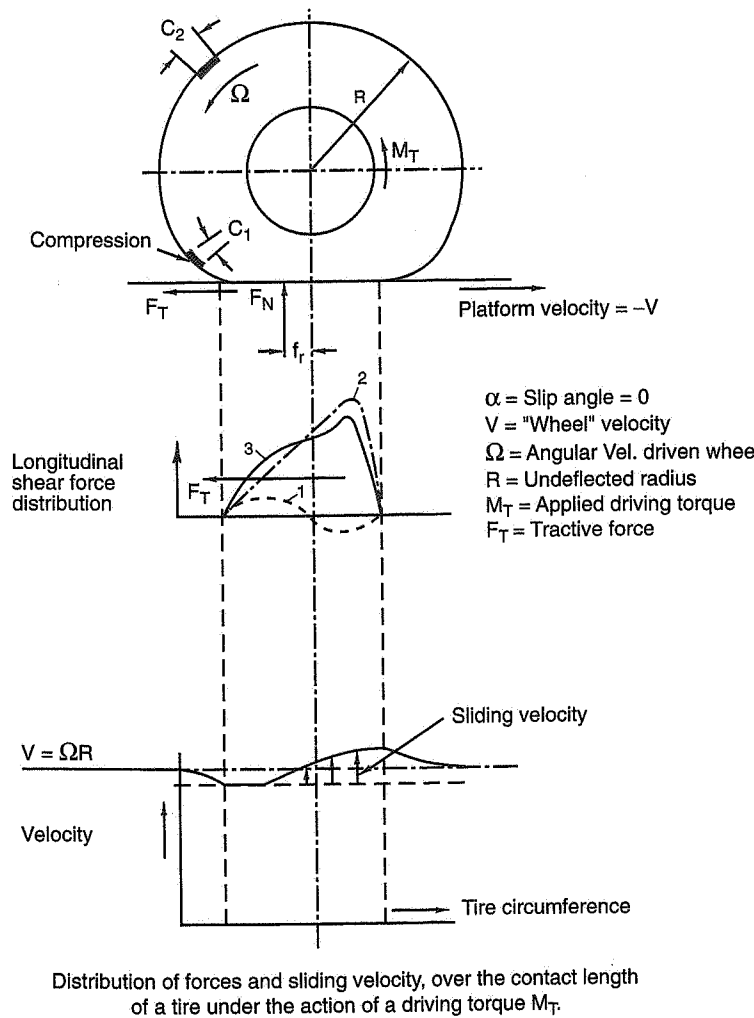


Figure 2.14 Tire print characteristics—driving (Ref. 33).

As indicated, the driving torque produces a forward reaction, i.e., the tractive force, F_T , from the road to the tire.⁸ This force moves the tire footprint forward relative to the axle, compressing the tread elements ahead of the print and deforming the tire in a circum-

ferential direction to accommodate. The compressed length C_1 may be compared to the uncompressed length C_2 . The compressed tread elements adhere to the platform (road) on entering the print. The shear stress (road to tire) is in the forward direction and tread elements are bent forward relative to the tire carcass. As more and more elements enter the print and move aft, into the region of increasing local load, the shear stress builds up in a linear fashion as shown by curve 2 of the figure.

In a free-rolling tire, longitudinal shear stresses also exist in the print. This is because the radius is forced to change as the elements enter the print. For a constant angular velocity, Ω_0 , the linear velocity at the circumference of the tire decreases as the radius changes resulting in a forward stress; this stress reverses in the last half of the print as the radius recovers. This stress distribution is approximately shown by curve 1. The net effect is to modify the stress pattern due to the tractive force, yielding a resultant such as curve 3. Direct superposition of curves 1 and 2 is questionable since sliding is occurring in part of the print.

The longitudinal shear force falls off as the rear of the print becomes unloaded. Sliding then occurs between the rear tread elements and the road—the elements which were bent forward now tend to straighten up. The longitudinal velocity in the print relative to the velocity of the undeflected tire is shown in the bottom of Figure 2.14.

This sliding in the print means that the revolutions/mile of a tire under a driving torque are greater than for a free-rolling tire.

Braking Force

Figure 2.15 is comparable to Figure 2.14 but the applied torque, M_B , is in the braking direction. The slip angle is again zero. This torque produces a braking force from the road to the tire, F_B . The force moves the print back relative to the axle, compressing the tread elements aft of the print. F_B also tends to pull and stretch those tread elements ahead of the print (compare C_3 with C_2).

For a modest braking force these elements will adhere to the road upon entering the print and will be bent backward by the rearward shear stress. As more and more elements enter the print and move aft under increasing load, the longitudinal shear force will build up linearly as indicated by curve 2. The free-rolling longitudinal shear force is given by curve 1. The approximate net shear stress is given by curve 3 (the sum of curves 1 and 2). As the print unloads toward the rear, sliding occurs between the tread elements and the road. Relative to the carcass the backward-bent elements tend to straighten up and the sliding velocity is shown by the bottom curve in Figure 2.15.

⁸ Tire forces and moments are generally considered as those which the road applies to the tire.

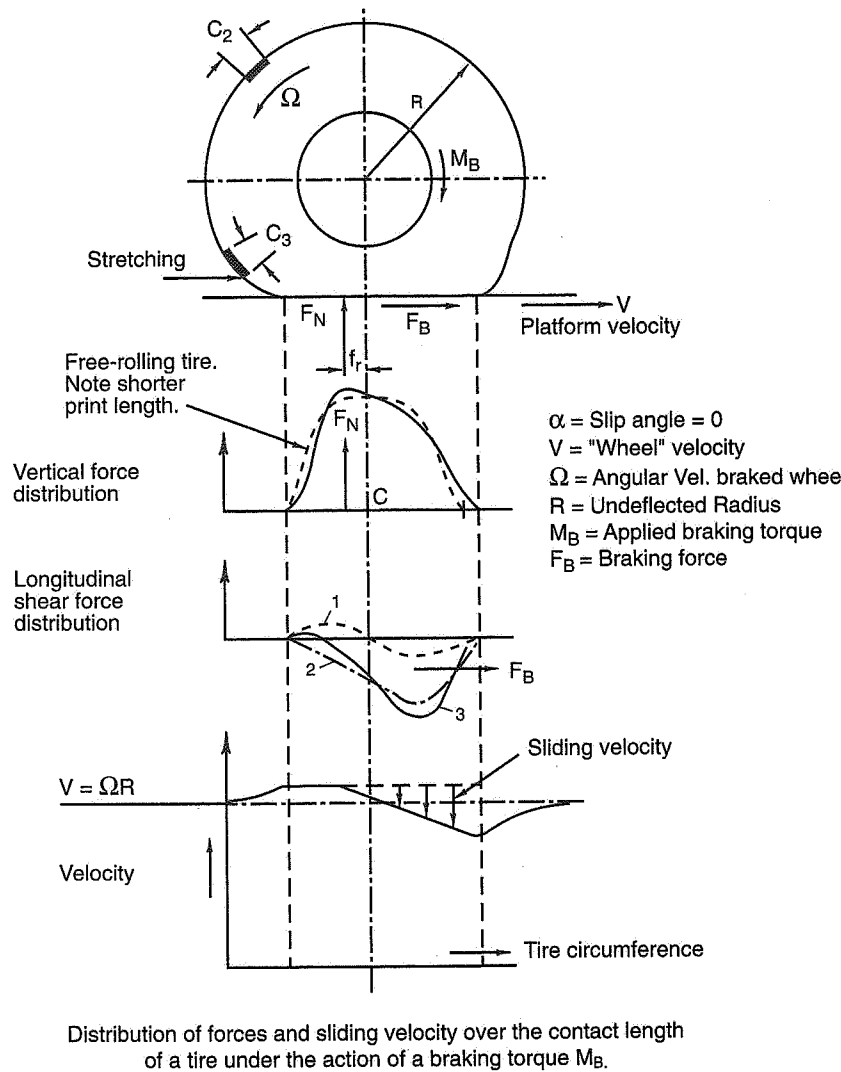


Figure 2.15 Tire print characteristics—braking (Ref. 33).

Slip Ratio

SAE J670 defines the longitudinal slip velocity, s , as the difference between the angular velocity of the driven (or braked) wheel, Ω , and the angular velocity of the free-rolling

wheel, Ω_0 , that is, $s = \Omega - \Omega_0$. SAE J670 further defines slip ratio as

$$SR = \frac{\Omega - \Omega_0}{\Omega_0} = \frac{\Omega}{\Omega_0} - 1$$

which can be expressed as a fraction or a percentage.

Now, $\Omega_0 = V/R_e$, where R_e is the effective radius of the free-rolling tire which can be calculated from the revolutions per mile. The slip ratio can thus be expressed as

$$SR = \frac{\Omega R_e}{V} - 1, \quad \alpha = 0$$

For free rolling, $\Omega R_e/V = 1$ and $SR = 0$; for locked braking, $\Omega R_e/V = 0$ and $SR = -1$.

If spinning is defined as $SR = +1$, then $\Omega R_e/V = +2$, which means that the peripheral speed is twice that of the free-rolling tire. This definition of spinning is arbitrary. The onset of spinning starts much earlier as subsequently discussed.

Tractive force F_T and braking force F_B are a function of slip ratio. As the slip ratio increases (numerically) from zero, the forces rise rapidly to a maximum which usually occurs in the range of 0.10 to 0.15 slip ratio, after which the forces fall off. Up to the peak the forces depend heavily on the elastic properties of the tread and carcass. After the peak the forces depend on a variety of factors such as tread composition, road texture, surface moisture, speed, tire temperature, etc.

Figures 2.16 and 2.17 are typical traction and braking slip ratio curves. This data was measured on a bias-ply passenger car tire; unfortunately, this data is rare and data on a modern racing tire was not available to the authors. The forces have been normalized by dividing by the peak force value in each case. For the traction case, note that the force falls off rapidly after the onset of spinning. This is for dry surface. Traction slip ratio curves can be obtained by recording drawbar pull against a dynamometer truck while recording test wheel rpm. Braking slip ratio curves can be measured with a trailer where the wheel is progressively braked. Both characteristics can also be measured in the laboratory, depending on the capability of the test machine.

Prior to the peak, an increase in slip gives an increased force which tends to damp the rotational velocity. Once a tire exceeds the slip ratio for peak force in either traction or braking, it becomes unstable and the wheel tends to either spin-up (traction) or lock (braking). Testing tires after the peak requires a high-performance servo control system on angular wheel speed. Based on the SAE definition of slip ratio, SR, the input to this control requires measurement of Ω , V and R_e . Since R_e is not measurable on an instant-

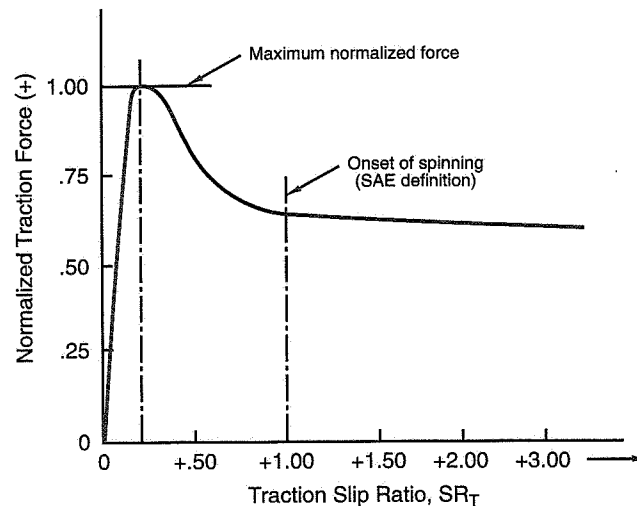


Figure 2.16 Typical traction—slip ratio curve; slip angle = 0°.

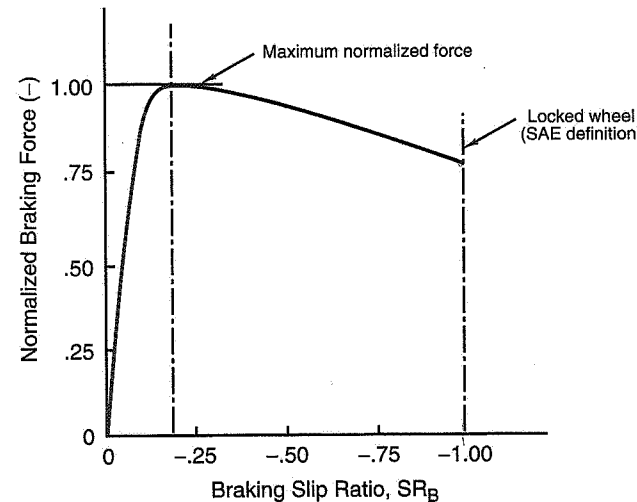


Figure 2.17 Typical braking—slip ratio curve; slip angle = 0°.

taneous basis, the Calspan TIRF uses the loaded radius R_ℓ , the height of the axle above the moving belt, and defines slip ratio as

$$SR = \frac{\Omega R_\ell}{V} - 1$$

When $\alpha \neq 0$, V must be replaced by $V \cos \alpha$ for both traction and braking definitions (see next section).

Definitions of Slip Ratio

A variety of slip ratio definitions are used worldwide. The following terms are used (some for just this section)

R_ℓ = height of the axle above the belt (road surface), loaded radius

R_e = effective rolling radius for free rolling at zero slip angle, from revs/mile

Ω = wheel angular velocity, radians per second

V = speed of the axle over the roadway, or belt surface speed

α = slip angle

$S, S_x, SR, K_x, \sigma_x, S_b, S_D$ = alternate definitions of slip ratio

The SAE J670 definition (Ref. 1) is

$$S = \left(\frac{\Omega R_e}{V \cos \alpha} \right) - 1$$

Calspan TIRF definition is

$$SR = \left(\frac{\Omega R_\ell}{V \cos \alpha} \right) - 1$$

An early definition used by Goodyear is

$$S_x = 1 - \left(\frac{V \cos \alpha}{\Omega R_e} \right)$$

Pacejka in Ref. 113 uses

$$\text{Practical slip quantity, } K_x = \left(\frac{\Omega R_e}{V \cos \alpha} \right) - 1$$

$$\text{Independent slip quantity, } \sigma_x = \left(\frac{V \cos \alpha}{\Omega R_e} \right) - 1$$

Sakai in Ref. 136 uses

$$\text{Traction, } S_t = \left(\frac{V \cos \alpha}{\Omega R_e} \right) - 1$$

$$\text{Braking, } S_b = 1 - \left(\frac{\Omega R_e}{V \cos \alpha} \right)$$

Dugoff, Fancher and Segel use the following in Ref. 42:

$$S_D = 1 - \left(\frac{\Omega R_e}{V \cos \alpha} \right)$$

Relationships among the various definitions of slip ratio follow:

$$S = K_x = -S_D = -S_b$$

$$S_x = -\sigma_x = -S_t$$

$$S = \frac{S_x}{1 - S_x} = \frac{-\sigma_x}{1 + \sigma_x}$$

$$S_x = \frac{S}{1 + S}$$

The SAE definition of slip ratio, S , may be computed from the Calspan TIRF definition, SR , as follows:

Let R_0 be the loaded radius for *free rolling at zero slip angle* for a corresponding speed and load. Also, let SR_0 be the corresponding slip ratio according to the TIRF definition. The effective rolling radius for free rolling at the same load and speed is

$$R_e = \frac{R_0}{1 + SR_0}$$

Then, for the case of nonzero slip angle and traction or braking, the SAE definition of slip ratio is given by

$$S = \left(\frac{\Omega R_e}{V \cos \alpha} \right) - 1 = \left(\frac{R_e}{R_\ell} \right) (1 + SR) - 1$$

where R_ℓ is the loaded radius and SR is the TIRF measurement of slip ratio. It is noted that $\Omega = \pi(\text{rpm})/30$, where rpm is that of the test wheel.

2.4 Combined Operation

For the race driver, the effect of traction and braking forces under cornering conditions is important. Although braking is initiated on the straight prior to a corner, it is generally carried on into the turn. Similarly, tractive effort may begin after the turn apex and continue onto the straight.

Sakai Data Plots

Comprehensive data on lateral and longitudinal force as a function of slip angle and slip ratio is relatively rare. Few facilities are available to run a comprehensive set of these tests, which are time consuming and costly. One published set of data (Ref. 136) was obtained by Sakai at the Japan Automobile Research Institute (JARI). This data was taken on a small passenger car tire at a load of 400 kg (882 lb.) and a speed of 20 km/h (12.4 mph). Although the tire and operating conditions are far from those of racing, this data gives a qualitative feel for the effects of combined slip angle and slip ratio. To a first order, tire forces/momenta are independent of speed.

In this data, Sakai defines longitudinal force as positive rearward (braking) and lateral force as positive to the right (right-hand turn). He defines two slip ratios, as described in the above tabulation of slip ratio definitions. The following table shows the difference between the SAE and Sakai definitions of slip ratio:

Slip condition	Sakai	SAE
Free rolling	0.0	0.0
Locked wheel braking	+1.0	-1.0
"Spinning" (2 × free rolling Ω)	-0.5	+1.0
"Spinning" (infinite Ω)	-1.0	$+\infty$

In order to give the reader a good understanding of the effect of combined slip angle/slip ratio on tire forces, four plots have been made from Sakai's published data. These are presented using his sign convention and his definitions of slip ratio.

Figure 2.18 shows the effect of slip angle on the relationship between the traction/braking forces and slip ratio. To reach peak traction/braking forces requires a higher and

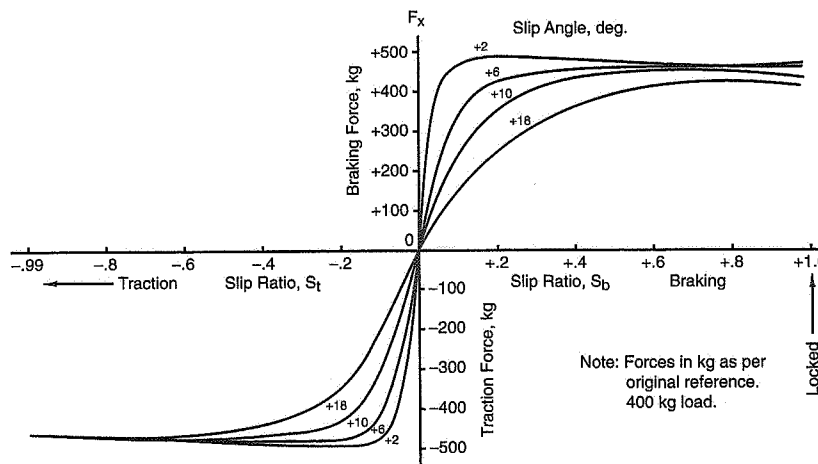


Figure 2.18 Braking and traction forces vs. slip ratio and slip angle (Ref.136).

higher slip ratio as the slip angle is increased. The peak value is somewhat lowered under braking.

Figure 2.19 presents the effect of slip angle on the relationship between lateral force and slip ratio. It will be noted that peak lateral force occurs under braking in the slip ratio range of 0.0 to +0.05, S_b . At any slip ratio the lateral force increases with slip angle, but at a progressively lower rate, as slip ratio (either traction or braking) is increased.

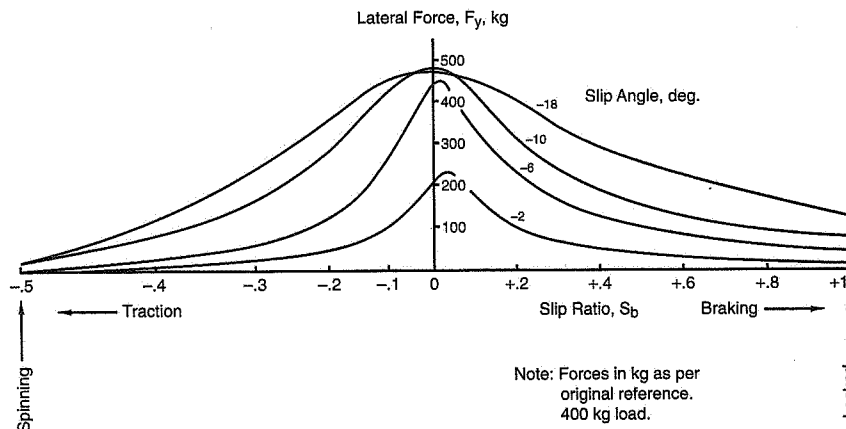
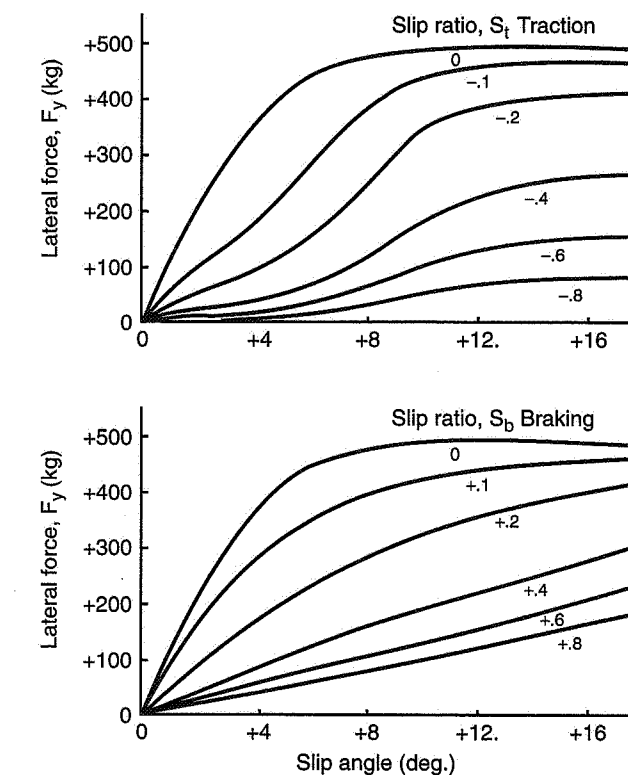


Figure 2.19 Lateral force vs. slip ratio and slip angle.

Figure 2.20 presents the same data plotted in a more familiar form—the cornering force curve (lateral force vs. slip angle) but with lines of constant slip ratio instead of constant load. It can be seen that the slope of the cornering force curve falls off rapidly with increase in traction or braking slip ratio.

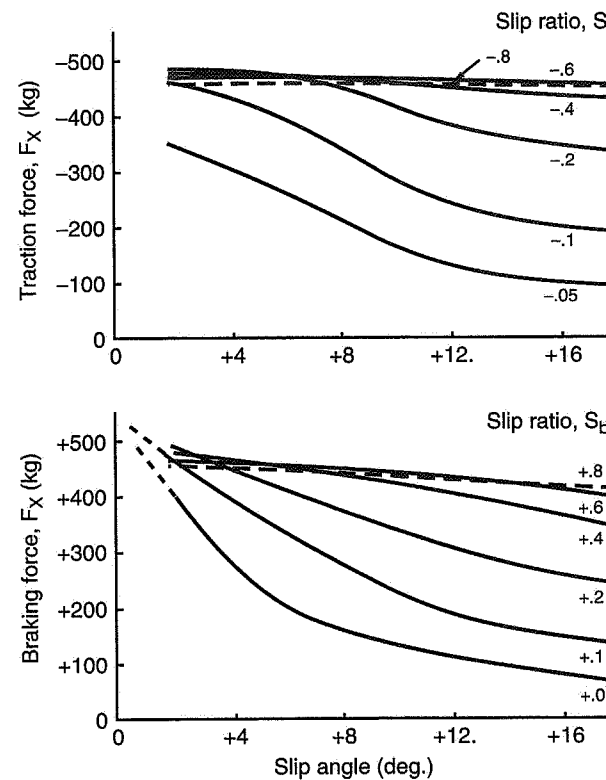


Notes: Force in kg as per original reference.
Lateral force is normal to wheel plane.
400 kg load.

Figure 2.20 Effect of slip angle and slip ratio on lateral force.

Figure 2.21 shows the effect of slip ratio on the traction/braking forces over the range of slip angles.

Figures 2.20 and 2.21 will be used in developing the complete friction circle, presented later in Figure 2.31.



Notes: Longitudinal force in kg as per original reference.
400 kg load

Figure 2.21 Effect of slip angle and slip ratio on traction/braking force.

Resultant Force vs. Resultant Slip Velocity

One can gain a more general understanding of the development of tire forces by noting that they all originate within the print as a result of some slip. Although it is convenient to think in terms of longitudinal and lateral forces, and slip ratio and slip angle (producing lateral slip), the tire only knows a resultant force and a resultant slip velocity. From the data of Figures 2.18 and 2.19 the resultant force and slip velocity have been computed and plotted in Figure 2.22. Some scatter due to the basic tire data and its manipulation is to be expected.

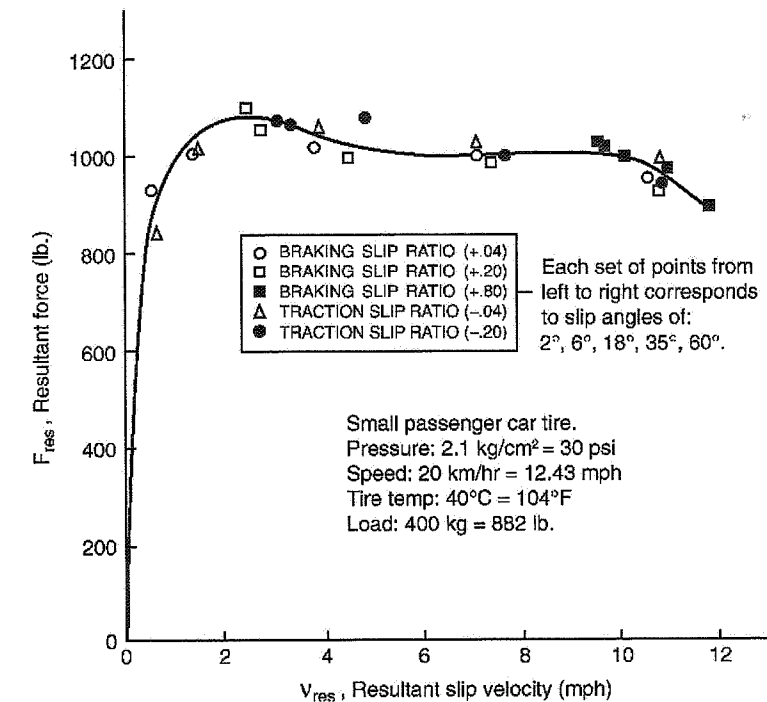


Figure 2.22 Resultant force vs. resultant slip velocity (Ref. 136).

The equations for the lateral and longitudinal slip velocity are

$$v_{\text{lateral}} = V \sin \alpha$$

$$v_{\text{longitudinal}} = V \cos \alpha - \Omega R_e = V \cos \alpha - V_B$$

where V_B is the circumferential velocity of the tire under traction or braking. (Note: V_B is related to traction and braking slip ratios—see Sakai under definition of slip ratio.)

The resultant slip velocity is

$$v_{\text{resultant}} = \sqrt{(v_{\text{lat}})^2 + (v_{\text{long}})^2} = \sqrt{V^2 + V_B^2 - (2V \times V_B \cos \alpha)}$$

The resultant force is

$$F_{\text{resultant}} = \sqrt{F_x^2 + F_y^2}$$

The peak of the resultant curve (Figure 2.22) is at 2.5 mph or at about 20% of the test velocity of 12.4 mph.

2.5 Camber Effects

In accordance with SAE terminology (Ref. 1), *camber angle*, ϕ , is defined as the angle between a tilted wheel plane and the vertical. The camber is positive if the wheel leans outward at the top relative to the vehicle, or negative if it leans inward. For testing isolated tires on tire testers, an SAE Tire Axis System has been defined and is discussed later in this chapter. In this system, the tilt of the wheel is referred to as the *inclination angle*, γ . The inclination angle is positive if the wheel is tilted to the right when viewed from behind the rolling tire.

In racing circles, tilt of a wheel is universally referred to as *camber*, with the sign conventions following SAE as above. The effect of camber on the tire forces and moments actually depends on the angle between the tire and a perpendicular to the ground—as opposed to the angle between the tire and a chassis reference. In the following figures, data is presented from several sources and generally refers to operating conditions that might be found at the outside front wheel of a car in a right-hand (+) turn.

Camber Force

In general, a cambered rolling pneumatic-tired wheel produces a lateral force in the direction of the tilt. When this force occurs at zero slip angle, it is referred to as *camber thrust*. A lateral force component due to camber can also occur at slip angles other than zero. Camber force is a function of the tire type, construction, shape, tread, pressure, load, tractive/braking effort, and camber and slip angles.

Experimental observations on a glass plate and simple theory indicate that camber thrust of narrow bias-ply tires arises from a lateral distortion in the print. When a stationary tire is pressed down onto the road at a camber angle, the center plane of the print is curved (see Figure 2.23(a)): When the tire is rolled at zero slip angle (b), a point entering the print is constrained by the road to move through the print on a straight path defined by the direction of motion. Thus the road applies forces to the tire which tend to remove the curvature in the stationary (nonrolling) tire print. The sum of these forces is the camber thrust.

It is possible to compare the lateral force produced by camber angle to that produced by slip angle. Because of the shape and size of the print distortion patterns, the lateral force generated in the linear (small angle) range by one degree of slip angle is greater than that generated by one degree of camber. For traditional bias tires the cornering stiffness ($\Delta F_y/\Delta\alpha$), is generally five to six times greater than the camber stiffness ($\Delta F_y/\Delta\phi$).

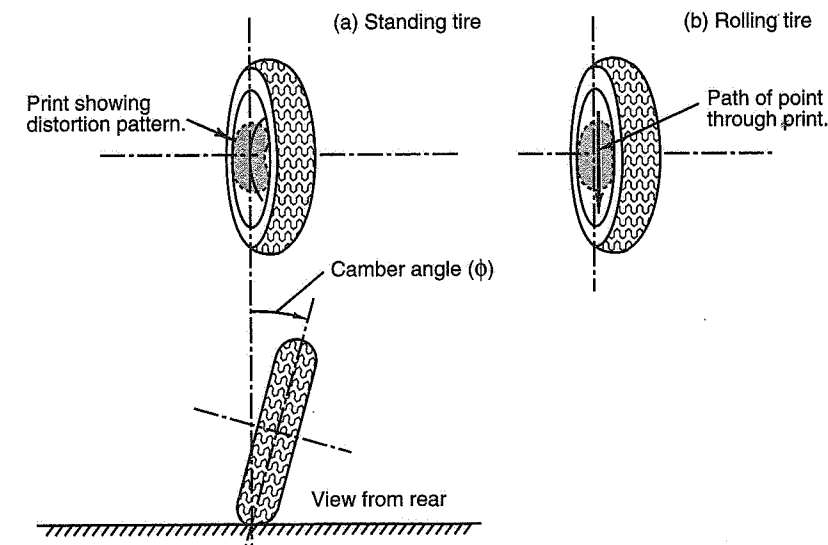


Figure 2.23 Distortion in print of a tire at a camber angle.

For radial tires the camber stiffness may be quite small since the lateral stiffness of the belt and the flexibility of the radial cord sidewall inhibit the kind of print distortion that gives rise to camber thrust. Such camber thrust as is generated may be due to distortion in the tread pattern or sidewall effects. Although wide bias and radial racing tires generate camber forces, the mechanism is not well understood. For wide street radial tires the camber forces tend to fall off at camber angles above 5°. For racing tires, the maximum force due to camber occurs at smaller angles. It is interesting to note that for rounded-cross-section motorcycle tires, camber produces useful lateral force up to perhaps 50°.

Aligning Torque due to Camber

Camber also affects the aligning torque (or pneumatic trail). The roughly triangular distortion pattern of the print due to slip angle (the lateral forces in the print increasing toward the back) gives rise to an aligning torque which is “stabilizing” in the linear range. On the other hand, aligning torques due to camber are generally quite small because of the fore and aft symmetry of the print distortion. In practice, small “destabilizing” aligning torques usually result when lateral force is generated by camber alone, i.e., the aligning torque due to camber tends to increase the slip angle. In combination with slip angle, the two effects tend to cancel and this may require an increase in mechanical trail to produce the desired centering effect.

Camber Roll-Off and Peak Lateral Force

In the linear range, camber thrust and lateral force due to slip angle are generally viewed as separate effects and are additive. This simply moves the cornering curve (lateral force vs. slip angle) up or down parallel to itself depending on which way the wheel is cambered. As the linear range is exceeded, the additive camber effect decreases or is said to "roll-off" (see Figure 2.24). Measurements made on a narrow bias-ply tire demonstrate that the peak of the cornering curve can move up when the tire is tilted into the turn while the peak generally moves down if the tire is tilted outward. Figure 2.25 shows this effect for round cross-section, slick bias-ply tires. This gain in max lateral force has since been confirmed by many other tests. Although no complete theory exists to explain the increase it is obviously associated with what happens in the print. Road-induced distortion due to **slip angle** is a maximum toward the rear of the print where local vertical forces are low; the largest distortion in the case of **camber** is near the center of the print where the local vertical forces are high. Slippage in the highly loaded center of the print is less likely than at the lightly loaded end of the print. This may help explain why higher lateral force is achieved when "aiding" camber is added to the slip angle. The actual conditions in the print under large slip and camber angles are very complex and are not fully explained by this simple physical picture.

Figure 2.26 is a plot of the maximum lateral force obtained on a Goodyear Eagle tire for various loads and cambers. As in Figure 2.25 the slip angle varies along each curve (the

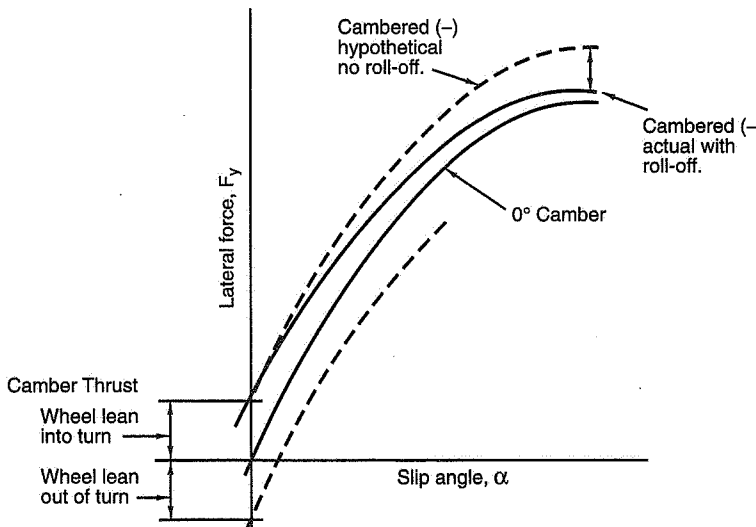
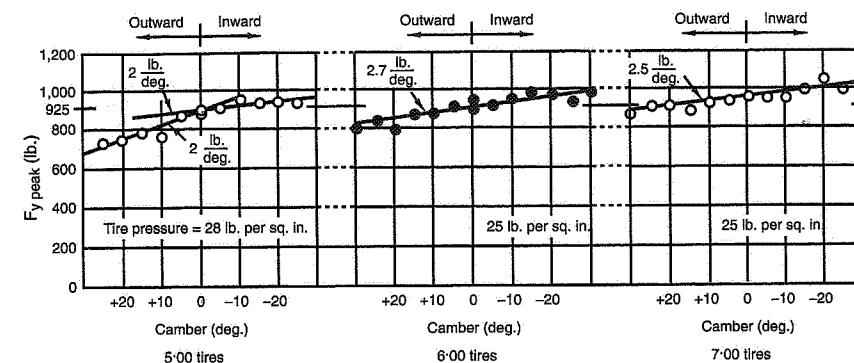


Figure 2.24 Camber thrust and camber roll-off at constant load.



Notes: The slip angle at each point on these curves is that which gave maximum lateral force.
925 lbs. load for all tires

Figure 2.25 Peak side force vs. camber (Ref. 46).

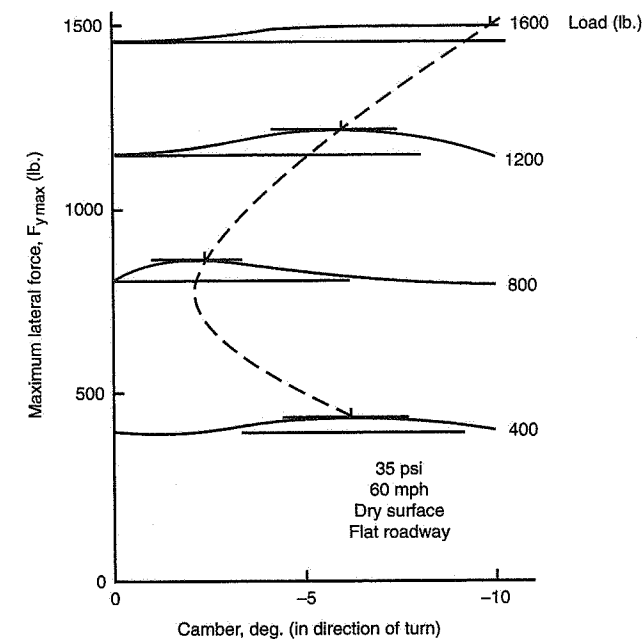


Figure 2.26 Peak lateral force vs. camber, P225/70R15 tire.

value with the max lateral force at each point is used). The highest lateral force values are all at some nonzero camber angle. The best camber angle increases with load, except for the light load where the data is probably less reliable. At 1200 lb. load, a 6% increase in max lateral force is obtained at -6° of camber.

Typical Cambered Tire Data

To illustrate the general effect of camber on lateral force over the full range of load and slip angle, three figures based on tests at Calspan TIRF of the Goodyear Eagle P225/70R15 tire are presented. The tire was tested at 35 psi pressure at 60 mph under dry conditions on this flat belt tire tester. Figure 2.27 is at 0° camber. The curves are labeled in terms of steer angle instead of slip angle; steering the wheels to the right is positive (+). Figure 2.27 indicates that the lateral force-producing capability of the non-cambered tire is about the same for right and left steer; the tire behavior is nearly symmetrical.

Figures 2.28 and 2.29 are for the wheel tilted at 5° and 10° to the right, respectively. In both instances the curves are asymmetrical. When the wheel is tilted to the right the lateral force produced by the right steer is greater than with left steer. The camber has the effect of rotating the set of curves in an counterclockwise direction around the origin. For these relatively wide tires, -5° of camber yields most of the gain in lateral force from camber.

With the exception of oval track cars (where both wheels on an axle may be tilted in the same direction), it is common to use negative camber (both wheels cambered inward) where the suspension permits. In the past with narrow, rounded bias tires it was common to see nearly 10° of negative camber on a rear swing axle (see bottom of page 614). With modern wide radials, the camber is restrained to, say, -5° for reasons of temperature, wear and performance.

Camber Optimization

Curves such as those of Figures 2.27, 2.28, and 2.29, or normalized versions, are useful for adjusting the camber to achieve maximum lateral force on a wheel at a known load and slip angle condition. Figure 2.30 is a plot of normalized lateral force vs. load for three camber angles all at 7° of steer angle in a right-hand turn. This steer angle was chosen as close to the peak for the three camber angles. Using this limited data, we can approximate the desirable camber for the outside front wheel for a range of vertical loads to maximize F_y/F_z .

All of the curves slope downward to the right, as was noted for vertical wheels in the earlier section on tire load sensitivity. The introduction of camber changes both the coefficient level and the load sensitivity (slope of curve). In this example, 5° of negative camber appears desirable at any load likely to be seen on the outside wheel. To truly find the optimum camber angle, data would be required at other intermediate camber angles near -5° .

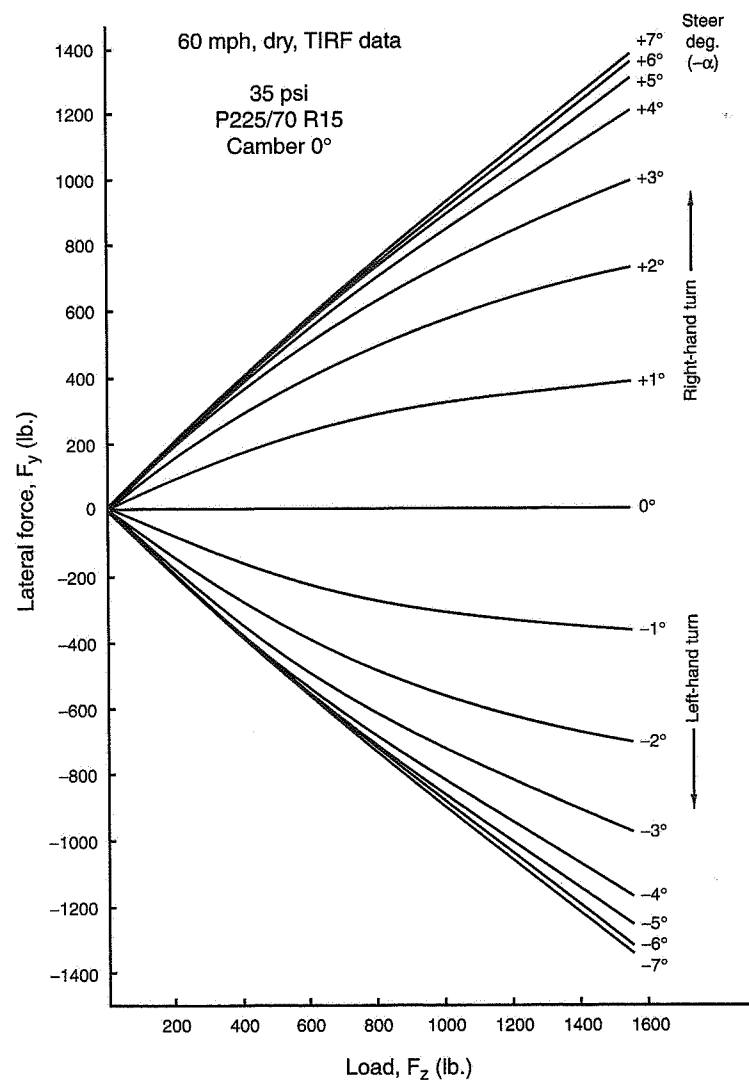


Figure 2.27 Lateral force at zero camber.

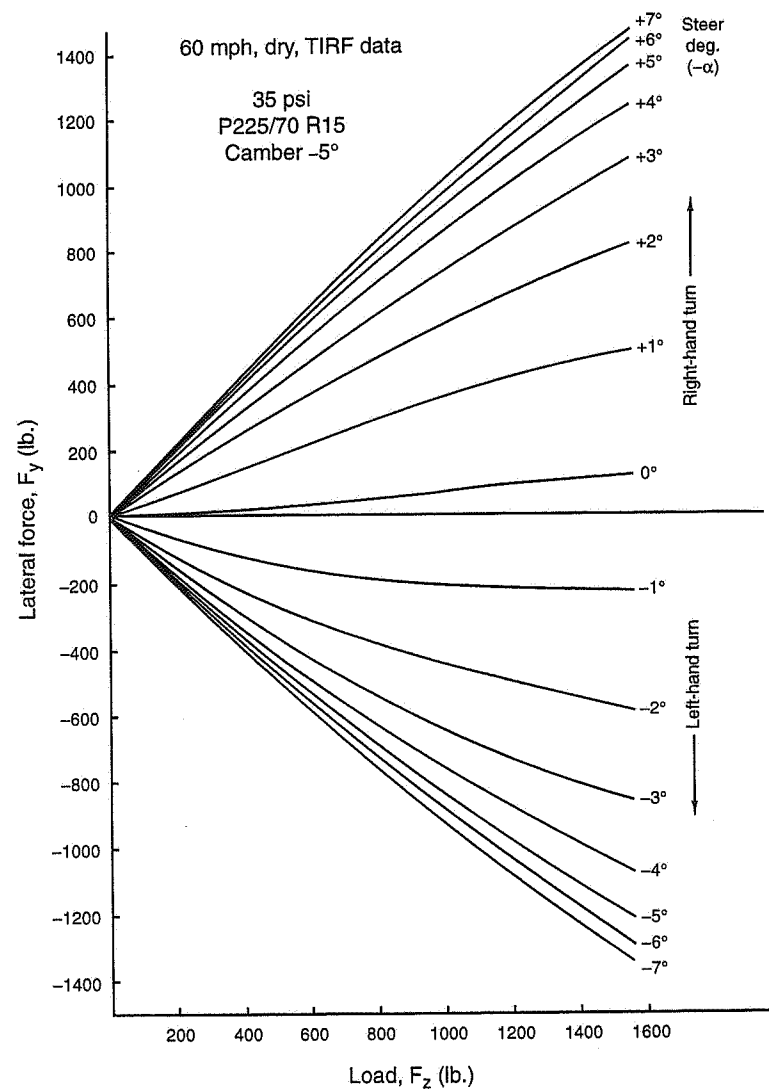


Figure 2.28 Lateral force at -5° camber, lean to right for LH front wheel.

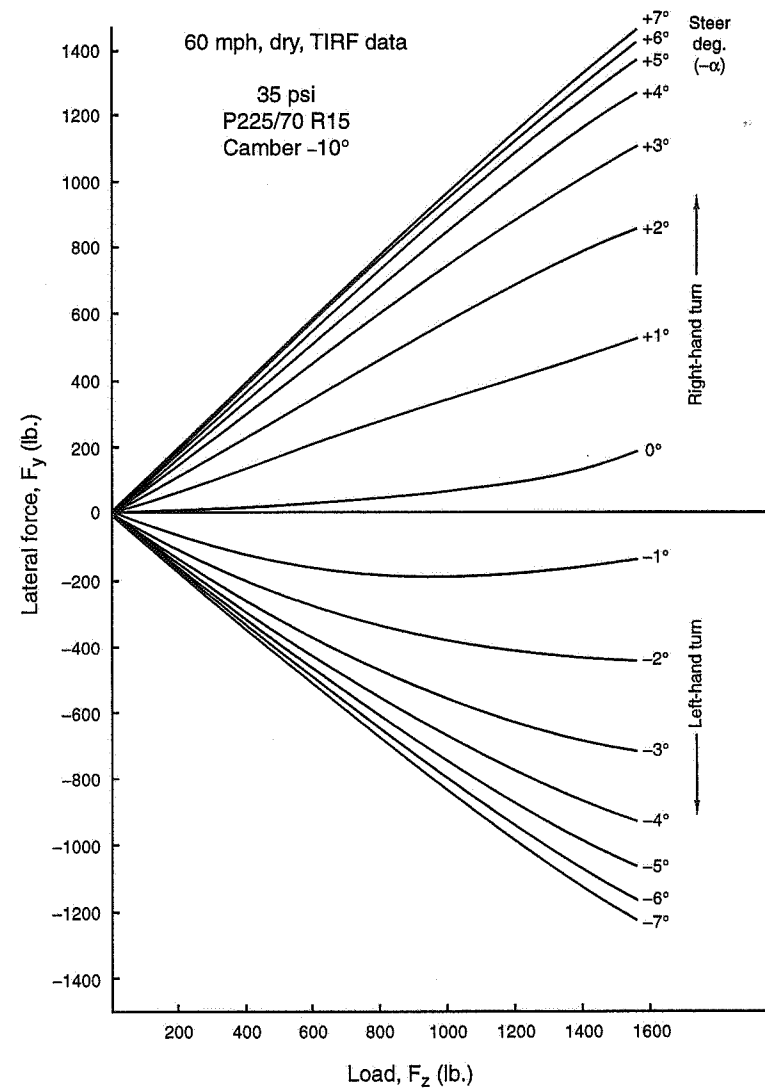


Figure 2.29 Lateral force at -10° camber, lean to right for LH front wheel.

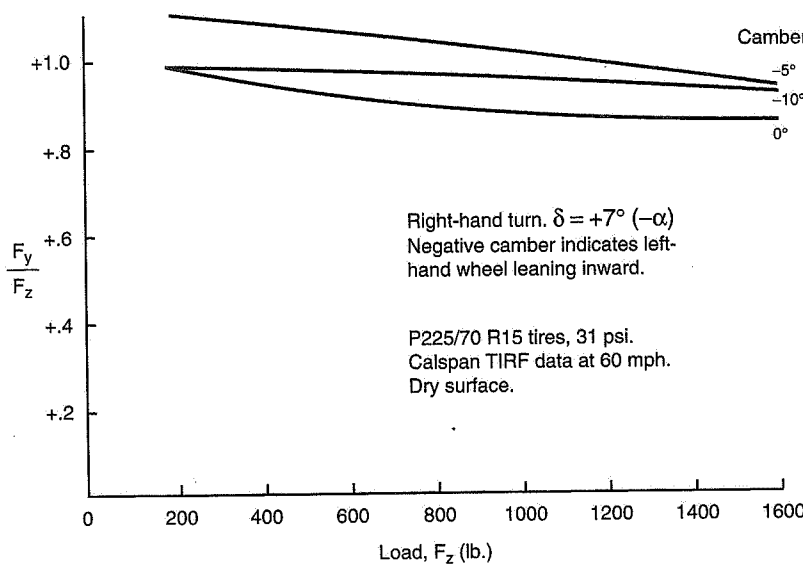


Figure 2.30 Load sensitivity for several camber angles.

In Chapter 7 the effects of camber, steer, load, and lateral load transfer on a pair of wheels on an axle are all combined.

2.6 Other Tire Effects

So far this section on tire mechanics has concentrated on forces, moments, and angles that relate the tire to the road. This section lumps together several other factors that affect tire performance.

Tire Pressure

Tire pressure is one of the easiest and most common changes made in setting up a race car. The range of permissible pressures is frequently set by the tire manufacturer generally for reasons of durability. Pressure affects the tire in several significant ways.

Tire performance at low slip angles and modest side forces is described by the cornering stiffness or the slope of the lateral force vs. slip angle curve of Figure 2.7. This slope is a measure of the tire's elastic properties—if the tire pressure is raised the carcass will get stiffer (less easy to distort) and the cornering stiffness will increase. For a given small slip

angle, an increase in pressure will give an increase in lateral force. By varying the pressures front to rear, modest changes in the under/oversteer balance of the vehicle can be achieved—a common example is the case of several rear engine, rear-heavy passenger cars which specify much higher tire pressures at the rear.

Tire performance at the peak of the curve (Figure 2.7) depends on the effective friction coefficient. As mentioned at the beginning of this chapter, grip is not very well understood but, in general, lowering the contact pressure between the rubber tread and the road raises the effective friction coefficient. Lowering the air pressure increases the size of the footprint and lowers the contact pressure in the print. However, too low an air pressure creates localized high pressure areas at the sides of the print due to the sidewall stiffness. The general idea is to set the air pressure such that the center tread (supported mostly by pressure) and the edges of the tread (supported by pressure and the sidewalls) carry a proportional share of the load.

Aligning torque is also affected by pressure. As the pressure is decreased, the print becomes longer and the center of lateral force moves rearward. When a tire loses air, steering effort for a given lateral acceleration turn is increased because of the decrease in cornering stiffness and the increase in aligning torque.

Tire drag will be decreased by an increase in pressure. There are two mechanisms of tire drag. The *rolling resistance* is a measure of energy lost in deforming the tire; with higher pressure, distortion and print size are reduced. Tire *induced drag* (drag resulting from cornering) will be reduced for a given required lateral force (below the limit) if the pressure is increased because the required slip angle is lower. This effect is discussed later in this chapter.

Ride, as is commonly known, is adversely affected by an increase in pressure—the tire spring rate rises and the tire contributes less compliance to the vertical springing of the vehicle. The vertical tire spring rate is critical in race cars with stiff springing (i.e., ground-effects cars) because the tire is a significant part of the total spring rate (perhaps 1/2).

Obviously, the best tire pressure is a compromise between the above factors. The best sublimit performance is achieved with higher pressures while maximum grip is achieved with somewhat lower pressures. The best pressure can be found only by experimentation, using the tire companies' recommendations for a starting point.

Tire Temperature

Tire temperature affects both the force-producing capability of the tire and also the life of the tire. The first question that must be considered regarding tire temperature is, "What temperature?" Working from the outside in, it is possible to measure:

- Different temperatures on the surface of the tire tread (surface probes or infrared sensors) or the surface of the sidewall
- Temperatures inside the tread or carcass (cords) with a needle probe as is commonly done by the race tire company representatives
- The contained air temperature (CAT) of the tire, which is an average temperature of the inside of the tire and rim (commonly done on indoor tire test machines)

The tire carcass is an elastic device that is partly responsible for the cornering stiffness. A change in temperature will change the modulus of elasticity of the rubber (unlike steel where this is constant over a large temperature range) and affect the cornering stiffness.

Tire pressure and temperature are interrelated—lower initial pressure results in more rubber distortion and higher temperature, which in turn results in higher “hot” pressure.

Tread compounding is a trade secret with the tire suppliers; compounds change with the application and with competition among tire companies. Both temperature history and time appear to affect tire grip but these effects are not consistent across a range of compounds.

Modern race tire tread compounds have an optimum temperature for maximum grip. If too cold, the tires are very slippery; if too hot the tread rubber will “melt”; in between is the correct temperature for operation. Unfortunately, the tire’s temperatures change continuously as the pressure, speed and operating forces vary. Again a compromise is needed.

Speed Effect

Tire performance varies with speed. Unfortunately, the effect is not consistent enough to be generalized. The only thing that seems likely is that tire force capability drops off as speed is increased. This drop-off may be gradual with increase in speed or abrupt in a narrow range of speeds. In some cases the lateral force capability increases slightly again as speed increases past a certain point.

Laboratory testing for speed effect requires separating speed effects from temperature effects. As the tire speed is increased at constant slip angle, the temperature increases during the test. As of this writing, there is no way to maintain constant temperature during a laboratory test; likewise there is no way to correct for the effects of temperature change on the measured forces and moments. Speed/temperature effects undoubtedly affect test results in ways that are expensive to determine at current tire test facility costs!

Conicity and Plysteer

As indicated in Ref. 4, tires have “non-symmetries due to fabrication and design” which create lateral force and aligning torque when a tire is tested at zero slip and camber angles. Two non-symmetries which occur in steady-state testing are *conicity* and *plysteer* which displace the measured curves from zero. On the vehicle this gives rise to steering/vehicle “pull” and “dog tracking.”

The following definitions are taken from Ref. 33, section 8.2.6, “Tire Nonuniformities” by A. Dijks.

Conicity—This term was apparently derived by considering a tire to assume the shape of a truncated cone... Based on geometry such a configuration would generate a force towards the apex of the cone regardless of which direction the tire or ‘cone’ was rotated. Thus conicity by definition is a force component which does not change direction with reverse rotation when measuring tire lateral force variation.

Ply steer—This component of the lateral force variation describes the influence of the plies in a tire in generating forces which could steer a vehicle from its intended straight line course. Ply steer by definition, is a force component which changes direction with reverse rotation, when measuring the tire lateral force variations.

Conicity is generally the result of an off-center belt in a radial tire. As well as the lateral force mentioned above, conicity also generates aligning torque in the same direction as the lateral force. Ply steer is apparently the result of the design of the plies in the belt. In this case, the aligning torque is in the opposite direction from the lateral force. Ply steer is generally a larger effect than conicity.

2.7 Friction Circle and Ellipse

In Section 2.3, Figures 2.20 and 2.21 illustrate the lateral force F_y and the longitudinal force F_x as functions of slip angle and traction/braking slip ratio. In this section (2.7) a single diagram is developed which combines the longitudinal and lateral forces. This diagram is composed of so-called friction ellipses and the friction circle. The friction circle represents the force-producing limit of the tire for a given set of operating conditions (load, surface, temperature, etc.). This diagram for a single tire/wheel is conceptually similar to the friction circle diagram for the whole vehicle.

Figure 2.31 is a plot of lateral force vs. longitudinal (braking/traction) force for a series of slip angles and slip ratios. Only the right half of the full circle diagram is shown. The data is from the Sakai paper referenced earlier. Unfortunately, these tests are not commonly run and no data of this type was available on a race tire. Lateral force is measured perpendicular to the wheel plane and longitudinal force is measured in the wheel plane.

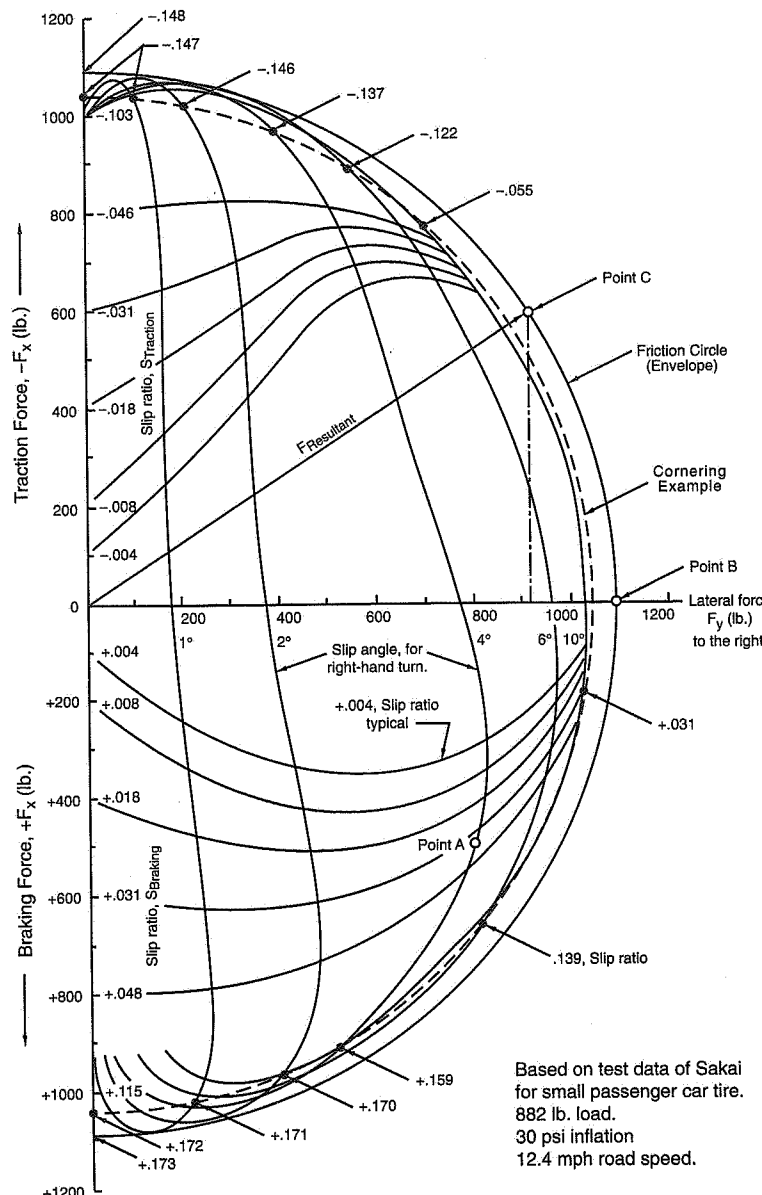


Figure 2.31 Friction circle diagram, right-hand turn.

General Description of the Diagram

At the origin the tire is free-rolling straight ahead with no longitudinal force (other than a small rolling resistance). The slip angle and lateral force are zero. Moving to the right along the horizontal axis increases lateral force and the corresponding slip angle lines are noted; the conventional lateral force vs. slip angle curve could be taken from the data on the horizontal axis.

The vertical axis represents longitudinal force and various slip ratios are marked along the scale. Note that + is down and braking while traction is up and - (Sakai convention). Points on the vertical axis could be used to develop the curves of slip ratio vs. longitudinal force.

The interesting part of the diagram is off axis, where combined traction/braking and lateral force are represented. For example, point "A" on the figure represents the force that is generated by 4° of slip angle and a slip ratio of about +0.036. This can be read off the force scales on the axes as 800 lb. of lateral force and 500 lb. of longitudinal force (braking).

In general, a circle is a close approximation to the boundary of the diagram—this "friction circle" represents the maximum force that the tire can generate under these operating conditions. For some tires, the outside envelope of this diagram may be slightly elliptical.

In racing, the tire is operated at or near the limit of the friction circle. At point "B" for example, the tire is giving pure lateral force at its best slip angle (13° slip angle gives this peak, although this curve is not drawn on the figure) of 1100 lb. If 600 lb. of tractive force is applied, the available lateral force drops to about 920 lb. at point "C." The combined force, the vector sum of the lateral and longitudinal forces, is still 1100 lb. as shown by the arrow labeled $F_{Resultant}$. From the right triangle formed by the components of $F_{Resultant}$, the Pythagorean Theorem can be used to calculate the length (force) from the origin to point "C."

$$F_{Resultant}^2 = F_x^2 + F_y^2$$

$$F_{Resultant} = \sqrt{600^2 + 920^2}$$

$$F_{Resultant} = 1100 \text{ lb.}$$

Note that the slip angle curves hook back as they approach the vertical axis. This indicates that points on these curves have exceeded the peak of the resultant force vs. resultant slip velocity curve, shown in Figure 2.22.

Cornering Example

As a preliminary to the discussion of the “g-g” diagram, in Chapter 9, the friction circle diagram (Figure 2.31) will be used to describe a racing cornering maneuver of a very simple vehicle. The friction diagram is drawn for a single tire and the car is simplified down to just this one tire, a “monocycle.” With only one tire, no load transfer is possible so the load is constant at the 882 lb. for the following example.

Recall that the limit for this tire is about 1100 lb. resultant force. We choose to take the corner at some small margin below this, at $F_{\text{Resultant}} = 1045$ lb. or 95% of the limit force. This is shown on the figure by a dashed line labeled “Cornering Example.”

If the turn were negotiated at 12.4 mph (the speed at which the tire data was obtained) the resulting slip velocity at 1045 lb. force would be 2.15 mph. Instead we choose to ratio the speed up—for example, at 100 mph the slip velocity increases by the ratio of the new to the original speed or $100/12.4 = 8.06$. The new slip velocity is $2.15 \times 8.06 = 17.34$ mph.

Before turn entry, the “tire” (monocycle) decelerates at 1045 lb. which translates to a slip ratio of +0.172. As the vehicle (tire) is turned in, lateral force builds up while braking force must reduce to maintain constant resultant force. The black dots at the intersections of the slip angle curves and the dotted 95% circle are labeled with the slip ratio at each point. By the time 4° slip angle is reached (the curve which also has point “A” on it), the slip ratio is +0.159—the brakes must be tapered off as the steering is tapered in. At the limit of cornering, the operating point is on the horizontal axis and the slip ratio is essentially zero.

As power is applied on turn exit, the slip ratio goes negative and the slip angle must decrease correspondingly. By the time the slip angle is down to 6° the slip ratio can be -0.122. At the end of the turn, the vehicle (tire) can accelerate at a slip ratio of -0.147 without any lateral force production. Throughout this example, the resultant force (the length of the force vector) on the vehicle has remained at a constant 1045 lb., only the direction of the force vector has changed.

Figure 2.32 shows the control that must be provided by the driver when traversing the example corner. Here, turn entry begins at the top of the figure with the driver applying just enough brakes to give the slip ratio of 0.172 (braking slip ratio is positive). As turn in progresses, the driver uses the steering and brakes to move along the curve. Keep in mind that the slip ratio is a function of brake torque and also steer angle while slip angle is likewise a function of steering and braking—both controls must be mixed to give the desired result! At maximum cornering, the slip ratio data in Figure 2.31 is not fine enough to fill in all the data points—our example driver probably coasts for some short distance around the apex before beginning to add power.

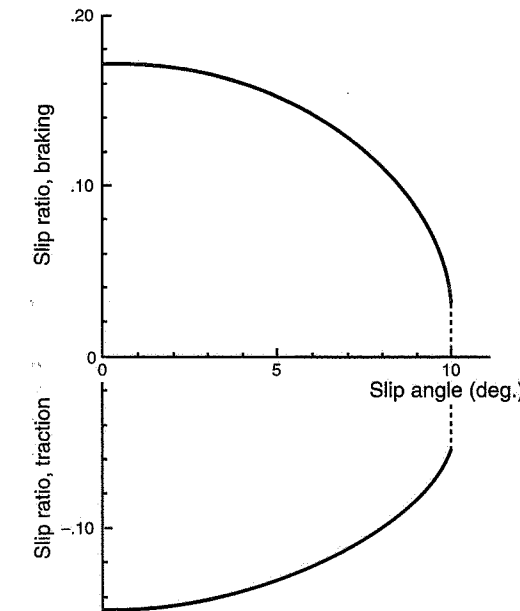


Figure 2.32 Slip ratio vs. slip angle for cornering example.

Summary

In this section the friction circle for one tire has been examined. The “g-g” diagram for the whole vehicle is a composite of the friction circle diagrams for all four wheels of the vehicle, taking into account load transfers (and other effects) which affect the size and shape of these four friction circles.

2.8 SAE Tire Axis System

Having reviewed tire behavior in general terms, we now turn to the specific force and moment components that are used to measure and present tire data by such testing facilities as Calspan Tire Research Facility (TIRF) and MTS Flat-Tracs.

The only external forces acting on a car are gravity, aerodynamic forces, and tire forces. The tire forces may be viewed as road forces acting on the car as a result of tire-road interaction. In this section we show how tire forces produce certain forces and moments and how traction forces (both driving and braking) and lateral forces result in thrust and

drag forces. Again, the algebraic signs assume that the road applies the forces and moments to the tire.

The tire axis system adopted for vehicle dynamics and tire work is that shown in Figure 2.33. This axis system, from SAE J670, has its origin at O, the center of the tire footprint (tire stationary). The origin, O, is at the intersection of the z axis with the road plane; a flat level road is assumed. The x axis is at the intersection of the wheel plane with the road plane. The z axis is vertical and passes through O. The y axis is perpendicular to x and z and lies in the road plane.

The figure shows the wheel at a positive inclination angle, γ , and a positive slip angle, α . R_ℓ is the loaded wheel radius, the distance from the center of tire contact to the wheel center measured in the wheel plane. It is not the effective rolling radius or revolutions/mile. The various forces and moments shown will be discussed in this section.

Slip angle, α , is + when the wheel is “slipping” to the right; this is negative steer, i.e., wheel steered to the left.

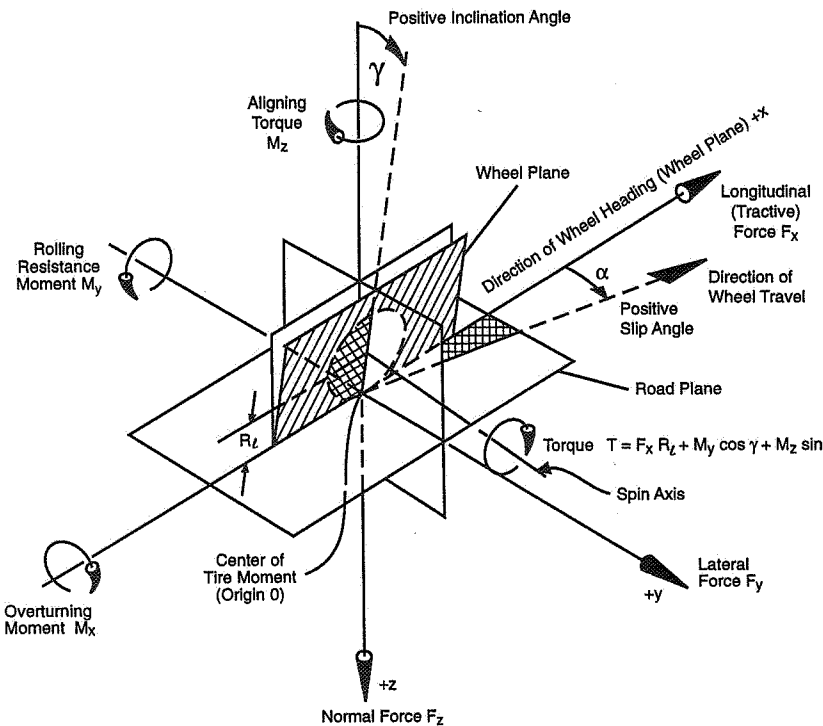
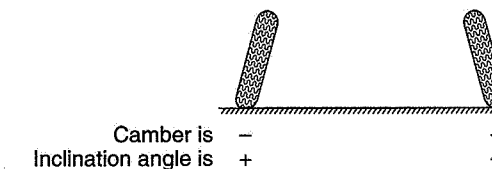


Figure 2.33 SAE tire axis system (Ref. 1).

Inclination angle, γ , has a different sign convention than camber angle:

When viewed from the rear of the car, if the tires are leaning like this:



Inclination angle is used for tire data; to use camber angle on a vehicle, the signs must be converted.

2.9 Discussion of Tire Forces

This section and the following section discuss tire forces and tire moments as defined by the SAE axis system. In addition, some analysis is given of certain combinations of these components that are significant to the vehicle as a whole. No detailed analysis will be made of the single resultant tire force/moment vector noted in the introduction to this chapter.

F_z : Normal Force (Load)

All tire forces and moments are a function of load as well as other operating variables. Race cars operate near the limit where tire load is particularly important. For a given set of tires, the load primarily determines the amount of force available to accelerate the vehicle, both laterally and longitudinally.

The normal force, F_z , and its road reaction, F_{zR} , also appear in M_x and M_y (as shown subsequently).

F_x : Tractive Force and F_y : Lateral Force

The mechanism for the generation of tire tractive forces, either in the driving or braking direction, has been discussed earlier in this chapter. It was shown that tractive force, F_x , which is in the direction of the wheel plane, is a function of longitudinal slip ratio, S . The way tires generate a lateral force (perpendicular to the wheel plane) was also treated. Now, these two forces are treated together because we are interested in how they affect vehicle *thrust and drag*. In short, we will be resolving tire F_x and F_y along V , the velocity direction.

The total thrust or drag is given by resolving the lateral and longitudinal forces along the velocity direction,

$$T \text{ or } D = F_x \cos \alpha - F_y \sin \alpha$$

We will first take a more detailed look at the interpretation of these two terms from the way that they are measured on a single tire in the laboratory. The discussion is based on Ref. 55 from Calspan TIRF.

Consider first the case when slip angle, $\alpha = 0$. A drag force, F_R , is produced at the road interface, the result of the rolling loss at the contact patch. This is commonly called "rolling resistance" for the special case where $\alpha = 0$. The force occurs at a distance R_ℓ , the loaded radius (not the effective radius) from the wheel center. If the tire is being driven by an input torque, T_{in} , it can be shown that F_R is given by

$$F_R = (SR + 1) \left(\frac{T_{in}}{R_\ell} \right) - F_x$$

where $SR = (\Omega R_\ell / V) - 1$ (slip ratio)

F_x = measured force along the x axis (+ driving, - braking, lb.)

Ω = angular velocity of the wheel (radians/sec.)

V = forward velocity (ft./sec.)

Note that SR is based on loaded radius, R_ℓ (for convenience in testing), and not on R_e as used in the SAE slip ratio definition. For free rolling, SR is not quite zero because of the Calspan definition of SR but it is usually very small.

If SR is taken as zero, the equation for F_R becomes

$$F_R = \frac{T_{in}}{R_\ell} - F_x$$

where T_{in} / R_ℓ is the force at the contact due to the input torque, T_{in} for a tire rolling with no loss due to deformation. The rolling resistance is then the difference between this force and the measured F_x .

Now, consider the case when the slip ratio is no longer zero. The relationship for F_R is now

$$F_R = \left[(SR + 1) \left(\frac{T_{in}}{R_\ell} \right) - F_x \right] \cos \alpha - F_y \sin \alpha$$

The term, $(SR + 1)(T_{in} / R_\ell)$, is due to the input driving torque with no deformation of the tire. The terms in the bracket, the difference between the measured F_x and

$(SR + 1)(T_{in} / R_\ell)$, constitute the rolling loss due to tire deformation. $F_y \sin \alpha$ is the induced drag due to the lateral force at a slip angle, α . F_R is the net drag force in the velocity direction. If the bracket is set to zero, $F_R = -F_y \sin \alpha$ and all of the drag is due to the lateral force component.

In the above it is stated that the terms in the bracket are the rolling loss due to tire deformations. This is probably not strictly true since there is local slippage in the print and local distortions as well as gross radial, longitudinal and lateral deformations of the tire carcass. With current tire test methods, there is no way to determine in detail how the losses occur or their relative magnitudes.

Reverting to the original relationship for thrust or drag,

$$T \text{ or } D = F_x \cos \alpha - F_y \sin \alpha$$

Referring to Figure 2.34, we can now say that:

1. $F_x \cos \alpha$ is the traction/braking component.
2. $F_y \sin \alpha$ is the induced drag component.
3. F_R is the net rolling resistance.

This shows these vector quantities for a driven wheel steered to the right, in a right-hand turn.

Figure 2.35 from Ref. 55 shows some typical test data. The net rolling resistance has been normalized by dividing by F_z , the load. From the standpoint of racing the import-

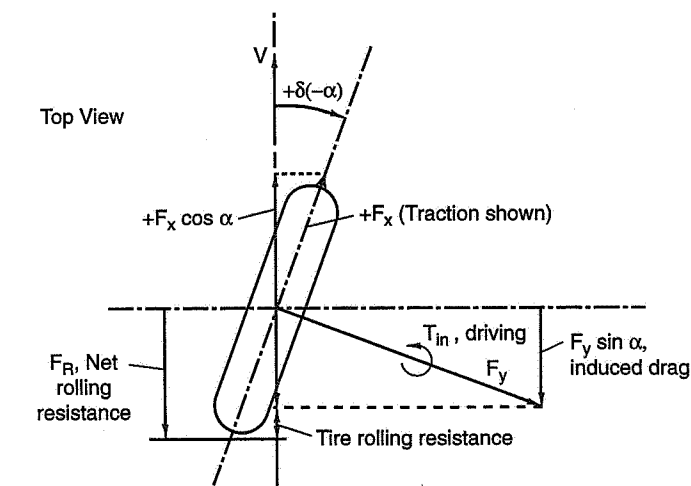


Figure 2.34 Components of the net rolling resistance, F_R .

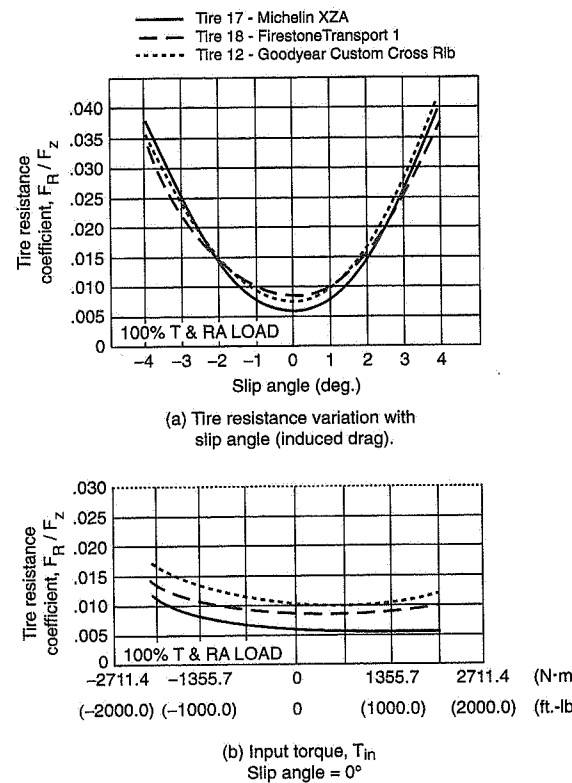


Figure 2.35 Tire resistance due to slip angle and input torque (Ref. 55).

ant component is the induced drag in part (a) of the figure. The drag due to traction/braking is small and is a function of tire design, pressure and temperature, all of which are usually determined by other considerations.

The induced drag is directly influenced by the slope and shape of the cornering force curve. A steeper slope and a sharper transition means that a given cornering force can be obtained at a lower slip angle. A recognition of this drag component by the Chevrolet / Chaparral Can-Am team led to the use of progressively wider tires, hence steeper cornering slope, as the season progressed. The increase in width at each race was sufficiently small to be undetected by the competition. This drag component has been called "induced" by its analogy to the aerodynamic lift and induced drag of a wing.

Lateral Force Induced Drag Example

In Figure 2.36 a two-wheel "bicycle model"⁹ of a coasting vehicle (no drive/brake torque) is depicted in a large radius cornering condition. The velocity vectors, lateral forces, and slip angles are shown. Resolving the tire lateral forces along the direction of the velocity vectors (i.e., path) at the wheels gives an induced drag of

$$D_{\text{induced}} = F_{yF} \sin \alpha_F + F_{yR} \sin \alpha_R$$

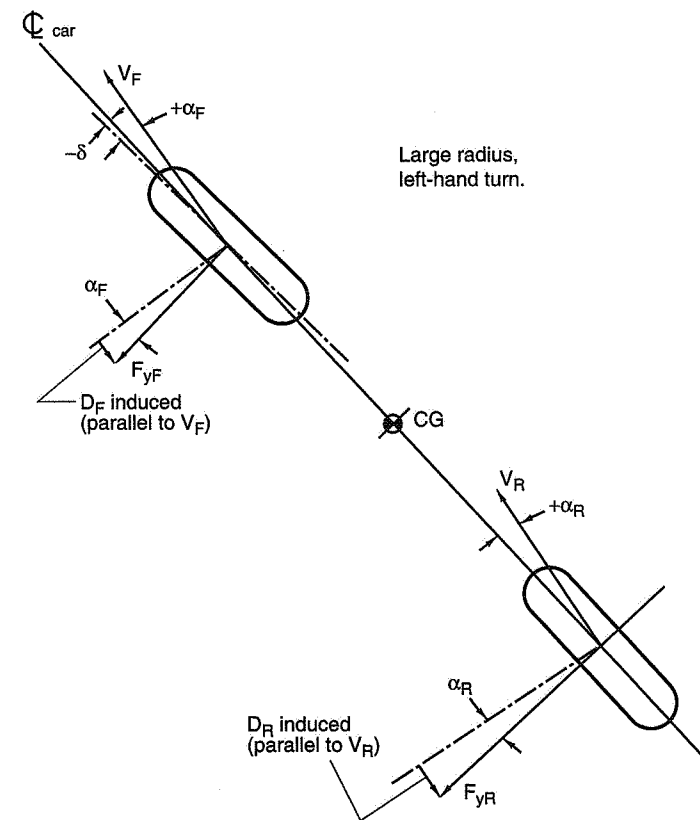


Figure 2.36 Lateral force induced drag—cornering vehicle.

⁹ The concept of the "bicycle model" is discussed in detail in Chapter 5.

To show the magnitude of the induced drag, the following example was run with a comprehensive four-wheel computer model. The race car is assumed to be in momentary steady-state at the apex of a turn at 220 mph. The radius of the turn is 840 ft. and the banking is 9°. The vehicle characteristics are:

Gross weight	1868 lb.
CG location	55.25% weight on rear wheels
Wheelbase	9.625 ft.
Front aero downforce	-911 lb., $C_{LF} = -0.528$
Rear aero downforce	-1903 lb., $C_{LR} = -1.015$
Reference frontal area	15.15 ft. ²

The total centrifugal force is 7190 lb., which is shared between the front and rear tracks in proportion to the CG location. The appropriate components of the centrifugal force and weight (banking), respectively, give the front and rear lateral tire forces in the plane of the road:

$$\begin{aligned} F_{yF} &= -3178 + 131 = -3047 \text{ lb.} \\ F_{yR} &= -3923 + 161 = -3762 \text{ lb.} \end{aligned}$$

The forces on the front and rear normal to the track are the sum of components due to, respectively, the centrifugal force, the weight, and the aero downforce:

$$\begin{aligned} F_{zR} &= 503 + 826 + 911 = 2240 \text{ lb.} \\ F_{zR} &= 621 + 1019 + 1903 = 3543 \text{ lb.} \end{aligned}$$

The effective friction coefficients (μ) front and rear are obtained by dividing the lateral force by the normal force:

$$\begin{aligned} \mu_F &= 3047/2240 = 1.36 \\ \mu_R &= 3762/3543 = 1.06 \end{aligned}$$

This seems reasonable; the front carries less load so the friction coefficient on the front should be higher, because of load sensitivity effects.

The computer program was also given tire data relating lateral force to slip angle (α). The average tire slip angles for the front and rear axles were calculated, along with vehicle slip angle (β) and steer angle at the front wheels (δ):

$$\begin{aligned} \alpha_F &= +2.5^\circ \text{ ("slipping" to the right)} \\ \alpha_R &= +1.4^\circ \text{ ("slipping" to the right)} \\ \beta &= +1.1^\circ \\ \delta &= -1.8^\circ \text{ (steer left, left-hand turn)} \end{aligned}$$

From this information and the lateral forces, F_{yF} and F_{yR} , the induced drag is computed as follows (β and δ are given for information only):

$$\begin{aligned} F_{yF} &= 3047 \times \sin(2.5^\circ) = 3047 \times 0.0436 = 133 \text{ lb.} \\ F_{yR} &= 3762 \times \sin(1.4^\circ) = 3762 \times 0.0244 = 92 \text{ lb.} \end{aligned}$$

Total induced drag, $D = 225$ lb.

The horsepower required to overcome this drag is

$$\begin{aligned} \text{Horsepower required} &= (\text{Drag in lb.} \times \text{speed in mph}) / 375 = (225)(220) / 375 \\ &= 132 \text{ horsepower} \end{aligned}$$

If engine power available at that speed is 700 horsepower, the tire induced drag uses 18.9%.

2.10 Discussion of Tire Moments

The tire moments will be discussed first in the context of zero γ (inclination angle) or α (slip angle); this will help in visualizing how the moments are generated. Later, we discuss the γ and α effects briefly.

M_z: Aligning Torque (or Moment)

Earlier in this chapter, the mechanism of aligning torque was shown to be a result of the lateral force distribution along the length of the tire footprint when there is a slip angle, α . It was also shown that the aligning torque (which for moderate slip angles below 2° to 6° depending on the tire) tends to turn the wheel so that the wheel plane (heading) rotates into its velocity vector (path).

The way wheel aligning torque is accounted for is illustrated in Figure 2.37.

In the 2DF model (see Figure 5.2) it is assumed that the tire sideforce due to α (which by definition is perpendicular to the wheel plane) passes through the center of the footprint. In actuality, it is behind that point by the pneumatic trail distance, t . The assumed position of the side force is valid if we add an aligning torque, of magnitude $F_y \times t$, around a vertical axis passing through the footprint center. In Figure 2.37 the torque will be counterclockwise—trying to make the wheel plane rotate in a direction to align itself with the velocity vector. In summary, aligning torque due to steer is in a direction to reduce the steer angle (stable). Aligning torque due to camber is usually in a direction to increase the steer angle (unstable).

The aligning torques associated with the wheels of a car are a weak function of inclination angle (camber), γ , and a strong function of slip angle, α , as shown earlier in this

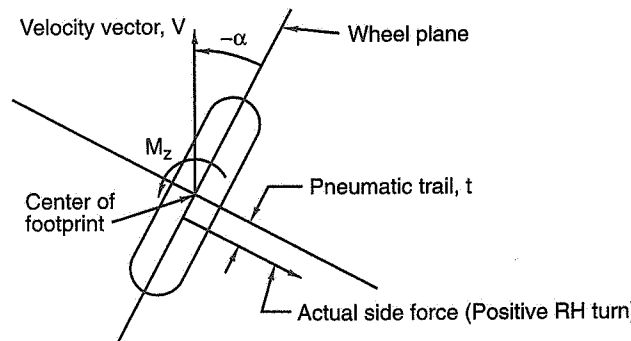


Figure 2.37 Aligning torque.

chapter. The aligning torques are externally applied by the road to the car and they figure in the yaw moment equation for a complete car. In these notes, M_z torques were ignored in developing the 2DF yaw response (in Chapter 5). The effect of M_z is in an understeer direction. Finally, it can be shown that aligning torque has a tiny component about the wheel spin axis but, for small γ this component is negligible.

M_x : Overturning Moment

An overturning moment about x is present whenever the road reaction force, F_{zR} (upward), is not in the same plane as the wheel load, F_z (downward). This is shown in Figure 2.38.

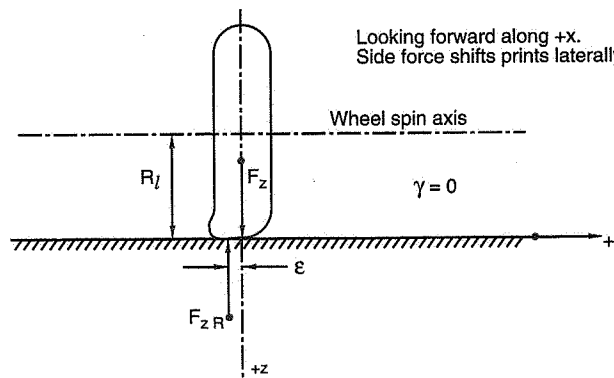


Figure 2.38 Tire overturning moment.

The road reaction force, F_{zR} , is out of the x - z plane, but, for vertical equilibrium, must equal F_z . The centroid¹⁰ of the upward road pressure is displaced by a distance, ϵ , as shown. The shift, ϵ , results when any set of conditions distorts the footprint laterally. This will occur if a side force is applied along the wheel spin axis.

The overturning moment is a pure couple of magnitude $F_z \times \epsilon$ lb.-ft. (or $F_{zR} \times \epsilon$, since $F_{zR} = F_z$). If a wheel is moving straight ahead with $\alpha = \gamma = 0$, the overturning moment is negligibly small and is produced mainly by tire imperfections. When α and/or γ are present, side forces are generated, resulting in footprint distortion and lateral shifting of F_{zR} . This shift affects the lateral weight transfer on an axle, and the effect can be large with wide tires. An analytical treatment of M_x as a function of α and/or γ is difficult and is not presented here; the practical source of information on overturning moment is from tire testing.

M_y : Rolling Resistance Moment

The term rolling resistance moment as used here is confined to the "resistance" to forward motion of a free-rolling wheel.¹¹ The free-rolling wheel is defined (see Ref. 141) as one that is towed (or pushed) straight ahead in an upright position with all applied moments (internal and external) about the wheel spin axis nearly zero.¹² Figure 2.39 shows the essential variables.

In Figure 2.39, F_T is the force required to tow the wheel at constant velocity, V . F_R is the rolling resistance force and is equal and opposite to F_T . Note that the free-rolling wheel produces no tractive force either driving or braking that is available to accelerate or brake the vehicle. The wheel load, F_z , is equal but opposite to the road reaction vertical force F_{zR} . Assume $T = 0$ (no applied torque), the road reaction resultant must pass through the spin axis (otherwise it would produce a moment about the spin axis); this establishes the distance d , where F_{zR} intersects the road plane. If F_R were zero, F_z and F_{zR} would be collinear; F_R (and F_T) exist because the periodic compression and expansion of the tread rubber (as the rubber goes through the contact patch) consumes energy.

For zero moment about the spin axis:

$$F_z d = F_R R_\ell$$

¹⁰ The footprint force F_{zR} is the resultant of the distributed force (i.e., pressure) over the footprint area (see Figure 2.23, for example). The point at which F_{zR} intersects the road plane is the centroid of the footprint pressure.

¹¹ Some treatments include the traction force moment about the spin axis.

¹² The free-rolling case is also that for which the longitudinal slip, s , is nearly zero.

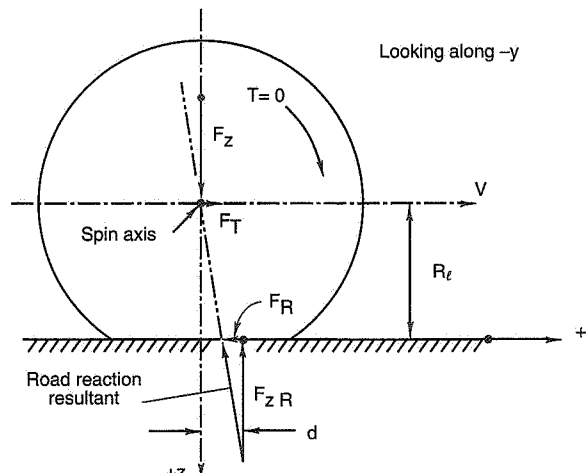


Figure 2.39 Free-rolling tire.

or

$$d = \left(\frac{F_R}{F_z} \right) R_\ell$$

To get some idea of the magnitude of the offset, d , we can go to Figures 14 and 18 of Ref. 141. For an H78-15 tire at 24 psi and 60 mph: $F_R = 19.2$ lb., $F_z = 1200$ lb., and $R_\ell = 13.7$ in.

Then, $d = (19.2/1200) \times 13.7 = 0.22$ in., which is small compared to a footprint length of, say, 6 in. Incidentally, a rolling resistance force of 19.2 lb. at a speed of 60 mph amounts to a power consumption of

$$(19.2 \text{ lb.} \times 88 \text{ ft./sec.}) / 550 \text{ ft.-lb./sec.} = 3.07 \text{ horsepower}$$

The term rolling resistance moment for a free-rolling wheel is a little deceptive. Consider the two-dimensional car in Figure 2.40 in which the driving wheel is at the rear and the free-rolling wheel (frictionless bearings) is at the front.

Assume, for a moment, that the driving wheel has no rolling resistance but the front wheel has a rolling resistance force of F_R (negative). This means that the rear wheel has

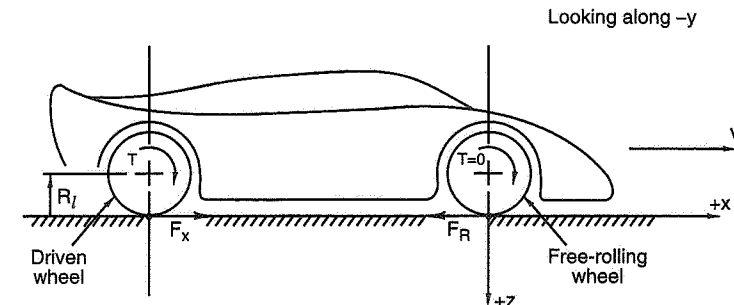


Figure 2.40 Rolling resistance torque.

to provide a tractive force, F_x , equal to F_R to cruise at constant velocity (neglecting aerodynamic forces). Hence the magnitude of the driving torque is

$$T = F_x R_\ell = F_R R_\ell = M_y$$

Thus, although the rolling resistance moment, $F_R R_\ell$, does not act around the spin axis of the front wheel, it has to be made up by the driving wheel. Now, if the driving wheel has an F_R of its own, its tractive force has to be increased to overcome its rolling resistance as well as that of the front wheel.

In order to get a feel for the magnitude of M_y we can go back to the previous example in which $F_R = 19.2$ lb. and $R_\ell = 13.7$ in. Then

$$M_y = (19.2 \times 13.7) / 12 = 21.9 \text{ lb.-ft.}$$

Going back to Figure 2.39 it is noted that the rolling resistance moment can also be written as $F_z d$ (a pure couple). Thus M_y increases with F_z —the variation being almost linear. The trends in the variation with load and speed are shown in Figure 2.41.

To this point, γ and α have been taken as zero. It can be shown that with an inclination angle (camber if the tire is on a vehicle) there is a cosy effect. Thus, in the literature (as in Figure 2.33) the rolling resistance moment is $M_y \cos\gamma$. For small γ this is a minimal effect; even if γ is as high as 10° , M_y is within 2% of $M_y \cos\gamma$. Given the data scatter on tire tests (performed on even the best of machines) the discrepancy is not worth worrying about. As for slip angle, α , there is probably a slight effect on M_y since the footprint is distorted laterally but the magnitude, like that with γ , should be small.

In summary, the rolling resistance moment, M_y , is of primary concern in power calculations since it manifests itself as driving torque to overcome F_R . Next we will show how this component of T (Figure 2.40), along with others, makes up a more complete torque equation.

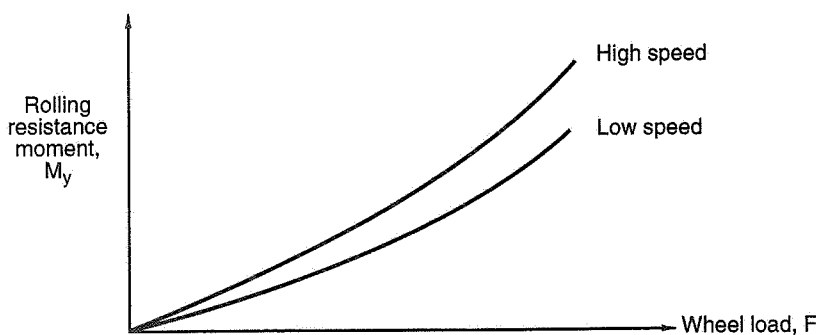


Figure 2.41 Rolling resistance moment as a function of load.

2.11 Torque About the Wheel Spin Axis

In Figure 2.33, SAE tire axis, a torque equation (in this case for driving traction) is given as

$$T = F_x R_\ell + M_y \cos \gamma + M_z \sin \gamma$$

which can also be written as

$$T = F_x R_\ell + F_R R_\ell \cos \gamma + M_z \sin \gamma \quad (2.1)$$

This equation is incomplete because it assumes no slip ratio, SR, as discussed in Section 2.3.

From the previous discussion of tractive and lateral force in Section 2.9, the following equation was developed for net rolling resistance including traction/braking and slip ratio:

$$F_R = \left[(SR + 1) \left(\frac{T_{in}}{R_\ell} \right) - F_x \right] \cos \alpha - F_y \sin \alpha$$

Solving for T_{in} gives

$$T_{in} = \frac{F_x R_\ell}{(SR + 1)} + \frac{F_R R_\ell}{(SR + 1) \cos \alpha} + \frac{F_y R_\ell \tan \alpha}{SR + 1} \quad (2.2)$$

Adding the inclination angle effect from Eq. (2.1) gives the following:

$$T_{in} = \frac{F_x R_\ell}{(SR + 1)} + \frac{F_R R_\ell \cos \gamma}{(SR + 1) \cos \alpha} + \frac{F_y R_\ell \tan \alpha}{SR + 1} + M_z \sin \gamma$$

Each term has a physical significance, respectively, from left to right:

- Output torque, + driving and – braking
- Rolling resistance torque, always –
- Induced drag torque, – when $\alpha \neq 0$, otherwise = 0
- Aligning torque component due to inclination angle, – when α and γ are positive

The tire axis system discussed here and the rather precise definitions associated with it are of interest primarily to tire and auto engineers, especially those engaged in tire design, testing and specification. To those who are primarily interested in car performance, chassis tuning and the like, the “bottom line” tire parameters of concern are those discussed earlier in this chapter—lateral force, aligning torque, and driving and braking traction—and how they interact and are influenced by such operating parameters as pressure, load, and temperature.

2.12 Goodyear Tire Data

The Goodyear Tire & Rubber Co. is known worldwide as the predominant supplier of race tires. As part of race tire development, they measure the force and moment producing capability of their product on laboratory machines and have provided the following tire data on several high-performance and racing tires, specifically:

- Lateral force (lb) vs. slip angle. This is the upper plot in Figures 2.42, 2.43, 2.44, 2.45, and 2.46.
- Aligning torque vs. slip angle. This is the lower plot in the same figures.
- Typical rubber durometer (hardness) readings, with a note on how this data is best used. See Table 2.1.

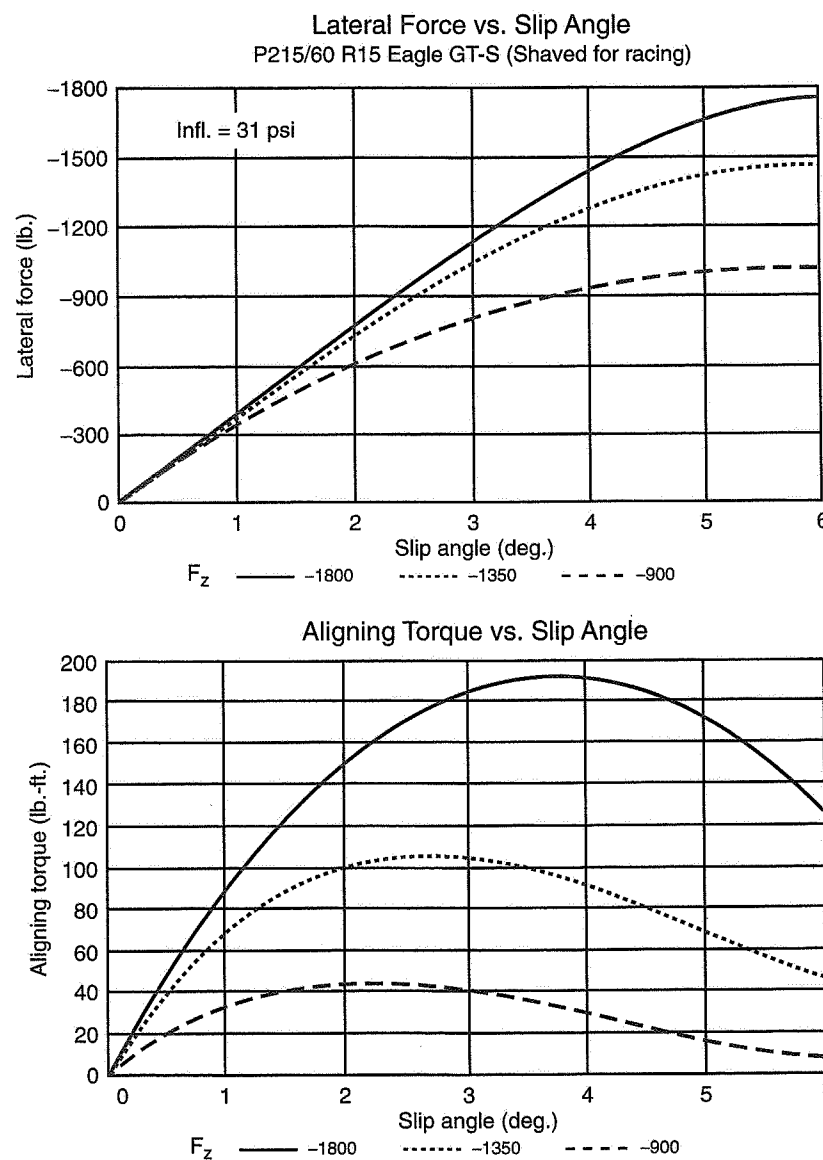


Figure 2.42 Goodyear data—Eagle GT-S.

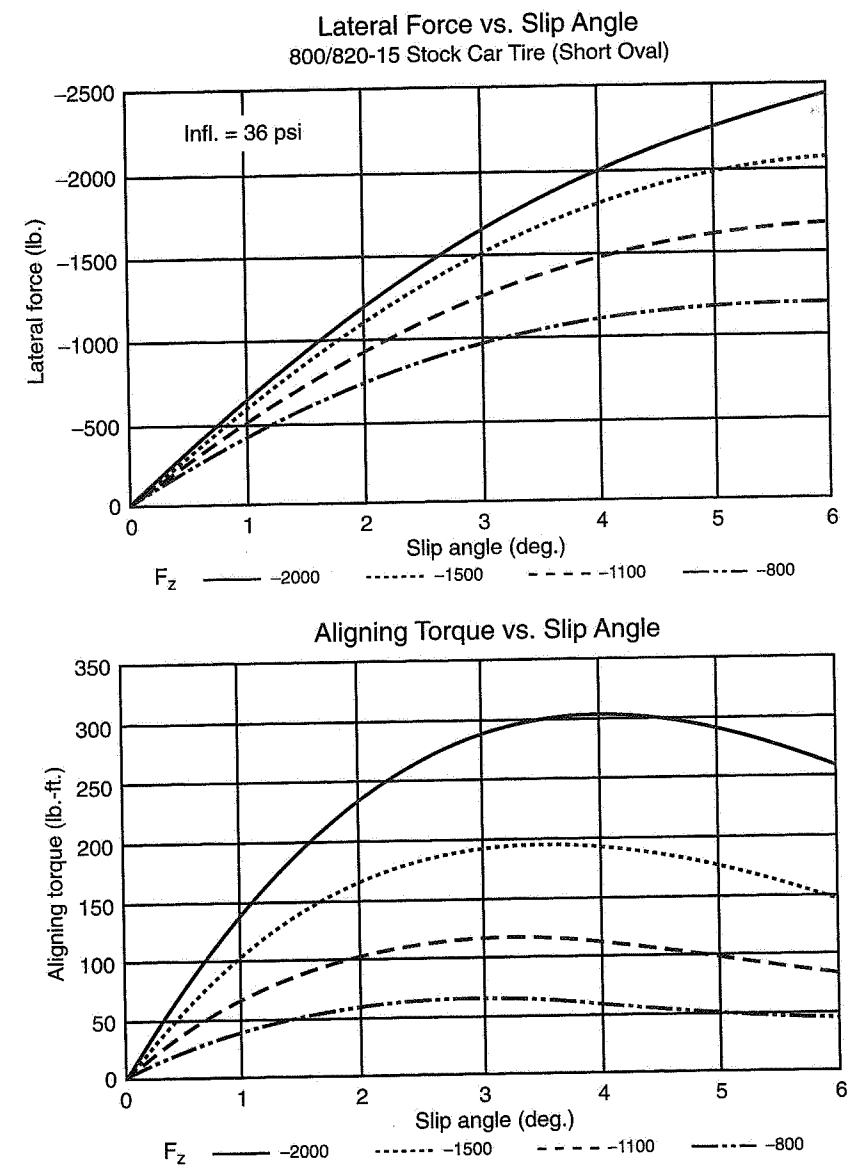


Figure 2.43 Goodyear data—Short Track Stock.

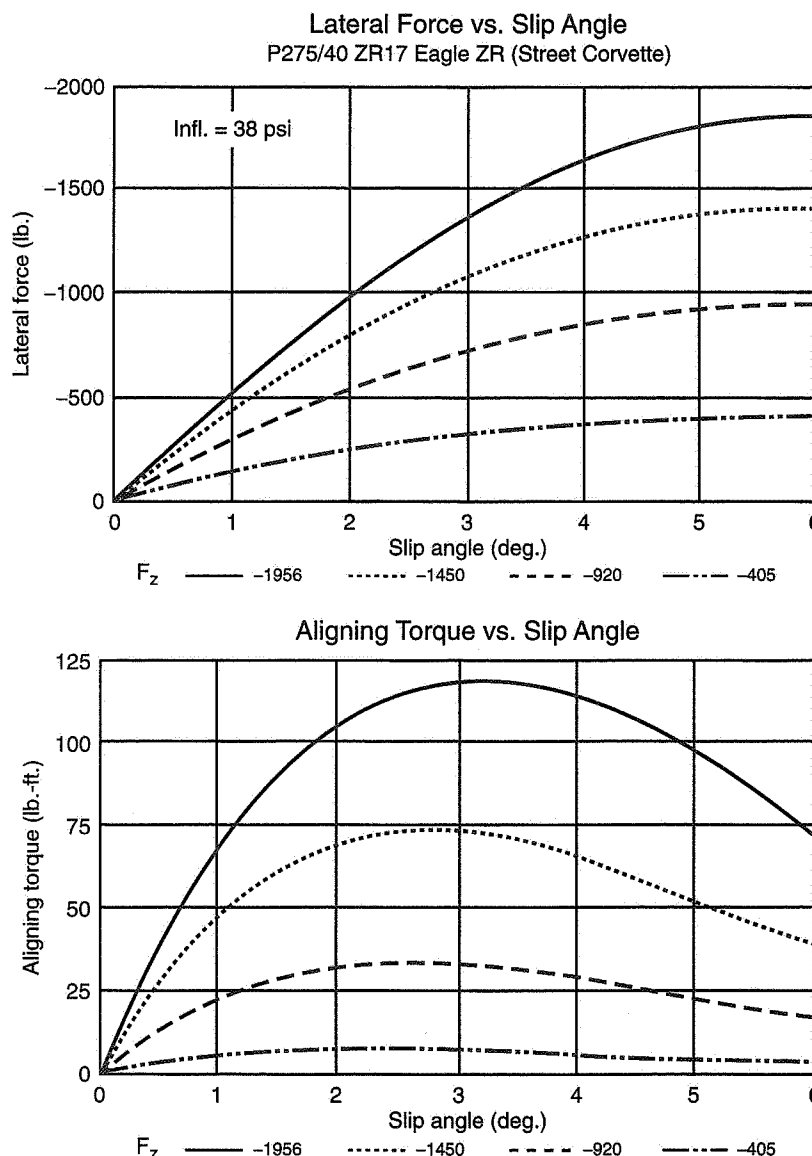


Figure 2.44 Goodyear data—Eagle ZR.

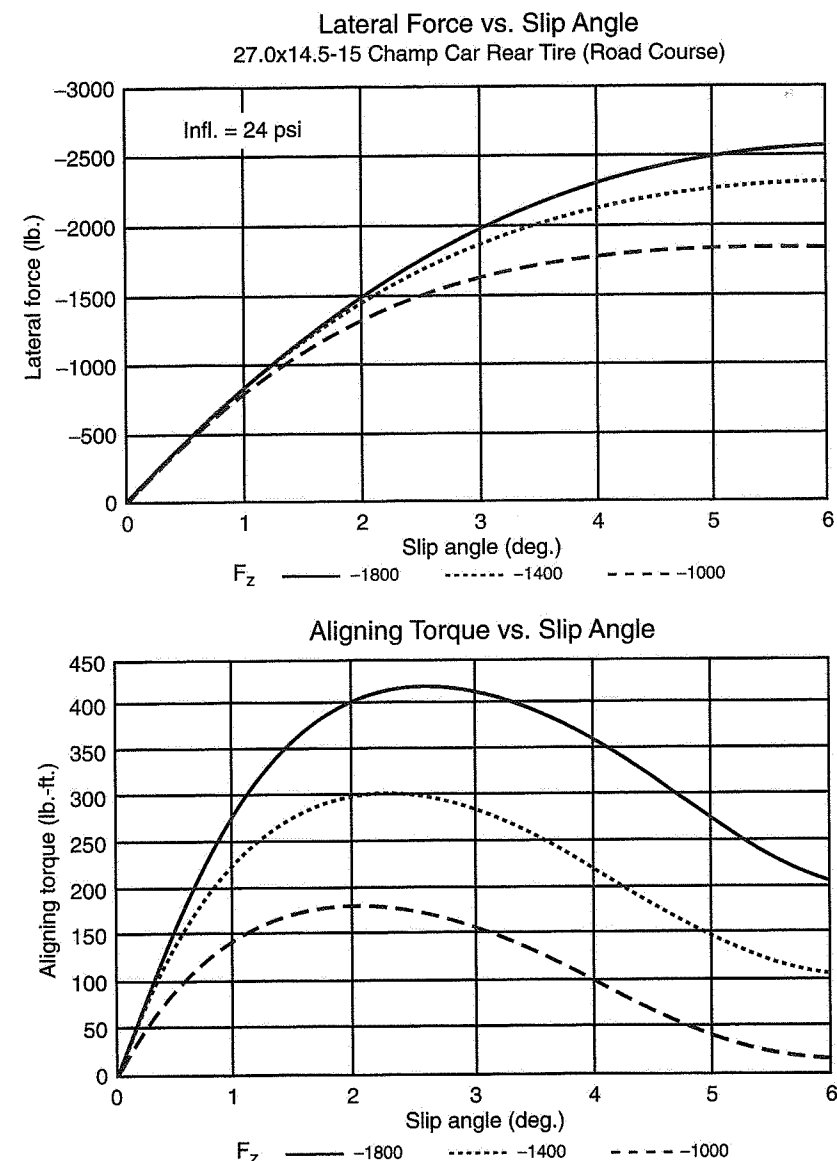


Figure 2.45 Goodyear data—Indy Car road course rear.

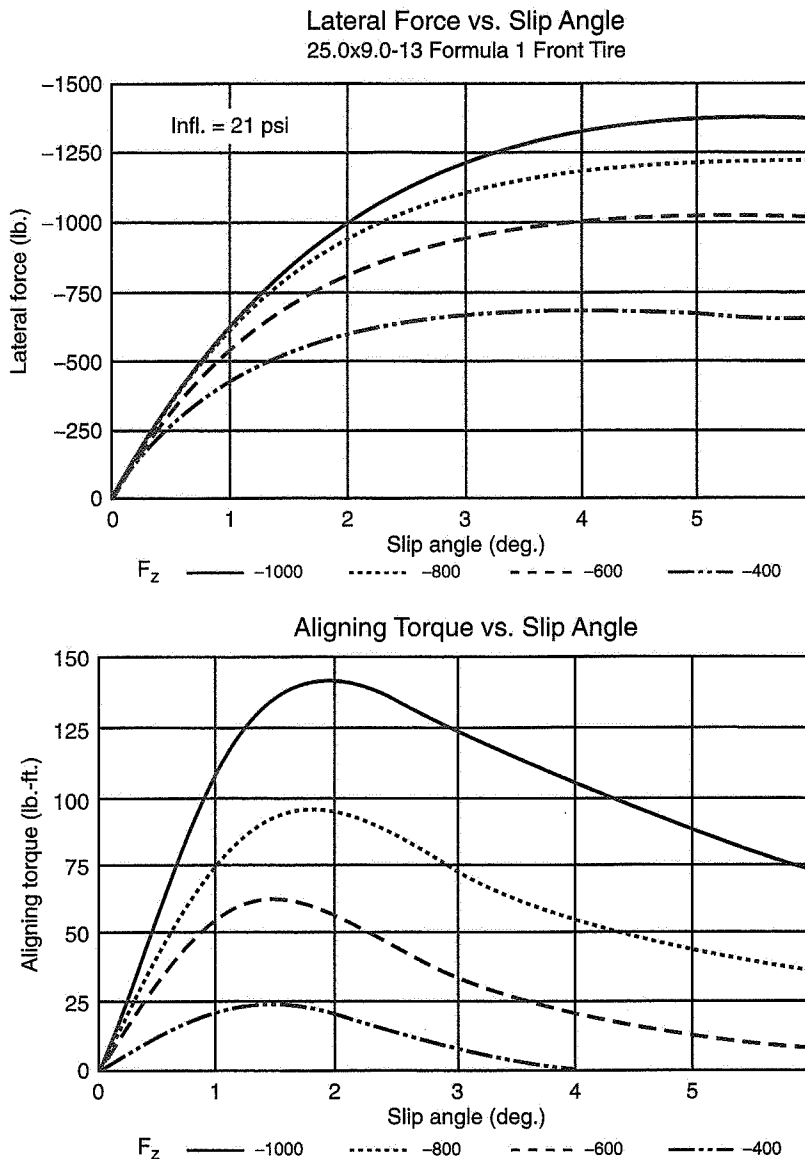


Figure 2.46 Goodyear data—F.1 front.

Table 2.1 Goodyear Data, Tread Compound Durometer Readings

Hardnesses listed are typical values measured on the Shore-A hardness scale, commonly used on plastic and rubber products. The values are also taken at room temperature and do not indicate how durometer readings change with respect to temperature.

The reader must also be cautioned not to correlate tread hardness (or softness) directly to traction. In many instances, more traction or cornering force may be obtained from a tire that has a higher durometer hardness. Tread compounding in racing is largely a matter of properly tailoring a compound to a specific application.

Still, the comparison of different tread hardnesses is of interest, if only to see how substantially compounds must vary between different types of racing if they are to work properly.

Type of Tire	Durometer (Shore A)
Eagle GT-S	65 - 80
Short Track Stock	60 - 75
Eagle ZR	60 - 75
Indy Car road course	55 - 70
Formula 1	50 - 65
Drag/Dirt	25 - 45

This tire data is “generic” in the sense that the race tires are described only by type of car (and position on the car). Thus the 800/820-15 Stock Car Tire is one of perhaps two dozen tire designs that are regularly provided for NASCAR sanctioned races. The intent is to make some typical real race tire data available for engineering use. The data will prove useful to anyone attempting to mathematically model race cars. Two possible uses are in a parameter study of different set-ups and a study of lap speeds and times. All vehicle simulations require some sort of “numerical tire.” That is the intent of this data.

Examining the plots, one can see that the cornering stiffnesses (C_α) vary widely and that some are more linear over a wider range of slip angles than others. Keeping in mind that C_α is the slope of the curves at $\alpha = 0$, one can see that for the maximum vertical loads given, the first three tires are fairly linear out to 4° or 5° but the last two begin to fall off at between 1° to 2° . As a matter of interest the C_α ’s for the five tires (at one load) are given in Table 2.2.

Table 2.2 Calculated C_α for Five Race Tires

Tire	Figure	Load lb.	Calculated C_α lb./deg.	lb./rad.
Eagle GT-S	2.42	1800	383	21,950
Short Track	2.43	2000	667	38,200
Eagle ZR	2.44	1955	533	30,600
Indy Road	2.45	1800	833	47,750
Formula 1	2.46	1000	750	42,975

The influence of load on C_α is marked. Using the concept of an “operating point,” say 2° , the F.1 tire (Figure 2.46) has a slope (at $\alpha = 2^\circ$) of about 285 lb./deg. at a 1000-lb. load, but only 90 lb./deg. at a 400-lb. load.

CHAPTER 3

Aerodynamic Fundamentals

“By god, we’ll build a plane so fast it’ll take six-penny nails to hold the paint job in place!”

“Granny” Granville
Gee Bee Aircraft
Granville Brothers



Introduction

Aerodynamic forces and moments, as well as the tire-road forces, affect “g-g” maneuvering performance (and stability and control). Unlike the tire forces which are primarily independent of speed, the aerodynamic forces increase rapidly with speed. For example, aerodynamic drag determines the vehicle’s performance characteristics at high speed including maximum speed, forward acceleration at the higher speeds, and braking deceleration.¹³ In addition to the direct effects of aerodynamic forces, the interaction of the aerodynamic and tire forces can have a large effect on lateral acceleration performance. For example, aerodynamic downforce (negative lift) increases the tire loads and this in turn increases the lateral force capability of the tires.

The race car aerodynamicist is confronted with such problems as:

- Reducing aerodynamic drag by external shaping, flow control, and efficient duct design for internal flow.

¹³ Modern open-wheel race cars have high enough drag that merely closing the throttle at top speed (200+ mph) will decelerate the car at about 1g.

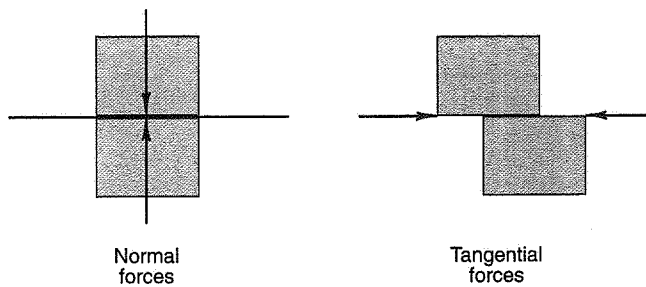
- Generating as much aerodynamic download and/or lateral force as possible, with the constraint that the drag not be too high.
- Wind tunnel testing, interpretation of wind tunnel test results and full-scale aerodynamic testing.
- Coping with aerodynamic/chassis coupling effects such as “porpoising” in ride height with ground-effects cars.

The intent of the present section is to review the origin and measurement of aerodynamic forces on full-size vehicles and on wind tunnel models. With this information the above problems can be approached from a more knowledgeable and fundamental point of view.

3.1 Properties of Air

The atmosphere is composed of a physical mixture of gases (78% nitrogen, 21% oxygen plus other gases and, on average, 1% water vapor—all by volume).

The interaction between the particles of a gas mixture, in this case air, are of two kinds: two particles can collide with each other with no sliding at the interface (producing “normal” or pressure forces) or two particles can slide by each other (producing “tangential” or shear forces). These interactions can be visualized if the air particles were cubes, as sketched below.



In reality, both types of interactions occur simultaneously but the relative magnitude of the two types of forces varies widely.

- In most of the air flowing around a body, the tangential or shear forces (which depend on the internal friction or viscosity of the air) are very small in comparison to the normal forces; the air particles interact with forces perpendicular to the line of contact (normal forces). *Streamlines* can be seen in smoke photos of this *free stream* airflow.
- In the thin layer of air next to a body, called the *boundary layer* (B.L.), the shear forces are important. In the boundary layer the air particles next to the body

adhere to the surface while the particles a short distance away are at *free stream velocity*. With this velocity gradient there are large sliding velocities and tangential forces in this layer.

- There is an additional situation in which an interaction occurs between the boundary layer and the free stream which can result in so-called *separated flow*. This turbulent and stalled condition results in high drag and loss of lift. Separated flow is characterized by a large amount of rotation which can arise only from tangential forces.

Before discussing these types of flow some measurable properties of air will be summarized.

Density

Air surrounds the earth in a layer that is many miles high. Air has mass and there is gravitational attraction between the air and the earth in accordance with Newton's law of gravitation. Again, because air has mass and is in the Earth's gravitational acceleration field, it exerts a force on the Earth's surface of approximately 14.7 pounds for each square inch of surface. This 14.7 pounds corresponds to the weight of a one-square-inch column of air from the Earth's surface to the top of the atmosphere; thus, the pressure at sea level is approximately 14.7 pounds per square inch (psi).

Air is a gas in which the particles are moving at random velocities. The energy of the particles is affected by temperature—the higher the temperature the greater the particle velocities and the wider the particle spacings. If the total number of particles in the one-square-inch column remain constant then the weight and pressure must also remain constant. If the temperature is increased, the inter-particle spacing increases and the column must get taller; if the temperature decreases the column gets shorter. In either of these cases, the number of particles per unit height will change; the *weight air density*¹⁴ which is the weight per unit volume will change with temperature.

Standard air density is defined for convenience in comparing measurements taken under different conditions. It is defined at specified pressure and temperature. For NACA/NASA Standard Atmosphere, for dry air at sea level, these are:

$$\begin{aligned} \text{Standard Pressure} &= 14.7 \text{ lb./in.}^2 = 2117 \text{ lb./ft.}^2 = 29.92'' \text{ of Mercury (Hg), absolute}^{15} \\ \text{Standard Temperature} &= 59^\circ\text{F} = 15^\circ\text{C} \end{aligned}$$

The *weight density* (specific weight) of air under these conditions has been measured as 0.07651 lb./ft.³, when the gravitational acceleration $g = 32.174 \text{ ft./sec.}^2$.

¹⁴ Sometimes called the specific weight.

¹⁵ This is the height of a column of mercury subjected to standard atmospheric pressure on the bottom and a vacuum on the top.

From $F = ma$, the mass/volume = specific weight/g and the *standard air mass density* is $\rho = 0.07651/32.174 = 0.002378 \text{ slug}/\text{ft.}^3$, where slug is in pound-sec.²/feet units.

The above standards are taken as a reference base in aerodynamic work. In reality, standard conditions rarely apply. The density of air changes in the following ways:

- **Change in temperature**—A change in temperature can be due to atmospheric temperature changes, or a localized condition such as air exiting a radiator. The change in air density due to temperature (at constant pressure) is given by the ratio of the absolute temperatures (original to present) in degrees Rankine (or Kelvin) times the original air density. Degrees Rankine are simply calculated by the addition of 460° to degrees Fahrenheit (for example, 59°F + 460° = 519°R). If the air exiting a radiator is 100°F above the surrounding air (at standard conditions) its weight density is given by the following:

$$\text{Density} = [(59^\circ + 460^\circ) / (159^\circ + 460^\circ)] \times 0.0765 = 0.0641 \text{ lb./ft.}^3$$

- **Change in pressure**—Air density is directly proportional to barometric pressure. A change in the barometric pressure can be either due to atmospheric weather conditions or due to a change in altitude (less air is stacked up above at higher altitudes). The change in air density due to barometric pressure is a direct ratio of the barometric pressure (present to original) times the original air density. The barometric pressure can be expressed in any consistent unit (e.g., pounds per square inch absolute, inches of mercury (Hg), etc.) to calculate this ratio.

The general law (Boyle's and Charles' Law) relating density, temperature and pressure is written as

$$\frac{\rho}{\rho_0} = \frac{p}{p_0} \times \frac{T_0}{T}$$

where the subscript "0" refers to the standard conditions mentioned above (with the temperatures given in absolute units) or to any desired baseline conditions.

Viscosity

Viscosity can be described as the "stickiness" of a fluid. For example, oil is more viscous than water. The viscosity of a fluid is determined by the forces created within the fluid when there are velocity differences within the fluid. The viscous forces are transmitted between the fluid and to any solid body through a thin boundary layer of the fluid that is attached to the body surface. The more viscous the fluid, the more force is transmitted to the body from the fluid. Conversely, the more viscous a fluid, the harder it is to move a body through the fluid. This can be demonstrated by slowly stirring a stick

through a heavy oil and through water. The units for absolute (or dynamic) viscosity, μ , are slug/feet-second.

The standard value of absolute viscosity for air at 59°F (15°C) is

$$\mu = 3.805 \times 10^{-7} \text{ slug}/\text{ft.-sec.} = 0.0000003805 \text{ slug}/\text{ft.-sec.}$$

The absolute viscosity of air (and other gases) rises slowly with temperature.

Kinematic viscosity, v , is the absolute viscosity, μ , divided by the density, ρ , i.e., $v = \mu/\rho$, which works out to be in units of ft.²/sec.

$$v = 0.00016 \text{ ft.}^2/\text{sec.}, \text{ for standard conditions}$$

One component of the Reynolds Number (RN), discussed later in this chapter, is the kinematic viscosity. There are situations where an aerodynamic force varies rapidly with a small change in RN, indicating a change in flow character. In these cases, the effect of temperature change on absolute viscosity as well as the effect of temperature change on density may be significant.

3.2 Bernoulli's Equation

Bernoulli's equation describes the conditions existing in the free stream, outside the boundary layer. It deals with pressure (normal forces) and velocity as air flows smoothly around a body. From this equation, it is possible to predict surface pressures and lift for many types of shapes, specifically those shapes where no separation is present and boundary layer growth is small. As drag depends on tangential forces (boundary layer effects) it is not treated by Bernoulli's equation.

As indicated earlier, the flow around bodies outside the boundary layer is predominantly nonviscous with normal or pressure forces between the air particles. For the subsonic speeds associated with race cars, the air density changes are small except in cases where large temperature changes occur (see the previous example of air exiting a radiator). Suppose that in flowing around the body of a vehicle the average air temperature increased by +10°. T_0 is 519°R absolute and the elevated temperature is 529°R. The density change is the ratio of $519/529 = 0.982$, less than 2%, which can be considered negligible.

Measurements of surface pressure changes on race cars in smooth flow conditions may locally reach 25 inches water column below the remote airstream, as measured by a differential pressure gauge or a U-tube (manometer) filled with water. To convert inches of water to pounds/foot² multiply by 5.2:

$$25 \text{ inches water} \times 5.2 \left[(\text{lb./ft.}^2) / \text{inch water} \right] = 130 \text{ lb./ft.}^2$$

Atmospheric pressure is 14.7 lb./in.² or $14.7 \times 144 = 2117$ lb./ft.².

$$\frac{\rho}{\rho_0} = \frac{2117 - 130}{2117} = \frac{1987}{2117} = 0.94$$

or, a 6% decrease in density for this fairly extreme condition. This density change would normally be considered negligible for a local condition.

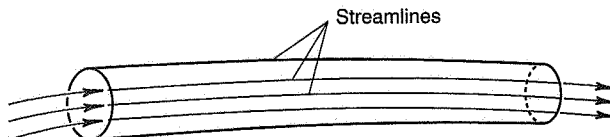
Therefore, the assumption is made that for smooth airflow outside the boundary layer the air is *nonviscous* and *incompressible*. These two assumptions define a "perfect fluid." An example of a perfect fluid is water—it is almost incompressible and has very low internal friction (viscosity). The following discussion of aerodynamics follows theoretical hydrodynamics.

Hydrodynamic theory enables the calculation of the flow field (the streamlines) and the associated velocity and pressure variations around smooth shapes such as wings and aircraft fuselages. This theory, for all its shortcomings, is a remarkably useful tool for the practical aerodynamicist.

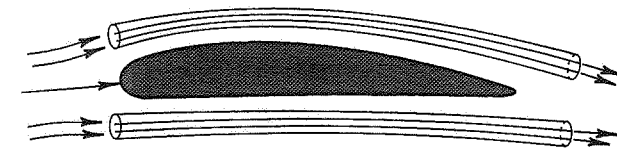
Bernoulli's equation gives us a means of relating velocity and pressure changes in the airstream. It is based on a perfect fluid and is really a statement of the conservation of energy in the fluid stream. It is instructive to develop it from first principles.

In aerodynamics, the principle of relative motion is assumed. Thus the air can be stationary with a body moving through it, or the body can be stationary with the air moving past it (as in a wind tunnel); the pressure/velocity relationships will be the same. For the following derivation the air is moving.

Consider a tube of air, a *stream tube*, made up of streamlines.

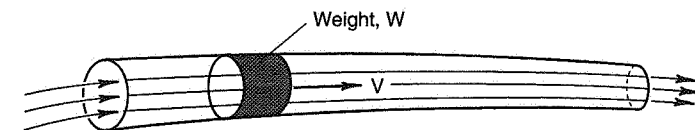


A streamline is the path of successive air particles in a steady flow. The outer surface of this tube is in effect a boundary since no air flows through it. The size and velocity of the tube will be described by Bernoulli's equation. Such tubes of air might, for example, pass over and under a wing. The cross-sectional area of these tubes will change with pressure changes as if they were elastic.



A stream tube is composed of a frictionless and incompressible fluid, and is an isolated system (no flow through the boundaries). Because of this the total energy must remain constant along its length but this energy can appear in different forms. In this situation three forms of energy are possible:

- **Potential energy** is associated with a height change of the fluid. It is given by Wz , where W is the specific weight and z is the height change. For automotive flow, this term is negligible.
- **Kinetic energy** is given by $(1/2)mV^2$, where m is the mass (in slugs) and V is the velocity in ft./sec. Consider a small volume (vol) of fluid in the stream tube of weight, W , and velocity, V , as shown below:

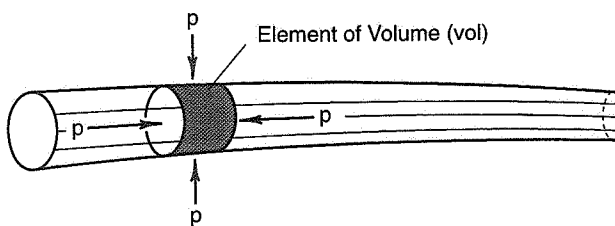


The kinetic energy of this small volume of fluid is

$$KE = \frac{1}{2} \left(\frac{W}{g} \right) V^2 = \frac{1}{2} m V^2 = \frac{1}{2} (\rho \times vol) V^2$$

This corresponds to the amount of work required to take this small mass of fluid and accelerate it to the velocity, V .

- **Pressure energy.** The stream tube is located in a fluid body which is under a static pressure at its outer boundaries (from the weight of all the air above it). This external pressure acts uniformly in all directions (as does pressure in any fluid) and the fluid element must be at an equal pressure to be in equilibrium. The pressure energy in the fluid element is equal to the work required to maintain its volume against the external pressure. This work is equal to $p \times vol$, where p is the external (and internal) pressure.



The total energy at a given position in the stream tube is

$$(p \times \text{vol}) + \left[\frac{1}{2} \rho (\text{vol}) V^2 \right]$$

In working with fluids it is convenient to think in terms of a unit volume. The total energy per unit of volume is

$$p + \frac{1}{2} \rho V^2$$

Bernoulli's equation says that this energy is constant along the stream tube, thus,

$$p + \left(\frac{1}{2} \rho V^2 \right) = \text{constant} = H$$

or

$$p + q = H, \quad \text{Bernoulli's equation}$$

$$\text{where } q = \frac{1}{2} \rho V^2$$

3.3 Discussion of Bernoulli's Equation

This section will discuss each of the terms, p , q , and H , in Bernoulli's equation in some detail, with particular reference to how they are measured. All of the terms in Bernoulli's equation have the units of pressure and any consistent units may be used such as inches of water, lb./in.², lb./ft.², etc. The atmospheric (barometric) pressure is frequently used as a reference pressure as will be noted.

Static Pressure— p is the pressure in the airstream (frequently referred to as *static* pressure). It is the pressure that would be measured by a barometer or other type of pressure gauge moving along with the airstream. Since it is not usually convenient to move an

instrument along with the airstream, the static pressure in a moving airstream is commonly measured with a static tube, shown in Figure 3.1. The holes are normally several diameters aft of the nose to insure that the flow is parallel to the tube wall (the tube must be oriented in the flow direction). The exact longitudinal location of the holes for a true static pressure measurement is determined experimentally as it is a function of the shape of the nose and details of the configuration. In the figure, the static pressure is referenced to atmospheric pressure.

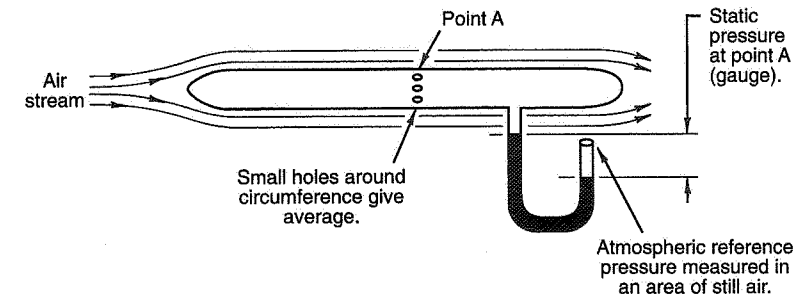


Figure 3.1 Static pressure tube, for measuring p in free stream.

The static pressure may also be measured by a flush pressure tap along the wall of a wind tunnel or on the surface of a body in an airstream, provided that the flow is attached and moving parallel to the surface, as shown in Figure 3.2. The principal requirement in measuring static pressure is that there be no direct component of the flow velocity into the static hole(s). The hole(s) must be flush and with no burrs around the sides to insure that the flow moves past smoothly.

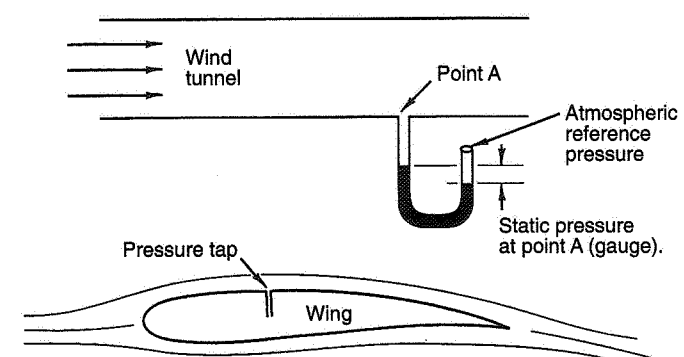


Figure 3.2 Static pressure tap, for measuring p along a surface.

When a pressure measurement is referenced to atmospheric pressure it is called *gauge* pressure. It could also be measured in an absolute sense by referencing it to a vacuum (for example, a diaphragm pressure gauge that is evacuated on one side). Gauge pressures lower than atmospheric are frequently called negative pressures. They are not negative pressures, merely pressures lower than the atmospheric reference pressure.

Dynamic Pressure— q is the *dynamic* pressure, the pressure that would be realized if the kinetic energy of the moving fluid at a given point were converted to a pressure. The pressure equivalent to the KE in the stream is the stop pressure; they are numerically equal. If a large flat plate is inserted into an airstream at right angles to the flow, as in Figure 3.3, then air particles moving in the column of air near the center would be decelerated to a stop at the plate and all of their kinetic energy would be converted to an increase in static pressure. This increase in static pressure is called the “*stop*” pressure, as pointed out above, numerically equal to the dynamic pressure, $(1/2)\rho V^2$.

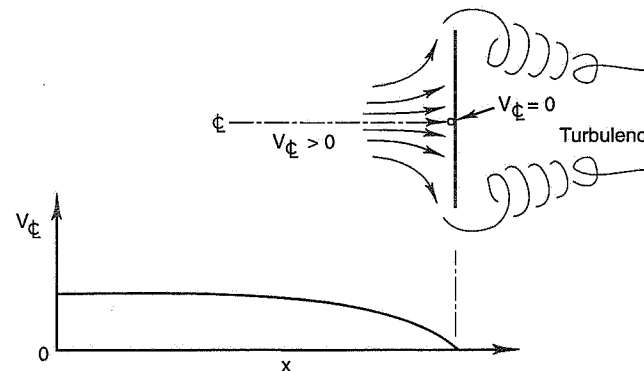


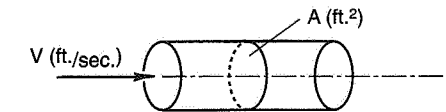
Figure 3.3 Dynamic or “stop” pressure, “q.”

The following formula can be used to compute the stop or the dynamic pressure:

$$q = \frac{V^2}{391} \approx \frac{V^2}{400}$$

where V is velocity in mph
 q is stop pressure in lb./ft.²

The stop pressure, q , can also be derived from the force required to decelerate an air column to zero velocity. Consider a cylinder of air, moving at velocity, V , with small cross-sectional area, A .



The volume of air passing a given point per second is $A \times V$ (units of ft.³/sec.); the mass per second is $\rho \times V \times A$ (in slugs/sec.). From $F = ma$, the force required to decelerate this mass to $V = 0$ is

$$\rho VA \times (\text{average velocity change}) = \rho VA \times \frac{V}{2} = \frac{1}{2} \rho V^2 A$$

$$\text{Stop pressure} = \frac{F}{A} = \frac{1}{2} \rho V^2$$

The dynamic pressure, q , is usually measured indirectly. Thus from Bernoulli's equation, $q = H - p$, where H is measured as described below.

Total Pressure— H is the *total* pressure, as defined by Bernoulli's equation, $H = p + q$. H is the total of the pressure and velocity energy in the fluid.

H can be measured by an open-ended tube, shown in Figure 3.4, in which the air is brought to rest at the nose of the tube (air is assumed incompressible at automotive speeds). The size of the tube, as indicated by experiment, is not critical. The measured pressure is called the *stagnation pressure*.

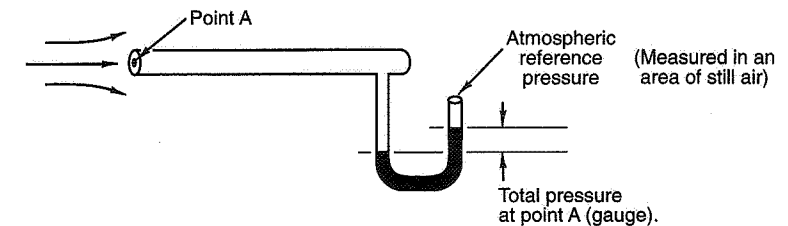


Figure 3.4 Total pressure tap, to measure “ H .”

The axis of the tube must be aligned with the direction of the airstream. This can be accomplished, for example, by building the tube into a weather vane, as shown in Figure 3.5. If the stream direction is known to be horizontal, this vane will rotate to line up with the flow.

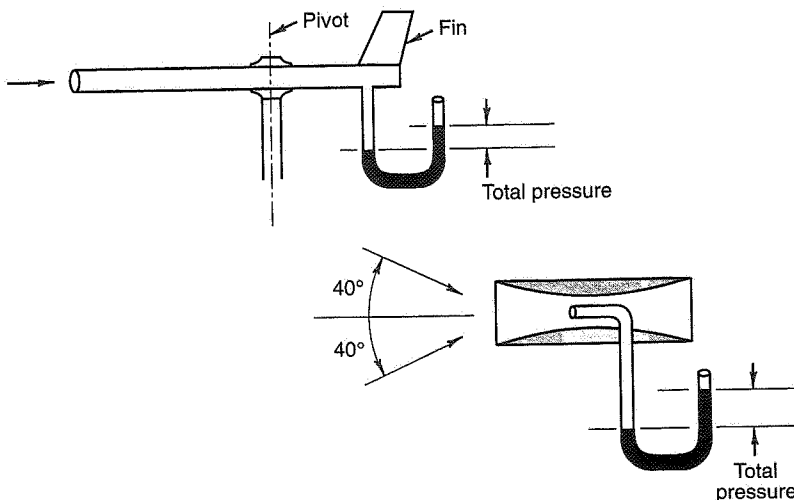
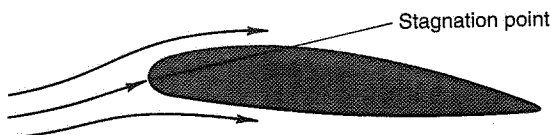


Figure 3.5 Weather vane, left, and Kiel tube, right, for measuring total pressure.

Other devices can be used to measure the total pressure if the flow direction is unknown. For example, a special total head tube called a Kiel Tube (Figure 3.5) works for $\pm 40^\circ$ from straight ahead. See Ref. 119 for more information on flow measuring devices.

Stagnation Pressure—Any time the air splits to go around a body in two or more different directions there will be a small region (point) of stagnation pressure equal to the static pressure plus the stop or dynamic pressure. That is, the stagnation pressure is equal to $p + q$. The stagnation point is shown on the wing below.



For a vehicle moving on the road (not in a wind tunnel), the static pressure, p , at the stagnation point is a special case and is equal to the barometric atmospheric pressure. This is because the flow has not been appreciably accelerated into a curved path by the body at the stagnation point. The streamline at the stagnation point is the border between the flows over and under the vehicle.

Dynamic Pressure and Velocity Measurement

If the total head, H , and the static pressure, p , are known at a point in the fluid, the dynamic pressure can be obtained by subtraction, as noted before:

$$q = \frac{1}{2} \rho V^2 = H - p$$

The conventional pitot-static tube type of airspeed indicator (Figure 3.6) is based on this principle. In the instrument shown, both the total and static sides are in effect vented to (measured relative to) atmospheric pressure. The instrument can be calibrated to read velocity, V , under known air density (temperature and pressure) conditions.

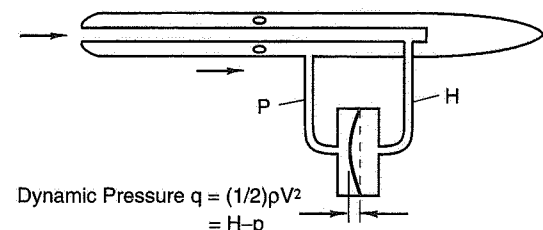
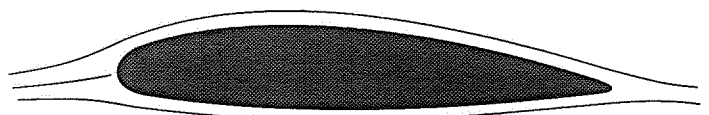


Figure 3.6 Pitot-static tube airspeed indicator.

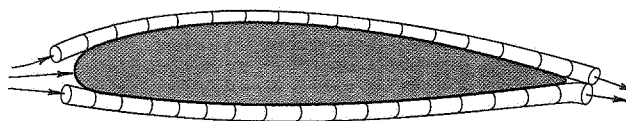
3.4 Pressure Distribution

Bernoulli's equation indicates that if the dynamic pressure is increased, the static pressure in the stream must decrease, or vice versa. An airfoil is a device which utilizes these pressure changes to generate force. With the airfoil shape shown below, the air must increase in speed as it goes over both the top and bottom surfaces, but more so over the top as the curvature and the distance traveled are greater.



It should be remembered that the air behaves as an incompressible fluid and the *condition of continuity* says that the same number of particles of air passing a cross-section of a stream tube near the leading edge of the wing must pass through a cross-section near the trailing edge. The stream tube will be thinner where the velocity of the air is higher,

over the thicker part of the airfoil. Typical stream tubes over the top and bottom of the airfoil are shown below.



The stream tubes behave as if they were elastic—as the air speeds up, the static pressure decreases and the tubes shrink in size. As the air slows down again toward the trailing edge the tubes expand under the increasing pressure. This is called *pressure recovery*.

The airfoil generates lift because the reduced pressure over the top of the wing is, in this case, greater than the reduced pressure under the bottom. The air is moving faster over the top. If the reduction in pressure, Δp , relative to the free stream pressure is plotted, the pressure distribution might look like Figure 3.7. Note that the pressure arrows are drawn perpendicular to the surface. This is a result of the assumption that there are no tangential (shearing) forces in the perfect fluid under discussion.

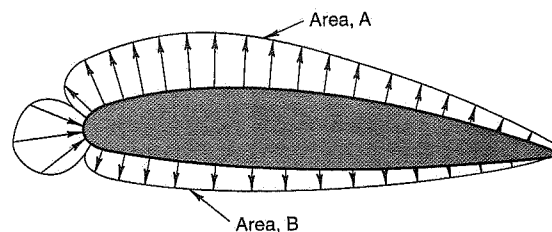
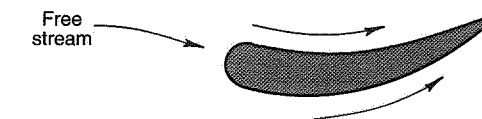


Figure 3.7 Pressure distribution around a wing.

The pressure distribution area A (in Figure 3.7) on the top of the airfoil is greater than area B, on the bottom, resulting in an upward lift. Pressure distributions can be measured experimentally by flush pressure taps in the wing surface to measure the static pressure at each point. The Δp arrows in the sketch are vectors—they represent both pressure and direction. If they were all added up by vector addition one might suspect that the sum would result in a pressure drag, that is, a force component in the downwind direction (relative to free stream). This occurs in the case of a real wing, but in the idealized case discussed here, the pressure recovery is complete and the sum of the pressure components in the remote stream direction is zero. The sum of the pressure components perpendicular to the free stream is not zero, in fact it is the lift of the airfoil.

Bernoulli's equation says that the kinetic energy in the airstream (the dynamic pressure or velocity head) can be exchanged for static pressure. The static pressure exerts a force on a surface and this is available for uses such as generating downforce. The downforce (lift) is limited by the magnitude of the dynamic pressure available. The quantity $(1/2)\rho V^2 = q$ determines the energy that is available to work with. The energy available increases with the square of the speed and directly with the air density.

The effectiveness of converting dynamic pressure to static pressure and lift, for example, depends on the shape of the body. The wing section shown below is very effective in creating downforce when it is angled to the free stream as shown. One may say that this wing has a high shape efficiency as regards down lift.



3.5 Consideration of Real Flows

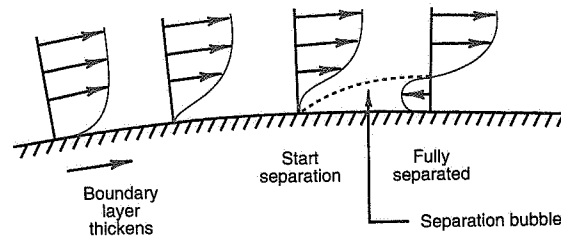
In the previous section, velocity and pressure relationships were treated for an ideal fluid moving around smooth body shapes such as airfoils. Air does not always act like a perfect fluid and few race cars are finely streamlined shapes. Flow conditions are seldom ideal. In Chapter 15 a number of types of airflow are characterized and discussed in detail. This section contains some general remarks on the characteristics of real airflows.

First consider the boundary layer of air at the body surface. In this layer the shear forces (viscous effects) are important. These forces tend to slow the airflow down and remove energy from the moving stream. This phenomenon depends on the distance that the air flows along the surface. The boundary layer tends to thicken along the length of the body, even if the body is very smooth. In practice, most boundary layers are *turbulent*. This means that the air particles in the boundary layer are moving with random velocities and are constantly changing distance from the body surface.¹⁶ This has the effect of distributing velocity energy throughout the layer which often helps to keep the boundary layer attached to the body and the free stream following the body contour.

As the air continues to move along the surface, the turbulent boundary layer will thicken further as the air in the boundary layer loses energy due to skin friction. This generally occurs on the aft part of the body where the free stream is slowing down and the pressure

¹⁶ Laminar boundary layers are not common on race cars; they are briefly discussed in Chapter 15.

is building up—the area of *pressure recovery*. The increased pressure and the lack of energy in the boundary layer can actually create a reversed flow at the surface, a condition known as *flow separation*.



Toward the rear end of typical automotive shapes the boundary layer can separate from the body and the flow will break down into large-scale turbulence known as the disturbed *wake* (see Figure 3.8). The thickening of the boundary layer and the formation of the turbulent wake is shown in the photograph in Figure 3.9.

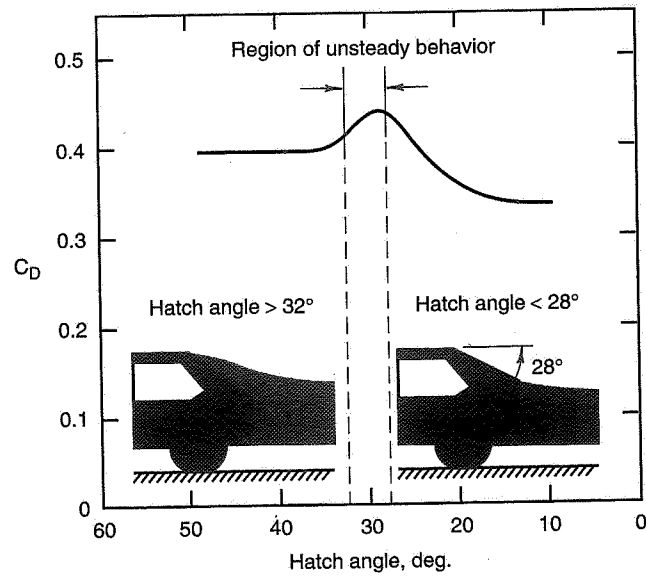


Figure 3.8 Critical behavior of a hatchback automobile (Ref. 70).

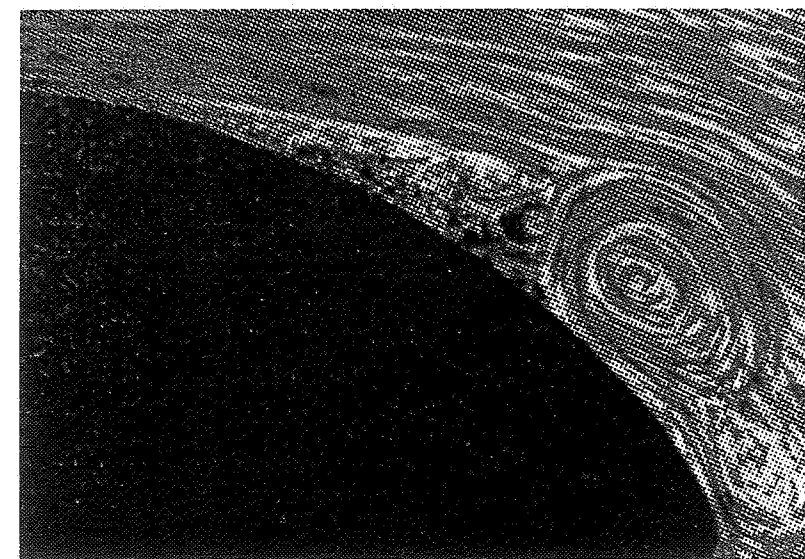
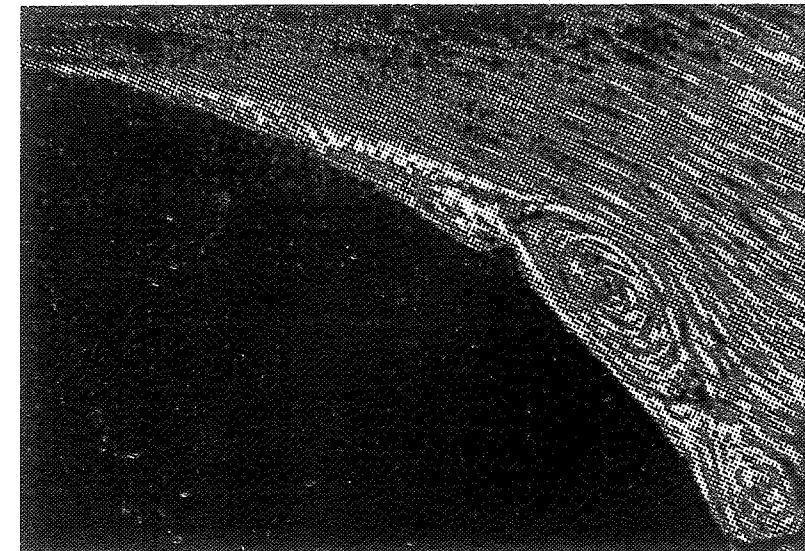


Figure 3.9 Turbulent wake formation (Ref. 79).

The forward part of a body is a boundary and forces the air to speed up to get around it. Once the maximum section is reached and/or the body shape recedes, there is nothing that forces the airflow to expand and follow the body shape except pressure and velocity changes within the stream tubes. Experience with wind tunnel design has shown that the air can only expand and follow a boundary slope of some 10° or less. If the diffuser section in a wind tunnel (see Figure 3.10) has a steeper angle the flow will separate from the wall with the creation of random turbulence. The same phenomenon is common at the rear of automobiles which vary from aircraft fuselages by being short bluff bodies. Smoke flow photos such as Figure 3.11 illustrate this type of separation. The white smoke "disappears" in the wake because it is thinned out by the turbulent mixing; the streamlines no longer exist in the wake.

Any sharp edge will result in separation. An infinite acceleration of the flow would be required to go around a sharp edge smoothly and that is not possible in a real fluid.

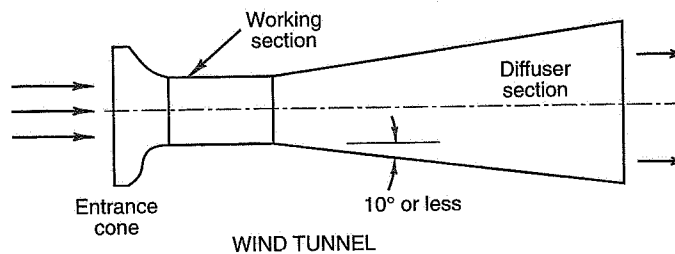


Figure 3.10 Simple wind tunnel showing diffuser angle.

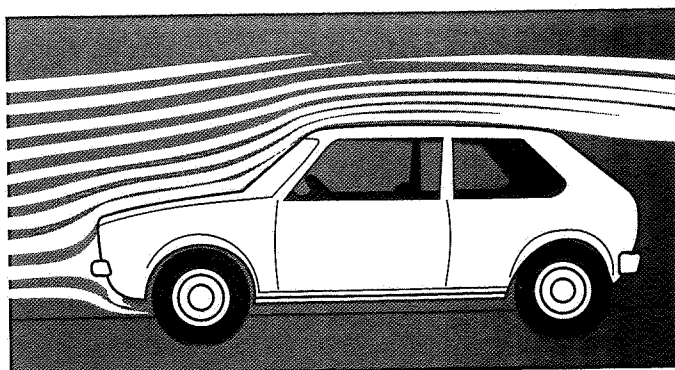


Figure 3.11 Streamlines in the center cross-section of a VW Rabbit (Ref. 151).

Separated flow is usually undesirable. The pressure in the wake region is low, increasing the pressure drag. Energy is required to maintain the turbulence and "drag along" the low-pressure region. This energy must come from the vehicle's power plant.

There are some exceptions to the rule that separation is undesirable. For example, on hatchback cars (refer back to Figure 3.8) with the rear end inclination angle steep (left side of figure), the flow separates at the roof. On hatchbacks with the rear inclination angle between about 28° to 24° , the flow separates at the lower edge of the hatch (right side of figure). The steeper hatch angle ($>32^\circ$) has lower drag. This phenomenon appears to be associated with the three-dimensional flow and the effect of vortices forming on the sides of the car at the rear. These vortices can induce favorable effects on the velocity field.

The mechanisms governing flow separation are only generally understood. Although great effort is being made to computer model aerodynamic flow, it is unlikely that the wind tunnel will become obsolete. Three-dimensional flows about bluff automotive shapes in close proximity to the ground are extremely complex. For the race car designer, the wind tunnel and full-scale development will remain the chosen tools for aerodynamic development for some time.

3.6 Aerodynamic Testing

Aerodynamic testing is the standard way to determine the characteristics of bluff bodies such as automotive shapes. This testing may take the form of model or full-scale wind tunnel testing or it may be done on the track with an actual vehicle. This section begins with a discussion of wind tunnel testing and Reynolds Number. Various test techniques that are usable on the track are discussed. The section concludes with a description of aerodynamic force and moment coefficients; these are widely used to compare one vehicle to another.

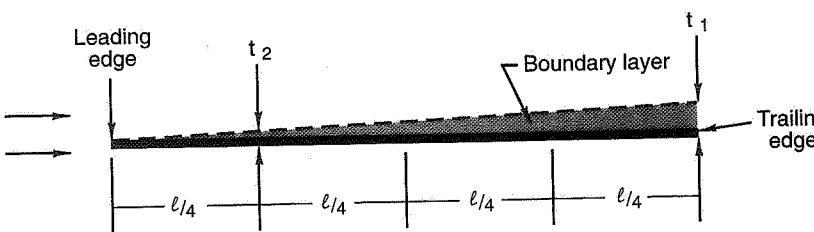
Wind Tunnel Testing

Wind tunnels are as old as the airplane; an early tunnel was built and used by the Wright Brothers. The size of the wind tunnel determines the largest model size that can be used. Some full-size tunnels have been built for small aircraft but generally aircraft aerodynamicists have used scale model tests. In the automotive case there are a number of tunnels suitable for testing the full-scale car (Lockheed-Georgia, MIRA in England and of course, the General Motors tunnel). If the actual vehicle and one of these expensive tunnels is available it is desirable to test at full size. This avoids the scaling problems with models but there are still problems of ground plane simulation, tunnel wall and blockage corrections, and speed corrections if the tunnel cannot reach racing speeds.

In the design stages of a new vehicle it is often necessary to test a model in a smaller, less expensive wind tunnel. In this case there are two specific problems that must be addressed: modeling the ground plane, and insuring that the model flow field is similar to the eventual full-size vehicle flow field:

1. The modern race car has very low ground clearance. The flow under the car and around the sides of the nose may be critical to lift and pitching moment. In real life the air is at rest relative to the road (for zero wind) and the vehicle moves past the road. In a conventional wind tunnel the air is not at rest with the "ground" and a boundary layer builds up in front of the test model. This can critically affect the airflow simulation under the model. This is not an easy problem to analyze and correct for—nor is the other solution, use of a moving ground plane to duplicate the real case where the air speed is zero relative to the road.
2. The second problem concerns "flow similarity" or the simulation in the tunnel of a flow pattern which generally corresponds to that of full scale. The theory of model testing says that the pattern of streamlines and separation locations should be geometrically similar for model and full-scale tests—a photo of one could be blown up to match the other. If the flow was frictionless with no boundary layer (ideal fluid) around both the car and the model there would be no problem. A boundary layer does exist and some other criterion for similar flow must be used.

Air blowing along a flat plate will create a boundary layer. This boundary layer will increase in thickness with distance from the leading edge of the plate.



If a 1/4-scale model of this flat plate were tested under the same airflow conditions, the boundary layer at the trailing edge would be t_2 in thickness instead of t_1 . Since the likelihood of boundary layer separation in the presence of pressure gradients on a real car depends on the **actual** thickness of the layer, it is apparent that the model is not a good simulation of full scale. Any separations that occur on the full scale should occur at the same scaled location on the model. To "convince" the flow to be similar on the model it may be necessary to use devices such as "trip wires" on the model, but the primary consideration is discussed below.

Reynolds Number

The basic condition for flow similarity between a model and a full-scale vehicle is that they are both at the same Reynolds Number (RN).

The Reynolds Number is defined as

$$\frac{VL}{v}$$

where V is the airstream velocity

L is an appropriately chosen length for characterizing the flow pattern
 v is the kinematic viscosity, μ/ρ , defined earlier

In the Properties of Air section at the beginning of this chapter it was pointed out that there are two kinds of interactions between air particles—normal and tangential. The first involve inertia (mass) effects and the second involve friction (viscous) effects. Reynolds Number similarity is based on the idea that if the ratio between these two kinds of interactions is constant the flow patterns will be similar.

A physical understanding of the RN is given below. The dynamic pressure, $(1/2)\rho V^2$, is the force per unit area that is realized if the kinetic energy of the moving particles is converted to a pressure by a collision with an object. It is an inertia force proportional to the dynamic pressure times the area on which it acts:

$$\rho V^2 \times L^2$$

where L is the chosen characteristic length.

The frictional force acting on a unit area is

$$\mu \times \frac{V}{L}$$

where μ is the absolute coefficient of viscosity

V/L is the rate the velocity is changing with distance through the fluid layers

Thus $\mu \times V/L$ is the frictional force per unit area, and

$$\left(\mu \times \frac{V}{L} \right) \times L^2 = \mu VL$$

is the actual frictional force.

The ratio of the inertia to the frictional force is proportional to

$$\frac{\rho V^2 L^2}{\mu VL} = \frac{\rho VL}{\mu} = \frac{VL}{v} = RN$$

To insure that flow patterns are similar between full-scale and model tests, the RN should be the same or at least as close as possible. Assuming that v is the same for both tests, then VL should also be the same for both tests. If the model scale is 1/4, the wind tunnel test speed would ideally be four times the vehicle speed. If it is not possible to meet this condition, it may be useful to repeat a test with several different speeds (= different RN) and note the variation of the measured forces. If flow separation is not a major problem or if other factors such as differences in surface roughness (between the full-scale and the model) do not exist, a test at other than true RN may suffice. Experience may also enable a "calibration" of full-scale and model results.

Flow Visualization

It is highly desirable to be able to "see" the streamlines in steady flow conditions and the extent of flow separation and wake size. This is true whether the test is performed in a wind tunnel or at the track. Several techniques are available for flow visualization. Although purely qualitative, flow visualization can indicate where problems exist and the extent of improvement when changes are made.

One of the simplest techniques is that of *tufting* in which short lengths (1-2 in. on a model, 4-6 in. full-scale vehicle) of yarn or heavy cotton thread are attached to the surface by tape at their forward ends. If the tufts are too long, "flag waving" may result. Sometimes the tufts are attached to pins that are an inch or so high if it is necessary to eliminate boundary layer effects. Figure 3.12 shows a tufted wing model in a wind tunnel.

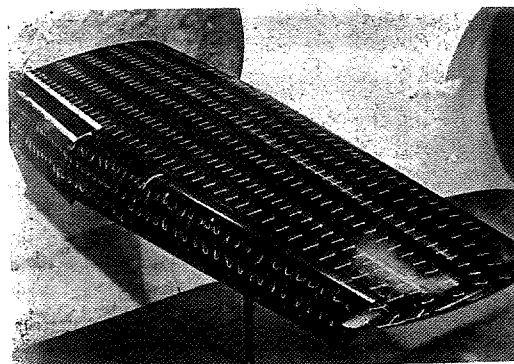


Figure 3.12 Tufts on a wing (Ref. 119).

Tufts can also be attached to a wire grid (plane perpendicular to the airstream) in a wind tunnel to determine wake conditions aft of a model. The extent and nature of the wake is closely related to the model drag. A typical grid installation is shown in Figure 3.13, along with a photograph of the tufts as disturbed by a swept wing model. This shows the generation of vortices aft of the wing tips. Vortex formations are common in the wake behind automobiles.

Long tufts are sometimes used to ascertain the entrance airflow conditions to ducts, for example.

Low-speed wind tunnels have utilized smoke to give a visualization of the flow patterns. Figure 3.14 shows a two-dimensional smoke tunnel and a typical flow picture.

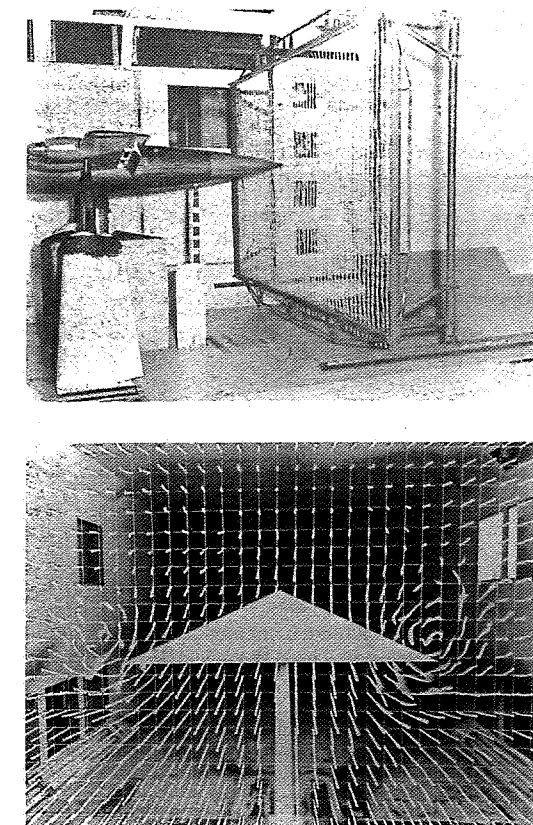


Figure 3.13 Tuft grid (Ref. 119).

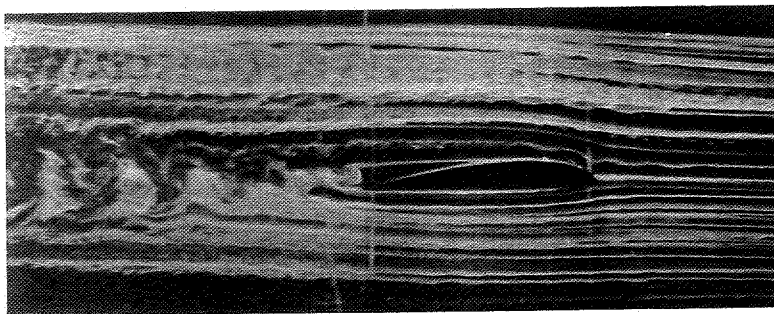
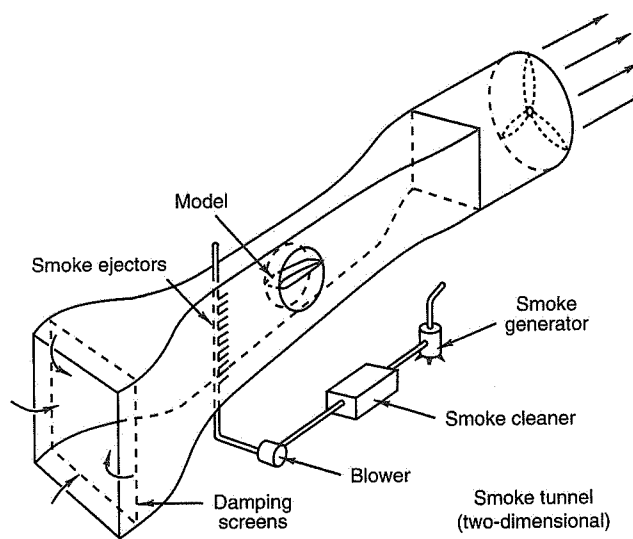


Figure 3.14 Smoke tunnel and smoke photo (Ref. 119).

Smoke can be generated in a number of ways. Titanium or tin tetrachloride (both poisonous if concentrated) will produce smoke (also poisonous) when brought into contact with moist air. Smoke tunnels have also used theatrical smoke and smoke from heated kerosene, rotted wood, or smoldering paper (with adequate ventilation for the carbon monoxide produced).

Still another technique for flow visualization is that of painting the surface of a model with a mixture of lampblack and kerosene. The tunnel is then started up, the flow stabilized and the tunnel shut off. The streaks of lampblack on the model are then observed or photographed.

Full-Scale Testing

The aerodynamic aspects of full-scale development are facilitated by the measurement of air velocity, static, dynamic, and total pressure, flow visualization and temperature using instrumentation and the theory discussed in this section. Generally the aerodynamic problems that have to be solved are related to one or more of the following:

- Drag reduction
- Downforce and its distribution
- Engine air intake duct efficiency
- Engine, oil, brake, transmission and differential cooling
- Crosswind stability and buffeting
- Driver ventilation

3.7 Pressure Coefficient, C_p

If p and V are the local static pressure and local velocity, respectively, at some point on a body, and p_∞ and V_∞ are their values in the remote stream, then from Bernoulli's equation:

$$p_\infty + \frac{1}{2} \rho V_\infty^2 = p + \frac{1}{2} \rho V^2$$

$$p_\infty + q_\infty = p + q$$

$$p - p_\infty = q_\infty - q$$

$$\frac{p - p_\infty}{q_\infty} = 1 - \frac{q}{q_\infty}$$

$$\frac{\Delta p}{q_\infty} = 1 - \left(\frac{V}{V_\infty} \right)^2$$

where p is referenced to p_∞ (the barometric pressure). Let $\Delta p/q_\infty$ be defined as a pressure coefficient, C_p , then

$$C_p = 1 - \left(\frac{V}{V_\infty} \right)^2$$

The relationship between V and V_∞ in an incompressible ideal fluid depends on the shape of the body, its orientation in the fluid stream, and the particular location on the

body. Once these are established, V/V_∞ is fixed as is C_p . The actual pressure at the point in question is then determined from

$$\Delta p = C_p q_\infty ; \quad p = \Delta p + p_\infty$$

Consider these two examples that show the range for C_p :

1. The local flow velocity, V , is reduced to zero near the center of a large flat plate perpendicular to the airstream:

$$C_p = 1 - \left(\frac{0}{V_\infty} \right)^2 = +1$$

This is the maximum positive value of the pressure coefficient.

2. The local flow velocity at a given point under a race car is moving at 200 mph while the car itself is traveling at 100 mph:

$$C_p = 1 - \left(\frac{200}{100} \right)^2 = 1 - 4 = -3$$

which is not an unrealistic value for a machine designed for aerodynamic downforce from the underside.

Consider the actual pressure and forces involved in these two examples. At 100 mph, $q_\infty = 100^2/391 = 25.6 \text{ lb./ft.}^2$. If the flat plate of the first example has an effective area of 1 ft.², the force in the drag direction is 25.6 lb. For flat plates of a few square feet in size the effective pressure coefficient is +1.17 because of flow separation around the edges¹⁷; this creates a lower pressure on the back of the plate.

For the underbody example, the pressure on the bottom of the car at the point in question is

$$\Delta p = -3q_\infty = (-3)(25.6) = -76.8 \text{ lb./ft.}^2$$

acting downward. If this acted on an area of 5 ft. \times 5 ft. = 25 ft.², the downforce would be

$$(25)(-76.8) = -1920 \text{ lb.}$$

or nearly a ton.¹⁸

¹⁷ see Ref. 62, p. 3-17.

¹⁸ The net force on the car has to take into account the pressure distribution on the top as well as the bottom. The force on top is likely to be upward. Both the top and bottom of the car must be strong enough to resist the aerodynamic loads; hoods and underpans have been known to fly off.

3.8 SAE Aerodynamic Axis System

Historically, wind tunnel facilities worldwide have used different nomenclature and reference axes. In order to "provide a common nomenclature for use in publishing road vehicle aerodynamic data and reports" the SAE Road Vehicle Aerodynamics Committee has published J1594, "Vehicle Aerodynamics Terminology" (Ref. 2). This committee includes international representation.

The axis system origin is located on the ground at mid-wheelbase and mid-track as shown in Figure 3.15.

x is positive forward

y is positive right

z is positive downward

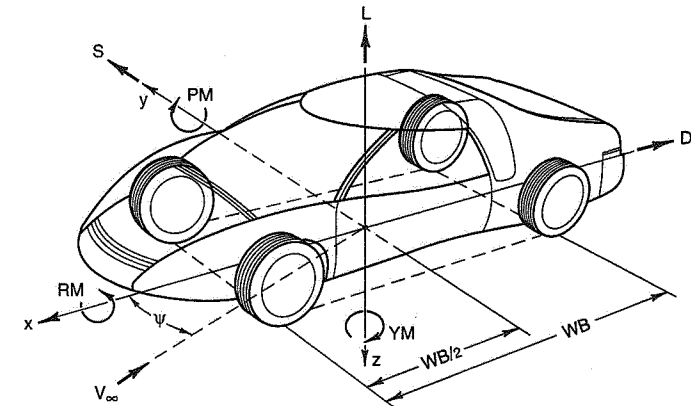
The additional equations shown on the figure allow transformation to forces and moments at the axle positions, thus

LF = component of aero lift at front axle

LR = component of aero lift at rear axle

SF = component of aero side force at front axle

SR = component of aero side force at rear axle



Aerodynamic Lift

$$LF = 0.5 \times L + PM/WB$$

$$C_{LF} = 0.5 \times C_L + C_{PM}$$

$$LR = 0.5 \times L - PM/WB$$

$$C_{LR} = 0.5 \times C_L - C_{PM}$$

Aerodynamic Side Force

$$SF = 0.5 \times S + YM/WB$$

$$C_{SF} = 0.5 \times C_S + C_{YM}$$

$$SR = 0.5 \times S - YM/WB$$

$$C_{SR} = 0.5 \times C_S - C_{YM}$$

Figure 3.15 SAE Aerodynamic Axis System (Ref. 2).

The great advantage to the use of coefficients is that once they are determined (as in a wind tunnel test) for a particular q , A , and WB , the forces and moments for other speeds, air densities, and body sizes can be calculated without further testing.

For tunnel tests of race cars, the coefficients are normally plotted against ride height (heave), pitch, and yaw angles, for various vehicle configurations.

It has already been noted that the nondimensional ratio, RN , can have a prominent effect on the flow pattern and, in fact, can change the force and moment coefficients. In the most general case, the coefficients depend on a number of other nondimensional ratios such as the Mach Number = V/V_{sound} , a length ratio for defining surface roughness, a velocity ratio for defining air turbulence, etc. Generally, the latter ratios are unimportant in automotive wind tunnel testing.

3.9 Aerodynamic Force/Moment Coefficients

Aerodynamic forces and moments are primarily due to pressure changes over the body surface. These pressure changes vary directly with the dynamic pressure of the free stream, q_{∞} . The actual forces are also proportional to some reference area which is related to the area upon which the pressure changes act (a reference area is used for convenience since it may be difficult to calculate the actual area). Finally, a coefficient must be introduced to take into account the effect of the body shape on the velocity distribution over the body and the orientation of the body in the fluid. The drag coefficient, C_D , is defined as

$$C_D = \frac{\text{Drag}}{Aq} = \frac{D}{Aq} = \frac{D/A}{q}$$

where D = drag in lb.

A = reference area in ft^2 , usually the frontal or the plan area of the vehicle

q = q_{∞} in lb./ft^2

C_D is nondimensional

Thus C_D is the drag per unit area per unit q_{∞} (the kinetic energy in the airstream available for conversion to pressure and force).

Moments and torques result from aerodynamic forces and depend on a reference length, WB (= wheelbase, ℓ).

The six forces and moments are then given by¹⁹

Lift, L = $C_L q_{\infty} A$ (positive upward, $L = -F_z$)

Drag, D = $C_D q_{\infty} A$ (positive rearward, $D = -F_x$)

Side Force, S = $C_S q_{\infty} A$ (positive to right, $S = +F_y$)

Pitching Moment, PM = $C_{PM} q_{\infty} A \times WB$ (positive nose up, $PM = M_y$)

Yawing Moment, YM = $C_{YM} q_{\infty} A \times WB$ (positive nose right, $YM = M_z$)

Rolling Moment, RM = $C_{RM} q_{\infty} A \times WB$ (positive right side down, $RM = M_x$)

¹⁹ The notation adopted in Ref. 2.

Vehicle Axis Systems

"Put the seat belts on the grandstands, we're going racing!" (Impression of the start of a race from the driver's seat.)

"Coach" Rollings
F-1 Tire Engineer



Introduction

At any given instant of time, a vehicle is subjected to a single force acting at some location and in some direction. This so-called external or applied force maintains the velocity or causes an acceleration of the vehicle. This force is made up of tire, aerodynamic, and gravitational force components. These different components are governed by different physical laws and it is not convenient to deal with this single force. Furthermore, these separate tire, aerodynamic, and gravitational force components act at different locations and in different directions relative to the vehicle chassis.

In order to calculate accelerations and velocities in directions of interest (such as fore and aft for performance or left and right for turning behavior), it is necessary to define axis systems to which the accelerations and velocities and the forces/torques causing them can be referred. Since we live in a three-dimensional world, three reference axes at right angles (90°) to each other which meet at a common point (the axis system "origin") are the basic and sufficient requirements for these axis systems.

This chapter was written by Fred Dell'Amico, MRA.

The common axis systems used in vehicle dynamics work in the United States have been defined by the Society of Automotive Engineers (SAE) and appear in Ref. 1. Their common use facilitates communication and uniformity of the technical literature. In order to properly relate changes in the motions of the vehicle and its components, as well as describe the vehicle path relative to the earth, there are two basic SAE vehicle axis systems. Two additional axis systems are used as required for the presentation of tire force and moment data (described in Chapter 2) and aero data (described in Chapter 3). These special axis systems can later be transferred to the vehicle axis system.

4.1 Two Types of Axis Systems

The two basic axis systems are described in the following sections.

Earth-Fixed Axis System

This system (the capital letter system) is fixed to the ground and the letters X - Y - Z are used to denote the three principal directions; X and Y are horizontal and at right angles to each other, Z is vertical downward. This earth-referenced axis system is used in this text only when it is necessary to reference some aspect of the vehicle motion to a fixed point or direction. In problems related to vehicle motion relative to the ground, it is common to start off with the origin of the vehicle axis system (described below), coinciding with the earth axis system origin. Frequently, the axes of the two systems will also coincide initially. The calculation or measurements will then indicate the relative motions of the two axis systems. However, it must be emphasized that the earth axes location and orientation are independent of the vehicle and are arbitrarily determined at the convenience of the user.

Vehicle Axis System

The Vehicle Axis System has its origin in aircraft usage. A review of the reasons for its adoption for automotive studies and the assumptions on which it is based are given below.

The first use of this axis system was by L. Segel in his classic paper, "Theoretical Prediction and Experimental Substantiation of the Response of the Automobile to Steering Control" (Ref. 144). The principal reason for its automotive as well as aircraft use is that it is *fixed* in the vehicle and moves with it. The inertia properties (moments and products of inertia) remain constant relative to this set of axes but would be variable if referenced to a set of axes fixed on the ground, for example. Not only would they be variable but they would lose in physical meaning to the engineer as the vehicle maneuvered.

Some confusion may arise because this axis system is referred to in different ways. Quite commonly it is called a "Moving Axis System" because it moves with the vehicle;

it is also labeled as "Body Axes" because it is fixed in the vehicle; frequently it is referred to as the "Stability Axes" or "Directional Control Axis System." The point to remember is that it is fixed in the vehicle and the inertia properties relative to it are taken as constant.

The next question is: Where is the origin of this axis system located and how are the axes oriented in the vehicle? This is discussed at length in Ref. 111, from which the following is abstracted. The automobile is considered as a two-mass system. The *unsprung mass* is taken as a rigid frame (with steerable wheels) and the *sprung mass* is considered as a rigid body. These two masses are "hinged" together at the roll axis and one variable, roll angle, specifies the relationship between the two masses. Figure 4.1 (from Ref. 111) shows these respective masses and how they are brought together in the complete car. Axes i_s and j_s come together in the complete car as i ; similarly j_s and j_u converge to j , and k_s and k_u to k .

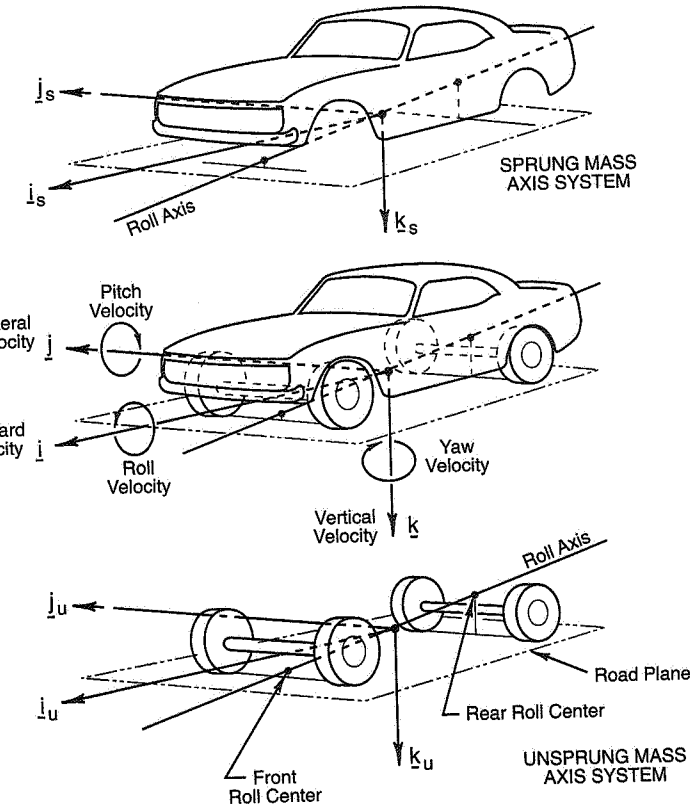


Figure 4.1 Axis systems used in determination of the vehicle axis system (Ref. 111).

Axes *i*, *j*, and *k* are relabeled as *x*, *y* and *z* (lower case) in the SAE system shown in Figure 4.2. The system is orthogonal (the axes are at 90° to each other) and is right-handed (i.e., a positive rotation about *x* rotates *y* into *z*, a positive rotation about *y* rotates *z* into *x*, etc.). The *x*-axis is horizontal and positive forward in the direction of motion when the vehicle is traveling in a straight line on a level road (road is assumed flat). The *x*-axis lies in the longitudinal plane of symmetry (vehicle assumed to have left-right symmetry). The *y*-axis points to the driver's right, is horizontal and 90° to the *x*-axis. The *z*-axis is perpendicular to the other two, is vertical and positive downward.

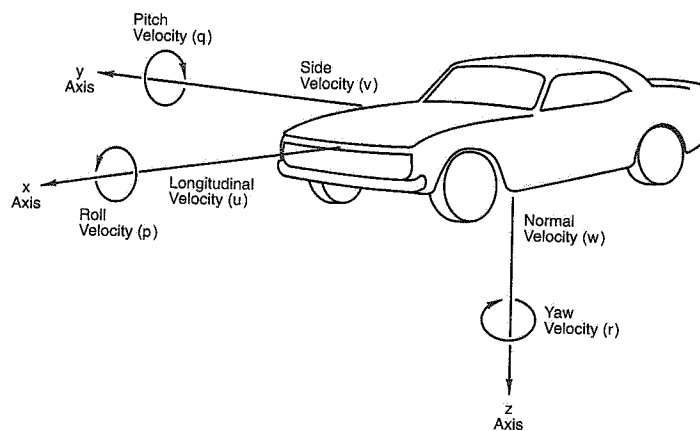


Figure 4.2 Vehicle axis system (Ref. 1).

The origin of the vehicle axis system (*x*, *y*, *z*) is the same for the sprung and unsprung masses, as indicated in Figure 4.1. It is located at the intersection of the vehicle roll axis (shown as a line sloping downward toward the front in Figure 4.1) and a line perpendicular to the road through the CG of the total vehicle, for a zero roll angle of the sprung mass.

It is usually assumed that the sprung mass rolls about the horizontal *x*-axis, rather than about the actual roll axis. (Equations have been developed for an inclined roll axis—see Ref. 111—but are infrequently used.) Also the origin of the system may, for particular purposes, be located elsewhere.

It is generally assumed that the “principal axes of the rolling mass are parallel to the body axes and that the center of gravity of the non-rolling mass is on the *x* axis” (Ref. 144).

Tire deflections are neglected and the plane of the wheel centers (equal-sized wheels front and rear) remains parallel to the ground.

4.2 Vehicle Motions

In vehicle dynamic studies of vehicle motion, it is customary for the user to fix certain operating variables. Thus a value can be assigned to the forward velocity and the tractive/braking force or longitudinal acceleration/deceleration. The motion of the unsprung mass can then be studied as a *perturbation* from the steady velocity condition; likewise the roll of the sprung mass can be studied in relation to the unsprung mass. These perturbations can be initiated by a control action or other disturbance such as a wind gust. For vehicle stability and control investigations the perturbation velocities of interest are

Forward velocity	<i>u</i>
Lateral velocity	<i>v</i>
Yawing velocity	<i>r</i>
Rolling velocity	<i>p</i>

For stability and control investigation, the pitch and vertical perturbations (*q* and *w*) are neglected. The so-called lateral-directional equations are in terms of *v*, *r* and *p*.

These perturbation velocity (linear and angular) components about the axes fixed in the vehicle must be measured relative to some reference. In aircraft practice it is customary to think in terms of another orthogonal axis system which follows the aircraft through its maneuvers and which at any given instance of time is coincident with the aircraft system but momentarily fixed in space. The perturbation velocities are measured relative to it. One might say that the reference axes are continually chasing the aircraft but can conveniently be momentarily stationary when the vehicle velocities are to be measured. This is, of course, equivalent to saying that the perturbation velocities are measured relative to inertial space.

If actual path along the ground is desired, the Vehicle Axis System is referenced to the Earth-Fixed Axis System as the initial condition. The various acceleration components (rates of change of the velocity component perturbations) are defined below along with the angular relationships associated with path analysis (see Figure 4.3).

1. **Longitudinal Acceleration** is the component of the vector acceleration of a point in the vehicle in the *x*-direction.
2. **Side Acceleration** is the component of the vector acceleration of a point in the vehicle in the *y*-direction.
3. **Normal Acceleration** is the component of the vector acceleration of a point in the vehicle in the *z*-direction.
4. **Lateral Acceleration** is the component of the vector acceleration of a point in the vehicle perpendicular to the vehicle *x*-axis and parallel to the road plane.

In steady-state condition, *lateral acceleration* is equal to the product of *centripetal acceleration* times the cosine of the vehicle's *sideslip angle*. Since in most

test conditions the *sideslip angle* is small, for practical purposes the *lateral acceleration* can be considered equal to the *centripetal acceleration*.

5. **Centripetal Acceleration** is the component of the vector acceleration of a point in the vehicle perpendicular to the tangent to the path of that point and parallel to the road plane.
 6. **Heading Angle (ψ)** is the angle between the trace on the X-Y plane of the vehicle x-axis and the X-axis of the earth-fixed axis system (see Figure 4.3).
 7. **Sideslip Angle (Attitude Angle, β)** is the angle between the traces on the X-Y plane of the vehicle x-axis and the vehicle velocity vector at some specified point in the vehicle. Sideslip angle is shown in Figure 4.3 as a negative angle.
 8. **Course Angle (v)** is the angle between the trace of the vehicle velocity vector in the X-Y plane and X-axis of the earth-fixed axis system. A positive course angle is shown in Figure 4.3.
- Course angle is the sum of *heading angle* and *sideslip angle* ($v = \psi + \beta$).

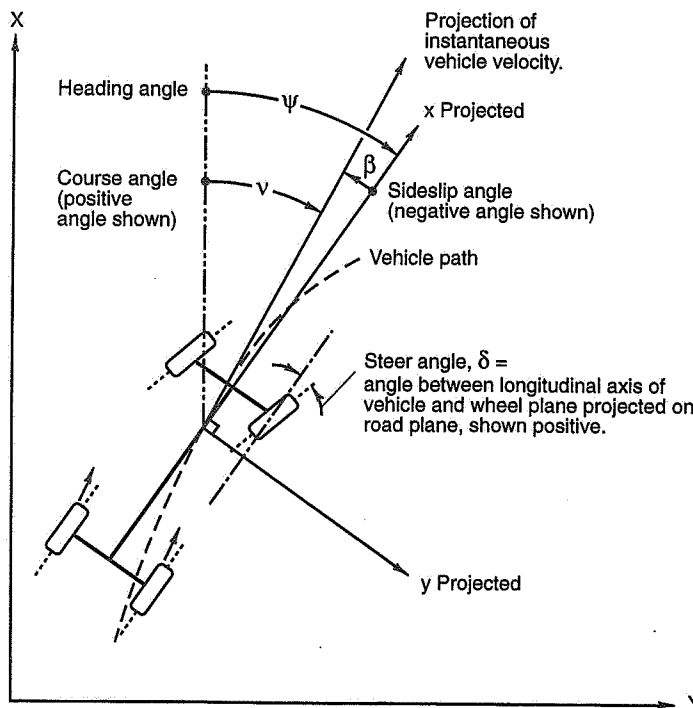


Figure 4.3 Heading, sideslip, course, and steer angles (Ref. 1).

9. **Vehicle Roll Angle** is the angle between the vehicle y-axis and the ground plane.
10. **Vehicle Pitch Angle** is the angle between the vehicle x-axis and the ground plane.

The force/moment components are defined below.

FORCES—The external forces acting on the automobile can be summed into one force vector having the following components:

11. **Longitudinal Force (F_x)** is the component of the force vector in the x-direction.
12. **Side Force (F_y)** is the component of the force vector in the y-direction.
13. **Normal Force (F_z)** is the component of the force vector in the z-direction.

MOMENTS—The external moments acting on the automobile can be summed into one moment vector having the following components:

14. **Rolling Moment (M_x)** is the component of the moment vector tending to rotate the vehicle about the x-axis, positive clockwise when looking in the positive direction of the x-axis.
15. **Pitching Moment (M_y)** is the component of the moment vector tending to rotate the vehicle about the y-axis, positive clockwise when looking in the positive direction of the y-axis.
16. **Yawing Moment (M_z)** is the component of the moment vector tending to rotate the vehicle about the z-axis, positive clockwise when looking in the positive direction of the z-axis.

4.3 Some Thoughts on Sign Conventions

In the SAE Tire Axis System (see Figure 2.33), the slip angle is defined as the angle between the wheel plane and the direction of wheel travel. In this system, if the wheel is moving forward to the left (as in a right-hand turn), the slip angle is negative but the lateral force is positive. Following this convention, the tire lateral force data is plotted in the fourth quadrant. In actual practice, users of tire data frequently plot cornering force in the first quadrant. This negative relationship between lateral force and slip angle can be confusing in the kinematic relationship between slip and steer angles.

Without proposing a change in the well-established SAE system, this note aims at clarifying some of the issues associated with this sign convention. In the SAE system, slip angles are assumed to be the result of a lateral velocity, v , in the presence of a forward velocity, u . For example, the rear tire slip angle is $\tan^{-1} v_R/u$ ($\approx v_R/u$ for small angles), where v_R is the local lateral velocity. If v_R and u are positive, the "slip" is to the right, α_R is positive, and the lateral force is to the left (negative), corresponding to a left-hand turn. But a slip angle can also be created by steering the wheel, or in aeronautical terminology, turning the wheel to a yaw angle. In fact, in the SAE system, a positive steer angle, δ , produces a positive lateral force. The wheel has been yawed to the right.

Of the two ways of creating an out-of-wheel-plane velocity component, the use of yaw angle has considerable logic for presenting data from tire tests. We have noted in Chapter 2, that the term “slip angle” is a questionable one since the wheel is not slipping laterally but rather is operating in a yawed-rolling condition. Defining “slip angle” in terms of a lateral/forward velocity ratio further perpetuates the notion that the tire is literally sliding sideways as a whole. In actual fact, because of the tire rolling motion, the print has areas composed of adhesion in the front and sliding in the rear. On tire testers, lateral slip velocity is never used to create the out-of-plane velocity; rather the wheel plane is steered (or yawed) relative to the belt velocity.²⁰

If the “slip angle” convention were replaced by yaw angle, the following would occur:

1. A positive yaw angle would line up with a positive rotation in the SAE System, i.e., a clockwise rotation looking forward. It would be compatible with the definition of positive steer angle.
2. In a RH turn, the yaw angles at the wheels would normally be positive as well as the lateral tire forces. The cornering curves would plot in the first quadrant.
3. The aligning torque data would plot in the fourth quadrant and the initial slope of the curve would be negative which is proper for a “stability” situation. That is, an increase in yaw angle would give a negative (or restoring) moment (the tire’s self-aligning torque).

So much for the tire itself, consider the motions of the vehicle and its interaction with the tires. In the SAE vehicle-fixed axis system, a lateral velocity to the right is positive—along the positive y axis. In a RH turn the vehicle experiences a lateral velocity to the left or negative in this axis system at speeds above the “tangent speed.” This aligns with what one senses in the vehicle. Furthermore, in a RH turn the yawing velocity of the vehicle is clockwise and positive—again aligning with one’s senses. The lateral velocity and the yawing velocity create lateral velocity components at the front and rear wheels. These velocities, together with the forward velocity, create yaw angle changes at the wheels which in turn account for the vehicle lateral and yaw damping. Thus a vehicle’s lateral velocity to the left (in a right-hand turn) gives rise to lateral force changes to the right, i.e., the vehicle damping-in-side slip. A positive yawing velocity results in a negative yawing moment, i.e., the vehicle damping-in-yaw. Without these damping effects a control or disturbance input would result in a continuously accelerated motion, which we know is not the case.

One final thought: SAE J1594, “Vehicle Aerodynamics Terminology,” uses an axis system which is similar to that of the tire axis system, except that the out-of-plane velocity vector is defined by a yaw angle, positive for clockwise rotation. This aligns with air-

craft wind tunnel practice. The aerodynamic forces and moments all follow aircraft practice and the data falls into the proper quadrant. Damping effects appear with proper signs.

For those who find the signs and plots associated with tire data difficult, slip angles can be replaced by yaw angles of opposite sign.

4.4 Symbol Conventions in this Book

In general, we have adopted the SAE Vehicle and Tire Axis Systems (of Ref. 1) and their associated symbols—thus X, Y, Z for the Earth-Fixed axes and x, y, z for the Vehicle and Tire Axes. The force (F) and moment (M) components of the Vehicle and Tire Axes are defined by subscripts referencing the particular axis. To distinguish between the Vehicle and Tire F/M components we have generally used **upper** case for the Vehicle subscripts and **lower** case for the Tire subscripts, thus F_X , M_X , ... refer to Vehicle components and F_x , M_x , ... refer to tire components. This is an arbitrary convention. In a book with so many authors and sources, it has been impossible to achieve a uniformity of symbols throughout and one must depend on context. In the particular case of lateral acceleration, we use $A_Y = a_y/g$, which again is arbitrary.

²⁰ The authors are aware of only one tire tester capable of direct lateral motions. This is located at the University of Michigan and was funded by Honda for motorcycle tire tests.

Simplified Steady-State Stability and Control

"It seems strange that the automobile industry went on for thirty-five years, building cars piecemeal this way with no real conception of the complete vehicle. Aircraft engineers, on the other hand, got busy from the very start, with wind tunnels and flight tests to find out how their vehicles actually operated."

Maurice Olley
ca. 1955



Introduction

This chapter begins with our approach to the driver-vehicle handling problem and explains why it is usually desirable to treat the vehicle part of the overall system. Our objective is to give the reader a mental framework for understanding vehicle behavior. To do this, we consider vehicle motions as composed of steady-state turning (this chapter) and dynamic (transient) maneuvering (next chapter). In each chapter, we first use a simplified mathematical model of the vehicle to develop some basic concepts after which we conclude with test results on real vehicles.

In the past and even today the terms understeer and oversteer have dominated considerations of automotive stability and control. It is one factor among a number that determine automobile motion behavior. In some situations it predominates, in

others it is much less important. Because it has been the central theme for so long, it has been described in a variety of ways. In this chapter we will cover various ways of expressing over/understeer physically and mathematically and leave it to the reader to choose a satisfying explanation.

To understand the mathematical models presented, some basic knowledge of tire and aerodynamic force development is necessary. These topics are treated in Chapters 2 and 3.

The material in this chapter forms the basis for the discussion of force-moment analysis in Chapter 8, where the full nonlinear car is analyzed by the MRA Moment Method.

5.1 Approach

In Chapter 1 it was concluded that one of the basic design requirements of a race car is the provision of control and stability characteristics that enable a skilled driver to operate at or near the “g-g” acceleration limits.

As the above requirement indicates, in real life the vehicle behavior and the driver’s capabilities are inseparably connected. The driver provides the intelligence to the “driver-vehicle” entity while the vehicle provides the maneuvering forces. Figure 5.1 illustrates this relationship in a generalized “block” diagram.

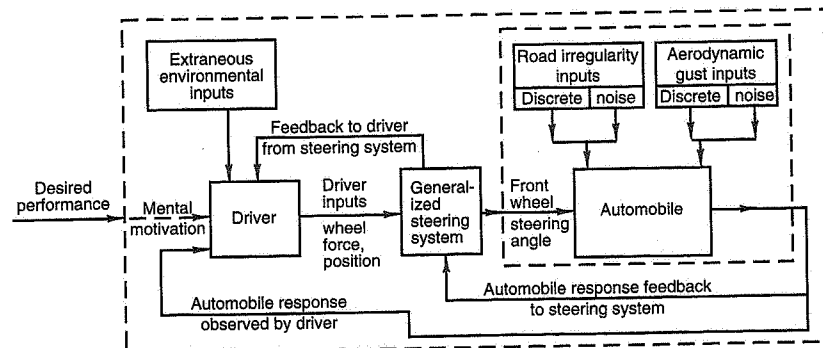


Figure 5.1 Generalized block diagram of driver-vehicle relationship.

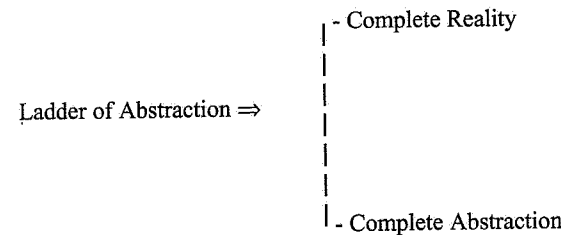
The driver is actuated by the several inputs of ‘mental motivation,’ ‘extraneous environmental inputs,’ ‘feedback from the automobile’s response’ (in terms of visual reference, lateral acceleration, yaw velocity, etc.), and ‘information returning via the steering system.’ The driver then applies steering force and position inputs through the steering system which, along with aerodynamic and road disturbances, initiates the car’s response.

The steering system is generalized because its characteristics may modify the driver’s inputs (i.e., power assist, nonlinear gearbox, etc.). For simplicity the throttle, brake, and any other control devices have been omitted from Figure 5.1. The behavior of the driver-vehicle system is technically called *handling*.²¹

Because of the difficulty of representing the driver in an analysis and because the driver’s characteristics are not subject to direct control, the engineer focuses on the control and stability of the vehicle component part of the system.

The ultimate reality of a vehicle’s control and stability can only be had by experiencing it. Thus the sum total of your sensory inputs when driving at your level of experience represents the reality of the automobile motions to you. Anything less than this—such as talking or writing about the car’s behavior—is an abstraction or approximation of reality. Engineering requires a compilation and communication of information if it is to specify, design and build certain characteristics into a vehicle. This in turn necessitates the development of formal, logical structures which are based, in varying degree, on abstractions. These enable us to obtain a mental “understanding” to the desired detail.

A concept which is helpful in approaching a subject as difficult as automobile stability and control is the “Ladder of Abstraction” sketched below (see Ref. 81).



Complete reality at the top is the functioning car, say, as the race driver experiences it, not what the driver may care to think about it. As we move down the ladder we move away from the physical car and make simplifying assumptions as to how it works; we may linearize its behavior or look at it in bits and pieces. Although the practicing engineer moves freely up and down the ladder, it is important to know one’s location on it. It is too easy to take mental constructs for reality.

The approach followed here is to start near the bottom of the ladder with an extremely simplified vehicle model. If the basic concepts can be clarified at a simple level they will carry through to a more realistic level. This is one justification for looking at the

²¹ “Handling” commonly refers to the directional stability and control of a vehicle. In technical circles, it generally refers to the behavior of the driver-vehicle combination in maneuvering tasks.

linear range of operation as opposed to starting with the nonlinear where the race car operates. It is difficult to explain some concepts except in the context of an elementary vehicle. Finally, race cars tend to be noncompliant, nonrolling and neutral steer—and can be approximated by a simple model in many respects.

5.2 The Elementary Automobile Defined

This representation of the automobile²² (often referred to as the “bicycle” model) is defined as follows:

- No lateral load transfer, i.e., the vehicle compressed to a single-track (hence, “bicycle” model)
- No longitudinal load transfer
- No rolling or pitching motions (of the body)
- Linear range tires
- Constant forward velocity (chosen by the user)
- No aerodynamic effects
- Position control
- No chassis or suspension compliance effects

As noted in Chapter 2, the tire cornering force curve (lateral force vs. slip angle) is treated as having linear, transitional, and frictional (breakaway) regions. The race car operates in all of these regions; in particular in the transitional and frictional regions during cornering. For this simple model, tire operation is in the linear regime only, corresponding to cornering at less than about 0.4g.

It is further assumed that the “vehicle” operates on smooth surfaces with no ride motions. We will use the small angle assumptions to simplify the equations unless otherwise noted. By “small angle assumption” we mean that, in radians, the sine of an angle is equal to the angle and the cosine of an angle is equal to one. This approximation works well for small angles; for example, at 20° the sine approximation is off by only about 2%; the cosine approximation is within 2% up to about 10°.

Position Control is defined in Ref. 1 as “that mode of vehicle control where restraints are placed upon the steering system input in the form of displacements ... independent of the control forces involved.” In actual vehicles the driver senses both position and force in unknown proportions. For analysis, several idealized control modes are used such as: “position” (or fixed), “force” (or free). Because of the slow steering ratios of passenger

cars it is reasonable to assume they are mostly driven in position control mode; vehicles with fast ratios (such as GP cars) may more nearly approach force control.

With this simple vehicle model, shown in Figure 5.2, we can investigate the effects of front and rear tire cornering stiffnesses, center of gravity (CG) location along the wheelbase, and geometric steer angle²³ on the yawing and sideslipping motions (which determine the path and attitude of the vehicle).

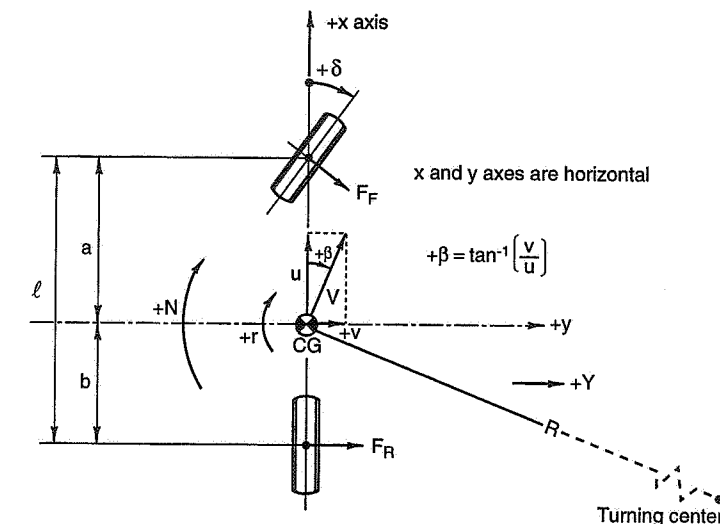


Figure 5.2 The “bicycle” model (two degrees of freedom).

For this representation of the vehicle, the two “degrees-of-freedom” are the motion variables, v (the lateral velocity) and r (the yawing velocity). The input variable is the front wheel steer angle, δ , which is under driver control.

When an automobile makes a turn it normally goes through three phases. The first is the turn entry, for example from a straight. In this phase the yawing velocity and the lateral velocity (relative to the vehicle y-axis as shown in Figure 5.2) build up from zero in straight running to their values in the steady turn. This is called the “transient turn-entry” phase where r and v are changing with time. The second phase is “steady-state cornering,” where r and v and the vehicle and tire slip angles are constant and the vehicle is moving along an unvarying path radius, R (or path curvature defined as $1/R$). The final

²² Identical to the linear two-degree-of-freedom (2DF) model shown later in this chapter.

²³ The steering angle (at the steering wheel) is the principal driver interface with the vehicle. Other interfaces such as at the throttle and brake control are not treated in this model.

phase is “turn exit,” where the yawing and lateral velocities are changing with time as they return to zero for straight running, “transient turn-exit.”

These phases are a useful idealization of a typical turn and the terms steady-state and transient will appear frequently in this chapter. Actual turns vary greatly: the steady-state phase may be very long compared to the transient phase (as in a “sweeper”) or be very short as at the apex of a tight turn (a “hairpin”). In a rapid lane change the right-left turns may merge to effectively eliminate the steady-state phase.

5.3 Steady-State Low-Speed Cornering Geometry

We begin by considering the geometry of very low-speed cornering in the steady-state phase only. Under these conditions where fore and aft and lateral accelerations are negligible, real vehicles behave like the previously defined “bicycle” model in that there is no body roll, lateral load transfer or related effects. The slip angles are zero and the front and rear wheels roll in their own planes so that turning is purely a geometric proposition. The front and rear wheels move on concentric circles, the front wheels are on the larger circle as shown in Figure 5.3.

The radius of turn is normally taken as the distance from the turning center to the center of gravity (CG) of the vehicle. For normal turns the small angle approximation, ℓ/R , is

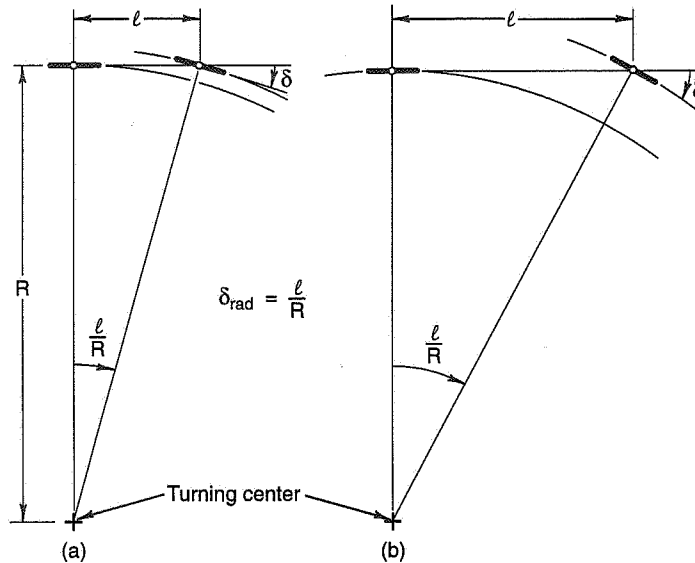


Figure 5.3 The wheelbase angle or “Ackermann steering angle.”

close to the required steering angle, δ (in radians). As the wheelbase, ℓ , is increased (as for example, doubled in Figure 5.3(b)), the steering angle increases in proportion for a constant turning radius. Other things equal, a long-wheelbase bus requires more steering angle than a passenger car.

The wheelbase angle, or as it is usually called in the technical literature, “Ackermann Steering Angle,” is then the geometric steer angle required for a car of wheelbase, ℓ , to track a turn of radius, R , at low speeds where the external forces due to accelerations are negligible. In addition to its operational significance, this Ackermann Angle is related to the basic yaw damping of the vehicle as will be explained later.

The Ackermann Steering Angle is not to be confused with so-called “Ackermann Steering” where the left- and right-hand front wheels are set up to give theoretically perfect steering at low speeds by being tangent to concentric circles about a turning center which lies on a line through the rear axle. Classic Ackermann steering is shown in Figure 5.4(a) and results in “toe out” of the outside wheel in a turn. One of its functions in the early days was to keep the front wheels from disturbing the gravel of ‘well-to-do’ owners’ driveways (according to Maurice Olley). “Parallel Steer” (b) is currently common and racing cars have frequently used “Reverse Ackermann” (c) geometry.

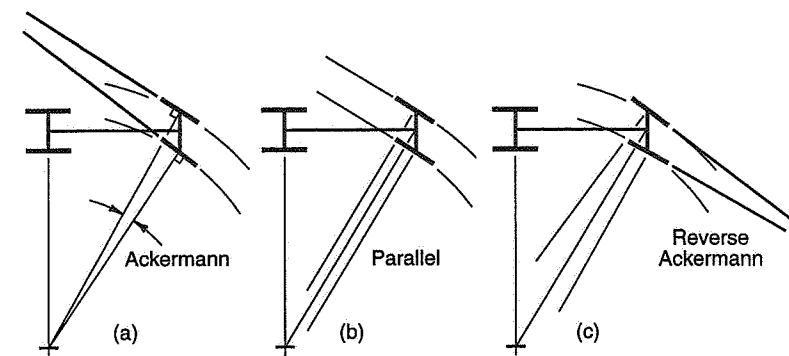


Figure 5.4 (a) Ackermann, (b) parallel, and (c) reverse Ackermann steering.

5.4 Steady-State Cornering of the Neutral Steer Car

The engineering definitions of neutral, understeer and oversteer can be developed with the bicycle model. These definitions apply to sublimit operation, generally in the linear range, and are not to be confused with the use of similar terms for behavior at the limit of adhesion (see Chapter 8). The distinctions will be discussed later as well as the relationship between “steer” characteristics and stability.

Consider what happens with the “bicycle” model when the cornering speed is increased such that the lateral acceleration can no longer be neglected. The centripetal acceleration, V^2/R , acts inward toward the turning center. The lateral force required to produce this inward acceleration is provided by the tires and has a magnitude of $(W/g) \times (V^2/R) = ma$, in accordance with Newton’s second law. Another way of treating this dynamic situation is to represent the presence of the acceleration by a hypothetical external force²⁴ equal to $-ma$ (acting in the opposite direction, i.e., outward). The system is then brought into equilibrium and treated as a static situation. The external force is called the *centrifugal inertia force*. The equilibrium achieved is identical to that of a ball on a string swinging around in a circle.

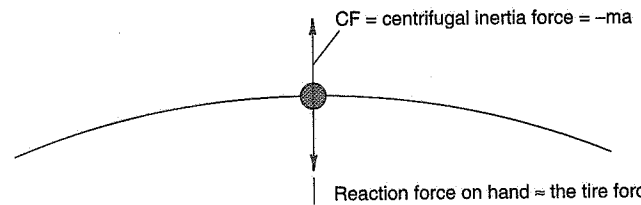


Figure 5.5 assumes that the fore and aft center of gravity of the vehicle is at the mid-wheelbase point ($a = b = \ell/2$). The front and rear tire cornering stiffnesses, C_F and C_R (in lb./deg. or lb./rad. of slip angle), for the pair of wheels at each track are the same, i.e., same tire size and pressure. The centrifugal force effectively pulling sideways on the vehicle must be reacted in a steady turn by the front and rear tire cornering forces which in this case are obviously equal. In general, the vehicle acts as a horizontal beam in lateral force and moment equilibrium, thus with the small angle assumption,²⁵

$$\text{Force Equilibrium: } CF = Y_F + Y_R = C_F \alpha_F + C_R \alpha_R$$

$$\text{Moment Equilibrium: } C_F \alpha_F a = C_R \alpha_R b \quad (\text{also called yaw moment balance})$$

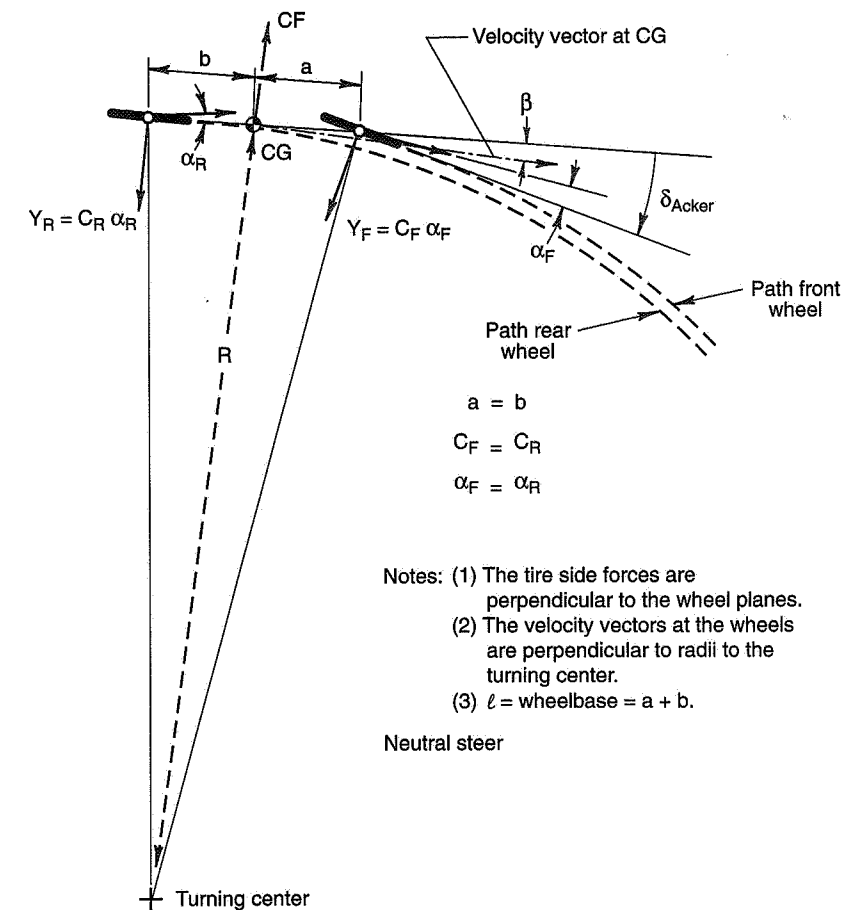
If $a = b$ and $C_F = C_R$, then $\alpha_F = \alpha_R$

Several interesting observations can be made from a comparison of Figures 5.5 and 5.3(a).

- The same steer angle is required to negotiate the same radius curve regardless of speed.

²⁴ The use of a hypothetical inertia force to achieve a “static” equilibrium is D’Alembert’s Principle. It is equivalent to writing $F - ma = 0$.

²⁵ Sine of the angle = the angle in radians.



- Notes:
- (1) The tire side forces are perpendicular to the wheel planes.
 - (2) The velocity vectors at the wheels are perpendicular to radii to the turning center.
 - (3) $\ell = \text{wheelbase} = a + b$.

Neutral steer

Figure 5.5 Turning with lateral forces.

- The vehicle slip angle is obtained by rotating the entire vehicle by the amount α_R (since in this simple model the plane of the rear wheels is always parallel to the chassis fore and aft centerline). This rotation establishes the *attitude* of the machine to its path. This angle, β , is normally measured between the chassis centerline at the CG and the tangent to the path. β is called the *vehicle slip angle* or *body slip angle*.
- In the situation shown the rear wheels are traveling on a smaller radius (R) than the fronts.

- The rotation that gives rise to the rear slip angle also steers the front wheels—in this case the front slip angle is the same as the rear.

To emphasize the last point, for the vehicle configuration chosen in this example (CG at mid-wheelbase and equal tire cornering stiffnesses front and rear), the slip angle required at the front to produce the force and moment equilibrium is obtained entirely from the rotation of the vehicle during the establishment of the rear slip angle. With this configuration, the steer angle, δ , is completely determined by the path curvature independent of the speed or lateral acceleration developed. In short, the steering angle remains at the Ackermann, $\delta = \ell/R$.

The vehicle configuration under discussion is termed *neutral steer* (NS) because as lateral acceleration (side force) is applied to the machine, it neither “oversteers” nor “understeers” the intended geometric path established by the Ackermann Steering Angle.

In Figure 5.6, some data is presented from a constant radius test on a vehicle that is close to NS. In this test, the car was driven around a circle of constant radius (in this case, 100 feet) at increasing speed and the steer angle and lateral acceleration recorded. The basic result from this test is a plot of steering angle vs. lateral acceleration as shown in the figure.

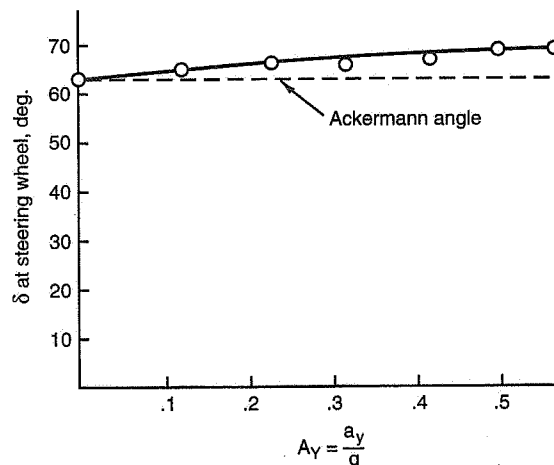


Figure 5.6 Research vehicle, constant radius test.

Because this vehicle is so close to NS the steering angle plotted is that of the steering wheel rather than that of the steered front wheels. The steering wheel angle departs from the Ackermann by only about 5° over the entire range of lateral acceleration. If this is divided by 14 (the steering ratio is 14 to 1), the front wheel departure from the Ackermann is only about 0.35°.

As side force or lateral acceleration is increased, as in the constant radius test, the slip angles increase. This follows from the force equilibrium equation shown earlier. If the cornering stiffnesses are constant, i.e., in the linear tire characteristics range, the slip angles must increase linearly with lateral acceleration. If the increase of front and rear slip angles is plotted against the lateral acceleration from the constant radius test (see Figure 5.7), the elementary NS car is characterized by curves of identical slope:

$$\frac{\Delta\alpha_F}{\Delta A_Y} = \frac{\Delta\alpha_R}{\Delta A_Y}$$

or

$$\frac{\Delta\alpha_F}{\Delta A_Y} - \frac{\Delta\alpha_R}{\Delta A_Y} = \frac{\Delta(\alpha_F - \alpha_R)}{\Delta A_Y} = 0$$

where Δ refers to a small quantity.

For the elementary NS car the rate of change of the difference between the front and rear tire slip angles with lateral acceleration is zero.

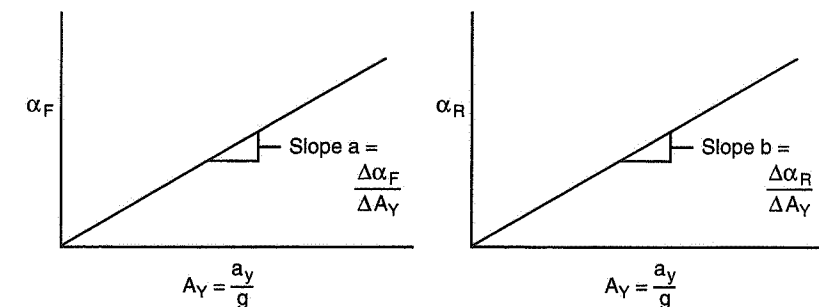


Figure 5.7 Variation of slip angles with lateral acceleration (NS).

For the simple “bicycle” model the actual front and rear slip angles are equal as well as the slopes. However, the important criterion for NS is that the rates of change with A_Y be the same.

Before leaving the simple NS car let us examine its behavior under an external disturbance. Suppose that the vehicle is traveling down a straight and level road with zero steering angle. Let us assume that it then runs onto a stretch of uniformly tilted road. If no change is made to the steering angle, one can expect that after the transient phase is over, the vehicle will be running on a straight line angled down the slope by the magnitude of the equal front and rear slip angles. The “heading” of the vehicle (in this case the angle

between the chassis and the road centerline) will remain zero. The angle of the path in the plane of the road is

$$\alpha_F = \alpha_R = \left(\frac{1}{C_F} \right) \left(\frac{W\phi}{2} \right) = \left(\frac{1}{C_R} \right) \left(\frac{W\phi}{2} \right)$$

This is illustrated in Figure 5.8.

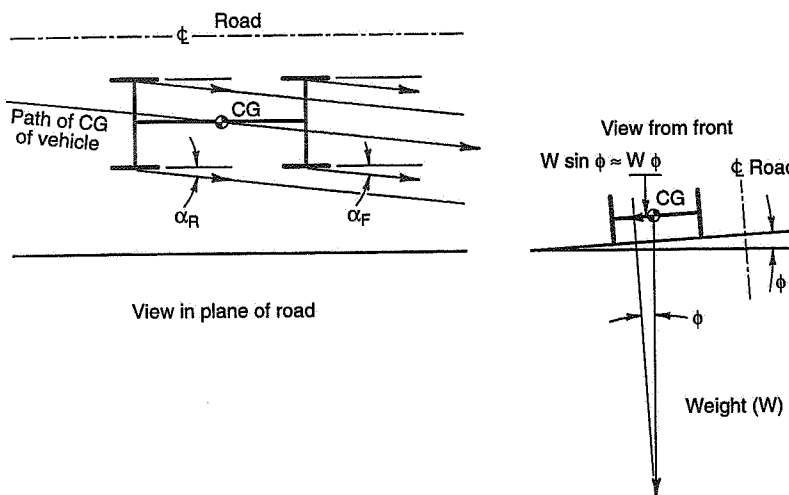


Figure 5.8 NS car on a tilted road.

Note that the attitude of the car remains parallel to the road centerline, but the path is down the slope. To run parallel to the road centerline, it is necessary only to rotate the vehicle to an angle equal to the tire slip angle (nose up the slope). The steering angle once steady-state is reached is still zero. The behavior of the NS car in a steady cross-wind would be comparable to its behavior on a tilted road if the resulting aerodynamic force were at the CG.

The lateral and directional degrees of freedom in the NS vehicle are *uncoupled* in the sense that the vehicle can be placed in sideslip as required to produce side force balance without requiring a change of steer angle to maintain directional moment balance. (This is not true of understeer and oversteer vehicles.)

We have dealt with the NS car at some length because it can be viewed as a "basic" vehicle with understeer and oversteer cars as departures from it. This will become clearer when the "tire damper" analogy is presented in a later section.

5.5 Steady-State Cornering of the Understeer Car

Consider now the simple "bicycle" model with the center of gravity located at 1/3 of the wheelbase aft of the front track. There is no significance to the 1/3 figure other than that it places the CG well ahead of the mid-wheelbase point. The static load on the front wheels is now 2/3 W and that on the rear 1/3 W; the front wheels are carrying twice the load of the rear. Assume that by changes in tire sizes and pressures the cornering slopes are equalized front and rear at the same numerical value utilized in the NS example. With the same wheelbase, the Ackermann Steering Angle for a given path curvature is the same as for the NS model. Let us examine what happens as the cornering speed is increased, and the vehicle experiences a centrifugal side force.

The vehicle acts as a horizontal beam or lever. The side force must be reacted at the individual tracks in inverse proportion to the CG to track distances (in ratio to the wheelbase). Thus the front track takes 2/3 of the cornering force and the rear 1/3. The cornering stiffnesses are identical front and rear, so the slip angle at the front must be twice that of the rear, $\alpha_F/\alpha_R = 2$. If we compare the lateral force balance for the present configuration with the NS configuration we will see that at the same lateral acceleration

$$\alpha_F = \frac{4}{3} \alpha_1 \quad \alpha_R = \frac{2}{3} \alpha_1$$

where α_1 = slip angle (same F and R) of the NS vehicle. These are shown as follows (where $WA_Y = a_y/g$):

For the NS vehicle,

$$WA_Y = 2C\alpha_1, \text{ since } C_F = C_R = C \text{ and } \alpha_F = \alpha_R = \alpha_1$$

For the present configuration,

$$WA_Y = C(\alpha_F + \alpha_R) = C(2\alpha_R + \alpha_R) = 3C\alpha_R = 2C\alpha_1$$

or

$$\alpha_R = \frac{2}{3} \alpha_1$$

also

$$WA_Y = \frac{3}{2} C\alpha_F = 2C\alpha_1$$

or

$$\alpha_F = \frac{4}{3} \alpha_1$$

Figure 5.9 shows the case when the turn radius, R_1 , is made equal to that of the NS configuration of Figure 5.5 (both figures drawn to the same scale with a very small turn radius). In these circumstances the vehicle attitude angle, β , is less by the reduction in the rear slip angle; the front slip angle that arises from this rotation is correspondingly less. If we take the slip angle of the NS car as reference, we lose $(1/3)\alpha_1$ from this rotation effect and this must be compensated for by an increase in steer angle, δ . However, we still need another $(1/3)\alpha_1$ to bring the front slip angle to the required value of $(4/3)\alpha_1$ and this must also be supplied by a further increase in steering angle.

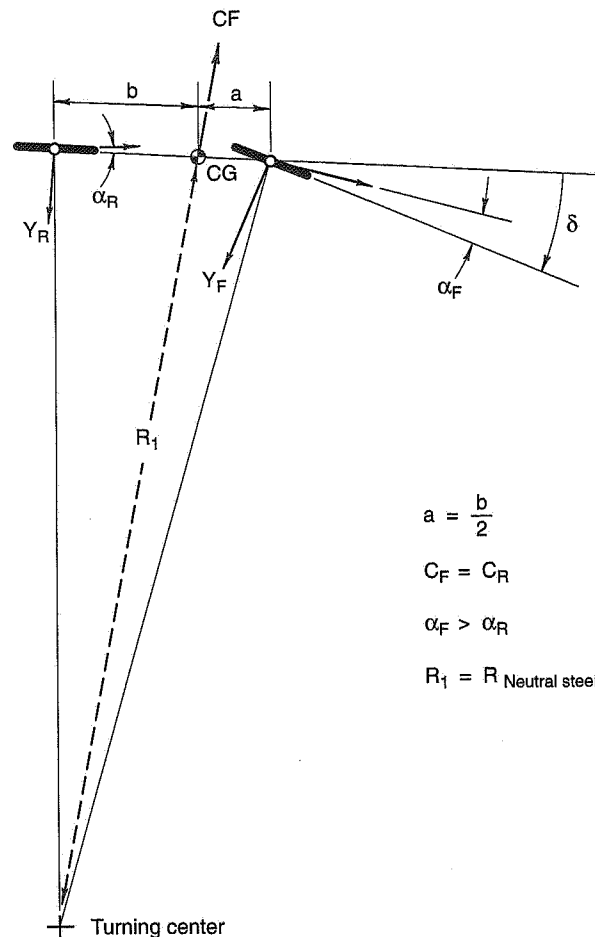


Figure 5.9 Turning with lateral forces, US car.

In short, the steering angle required to maintain the specified radius is $(2/3)\alpha_1$ more than for the NS car. This increase arises from the difference between the front and rear slip angles—the Ackermann Steering Angle has remained unchanged (same ℓ and R). Slip angles are merely steer angles as far as the vehicle knows; in this case the front slip angle, $\alpha_F = (4/3)\alpha_1$, is trying to steer the vehicle out of the turn while the rear slip angle, $\alpha_R = (2/3)\alpha_1$, is trying to steer the vehicle into the turn. The net steering effect is the difference of $\alpha_F - \alpha_R = (4/3)\alpha_1 - (2/3)\alpha_1 = (2/3)\alpha_1$ in the direction of turning out of the turn (the front track predominates as would be expected with the forward CG).

The total steering angle is given by the relationship

$$\delta = \delta_{\text{Ackermann}} + (-\alpha_F + \alpha_R)$$

or

$$\delta = \frac{\ell}{R} + (-\alpha_F + \alpha_R)$$

Note: The α 's are normally negative in a RH turn (SAE convention).

This is the basic relationship covering the steady-state steering of the elementary automobile. For complex real vehicles additional steer effects must be taken into account as well as the slip angle difference due to the CG location. In general most of the effects which change the slip angles are proportional to lateral acceleration, for example, roll steers and compliance (deflection) steers.

In Figure 5.9, the steering angle, δ , was adjusted to compensate for the different slip angle required to maintain the same radius as the neutral steerer. Suppose the steering angle had been left at the Ackermann corresponding to the turn radius of Figure 5.5. This situation is shown in Figure 5.10.

It is apparent that the radius of the turn has increased appreciably, since the steering angle is now δ_{Acker} instead of $\delta_{\text{Acker}} - (2/3)\alpha_1$ (note: α_1 is – for RH turn). In order to maintain the same CF, hence Y_F , Y_R , and slip angles, the speed on the larger radius has been increased by the square root of the new radius over the old (about 15% in the example).

The important point to note is that at the same lateral acceleration and steer angle the turn radius of the forward CG machine is greater than that of the NS vehicle. The forward CG machine is termed ***understeer*** (US)—as lateral acceleration (i.e., side force) is applied it “understeers” the geometric path established by the Ackermann Steering Angle.

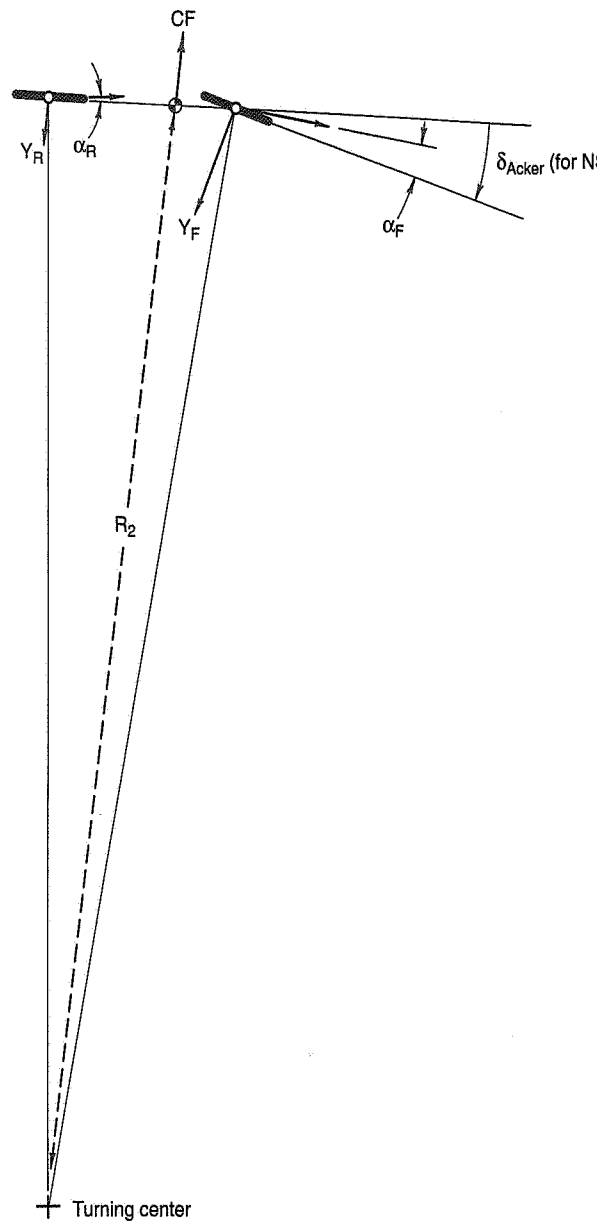


Figure 5.10 Turning with lateral forces, US car, $\delta = \delta_{\text{Ackermann}}$ (for NS).

Conventional passenger cars are almost all modest to heavy understeerers. Figure 5.11 shows some typical constant radius test data for such a machine. Beyond about 0.4g the data becomes nonlinear because of tire and suspension properties.

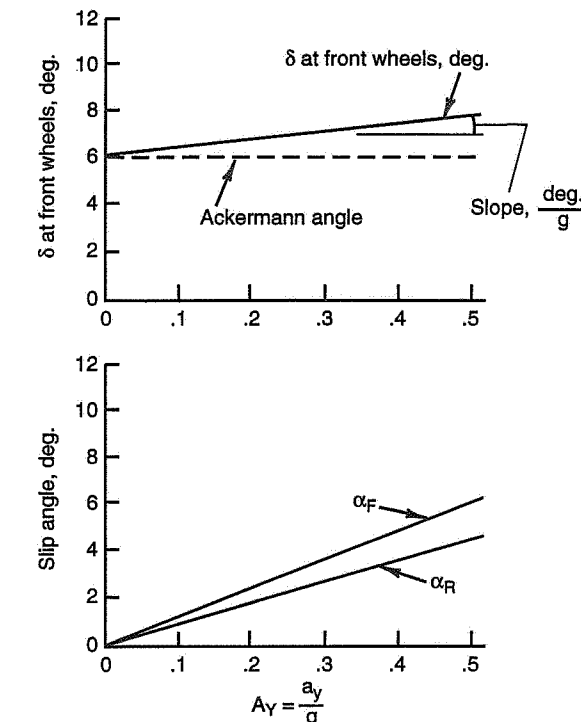


Figure 5.11 Constant radius test for US car.

One measure of the amount of US is the slope of the constant radius skid pad curve (see Figure 5.51a or Chapter 11.7). The steer relationship for the elementary vehicle was given as

$$\delta = \frac{\ell}{R} + (-\alpha_F + \alpha_R)$$

Since $(-\alpha_F + \alpha_R)$ is a function of lateral acceleration, we may take the slope

$$\frac{\Delta\delta}{\Delta A_Y} = \frac{\Delta(-\alpha_F + \alpha_R)}{\Delta A_Y}, \text{ deg./g}$$

as a measure of US.

For reasons of clarity we have discussed US in terms of the longitudinal CG location with equal cornering stiffness F and R. This may be generalized by pointing out that any modifications which affect the rate of change of the front and rear slip angles with lateral acceleration will change the steady-state UO (under/oversteer) properties of the vehicle. It is the difference, $(-\Delta\alpha_F/\Delta A_Y + \Delta\alpha_R/\Delta A_Y)$, that counts. These slopes can be affected by a large number of design factors including tire size and pressure, roll and compliance steers, camber effects, longitudinal and lateral load transfer, aerodynamic loading, and others.

5.6 Steady-State Cornering of the Oversteer Car

We have examined the steering properties of NS and US cars due to front and rear slip angle changes under side force (i.e., lateral acceleration). On the neutral steer car the rates of change of α_F and α_R with A_Y are identical and the car corners on the geometric Ackermann Steering Angle. On the understeer car the rate of change of α_F with A_Y exceeded that of α_R with A_Y and either the path radius, R, increased with lateral acceleration or more steer angle was required to hold the radius.

It is easy to anticipate the steering behavior of the *oversteer* (OS) car. In this machine the rate of change of rear slip angle with A_Y is greater than the rate of change of the front slip angle; the slip angle steer at the rear predominates and the car "oversteers" the intended geometrical path established by the Ackermann Steering Angle.

Figure 5.12 depicts the steady-state cornering situation to the same scale and turn radius as Figures 5.5 and 5.9 for the NS and US cars. The CG of the OS car is at $2/3 \ell$ aft of the front axle and F and R cornering stiffnesses are assumed equal.

It will be noted that the vehicle attitude angle, as determined by the rear slip angle, is greater than for either the NS or US cases. The front slip angle that arises from this chassis rotation is correspondingly greater and, in fact, is considerably larger than is required to maintain the radius. Using the slip angle α_1 of the NS car as a reference, the rear track reacts twice the side load of the front track and the slip angles must be

$$\alpha_F = \frac{2}{3} \alpha_1 \quad \alpha_R = \frac{4}{3} \alpha_1$$

where α_1 = slip angle (same F and R) of the NS vehicle.

The rotation effect ("tail swing") adds a $(1/3)\alpha_1$ surplus at the front which must be compensated for by a reduction in steer angle. However, a further reduction is required in α_F

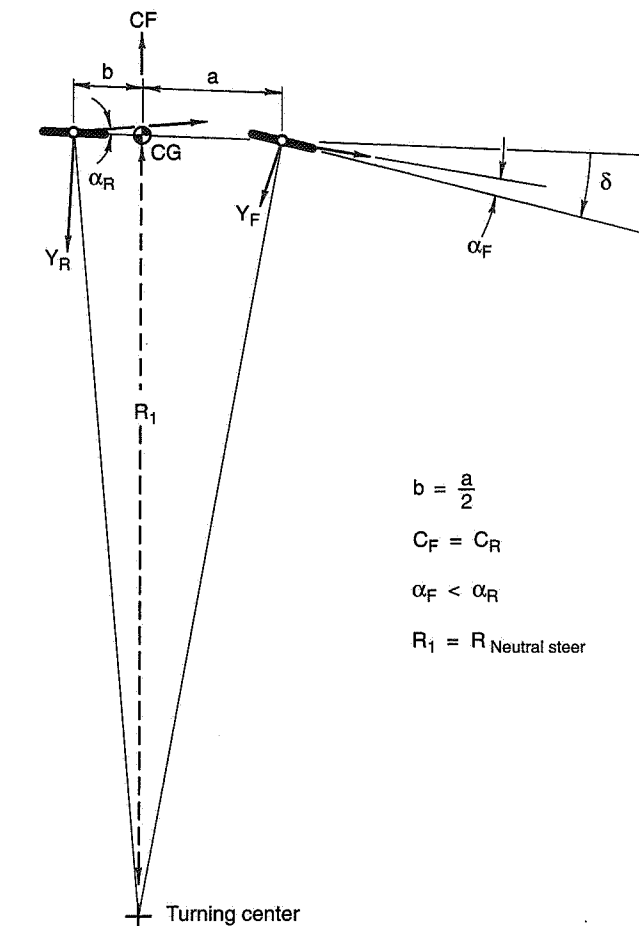


Figure 5.12 Turning with lateral forces, OS car.

by $(1/3)\alpha_1$ and this again must be supplied by a further reduction in steer angle. Thus the required δ is given by

$$\delta = \frac{\ell}{R} + (-\alpha_F + \alpha_R) = \frac{\ell}{R} + \left(\frac{2}{3}\right)\alpha_1$$

and the steer angle of the OS car is $(2/3)\alpha_1$ less than for the NS car and $(4/3)\alpha_1$ less than for the US car. (Note: α_1 is – for RH turn.) In short, an oversteerer corners at a more nosed-in attitude but at a lesser steering angle by comparison to “comparable” NS and US vehicles.

If the steering angle had been left at the Ackermann corresponding to the turn radius of Figure 5.5, the result is shown in Figure 5.13.

This rearward CG machine is termed *oversteer* (OS) because as lateral acceleration is increased, it “oversteers” the geometrical path established by the Ackermann Steering Angle.

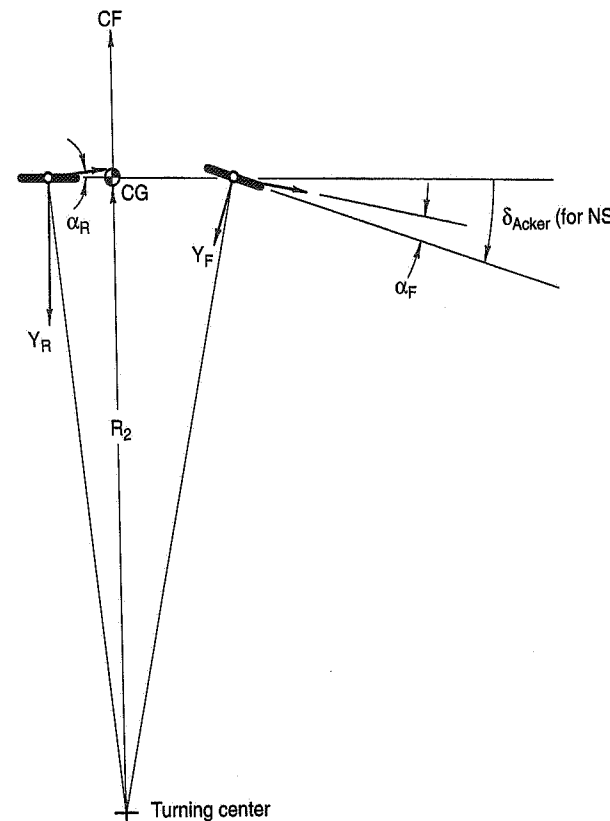


Figure 5.13 Turning with lateral forces, OS car, $\delta = \delta_{\text{Ackermann}}$ (for NS).

In discussing the Neutral Steer car, we examined its behavior under an external disturbance, for example, a uniformly tilted road. We found that in the steady-state the NS vehicle would run down the road on a straight but angled path. The path must be straight because the front and rear slip angles are equal. On the US and OS vehicles, the front and rear slip angles are not equal and a path curvature must result. On the US vehicle the front slip angle predominates and the vehicle turns down the inclined road, whereas on the OS vehicle the rear slip angle steer predominates and the vehicle tends to turn up the slope. These behaviors are shown in Figure 5.14 ($\delta = 0$ in all cases).

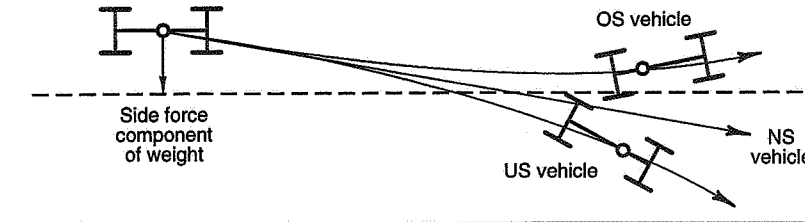


Figure 5.14 Steer behaviors on tilted road.

Concluding this discussion of geometric steer characteristics, we note that the resulting motion of the vehicle depends on the front and rear ends. Thus, the vehicle motion is determined by the steer and slip angles at the two ends of the machine. Thought of in these terms, the motions would reduce to geometry. The predominant reason for becoming involved with dynamics (acceleration effects, see Chapter 6) is that the tires are laterally flexible, with the slip angles determined by the external forces. The greater the cornering stiffnesses, the more nearly the automobile approaches the lateral fixity of a railroad train and the less susceptible it becomes to external forces and the more it is understandable in simple geometric terms.

In analyses of automobile motions, it is usual to set up a single reference axis system with the origin in the car at the CG. Such a procedure tends to obscure the relatively great independence that exists between the front and rear tracks in determining vehicle motions. Unlike an airplane where the downwash from the wing exerts a major influence on the angle of attack of the air at the horizontal tail surface, the slip angles at the front and rear wheels of an automobile are fundamentally coupled through the chassis rigidity. There are many things that can be done to change the individual front or rear steer characteristics, and the development engineer frequently thinks of the front and rear of the car separately.

5.7 Equations of Motion

The equations of motion will be developed for the Elementary Automobile ("bicycle") model. This is a linear model with two degrees of freedom (2DF) which enables the calculation of the motion variables as a function of the forces and moments acting on the vehicle. Referring to Figure 5.2, the motion variables of interest are forward velocity, u , lateral velocity, v and yaw rate, r . Yaw rate, r , is the angular velocity of the vehicle around a vertical axis passing through the CG. The vector sum of u and v is the path velocity, V , which is perpendicular to the turn radius, R . The x -axis of the car is at body slip angle, β , with V . For straight-ahead motion $\beta = 0$ and R is infinite. The total side force is Y and the yawing moment about the CG is N .

In vehicle dynamics work, V is usually left as an "open variable" (i.e., independent variable); thus we assign values to it and calculate how the other variables turn out. Also, since $V \approx u$, the two remaining dependent variables are r and v . This is why it is called a two-degree-of-freedom model. The other assumptions defining this elementary car model have been summarized in Section 5.2.

The reference axis system (vehicle axis system) is fixed in the vehicle with the origin at the vehicle CG. (Chapter 4 offers a more detailed discussion of this axis system.) The essential features are that changes (perturbations) in the dependent variables are measured relative to inertial space and the moments and products of inertia are constant. If the actual path of the vehicle relative to ground is required, an additional earth-fixed reference system is required. Table 5.1 summarizes the terminology and units.

The differential equations of motion follow from Newton's second law:

$$\begin{aligned} T &= I\alpha \quad (\text{where } \alpha = \text{angular acceleration}) \\ F &= ma \end{aligned}$$

In our application, these become

$$N = I_z \frac{dr}{dt}$$

$$Y = ma_y$$

where N and Y are the resultant yawing moment and lateral force that the tires apply to the vehicle (aerodynamic forces are not included in the elementary vehicle). They are the "unbalanced" moment and force causing the angular and linear accelerations. The right-hand sides of the equations are called the inertia terms.

Let us first develop the inertia terms for our vehicle axis system.

Table 5.1 Terminology Used in Equations of Motion

Term	Symbol	Units	Sign
CG location	a, b	ft.	always +
Wheelbase	ℓ	ft.	always +
Mass of vehicle (W/g)	m	slugs	always +
Weight of vehicle	W	lb.	always +
Gravitational acceleration	g	ft./sec. ²	always +
Yawning moment of inertia ($k^2 M$)	I_z	slug-ft. ²	always +
Radius of gyration in yaw	k	ft.	always +
Yawning moment	N	lb.-ft.	+ for clockwise
Lateral force (also F_y)	Y, Y_F, Y_R	lb.	+ to right
Lateral acceleration	a_y	ft./sec. ²	+ for RH turn
Lateral acceleration (a_y / g)	A_y	g	+ for RH turn
Path radius	R	ft.	+ for RH turn
Path curvature	$1/R$	1/ft.	+ for RH turn
Vehicle velocity ($\sqrt{u^2 + v^2}; V \approx u$)	V	ft./sec.	+ for forward
Yawning velocity	r	radian/sec.	+ for clockwise
Lateral velocity	v, v_F, v_R	ft./sec.	+ to right
Longitudinal velocity	u	ft./sec.	+ for forward
Steer angle front wheels	δ	radian	+ for clockwise
Slip angles	α_F, α_R	radian	+ for slip to right
Vehicle slip angle at CG	β	radian	+ for slip to right
Cornering stiffnesses (two tires)	C_F, C_R	lb./radian	always -
Total cornering stiffness ($C_F + C_R$)	C	lb./radian	always -
Ackermann Angle	ℓ/R	radians	+ for RH turn
Stability factor	K	$\frac{1}{(\text{ft./ sec.})^2}$	+ for US
Centrifugal force	CF	lb.	- for RH turn
Overall steering ratio	G	deg./deg.	always +

The $I\alpha$ term in our notation is

$$I_z \frac{dr}{dt} = I_z \dot{r} \quad (5.1)$$

where r is referenced to inertial space. dr/dt in calculus notation is the rate of change of yawing velocity with time (or angular acceleration). This time derivative can also be written \dot{r} . r and \dot{r} can be measured by appropriate gyroscopic instruments located in the automobile. I_z is the moment of inertia about the z-axis.

The expression for " a_y " in the vehicle axis system is

$$\begin{aligned} a_y &= Vr + \dot{v} \\ &= Vr + V\dot{\beta} \quad (V = \text{constant}) \\ &= V(r + \dot{\beta}) \end{aligned} \quad (5.2)$$

a_y consists of two terms. The first is the centrifugal force term and the second is the direct lateral acceleration term.

Consider the following: If an automobile is in a steady turn on a path radius, R , the centripetal acceleration is V^2/R . Since $r = V/R$, the centripetal acceleration is Vr . To sustain this constant lateral acceleration the vehicle operates at a constant slip angle β (i.e., $\dot{\beta} = 0$). The lateral velocity component, v (in Figure 5.2) is also constant since V and β are constant. Thus in this axis system there is a steady component of lateral velocity in a steady turn.

In a transient maneuver, the lateral velocity, v , and hence β , are no longer constant and a direct lateral acceleration component \dot{v} can exist. The total lateral acceleration is the sum of that due to path curvature and that due to \dot{v} .

Another way to think of this lateral acceleration relationship during a transient is to note that in this 2DF system the two basic variables, v (or β) and r , are coupled. In Figure 5.15 consider an initial condition in which the vehicle CG is at Point A in a steady turn of radius R_1 . The acceleration due to path curvature is $V^2/R = Vr_1$. If we initiate a transient condition by a pulse of lateral acceleration, \dot{v}_1 , the radius will decrease as a lateral velocity and displacement buildup. This in turn, will change the centripetal acceleration, Vr_1 , to Vr_2 since r is inversely proportional to R . The relationship is not a simple one since a double integration is involved in going from a \dot{v} to a change in R (i.e., ΔR).

Unbalanced Forces and Moments

The so-called unbalanced forces and moments causing acceleration arise totally from the tires in this simple model. Since load transfer, camber and aerodynamic effects are omitted, only slip angle effects need to be included at the appropriate static loads.²⁶ The slip angles are functions of the two basic motion variables, v (or β) and r . The relationships are developed below.

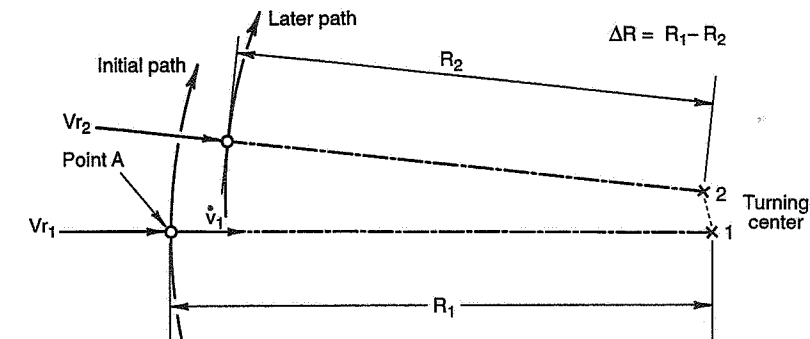


Figure 5.15 Acceleration components in a transient.

Figure 5.16 shows the velocities at the rear tire. If the vehicle experiences a V ($V = u/\cos \beta \approx u$) and v at the CG, the rear tire will also experience them. If the vehicle experiences a positive r about the vertical z-axis, the rear tire will experience a lateral velocity component, $-br$, where b is the distance from the CG to the rear axle.

$$\begin{aligned} \alpha_R &= \frac{v - br}{V} = \frac{v}{V} - \frac{br}{V} \\ \alpha_R &= \beta - \frac{br}{V} \end{aligned} \quad (5.3)$$

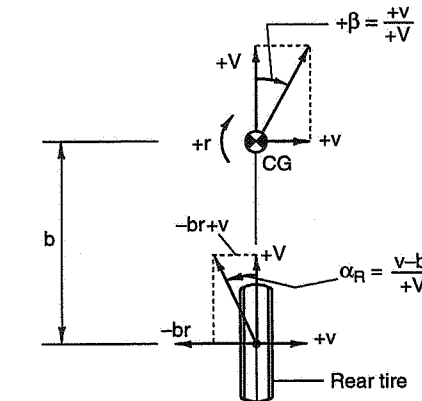


Figure 5.16 Velocities at rear tire.

²⁶ An extension of this model could include constant aerodynamic downforce at the front and rear and also longitudinal load transfer effects associated with constant longitudinal acceleration.

For the front tire, the slip angle will have three components due to vehicle slip angle, β , yawing velocity, r , and steering angle, δ —see Figure 5.17.

$$\begin{aligned}\alpha_F &= \frac{v + ar}{V} - \delta = \frac{v}{V} + \frac{ar}{V} - \delta \\ \alpha_F &= \beta + \frac{ar}{V} - \delta\end{aligned}\quad (5.4)$$

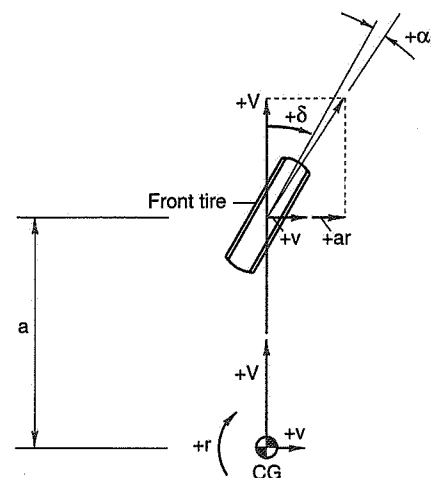


Figure 5.17 Velocities at front tire.

The small angle assumption was used in deriving Eqs. (5.3) and (5.4); the angles are in radians and the sign conventions are those of Figure 5.2.

According to our assumption, the lateral tire forces vary linearly with slip angle. The lateral tire forces at the front and rear tracks are

$$\begin{aligned}Y_F &= C_F \left(\beta + \frac{ar}{V} - \delta \right) = C_F \beta + C_F \left(\frac{ar}{V} \right) - C_F \delta \\ Y_R &= C_R \left(\beta - \frac{br}{V} \right) = C_R \beta - C_R \left(\frac{br}{V} \right)\end{aligned}$$

The total lateral tire force, Y , is then

$$\begin{aligned}Y &= Y_F + Y_R = C_F \beta + C_F \left(\frac{ar}{V} \right) - C_F \delta + C_R \beta - C_R \left(\frac{br}{V} \right) \\ Y &= (C_F + C_R) \beta + \frac{1}{V} (aC_F - bC_R)r - C_F \delta\end{aligned}\quad (5.5)$$

The total tire yawing moment about the z-axis through the CG is

$$\begin{aligned}N &= N_F + N_R = Y_F a - Y_R b \\ &= C_F a \beta + C_F \left(\frac{a^2 r}{V} \right) - C_F a \delta - C_R b \beta + C_R \left(\frac{b^2 r}{V} \right) \\ N &= (aC_F - bC_R) \beta + \frac{1}{V} (a^2 C_F + b^2 C_R)r - aC_F \delta\end{aligned}\quad (5.6)$$

Y and N are the unbalanced forces and moments acting on the vehicle from the tires.

The Derivative Notation

The derivative notation comes from aeronautical practice. It was used in the earliest linear analyses of aircraft stability and control and was initially applied to the automobile by Segel in 1956 (Ref. 144). The derivatives are slopes of force/moment curves against motion variables β , r and δ . They relate the forces and moments to small excursions of these variables. In this linear system they can be considered separately; as a group they define the unbalanced forces and moments due to the tires. In the aeronautical case, the individual derivatives have been measured in specialized wind tunnel and flight tests; aero engineers think about stability and control in “derivative” terms. In both the auto and aero cases the derivatives have a physical significance.

The lateral tire force and yawing moment are linear functions of β , r and δ (since C_F , C_R , a , b , V are constants). In a linear situation such as this, the principle of superposition holds and the components due to β , r and δ are additive. Expressed mathematically, Y and N can be written

$$\begin{aligned}Y &= f(\beta, r, \delta) = \left(\frac{\partial Y}{\partial \beta} \right) \beta + \left(\frac{\partial Y}{\partial r} \right) r + \left(\frac{\partial Y}{\partial \delta} \right) \delta \\ Y &= Y_\beta \beta + Y_r r + Y_\delta \delta\end{aligned}\quad (5.7)$$

$$N = f(\beta, r, \delta) = \left(\frac{\partial N}{\partial \beta} \right) \beta + \left(\frac{\partial N}{\partial r} \right) r + \left(\frac{\partial N}{\partial \delta} \right) \delta$$

$$N = N_\beta \beta + N_r r + N_\delta \delta \quad (5.8)$$

The constant partial derivative slopes, $\partial Y/\partial \beta$, $\partial Y/\partial r$, $\partial Y/\partial \delta$, $\partial N/\partial \beta$, $\partial N/\partial r$, $\partial N/\partial \delta$, are the *stability and control derivatives*, usually expressed in the short-hand notation, Y_β , Y_r , Y_δ , N_β , N_r , N_δ .

By comparing Eqs. (5.5) and (5.6) with (5.7) and (5.8), the stability derivatives can be calculated for this simple vehicle in terms of front and rear tire cornering stiffness, the longitudinal location of the CG (a and b) and the velocity, V, as follows:

$$Y_\beta = C_F + C_R$$

$$Y_r = \left(\frac{1}{V} \right) (aC_F - bC_R)$$

$$Y_\delta = -C_F$$

$$N_\beta = aC_F - bC_R$$

$$N_r = \left(\frac{1}{V} \right) (a^2 C_F + b^2 C_R)$$

$$N_\delta = -aC_F \quad (5.9)$$

Equations of Motion

The complete *equations of motion* in derivative notation are obtained by combining Eqs. (5.1), (5.2) and (5.7), (5.8).

$$I_z \dot{r} = N_\beta \beta + N_r r + N_\delta \delta$$

$$mV(r + \dot{\beta}) = Y_\beta \beta + Y_r r + Y_\delta \delta \quad (5.10)$$

5.8 Physical Significance of the Derivatives

Now that we have the equations of motion in derivative form it is appropriate to discuss the physical significance of the individual derivative terms found on the right-hand side of the equations. It is very useful to be able to think in terms of these derivatives, as aircraft engineers have been doing since the turn of the last century.

Yawing Moment Derivatives

Consider the yawing moment derivatives first:

N_δ This derivative is the proportionality factor between the yawing moment and the steering angle. It is the *control moment* derivative. It increases with the cornering stiffness of the front tires and their distance from the CG. It is always positive.

N_r This derivative is the proportionality factor between the yawing moment on the vehicle (produced by the tires) and the yawing velocity of the vehicle. It is the *yaw damping* derivative. It is always negative, i.e., damping, in the linear range of the tires. It is exactly analogous to an angular viscous damper, always trying to reduce the yawing velocity. It is a function of the front and rear cornering stiffnesses, the distances from the front and rear wheels to the CG squared and is inversely proportional to forward velocity. N_r is theoretically infinite at zero velocity since a small yawing velocity, r , will produce an infinite change in $\alpha_F = ar/V$ and $\alpha_R = br/V$. N_r is zero at infinite speed. For a simple vehicle with C_F and C_R independent of load, it has its smallest magnitude when the CG is at the midpoint. The fall off in steady-state directional stability with speed is frequently attributed to changes in understeer, but is more properly attributed to the reduction in yaw damping.

N_β This is the "static" *directional stability* slope or under/oversteer derivative. On this simple vehicle it is the difference between the moment (about the CG) produced per unit β , by the rear and front wheels, i.e., $-bC_R$ and aC_F . It is a pure "weathercock" effect. If the rear wheels (stabilizing) produce a greater moment slope than the front wheels (destabilizing), the vehicle is stable and wants to reduce β . N_β is basically independent of speed. One mechanical analogy for N_β is that of a "spring" between the velocity vector and the chassis centerline, as indicated in Figure 5.18.

With a positive N_β , the vehicle is always trying to align itself with the relative velocity vector, thus US. Since the relative velocity is created by the vehicle, it is sort of analogous to a weathervane which blows in its own face!

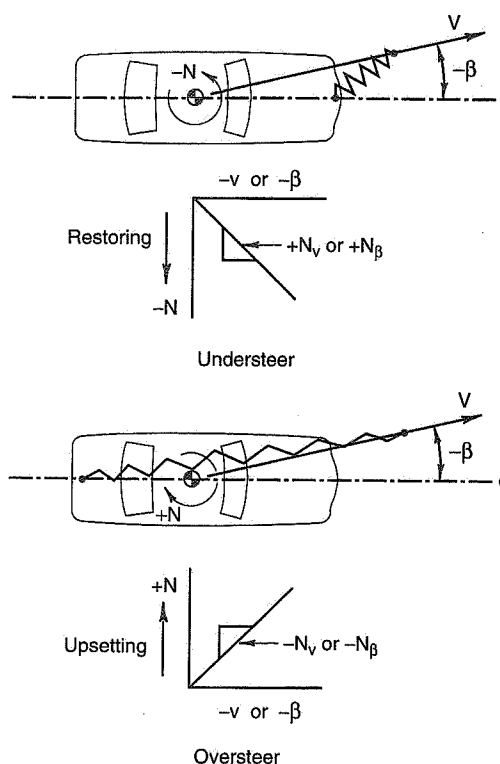


Figure 5.18 The understeer/oversteer spring.

Lateral Force Derivatives

We will now consider the lateral force derivatives:

- Y_δ This derivative is the proportionality factor between the side force from the front wheels due to steering and the steer angle; in short, the side (lateral) force due to steering—the *control force derivative*. It is always positive.
- Y_β This is the side (lateral) force slope. It is similar to the slope of the lateral force vs. slip angle curve for a single tire, but it is the slope of the lateral force curve for the entire vehicle. As such, it is a measure of the rate that lateral force is developed as the vehicle is sideslipped. Since the slope Y_β is always negative in the linear range, i.e., a negative lateral force for a positive sideslip velocity, it corresponds to the rate in a linear damper and is called the *damping-in-sideslip*.

- Y_r This derivative is the side force due to yawing velocity and arises from the difference in the lateral tire forces that comprise N_r . The sign of Y_r follows that of N_β . Y_r is inversely proportional to V . In general, Y_r is small. It is called the *lateral force/yaw coupling derivative*.

In summary, in this simple vehicle there are six derivatives, two associated with control, two with damping, and two cross-coupling between the two degrees of freedom, as shown in Table 5.2.

Table 5.2 The Derivatives
(Simple Two-Degree-of-Freedom Automobile)

Derivative	Name	Nature
N_δ Y_δ	Control Moment Derivative Control Force Derivative	Control
N_r Y_β	Yaw Damping Derivative Damping-in-Sideslip Derivative	Damping
N_β Y_r	Static Directional Stability Derivative Lateral Force/Yaw Coupling Derivative	Coupling

5.9 Steady-State Responses

We will now solve Eqs. (5.10) for the steady-state turning behavior of the 2DF vehicle. In steady turning, \dot{r} and $\dot{\beta}$ (or \dot{v}) = 0, and the equations become

$$\begin{aligned} mVr &= Y_\beta\beta + Y_r r + Y_\delta\delta \\ 0 &= N_\beta\beta + N_r r + N_\delta\delta \end{aligned} \quad (5.11)$$

In a steady turn, $r = V/R$. Substituting and rearranging gives

$$\begin{aligned} -Y_\delta\delta &= Y_\beta\beta + \left(VY_r - mV^2\right)\left(\frac{1}{R}\right) \\ -N_\delta\delta &= N_\beta\beta + VN_r\left(\frac{1}{R}\right) \end{aligned} \quad (5.12)$$

Response to Control

The linear steady-state control response characteristics are given as a series of ratios:

Curvature response defined as	$(1/R)/\delta$
Yawing velocity response defined as	r/δ
Lateral acceleration response	$(V^2/R)/\delta$
Sideslip angle response defined as	β/δ

Eqs. (5.12) will be solved simultaneously for the curvature response by eliminating β , leaving the equations in terms of $1/R$ and δ . Solve for β in the second equation and substitute into the first equation.

$$\begin{aligned}\beta &= -\left(\frac{N_\delta}{N_\beta}\right)\delta - V\left(\frac{N_r}{N_\beta}\right)\left(\frac{1}{R}\right) \\ -Y_\delta\delta &= -\left(\frac{Y_\beta}{N_\beta}\right)N_\delta\delta - V\left(\frac{Y_\beta}{N_\beta}\right)N_r\left(\frac{1}{R}\right) + (VY_r - mV^2)\left(\frac{1}{R}\right)\end{aligned}$$

or

$$\begin{aligned}\left[\left(\frac{Y_\beta}{N_\beta}\right)N_\delta - Y_\delta\right]\delta &= \left[(VY_r - mV^2) - V\left(\frac{Y_\beta}{N_\beta}\right)N_r\right]\left(\frac{1}{R}\right) \\ (Y_\beta N_\delta - N_\beta Y_\delta)\delta &= [N_\beta(VY_r - mV^2) - VY_\beta N_r]\left(\frac{1}{R}\right)\end{aligned}$$

and

$$\begin{aligned}\frac{1/R}{\delta} &= \frac{Y_\beta N_\delta - N_\beta Y_\delta}{N_\beta(VY_r - mV^2) - VY_\beta N_r} \\ &= \frac{Y_\beta N_\delta - N_\beta Y_\delta}{V(N_\beta Y_r - N_\beta mV - Y_\beta N_r)}\end{aligned}$$

or

$$\frac{1/R}{\delta} = \frac{Y_\beta N_\delta - N_\beta Y_\delta}{VQ} \quad (5.13)$$

where

$$Q = N_\beta Y_r - N_\beta mV - Y_\beta N_r \quad (5.14)$$

Further, since $r = V/R$, the r response is

$$\frac{r}{\delta} = V \frac{1/R}{\delta} = \frac{Y_\beta N_\delta - N_\beta Y_\delta}{Q} \quad (5.15)$$

and the lateral acceleration response is obtained by multiplying Eq. (5.13) by V^2 :

$$\frac{V^2/R}{\delta} = \frac{V(Y_\beta N_\delta - N_\beta Y_\delta)}{Q} \quad (5.16)$$

Finally, the sideslip angle response is obtained by eliminating r from Eqs. (5.11):

$$\frac{\beta}{\delta} = \frac{Y_\delta N_r - N_\delta(Y_r - mV)}{Q} \quad (5.17)$$

Response to Applied Side Force

Now, it is also possible to obtain the steady-state responses of the car to an *applied side force* at the CG (such as driving on a cambered road). If this side force is $+F_y$ and if the steering angle is taken as zero, Eqs. (5.12) become

$$-F_y = Y_\beta\beta + (VY_r - mV^2)\left(\frac{1}{R}\right)$$

$$0 = N_\beta\beta + VN_r\left(\frac{1}{R}\right)$$

The response relationships are

$$\frac{1/R}{F_y} = -\frac{N_\beta}{VQ} \quad (5.18)$$

$$\frac{r}{F_y} = -\frac{N_\beta}{Q} \quad (5.19)$$

$$\frac{V^2/R}{F_y} = -\frac{VN_\beta}{Q} \quad (5.20)$$

$$\frac{\beta}{F_y} = +\frac{N_r}{Q} \quad (5.21)$$

Response to Applied Yawing Moment

Similarly, the steady-state response relationships may be found for a *steady, externally applied yawing moment, +N*:

$$0 = Y_\beta \beta + (VY_r - mV^2) \left(\frac{1}{R} \right)$$

$$-N = N_\beta \beta + VN_r \left(\frac{1}{R} \right)$$

The response relationships are

$$\frac{1/R}{N} = \frac{Y_\beta}{VQ} \quad (5.22)$$

$$\frac{r}{N} = \frac{Y_\beta}{Q} \quad (5.23)$$

$$\frac{V^2/R}{N} = \frac{VY_\beta}{Q} \quad (5.24)$$

$$\frac{\beta}{N} = -\frac{(Y_r - mV)}{Q} \quad (5.25)$$

Since we are dealing with a linear system, the effect of, say, a simultaneous application of side force and yawing moment can be found by merely adding the appropriate responses. For example, the response in path curvature to an aerodynamic gust which has a lateral force component F_y at the CG and a moment N about that point is

$$\frac{1}{R} = -\left(\frac{N_\beta}{VQ} \right) F_y + \left(\frac{Y_\beta}{VQ} \right) N$$

$$= -\frac{1}{VQ} (N_\beta F_y - Y_\beta N)$$

5.10 Neutral Steer Responses

Steer properties of the automobile have been defined in various ways. We will use the derivative definitions but show that they correspond to other definitions. Thus for neutral steer (NS), $N_\beta = 0$, i.e., the static directional stability is zero. This says that if the vehicle is thought of as a weathervane in β , no moment arises on the vehicle when a β exists (with δ and $r = 0$). There is no directional spring in the analogy previously given; the yawing moment from the front pair of wheels due to β is equal and of opposite sign to that from the rear pair of wheels.

With $N_\beta = 0$, Q from Eq. (5.14) becomes $-Y_\beta N_r$, the product of the two damping derivatives. The response relationships reduce to the following.

Response to Control—Neutral Steer

$$\frac{1/R}{\delta} = -\frac{1}{V} \frac{N_\delta}{N_r} \quad (5.26)$$

$$\frac{r}{\delta} = -\frac{N_\delta}{N_r} \quad (5.27)$$

$$\frac{V^2/R}{\delta} = -V \frac{N_\delta}{N_r} \quad (5.28)$$

$$\frac{\beta}{\delta} = -\frac{Y_\delta}{Y_\beta} + \frac{1}{V} \frac{N_\delta}{N_r} (Y_r - mV) \quad (5.29)$$

Response to Applied Side Force—Neutral Steer

$$\frac{1/R}{F_y} = 0 \quad (5.30)$$

$$\frac{r}{F_y} = 0 \quad (5.31)$$

$$\frac{V^2/R}{F_y} = 0 \quad (5.32)$$

$$\frac{\beta}{F_y} = -\frac{1}{Y_\beta} \quad (5.33)$$

Response to Applied Yawing Moment—Neutral Steer

$$\frac{1/R}{N} = -\frac{1}{VN_r} \quad (5.34)$$

$$\frac{r}{N} = -\frac{1}{N_r} \quad (5.35)$$

$$\frac{V^2/R}{N} = -\frac{V}{N_r} \quad (5.36)$$

$$\frac{\beta}{N} = +\frac{(Y_r - mV)}{Y_\beta N_r} \quad (5.37)$$

The control responses, (path curvature, yaw velocity and lateral acceleration) for the NS car depend on the control moment, N_δ , the yaw damping, N_p , and the velocity, V .

From Eq. (5.27),

$$\delta N_\delta = -r N_r \quad (5.38)$$

which says that in a steady turn the control moment just balances out the yaw damping moment.

Ackermann Relationship—Neutral Steer

The conventional relationship for the Ackermann angle can be derived from the NS car responses at low lateral acceleration when the vehicle is tracking at the Ackermann steer,

and $\beta = 0$. From Eqs. (5.27) and (5.9),

$$\begin{aligned} \frac{r}{\delta} &= -\frac{N_\delta}{N_r} = \frac{aC_F}{(a^2C_F + b^2C_R)(1/V)} \\ &= \frac{VC_F}{\left(aC_F + \left(\frac{b}{a}\right)bC_R\right)} \end{aligned}$$

Since,

$$N_\beta = aC_F - bC_R = 0, \text{ and } \frac{b}{a} = \frac{C_F}{C_R}$$

$$\frac{r}{\delta} = \frac{VC_F}{aC_F + bC_F} = \frac{V}{\ell} \quad (5.39)$$

and

$$\delta = \frac{\ell}{V/r} = \frac{\ell}{R}, \text{ the Ackermann Relationship} \quad (5.40)$$

Normally, as noted earlier, the Ackermann angle is thought of as the geometric steering angle required at low speed (i.e., low lateral acceleration) for a vehicle of wheelbase, ℓ , to track a circle of radius R . Another interpretation of the Ackermann angle can be found by substituting the Ackermann steering angle, ℓ/R , into Eq. (5.38), thus

$$rN_r = -\left(\frac{\ell}{R}\right)N_\delta$$

Here it is apparent that the Ackermann Steering angle, ℓ/R , is just that angle required to overcome the yaw damping moment, rN_r , for a neutral steer vehicle at any speed. This relationship was first derived by Dave Whitcomb and reported in Ref. 92.

Summary of Neutral Steer Behavior

The neutral steer two-degree-of-freedom vehicle has zero responses with respect to an applied force input at the CG (such as running on a cambered road) with the exception of the vehicle slip angle, β . For equilibrium in the steady-state, the vehicle must run off at a slip angle given by Eq. (5.33):

$$\beta = -\frac{F_y}{Y_\beta}$$

Y_β is equal to $C_F + C_R$ or the total tire cornering stiffness, C . Maximizing C results in minimum β or minimum response to disturbance.

A further observation may be made from the NS car responses. When a yawing moment is applied to the car (say from a side gust acting at a center of pressure ahead of the CG), all of the responses (Eqs. (5.34)-(5.37)) are proportional to $1/N_r$. This suggests that an effective way to minimize steady-state gust response is to maximize N_r through the use of high cornering stiffness tires (as is well known). Unfortunately,

$$N_r = \left(\frac{1}{V}\right)(a^2C_F + b^2C_R)$$

and goes down linearly with V , the tires becoming less effective dampers at higher speeds. Increasing a and b or the wheelbase, ℓ , is another way to reduce response to a yaw disturbance.

5.11 Understeer and Oversteer Responses

The general curvature response to a steer angle, (Eq. (5.13)) is

$$\begin{aligned} \frac{1/R}{\delta} &= \frac{Y_\beta N_\delta - N_\beta Y_\delta}{VQ} \\ &= \frac{Y_\beta N_\delta - N_\beta Y_\delta}{V(N_\beta Y_r - N_\beta mV - Y_\beta N_r)} \\ &= \frac{1}{V(N_\beta Y_r - Y_\beta N_r)} - \frac{N_\beta mV^2}{(Y_\beta N_\delta - N_\beta Y_\delta) - (Y_\beta N_\delta - N_\beta Y_\delta)} \end{aligned}$$

By substituting the expressions for the derivatives (Eq. (5.9)) into the first term in the denominator we find that

$$\frac{V(N_\beta Y_r - Y_\beta N_r)}{(Y_\beta N_\delta - N_\beta Y_\delta)} = a + b = \ell, \text{ the wheelbase}$$

The equation becomes

$$\begin{aligned} \frac{1/R}{\delta} &= \frac{1}{\ell - \frac{N_\beta mV^2}{(Y_\beta N_\delta - N_\beta Y_\delta)}} \\ &= \frac{1/\ell}{1 + \left(\frac{1}{\ell}\right)\left(\frac{mN_\beta}{(N_\beta Y_\delta - Y_\beta N_\delta)}\right)V^2} \\ \frac{1/R}{\delta} &= \frac{1/\ell}{1 + KV^2} \end{aligned} \quad (5.41)$$

where

$$K = \left(\frac{mN_\beta}{\ell(N_\beta Y_\delta - Y_\beta N_\delta)}\right)$$

or

$$K = \frac{m}{\ell} \left(\frac{N_\beta / (-Y_\beta)}{N_\delta - (N_\beta / Y_\beta) Y_\delta}\right) \quad (5.42)$$

K is termed the *stability factor*.

The yawing velocity response to steering is obtained by multiplying the curvature response by V , thus,

$$\frac{r}{\delta} = \frac{V/\ell}{1 + KV^2} \quad (5.43)$$

Note that K depends on the derivatives, which for the simple model are independent of speed. For more complex models K and V may not be independent (for example, when aero downforce is included).

Stability Factor, K

An examination of Eqs. (5.41) and (5.43) indicates how the steady-state curvature and yaw velocity responses vary with forward velocity. As Segel points out, in Ref. 144, if K (which is a constant depending only on the vehicle mass, wheelbase and stability derivatives) is zero, the curvature and yaw velocity control responses become those for the neutral steer car as given by Eqs. (5.40) and (5.39), i.e.,

$$\frac{1/R}{\delta} = \frac{1}{\ell} \quad \text{and} \quad \frac{r}{\delta} = \frac{V}{\ell}$$

If K is not zero these responses are modified in a way which depends on the algebraic sign of K. By substituting the expressions for the derivatives of this simple model (as given by Eq. (5.9)) into the denominator of K, we see that it is always positive, thus,

$$N_\delta - \left(\frac{N_\beta}{Y_\beta} \right) Y_\delta = \left[-aC_F - \left(\frac{aC_F - bC_R}{C_F + C_R} \right) (-C_F) \right] = -\frac{C_F C_R \ell}{C_F + C_R} \quad (5.44)$$

which is positive since C_F and C_R are always negative.

Thus the sign of K is determined by the numerator, $m(N_\beta - Y_\beta)$. Since Y_β is always negative, the numerator takes the sign of N_β , the "static" directional stability or "directional stiffness," which can be positive or negative. If K is positive (positive directional stiffness) then both the curvature and yaw velocity responses tend to decrease with speed. These trends are shown in Figures 5.19 and 5.20. The curves shown are for single plus and minus values of K. Larger values of K would give still more pronounced fall-off in response (for +K) or increase in response (for -K). In all cases, the derivatives which make up K are independent of speed. In particular, note that N_β , the directional stiffness, is constant with speed (for this simple model without secondary effects).

A physical understanding of K can be obtained as follows:

Suppose one were to apply a pure side force, Y_0 , at the CG and steer so that $r = 0$. In this case,

$$\sum Y = Y_0 + Y_\beta \beta + Y_\delta \delta = 0, \text{ in the steady-state}$$

and

$$\sum N = N_\beta \beta + N_\delta \delta = 0$$

then,

$$Y_0 = -Y_\beta \left(\frac{-N_\delta}{N_\beta} \right) \delta - Y_\delta \delta = \left[\left(\frac{Y_\beta N_\delta}{N_\beta} \right) - Y_\delta \right] \delta$$

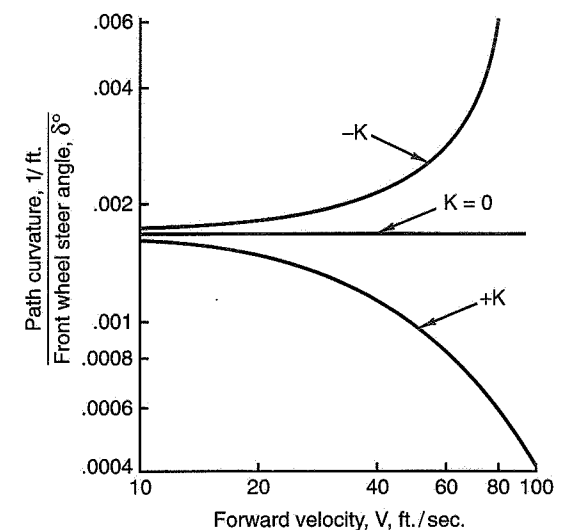


Figure 5.19 Path curvature response (Ref. 92).

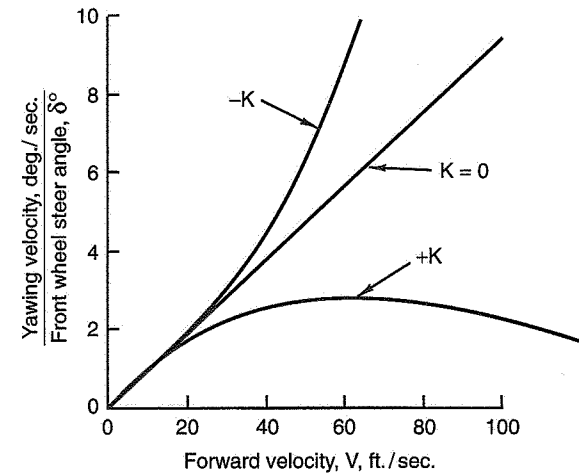


Figure 5.20 Yawing velocity response (Ref. 92).

or

$$\frac{\delta}{Y_0} = \frac{-N_\beta}{N_\beta Y_\delta - Y_\beta N_\delta} = -\left(\frac{\ell}{m}\right)K$$

Thus the steer angle required to keep the car from turning, under the action of the side force, Y_0 , is proportional to the negative of the stability factor, K .

SAE Steer Definitions

SAE J670 (Ref. 1) gives the following definitions for understeer and oversteer (as related to conventional skid pad tests):

- US—"A vehicle is *understeer* at a given trim if the ratio of the steering wheel angle gradient to the overall steering ratio is greater than the Ackermann steer angle gradient."
- OS—"A vehicle is *oversteer* at a given trim if the ratio of the steering wheel angle gradient to the overall steering ratio is less than the Ackermann steer angle gradient."

By rearrangement of Eq. (5.41) and introducing overall steering ratio, (G), we obtain

$$\frac{\delta_{SW}}{(V^2/R)G} = \frac{\ell}{V^2} + \ell K$$

where, ℓ/V^2 is the *Ackermann steer angle gradient*, $\frac{d(\ell/R)}{d(V^2/R)}$.

If K is positive, the vehicle is *understeer*; if K is negative the vehicle is *oversteer*. This constitutes the relationship between the stability factor, K , and the SAE definitions of understeer/oversteer.

Neutral Steer Point

The *Neutral Steer Point* (NSP) for this simple vehicle is defined as the point along the chassis at which an external lateral force can be applied which produces no steady-state yaw velocity. (This definition aligns with that of SAE's for the more complex rolling vehicle.)

Consider Figure 5.21: Assume $\delta = 0$ (no steer) and apply a lateral force, Y_0 , at d from the front axle. The requirement is that $r = 0$ in steady-state which also implies that $I_z \dot{r} = \Sigma N = 0$. Then, from Eqs. (5.10),

$$\sum Y = Y_0 + Y_\beta \beta$$

$$\sum N = -(d - a)Y_0 + N_\beta \beta = 0$$

Hence

$$\beta = (d - a) \frac{Y_0}{N_\beta}$$

and

$$\sum Y = Y_0 \left[1 + (d - a) \frac{Y_\beta}{N_\beta} \right]$$

but

$$\sum Y = mV(r + \dot{\beta}) = mVr, \text{ in steady-state}$$

and since $r = 0$,

$$\sum Y = 0 \quad \text{and} \quad d = a - \frac{N_\beta}{Y_\beta}$$

Nondimensionalizing by the wheelbase gives

$$NSP = \frac{d}{\ell} = \frac{a}{\ell} - \left(\frac{N_\beta}{Y_\beta} \right) \left(\frac{1}{\ell} \right) \quad (5.45)$$

This is the general relationship for the NSP in terms of the stability derivatives.

For our 2DF model, from Eq. (5.9),

$$N_\beta = aC_F - bC_R$$

$$Y_\beta = C_F + C_R$$

$$d = a - \frac{aC_F - bC_R}{C_F + C_R} = (a + b) \left(\frac{C_R}{C_F + C_R} \right)$$

$$NSP = \frac{d}{\ell} = \frac{C_R}{C} \quad (5.46)$$

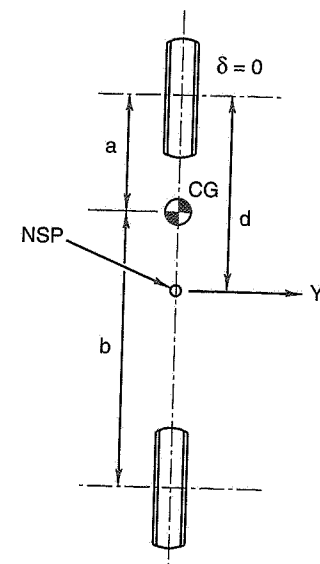


Figure 5.21 Neutral steer point.

Static Margin

The static margin (SM) for this simple vehicle is defined as the horizontal distance along the chassis between the neutral steer point and the center of gravity, divided by the wheelbase. (This definition aligns with that of SAE's for the more complex vehicle with a roll degree of freedom.)

$$SM = \frac{d - a}{\ell} = \frac{d}{\ell} - \frac{a}{\ell} = NSP - \frac{a}{\ell} \quad (5.47)$$

From Eq. (5.45), the static margin in terms of the stability derivatives is

$$SM = -\left(\frac{1}{\ell}\right)\left(\frac{N_\beta}{Y_\beta}\right) \quad (5.48)$$

For our 2DF model,

$$SM = -\left(\frac{1}{\ell}\right)\left(\frac{aC_F - bC_R}{C_F + C_R}\right) = \frac{-(a/\ell)C_F + (b/\ell)C_R}{C} \quad (5.48a)$$

Referring back to Eq. (5.48) it is interesting to note that since $N_\beta = \partial N / \partial \beta$ and $Y_\beta = \partial Y / \partial \beta$, the static margin can be expressed as

$$SM = -\left(\frac{1}{\ell}\right)\left(\frac{\partial N}{\partial Y}\right) \quad (5.49)$$

SM is an indication of the sense and amplitude of the yawing moment associated with the applied side force. Since Y_β is always negative, the SM has the sign of N_β . If a positive side force is applied (RH turn) and the resulting yawing moment is negative, the vehicle has a positive static margin and is understeer. Physically, the yawing moment is trying to reduce the applied side force at the CG. Thus the SM is an alternative way of specifying under/oversteer.

The relationship between K and the SM, in derivative terms, may be deduced by combining Eqs. (5.42) and (5.48), thus:

$$K = \frac{SM}{\left(\frac{1}{m}\right)\left[N_\delta - \left(\frac{N_\beta}{Y_\beta}\right)Y_\delta\right]}$$

Olley Definition

The earliest definition of under/oversteer dates back to Maurice Olley (Ref. 112). He defines the steer properties in terms of the path taken by a vehicle (initially running in a straight path with zero steer angle) when subjected to a steady side force at the CG.

The equations of motion for our 2DF vehicle with a steady side force, $+F_y$, located at the CG are

$$\begin{aligned} mV(r + \dot{\beta}) &= \beta Y_\beta + r Y_r + F_y \\ I_z \dot{r} &= \beta N_\beta + r N_r \end{aligned}$$

For steady-state, these become (on rearrangement)

$$\begin{aligned} r(mV - Y_r) &= mVr = \beta Y_\beta + F_y \\ \beta &= -\frac{r N_r}{N_\beta} \end{aligned}$$

where Y_r is negligible compared to mV .

Combining these two equations and solving for the path response to side force input gives

$$\frac{(1/R)}{F_y - (mV^2/R)} = \frac{N_\beta}{VN_r Y_\beta} \quad (5.49a)$$

mV^2/R is the centrifugal force and $F_y - mV^2/R$ is the total side force acting on the vehicle. VN_r is independent of speed since tire slip angles depend on r/V , not on r alone. The denominator of the expression is always +, so that the sign of the response depends on the sign of N_β .

Olley states that the vehicle is understeer if under the applied side force the path curves away from the applied force. This will occur if N_β , the static directional stability, is positive. For a positive N_β the turning center is to the right for a positive F_y and the effective side force is reduced by the centrifugal force. If N_β is 0, there is no change in the path and, as shown earlier, the vehicle is NS. If N_β is negative the centrifugal force acts in the same direction as the applied force, F_y , and the center of curvature is on the other side of the car while the curvature itself is increased.

Figure 5.22 (taken from the Segel paper referenced earlier) illustrates these paths. A simple way of checking the steer tendencies of a car is to drive it along a sloping road and (with $\delta = 0$) note the path. If it runs down the slope under the lateral weight component it is US, or OS if it tends to run up the slope.

Slip Angle and Effective Slip Angle Steers

The Olley definition of under/oversteer is an excellent introduction to the concept of slip angle and effective slip angle steers and subsequently to the Bundorf Cornering Compliance concept.

The application of a steady side force at the CG must be equilibrated by side forces in the opposite direction at the front and rear tracks. These side forces are inversely proportional to the distances of the tracks from the CG. These side forces produce (in the simple 2DF vehicle) slip angles which are proportional to the side forces and inversely proportional to the their cornering stiffnesses. These slip angles, as far as the direction of motion of each end of the vehicle is concerned, act exactly like the steer angle of a wheel with infinite cornering stiffness. Thus the velocity vector at the front track is angled to the chassis (of this simple vehicle) at the front slip angle, and similarly for the rear. The path of the vehicle in the Olley test is determined by the relative steer effect of the front and rear *slip angle steers*, $(-\alpha_F + \alpha_R)$. For example if the CG is at mid-wheelbase, the side force reaction front and rear will be equal. If the cornering stiffness of the front tires is less than the rear tires, the front tires will steer the vehicle away from its initial path faster than the rear tires will steer it back, and the vehicle is understeer.

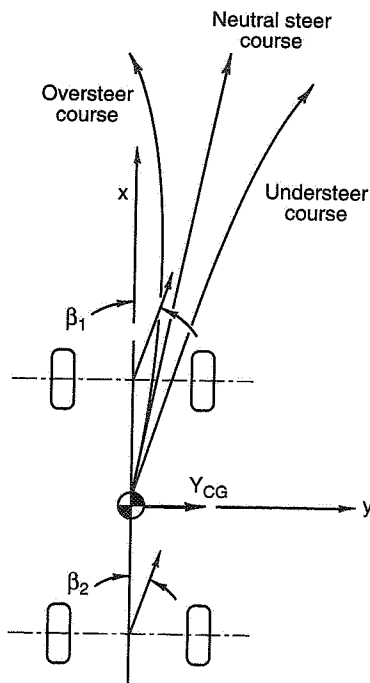


Figure 5.22 Under/oversteer representation of vehicle stability (Olley).

In the case of real automobiles, the direction of motion of the ends of the vehicle also depend on such items as roll steer, suspension deflection steer, camber changes, lateral and longitudinal load transfer, traction/braking effects, etc. These may be accommodated by working out or measuring "effective slip angle steers," and their difference $(-\alpha_{Fe} + \alpha_{Re})$.

Consider now the slip angle steers in the context of steer maneuvers such as conventional skid pad tests. From Eqs. (5.3) and (5.4), derived from the turning geometry,

$$\alpha_F = \beta + \frac{ar}{V} - \delta \quad (5.4)$$

$$\alpha_R = \beta - \frac{br}{V} \quad (5.3)$$

Then,

$$\begin{aligned}-\alpha_F + \alpha_R &= -\beta - \frac{ar}{V} + \delta + \beta - \frac{br}{V} \\ \delta &= \frac{r\ell}{V} + (-\alpha_F + \alpha_R) = \frac{\ell}{R} + (-\alpha_F + \alpha_R)\end{aligned}\quad (5.50)$$

for a constant radius skid pad test. For the constant throttle (constant speed) test the first term becomes $(\ell/V^2)(V^2/R)$.

The general curvature response, Eq. (5.41), can be rewritten:

$$\delta = \frac{\ell}{R} + \frac{\ell KV^2}{R}$$

where

$$\ell K = \frac{mN_\beta}{N_\beta Y_\delta - Y_\beta N_\delta}$$

Comparing this with Eq. (5.50) yields

$$-\alpha_{Fe} + \alpha_{Re} = \frac{\ell KV^2}{R} \quad (5.50a)$$

$$K = +\frac{1}{\ell} \left(\frac{-\alpha_{Fe} + \alpha_{Re}}{V^2/R} \right), \text{ the stability factor} \quad (5.51)$$

where the α 's can be considered as "effective," i.e., α_{Fe} and α_{Re} .

Thus the rate of change with lateral acceleration of the effective slip angle difference is also a measure of under/oversteer.

K and the difference of the effective slip angle steers, $(-\alpha_{Fe} + \alpha_{Re})$, can also be related to the static margin, SM , as follows. In derivative terms, K is defined by Eq. (5.42):

$$K = \frac{m}{\ell} \left(\frac{N_\beta / (-Y_\beta)}{N_\delta - (N_\beta / Y_\beta) Y_\delta} \right)$$

Introducing the SM from Eq. (5.48),

$$K = \frac{m}{\ell} \left(\frac{-\ell \times SM}{(N_\beta Y_\delta / Y_\beta) - N_\delta} \right)$$

If the relationships for the derivatives of the simplified vehicle, Eqs. (5.9), are substituted into the denominator of the above equation, it will be found to equal

$$\ell^2 C_F \left(\frac{C_R}{C} \right)$$

where $C = C_F + C_R$.

Then

$$K = \frac{m(-\ell \times SM)}{\ell^2 C_F (C_R / C)}$$

$$\text{or } K = -\frac{1}{g\ell} \frac{C/W}{(C_F/W)(C_R/W)} SM \quad (5.51a)$$

where W = vehicle weight.

From Eq. (5.51), rearrange to

$$\begin{aligned}-\alpha_F + \alpha_R &= K\ell \left(\frac{V^2}{R} \right) \\ &= -\frac{C/W}{g(C_F/W)(C_R/W)} SM \left(\frac{V^2}{R} \right) \\ &= -\frac{C/W}{(C_F/W)(C_R/W)} SM(A_Y)\end{aligned}\quad (5.52)$$

where α_F and α_R can be considered as effective steers if the slopes C_F and C_R are corrected for the additional effects noted earlier.

Bundorf Cornering Compliances

Starting with Eq. (5.51),

$$\begin{aligned}
 -K\ell \left(\frac{V^2}{R} \right) &= \alpha_F - \alpha_R \\
 &= \frac{F_F}{C_F} - \frac{F_R}{C_R} \\
 &= \frac{F(b/\ell)}{C_F} - \frac{F(a/\ell)}{C_R} \\
 &= \left(\frac{W(b/\ell)}{C_F} - \frac{W(a/\ell)}{C_R} \right) \frac{F}{W} \\
 &= \left(\frac{W_F}{C_F} - \frac{W_R}{C_R} \right) A_Y
 \end{aligned}$$

where F_F and F_R and F are lateral forces

W is the gross weight

C_F, C_R are the respective cornering slopes

Since

$$-\ell K \left(\frac{V^2}{R} \right) = -\ell K \left(\frac{V^2}{gR} \right) g = -\ell K A_Y g$$

$$\ell K = -\left(\frac{W_F/C_F}{g} - \frac{W_R/C_R}{g} \right)$$

$$57.3 (\ell K) = D_F - D_R \quad (5.53)$$

where D_F and D_R are the Bundorf cornering compliances (Ref. 28) at the front and rear, respectively, in deg./g.

For the simple 2DF model the slip angles/g are the cornering compliances. Effective slip angles/g cover the more complex real vehicle. US at front increases D_F ; US at rear decreases D_R (the sign convention established by Bundorf).

For either the Olley applied force test, or for the steered path tests (constant radius or constant speed), the cornering compliances determine the steer characteristic. A virtue of the cornering compliance concept is that the various effects which contribute to D_F and D_R can be evaluated separately and summed. The difference between D_F and D_R then yields a numerical measure of under/oversteer in degrees/g referred to as the *understeer gradient*. Summing these separate effects (such as tire/weight, roll steer and camber, deflection and aligning torque steer, etc.) is called the *understeer budget*. The system is linear and the effects are additive.

An example of an understeer budget for a passenger car is given below:

	Front D_F , deg./g	Rear D_R , deg./g
Weight distribution effect, i.e., tire cornering stiffness	7.2	6.6
Aligning torque on rigid body	0.1	-0.1
Roll camber	1.2	0.0
Roll steer	0.5	-0.5
Lateral force deflection steer compliance	0.2	0.2
Aligning torque deflection steer compliance	<u>1.3</u>	<u>0.1</u>
Cornering compliances	10.5	6.3
Total understeer, $D_F - D_R = 4.2$ deg./g		

In derivative terms the understeer gradient is

$$UG = W \left(\frac{N_\beta}{Y_\delta N_\beta - N_\delta Y_\beta} \right) 57.3 \text{ deg./g}$$

To estimate the magnitude of the linear component terms in D_F and D_R see Ref. 27.

Using the **derivative** approach, it is similarly possible to sum up the individual effects at the front and rear tracks. There are only four derivatives involved ($N_\beta, Y_\beta, N_\delta, Y_\delta$) in K . The front axle contributes to all four of these and the rear axle to two. The fundamental virtue of working with the derivatives is that they are physically understandable in terms of the actual forces and moments which produce the control, stability, and damping. The aircraft industry in its wind tunnel testing performs the equivalent of under/oversteer budgets when it ascertains the contributions of the wing, the vertical tail, the fuselage, powerplant thrust effects, etc., on the static directional stability, N_β .

Bundorf Cornering Compliances

Starting with Eq. (5.51),

$$\begin{aligned}
 -K\ell \left(\frac{V^2}{R} \right) &= \alpha_F - \alpha_R \\
 &= \frac{F_F}{C_F} - \frac{F_R}{C_R} \\
 &= \frac{F(b/\ell)}{C_F} - \frac{F(a/\ell)}{C_R} \\
 &= \left(\frac{W(b/\ell)}{C_F} - \frac{W(a/\ell)}{C_R} \right) \frac{F}{W} \\
 &= \left(\frac{W_F}{C_F} - \frac{W_R}{C_R} \right) A_Y
 \end{aligned}$$

where F_F and F_R and F are lateral forces

W is the gross weight.

C_F, C_R are the respective cornering slopes

Since

$$-\ell K \left(\frac{V^2}{R} \right) = -\ell K \left(\frac{V^2}{gR} \right) g = -\ell K A_Y g$$

$$\ell K = -\left(\frac{W_F/C_F}{g} - \frac{W_R/C_R}{g} \right)$$

$$57.3 (\ell K) = D_F - D_R \quad (5.53)$$

where D_F and D_R are the Bundorf cornering compliances (Ref. 28) at the front and rear, respectively, in deg./g.

For the simple 2DF model the slip angles/g are the cornering compliances. Effective slip angles/g cover the more complex real vehicle. US at front increases D_F ; US at rear decreases D_R (the sign convention established by Bundorf).

For either the Olley applied force test, or for the steered path tests (constant radius or constant speed), the cornering compliances determine the steer characteristic. A virtue of the cornering compliance concept is that the various effects which contribute to D_F and D_R can be evaluated separately and summed. The difference between D_F and D_R then yields a numerical measure of under/oversteer in degrees/g referred to as the *understeer gradient*. Summing these separate effects (such as tire/weight, roll steer and camber, deflection and aligning torque steer, etc.) is called the *understeer budget*. The system is linear and the effects are additive.

An example of an understeer budget for a passenger car is given below:

	Front D_F , deg./g	Rear D_R , deg./g
Weight distribution effect, i.e., tire cornering stiffness	7.2	6.6
Aligning torque on rigid body	0.1	-0.1
Roll camber	1.2	0.0
Roll steer	0.5	-0.5
Lateral force deflection steer compliance	0.2	0.2
Aligning torque deflection steer compliance	1.3	0.1
Cornering compliances	10.5	6.3
Total understeer, $D_F - D_R = 4.2$ deg./g		

In derivative terms the understeer gradient is

$$UG = W \left(\frac{N_\beta}{Y_\delta N_\beta - N_\delta Y_\beta} \right) 57.3 \text{ deg./g}$$

To estimate the magnitude of the linear component terms in D_F and D_R see Ref. 27.

Using the derivative approach, it is similarly possible to sum up the individual effects at the front and rear tracks. There are only four derivatives involved ($N_\beta, Y_\beta, N_\delta, Y_\delta$) in K . The front axle contributes to all four of these and the rear axle to two. The fundamental virtue of working with the derivatives is that they are physically understandable in terms of the actual forces and moments which produce the control, stability, and damping. The aircraft industry in its wind tunnel testing performs the equivalent of under/oversteer budgets when it ascertains the contributions of the wing, the vertical tail, the fuselage, powerplant thrust effects, etc., on the static directional stability, N_β .

5.12 Significant Speeds

In this section, several significant speeds will be derived using the derivative approach. Maurice Olley was the first to discover the critical speed beyond which some vehicles become divergently unstable. More recently, it is recognized that this is the speed at which the stability index changes sign. Various other interesting speeds have been noted in the technical literature and are covered here.

Ackermann Speed

The Ackermann Speed can be defined as a turning speed so low that the lateral acceleration (and centrifugal force) has a negligible effect in producing lateral velocity, v , and tire slip angles. The vehicle turns on a path whose center is determined by the intersections of perpendiculars from the front and rear wheel planes as shown in Figure 5.3. With the small angle assumption, the Ackermann Steer Angle is ℓ/R radians.

Even at this low speed, the vehicle is traveling on a curved path and there are slip angles induced by the curved path. It was demonstrated under the subsection titled "Ackermann Relationship—Neutral Steer" that in this turning situation the control moment due to the Ackermann Steer is just that required to overcome the yaw damping moment. Referring to Figure 5.3, the path curvature is $1/R$. This curvature times the wheelbase determines the steer angle since the front wheels are tangent to the path. The control moment is obtained by multiplying this product by the front cornering stiffness and the moment arm, ℓ , thus,

$$\delta N_\delta = \frac{1}{R} \ell C_F \ell = C_F \left(\frac{1}{R} \right) \ell^2 = C_F \left(\frac{r}{V} \right) \ell^2$$

where r is the yawing velocity.

The yaw damping moment comes from the front wheels. The slip angle at the front wheels is $-r\ell/V$ and the yaw damping is obtained by multiplying this by the cornering stiffness and the moment arm, thus,

$$r N_r = -C_F \left(\frac{r\ell}{V} \right) \ell = -C_F \left(\frac{r}{V} \right) \ell^2$$

$$\therefore \delta N_\delta = -r N_r$$

Tangent Speed

At low speed on a circle, the rear tires travel on a smaller radius than the front (track a smaller circle). As the speed is increased and side force and slip angles build up there

comes a point where the front and rear tires track on the same circle. The chassis centerline is tangent to the path and the vehicle slip angle, β , measured at the CG is zero. This speed is termed the *tangent speed*. Above this speed the rear wheels travel on a larger radius than the front and the vehicle assumes a "nose-in" attitude. The tangent speed is a function of the rear cornering stiffness, the vehicle mass, wheelbase, and CG location. For passenger cars it is generally between 25 and 35 mph. For race cars with high rear cornering stiffness and low mass it can be much higher. The concept of tangent speed is from Fred Dell'Amico in Ref. 40.

The general β response to control is given by Eq. (5.17):

$$\beta = \frac{\delta}{Q} (Y_\delta N_r - N_\delta (Y_r - mV))$$

From the lateral acceleration response to control, Eq. (5.16):

$$\delta = \frac{(V^2/R)Q}{V(Y_\beta N_\delta - N_\beta Y_\delta)}$$

Substituting (5.16) into (5.17) to eliminate δ gives, after rearrangement,

$$\beta = \frac{(V/R)[Y_\delta N_r - N_\delta (Y_r - mV)]}{V(Y_\beta N_\delta - N_\beta Y_\delta)}$$

At the tangent speed, $\beta = 0$. Since tangent speed (V_t) is higher than the Ackermann Speed, the only way to make the above equation equal to 0 is to set

$$Y_\delta N_r - N_\delta (Y_r - mV) = 0$$

Solving for V_t , the tangent speed is

$$V_t = \left(\frac{-1}{m} \right) \left(\frac{Y_\delta N_r}{N_\delta} - Y_r \right) = \left(\frac{-g}{W} \right) \left(\frac{Y_\delta N_r}{N_\delta} - Y_r \right) \quad (5.54)$$

A physical explanation of this relationship follows: Since $\beta = 0$, the only derivatives involved are those due to δ and r . The two moment derivatives are N_r and N_δ . The control moment equilibrates the resisting moment arising from the curved path, thus moment balance is

$$\delta N_\delta = -r N_r$$

The lateral force balance involves three terms: δY_δ , $r Y_r$, and the centrifugal force, CF . Neglecting signs, $CF + \delta Y_\delta + r Y_r$ must equal zero. Consider the first term in the bracket of Eq. (5.54):

$$\frac{Y_\delta N_r}{N_\delta} = Y_\delta \left(\frac{r N_r}{\delta N_\delta} \right) \left(\frac{\delta}{r} \right) = -Y_\delta \left(\frac{\delta}{r} \right)$$

Then

$$V_t = \left(\frac{-g}{W} \right) \left(Y_\delta \left(\frac{\delta}{r} \right) - Y_r \right) = \left(\frac{-g}{W r} \right) (\delta Y_\delta - r Y_r)$$

but

$$r = \frac{V_t}{R}$$

and

$$V_t = \left(\frac{-g R}{W V_t} \right) (\delta Y_\delta - r Y_r)$$

$$\left(\frac{W}{g} \right) \left(\frac{V_t^2}{R} \right) = -(\delta Y_\delta + r Y_r) = CF$$

If the relations for the derivatives for this simple vehicle (Eqs. (5.9)) are substituted into Eq. (5.54),

$$V_t = \sqrt{-\frac{\ell g b C_R}{W_a}} \quad (5.55)$$

where C_R is always negative.

The significance of tangent speed lies in its relationship to transient response time. The higher the tangent speed the shorter the lateral response time to 90% of steady-state following a step input. One way to show this is as follows: Eq. (5.55) can be rewritten as

$$V_t = \sqrt{-\frac{gbC_R}{W_a/\ell}} = \sqrt{-\frac{gb}{W_R/C_R}} = \sqrt{-\frac{b}{D_R}}$$

where D_R is the rear Bundorf compliance as defined by Eq. (5.53).

Bundorf has shown (in the paper referenced earlier) that for this simple model with a fixed value of the front cornering compliance, D_F , the lateral acceleration response time increases rapidly with an increase in D_R . A higher rear cornering compliance corresponds to a lower V_t .

Critical Speed

At the *critical speed* the car becomes divergent, that is, a small steering input results in very large (theoretically infinite) responses in terms of path curvature, $1/R$, yawing velocity, r , lateral acceleration, V^2/R , or vehicle slip angle, β . Eqs. (5.13) through (5.17) gave us the general control responses of our 2DF vehicle and may be used to investigate the critical speed. All of the responses may be made infinite by making Q (which appears in the denominator) zero. Let us examine the implications of making $Q = 0$.

$$Q = N_\beta Y_r - N_\beta m V - Y_\beta N_r = 0$$

Hence,

$$V = \frac{N_\beta Y_r - Y_\beta N_r}{N_\beta m}$$

But, Y_r and N_r are proportional to $1/V$, so we can write

$$V_{\text{Crit}}^2 = \frac{N_\beta (V Y_r) - Y_\beta (V N_r)}{N_\beta m}$$

$$V_{\text{Crit}} = \sqrt{\frac{N_\beta (V Y_r) - Y_\beta (V N_r)}{N_\beta m}} = \sqrt{\frac{-1}{K}} \quad (5.56)$$

A physical understanding of V_{Crit} follows.

Normally, $N_\beta Y_r$ is negligible compared to the other terms (since Y_r is small, particularly for any vehicle close to NS). Therefore

$$-N_\beta m V - Y_\beta N_r = 0 \quad (5.57)$$

The condition then for the responses to become infinite is that $-N_\beta m V$ added to $-Y_\beta N_r$ be zero. Can this occur for an US car? See Figure 5.23 where the individual terms are plotted against speed.

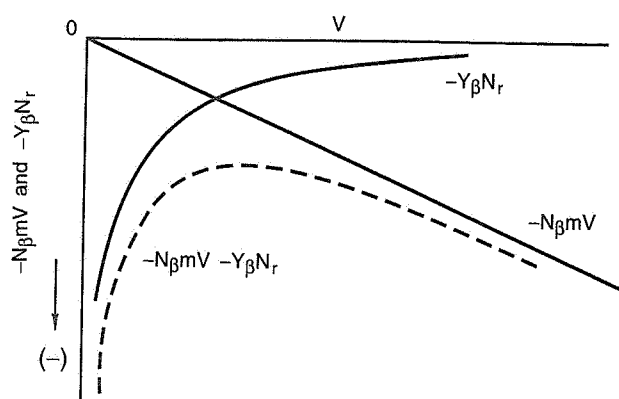


Figure 5.23 US speed relationships.

- For understeer, N_β is + which means that $-N_\beta mV$ will be negative and increase linearly with V .
- The term $-Y_\beta N_r$ will always be - (since Y_β and N_r are damping terms and always -) and it will decrease with V since $N_r \approx 1/V$.
- At zero V , $-Y_\beta N_r$ will be infinite as N_r is infinite.

The sum of $-N_\beta mV$ and $-Y_\beta N_r$ is obviously never 0, in fact it is always negative; thus the responses never become infinite and **there is no critical speed for an understeer car**.

For a neutral steer car, $-Y_\beta N_r$ has a finite value and $-N_\beta mV$ is 0 (in Eq. (5.57)) and their sum is finite. However $-Y_\beta N_r$ is approaching zero with increasing V (see Figure 5.23) so that it might be said that a critical speed exists for the NS car at infinite velocity. A neutral steer car **does not have a real critical speed** because of the damping in the system as represented by $Y_\beta N_r$.

Consider the oversteer automobile. In this case N_β is - and the term $-N_\beta mV$ is positive, and increases with velocity. The situation is depicted in Figure 5.24.

Here a critical speed is possible, at the velocity at which the two terms are equal. The damping term is decreasing because N_r is decreasing with speed, which is directly the result of the reduced slip angles which the tires experience for a given yawing velocity as the speed increases, i.e., the effectiveness of the tires as a yaw damper decreases.

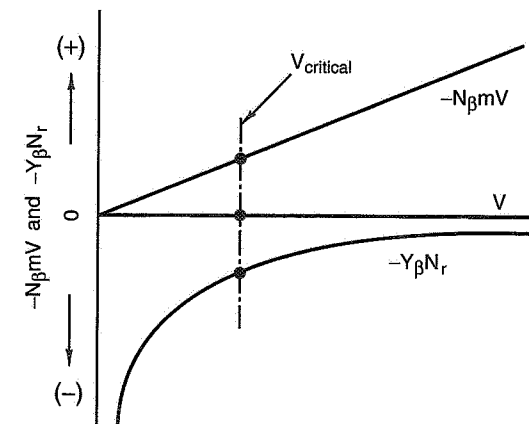


Figure 5.24 Critical speed relationships.

This simple analysis can be carried further to shed more light on the situation prevailing at the critical speed. From Eq. (5.57) we can write

$$-N_\beta mV = Y_\beta N_r = CN_r$$

or

$$-N_\beta = \left(\frac{C}{mV} \right) N_r \quad (5.58)$$

where $C = C_F + C_R$.

Now let us assume that this vehicle with fixed control (i.e., no steering input) and at the critical speed experiences a small disturbance which curves the path generating a centrifugal disturbing force at the CG. The sideslip response to such a force is given by Eq. (5.33) which is not only correct for a NS car but is approximately correct for a car with modest \pm values of N_β . Thus,

$$\frac{\beta}{F_y} = -\frac{1}{Y_\beta} = -\frac{1}{C}$$

or

$$C = -\frac{F_y}{\beta}$$

Substituting this into Eq. (5.58) gives

$$-N_\beta = -\left(\frac{F_y}{\beta mV}\right)N_r$$

or

$$-\beta N_\beta = -\left(\frac{F_y}{mV}\right)\left(\frac{r}{r}\right)N_r = -\left(\frac{F_y}{CF}\right)rN_r$$

but

$$\left(\frac{F_y}{CF}\right) = -1.0$$

and

$$\beta N_\beta = -rN_r \quad (5.59)$$

This says that at the critical speed the actual OS moment, βN_β is just equilibrated by the yaw damping moment, rN_r .

The above conclusion can be arrived at in another manner which may be of further help in visualizing the physical situation at the critical speed. We have noted in Figure 5.24 that one has a critical speed because the yaw damping is decreasing with speed while the static directional instability term is increasing. If a disturbance produces path curvature, the OS tends to increase the curvature and the yaw damping tends to prevent it. At the critical speed the effects are equal but at higher speed the OS predominates. Let's look at this from the standpoint of a skid pad test being run at the critical speed. The basic skid pad equation for the constant radius test is

$$\delta = \delta_{Acker} + (-\alpha_F + \alpha_R) \quad (5.50)$$

but

$$\delta_{Acker} = \frac{\ell}{R} = -r\left(\frac{N_r}{N_\delta}\right) \quad (5.60)$$

Also the steering angle required to counteract the oversteer effect as represented by $-(\alpha_F - \alpha_R)$ is given by

$$\delta_{OS}N_\delta = -\beta N_\beta$$

or

$$\delta_{OS} = -\beta\left(\frac{N_\beta}{N_\delta}\right) \quad (5.61)$$

Substituting Eqs. (5.60) and (5.61) into (5.50), and noting that at the critical speed the steer angle required is zero, gives

$$0 = -r\left(\frac{N_r}{N_\delta}\right) - \beta\left(\frac{N_\beta}{N_\delta}\right)$$

or

$$\beta N_\beta = -rN_r$$

which checks with Eq. (5.59).

Also, $\delta_{Acker} = (\alpha_F - \alpha_R)$ at the critical speed. The steer angle is equal to the Ackermann for neutral steer but equal to zero for the critical speed. At the critical speed the slip angle difference sustains the wheelbase or path curvature angle, i.e., the Ackermann.

Characteristic Speed

A characteristic speed has been proposed by General Motors as one way to measure the amount of understeer. We will first discuss it in terms of the steer equation.

For the constant throttle (constant speed) / variable radius test, Eq. (5.50) becomes

$$\delta = \left(\frac{\ell}{V^2}\right)\left(\frac{V^2}{R}\right) + (-\alpha_F + \alpha_R)$$

For two different speeds, the first (Ackermann) term plots as shown in Figure 5.25.

The second term, the slip angle difference, is independent of speed (when tire forces and vehicle parameters are speed independent) but varies linearly with lateral acceleration. The slope of the curve is a function of US as shown in Figure 5.26.

Now for any given amount of US there is some speed at which the δ_{Acker} will just equal the δ due to slip angle difference. This speed is called the *characteristic speed* and it is apparent that the more US there is, the lower this speed will be. The speed can then be taken as a measure of the amount of US (some North American passenger cars have a characteristic speed as low as 40 mph). At the characteristic speed the steer angle required is just twice the steer angle of a NS car at the same speed, since the NS car turns at the Ackermann steer angle.

To express these conclusions in derivative form, consider an US car and a NS car at the same speed and lateral acceleration. What is the moment balance in the US car at its characteristic speed? The control moment on the US car must be $2\delta_{Acker}N_\delta$. Since V^2/R

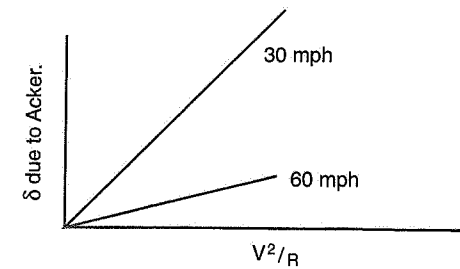


Figure 5.25 Ackermann term, constant throttle test.

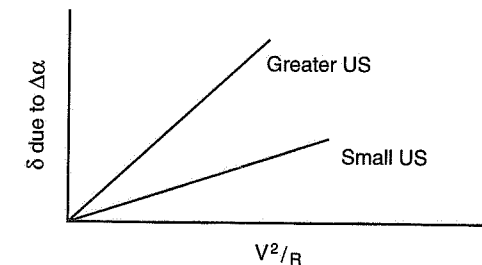


Figure 5.26 Slip angle difference term.

and V are the same for the two vehicles, the yawing velocity, r , and the yaw damping moment, rN_r , will be the same (this assumes the same N_r , although N_β is different). We know, however, that for the NS car,

$$\delta_{\text{Acker}} N_\delta = -rN_r$$

Hence, for the US car,

$$2\delta_{\text{Acker}} N_\delta = 2(-rN_r)$$

Since $-rN_r$ is the same on both cars, an additional moment $-\beta N_\beta$ must occur in the moment balance. Thus

$$2\delta_{\text{Acker}} N_\delta = -rN_r - \beta N_\beta$$

where $\beta N_\beta = rN_r$.

This says that at the characteristic speed for US, the understeer moment, βN_β , is numerically equal to the yaw damping moment. They are of the same sign and opposed to the control moment.

It is interesting to note that at the same speed and lateral acceleration, a change in sign of N_β to an oversteer moment produces a vehicle at its critical speed (see Eq. (5.59)) with a steer angle of zero. These relationships are summarized in Figure 5.27. The general expression for V_{Char} in terms of derivatives is

$$V_{\text{Char}} = \sqrt{\frac{-N_\beta(VY_r) + Y_\beta(VN_r)}{N_\beta m}} = \sqrt{\frac{1}{K}} \quad (5.62)$$

Figure 5.28 shows the yaw velocity response to control input. The response reaches a maximum for the US car at its characteristic speed. This response is one-half that of the comparable NS car at the same speed. It is also the speed at which the response of the OS car goes to infinity, its critical speed (where N_β is equal in magnitude but opposite in sign to the US car).

Condition	δ	Equilibrium equation	Sense of moments in RH turn
Characteristic speed for US	$2\delta_{\text{Acker}}$	$\delta N_\delta = -\beta N_\beta - rN_r$	$\beta N_\beta = rN_r$
NS	δ_{Acker}	$\delta N_\delta = -rN_r$ $N_\beta = 0$	$\beta N_\beta = 0$
Critical speed for OS	0	$\beta N_\beta = -rN_r$	$\delta N_\delta = 0$

Figure 5.27 Simple 2DF car, moment components.

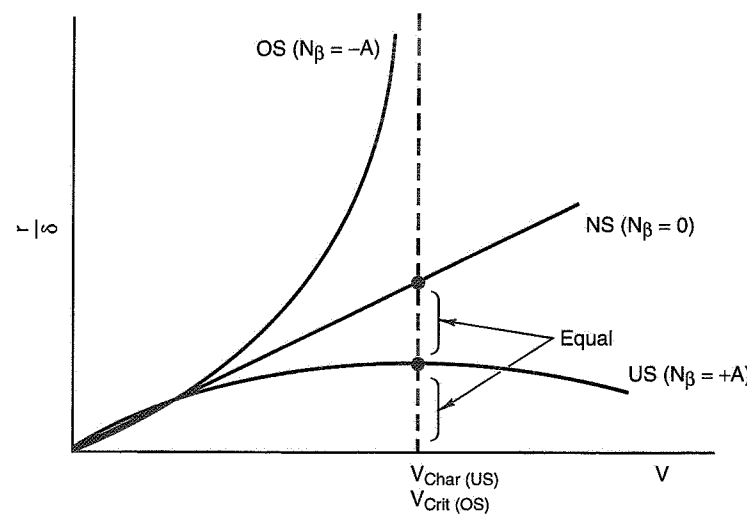


Figure 5.28 Yaw velocity response to control.

Stability Factor and Critical/Characteristic Speeds

The yaw velocity response to control in terms of K is given by Eq. (5.43):

$$\frac{r}{\delta} = \frac{V/\ell}{1 + KV^2}$$

At the critical speed this response is infinite and the denominator of Eq. (5.43) must be zero.

$$1 + KV^2 = 0$$

and

$$V_{\text{Crit}} = \sqrt{\frac{-1}{K}}$$

as noted earlier.

To find the speed at which r/δ is a maximum (characteristic speed for US), we write Eq. (5.43) as follows:

$$\frac{r}{\delta} = \frac{1/\ell}{1/V + KV}$$

The denominator now contains all the speed terms and should be minimized; let $f = 1/V + KV$.

$$\frac{df}{dV} = \frac{-1}{V^2} + K = 0 \quad \text{and} \quad \frac{1}{V^2} = K \quad \left(\text{or} \quad \frac{1}{V} = KV\right)$$

or

$$V_{\text{Char}} = \sqrt{\frac{1}{K}} \quad (5.63)$$

The function f is a minimum where $1/V = KV$ as shown in Figure 5.29. For engineering calculations, in terms of static margin:

$$V_{\text{Crit}} \text{ (or } V_{\text{Char}}) = \text{sgn(SM)} \times 3.87 \sqrt{\frac{I/C_F C_R/C}{W \times \text{SM}}} = \text{sgn(SM)} \times 3.87 \sqrt{\frac{C_0}{\text{SM}}} \ell, \text{ mph} \quad (5.64)$$

where $C_0 = \left(\frac{1}{W}\right)\left(\frac{C_F C_R}{C}\right)$, note that C_0 is a negative quantity.

The C's are in lb./radian and SM in fraction of the wheelbase, see page 225 for the sign convention of SM.

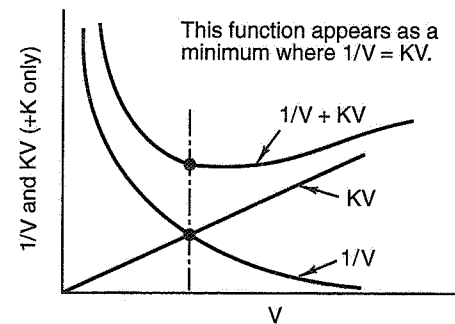


Figure 5.29 Minimizing $f = 1/V + KV$.

The Tire as a Damper—Analogy

There is an analogy (first suggested by A.G. Fonda, personal communication) which is useful in acquiring a further physical feel for the derivatives. In Figure 5.30, a simple tire is shown moving with a resultant velocity, V , at a slip angle, α .

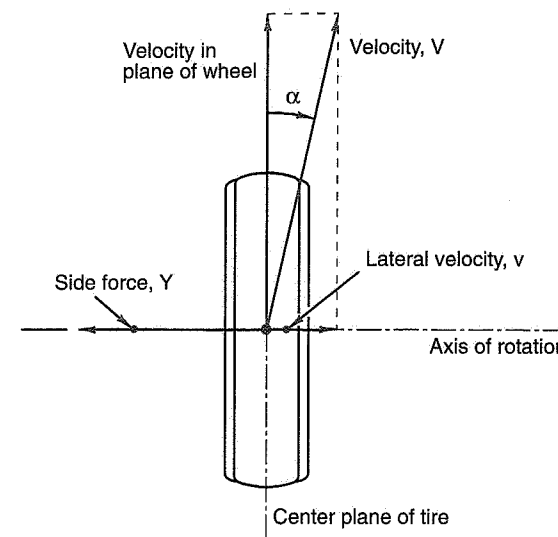


Figure 5.30 Tire lateral velocity and side force.

If the velocity in the plane of the wheel is assumed constant (a common assumption in stability and control analyses), the lateral velocity, v , is directly proportional to the slip angle, α . Thus the existence of a slip angle presupposes a lateral velocity (perpendicular to the wheel plane) or vice versa. Although it is common to use the variable, α , for side forces, lateral velocity, v , is probably more fundamental and more closely related to braked and powered wheels, as well as free rolling. The side force developed as the result of the lateral velocity is along the same line of action but in the opposite direction; the tire is behaving like a lateral hydraulic damper (shock absorber). For the small slip angle range,

$$Y = C_\alpha \alpha = C_\alpha \left(\frac{v}{V} \right) = \left(\frac{C_\alpha}{V} \right) v$$

where C_α is the tire cornering stiffness and (C_α/V) is the "damper" constant—the factor of proportionality between lateral velocity and lateral force.

This lateral damper may be visualized as replacing the tire (for lateral forces) by traveling along at the wheel speed relative to the ground with one end anchored to ground as is the moving tire patch. When a car is set in a turn with typical nosed-in attitude, it is easy to visualize the tires as "slipping" sidewise relative to the car centerline, acting as long continuous dampers with the road. Note that the "damper" constant decreases with forward speed, V .

Since $C_\alpha = \partial Y / \partial \beta$, the damper constant is the damping-in-sideslip derivative divided by the constant forward velocity, i.e.,

$$\left(\frac{1}{V} \right) \left(\frac{\partial Y}{\partial \beta} \right) = \frac{Y_\beta}{V}$$

Using the tire-damper analogy, we will now develop the concepts of damping center, damping-in-sideslip, and yaw damping.

Damping Center

Now consider our "bicycle" model subjected to an applied (external) side force from whatever cause, for example, an aerodynamic side force. Assume that the front and rear tires have different cornering stiffnesses, i.e., different lateral damper characteristics. Figure 5.31 represents the situation with the tires replaced by their analogous dampers.

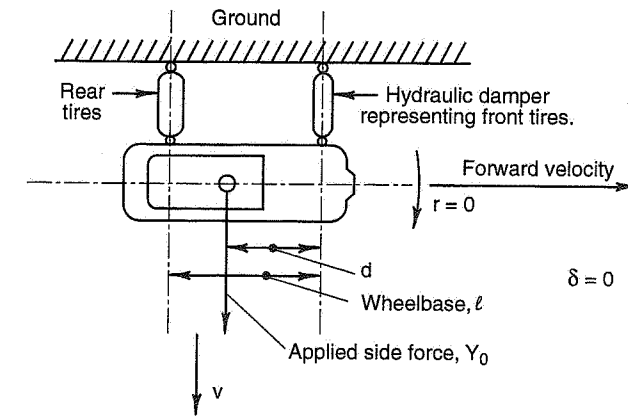


Figure 5.31 Tire damper side force—2DF automobile.

We wish to locate the position of the applied side force along the chassis which results in yaw moment trim ($\Sigma N = 0$) in a steady-state situation with $r = \delta = 0$. Let the applied side force be Y_0 and let its location for the above conditions be a distance, d , aft of the front axle. If the tires had equal damper constants and the applied side force was at the mid-wheelbase, no yawing moment would result. If the tires are of unequal damping constants, the point of application of the applied side force for zero yawing moment will be closer to the end of the stiffer tire damper. This point is found by taking moments, such that the moments of the F and R tire damper about this point are equal but of opposite

sign. This point is logically termed the *damping center*. The damping center is found as follows where Y_F and Y_R are the front and rear tire side forces, respectively:

$$Y_F d = Y_R (\ell - d) = Y_R \ell - Y_R d$$

or

$$d(Y_F + Y_R) = Y_R \ell$$

and

$$\frac{d}{\ell} = \frac{Y_R}{Y_F + Y_R} = \frac{(C_R/V)v_R}{(C_F/V)v_F + (C_R/V)v_R}$$

But since $v_R = v_F$, when $r = 0$,

$$\frac{d}{\ell} = \frac{C_R/V}{C/V} = \frac{Y_{\beta R}/V}{Y_{\beta F}/V} = \frac{\text{Rear Damper Constant}}{\text{Total Damper Constant}}$$

= Damping center location in fraction of wheelbase aft of the front axle

The damping center is analogous to the neutral steer point (NSP) derived earlier. Thus the static margin can be viewed as the distance between the damping center and the vehicle CG.

Damping-in-Sideslip

If the vehicle is pulled sideways by a force at the damping center (NSP), it will move directly sideways and an opposing force will be developed by the tires acting as "dampers." If the vehicle is moved sideways at a series of lateral velocities and the damping forces measured, a plot of the force vs. velocity may be constructed as in Figure 5.32.

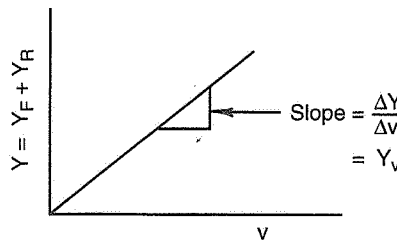


Figure 5.32 The damping-in-sideslip.

The slope of this curve, the effective lateral damping constant for the vehicle, is

$$\frac{\partial Y}{\partial v} = \frac{C}{V} = \frac{Y_v}{V}$$

vY_v denotes that part of the total side force on the vehicle arising from v . The damping-in-sideslip is always trying to reduce the lateral velocity of the car. This is the situation of a car on a tilted road. The reason the car achieves a steady sloping path down the road camber and does not continue to accelerate laterally under the action of the weight component ($W\phi$), is that slip angles, and hence opposing tire side forces, are developed. Using the damping-in-sideslip concept, one may say the lateral velocity of the car down the tilted road produces a lateral damping force which at some lateral velocity, v , equals the weight component ($W\phi$), where ϕ is the road tilt.

Damping-in-Yaw

The concept of yaw damping follows naturally from the tire-as-a-damper concept. Suppose a yawing moment, from a road or wind disturbance, is applied to a car and a yawing velocity about the CG results. The dampers representing the tires will react in opposite directions developing forces which in turn create moments about the CG opposing the yawing velocity. Since the damping effect is large in the nonskid regime, the yawing velocity will rapidly settle down to an equilibrium or steady-state value. Figure 5.33 depicts the yaw damping effect.

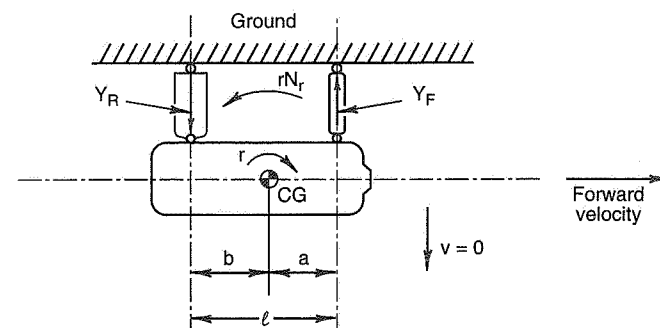


Figure 5.33 Damping-in-yaw.

As developed earlier, the damping-in-yaw can be written as

$$N = \left(\frac{\partial N}{\partial r} \right) r = rN_r = \left[\left(\frac{C_F}{V} \right) a^2 + \left(\frac{C_R}{V} \right) b^2 \right] r$$

In a steady turn, $r = V/R$ and the actual yaw damping moment is

$$\begin{aligned} N &= rN_r = \left(\frac{V}{R}\right) \left(\frac{1}{V}\right) (C_F a^2 + C_R b^2) = \left(\frac{1}{R}\right) (C_F a^2 + C_R b^2) \\ &= \left(\frac{gA_Y}{V^2}\right) (C_F a^2 + C_R b^2) \end{aligned}$$

For a turn of given lateral acceleration the yaw damping moment decreases as the velocity squared. N_r varies inversely with velocity and this holds true for the more complete model including the roll degree of freedom, compliances, camber, etc.

Note: In aeronautical circles it is customary to drop the term "derivative" and simply refer to N_r (for example) as the "yaw damping." Similarly, N_β and Y_β are the "static directional stability" and "lateral damping." It is understood that the actual moment or force is obtained by multiplying the derivative by the variable (for example, rN_r).

Generalized Yaw Moment

Using the "damper" analogy it is possible to work out (for the linear 2DF car) a single expression for the steady-state untrimmed yaw moment ($N \neq 0$). This is the yaw moment available for angularly accelerating the vehicle in maneuvers, thus,

$$\begin{aligned} N &= -\left(\frac{C_F C_R}{C_F + C_R}\right) \left(\frac{\ell}{V}\right) (v_\delta - v_{\ell/R} - V_{\alpha F} + V_{\alpha R}) \\ N &= -\left(\frac{C_F C_R}{C_F + C_R}\right) \ell (\delta - \ell/R - \alpha_F + \alpha_R) \\ N &= -\left(\frac{C_F C_R}{C_F + C_R}\right) \ell (\theta) \end{aligned}$$

where N = yawing moment

ℓ = wheelbase

V = vehicle velocity

v_δ = lateral velocity component at the front wheels due to steer angle, δ

$v_{\ell/R}$ = lateral velocity component at the front wheels due to the Ackermann angle, ℓ/R (the path curvature effect)

$V_{\alpha F}$ = lateral velocity component at the front wheels due to front slip angle, α_F

$v_{\alpha R}$ = lateral velocity component at the rear wheels due to rear slip angle, α_R
 θ = total effective steer angle

$C_F C_R \ell / (C_F + C_R)$ has the dimensions of a torsional spring constant (lb.-ft./rad.), which when multiplied by an effective steer angle (θ) gives the unbalanced yaw moment, N . Thus the vehicle appears to be acting like a torsional spring. This interpretation will be reinforced later in the dynamic analysis of this 2DF system. Referring back to the first equation above, one might interpret $C_F C_R / (C_F + C_R)$ as a damping constant of the front and rear tires acting as lateral dampers in parallel.

5.13 Static Stability and Control

Up to this point we have been analyzing an elementary automobile under linear steady-state equilibrium conditions in terms of (1) its geometrics/kinematics and (2) its steady-state response relationships using force/moment derivatives. With these tools we have reviewed a number of traditional concepts such as the Ackermann effects, over/understeer, neutral steer point, stability margin, stability factor, effective steer, cornering compliance and significant speeds. A consideration of the forces and moments which act on the automobile in a non-equilibrium, out-of-trim condition, leads to a conceptually new approach to automobile stability and control analysis, namely automobile *statics*. Automobile statics enables us to move into the nonlinear range of operation, and develop analytical tools which are simpler and more suitable for many design applications than the full dynamic analysis. Statics will be introduced in this section, but a comprehensive discussion of the technology is in Chapter 8, Force - Moment Analysis.

The traditional notions of car stability and control derive from proving ground tests, with emphasis on motion variables. The concepts of automobile statics, on the other hand, have their origins in aircraft wind tunnel testing and associated design procedures. The term *statics* implies that we are dealing with the unbalanced forces and moments available for stabilizing or maneuvering the vehicle. Thus in a wind tunnel test, the model is tested over a range of attitudes to the relative wind direction, and the forces and moments measured, without regard for those particular conditions where force/moment equilibrium exists. This procedure is also used in ship model basin testing and in the tire tester. In short, the force and moment producing capability of the device under test is being assessed. Statics technology refers to the use of these force/moment data in developing useful stability and control concepts, evaluations, and design procedures.

It is obvious that a complete description of automobile motions can only be obtained from the time solution of the dynamic equations. However, there is abundant evidence, from both aircraft and automotive experience, that satisfactory handling is usually assured if static requirements are met. High-performance aircraft are still basically designed and tailored by wind tunnel tests. The relatively high damping of the position control airplane and automobile tends to emphasize the importance of statics. In any event, satisfactory static behavior is a prerequisite to dynamic performance. Finally, successful

race car designers and tuners approach handling problems in static terms which are physically understandable; when these fail, more complex dynamic analysis may be required.

In the next sections we will examine some static control and stability concepts using the "bicycle" model. In order to relate these concepts to the previous material in this chapter, linear range examples will be used.

Static Directional Stability

Basically, the term *static stability* refers to the tendency of a system to return to a previously established equilibrium when disturbed. One cannot talk about stability without first having established the equilibrium or initial trim. The initial trim can be defined by the control position, a steady-state attitude or acceleration. Figure 5.34 illustrates some trim and stability situations for simple devices.

In Figure 5.34a(1), the three-sided solid is obviously in trim. If disturbed angularly as in a(2), it will, on release, return to the original trim of a(3). This tendency to return (the moment of the weight about one corner) is the static stability.

In Figure 5.34b, the same solid is disturbed to a larger angular position. The weight vector passes beyond the corner and if released the solid tends to go to another trim, i.e., to a trim different from the original trim. It appears that this solid possesses "static stability" with respect to more than one trim (there are three faces and three trim positions). The trim position it will return to depends on the magnitude of the disturbance. This multiple trim situation is shown only to illustrate that it is easy to confuse stability and trim. Thus in b with the amplitude disturbance shown, the solid is no longer stable with respect to the initial trim but it is "statically stable" with respect to another trim. This is a device in which the stability at trim is very large.

In Figure 5.34c(1) a roller is shown at trim. When the roller is disturbed to the position of c(2) the weight component tangent to the curved track gives the roller "static stability" with respect to the initial trim. If the roller is then released, it will not immediately return to trim but will, in all probability, "overshoot" as shown in c(3). After an oscillation or so, it will settle down at its initial trim. This illustrates what is referred to as *dynamic stability*; a device or system possesses dynamic stability if any oscillations that occur on approaching a trim are damped out (this also includes the case where the damping effect is so great that no oscillation occurs). If the roller has zero effective damping then it will oscillate indefinitely. If the oscillations should increase in amplitude (as they may in certain coupled systems) the system is "dynamically unstable." The question of dynamic stability or instability cannot arise unless the system is first "statically" stable with a tendency to return to some trim.

In Figure 5.34d, three examples are presented of devices which possess "static instability," i.e., any disturbance will result in a divergence. In each case, a precarious trim ini-

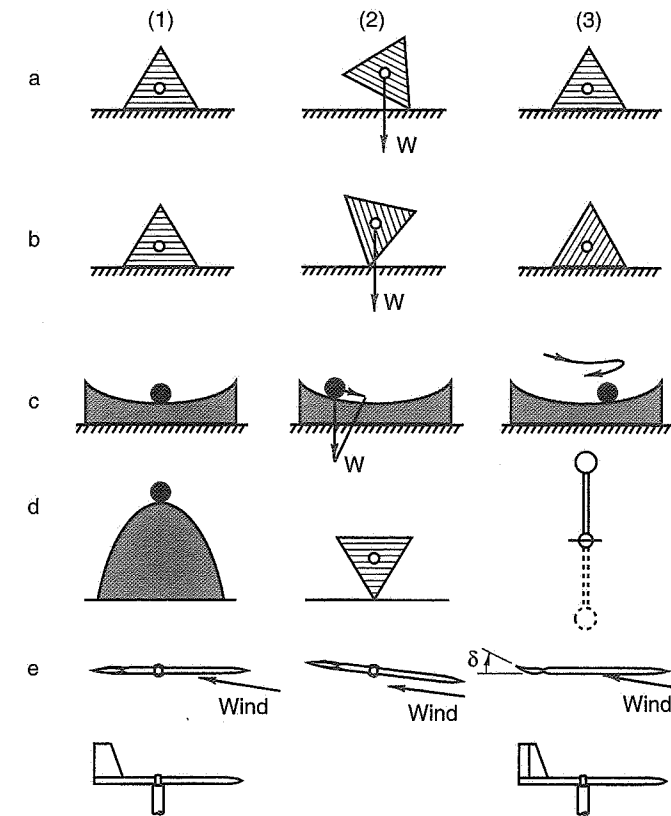


Figure 5.34 Trim and stability.

tially exists (this is called an "unstable trim") from which, if the smallest disturbance occurs, the device will diverge indefinitely or until it arrives at some stable trim.

In Figure 5.34e, we have a weather vane initially at an angle to the wind. Upon release it aligns itself (achieves a stable trim) with the wind, probably with very little overshoot since the restoring moment in relation to the aerodynamic damping effect is generally small. Here we have a situation in which static stability and trim exist in relation to the relative wind which is constantly shifting in relation to compass heading, i.e., an earth-oriented reference. By installing a "rudder" or movable surface on the vane it is possible to change the trim position relative to earth axes. In e(3) this adjustable surface has been moved to the angle δ and the vane is now made to trim (re: earth axes) in an untrimmed position of the first figure. This illustrates the possibility of having movable elements in

a device for adjusting the trim (example: trim tabs on airplanes). It also illustrates the close relationship between “trim” and “control”; they are the same type of thing but differ in their operational functionality.²⁷

Returning to the elementary automobile, let us assume it is initially traveling down a flat, straight road under a no-wind condition. The steering control is set at $\delta = 0$ and the path and the heading of the car are aligned with the road. This is the *trim condition*. Now, assume the car strikes a momentary bump in the road such that its heading (i.e., the angle between the centerline of the car and the centerline of the road) is no longer zero. Take as an “initial condition” the situation where the car has just left the bump (disturbance) and finds itself at an angle β to the road centerline. We will now examine the behavior of neutral, understeer, and oversteer cars starting from this “initial condition.” (Note: The steering angle δ remains fixed at 0, at the trim position prior to the bump.) The “initial condition” for the NS car is shown in Figure 5.35.

In the situation shown, the front and rear slip angles are the same and equal to β . These slip angles produce Y_F and Y_R which also are equal. The total tire side force ($Y_F + Y_R$) accelerates the vehicle laterally to the right with a magnitude $A_Y = a_y/g = (Y_F + Y_R)/W$. We may treat this situation as a quasi-static one by applying d’Alembert’s Principle in which the system is placed in lateral force equilibrium by applying an inertia force, $W \times A_Y$, at the CG and in the opposite direction to A_Y . This force is shown acting to the left in Figure 5.35. Let us now examine the directional moment equilibrium by taking moments about any point such as the CG or one of the axles. It is found that the system is in moment equilibrium: no tendency exists to rotate the vehicle in a direction of increasing or decreasing β . In accordance with the idea of “static stability” as developed with Figure 5.34, the car of Figure 5.35 exhibits neutral static stability in the angular (vehicle slip angle) variable β with respect to its initial trim of $\beta = 0$. The car is indifferent as regards β and will stay at whatever vehicle slip angle to which it is disturbed. In an actual vehicle in this situation on the road the path will not remain parallel to the centerline of the road but will move off at a slight angle to the right under the action of the tire side forces. However, if one takes a NS vehicle on ice and throws it into a yawed condition (i.e., $\beta \neq 0$) and then rapidly moves the control back to $\delta = 0$, the vehicle will travel on a straight path close to its original path with no tendency for β to change.

In the above example, it is shown that a simple vehicle with **neutral steer characteristics** also exhibits **neutral static stability characteristics**, i.e., any tendency to return toward an initial trim is lacking. Since β is the vehicle slip angle, a neutral steer vehicle can now be seen as one which develops no yawing moments to reduce β to 0 or to some other β trim. If N represents an unbalanced yawing moment which arises when the vehicle is disturbed in β , the condition for neutral stability (or neutral steer) is that $\Delta N/\Delta\beta = 0$. The vehicle reacts like the weather vane of Figure 5.34(e) with an additional forward “tail” on it. It would then be indifferent to the wind angle. Similarly, the neutral stability

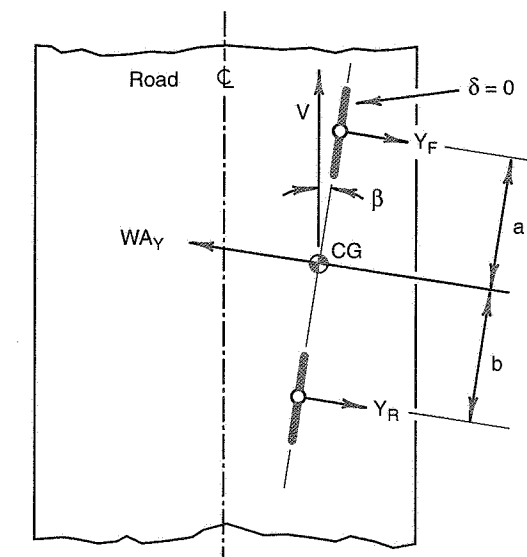


Figure 5.35 NS car directionally disturbed.

car is indifferent to vehicle slip angle and shows no tendency to “weathercock”—to try to align the vehicle centerline with the direction of motion.

Figure 5.36 shows an US car with the same “initial condition” as for the NS case.

In this vehicle, the front and rear cornering stiffnesses are adjusted to be the same and the CG is placed 1/3 of the wheelbase aft of the front axle ($a = b/2$). Due to the disturbed β , the slip angles front and rear will again be β and the side forces, Y_F and Y_R , will be equal and the same as before. However, an unbalanced yaw moment exists, thus,

$$N = aY_F - bY_R$$

The sign convention shown in Figure 5.36 was used in writing down this equation. Since $Y_F = Y_R$ and since $b = 2a$, it is apparent that $-bY_R$ dominates and the unbalanced moment, N , is negative or in a direction to try to rotate the vehicle to reduce the initial β disturbance. This vehicle with **understeering characteristics in a steady turn** exhibits a **stable static stability characteristic**. It “weathercocks” in a direction to reduce vehicle slip angle; its behavior is analogous to the simple weather vane of Figure 5.34. If such a vehicle is thrown into a slide (most easily demonstrated on a low-coefficient surface), it tries to reduce its slip angle and align itself with the direction of motion. If it were possible to place this vehicle at a series of vehicle slip angles, β , and measure the unbalanced

²⁷ The steering wheel on an automobile performs both a “trim” and “control” function.

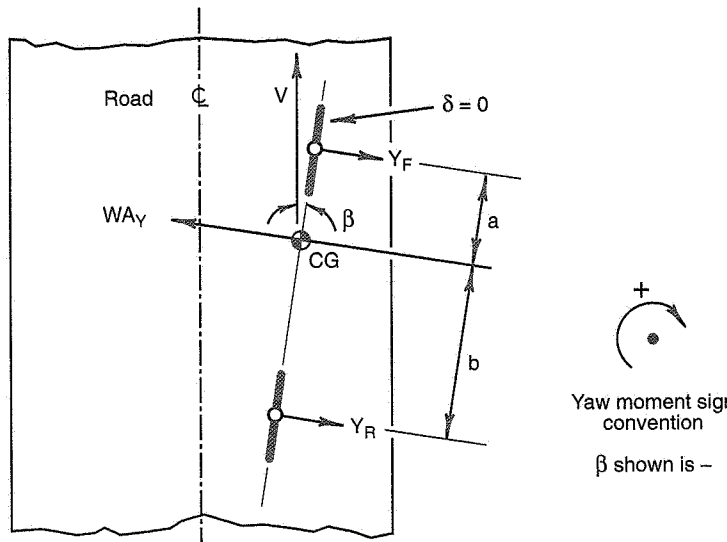


Figure 5.36 US car directionally disturbed.

yawing moment, one would obtain (in the linear tire range) the curve of Figure 5.37 (sign conventions as for Figure 5.36).

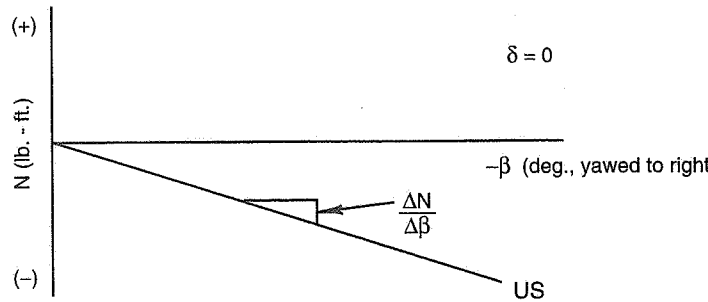


Figure 5.37 Static stability curve for US car.

The slope $\Delta N / \Delta \beta$ is negative by these sign conventions for the US car and the magnitude of the slope is a measure of the amount of US or static directional stability. Since $\delta = 0$ the vehicle is trimmed at $\beta = 0$, where the unbalanced moment, N , is zero (by definition the moment is zero at trim). $N = 0$ is the most general condition for trim of an automobile.

This way of looking at US is comparable to the measurement of aircraft stability in a wind tunnel (as noted earlier, the terminology "static stability" comes from that source), although in the aircraft case the moments arise from aerodynamic forces (instead of tire forces). The model is yawed through a series of angles and the moments are measured and plotted. If the plot of these unbalanced aerodynamic moments indicates the model has a restoring tendency, it is said to have "static directional stability."

The OS case is illustrated in Figure 5.38. In this case, it is apparent that the balance of moments tends to increase β . If moments are taken about the CG, $+aY_F$ is numerically greater than $-bY_R$ and the car tries to rotate to the right. If the unbalanced yawing moment were measured for a series of vehicle slip angles, β , the curve would have a positive slope; $\Delta N / \Delta \beta$ would be +.

In summary, the yaw moment behavior for the NS, US, and OS cars is given in Figure 5.39.

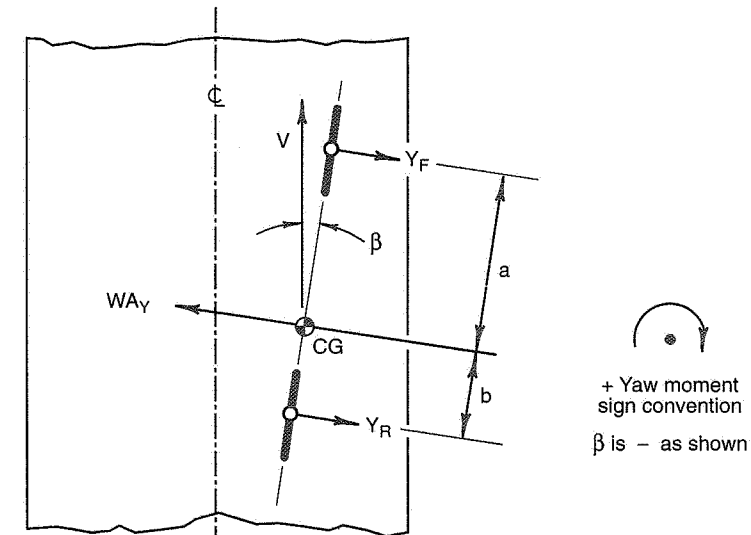


Figure 5.38 OS car directionally disturbed.

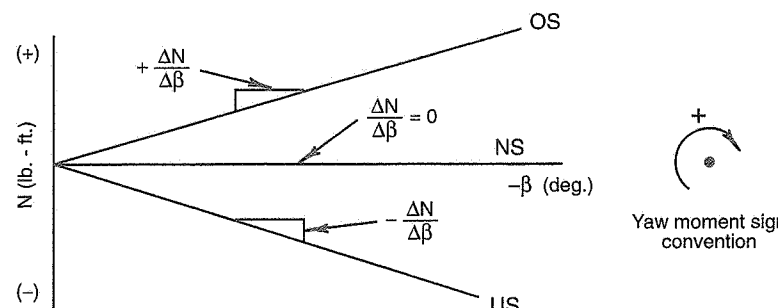
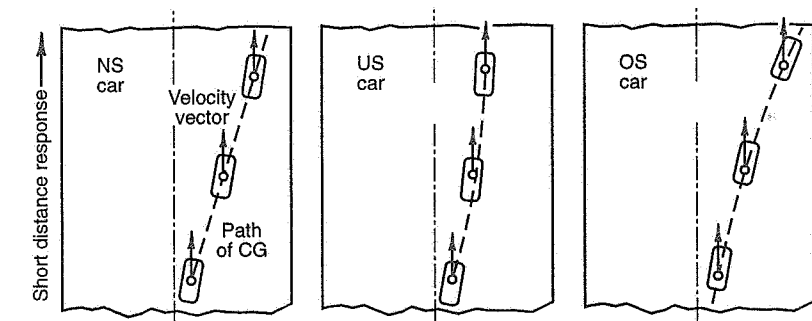


Figure 5.39 Static directional stability.

It has been shown that there is a correspondence between the steering characteristics of automobiles in steady turns and their directional restoring tendency when disturbed in β . This latter tendency, referred to as "static stability," is a necessary condition to complete dynamic directional stability, and can be measured by the slope of the unbalanced yaw moment curve. In the case of the steering characteristics and the moment characteristics steady-state conditions exist.

In the examples shown of the moment approach, resort was made to certain artificialities in order to isolate the effect of interest; thus d'Alembert's Principle was utilized to place the car in lateral force equilibrium so that the yaw equilibrium could be examined alone. Furthermore, quasi-steady conditions were assumed in a situation which in reality would be changing with time. If one were to take the NS, US, and OS vehicles discussed above and examine their more nearly actual behavior following the road bump disturbance, their paths and attitudes would be qualitatively as shown in Figure 5.40. In actuality the behavior depicted in Figure 5.40 is not exactly what occurs on the real automobile. While the vehicle slip angle tends to change in the manner suggested and the paths do bend off to the right, powerful tire damping factors enter which modify these pictures considerably.

There is a very important point that can be drawn from Figure 5.40, namely, that when the disturbance is over and steady-state has been restored, the car will not be traveling on the road center line nor headed in that direction. There is nothing in the car which knows the compass heading of a given road. When one talks "stability" of an automobile, one is really talking about the tendencies and abilities of the car to reduce its slip angle (or side force or lateral acceleration) to some trim value, usually zero. This is one reason why car "stability" is confusing. It does not necessarily help in maintaining a course down a road and, as we have already noted, an excess of US tends to make a car run down the camber (of a tilted road). However, passenger vehicle experience indicates that it is desirable to have some inherent tendency in the vehicle toward maintaining the resultant velocity vector in the longitudinal plane of the vehicle.



Note: Vehicle size relative to road is scaled down for convenience in showing behavior.

Figure 5.40 Motions of cars following a disturbance in vehicle slip angle, on a flat road.

Static stability arises from the balance of the yawing moments on the car due to vehicle slip angle. The forces and moments from the rear track are stabilizing (analogous to the vertical tail on an airplane or weather vane) whereas the front track forces and moments are destabilizing. This is why, in part, that a car becomes unstable when a rear tire blows and the cornering stiffness at that end of the vehicle is reduced. If both tires blew out on the front, the vehicle would become very US. When only one tire blows out on the front, the car also becomes more US but a still more prominent effect from the driver's standpoint may be the trim change occurring in the steering system (due to aligning torque effects). If the rear wheels are spun on ice (through excessive driving torque), the static directional stability, as well as some damping effects, are drastically reduced and the car becomes OS and unstable. If the brakes are locked up on the front, the side force vs. slip angle slope of the front tires approaches zero, the destabilizing effect of the front track is reduced, and the vehicle plows ahead in a very stable, understeering condition. This is an example of extreme stability which may not be so desirable if one is engaged in an avoidance maneuver.

Static Directional Control

Static directional control is the control moment on the vehicle as a result of steering the front wheels. Figure 5.41 illustrates this with the simple "bicycle" model.

Assume the vehicle is moving down the road at velocity, V , and the front wheels are rapidly moved to a steer angle, δ_1 . The situation shown in Figure 5.41 could exist momentarily if δ_1 were applied rapidly enough (step input). It could also exist if the vehicle were put in equilibrium with a d'Alembert force and moment. In either event, the front tire side force creates a control moment about the vehicle CG of

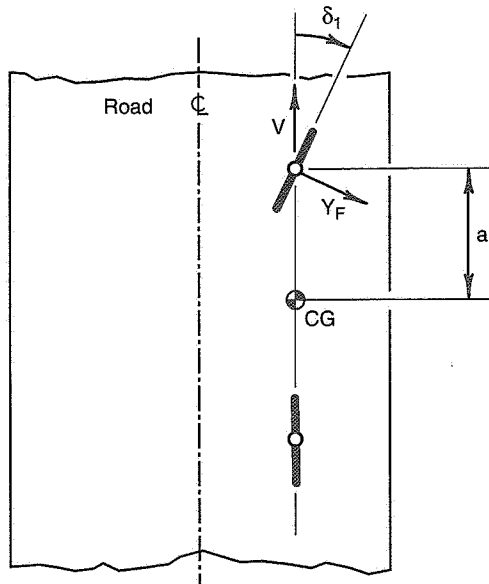


Figure 5.41 Steering control moment.

$$N_{\text{control}} = Y_F \cos \delta_1 \times a$$

or for small angles,

$$N_{\text{control}} = Y_F a = \left(\frac{\Delta Y_F}{\Delta \alpha} \right) \delta_1 a = C_F \delta_1 a$$

where C_F is the cornering stiffness of the front tires.

Since, as noted earlier, it is possible in linear systems to add the effects of the separate variables (the principle of superposition), let us add this control action to the static stability curve for the US car of Figure 5.37. The result is shown in Figure 5.42.

The effect of the constant control moment for this simple linear vehicle is to move the stability curve up by an amount of the control moment. The control action will ultimately result (as the vehicle rotates due to the control moment) in a new β trim, β_1 . The path by which it gets there is sketched on the figure. What happens is that as the vehicle rotates, both the control and stability moments are acting on the vehicle and at β_1 they become equal and opposite. The stability moment tries to reduce β and the control moment

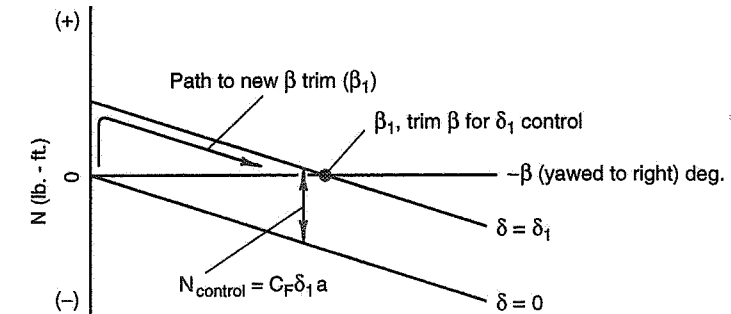


Figure 5.42 Static stability and control, US car, constant speed.

increases it. This is a simple example of the interaction of stability and control moment components.

5.14 Steady-State Path Curvature Stiffness

There is another effect which produces a large yawing moment component on the car. This effect can be described geometrically as a path curvature stiffness.²⁸ In any steady turning situation where a centrifugal force is present, the vehicle is on a curved path. When the vehicle is placed on this curved path (with $\delta = \beta = 0$, since interest is in the effect of path curvature only—justified in the linear, superposition context), there are “curve-induced” slip angles at the front and rear wheels as shown in Figure 5.43.

These slip angles produce lateral forces in the direction shown which in turn produce a moment about the CG tending to turn the vehicle out of the curved path. This moment is

$$N_{1/R} = Y_F \times a + Y_R \times b = C_F \alpha_F \times a + C_R \alpha_R \times b$$

where $1/R$ is the path curvature.

The moment, $N_{1/R}$, can be shown to be inversely proportional to the turn radius R . That is, the tighter the turn the larger $N_{1/R}$. The units of $N_{1/R}$ are lb.-ft. per $1/R$, hence the term *path curvature stiffness*; to stay on path there has to be a moment due to δ of $\delta C_F a$ in the positive direction to equilibrate the path curvature stiffness.

If one has ever tried to push a car or even a rubber-tired model around a curved path without steering, the magnitude of this moment can be appreciated. In F/M terms this is

²⁸ This was first defined in this terminology by Fred Dell'Amico in Ref. 40.

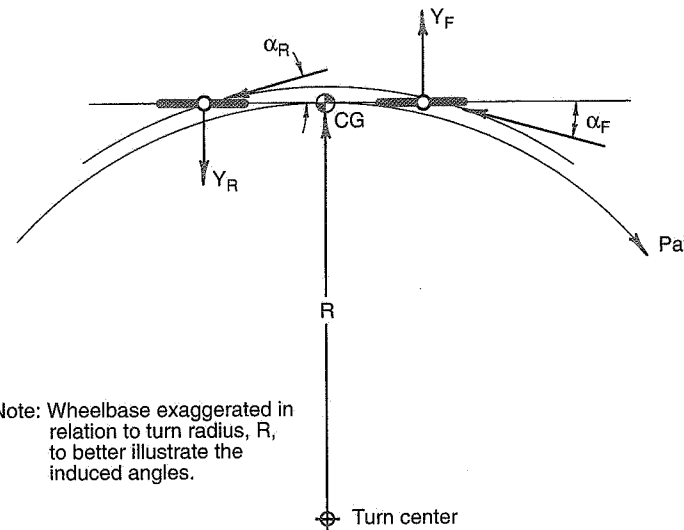


Figure 5.43 Slip angles induced by path curvature, vehicle at $\beta = \delta = 0$.

exactly the moment that must be overcome by the Ackermann steering which produces a counteracting moment in the opposite direction.²⁹ In Figure 5.44, the vehicle is oriented on a turning circle of radius R such that its centerline is tangent to the circle at the rear wheel (rear slip angle = 0) and the rear wheel produces no lateral force or moment. The front wheel is set at the Ackermann and produces all of the control yawing moment, namely $Y_F \cos \delta \times \ell$, or for small angles, $Y_F \ell$. This equals the path curvature stiffness moment.

Yaw Damping

Apart from its relationship to the Ackermann angle, the yaw damping produces the largest stabilizing moment on the vehicle in a steady turn or disturbance. It also accounts for the decrease experienced in directional stability as the speed is increased. This important concept is developed in simple terms below, referring to Figure 5.45.

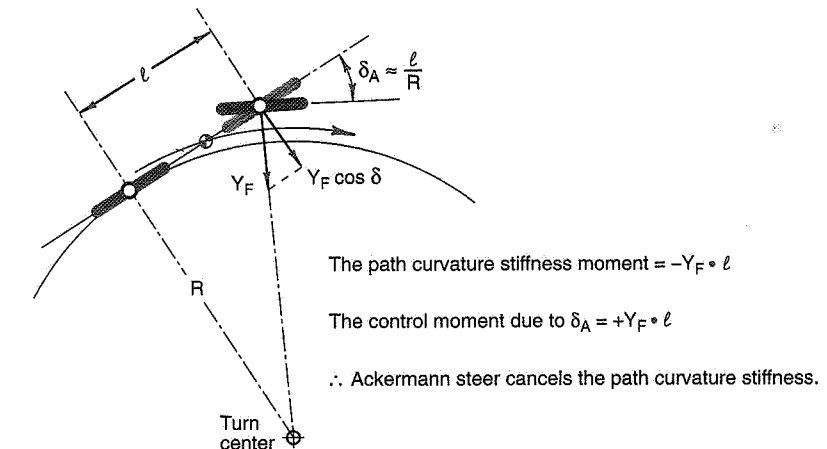


Figure 5.44 Yaw moment due to Ackermann steer angle.

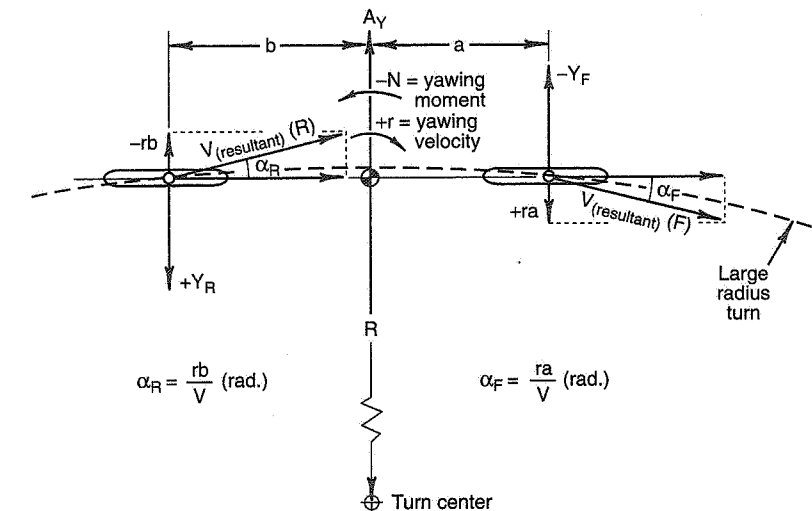


Figure 5.45 Path curvature stiffness and yaw damping.

²⁹ First pointed out by David Whitcomb in Ref. 92.

The vehicle is in a steady turn at a constant V and A_Y . Thus r is also constant since

$$r = \frac{V}{R} = A_Y \left(\frac{g}{V} \right)$$

where r is in radians/sec.

The yawing velocity produces lateral velocities at the front and rear wheels of $+ra$ and $-rb$, respectively. The vector addition of these lateral velocities with forward velocity, V , results in induced slip angles at the front and rear of α_F and α_R , as shown in Figure 5.45. These in turn give rise to $-Y_F$ and $+Y_R$, lateral forces at the wheels. Together they produce the negative yawing moment, N :

$$-N = Y_F a + Y_R b = C_F \alpha_F a + C_R \alpha_R b$$

$$-N = \frac{C_F r a^2}{V} + \frac{C_R r b^2}{V} = \frac{r}{V} (C_F a^2 + C_R b^2)$$

$$N = \left(\frac{\Delta N}{\Delta r} \right) r = \frac{-r(C_F a^2 + C_R b^2)}{V}$$

This moment tends to decrease any yawing velocity, r . It is analogous to a rotational dashpot (damper). It increases with a^2 and b^2 and with the cornering stiffnesses, C_F and C_R . Also it decreases with forward velocity, V . In line with aircraft practice it is called *yaw damping* and defined as $\Delta N/\Delta r$, the rate of change of moment with yawing velocity. In steady-state, it is equivalent to the path curvature stiffness.

Stability Index

In Figure 5.42, the static stability moment, $(\Delta N/\Delta \beta)\beta$, and the control moment, $(\Delta N/\Delta \delta)\delta$, were plotted on a single diagram of N vs. β . The vehicle was assumed to be moving along a straight path at various β with two positions of the steering control $\delta = 0$ and δ_1 . By replotted this diagram against lateral acceleration, A_Y , for curved paths, it is possible to add in the moment, $N_r r$, the yaw damping effect. The diagram could be plotted for a constant forward speed, V . At each lateral acceleration, there is a yawing velocity, $r = (A_Y \times g)/V = A_Y \times \text{constant}$, which gives rise to the moment component $(\Delta N/\Delta r)r = N_r r$. Such a plot is shown in Figure 5.46.

The total moment, N , is now comprised of three parts: that due to β (UO), that due to δ (control), and that due to r (yawing damping or path curvature stiffness).

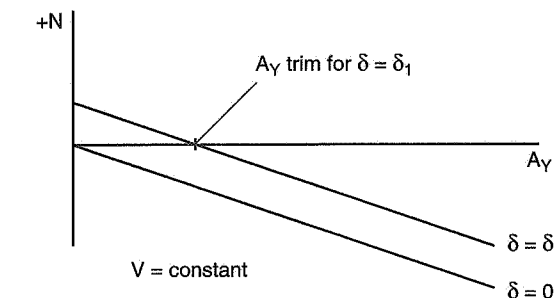


Figure 5.46 Static stability, control, and yaw damping.

With the addition of constant β lines in Figure 5.46 and additional δ lines to cover the operating range, this figure is the basic $N-A_Y$ diagram of the Moment Method referenced in Chapter 8. Whereas the slope of the δ lines in Figure 5.42 are $\Delta N/\Delta \beta$, a measure of static directional stability (UO), the slope of the lines in Figure 5.46 are the sum of the effects $\Delta N/\Delta \beta$ and $\Delta N/\Delta r$. This latter slope is referred to as the *stability index* (SI).

The SI is an absolute measure of the total steady-state directional stability when A_Y is taken as the operating variable. In the linear range it is usually expressed in nondimensional terms, thus,

$$\begin{aligned} SI &= \left(\frac{dN}{dA_Y} \right) \left(\frac{1}{W\ell} \right) = \left(\frac{dC_N}{dA_Y} \right) = \left(\frac{W}{C} \right) \left(\frac{\partial C_N}{\partial \beta} \right) + \left(\frac{g}{V} \right) \left(\frac{\partial C_N}{\partial r} \right) \\ &= \left(\frac{W}{C} \right) C_{N_\beta} + \left(\frac{g}{V} \right) C_{N_r} \end{aligned} \quad (5.65)$$

where C_{N_β} = Static stability derivative (UO) in nondimensional form ($C_N = N/W\ell$)
 C_{N_r} = Yaw damping derivative
 C = Total cornering stiffness
 W = Vehicle weight
 A_Y = lateral acceleration in "g" units

The condition $SM = 0$ (or $C_{N_\beta} = 0$) determines the boundary between under/oversteer. The condition $SI = 0$ (or $V = V_{\text{Crit}}$) determines the boundary between maneuver stability and divergent instability. The characteristic speed (V_{Char}) is the speed at which the stability index is twice the static margin, $SI = 2(SM)$.

Automotive vs. Aircraft Practice

There are direct analogies between automobile and aircraft stability and control concepts as tabulated below:

<u>Automobiles</u>	<u>Aircraft</u>
Neutral steer point	Fixed control neutral point
Static margin	Fixed control static margin
Critical speed	Fixed control maneuver point
Stability index	Fixed control maneuver margin

The concepts of free or force control, static and maneuver stability as used for aircraft have yet to be precisely defined for automobiles.

Ref. 93, by Milliken, Dell'Amico, and Rice, 1976, introduced the application of static concepts to the automobile. In this form of the MRA Moment Method, these concepts are being increasingly used in passenger and racing car design and analysis. For those interested in acquiring a broader knowledge of vehicle statics, we can also recommend several aeronautical texts: Ref. 66 is a highly concise yet comprehensive presentation and is highly recommended. Ref. 115 is a comprehensive presentation of longitudinal and directional statics as practiced in aeronautical engineering circles. Ref. 43 is a comprehensive coverage of aircraft statics, stability derivatives and advanced aspects of airplane stability and control. A substantial part of other standard texts on aircraft stability and control is also devoted to statics.

Static Margin, C_0 Presentation

Fred Dell'Amico in Ref. 40 has taken a slightly different approach to solving the linear two-degree-of-freedom steady-state Eqs. (5.5) and (5.6). These equations represent the unbalanced force and moment acting on the vehicle (from the tires) in the generalized out-of-trim case. This approach nicely shows the variation of static stability with speed.

It is convenient first to normalize N by dividing (5.6) by $W\ell$ and to normalize Y by dividing (5.5) by W. The quantities $C_N = N/W\ell$ and $C_Y = Y/W$ are then nondimensionalized yaw moment and side force coefficients.

With this change, one can solve for β in (5.5) and insert its value in (5.6). The following is obtained, after some manipulation:

$$C_N = -SM C_Y + \frac{C_F C_R}{(C_F + C_R)W} \left(\frac{r\ell}{V} \right) - \frac{C_F C_R}{(C_F + C_R)W} \delta \quad (5.66)$$

where SM is the 2DF static margin, given by $\frac{bC_R - aC_F}{\ell(C_F + C_R)}$.

Assume next that the total side force produced by the tires (Y) is always equal to the centripetal acceleration force, mVr . C_Y is then equivalent to the lateral (centripetal) acceleration in units of g, denoted A_Y , and yaw rate, r, is a dependent variable given by

$$Y = \left(\frac{W}{g} \right) Vr ; \quad r = \left(\frac{Y}{W} \right) \left(\frac{g}{V} \right) = C_Y \left(\frac{g}{V} \right) = A_Y \left(\frac{g}{V} \right)$$

Also letting

$$\frac{C_F C_R}{(C_F + C_R)W} = C_0 \quad (5.66a)$$

and substituting for r, Eq. (5.66) becomes

$$C_N = -SM A_Y + C_0 \left(\frac{\ell g}{V^2} \right) A_Y - C_0 \delta \quad (5.67)$$

Eq. (5.67) is the fundamental C_N - A_Y relationship. For a given speed, V, A_Y , and δ can be thought of as the independent variables, and C_N the dependent variable.

A plot of Eq. (5.67), in which δ is fixed at some arbitrary value and the condition that $Y = mVr$ is met by varying β , is shown in Figure 5.47. Each point on the curve of the figure is associated with a value of β which can be found by inserting the C_N - A_Y coordinates in the normalized version of Eq. (5.6), with the above substitutions and definitions, and solving for β . That expression is

$$C_N = -SM \left(\frac{C_F + C_R}{W} \right) \beta + \left(\frac{gN_r}{W\ell V} \right) A_Y - \left(\frac{aC_F}{W\ell} \right) \delta$$

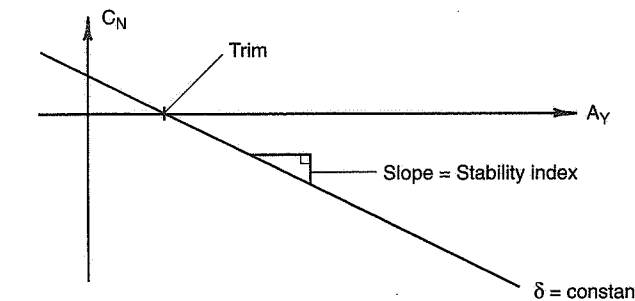


Figure 5.47 Stability plot: C_N - A_Y with constant V and constant δ .

Variation of Stability Index with V

Since V and the static margin appear explicitly in Eq. (5.67), it is possible to explore the C_N - A_Y plot as a function of V as well as of SM , remembering that $SM = 0$, $SM > 0$, and $SM < 0$ correspond to the neutral steer (NS), understeer (US), and oversteer (OS) car, respectively.

(a) The Neutral Steer Car

For the neutral steer car, $SM = 0$ and Eq. (5.67) becomes

$$C_N = C_0 \left(\frac{\ell g}{V^2} \right) A_Y - C_0 \delta$$

To clearly see the influence of velocity on stability, we can let $\delta = 0$ as in Figure 5.48. The C_N - A_Y plot shows that the neutral steer car is stable at all speeds, that its lateral-directional stability decreases as the speed is increased, and that it approaches neutral stability at very high speed.

(b) The Understeer Car

For the understeer car, $SM > 0$ and Eq. (5.67) applies as it is. Figure 5.49 shows the influence of velocity on stability (as before, $\delta = 0$). For the US case, the various parameters are

$$SI = \left(\frac{\partial C_N}{\partial A_Y} \right)_{\delta=\text{constant}} = -SM + C_0 \left(\frac{\ell g}{V^2} \right) \quad (5.68)$$

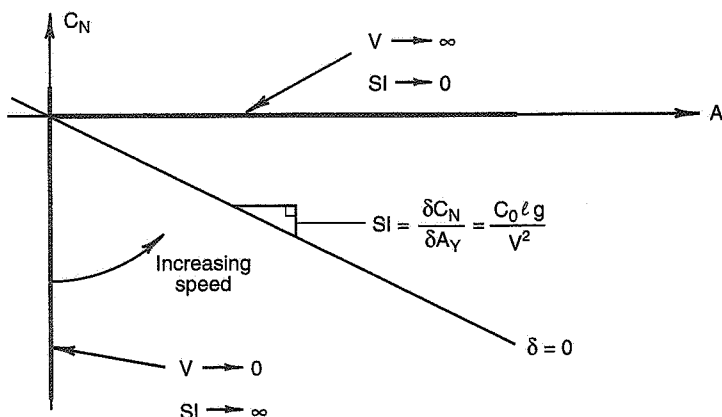


Figure 5.48 Stability plot: C_N - A_Y ; $\delta = 0$; neutral steer car.

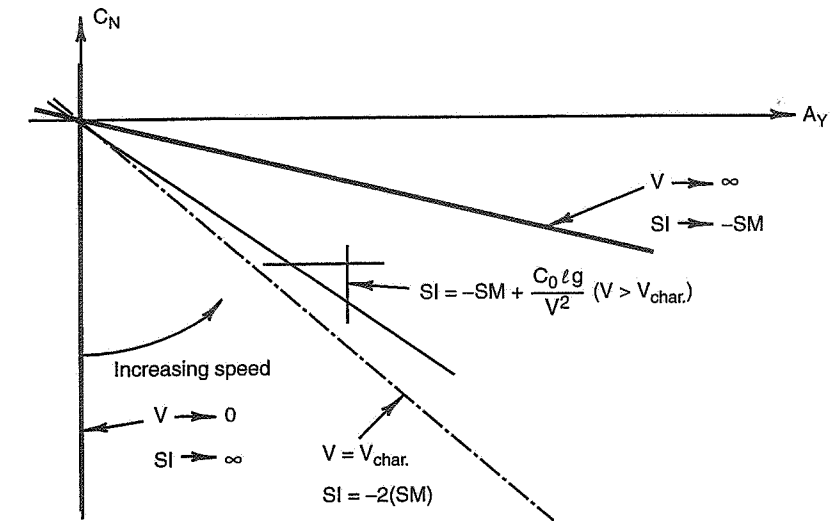


Figure 5.49 Stability plot: C_N - A_Y ; $\delta = 0$; understeer car.

Since characteristic speed is that speed at which the steer angle of an US car is twice the steer angle of a NS car (i.e., twice the Ackermann angle), it can be shown that

$$SI = -SM + \left(\frac{C_0 \ell g}{\ell g (C_0 / SM)} \right) = -2SM$$

This relationship is shown in Figure 5.49.

(c) The Oversteer Car

For the oversteer car, $SM < 0$ and Eq. (5.67) applies as it is. The C_N - A_Y stability plot is similar to those for the NS and US except that, now, the stability index can be positive. Figure 5.50 shows how stability varies with velocity ($\delta = 0$). The OS car is stable up to its critical speed, V_{Crit} . At V_{Crit} it is neutrally stable ($SI = 0$), and at speeds above V_{Crit} it is unstable ($SI > 0$), as shown in Figure 5.50. The stability index is

$$SI = \left(\frac{\partial C_N}{\partial A_Y} \right)_{\delta=\text{constant}} = -SM + C_0 \left(\frac{\ell g}{V^2} \right)$$

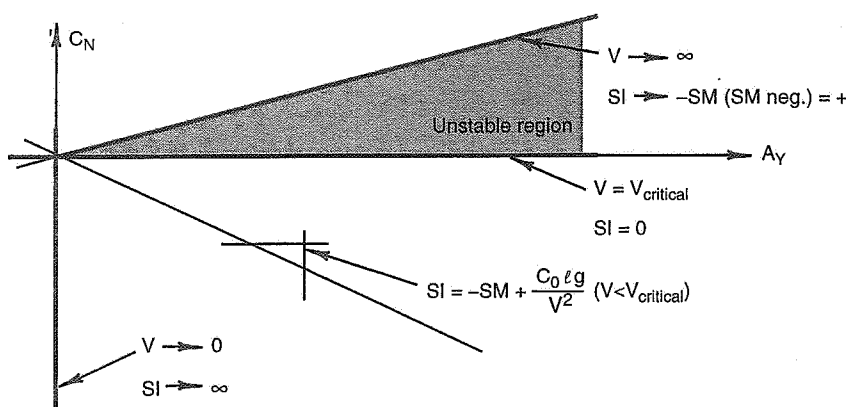


Figure 5.50 Stability plot: C_N - A_Y ; $\delta = 0$; oversteer car.

At very high speeds the second term approaches zero and the first term is positive (i.e., SM is negative).

Figures 5.48, 5.49, and 5.50 give a good feel for the variation of the static stability ($SI = \partial C_N / \partial A_Y$) with speed for the three cases. The general equation for the stability index has two terms: the first term, the static margin, does not vary with speed, while the second term, $C_0(\ell g/V^2)$ does. By comparing Eq. (5.68) with (5.65), we see that

$$SM = -\left(\frac{W}{C}\right)C_{N_\beta}$$

$$C_0 = \left(\frac{V}{\ell}\right)C_{N_r}$$

These are the relationships between the static margin (SM) and C_0 and the derivatives. Thus SM is proportional to the static "weathercock" stability and C_0 is proportional to the yaw damping. SM and C_0 are nondimensional.

5.15 Steady-State Response Data

Having examined the steady-state behavior of simple linear math models we now move up the Ladder of Abstraction to the measured performance of real vehicles. A variety of steady-state directional control tests have been developed by the SAE and the International Organization for Standardization (ISO) through its Technical Committee/Subcommittee, TC22/SC9. These procedures are given in Refs. 8 and 3 and are under continuous devel-

opment. Of the various test methods described, two are most commonly used: the constant radius - variable speed test and the constant speed (in practice, constant throttle)/variable radius test.

The general expression for understeer gradient (UG) in terms of K is

$$UG = \frac{d\delta}{dA_Y} = 57.3 K \text{ deg./g} \quad (5.68a)$$

In the constant radius (circle) test, the primary measurement is the steer angle required to keep the vehicle on the circle at various speeds. The understeer-oversteer gradient is equal to the steer angle gradient measured at the front wheels (δ/A_Y , deg./g) since there is no change in Ackermann angle on a constant radius. In practice the steering wheel angle gradient is normally measured and converted to the front wheels by dividing by the overall steering ratio. In this test, the speed, and thus the road load power (rolling + aero drag) required to maintain constant speed, is changing. The variation in tractive effort affects the test results when compared to the constant speed/throttle test. For low-speed passenger cars, this effect is secondary but it cannot be ignored at high speed. Likewise, aero download effects will change with speed in this test, assuming a large enough circle to attain a high speed.

In the constant speed - variable radius test, the understeer-oversteer gradient must be found from the difference of the steer angle gradient and the Ackermann angle gradient, understeer if the former is greater than the latter. In this test a series of runs are made at a constant speed or constant throttle. On each run, starting from a straight path, a step steer (rapid change in steer angle) is applied and held until the vehicle reaches steady-state. The step steer magnitude is increased on each run. Only the steady-state data is used for the steady-state response analysis. The Ackermann angle gradient is determined as follows:

$$\text{Ackermann angle, } \delta_{\text{Acker}} = \frac{\ell}{R} \quad (\text{small angle approximation})$$

$$\text{Lateral acceleration, } A_Y = \frac{V^2}{gR}, \text{ in g units}$$

$$\text{or } R = \frac{V^2}{gA_Y}$$

$$\text{Hence, } \delta_{\text{Acker}} = \left(\frac{\ell g}{V^2}\right) A_Y$$

$$\text{Ackermann angle gradient, } \frac{d\delta_{\text{Acker}}}{dA_Y} = \frac{\ell g}{V^2}$$

δ_{Acker} in radians, ℓ in ft., and V in ft./sec.

$$\text{or, } \frac{d\delta_{\text{Acker}}}{dA_Y} = \frac{858\ell}{V^2}, \text{ deg./g}$$

δ_{Acker} in deg., ℓ in ft., and V in mph

Figure 5.51 shows typical plots from (a) constant radius and (b) constant speed tests. These are tests that are typically performed by auto manufacturers with a full complement of on-board instrumentation. The recommended instruments are fully described in the test procedures. The constant radius test is unique because it will generate useful data with a minimum of instruments—a protractor on the steering wheel to measure δ_{SW} and a stopwatch to time laps of the circle. From the “lap” times, speed and lateral acceleration can be calculated.

When these tests are performed with a full complement of instruments the data is often reduced to response ratios. The most common are

- Understeer gradient, deg./g (can be approximated without fancy instruments)
- Steering sensitivity, g's/100° SW (steering wheel) angle
- Roll gain, deg./g
- Sideslip gain, deg./g (β = sideslip angle)

These are usually measured as slopes of the response curves at 0.15g in the linear range of tire performance. General Motors Proving Ground, for example, uses the constant speed test and for passenger cars has standardized on a test speed of 100 km/h (62 mph). Ref. 129 summarizes the results of measurements on 169 cars. The averaged results are given in Table 5.3. Further tests have been run on an international group of sports cars and these are averaged in Table 5.4. When compared to the passenger cars, sports cars have greater steering sensitivity, less understeer, and lower roll gradients.

Formal response test results for race cars are generally not available in the literature. Much of the response information required should be available to professional teams with on-board instrumentation systems. Race cars are likely to have higher steering sensitivity, negligible understeer at realistic speeds (and power level for road load), lower roll gradient (especially with ground-effects cars and/or active suspension), and low sideslip gain (because of the high cornering stiffness tires).

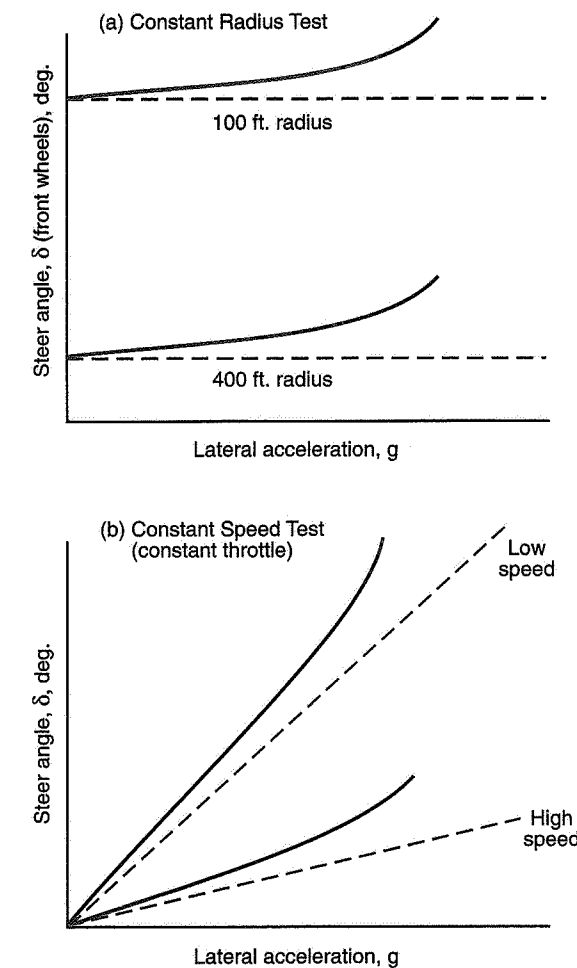


Figure 5.51 Steady-state response tests.

Table 5.3 Response Parameters, Test Speed = 62 mph

	Origin	Minimum	Average	Maximum
Steering Sensitivity (g's/100° SW)	Domestic	0.57	1.01	2.15
	Foreign	0.77	1.20	1.90
Understeer (deg/g)	Domestic	0.7	4.4	8.2
	Foreign	1.3	2.6	5.8
Roll Gradient (deg/g)	Domestic	3.0	6.4	11.0
	Foreign	2.9	7.1	9.6

Table 5.4 Sports Car Response Parameters

	Minimum	Average	Maximum
Steering Sensitivity (g's/100° SW)	0.94	1.38	1.94
Understeer (deg/g)	1.17	2.61	5.53
Roll Gradient (deg/g)	3.47	4.78	7.01
Sideslip Gain (deg/g)	0.78	2.22	4.79
The number of vehicles averaged = 12			
Speed = 62 mph			

Steering Sensitivity

The *linear* steering sensitivity is a function of the under/oversteer gradient and the speed. From the SAE definition,

$$UG = \left(\frac{d\delta_{SW}}{dA_Y} \right) \left(\frac{1}{G} \right) - \frac{d\delta_{Acker}}{dA_Y} = \frac{d\delta}{dA_Y} - \frac{858 \ell}{V^2} \quad (5.69)$$

where the three gradients are in deg./g at the front wheels
 δ defined as δ_{SW}/G
 ℓ is in ft.
 V is in mph

Solving this for $dA_Y/d\delta$,

$$\frac{dA_Y}{d\delta} = \frac{1}{UO \text{ gradient} + (858\ell/V^2)}$$

or, steering sensitivity in g/100° $\delta_{SW} = (100/G)(dA_Y/d\delta)$. G is overall steering ratio.

Figure 5.52 presents steering sensitivity, $dA_Y/d\delta$, as a function of speed, UO gradient, and wheelbase. Race cars are usually close to neutral steer (zero deg./g), and, unlike cars with some small amount of understeer, have very sensitive steering at high speed. Minimizing changes in steering gain with speed by use of understeer is generally viewed as desirable for passenger cars. The race car must be near neutral steer (to develop maximum lateral acceleration) and high steering sensitivity is the result.

Consider a (hypothetical) Grand Prix car with a 108" wheelbase cornering at 50 mph and 150 mph in a 2g turn (see the neutral steer line on Figure 5.52). The results are given in Table 5.5. The level of steering sensitivity can be changed by adjusting the steering ratio but the change in gain with speed remains (assuming a rack-and-pinion steering system). As shown in the table, the race driver lives with a gain change of about 9 to 1 and the gain level is 2 to 10 times higher than that of passenger cars.

Nonlinear Response Characteristics

The response ratios discussed previously were measured at low lateral acceleration ($A_Y \approx 0.15g$). It is common in proving ground tests to measure the steering wheel angle to higher steady-state lateral accelerations, approaching maximum lateral capability. Figure 5.53(a) shows test results from a popular sports car, c. 1980. Note the increase in steer angle at high lateral accelerations which has occasionally been interpreted as an increase in directional stability.

Assume (for the moment) that the concept and definition of understeer gradient, Eq. (5.69), applies at operating points in the high lateral acceleration range. Then we can calculate the understeer gradient by taking slopes in this range and correcting these to the front wheels ($G = 17.3$) and removing the Ackermann gradient ($\ell = 8.17$ ft., test speed = 62 mph). This gives a plot of "understeer" gradient as shown in Figure 5.53(b). This curve shows a constant gradient up to about 0.4g, after which it increases markedly as max lateral (0.83g) is approached. Thus it might be concluded that the vehicle is becoming very stable as max lateral is approached.

If the steering sensitivity is calculated from these test results as in Figure 5.54, it will be seen that the steering sensitivity is falling off as max lateral is approached, and, in fact, has become about zero at max. Thus the upsweep in the understeer gradient is totally

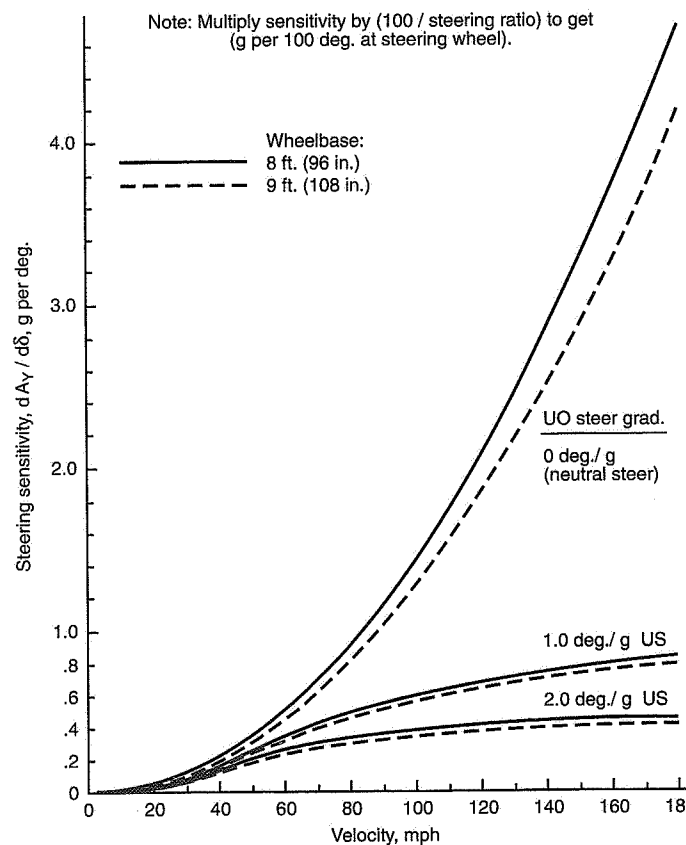


Figure 5.52 Steering sensitivity vs. speed.

Table 5.5 Grand Prix Response Parameters

	50	150
$dA_y/d\delta$ at front wheel	0.32	2.88
$dA_y/d\delta$ at steering wheel	0.021	0.192
Steering wheel rotation for 2g turn, deg. (15:1 steering ratio)	95.2	10.4
Rim movement for 12" dia. steering wheel, in.	9.9	1.1
Steering sensitivity (g's/100° SW)	2.13	19.2

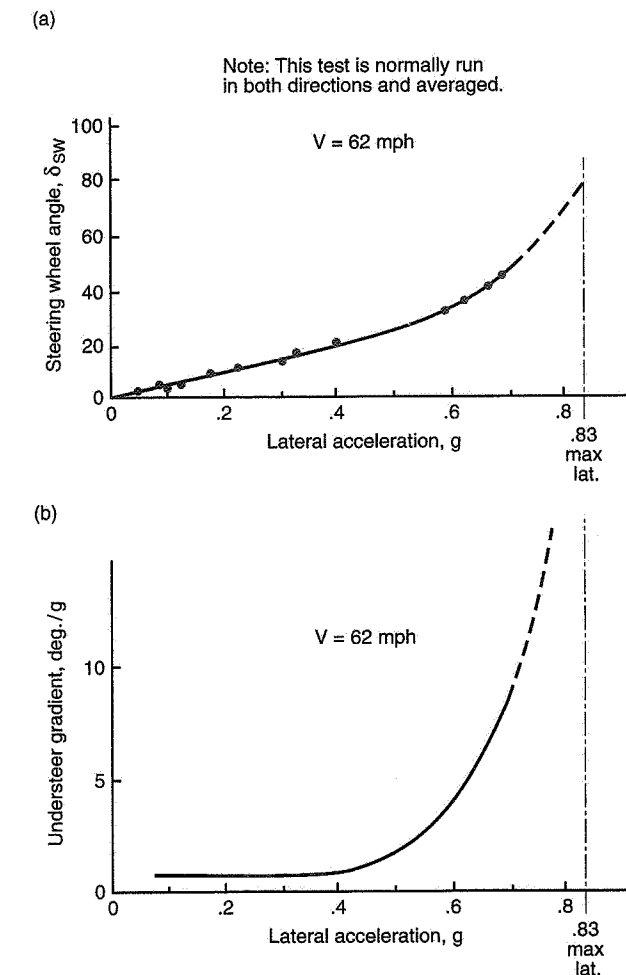


Figure 5.53 Steady-state steer test and "understeer" gradient.

due in this case to the fall off of the steering sensitivity as the front tires approach the peak of the cornering force curve.

The use of steer angle, δ , in steady-state response tests implies that the static directional stability and yaw damping moments are being measured in terms of the control moment instead of a more absolute measure. This is satisfactory in the linear range but as the

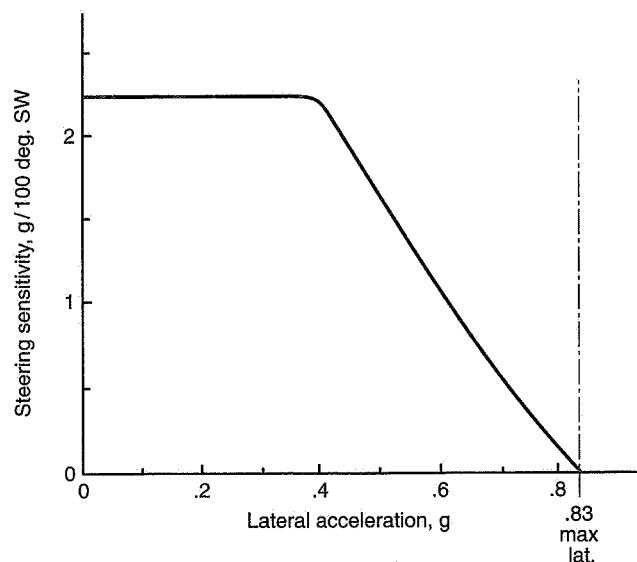


Figure 5.54 Steering sensitivity vs. lateral acceleration, steady-state test.

nonlinear range is entered, one is never sure if the change in slope is due to stability, damping, or control.

Expressed in derivative terms (for the linear range),

$$\frac{d\delta}{dA_Y} = \left(\frac{W}{C} \right) \left(\frac{C_{N_\beta}}{C_{N_\delta}} \right) + \left(\frac{C_{N_r}}{C_{N_\delta}} \right) \left(\frac{g}{V} \right)$$

where C_{N_β} = Static stability derivative in nondimensional form

C_{N_r} = Yaw damping derivative

C_{N_δ} = Control moment derivative

It is obvious that C_{N_β} and C_{N_r} are being measured in C_{N_δ} units. In the nonlinear range it would be most desirable to deal with actual forces and moments or use operating point techniques where local slopes and derivatives are of interest.

The dramatic reduction in steering sensitivity as the limit is approached has a strong effect on race driving technique. This is documented in the following quotation by Stirling Moss (Ref. 104) (emphasis added by the authors):

Few people outside racing can appreciate that race driving is not like driving on the road at all. A racing car is always in an attitude at corners, never pointing as directly fore-and-aft in its line of travel as a road car would be in normal motoring. The racing car is sliding, to some degree, nearly all the time, but to be quick the best drivers try to do the slides and drifts with the least drag possible at moments when drag doesn't matter. One can put the car into a Kristie—a broadside as in ski-ing—to slow it into corners. But once one has presented the car to a very high-speed corner it's rather like throwing a dart—when it has left your hand you can't do a thing about its path. If you present a car accurately to such a corner it will track through in a long drift on virtually a predestined trajectory. You can make tiny adjustments, but once you have presented it to the corner you can only adjust the trim, not make major changes of direction—not if you are on the limit.

Steering is used to present the car, then to compensate for the throttle, because as one opens the throttle, and the car starts to slide you may have to use the steering wheel to compensate—to balance the power. I would describe the steering wheel as the presenter and the balancer really.

Current race cars using high cornering stiffness tires do not experience the large "drift" attitudes associated with cars of Moss' era, but the steering near the limit is still marginal. A high level of skill and experience is required to consistently corner these cars at high lateral accelerations. For further information on steady-state skid pad testing, see Chapter 11.

5.16 Steady-State Nonlinear Analysis

Analysis and on-board instrumentation are being used in design and tuning by professional racing teams. Specialized computer programs such as the MRA Moment Method enable prediction of the stability and control of a race car given accurate chassis, tire, and aero data. Lap time prediction, including details of performance around the circuit are approaching a level of sophistication useful for chassis tuning. These are theoretically possible but their achievement will depend on acceptable model complexity, cost to use, available input data, the degree to which it is necessary to simulate the driver and advances in computer technology.

In 1963 an analysis of the steady-state turning behavior of a rear drive automobile was performed by Radt and Pacejka (Ref. 122). This analysis utilized a comprehensive nonlinear representation of the automobile with the following degrees of freedom:

- Longitudinal Velocity
- Lateral Velocity
- Yawning Velocity

Roll Angle of the Sprung Mass

Roll Angle of Front and Rear Unsprung Masses

The solutions, which were carried out on a large (at the time) digital computer, cover the complete linear and nonlinear range, up through max lateral. The effects of nonlinear tire characteristics, lateral load transfer, rear driving thrust, and nonlinear roll behavior on the steady-state turning performance were studied.

The results indicated that the linear representation of the vehicle as developed by L. Segel in Ref. 144 is satisfactory to about 0.3g. Above this lateral acceleration a nonlinear model is required.

Of particular interest to racing, the study explored the effect of large driving thrust at high lateral accelerations, near and at the limit. Figure 5.55 shows the result on path radius of total driving thrust at various steer angles. Steer angles of 8° and 16° give lateral accelerations very close to peak at high thrust levels. It will be noted that as the driver increases throttle setting (at 8° and 16°) there is initially an increase in path radius—the vehicle is beginning to plow due to the longitudinal load transfer which is unloading the front wheels. As the driving thrust is increased still further, the lateral force at the rear tires is reduced (friction ellipse effect) and the vehicle starts to spin (reduced path radius).

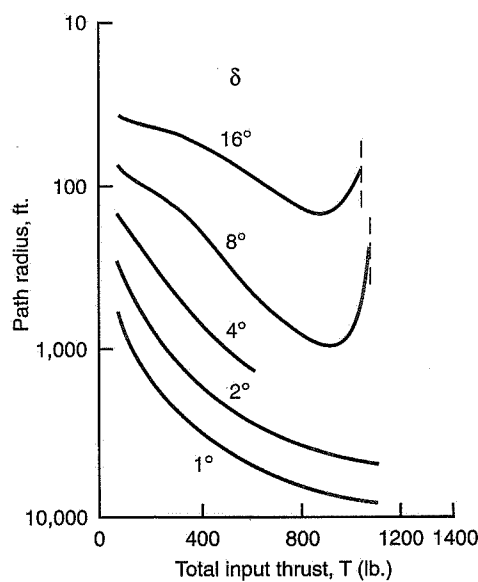


Figure 5.55 Path radius, R , vs. total input thrust, T .

The results of this study enable a detailed look at the forces on a vehicle with various levels of tractive effort (see Figure 5.56). In this figure, the forces and operating conditions are shown graphically, where

T	Total input driving thrust
F_z	Vertical tire force
A_y	Lateral acceleration
β	Vehicle slip angle
R	Radius of turn
r	Yaw rate about the turning center
V	Forward velocity
δ	Steer angle, fixed at 8°

The tire forces (lateral and tractive) are shown as arrows at the individual wheels.

To appreciate this analysis from the standpoint of racing, it should be remembered that at each level of driving thrust the vehicle is in a trimmed steady-state turn (in balance, yawing moment $N = 0$). Thus the operating conditions correspond to the middle phase of a racing turn near the apex. The next requirement for this phase of a racing turn is to be traveling as fast as possible.

Figure 5.57 is a plot of the vehicle responses which are shown graphically in Figure 5.56 for $\delta = 8^\circ$. The maximum cornering speed (98 mph) for this steer angle occurs at Point A, when the vehicle is traveling on a radius of 939 ft. The corresponding lateral acceleration is 0.67g and β is -6° . Other data indicate that both the front and rear tires are slightly below the peak. Thus this condition would be appropriate for race operation in the middle (steady-state, balanced) phase of a turn.

It will be noted that a somewhat higher lateral acceleration would be obtained if the driving thrust were increased to 1040 lb. When this is done the turn tightens markedly (to a radius of 476 ft.), the vehicle attitude, β , increases rapidly to -10.4° , and the speed falls off to 73 mph. The vehicle is still balanced, precariously, since the front and rear slip angles are essentially at the peak and any more β would put them over. An examination of Figure 5.56 shows that as β and A_y increase, the longitudinal component along the car axis of the centrifugal force increases. This component is in the nature of an *induced drag* which must be equilibrated in a steady turn by driving thrust. Less thrust is then available to overcome rolling resistance and aerodynamic drag and the equilibrium speed is reduced.

This pioneering work by Radt and Pacejka indicated that **yaw balanced, steady-state racing turns could be studied** with a comprehensive, nonlinear model and enough data on the chassis, tires, and aerodynamics. By varying the vehicle, tire, and aerodynamics it would be theoretically possible to optimize the vehicle configuration for various severity corners. At this level of analysis, the turn entry and exit phases were not included. This work preceded the Moment Method analysis.

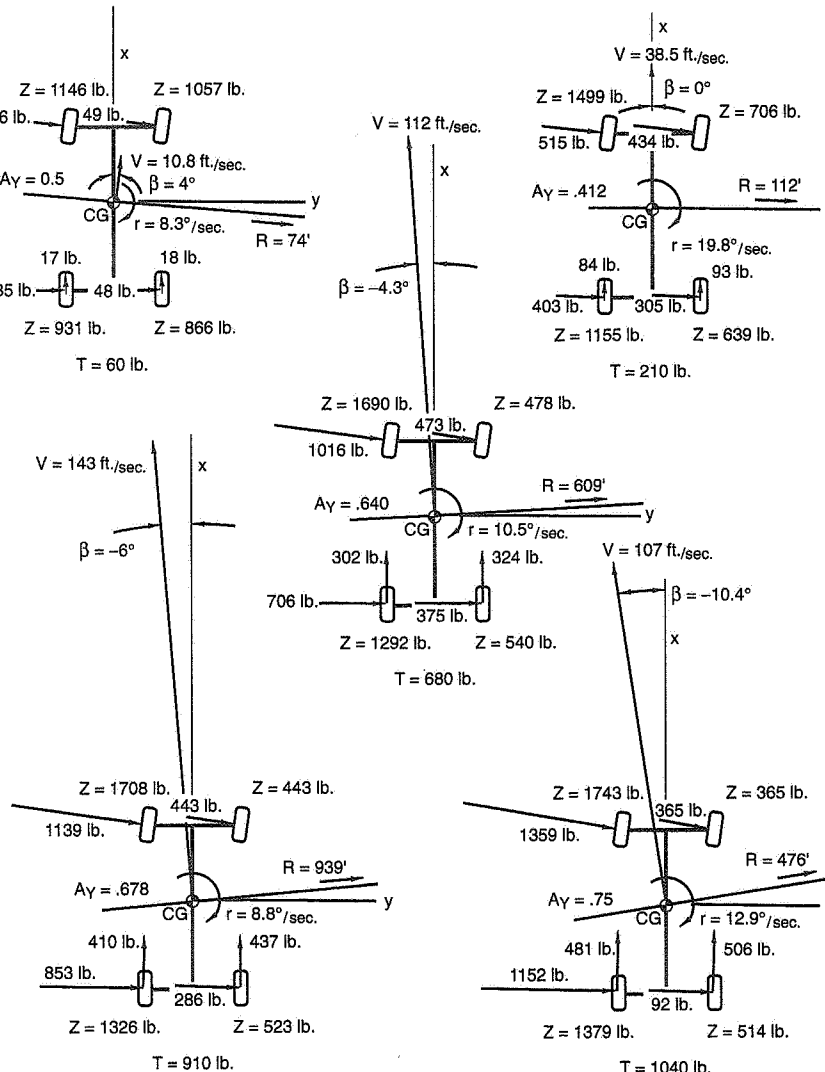


Figure 5.56 Plan view of vehicle showing responses and tire forces ($\delta = 8^\circ$).

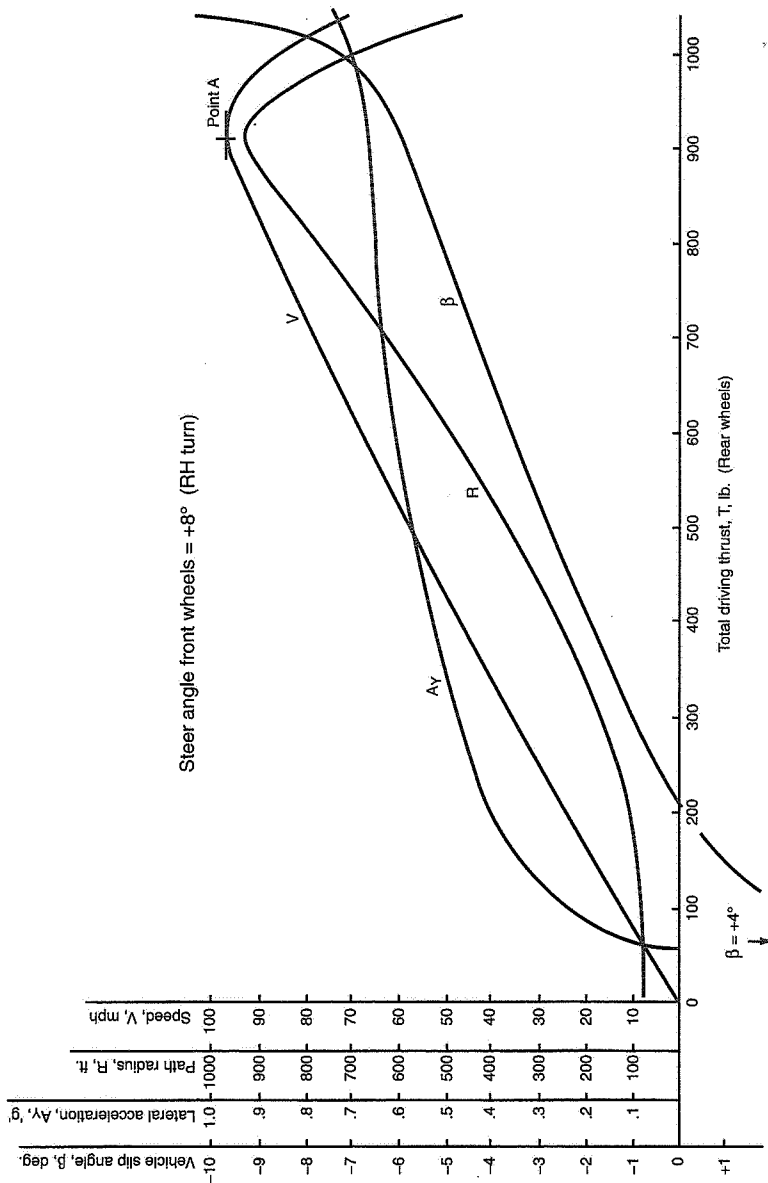


Figure 5.57 Plot of vehicle responses vs. driving thrust.

5.17 General Conclusions on Steady-State

In this chapter we have discussed a number of ways of looking at steady-state stability and control. A very simple, understandable model has been used. This model is not adequate for calculating the behavior of real cars; this is reserved for later discussion as in, for example, Chapter 8. We have shown that there are many ways of expressing the physical concept of understeer-oversteer (UO). In general, the mathematics of these different techniques are equivalent, but they differ as models for physical understanding.

It is first necessary to distinguish between UO in the linear range (where the tires are operating on the elastic portion of their cornering curves) and UO near the limit where tire frictional characteristics dominate. The linear range is of particular interest for passenger cars and is normally considered to be in the $\pm 0.35g$ lateral acceleration range—this covers most highway use. The nonlinear range (which varies with load) and the directional balance are most important to race car performance and handling. In both cases the terms understeer and oversteer are apt in the sense that the vehicle “under” or “over” steers the Ackermann path, while neutral steer is the boundary between the two.

The physics of **linear** UO and **limit** UO differ. The former is primarily concerned with tire distortion effects due to slip and camber angles while the latter is mainly concerned with frictional or grip characteristics. Thus **linear** UO involves tire carcass construction features while **limit** UO adds concern for the tread material compound. Tire load is important in both ranges as it affects both lateral forces due to slip/camber (linear range) and friction level (limit range).

By way of summary, we have discussed the following approaches to UO steer and their relationships. Before using any of these equations, reference should be made to the appropriate section to clarify assumptions and limitations.

1. Understeer Gradient (UG)

For SAE/ISO, steady-state response tests:

a. Constant radius—variable speed

$$UG = \frac{d\delta}{dA_Y} = 57.3 K \ell g, \text{ deg./g} \quad (5.68a)$$

b. Constant speed (throttle)—variable radius

$$UG = \frac{d\delta}{dA_Y} - \frac{858 \ell}{V^2} = 57.3 K \ell g, \text{ deg./g} \quad (5.69)$$

where the gradients are in deg./g at the front wheels defined by $\delta = \delta_{SW}/G$
 G is overall steering ratio (linear)
 ℓ is in ft.
 V is in mph

Additional expressions for UG:

$$UG (\text{deg./g}) = -57.3 \left(\frac{SM}{C_0} \right) = 57.3 W \left(\frac{N_\beta}{\ell C_F C_R} \right)$$

Neutral steer, $N_\beta = 0$, $UG = 0$
 Understeer, $N_\beta > 0$, $UG > 0$
 Oversteer, $N_\beta < 0$, $UG < 0$

$$UG (\text{deg./g}) = 57.3 \left(\frac{W}{\ell} \right) \left(\frac{a}{C_R} - \frac{b}{C_F} \right)$$

Increasing a and $C_F \rightarrow$ decreased UG
 Increasing b and $C_R \rightarrow$ increased UG

SM, C_0 and K defined below.

2. Static Margin (SM)

$$SM = -\frac{1}{\ell} \left(\frac{aC_F - bC_R}{C_F + C_R} \right) = -\frac{(a/\ell)C_F - (b/\ell)C_R}{C} \quad (5.48a)$$

Neutral Steer SM = 0
 Understeer SM > 0
 Oversteer SM < 0

$$SM = \frac{d}{\ell} - \frac{a}{\ell} = NSP - \frac{C_R}{C}$$

3. Stability Factor (K)

$$\frac{r}{\delta} = \frac{V/\ell}{1 + KV^2}, \text{ defines K} \quad (5.43)$$

See note following the derivation of Eq. (5.43).

$$K = \frac{-SM}{C_0 \ell g} , \quad \frac{1}{(\text{ft./sec.)}^2} \quad (5.51a)$$

$$\text{where } C_0 = \frac{1}{W} \left(\frac{C_F C_R}{(C_F + C_R)} \right) , \text{ definition of } C_0 \quad (5.66a)$$

C_0 is nondimensional.

C_0 is always $-$, K takes the sign of SM .

$$\text{Thus, } \frac{r}{\delta} = \frac{V/\ell}{[1 - (SM/C_0)(V^2/\ell g)]} , \quad (V^2/\ell g) \text{ is nondimensional.}$$

4. Characteristic speed for Understeer

$$\text{Is when } \frac{r}{\delta} = \frac{1}{2} \left(\frac{V}{\ell} \right) = \frac{1}{2} \left(\frac{r}{\delta} \right)_{\text{NS}}$$

$$\text{Occurs when } \left(\frac{SM}{C_0} \right) \left(\frac{V^2}{\ell g} \right) = -1$$

$$V_{\text{Char}}^2 = \left(\frac{C_0}{SM} \right) g \ell = \frac{1}{K} \quad (5.63)$$

5. Critical speed for Oversteer

Is when $r/\delta = \infty$

$$\text{Occurs when } \left(\frac{SM}{C_0} \right) \left(\frac{V^2}{\ell g} \right) = +1$$

$$V_{\text{Crit}}^2 = - \frac{1}{K} \quad (5.56)$$

For engineering use,

$$V_{\text{Char or Crit}} = 3.87 \sqrt{\left| \frac{C_0}{SM} \right| \ell} , \quad \text{mph} \quad (5.64)$$

6. Olley Definition

The vehicle is US if the path curves away from a side force applied at the CG ($\delta = 0$). If it curves toward the side force it is OS and NS if the path is straight (see Figure 5.22).

$$\frac{1/R}{F_y - mV^2/R} = \frac{N_\beta}{VN_r Y_\beta} \quad (5.49a)$$

where $F_y - mV^2/R$ = total side force
 VN_r is independent of speed

7. Effective slip angle steers (α_{Fe} , α_{Re})

When lateral force is imposed on a simple vehicle, the front and rear slip angles "steer" the vehicle and account for departures from the Ackermann. They determine the path curvature noted in the Olley test definition. In real vehicles the directions of motion of the front and rear still define departures from the Ackermann but these motions depend on a large number of design characteristics. The motions at front and rear can then be expressed as effective slip angle steers,

$$-\alpha_{Fe} + \alpha_{Re} = \frac{\ell KV^2}{R} \quad (5.50a)$$

If $K > 0$, $(-\alpha_{Fe} + \alpha_{Re}) > 0$, $\alpha_{Fe} > \alpha_{Re}$ US
If $K < 0$, $(-\alpha_{Fe} + \alpha_{Re}) < 0$, $\alpha_{Fe} < \alpha_{Re}$ OS
If $K = 0$, $(-\alpha_{Fe} + \alpha_{Re}) = 0$, $\alpha_{Fe} = \alpha_{Re}$ NS

8. Bundorf Cornering Compliances D_F , D_R

Understeer gradient (UG) = $D_F - D_R$, deg./g (see Section 5.11)

D_F = front cornering compliance, deg./g = $57.3 W_F / C_F$ (C_F in lb./rad.)

D_R = rear cornering compliance, deg./g = $57.3 W_R / C_R$ (C_R in lb./rad.)

where C_F and C_R are for front and rear wheel pairs and where US effect at front increases D_F (+) and US effect at rear decreases D_R (-)—a Bundorf sign convention.

For the simple model, D_F and D_R are α_F/g and α_R/g . For more complex models they are sideslip angles/g.

9. Static Directional Stability

Slope of yawing moment curve $N_\beta = dN/d\beta$ for constant δ and operating conditions. This is also referred to as directional spring or weathercock effect (see Figure 5.18).

In coefficient form, $C_{N_\beta} = dC_N/d\beta$

10. Stability Index, SI

Slope of yawing moment curve dN/dA_Y for constant δ and operating conditions.

$$SI = \left(\frac{\partial C_N}{\partial A_Y} \right)_{\delta=\text{constant}} = -SM + C_0 \left(\frac{\ell g}{V^2} \right) \quad (5.68)$$

Comparison with Aeronautical Usage

In aircraft technology a strong distinction between normal operation and stall behavior exists—there is little commonality in the language of these two regimes. This has not been true for automobiles **but it would certainly be desirable**. Race driver terminology of “plow or push” and “spin or loose” is, in our view, preferable to “final UO” but it is difficult to break long-established linguistic habits.

The conventional concept of UO as expressed in the SAE/ISO definition stems from proving ground testing. We prefer more absolute definitions of UO related to the forces/moments acting on the vehicle. Thus we incline toward the derivatives and statics, i.e., aircraft practice. We feel that N_β , the rate of change of yawing moment with β , an obvious weathercocking effect, is a good physical way of thinking about linear or operating point static stability. The stability index, the rate of change of yawing moment with lateral acceleration, is an absolute measure of static directional stability when referred to A_Y as the operating variable. In general the application of “statics” to the automobile opens up a wide range of highly developed aircraft technology involving such concepts as yaw damping (path curvature stiffness) and lateral damping.

Understeer and the Driver

What is the significance of linear “fixed control” understeer to the driver and how is it sensed? Ordinary drivers are not particularly conscious of steering wheel position so it seems unlikely that they will sense UO as measured in the SAE/ISO tests. This is particularly true since steering ratio will change from vehicle to vehicle.

Understeer promotes more constant steering gain over the speed range which seems desirable, but again it seems unlikely that this will be detected directly. Successful passenger vehicles have been operated with a wide range of linear understeer, even modern practice varies between 2 and 8 deg./g.

As discussed in the next chapter, the level of understeer has an effect on the transient response times—the response of yaw velocity and lateral acceleration to steering input. Here there is evidence that the average driver can detect excessive response times as well as too rapid response (or steering sensitivity). Understeer has a marked effect on shortening the response time. Understeer also affects disturbance response and straight running.

The conventional automobile is successful in the hands of a wide range of drivers and operating conditions for a variety of reasons: inherently high directional and lateral damping in the tire linear range, response times appropriate for human controllers, and some modest amount of directional stability.

Simplified Transient Stability and Control

"To see Nuvolari in his hey-day, chin out, sitting well back in the driving seat, his outstretched hairy brown arms flashing in the sun as he made his blood-red Alfa perform seemingly impossible antics, not once but corner after corner, lap after lap, the tyres screaming and the crowd yelling themselves hoarse, was quite fantastic."

George Monkhouse
in "Grand Prix Racing"

"A jerky little twist can throw you into that long, long slide. A slow large turning of the steering wheel can (ha! ha!) have the same effect."

Grampaw Throttlebottom
on *Sportive Automobilism*
(a.k.a. Miles Collier)



Introduction

In this chapter we examine the transient (or dynamic) maneuvering associated with turn entry and recovery. Here, such motion variables as yawing and lateral velocity and path

In this chapter, Fred Dell'Amico, MRA, wrote the second section, "The Spring-Mass-Damper System." The third section, "Dynamic Stability—Two-Degree-of-Freedom Automobile" is based on Ref. 127 by Roy Rice.

curvature are changing with time. In keeping with the previous chapter on steady-state response we will initially deal with the behavior of small perturbation models (mainly the “bicycle” model). This will be followed by transient response data on real cars, including some free control response data. Finally, some description of nonlinear analytical modeling will be given to show the evolution of the very comprehensive models currently in use for realistic vehicle dynamics simulation.

This discussion assumes fixed (or position) control of the steering wheel. This means that the driver input does not react to steering torques generated by the car—the driver obtains a steer angle regardless of steer torque. The opposite extreme is force/free control where the driver commands a torque (or zero torque for free control) and pays no attention to the position of the steering wheel.

In the real world, of course, cars are controlled by a combination; the proportion of fixed and force control vary with the driver, vehicle, and driving task. The fixed control assumption has been used to date in most theoretical and experimental work. The fixed control assumption avoids modeling the driver in detail, a very complex problem.

6.1 Approach

The analysis of linear mechanical systems that exhibit time-varying (dynamic) responses is a well established discipline. It begins with the mathematical equations of motion which are an expression of Newton’s laws as discussed in Section 5.7 for the two-degree-of-freedom “bicycle” model. In Section 5.9 these equations were solved simultaneously for the steady-state turning situation by setting \dot{r} and $\dot{\beta}$ (or \dot{v}) = 0. That is, steady-state turning was defined as **no** time variations in the motion variables, r and β (or v). We are now interested in solving these equations for the case in which r and β can vary with time.

One classical way of solving these equations to yield the time responses (or time histories) of the motion variables to a control input is the Laplace transform. By rewriting the equations in terms of the Laplace operator, transfer function relationships can be derived which establish the ratio between the output (or response) variable, such as yaw rate, and the control input, δ . By use of the inverse transforms, which have been worked out for a large variety of Laplace transfer functions, one can obtain the actual time responses.

A rigorous discussion of Laplace transform mathematics is beyond the scope of this book, but a few observations will be helpful in understanding some of the material in this chapter. The transfer functions, relating output to input, appear as a ratio. The denominator of this ratio is called the “characteristic expression” and it determines the inherent stability of the system, i.e., how it behaves if momentarily disturbed and then left alone. Think of a simple pendulum which is slightly displaced and then released to come back toward its equilibrium position. The nature of the return to equilibrium depends on two

basic properties of the system, *the undamped natural frequency* and the *damping ratio*, both of which can be determined from the denominator or characteristic expression of the transfer function.

The numerator of the transfer function is related to the nature of a disturbance or input applied to the system. Rather than let the pendulum return to center under the action of gravity, one could push on the pendulum in various fashions as it tries to seek its natural equilibrium. These “forcing functions” or controlling actions will affect the overall response of the system. A poorly damped pendulum which is displaced and released will overshoot and oscillate once or twice before settling down to a stop; if the correct external “control” force is applied in the right direction and at the right time, the pendulum can be forced to stop at its final position with no overshoot.

In general, the lateral and directional responses of automobiles depend on both the inherent stability and the disturbance or control, i.e., the relative value of the numerator and denominator of the transfer function.

In the next section we will examine the natural (or inherent behavior) of a simple single-degree-of-freedom system which will clarify the concepts of frequency and damping.

6.2 The Spring-Mass-Damper System

Introduction

In this section we will review the statics and dynamics of the spring-mass-damper (SMD) system. As shown in Figure 6.1, the SMD system—in this case a rectilinear system—consists of a mass, m , whose motion under an applied force, F , is desired. The resistive forces are the mass’s inertial reaction force, ma ,³⁰ a spring force, and a viscous damper force.

The SMD system is of considerable significance in engineering because many simple systems in the real world are very closely approximated by a SMD system. Two familiar examples are

- A storm door in which the door (mass) is closed by a spring force and a piston/cylinder is used to dampen or slow down the closure (in this case the applied force, F , is zero).
- The suspension system for a wheel on an automobile, in which case the shock absorber is the damper.

³⁰ Newton’s second law.

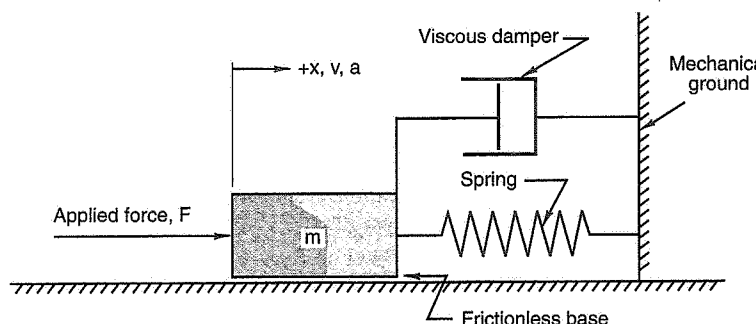


Figure 6.1 Spring-mass-damper system.

In addition to many nearly exact duplications of the SMD system which, incidentally, is a linear system (Figure 6.1), there are numerous applications in which the dynamics of rigid bodies are closely approximated by the SMD system—including the lateral/directional response of a simple automobile to steering inputs.

The SMD system of Figure 6.1 is idealized in that the frictional force has been assumed to be zero. If the frictional force is constant it merely subtracts from the applied force, F ; if it is a variable the system becomes nonlinear and more difficult to analyze. In Figure 6.1 the relevant forces acting on the mass are

- Applied force = F (lb.)
- Resistive forces
 - Inertial reaction = $ma = (W/g)(a)$, lb.
 - Spring force = $K'x$ (lb.), where K' is the spring constant in lb./ft. (or lb./in.) and x is the displacement of the mass in feet (or inches)³¹
 - Damper force = CV , where C is the damper constant in lb. per ft./sec. (or lb. per in./sec.), and V = Velocity in ft./sec. (or in./sec.)

The equation of motion is therefore

$$F = Wa/g + CV + K'x \quad (6.1)$$

Thus, the resistive forces are proportional to acceleration, velocity, and displacement. It should be noted that while the force, Wa/g , is always exact and while the force, $K'x$, is

close to being exact in most cases (because the spring rate is fairly constant), the damping force, CV , is sometimes inexact—owing to a C that is not strictly linear. Such may be the case, for example, for a shock absorber; if the slope of the f vs. V curve (which is what C is) is not constant, one has to use a linear approximation to apply Eq. (6.1).

Another example of the SMD system is shown in Figure 6.2.

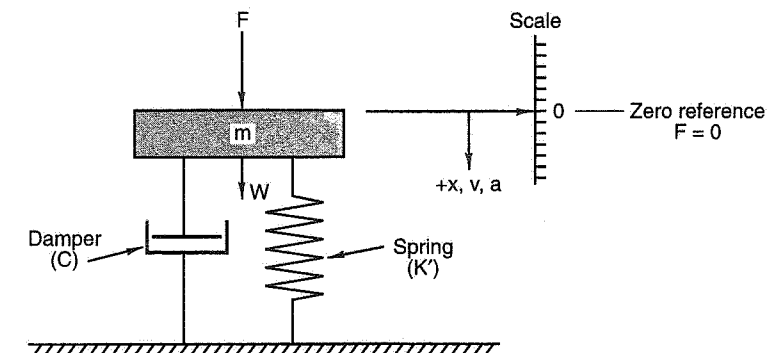


Figure 6.2 Another SMD system.

For our purposes the system of Figure 6.2 is of greater interest than that of Figure 6.1 because it is a crude approximation to a wheel suspension system (the tire spring is omitted). In this case there is a weight force, W , acting downward but no friction force.³² The weight force, W , can be taken out of the picture by using the “at rest” position of the mass on the spring as the zero reference for displacement measurement. For example, if the spring rate, K' , is 50 lb./in. and the mass weighs 100 lb., the zero reference is $100/50 = 2.0$ in. as measured from the spring’s free end when it is unstressed (i.e., undeflected). With the zero reference thus established the equation of motion of the system of Figure 6.2 is exactly that of Figure 6.1, i.e., Eq. (6.1).

Statics

The statics of the SMD system are quite straightforward. If a constant force, F_1 , is applied (it could be another W placed on top of the first one), the mass will be pushed down to some steady-state value of x , say x_1 , given by $x_1 = F_1/K'$. Thus, if $F_1 = 200$ lb. and $K' = 50$ lb./in.,

$$x_1 = F_1/K' = 200 \text{ lb.}/(50 \text{ lb./in.}) = 4 \text{ in.}$$

³¹ Note that K' is used to distinguish this spring constant from K , the stability factor.

³² Not true for an actual wheel suspension system.

Since acceleration and velocity are zero in the steady-state, inertial reaction and damping forces are also zero.

Dynamics

The dynamics of the SMD system are far more interesting than its statics. There are two important parameters that completely define the dynamics of the SMD system: these are its *undamped natural frequency* and its *damping ratio*.

Undamped Natural Frequency

The undamped natural frequency, ω_n , is given by the expression

$$\omega_n = \sqrt{K'/m} , \text{ in radians/sec.} \quad (6.2)$$

(divide by 2π or 6.28 to get Hz or "cycles per second")

The undamped natural frequency, usually shortened to "natural frequency," is the frequency at which the mass will oscillate about the zero reference if the mass is pushed down (or pulled up) and then let go. Theoretically, the oscillation will go on indefinitely since there is nothing to dissipate the original energy stored in the spring at its initial deflection (the spring is assumed to dissipate no energy). In the above example ($F_1 = 200$ lb., $K' = 50$ lb./in., $x_1 = 4$ in.) the natural frequency is:

$$\begin{aligned}\omega_n &= \sqrt{50 \text{ lb./in.} / [200 \text{ lb.} / (32.2 \times 12 \text{ in./sec.}^2)]} = \sqrt{96.6/\text{sec.}^2} \\ &= 9.83 \text{ rad./sec.} = 1.57 \text{ Hz}\end{aligned}$$

Note: 32.2 is the acceleration due to gravity in ft./sec.²; it must be multiplied by 12 to work in in./sec.²

Since $C = 0$, the natural frequency is a function only of the mass and the spring rate. As damping is added, frequency (ω_n) tends to reduce with increased C (that is, if damping is light and oscillatory behavior is occurring).

Damping Ratio

The damping ratio is a convenient mathematical tool that shows the influence of the damping constant, C , on transient response. In the previous section the mass was pushed downward and then let go. Because the damping was zero ($C = 0$) the mass oscillated about its zero reference value. With nonzero damping the transient that takes place, in

x , between the time that the force is removed and the mass comes to rest, at $x = 0$, will vary in accordance with the damping ratio, ζ ; it is given by

$$\zeta = \frac{1}{2} \left(\frac{C}{m\omega_n} \right), \text{ dimensionless} \quad (6.3)$$

If Eq. (6.2) is inserted in Eq. (6.3),

$$\zeta = \frac{1}{2} \left(\frac{C}{\sqrt{K'm}} \right) \quad (6.4)$$

Note that the ζ is directly proportional to C . This equation can be solved for C and used in reverse, if a ζ is known (or desired):

$$C = \zeta \times 2 \times \sqrt{K'm} \quad (6.5)$$

The ζ is useful because its value reveals the following transient characteristics:

- (a) If $\zeta = 0$ This results when $C = 0$. As noted above the mass oscillates indefinitely about the zero reference. In real systems there is always some form of energy dissipation so that, in time, $x = 0$ is reached.
- (b) If $\zeta < 1$ The system is said to be *underdamped*; it will oscillate about the zero reference but with a decreasing amplitude and eventually reach steady-state at $x = 0$.
- (c) If $\zeta = 1$ The system is said to be *critically damped*; the mass will return to $x = 0$ smoothly, without under/overshoot. If we set Eq. (6.4) equal to 1.0 and solve for C we find that the damping constant needed for critical damping is

$$C = 2\sqrt{K'm} , \text{ lb./in./sec.}$$

- (d) If $\zeta > 1$ The system is said to be *overdamped*; the mass returns smoothly to $x = 0$ but more slowly than the critically damped case.

All four of these cases are shown in Figure 6.3.

In all of the above we have concentrated on rectilinear systems. The theory for rotational (torsional) systems is identical, except that angular displacement is involved and the spring-mass-damper units are different (the units of ω_n and ζ are unchanged). The analogous parameters in the two kinds of motion are shown in Table 6.1.

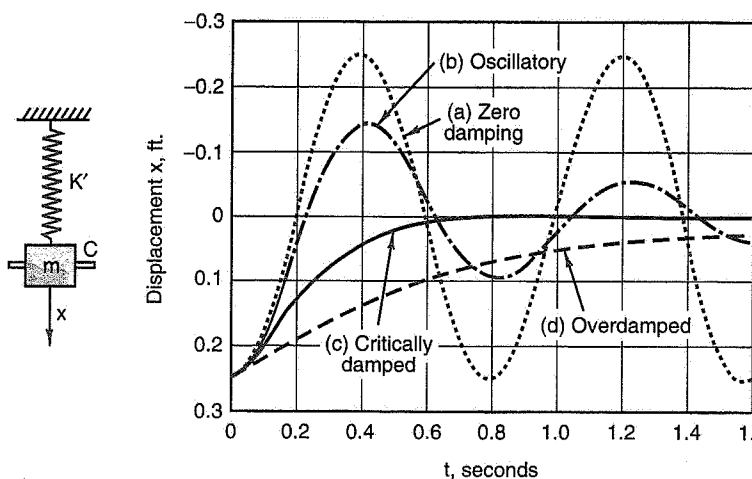


Figure 6.3 Effect of damping ratio on transient response of spring-mass-damper system.

Table 6.1 Comparison of Rectilinear and Rotational Dynamics

Rectilinear	Rotational
Applied force, F (lb.)	Applied Torque, T (lb.-ft.)
Inertia reaction force, ma (lb.)	Inertia reaction moment, $I\alpha$ (lb.-ft.) (α = angular acceleration, in rad./sec. ²)
Damping force, Cv (lb.)	Damping moment: C in lb.-ft./rad./sec. multiplied by angular velocity in rad./sec.
Spring force, $K'x$ (lb.)	Spring torque: K' in lb.-ft./rad. multiplied by displacement angle in radians

Suspension System Example

For illustrative purposes we will use a simplified example that avoids suspension system kinematic complexities. Assume a symmetrical car with a total weight of 2200 lb.; the chassis weight is 2000 lb. (500 lb. or 15.53 slug mass on each wheel) and the wheel unsprung weight is 50 lb./wheel or 1.55 slug mass. Also assume that the ride rate at each

wheel is measured and is 375 lb./in. and that the tire spring rate is known to be 2000 lb./in. at the desired tire pressure. We can now make some calculations on a "quarter-car" basis (see Figure 6.4).

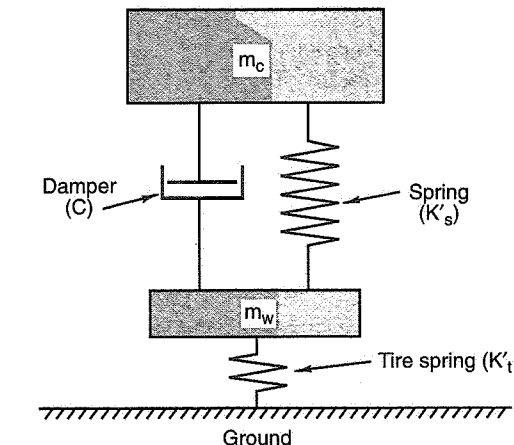


Figure 6.4 "Quarter-car" SMD system.

Static Deflection—This is 500 lb./375 lb./in. = 1.33 in.

Chassis Natural Frequency, ω_c —The measured ride rate, as defined in Ref. 1, takes into account the suspension spring (in the wheel plane), with rate K'_s , and the tire spring with rate K'_t . If the measured ride rate, K'_R , is 375 lb./in. and the tire rate is measured separately at 2000 lb./in., the suspension rate can be found from (see Chapter 21)

$$K'_R = \frac{K'_s K'_t}{K'_s + K'_t}$$

where K'_R is the composite rate for two springs in series.

Then

$$375 = \frac{K'_s (2000)}{K'_s + 2000}$$

from which, $K'_s = 462$ lb./in.

For the chassis natural frequency, use the suspension rate and the chassis mass and apply Eq. (6.2). Thus,

$$\omega_c = \sqrt{\frac{K'_s}{m_c}} = \sqrt{\frac{462}{15.53/12}} = 18.9 \text{ radians / sec.}$$

$$18.9/2\pi = 2.9 \text{ Hz (wheel stationary)}$$

Wheel Natural Frequency, ω_w —To compute the wheel natural frequency (often called the wheel hop frequency), it is necessary to take into account K'_s and K'_t because the wheel oscillates between the suspension and tire springs. Although these two springs are on opposite sides of the wheel/hub/knuckle mass, the mass would feel the same force if the two springs were in parallel on one side of the mass. In other words, the two springs, K'_s and K'_t , are in parallel and their composite rate is their sum.

$$\omega_w = \sqrt{\frac{(K'_s + K'_t)}{m_w}} = \sqrt{\frac{462 + 2000}{1.55/12}} = 138 \text{ radians / sec.}$$

$$138/2\pi = 22.0 \text{ Hz (chassis stationary)}$$

Shock Absorber for Sprung Mass—Now suppose we wish to use a shock absorber whose damping constant, C , is such that the chassis motion is only slightly underdamped. If we use a ζ of 0.9 then, from Eq. (6.4),

$$0.9 = \frac{1}{2} \left(\frac{C}{\sqrt{K'_s m_c}} \right) = \frac{1}{2} \left(\frac{C}{\sqrt{462 \times (15.53/12)}} \right)$$

from which

$$C = 0.9 \times 2 \times \sqrt{462 \times (15.53/12)} = 44 \text{ lb./in./sec.}$$

Shock Absorber for Unsprung Mass—We can next ask the question: What does this value of C do to the wheel hop mode (with respect to a stationary chassis)? Eq. (6.4) provides the answer:

$$\zeta = \frac{1}{2} \left(\frac{C}{\sqrt{(K'_s + K'_t)m_w}} \right) = \frac{22}{\sqrt{2462 \times (1.55/12)}} = 1.23$$

In the course of choosing a damping ratio to keep chassis motion under control—that is, non-oscillatory—the wheel motion is usually slightly overdamped. The masses and

spring rates in passenger car suspension systems are proportioned such that both the chassis and the unsprung mass are reasonably damped in ride by the same shock absorber.

Warning—Coupled vs. Uncoupled Systems

By assuming that one element is stationary in the above treatment we have, in effect, uncoupled the chassis and wheel. In actuality the chassis/wheel system is coupled and the oscillatory modes are complex, depending on whether the two modes (ω_c and ω_b) are in-phase or out-of-phase. Suffice it to say that the above approach yields good approximations; more sophisticated treatments can be found in the literature (see, for example, Ref. 18).

6.3 Dynamic Stability—Two-Degree-of-Freedom Automobile

Returning now to the simple 2DF model (bicycle model), we can draw some parallels with the spring-mass-damper system. In the Approach section earlier in this chapter, it was noted that the denominator of the transfer function, the “characteristic expression,” determines the inherent stability of the system; this can be described by the *undamped natural frequency* and the *damping ratio*. If we compare the transfer functions of the equation of motion for the spring-mass-damper system and the equations for the 2DF model (solved simultaneously), the form of the denominators is precisely the same. The correspondence between the inertia, spring, and damping coefficients is given in Table 6.2 (see also Section 6.5).

Table 6.2 Inertia, Damping, and Spring Coefficients

	Inertia	Damping Coefficient	Spring Coefficient
Simple spring-mass-damper system	m	C	K'
2DF automobile in derivative notation	I_z	$C = -N_r - \frac{I_z Y_\beta}{mV}$	$K_T = N_\beta + \frac{Y_\beta N_r - Y_r N_\beta}{mV}$
2DF automobile in physical parameters of the derivatives	I_z	$C = -(a^2 C_F + b^2 C_R) - I_z \frac{(C_F + C_R)}{mV}$	$K_T = (a C_F - b C_R) + \frac{\ell^2 C_F C_R}{mV^2}$

From the equations in the table, the natural frequency, ω_n^2 , and a damping ratio, ζ , can be calculated, thus,

$$\omega_n^2 = \frac{\text{Spring Coefficient}}{\text{Inertia}} = \frac{K_T}{I_z}$$

$$\zeta = \frac{1}{2\omega_n} \left(\frac{\text{Damping Coefficient}}{\text{Inertia}} \right) = -\frac{1/2(C/I_z)}{\sqrt{K_T/I_z}}$$

Natural Frequency

As summarized at the end of the preceding chapter on steady-state stability, there are a number of related ways of expressing under/oversteer. We have selected several of these in developing Table 6.3.

Table 6.3 US/OS Factor and Natural Frequency in Yaw

Under/Oversteer Factor	Natural Frequency, $\omega_n^2 =$
Stability Factor (K)	$\frac{C_F C_R \ell^2}{m^2 k^2 V^2} (1 + KV^2)$
Understeer Factor (\bar{K})	$\frac{C_F C_R \ell}{m^2 k^2 V^2 g} (\ell g + \bar{K}V^2)$
Stability Index (SI)	$\frac{(C_F + C_R)\ell}{mk^2} (\text{SI})$
Static Margin (SM)	$\frac{(C_F + C_R)\ell}{mk^2} \left(\frac{C_0 \ell g}{V^2} - SM \right)$
Cornering Compliance (D)	$\frac{C_F C_R \ell}{m^2 k^2 V^2 g} (\ell g + (D_F - D_R)V^2)$

(continued)

Table 6.3. US/OS Factor and Natural Frequency in Yaw (cont.)

where $K = -\left(\frac{SM}{C_0 \ell g}\right)$, $1/(\text{ft./sec.})^2$ (classical stability factor)

$\bar{K} = \left(\frac{SM}{C_0}\right)$, nondimensional

$\frac{K}{g} = K\ell$, $1/g$

$$UG = 57.3 K\ell g = D_F - D_R$$

$$D_F - D_R = 57.3 \frac{\bar{K}}{g} = 57.3 K\ell$$

k = radius of gyration in yaw

There are many observations that one can make about the car's transient response. If we recognize that high values of ω_n are desirable for fast response, then we can look at the factors which constitute ω_n and evaluate their effects. Thus,

$$\omega_n^2 = \frac{C_F C_R \ell^2}{m^2 k^2} \left(\frac{1 + KV^2}{V^2} \right) \quad (6.6)$$

is one form of the equation of interest from Table 6.3.

In the $C_F C_R / m^2$ term, we have a form of the total cornering coefficient, C/W. Its value should be large for rapid response—that is, lots of tire and light weight. Further, it suggests that for a given total cornering stiffness ($C_F + C_R$), equal values front and rear are best from this standpoint. The distribution effect is a relatively weak one, however. A difference of 20% between C_F and C_R , i.e., $C_F = 0.8C_R$, for the same total value, gives a loss in their product of only 1%. To give some idea of reasonable values for this factor, a few representative vehicles are listed in Table 6.4).

Table 6.4 Total Cornering Factor

Vehicle	$C_F C_R / m^2 (\text{ft.}^2/\text{sec.}^4)$
Full-size station wagon	1.55×10^4
Full-size sedan	2.05×10^4
Small sports car	4.45×10^4
Large American sports car	9.75×10^4
Current F.1 Grand Prix	$(100 \text{ to } 200) \times 10^4$

One might want to think of this term as the lateral motion equivalent of the performance factor, power-to-weight ratio. It is a measure of the cornering power with respect to the mass of the vehicle.

The next factor is a geometry to inertia ratio—a form of the k^2/ab ratio (inverted). It indicates how the weight is distributed along the length of the car. For good response, ℓ^2/k^2 should be large. Interpreted physically, it suggests that vehicle weight should be kept within the wheelbase; large overhangs result in increased values of k^2 for a given weight. Values may range from about 3 for large station wagons and cars, 5 for small sports cars, and up to 7.5 for current F.1 cars.

The third factor is $(1 + KV^2)/V^2$. It shows how the transient response can be affected by the stability factor and demonstrates that the under/oversteer characteristic of the car (basically a steady-state consideration) is also involved in the transient dynamics. There are a number of ways to look at this. First, note that increasing velocity always works toward decreasing the natural frequency, the effect of the V^2 term in the denominator. This is what happens with the NS car for which K is zero. Positive values of K (the understeer configuration) help mitigate this trend while negative values (oversteer) supplement the effect. At that speed for which $KV^2 = -1$ (the critical speed), response time as well as the steady-state gain become large—the vehicle tends to spin in the fixed control mode.

It may be more satisfactory to view the natural frequency in a form which can be derived from Eq. (6.6):

$$\omega_n^2 = \frac{C_F C_R \ell^2}{m^2 k^2 V^2} + \left(\frac{a C_F - b C_R}{m k^2} \right) \quad (6.7)$$

The first term defines the natural frequency for the neutral steer car; the second term modifies this frequency upward or downward according to its sign (i.e., for under or oversteer) and is independent of speed. For a current F.1 car, NS, this simple formula gives $\omega_n \approx 3$ Hz at 100 mph and 1.5 Hz at 200 mph.

Yet another way to view the effect is that KV^2 acts as a wheelbase stretcher (or shortener). One might think of it as a modifier to ℓ in Eq. (6.6). Then, at the characteristic speed, where $KV^2 = 1$, the **apparent** wheelbase of the car is 1.4 times the **true** wheelbase of a neutral steerer. Conversely, at critical speed for the oversteer car, the apparent wheelbase is zero, since $KV^2 = -1$ for this condition.

Damping

The other factor of interest in the characteristic equation is the damping term. Although an equation giving ζ (damping ratio) explicitly can be written, it is rather cumbersome. Instead, we can write a simplified equation for the lateral and yaw damping as

$$2\zeta\omega_n = - \frac{m(a^2 C_F + b^2 C_R) + m k^2 (C_F + C_R)}{m^2 k^2 V} \quad (6.8)$$

If we assume the completely balanced NS car ($C_F = C_R$, $a = b$ and $k^2/ab = 1$), the expression will collapse to

$$2\zeta\omega_n = - \frac{4C_F}{mV}$$

With these parameter values, ω_n is equal to $2C_F/mV$ and ζ turns out to be equal to 1 (i.e., critically damped). And, in fact, neutral steer vehicles, even when the values of the parameters do not satisfy our assumption, are very nearly critically damped at all speeds. Understeer vehicles are underdamped at all speeds; oversteer vehicles are overdamped.

Numerator Terms

Each of the transfer functions, as developed in Ref. 123, contains frequency-sensitive terms in the numerator. While these do not affect the system stability, they do influence the transient response (and of course the frequency response as well). The degree of this influence depends on the relative values of the terms in the numerator and denominator, and we find that for reasonable values of the car's parameters, the effect of the derivative terms in the numerator is important.

6.4 Single-Degree-of-Freedom Analysis

Those modern race cars which develop high downforce from ground effects are severely limited in terms of roll, pitch, and ride height changes. These cars can be approximated by the simple 2DF model in the sense that their motions can be described in terms of yawing and lateral velocities. The overall dynamic motions of the vehicle (not high

frequency vibrations) are strongly influenced by the lateral and yaw dampings, the inertia characteristics, and by speed/traction effects.

Some physical understanding of the importance of the damping terms can be shown by considering two special cases, from Ref. 92, paper no. 5.

Sideslip Response to a Lateral Force, Zero Yawing

From the lateral force equation for the "bicycle" model (Eq. (5.10)), for $r = 0$, set $Y_\delta \delta = F_y$.

Substitute, $\beta = v/V$, and rearrange:

$$\left(\frac{Y_\beta}{V}\right)v - m\dot{v} = -F_y \quad (6.9)$$

The time solution is

$$\frac{v}{F_y} = -\frac{V}{Y_\beta} \left(1 - e^{\left(Y_\beta/mV\right)t}\right) \quad (6.10)$$

This response is shown in Figure 6.5. It is exponential, convergent because Y_β (the damping in sideslip) is negative. The steady-state response magnitude increases with speed. The time to reach approximately 63% of steady-state is

$$t_{1/e} = \frac{-mV}{Y_\beta} \quad (6.11)$$

Several implications of this response relationship depend on the type of input force, F_y . Consider first a lateral side wind gust. If Eq. (6.10) is integrated to give a lateral displacement per unit wind force, it will be seen that a minimum response rate will occur if the response time is large and the steady-state response is small. For a given V/Y_β , the larger the mass the longer the response time, but, the steady-state response is independent of mass. For F_y from a change in road tilt (camber), both the response time and the steady-state response depend on m/Y_β , hence any increase in response time also increases the steady-state response. In this situation a high value of Y_β is desirable—large total tire cornering stiffness. In maneuvering, short response time and low steady-state sideslip is desirable; the vehicle goes where it is pointed. This is achieved by a high value of Y_β and a low mass for this simple model.

A lane change maneuver on a current F.1 car indicates the very rapid response and damping to steady-state, particularly at the lower speeds. Both the response time and

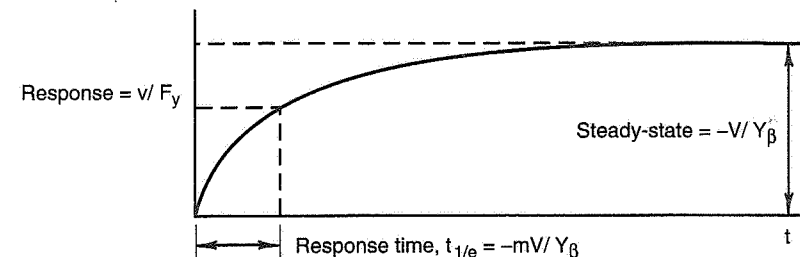


Figure 6.5 Transient sideslip response to side force, F_y ($r = 0$).

steady-state response increase with speed. The following values were calculated for a current F.1 car of 1719 lb. G.W. with front/rear axle cornering stiffnesses of 700/1250 lb./deg. It is assumed that a 2g maneuver can occur in the linear range of these tires.

	100 mph	150 mph
Response time	0.070 sec.	0.105 sec.
Steady-state lateral velocity for a 2g lateral force input	4.51 ft./sec.	6.77 ft./sec.
Δ Sideslip angle	1.76 deg.	1.76 deg.

Yaw Response to Steer Angle, Zero Sideslip

In this case, the model can yaw relative to its velocity vector but there is no lateral velocity, v , in the vehicle fixed axis system. In effect, it has infinite damping in sideslip. The situation is shown in Figure 6.6. The heading angle, ψ (positive when the vehicle is yawed to the right), gives rise to a moment:

$$N = aF_{YF} - bF_{YR} = -(aC_F - bC_R)\psi$$

Thus, $\partial N / \partial \psi = N_\psi = -(aC_F - bC_R) = -N_\beta$. The equation of motion in this single degree of freedom is

$$I_z \ddot{\psi} - N_r r - N_\psi \psi = N_\delta \delta \quad (6.12)$$

When this equation is solved by the Laplace operator, the denominator (characteristic) indicates that several types of response are possible depending on the relative magnitudes and signs of the derivative terms in relation to the yaw inertia, I_z .

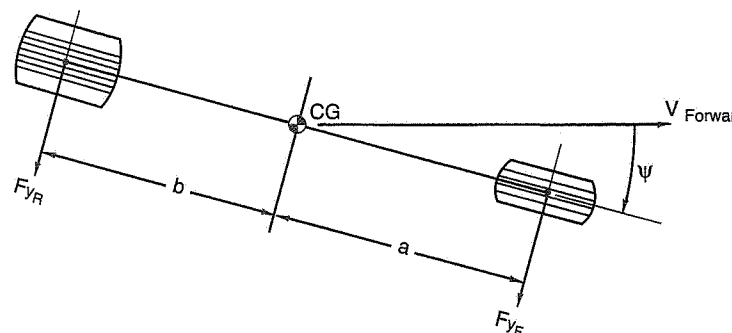


Figure 6.6 Yawing motion definitions.

- If N_ψ is positive ($N_\beta -$), yawing motion is divergent or oscillatory unstable.
- If N_ψ is zero ($N_\beta = 0$), yawing motion is neutrally stable.
- If N_ψ is negative ($N_\beta +$), yawing motion is convergent or a damped oscillation.

Note, for a 2DF vehicle it was shown that the vehicle can remain stable with a negative N_β up to the critical speed, due to high damping in sideslip. In this single degree of yaw motion model, the sideslip motion does not exist and instability occurs as soon as N_β becomes negative. This is an example of the interaction of the single-degree-of-freedom modes in producing the two-degree-of-freedom motions.

N_ψ ($= -N_\beta$) is the “index of stability” of yawing motion. The motion is exponential or oscillatory and this is determined by the relationship between the stability/damping terms and the yaw inertia. If,

$N_r^2/4I_z > -N_\psi$, the motion is convergent and exponential.

$N_r^2/4I_z < -N_\psi$, the motion is oscillatory.

Since N_r decreases inversely with speed, there will be some speed at which

$N_r^2/4I_z = -N_\psi$, and the motion changes character.

When the response is exponential, the motion following a step input is primarily a function of $2I_z/N_r$ —long response times occur for cars having large I_z and low N_r . Both of these terms, yaw inertia (polar moment of inertia) and yaw damping, tend to vary as the square of the wheelbase. Thus, varying the wheelbase is not an effective way to change the response time. The appropriate way to reduce the response time for a given wheel-

base is to reduce the radius of gyration (I_z) and increase the tire cornering stiffness, as in modern race cars.

An interesting approximation to the term $2I_z/N_r$ can be derived. For the case of $a \approx b$ and $C_F \approx C_R$,

$$N_r \approx \frac{\ell^2 Y_\beta}{4V} = +\frac{a^2 Y_\beta}{V}, \text{ and } I_z = mk^2$$

Then,

$$\frac{2I_z}{N_r} = +\frac{2k^2 m}{a^2 Y_\beta / V} = +2 \left(\frac{mV}{Y_\beta} \right) \left(\frac{k^2}{ab} \right)$$

where $-mV/Y_\beta$ is the response time for the single-degree-of-freedom side slip case. This says that the two single-degree-of-freedom cases are coupled by the k^2/ab ratio.

When the response is oscillatory, the natural frequency and damping ratio for the yaw/zero sideslip model are

$$\omega_n^2 = \frac{-N_\psi}{I_z}$$

$$\zeta^2 = \frac{-N_r^2}{4I_z N_\psi}$$

Since N_ψ is negative for stability, both ω_n and ζ are positive quantities. The natural frequency will increase with the static directional stability, N_ψ , and decrease with increase in I_z . This frequency is independent of speed. The damping ratio decreases rapidly with speed (since N_r varies inversely with speed). The damping ratio also decreases with increase in I_z and N_ψ .

To summarize, the characteristics of these two single-degree-of-freedom models are strongly influenced by the lateral damping and yaw damping, respectively. The damping terms depend on the tire cornering slopes and are large in the linear range, but decrease as the limit is approached. This effect, combined with the decrease in yaw damping with speed has an effect on race car behavior at the limit.

6.5 Two-Degree-of-Freedom Normalized Response Charts

In Ref. 123, Dr. Radt develops a 2DF derivative model for “illustrating the relationships between the stability derivatives and parameters of the dynamic response.” This model,

following from a three-degree-of-freedom model, reduces the dynamic response from fourth order to second order, i.e., to a spring-mass-damper system.

The mathematical development starts with Eqs. (5.10). The moment equation is solved for β which is then differentiated to get $\dot{\beta}$. These are substituted into the force equation of (5.10) to give a single differential equation in yaw rate, r , and its derivatives.

The steady-state yaw rate, r_0 , is obtained by setting the first and second derivatives of yaw rate to zero and normalized by dividing by the steady-state steer angle, δ_0 . When this equation is combined with the differential equation in r , a single expression for r/r_0 results:

$$I_z \left[\frac{d^2(r/r_0)}{dt^2} \right] + C \left[\frac{d(r/r_0)}{dt} \right] + K_T (r/r_0) = Q \quad (6.13)$$

$$\text{where } C = - \left[N_r + \frac{(I_z Y_\beta)}{mV} \right]$$

$$K_T = N_\beta + \frac{Y_\beta N_r - Y_r N_\beta}{mV}$$

$$Q = K_T \left[\frac{1 + (mVN_\delta)(d(\delta/\delta_0)/dt)}{Y_\delta N_\beta - Y_\beta N_\delta} \right]$$

On examination, Eq. (6.13) can be recognized as similar to the linear equation for a damped torsional pendulum:

$$I \left(\frac{d^2\theta}{dt^2} \right) + C \left(\frac{d\theta}{dt} \right) + K_T \theta = Q \quad (6.14)$$

$$\begin{aligned} \text{where } \theta &= \text{Rotational displacement} \\ I &= \text{Rotational moment of inertia} \\ C &= \text{Torsional damping} \\ K_T &= \text{Torsional spring rate} \\ Q &= \text{Applied torque} \end{aligned}$$

Eq. (6.13) for the 2DF model (which couples yaw rate and sideslip) compares to Eq. (6.14) for the torsional pendulum in the following manner: The effective inertia is the same in both equations; the equivalent torsional damping in (6.13) contains both yaw damping

and damping in sideslip; the equivalent torsional spring in (6.13) contains the static directional stability and a second term which depends on the damping derivatives. The damping derivatives decrease with velocity and the second term in the equation for K_T , the spring term, can be shown to decrease as velocity squared.

By analogy between Eqs. (6.14) and (6.13), one may recognize the *undamped* natural frequency, ω_n , and the damping coefficient, ζ , as

$$\omega_n^2 = \frac{K_T}{I_z} = \frac{N_\beta}{I_z} + \frac{Y_\beta N_r - Y_r N_\beta}{mVI_z}$$

ω_n in radians/sec., and

$$\zeta \omega_n = \frac{C}{2I_z} = - \frac{N_r/I_z + Y_\beta/mV}{2}$$

$$\omega = \omega_n \sqrt{1 - \zeta^2}$$

Step Response Charts

Using Laplace transform techniques, we can solve for the time (t) response to a step change in steer angle. The vehicle starts in straight-ahead motion, and at time zero a step steer is applied. The equations are developed for r/r_0 and β/β_0 for the underdamped (oscillatory) case where $\zeta < 1.0$ and for the overdamped case $\zeta \geq 1.0$. In addition, relationships are developed for

- Response time to 90% of steady-state, 1st crossing
- Time to peak
- Percent overshoot

The solutions for r/r_0 and β/β_0 are in terms of $\omega_n t$ and ζ and a time constant, τ . The solutions for r/r_0 and β/β_0 are identical except for different values of τ , namely τ_r and τ_β which are defined in terms of the derivatives:

$$\tau_r = \frac{mVN_\delta}{Y_\delta N_\beta - Y_\beta N_\delta}$$

$$\tau_\beta = \frac{-I_z Y_\delta}{mVN_\delta - Y_r N_\delta + Y_\delta N_r}$$

The results of numerical calculations are presented in six charts, Figures 6.7 through 6.12.

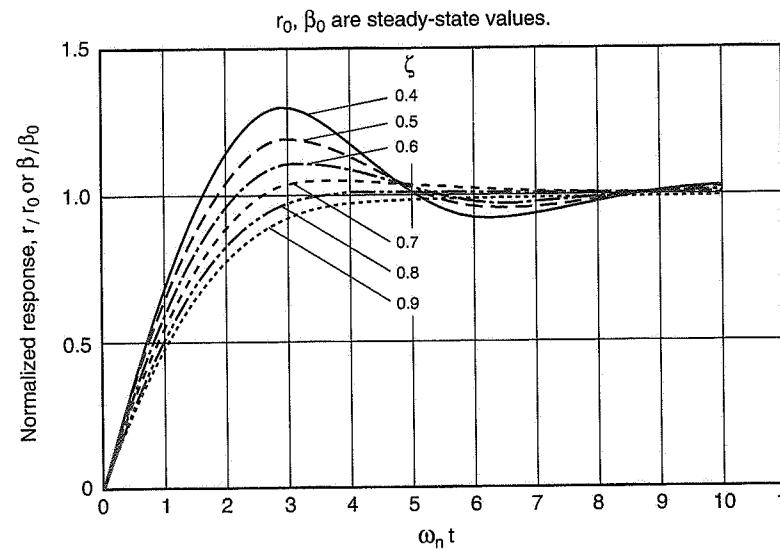
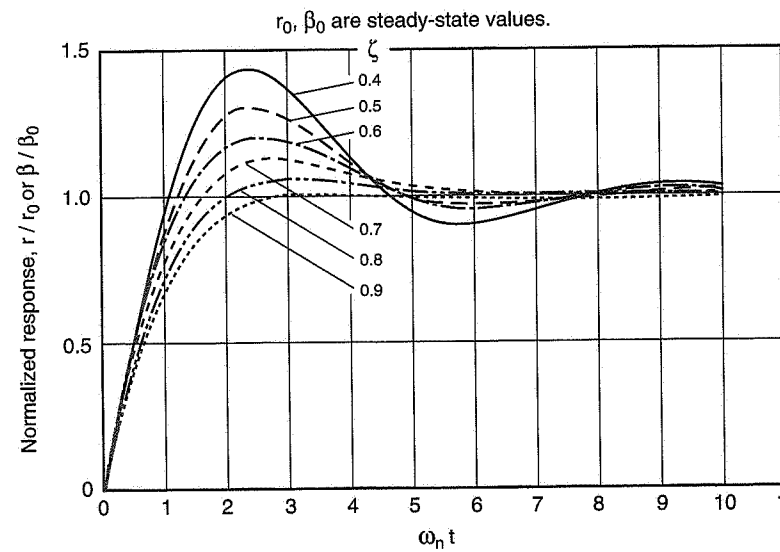
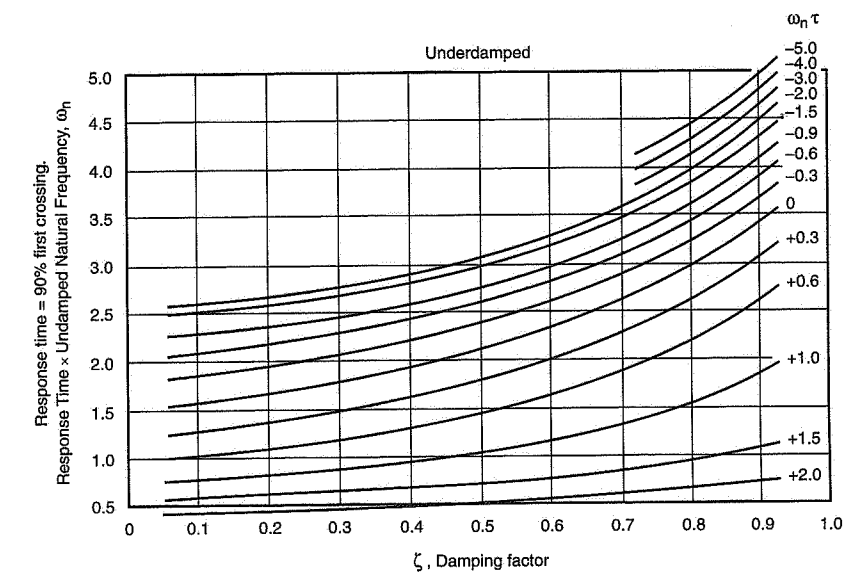
Figure 6.7 Normalized responses, $\omega_n\tau = 0.5$.Figure 6.8 Normalized responses, $\omega_n\tau = 1.0$.

Figure 6.9 Response time, underdamped case.

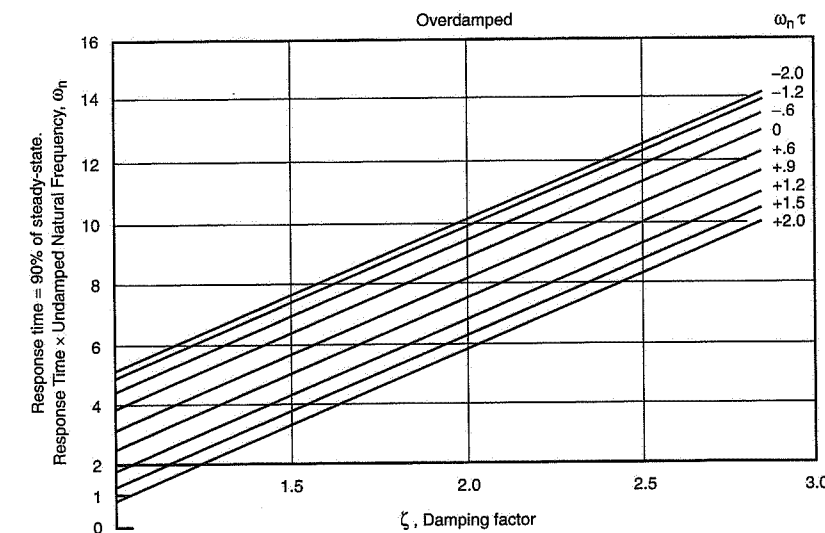


Figure 6.10 Response time, overdamped case.

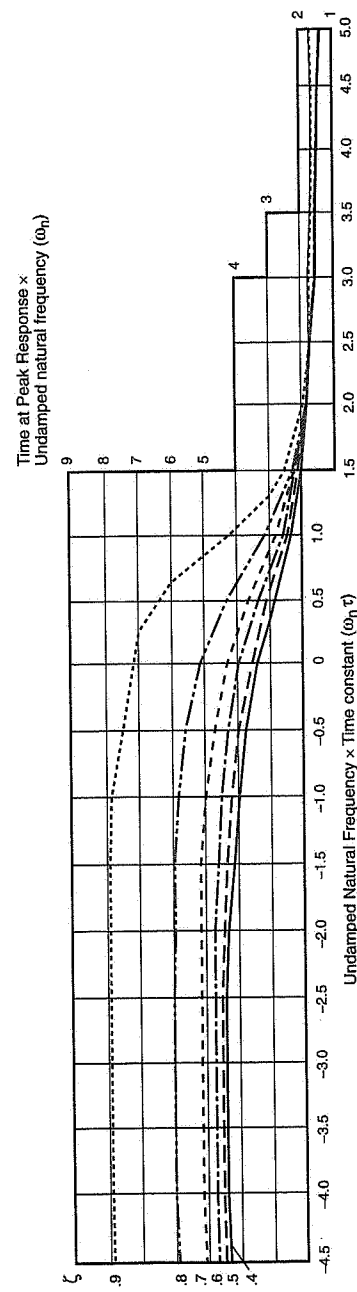


Figure 6.11 Time to peak response.

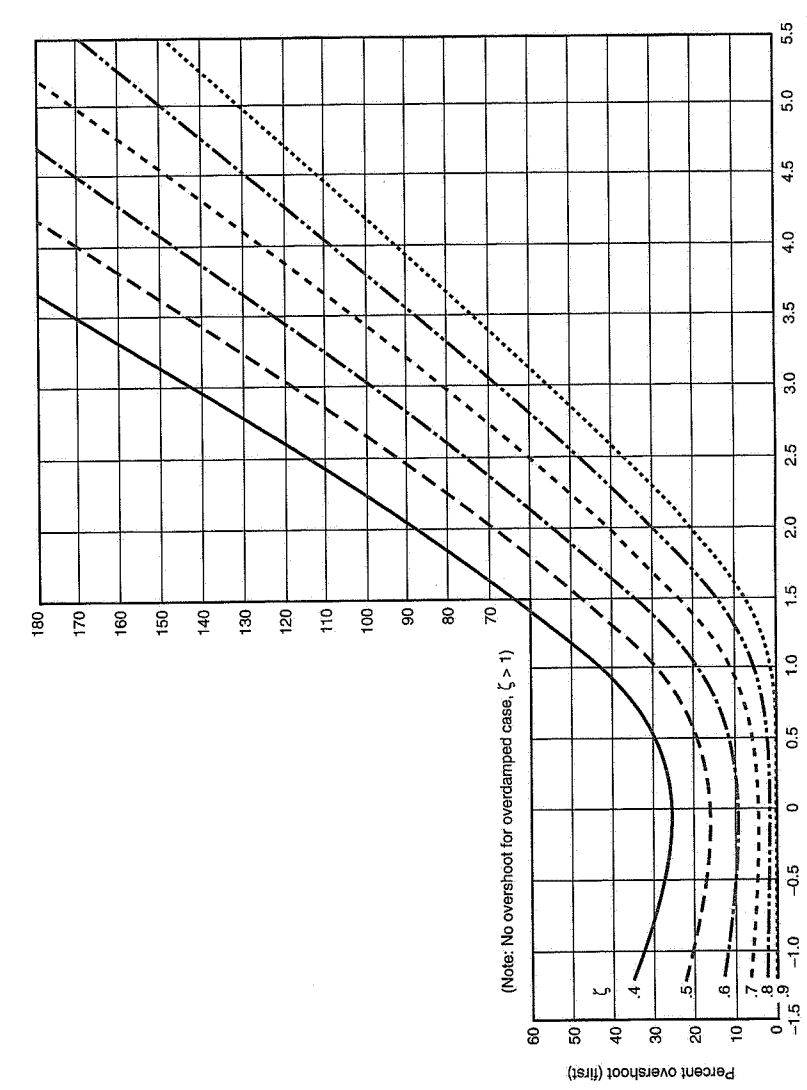


Figure 6.12 Percent overshoot.

Step Response Examples

First Example

Small front-wheel-drive car, same tires front and rear.

$$\begin{aligned} W &= 2000 \text{ lb.} & W_F &= 1300 \text{ lb. (65\%)} \\ m &= 62.11 \text{ slugs} & W_R &= 700 \text{ lb.} \\ I_z &= 832 \text{ slug-ft.}^2 \quad (k^2/ab = 0.85, k = 3.66 \text{ ft.}) \\ \ell &= 8.33 \text{ ft. (100 in.)} & a &= 2.92 \text{ ft.} & b &= 5.41 \text{ ft.} \end{aligned}$$

Tires: $C_F = -240 \text{ lb./deg.} = -13,752 \text{ lb./radian}$
 $C_R = -200 \text{ lb./deg.} = -11,460 \text{ lb./radian}$
 C_F, C_R are for two front or rear tires

$$\text{Understeer Gradient} = 57.3 (W/\ell) [(a/C_R) - (b/C_F)] = 1.91 \text{ deg./g}$$

$$\text{Derivatives: } Y_\beta = C_F + C_R = -25,212 \text{ lb./rad.}$$

$$Y_r = (1/V) (aC_F - bC_R) = +(1/V) 21,843 \text{ lb.-sec./rad.}$$

$$Y_\delta = -C_F = +13,752 \text{ lb./rad.}$$

$$N_\beta = (aC_F - bC_R) = +21,843 \text{ lb.-ft./rad. (stable)}$$

$$N_r = (1/V) (a^2C_F + b^2C_R) = -(1/V) 452,667 \text{ lb.-ft.-sec./rad.}$$

$$N_\delta = -aC_F = +40,156 \text{ lb.-ft./rad.}$$

Calculations for two speeds, 40 and 80 mph:

	40 mph 58.7 fps	80 mph 117.4 fps
Undamped natural frequency, ω_n	9.36 rad./sec. 1.49 Hz	6.45 rad./sec. 1.03 Hz
Natural frequency, $\omega = \omega_n \sqrt{1 - \zeta^2}$	4.72 rad./sec.	5.02 rad./sec.
Damping factor, ζ (nondimensional)	0.864	0.628
Time factor (yawing), τ_r	+0.112 sec.	+0.224 sec.
Time factor (sideslipping), τ_β	-0.45 sec.	-0.049 sec.

From Figures 6.9 through 6.12 obtain:

	40 mph		80 mph	
	Yawing r	Sideslip β	Yawing r	Sideslip β
$\omega_n \tau$	+1.03	-4.21	+1.42	-0.32
ζ	0.86	0.86	0.63	0.63
Response time $\times \omega_n$, 90% (Fig. 6.9)	1.62	4.63	0.84	2.70
Response time to 90% first crossing, sec.	0.17	0.49	0.13	0.41
(Time at peak) $\times \omega_n$ (Fig. 6.11)	3.55	7.14	2.21	4.31
Time to peak, sec.	0.38	0.76	0.34	0.67
Overshoot % (Fig. 6.12)	3.0	1.5	29.0	8.0

The undamped natural frequency, ω_n , is 30% less at 80 mph than at 40 mph and the damping has decreased by a comparable amount. The natural frequency, ω , was actually increased slightly to 5.02 rad./sec. at 80 mph from 4.72 at 40 mph. The response times to 90% and peak are slightly shorter at the higher speed in both yaw and sideslip. Time to peak response is about 2.4 times the response time (90%) for yaw and approximately 1.6 for sideslip. Increasing the damping factor decreases the overshoot in all cases, while increasing the time to peak response.

Second Example

Formula 1 car (c. 1993)

$$\begin{aligned} W &= 1719 \text{ lb. (driver & fuel)} & W_F &= 688 \text{ lb. (40\%)} \\ m &= 53.38 \text{ slugs} & W_R &= 1031 \text{ lb.} \\ I_z &= 639 \text{ slug-ft.}^2 \quad (k^2/ab = 0.55, k = 3.46 \text{ ft.}) \\ \ell &= 9.52 \text{ ft. (114.2 in.)} & a &= 5.71 \text{ ft.} & b &= 3.81 \text{ ft.} \end{aligned}$$

Tires: $C_F = -543 \times 2 = -1086 \text{ lb./deg.} = -62,228 \text{ lb./radian}$
 $C_R = -843 \times 2 = -1686 \text{ lb./deg.} = -96,608 \text{ lb./radian}$

Assume these cornering coefficients take into account aerodynamic downforce up to, say, 1g cornering.

Understeer Gradient = $57.3 \text{ (W/l)} [(a/C_R) - (b/C_F)] = 0$, neutral steer

Derivatives: $Y_\beta = C_F + C_R = -158,836 \text{ lb./rad.}$
 $Y_r = (1/V)(aC_F - bC_R) = +(1/V) 12,754 \text{ lb.-sec./rad.}$
 $Y_\delta = -C_F = +62,228 \text{ lb./rad.}$
 $N_\beta = (aC_F - bC_R) = 0 \text{ lb.-ft./rad.}$
 $N_r = (1/V)(a^2C_F + b^2C_R) = -(1/V) 3,429,449 \text{ lb.-ft.-sec./rad.}$
 $N_\delta = -aC_F = +355,322 \text{ lb.-ft./rad.}$

Calculations for two speeds, 60 and 180 mph:

	60 mph 88 fps	180 mph 264 fps
Undamped natural frequency, ω_n	45.4 rad./sec. 7.23 Hz	15.1 rad./sec. 2.41 Hz
Damping factor, ζ (nondimensional)	1.04	1.04
Time factor (yawing), τ_r	+0.030 sec.	+0.089 sec.
Time factor (sideslipping), τ_β	-0.049 sec.	-0.009 sec.

From Figure 6.10 obtain:

	60 mph		180 mph	
	Yawing r	Sideslip β	Yawing r	Sideslip β
$\omega_n \tau$	+1.36	-2.23	+1.34	-0.14
ζ	1.04	1.04	1.04	1.04
Response time $\times \omega_n$, 90% (Fig. 6.10)	1.90	5.20	1.80	4.20
Response time to 90% first crossing, sec.	0.04	0.11	0.12	0.28
Vehicle overdamped, no peak—long time to steady-state	0	0	0	0
Overshoot %				

The F.1 car is overdamped and thus has nonoscillatory responses over the speed range. The yaw velocity response times to 90% of steady-state are very short at both 60

and 180 mph (longer at 180). The time to steady-state was not calculated but is probably long compared to the response times. Since $N_\beta = 0$, the critical speed is infinite and the vehicle is NS over its speed range. This means that the yaw and sideslip motions are largely uncoupled.

For steady-state and $N_\beta = 0$, we have from Eq. (5.11),

$$N_\delta \delta = -N_r r$$

Now, $r = V/R$, or $Vr/g = V^2/gR$ = lateral acceleration, g units. Assuming a steering ratio, $G = 12$, let us calculate the steering wheel angle for a steady turn at 1g at $V = 60$ and 180 mph.

	60 mph 88 fps	180 mph 264 fps
$r = (1)(32.2)/V$	rad./sec. deg./sec.	0.37 21.0
N_r	lb.-ft./rad./sec. lb.-ft./deg./sec.	-38,971 -680
rN_r	lb.-ft.	-14,419 -1559
N_δ	lb.-ft./rad. lb.-ft./deg _{FW}	+355,322 +6201
$G = 12$	lb.-ft./deg _{SW}	+517 +28
$\delta_{SW} = -rN_r/N_\delta$, deg. for 1g turn		+517 +3

Since N_δ remains constant with speed, the decrease in steering angle required to accomplish a 1g turn at 180 mph is due to the fall-off in the yaw damping, rN_r . In a steady turn, the actual moments on the car due to yawing velocity and steering angle are equal. Because the control derivative, N_δ , is very large; only a relatively small steering angle is required to equilibrate the yaw damping. Because the F.1 car is neutral steer, only two moments determine its behavior, the yaw damping and control. For the previous small fwd car example, the static stability moment, N_β , must be taken into account.

As will be discussed in the next section, these step response estimates can be applied to other operating points, provided the initial conditions have been determined by some means, for example, a simulation of a constrained test like MRA Moment Method.

6.6 Notes on Stability Derivative Concept

The stability derivative concept has been extensively utilized in the linear analysis of Chapter 5 and in this chapter. As noted earlier, it was originally applied to the automobile by Leonard Segel in Refs. 92 and 144, in 1956. Segel's analysis was for the linear range of automobile maneuvering as defined by the linear slope of the tire's cornering force curve, which in the normal automobile covers operation up to about 0.35g lateral acceleration. The use of derivatives has frequently been assumed to be applicable only to the linear range as defined above. The origin of the derivative concept and its much greater utility are discussed below.

Stability derivatives had their origin in the analysis of aircraft stability and control. The original equations of motion were published in 1911 (see Ref. 25). These equations which used stability derivatives were for small perturbations about an initial operating condition. There was nothing which suggested that they applied only to the linear range of aircraft flight as defined by the linear portion of the lift curve. Although operating conditions were initially taken in straight flight, by 1915 they were extended to the case of steady turning by researchers at the Royal Aircraft Factory in England. At the same time wind tunnel techniques were developed for measuring the angular, control, and rotary derivatives, and at a somewhat later date, test techniques were devised for assessing the derivatives on full-size aircraft in flight.

The derivative concept has been in use in aircraft engineering to the present day. It has been the basis of analysis of stability and control, for designing stability augmentation (active controls) and automatic control, and for physically understanding aircraft motions. The derivative equations of motion have been applied at operating points over the full flight maneuvering range including stall and even spin conditions.

The final assessment of passenger car behavior is accomplished by test drivers in closed-loop handling maneuvers. A significant part of this evaluation, other than large amplitude safety maneuvers, concerns the behavior of the vehicle under ordinary driving conditions where most of the vehicle's life is spent. Here one is concerned with on-center handling and maneuvering under small control and disturbance inputs. The race driver is also concerned with the effect of small control and disturbance inputs when operating near the cornering limit. In both instances there is a need to establish a correlation between driver subjective feel and objective vehicle behavior. The derivative concept appears particularly promising for this correlation especially when it can be applied to the control forces as well as the control motions.

6.7 Transient Response Data

A variety of transient response tests have been developed based on different types of control inputs. For example, ISO International Standard 7401 (1988) considers step,

sinusoidal, random, and pulse steer inputs. This discussion will be based on the commonly used step/ramp steer input.

The test procedure is to establish a constant speed in a straight line. To quote ISO 7401:

... a steering input shall be applied as rapidly as possible to a preselected value and maintained at that value for several seconds or until the measured vehicle motion variables reach a steady-state. No change in throttle position shall be made, even though speed may decrease.

Data is taken in left- and right-hand steps and usually for a series of step magnitudes. An adjustable steering stop enables rapid manual inputs without overshoot.

Figure 6.13 illustrates a typical step/ramp input and response/output. The time to 90% of steady-state is generally defined as the *rise time*. Several responses may be measured, the most common being the yaw velocity, lateral acceleration, sideslip (β) and roll angle. Tests are normally run at 100 km/h (62 mph) but other speeds are also used. Although the ISO procedure calls for straight running at the start of the test, it is also possible to start from steady-state on some fixed-radius turn. Some typical response data for a street performance car are shown in Figures 6.14 through 6.16. The yaw velocity rise times are approximately 0.2 sec. and the lateral acceleration rise times are typically twice as long. It is the numerator term in the yaw rate transfer function which accounts for the quicker response in this variable than is achieved in lateral acceleration.

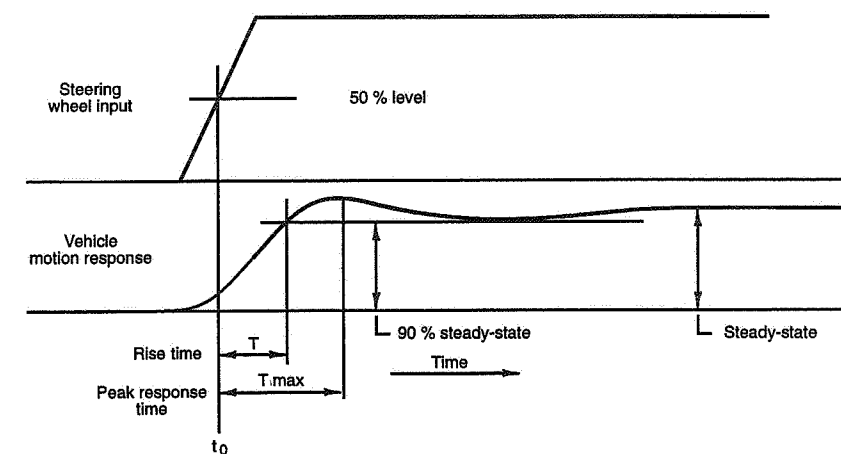


Figure 6.13 Rise time and peak response time (Ref. 9).

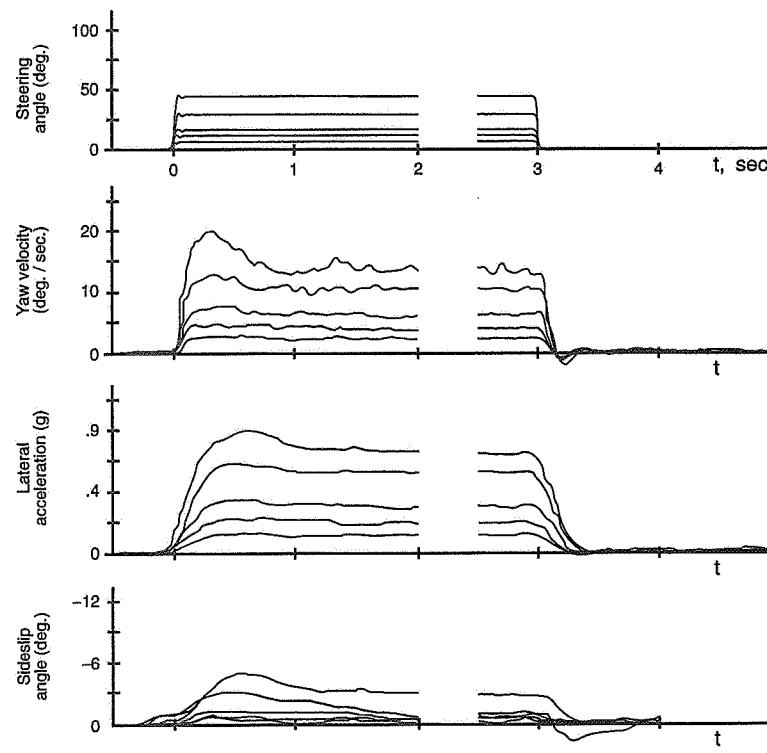


Figure 6.14 Transient response to ramp steer inputs, $V = 62$ mph.

The results of a survey of lateral acceleration rise time for domestic and foreign passenger cars performed by General Motors (1984) are given below:

	Origin	Minimum	Average	Maximum
Lateral acceleration rise time (sec.)	Domestic	0.28	0.41	0.77
	Foreign	0.24	0.37	0.51

In general the rise times decrease with more US at the expense of some overshoot. This overshoot increases with speed due to a decrease in damping but the amount of overshoot in passenger cars is not viewed as significant. Rise times longer than those above may be undesirable—the vehicle never seems to settle down and a driver-

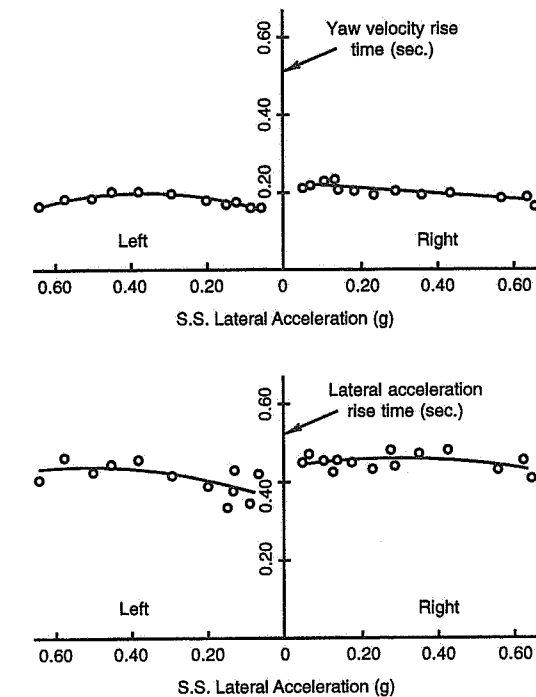


Figure 6.15 Yaw velocity / lateral acceleration rise times, from straight path, 62 mph.

induced oscillation may occur. An overloaded (rear load) station wagon (OS) is a case in point.

Yawning velocity rise times for sports and GT cars fall in the minimum passenger car range or shorter; values have been measured in the 0.11 to 0.14 sec. range.

Steering gain and response times are frequently confused and subjectively misinterpreted. SAE defines control gain as the ratio of steady-state lateral acceleration to the steering wheel angle input (g's/deg.). Rise time is a measure of the time to 90% steady-state from a step steer input (seconds). More gain (typically faster steering ratio) will result in a larger steady-state response but the time to reach 90% will remain about the same (linear system).

Unfortunately, response measurements on race cars are rare, but this does not mean that rise time is unimportant. For example, a recent project at MRA looked at rough road performance of a race car in terms of handling/roadholding instead of ride. Ideally,

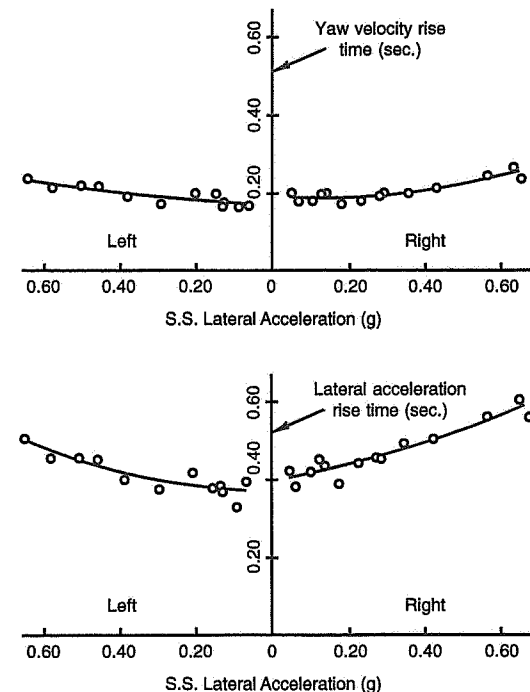


Figure 6.16 Yaw velocity / lateral acceleration rise times, from curved path, 62 mph.

race cars would always move from one steady-state condition to another—why waste time in a transient? This suggests short response times, not only for handling as discussed here, but for every part of the car, i.e., engine throttle response, transmission shift time, etc.

Force/Free Control Response

To properly study on-center handling and cars with quicker steering ratios, modeling and testing of force/free control are required. Free control testing is indicative of the force control since the steering system response is the result of the torques originating at the tires and the details of the steering system (manual or power, rack/box, linkage, etc).

Figure 6.17 is the result of a free control test in which the steering wheel was released from an initial condition of steady-state cornering. It demonstrates the dynamics of the

steering system—in this case a nonpowered one. The dynamics of the system are affected by the inertia of the steering wheel, the steering ratio, the spring and damping characteristics of the system components, and the kingpin torques from tire forces and gyroscopic forces.

Race cars have quicker steering systems than street cars, often 12:1 or faster, and smaller steering wheels (less inertia). Also, there is more emphasis on good force feedback for the driver. Future analysis of race car handling will have to involve the force control mode, and suitable models will be required.

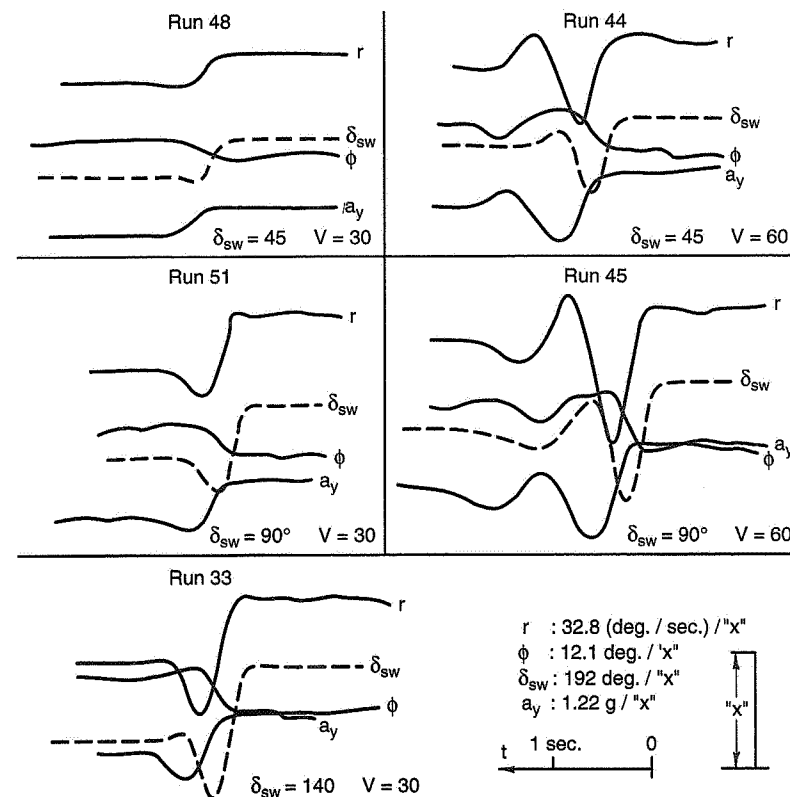


Figure 6.17 Typical free control data records.

6.8 Early Analytical Approach

One of the earliest analytical studies inspired by racing is Radt's "Motions of Skidding Automobiles" (Ref. 121) from 1960. In this effort a "bicycle" model was used but with a tire representation that took into account the nonlinearity of the cornering force curve and the effect of traction/braking via the friction circle. Performed on an analog computer, it enabled the calculation of steady-state turning behavior at high laterals and transient (time) responses of limit behavior. Both rear- and front-wheel drive were investigated.

Figure 6.18 (from the above report) depicts the effect of driving thrust on steady-state cornering at a constant speed, for various front-wheel steer angles, δ . The vehicle is in a RH turn.

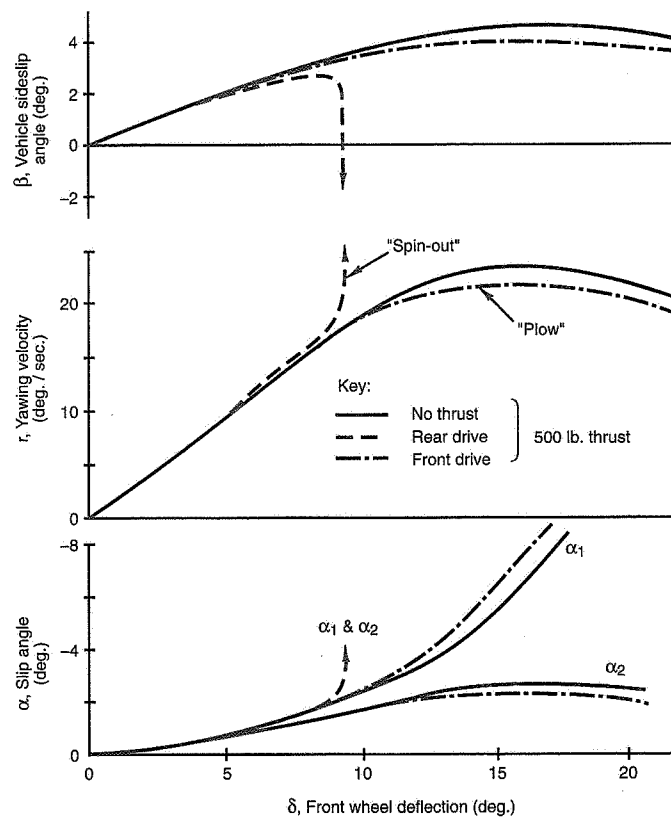


Figure 6.18 Effect of front- and rear-wheel driving thrust on steady turning at low speed.

This figure clearly shows the spinning and plowing behavior of rear- and front-wheel-drive cars when the limit is reached, in this case by too much "steer" (too tight a radius) for a given speed. Spinout is indicated by a rapid increase in yawing velocity in the direction of the turn; plow, by a fall-off of the yawing velocity. The slip angles are also shown (but with this model no effects of lateral weight transfer were included).

Figure 6.19 shows the effect of front- and rear-wheel driving thrust on a transient response to a front-wheel step steer (at the same speed as for Figure 6.18). In addition to the yaw velocity and vehicle sideslip responses, the change in heading (relative to earth axes) is also plotted. The step size is such that for a coasting vehicle and for the front drive, a steady-turning velocity and sideslip is reached after about one second. For the rear drive, whose lateral force capability is degraded by the driving thrust, the vehicle spins out. The front drive has a slightly reduced response over the zero driving thrust case (plowing).

Figure 6.20 examines spin recovery characteristics for the rear drive (at a higher speed and smaller step input than for Figure 6.19). The recovery technique is one of merely neutralizing the steer angle at two ("early" and "late") times in the transient. If recovery is initiated at 1.54 sec. after the step input, the yaw velocity decreases to zero and the heading angle stabilizes at 20 deg. If the attempt is initiated later, at 1.76 sec., the vehicle continues to spin out.

In order to demonstrate how important the driver characteristics are in limit operation where incipient spin may occur (due to excess speed, too much throttle application of rear drive, disturbance, etc.), a simple driver model was added to the simulation. The model assumed that a perfect driver responded to heading angle, ψ , in a closed-loop control such that

$$\delta = k\psi$$

where δ is the driver's steer angle
 ψ is the heading angle
 k is a gain constant

However, it was recognized that the real driver cannot respond immediately to a change of heading because of perception and neuromuscular delays, and a linear first-order time lag (represented by τ) was added to the above equation, thus,

$$\tau\dot{\delta} + \delta = k\psi$$

This says that the total δ in response to ψ has a rate component which depends on the lag time constant τ . Two values of τ were used, 0.1 and 1.0 sec., corresponding to fast and slow responding drivers.

In Figure 6.21, at modest speed, a spin is induced by increasing the steer angle to some 12.5° in 2 sec. with 500 lb. of driving thrust (rear drive) with no driver action. The re-

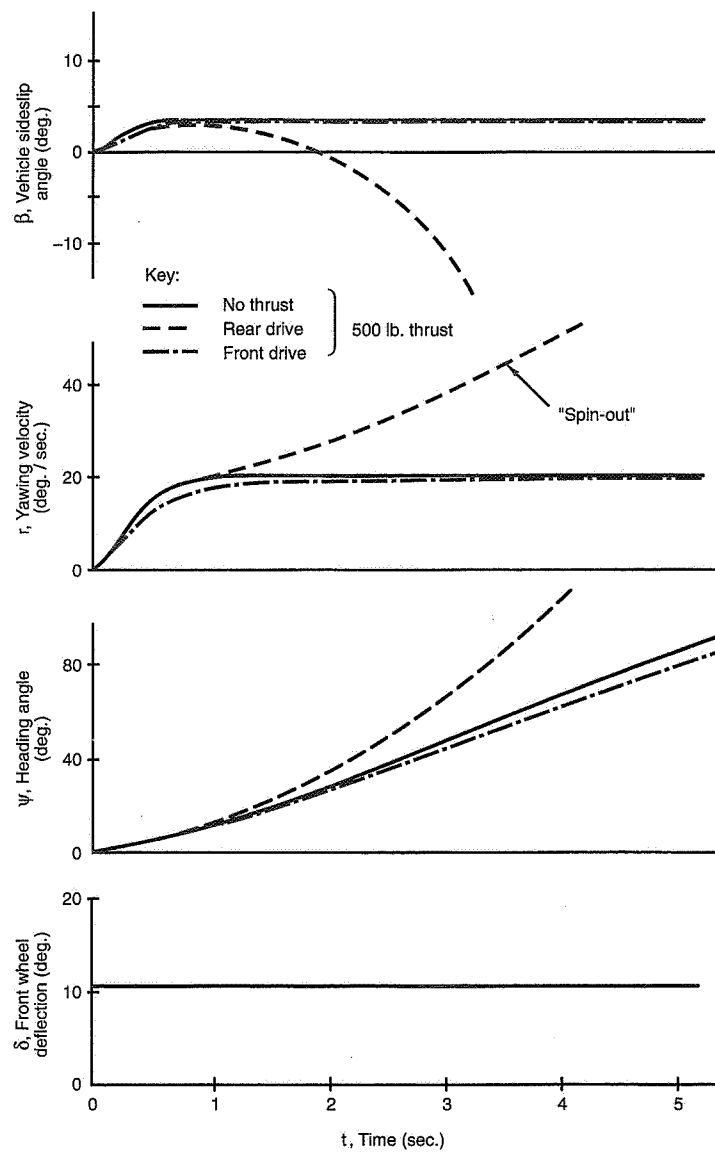


Figure 6.19 Effect of front- and rear-wheel driving thrust on step steer response.

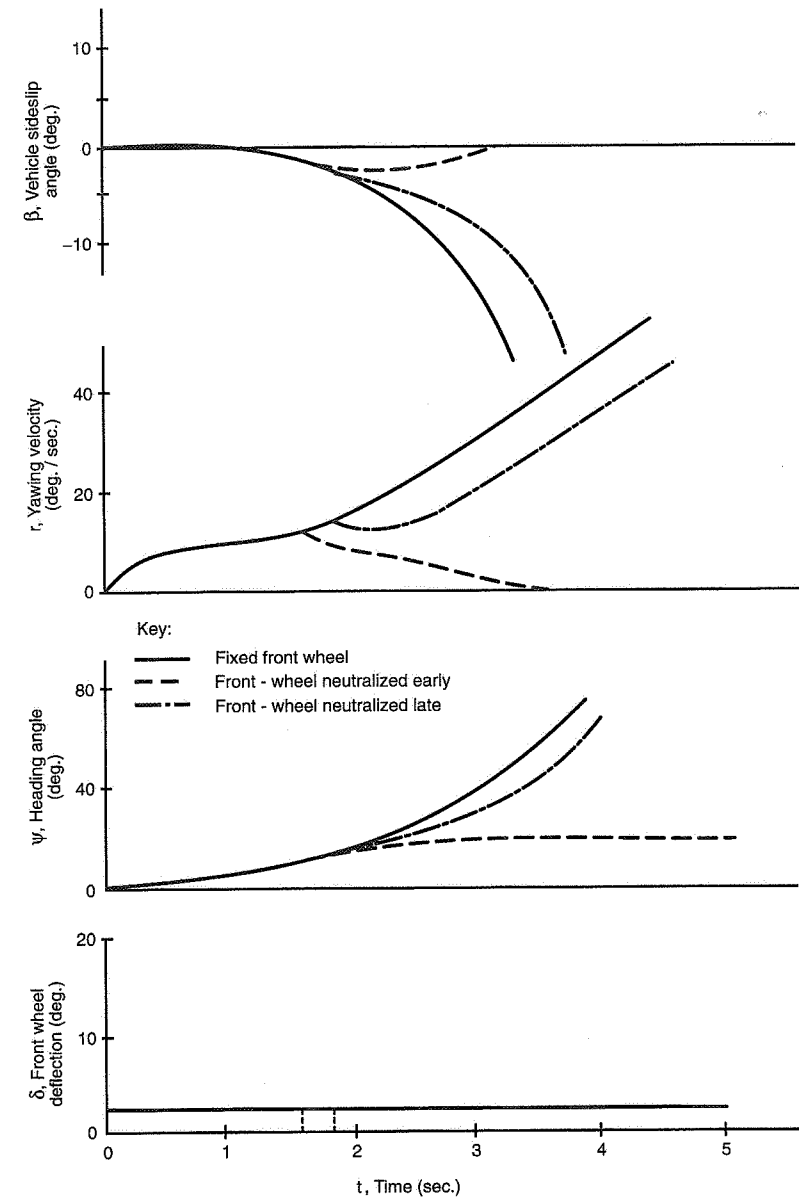


Figure 6.20 Neutralizing steering on "spin" recovery,
rear-wheel driving thrust = 500 lb.

responses in this case are the solid curves. The driver is then introduced with the two time lags. Both "drivers" are able to reduce the yaw velocity and recover, although the slow driver overshoots slightly and uses a small amount of negative steer angle to stabilize the heading angle.

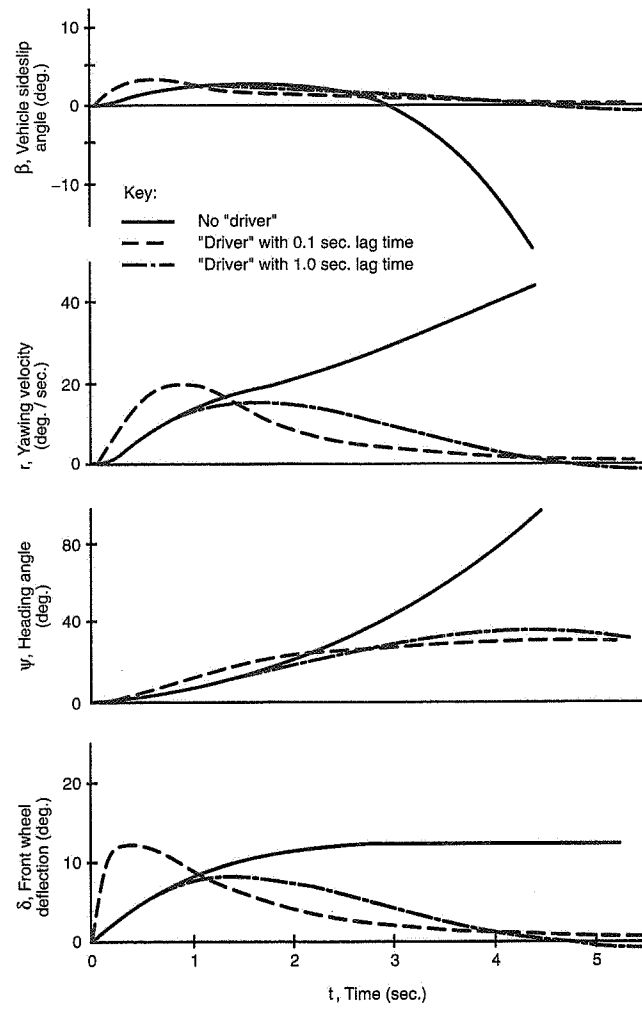


Figure 6.21 "Spin" recovery by simulated "driver" at low speed.

In Figure 6.22, at a higher speed, the drivers have considerable difficulty in spin recovery:

Slow driver, low gain (small k): Unsuccessful in avoiding spin.

Slow driver, high gain (large k): This driver stops a spinout to the right but over-controls and spins out to the left.

Fast driver, high gain (large k): Recovers from spin in a damped oscillation. Large control action in first 2 sec. and return to neutral.

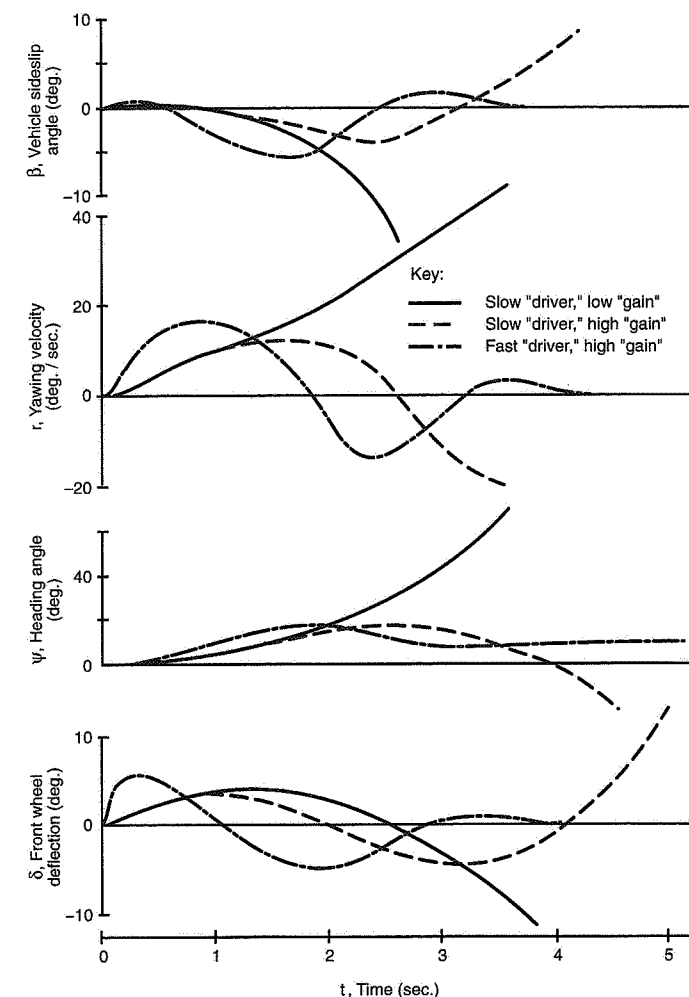


Figure 6.22 "Spin" recovery by simulated "driver" at higher speed.

The qualitative conclusions from this figure align with experience. Thus a fast-responding, high gain driver has the best chance of correcting rear breakaway but may have difficulty in avoiding an induced oscillation. In aircraft terminology this is called a "pilot induced oscillation" or PIO.

The early mathematical model used in Ref. 121 has been updated by Dr. Radt at MRA, where it is now called the Simplified Vehicle Dynamics Model (SVDM). This model is very flexible and has been useful in studying a number of problems including driver control of high-powered rally cars (for Ford of England, early 1980s), rear steer (four-wheel steer) algorithms and four-wheel drive. It has also formed the basis of the real-time model used in a simple simulator. The manual that accompanies the computer program includes documentation of the governing equations (over 200), making SVDM very useful as a learning tool.

6.9 Advanced Vehicle Dynamics Models

A survey of the literature indicates that a large variety of simulations of automobile motions exist. To this list could be added many unpublished, proprietary models available at the car companies and research establishments. These models differ in terms of the degrees of freedom involved and the level of their representation of the chassis/suspension, tires, driveline/differential, brake system, aerodynamics, etc. The choice of model depends on its underlying assumptions in relation to its intended use. In this book, for example, we have utilized derivative models based on small perturbations to explain automobile motion in physical terms.

To accurately predict the motions of a complete automobile over the full operating range of lateral acceleration and yaw rate requires a large amplitude, nonlinear model with multi degrees of freedom and detailed representation of the physical components of the automobile. There are not many models that meet this requirement that have also been validated against proving ground experiments. Some models of this caliber are described below.

The McHenry Model

In the mid-1960s, Raymond McHenry of Cornell Aeronautical Laboratory (CAL, now Calspan), started the development of a "computer simulation of general three dimensional automobile dynamics for the study of accident related maneuvers on irregular terrain." The development was government sponsored and continued for over six years in a series of phases. A progress report is given in Ref. 88. The model consists of 15 degrees of freedom—six rigid body motions of the sprung mass, four suspension deflections of the unsprung masses relative to the sprung mass, one steer degree of freedom, and four rotational degrees of freedom for wheel spin. In the course of the development extensive

correlation was accomplished with large amplitude maneuvers such as skidding on dry pavement and jumping ramp-to-ramp as done in automotive thrill shows. The model was also used to develop the special ramp shapes required to perform a spiral jump; the vehicle was launched from a spiral ramp, performed a 360-degree barrel roll in the air, and landed on another reversed spiral ramp.

The McHenry model may be classified as a phenomenological, lumped parameter simulation in which the various components of the vehicle and the tires were represented by equations theoretically and/or empirically based. As well as output listings, it also included computer graphic output. This model, eventually known as HVOSM (Highway-Vehicle-Object Simulation Model), was a pioneering effort, widely copied, and still extensively utilized in accident-related work.

Chevrolet DK-4 Model

One offshoot of the HVOSM development was the DK-4 model sponsored by Chevrolet in the 1967-68 period. This model was developed at CAL by R. Douglas Roland working closely with McHenry and his associates (Ref. 131). This model was directed toward "the simulation of transient nonlinear cornering on roadways which vary in elevation, camber and curvature, for axle rear suspension and independent rear suspension vehicles." The model included capability for open-loop driver input and also a preview-predictor driver model for closed-loop simulation including modes for path following, speed control, and skid recovery.

Since the expressed use of DK-4 was for automobile stability/control and handling design/development, comprehensive simulation of all significant elements of the vehicle configuration were included. The wide variety of inputs available are partially summarized as follows:

- Chassis data from tests on a kinematic and compliance test facility (Ref. 109) which generates nonlinear plots of suspension geometry and compliance. Depending on the particular item, either functional relationship or tabular lookup is used to model the physical test data.
- Wind tunnel force and moment data.
- Tire force and moment data, entered in tables for lateral/longitudinal force and aligning torque as functions of load, slip angle, camber, and tractive force.

Chevrolet and CAL worked closely together to insure accurate representations of vehicle components and consistent sign conventions throughout the program.

MRA Moment Method (MMM)

MMM is not time based like the previous models discussed but it was initially written using the basic equations developed for DK-4. Again, it was originally coded for mainframe computers. At MRA, the original program was first ported to a personal computer and then extensively rewritten and improved. Starting in the mid-1980s, MRA has continued to improve MMM by the addition of post-processing and other features to improve its utility as an interactive tool for design/development of vehicle handling for any type of automobile, passenger car to race car.

Vehicle Dynamic Simulation (VDS)

This MRA development is a logical successor to DK-4, but runs on personal computers. It generates time histories of vehicle motion and includes the capabilities of DK-4 as well as a comprehensive plotter capable of showing the gross motion of the vehicle and also detailed operating conditions at each wheel. Over 100 internal variables are available for plotting.

One MRA customer has validated VDS against proving ground (PG) tests. This was done with a passenger car using state-of-the-art instrumentation (in 1993-4); some of the results are shown in Figures 6.23 and 6.24. We have chosen a lane change maneuver, but other maneuvers indicate good correlation as well. Some of the steps required to make the comparison include:

- Instrument the sample vehicle and record PG data; select a good clean test run for each type of maneuver.
- Develop the vehicle model from dimensional data (wheelbase, track, etc.), weight data (CG locations—sprung/unprung), inertia tests (swing the vehicle), chassis test (static kinematics and compliance rig data on the sample), and damper tests (this data was somewhat suspect). We are assured that this data was used directly, no “fudging” was done to improve the correlation.
- Measure tire data in the laboratory, smooth and reduce the data to the correct form for VDS input. Likewise for aero data from the wind tunnel.
- Digitize steer angle vs. time data from the chosen PG test run—this forms the control input (in tabular form) to VDS. We have included the steer comparison to show that a fairly large lookup table was used to match the control input from the PG test run. Same for throttle input (which was constant for this run).
- Run VDS and overplot the model results with the instrumented car results, as seen in the figures. It was suspected that the ~10% error in the first peak in the yaw rate response was due to dynamic flexibility in the steering system; the error in roll velocity was attributed to damper data.

Correlation involves a fair amount of work but the results are worthwhile. Now that a baseline VDS data set is correlated, vehicle parameters can be modified in the model with reasonable assurance that the results will agree with actual built cars. When compared to the cost of prototyping and testing parameter changes on a real car, the simulation method is considerably faster and cheaper. It also allows the engineer to try many “what if’s” before a prototype is built. For racing application, the high cost of testing makes this approach very attractive to those teams with in-house engineering.

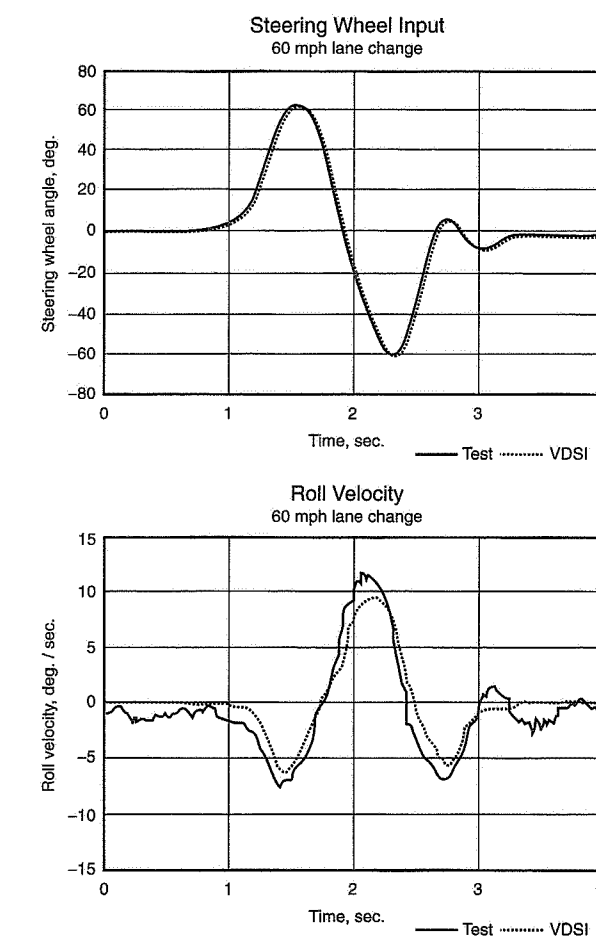


Figure 6.23 VDS correlation—1.

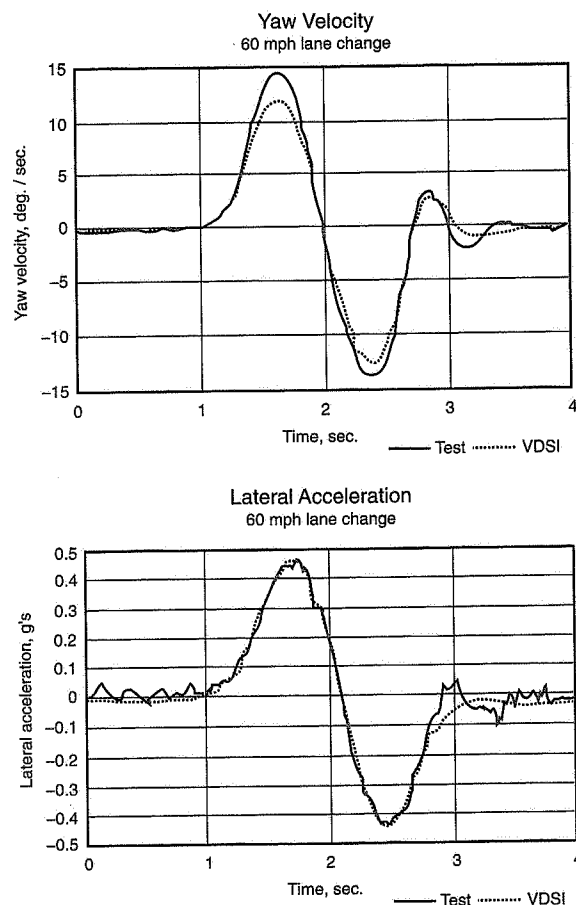


Figure 6.24 VDS correlation—2.

Recent MMM and VDS model developments have been accomplished by Dave Segal with software testing and documentation assistance by Doug Milliken. The correlation was performed by an MRA customer who wished to remain anonymous.

Using Advanced Vehicle Dynamics Simulations

As can easily be seen from a look at the mathematics throughout this book, vehicle dynamics modeling is complex; in fact, the level of analysis presented here is still simplified

from that used in the above simulations. If a high degree of accuracy is desired then computer simulations of automobiles will also be complex. The user of these models is responsible for the quality of the input data, to avoid the "garbage in / garbage out" syndrome. The following items summarize our experience in using these models to simulate a broad variety of vehicles:

- The user(s) should be a competent vehicle dynamicist with the ability to form mental connections between measured (or simulated) input data and the physical hardware. The user should also be specifically trained on the model—MRA includes this training with every model sold.
- Input data for suspension parameters needs to be in the form of raw data response plots, not curve fits calculated by the test facility. This lets the user decide what portion of the data to use for the particular problem. It also gives the user a chance to check the original data; we occasionally find errors in this data and request a retest.
- Take a great deal of care in establishing the baseline model for a particular study. We often use two people to cross-check each other on both the magnitude and especially the sign conventions of all the input data items (this can be hundreds of numbers, depending on the project and the model used).
- Raw tire data as it comes from tire test facilities can rarely, if ever, be used without further conditioning. If the raw data has already been processed, it is vital to understand how it was processed. Laboratory tire testing is still part science and part art. For example, consider that the tire temperature (surface and carcass) changes during testing and also that tire samples must be changed during a test because of tread wear. Unprocessed tire data will usually produce irregular vehicle simulation results, making it difficult to draw conclusions about the vehicle.
- It must never be forgotten that the purpose of these comprehensive models is to make design decisions between small configuration changes. That is why the models are so detailed.

If the original work by McHenry (which led to HVOSM) is taken as a starting point, there is now about 30 years of experience in writing and using these models. Based on our customer feedback, these models produce realistic, reliable simulations of handling for design and development use.

Steady-State Pair Analysis

"My boss told me 'You'll go down in history as the man who introduced understeer into England, making cars run straight in a country that has nothing but crooked roads!'"

Harry Grylls, Chief Engineer
Rolls-Royce Motor Cars, ca. 1956



Introduction

In previous chapters, stability and control of the automobile has been examined using an elementary model—the “bicycle model”—which used a single (linear) tire on each end and did not roll (or lean) when turning. Pair analysis is a first step up, moving from single tire performance to two tires. The pair analysis technique can also be used to prepare tire data to make the bicycle model more realistic. In this chapter we move up the “Ladder of Abstraction” toward reality but still stop short of an analysis of the complete vehicle.

Remember that the forces produced by a tire depend on the tire operating conditions and that tires are measured on test rigs by varying these operating conditions. In a “pair analysis,” steady-state lateral force performance is calculated for a pair of tires on a single track/axle (the front or rear pair), using data measured on a single tire. The operating conditions for each tire of the pair are established using data on the car including load

The Pair Analysis computer program and related material discussed toward the end of this chapter was written by Dave Segal at MRA with support by Goodyear.

transfer and wheel orientations. The analysis is steady-state for two reasons: first, steady-state performance is generally adequate for handling studies, and second, transient tire data is scarce.

"Pair analysis" may be a practical alternative to more complete "computer modeling" for race car development since the objective is usually one of increasing the lateral force capability of either the front or rear track. In this approach, one can explore the effect of changes in those design and operational factors which may be practically modified. The relative results of such calculations may be more important than the absolute magnitude.

There is considerable justification for track (or wheel-pair) analysis.

- The only direct connection (except in four-wheel-drive) between the front and rear tracks is the chassis—vehicle behavior is determined by the relative performance of the front and rear tracks. For example, the yawing moment on the vehicle is simply the difference between the total lateral forces at the front and the rear, times their respective distances from the CG.
- The total lateral tire force is the sum of the lateral track forces.
- Some vehicle characteristics are largely determined by only one track; for example, in vehicles with steerable front wheels only, the steering moment comes totally from the front. Yaw response time, on the other hand, is largely controlled by the rear track (the time for the rear slip angles to stabilize after a step steer at the front).

Finally, when track analysis is combined with the "bicycle model" it gives a good physical feel for car performance.

We begin with a summary of some of the important design and operational factors which contribute to the differences in behavior of a real vehicle and the elementary model. The chapter continues with discussion of the pair analysis calculation procedure and concludes with a discussion of a pair analysis computer program and some calculated sample data.

Model to Reality

Numerous factors in the real vehicle change the track performance over that assumed in the elementary model. These factors primarily modify the lateral force through one or more of the following: tire loads, slip angles, camber angles, and longitudinal slip ratios, which are discussed below:

Static Wheel Loads—These are the result of the gravitational acceleration, A_z , acting on the mass of the vehicle. Any change in the mass distribution longitudinally or laterally will affect the individual static wheel loads.

Longitudinal Load Transfer—The loads on the front and rear tracks change when steady braking or accelerating forces are applied at the tire/ground contact. These load changes occur because the D'Alembert inertia force (due to acceleration, A_x) acts at the CG which is above ground level; the couple thus induced must be reacted by vertical forces at the tires. Suspension anti-forces tending to lift, dive, or squat the vehicle under acceleration may change the CG height; this must be considered in an accurate calculation.

Lateral Load Transfer—In a steady turn the lateral tire forces acting at the ground and the lateral inertia force (due to acceleration, A_y) produce a rolling moment which is reacted by changes in vertical wheel loads. The total rolling moment is distributed between the front and rear pairs of wheels. The distribution is performed in two parts. The first part involves the rolling of the body on the suspension springs about the roll axis of the suspensions. This part (the lateral inertia force times the vertical distance between the CG and the roll axis) is distributed to the front and rear tracks in proportion to the suspension roll stiffnesses. This is referred to as *roll couple distribution*. The second part (the lateral inertia force times the distance between the roll axis and the ground) is distributed in inverse proportion to the distance between the CG and the tracks and in direct proportion to the roll center heights at the tracks. Here again the details of the suspensions must be taken into account for accurate results. The roll centers may move laterally and vertically in a nonlinear fashion and affect the distribution of the load changes between the wheel pair. The details of longitudinal and lateral load transfers are covered in Chapter 18.

Anti-Roll Bars—These are usually in the form of a torsion bar spring which connects the vertical motions of the left and right wheels. No twist of the torsion bar takes place if the wheels move up and down together (ride), but in roll the bar is twisted as one wheel moves down and the other up from some initial position. Twisting of the bar adds load to one wheel and removes it equally from the other. Anti-roll bars change the distribution of the lateral load transfer between the front and rear tracks, and also reduce the body roll angle and add to the one-wheel bump rate of the suspension.

The opposite of the anti-roll bar is the Z-bar. When a Z-bar is added to an existing suspension it increases the spring rate in ride without changing the lateral load transfer taken on that end of the car. Anti-roll bar calculations are covered in Chapter 16 and their effects on wheel loads are in Chapter 18.

Wedge or Diagonal Weight Jacking—This results in a change in the static load on the wheels of an axle (one wheel carries more load while the other carries less). The total load on the axle remains the same unless the CG is moved. A change in left-right load on one track results in the opposite change in load distribution on the other track. In short, increasing the spring preload (jacking) on the RH front wheel tends to rotate the body about a diagonal axis through the LH front and RH rear wheels—hence the term

diagonal weight jacking. Because the weight of the car is fixed, increasing the preload on the RH front wheel means that the RH front and the LH rear wheel will carry more load than the sum of the LH front and the RH rear.

Stagger—This is the difference in diameter between the tires on a track (axle). It is usually measured as the difference in tire circumference and controlled by tire selection. Depending on the tire design there may or may not be a range of diameters available due to manufacturing tolerances and changes during use. As far as tire loads are concerned, stagger has the same type of effect as diagonal weight jacking. Stagger on a **drive axle** results in a direct vehicle yawing moment; this varies with the type of differential used in the axle.

Engine Torque Reaction—Unless the final drive unit is mounted on the chassis (independent or deDion type suspension), the engine torque reaction passes into the suspension springs and produces “diagonal” load changes on the wheels. Jacking, stagger, and engine torque reaction are covered in Chapter 18.

Geometric Steers and Cambers—Because of the suspension and steering system geometry, steer and camber changes can occur as the wheels travel in ride. The various effects are defined separately in terms of the body motions:

Ride Toe (or bump steer)	Ride Camber
Roll Steer	Roll Camber
Brake Steer	Brake Camber
Acceleration Steer	Acceleration Camber

In addition, steer and camber changes occur due to deflections in the suspension and steering system under the application of lateral forces and aligning torques at the wheels:

Lateral Force Compliance Steer
Lateral Force Compliance Camber
Aligning Torque Compliance Steer
Aligning Torque Compliance Camber

In race cars, the compliances are generally minimized by design through the elimination of rubber bushes, etc. (see Chapter 23). It should be noted that structural compliances in the presence of large cornering loads can make significant changes in wheel operating conditions.

Longitudinal Slip Ratio—As discussed at the end of Chapter 2, the lateral force capability of a tire is reduced by the application of a driving or braking force. Friction circle effects on driven or braked tires can be taken into account in calculating the lateral track force performance.

Brake distribution, differential characteristics, and application of such devices as anti-lock/anti-spin must be taken into account for accurate calculations (see Chapter 20).

Suspension Springs—In some classes of racing, suspension springs are changed to tune the chassis. These changes will usually affect the loads at the wheels and change performance.

Shock Absorbers—For steady-state analysis, the shock absorber forces are neglected. They are obviously important when transient analyses are performed.

7.1 Pair Analysis Procedure

A simple procedure for calculating the lateral performance of a pair of tires on a track is described below. It is amenable to “hand calculation” and, in a more comprehensive form, to a computer program. Any calculation of this type assumes the availability of tire data. If slip ratio effects are not involved, lateral force versus slip angle for a series of loads is sufficient. Complete tire data for braking and traction slip ratios and slip angles at various loads is very rare but some data such as the friction circle limit and load sensitivity may be available or estimated.

Figure 7.1 shows a wheel pair (two tires on a track) as seen from the rear in a right-hand turn. The turning center is off to the right. The subscript “a” can take the value of “F” or “R” to indicate front or rear axle. Assume a RH turn for all of the analyses in this section.

That part of the total rolling moment of the vehicle about the ground which is taken at the track in question can be represented by the inertia force (centrifugal), $W_a(a_y/g)_a$ ($= W_a A_{Y_a}$) times the distance h_e , the height of a fictitious “center of gravity” for the track.

Summing moments and forces in Figure 7.1 gives

$$\text{Moment about Point A: } L_L \left(\frac{t}{2} \right) - L_R \left(\frac{t}{2} \right) - W_a (A_Y)_a \times h_e = 0$$

$$\text{Vertical Forces: } W_a = L_L + L_R$$

from which

$$\frac{(t/2) \times (L_L - L_R)}{W_a} = (A_Y)_a \times h_e$$

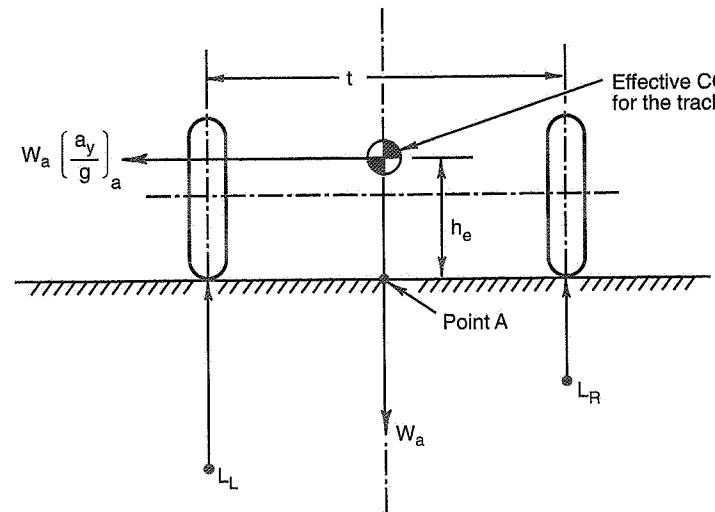


Figure 7.1 Wheel pair on a single track.

The Fraction Load Transfer, FLT, is defined as

$$\text{FLT} = \frac{L_L - L_R}{W_a} = \frac{\Delta L}{W_a} \quad (7.1)$$

where $\Delta L/2$ = load transferred from the inside wheel to the outside wheel.

When $\text{FLT} = 1.0$, all of the load has been transferred to the outside wheel. Substituting FLT into the previous equation gives

$$\text{FLT} = 2(A_Y)_a \times \frac{h_e}{t} \quad (7.2)$$

In the general case, W_a should take into account any changes in static wheel loads plus longitudinal load transfer if the situation of interest involves longitudinal acceleration. Jacking (wedge), stagger, and engine torque reaction will offset only the initial wheel loads (change the trim loads). $(A_Y)_a \times h_e$ represents the total moment in the track about the ground Point A. If one is analyzing a single track of a given vehicle then $(A_Y)_a \times h_e$ can be determined from the lateral load transfer distribution as outlined in Chapter 18 or the equations given later in this chapter. In cases where the performance of a pair of wheels is being studied without reference to a particular vehicle configuration, the parameter, h_e or h_e/t , is a convenient way to represent changes in the lateral load transfer.

The calculations proceed as follows:

The actual wheel loads are calculated for a series of values of FLT (such as 0, 0.10, 0.20, to 1.0) for the given track load, W_a , from Eq. (7.1). A series of steer (negative slip angles) are then chosen (such as 0° , $+1^\circ$, $+2^\circ$ to 10°) which cover the performance range of interest. In general, the steer (slip) angles of the two wheels will be different because of initial toe and Ackermann/reverse Ackermann geometry. In this case, a reference steer is specified which is an average of the left and right wheel steers (no absolute steer reference exists for a single track) but the individual steer (- slip) angles are used when entering tire data.

In the most general case, suspension geometry effects (some or all of them) could be introduced before entering the tire data. This requires chassis data, such as that obtained on Chevrolet's Vehicle Handling Facility for ride, roll, and longitudinal force effects on steer and camber. Some of these effects can be deduced from suspension design layouts. These geometric and compliance steer and camber changes are expressed as a function of lateral and longitudinal accelerations. The complexity of introducing these effects, however, practically eliminates hand-calculation and requires a computer program.

At this point the tire data is entered and the lateral force for LH and RH tires is obtained for the finalized steers, cambers, and loads. Longitudinal slip ratio (Circle Diagram) effects are taken into account if studying a driving/braking case (assuming adequate tire data).

The lateral track force is the sum of the lateral forces of the two wheels, which is then multiplied by the cosine of the reference steer angle to give the lateral force in the direction of the turning center. This force divided by W_a is the lateral acceleration of the track ($(A_Y)_a$). A plot of $(A_Y)_a$ vs. FLT with reference steer angle as the parameter represents the potential of the tires for producing lateral "axle" force for the track configuration over the range of steers and FLTs . This is the basic output of the track analysis. This is called the *lateral force potential diagram*.

The actual load transfer experienced on the track depends on the track width and the rolling moment produced by the lateral acceleration acting at the fictitious CG height, h_e , as given by Eq. (7.2) above. This relationship enables diagonal operating lines to be drawn on the tire potential diagram for various values of h_e/t , the lateral load transfer parameter.

A final step involves the transfer of the lateral accelerations obtained for the various steer angles at the intersections with an h_e/t line, to a plot of lateral acceleration for the track against the average steer angle. This curve is the *cornering coefficient curve for the track (cornering force/W_a)* and shows the effect of load transfer, geometric and other factors in modifying the single tire characteristics. It is a measure of how well the vehicle track configuration utilizes the tire lateral forces.

Figure 7.2 shows an example of (a) the “potential” diagram and (b) the corresponding cornering coefficient (= lateral acceleration for the track) for a small research vehicle.

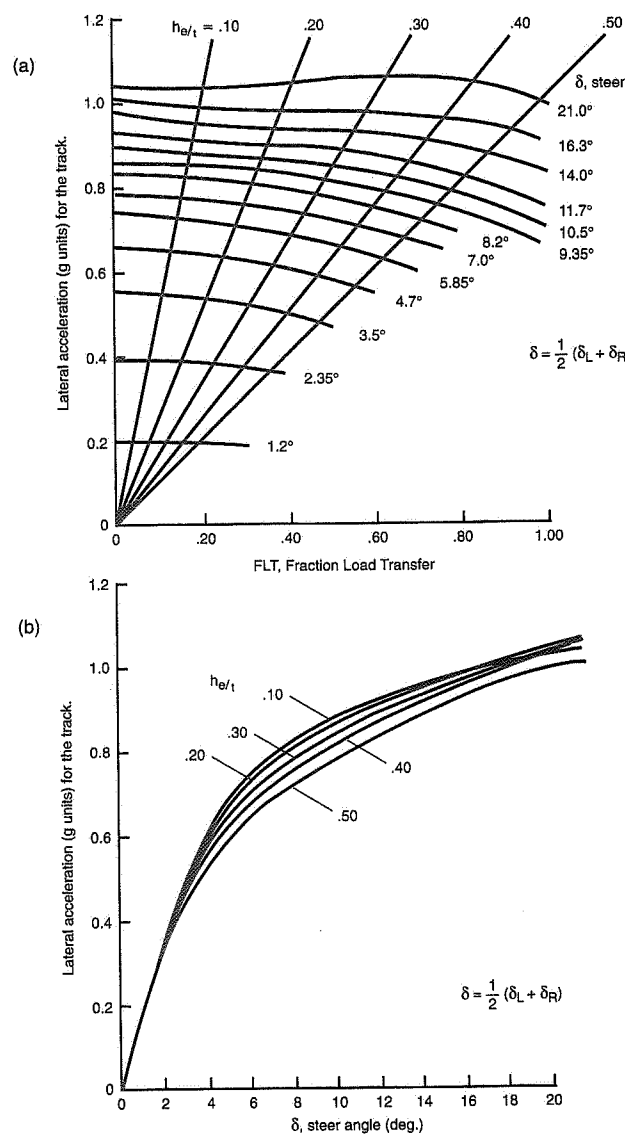


Figure 7.2 Ackermann steer, 0° camber, 0° toe.

7.2 MRA Computer Program

To extend and formalize the pair analysis concept, a computer program has been written. The program calculates axle lateral force for either the front or rear pair of tires. It also allows the user to input characteristics for the other end of the car, in which case it will calculate and use the correct total lateral weight transfer distribution for the whole car.

The computer program has the specific capabilities listed below. The first four items are available from suspension tests on a K & C (kinematic and compliance) rig such as Chevrolet VHF or MTS K & C. Force and moment tire data must be available from a tire tester such as Calspan's TIRF.

- Roll center heights vary as a function of roll angle.
- Roll stiffnesses vary as a function of roll angle.
- Steer-steer (Ackermann) and roll-steer effects are included.
- Roll-camber of the wheels is considered.
- Laterally offset CG is allowed.
- Braking/driving torque proportioning is included.
- Axle torque specification or longitudinal acceleration target allows study of either constant driving/braking conditions or road load (RL) power.
- Tire slip angle drag relative to the centerline of the car is calculated.
- Different tires on an axle are allowed.

In the simple pair analysis calculation procedure of the previous section, the track lateral acceleration acts at an “effective” CG height, h_e . For the computer program the effective height depends on the vehicle CG location, roll rate and distribution, roll center locations and unsprung weights. It is developed as follows:

From Eqs. (7.1) and (7.2),

$$\frac{(L_L - L_R)_a}{W_a} = \text{FLT} = 2A_Y \frac{h_e}{t_a}$$

or

$$h_e = \frac{t_a(L_L - L_R)_a}{2W_a A_Y}$$

To obtain h_e , we need to develop the total load transfer for a given track, where the subscript a refers to “F” or “R” axle as chosen by the user.

P_K = Fraction of total roll stiffness on active axle

$$P_K = \frac{K_a}{K_F + K_R - W_S H_S + W_S y'' A_Z}$$

where K_a = active axle, roll stiffness

K_F, K_R = F and R axle, roll stiffness

W_S = sprung weight

H_S = sprung weight CG above roll axis

y'' = lateral offset of sprung mass CG

(positive to the right)

Total load transfer on axle "a" is

$$(L_L - L_R)_a = \left(P_K H_S W_S + W_{S_a} Z_{R_a} + W_{U_a} Z_{W_a} \right) \frac{2A_Y}{t_a}$$

where W_{S_a} = sprung weight active axle

W_{U_a} = unsprung weight active axle

Z_{R_a} = roll center height at active axle

Z_{W_a} = height of active axle unsprung weight

(Both Z's are + above ground)

Then,

$$h_e = \frac{P_K H_S W_S}{W_a} + \frac{W_{S_a} Z_{R_a}}{W_a} + \frac{W_{U_a} Z_{W_a}}{W_a}$$

Once h_e is known for this more complete model of the real vehicle, the pair analysis proceeds as for the simple case given in the previous section.

7.3 Example Calculations

These calculations were performed with the MRA computer program for the front "axle" of a front-drive sports performance sedan with the following base configuration:

$G_W = 3570$ lb. (65% front)

$\ell = 113$ in., wheelbase

$h = 21$ in., total CG height

$t_F = t_R = 61.8$ in., track width

$K_F + K_R = 1124$ lb.-ft./deg. (62% front), total roll stiffness

$z_{RF} = 3.8$ in., roll center height at front axle

0° static toe, 0° roll steer, parallel steer, 0° static camber, 50% camber compensation

Tires are Goodyear Eagle P225/50VR15

The following test cases were run:

Test number	Showing effect of:
1	Static camber
2	Camber compensation
3	Roll rate distribution
4	Front roll center height
5	Static toe
6	Static CG height
7	Drive torque
8	Drive torque split (left-right)

The conclusions are fairly obvious from Figures 7.3 and 7.4. The highest normalized lateral force and cornering stiffness for the track is obtained with

- -2° static negative camber
- 100% camber compensation
- 42% roll rate distribution on the front track
- 7.8 in. above ground
- 1° toe-in
- 19 in. static CG height (minimum)
- 0 drive torque
- 100% drive torque to outside wheel

where each of these effects was compared separately to a base configuration.

7.4 Lateral Load Transfer—Discussion

Because of the nonlinearity of tire lateral force versus load curves (for constant slip angles), transferring load from the inside to the outside tire on an axle invariably results in a decrease in lateral track force—when compared to the same axle with no load transfer. The utility of the conventional anti-roll bar for increasing US when installed on the

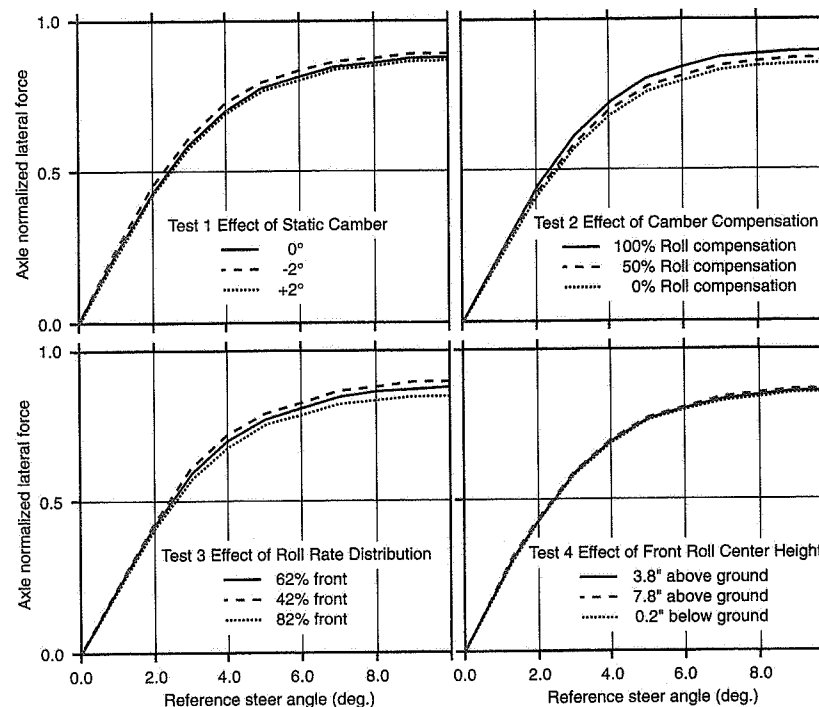


Figure 7.3 Axle pair analysis—1.

front suspension follows from this nonlinear tire characteristic. It should be noted that the US is obtained at the expense of total cornering force of the vehicle. This reduction in track lateral force with load transfer is well illustrated in the “lateral force potential diagram” of Figure 7.2(a) where the slip angle lines slope downward to the right as the fraction load transfer (FLT) is increased.

The question may be asked: Is it possible to find a configuration in which increasing lateral load transfer actually increases the lateral force for the track, i.e., to have the slip angle lines on the potential diagram slope upward to the right with increasing FLT? If this was practical an anti-roll bar on the rear suspension would increase US while building up the total side force. One configuration which meets this condition is the use of highly negatively cambered tires (wheels tilted inward relative to the vehicle). Using TIRF measured data on 5.00-16 motorcycle tire data with toe-out and reverse Ackermann steer and -15° of camber on each wheel, the results shown in Figure 7.5 were obtained. This figure may be compared directly with Figure 7.2.

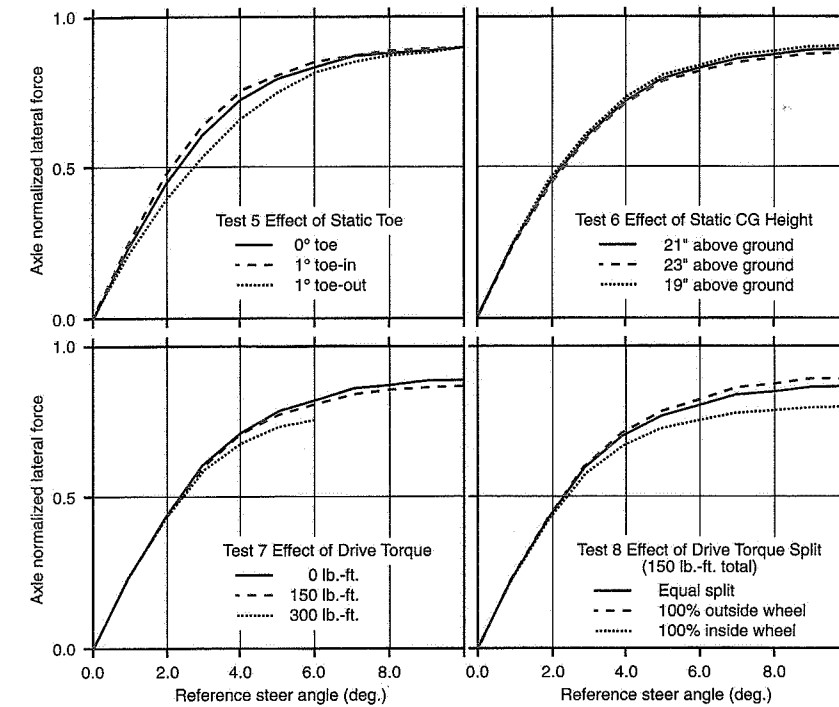


Figure 7.4 Axle pair analysis—2.

This very high camber configuration cannot be used with current wide race tires. Also, it was noted that rolling resistance increased with this high camber. However, analysis of tire data on P225/70R15 performance tires exhibited the same behavior as the motorcycle tires provided the negative camber was limited to -5° . An improvement in maximum lateral acceleration of the track of some 5% over vertical wheels was obtained. Race cars tend to utilize negative camber in amounts depending upon tire width, edge temperature, etc.

The basic reason for the improvement of track performance with load transfer on negative camber goes back to the cambered tire data shown in Chapter 2. Thus the incremental lateral force due to camber tends to increase directly with load which compensates for the nonlinear behavior of lateral force due to slip angle.

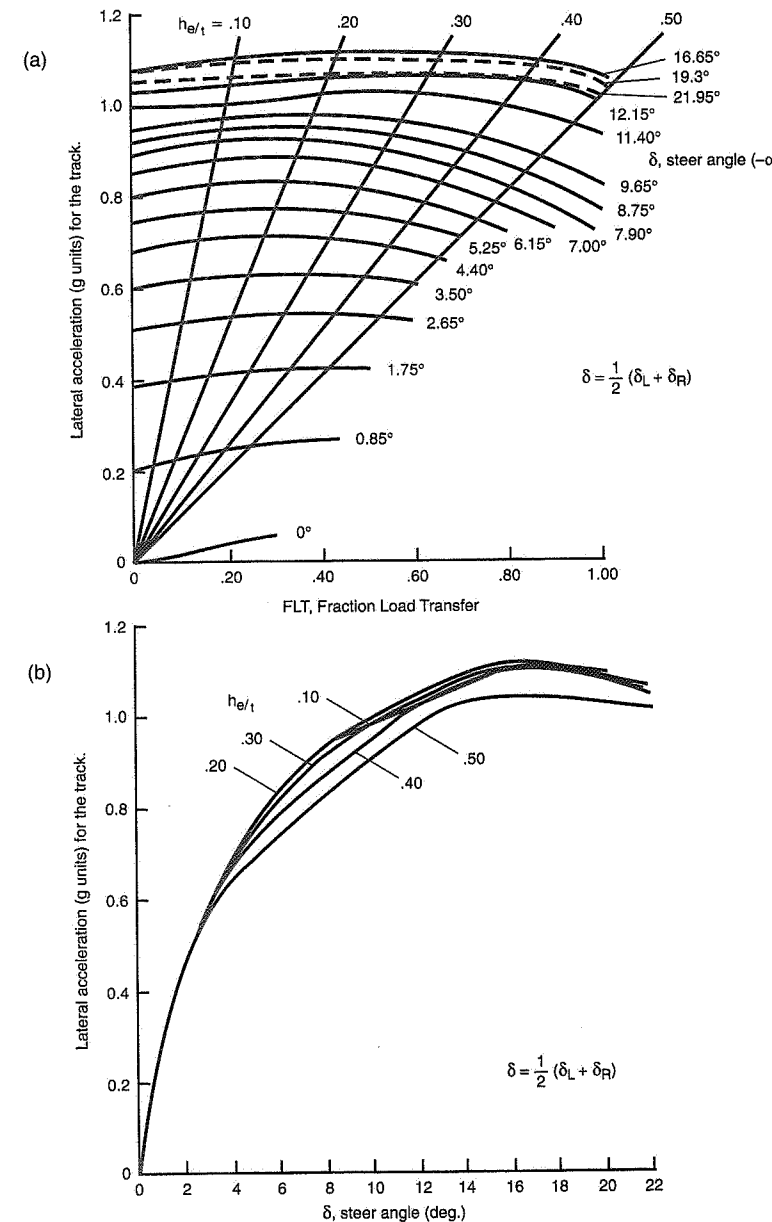


Figure 7.5 Reverse Ackermann steer, -15° camber, 1° toe-out/wheel.

CHAPTER 8

Force - Moment Analysis

*"Each technique has its share of proponents,
Milliken and I favor the Method of Moments.
For cars of all sizes,
their performance it analyzes,
and it handles nonlinear components."*

Roy S. Rice
on the occasion of presenting a paper
at SAE on the Moment Method



Introduction

In this chapter, the overall forces and moments which act on the automobile are used to analyze its stability, control, and maneuvering performance. The analytical approach is called MRA Moment Method technology; it originated from racing experience, aircraft wind tunnel, and other types of constrained testing. As a technique, it stands between those concerned with steady-state turning (Ref. 122) and those involved in the complete

The force-moment concept was originally proposed in a 1952 CAL memo, "Long Range Automotive Stability & Control Research Program," by Bill Milliken. The first F-M measurements (using a tethered skid pad, 1955) yielded UO, control moment, etc. An analytical approach was initiated with GM Engineering Staff by memo to Winchell/Bidwell, 1969. The MRA Moment Method has been in continuous development since by Roy Rice, Fred Dell'Amico, Doug Roland (CAL/Calspan), Dennis Kunkel (CAL/GM) and others (Ref. 93). Recent major advances in the computer program and post-processing/interpretation have been accomplished by Dave Segal and Doug Milliken, including specific applications to racing.

dynamics (Refs. 88, 131, 32, and 85). The distinctions will become clearer in the following discussion.

8.1 Approach

The force and moment concept will first be described in the context of a simplified constrained model test. The basic premises underlying the method will be described, followed by a brief summary of earlier constrained testing experience. Next follows a review of an implementation of the MRA Moment Method (MMM) as a computer program and the related theory for full-scale indoor MMM testing machines.

In describing the results from this type of analysis, particular emphasis will be given to unique graphical presentations (diagrams). These diagrams are a "portrait" of the maneuvering performance of the vehicle over the full lateral acceleration range for given sets of operating conditions.

Limit cornering and behavior are covered in the next section as a preliminary to two examples of race/sports car analysis by MMM. The first example illustrates the changes which occur in the diagrams with vehicle operating conditions such as speed, road load (RL) power, acceleration and braking. This illustrates the problem of compromising the vehicle set-up for the wide range of conditions met in circuit racing. The second example focuses on the effect of changes in a sports car configuration and their interpretation through the diagrams.

Experience has shown that the interpretation of MMM diagrams can be enhanced by a detailed knowledge of what is happening at each individual wheel at any point on a diagram. This is accomplished by a post-processing routine called "Friction Circle." Several examples of these are given in the sports car example where they serve as a logical lead-in to the overall vehicle "g-g" diagram in the next chapter.

8.2 Constrained Testing

The Moment Method is based on the assumption that most of the stability and control characteristics of interest to the automotive engineer can be obtained from a study of the **steady-state forces and moments** on the vehicle. These forces and moments are not only those associated with equilibrium (balanced) conditions, but those "**unbalanced**" forces and moments which are available for linearly and angularly accelerating the vehicle in maneuvers.

The constrained test underlying MMM can be described by referring to Figure 8.1, which shows an elementary vehicle model constrained on a model flat-belt tire tester. Imagine that the model is a real car and that it is being supported on a large belt which can move at real car speeds. Also assume that driving and braking forces can be applied to the

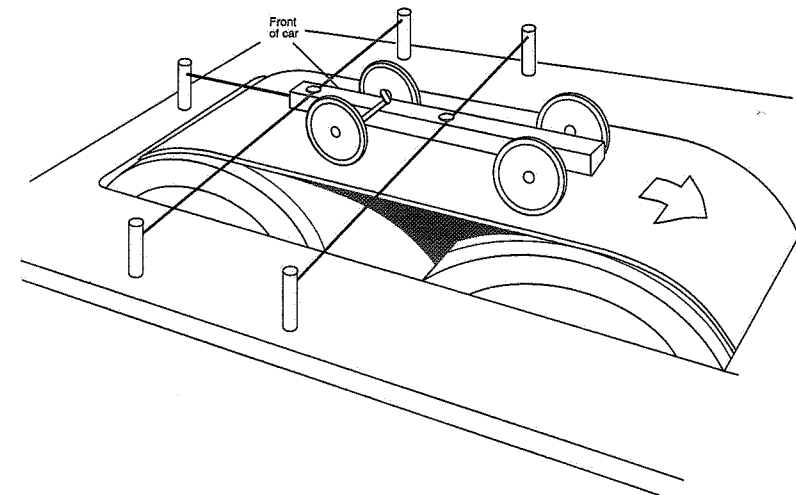


Figure 8.1 Constrained model on moving belt.

roadway by the engine/driveline and brakes of the vehicle. Aerodynamic forces and moments are not present but it is conceivable that the device could be located in a full-scale wind tunnel.

The forces and moments on the model can be measured in the constraint system. In Figure 8.1, the constraint system consists of three wires: one to constrain the vehicle longitudinally to react the tractive or braking forces, and two lateral wires, one at the front of the car and the other at the CG. The sum of the forces in the two lateral wires gives the total lateral force on the car; the force in the front lateral wire times the distance to the CG gives the yawing moment on the vehicle. Newton's second law for linear and angular accelerations states that:

$$F = ma = (W/g)a \quad \text{or} \quad F/W = a/g, \text{ linear acceleration}$$

$$M = I\alpha \quad \text{or} \quad M/I = \alpha, \text{ angular acceleration}$$

D'Alembert's principle states that the presence of a steady acceleration on a body can be represented by applying a **reversed effective inertia force (or moment)** to it, thus bringing it to rest, i.e., in static equilibrium. The sum of the forces (or moments) will equal zero:

$$a/g - F/W = 0$$

$$\alpha - M/I = 0$$

In the case of a constrained model in static equilibrium, a force in the longitudinal wire, divided by the vehicle weight, can be interpreted as a steady longitudinal acceleration of magnitude F/W , in "g" units. This is the situation on a chassis dynamometer—the restraint forces would be used to accelerate the vehicle if it was not restrained. Similarly, the lateral force divided by the weight is equivalent to a steady lateral acceleration. Finally, the yawing moment divided by the moment of inertia in yaw corresponds to a steady yawing acceleration. Thus simulations of constant acceleration can be had on a constrained tester.

The simple three-wire constraint system of Figure 8.1 assumes the wires are sufficiently long that the model is free to heave, pitch, and roll through ranges comparable to those experienced by real vehicles. **This is necessary for insuring appropriate vertical tire loads and their distribution.** With this constraint the vertical tire forces depend on the static weight and the longitudinal and lateral weight transfers—the model is free to react to simulated vertical, longitudinal, and lateral accelerations. This is a feature of the MMM constraint system that differs from a wind tunnel balance (for example) which constrains the model in all six degrees of freedom.

History of Constrained Testing

In addition to the wind tunnel, other well known examples of constrained testing are the tire tester, kinematic and compliance testers,³³ and the ship model basin. There is also a history of constrained tests of full-size automobiles at various proving grounds. Figure 8.2 illustrates several of these which are described below:

- (a) This is the earliest tethered test known to the authors. It was performed at General Motors about 1950 by Tom Charmichael. Known as the "Maypole" test it was originally used for determining the cornering forces of the front tires. Forces were measured by proving rings in the cables. This test was repeated on ice by CAL in 1955. The slip angle of the vehicle was adjusted by changes in the cable lengths and tests were run over the full range of steer angles (provided the speed was sufficient to keep the cables tight). The static directional stability, roll steer, and control moments were deduced from these tests.
- (b) In 1963 a "simulated" roadability test was performed by Chevrolet in which a car was tethered to a pole in the center of a circle. The test was run at very low speed and the centrifugal force was simulated by a cable connecting the test vehicle CG to a heavy vehicle driving on the same radial line on a larger circle. The test enabled low-speed observation of suspension behavior under realistic cornering forces.
- (c) In this scheme, a vehicle was tethered to a railcar via a single link permitting freedom in roll and yaw. The single link also enabled the test vehicle to accelerate "ahead" or decelerate "behind" (using its engine/brakes) such that the link sloped

³³ Such as Chevrolet Vehicle Handling Facility (VHF) and the MTS K & C rig.

forward or aft relative to the railcar. Thus the link measured the D'Alembert force. The test could simulate straight running or turning with or without steady longitudinal acceleration. However, the test vehicle is unconstrained in yaw and this test does not give unbalanced yaw moment data.

- (d) The MIRA (England) tethered testing technique was originally conceived in the early 1960s by David Hodkin, and remained in operation into the 1970s. A rigid fore and aft tethering link was used but the vehicle was free to roll and yaw about the CG attachment point. The tests were run at low speed thus reducing tire wear. Steady-state conditions could be maintained under traction and braking conditions. Again, as in (c) above, no unbalanced yawing moments could be measured and the information deduced from a test was comparable to that obtained in free steady-state proving ground tests.

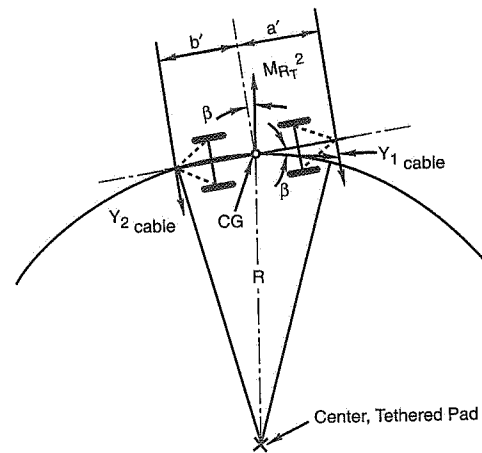
8.3 Computer Program

The development of complex MMM computer programs was initiated in 1976 under a contract from General Motors. For reasons of size, cost, and complexity it did not appear practical at that time to develop a full-scale constrained indoor tester, although an extensive engineering study was made of such a device. Therefore, the test was simulated by a computer program. This simulation was designed to utilize nonlinear tire, aerodynamic, and chassis data as they were currently measured and available in the industry. This simulation was based on a full-dynamic mathematical model by the elimination of the acceleration terms and the insertion of the constraining forces and moments.

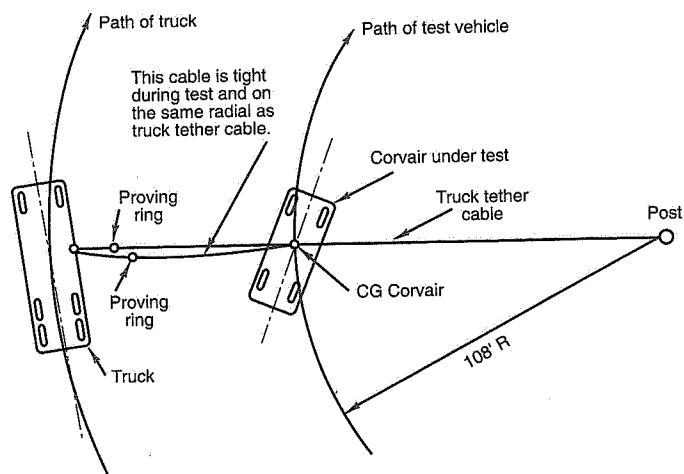
The program used for the computations in this book is the third major revision of MMM, running on an IBM-compatible PC. This model has 14 degrees of freedom (6 chassis, 4 vertical unsprung, 4 wheel rotations). It incorporates a rather complete nonlinear representation of the suspension (left-right symmetric or asymmetric) including:

- Separate ride spring and bump stop rates
- Anti-roll bar rates
- Steer-steer and steer-camber
- Ride steer and ride camber
- Compliance steer and compliance camber due to lateral force, tractive/braking force, aligning torque, and overturning moment
- Roll and swing center effects (anti-roll, anti-pitch, etc.) as functions of lateral force, tractive/braking force, aligning torque and overturning moment

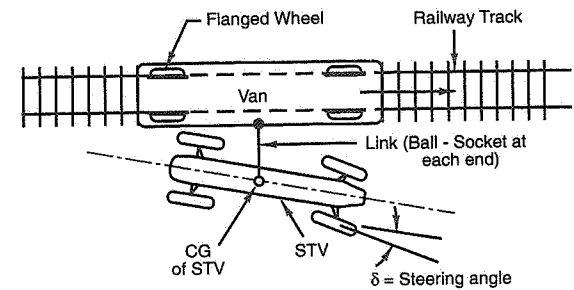
Various tabular tire models that use experimentally determined tire data are incorporated. This generates lateral force, aligning torque, and overturning moment as a function of normal load, slip angle, camber angle, and traction/braking. The simulation is exceptionally



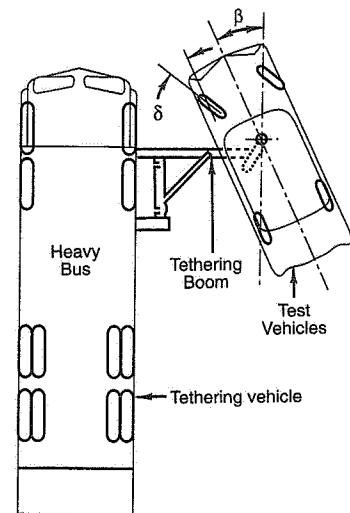
(a) Tethered Skid Pad Force Diagram



(b) Chevrolet Simulated Roadability Test

Figure 8.2 Constrained proving ground tests on automobiles.

(c) Chevrolet Constrained Linear Test



(d) MIRA Tethered Testing Technique

Figure 8.2 Constrained proving ground tests on automobiles (continued).

versatile in terms of its ability to handle front, rear, and 4WD configurations, various differentials, asymmetrical tire configurations, etc. The nonlinear data is input as fitted polynomials and/or lookup tables, depending on the particular data item.

This computer simulation has proven its usefulness in "up front" analysis of vehicles in the design stage and also in studies to improve existing vehicles. A computer simulation gives the engineer the ability to rapidly change a large number of parameters independently, something that is often impossible to do in hardware. After a baseline configuration is modeled, parameter changes can be rapidly evaluated.

An ideal combination of development tools would be the computer program in combination with a laboratory MMM test machine. The MTS Flat-Trac Roadway Simulator™, the first of which was completed in 1994, has an MMM capability similar to the earlier

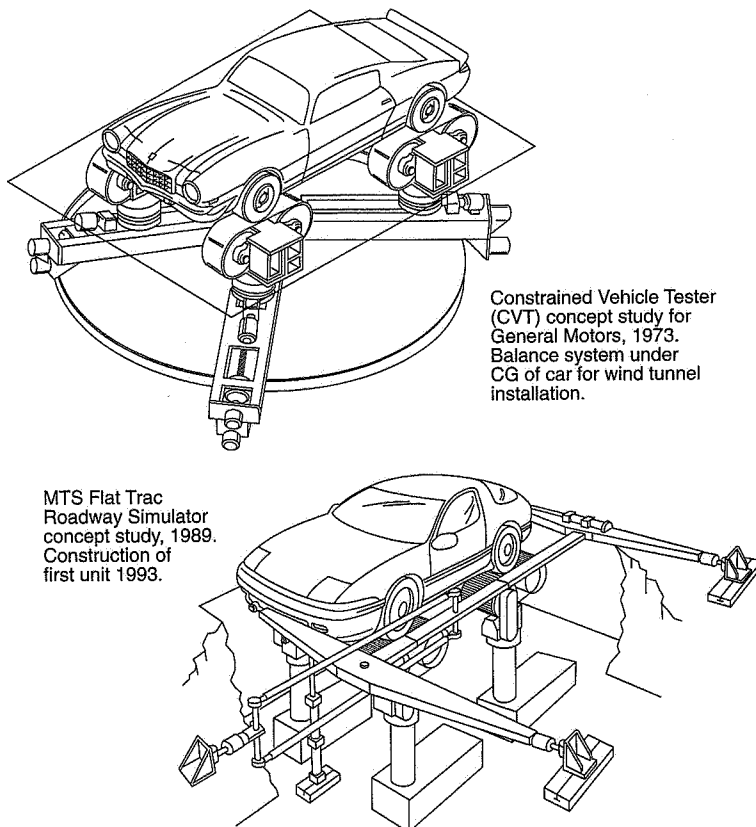


Figure 8.3 Full-scale test devices for making MMM measurements.

work for General Motors. Figure 8.3 illustrates the MTS machine and its conceptual predecessor. In both of these devices, four flat belts are used so that different wheel speeds, longitudinal slip ratios, and steers are available.

8.4 Moment Method Results

The results of MMM computer runs can be presented in tabular form or as diagrams and plots from post-processing routines. To explain the application of the method to racing we will focus on the diagrams. These are specialized plots presenting the measured (or computed) forces and moments from a constrained test or simulated test. In principle, the diagrams are similar to those from wind tunnel tests which portray the variation of vehicle aerodynamic forces and moments as functions of attitude (angles of attack or yaw) and control positions.

In automobiles, the yawing moment, N (or coefficient $C_N = N/W\ell$), is a very important parameter. As noted in Chapter 5, steering control, directional stability, and yaw damping can all be defined in yawing moment terms. The lateral force, Y (or coefficient $C_Y = Y/W$), is of equal importance since it determines the path of the vehicle. Thus it is logical to plot C_N vs. C_Y as the coordinates of an MMM diagram. In steady-state turning maneuvers, C_N and C_Y are functions of the vehicle attitude angle, β , and the steer angle, δ . As independent variables, they determine the front and rear slip angles, hence lateral tire forces, lateral weight transfers, etc., which define steady-state turning maneuvers. By testing over the full range of δ and β , the maneuvering characteristics of the vehicle can be diagramed for road load or different amounts of driving or braking longitudinal acceleration.

Example of Diagram Build-Up (C_N - A_Y)

To show how an MRA Moment Method diagram is developed and interpreted we will use data from the constrained model of Figure 8.1 to build up the diagram presented as Figure 8.6. For this example calculation a simplified MMM with only one type of solution is used and the assumption is made that all of the lateral force generated by the tires is used to balance the centrifugal force in turning:

$$C_Y = Y/W = A_Y$$

The vehicle is said to be "trimmed" in lateral force. Thus the coordinates of the diagram are now C_N vs. A_Y with δ and β as parameters.

The diagram will be developed for a right-hand turn, constant speed, and road load (RL) condition. Since $A_Y = V^2/gR$ and since V is constant, the horizontal axis may be viewed as path curvature (or path radius). The diagram then portrays the variation of yawing moment for all radius turns from straight ahead to the tightest possible at the given speed. This type of operation is related to the SAE/ISO Constant Throttle skid pad test described

in Ref. 3 (also called J-turn test), but the test procedure covers only trimmed (equilibrium) conditions while the diagram covers all trimmed and untrimmed situations. The resulting diagram is referred to as the C_N - A_Y diagram. Since the directional stability can be determined for any path curvature it is also referred to as the "stability diagram."

The model tester (of Figure 8.1) does not simulate path curvature and the geometric effects this has on slip angles. To keep it simple, we will omit these small induced slip angle corrections for this first example. The model characteristics are:

Wheelbase	8"
CG location	mid-wheelbase, $a = b = 4"$ or $a/\ell = b/\ell = 0.5$
Weight	1.66 lb. (half on front track and half on rear)

The cornering force curves for the model tires were measured and are given in Figure 8.4.³⁴ The rear tires have higher cornering stiffness than the front; thus linear understeer is anticipated.

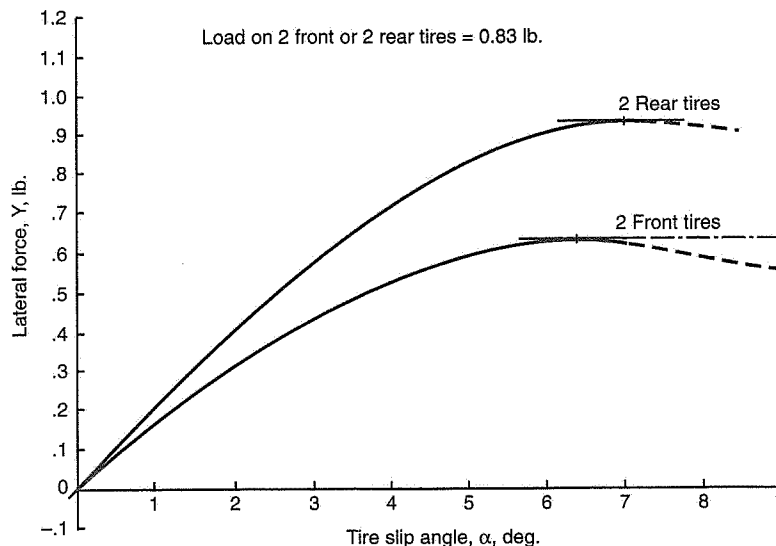


Figure 8.4 Cornering force curves for model tires.

³⁴ Note that α is used as a positive quantity; it is actually negative in the SAE system.

In building up the diagram, consider first a situation in which the vehicle slip angle, β , is held at zero, while the front wheels are progressively steered to the right (see Figure 8.5(a)). The lateral force from the front wheels can be moved back to the CG by the addition of a yawing moment, $C_{Y_F}(a/\ell)$. The data are presented in Table 8.1. These data are then plotted on the upper part of Figure 8.6 as line (a). This line is also labeled $\beta = 0$. As more and more steer angle is applied, the front tire lateral force moves up the cornering force curve (Figure 8.4) until it saturates at slightly over 6° —the upper end point on line (a) of Figure 8.6. This is one point on the front tire limit. The line (a) represents the control moment available at various lateral accelerations for $\beta = 0$.

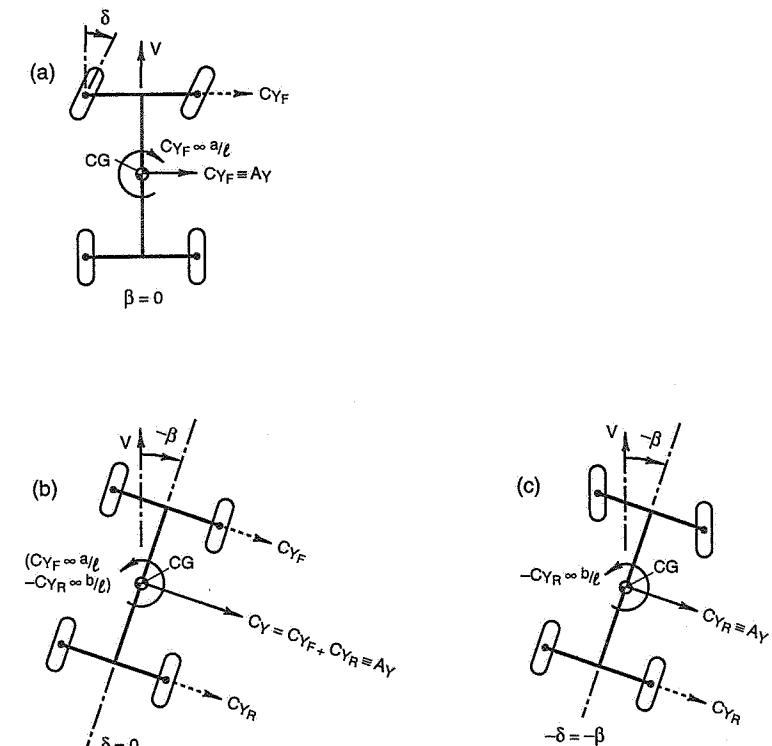
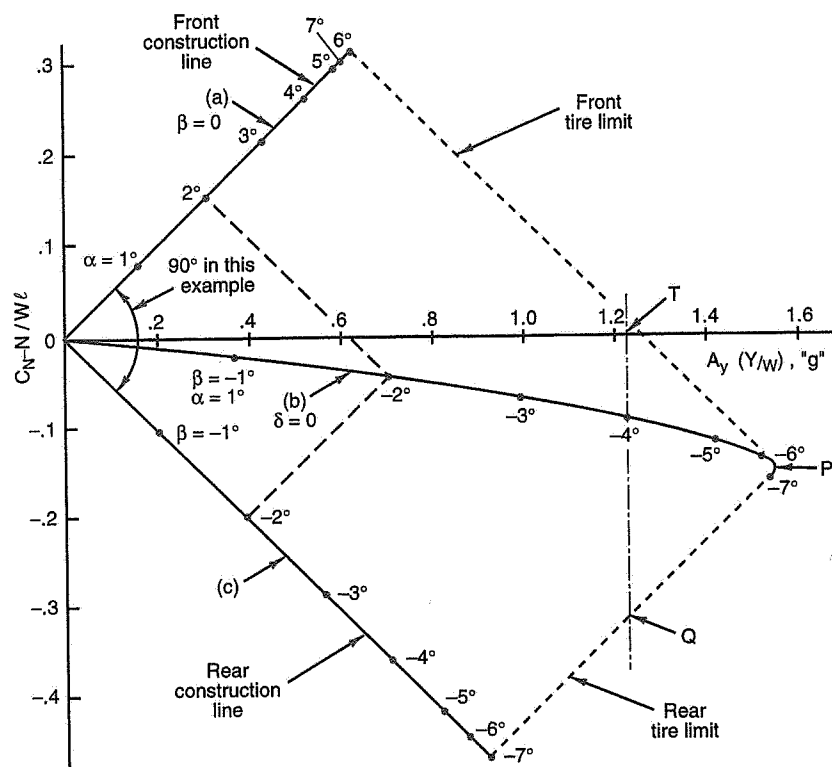


Figure 8.5 Build-up of C_N - C_Y MMM example.

Table 8.1 Model Data for $\beta = 0, \delta$ Varies

$\alpha_F^\circ \equiv \delta^\circ$	$C_{Y_F} \equiv A_Y$	$C_N = C_{Y_F}(a/\ell)$
1	0.160	0.080
2	0.308	0.154
3	0.427	0.214
4	0.525	0.263
5	0.595	0.298
6	0.627	0.314
7	0.614	0.307

Figure 8.6 C_N-C_Y example, right-hand turn, RL power.

Consider now a second situation in which steer angle, δ , is held at zero while the vehicle slip angle, β , is varied progressively in the negative direction by rotating the whole vehicle to the right, as in a RH turn (see Figure 8.5(b)). This data from Table 8.2 is plotted below the horizontal axis in Figure 8.6 as line (b), also labeled $\delta = 0$. As more and more negative β is applied, the front and rear tires move up their respective cornering force curves (Figure 8.4). The front tire saturates at slightly over $\beta \approx -6^\circ$ which gives us another point on the front tire boundary. The rear tires saturate at $\beta \approx -7^\circ$ which gives us a point on the rear tire boundary. The front tires fall off faster than the rears after saturation, so the front tire boundary bends down slightly to meet the rear boundary. The max lateral acceleration in an untrimmed condition $N \neq 0$ is 1.55 at a $\beta \approx 6.5^\circ$. The slope of line (b) taken at straight-ahead trim ($C_N = 0, A_Y = 0$) is a measure of the *directional stability*, dC_N/dA_Y ; a disturbance in A_Y results in a yawing moment tending to return the vehicle to its initial trim.

Table 8.2 Model Data for $\delta = 0, \beta$ Varies

$\alpha_{F,R}^\circ \equiv -\beta^\circ$	C_{Y_F}	C_{Y_R}	$C_Y = C_{Y_F} + C_{Y_R}$	$C_{N_F} = C_{Y_F}(a/\ell)$	$C_{N_R} = C_{Y_R}(b/\ell)$	$C_N = C_{N_F} + C_{N_R}$
1	0.160	0.207	0.367	0.080	-0.104	-0.024
2	0.308	0.395	0.703	0.154	-0.198	-0.044
3	0.427	0.569	0.996	0.214	-0.285	-0.071
4	0.525	0.713	1.238	0.263	-0.357	-0.094
5	0.595	0.827	1.422	0.298	-0.414	-0.116
6	0.627	0.900	1.527	0.314	-0.450	-0.136
7	0.614	0.928	1.542	0.307	-0.464	-0.157

A third situation considered is that in which the vehicle is rotated in β but at each β the front tires are steered back to zero slip angle. Thus all of the lateral force and yawing moment will come from the rear tires. The physical situation is sketched in Figure 8.5(c), the data is given in Table 8.3, and is plotted in Figure 8.6 as line (c). The lower endpoint of this line represents saturation of the rear tires at $-7^\circ \beta = 7^\circ \alpha$; the rear tires are on the peak of the cornering force curve.

This gives us two points on the rear tire boundary. Several interesting observations may be made:

- Lines (a) and (c) are called *front and rear construction lines* (as they are useful in constructing MMM diagrams). More importantly, when the vehicle operation is on line (a), all of the force and moment comes from the front pair of wheels; when the vehicle operation is on line (c), all of the force and moment comes from the rear wheels. The slope of line (a) is $C_{N_F}/C_{Y_F} = C_{Y_F}(a/\ell)/C_{Y_F} = a/\ell$; the slope of line (c) is $C_{N_R}/C_{Y_R} = C_{Y_R}(b/\ell)/C_{Y_R} = b/\ell$. Since a/ℓ and b/ℓ are equal in this example, the angle between the front and rear construction lines is 90° , as indicated in Figure 8.6.

Table 8.3 Model Data for $\alpha = 0, \beta$ Varies

$\alpha_R^\circ \equiv -\beta^\circ$	$C_{V_R} = A_Y$	$C_{N_R} = C_{V_R}(b/\ell)$
1	0.207	-0.104
2	0.395	-0.198
3	0.569	-0.285
4	0.173	-0.357
5	0.827	-0.414
6	0.900	-0.450
7	0.928	-0.464

- Line (b) has force and moment components from both the front and rear wheels of the car. Thus a point on line (b), say at -2° , can be obtained by vector addition of the contributions of the front and rear wheels. At this point we had 2° of slip angle on the front and -2° of $\beta \equiv \alpha_R$ on the back. The dashed lines show the vector addition. To confirm this vector addition, one can achieve the same results by adding up the lateral (A_Y) force/moment components of the front and rear wheels.
- We know that the endpoints of lines (a) and (c) represent saturation of the front and rear tires, i.e., they are on the peaks of their respective cornering force curves. By adding them up vectorially we can show the maximum force/moment capability of the vehicle configuration. Such a point is shown at P in Figure 8.6.
- For a vehicle to be in steady-state equilibrium (i.e., trimmed), the yawing moment, C_N , must equal zero. Although point P occurs at a lateral acceleration of $1.54g$ it cannot be achieved under equilibrium conditions, but only in a momentary "steady" condition reached from a dynamic maneuver.
- The maximum trimmed lateral acceleration is at point T, with a value of approximately $1.23g$. At point T, the front tires are saturated but a large excess of yawing moment remains from the rear of about $C_N = -0.31$ as shown at point Q. Thus the vehicle will "plow" at the limit. Actually a good measure of "final under/oversteer" is the distance from point P to the A_Y axis. If point P is below the axis (for RH turn) "final understeer" (plow) will occur; if P is on the axis the vehicle will drift (neutral), and above the axis there is "final oversteer" (spin).

Moment Method Diagrams

The above example of the basic construction of a C_N - A_Y diagram indicates the strong connection between the features of the diagram and the physical behavior of the vehicle. Properly understood and interpreted, the diagram is a "portrait" of vehicle maneuvering potential for specific operating conditions.

Figure 8.7 is a typical four quadrant C_N - A_Y diagram which covers all combinations of maneuvering in both left- and right-hand turns. The δ lines are labeled in terms of steering wheel angle. Each intersection point of δ and β lines is solved by the computer program. We have already shown that the front construction line represents the force and moment from the front wheels; similarly for the rear construction line. Any point on a construction line represents the lateral force and moment components corresponding to a slip angle at that pair of wheels. To obtain the total force/moment for a set of front and rear slip angles, one adds up the appropriate F and R force components obtained on the construction lines for each slip angle combination. For use of the diagram it is more convenient to think in terms of δ and β instead of α_F and α_R . Fortunately δ , β , α_F and α_R are related by the kinematic wheel relationship

$$\alpha_F = \beta + a/R - \delta \quad \text{and} \quad \alpha_R = \beta - b/R$$

These permit the use of δ and β instead of α_F and α_R for labeling the grid of the diagram.

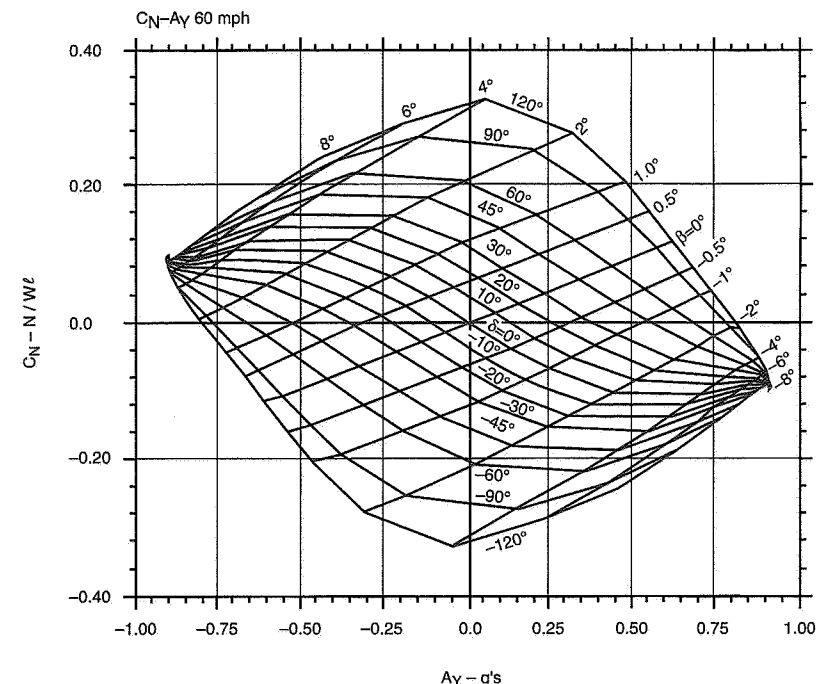


Figure 8.7 Typical four quadrant MMM diagram.

The C_N-A_Y diagram covers all constant-speed maneuvering. As discussed in Ref. 94, such steady-state parameters as understeer, stability index, steering sensitivity, roll and sideslip gains, etc., can be deduced directly from the diagram. They are associated with operation on (or small departures from) the trim line ($C_N = 0$). Max lateral acceleration and limit behavior have already been mentioned. The term *stability index* has its origin in the C_N-A_Y MMM diagram. It is defined as the slope of a δ line through trim and is a measure of the true static (steady-state) directional stability. Reference should be made to Chapter 5, where this concept and its companion, path curvature stiffness, are discussed.

Another diagram which is used in race car analysis is called C_N-C_Y . While C_N-A_Y corresponds to constant-speed maneuvering on different radii, the C_N-C_Y represents maneuvering (turning) on a constant radius at varying speeds. This is related to the constant-radius proving ground test (circle test) for vehicle operation on the trim line. The diagram can be drawn for any given radius, including infinite, which is a straight path.

In the C_N-A_Y diagram, all of the lateral force coefficient, C_Y , is utilized in reacting the centrifugal acceleration, thus $C_Y \equiv A_Y$, or the vehicle is in lateral force trim (equilibrium). In the C_N-C_Y diagram this restriction is no longer present and the lateral force can be used to react the centrifugal force on a given constant radius at varying speeds, or to react a lateral wind or the lateral component of the weight on a tilted (cambered) road. Thus C_N-C_Y is somewhat more generalized than C_N-A_Y . In the two examples given later in this chapter, the C_N-A_Y diagram is used to simulate operation on a road course with a large variety of corners and operating conditions. The C_N-C_Y diagram is used when interest lies in optimizing the performance on a given corner. C_N-C_Y has been successfully used for analysis (and prediction) of performance on high-speed oval track turns.

Steady-State Defined

It has been noted that MMM diagrams can be developed for conditions of longitudinal acceleration (traction or braking) as well as road load (RL). Since the MMM is implicitly based on steady-state conditions and since longitudinal acceleration results in a change in steady-state conditions, some explanation of "steady-state" is in order.

Steady-state as used in MMM context means that certain significant variables are constant. Two such situations are

- (1) Linear motion at constant speed
- (2) Cornering at constant speed

In (2) above, the significant variable is lateral acceleration which is constant. Both (1) and (2) are conditions which remain constant for an indefinite time period. Thus we can say that they are "steady, steady-state."

Two other conditions can be defined as steady-state:

- (3) Linear motion at constant speed and constant longitudinal acceleration
- (4) Cornering at constant speed and constant longitudinal acceleration

These conditions can exist, but not for long; they are referred to as "momentary steady-state." They are useful "snapshots" which can be taken at various times in a longitudinally accelerated condition. The Can-Am car example will illustrate the effect of steady (but momentary) traction and braking on the diagram.

Table 8.4 is a summary of MMM diagrams currently in use. Other diagrams have been developed for various special purposes.

Maneuvering on the Diagram

On the C_N-A_Y diagram the coordinate C_N is proportional to angular acceleration, α :

$$N = I\alpha$$

and

$$C_N = I\alpha/W\ell$$

where I , W and ℓ are constant for a given vehicle configuration.

Thus the C_N-A_Y diagram is equivalent to a plot of **angular acceleration vs. lateral acceleration**, two quantities which define maneuvering. Off the horizontal axis, the yawing moment, N , is available for creating an angular acceleration, hence a dynamic maneuver. For example, assume a step steer of 90° is so rapidly applied that no rotation of the vehicle occurs and β remains at zero for an instant. The vehicle then finds itself with an unbalanced yawing moment and associated angular and lateral accelerations. In a short time, rotation and β occur and the vehicle starts to move toward a new trim. By appropriate integration, taking into account the path curvature change, the vehicle may be tracked on the diagram to its new steady-state equilibrium. This is termed *maneuver tracking*.

Consider the maneuvering excursions that are likely to occur in racing. A racing turn is composed of three phases—the transient "turn-in" with associated braking, the steady-state phase (often near the corner apex), and the transient recovery to straight path with longitudinal acceleration. In the middle phase, near the apex, the vehicle is momentarily traveling at a constant speed on a constant radius such that its angular yawing velocity (rate of change of heading) is **constant**. This is one definition of steady-state turning. The constant speed also implies that the lateral acceleration is constant; $N = 0$ and the car is in balance.

Table 8.4 Summary of MRA Moment Method Diagrams

Mode Designation	Speed Specification	Path Radius Specification	Longitudinal Force Specification	Lateral Force Utilization	Related Test Procedure	Comments
$C_N A_Y$, Road load	Desired constant speed	Variable with A_Y , over operating range	Road load, $A_X = 0$ along path	Lat. force used for lat. accel., $C_Y = A_Y$	SAE & ISO constant throttle variable radius test	Tractive effort at drive wheels varies secondarily over diagram
$C_N A_Y$, engine overrun, braking/ traction	Desired constant speed (momentarily)	Variable with A_Y over operating range	Mode 1: Fixed X force on vehicle axis Mode 2: Fixed A_X , by tractive effort at driving wheels	Lat. force used for lat. accel., $C_Y = A_Y$	Mode 1: Used for braking studies. A_X varies somewhat over diagram Mode 2: Used for engine overrun and traction or acceleration studies	
$C_N C_Y$, Finite radius, engine overrun, braking/traction	Variable with A_Y over operating range	Desired constant radius	Road load, $A_X = 0$ along path	$C_Y = A_Y$, where A_Y produced by speed change on constant radius	SAE & ISO constant radius variable speed test	Secondary effects over diagram due to tire and aerodynamic speed dependencies
$C_N C_Y$, Finite radius, engine overrun, braking/traction	Variable with A_Y over operating range but invariant with longitudinal force.	Desired constant radius	Mode 1: Fixed X force on vehicle axis Mode 2: Fixed A_X , by tractive effort at driving wheels	$C_Y = A_Y$, where A_Y produced by speed change on constant radius	MIRA Tethered Test with yaw balance	Secondary effects over diagram due to tire and aerodynamic speed dependencies

Table 8.4 Summary of MRA Moment Method Diagrams (continued)

Mode Designation	Speed Specification	Path Radius Specification	Longitudinal Force Specification	Lateral Force Utilization	Related Test Procedure	Comments
$C_N C_Y$, Infinite radius, Road load	Independent of speed except for secondary effects due to tire and aerodynamic speed dependencies	Straight path, $R = \infty$	Road load, $A_X = 0$ along path	Unsigned	MIRA Tethered Test with yaw balance	Most unrestricted and basic form of Moment Diagram; pure force/moment producing capability of vehicle with no path curvature effects
$C_N C_Y$, Infinite radius, engine overrun, braking/ traction	Independent of speed except for secondary effects due to tire and aerodynamic speed dependencies	Straight path, $R = \infty$	Mode 1: Fixed X force on vehicle axis Mode 2: Fixed A_X , by tractive effort at driving wheels	Unsigned		Only restricted by the specifications of longitudinal force. No path curvature effects.

In the turn-in and powering-out phases, the angular velocity is not constant, changing from zero at the start of the turn, for example, to a steady-state value at the apex. Thus angular acceleration exists. As indicated above, when a mass is angularly accelerated a moment is required to overcome its angular inertia. This moment, N_a , must be supplied by the vehicle's steering control, the lateral tire forces at the front wheels times the moment arm, a , to the CG. We wish to estimate how large this inertia moment, N_a , is relative to other yawing moment components on the vehicle. If it is small enough to be neglected in practical cases, the turn-in and powering-out phases of a turn can be treated as true steady-state.

Assume a race car configuration as follows:

W	1800 lb.
ℓ	Wheelbase, 8 ft.
CG	60% of ℓ , aft
a	4.8 ft.
b	3.2 ft.
Radius of Gyration	$0.8 \times 4.8 = 3.84$ ft.
Moment of Inertia, I	824.5 slug-ft. ² (= lb.-ft.-sec. ²)

Further assume that this vehicle transitions from a straight path into each of two turns—one of 100 ft. radius, the other of 1000 ft. radius. In the steady turns, the vehicle is to develop 1.2g laterally (its speeds in the steady turns are 42.4 and 134.0 mph). A reasonable spiral turn entry was used in the calculations. The results below are the calculated angular inertia moments:

For 100 ft. radius turn, $N_a = 206$ lb.-ft.

For 1000 ft. radius turn, $N_a = 20.6$ lb.-ft.

Expressed as a yawing moment coefficient by dividing by $W\ell$, we have

For 100 ft. radius turn, $C_{Na} \approx 0.010$

For 1000 ft. radius turn, $C_{Na} \approx 0.001$

On a typical race car of this size, 1° of front wheel steer will produce a yaw moment of over 1400 lb.-ft. or a coefficient of 0.096. Thus it seems safe to assume that the inertia moment is small enough to neglect, particularly as it falls off rapidly at higher speeds. It is easy to establish whether or not the inertia moment is important in a particular case.

Experience in racing suggests that the smoothest driving techniques (which minimize angular acceleration) produce the highest speeds. Successful drivers at Indianapolis, for example, are known for their sensitive driving and smooth transitions; they appear reluctant to give away lateral tire force for angularly accelerating the vehicle, preferring to move carefully from one steady-state condition to another. In MMM terms, drivers on

high-speed corners—road courses or ovals—operate very close to the trim line, $N = 0$, unless tactics or emergencies dictate otherwise.

There are some forms of racing, i.e., Pro-Rally, where large excursions over the MMM diagram occur. Often, large control moments are used to produce β opposite to that required for an upcoming corner. This then allows a rapid rotation of the vehicle into a high β attitude for the turn (dirt-track slide). It would be interesting to analyze the maneuvering of some of the top rally drivers by the MMM technique.

8.5 Limit Behavior

Yaw moment balance ($N = 0$) is a requirement for steady cornering, otherwise the vehicle would be subjected to an unbalanced moment ($N \neq 0$) initializing an angular acceleration. It is apparent that yaw moment balance (trim) can be obtained with either the front or rear track at (or close to) its tire force peak. For the highest cornering speed it is obviously desirable to have the front and rear tracks peak simultaneously to use all of the potential cornering force of the vehicle. The behavior of the vehicle at the limit is then one of drifting, or sliding laterally, and the vehicle is said to be *neutral*.

Chassis tuning or setting-up the vehicle has the objective of achieving neutral or near neutral cornering behavior, unless special circumstances and driver preference dictate otherwise.³⁵ In any event, it will be impossible with a passive suspension to obtain neutral cornering under all operating conditions (such as cornering under traction and braking).

A vehicle with one end reaching the limit first will tend to push (plow) or become loose (spin). The machine that pushes is frequently said to have “final understeer”; the machine that spins “final oversteer.” Although the machine’s behavior is reminiscent of over/understeer in the tire’s linear range of operation, the physical situation is different and the two should not be confused. They have different handling implications and different causes.

Stability and Control

The concept of under/oversteer (UO) is associated with the linear range of tire operation where the forces arise from elastic tire distortion in the print. Lateral tire force is approximately proportional to slip angle (at constant load, etc.) in the linear range. The alternative ways of defining UO have been discussed in Chapter 5, but they all involve a

³⁵ At very high speeds, super-speedways for example, spin recovery may be practically impossible and the cars are deliberately set-up for some push (plow) at the limit. Here cornering speeds are power limited, not lateral force limited.

slope taken at some particular trim. One physically satisfying way of thinking of understeer is the weathercock analogy. Understeer is the tendency of the vehicle to align its axis with its velocity vector (to reduce vehicle slip angle, β). This simply says that the restoring moment from the rear track (from the lateral tire forces due to β) is greater than the destabilizing moment from the front track. In order to obtain a slope, the resulting moment is measured over a small range of β . If N is the yawing moment component due to β , $\Delta N / \Delta \beta$ is a measure of linear understeer. It is positive for understeer, zero for neutral, and negative for oversteer (using SAE sign conventions).

Final under or oversteer occurs in the transitional and frictional ranges of tire operation (see Figure 8.8) when one end of the vehicle is reaching its limit lateral force capability. In dry conditions the lateral force output then remains essentially constant; for wet it can fall off. Slip angle ceases to be the significant variable at that end of the vehicle and control passes to the other end of the machine. Consider the case where the limit is first reached at the front: changes in β no longer increase the destabilizing moment from the front. The stabilizing moment from the rear takes over, the path tends to straighten and the vehicle aligns itself with the path. With front steer, control moments can no longer be generated. In these circumstances, about all the race driver can do is slow down or break traction on the rear tires with power. When the limit is first reached at the rear, increase in β results in no further stabilizing moment from the rear and the destabilizing

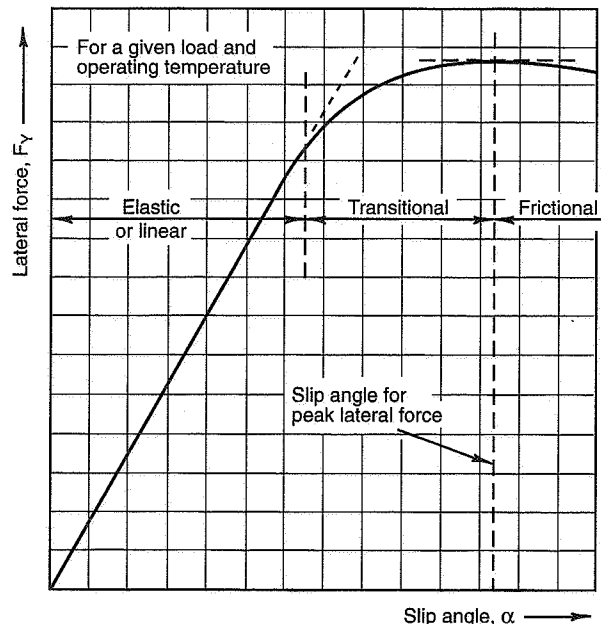


Figure 8.8 Lateral force vs. slip angle for a racing tire.

moment at the front takes over. Steering control remains and driver control action may avert a spin.

Roughly half of the lateral and yaw dampings are lost when either end of the vehicle breaks away, so the driver may induce (in a recovery attempt) a PIO (in aeronautical terminology, a “pilot induced oscillation”). The old racing adage then applies: “Keep fighting it son, you may make it yet!”

When one end (of the vehicle’s tires) is in the frictional range and the other end is in the nonlinear transitional range the physical situation is very different from the linear elastic low-lateral acceleration case. It seems best to avoid the terms “final over/understeer” and use the race driver’s descriptive terms push (plow) and loose (spin) for limit behavior.

The range of linear over/understeer can be defined for dry surfaces in terms of lateral acceleration (say from 0 to 0.3–0.4g). With the high-powered rear-drive race car, a loose (spin) condition can occur at any lateral acceleration (even zero) if the drive tires are spun up in a low gear. Similarly, a high-powered front drive could be made to push (plow) if traction is broken on the front. Improper brake balance which locks up the front or rear will also result in push or spin.

Trim at the Limit

When one end of the vehicle is at the limit (on the peak of its cornering force curve), “trim” can still exist. For example, if the front end of the vehicle reaches the limit, the peak force remains and the vehicle can continue around the corner for which it is trimmed. Control in the sense of the “ability to tighten the turn” or cope with small disturbances has largely disappeared. Recovery from the turn can be initiated by steering to reduce the slip angle below the peak. The trim associated with this situation is called a *stable trim*.

If the rear end reaches the limit first, the vehicle can continue the turn in which it is trimmed, but inherent stability against small disturbances is no longer available. The trim associated with this situation is an *unstable trim*.

If both ends are on the peaks, neither steering control nor stability are available to the driver. This explains Stirling Moss’s contention that if a car is set up for max cornering (drift at the limit), once the car is presented to the corner the vehicle will go through on a predestined trajectory “like a thrown dart.” Changes in power in conjunction with small steering motions may permit some adjustments in trim.

Thus we see that sub-limit concepts of **stability** and **control** do not easily apply to limit operation. Limit operation is more analogous to stalling in an airplane. In this regime pilots and engineers talk of stall characteristics in terms of stall warning, pitch and roll

behavior, and recovery techniques, which compare to skid warning, breakaway characteristics, and recovery for the automobile.

The following analogies may be helpful in thinking about these operating regimes. In Chapter 5, the behavior of a pneumatic tire in the linear range has been compared to a hydraulic damper. Thus, at constant forward velocity the lateral force is proportional to the slip angle which is in turn proportional to lateral velocity. The lateral force is along the same direction but opposite in sign to the lateral velocity.

At the peak of the idealized cornering force curve of Figure 8.9, the analogous damper is the Coulomb type, namely a friction damper which puts out a constant force independent of lateral velocity (or slip angle at constant speed).

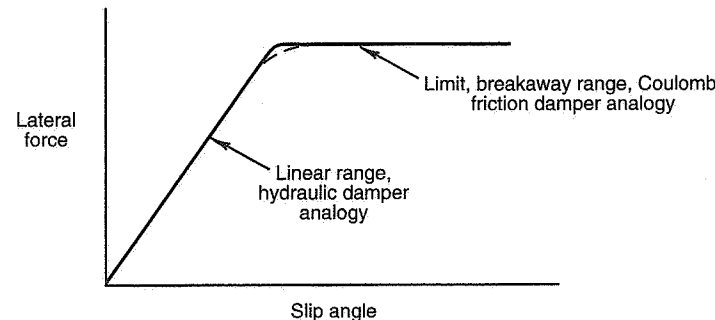


Figure 8.9 Idealized cornering force curve.

The lateral force at the peak of the cornering force curve is of frictional nature, as opposed to the tire distortion in the linear range. For tires, the relationship is nonlinear with the effective coefficient falling off with increase in load (tire load sensitivity). The **peak adhesion or grip** depends on tire print size and shape, tire material and hardness, temperature, surface conditions, etc. The details of what goes on in the print are still not fully understood (see Chapter 2). If the peak tire lateral force was a linear function of load, the race car would tend to be neutral and remain so with changes in longitudinal CG position and LLTD (Lateral Load Transfer Distribution). With this hypothetical tire, moving the CG aft, for example, would increase both the centrifugal force component taken by the rear track and the lateral tire force, in proportion. Transferring load from the inside to the outside wheels would be ineffective in changing the lateral track force since the loss on the inside wheel should be fully compensated by the increase on the outside wheel. It is the variation of the effective friction (or adhesion, grip) coefficient on actual tires that facilitates chassis tuning.

For any automobile there should be a smooth progression in the lateral forces and slip angles at the front and rear tracks when the vehicle traverses a turn at the limit. Figure

8.10 shows the cornering curves for the front and rear of a rear-drive sports sedan with performance tires. The vehicle is cornering at 60 mph under RL conditions and the curves correspond to zero yawing moment; the vehicle is trimmed and in balance. Max cornering is reached when the front tires are saturated (reach the peak of the front cornering force curve) at Point A. At this point the average front slip angle is 8° and the average rear slip angle is 4° (Point B). The lateral acceleration is about $0.86g$. The vehicle "pushes" since the rear tires have not peaked.

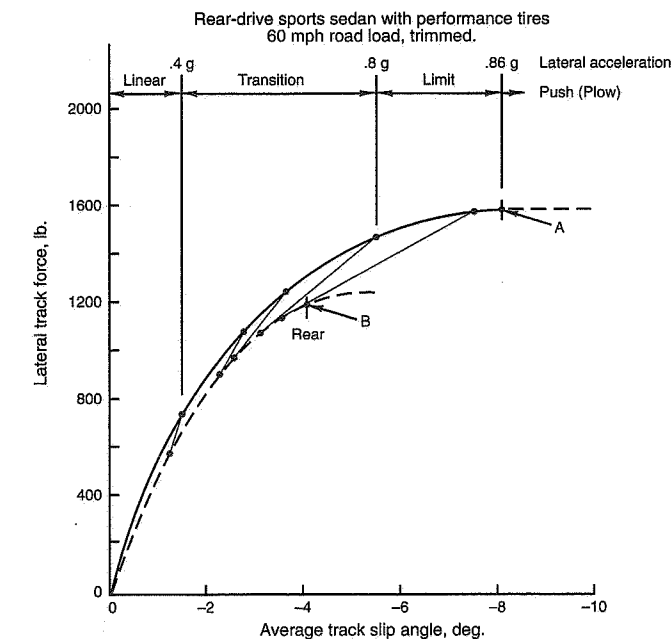


Figure 8.10 Cornering forces for the front and rear tracks.

The tire operating regimes are indicated at the top of the figure. In the **linear range**, stability may be assessed in over/understeer terms; in the **transition** range over/understeer can be used in an "operating point" context, through localized slopes; above $0.8g$ the vehicle is in the **limit** region and its behavior can be described in "breakaway" terms as indicated earlier.

Linear vs. Limit Characteristics

These characteristics depend on different physical phenomena and a variety of combinations are possible. This can be illustrated by an elementary car model in which only the

fore and aft CG location (a and b) and friction coefficients at the front and rear tires (μ_F and μ_R) are varied. The tire cornering curves are idealized as in Figure 8.9 by two linear line segments, and the vehicle weight and wheelbase are fixed.

Figure 8.11 shows the resultant F-M envelope for a few combinations of the independent variables. Note that the maximum value of lateral force for which the vehicle can be

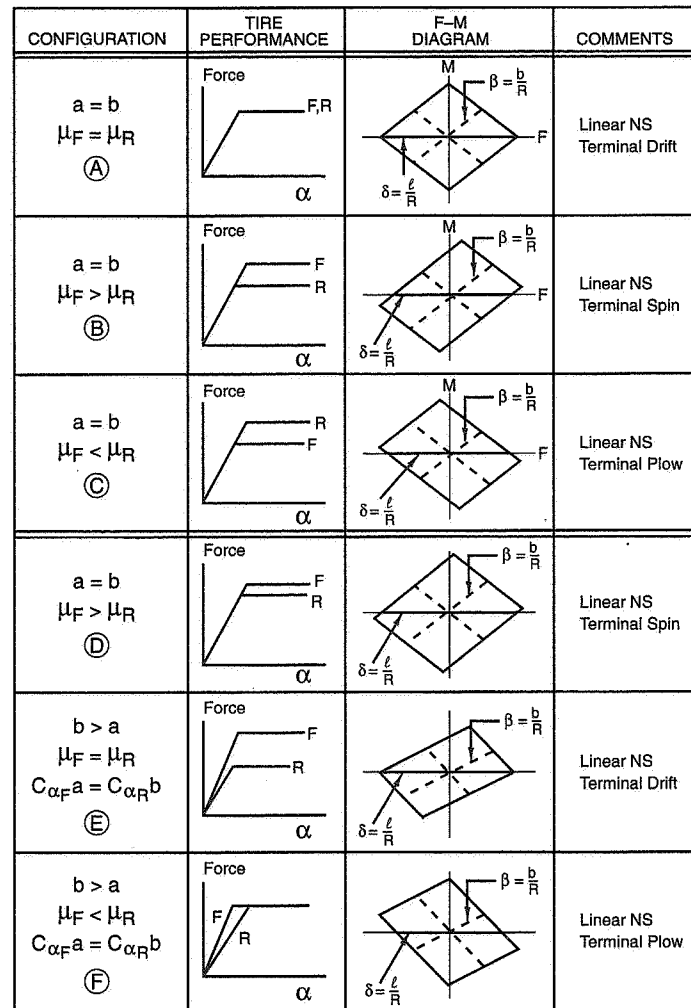


Figure 8.11 Force-moment envelopes.

trimmed is dependent only on the smaller of the μ 's; their relative values dictate whether the vehicle will spin $\mu_F > \mu_R$, drift $\mu_F = \mu_R$, or plow $\mu_F < \mu_R$ at the limit of performance. Note that the maximum values of control moment and total side force are equal for the first three cases in Figure 8.11 because the values of $\mu_F + \mu_R$ for all cases are equal.

Case D shows the condition for which μ_F has been increased and μ_R is unchanged from Case A; here the size of the diagram is increased in both axes although the maximum trimmed force remains the same. Case E illustrates a combination of tire performance (spin) and vehicle geometry (US) which produces linear NS and terminal drift at the same value of trim maximum force as Case A. With the same geometry and tire cornering stiffness as Case E (retaining neutral steer characteristic), Case F demonstrates reduced maximum trim force at the same value of maximum available force, resulting in plow.

These samples obviously represent only a few of the many possible combinations of the primary vehicle parameters. It would be interesting to develop a complete catalog of these diagrams for a variety of operating conditions of a given basic vehicle.

8.6 N-A_Y, Race Car Example

The vehicle used in this example is the Chaparral GS 2G which had a very successful season in Can-Am racing in 1967. This car was extensively tested by Chevrolet and excellent chassis, tire and aero input data were available. Furthermore the full-scale handling characteristics had been measured, along with driver comment. Finally, the vehicle had an adjustable wing at the rear, permitting a comparison with and without additional downforce.

Pertinent characteristics of this rear-drive vehicle are given below:

W	1950 lb. (1/2 fuel)
CG	66% wheelbase, aft
a	4.95 ft.
b	2.55 ft.
ℓ	7.5 ft.

Detailed data were available on brake balance, lateral weight transfer distribution, aerodynamic download/drag, and tires, including friction coefficient as a function of load and speed.

N-A_Y diagrams were calculated for the conditions shown in Table 8.5 and the diagrams are identified by this table. N is the actual yawing moment at the CG, in lb.-ft.

Table 8.5 Moment Method Run List

Condition Number	Speed, V mph	Aero Configuration	Fraction Lat. Load Trans. on Front	Front Brake Force, lb.	Rear Brake Force, lb.	Thrust Force Rear, lb.	Steady Longitudinal Acceleration, g's
B ₁	B ₂	D ₂					
1	40	Trimmed	0.80	0	0	0	0
2	100	Trimmed	0.80	0	0	0	0
3	100	Trimmed	0.80	0	0	1280	0.66
4	100	Spoiled	0.80	975	975	0	1.00
5	100	Trimmed	0.50	0	0	0	0
6	140	Spoiled	0.80	0	0	0	0

The notation (under "Aero Configuration" in the table) of "Trimmed" means that the rear wing was set horizontal. "Spoiled" means that the wing was set with the nose down to give maximum downforce (approx. 25°). In the table and related figures, "FRC" is the fraction lateral load transfer taken on the front. $B_1 = B_2 = D_2 = 0$ indicates RL power. If B_1 , B_2 , or D_2 is other than zero, the actual braking or driving force at the ground is given. The δ on all the diagrams is steer angle at the front wheels.

Figure 8.12 is a baseline diagram, 40 mph, RL, with the wing trimmed. At this condition the maximum trimmed lateral acceleration is 1.28g (Point A). Trimmed means the vehicle is in "yaw moment balance" with $N = 0$. Remembering that the upper boundary (B) represents the maximum lateral force from the front tires, it is seen that the max trimmed lateral acceleration is determined by the front tires. The rear tires are still capable of producing some 600 lb.-ft. of yawing moment (Point C). If the driver attempts to corner harder than 1.28g by some dynamic maneuver, the vehicle will plow (push). The rear tire maximum force boundary is shown at (D).

Whether the vehicle plows or spins is indicated by the location of the point of intersection of the front and rear tire boundaries (on this diagram, Point E). The rule is: if this point falls below the $N = 0$ axis the car plows; above the axis the car spins; if on the axis the car drifts (is neutral). The vertical distance the point is from the axis is a measure of the plow/spin tendency, the unbalanced moment. This is an example of why race cars are tuned to be neutral at the limit. It means that all of the front and rear cornering force is being used, the two ends of the car peak together and the maximum lateral acceleration is achieved under "moment balanced" conditions.

The control available to the driver at any lateral acceleration may be evaluated in terms of the maximum yawing moment that can be applied to the car through the steering. Let us assume the vehicle is in a RH turn at 0.6g and the driver wishes to tighten the turn rapidly. If the steering is applied rapidly enough the vehicle slip angle, β , remains unchanged—the vehicle has not rotated. Starting with an initial steer angle of about 2° (Point F), we read up the constant β line (-1.0β), to the front tire boundary (at Point G). At this point

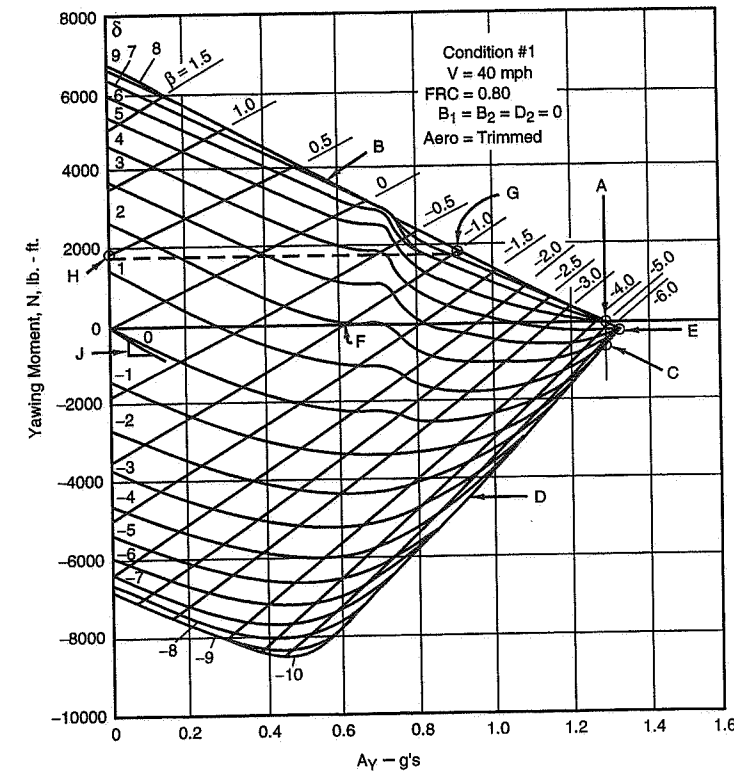


Figure 8.12 Chaparral, condition #1.

the driver has applied a steering moment of about 1800 lb.-ft. (Point H), or a lateral force at the front track of $1800/4.95 = 364$ lb. If this steer angle is held, the vehicle would start to rotate clockwise, moving down the front tire boundary and finally retrimming at Point A. Of course no driver would apply such a step of control (about 8° of δ , measured at the front wheels), but the distance from Point F to Point G and the associated yawing moment is still a measure of available control.

As noted earlier, when the lateral acceleration increases, the driver's control decreases. More of the lateral force from the front and rear tires is required to balance the centrifugal force. At max trimmed lateral (Point A), the driver has (in this case) no control left for tightening the turn, but can widen the turn by backing off on steering and getting below the peak of the front tire cornering force. The great reduction in control at the limit of a neutral car explains the quote by Stirling Moss of the "predestined trajectory."

In Figure 8.12, the δ curves have a curious "bump" in the vicinity of $0.7g$. By looking at the data tabulation, it was found that the vertical force on the inside front tire had dropped to zero. The wheel had come off the ground because of the large fraction of the lateral load transfer on the front track (80%). From there on the car was a three-wheeler, with a momentary increase in stability.

In racing, most interests center on limit cornering behavior, but all of the sub-limit parameters for judging stability and control can be deduced from the diagram. In particular, the directional stability (of interest on fast straights and bends) is given by the slope of a δ line as it passes through trim. For example, the slope shown at J is a measure of the true directional stability in straight running (this slope is referred to as the *stability index*—see Chapter 5).

Figure 8.13 illustrates what happens when the speed is increased to 100 mph, RL, with all other conditions unchanged. The size of the diagram is about the same; it depends on

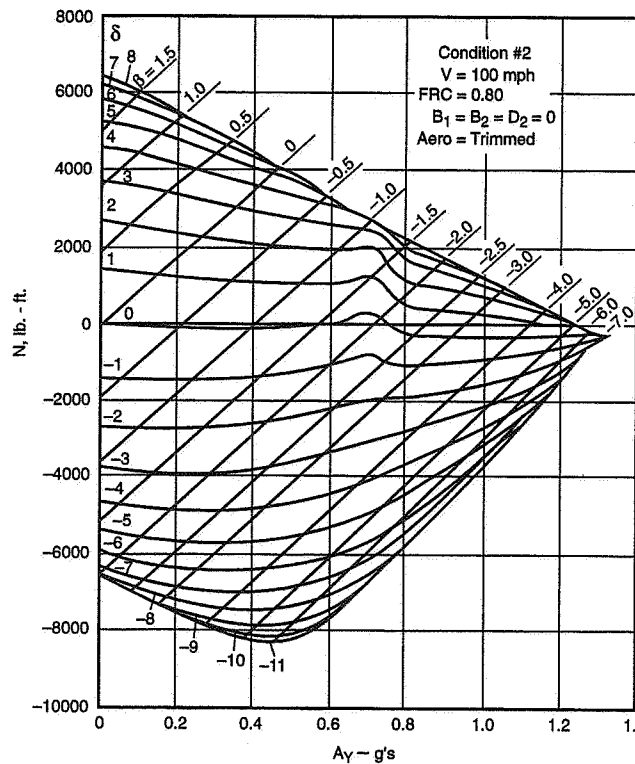


Figure 8.13 Chaparral, condition #2.

the tire friction coefficient. The maximum lateral is reduced slightly to $1.25g$ and there is a slight increase in push at the limit. The major difference is the slopes of the δ lines which are now nearly horizontal in the operating range near $N = 0$. This drastic change in directional stability is due to the decrease in yaw damping (a component of the stability index) with speed. Physically, it is due to the reduction in path curvature for a given lateral acceleration as speed is increased. Slip angles induced by path curvature are stabilizing (again, see Chapter 5).

Figure 8.14 at the same speed (100 mph) shows what happens when the vehicle is accelerated with a tractive force (above road load) of 1280 lb. or $1280/1950 = 0.66g$. The size of the maneuvering area is markedly decreased as load is transferred off the front tires (lowering the front boundary) and the lateral force potential at the rear is decreased via the friction ellipse relationship (which moves the rear boundary up). The max trimmed (balanced) lateral acceleration is now $0.87g$ and the vehicle is a strong plow at the limit. This condition is one that could occur in the final phase of a turn.

It is interesting to note that the directional stability as measured by the slope of the δ lines is increased over that of Figure 8.13. Two effects are present, the transfer of load to the

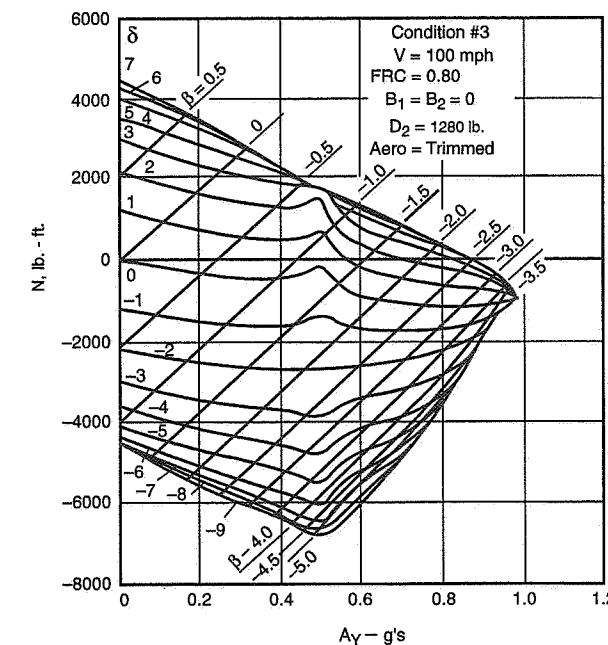


Figure 8.14 Chaparral, condition #3.

rear (increasing stability) and the friction ellipse effect at the rear (decreasing stability). In this case, the former predominated. The inside front tire now lifts off the ground at a lower lateral acceleration because of the longitudinal load transfer.

Figure 8.15 illustrates the effect of 1.0g braking, $(975 + 975)/1950 = 1.0$, which could occur in the initial phase of a turn. The speed is still 100 mph but the rear wing has been rotated down for max aero downforce. The vehicle is highly unstable. At the limit, the car exhibits a strong spinning tendency, with the apex of the diagram well above the N = 0 line. In order to trim the vehicle at max lateral in a turn, some $8^{\circ}\text{--}9^{\circ}$ of reverse steer is required; this is referred to as an *unstable trim*. Practically, it would probably be impossible to corner with this amount of braking at much above 0.85g. The driver can generate control moments in this range but it takes skilled closed-loop control to hold a trim. In effect the driver must augment the stability to maintain trim.

The "bump" in the δ lines in the 0.3-0.4 lateral acceleration range appears due to inside front wheel lockup. The accurate simulation of limit brake performance is very difficult and has been improved in subsequent versions of the program.

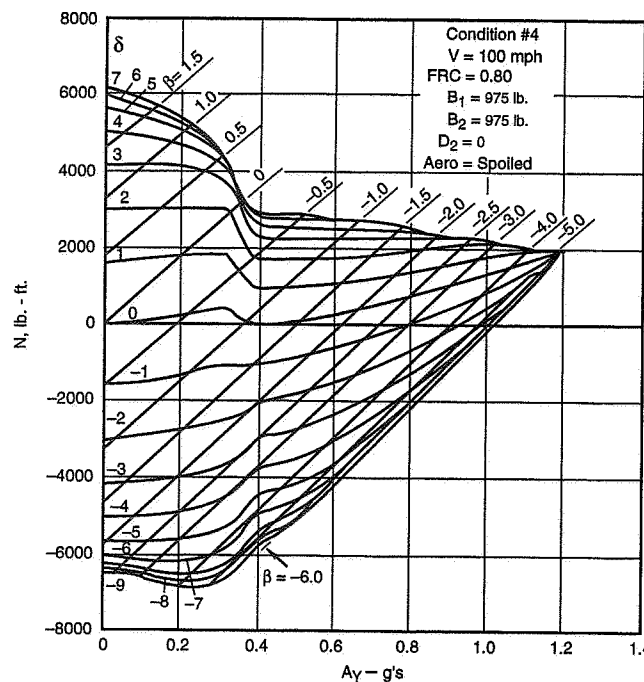


Figure 8.15 Chaparral, condition #4

Figure 8.16 illustrates the effect of changing the lateral load transfer distribution. Comparison should be made with Figure 8.13. In the latter, 80% of the LLTD was taken on front and the inside front wheel lifted off around 0.7g. When the LLTD on the front was reduced to 50% the wheel lift-off occurred at about 1.2g, very near max lateral (obviously not a desirable thing for control near the limit). If LLTD on the front was reduced to say 40%, wheel lift-off would be avoided.

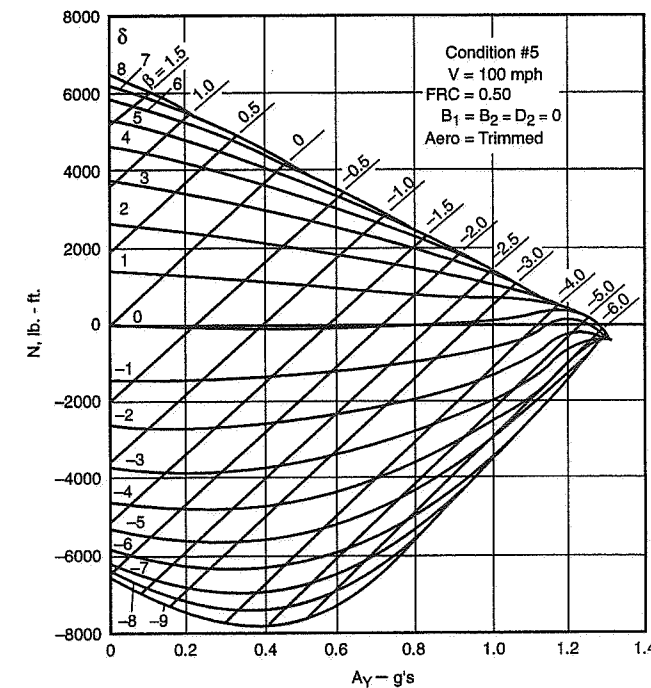


Figure 8.16 Chaparral, condition #5

In a final Chaparral figure, 8.17, the dramatic effect of aerodynamic downforce is illustrated. In this case the diagram is for 140 mph and the rear wing is turned down ("spoiled"). The max trimmed lateral is 1.4g. The vehicle exhibits modest plow which is generally desirable at the higher speeds. Also, as the internal δ lines indicate, some small stability exists at accelerations above 0.9g. The size of the diagram—the maneuvering area—has been increased markedly over all the other operating conditions explored. The increase in size of the diagram is due to increasing both the front and rear boundaries, which together increase the maximum trimmed lateral; it also means that both the destabilizing and stabilizing moments from the front and rear have increased in about equal proportions thus maintaining a near neutral vehicle.

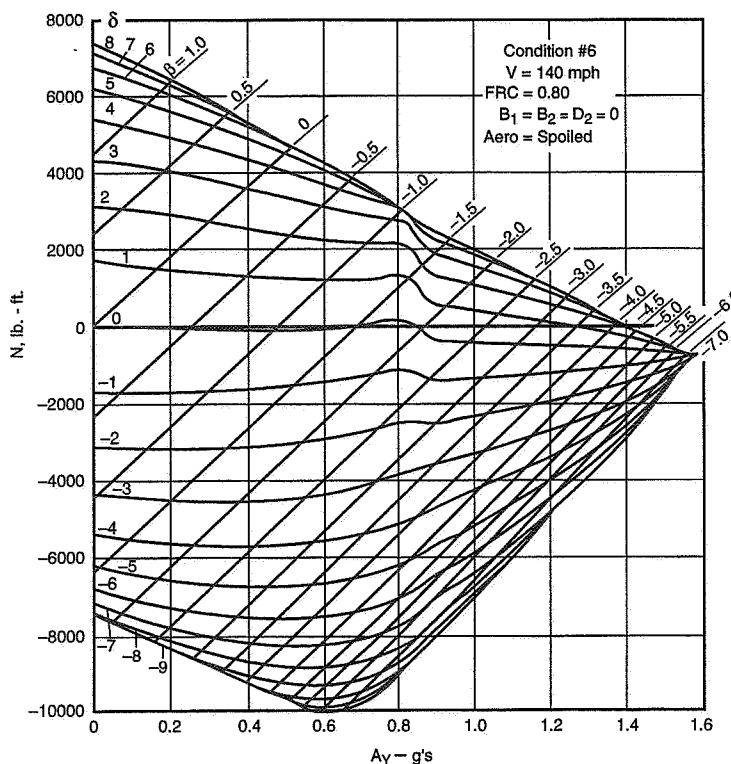


Figure 8.17 Chaparral, condition #6.

The drivers of the Chaparral felt that the set-up depicted by these MMM diagrams gave a reasonable compromise of the various operating conditions. It was certainly a race-winning one.

It should be noted that most race car operation is close to the $N = 0$ axis. The better professional drivers are known for their smooth control application, thus they are in a near steady-state condition most of the time. Heavy braking may be an exception. Also evasive or emergency maneuvers may require substantial control moments.

Finally, operation very close to the limit at high speed with wind and road disturbances can be a delicate affair requiring trim corrections by throttle and steering. As Miles Collier noted many years ago, in the cars of that era, driving near the limit where the distribution of the loads on the wheels is so important is a bit like "dancing along on a four-legged table."

8.7 C_N - A_Y , Sports Car Chassis Tuning Example

The intent of this example is to illustrate use of MMM in a brief parameter study. We will first define in some detail a baseline vehicle. Next we will show the characteristics of this vehicle over the full lateral acceleration range making use of MMM post-processing for steady-state trimmed parameters and "friction circles." Then we focus on the end of the C_N - A_Y diagram and show the changes in limit behavior that occur with physical changes in the vehicle.

The vehicle used in this example is a large sports car defined by the following baseline configuration. The list indicates the sort of comprehensive input available with MMM.

Rear drive	
Wheelbase, ℓ	98 in. (8.17 ft.)
Track F, R	55 in.
Gross weight	3000 lb. CG location 54% on front
Front track weight	1620 lb. (810 lb./wheel), $a = 45$ in.
Rear track weight	1380 lb. (690 lb./wheel), $b = 53$ in.
CG height	19 in.
Front spring rate	200 lb./in. at wheel = 93 cycles/min.
Rear spring rate	167 lb./in. at wheel = 92.5 cycles/min.
Steering ratio, G	16 to 1, parallel steer
Static toe, F & R	0
Bump steer, F & R	0 (to keep things simple)
Static camber, F & R	0
Bump camber, F & R	1°/inch ride travel
Lat. force compliance steer, F	-0.09°/1000 lb. lat. force (US)
Lat. force compliance steer, R	-0.20°/1000 lb. lat. force (OS)
Lat. force compliance camber, F	-0.6°/1000 lb. lat. force (US)
Lat. force compliance camber, R	-0.6°/1000 lb. lat. force (OS)
Traction/braking compliance steer	Nearly 0
Aligning torque compliance steer, F	+0.5°/100 lb.-ft. torque (US)
Aligning torque compliance steer, R	+0.1°/100 lb.-ft. torque (OS)
Aligning camber stiffness, F & R	Very high
Anti-dive	150 lb. jacking force/1000 lb. longitudinal force
Roll center height, F & R	3 in.
Anti-roll bar on front such that total roll rate, F = 1400 lb.-ft./deg.	
No roll bar on rear, total roll rate, R = 390 lb.-ft./deg.	
Roll gradient	2°/g

Aero frontal area	20 ft. ²
Drag coefficient, C_D	0.280
Lift coefficient F, C_{LF}	0.136 up
Lift coefficient R, C_{LR}	-0.080 down (rear deck spoiler)

Tires Goodyear P225/50 VR15 F & R

(Note that these have characteristics similar to the P215/60 VR15 shown in Chapter 2. No overturning moment data was available for these tires so this was omitted in this example calculation.)

The baseline operating condition is 100 mph, road load. This means that power is supplied to maintain 100 mph regardless of the amount of turning.

Baseline Configuration Behavior

Figure 8.18 presents the four quadrant (left- and right-hand turns) C_N - A_Y diagram for the baseline configuration, 100 mph, RL with the δ and β lines based on SAE sign conven-

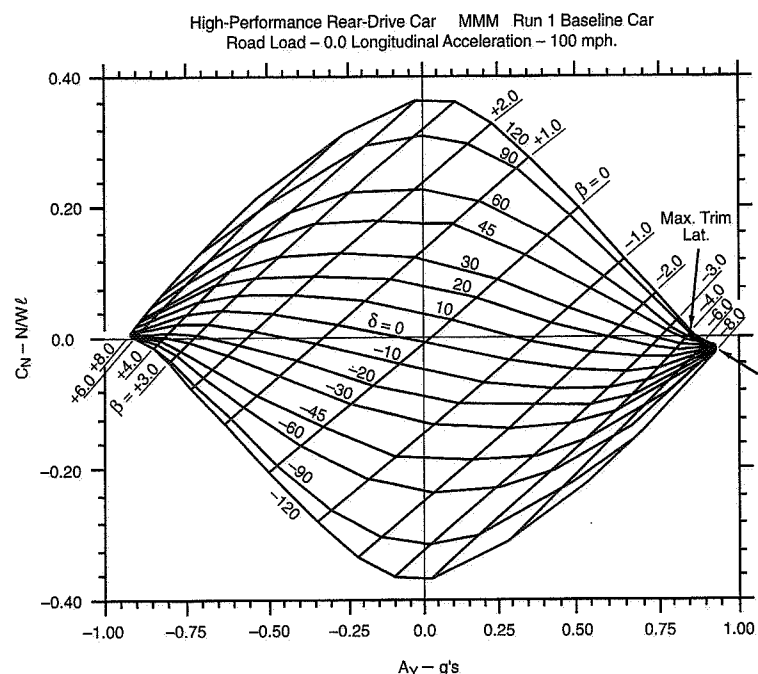


Figure 8.18 Sports car, baseline.

tion indicated. This diagram indicates a well-behaved vehicle, stable over the lateral acceleration range as indicated by the slopes of the δ lines as they cross $C_N = 0$ (trim), with a slight amount of "plow" at the limit—Point A falls below the $C_N = 0$ axis. Max lateral trim is 0.88g. At this point the front tires have saturated but the rears are still capable of producing -0.05 more yawing moment coefficient. In terms of actual yawing moment,

$$N = (-0.05)(3000)(8.17) = -1226 \text{ lb.-ft.}$$

or 150 lb. of lateral force at the front and rear tracks tending to "push" the car out of the turn.

Figure 8.19 gives the roll angle for all of the δ - β solution points, trimmed and untrimmed. Its slope is the roll gain, slightly over 2°/g for the baseline case.

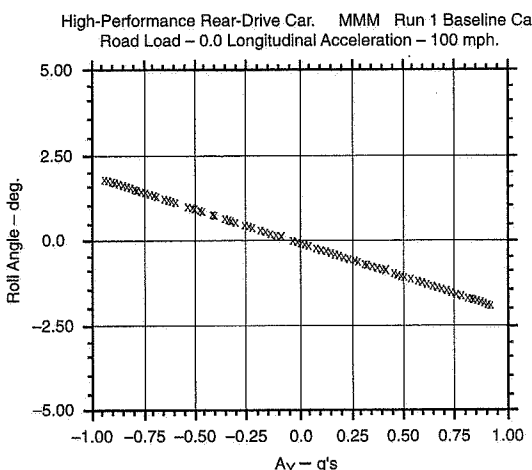


Figure 8.19 Roll angle vs. A_Y .

MMM post-processing interpolates along the $C_N = 0$ line to find steady-state trimmed values for a number of parameters over the full lateral acceleration range, these are discussed below:

- Figure 8.20, steer angle corresponds to the SAE Constant Speed (throttle) Skid Pad Test. The slope of this curve in the linear range is the US (shown later in Figure 8.23). The "turn-up" at the end is due to a reduction of the control effectiveness as the front tires approach the peak of the cornering force curve.

- Figure 8.21, **stability index** is a measure of the true static directional stability which includes the US moment and the yaw damping moment (see Chapter 5). It is essentially constant up to about 0.7g after which the vehicle starts to plow as the limit is approached.
- Figure 8.22, **trimmed sideslip** indicates the variation of vehicle sideslip, β , measured at the CG. At this high speed (large radius), β is very nearly equal to the rear slip angle, except for the effects of any compliance and kinematic steers in the rear suspension.
- Figure 8.23 gives the **understeer gradient** as a function of lateral acceleration, although US is normally defined as a linear range (0.2g) characteristic. For this vehicle the gradient is about $1^\circ/g$ on-center and $2^\circ/g$ at 0.55g. These numbers are low for this category of car, which typically falls more in the $2^\circ/g$ to $3^\circ/g$ range on-center.
- Figure 8.24 shows the **steering sensitivity** as defined by General Motors in g/100° of steering wheel angle. The sensitivity is high (about 3.8 on-center), again probably too high for a production sports car. It falls off to near zero at max lateral.

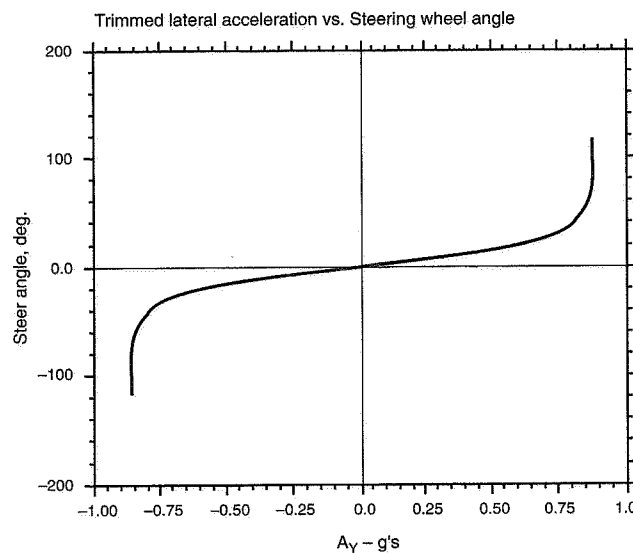


Figure 8.20 Steer angle response.

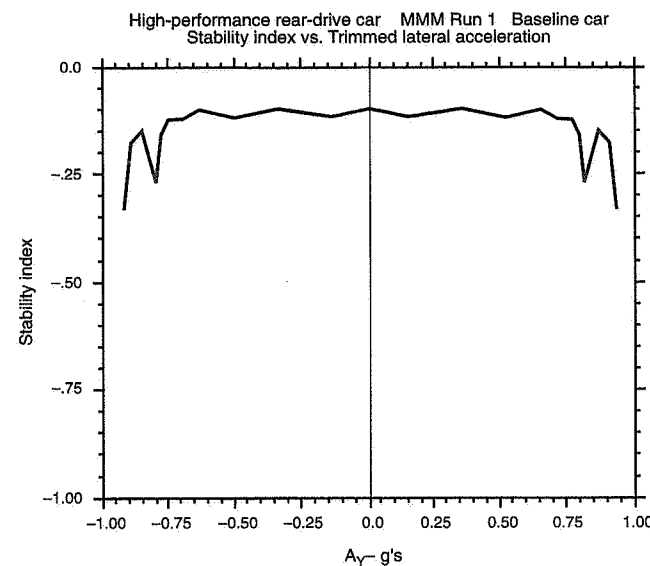


Figure 8.21 Stability index.

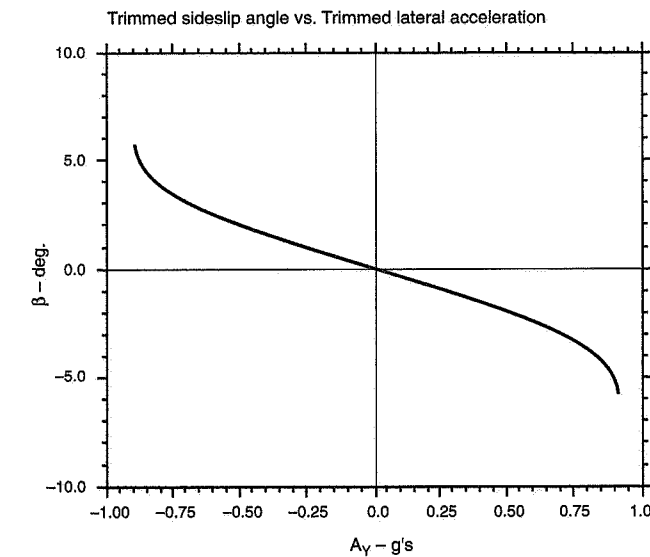


Figure 8.22 Trimmed sideslip angle response.

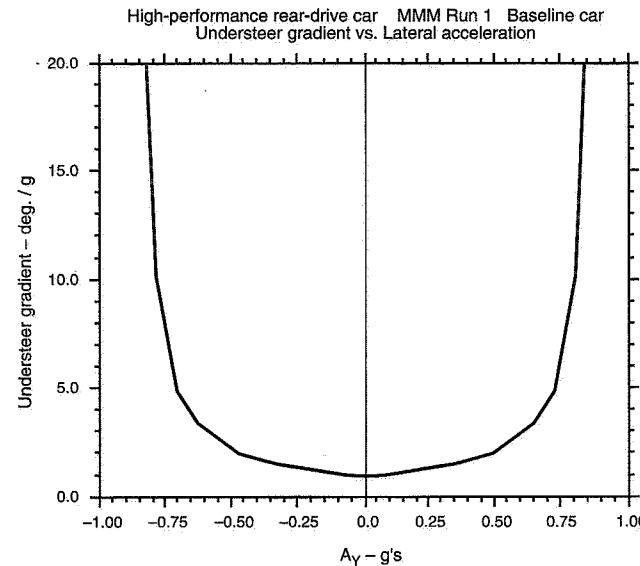


Figure 8.23 Understeer gradient.

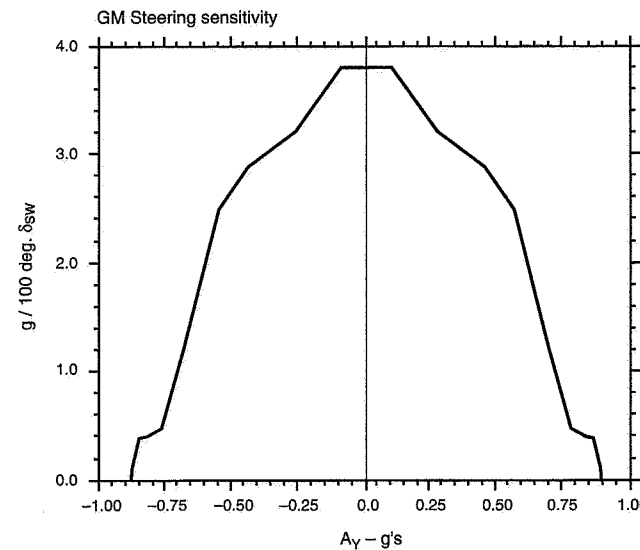


Figure 8.24 GM steering sensitivity.

MMM post-processing allows the user to interact with a solution data set to produce "friction circles" for any point on the maneuvering diagram. This shows detailed operating conditions at each wheel (see Figure 8.25). The first plot is for straight ahead and the other is near max trimmed lateral. Each plot shows a friction circle (ellipse) at each wheel location which represents the boundary of the resultant horizontal force available at that wheel, based on the current load and friction coefficient. In addition, an arrow is shown which represents the resultant horizontal force actually being generated at that wheel.

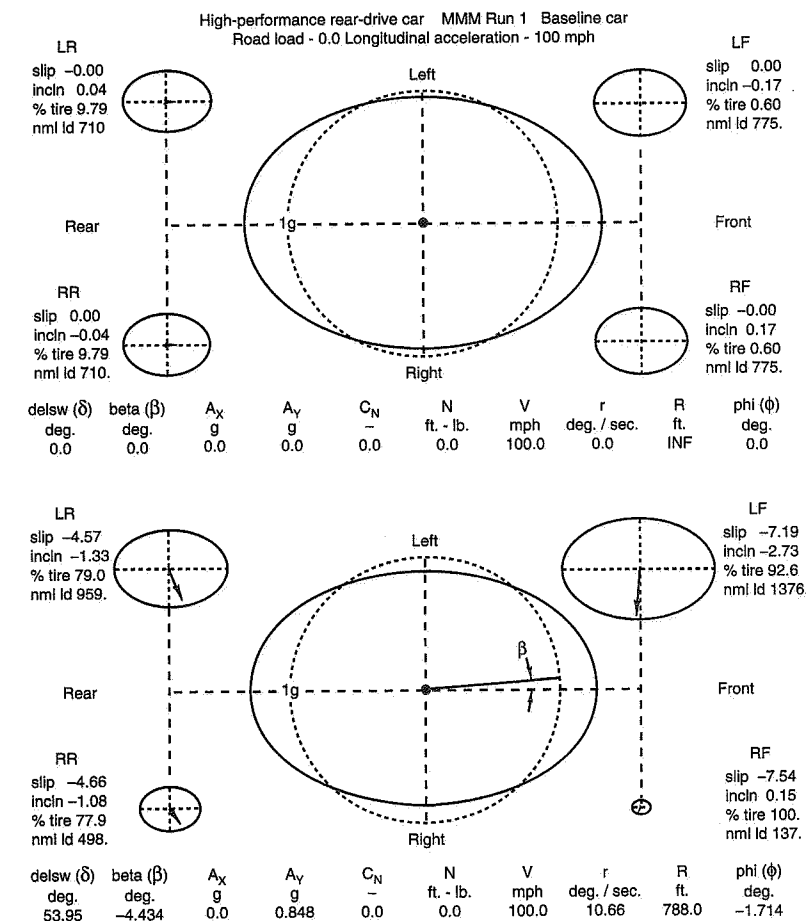


Figure 8.25 Friction circles, baseline.

For the first plot, $A_Y = 0$, there is no lateral force at any wheel and the small longitudinal force shown at the rear is just enough to overcome aero and rolling drag at 100 mph. For the lower plot, $A_Y = 0.848$, the vectors are very close to the boundary, and the inner front wheel is saturated (%tire = 100). The front wheel vectors are swung rearward due to slip angle drag. On the rear, the vectors are short of the limit and are swung forward because of the tractive effort required to maintain 100 mph (RL). Detailed wheel operating conditions are tabulated at each wheel position and the vehicle operating conditions are listed at the bottom of the diagram.

In the center of the diagram is an ellipse approximating the potential "g-g" diagram without any weight transfer. A 1g reference circle is shown dotted; note that these tires have much greater longitudinal force capability than lateral force capability. The line from the center shows the vehicle path or vehicle slip angle, β .

Limit Behavior

Figure 8.26 is an enlargement of the tip of the baseline configuration diagram, with the δ and β lines identified. The characteristics at the limit are defined by several parameters shown on this figure:

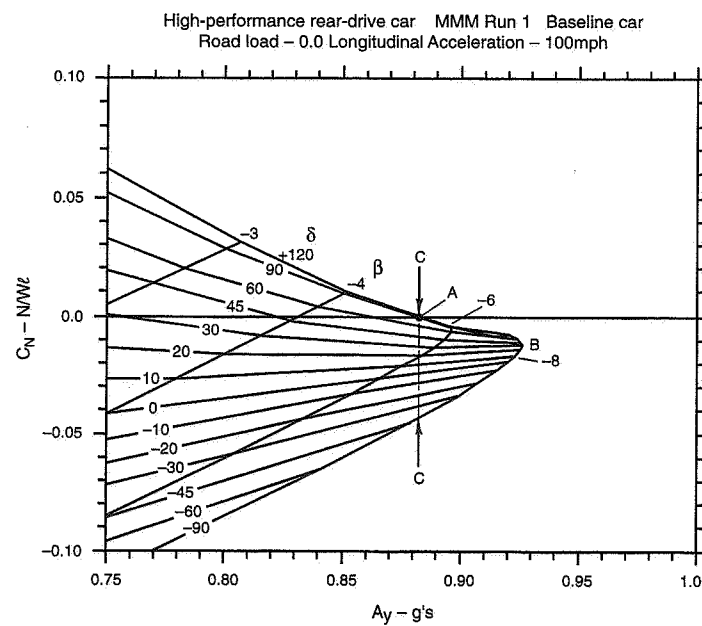


Figure 8.26 Baseline, rescaled to show peak.

1. Maximum trimmed lateral acceleration (Point A) = 0.881.
2. Maximum untrimmed lateral acceleration (Point B) = 0.926.
3. Residual moment coefficient at maximum trimmed lateral acceleration, distance C—C = -0.042 (at rear, thus push).
4. Stability at maximum trimmed lateral acceleration, the slope of the δ line through Point A = $-0.083 C_N/g$ (stable).

For this example, we have made eight separate (somewhat arbitrary) changes in the vehicle configuration from the baseline to illustrate the effect on the end of the C_N-A_Y diagram. The operating condition has remained constant at 100 mph, RL. Table 8.6 summarizes the changes that were made and lists several parameters, as measured from the diagrams, which define characteristics at the limit. Figure 8.27(A) through (H) are the corresponding C_N-A_Y diagrams. In addition a friction circle diagram at $A_Y = 0.848$ is shown for each configuration on Figure 8.28(A) through (H). In cases (A) and (B) we changed the roll stiffness and the roll gain was measured for these two runs.

This example indicates how one might approach the problem of setting up a car on paper, but it does not illustrate the full process. In particular, runs should be made with various operating conditions such as turn entry (braking and turning) and turn exit (power and turning) in order to achieve a suitable compromise. Numerous small configuration adjustments can be studied.

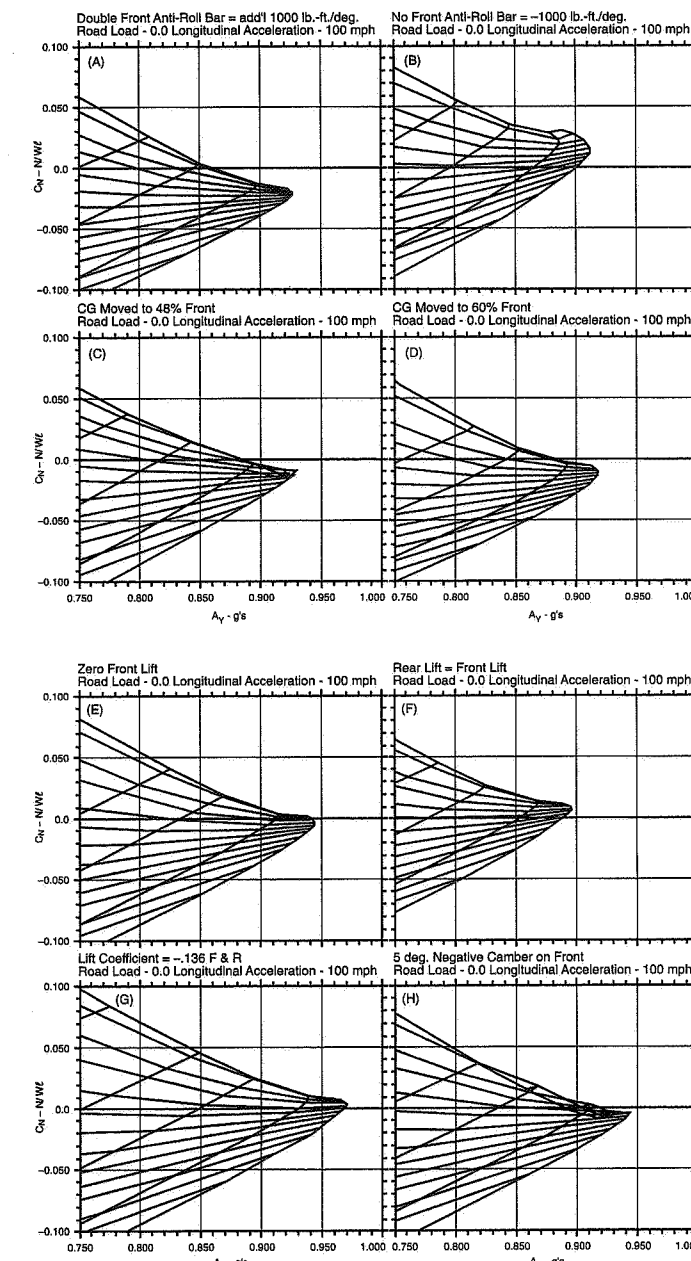
Following are some comments on the results summarized in Table 8.6:

1. The effect of changes in front anti-roll bar, (A) and (B), are in the expected direction. Removing the bar completely has a substantial effect on the roll gain.
2. Moving the CG forward and aft of baseline, (C) and (D), results in only small changes in limit behavior and max trimmed lateral, for this particular car. The change in stability with aft CG is small; in the case of forward CG, the push unchanged from baseline, but the tractive effort at the rear reduces the stability slightly which can be seen by examining the friction circles.
3. Reducing the aero lift on the front (E) increases max lateral as would be expected and results in a vehicle which is near neutral at the limit. Equalizing aero lift (F) (not downforce) at front and rear results in a loose (unstable) condition at the limit.
4. Supplying a large aero downforce at F and R (G), increases maximum trimmed lateral and in this case results in a near neutral vehicle at the limit.
5. Adding negative camber at the front (H) (relative to the baseline) gives an increase in maximum trimmed lateral and a decrease in stability, as would be expected.

Table 8.6 MRA Moment Method Parameter Study

High-Performance Sports Car. R.L. - Zero Longitudinal Accel. 100 mph.
Each Configuration Shows Change from Baseline.

Figure No.	Configuration	Residual Moment Coefficients				
		Max. Trim Lateral, g	Max. Untrim Lateral, g	Mom. Coeff. at Max. Trim (Nondimen.)	Stability at Max. Trim, C_N/g	Roll Gradient deg./g
	R.L. 0 Longit. Accel. Baseline	0.881	0.926	-0.042 at Rear (Push)	-0.083 Stable	2.10
(A)	Double F. Anti-roll bar. (Add 1000 lb.-ft./deg.)	0.864	0.926	-0.057 at Rear (Push)	-0.091 Stable	1.25
(B)	Remove F. Anti-roll bar.	0.899	0.912	+0.028 at Front (Spin)	+0.066 Unstable	5.00 On-center
(C)	Move CG to 48% F. (From 54% F.)	0.890	0.932	-0.036 at Rear (Push)	-0.082 Stable	
(D)	Move CG to 60% F.	0.879	0.920	-0.042 at Rear (Push)	-0.078 Stable	
(E)	Reduce F. Aero Lift to Zero.	0.940	0.943	-0.006 at Rear (Push)	-0.008 Stable	
(F)	Make F. Aero lift = R. Aero lift. (i.e., Remove Rear Spoiler)	0.887	0.895	+0.011 at Front (Spin)	+0.040 Unstable	
(G)	Make Aero Downforce Coeff. F & R = -0.136	0.969	0.970	+0.003 at Front (Spin)	+0.009 Unstable	
(H)	Add 5° Negative Camber on F.	0.918	0.942	-0.025 at Rear (Push)	-0.036 Stable	

**Figure 8.27** MMM parameter study results.

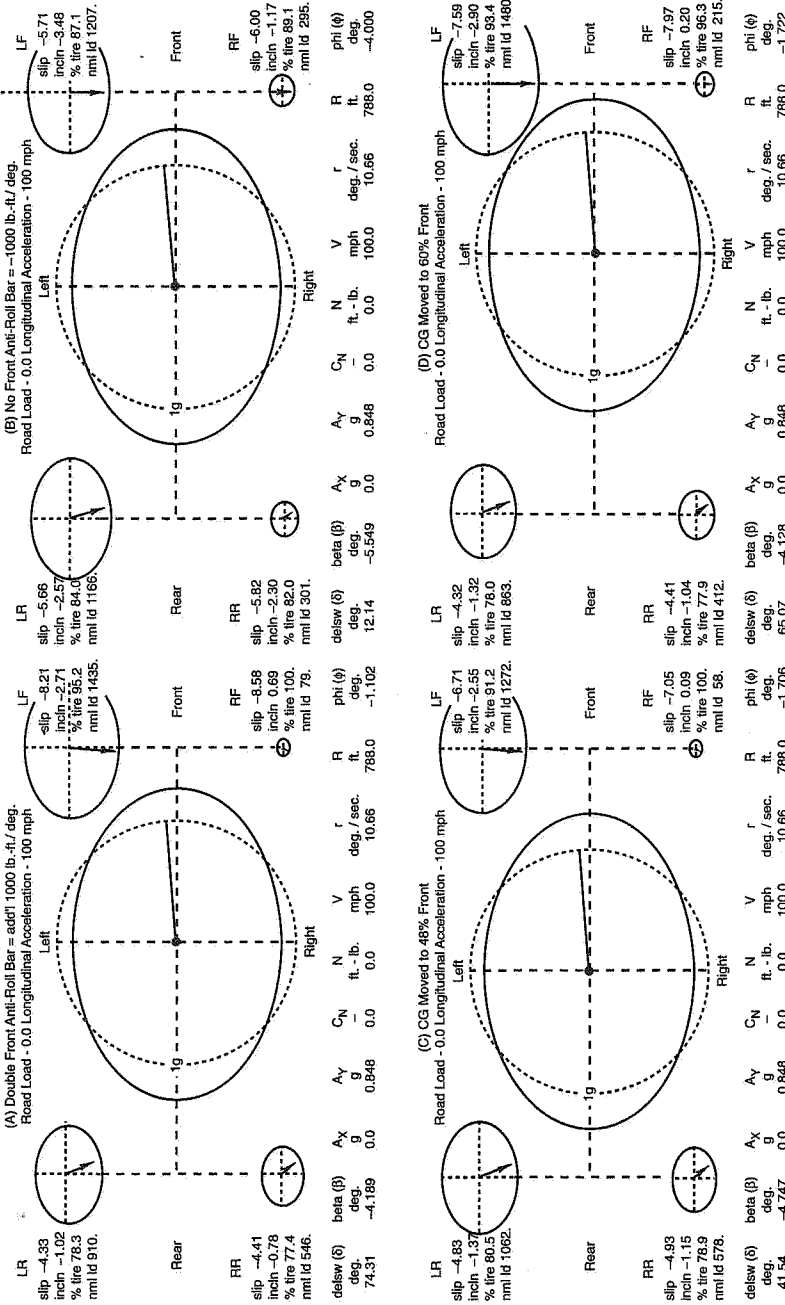


Figure 8.28 MMM study, near-limit friction circles.

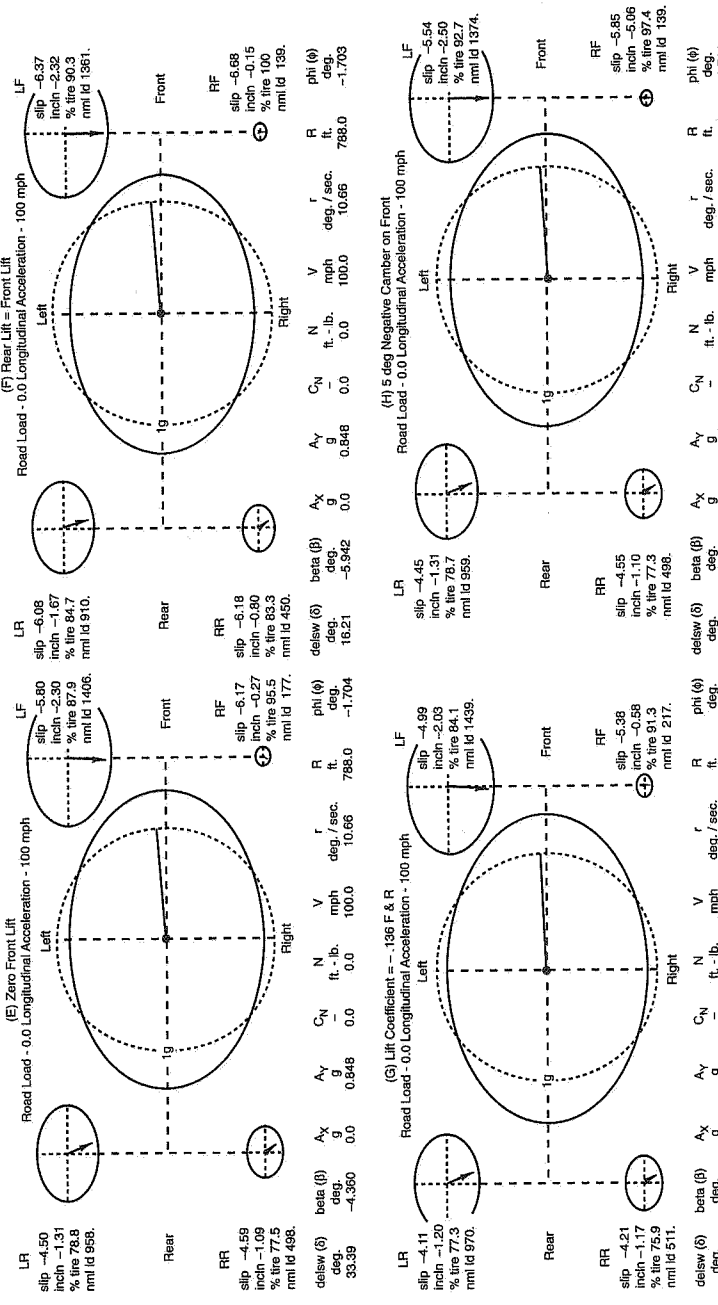


Figure 8.28 MMM study, near-limit friction circles (continued).

8.8 Lap Time Analysis

Previous sections have discussed the use of MMM (trimmed and untrimmed steady-state analysis) for studying a car in a variety of isolated maneuvers. In this section we discuss the use of steady-state trimmed analysis to simulate a racing lap, beginning with early manual calculations and extending to current computer simulations. The basic assumption behind this technique is that race drivers drive very smoothly; in most situations, trimmed steady-state is a very good approximation of the actual behavior of the car. First, we look back at early lap time calculations and then move to the current computer simulation.

Since the earliest days of racing, cars have been developed using lap time as a measure of progress. The first and most consistently used piece of "instrumentation" was the stopwatch for interval/segment times as well as whole lap times.

It appears likely that Mercedes-Benz was the first to develop an analytical simulation of race car circuit performance. As the following quote by Sterling Moss (from Ref. 105) indicates, it was regularly used in the 1954-55 post-WWII period and may have been available in a less-developed form in the 1937-39 period.

And then behind all this there was, of course, a race analysis department. If you should wonder what on earth this might be, or do, let me say that every course was mathematically dissected and the speed at every point calculated together with the required gear in every section. From this it was child's play to tell the driver what he should do, where he should do it, and what sort of lap speeds he should achieve. So if you started by saying that on a certain corner you were coming out at 5,500 r.p.m. and you would prefer 5,300 r.p.m., in next to no time the gear ratio would be changed so that without altering your road speed this is how it would be. But then somebody else would say: "My dear chap, you're going too slow there, on *that* ratio you really ought to be coming out at 5,450." And, my God, when you took it seriously out of it you came at 5,450. Or perhaps 5,500 if you wished to prove that slide rules are not always infallible.

And then, of course, during a race all your lap times would be logged but in addition Neubauer used to mark your gear changes and time them; by doing this through a race he would know if an engine was losing tune or if the driver was trying harder. He was that much on the ball.

An independent analysis of circuit performance was performed at Cornell Aeronautical Laboratory (CAL) in the 1954-56 period for the Lime Rock circuit (as requested by John Fitch) and for the third Watkins Glen circuit (the first permanent circuit at the Glen). The purpose of the latter analysis was to insure a 100 mph lap, thus making it one of the fastest USA circuits of that era. Both of these analyses were limited by the hand calculations used.

A simple manual calculation procedure breaks the lap into straights and constant-radius turns. First the limiting speeds on each turn are determined by knowing the max lateral acceleration and using the simple formula $V = \sqrt{A_Y R_g}$; once the turn speeds are known, the time in each turn can be calculated. Then max longitudinal tire friction for accelerating/braking and engine power are used to calculate the time to travel down each straight including the requirement that the car must be traveling at the right speed to make the next corner. Analysis was easier before aerodynamic download—friction coefficients for cornering, accelerating, and braking were essentially independent of speed, and once measured could be used at all points on the track. Now the performance of the car is very much a function of speed and a computer is required if the problem is to be solved in a reasonable amount of time.

In 1971 the Watkins Glen GP circuit was enlarged and improved by an additional one-mile section and other changes. At the request of WGGP Executive, Malcolm Currie, a computer analysis was performed at CAL by R.D. Roland and C.F. Thelin under the general direction of W.F. Milliken, Head, Transportation Division. This analysis was reported in Ref. 132. The circuit was accurately represented in terms of elevation, grade, and banking. The vehicle was taken as a point mass with overall acceleration limits as shown in Figure 8.29, an early use of the "g-g" diagram. These limits were based on experience with Can-Am cars. Comprehensive performance profiles were calculated for the then-current Grand Prix car, as indicated in Figure 8.30.

Starting with the general analyses techniques summarized above, Milliken Research Associates (MRA) has been developing and progressively improving a circuit simulation since 1982.

1. RCSIM (Race Circuit Simulation) used a "bicycle" model (as described earlier in Chapter 5) to represent the vehicle. This improvement over the earlier point-mass representation allowed more realistic modeling of driving and braking weight transfer and the associated tire load changes (including tire load sensitivity effects). Brake balance (and torque split for 4WD) could be fixed or automatically balanced for every station around the track. This simulation was intended only to give lap times but it also correlated well with segment (corner) times on two different F.1 circuits. Development by Peter and Doug Milliken (1982).
2. Pathopt (Path Optimizer) used a point mass representation of the vehicle and a survey of the left and right edges of the roadway to compute an "optimum" path (minimum time) around a track. The generated path was then used as raceline data input to RCSIM. This was particularly useful for new (street) circuits where no established line existed. Development was by Peter Milliken (1984). For established circuits, we anticipate that the race line can be "drawn" by looking at the actual path taken by the driver with a modern in-car instrumentation system.

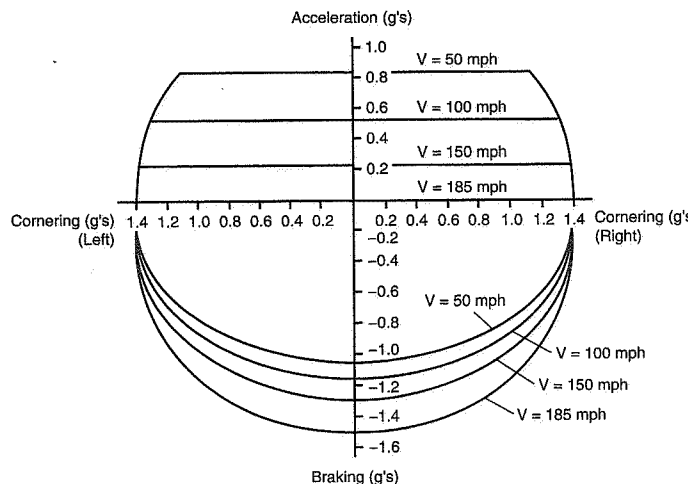


Figure 8.29 Formula 1 car performance envelope, c. 1971.

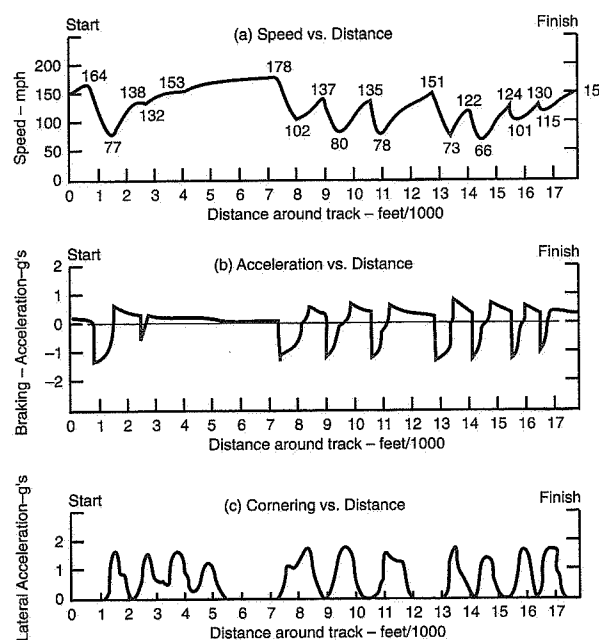


Figure 8.30 Formula 1 performance profile on Watkins Glen fourth circuit.

3. RCSIM-2 expanded the vehicle model to four wheels by use of the pair analysis technique and added slip and camber angles to the tire representation. By including slip angle drag effects ("induced drag"), this version was the first to give realistic corner speeds on superspeedways (power limited turns). Some suspension parameters were also introduced into the model. This and subsequent versions have been developed by Dave Segal with support from Doug Milliken (1989).

4. LTS (Lap Time Simulation) is a further development of RCSIM-2. The vehicle representation is expanded to a better four-wheel model. Engine modeling and gear shifting (with adjustable shift time) is added to the constant power engine (continuously variable transmission) simulated in earlier versions. Additional suspension detail and additions to the aero force representation are also included (1991-present).

The current LTS is a very complex, nonlinear model with numerous layers of iterative solvers to deal with real tire and vehicle data. It is approaching the point where it can be used to guide car set-up, provided reliable input data is available. The race track is broken into sections of arbitrary length (typically 10 to 50 ft. long) and each section of the track is described by turn radius, bank, grade, vertical curvature, and local friction coefficient. Steady-state trimmed solutions are generated at each section of track by the LTS program using much of the same basic technology as MMM. Output consists of a listing of about 30 variables for each section of race track. This data can be plotted against track geometry (station), time (from the start-finish), or distance (along the path), similar to the output of an in-car data acquisition system.

“g-g” Diagram

“A method for characterizing the performance of the driver-vehicle system, including the influence of roadway surface conditions... a means for quantifying the capability envelope of the car and demonstrating how much of this capability is utilized by the driver in the performance of driving tasks.”

Roy S. Rice
Vehicle Research
Calspan Corporation



Introduction

The concept of the “g-g” diagram as a measure of driver/vehicle/circuit performance was introduced in Chapter 1. It was concluded that race cars should have large “g-g” maneuvering diagrams throughout their performance envelope and that race drivers should operate close to the diagram boundaries. In this chapter we will look at the evolution of the “g-g” diagram and then examine its various uses with specific experimental and analytical examples. The chapter concludes with some historical notes.

9.1 Conceptual Development

The notion of a tire friction circle was introduced in Chapter 2. The idea is that no matter what combination of steering and braking or driving torques (more fundamentally, slip angle and slip ratio) is applied to a wheel, the maximum horizontal force that the tire can

produce is limited by the tire/road friction coefficient times the load on the wheel. This says that the horizontal force is independent of direction and can be represented by a *friction circle* with radius determined by load and friction coefficient. The concept is somewhat idealized and departures from a circle may occur due to tread pattern, print shape as affected by camber, etc. Its exact size is not easy to determine. Nevertheless, the friction circle concept is a very useful one.

Roy Rice, in Ref. 128, points out that "conceptually the tire friction circle can be applied to the whole automobile by collapsing the four wheels into a single equivalent car/road interface...." This could be called the *vehicle friction circle*. If the coefficient of friction was independent of load, that is, the load sensitivity was zero and the same coefficient applied at all wheels, the vehicle friction circle radius would be determined by the coefficient of friction times the vehicle weight.

In actual fact, a real automobile cannot reach the boundary of the vehicle friction circle, as defined above, for the following reasons:

- **Traction Limitations**—Most vehicles are power limited (over much of the gear-speed range) and cannot produce the slip ratio for maximum resultant force over part of the diagram.
- **Load Transfer Effects**—During maneuvering there are longitudinal and lateral load transfer effects which result in large load changes at the wheels. The lateral and longitudinal forces from the tires are not linearly related to these load changes, as discussed in Chapter 2. The load changes, through the tire load sensitivity, also change the local friction coefficients.
- **Suspension Effects**—Camber and compliances due to the suspension geometry and to rubber bushings and mechanical deflections can change the wheel orientations, which in turn affect the tire forces.
- **Limiting Stability Balance**—The operating conditions at the four wheels or "axles" are such that they seldom reach their limit at the same time. Thus an understeerer at the limit plows off on front while the rear is still hanging on. Obviously the full utilization of the vehicle friction circle is not achieved. This effect may be minimized on race cars, where close to neutral steer at the limit is sought.
- **Brake Balance**—This may inhibit use of friction limit by both front and rear tires simultaneously.

By use of a comprehensive computer model such as the MRA Moment Method (MMM), the friction circles at the four wheels and the corresponding point on the vehicle friction circle may be computed for a particular vehicle operating condition. Figure 9.1 shows an example of a large rear-drive sports car cornering at 0.76g under dropped throttle and moderate braking. The vehicle is in equilibrium in a RH turn. On the diagram,

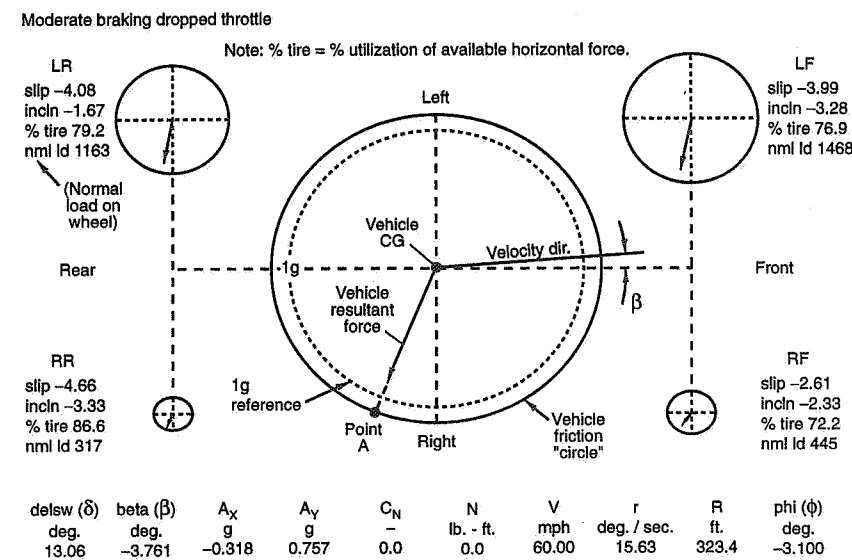


Figure 9.1 RWD, braking and D.T.

- The resultant horizontal force vector at each wheel is shown.
- A friction circle is drawn for each wheel. Its radius is the maximum force available for the load on the wheel (i.e., at each wheel, load \times friction coefficient is calculated). Slip and camber (inclination) angles are also tabulated for each wheel.
- Note that the inside rear wheel is utilizing all the available force, while the other wheels are short of their limits.
- Add up the longitudinal and lateral components of the force vectors at the wheels to construct the *vehicle resultant force vector* for this operating condition.
- Sum the radii of the friction circles at the wheels to find a Point A on the vehicle friction circle. The solid circle (taken as actually slightly elliptical) drawn through Point A corresponds only to this particular operating condition.

Later we will show what this diagram looks like when it is developed for various combinations of lateral and longitudinal accelerations with all of the load transfer, suspension effects, etc., included.

The final step to constructing the "g-g" diagram is to convert to "g units," normalizing the resultant forces by dividing by the weight on the wheels (or vehicle). A 1.0g refer-

ence circle is shown dotted in Figure 9.1. (Note: Figures such as 9.1 are available from MMM postprocessing, further examples are given in Chapter 8.)

9.2 General Uses

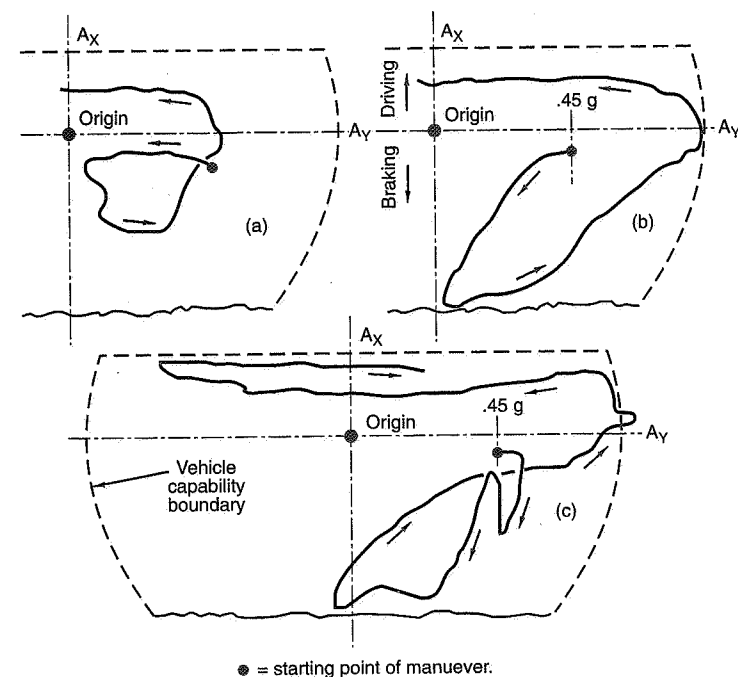
The most complete summary of the various uses of the “g-g” diagram has been given by R.S. Rice in Ref. 128 of 1970 and in Ref. 126 of 1973. He points out that there has long been a need for relating “driver’s actions with car’s performance capability ... including the effect of road surface conditions on overall system behavior.” The virtue of the “g-g” presentation is that it moves away from the limitations of vehicle stability and control into the area of **handling task performance**. Thus it is not only a means of quantifying the maneuvering envelope of the car but for demonstrating “how much of this capability is utilized by the driver in the performance of driving tasks.”

The “g-g” diagram has seen two general uses:

- Plotting a particular task performance.
- Determining the maneuvering area utilized by the driver/vehicle in a comprehensive series of tasks (i.e., laps on a race course).

Figure 9.2, taken from Ref. 126, illustrates the performance of three different drivers in the following specific maneuver: starting from a large radius RH bend, at 50 mph and 0.45g lateral, transitioning through a short straight while braking down for a tight 90° right hander. Driver (a) utilizes only a small part of the vehicle’s envelope; driver (b) reaches the vehicle’s envelope in lateral acceleration at a point where the longitudinal acceleration is approximately zero; driver (c) is more aggressive and loses control in the tight RH corner and experiences a large lateral acceleration to the left while attempting to recover.

An example of the second type of general use is given in Figure 9.3. Here longitudinal and lateral accelerometers were installed in a conventional passenger car and a recording was made under normal driving conditions over a period of time. It will be seen that this driver rarely exceeded a 0.25g circle, with a heavy concentration along the longitudinal and lateral axes. The record shows a minimum of **combined** lateral and longitudinal acceleration. The occasional peak of about 0.4g is generally in the braking direction. The only approach to the actual limits of the vehicle were in pure forward acceleration (power limited) at about 0.3g. This is one example of a driver’s “willingness” limits; the driver’s “capability” limits probably utilize more of the diagram’s area, but average highway drivers are unlikely to fill in the combined lateral and longitudinal portions of the “g-g” diagram.



● = starting point of maneuver.

Figure 9.2 Maneuvering performance of different drivers.

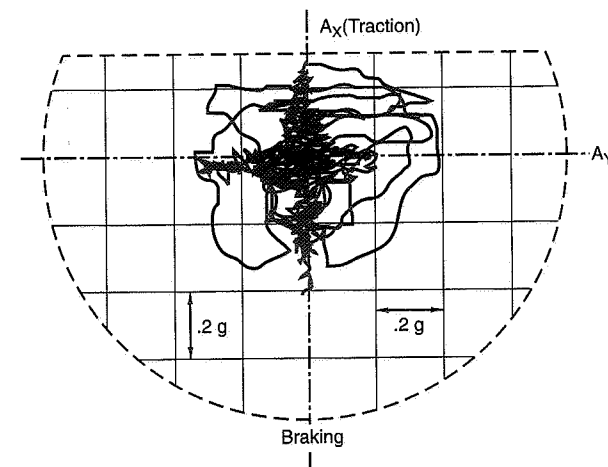


Figure 9.3 On-road maneuvering (typical driver).

9.3 Vehicle Capability

In the application of the “*g-g*” diagram to racing, it is desirable to know the “theoretical” limit of the vehicle for given operating conditions. The term “theoretical” denotes the ultimate vehicle limit, or, the limit with a “perfect” driver. Two possibilities exist for estimating this limit—experiment or analysis. In Chapter 1 we had acceleration data on three world-class Grand Prix drivers (Andretti, Stewart, and Peterson) on the same circuit in the same car. Since it was known that these drivers could reach the vehicle’s limits, a smooth boundary around their measured performance was taken as the vehicle’s capability. This boundary applies only to this one circuit and the speeds and accelerations associated with it. Note that large parts of the presumed boundary were not reached.

It is a difficult task to accurately establish the vehicle “*g-g*” boundary experimentally. Two operating variables affecting the size of the diagram are aero downforce and drag—both increase with speed squared. As speed is increased, downforce improves cornering while drag reduces forward acceleration and improves braking. This suggests a three-dimensional figure where the third axis is speed as a true representation of the “*g-g*” capability.

Figure 9.4 illustrates several attempts to estimate the vehicle capability from limited experimental and theoretical information:

- (a) Estimate of F.1 car capability envelope as used in the Watkins Glen circuit analysis, Ref. 132. In 1971, aero downforce was only beginning to be exploited.
- (b) From Ref. 161 (1983) by Paul Van Valkenburgh on the use of the “*g-g*” diagram in racing. Again, extreme aero downforce is not considered.
- (c) From Ref. 167 (1984) by Peter Wright. Here, the increase in the limit due to aero downforce is included.

To our knowledge, the first attempt to accurately calculate the “*g-g*” boundary for real vehicles, taking into account all the factors listed in Section 9.1 (traction limitations, load transfer effects, etc.) was made by Dave Segal, MRA, in 1991. Two diagrams were calculated, the first for a high-performance sports sedan with rear-wheel drive and 54% front weight distribution (Figure 9.5), and the second for a comparable front-wheel drive with 64% front weight distribution (Figure 9.6). The calculations were for constant 60 mph; normal aerodynamic forces for such vehicles were included. The plots are for RH cornering.

Each figure is based on ten individual MRA Moment Method (MMM) simulation runs (see Chapter 8), each at a different level of drive torque or brake line pressure. The diagrams consist of a series of basically horizontal lines of constant drive torque (or brake pressure) plotted against longitudinal and lateral acceleration. Each solution point repre-

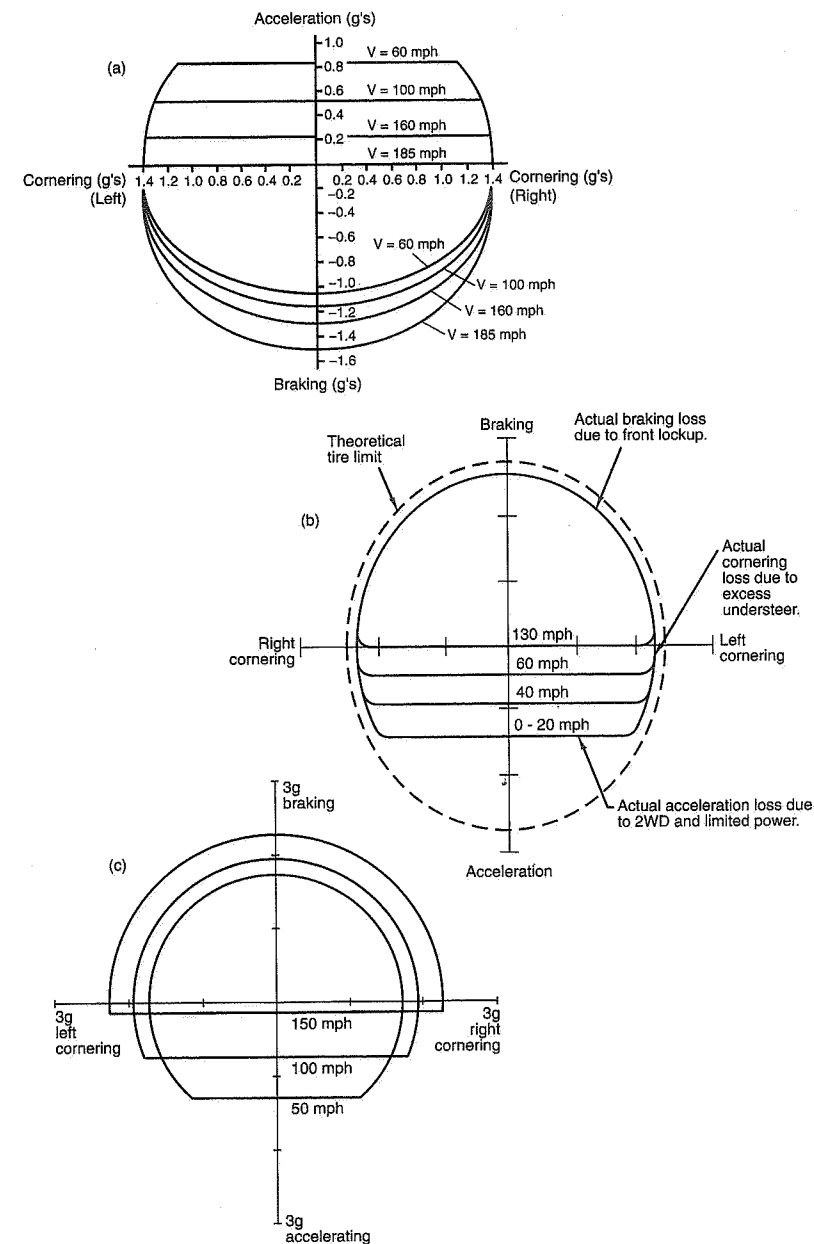


Figure 9.4 Vehicle “*g-g*” estimates.

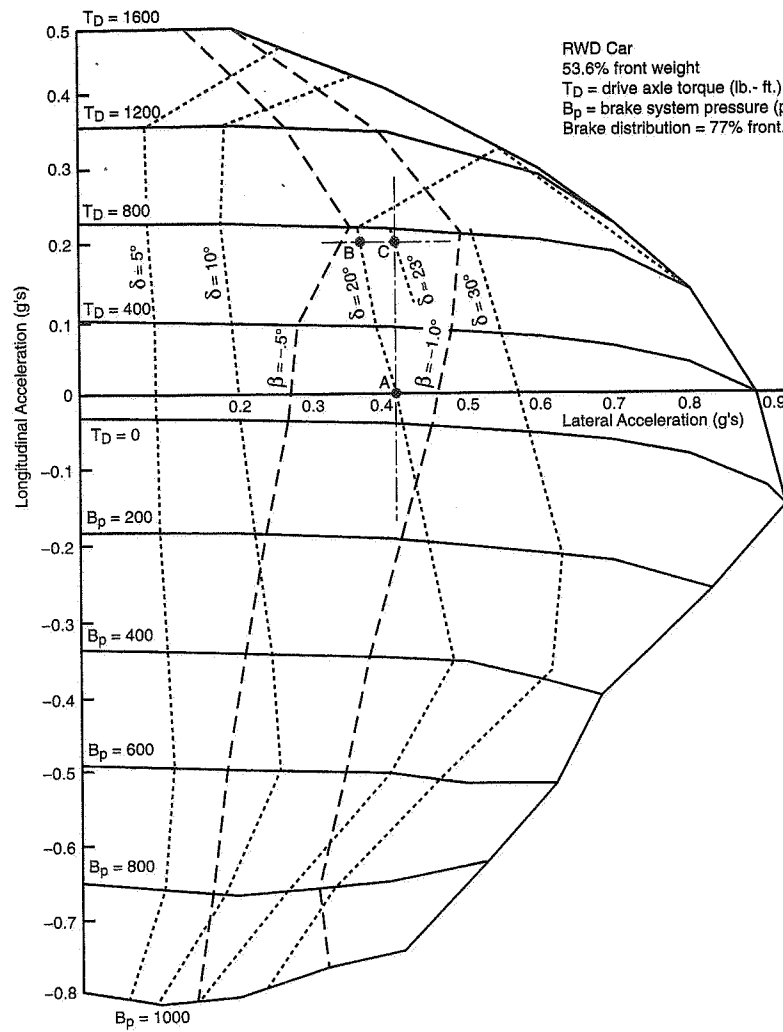


Figure 9.5 "g-g" diagram, rear-wheel drive.

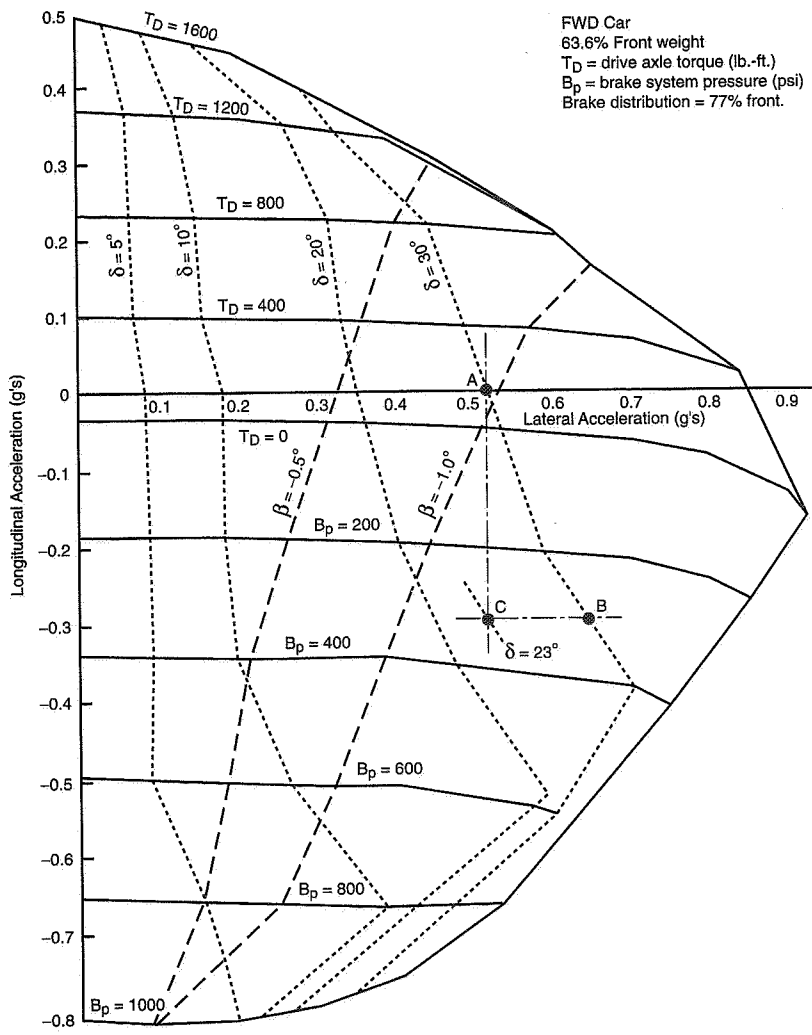


Figure 9.6 "g-g" diagram, front-wheel drive.

sents momentary steady-state cornering while accelerating/braking at a (momentary) constant speed. For example,

- The $T_D = 0$ curve represents a free-wheeling car cornering at various lateral acceleration levels; this curve is offset from zero longitudinal g by aero drag and rolling resistance and tends toward increased negative longitudinal acceleration because of the increase in vehicle sideslip drag at higher lateral g.
- The zero longitudinal acceleration axis represents road load—enough driving torque to overcome all drag elements to maintain zero longitudinal g (constant speed) while cornering.
- The rightmost periphery of the diagram represents the maximum trimmed lateral acceleration at different levels of longitudinal acceleration.

The maximum lateral acceleration for both vehicles occurs with zero drive torque. As expected, the diagrams are neither circular nor elliptical because of the many factors which influence acceleration performance. Future work includes automated “g-g” diagram generation from MMM vehicle and tire data.

An interesting feature of Figures 9.5 and 9.6 is the internal δ (steer angle) and β (vehicle slip angle) lines which were computed as part of the MMM solutions. They provide a numeric measure of longitudinal trim change sensitivity of the car—that is, what happens to lateral trim as longitudinal trim is changed. For example, for the RWD car of Figure 9.5, if we are cornering at road load at 0.41g lateral at a steering angle of 20° (Point A) and suddenly accelerate to a level of +0.2g with fixed steering, the lateral acceleration is reduced to 0.36g (Point B). This implies an increased path radius. To maintain the same lateral trim (Point C), the steering must be increased to some 23°. In Figure 9.6, an example of trim change due to braking is shown. Starting at a trim of 0.5g lateral, the application of 0.3g braking increases the lateral acceleration trim to 0.63g at constant steer of 30°. To maintain the original trim the steer angle must be reduced to 23°. Thus, the internal lines cover all the changes due to throttle and brakes. It appears practical to map out other variables such as load transfers and slip angles on these diagrams.

9.4 Race Car Applications

Overall Driver-Vehicle-Circuit Performance

Figure 9.7 (from Peter Wright, Team Lotus) is an example of “g-g” diagram use for a comprehensive task. It was recorded by Senna in a practice run on a dry circuit at Adelaide, Australia, in 1987. It will be noted that he consistently reached about 1.8g forward acceleration and about 3.0g braking and lateral accelerations in the vicinity of 2.5g. When accelerating he was able to maintain high levels of lateral acceleration, i.e., fill out the combined acceleration area. During braking he was less successful in filling out the combined area because the vehicle was unstable.

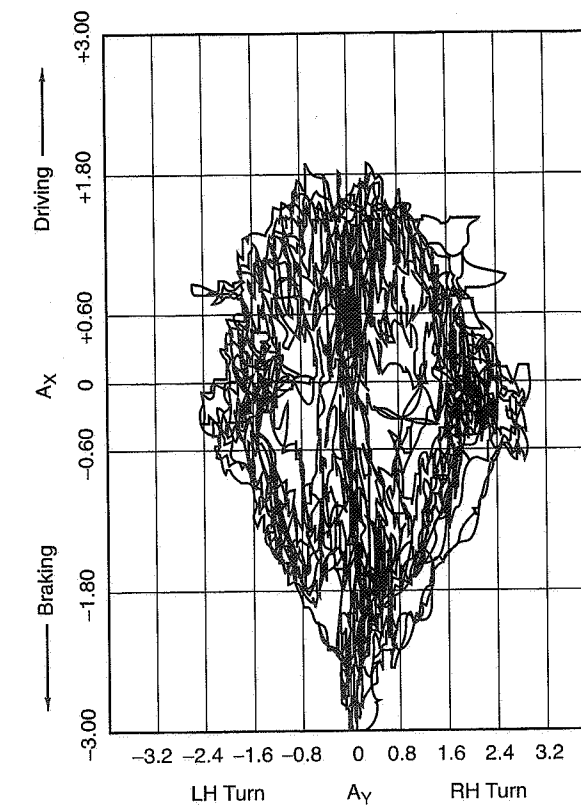
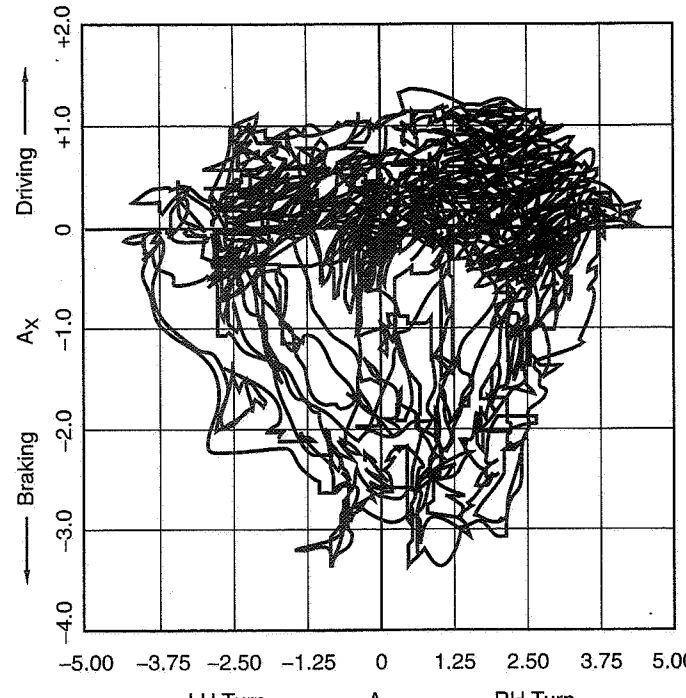


Figure 9.7 Adelaide, 1987, Senna.

This diagram is a measure of overall “driver-vehicle-circuit” performance with no attempt to control any of the driver, vehicle, or circuit variables, for example, speed and associated aero downforce.

Figure 9.8 is a comparable diagram taken some six years later. The longitudinal performance is about the same but considerably higher lateral accelerations are attained probably due to higher speeds and more aero downforce. This diagram is well filled out in the combined braking lateral area.



Qualifying, dry circuit, from Peter Wright.

Figure 9.8 Silverstone, 1993, Herbert.

Effect of Speed—Calculated

To isolate the effect of speed (and aero downforce), we used the MRA Lap Time Simulation program (LTS) to compute the acceleration performance of an Indy car (1992) on the Belle Isle circuit during a 105 mph average speed lap. A "perfect" driver with a shift time of 0.1 sec. was assumed. Figure 9.9 shows all of the calculated points which range from a speed of 46 mph to 167 mph. Note that directional instability under hard braking does not affect the "ideal" driver the same way as a human driver.

Figures 9.10 and 9.11 illustrate the operating points in three different speed bands, namely, 46-86 mph, 86-127 mph, and 127-167 mph, respectively.

Another scheme for showing the effect of speed (hence, aero downforce) is to plot the longitudinal and lateral accelerations against speed. Figure 9.12 uses data from the same

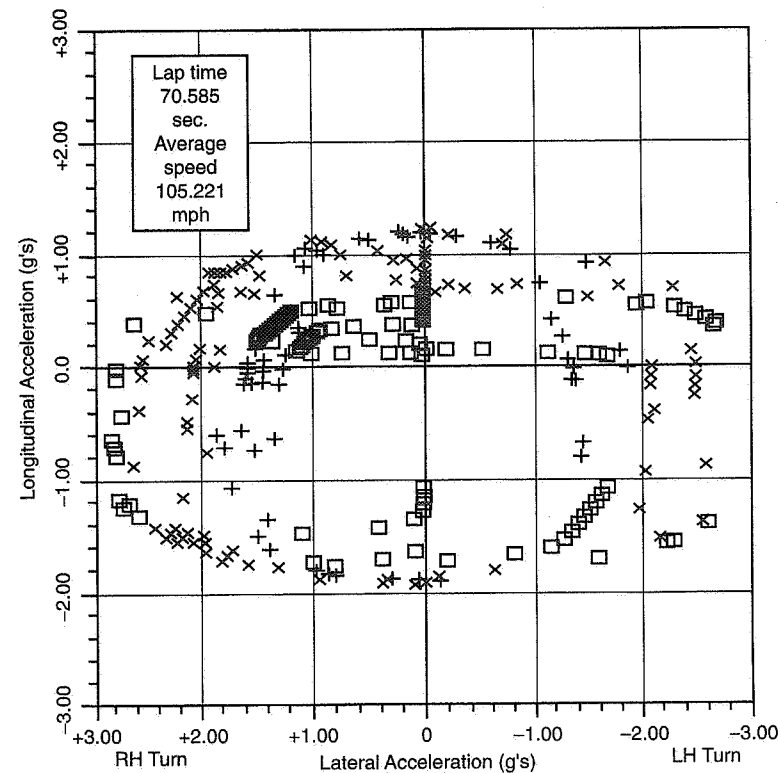


Figure 9.9 Belle Isle, 1992, LTS calculations.

qualifying lap as Figure 9.8. This figure shows that increasing speed increases the available lateral acceleration. From 60 to 180 mph the peak lateral acceleration increases from 1.88 to 4.58g, somewhat less than the square of the speed, probably because of tire load sensitivity. The braking deceleration increases with speed and the driving acceleration decreases with speed as would be expected.

g-Analyst®

A significant recent development is the "g-Analyst," a precision instrument available at modest cost for measuring and recording acceleration data. Prior to this, specialized instrumentation has been used by test and research groups for recording these diagrams. The "g-Analyst" utilizes the output of three accelerometers with a resolution of $\pm 0.01\text{g}$.

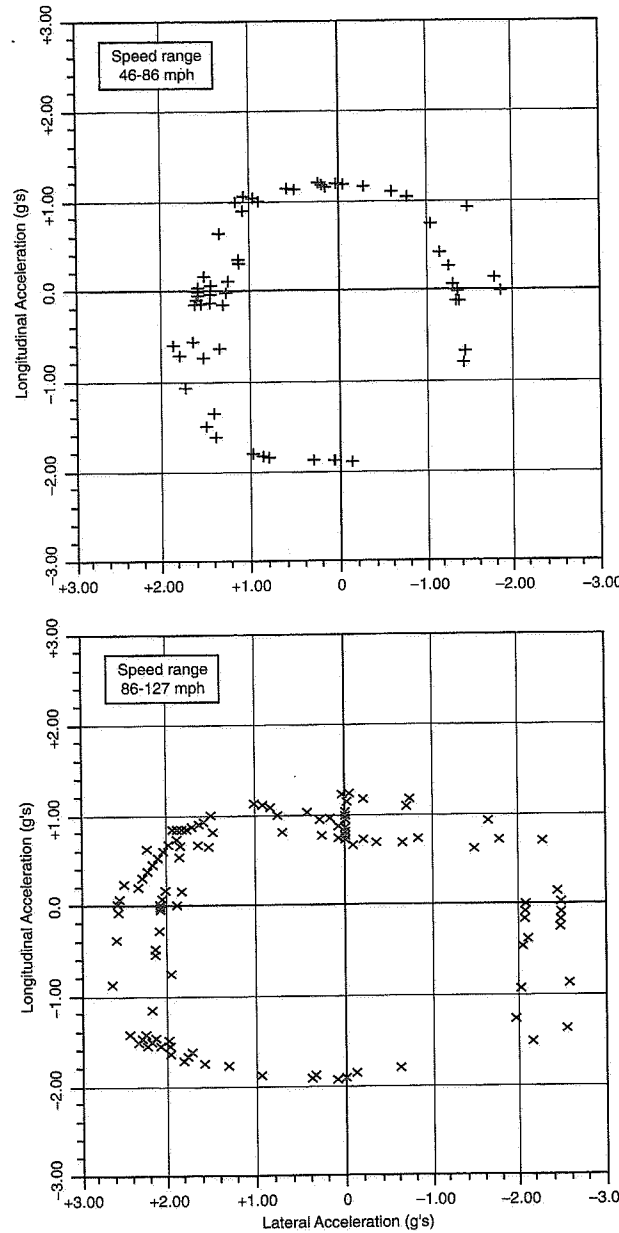


Figure 9.10 Belle Isle, speed segregated (lower speeds).

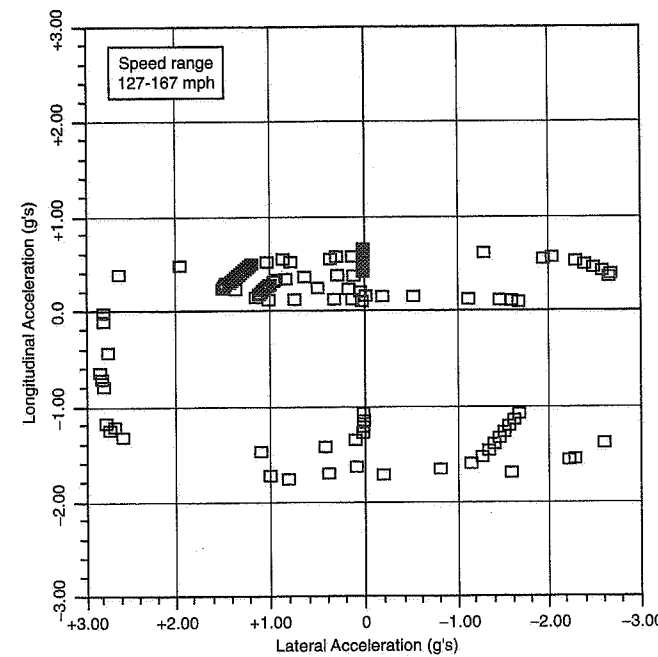


Figure 9.11 Belle Isle, speed segregated (higher speed).

Data is recorded at the rate of ten samples/sec. and can be stored, processed, and plotted in various ways. The device is useful in a variety of applications—driver training, vehicle tuning, vehicle research, etc. The manufacturer, Valentine Research, is listed under Ref. 91.

9.5 Historical Notes

At the request of Mike Valentine, a brief history of the friction circle and "g-g" diagram was incorporated in the g-Analyst "Learning Guide" (Ref. 91). Since the publication of the Learning Guide, some additional information has come to light and a more complete history is presented here.

In the period 1953-55, Joy and Hartley of Avon Ltd. performed a very comprehensive test of passenger car tires on a steel drum (Refs. 72 and 73). The published data was analyzed by Albert G. Fonda, an engineer in the full-scale division of Cornell Aeronautical Laboratory, and published in a memorandum of August 29, 1957 (Ref. 47). Figure 9.13, taken from this memorandum, appears to be the earliest friction circle plot including

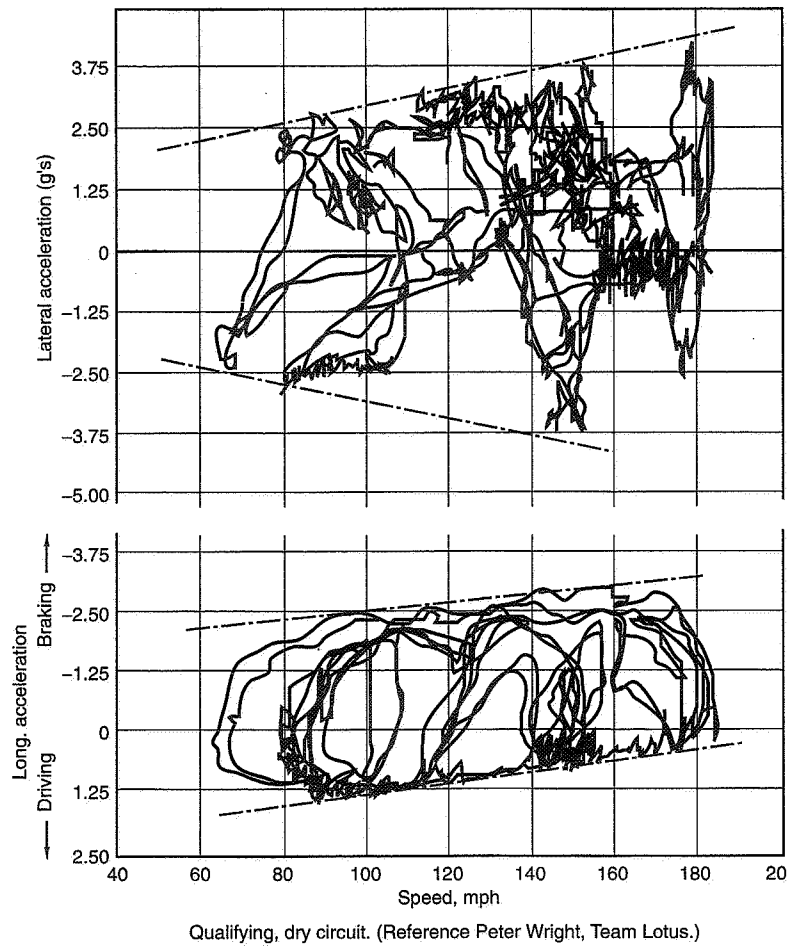


Figure 9.12 Silverstone, 1993, Herbert.

"friction ellipses" at various slip angles. On the same figure he plotted aligning torque for various slip angles and longitudinal force. The friction circle plot was limited by the data to one-half of the circle. Fonda's comments are that "this figure was assembled from four separate Avon figures in order to show the relationship of effects. The net vector $F_Y \rightarrow F_X$ is assigned a maximum value of 1.0 F_Z by Avon, but this limit may not even be a circle much less have this radius." In this same memorandum, Fonda introduces the idea of pneumatic trail (M_Z / F_Y), which again appears to be a "first." He also used the term "cornering stiffness" as opposed to the then commonly used "cornering power."

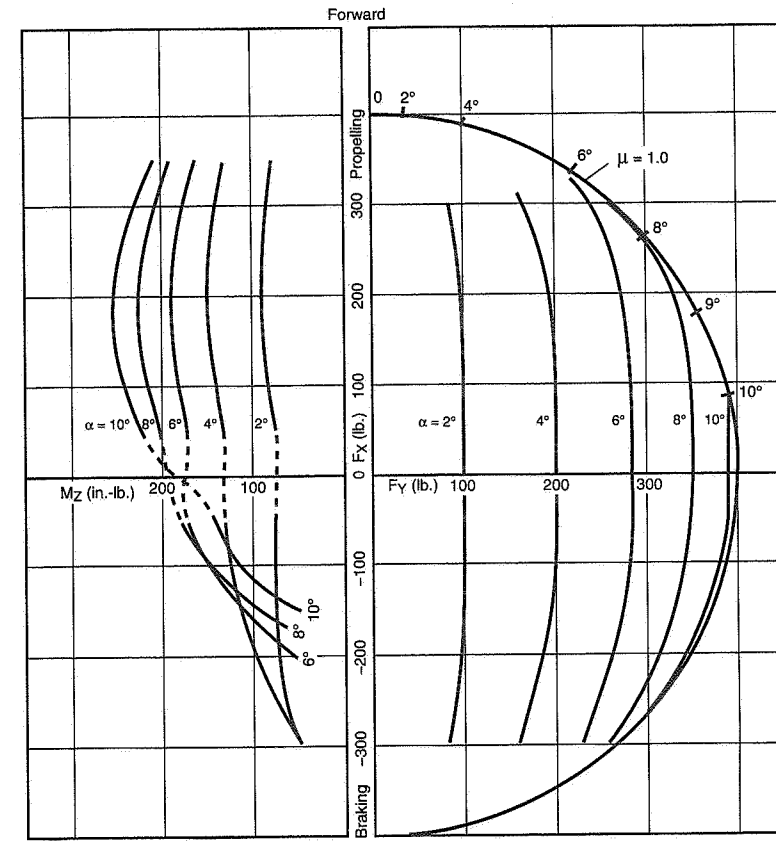


Figure 9.13 Longitudinal force vs. side force and torque (Ref. 47).

In 1955 the Air Force-CAL On-Road Tire Tester was commissioned. This machine, sponsored by the U.S. Air Force, was developed at CAL and featured the first 6-component balance system. It had a large load capacity and slip and camber ranges of $\pm 30^\circ$. Fonda became the operating project engineer on this machine and carried out a series of pioneering investigations, an early one of which is reported in Ref. 92.

Based on his tire tester experience, Fonda (circa 1958) installed a two axis x-y pen recorder in a Corvette on loan from General Motors, and obtained the "g-g" diagram shown in Figure 9.14. This appears to be the earliest "g-g" diagram measured on a vehicle. Fonda subsequently moved on to other areas of engineering; it is time to recognize his pioneering status in the tire and vehicle testing area.

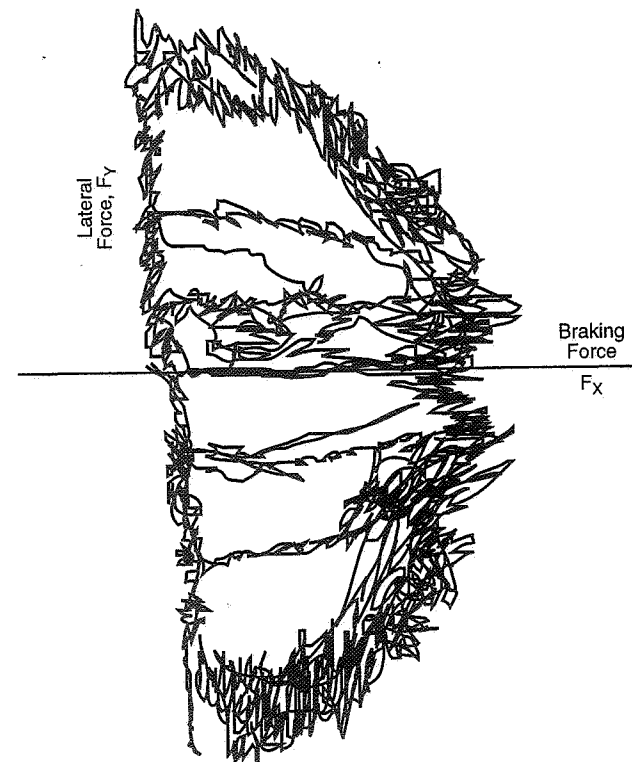


Figure 9.14 Corvette tire "g-g" diagram, 1958.

Following Fonda's work in 1957-58, the progression of development and application appears as follows:

- 1960: Earliest open-literature published reference to tire friction circle: Radt and Milliken (Ref. 121).
- 1960: Stirling Moss had developed, and was utilizing on the 2-1/2 litre Lotus Climax, the cornering technique which exploited the full area of the vehicle "g-g" diagram. The following quotation is from Ref. 105:

But was even the latest point on the straight the latest effective point to keep the brakes on? Gradually, and carefully, feeling my way I came to the conclusion that this was not so and that if one of the objects of turning on power on a corner was to lessen the ability of the rear tyres to take side thrust, why could not this be done by putting braking torque through the tyre-case rather than engine torque?

More, perhaps, by instinct backed by practice than by intellectual exercises, I found that, against all my previous teachings, the only real way for me to get round corners was to keep the brakes on pretty hard right up to the apex and then in a flash to get over on to the throttle so that at one moment the rear wheels were absorbing braking thrust and almost instantaneously afterwards power thrust. And, of course, these two torques, or thrusts, had to be about equal if one was going to properly balance the car and set it up; one had to be steering the right course at the same time, so it was all a bit of a juggling act performed in three or four seconds and not really something that could be recommended to a novice who was likely to find himself surprised enough by taking a corner perhaps twice as fast as he would normally have done. But I felt this was the answer for me and whereas in previous years any advantages I had had came from quickness of eye and muscular reaction, coupled, I think, with good computing power as to how far one could keep going down the straight before braking, I had now evolved something which was genuinely new and maybe superior to just performing well with an established method.

The great merit of the Lotus was that it was so responsive that it was simply an extension of the driver and, if it was not doing just what you wanted it to do, then there were a host of adjustments that could be made.

- 1965: From unpublished notes, it seems likely that Chevrolet R&D under Frank Winchell, and Jim Hall of Chaparral Cars, were thinking in terms of the overall acceleration capability of race cars. For a practical description of the work which came out of this period see Ref. 162. In this book a strip chart is shown with lateral and longitudinal acceleration right next to each other, but no direct "g-g" recordings. These recordings were made in the Chevrolet R&D telemetry van, one of the earliest comprehensive data recording systems used in racing, developed by Don Gates and commissioned in 1969.
- 1968-69: Mark Donahue had the opportunity of driving a Z28 Camaro on a course laid out on General Motors Proving Ground "Black Lake."³⁶ The Camaro was instrumented and data recorded in Gates' van. It was there that Donahue began to develop the full "g-g" diagram cornering technique (see Ref. 41). To quote Donahue:

But I was beginning to find out just how much there was to learn about the vehicle dynamics of race cars.

Possibly the most important concept was the "friction circle" technique of driving. Basically, that is the knowledge that the car—or its tires—has relatively equal traction capabilities in any direction, whether accelerating, braking or cornering. The theory is that you get maximum performance when you pass from one condition to the other without going through the center of the circle. In other words, the fastest way into a corner is to gradually trade off braking traction versus cornering traction, until all traction is being used in

³⁶ The Black Lake facility has a fairly smooth surface. One recent attempt to test a race car (that we are aware of) failed to develop realistic tire temperatures.

cornering. I began calling that the "American technique" as opposed to the traditional "European technique" of braking, cornering, and accelerating totally independently. I still think that "filling the circle" is one of the hardest things a racing driver has to do. Few drivers are aware of the theory, but most have a natural tendency to do it anyhow.

The value of having Black Lake to drive on at that point in my education was that it made my mistakes harmless. I can't take risks like that on a racetrack, where it's critical. That's just not my style. But there was nothing to run into on Black Lake. I could skid off the course and just slide forever. I knew that was a tremendous opportunity to learn the upper limits of both me and the car, and I was really being selfish at that point. I was going to run there until they kicked us out—and I don't think we left until we eventually wore out the motor.

- 1970: The first published use of the "g-g" diagram was by Rice and Alianello (referenced earlier). Their work had begun in 1968-69. In 1970 Mark Donahue and Don Cox visited CAL in Buffalo, and Donahue recorded his "g-g" signatures on the instrumentation developed by Rice and Alianello.
- Circa 1970: Internal papers were prepared in the Isuzu Motors Ltd. research department (Refs. 107 and 108). These papers are undated and contain no references to previous work, nor do we remember how we came in possession of them. Figures 9.15 and 9.16 show two experimentally measured "g-g" diagrams and also the "g-g" diagram used in the analysis. They also developed a computer program and predicted and confirmed lap times on several circuits. We believe that this work was done in about 1970 but whether it proceeded or followed the Watkins Glen analysis (below) is unknown. In any event, it is a remarkably complete analysis and the lap time simulation is comparable to those we enjoy today.
- 1971: Roland and Thelin, "Watkins Glen Computer Simulation of Circuit Performance" (Ref. 132)—a very complete analysis of the improved circuit. This was preceded by a simpler analysis of the Lime Rock Circuit as requested by John Fitch in 1970.
- 1973: Rice, SAE Paper No. 730018 (Ref. 126).
- 1983: Van Valkenburgh, *Road & Track* article (Ref. 161).
- 1984: Wright, *Road & Track* article (Ref. 167).

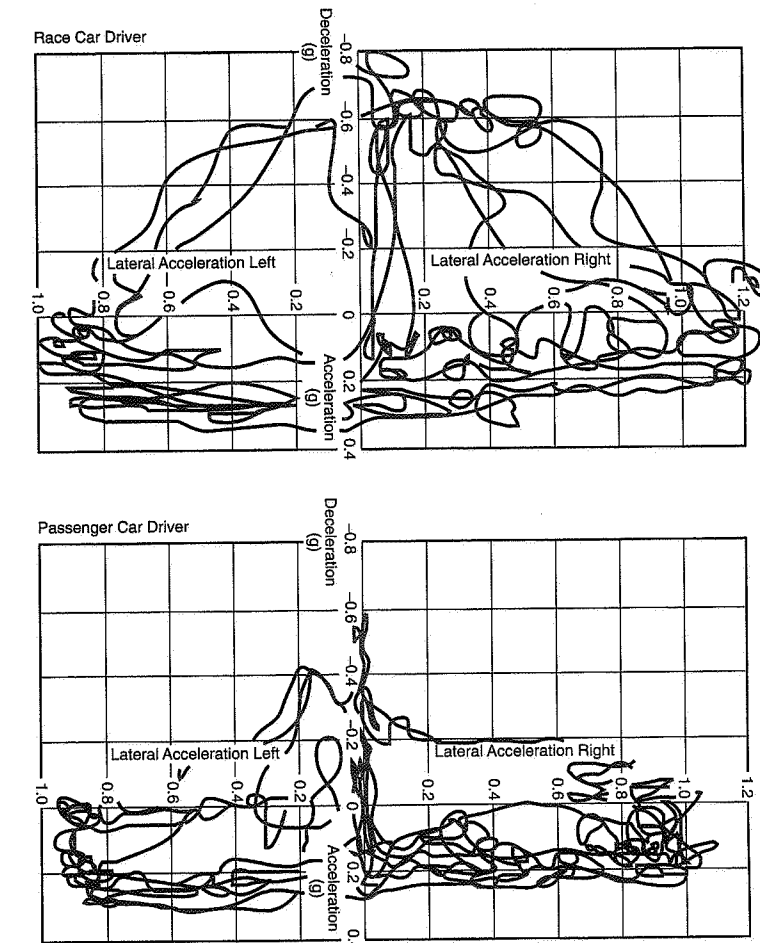


Figure 9.15 "g-g" diagrams from Isuzu, c.1970 (Ref. 108).

Race Car Design

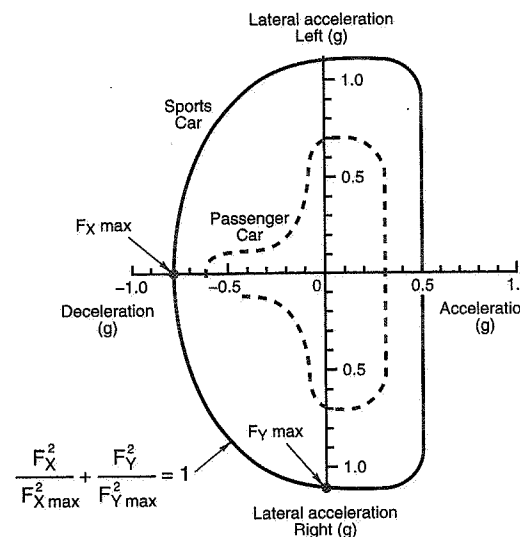


Figure 9.16 "g-g" diagrams from Isuzu, continued.

"In automotive design a straight line is the most awkward path to follow between two points."

Maurice Olley



Introduction

The process of design is not sequential but rather one of multiple stages of revision and refinement. This chapter briefly outlines a design procedure for a new race car, including the use of some of the analytical tools described elsewhere in this book. It is based on experience with several race teams and on project engineer responsibility for analysis/design/build/test of a number of specialized research vehicles. Many excellent books are available for further reading on race car design; for example, Ref. 38, by Costin and Phipps, was written at the beginning of the modern era of stressed skin chassis and mid-engine designs. Other books the authors have found useful include Refs. 148, 150, 152, 157, and 164.

It is important to recognize the relationship between available resources and expectations. For example, it will be difficult to design an Indy car with resources only sufficient for a Formula Vee. Resources include budget, time, past experience, engineering facilities (shop, fabrication, computing, test, instrumentation), etc. With ingenuity, one type of resource can be substituted for another. When starting a design project, it is well to assess one's resources to avoid frustration and compromise at a later time.

Compared to production car design or large aircraft design, race car design is on a smaller scale. A single designer, given a strong enough personality, can still track an initial concept through to hardware. The designer can make the conceptual sketches or layouts, perform (or specify) some “proof of concept” analysis, direct the detailed drafting, follow the fabrication and assembly, and plan and evaluate the prototype testing, using both predictive tools and test data from in-car instrumentation.

Some of the best stories in racing are about efforts that have succeeded in spite of unbalanced resources. In the past, projects have been driven through to successful completion by lone, exceptional individuals. With the sophistication of current race cars, this is more the exception than the rule—coordination of design, engineering and research teams is required at the top levels of pro racing.

10.1 Constraints and Specification

Constraints are external boundaries within which the designer must work. The vehicle rules and the competition rules are primary constraints. The designer must be thoroughly familiar with these rules (and unwritten rules in some cases). There are many additional practical constraints such as available components (especially tires, engines, drivetrains, brakes, etc.). The successful designer arrives at a realistic interpretation of the various constraints as they are applied in practice. The designer also realizes that to be successful in competition it is necessary to work to the absolute limits of the constraints.

The specification is the outline of the detailed objectives of the design including items such as:

Performance—For a new design, it is necessary to lay out performance goals, admitting that they will be changed in development. These could include acceleration capability in all directions (“g-g”), top speed, fuel consumption, tire consumption, and cooling requirements. These specifications are generally arrived at by simple calculations, rules of thumb, or perhaps carry over from a previous similar design.

Handling—The design must have handling qualities that allow the performance envelope to be used by the driver. This involves specifying details of the steering system, other controls, suspension system, and the chassis stiffness and body aerodynamics (drag and downforce). Based on the authors’ experience in working with a number of race teams, there is much more analysis that could be done at this stage toward optimizing the preliminary design.

Structure—Overall torsional and bending stiffness and local strength required to deal with the maximum loads from side force, braking force, bump, aerodynamic loads, engine torque reaction, etc., can all be estimated as part of the specification. We are aware that a number of teams are using advanced structural models (i.e., finite element), especially where there are rules on vehicle crush (crash testing).

Driver Accommodations and Safety—Good vision, adequate cockpit size, comfortable seating and restraints, moderate cockpit temperature, etc., all contribute to driver performance. Responsible design calls for the best in fire equipment, rollover and structural crash protection, fuel cells, and other mandated safety equipment.

Tires—The tires on a car perform a similar function to the wings on an airplane. In many racing classes the choice of tires is limited, effectively limiting the performance of the car. It is often said that race car design is all about optimizing the use of the tires.

Adjustable (tunable) Features—The required set-up for different race situations cannot be predicted and some adjustment capability must be provided in the design. Typical adjustments include:

- Weight Distribution—movable ballast, fuel capacity, burnoff (CG travel), and adjustable wheelbase.
- Aerodynamics—different wings and wing settings, suspension adjustment of car attitude and ride height.
- Suspension—ride height, body attitude, wheel loads (springs, anti-roll bars), damping, static settings (toe, camber), geometry (variable swing arm length and roll center height), and others.

Here is a place where parameter studies (using whole vehicle computer modeling) can be very helpful. With simulation it is possible to make many changes in a short time—simulation is cost effective. It is also possible to vary just one parameter without changing any others, something that is usually very hard to do with a real car in a test program.

10.2 A Design Process

There are many compromises in the overall design of a successful race car. As it is practically impossible to design something this complicated in a continuous (sequential) fashion, the design is continually reviewed and refined in a series of stages. A balanced approach starts with the overall concept, proceeds to preliminary design followed by stages of refinements and finally detailing to the required level. Parallel design concepts (different solutions to the same problem) and iterations (repeated modifications of a design until satisfactory) occur at each stage.

Design includes consideration of the fabrication techniques and design of required manufacturing tooling. This “simultaneous engineering” can save time and money when the car is built, and later serviced.

The design process is helped by brainstorming—discussions with other people involved in building and campaigning the car. This helps ensure that nothing is overlooked and often results in useful improvements.

Unbalanced designs are designs that emphasize one feature. There are cases where these have proven successful when the one feature is exceptionally good, for example, cars with outstanding handling but average engines. A car with an outstanding power/weight ratio relative to the competition may win even if the rest of the design is only fair. When competition is close, the right combination is necessary.

Preliminary Design

The goal of preliminary design is to fix the general arrangement of components in the car. The preliminary design aims at satisfying the packaging requirements (components, openings for driver and duct work, etc.) and the other specifications including the weight and balance requirements for handling. Depending on the specific rules, special body shapes for aerodynamic download may well determine much of the package outline. If ground effects are allowed, preliminary aero testing (wind tunnel) will determine much of the package outline.

Preliminary design starts by gathering data on all the components to be used in the car. If real data is not available, it must be estimated. Most important are component size and weight. The dimensions are used to make rough layouts of the location of the components, typically starting with the side view. The weights of the components are then used to estimate the overall weight and the location of the CG.

With some work, it is usually possible to compromise locations of the major components with the required CG location and allow everything to be packaged. The desired CG location depends on the neutral steer point (choice of tires), center of aerodynamic downforce, required load on the driving wheels for traction, and required load on the steering wheels for control. To reduce weight transfers (and directional trim change) the CG must be as low as possible (except in certain cases where weight transfer may be useful, i.e., drag racing).

As the side view progresses, top and front/rear views can be developed. Some of the major considerations at this stage include:

- Wheelbase and track, including adjustment ranges
- Ride height/ground clearance
- Planning for aerodynamic development and overall body shape
- Cooling for engine, transmission, oil, brakes, driver (radiators and ducting)
- Fuel, water, and oil tank locations and shapes
- Accessibility for maintenance and pit work
- Type of suspensions (leave enough space)

- Type and shape of overall structure
- Space for the driver

Wheelbase and track affect basic handling. Generally, a wider track gives a larger maximum lateral acceleration. A short wheelbase improves maneuvering while a long wheelbase increases the directional damping. See Chapter 5 for more on this topic.

A mock-up of the general arrangement is often used to check for interferences and complement the drawing process. This can use real components (engine, transmission, wheels/tires, etc.) when they are available. Race cars are often very dense; a compact package is usually desirable and a mock-up helps with the three-dimensional fitting process.

At this point there is a good idea of the overall size and mass distribution of the vehicle. A new CG estimate can now be made and, if necessary, adjustments can be made to the preliminary design.

Detailed Design and Analysis

Prior to detailing, the preliminary design should generally meet the constraints and specifications. From the preliminary design the following data is available:

- Overall dimensions and component locations
- Body shape from preliminary wind tunnel test results and other considerations
- Weight and CG location and desirable adjustment range.
- Power curves from engine builder
- Tire data from tire manufacturer

It is now possible to proceed with the detailed design and analysis. These two efforts proceed in parallel—data from each is required to finalize the other.

An early priority, if further wind tunnel testing is planned, is the wind tunnel model drawings and construction of the model. The scale and sophistication of the model will depend on the available tunnel and test objectives. Aerodynamic downforce development is often done in a tunnel with a moving belt and rotating wheels. Comparative results for downforce, pitch, and yaw have been obtained in small tunnels at modest speeds. Drag measurements benefit from higher Reynolds Numbers achieved by larger scale models and higher test speeds. If resources permit, aerodynamic development may be performed on the prototype in a full-scale tunnel at realistic Reynolds Numbers. In all cases, it is desirable to study the flow conditions around the model/vehicle as well as measuring the forces and moments.

All the components of the vehicle attach to the chassis (monocoque tub, space frame, or whatever). This is designed early in the process, with understanding that it may be modified as the rest of the design proceeds. Other detailed design effort includes:

- Suspension geometry, springs, shocks, and anti-roll bars
- Steering geometry and location of steering gear
- Cockpit layout, seat, restraints, control locations, instruments, etc.
- Engine mounting—possibly a structural part of the chassis
- Various systems—cooling, oil, brake, fuel, safety

Stress analysis and component reliability (fatigue) tests are a part of the detailed design effort. Even simple stress analysis is better than none, especially when previous experience is not available to size components. Key to effective stress analysis is knowledge of the loads experienced. Load and safety factors for stress analysis are usually based on previous experience but strain measurements and engineering analysis can also provide load data. Many components are designed for stiffness as opposed to strength.

It is still possible that a conflict will arise, forcing a return to another preliminary design cycle. For example, there may be clearance problems after a part is sized for the required strength/stiffness, or, wind tunnel tests may indicate a change in shape requiring certain components to be moved.

Decisions must be made on the amount of detailing versus shop floor design. Even for top level teams, the resources and time available do not permit the level of detail engineering and design used for production cars or aircraft. Dedicated fabricators, machinists, and mechanics are an invaluable resource.

Analytical tools are available to assist the designer. Useful programs can be developed for small computers; for example, suspension geometry, spring, and anti-roll bar calculations, simple stress analysis, performance, etc., are all fairly easy to program.

Setting up race cars for particular circuits remains a major problem. The objective is to arrive at a configuration with maximum cornering performance and good handling. As noted earlier, adjustments are provided for tuning the chassis but will be of little use if the basic design and ranges of adjustment are too far off to satisfy the different circuit requirements. Total vehicle dynamic analysis is useful to ensure that the basic design and range of adjustments are reasonable for handling. In some cases, different cars will be required to meet the varying requirements of different tracks.

Testing and Development

"What's wrong, here's a night and nobody's working."

Raymond Mays
quoted by Tony Rudd

"The torsional stiffness measured ... was 240 lb ft per degree."

Tony Rudd
on a mid-1950's F.1 car
(Both quotes from Ref. 135)



Introduction

In Chapter 1 it was concluded that the basic design requirements of a race car are:

- Provision of the largest vehicle "g-g" maneuvering areas throughout the speed range.
- Control and stability characteristics that enable a skilled driver to operate at or near these acceleration limits.

Once a car is designed and built, it is up to the development and race crews to adjust/tune/modify the car until it reaches its potential. Now a driver is required, and based on earlier definitions we are now discussing handling (driver in the loop), not just vehicle dynamics. We begin this chapter with discussions of the driver-vehicle relationship and desirable vehicle characteristics. Next, some testing fundamentals are discussed along

with test program planning and methodology. The chapter ends with a description of skid pad testing.

11.1 Driver-Vehicle Relationship

Motor racing, unlike ordinary highway driving, is very much an athletic endeavor. Circuit performance depends on an intimate relationship between the driver and the vehicle characteristics. If “handling” is defined as the maneuvering performance of the driver-vehicle system (the conventional definition), then the interdependence between the driver and the vehicle is far greater in the racing situation than on the highway.³⁷ This is well documented in the following quotation by Stirling Moss (Ref. 104) (bold emphasis ours):

Few people outside racing can appreciate that race driving is not like driving on the road at all. A racing car is always in an attitude at corners, never pointing as directly fore-and-aft in its line of travel as a road car would be in normal motoring. The racing car is sliding, to some degree, nearly all the time, but to be quick the best drivers try to do the slides and drifts with the least drag possible at moments when drag doesn't matter. One can put the car into a Kristie—a broadside as in ski-ing—to slow it into corners. But once one has presented the car to a very high-speed corner it's rather like throwing a dart—when it has left your hand you can't do a thing about its path. If you present a car accurately to such a corner it will track through in a long drift on virtually a predestined trajectory. You can make tiny adjustments, but once you have presented it to the corner you can only adjust the trim, not make major changes of direction—not if you are on the limit.

Steering is used to present the car, then to compensate for the throttle, because as one opens the throttle, and the car starts to slide you may have to use the steering wheel to compensate—to balance the power. I would describe the steering wheel as the presenter and the balancer really.

Since it is so difficult to represent the characteristics of drivers in analytical engineering terms, it has become common in the development of vehicle dynamics to separate out the vehicle component and look at its stability and control independent of the driver. This is an abstraction of the real situation; it works well for the development of ordinary vehicles where the connection between driver and vehicle is limited but is far less satisfactory for the racing situation. This reservation applies to much of the material in this chapter.

The motion behavior of a vehicle can be thought of as depending on four sets of force actions: control, stabilization, damping, and disturbance. *Control* is an intentional action on the part of the driver in the direction of task accomplishment. *Stabilization* is a force action which tends to resist a change of vehicle attitude to its path. *Damping* resists a

³⁷ Simple observation of the level of concentration and activity required to drive a race car compared to a passenger car illustrates this point.

change in lateral and yawing velocities. *Disturbance* is a force action tending to move the vehicle away from its momentary trim (and usually away from task accomplishment).

Control is the result of the driver's intelligence in processing sensed information and memory recall of experience, transmitted to the vehicle through the controls. It represents the driver's best efforts in positive task accomplishment. Stabilizing actions, on the other hand, can be helpful in some situations and detrimental in others. Thus an excess of weathercock stability (understeer) can inhibit the vehicle's response in one maneuver or assist in a different maneuver. Damping generally has a positive effect in shortening the response time to steady-state and resisting externally induced motions. Disturbances from wind and road normally interfere with task accomplishment.

The roles of the driver and vehicle can now be stated:

- The driver's basic responsibility is that of establishing the appropriate path and speed in the presence of disturbances from wind, road, and traffic.
- The fundamental contribution of the vehicle is one of facilitating the driver in this guidance function.

Since the vehicle is not intelligent and cannot be optimized for all tasks, there will be occasions when the vehicle fails to facilitate the driver's intentions. In these situations the driver must compensate through additional control action, referred to as driver *response augmentation*.

11.2 Desirable Vehicle Characteristics

It is possible to state in general terms how the stability and control characteristics of the conventional passenger car can facilitate the driver's guidance task. The vehicle can perform this function by:

- Minimizing response to external disturbances (wind and road).
- Ensuring satisfactory control response characteristics.
- Ensuring no major or uncontrollable instabilities.
- Providing satisfactory information flow to the driver.
- Providing reasonable max “g” limits, skid warning, acceptable breakaway behavior and recovery.
- Remaining consistent in behavior with changing environmental conditions such as rough surface, change in road surface coefficient, etc.

The above specification of desirable stability and control characteristics is much less applicable to the race car. With a wider speed and acceleration range and operation in the

tire nonlinear/limit region, conventional concepts of stability and response are not as well defined. The task structure in racing is complex and constantly changing during a race (and from circuit to circuit). The vehicle's contribution to "handling" is seldom ideal and more *response augmentation* is required of the driver.

To cope with the changing operating environment, race car design has evolved in the direction of more chassis adjustability rather than toward a specification of stability and control. Nevertheless, the overall trend is to facilitate the driver's guidance function. For example, in order to achieve the highest average cornering acceleration, race car set-ups are compromised in the direction of "neutral steer" at the limit. This tends to reduce the response to road disturbances and oscillatory instability at high speeds.

In order to achieve a high max lateral, current tire designs are wide, with low aspect ratio (tire height/width, expressed in percent). Wide tires have advantages and disadvantages. On the plus side, the resulting high cornering stiffness increases the lateral and yaw damping which promotes desirable sublimit control response at high speeds. On the minus side, wide tires reach peak lateral force at relatively small slip angles, thus break-away warning is poor. In addition, wide tires are more susceptible to road irregularities.

As a final generality, considerable experience suggests that extremely maneuverable vehicles such as race cars and fighter aircraft should have large control capability, minimum mass and rotational inertias, high damping and small static directional (attitude) stability. This results in fast and well-damped behavior with responses approaching first order (exponential).

11.3 Fundamentals of Testing

Testing and development broadly falls into several categories:

- **New vehicle shakedown**—Some running time to insure vehicle integrity and to build driver confidence in the new vehicle. Check-out of all the systems (engine, transmission, brakes, cooling, etc.). More running will establish vehicle reliability. At this point, the vehicle is ready for development and tuning.
- **Development**—Exploring the potential of various changes and adjustments in the vehicle configuration. This is often a luxury that is not practically available.
- **Reliability testing**—Pre-running races to test the "whole vehicle" endurance. At the same time, component life (i.e., tires and brakes), and fuel consumption can be determined.
- **Qualifying and race set-up**—Fine adjustments to match the vehicle to a specific track (and track conditions) and to match the vehicle to the driver. The objective is to optimize the driver-vehicle combination.

The ultimate objective of any race car testing and development program is to assist in winning races. This means fast qualifying and race lap times, satisfactory handling, and reliability. Test results can help set up the car in the short time that is available for practice. For test purposes, the single number "lap time" is not very much information; there are other measures of car performance that can be used to study the problem in greater detail.

The development of passenger cars for sublimit and occasional limit maneuvering can be accomplished with a series of stylized tests (see Refs. 3, 8, and 9). For race cars, stylized tests have limited utility. For road racing cars with low/modest speed cornering, circular skid pad tests may be a good starting point for development. For higher speeds and banked tracks, skid pad conditions are too far from reality and development must be done on the track. The choice of development program is heavily determined by the speed/power of the car and the type of competition.

As mentioned in Chapter 10, available resources and facilities determine the amount and type of testing that will be done.

Laboratory Testing

In the past, the only tool available for performance evaluation at the race track beyond the stopwatch and tire pyrometer was subjective driver comment (qualitative). This was true for all but the most highly funded teams. The trend is toward the use of more instrumentation, much of it electronic and microcomputer based. The use of instrumentation makes testing *quantitative*.

It is interesting to note that progress made in the engine field is largely the result of highly instrumented dyno testing. Dynamometers and associated instrumentation are recognized as a necessary tool for engine work; no serious development occurs without one. Chassis testing still lags engine development for lack of detailed quantitative data and interpretation. The chassis test equivalents to engine dyno facilities are not generally available to race teams. They are available to passenger car manufacturers, who have trained staff to perform the testing. Ideally, three types of information are necessary to establish chassis subsystem performance:

- **Tire data at real speeds and temperatures**—Perhaps the most difficult to obtain, unless it is available from the tire manufacturer.
- **Chassis geometry, compliance, mass and inertia properties**—These physical tests often require large (expensive) equipment but many of these numbers may be estimated, provided that the numbers are used with engineering judgment.
- **Aerodynamic (wind tunnel) data**—This is the only type of data that can be reasonably developed from scale models, reducing the testing expense.

A practical alternative to indoor testing is to instrument the car and then analyze the data. On one hand, this is more “realistic” than lab tests, but track test data is often difficult to interpret because of variability in operating conditions. Regardless of its source, vehicle data is complex and elaborate analysis is required to take full advantage of it.

There is still the feeling that handling is a mystery; with enough instrumentation, testing and analysis, race car handling will yield to engineering understanding.

11.4 Track Test Program Planning

The first step in test planning is reserving a circuit/track for some period of time. The schedule should ensure that the car is ready to run when it reaches the test facility—shop work is best and cheapest done in the shop. This is possibly the most basic rule in testing and one which is often hard to adhere to.

Instrumentation (if any is to be used) must be arranged well in advance. Instrumentation manufacturers seldom work to race car schedules and their products are costly. The amount of instrumentation depends on the testing time available; if this is to be a first instrumented test it is advisable to allow several days to debug the installation. Once the team has an understanding of the use of instruments it is possible to accomplish a great deal in a short test period. An alternative is to hire a specialist firm to instrument the car and interpret the data.

A wide variety of transducers and recording equipment is available. Much of this equipment will work satisfactorily in the race car electrical noise and vibration environment. Some instrumentation gives quick readout during the test—the standard is the stopwatch. Other instrumentation will provide more comprehensive data for later analysis. Time must be allowed in the schedule for mounting, wiring, and calibrating.

The items that can be adjusted on a race car are generally well known and are treated elsewhere in this book.

Race car testing is “running laps” with a variety of configurations. A list of configurations to test should be part of the planning. At the track, the desire is always to try to improve the set-up (faster, better handling) and the test program may only be a guide.

11.5 Test Methodology

The “scientific method” addresses the issues of “good data” versus “bad data” and provides a framework to ensure the former. With instrumentation in a harsh environment such as a race car/race track, it is all too easy to get bad data. Bad or misleading data is possibly the most confusing thing that can happen in a test session. First it is necessary to define a few terms.

1. *Accuracy* is an instrument’s agreement with recognized standards. For example, a watch can be said to be accurate to within 1 second per month. This means that comparison of the watch to a time standard will always be within the 1 second during the month. Basic accuracy data will be provided in the manufacturer’s specification.
2. *Resolution* is the smallest change that the instrument can measure. In the case of a watch it may be 0.01 second. For other sensors, for example, accelerometers, the resolution may be “infinitesimal” and then the resolution depends on the recording system to which the sensor is connected.
3. *Hysteresis* describes the case where the output depends on the history of inputs. Ideally, instruments have no hysteresis. Race cars **do** have hysteresis; for example, the measurement of ride height depends on how much stiction is in the suspension and how the car was bounced or rolled out.
4. *Precision* has to do with the whole measuring process and random variations within it. For example, the imprecision in manual stopwatch timing depends on the operator and may be 0.1 second. For a single measurement (one lap time) the precision can be based only on the past history of that type of measurement. Automatic systems usually have more precision than manual ones.
5. *Calibration* is setting the output (for a given input) of an instrument equal to some known standard. Instrumentation must be adjusted and checked to ensure that data is accurate. If data is to be recorded, good calibration of the recording equipment can be time consuming. For very bad sensors there may be a question of linearity; in this case it is necessary to calibrate at a number of different input conditions and keep a calibration curve for use in reducing the data.
6. *Gain* is defined for linear systems as the ratio of output to input. In the case of electronic measurements it is often expressed in terms of volts per measured quantity, for example, 2.5 volts/1g might be the calibration of an accelerometer.
7. *Offset* describes the difference between zero input and zero output of an instrument. The above accelerometer may have an output of +5 volts at zero g, in this case, +1g may be represented by +7.5 volts and -1.5g by +1.25 volts. See Figure 11.1 to see what this gain and offset looks like.
8. *Noise* is the presence of other signals (or data) mixed in with the desired measurement. Noise sources are common in race cars; for example, accelerometers will measure engine vibration along with lateral acceleration. Noise is the enemy of good data and a combination of mechanical isolation of sensors and careful electrical shielding and grounding is required to reduce noise (increase signal-to-noise ratio).

The goal of any test session is to gather good data on different vehicle configurations. A further goal is to be able to make use of this data in set-up at a future date. An effective test session will do both.

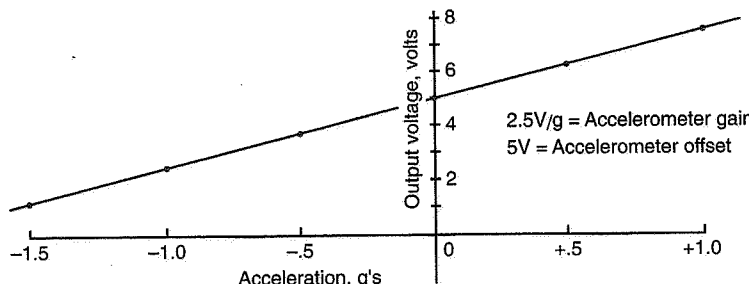


Figure 11.1 Gain and offset for an accelerometer.

Besides having good instruments, some principles of obtaining good data include:

1. Make one change at a time. If two changes are made at once it is usually impossible to determine the effects of either. Once testing has given a good understanding of a particular vehicle, then multiple changes may be made with a better chance of success.
2. Return to a baseline configuration to “calibrate” factors that are not under control, for example, tire wear and track temperature.
3. Be aware of the effects that different changes make. A single mechanical change can have multiple effects. Measuring the set-up that is used for each test is the only way to control this. Some things that can be measured for each configuration include:
 - Tire pressure
 - Alignment—camber, toe and caster
 - Weight on each wheel
 - Trim or ride heights
4. A special form, prepared in advance, is convenient for recordkeeping. To be able to use the data later it is important to keep good records of:
 - Configuration details—a big list
 - Environmental conditions—temperature, wind, track condition
 - Driver comments—as specific as possible
 - Lap times / tire temperatures / other data.

Full-scale Aero Testing

The aerodynamic aspects of full-scale development are facilitated by the measurement of air velocity, static, dynamic, and total pressure, flow visualization, and temperature using instrumentation and the theory discussed in Chapter 3. Generally the aerodynamic problems that have to be solved are related to one or more of the following:

- Drag reduction
- Downforce and its distribution
- Engine air intake duct efficiency
- Engine, oil, brake, transmission, and differential cooling
- Crosswind stability and buffeting
- Driver ventilation

11.6 Some General Notes on Development

Development or tuning is an optimization process. If the process is well organized (and well funded) it will take the form of making theories and running tests to prove (or disprove) them. The reason that the process is so complex is that there are too many variables to test, not enough data, and little in the way of techniques to assemble the available data into something useful. Some general principles that may help are given here.

It is important to have a good explanation or at least a theory for each problem area. A large quantity of data will make little sense if there is no broad way to make cause-and-effect relationships between different items. A fairly complex theory that represents parts of reality (given its fundamental limitations) is the two-degree-of-freedom vehicle discussed in Chapter 5. This theory has been tested, in the sense that cars developed with the 2DF theory generally behave as the theory predicts. This theory may require too much data to be useful in the real world but an understanding of this broad theory helps to direct the thinking process.

An example of a less complex theory is: If the tire rubber works equally hard on all four wheels then the car will be balanced, or at least the tires will wear out evenly. Following this theory leads to the common practice of measuring tire carcass temperature, with the intent of determining the energy input into the tires. This theory needs modification if different compounds or sizes are used, but the general idea of a conceptual framework is still useful.

Theories are made up to explain the otherwise inexplicable. Great care must be taken with theories that pertain to very specific circumstances. For example, if a particular car laps faster with stiffer springs, a possible first theory might be to “stiffen up” all cars—to make them faster. The problem with this theory is that the first car (that the theory was

based on) may have had a large amount of bump steer. With this extra data it becomes obvious why it was desirable to limit the wheel travel in bump—every little bump was disturbing the path. At this point it is necessary to clear out the old theory and start again.

Linear systems analogies often make reasonable theories if properly applied. If a system is linear it means that a small change makes a certain difference and a larger change in the same direction makes a proportionately larger difference. The trick to using this tool is in choosing the right measurement. A change in the balance of the car (plow vs. spin) may be easily detected in the change in steering wheel position on a given steady turn, but the same change may not be so easy to see in the overall lap time.

When checking a theory it often helps to reduce the complexity of the experiment. For example, low-speed handling is influenced by chassis set-up, a complex problem. At high speeds, the size of aero forces can be large (depending on the vehicle and the speed) and another set of aerodynamic explanations must be added in to understand handling. Thus sorting out trends (if not actual numbers) in the chassis set-up is much easier to do at low speeds. Simplifying even more to a continuous turn (skid pad) may be a good starting point.

It is important to recognize that there is a difference between steady-state characteristics that apply at the turn apex and transient characteristics on turn entry and turn exit. Establishing neutral steady-state turning characteristics is the first step in balancing the car. The steady-state condition occurs at mid-turn. From there the turn entry and exit transients can be developed.

The most complex theories are mathematical calculations run on computers. The principle of “garbage in/garbage out” is most obvious here. Data from the lab test facilities mentioned above makes it almost necessary to use a comprehensive computer model. The alternative of working backwards from vehicle test data to arrive at tire, chassis, and aero data is full of uncertainties.

Possibly the hardest data to use, and the only data that is always available, is subjective data—driver comments. The aircraft industry has gone to great lengths to establish standards for pilot comment (see Ref. 37). The two main principles described in this reference are:

- **Restrict subjective rating to very specific items.** Test pilots fly specified maneuvers and rate the different parts of each maneuver.
- **Use a standard scale for all ratings** (Ref. 37 uses 1-best to 10-worst); automotive raters have tended to use 1-worst, 10-best. The pilot rating scale is a very well-developed engineering tool and this reference is recommended.

In the race car case, test drivers must distinguish where on the track (turn entry, dropped throttle, a bump in the road, etc.) a problem is occurring and report it accurately. Simple comments such as “it’s loose” have little meaning until more is known.

11.7 Circular Skid Pad Testing

Skid pad testing is a common way to measure steady-state vehicle characteristics. Standard test procedures used by the auto industry for production vehicles have been compiled into an SAE Recommended Practice (Ref. 3). The aim of the industry standard tests is to measure the *understeer gradient* of a vehicle at moderate lateral acceleration conditions. For racing, the skid pad has two main uses:

- Balancing the vehicle near maximum lateral acceleration—as is found at the apex of a slow corner.
- Increasing the maximum lateral acceleration at low speeds.

At higher speeds aerodynamic forces and their distribution are important and aerodynamic development cannot be done with a low-speed skid pad test.

Briefly, SAE describes a test where the vehicle is driven on a constant radius circle (minimum 100-ft. radius) at a range of speeds starting from very slow (to establish the geometric steer required to negotiate the turn—the Ackermann angle) to near the limit of the vehicle. The speed is increased in small increments and each speed is held constant until a steady-state data point is obtained. At each speed a number of measurements are made:

1. Steering wheel angle—required
2. True vehicle speed—required (5th wheel or timed laps)
3. Lateral acceleration—optional (can be calculated from speed and radius)
4. Roll angle—optional
5. Yaw rate (velocity)—optional (measures the rate of turning)

Data from a constant radius test is shown in Table 11.1 along with the formula for calculating lateral acceleration and other data from the test. This data is plotted in Figure 11.2.

From the plot it can be seen that the steer required to stay on the circle increases with speed; this vehicle is understeer. The slope of the curve gives the amount of understeer. The straight line slope is approximately 9° of steering per 0.5g lateral acceleration or $18^\circ/g$ of understeer at the steering wheel. A more common description of understeer is at the front wheels and to convert it is necessary to divide by the steering ratio. $18^\circ/17^\circ \approx 1.1 \text{ deg./g}$ of understeer at the front wheels.

Table 11.1 Data and Data Reduction from Skid Pad Test

V mph	V ft./sec.	δ_{SW}	V^2/Rg
0.00	0.00	66.00	0.00
20.00	29.33	71.00	0.23
25.00	36.67	72.00	0.35
30.00	44.00	78.00	0.51
35.00	51.33	83.00	0.69
39.50	57.93	111.00	0.88

Steering Ratio = 17:1

$V = \frac{2 \times 3.14159 \times \text{Radius (ft.)}}{\text{lap time (sec.)}}$

This gives V in ft/sec.

Lateral acceleration = V^2/Rg

where: V is velocity in ft/sec. (ft/sec. = mph \times 1.4667)
R is the radius of turn = 118 ft. in this case
g (acceleration due to gravity) = 32.2 ft./sec.²
 δ_{SW} is Steering wheel angle, degrees

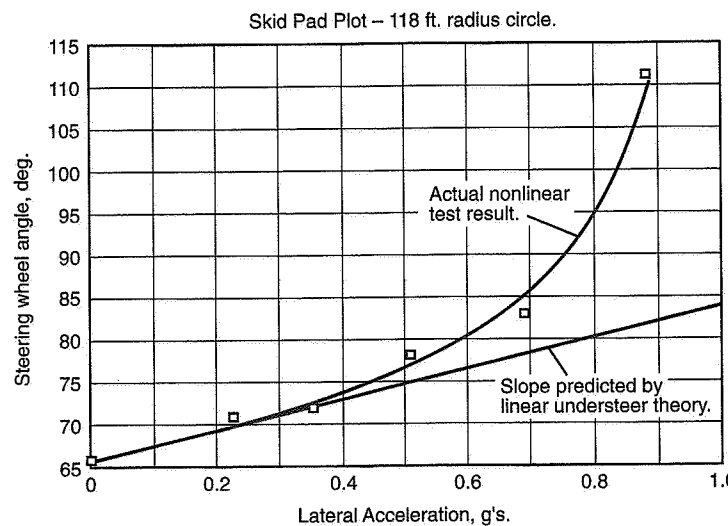


Figure 11.2 Skid pad plot.

If the understeer is desired at some other lateral acceleration it is necessary to take the slope of the skid pad plot at that point and repeat the calculation. Note that the high lateral acceleration end of the curve is very steep. This indicates that this vehicle is plowing at the limit, if the curve is vertical, an increase in steering wheel angle will not give a corresponding increase in lateral acceleration.

For race car development, most of the time on the skid pad circle will be at or near the limit. While the plot of Figure 11.2 shows one data point at 0.88g lateral acceleration, in fact the vehicle was averaging this amount of steer and averaging this lateral acceleration for a complete lap; this data is not steady-state in the strict sense of the term. Varying conditions around the circle require small adjustments by the driver in steering and throttle to keep the vehicle at max lateral. Smooth driving technique is important to good data at the limit.

In a development program small changes are made in car set-up and the effect is noted on speed (or lap time). Unfortunately, the tuning process is confused by several variables that are not easily controllable. The most important of these are:

1. Tire wear will be rapid at high lateral accelerations; the tires will not be the same tread depth from run to run.
2. Tire temperature varies with the amount of run time. It is advisable to always run each configuration for the same number of laps and to monitor tire temperature for each run. Depending on the tire, performance may be affected by the number of heating/cooling cycles.
3. Air temperature and track temperature both affect tire performance.
4. Fuel burn-off affects weight distribution and total weight.
5. The tires may deposit rubber on the surface making it stickier. Also, the pad surface may vary around the circle.
6. The driver must be very smooth and consistent to generate good data.

Keeping good records of all the lap times and changes is extremely important if any conclusions are to be drawn from a day at the skid pad.

Some other points to keep in mind are:

1. Watch the oil pressure: Constant turning in one direction may uncover the oil pump pick-up.
2. Continuous running at high lateral accelerations will cause very rapid tire wear; a set of street tires can be worn out in less than a day.
3. Electronic timing of every lap is best. The intervals are so short that manual timing introduces large errors.
4. For road racers, test in both directions to check symmetry (or lack of symmetry).

Chassis Set-up

“... leaping and bounding out of control, in every corner it went from understeer to oversteer, and when the brakes were applied the rear axle banged into the chassis.”

Mark Donohue

*On the handling of an “unsorted” sedan
(from Ref. 162)*



Introduction

In this chapter we discuss specific problems that may arise in tuning an existing car for a given race track. The list of problems discussed and the possible solutions offered are based on the authors' experiences and are by no means complete. As far as we know, the suggested remedies are accurate but there will always be exceptions; **the following material should be treated as a guideline, not as “gospel.”**

When discussing car set-up it is necessary to make the distinction between changes that will always improve the performance of the car (make all of these first) and changes that tune or balance the car (these have trade-offs). In the first category are things like more power and stickier tires; the second category includes small changes in such things as spring rates or anti-roll bars. It takes both good initial design and careful tuning to produce a successful car.

One major cause of handling problems, suspension/component/chassis compliance (or flexibility) is not discussed in this chapter at all, because it is more a function of the

vehicle design. As noted in the quote at the start of Chapter 23, every engineering material is flexible to some degree. Loads in various parts of a car can be surprisingly large, leading to unexpected distortion. Compliance often occurs in components that are structurally in bending, instead of straight compression/tension. **With unknown and/or excessive compliance, it will be very difficult to predict any aspect of race car performance.** Cars that have large compliances (often unknown by the team) are often unresponsive to the standard changes to which other cars respond.

This chapter is keyed to several tables. Tables 12.1 and 12.2 list the principal chassis adjustments that can be made on a modern race car. You can consult Table 12.3 with a known problem in mind, and it will point to changes that should have a large influence on the problem. The challenging part of racing set-up is that **everything affects everything else.** A change made to improve one aspect of performance of a car can easily degrade its overall performance. The best lap time is made with the set-up that is the best compromise for the circuit as a whole, including the driver. Table 12.4 puts this into perspective by pointing out some of the effects that will occur when a particular change is made to improve some particular problem.

Given the differences between cars, this set of tables can only be considered a starting point in the set-up process. Ideally, enough testing will be done to put numbers on the size of the effect of a given change. This test data will be invaluable at the track when time is short.

12.1 Set-up

Racing is all about driving the vehicle at its limits, near the boundary of the “g-g” diagram. Finding a vehicle configuration which can be driven to produce this desired performance is referred to as *setting up* or *chassis tuning*. It is a difficult task requiring many compromises to fit each circuit and the driver’s capabilities and preferences. Often it will not be possible to achieve the optimum set-up in the available testing and practice time and the driver will have to allow for the vehicle deficiencies that remain.

The principal objectives in setting up the car are:

1. Cornering balance (neutral steer) under max lateral conditions.
2. Compromise between cornering performance and drag on high-speed tracks.
3. Eliminating specific control and stability problems at any points on the circuit as reported by the driver.

The traditional set-up procedure is to make changes in vehicle adjustments based on subjective driver comments, and lap and segment times. These might be supplemented with remarks from observers stationed at various points around the track and tire temperature measurements taken in the pits.

The professional racing approach to set-up has become much more sophisticated in recent years. In the first place, the cars have become more adjustable. Second, electronic on-board and track-side instrumentation is being used by most well-financed teams. Services of this type are also available on a rental basis. When the stakes are high enough, *set-up* approaches *design* and major overnight changes may be made in the vehicle. For example, extensive modification might be applied to an aerodynamic surface or several alternatives may be made available.

Table 12.1 Principal Chassis Tuning Items

- | |
|--|
| <ol style="list-style-type: none"> 1. Tires <ol style="list-style-type: none"> a. Different designs, sizes and front/rear combinations b. Tire pressures/tire temperatures c. Stagger (different tire circumference) frequently used across an axle d. Rim widths and offsets (possible track change) e. Static alignment (toe, camber, caster) 2. Static Wheel Loads <ol style="list-style-type: none"> a. Longitudinal CG location (shifting ballast) b. Lateral CG location (shifting ballast) c. Wedge, diagonal weight jacking, or warp (changes in spring preload) 3. Lateral Load Transfer Distribution (LLTD) <ol style="list-style-type: none"> a. Roll couple distribution front to rear b. Roll center heights (front and/or rear) c. Ride spring rates d. Anti-roll bars or Z-bars e. Progressive rate springs, linkages and bump stops (Notes: Coupling occurs with ride height changes when progressive rate linkages are used. Cockpit adjustment of LLTD may be provided.) 4. Ride Height and Body Attitude (Roll and Pitch) <ol style="list-style-type: none"> a. Wheel orientation changes via suspension geometry <ul style="list-style-type: none"> • Camber curves • Ride (bump)/roll steer • Anti-dive/squat • Steering geometry • Wheel travel b. Aerodynamics (function of ride height and body attitude) |
|--|

Chassis Adjustment

Tables 12.1 and 12.2 cover the principal items that are used in tuning the chassis. No such list can be viewed as final, since competition experience and ingenuity are continually producing new ideas.

An examination of the list in Tables 12.1 and 12.2 will indicate that the major part of tuning is concerned with maximizing the lateral tire forces while achieving the proper balance. Items 1-4 in Table 12.1 are directly concerned with the **tires themselves, desirable wheel orientations, and tire loads**. The aerodynamic lift/downforce of item 1 in Table 12.2 is an important component of the vertical tire loads when aero

Table 12.2 Additional Principal Chassis Tuning Items

1. Aerodynamic Forces and Moments
 - a. Lift/downforce
 - b. Drag
 - c. Pitching and yawing moments (Note: As affected by size, shape, angle of wings, car shape/underbody, internal air flow, etc.)
2. Brakes
 - a. Distribution, front to rear
 - b. Cooling
3. Driveline
 - a. Gearing
 - b. Differential(s), type and functional behavior
 - c. Spool
 - d. Engine performance characteristics
4. Dampers
5. Driver/Vehicle Interface
 - a. Steering ratio
 - b. Pedal forces and movements
 - c. Force feedbacks (kickback, oscillations)
6. Compliances
 - a. Chassis and suspension stiffness maximized by design
 - b. Suspension compliances are not adjustable for tuning (as in road cars)

devices are allowed. Brake distribution, item 2 in Table 12.2, affects control and balance via modification to the tire loads and through the friction circle. Driveline characteristics acting through the interaction of longitudinal and lateral tire slip can significantly affect the available lateral tire forces. Finally, dampers have some direct control on tire loads under rough road and transient conditions.

Although it is generally desirable to make one configuration change at a time, there are interactions between changes which must be understood.

12.2 Primary Set-up

Table 12.3 is a **first cut** at the major problem areas for high-performance / racing cars. Down the left side of the table is a list of different operating conditions and across the top is a list of items that can be changed. The numbers in the chart correspond to the numbered paragraphs in this section on Primary Set-up. The choice of which relationships to discuss was made on the basis of "most likely to affect performance." As an aid to understanding, we recommend that the reader stop and create a mental picture for each situation.

The changes along the top of the table are ordered from left to right in approximate mechanical difficulty. Changes on the left side of the table require a fair amount of effort and may need to be designed into the car; those on the right are items that can be changed relatively easily in tuning the car.

1. **The Effect of CG Location on Straight Line Braking**—When the brakes are applied, load is transferred from the rear tires to the front tires. The higher the CG, the more is transferred for any given deceleration. Tires are load sensitive, thus theoretical best braking occurs with the tires evenly loaded (if the tires are the same on both ends of the car). For the typical RWD or FWD road car (with initial forward load bias) this says that to improve the absolute level of braking, the CG should be as low as possible and moved toward the rear of the car. Clearly this is not always feasible for FWD race cars but it should be taken into account when a car is being designed.
2. **The Effect of Tires and Rim Sizes on Straight Line Braking**—To the extent that changing the tires/rims changes tire/road friction properties, the braking performance will be affected. The end with the stickiest tires can generate relatively more braking force for the load on it.
3. **The Effect of Brake Balance on Straight Line Braking**—Brake balance is the name given to the proportioning of brake force (or brake torque) to the front and rear tires. The brake balance to give "correct" proportions of braking to the front and rear (relative to their potential) varies with deceleration rate. The harder the stop, the more heavily loaded will be the front wheels and the more braking effort they can support. Likewise, the rear tires are unloaded as the deceleration

Table 12.3 Key to Primary Set-up Guide

	CG Location	Roll Center Location	Anti-Pitch Geometry	Steering Axis Geom.	Camber Effects	Ride/Roll Steer	Aerodynamics	Differential	Tire & Rim Sizes	Ride Spring Rates	Ride Height	Brake Balance	Roll Stiffness Dist.	Dampers
Low-Speed Steady-State:														
Straight Line Braking	1								2		3			
Braking & Cornering	4	5									6	7		
Cornering	8	9			10				11				12	
Acceleration & Cornering								13					14	
Straight Line Acceleration	15		16					17						
High-Speed Steady-State:														
Straight Line Braking						18					19			
Braking & Cornering						20					21			
Cornering						22								
Straight Line Acceleration						23								
Transient Behavior:														
Dropped Throttle in a Turn	24				25	26							27	
Braking in a Turn	28									29				
Poor Road			30	31				32	33				34	
Control Characteristics:														
Steering Force & Ratio				35			36							
Steering Kickback			37			38	39							

increases and they must have less braking force. This is accomplished in several ways: Either the brake balance is fixed and is biased heavily toward the front, which means the rears don't do their share on relatively gentle stops, or various types of proportioning valves are used to limit hydraulic pressure to the rear brakes to prevent premature locking. Finally, an anti-lock system may be fitted.

When the brakes are not correctly set up (for racing) one end will lock up before the other. If the rears lock first, the car will tend to spin, based on the destabilizing side force that the still-rolling front tires provide. If the fronts lock up first, steering control will be lost and the car will go straight or slide down the camber

of the road. Because the desirable brake balance varies with the deceleration, different brake balances are required on different coefficient of friction surfaces. For example, snow gives little absolute braking capability and the best brake balance will be very close to the fore-aft static weight distribution. Where possible, it is desirable to fit some sort of brake balance adjustment to race cars to allow tuning of the brakes to different surfaces and conditions.

4. **The Effect of CG Location when Braking and Cornering**—The result of combined braking and cornering on turn entry is to load the outside front wheel very heavily (perhaps as much as one half the weight of the car). At the same time, the inside rear wheel is lightly loaded. The higher the CG, the more load will be transferred. This situation will be exaggerated if the CG is forward to begin with. The heavily loaded outside front tire will be operating at a relatively low coefficient because of load sensitivity. Assuming the car has been otherwise set up, a low and rearward CG position is going to keep the tires most evenly loaded on turn entry, and this will give the best performance.
5. **The Effect of Roll Center Location when Braking and Cornering**—Roll center heights front and rear partially determine the way the roll moment on the car from lateral force is distributed. Lowering the roll center on one end will lower the roll moment resisted by that end; the wheels on that end will be more evenly loaded in cornering compared to the other end of the car. For example, assume that the car is loose on turn entry; the idea is to sacrifice grip on the front to increase grip on the rear. The outside front is taking the largest share of the load and increasing the front roll resistance by raising the front roll center will further degrade it to help the rear stick proportionately better. Additional help can be obtained by lowering the rear roll center height as well. It should be noted that "too high" a roll center leads to jacking.
6. **The Effect of Brake Balance on Combined Braking and Cornering**—The correct brake balance for straight line stopping may not be appropriate on turn entry. The outside front tire is very heavily loaded and generates relatively more lateral force than the rear leading to spin. This is true even though the front is operating at a lower coefficient (due to load sensitivity). Thus, too much rear brake bias may be described as "loose coming into the turn."
- Some production cars have almost no rear brake bias (to prevent accidental spins) and the sometimes-used practice of trail braking (braking while on the throttle in a front-wheel drive) has a compensating effect. The engine power reduces the braking on the front wheels while the rears are still receiving a normal amount of braking force. The result is that the rear tires are saturated and the car begins to spin; carefully controlled, this can be used to get the tail out on entry to tight corners.
7. **The Effect of Roll Stiffness Distribution when Braking and Cornering**—The roll stiffness distribution is the other way of changing the loads on the wheels under lateral force. Roll stiffness can be raised by increasing anti-roll bar stiffness or increasing spring stiffness. Again, assuming the car is loose on turn entry, it is appropriate to resist more of the body roll moment on the front. Higher

front roll stiffness will do this. If the car has a "rising rate" spring installation, the front roll stiffness increases when the vehicle pitches forward.

For front-wheel drive the problem may be reversed, if the CG of the car is so high and/or forward that the inside rear wheel is off the ground, the rear of the car is already offering all the roll stiffness it can and further changes in rear roll stiffness will have no effect.

8. **The Effect of CG Location on Steady-State Cornering**—A neutral car is best for steady-state cornering. By tuning, cars with a range of CG positions near the center of the car (and same tires front and rear) can be made to be neutral. If the CG is forward, the lightly loaded rear end will stick better than the front (because of tire load sensitivity) and the rear end must be degraded to bring the car back to neutral (this ignores the friction circle effect which can degrade the drive tires a great deal, even at road load power). The best use of equal-sized tires in steady-state cornering is made with the CG near the center of the car.
9. **The Effect of Roll Center Location on Steady-State Cornering**—If the car is forward weight biased, a rear roll center higher than the front will tend to make it neutral. If both roll centers are so low (i.e., on the ground) that the car has a large amount of body roll, absolute cornering performance may be affected through adverse tire camber. It is necessary to strike a compromise here because too high a roll center leads to jacking (and lateral tire scrub on bumps), an undesirable characteristic.
10. **The Effect of Camber on Steady-State Cornering**—It is desirable to have a small amount of negative camber (top of the tire leaning toward the center of the car) on the outside wheels. This produces the maximum lateral force from the two outside tires. Tire temperature taken across the tread width is commonly used to set static camber; the camber is changed until the temperature is roughly the same across the tread width. For race courses where the direction of turn is always (or mostly) the same, positive camber on the inside wheels will also help. Camber can also be used to balance the car.
11. **The Effect of Tire and Rim Sizes in Cornering**—Cornering stiffness is often a function of tire/rim size, aspect ratio, and width. As has been mentioned earlier, higher cornering stiffness tires require lower slip angles to produce a given amount of lateral force. Lower slip angles means lower "induced drag" or scrub and less speed loss in cornering. The optimum rim width may also play a part in maximizing the total grip available from a given tire.
12. **The Effect of Roll Stiffness Distribution on Steady-State Cornering**—For a symmetrical car (50% weight on the front wheels, 4WD, etc.), the roll stiffness would ideally be the same on front and rear, if steady cornering were to be optimized. In 2WD cars, the drive degrades the lateral force capability at that end and the roll stiffness is biased toward the undriven end. Many suspensions (especially rear) have an anti-roll bar "built-in" (twist axles). These double-duty suspensions require care in calculating the roll stiffness.

13. **The Effect of Differential Type on Acceleration Out of a Corner**—With an open differential the lightly loaded inside wheel is free to spin up under power if enough torque is available. This limits the available acceleration. Limited slip differentials have been used with varying success. It is unlikely that the simple addition of such a differential will be successful. As with any major change, a period of development must be gone through to make the new set-up work. The type of limited slip differential chosen will be very important. Undesirable jerkiness occurs with many types and experience has shown this to be undesirable for combined acceleration and turning.

The locked rear end or spool is another common solution to the problem of wheel spin. Because the locked axle has high resistance to yaw, more front cornering power may be required to keep the car neutral. If all the turns are the same direction, stagger (differential tire circumference) may be used to "split the difference" between low drag when straight running and when turning.

14. **The Effect of Roll Stiffness Distribution on Acceleration Out of a Corner**—Roll stiffness is the easy way to change lateral load transfer distribution. For rear-wheel drive the tendency is to spin the inside rear; more roll stiffness on the front (less on the rear) will help this. On the other hand, acceleration from low speed can reduce the front tire load so much that the car plows.

For front-wheel drive, if the inside front wheel is spinning on acceleration out of a low-speed corner, more rear roll stiffness will help if the inside rear wheel isn't in the air.

15. **The Effect of CG Location on Straight Line Acceleration**—The CG location determines the point of wheel spin. As the CG is moved further rearward in a rear-drive car, the traction available increases. CG further forward in a front-drive car increases traction available. Traction is a problem at low speeds (low gearing = high torque) with high-powered cars and on slippery surfaces.

The need to move the CG to get traction with a FWD is exaggerated when compared to a RWD because load is shifted off of the front tires on acceleration. The CG should be as low as possible to minimize this undesirable weight transfer. All of the other requirements for a good handling car suggest that the CG should be toward the center of the car; the traction requirement of front-wheel drive forces a compromise in CG position. That is, put the CG as far back as you can and still get enough traction.

16. **The Effect of Anti-Pitch Characteristics on Straight Line Acceleration**—Rear-drive cars, especially those for drag racing, may profit from rear lift (anti-squat). This raises the CG and increases weight transfer to the rear wheels on acceleration. The lift effect is created by choosing the rear suspension attachment points to give a high pitch center; the torque reaction from the driving wheels lifts the car. On a FWD, such lift is detrimental to acceleration. Although anti-lift geometry is possible for the front suspension (namely, the wheel moves forward on bump) it leads to harshness and is generally avoided. Some

FWD front suspensions have lift built in (as an aid to good ride); this may be removed for high-performance use. On acceleration, the rear of a FWD will squat; there is no torque reaction available to counteract this.

17. **The Effect of Differential Type on Straight Line Acceleration**—If both tires are on similar coefficient pavement at similar vertical load, the differential type should not affect straight line acceleration capability (wheel spin limited). This is true of most independent suspensions and some torque tube solid axles. With solid rear axles this is not true because the wheel loads differ on acceleration.

With the differential partially locked, small differences in tire size may cause the car to pull on acceleration (especially true on some front drives). This can be diagnosed by swapping the tires; if it pulls the other way, the wheels are being locked to the same rpm by the differential and the tires differ in circumference.

18. **The Effect of Aerodynamics on High-Speed Braking**—Aerodynamic drag helps the brakes at high speed. As an extreme example the Formula One cars of a few years ago had enough aero drag to decelerate at two-thirds of a "g" at 170 mph with no brakes at all! The same ground-effects cars could brake at over five g's because of aero down load. The aero down load distribution front to rear will partially determine the best brake balance and this may change with speed.

19. **The Effect of Brake Balance on High-Speed Braking**—Best brake balance at high speeds will be different than at low speeds because of aerodynamic forces. If the brake balance is biased toward the rear (relative to the balance required for four-wheel simultaneous lockup), the rear wheels may lock and the car will tend to swap ends (hard to control at high speed). Brakes heat up when slowing the car, especially if the stop is from high speed. If different brakes are used front and rear, the brake balance may change as the car slows down and the brakes heat up, if the brake linings change coefficient of friction.

20. **The Effect of Aerodynamics on Combined Braking and Cornering at High Speed**—Aerodynamic down load (or lift) affects the stability of the car at high speed. If down load is available at the rear, it will help keep the rear wheels stuck down and make the car stable. If down load is available at the front, it will tend to destabilize the car and aid turn-in. An appropriate balance between aero down (or lift) loads must be reached.

21. **The Effect of Brake Balance on Combined Braking and Cornering at High Speed**—Best brake balance for high-speed turn entry is different than for straight braking. Too much braking on the lightly loaded rear degrades already marginal amounts of lateral force; this may lead to spin. For front-heavy cars ideal brake balance puts more braking on the front as the car corners harder. At high speed it is unlikely that the driver will want to get the tail out very much; it is generally better to go into high-speed bends with the front tires limiting slightly.

22. **The Effect of Aerodynamics on High-Speed Steady-State Cornering**—If there is down load available it will improve corner speeds. High-speed corners are often power limited: at full throttle the car slows down due to tire induced

drag (scrub). Aero down load will reduce tire slip angles (tire induced drag), but aero down load often adds aero drag. The question is: Is the reduction in tire drag more than the increase in aero drag?

At high speed the road load power (the power required to maintain constant speed) is much greater due to aerodynamic drag. The drive axle tire side force may be limited by friction ellipse effects.

Direct side force from vertical surfaces may also be used. This adds the aero induced drag to the tire induced drag and it is likely that the aero induced drag will be higher. In other words, direct aero side force may not be very useful on low-powered cars.

23. **The Effect of Aerodynamics on High-Speed Straight Line Acceleration**—Aerodynamic drag (and to a much lesser extent other losses) limits the top speed of cars. Lowering the drag will allow a higher terminal velocity. What is not so commonly realized is that at high speeds the available forward acceleration is a function of the air drag as well as the power. At high speed the air drag has a large effect on the available acceleration.

24. **The Effect of CG Location on Dropped Throttle in a Turn**—When the throttle is lifted in a turn, several things happen at once. Load is shifted onto the front wheels and off the rear wheels by engine braking. The amount of load shifted is determined by the CG height, wheelbase, and the motoring torque. The immediate effect of this load shift is to increase the front tire lateral force and decrease the rear lateral force. The key here is "immediate" because the load shift happens quickly enough that the tire slip angles stay the same. A careful look at tire data will show what is happening. The result is that the front end "tucks in" and/or the rear end comes out. In extreme cases the car will spin if the driver does not take corrective action. Lowering the CG reduces this effect.

25. **The Effect of Ride and Roll Steer on Dropped Throttle in a Turn**—When the throttle is dropped, the car pitches forward. It is possible to arrange the ride steer to change the wheel steer angles on pitch to reduce the effect of dropped throttle. Toe-out with bump travel on the front end will reduce the steer angle on the outside front wheel. This will reduce the front side force and lower the amount of tuck in. In moderate turns, some toe-in on rebound at the rear will reduce the effects of dropped throttle as well.

At high lateral accelerations it is not so easy to correct dropped throttle effect with ride steer. The rear tire slip angles need to be increased to give more lateral force to make up for the decrease in load. The problem is that the tire is almost at its peak already and increasing the slip angle may not increase the side force available. The problem with ride/roll steer is that it is undesirable for much of the rest of operation. In general, geometric and compliance steer effects are ineffective at high lateral accelerations.

26. **The Effect of Differential Type on Dropped Throttle in a Turn**—The differential type affects dropped throttle behavior. An open differential that distributes the torque evenly from side to side will probably have the least effect on dropped throttle behavior. A differential that remains locked (possibly due to some preload) when throttle is dropped produces a stabilizing yawing moment or “yaw damping” moment. Some limited slip differentials may put shock loads into the drivetrain when they lock and unlock. This can have effects that are hard to predict.
27. **The Effect of Dampers on Dropped Throttle Behavior**—When the throttle is dropped in a turn, the body of the car pitches forward and the loads on the front and rear track change over a short period of time. Soft dampers will stretch out this transient and the dropped throttle response will not be so sudden. Overall, however, soft dampers can have an adverse effect on control.
28. **The Effect of CG Location While Braking in a Turn**—When the brakes are first applied, a large amount of load shifts from the rear to the front axle. This changes the tire operating loads and side forces and the car tucks in. Lowering the CG reduces the load change on braking.
29. **The Effect of Brake Balance While Braking in a Turn**—The large transient effect of brake application is to transfer load forward and change the loads on the tires. Brake balance also can affect this transient through the friction ellipse effect. If the rear of the car is “coming around” too much on brake application, shifting the brake balance forward will reduce the side force available from the front tires and effectively increase the side force at the rear. Lockout or proportioning valves can change this behavior but require adjustment for different track friction coefficients.
30. **The Effect of Steering Axis Geometry on Poor Road Behavior**—Kingpin inclination and kingpin lateral position determine the scrub radius measured at the ground. It has become popular to design FWDs (in particular) with “negative scrub radius.” This tends to stabilize the car in straight running when the two wheels are on different coefficient surfaces under braking or traction. For poor-road straight running, this is probably a good thing.
- Undriven front axles ideally have a small scrub radius. This reduces steering torques due to one-wheel bumps. Unfortunately, large brakes and suspension links often conflict with centering the tire print on the kingpin. In this case the steering system must be designed to accept these shock loads.
- The caster angle and longitudinal kingpin location determine the trail. The trail is commonly measured on smooth surfaces but on rough roads the tire contact patch can effectively move forward and the trail disappear or reverse. To avoid this, extra trail may be an appropriate modification for cars that have little to start with.
31. **The Effect of Ride or Roll Steer on Poor Road Behavior**—Ride steer is a geometric effect which results in the wheels steering with ride motion. Ride/roll

steer is often built into production cars to influence low lateral acceleration handling. Small changes in the wheel steer angles will have little effect on the limit handling because the tires are nearly saturated. What ride steer will do is steer the car with bump travel when traveling straight; this is why most racing cars have been *bump steered*, the name given to the process of adjusting the steering linkage to minimize bump steer. This is especially important if the ride height has been changed from stock or the suspension geometry modified.

Ride steer and roll steer are closely related but they load the steering system (and box/rack mounts) in different directions depending on the detailed geometry. If there were no compliance in the steering system or suspension, ride steer and roll steer would be just a function of the wheel ride position to the chassis. In reality this is not often true.

32. **The Effect of Ride Rates on Poor Road Behavior**—The spring rates or ride rates must be chosen to match the terrain and the wheel travel must be chosen at the same time. A reasonable ride rate will keep the suspension off of the bump stops most of the time but not be so stiff that the bump stops are never reached (except on very smooth tracks). In fact, progressive bump stops may be considered part of the spring rate—a highly nonlinear part. Contact with a solid bump stop is upsetting to the car in any circumstance.

If nonlinear ride springing is used (often through “rising rate” geometry) it has the effect of a smoothly progressive bump stop.

33. **The Effect of Ride Height on Poor Road Behavior**—If the car is lowered it is likely that there will be less suspension travel. To keep from bottoming on rough roads, the spring rate must be raised or the dampers stiffened. This in turn will change the ride and handling. Changing the ride height (up or down) will often change the ride steer or ride camber characteristics.

34. **The Effect of Dampers on Poor Road Behavior**—The best damper settings (adjustable dampers) for rough road will control the body motion to keep the car fairly level but allow the suspension to follow the surface. Dampers adjustable in bump and rebound separately are best for this. It can be difficult to sort out the difference between dampers that are too stiff and springs that are too stiff.

35. **The Effect of Steering Axis Geometry on Steering Wheel Force and Ratio**—Steering forces (with manual steering) at the steering wheel come from the tire self-aligning torque, from the mechanical trail, and from steering gear friction. The forces at the wheels are divided by the steering ratio before they reach the driver; the forces can be very large at the front wheels in a turn. If any aspects of the steering geometry are changed it is likely to affect the steering force characteristics.

Some examples: If caster angle is increased the self-centering torque will increase. If kingpin inclination is changed the rise and fall of the front end with steering will change—this may affect steering forces at low lateral accelerations. The rise and fall of the wheels changes the diagonal wheel loading similar to

"wedge." If the scrub radius is changed the parking-lot-speed force levels will change. Simple changes like tire diameter, wheel offset, and ride height will affect the front-end geometry. If the steering ratio is not satisfactory, the steering arm(s) length can be changed. Bump steer may be changed by steering arm changes; in particular, changing outer ball joint height is a standard method of changing ride steer.

36. The Effect of Tire and Rim Sizes on Steering Wheel Force and Ratio—

Changes in tire cornering stiffness change the effective steering ratio. A tire that has a steep cornering force curve needs less slip angle for a given lateral force than a softer tire. The steer angle required for a given corner is the sum of the Ackermann angle (depending on radius-of-turn and wheelbase) and the slip angle; reducing the slip angle required "speeds up" the steering. Simply changing the rim width can change the cornering stiffness; changing to larger size or wider tires will likely raise cornering stiffness. Steering wheel force will be affected if tires are fitted that have different aligning torque characteristics.

37. The Effect of Steering Axis Geometry on Steering Kickback—

In general, race cars with little scrub radius will track well over rough roads. On smooth tracks, larger scrub radius (perhaps due to interference between wheel/knuckle/brakes) can be tolerated.

For the special case of FWDs, a slight amount of negative scrub radius gives the steering a self-correcting feature in straight line operation. If one wheel has more traction than the other while accelerating or braking, it would tend to yaw the car, but the difference in tractive force turns the front wheels slightly to compensate. This may result in small steering wheel motions on rough or slippery surfaces but the car will tend to keep tracking straight. For a front-drive race car with high power, negative scrub radius may not be so desirable because of combined cornering and braking/accelerating. The heavily loaded outside wheel will dominate the steering force and the driver may be fighting the wheel with power changes. Moving toward centerpoint steering will improve this.

38. The Effect of Differentials on Steering Kickback—

For FWD race cars. If any limited slip differential is fitted that locks-up or unlocks suddenly, it will be reflected to the steering. If there is any scrub radius, the change in drive torque will produce a torque about the kingpin which will be noticed at the steering wheel. Even with centerpoint steering a change in engine torque will change the tire self-aligning torque and this will change the steering force in a turn.

39. The Effect of Tire and Rim Sizes on Steering Kickback—

The early wide street tires had a tendency to "nibble"; that is, follow longitudinal ridges in the road. While this has been improved, the current use of very wide tires has brought it back. If this is a problem, little can be done but play with tire pressures or change to narrower tires.

12.3 Secondary Set-up

Table 12.4 refers to the numbered and lettered paragraphs that follow. This table shows some side-effects that can occur from a change in set-up. To use the table, enter on the left side with the proposed change and then refer to the lettered items to see the effect of this change on the various aspects of performance listed across the top of the chart. If nothing else, the wide variety of effects and consequences should highlight the fact that set-up is all about compromise.

1. Moving the CG Position

- A. Straight line braking will be best when the tires are evenly loaded. This means an aft CG is best for equal-sized tires. For a forward CG, larger front tires are needed for best braking. A lower CG will reduce weight transfer.
- B. Lowering the CG will reduce weight transfer (and improve performance) on turn entry (combined cornering and braking). The outside front tire will be the most heavily loaded. The best CG position is again aft for equal-sized tires, and moves forward as the front tire size is increased.
- C. The highest lateral acceleration (best steady-state cornering) will be had with a neutral car. For equal-sized tires this is easiest with a CG near center.
- D. For best acceleration out of a corner, wheel spin must be avoided. This implies a rearward CG position for RWD and a forward CG position for FWD. The FWD has a conflict with A-C above; higher-powered FWDs will need more weight forward; the acceptable range seems to be 60% to 70% (or possibly more) load on the front wheels as the power-to-weight ratio goes up. The upper end is appropriate for cars with 10 lb./hp or less.
- E. Again, the CG must be toward the drive wheels for traction.
- F. High-speed straight line stability implies understeer in the low lateral acceleration range. A CG forward of the neutral steer point is understeer and stable.
- G. Turn-in (transient response to step steer) will be improved as the CG is moved forward and the front tires do more of the cornering. Note that "turn-in" may also have other definitions.
- H. Dropped throttle tuck-in will be reduced by lowering the CG.
- I. Braking in a turn will result in tuck-in if the brakes are balanced aft. Lowering the CG will reduce the load shift when the brakes are applied, and reduce the size of the transient.
- J. Rough road tracking calls for an understeering configuration—forward CG location.
- K. Rough road cornering set-up will depend on driver style. For those who are content to plow around corners, a forward CG is appropriate. If a tail-out attitude is desired a more central CG location is called for.

Table 12.4 Key to Secondary Set-up Guide

	Steady-State Characteristics:				Transient Characteristics:				Control Characteristics:				
	Straight Line Braking	Braking & Cornering	Cornering	Acceleration & Cornering	Straight Line Acceleration	High-Speed Stability	Turn-In	Dropped Throttle in a Turn	Braking in a Turn	Rough Road Tracking	Rough Road Cornering	Steering Force & Ratio	Steering Kickback
1. CG Position	A	B	C	D	E	F	G	H	I	J	K	L	M
2. Roll Center Location		A	B	C			D	E	F	G			
3. Anti-Pitch Geometry	A	B		C	D			E			F		
4. Steering Axis Geom.		A	B	C		D	E			F		G	H
5. Camber Effects		A	B	C		D	E			F			G
6. Ride/Roll Steer	A	B	C	D	E	F	G	H	I	J	K		
7. Differential				A	B			C	D	E	F		G
8. Track Width		A	B	C				D	E	F			
9. Tire & Rim Sizes	A	B	C	D	E	F		G	H		I	J	
10. Ride Spring Rates	A	B	C			D			E	F			
11. Roll Stiffness and Roll Stiffness Dist.		A	B	C		D	E	F	G	H	I		

- L. Moving the CG forward will increase the steering force at low speeds (parking) and also in corners as there is more lateral force at the tire and thus more moment about the kingpin.
- M. If a front-drive car is lowered to lower the CG, the driveshaft angles will change. This means that different amounts of torque reaction (likely more) will be present at the hub and thus in the steering. If the driving torque varies from one side to the other, kickback in the steering will be present.

2. Moving the Roll Center Positions

- A. Lowering the front roll center or raising the rear will make the rear take more roll couple and the rear will saturate sooner. Balancing the brakes to give more on the rear may have the same effect.
- B. As 2A but not confused with brake balance. The roll center locations will probably not be easy to change once the car is built; they need to be considered at design stage.
- C. For best acceleration for a FWD car out of a corner the front wheels need to be evenly loaded. This will happen if the rear is taking as much roll couple as possible, when the inside rear wheel is off the ground. A rear roll center higher than the front will help achieve this. The situation for the rear drive is just opposite.
- D. During turn-in, the roll center heights determine the proportion of lateral load transfer that is passed through the suspension linkage. The rest of the load transfer is passed through the springs and anti-roll bars as the vehicle rolls. Raising the roll centers gives an anti-roll effect and reduces body roll. High roll centers lead to jacking (the whole car rises when lateral force is applied) and lateral wheel travel on bump; these are undesirable.
- E. Dropped throttle tuck-in will be decreased if the rear roll resistance is reduced or the front increased. This can be done by lowering the rear roll center or raising the front roll center. This will make the car more understeer; more of the total roll moment will be resisted on the front.
- F. Tuck-in under braking in a turn is similar to dropped throttle. The problem is always present in cars that are balanced near neutral steer at zero longitudinal force. In FWDs there are conflicting requirements for traction out of the corner which call for even front wheel loads (low roll center height).
- G. Rough road tracking will be best when the suspension contributes the minimum disturbance to the vehicle. Roll centers near the ground give low lateral wheel motion with ride travel and minimize lateral “shake” on rough roads.

3. Changing the Anti-Pitch Geometry

- A. Adding some anti-dive to the front will reduce the pitch down on braking; likewise anti-lift will stop the rear from rising on braking. Anti-pitch is roughly analogous to the anti-roll effect that comes from raising the roll centers. The body attitude (pitch) will have little effect on the amount of braking available unless the car pitches so much that the suspension travel is used up and the wheels are against the bump stops; tire traction decreases when the load is fluctuating. Some dive is desirable as a cue to braking level, according to competition drivers.
- B. Anti-dive geometry puts braking loads through the suspension and tends to add stiction to the suspension. This is usually not desirable.

- C. Anti-squat (RWD) and Anti-lift (FWD) geometry is similar; engine torque reaction changes the ride height. Some FWD sedans come with the opposite—the suspension pick-up points are such that the front wheels move back on bump travel. This is done to improve ride but has the side-effect that the front end rises on acceleration. Excessive pitch on turn exit is probably undesirable.
- D. Anti-pitch geometry affects the absolute amount of traction available on a rear drive in two ways. By increasing the transient loading on the drive wheels it may help prevent wheel spin, and by raising the CG height it promotes rearward weight transfer. Tractive force “anti’s” work on engine torque reaction. On RWDs, the front end will rise on acceleration since no anti-effect can be incorporated. On FWDs, the rear end will lower on acceleration for the same reason.
- E. The transient when braking in a turn will be more sudden if anti-dive is added. With more anti-dive, more of the load shifted to the front wheels (from the rear wheels) will be carried in the suspension members and less in compression of the springs.
- F. When anti-dive/lift is added to the front suspension, it may have the side-effect of changing the trail and/or caster angle with bump travel. This will change the steering force with ride height—not desirable.

4. Changing the Steering Axis Geometry

- A. In combined braking and cornering the outside front wheel is heavily loaded and it will dominate the steering torque. In conventional FWDs, negative scrub radius (kingpin axis intersects the road outside of the center of the tire patch) will tend to give steering in the oversteer direction. The opposite is true of positive steering offset, as used in most rear-wheel-drive cars.
- B. In steady cornering the trail and the pneumatic trail (aligning torque) determine the steering force. More trail equals higher force level and more spin back. Too much trail will mask the aligning torque. The self-aligning torque is a valuable signal of front tire breakaway; it first increases with lateral force and then decreases or reverses as the tire reaches its limit. With a modest amount of trail the driver can sense this as a reduction in steering force.

Reverse-Ackermann geometry (usually obtained with the steering linkage in front of the front axle) will give more steer angle to the outside front wheel than the inside. This is appropriate for high-performance use because the outside wheel has more load on it and reaches its peak at a higher slip angle than the inside, lightly loaded wheel. With conventional Ackermann steering geometry the inside front tire is dragged around corners at a slip angle over its peak. Parallel steering may be a reasonable compromise for cars that will be street driven. Reverse-Ackermann results in high rolling resistance at low lateral accelerations.

- C. For FWDs, as in the braking case, negative scrub radius is not useful when accelerating out of a turn. In this case the outside wheel dominates and steers in the un-

- dersteer direction—the FWD is almost certainly understeering enough at this point already.
- D. For high-speed stability in the presence of road disturbances, zero or slight negative scrub radius is desirable.
- E. In tight turns, turn-in will be helped if the kingpin inclination (front view) and the caster angle (side view) are large. This gives negative camber with steer on the outside wheel which helps front adhesion. It is important to put this in perspective by finding out just how much steer the driver uses on the track; the effect is very small at small steer angles.
- F. Rough road tracking is good with negative scrub radius. A random longitudinal bump load on a front wheel will tend to yaw the car and at the same time the wheel will steer to counteract the yaw moment.
- G. Steering force goes up as trail is increased. Steering force at parking speeds goes up as scrub radius decreases—highest at centerpoint steering. If the steering arm is changed in length, the steering ratio is changed and it is likely that the amount of Ackermann (or reverse Ackermann) is changed.
- H. As the scrub radius moves away from centerpoint steering the amount of steering kickback will increase.

5. Changing the Camber—Note: Camber effects are much less with radial tires than with bias tires.

- A. The camber on turn entry is affected by the roll camber, ride camber, lateral force compliance camber, steer-camber (on the front), and the static camber. It is unlikely that the camber will be correct over the range of combined operation, from hard braking / light cornering to hard cornering / light braking. It is common to use temperature across the tread as an indicator of a good camber setting but this is only an average of a range of conditions.
- B. Camber has been found to affect tire performance over the whole slip angle range. The correct negative camber will optimize the tire lateral force. For oval tracks or other circuits where the car turns one way, both wheels can be “leaned into the turn.”
- C. On turn exit, plow is often the problem. The actual camber is a function of those items mentioned in A. above. Ideally the camber would change from best camber for cornering at the apex to zero for acceleration once the turn is finished. In reality the tire is not often at “best camber.”
- D. Camber thrust increases with load. Consider a pair of negatively cambered front wheels: when a disturbance transfers some load to, say, the left wheel, the left tire camber thrust to the right increases and the car starts to turn right. This in turn increases the load transfer to the left and so on. To counter this tendency to wander,

a little toe-out is often necessary (depending on the tire construction this might be on the order of 10% of the camber angle).

- E. For best turn-in the front tires probably want to be at best camber before the turn starts. This implies that static camber be set fairly high. If the turn is initiated under braking the ride camber from pitch down will add.
- F. If the suspension design gives much camber change with ride travel the camber thrust that results will give poor rough road tracking.
- G. If the suspension design gives camber change on bump travel the steering will kick back (or possibly tramp/shimmy) over bumps. This is because the wheels act as gyroscopes and the reaction torque to a camber change is around the kingpin. This is a problem with suspension designs that have rapid camber change with one wheel bump, like solid axles and swing axles; it is also possible to get short swing arm lengths with independent designs in the search for "camber compensation" to correct for camber "lost" due to body roll angle.

6. Changing the Ride/Roll Steer Characteristics

- A. Under hard braking, ride steer will only disturb the car. If the wheels steer (toe) with dive (on the front due to braking) they will be using up some of the friction circle fighting against each other.
- B. Roll and ride steer will change the attitude of the car in racing-turn entry but the tire slip angles (except for effects that steer one side more than the other) will stay the same. This is not the case for maneuvering below the limit where the under/oversteer can be greatly modified by ride and roll steer.
- C. In limit cornering, steering the wheels with roll steer (front or rear wheels) will simply cause the car to corner at a different attitude angle to the path. In sublimit maneuvers, it is this reorientation of the car that drivers sense as roll understeer or roll oversteer.
- D. In turn exit (at the limit), the front tires will be saturated due to light load (unless traction is broken with excess power on the rear). Changing the angles of front or rear wheels will not change the fact that the rear tires still have margin left while the front tires are limiting.
- E. As in braking, it is important that the tires are pointing straight ahead for best traction. Any ride steer with pitch (due to longitudinal acceleration) will only hurt performance.
- F. If the front wheels steer on one wheel bump (ride steer) the car will not track well, especially if high cornering stiffness tires are fitted. With racing tires, small steer angles can give surprisingly large side forces.
- G. Roll steer can modify the amount of steering required for turn-in. To give an example, as a car with roll understeer is turned-in it begins to roll, the body-roll

steers the wheels out of the turn, and the driver must add more steering to compensate.

- H. At lower lateral accelerations, ride/roll steer can influence dropped throttle behavior. When the throttle is dropped in a turn, the car pitches forward and roll understeer (front end) will correct for the tuck-in. At high lateral accelerations, steering on the rear will have little effect—the rear tires are unloaded and will be at or near their limits. Roll understeer on the front may tend to alleviate tuck-in.
- I. Ride/roll steer can affect the car while braking in a turn if the tires are not saturated (low braking and lateral forces). The situation is similar to dropped throttle. In maneuvers near the friction circle limit, roll understeer will have some effect if used on the front of the car. Load and camber are the variables that affect the size of the friction ellipse, not steer angle.
- J. Ride or bump steer is very distracting when trying to negotiate a rough road, especially with tires that have high cornering stiffness.
- K. For rough road cornering some roll understeer may be desirable. As an outside tire hits a bump the load on it (and the side force it is producing) increases. If the front wheel steers out as it moves up it will tend to compensate and the car will tend to hold a smooth path. On the rear, toe-in with bump has a similar effect.

7. Different Types of Differential

- A. When accelerating out of a corner the drive wheels are unevenly loaded and traction on the inside wheel is limited to a lower value than the outside wheel. Different types of differentials are available which may help in this situation. Ideally, both drive wheels would be fitted with an anti-spin device that would apply the maximum driving torque to each tire, given the load and slip angle of operation. The inside wheel wants to be at a lower rpm (less load and smaller radius of travel) than the outer but this seems to be beyond the computation ability of mechanical devices. The best that limited slip differentials will do in this situation is lock the two axles to the same speed. The worst type of differential for this situation is the standard "open" diff; it will allow the inside wheel to spin up and limit the driving torque on each wheel to that of the spinning wheel. A full treatment of types of differentials is found in Chapter 20.
 - B. For independent suspensions the differential is less critical for straight line acceleration. Loads on the tires are even (independent suspension) and the same torque is applied to each axle. If the two wheels are locked together, small differences in tire size may steer the car. This acceleration-torque-steer is found primarily on FWDs due to compliance and asymmetry in the steering and suspension.
- For solid axle suspension, the wheel loads are uneven on acceleration unless some torque reaction device is used. A limited slip differential or spool certainly helps in this case.

- C. When the throttle is dropped in a turn, the front tires are loaded up and they produce more side force (destabilizing) than they did when the power was on. An open diff probably has the least effect in this situation; the driving torque (present before the throttle is dropped) and the motoring torque are split evenly between the drive wheels. If the drive wheels are locked (or partially locked) under power (by a limited slip diff), and they unlock when the power is removed (a characteristic of certain differentials), relatively more side force will suddenly be available. A diff that remains locked with the throttle dropped will add "yaw damping."
- D. While braking in a turn it is most desirable to have anti-lock. Barring that, a differential that keeps both wheels turning at the same speed (regardless of braking) will help prevent lockup. This would be one of the fixed preload types of limited slip.
- E. For best rough road traction (and probably directional control) some sort of anti-lock differential will keep an unloaded wheel from spinning up and then disturbing the car when it lands.
- F. For FWDs, a limited slip differential may be some help in rough cornering. On the minus side a differential that is locking and unlocking the front axle will make steering difficult. Ideally the limited slip differential would be smooth in operation.
- G. For FWDs, any type of differential that dynamically changes the torque on the two wheels will give a steering reaction. This reaction will add to any torque reaction caused by angularity of the driveshafts due to steer angle or other misalignment such as that caused by ride travel.

8. Changing the Track Width

- A. Increasing the track width reduces the load transfer on turn entry. With the tire loads more evenly distributed the tires can produce more force (load sensitivity).
- B. In steady-state cornering the track width and the CG height determine the total lateral load transfer. Increasing the track reduces the load transfer. This will improve lateral acceleration capability.
- C. If the track is increased the load transfer is decreased and this may allow more of the total roll resistance to be taken on the non-driving end of the car before wheel lift. This will give more equal loads on the drive wheels for acceleration on turn exit.
- D. Increasing the track will improve the braking in a turn performance by increasing the max lateral force available.
- E. Bumpy road tracking may not be improved by a track width increase. The yawing and rolling moment from hitting a one-wheel bump is increased and the car may tend to be re-aimed more severely than with a narrower track.

- F. Track width increase will help rough road cornering. More even wheel loads improve tire performance. Less lateral load transfer gives less body roll and this means there is more suspension travel available before hitting the bump stops.

9. Tires and Rims

- A.-H. Tires dominate race car chassis set-up. Small changes in tire performance through tire (or rim) width, compound, pressure, camber, load, ambient and track temperature, stagger, etc., are always happening, even when not desired. In general, the end of the car that is limiting performance is the one that needs improved grip, and occasionally this can be found. If the car cannot be balanced by improving one end, it may be balanced by degrading the other end; this is commonly done by increasing roll stiffness, etc.

Improving the tire performance on the non-limiting end is less likely to improve overall performance, except on power-limited high-speed turns where any reduction in slip angles reduces the tire induced drag.

- I. Steering torque at the kingpin (ignoring steering system losses) is a function of front end geometry and tire self-aligning torque. If the trail is not so large that it swamps out the self-aligning torque, changing tire size or construction will likely change the steering force characteristics. The effective steering ratio (at the steering wheel) includes the tire cornering stiffness. For example, radial tires usually have higher cornering stiffness than bias tires and they require less steering wheel motion for a given maneuver (at speed).
- J. Steering kickback can occur with very wide tires. This nibbling over ridges in the road was severe in the past but has been much improved by changes in tire design. Very wide (50 or wider series) tires may still nibble in certain situations.

Often, wide rims have different offset than stock rims and do not preserve the original scrub radius. If the center of the print is not near the kingpin intersection with the ground, steering kickback can be expected on rough roads.

10. Changing the Ride Spring Rates

- A.-C. Ride spring rates affect the lateral load transfer distribution. Lowering the ride rates on one end will even out the loads on that end (assuming that both wheels are on the ground) and this will raise the lateral force available from that end of the car. Stiffer springs than fitted to production cars generally limit the amount of body motion in pitch and roll and this is desirable for racing. Race cars often wind up with the undriven end very stiffly sprung relative to the driven end; this keeps drive wheels more evenly loaded for traction.
- D. Stiffer springs will speed up the response in turn-in. With stiffer springs the car does not take as long to get to steady-state roll angle and this aspect of the trans-

sient is improved. For cars that have poor suspension geometry (excessive ride steer and ride camber), stiffening up the springs effectively removes some of the "disturbance" from these effects.

- E. For rough road operation spring rates are very important. It is necessary to take advantage of all of the suspension travel to keep the wheels on the ground as much as possible. If a flat ride (that is, the car lands flat after crossing a bump) is desired the spring rates must be adjusted to give slightly higher undamped natural frequency on the rear than on the front, i.e., approximately 10% stiffer on the rear. This often is not possible because of the high front spring rates required for front roll stiffness.
- F. Rough road cornering is influenced by the smooth surface behavior (under/over-steer). However, if one end of the car is more stiffly sprung or has higher unsprung weight, the wheels on that end will spend less time on the ground and that end will limit performance. If the springs are not stiff enough the car may hit the bump stops with a combination of roll in a turn and one wheel bump.

11. Adjusting the Roll Stiffness and Roll Stiffness Distribution

- A. If the car is loose on turn entry (and the driver cannot make use of this effect), more front roll stiffness (or less rear) will make the rear tire loads more equal and help the problem, if all four wheels are still on the ground.
- B. Adjusting the anti-roll bars is a common way to change the stability of a car in a steady turn. This works through the load sensitivity of the tires—a pair of unevenly loaded tires has degraded lateral force performance compared to the same tires with the same total load split evenly between them. Thus, to degrade lateral force capability of the front end of a car the anti-roll bar is stiffened on that end. This works until the inside front wheel is off the ground and the front track can provide no additional roll moment.
- C. For best traction on acceleration out of a corner the drive wheels need to be evenly loaded. Taking as little roll moment on the driven wheels as possible gives the desired effect—low roll stiffness on the drive axle. However, if the roll resistance of the suspension is reduced too much, excessive body roll will become a problem.
- D. Anti-roll bars do not have much effect at low lateral accelerations (low amounts of lateral load shift to distribute between the front and rear tracks). If straight running is a problem, it is unlikely that changing the roll couple distribution will help.
- E. Stiffening the car in roll will improve turn-in by reducing the roll angle of the car (and the time to get the car set to a new roll angle).
- F. If the car has a large dropped throttle response, increasing its basic stability will give a greater margin before spin (by increasing the rear grip available). Higher front roll stiffness (or lower rear roll stiffness) will accomplish this. Higher total

roll stiffness reduces transient response time by increasing the rate that load changes occur at the tires.

- G. Braking in a turn adds a large forward load shift to the lateral load shift due to cornering. This degradation of rear grip is sometimes used by drivers to get vehicle slip angle on turn entry. Roll stiffness tuning is effective in changing the stability because it changes tire operating conditions, for example, increasing the roll stiffness will reduce the body roll angle and this in turn may give more favorable tire camber (and more grip).
- H. For best rough road tracking, little additional roll stiffness (beyond that from the ride springs) is desirable. Anti-roll bars attempt to force the wheels on an axle to move together; this reduces the independence of the suspension action and increases the one-wheel bump rate.
- I. H, above, is true for rough road cornering as well. Best grip is with the four wheels following the road. If the car rolls so much that suspension travel is used up on the outside wheels then the roll stiffness must be increased.

Historical Note on Vehicle Dynamics Development

"Progress, far from consisting in change, depends on retentiveness... Those who cannot remember the past are condemned to fulfil it"

George Santayana
Life of Reason, 1905-6



The major developments in automotive vehicle dynamics technology have taken place in the last 60 years—within the lifetime of a number of the principal contributors. The core activity occurred at General Motors or under its sponsorship, with numerous contributions from other sources, notably Goodyear and Dunlop, and other tire and car companies. With a few exceptions where a racing motivation existed, the objective of these developments came from a desire to better understand passenger car behavior.

Vehicle dynamics is an exciting subject particularly if one has been involved in its development. Our participation started in the late 1940s and has continued through to the present. During this period we have had an opportunity to meet, know and work with many of the pioneers. In the present chapter we will attempt to give the reader a first-hand account of some of the key personalities—in part in their own words—and their

accomplishments. Hopefully we can impart some of the atmosphere which prevailed as each new advance in the picture fell into place.

This chapter is by no means a complete history of vehicle dynamics development but rather a personal account as we have experienced it. We have chosen to cut off these notes at around 1985. Before that time much of the basic theory had been developed as well as some comprehensive models and computer programs used on mainframes for research and development purposes. With the advent of the personal computer, circa 1980, we were to see a major step forward in the application of the theory to vehicle design problems. Only recently have vehicle dynamics tools been exploited at the conceptual design level.

For a more detailed account with references to the literature, see the first paper in Ref. 92 and Ref. 145.

Bill Milliken

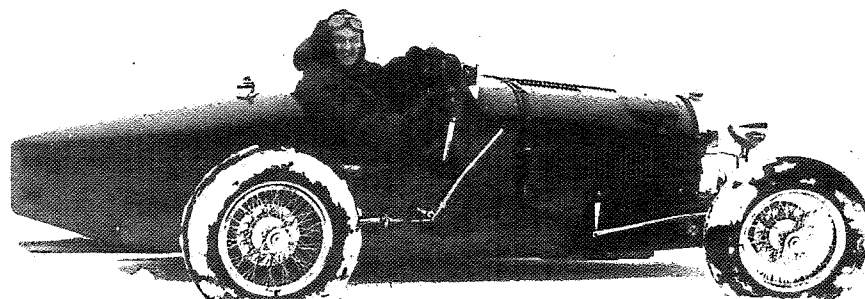


Figure 13.1 Bill Milliken and Type 35 Bugatti.

For me it all began when I drove my newly acquired Type 35 Bugatti up in front of the old Flight Research hangar of the Cornell Aeronautical Laboratory (CAL) in Buffalo in the fall of 1946. In those days, I was manager of Flight Research and we were engaged in some very advanced aircraft dynamics research for the Air Force. This resulted in the first ever frequency response measurements in flight and the invention of the variable stability airplane, the predecessor of fly-by-wire flight control systems of modern mili-

tary and large commercial aircraft. I kept my Bugatti in the flight hangar and took advantage of the top technicians to maintain it.

The post-war resurgence of road racing in this country had not yet started so I entered the Bug in the only alternative, the 1947 Pikes Peak Hill Climb, and then in 1948 in the first Watkins Glen event on the old circuit. It was the beginning of 15 years and 110 races with a variety of interesting machinery including two four-wheel drives and an early installation of a torque converter in a race car. But more importantly it led to a research program in automobile vehicle dynamics.

One doesn't engage in motor racing for long to realize that handling is a vital part of success. Dave Whitcomb, one of our top dynamicists in Flight Research, had also engaged in racing and we soon became interested in what was known about the vehicle dynamics of automobiles. Automobiles had been around longer than aircraft and we imagined that there must be a "textbook" which would answer the questions that arose from our racing experiences. A literature survey was not too revealing, so in 1952 we decided to satisfy our curiosity by a visit to several car companies in Detroit. Our meeting at the GM Proving Ground proved crucial.

Although we didn't appreciate it at the time, the GM group at the meeting, consisting of Maurice Olley, Bob Schilling, Ken Stonex, von Pohleus, and Tom Carmichael, was responsible for much of the progress that had been made in vehicle dynamics to that date. Since we had called the meeting I was asked to recount our work in aircraft dynamics. Suddenly, in the course of this recitation, Olley literally jumped to his feet and shouted, "We should do it," meaning, as we soon found out, that GM should engage our services for applying techniques successfully used for aircraft to the automobile—specifically for the analysis of transient behavior. Thus it was that the next day found us with an initial \$25,000 contract to be administered by Bob Schilling, Head of the Mechanical Engineering Department in the GM Research Laboratory Division. This funding increased to about \$100,000/year until, in 1958, we received a five-year contract for \$0.5 million. But before recounting GM's in-house activities during this period and ours at CAL, let us turn to the pioneering work of Maurice Olley and his associates in the preceding 20 years, namely 1930-1950.

It is difficult to describe the immensity of the accomplishments of the Olley group during those years. They were starting from state zero with only meager experimental and analytical tools. But Olley had a strong grounding in the fundamentals of mechanics and the pragmatic approach of a practical engineer, plus an enthusiasm and imagination that knew no bounds. By simple experiment, by some simple analysis, and by a great deal of thinking, he was to lay the foundation for all that followed. The Olley story deserves a book; we at CAL had started one under GM sponsorship which we had hoped to finish before his death in 1972. Unfortunately it was curtailed for possible litigation ramifications and has yet to be written. The next section is an abstract of parts of our draft.

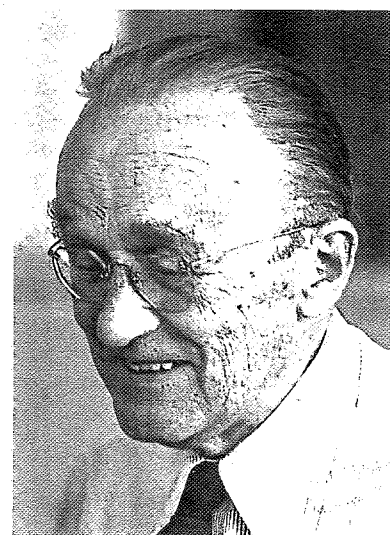
Maurice Olley

Figure 13.2 Maurice Olley.

Maurice Olley's life coincided with the development of the automobile. Born in 1889, only four years after the original Benz gasoline-powered tricycle, he was, to quote from his own "Reminiscences," practically raised on the Holyhead Road in North Wales. He was to write that:

...this was the highway from London along which the Royal Mail coaches had travelled with the Irish mail, before the railways came. It was one of the historic roads of the Island, meeting up on the English plain with the great Roman road system, up which the military supplies came to Chester and the Wall, the very frontier of civilization. But this highway lay white and silent, grass-grown along the edges and almost empty of life. It served as a convenient playground and cycle track and a connecting road for farmers. But at the turn of the century [when Olley was approaching his teens], the Holyhead Road began to show signs of reviving life. What young boy would not have been interested in these strange vehicles, conducted by people wearing goggles and overalls, usually very dirty? The contraptions were obviously unreliable. They frequently stood at the roadside, regarded skeptically by their owners. Then, after furious effort with a starting handle, which looked like winding up an oversize clockwork toy, would burst into heaving life and explode themselves away out of sight.

That early excitement and enthusiasm for the automobile characterized Olley's entire life. Having served a five-year apprenticeship as a machine tool builder, he went on to the drawing office at Rolls-Royce and subsequently to work as a designer for Sir Henry Royce. There he designed everything from generators to connecting rods, reduction gears, and office furniture. World War I found him in the United States as liaison for Rolls-Royce's participation in the Liberty engine program. Then after the war he served in various engineering capacities with Rolls-Royce in Springfield, Mass., when they decided to build cars in this country. That enterprise ended in 1930, and Olley, then 41 years of age, found himself in Detroit where he joined Cadillac.

The next ten years were probably the most interesting and creative ones in his entire career. He was to note that in the 25 years preceding his affiliation with Cadillac, the engineers had ruled the roost.

That uncertain contraption of 1905 had become the classic design of automobile, an almost perfectly reliable mechanism, but built by engineers to please themselves, and with little or no regards for the passengers. There had been sporadic attempts to make the vehicle ride decently, but little had been done. The rear passengers functioned as ballast, stuck out behind the rear wheels. Steering was frequently unstable and the front axle with front brakes made shimmy almost inevitable. All of the parts functioned perfectly but when put together the whole was seldom satisfactory. So, from there onward, there was a continual struggle to improve the vehicle as a **whole**.

Many of us remember Olley for his handling work but it is important to realize that his contributions in that area came about as part of his concern with the automobile in its totality. His interests ranged from technical details and production processes, to its functional and appearance aspects, and on to its philosophical impact on society.

In the 1920s Rolls-Royce had become intensely interested in ride. In those days British roads were smoother than those on the continent or in the United States and complaints were received from their export customers. Olley was aware of this and was determined to find ways of improving ride when he joined Cadillac. Although he was guided by the theoretical work of Rowell and Guest (Refs. 134 and 54), his approach was essentially experimental. Thus, he introduced the first bump rig into Detroit for producing synthetic ride in the laboratory and he swung vehicles to determine their pitch inertias. Finally, in 1932, he built his famous "K² Rig," a large limousine on which by movable weights front and rear he could "produce changes in relative deflection of the front and rear springs and in the moment of inertia." Henry Crane, Alfred P. Sloan's principal technical advisor, was a friend and frequent passenger in the K² vehicle. No instrumentation was used, as at that stage they were attempting to evaluate those characteristics which subjectively produced the best ride.

In Olley's words, "the K² rig was telling us, in no uncertain terms, that a **flat ride** was desirable and possible with softer springs on the front than on the rear." But softer

springing on a beam axle had inevitably led to shimmy and questionable handling. They soon concluded that independent front suspension was a next logical step and implemented this conclusion in two experimental Cadillacs, one with a Dubonnet and the other with a double wishbone type. L.P. Fisher liked to accuse Olley of being the first man at GM to spend a quarter of a million dollars on two experimental cars!

The idea of independent wheel suspension was not new. As Maurice Platt, former chief engineer of Vauxhall pointed out, Hans Ledwinka of Tatra must rank as the principal pioneer of independent suspension, having produced a successful vehicle with four-wheel independent as early as 1925, with Daimler-Benz following in 1930. Olley was aware of Sensaud de Lavaud's 1928 paper on "The Problems of Independent Rear Wheels," although Olley cautioned, "don't be deceived by his beautiful use of the French language—not all of his theories are sound."

In any event, the experimental Cadillacs were ridden by engineers and executives of the corporation and there was agreement that they offered something very special in the way of ride and handling. Cadillac adopted the suspension, followed by Buick, Chevrolet, Oldsmobile, and Pontiac, circa 1933. O.E. Hunt, Vice President of Engineering at Cadillac, had tried to dissuade Chevrolet, claiming there weren't enough centerless grinding machines in the whole U.S. to grind the wire for the coil springs, but Bill Knudsen went ahead anyway and Boss Kettering stated categorically that "we can't afford not to do it."

Thus, in three short years after reaching Cadillac, Olley became responsible for the introduction of the independent front suspension in the United States. In March 1934, he presented his SAE paper entitled, "Independent Wheel Suspension—Its Whys and Wherefores." Bob Schilling, one of the pioneers in handling and an associate of Olley's, referred to the independent suspension development as "an enormous engineering accomplishment—a mixture of systematic experiment and reasoning—a classical example of the scientific method and proper engineering—the beginning in fact of real suspension engineering." It was also the beginning of a systematic attack on automobile stability and control.

With the independent suspension came handling problems associated with steering geometry, roll steer, compliance effects, etc., not encountered before, nor was the wishbone suspension completely free of shimmy. In the early application of the short long arm suspension (SLA), numerous steering system problems were common. Olley and his associates at Cadillac tackled these handling problems with the same thoroughness and enthusiasm that had enabled success in ride.

In 1925, the Frenchman George Broulhiet had advanced the tire slip angle concept in a paper entitled, "The Suspension and the Automobile Steering Mechanism." Subsequently, three Germans, Becker, Fromm, and Maruhn, in an investigation of the vibration of automobile steering mechanisms, performed tire measurements on a rotating steel drum, showing the relationship between the tire forces and the slip angle and load. Olley was

aware of this work and requested similar measurements of R.D. "Cap" Evans at Good-year. Evans' work marks the beginning of tire drum testing in this country. Olley has noted that he was also familiar with Ralph Moyer's early skid resistance measurements at Iowa State, circa 1934, and the work of Bradley and Woods in England on the motions of vehicles with locked wheels, 1930.

It is not easy to summarize the activities of the Cadillac group in the 1934-39 period since they involve so many parallel explorations and investigations. It must rank as one, if not the most, creative periods in the history of automobile handling and out of it came the conceptual basis for handling design to the present day. Olley had surrounded himself with such men as Bob Schilling, von Pohlemus, and Henry Fuchs, and together they represented a formidable experimental and analytical team. Unlike much intensive development work, it was well documented, much of it by Olley himself, replete with bits of philosophy and "Olleyisms" such as: "In automobile design a straight line is the most awkward path to follow between two points."

In 1934 Olley produced a small internal report entitled, "Stable and Unstable Steering." In it he considers what happens when a lateral force disturbance is applied at the CG. Based on the tire tests of Evans, he works out the simple oversteer/understeer equations and derives the expression for critical speed. They had coined the term "oversteer" in 1931 observing that "a car which had steering geometry such that when it rolled to the right it steered to the left, could not be safely handled on the road." He now extended the concept to include the effect of weight distribution and tire characteristics. When a side force is applied to a car, if it turns away from the force it is oversteering, and conversely for understeering. The Bundorf/Leffert Cornering Compliance Concept, still widely used in design for assessing the contribution of understeer factors, is related to this Olley view of understeer. In the same report, Olley concludes that the camber effect of SLA suspensions is stabilizing on the front but destabilizing on the rear. He also discusses geometrical roll steer, overloaded rear tires, and the fact that compliance in the steering may be a useful design variable when cars are basically more stable. But this report is specifically mentioned as perhaps the earliest in the literature to discuss oversteer/understeer.

In 1937 Olley reviewed the handling activity of the preceding few years in a report entitled, "Suspension and Handling." By any standards the work that this represents is an impressive accomplishment. Conceptually and in terms of physical understanding it covers a large part of what is used today in handling design.

Some of the subjects covered were:

1. Understeer in relation to straight running.
2. The effects of load, pressure, traction and braking, and drum curvature on lateral force tire data.
3. The slip angle as the principal cause of tire wear.
4. The aligning torques due to slip and camber and the variables affecting them.

5. Parallel versus Ackermann Steer.
6. Stabilizer bars and their use on front and rear.
7. Factors contributing to understeer.
8. Steering effort in relation to straight running and how the aligning torque working through the compliances can improve directional sense.
9. The geometric steers.
10. Skid pad tests.
11. "Handling" as composed of a *car* part and a *driver* part.
12. The distribution of the roll couple.
13. The tire load and load transfer sensitivities.
14. Problems of combined ride and handling.

By 1937 the skid pad, an innovation by the Cadillac group, was a well-developed testing tool. Page after page of plots of steering angle versus speed on the circle are extant. Tests were performed on their own cars and many competitive ones for a great variety of off-design conditions. There was much to be learned from these tests and, as Olley wrote to a colleague at Vauxhall, "don't let anyone persuade you that the skid pad tests don't mean anything. They mean pretty nearly everything if we will just take the trouble to interpret them. I am bedeviling Bob Schilling and Henry Fuchs on their interpretation." He later notes that his objective is to predict skid pad results for new cars from known tire and vehicle data. It should also be mentioned that by this time results were coming in from Dr. A.W. Bull's tire tests at U.S. Rubber, again inspired by Olley. These were the earliest data in this country on traction/braking and drum curvature effects, and were later published in "Tire Behavior in Steering," SAE 1939.

From their skid pad tests, Olley was gradually building up a specification for a desirable handling car, concluding at that time that an understeer of at least $2^\circ/g$ was needed in the linear range and that the curve should turn up smoothly at the end to give modest plow at the limit. The roll angle should not exceed 6° . In addition, he was beginning to look at factors important to the driver such as centrifugal caster, friction, and steering flexibility—in short, steering effort and centering. Finally, he discusses wind handling, a subject receiving some impetus through Dr. Kamm's work at the Stuttgart Research Institute for Vehicle Sciences, initiated in 1925 and continued up to World War II.

In summary, Olley stresses their objective as achieving a car with a sense of direction (on-center handling, as we call it today) and a car that can be maneuvered easily under all conditions.

There are many colorful stories which have come down from this period of handling activity. One day Olley, Phil Pretz, and Bill Burnett, while testing a car, crossed a railroad track just missing a train. Olley stuck his arm out a window, pointed a finger at the engi-

neer and yelled, "Here's one you didn't get, you old S.O.B.!" On another occasion to emphasize some aspect of driver behavior, he challenged an associate to drive a car with a reversed steering gear such that steer to the left gave turn to the right. The associate performed surprisingly well on this car, got into his own vehicle, and crashed!

It may appear as if Olley's concentration was exclusively upon steady-state handling; far from it. From the beginning he was greatly concerned with the transient conditions of turn entry and maneuvering, and by 1938 he and Bob Schilling had a clear, if qualitative, picture of what went on after a step steering input. In a remarkable document entitled, "Handling Factors—1938," Schilling describes in much detail the sequence of events for cars of various characteristics following a step input. The presentation shows path and attitude variations and the characteristic shape of the lateral acceleration transient. One wonders how many handling engineers of today have as clear a physical understanding of this aspect of vehicle dynamics. Schilling also discusses the probable effect of roll axis location, roll rates, roll couple distribution, suspension geometry, shock absorber effects, etc., on the transient.

Two years later, Ken Stonex of the G.M. Proving Ground staff published an open literature report on the skid pad technique and also described the famous "checkerboard" test from which transient behavior was determined by photographing a grid on the ground as the car maneuvered over it. This is generally credited as being the earliest measurement of automobile dynamic behavior.

World War II temporarily curtailed Olley's activities in handling, but in 1945 he returned to Vauxhall where he consulted in suspension design and the next year presented his classic paper, "Road Manners of the Modern Car," at the Institution of Automobile Engineers in London. According to Maurice Platt, Olley's work had a large influence on European designers who had not fully appreciated the implications of independent suspension. Olley also gave invaluable assistance to Dr. Fogg in the planning stages of MIRA (Motor Industry Research Association), resulting in the high priority given to the skid pad installation. In 1952, Ed Cole invited Maurice to head up the new Chevrolet R&D section, a position he held until 1955 when he was officially retired at age 66. But Maurice never retired in the conventional sense and for several years he continued to appear at Chevrolet where he wrote up his knowledge of suspension design and handling in a series of monographs published in 1961 through 1963. Later he lectured at the General Motors Institute and engaged in consulting. His interest in automobile design and handling remained unabated and he carried on a wide correspondence with researchers and practitioners in these areas worldwide. My own Olley file contains hundreds of letters, all hand-printed, in beautiful English and enlivened with sketches.

In the time span of Olley's more active work in handling, there were other investigators who made notable contributions in *specialized* areas. One thinks of Lippman's pioneering measurements in tire dynamics, 1954; the development of tire theory by von Schlippe and Dietrich and Temple; the flood of experimental and analytical contributions by Eric Gough; and Lind-Walker's 1950 paper on "Directional Stability," a fascinating contribu-

tion introducing the aircraft concept of the *neutral steer point* to the automobile and pointing up the desirability of front-wheel drive and the importance of aero drag for the small economy car.

But the unique feature of Olley's work was its comprehensiveness and overall view. Olley once wrote: "It seems strange that the automobile industry went on for thirty-five years, building cars piecemeal this way with no real conception of the complete vehicle." If there is any one engineer who was to change this viewpoint it was Maurice Olley.

Olley was not only a creator but a facilitator. His enthusiasm, openness, and willingness to impart his knowledge to others lengthened his reach so that his influence became worldwide. On the evening of our meeting at the GM Proving Ground, Dave Whitcomb and I wound up at Olley's apartment with Bob Schilling. Maurice spread out a number of large drawings on the floor and with them answered many of our questions. Olley became a close friend, as did Schilling, and we met on numerous occasions in Detroit and Buffalo and carried on a voluminous correspondence. Olley's personality was one of quiet maturity. He was a great conversationalist and when he visited Flight Research he would sit down in our one comfortable chair and the rest of us would gather around. He was fascinated with car behavior and his fascination was infectious. Although he worked for large organizations and was a great supporter of GM, he remained a free-agent; he held titles but he was never bound by them. If the occasion warranted, he was well received on the 14th floor of the GM Building.

Bob Schilling was one of Olley's closest friends and collaborators. Trained in Germany, he had an extensive design experience and a characteristic thoroughness. I always had the feeling with Bob that I was in the presence of a really great engineer.

Leonard Segel

The contract from General Motors for research in automobile stability and control using aircraft technology began early in 1953 in CAL's Flight Research Department. It was placed under the direction of Leonard Segel as Project Engineer. Len had obtained an aeronautical degree from the University of Cincinnati in 1947 and had immediately accepted a job in Flight where he was engaged in projects for the military that involved the dynamic equations of motion and their use in the analysis of flight tests. He was an excellent choice with the appropriate aircraft experience and the strong analytical capability required for laying down a lasting theoretical foundation. As noted earlier the basic research for GM was extended and continued until 1963, and Segel remained the project engineer for the entire period.

Segel's reflections of his involvement in the GM program are given in Ref. 145 and quoted below. I have singled out our presentations at the Institution of Mechanical Engineers (IME) in 1956 as a watershed event which deserves a separate discussion; also

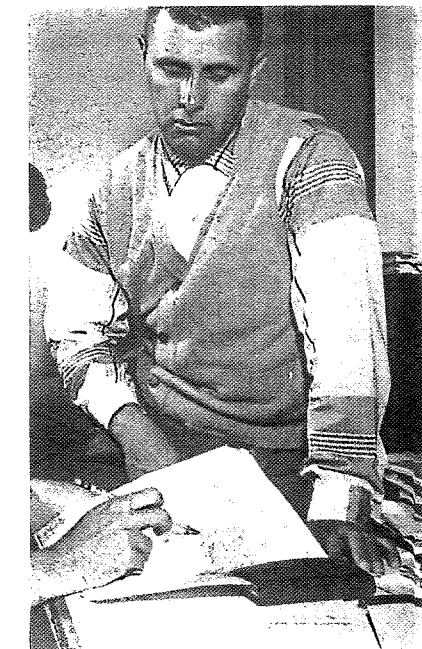


Figure 13.3 Leonard Segel.

there were concurrent activities at CAL and at GM of an important nature apart from our program for GM.

At the very beginning, I can recall that our primary concern was the level of knowledge which existed with respect to the forces and moments generated by the pneumatic tire. Since we were planning to use a 1953 Buick in the test program, we arranged for U.S. Rubber to conduct tests on the tires used on the Buick. Their tire dynamometer employed a rolling drum, as was the case in most tire companies at that time. Consequently, we knew that the data to be acquired would not be equivalent to the characteristics which prevail on a flat surface. There were many other questions facing us and we searched desperately for literature which would enlighten us on the mechanical characteristics of tires relevant to directional stability and control behavior.

Fortunately, we found a British report written by Hadekel (1952) which addressed many of the issues which concerned us. This report became our "bible." To me, it was equivalent in many respects to the large body of air-

foil data that had been produced by the National Advisory Committee for Aeronautics (later to become NASA) for the benefit of all who were working in the field of applied aerodynamics and flight mechanics.

A major question was whether we could justifiably make the quasi-static tire assumption which had been universally adopted by earlier researchers, e.g., Rieckert, Rocard, and Schilling. Fortunately, the report by Hadekel contained information relevant to this question. We discovered that during the war years a German engineer (working at Junkers Aircraft) had addressed the problem of aircraft landing gear shimmy and had developed a simple structural model of the pneumatic tire (von Schlippe and Dietrich, 1941). In this model the tire is represented as a massless taut string on an elastic foundation. It reveals that the lag between tire side force and tire slip angle is, to the first order, a function of the distance rolled after a change in slip angle has occurred. A decade later, just prior to the research being initiated at CAL, a young chemical engineer in U.S. Rubber's research department conducted some measurements on a tire-vehicle system which led him to conclude that a tire had to roll a short distance before achieving its steady-state side force (Lippman, 1954); it should be noted that Lippman was unaware of von Schlippe's work. Given the findings of von Schlippe and Lippman, it became apparent that one could neglect the small time delay associated with the transient lateral deformation of the tire provided motor vehicles are traveling at highway speeds and the rate of change of slip angle is not too large.

Having satisfied ourselves that the quasi-static tire assumption was reasonable we decided that our first efforts toward modeling the motor car should be restricted to investigating (1) the stability of the automobile with the front wheels held fixed and (2) the response to a displacement of the front wheels. The stability with steering wheel unconstrained and the response to a steering moment would be left to follow-on studies. Clearly we were influenced by the practice of the aircraft stability and control analyst of differentiating between "fixed" and "free-control" stability.

In deriving the equations of motion of a motor car assumed to consist of (1) a nonrolling mass, free to yaw and sideslip, and (2) a rolling mass, constrained to roll about an axis fixed in the nonrolling mass, we took our cues from aeronautical practice, even though we were dealing with a linked two-mass system rather than a single mass. Calculations readily showed that the gyroscopic moments created by the angular rotation of the moment of momentum vectors associated with the rotating wheel masses were negligible in comparison to the moments deriving from the tires. (At a later date the methods of analytical mechanics were employed to derive the inertial reaction terms in a more rigorous fashion.) In addition there were a host of laboratory methods which had to be developed for measuring the various properties of the test

car, viz., locations of mass centers, yaw and roll moments of inertia, heights of front and rear roll centers, roll stiffness of the suspension, roll damping constant, kinematic properties of the front and rear suspensions determining steering and inclination of the front and rear wheels as a function of body roll, etc. To the extent that some of these properties have an influence on the statics of turning, we were able to obtain some of the needed information from General Motors. However, we were not inclined to accept a number or value from an outside party without verifying the accuracy of the information ourselves.

In order to measure lateral acceleration, yaw and roll velocities, and angular displacements of the front wheels and the roll displacement of the rolling mass, we resorted to the instrumentation practice that had been developed for measuring aircraft motions in space. A key element of this practice involved the use of oscilloscopes with galvanometers that could be placed in a circuit whose dynamic response could be adjusted to filter out signal content above a certain frequency. Thus it was necessary to dynamically calibrate each measurement channel so as to establish the frequency response of each motion transducer, in conjunction with a specific galvanometer and its associated circuitry. To a very large extent it was this practice that required that all measurements made in the time domain be converted to the frequency domain. (Although such a conversion would have been unnecessary if we had used a harmonic forcing function to determine the frequency response of the tire-vehicle system, we had learned from our aircraft experience that the test activity is much more efficient when an aperiodic forcing function containing the frequencies of interest is used.) Recall that the time frame was the early fifties. With digital and analog computers in their infancy, it was a major undertaking to integrate either linear or nonlinear differential equations in order to obtain time histories which could be compared with actual measurements. On the other hand, it was relatively straightforward to evaluate the transfer function, i.e., the frequency response of a system described by linear differential equations.

It is worth noting that the above mentioned adoption of a test procedure employing step- and pulse-like steer inputs to a motor car also means that testing was made more efficient at the expense of making the data processing task more laborious. At that time analog to digital conversion devices did not exist, meaning that a large number of manhours had to be used to measure distances on an oscilloscope record (at many intervals of time) for subsequent conversion to engineering units. Fortunately, we were able to avoid this very time consuming task plus the task of harmonically analyzing the input and output signals by using a mechanical harmonic analyzer. The analyzer available to CAL contained five spheres which on rolling on a flat surface became integrating devices comparable to the mechanical integrators used by Vannevar Bush in his mechanical differential analyzer, more popu-

larly known as an "analog computer." A human operator followed the analog trace of an input or output signal by controlling the vertical motion of a pair of crosshairs while a motor slowly drove the crosshairs horizontally whenever the operator closed a switch. A single traverse of the signal trace yielded five harmonic amplitudes and phase angles. On changing the gears associated with each sphere and repeating the operation, five more harmonics could be determined and so on. Clearly, the process was much less efficient then, than the very same process is today.

The Flight Research Department of the Cornell Aeronautical Laboratory was located in one corner of the airport serving the city of Buffalo. Since the airport was not particularly level, vehicle test activity had to be restricted to days in which the inactive runways were deemed suitable, in that prior measurements of the grade and cross-section had shown that their departure from a horizontal surface was sufficiently small. Whereas we had a radio transmitter to contact the aircraft controllers on duty, they had to use their light gun to give us a signal to proceed. Two people were needed to conduct the tests; myself as the driver who created the input disturbance and an assistant who (1) operated the accelerator pedal to maintain a desired constant speed and (2) turned the recording system on and off as appropriate. I recall that I was particularly concerned about insuring that tire inflation pressures be held constant as the tests proceeded since the test data supplied by the U.S. Rubber Co. made it quite clear that the tire properties were very much a function of the "hot" inflation pressure. To this end, we made passes up and down the runway to heat the tires up prior to gathering test data. As the tests proceeded and tires heated further, I would periodically stop the car and check the inflation pressures with a very sensitive pressure gage and bleed off air pressure as required. Since tests were made at four or five different levels of understeer gradient, achieved in part by differential inflation pressures fore and aft, it was necessary to monitor these differential pressures very carefully in order to maintain the understeer gradient at the desired level.

Notwithstanding the above efforts to ensure the tire stiffness properties remain constant, the stiffness properties were in fact increasing with time as a result of the tread wear which occurred during the dynamic tests and particularly during the "skid pad" test performed midway in the program. In retrospect, it was possible to show that the agreement between theoretical calculations and measurements could be improved substantially by accounting for the effects of tire wear. Measurements were conducted on the worn tires with the over-the-road dynamometer developed at CAL, under sponsorship of the U.S. Air Force.

The accomplishments achieved at that point were:

- (a) development of a linear mathematical model describing the motor car's response to front-wheel steer displacement and verification of its validity by full-scale response tests
- (b) demonstrating that a roll, yaw and sideslip degree of freedom are necessary and sufficient to explain and predict a motor vehicle's response to steer displacement of its front wheels
- (c) performance of an eigenvalue analysis indicating the changes in dynamic stability caused by an increase in speed when the vehicle is understeer or oversteer
- (d) development of an approximate factorization of the characteristic equation of a four-wheeled motor car to obtain closed-form solutions for the undamped natural frequencies and damping ratios of the two modes of motion, identified as a "directional" mode (consisting mainly of yawing and sideslipping) and a "rolling" mode (characterized by substantial rolling as well as yawing and sideslipping)
- (e) development of an analytical expression for understeer gradient in terms of the mechanical and kinematic properties of the running gear and of the front and rear suspensions
- (f) mathematical explanation of the manner in which (1) the understeer gradient influences the transient response to steering and (2) the system becomes dynamically unstable when the vehicle is oversteer and is being operated at or above the critical speed
- (g) demonstration of the validity of the quasi-static tire assumption, provided the steering input and other disturbances are characterized by time histories whose frequency content does not exceed two cycles per second and vehicle velocities are representative of highway speeds
- (h) conversion of von Schlippe's equations (describing the dependency of tire side force on distance rolled) to the frequency domain, thereby defining the frequency response of the tire (Segel, 1966), making it possible to explain discrepancies in amplitude and phase noted between theory and experiment at frequencies above two Hz
- (i) noting that the inability of the tire to produce a side force instantaneously following a step change in slip angle, is responsible for the initial slope of the yawing velocity response to a step change in steer angle being zero rather than finite.

Other Activities at CAL (1953-1956)

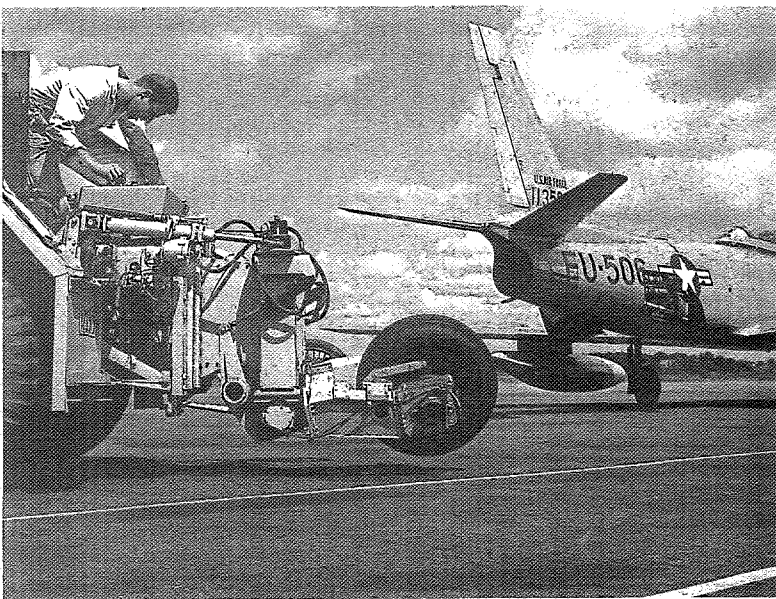


Figure 13.4 Air Force—CAL six component tire test rig.

Having established a core program under GM sponsorship, we were able to consider an expansion into related automotive areas. The pneumatic tire, unlike many products, cannot be easily specified. Measuring tire forces is a long and costly job fraught with problems of wear and temperature control. Nevertheless, the analysis of automobile stability and control is totally dependent on tire data. I was determined to do something about it, and in 1953 promoted through our Air Force contacts a program to develop an on-road tire tester for nose-gear tires and, although we didn't advertise our interest, automobile tires as well. This machine was developed at CAL by Bill Close, a Scotsman (British-American) aircraft designer who I had met at the first Watkins Glen event and who was later to become famous for organizing the timing and scoring team for the U.S. Grand Prix races. He was supported by Cliff Muzzey, an all around mechanical/electrical/aeronautical engineer who came out of the Draper Instrumentation Laboratory at MIT. The machine they developed pioneered a whole variety of advances in tire testing. The test tire was supported on a first-time six-component strain gage balance based on wind tunnel practice which was attached to the back of a twin rear axle military vehicle. The tire was loaded by a "zero-rate spring" (a nitrogen cylinder) up to 3000 lb., and slip and camber angles of $\pm 30^\circ$ were available. The machine was commissioned in October 1954 and

was continuously in use on programs for tire companies into the mid-1960s. Al Fonda was made responsible for its operation and, as recounted in Chapter 9, appears to have used it to measure the tire friction circle for the first time.



Figure 13.5 Dave Whitcomb.

The idea of a Vehicle Dynamics Department had been germinating since 1954 and was finally sold to CAL management in 1956. I became its manager with Dave Whitcomb as assistant department head.

Organizational changes affecting research in car stability and control were taking place at General Motors. Our contracts work had been monitored by Bob Schilling with unofficial but important inputs by Maurice Olley. In 1955, GM appointed Joe Bidwell as head of the engineering mechanics department and from there on he became our official contact. He was to build up a large in-house vehicle dynamics group (of which more later).

With responsibility for CAL's new vehicle dynamics department, Dave Whitcomb and I were anxious to promote it. We were well aware of the seminal nature of Len Segel's work and the uniqueness of the AF-CAL tire tester. What better way to establish a reputation than to publish papers in our technical society. Interestingly enough, GM's Joe Bidwell placed no restrictions on the publication of Segel's work. In fact, GM viewed R & D in basic vehicle dynamics as fundamental knowledge removed from immediate design application and in nowise proprietary, although they reserved the right in their contract to revert to Commercial Confidential if warranted. However, when SAE was apprised of the mathematical nature of a paper on the dynamic response of the automobile to steering control, they rejected it (things have changed since!). At this juncture Olley and Schilling entered the picture. Olley contacted the Institution of Mechanical

Engineers (IME, London) who were more than interested in comprehensive papers on our work. Schilling was instrumental in arranging for a summary paper by Len at the Atlantic City Summer Session of the SAE, 1956.

IME Papers, 1956

Undoubtedly out of their great respect for Maurice Olley and his work, the IME set out to make the presentation of our papers in England a memorable event. The five papers consisted of a general introduction to our overall research program and the state of the art,

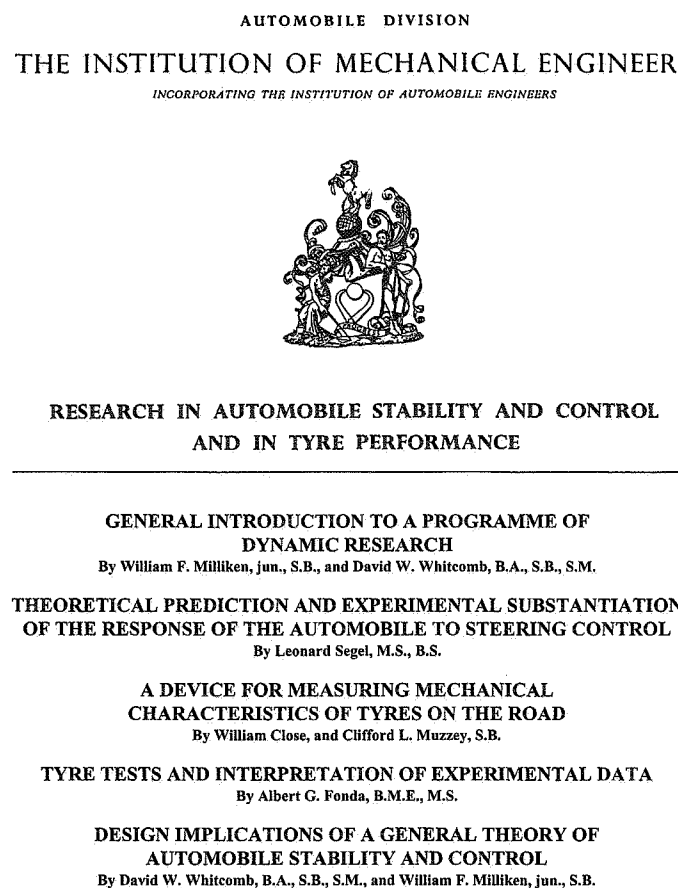


Figure 13.6 Cover of "The IME Papers."

Segel's linear analysis of the automobile response to steering, two papers on the tire tester development and measurements taken with it, and a final paper by Whitcomb using a two-degree of freedom linear analysis directed toward design implications. We delivered the drafts in late August 1956 and the IME assigned an editor, Miss Dorothy Cridland, who did a monumental job of checking all references and material, tightening up the texts and converting the spelling into the good King's English. In addition, she later took all of the papers, discussion material and author's answers and incorporated the whole into the 140-page publication known in the USA as "The IME Papers."

Our team of five authors and wives converged on London in early November 1956. The authors met with Reg Main, secretary of the Institution at headquarters. We were to present the papers in London, Coventry, and Luton (Vauxhall). Jaguar and Humber made cars available to us during our stay in England and we took the opportunity to visit such facilities as Rolls-Royce in Crewe and MIRA.

The initial presentation in London was at a General Meeting on November 13, 1956. The meeting was chaired by A.G. Booth, chairman of the automobile division, IME. Over 90 people attended, including such well-known figures in the automobile/tire industry as Donald Bastow, Eric Gough, David Hodkin, and Harry Grylls. The discussion was lively to say the least. After the meeting, we were taken to the Royal Automobile Club for dinner and toasts.

The subsequent sessions in Coventry and Luton were equally fruitful and we formed lasting friendships with Harry Grylls, Eric Gough, Maurice Platt, John Ellis, and others which enabled us to exchange progress in subsequent years.

CAL bought one thousand copies of the summary document and all but a couple dozen have since been distributed.

The IME awarded Len Segel the Crompton-Lanchester Medal for his paper, "Theoretical Prediction and Experimental Substantiation of the Response of the Automobile to Steering Control," the first time this award had gone outside of England.

It is interesting to note that the two-degree-of-freedom analysis of Whitcomb's has become the way most engineers think of the car in physical terms. The addition of the roll mode (undesirable in any event as shown by active car experience) makes it difficult to sort out primary effects on the motion.

Joe Bidwell

In 1955 GM began to build up their in-house capability in vehicle dynamics research under the direction of Joe Bidwell at the Research Laboratories Division. For the next eleven years in GM Research and subsequently in Engineering Staff, a substantial group

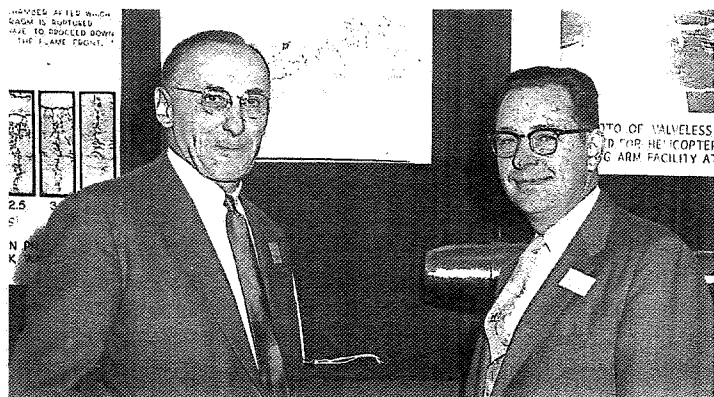


Figure 13.7 Bob Schilling and Joe Bidwell.

of highly competent engineers continued to expand the knowledge of vehicle dynamics. Joe Bidwell has recently summarized his memories of those interesting years and the following is his unabridged story.

My personal involvement with vehicle dynamics started in July of 1955 when I was appointed Head of the Engineering Mechanics Department at General Motors Research Laboratories. My career at GMR started in 1942 after graduation from Brown University with a degree in mechanical engineering. Except for a period during World War II when I was assigned to Naval Research Laboratories separating uranium isotopes, my work at GMR had dealt mainly with oil film lubrication, wear, rubbing and rolling surfaces and other tribology problems. The Engineering Mechanics Department had additional project responsibilities, but the staff devoted to vehicle dynamics varied from perhaps 20 to 50 during its stay at GMR and following its move to Engineering Staff in 1966. My everyday involvement with vehicle dynamics ended in 1972 when I was assigned to Central Office as Assistant to Ed Cole, but my interest has continued to the present.

While the rest of these comments will deal with the period after 1955, [let me say] a few words about where the science of vehicle dynamics stood at that time.

Prior to the early 1930s, automobile directional control was understood mainly from the geometric standpoint. Recognition of the "slip angle" of pneumatic tires was the first major step in the development of an understanding of the directional behavior of automobiles. This concept led to rapid development of simple steady-state linear directional control models as well as the devel-

opment of experimental procedures such as the "skid pad" test. I don't have an accurate chronology of events, but well before 1955 Maurice Olley had developed a comprehensive analysis of steady-state directional control including the effects of suspension design. As early as 1936 Kenneth Stonex at the GM Proving Grounds had developed instrumented skid pad tests and measured steady-state steering behavior. He had also mounted a motion picture camera on top of a car and ran steering tests on a checkerboard painted on the road; photogrammetric analysis was used, frame by frame, to determine transient response characteristics! Ball and disk mechanical analog differential analyzers had been used to look at simplified quarter car ride models.

Bob Schilling, who headed the Engineering Mechanics Department before me, was a competent analyst and had already written the basic directional control equations (but not in the derivative notation used by Segel). He had also contracted with the Cornell Aeronautical Laboratories to apply their aircraft stability and control technology to the automobile. When I succeeded Schilling both our contract and in-house vehicle dynamics work were expanded. Bob Kohr supervised most of this activity at the time. The period from 1955 to 1966 (when my department was transferred to Engineering Staff) was especially productive. In the following narrative I have tried to recall the individuals primarily concerned with specific programs, however I should emphasize that the entire group interacted and contributed to the success of the overall activity. If I have overlooked someone, I apologize—it is the result of poor memory. The most accurate record lies in the files of the many reports written and in the libraries of GMR and Engineering Staff along with SAE papers.

Since I was new to the field, I quickly became aware of a communication problem. Words were not universally used to mean the same thing. One of our first efforts was to develop a terminology based on quantitative definitions. Bob Kohr, Don Nordeen, and Tom Bundorf made major contributions to this work which ultimately resulted in the adoption by SAE of J670, "Vehicle Dynamics Terminology." I considered this accomplishment very important. It standardized definitions of tire forces and moments, established a vehicle axis system, and force and moment definitions and provided quantitative definitions of steady-state terms such as "understeer," "oversteer," and "stability," and many other terms which had frequently been used ambiguously.

A word about the Society of Automotive Engineers: SAE Technical Committees provided a forum for experts in various aspects of vehicle technology to discuss common technical problems and develop standardized test procedures. In 1955 there was no Technical Committee devoted to vehicle dynamics. A couple of years after joining the Engineering Mechanics Department, I

was able to get an existing SAE committee, the Riding Comfort Committee, to expand its scope to include directional control and it was renamed the Vehicle Dynamics Committee. My first effort was to get our vehicle dynamics terminology integrated into the original J670, first published in 1952, which had up to then included only ride related terms. This greatly revised terminology was finally published in 1965 as SAE J670a "Vehicle Dynamics Terminology." SAE Committees do not act fast. I served as chairman of this committee for several years and, with the contributions of many talented members, it served to standardize tire testing equipment and many steady-state and transient test procedures developed by GM and other industry participants. In later years there was considerable interaction with the International Organization for Standardization [ISO] on test procedures. They do not act rapidly either.

We procured a large electronic analog computer about 1960 which Bob Kohr utilized to solve the transient directional control equations which we were developing. The analog computer was well suited to simulating the dynamic vehicle response although nonlinearities presented problems. These were later attacked by Dick Valentine using a "hybrid" computer that utilized digital techniques to represent the nonlinearities.

We also constructed a "ride simulator"—a car body mounted on electro-hydraulic servos and driven by a ride model programmed in the analog computer—to evaluate subjective opinions of changes in suspension design with reproducible road inputs. The mechanism provided three degrees of freedom, pitch, bounce and roll. The analog computer provided the ability to calculate the ride motions and drive the servos in real time which was not possible with the digital computers of that era.

The ride simulator was supplemented by the development of a road profile measuring device. The road profilometer consisted of two bicycle-like wheels, one in each track, mounted in a truck which could be operated at about 30 mph to measure and record the vertical displacements of the two wheel tracks from an inertial reference. These data served as road inputs to the analog computer. This device found additional applications for airport runway and highway inspection and is still being manufactured.

Recognizing the need for subjective evaluation of vehicles for both ride and handling and the need to study driver interactions with the vehicle, I started a "human factors" group of engineering psychologists to conduct these studies. This group varied in size from two to five over the period. Paul Olson was one of the longstanding members along with Rudy Mortimer and Bob Bierley. One of the principal goals of this group from the start was to develop tests to quantitatively evaluate driver-vehicle performance (which I define as "han-

dling" as opposed to "vehicle dynamics" or the response of the mechanical system to control or disturbance inputs). Quantitative measures can be either objective or subjective and both can be useful. Tasks such as tracking a wavy lane or constrained lane change maneuvers were among the first tried. The response characteristics of production vehicles were varied by modifying tire properties, weight distribution and mechanical components such as steering gear. We evaluated the spacing-control performance of drivers in a single lane of traffic as a function of traffic variables to provide driver models for Bob Herman's group in their pioneering analytical study of single lane traffic flow.

The development of task performance tests were given a boost after the birth of the National Highway Traffic Safety Administration about 1967 with their ridiculous "safety" proposals such as a standard on "overall steering ratio" which had absolutely no relation to safety. Richard Denzer, working at the Milford Proving Grounds, structured several tasks involving simulation of potential accident situations and conducted tests with cars having a wide range of response characteristics and using average drivers. I think I can accurately and briefly summarize the results of all of this work in the following statements:

1. Task performance differences can be quantified.
2. Drivers learn and adapt rapidly to vehicle differences.
3. Performance differences among drivers is far greater than among cars.
4. It is still questionable how task performance relates to real world safety.

Perhaps one of our most significant developments was a flat bed tire tester to permit measurement of the six force and moment components of experimental tires. Bob Van House was responsible for its design and construction. It was a slow speed, flat bed design with the axle and tire mounted on a balance system. The slip angle and camber angle were adjustable over a wide range and a hydraulic motor could produce driving or braking torques. Several were ultimately built for tire manufacturers.

The tire tester, while it provided reams of tire force and moment data, would not have been nearly as useful had it not been for the development by Don Nordeen of a "language" for characterizing tire performance. About 1963 he reduced the voluminous data to three normalized functions of slip angle: (1) normalized lateral force, (2) normalized load transfer sensitivity and (3) normalized load sensitivity, and showed how these could be used to predict vehicle response. This technique provides a means for quantitatively communicating desired properties to tire manufacturers and continues to serve as the basis for force and moment specification in the GM Tire Performance Criteria.

Our work covered all aspects of vehicle control (steady-state and transient analysis and experimental measurement techniques), task performance tests, tire properties, and even vehicle hardware. Roy Cataldo and I were deeply involved in this latter area. Shortly after my arrival we began development of electro-hydraulic servos to permit study of unique steering systems. In early 1958 we installed a system we named "Unicontrol" in a Chevrolet convertible. This system used a single four-inch stick with a weighted ball on top and mounted in the side door panel (not unlike the sidarm controls now used in some fly-by-wire aircraft). Steering was controlled by side to side motion of the ball, braking by rearward motion, and throttle by forward motion. The steering sensitivity was made a function of speed. A given lateral displacement commanded about the same lateral acceleration at any speed (above some minimum). It might be noted that this is approximated by the lateral acceleration gain of a conventional car operating above its characteristic speed. The weighted ball provided extremely fast free control response since its accelerometer effect drove the front wheels to center when released.

The steering servo also permitted automatic guidance by tracking a path defined by the magnetic field around a wire buried in the pavement. We had a couple of miles of guidance cable in the test track at the GM Tech Center and later, working with RCA, built a short loop track with sensors in blocks to detect the presence of a vehicle. This system, demonstrated in April 1960, utilized two cars which followed the road path and braked to avoid collision automatically. Thirty plus years later, similar programs are being conducted under the current Intelligent Vehicle Highway Systems program. In a paper given in January 1959, I had predicted (rashly) that we would have such systems in operation by 1980!

Although aerodynamics of automobiles is generally thought of in relation to drag and fuel economy, the yawing moment produced by a wind vector not aligned with the direction of motion can produce sizable disturbance forces. The study of this effect involves two components, the determination of the yawing moment and side force as from wind tunnel tests and the determination of the disturbance produced. The measurement of the disturbance had previously been studied by setting up a crosswind using aircraft engines and propellers alongside a straight road section to produce a pulse as the car was driven through. One of the limitations of this procedure was that the aerodynamic effects could only be modified by physical changes to the vehicle body. To circumvent this limitation we contracted with CAL to build a small (200 pound thrust) hydrogen peroxide rocket motor. We could mount the motor at the vertical and longitudinal location which would produce the yawing moment we wished to simulate and instrument the vehicle to measure the input pulse and response and thus evaluate the potential advantages of modified aerodynamics.

About 1956 we contracted with CAL to construct a "variable stability vehicle." This vehicle, which incorporated both a front wheel position and a steering wheel force servo, was intended to simulate varied directional response characteristics for use in driver studies to replace the physically modified vehicles generally used. The front wheels were not directly connected to the steering wheel but were positioned by the electro-hydraulic servo responding to combinations of steering wheel position and motion sensor inputs. While the vehicle proved useful for some purposes, the steering force servo was not completely satisfactory and the range of response attainable was limited by the ability to steer only the front wheels. Handling tests continued to be conducted with modified production cars.

In the early to mid-60s we initiated an in-house program to develop a "variable response vehicle." This differed from the earlier vehicle both in concept and in hardware. The concept was to build a vehicle that could track a "reference model" generated by a small analog computer in the vehicle. The control inputs would go into the computer-simulated vehicle and the calculated responses would be matched by the VRV. The hardware required to implement this plan required the ability to steer both the front and rear wheels via electro-hydraulic servos. Associated sensors to measure lateral acceleration and yaw to match the model outputs were also required. In addition a steering wheel servo provided both variable force and displacement control sensitivity. The complexity of the system resulted in a long development time and difficulty in use. The reference model control was never very successful due to the structural flexibility of the vehicle limiting bandwidth. However, the ability to control sideslip and yaw independently and feed back motion sensor inputs permitted the study of unique control systems. Although this was an extremely flexible piece of equipment, its experimental use was limited by its complexity to experiments which could not be done with simply modified production vehicles.

Throughout this period from 1955 to 1972, there was a continuous effort to develop more and more comprehensive analytical models of vehicle dynamic behavior. At GMR Bob Kohr and Don Nordeen and their coworkers headed this activity. Both the analog/digital hybrid and later improved digital computers were used to solve the increasingly complex dynamic equations.

However, while sophisticated models might predict the response of a simulated vehicle in a specific circumstance, it was difficult to get an understanding of why it behaved as it did without going back to simplified models where the influence of individual design factors could be visualized. Tom Bundorf contributed a great deal to this understanding by his introduction of the "cornering compliance concept." Basically, the idea is to evaluate the contribution of each of the individual design parameters—roll steer, cornering stiffness,

At first glance this way of looking at design influences on directional behavior appears limited to linear steady-state conditions. Bundorf demonstrated that insight into their impact on transient response (for a nonrolling model) can be gained by looking at not only the total understeer but at the front and rear components. Understeer at the front produces faster response than an equivalent amount at the rear. Including the roll mode introduces the additional complexity of the roll dynamics. Bundorf also showed how cornering compliances are related to the linear steady-state parameter, characteristic speed. Characteristic speed is an alternative means for characterizing understeer in the linear range and is the speed at which the steering sensitivity is just one half that of a neutral steer car. This is somewhat analogous to the critical speed of an oversteer car where its gain becomes infinite.

Supplementing steady-state and transient analysis, a great deal of effort was applied to experimental procedures and instrumentation for accurately measuring the response of vehicles. Dick Rasmussen was responsible for much of this work. Although the "skid pad" test had been used for many years, its interpretation had been based largely on the assumption that front and rear tire slip angles were the significant factors. Two other test procedures and associated instrumentation were devised to obtain data similar to that of the constant radius turn. Both the "constant speed" and "constant steer angle" tests required less driver skill and reduced variability. Instrumentation to simplify and speed data analysis was devised.

Several transient test procedures were evaluated but the most used was the step steer input. This test is relatively simple to conduct, is not dependent on driver skill and provides useful vehicle evaluation. In the early part of this work, on-board instrumentation created problems due to the weight and power requirement of the recording equipment to record outputs from the accelerometers and gyros.

Looking back I couldn't imagine a more talented, dedicated and productive bunch of people to have worked with—not just those I've mentioned, but every engineer, mechanic and technician. They all contributed to expanding the understanding of the control behavior of road vehicles and drivers that will continue to benefit automobile design for many years in the future.

In his account, Joe Bidwell has noted the 1956 Buick Variable Stability vehicle developed at CAL for General Motors. Although this vehicle suffered from servo problems, it remains (to the best of our knowledge) the first variable stability automobile and hence a

landmark effort. Similarly, the GM Variable Response Vehicle with reference model control was a pioneering effort which introduced servo control of the rear wheels, years before it was "re-invented." The original CAL/GM vehicle was described in a paper entitled, "The Variable-Stability Automobile," by L. Segal and R.T. Bundorf, given February 1965 at the Detroit SAE Section. Variable stability vehicles are still the "chosen instrument" for handling qualities work and they have yet to be fully exploited.

In the interest of historical completeness, we should mention that an earlier vehicle, a 1954 Buick, was equipped with a variable "feel" servo steering system (suggested by Schilling). On this car, the control forces could be made a function of lateral acceleration and yaw velocity in various proportions.

1963-1976, Changes and Activities at CAL and GM

After the completion of our large contract with GM in 1963, vehicle dynamics research at CAL was reorganized by the formation of a Transportation Division. This was composed of two departments, Transportation Research (under Bob Wolf and Ed Kidd) and Vehicle Research (under King Bird and Fred Dell'Amico); the author was appointed division head. In 1966 Joe Bidwell moved to GM Engineering Staff where he remained until 1972. GM internal research in vehicle dynamics continued at a high level as noted earlier, and we at CAL received continued GM sponsorship on a project-by-project basis.

Although in earlier years we worked in sort of an academic research atmosphere, this started to change in the early 1960s. Some major events were: the Corvair litigation, our involvement with the Chevrolet Chaparral project, the National Traffic and Motor Vehicle Safety Act of 1966, the formation of the National Highway Traffic Safety Administration (NHTSA), and Frank Winchell's appointment as Vice President GM Engineering Staff in 1972. As hectic as they were, very substantial advances in vehicle dynamics technology took place during those years. The linear model developments (in the 1950s) had yielded a fundamental understanding of the lateral/directional motions of the automobile but were not adequate for design purposes. The developments necessary for practical application in large-amplitude computer-based models occurred in this period.

Frank Winchell

I first met Frank Winchell in the fall of 1964. Frank was then in charge of Chevrolet Research and Development located in the Chevrolet Engineering Center in Warren, MI. For some time Maurice Olley had been after me to meet Winchell—"you've got to see how Frank builds experimental cars and what he is learning." So we talked—a lot about race cars—and Mauri Rose³⁸ gave me a tour of the shop. I was beginning to sense the

³⁸ Three-time Indy 500 winner.

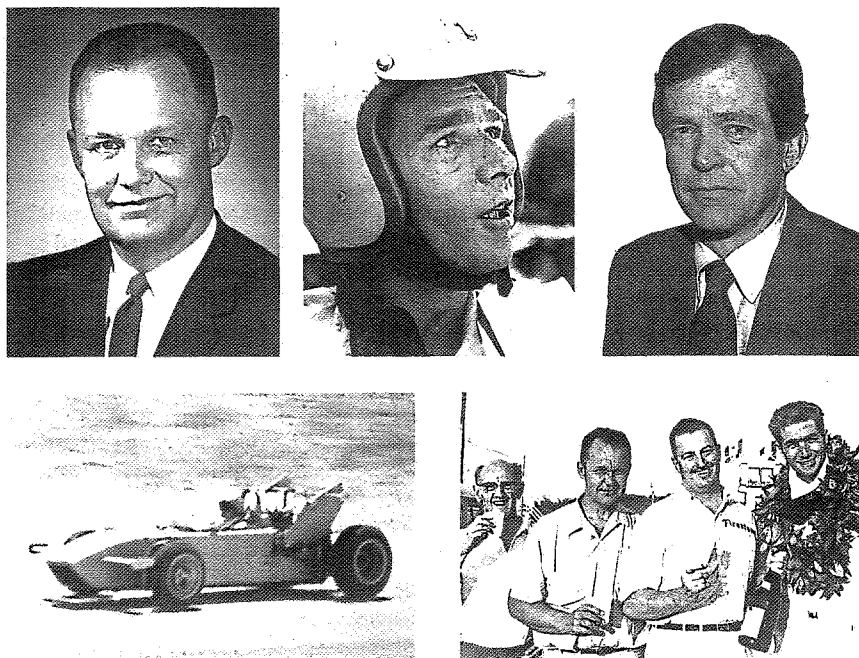


Figure 13.8 (upper left to right) Frank Winchell, Jim Hall, Jim Musser.
 (lower left) STV at Midland with front and rear wings, 1964.
 (lower right, l. to r.) Bill Milliken, Frank Winchell, Hap Sharp, Jim Hall
 at Watkins Glen.

level of reality and the type of thinking that characterized Winchell and the R&D group he had built. At lunch we got into an argument about 4WD cars. I had raced two of them and imagined they were the race car of the future. Winchell, who had met Jim Hall in 1962 and was already involved with Chaparral, thought otherwise. It was the first of a number of stormy encounters and correspondence which ultimately led to a profound and enduring friendship. When I met with Frank a couple of months after our initial luncheon, he had built up a prototype 4WD car and tested it!

It is impossible to talk about Frank Winchell's work and accomplishments without some understanding of his character. He is an absolutely straightforward independent thinker. What he says is what he believes—there is no hidden agenda. On the surface he is tough and competitive and has scared off some people, but most who have worked with him are his staunch admirers. Largely self taught, his engineering and creative abilities operate at a fundamental level, and his approach is heavily experimental. Referring to Galileo he once said, "The greatest act of humility I ever heard of was that of a man in a great cathe-

dral who, in the presence of infinite knowledge and wisdom, occupied himself with the swaying of a chandelier, counting the regularity of its period with his pulse."

In 1965, I was invited to become a consultant to Chevrolet R&D, an arrangement with Frank that lasted until his retirement in 1982. The original intent was to assist in the Corvair defense.

Early in 1965, a small group including Jim Hall, Jim Musser, David E. Davis, Jr. (then of *Car & Driver*), and I convened at Chevrolet for a review of handling fundamentals. It was Frank's contention that the essential physics of handling could be understood by applying Newton's laws, using vector and free-body diagrams, along with a basic understanding of tire elastic and frictional (limit) properties. In addition, the car's behavior could be demonstrated with elementary mechanical models and analogies to a variety of common mechanical devices. Winchell proved an inspiring instructor. By use of all kinds of simple demonstrations he turned the event into an *experience* as opposed to an academic exercise. He drove home the physics of a basic car, after which one could elaborate with all of the secondary effects without becoming lost in the details. A tremendous asset for a vehicle dynamicist.

At that time, the Corvair opponents were claiming a rear-heavy car would always break-away rear first. Using a simple model car with adjustable CG, and movies of real cars on the proving ground, Frank was able to demonstrate the basic physics behind understeer, oversteer, and neutral steer both sublimit and at the limit. CG location was only one of the determining factors, among many.

In the course of the week many of the features contributing to Chaparral performance were discussed. Hall and Davis later published a series of *Car & Driver* articles, "What Makes Cars Handle?" (Ref. 57), which still remains as a sound statement of the logic behind the general configuration of the modern race car.

Up to this time, Chevrolet and Chaparral had concluded that the fastest way around a circuit was to minimize transients and go from one steady-state to another as fast as possible. The development problems they had encountered were solved by thinking along steady-state lines. Nevertheless, they were curious about "dynamics" and its possible importance. So arrangements were made for Winchell, Hall, and me to take the variable stability airplane course at CAL, probably the best hands-on way to learn about dynamic effects. A B-26 had been modified with servo control to an "in-flight simulator" and the frequencies and dampings of the basic modes of motion could be varied in flight; control forces and motions could also be varied. This device had proven to be an effective tool for training Air Force and Navy test pilots in flight dynamics. Giff Bull, CAL's instructor/pilot, gave us a full week of ground school and flight demonstrations. In the evening we struggled with the dynamics of a "bicycle model," drank beer, and compared notes. Interestingly enough, the experience reinforced my belief that automobile "statics" was an important area to develop—race cars being more steady-state than most people imag-

ine. This led to the initiation of the Moment Method some four years later. As he boarded his return flight to Detroit, Winchell's parting comment was, "If you ever find a situation where $F = ma^2$, I'll accept a collect phone call!" Later that year, we made the first of several visits to Midland, Texas, Jim Hall's Rattlesnake Raceway headquarters.

Chevrolet R&D and Chaparral

The collaboration of Chevrolet R&D and Chaparral in the 1962-66 period ranks as one, if not the, most effective and creative episodes in the history of automobile racing. It must be remembered that both groups were going concerns before their association. Winchell's R&D was a mature group of outstanding designers, engineers, fabricators, mechanics, and testers with all the facilities for rapidly building prototypes and evaluating them. Hall and Sharp had their own development staff and private race track and were deep into the racing scene. Hall had an engineering degree and had flown high-performance aircraft. Hap Sharp was a man of great natural intelligence. All four principals—Winchell, Hall, Musser, and Sharp—were results-oriented and used to operating fast with parallel developments. Involved in Can-Am racing with a largely free formula, they were unencumbered with arbitrary regulations and could go for the optimum engineering solution.

The following is a first-hand account of the Chevrolet-Chaparral collaboration recently written by Frank Winchell with the help and cooperation of Jim Hall and Jim Musser (Hap Sharp died some years ago). Because of the General Motors policy at the time of "no racing," it was never possible to tell the story with proper recognition of all parties involved. The authors of this book are immensely pleased to be able to include this first-ever authentic account of Chevrolet-Chaparral racing.

By way of introduction, I had the opportunity—as a sort of independent observer—to witness the operation of the Chevrolet-Chaparral collaboration in both Midland and Detroit. It appeared to me as a near perfect amalgamation of the complementary talents of a number of very smart people, motivated by the single goal of winning by learning. It was an extraordinary team effort in which the contributions of the individual were transcended by the team's goal. Its seminal accomplishment was the introduction of aerodynamic downforce which has changed the face of racing and enabled the remarkable circuit performance we see today—230+ mph laps at Indy, for example. Certainly other competitors had used ducktails and spoilers to reduce aerodynamic lift but it was a gigantic conceptual step to use aerodynamics to intentionally load up the tires without adding appreciable weight. From that day on the race car became a hybrid vehicle—part conventional car, part aerodynamic. Their follow-up achievement was to put the downforce directly into the suspension which, if permitted today, would eliminate most of the irrationalities of the modern high downforce race car.

Here is the story in Frank Winchell's words:

Background

I followed Maurice Olley and Bob Schilling as director of Chevrolet Research and Development. Olley retired and I became Schilling's assistant in 1959. In 1960 Schilling went to Opel and I became director.

Maurice Olley was the most knowledgeable automotive engineer I had ever known. He was particularly knowledgeable in the field of ride and handling. Schilling was about the second most knowledgeable engineer I ever knew.

I didn't know anything about anything related to vehicle dynamics.

I had some experience in military aircraft engines, heavy-duty automatic transmissions for military vehicles, and participated in the development of the Cadillac T-41E1 tank. I came to Chevrolet in '52 and was involved in the design and development of automotive transmissions until I went to Chevy R&D in '59.

Unfortunately Schilling was there less than a year. Fortunately, Maurice used to drop by for a visit about once a month. I was the keeper of his papers. He used to come in and browse through all his old stuff and tell me about interesting and amusing things that went on in the course of the evolution of the automobile and the airplane. He was an exceptional freehand illustrator, a writer and a wit. I liked him. So did everyone else. Fortunately, Olley and Schilling had surrounded themselves with some really good people. So did I. Musser was the best.

From Maurice I became acquainted with his old friend and colleague Bill Milliken, a long time researcher in the stability and control of everything from submarines to airplanes, a guy who had built, flown, and crashed his own airplane before he was 20. He was an ex-racer and, at the time, head of a division of the Cornell Aeronautical Laboratory. I found him a valued consultant and engaged his erudite insights and analytical efficacies³⁹ for the next thirty-some years.

For reasons unknown to me, in early 1960 I got fingered to help the legal staff in the preparation of the defense of the Corvair. The alleged defect being that it would "suddenly and unexpectedly go out of control and roll over."⁴⁰ As its transmission engineer, I was clean and blameless. Further, I didn't know "sicum" about handling and had never been in the same room

³⁹ I think that is what it was.

⁴⁰ My wife and two kids had Corvairs—to my knowledge none of them ever got one upside down.

with a lawyer. What I did have was a very informal organization, a super model shop and some very capable engineers and craftsmen that were not burdened by production deadlines.

It turns out that, while a great deal was known about stability and control in the normal driving range, below 0.3g's, what was known about the behavior of an automobile above 0.3g was mostly "seat of the pants." To my knowledge there was nothing in the library of any attempt to quantify the limit or the character of an automobile at anywhere near the limit of control. Even less was known about the driver, particularly at anything above 0.3g's.

Passenger cars and drivers never intentionally run at the limit of control. Racing cars and racing drivers run at the limit of control all the time. Research in vehicular control and racing are accordant activities. While never actively involved in racing, as a one-time resident of Speedway, Indiana, I had been keen on it since about the age of nine.

With the advent of Ralph Nader and others like him, came the proclamation that "Speed Kills!"—a revelation that made a lot of sense to the public relations people in General Motors. We were subsequently directed to halt any and all activity related to motor racing—irrespective of the obvious fact that the primary objective of motor racing is accident avoidance, crashworthiness, and getting from point A to point B in the least time and with the least effort—a basic objective that has possessed both man and beast since the beginning of time. You can't get there if you can't keep it on the race track and killing drivers tends to have a negative effect on team spirit.

As the designated "expert" witness for the Corvair defense, I made a concerted effort to experience and to understand the dynamics of both the car and driver at the limit of control. That meant putting numbers on the coordinates of stability and control.

In short, if I had known **anything** about ride and handling and if I had **not** been fingered by the legal staff, what follows would not have happened.

The Corvair

Mauri Rose was a Chevy R&D technician. In the beginning he, Jim Musser, and I spent a lot of time on the skid pad with a lot of cars, the principal reference cars being the Falcon, the Volkswagen, and the Renault. We found that the limit of control was about the same for all cars; the front engine rear drives terminated in understeer and the rear engine rear drives terminated in oversteer, all at about 0.6g's. The cars were run on a 108-ft. radius circle. The

limit of control was calculated from the recorded lap times. We quantified the limit of control and the characteristic of **every passenger car configuration** on the road at that time.

Starting from nowhere, I remember:

- Olley was the guy that clued me about slip angles and roll couple distribution.
- Musser was the guy on chassis torsional stiffness and suspension geometry.

It became evident that it was the magnitude and relative rate of change of front and rear slip angles that fixed the limit of control, not the coefficient of friction. With enough torsional stiffness and appropriate roll couple distribution we found we could set up most any car so that it terminated in neutral steer and effect an extension of the limit of control—with "state-of-the-art" tires.

The Start

That revelation led to tire development. The first attempts at increased lateral stiffness began with wider rims, reduced tread depth, and higher pressures. Working with the tire companies, subsequent developments added structure and compounding. The wide, low-profile tires resulted in marked improvements in lateral stiffness and reduced slip⁴¹ angles. With proper front and rear balance, good controllability could be achieved right up to the limit of adhesion.

A lot of stuff was built to quantify tire performance right out to the limit of adhesion. A lot of stuff was built to quantify car/driver performance right out to the limit of control. A lot of time and energy went into trying to close the "hypothesis/observation" loop.⁴²

It soon became evident that, with the tractive vector on the rear wheels, maximum lateral acceleration requires that the inside rear carry as much of the total normal force, thru the corners, as possible. That meant:

- A wide track and a low CG.
- Roll centers and roll axis on the ground (to prevent jacking).

⁴¹ The path of the front wheels accommodate changing slip angles by the rotation of the steering wheel. The rear wheels require rotation of the entire mass of the car.

⁴² "A guy with a hypothesis and no observation to back it up, has got 'nuthin.' A guy with an observation and no hypothesis to back it up, is also 'bare assed.'"

- A set of rear tires with all the lateral stiffness you could get. With the wide, low profile tires, that meant keeping them essentially “perpendicular” to the road in the corners.
- All the roll stiffness you could get on the front (near zero normal force on the inside front at max lateral acceleration).
- Develop a front tire with enough lateral stiffness to keep the car at near neutral steer at the limit on the low-speed skid pad. (This was not a big deal because, with the weight bias of a rear engine rear-drive car, even with all the front normal force in the outside front, it took less lateral stiffness on the front than the rear.)

In the beginning there was no tire data at or near the limit of adhesion. There wasn't even any tire lab, anywhere, capable of producing it. R&D did a lot of work in developing some pretty basic equipment and instrumentation for the purpose of understanding and quantifying the components of the tire - chassis - driver - road “equation,” including:

- A glass floor and a mirror so we could watch the slip angles develop.
- A scale model of a tire testing rig where we could introduce varying vertical, longitudinal, and lateral forces and measure the resulting slip angles.
- 3/8 plastic scale models of chassis structure.
- A scale model of a car with a variable vertical and longitudinal CG, roll couple distribution, longitudinal and lateral side forces, and tire stiffness, front and rear.
- A full-scale trailing arm “merry-go-round” tire tester with variable normal and longitudinal forces at lateral accelerations up to and including the limit of adhesion.
- Equipment for tracking and quantifying the path, attitude, speed, and elapsed time of the test car through various interesting segments of the course.
- Instrumentation for the graphical recording of speed and distance.
- Water-soluble dye was used to extract the path, attitude, and speed of the car at any or every point on the track.⁴³

⁴³ Nozzles were located along the longitudinal centerline, one under the front axle, one under the rear axle, and one under the CG. The stream under the CG was interrupted at precise intervals by a rotating valve. Speed at any point could be calculated by dividing the length of the mark by the interval. The radius at any point was indicated by the angle between the front and rear wheels of a tricycle tracking the path of the CG. With the wheelbase known, the attitude of the vehicle and the rear slip angles were determined by the separation of the front and rear axle paths. The on/off switch was in the cockpit so when the driver was up and running he could lay down what was going on whenever he was ready.

- A suspension test vehicle (STV). A single-passenger, high-performance, slab-sided structure accommodating any feasible suspension geometry.
- The construction of a safe, 1g/100 mph skid pad.
- Sober⁴⁴ and drunk driver tests in accident avoidance situations.
- A “limit of control” driver training school.⁴⁵

To get a finger on the state of the art of “stability and control,” we bought a Lotus Formula Jr. and a championship go-kart. Both were incredible. The Lotus F Jr. was, at the time, maybe the best handling car ever. The go-kart was a riot and, at low speeds, capable of lateral accelerations equal to any race car. We rented the Waterford Hills race track a few miles north of our shop. Mauri Rose, Jim Musser, and I spent a lot of time out there with the Lotus Jr. and other vehicles. The track was secluded and handy but short and slow—no long straights or big turns.

XP 777—(Monza GT)

About that time, we figured that we were not only in a position to defend the Corvair, but that we knew enough to develop a sports car with handling qualities substantially better than what we knew to be the state of the art.

We built three. Jim Musser was the project engineer. He ended up with a stiff steel monocoque with ‘wide’ rims and a hopped-up Corvair engine behind the rear axle—and the roll couple distribution to go with it. All the development work was done with the bare chassis. In the end, it exceeded anything we knew of. It was neutral at the limit and turned over 0.8g's. Bill Mitchell was keen on it, and Larry Shinoda did a really slick, good-looking body. It was called the XP777.

The Meeting of June 17, 1962

Mitchell was big on high-performance cars and attended a lot of road races, often showing some of the big, loud, “hairy”-looking cars he and his people liked to build. He wanted to take the XP777 to Elkhart Lake for the June '62 Road America race. Musser and I went along. It was driven on the parade lap and got a lot of attention at the show after the parade. Jim Hall was one

⁴⁴ Almost everybody panicked at about 0.3g's, locked up the brakes, cranked in full steer, and slid into a dummy that could have been missed at lateral accelerations well within the limits of the car.

⁴⁵ Still used by various police organizations, I think.

of the interested parties. Hall and Musser, both engineers, had a long and detailed discussion standing over the car. Musser later introduced me to Hall and his partner, Hap Sharp. Like everyone else in that series, they were running front engine rear-drive 'sports' cars. Colin Chapman had, by then, established the rear engine rear-drive monocoque as the way to go. Hall and Sharp knew it was the way to go and had a fiberglass monocoque in the process.

That chance meeting was the beginning of a long and mutually productive relationship.

Here was an engineer, a successful racing driver, a guy with his own shop, his own race track; a guy with the means to build and develop his own cars, a guy operating out of a remote little place in far away Texas who knew that $F = ma$. My mother would have known what to do—he and Hap wanted to build a MERD Chaparral that would blow the doors off everything on the track, we wanted to build a MERD Corvette that would blow off everything on the road. It looked like it would be fun, the Corvair thing looked like it was in the bag, and there was the good chance we would make a contribution to the art and science of stability and control—an end that, in my mind, would certainly justify the means.

Hall went to Europe to drive F1 cars. He was gone for that one season. While he was away, Hap came to town with a proposition. I don't remember exactly what it was but I liked it.

Penske came in some time later. He was a top driver and a persistent competitor. He drove a Cooper F1 MERD space frame, modified for the series, called the "Zerex Special."⁴⁶ He was running an iron Chevy V8. He worked for ALCOA, and one day he called to say that if we could get him the patterns for an aluminum Chevy block, he could get them cast. (It was an engine we visualized for the MERD Corvette.) He got the patterns. He cast the blocks. We machined, built, tested and made the engines available to both he and the Hall/Sharp team. It soon became apparent that we could not support both operations. Penske drove a number of races with Jim and retired as a driver in December 1964.

I understood why we were out of racing. It didn't make any sense and I thought there was far more to be gained than lost. The immediate chain of command at the time was Goodman, Cole, and Knudsen. I didn't tell them we were not doing what we were doing and I don't remember them ever ask-

ing me if we were doing it. It was not something that would embarrass GM. We showed them a lot of the stuff we had built and done in the process of trying to understand vehicle dynamics; the models and rigs we built for helping the lawyers to ask good questions and to spot bad answers. They knew about the XP777 and the experimental rear engine rear-drive Corvette. There was no problem in developing a sports car for the street. We were just not supposed to be supporting any racing operation.

The 1st V8 MERD Monocoque and the move to Midland

At the time of the Elkhart Lake meeting, Hall and Sharp had a MERD Chevy V8 fiberglass monocoque in the process of construction. When we got back, Musser started a MERD Chevy V8 steel monocoque. Conceptually, Musser's car was the same as the XP777 except it accommodated the Chevy V8 ahead of the rear axle—a stiff monocoque, anti-roll, anti-pitch, anti-camber, anti-jack suspension geometry, wider stiffer tires, neutral steer roll couple distribution, etc. In January of '64, all the instrumentation, and all the car and tire test work were moved to Midland. Performance monitoring photo cells were planted at points of interest around the course. The tire tester was set up and a 100-ft. radius skid pad built. For a couple of reasons Musser and I, both novice drivers, knew that getting hurt would not be good. The outside of the turns were grassed and irrigated so there was room to get off the track without getting into the sand and upside down. The first move included the Suspension Test Vehicle, the Lotus Formula Jr., and the Cooper. It was a good move. It beat the hell out of Waterford. It beat the hell out of the Milford Proving Ground and the GM Tech Center, etc., combined.

In the course of all that followed, we got acquainted with a number of racing drivers—people who drove at the limit for a living. They were a potential source of impressive expert testimony. There was Hall, Sharp, Penske, Stirling Moss, Fangio, Phil Hill, and others, all familiar with the behavior of conventional FERD, MERD, and RERD passenger and racing cars. All of them supported GM's position that the Corvair was state of the art. Hall did a piece for *Car & Driver* on the fundamentals of stability and control. In preparation for the possibility of being called to testify, Moss and Fangio spent considerable time at the GM proving ground driving the Corvair, the VW, the Renault, the Ford Falcon, etc. Stirling Moss was called and gave testimony in one of the California cases.

The end product of this Chaparral / Chevy effort led to:

- An unprecedented extension of the art and science of vehicle dynamics, particularly at the limit of control, particularly for racing cars.
- The complete exoneration of the Corvair.

⁴⁶ He covered the F1 chassis and wheels with a two-passenger body with him in the middle and a seat for an underaged midget by his side.

- An unprecedented road racing record by Chaparral Cars.
- Sadly, the ultimate conclusion by GM that a midship engine sports car was not a practical configuration for street use.

For me, the Chevy R&D / Chaparral experience was easily the best of my professional career. The principals were Jim Hall, Hap Sharp, Jim Musser, and me—backed by some of the best engineers and craftsmen anywhere. Motor racing was the compendium of the process of natural selection; it was about as close to a ‘free market’ mechanism as you could get—a definitive objective, intense competition, no constraints, and a nice tight little loop that paid every Saturday. As competitors, we had it all: the money, the place, the tools, the energy, the incentive, the talent, and the freedom to do whatever we figured would get us across the line first.

That it went off as well as it did was not evidence that there were no fistfights, but the potential and the excitement of the learning process and beating the hell out of the best in the business was a dominating influence on the way we all behaved. Who sparked what was not a concern then or, to my knowledge, now. What happened was that we got it all together; that it got sparked was inevitable. But, without exception, Jim Hall was the guy who said what went on the car on race day. It would not have worked any other way.

A lot of energy was spent in trying to put numbers on significant variables and to figure out quick and easy ways to find out if the hardware was producing numbers consistent with Newton’s prognostications. It began with the understanding that the ultimate objective was minimum drag, minimum mass with the lateral and longitudinal vector sum equal to the normal force times the coefficient of friction—at every point on the course—and with the stability and control to get there and to stay there—an approachable objective. The Chaparrals came closer than the rest.

Of the various devices used to measure performance, the most revealing was a simple rev counter on the front wheel. The supporting instrumentation converted the blips to speed and distance. The paper was driven by distance and the pen by speed. Since the distance was constant, traces of various lap times could be directly overlaid. We were the early pioneers of On-Board Instrumentation. These early efforts were simple and effective.

A standard automotive 8-track tape recorder simply recorded the tone from the magnetic pick-up at the front wheel. The playback produced a plot of speed vs. distance for each lap. The unit was used at every race track including tire tests at Indy. Speed/distance maps were plotted for every track on the circuit. With this instrumentation, accurate measurements of the lap time

effects could be made for various vehicle changes. For stated reasons, on race weekend, Hall would make tape recordings during practice, take the recorder to a phone booth, call R&D and play it back. The tone was converted to the speed vs. distance plot so that modifications were easily quantifiable.

With this instrumentation, the relative significance of developments in longitudinal and lateral acceleration were easily and directly quantified.

Longitudinal

Deceleration

The sum of all the braking intervals on any given track is a very small part of the total lap time. Gains due to increases in brake performance are therefore relatively small.

Brakes were essentially state of the art:

- Torque was balanced front and rear in proportion to the dynamic normal forces. The energy capacity and the dissipation rates allowed these torques to be consistently maintained.
- Subsequently, the adjustable wing at the rear became a significant reservoir for braking energy.
- The development of the wide rims for cornering stiffness brought on a brake cooling problem. The problem was relieved with an open cast aluminum wheel with tangential spokes cantilevered off the hub.⁴⁷

Acceleration

Acceleration gains were more significant because the vehicle operates in this mode for longer periods of time. However, gains were something less than what might be expected because the gain in speed does not start until exiting the turn and requires earlier braking going into the next turn.

- Except for the aluminum block, the engines were, essentially, state of the art.

⁴⁷ It happens that some years back, Chevy released a torque converter turbine with radial spokes. In time they broke, regularly. One morning on the way to work I realized I was following an old model A Ford with a rear-mount spare wire-spoked wheel. It took about 30 miles to finally see what I was looking at. We put the spokes in tension and fixed the turbine and subsequently the brakes on the Chaparral.

- The torque converter, the so-called “automatic transmission,” was a new development.⁴⁸ The characteristics of this torque converter were tailored to the engine torque curve so that the WOT tractive effort was at the limit of adhesion right up to the peak torque of the engine—with no ratio changes. The “automatic” allowed the driver to keep both hands on the wheel, his left foot poised on the brake and the right foot on the throttle. He could get into the corner deeper and come off of it quicker. The left foot on the brake, the right on the throttle and both hands on the wheel afforded better control, particularly in traffic. Later, with increasing competition and for some tracks, ratio changes were added. We ended up with as many as three speeds—all manual, clutchless shifts.

Lateral

Gains in lateral acceleration showed far more potential than any gain in longitudinal acceleration. An increase in cornering speed, given any longitudinal performance, is an increase in speed at every point on the course.

Most of the emphasis in motor racing, up to this point, had been directed at the length of the **longitudinal** vector. Because of our involvement with the Corvair, the better part of the Chevy R&D energy had been directed at the length of the lateral vector.

The recognition that the force between the tire and the road could be substantially increased via aerodynamics without a corresponding increase in mass led to maybe the biggest advance in racing technology—easily accounting for the biggest single reduction in lap times in the history of the sport.

While the longitudinal vector on the tractive wheel increases with the square of the speed, so does the aerodynamic downforce. Such being the case, **neutral steer is achievable at any speed and with increasingly higher lateral accelerations. But because of the increasing length of the tractive vector with speed, for neutral steer the downforce on the tractive wheels must increase at a higher rate than on the rolling wheels.**

Aerodynamic downforce became the dominant interest of the R&D / Chaparral team.

While most drivers and builders had little regard for the low-speed skid pad, it was perhaps the most important tool for setting up a car for maximizing

lateral acceleration. The convention, at the time, was to set up for neutral steer in the high-speed turns and tolerate strong understeer and limited lateral acceleration in the low-speed turns. Now it became clear that the car should be set up for neutral steer and maximum lateral acceleration in the low-speed turns adjusting aerodynamic downforce to maintain neutral steer and increased lateral acceleration at high speed.

The tire test machine was designed to measure the slip angles right out to the limit of adhesion. It was a merry-go-round with a long radial arm to which was fixed a trailing arm that held the test wheel and tire. The speed was controlled by someone riding the radial arm sitting directly over the axis of rotation. The rig was powered by a gasoline engine driving a wheel near the outer end of the radial arm. The normal load on the test tire was controlled by the use of lead ballast. The lateral forces were calculated from the speed and radius of the path of the tire. The slip angles were indicated by the angular position of the trailing arm. The equipment plotted slip angles vs. side forces for various normal forces right out to the limit of adhesion.

The approach was to select tire sizes, rim widths, and roll couple distribution to achieve maximum lateral acceleration on the skid pad in both directions making the car as neutral as possible. Since speeds on the skid pad are low, aerodynamics were not a factor. Having maximized the g's on the skid pad, the car would be taken to the track's high-speed turn where the rear downforce was adjusted for neutral steer. The limitation was always the downforce in front; there was no problem in getting enough on the rear to balance the front. The attempt was made, however, to minimize the drag-to-downforce ratio. The drag force reduced speed and the drag moment reduced the front downforce and hence maximum lateral acceleration.

In early tests, cars would typically do better in one direction than the other. To balance right and left, the car was mounted on individual wheel scales with a driver and half a load of fuel on board. The threaded collars supporting the springs on the shocks were adjusted so that no weight was jacked corner to corner. This was done with the roll stabilizer links disconnected. The lengths of the stabilizer links were then carefully adjusted so that when they were reattached there would be no twist in the bar. Cars set up in this manner achieved the same lateral acceleration in both directions.

A torsionally stiff chassis was an absolute essential in effecting the roll rate and roll couple distribution required for stability and control at high lateral accelerations. For a sprung mass roll rate of 300 lb.-ft./deg., R&D shot for and ended up with a 3000 lb.-ft./deg. aluminum structure that weighed just 57 lb. Key to this achievement was the use of a simple 3/8 scale plastic model. (The unlettered act of simply twisting the model between the palms of both hands probably stimulated more ideas than any of today's computer

⁴⁸ Sharp asked a lot of good questions. One of these was, “Why do we have to have so many damn gear ratios?”

models. Construction was quick and easy and facilitated confirmation of a lot of ideas that would otherwise not have been explored.) To our knowledge, the efficient utilization of space and mass in chassis structure afforded by this process has not been exceeded.

The suspension geometry was worked out on the Suspension Test Vehicle. The wheel base was 100", the tread 60" and the CG height was 13-14".

- The front was SLA independent, with a swing arm length of 75" in both planes with the lateral instant center on the ground to prevent jacking. 33% anti-dive turned out to be a reasonable compromise.
- The rear was essentially the same as the front. The lower rear ball joint was actually the steering arm end. For pitch considerations, the rear was set up for 100% anti-lift and 100% anti-squat. The resulting toe changes were easily nulled by adjusting the upper and lower tie rod lengths.

The Evolution of Aerodynamic Downforce

- 1962—Hall experienced front lift on the T&B FERD Chaparral 1. Although a number of things were tried, the problem was never completely eliminated.
- October '63—The new Chaparral 2 had a body with an inverted airfoil profile with a high leading edge (a Bill Mitchell idea). Hall had done much of the preliminary development with the bare chassis, with very encouraging results. But, when the body went on, the wheels came off, and, at 120 mph the fronts were in the air.⁴⁹

⁴⁹ Bill Mitchell probably sold more cars for GM than anybody in its history but he didn't know, or care, if $F = ma$ or not. He was, at the time, the most powerful executive in the corporation. He scared almost everybody, Shinoda and I excepted. He liked big toothy grills, fake portholes and big airscops that were hooked up to nothing. If chrome had not been invented by the time he got there, nobody would have ever heard of him. He had no idea at all what a car wanted to look like. He tried to make them look like sharks and P-38's. He didn't like anything that looked functional. If he couldn't disguise it, he covered it up, particularly if it was a screw, any screw. But he was bananas for horsepower. If it was big and shiny, smoked the tires and made a lot of noise, it was a car. Americans agreed—in droves. His "designs" were the paragon of the industry. Everybody tried to make theirs look like his. I was in his corner, I just didn't think it was going to last forever.

Of all the things he didn't know about, aerodynamics probably heads the list. Few in the industry knew much more. As V.P. of GM Engineering Staff, I proposed to build a full-scale wind tunnel. To no one's surprise and for conspicuous reasons, a number of brawls ensued. Bill won 'em all. The chairman pacified him by agreeing to let him run it. At Bill's insistence they had changed the name from Styling to Design Staff so it was clearly the proper thing to do.

In any event, his idea of an "inverted airfoil" profile for a racing car would have worked out well if the CG had been high enough, say 50 feet.

- Jim called about a week before the '63 Riverside race. He brought it in and we pop riveted a 'dam' in front to divert the air around the body rather than letting it pile up underneath. The first run sucked the skins right down on the tires and about set them on fire. Subsequent modifications relieved the excess downforce. A laid-up fiberglass equivalent was installed and Hall made the race, the first for the Chaparral 2. He was the quickest but went out with an electrical fire.
- The 'Riverside dam' was ugly and had a lousy drag coefficient. It was a quick fix for the Riverside race late in '63. When the season was over, Hall set about doing a new nose, lowering the aero parting line at the leading edge, and ducting the air from under the nose through the radiator and out the top. Unlike the dam, the new nose resulted in increasing oversteer with increasing speed. Calibrated rods through the fenders and off the front uprights showed increasing downforce with increasing speed. Recognizing the problem, Jim developed a lip on the back to balance the downforces in front so that the car was neutral steer at all speeds.
- Spring '64—Musser experienced front lift on the first aluminum monocoque R&D MERD V-8 at 170 mph. (The leading edge was much lower than the original Chaparral 2.) The entire front section was held down by springs at the rear, which allowed that end of the section to lift off the body. Had the section been bolted down, the lift probably would not have been apparent. Musser surveyed the top and bottom of the skins with a water manometer and vented the high-pressure areas under the skin to the low-pressure areas on top. It was expected that this change would result in less drag than the quickie dam we put on the Chaparral 2. The car ended up with about 100 lb. downforce.
- Although we had begun to utilize aerodynamic downforce for balance and for gains in lateral acceleration, we had not yet realized the enormous potential of aerodynamic downforce in the overall performance of racing cars—lateral and longitudinal acceleration.
- The revelation that there was a way to increase the normal force without a corresponding increase in mass was about as elementary and as profound as Newton's revelation under that apple tree. I imagine he probably laid there for a while after he got hit. I think we laid there a while too—if I had been conscious when we smoked those tires, I would have stepped back and hollered, "EUREKA! Get some big springs in there and stick a wing on the back." I didn't and I don't remember anybody else making the right kind of noises either.
- Some time later, the Cooper took a couple of corners faster than our data indicated it was capable of doing. It got through the traps at high-

er lateral accelerations than we knew it should. I have a recollection of us standing around there trying to figure out what caused it. The only thing we found that looked funny was a strip of square tubing, maybe a $1/2'' \times 1/2''$ or more, on the bottom pan across the width of the car at the CG.⁵⁰ Somebody wondered if it could have caused a depression in the air pressure under the big area of the bottom pan. We experimented with various strips at various places and various angles on the Chaparral with no significant results. But it has been in my mind for a lot of years that that was when we got hit, when we began to realize the potential of aerodynamic downforce. At the time, I had never seen any evidence that Chevy, Cooper, Chapman, Cunningham, Ferrari, Troutman & Barnes, Chaparral Cars, or anybody else had been hit. Yeah, I know Ferrari had a lip on the back of something a long time ago. So? Whatever it did couldn't have been much and they didn't show any evidence of recognizing its potential.

- Whenever it was, and whatever hit us, it was we who put ourselves in the position to get hit, and we were the first to show any evidence of having been awakened by it.

In any event, it worked and the other teams continued to gather around every Saturday looking for what the Chaparral had that they didn't have. The process continued. Gains were incremental but the Chaparral led the way.

The Front

- The evolution began with the dam—a diverter, causing the air to go around rather than under the car.
- The leading edge was lowered.
- The air was ducted from under the nose through the radiator and out at the high-velocity, low-pressure areas above.
- Vents were added.
- The mustache replaced the dam.
- The radiator was moved to the back and the duct opened for higher air-flow and higher down force (see below).

But the front remained the limiting factor in total downforce. Getting what it took in the back to balance all that we could get in the front was no problem.

⁵⁰ It had been used to mount a nozzle for spraying dye on the track to show the path of the CG.

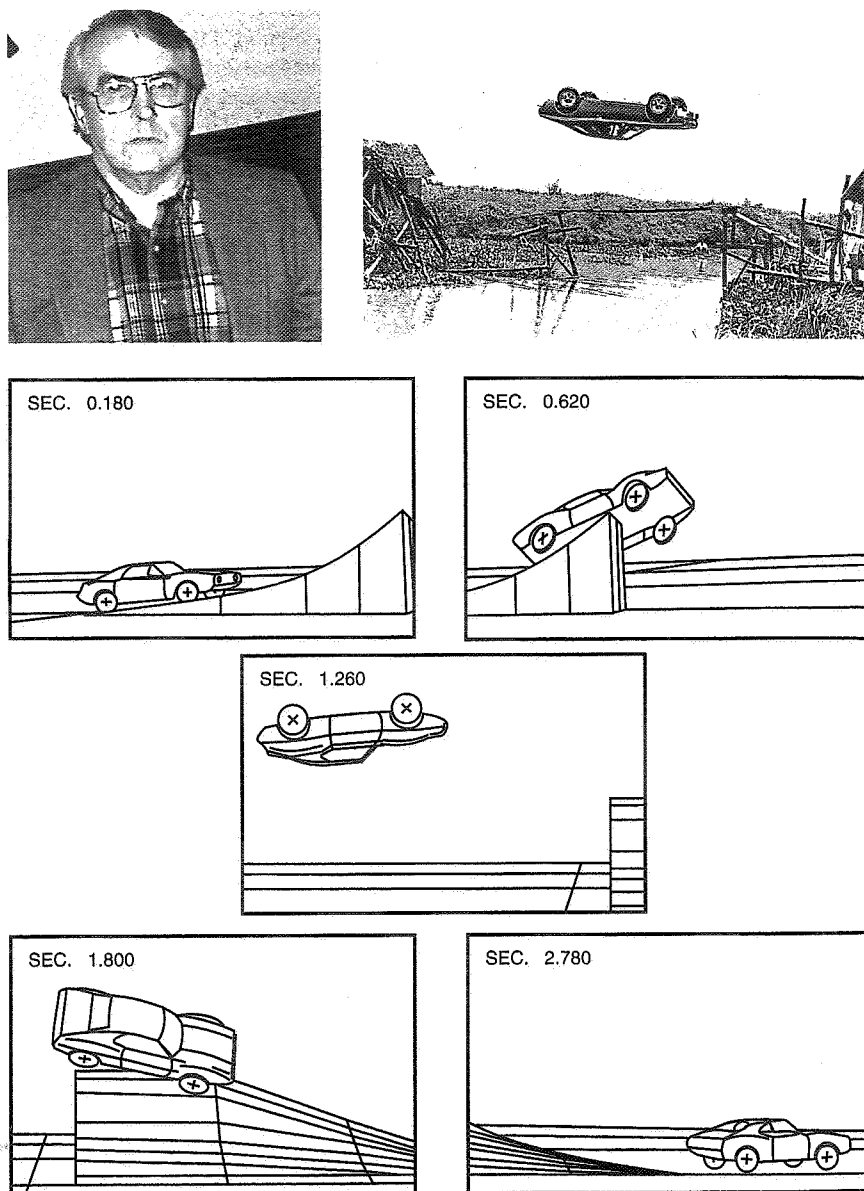
The Back

- The back began with a relatively small lip fixed to the rearmost part of the body.
- Next was an overlapped lip. While the angle was fixed, the height could be adjusted in the pre-race set-up to balance whatever downforce was achievable in the front.
- With increasing gains in downforce in the front came a larger rear wing, standing above the body; the angle of attack was adjustable for pre-race set-up.
- Increasing downforces resulted in increasing drag. Logically, the next step was a wing design that allowed the angle of attack to be trimmed for minimum drag by the driver, in the course of the race.⁵¹
- Predictably, the downforces got so high and the springs so stiff the mass was essentially unsprung. As the roll rate increased, the roll couple distribution became very sensitive and difficult to maintain. Logically, the next step was to take the rear downforces directly onto the wheels, retaining the trim control described above.

With the rear wing trimmed for minimum drag, at increasingly higher speeds, the downforce increased much faster in the front than in the rear so that the car was potentially unstable. To correct this, a valve was incorporated in the duct in the front and connected to the linkage operating the rear wing, so that when the driver released the pedal **entering the corner, both ends of the car went to the high downforce position**, i.e., the valve opened in front and the wing in back went down. When the driver depressed the pedal **coming off the corner, both ends of the car went to the low downforce position**, i.e., the rear wing went to the minimum drag, minimum downforce position and the front valve closed enough to reduce the downforce and balance out the car for high speed. Both positions of both the front valve and the rear wing were adjustable for pre-race set-up.

On Saturday, they started gathering around again. Copies began to show up on F1 cars. Some of the wings blew off. Before they could figure out how to get them to stay on, they were banned. Too bad... Newton would have barfed.

⁵¹ The wing pivot was set behind the center of pressure so that, unattended, the wing stayed in the max downforce, high drag position. With the torque converter (no clutch) the driver's left foot was free to brake. Coming off the corner and down the straight he could release the brake and depress the wing pedal for max speed and acceleration. In approaching the corner, on releasing the wing pedal to apply the brake, the wing would return to the max downforce, high drag position.

Ray McHenry—The Comprehensive Models*Figure 13.9 Ray McHenry and the Spiral Jump.*

McHenry joined the Vehicle Dynamics Dept. at CAL in 1961 and later transferred to the Transportation Division where he remained until 1978 as a Staff Scientist.

Ray is an extraordinary engineer by any standards, combining a solid understanding of the mathematical foundations of vehicle dynamics with the empirical approach of the practical engineer and designer. As one of his co-workers has said, McHenry was "results oriented." He would utilize closed-form theory when available but was never stopped by its limitations, pressing on with the incorporation of experimental data from a variety of sources to a good engineering result. Highly competitive, armed with a good sense of humor, anxious to tackle the tough problems, Ray was able to pioneer a variety of models in crash simulation and vehicle dynamics in general.

In light of his subsequent accomplishments, his background prior to coming to CAL is enlightening. It is summarized below in his own words.

Early fascination with automobiles and curiosity about how they were designed, particularly the suspensions and steering systems. While in grade school and high school, built several small vehicles with bicycle wheels and single-cylinder engines.

Father and older brother always had ongoing creative projects on mechanical devices and gadgets, such as wood-splitters, snow blowers and farm tractors. Desire to 'join the team' demonstrated through attempts to perform useful design calculations.

Trained in aircraft and engine mechanics in U.S. Air Force. Served as a helicopter crew chief. Active duty 1946 through 1949.

B.S. Engineering Physics, minor in Mechanical Engineering, University of Maine, 1953, M.S. in Automotive Engineering, Chrysler Institute, 1955. Thesis on vehicle parameters needed for vehicle dynamics analysis, measurement procedures.

Worked for Mr. Robert Janeway in the Vehicle Dynamics Department at Chrysler. The learning experience of working with Mr. Janeway, in terms of the application of engineering theory to practical design problems, is considered to have been extremely valuable.

Served as principal operator of one of the first analog computers in the automotive industry while at Chrysler. Applications to vehicle ride dynamics. Also participated in early (1954) applications of digital computers to specific design problems (e.g., leaf spring design) and to the ride dynamics of automobiles. The early digital applications to vehicle dynamics involved overnight runs on digital computers in the Chrysler accounting department.

Worked as a senior design engineer at Ford Motor Company. Design and fabrication of prototype suspension components. Evaluation of ride and handling characteristics of experimental vehicles. Measurement of suspension properties of production, prototype and competitive vehicles.

Of his several comprehensive models, the Highway-Vehicle-Object Simulation Model (HVOSM) has had the greatest impact on vehicle dynamics. This was developed for the Bureau of Public Roads to study single vehicle accidents (Ref. 88). This model, developed over a several year period, has fifteen degrees of freedom (six rigid body sprung mass, four suspension deflections, one steer, and four wheel rotations), is large amplitude and fully nonlinear. There is also detailed terrain representation and an associated driver model.

HVOSM and directly related successors moved technology into the application level for real vehicles.

With characteristic thoroughness, McHenry insisted on an extensive experimental validation which involved all of the usual testing tasks plus some dramatic maneuvers such as those utilized in automobile thrill shows. Not content with the successful simulation of a normal ramp jump, Ray conceived of the "spiral jump" in which the vehicle takes off from a "spiral ramp," does a complete barrel roll in the air and lands on a "reverse spiral ramp." Using the model and an early application of computer graphics he designed the ramps which were then constructed and the maneuver demonstrated at the CAL testing area.

For the development of HVOSM, McHenry received the Crompton-Lanchester Medal as well as the Safety Award in Mechanical Engineering, both from the IME, in 1969.

HVOSM was widely (and in one case unscrupulously) copied but there is no question that it was McHenry who had the vision and the talent to create this technology.

A major offshoot of HVOSM was the development of DK-4 for Chevrolet which occurred in 1970-71. This model (Ref. 131) was authored by R. Douglas Roland, Jr., of the CAL Vehicle Research Department. The mathematical basis of HVOSM was utilized but the emphasis was on vehicle stability and control as opposed to single vehicle accidents. The model was developed in close cooperation with Chevrolet, in the person of Ernie DeFusco. The chassis, tire, and aerodynamic inputs were incorporated in formats commonly used by GM.

DK-4, in turn, was to serve as part of the basis for the comprehensive implementation of the Moment Method by Dennis Kunkel in 1975. Since the Moment Method involves steady-state nontrimmed forces and moments, its solution process is different than that of the time-based DK-4.

HVOSM, DK-4, and the Moment Method were originally programmed for IBM mainframes. All three were ported to IBM-PC by D. J. Segal in 1985-86, with extensive additions (to be discussed later) to the Moment Method. Dave Segal had earlier collaborated with McHenry in the development of HVOSM and crash simulation developments.

Finally, in the sequence of things, the current MRA Vehicle Dynamics Simulation (VDS) has its roots in DK-4—the culmination of over 30 years of large, comprehensive vehicle model developments.

Calspan Tire Research Facility (TIRF)

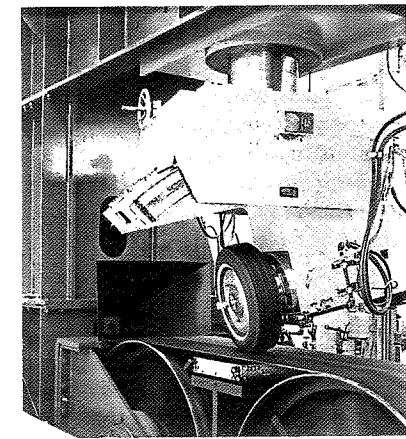
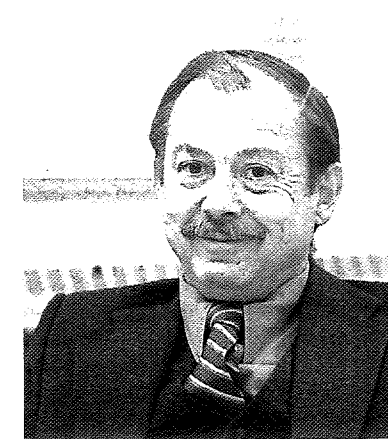


Figure 13.10 King Bird and TIRF.

The study of automotive vehicle dynamics requires force/moment tire data. We have already noted that CAL had pioneered a modern tire tester in the Air Force—Cornell on-road machine of 1954—a machine that produced reliable six-component data for the full range of free-rolling tire operation up to 40-50 mph. Later Bidwell had carried tire tester development further in a flat bed laboratory machine which permitted tests under traction and braking at low speeds. By 1967 it became apparent to Cornell Lab / Calspan Transportation Research that there was a need for a much higher-performance indoor tire tester.

The history of the promotion, design, and development of such a machine, located at Calspan in Buffalo, NY, is well documented in a memorandum by King D. Bird, "Summary of Tire Research Facility (TIRF) Case Study," of December 1972. Bird, then head of the Vehicle Research Department, was almost totally responsible for TIRF, obtaining

sponsorship, making design and development decisions, and bringing the facility to operational status. He was ably assisted by his project engineer, Jim Martin.

The specification for this facility insured a quantum jump in the technology. It was to be an indoor, flat surface machine with a load capability for passenger car tires of 4000 lb. and up to 12,000 lb. for truck tires. Very large slip and camber angle ranges and high accuracy strain gage balances (six-component), substantial traction and braking capability, and a speed up to about 180 mph were specified. Computer operation and data processing were planned from the beginning.

After a trip by Bird to Europe in December 1967 where various tire research facilities were visited, discussion got underway as to the basic configuration. Early in February the decision was made to use a rotating belt for the roadway surface. The eventual specification was for a steel belt 30 inches wide running on 67-inch diameter steel drums, the belt to be coated with various surface materials to provide desired friction coefficients. Under the test tire, the belt was to be supported by an air or fluid bearing. This configuration, which proved to be desirable, offered some difficult technical problems, for example: How would the belt be restrained laterally under several thousand pounds of side force from the test tire? Could a bearing be developed which would maintain the belt essentially flat under the test tire and still support high normal loads? Could a scheme be devised for putting a water film of controlled thickness on the belt for wet tests?

All of these problems were ultimately solved and, in part, demonstrated on a 1/4 scale model of the drum/belt assembly which was completed in 1968. The lateral belt tension was solved by first analyzing why belts tend to ride on the high part of crowned drums. The mechanism proved to be related to the way tires develop lateral force from slip and camber angles. The solution adopted by Calspan permits one drum to tilt (against a stiff spring) about an axis perpendicular to the drum axis, under the lateral force from the test tire. George Duryea (CAL, Calspan) made major technical inputs to the basic design of the facility. Incidentally, George is the grandson of pioneer automaker J. Frank Duryea, winner of the first race in the U. S. (see *Carriages Without Horses*, Scharchburg, SAE R-127, 1993).

The problem of financial sponsorship for this facility was equally difficult. It was accomplished by a phase I feasibility and design study in which the following companies contributed \$10,000 each:

GM	Goodyear	Dunlop (USA)
Ford	Goodrich	Armstrong
Chrysler	Uniroyal	General Tire
AMC	Calspan	

The second phase was financed equally by Motor Vehicle Manufacturers Assn. (MVMA) and Rubber Manufacturers Assn. (RMA) plus a \$100,000 sole source contract from

NHTSA for shakedown of the facility. Forty meetings outside of town were required to bring in the sponsorship. To avoid any collusion (anti-trust regulations), the contributions totaling some \$670K from MVMA and RMA were made as gifts to Calspan.

The TIRF facility became operational in January 1973 and has been in continuous operation ever since—over 20 years. After its shakedown period, an experimental validation was performed against other test facilities located at Firestone, Ford, General Motors, General Tire, Goodrich, Goodyear, Uniroyal, and University of Michigan (HSRI). There was a considerable spread in the data from the other machines (the largest spread occurring for the on-road machines). Data from TIRF fell close to the mean data from the other machines and hence suggested that “within the evaluated performance range, TIRF was indeed a valid test facility.”

There is no question that TIRF set a new standard in tire testing facilities. It pioneered flat belt technology and high-speed testing. The features of the machine have been widely copied including the belt tracking principle, the air and water bearing (Calspan uses an air bearing but also produced the earliest design of a water bearing). Using the basic features of TIRF, MTS Systems Corporation has developed a production tire test facility, the FLAT-TRAC, which has been widely sold and hence increased the availability of reliable tire force and moment data.

Moment Method (Force-Moment Analysis)

For one who worked in the aircraft industry for 20 years and was literally brought up with wind tunnels,⁵² it was no stroke of genius to envision the importance of automobile “statics,” the analysis of the balanced and unbalanced (untrimmed) forces and moments on the automobile. In fact, the development of static theory and substantiation by test was listed in a general research plan put together by the author in 1952, at the beginning of our research for General Motors. Why we failed to push “statics” after our initial success with the linear dynamics can be explained only by a preoccupation with aircraft dynamics and our distance from the automobile design process where statics really pays off. The only exception was the constrained test program (tethered skid pad) performed at Pine Lake, Wisconsin, during the National Safety Council Winter Driving Program in 1955. Thus it was some 14 years before we seriously undertook the study of “statics” in 1969. By that time Frank Winchell and Joe Bidwell had both moved to GM Engineering Staff. The subject was reopened in a memorandum to Bidwell titled, “Static Directional Stability of Automobiles - Moment Measurement Technique” (5/19/69) in which we reviewed general wind tunnel practice, the limited experience with automobile proving

⁵² Bill Milliken constructed the first small wind tunnel (W.T.) at the University of Maine in 1931, worked for two years at MIT as W.T. assistant, liaisoned W.T. programs for Vought, Vought-Sikorsky, Boeing and Avion (Northrop) in various tunnels including: Sikorsky, Propeller Research Tunnel, 7 x 10 ft. NACA Langley, 20 ft. NACA Ames, GALCIT at Cal Tech, etc.

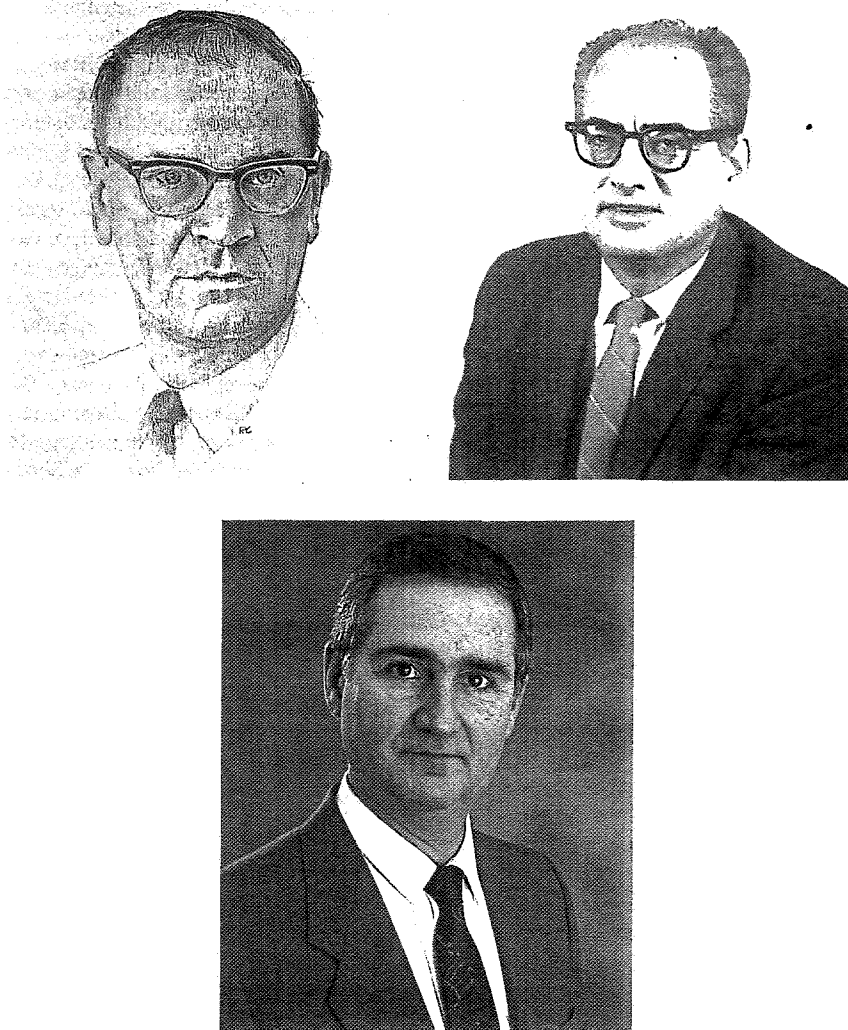


Figure 13.11 Roy Rice, Fred Dell'Amico, and Doug Roland.

ground constrained testing, the special requirements of an automobile constraint system and a simplified closed-form calculation procedure. In a subsequent session with Winchell and Bidwell, we were given the green light to go ahead on our consulting agreement.

Using available data for Chaparral GS 2G, 1967 Can-Am car, a paper spreadsheet of over 40 columns, and a slide rule, the first N-A_y diagram was produced by the author over a two-month period (a labor-intensive process of some 10 hours/point!). For these calculations, a lateral acceleration and hence a trimmed lateral force and an untrimmed yaw moment were initially assumed. The closed-form procedure resulted in the corresponding steer angle, δ , and chassis attitude, β (also α_F and α_R).

After that, the activity on automobile statics was placed in the CAL Vehicle Research Department under King Bird, where in the ensuing years a great deal of talent was brought to bear on the subject. This consisted in broadening the concept, developing a variety of computer programs of increasing sophistication, conceptualizing and investigating an indoor Constrained Vehicle Tester (CVT), plus a great deal of effort on the interpretation and theory behind the diagrams—in short, the development of a statics technology.

Most of this effort, which continued until 1976 when I retired from Calspan and set up MRA, was supported by Winchell, GM Engineering Staff. It was Frank's unvarying philosophy that if some fundamentally sound technology came along, GM should know about it and be involved.

Some of the specific accomplishments during this period and the people involved were:

1. Development of a simplified nonlinear Moment Method (MM) computer program which enabled calculation of diagrams under traction/braking conditions—Roland (1970).
2. Development of a MM program based on a linear tire cornering characteristic with a horizontal friction limit enabling an understanding of the limit end of the diagram—Roland (1970).
3. Experimental demonstration (with scale model vehicle and roadway) of the constraint system—Dell'Amico (1970).
4. Proposals to develop Constrained Testing techniques (resulted in contracts from Engineering Staff)—Rice, Dell'Amico, Roland and others (1970-72).
5. Report, "Steady-State Stability of the Automobile—An Approach Based on a Method of Tethered Vehicle Testing using a Yaw Constraint"—Dell'Amico (1971). A major advance introducing the stability index and path curvature stiffness concepts.
6. Report, "The Constrained Vehicle Tester (CVT)—A Device for Obtaining Stability and Control Data on a Full-Scale Automobile," in two parts—Dell'Amico, Rice and Romeo (1973). This report describes flat-belt roadway units controllable in speed and direction, wind tunnel and laboratory versions of the CVT, the CAL constraint system, sizing and test variables, earliest discussion of the

constrained transient, etc. This technology was much later transferred to MTS Systems Corp. and is the basis for the Flat-Trac Roadway Simulator.

7. Report, "The Constrained Vehicle Tester—Phase 2," a study of attachment point methods and error analysis—Dell'Amico and Massing (1975).
8. Report, "Development of Moment Method Computer Simulation Program based on DK-4"—Kunkel (1975). This was the beginning of a comprehensive MM computer program, a simulation of the CVT. Kunkel was a member of the CAL Transportation Safety Department at that time.
9. Report, "Moment Method Analysis of a Vehicle with Highly Cambered Wheels Using Computer Simulation"—Kunkel (1975). The vehicle, MX-1, had been tested on Chevrolet's VHF (kinematics and compliance tester) and comprehensive tire test data was available from TIRF.
10. By 1975, Rice, Dell'Amico, and others had developed the more generalized C_N-C_Y diagram and the still more fundamental plot for infinite radius.
11. SAE Paper No. 760712, "The Static Directional Stability and Control of the Automobile," by Milliken, Dell'Amico and Rice (1976). This was the first of a number of papers describing static technology (Refs. 93 and 94).

Roy Rice (CAL, Calspan) was a great proponent of the Moment Method. He viewed the moment diagrams as literally portraits of the stability and control of the vehicle and had gone far in developing a feel for diagram changes resulting from changes in the vehicle configuration. He was the first to integrate a transient on the diagram, work out the trim

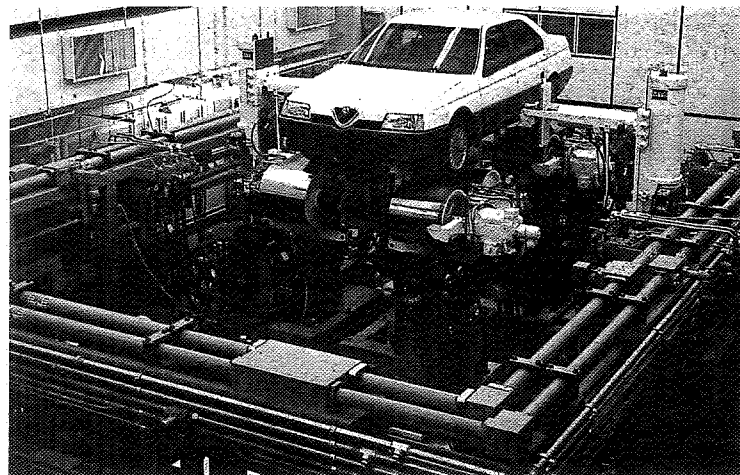


Figure 13.12 MTS Flat-Trac Roadway Simulator.

change technique, and come up with the "grid" idea where one starts with a fundamental grid of α_F , α_R and builds up to the full Moment Method plot. Rice was a dynamicist of the first order having worked on early missile control systems, but his enthusiasm for the Moment Method for understanding car control was unbounded. His ability to interpret the convolution of a diagram was comparable to that of a top aerodynamicist interpreting a wind tunnel pitching moment curve.

By the start of MRA (1976), the technology had reached an application stage. MRA acquired contracts for development work from Goodyear, Rolls-Royce, Chevrolet (Corvette), Bridgestone, Ford, Nissan, Fiat, Cadillac, etc., and was able to utilize Rice's capability by subcontract to Calspan.

As noted in Chapter 8, Dave Segal made the next major step by converting the mainframe program to IBM-PC (on a contract from Terry Satchell, then at GM, C-P-C North) and adding a variety of post-processing, thus making a computer program available for car and tire companies and race teams (earlier on, Goodyear had acquired a mainframe version). Dave is also a great proponent of vehicle statics, having gained so much insight into car control from his development and use of the Moment Method.

Peter Wright

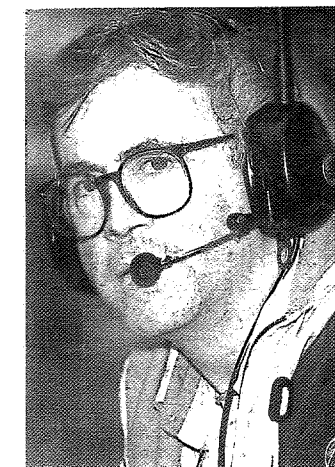


Figure 13.13 Peter Wright (left) and David Williams.

In late 1981, I called on Tony Rudd, then Corporate Research Director at Lotus Cars in England. We had become acquainted at the U.S. Grand Prix at Watkins Glen. Dur-

ing my visit, Tony introduced me to Peter Wright. It was a chance meeting but made to order—one that resulted in all kinds of good things on business, technical, and personal levels. We obviously shared a great interest in the engineering aspects of racing.

Once the idea of using aerodynamic downforce to improve performance was introduced by Chevrolet R&D / Chaparral, there was rapid acceptance by the racing fraternity, followed by high-mounted wing failures and legislative action. Probably no one was more conscious of the value of downforce, nor more anxious to bypass these constraints, than Colin Chapman. The idea of attaining a reduction in pressure on the large bottom area of a car was attractive, but no one had done it.

Peter Wright's career to that point had been a varied one, hardly lacking in excitement. A graduate of Cambridge, he had worked for BRM under Rudd. Later he was employed by Specialized Mouldings, fabricators of race car bodies, where he designed and supervised the construction of a wind tunnel. Still later he worked for Colin Chapman as a consultant in his molded power boat enterprise. Peter subsequently became Research Director for Team Lotus and finally gravitated to Lotus Engineering (the engineering consultancy). At one time he knocked off for a year or so to try farming! When I met him he was still working as a consultant, maintaining a characteristic degree of freedom in his thinking and action.

At the instigation of Chapman and Rudd, Peter and a small group of associates did the research that led to techniques for generating aerodynamic downforce by careful shaping of the car bottom. The technical aspects of this achievement are described elsewhere in this book; suffice it to say that it led to downforce levels in multiples of the static vehicle weight and unheard of cornering performance gains. The research was performed with modest equipment in a low-speed tunnel with a moving belt ground-plane, required by the small "ground" clearance. It was a classic example of talent, ingenuity, experience and persistence—as opposed to extensive facilities—leading to a major breakthrough.

I was aware of Peter's ground-effects accomplishments when we met but by that time he was involved in another development so "secret" that I was given only the sketchiest outline. As the story came out later, the level of downforce mentioned above required high suspension stiffness resulting in driver fatigue and requirements for smoother circuits. To cope with these, Chapman came up with his famous double suspension system, embodied in the Lotus 88—a remarkable and costly development in which Peter had played a part. This car was banned and Chapman lost the legal battles that ensued. Thus Lotus was still seeking a way to support high downforce while maintaining reasonable ride. An original approach to this came about as follows:

The Flight Instrumentation laboratory of the Cranfield College of Aeronautics in the person of David Williams had developed an in-car instrumentation system for Team Lotus. David Williams is a remarkable controls engineer, largely self-taught. Among his

accomplishments was the control system for the first variable stability aircraft in England and the modifications to the Harrier control after the Falkland experience.

Thus it is he who is credited with suggesting that an *active* suspension system could be designed which would support high downforce and still yield a satisfactory ride. Colin Chapman agreed to a modest budget and the use of an Esprit, and Williams and Wright got underway. Peter supplied the vehicle modifications and David developed the electro-hydraulic system and algorithms. State-of-the-art aircraft components and technology were used.

Unlike previous active vehicles such as the CAL/GM variable stability cars, the Lotus/Cranfield vehicle employed load control and the separation of ride motions into four primary modes—heave, pitch, roll, and warp. A test rig using real components enabled the development of stable control of the high-frequency motion of the unsprung masses. Although the electronics were carefully analyzed, no attempt was made to model the complete vehicle and control system. Rather the system was developed and modified in actual on-road testing largely carried out by Wright and Williams. It was a typical race car approach and cut out months of development time. The performance of this fully active load system was a revelation. Conceived as a ride system, it gave astounding control over handling.

At the time I met Peter, they were sorting out potential applications for active control beyond racing. About a year later we met in London and Hethel and worked out a contract whereby I was to assist Lotus in promoting active prototype developments for American firms, notably car and tire companies. Continuing development of active technology remained with the Lotus and Cranfield groups until the formation several years later of Moog-Lotus.

Although a fully active Lotus system has yet to appear on a production passenger car, active technology has had major impact on vehicle dynamics and what it may be like in the future. Having been involved in the application of servo control technology to aircraft in the form of control augmentation, I predicted in 1950 in a paper at the Royal Aeronautical Society in England, that sooner or later we could expect military and large commercial aircraft would be fly-by-wire in fully servoed systems. It has taken 30+ years, but was inevitable. The gains are so enormous that they cannot be ignored. Fundamentally it seems to me that a similar course is likely for the automobile. The effect on ride and handling of a fully active system completely changes one's perspective of vehicle dynamics. Over/understeer is no longer a fixed characteristic but can be made fully adjustable to some functional relationship or by the driver. With appropriate sensing, the yaw damping of the vehicle can be made constant with speed, instead of falling off. Load control of breakaway characteristics is now possible. Active control can have a major effect on pavement life since it tends to maintain constant wheel loads. For the technically inclined, active control completely generalizes the equations of motion removing the limitations of a fixed set of derivatives. How far one can go from there is

illustrated by recent research airplanes which have been flown to 70°-80° angle of attack and remained maneuverable.

The impact of the Lotus fully active system had fanned out in many directions:

1. Until a change of regulation, active controls of various types had become common on Grand Prix cars.
2. Active control has spurred an interest in semi-active and adaptive ride systems for production cars. Here the emphasis has been on body motion control.
3. Active and semi-active components such as shock absorbers have been inspired by the performance of the fully active systems. This is also true of developments in rear steer and the potential of active differentials.
4. Active/adjustable prototypes are the "chosen instrument" for studying handling—the driver-vehicle relationship. If we are to ever develop (as the aircraft industry has) a handling specification, it will be implemented with variable control vehicles.

Thus it is that the work of Peter Wright and David Williams has added a dimension to vehicle dynamic technology of far-reaching consequences.

In 1954, an Automotive Symposium was held at Cornell Aeronautical Laboratory in Buffalo and Figure 13.14 was taken of the participants.

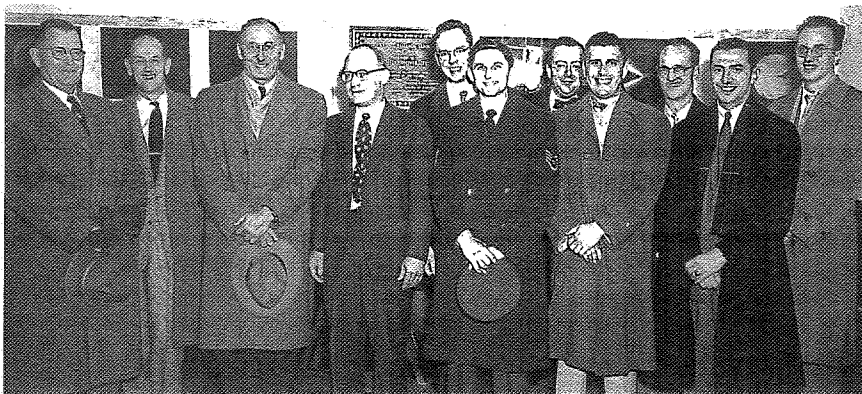


Figure 13.14 CAL, February 5, 1954. (l. to r.) Dr. W. Kamm, Bill Milliken, Bob Schilling, Ed Dye, Dave Whitcomb, W. Cyrus, Cliff Nuttall, Len Segel, Bill Close, Ernie DeFusco, Al Fonda.

Part II

Tire Data Treatment

"These nondimensional coefficients are the primary language of applications in aerodynamics ... with a small amount of analysis, we have saved a huge amount of effort."

John D. Anderson, Jr.
University of Maryland (Ref. 15)



Introduction

As Anderson notes in the quote above, aerodynamicists have been very successful in reducing voluminous aircraft force and moment test data to nondimensional coefficient form. These coefficients are based on normalization by the dynamic pressure and a characteristic area and length. Thus the coefficients enable the forces/momenta to be determined for any vehicle size and operating condition.

Tires on automobiles and wings on aircraft perform similar functions, but until fairly recently automotive engineers have generally represented the results of tire tests in pounds and foot-pounds in look-up tables with interpolation routines.

In this chapter we first discuss some of the problems of obtaining high-quality tire data, then we give an overview of tire data nondimensionalization—an efficient way to handle tire force/moment data for vehicle analysis of race (and production) car handling.

This chapter was written by Dr. Hugo Radt, MRA, the originator of the tire nondimensionalizing technique. Dr. Radt and the authors wish to acknowledge substantial support by Goodyear and Chrysler for the development of the nondimensional technique.

A typical test for forces and moments on a single tire includes variations of slip angle, load, camber angle, and traction/braking at one inflation pressure and speed. Assuming no means for combining or correlating data at different test conditions, a complete test for one tire typically would include 17 values of slip angle at 6 loads, and 5 camber angles. Traction/braking tests are usually performed by sweeping through the longitudinal force while holding the other test conditions fixed; this test schedule would require 510 such traction/braking sweeps. Clearly, this would be too costly and would require the use of many tires because combinations of high slip angle, high load, and large traction or braking forces yield rapid tire wear on the test machine. Problems of repeatability also occur when multiple tires are used to obtain one complete set of data. Furthermore, similar sets of tests would have to be repeated if the front and rear tires on the race car are different and if the effects of tire inflation are critical.

Another problem area is the treatment of tire data so that it can be used in the analysis and simulation of vehicle handling. Tables of raw data can be voluminous and require polynomial or spline fits for interpolation between data points. Accuracy may be lost and "jumps" or "bends" may occur in the resulting plots when a change of longitudinal force occurs. An empirically derived fit to tire data, referred to as the "magic formula," has been successful in matching much of the raw data. However, the parameters (constants) of the fit are difficult to obtain and require cross plotting to obtain effects of more than one variable at a time.

14.1 Tire Data Nondimensionalization

An alternative approach is called *Tire Data Nondimensionalization* because it makes use of ratios of the raw data in such a way that the dimensions of the data are eliminated. For example, dividing the lateral force by the product of friction coefficient times load makes the resulting "normalized lateral force" nondimensional. The major objectives of using these nondimensional or normalized variables are to:

- Reduce test time and cost.
- Produce less wear during testing.
- Improve tire data accuracy by smoothing the data for combined conditions and performing fewer tire changes during testing.
- Provide simple, accurate representations of tire data for vehicle simulations.
- Allow potential for including variations of surface friction.
- Provide for straightforward and accurate interpolation of data between loads and potential for extrapolating the data to higher or lower loads than those used during the test program.

- Allow for comparison of the purely nonlinear behavior of different tires or the same tire under different operating conditions.

The approach used in tire data nondimensionalization is to:

1. Combine tire lateral force vs. slip angle data, as functions of load, into single curves for all loads in the range from near zero load to twice the tire rated load or to the maximum load expected during racing. Similarly combine data on self-aligning torque and overturning moment for different loads.
2. Combine slip and camber angles into one effective camber/slip variable, for small camber angles (up to about $\pm 10^\circ$). **Note:** In this chapter, camber angle is used interchangeably with inclination angle (see Figure 2.33 for the strict definitions).
3. Combine slip ratio for traction/braking with slip angle and camber angle to provide one effective resultant slip variable.

14.2 Pure Slip Characteristics

Pure slip characteristics refer to lateral force, self-aligning torque, and overturning moment as functions of load and one of either slip angle or camber angle. Also included are longitudinal force (traction/braking) as a function of load and longitudinal slip ratio.

Slip Angle and Load

Several semi-empirical theories of tire mechanics yield the following relations between dimensionless force and slip angle and between dimensionless self-aligning torque or overturning moment and slip angle.

The nondimensional or normalized lateral force, \bar{F} , is defined by

$$\bar{F} = \frac{F_y}{\mu_y Z} \quad (14.1)$$

Similarly, nondimensional or normalized self-aligning torque, \bar{M}_z , is

$$\bar{M}_z = \frac{M_z}{T_z \mu_y Z} \quad (14.2)$$

and the normalized overturning moment, \bar{M}_x , is

$$\bar{M}_x = \frac{M_x}{P_x \mu_y Z} \quad (14.3)$$

while a normalized slip angle is defined as

$$\bar{\alpha} = \frac{C \tan \alpha}{\mu_y Z} \quad (14.4)$$

That is, \bar{F} , \bar{M}_z , and \bar{M}_x are each functions of $\bar{\alpha}$, independent of the load, because load, Z , is already included in the above relations as well as in determining the (lateral) friction coefficient, μ_y , cornering stiffness, C , pneumatic trail, T_z , and overturning trail, P_x .

Pneumatic trail is the ratio of self-aligning torque to lateral force for small slip angles, while overturning trail is the ratio of overturning moment to lateral force, again for small slip angles. The reasoning behind selection of these particular dimensionless forces and moments and the normalized slip angle is provided in Ref. 124, which discusses several semi-empirical theories.

Before normalizing and plotting tire data, we first take an average of lateral forces between positive and negative slip angles, taking into account the fact that the direction (sign) of the lateral force changes when slip angle changes sign. This averaging process eliminates the values of lateral force at zero slip angle caused by tire asymmetries called *conicity* and *ply steer*. A similar averaging is done for self-aligning torque and overturning moment. Conicity and ply steer effects can be reintroduced, for small slip angles, when performing calculations using nondimensional data fits, but are really of little interest for the race car where one is more concerned about high slip angle behavior.

Figures 14.1 and 14.2 show data points at five different loads, for \bar{F} vs. $\bar{\alpha}$ and \bar{M}_z vs. $\bar{\alpha}$, respectively, for a P195/70R-14 tire. All the data points fall close to the solid curve. This solid curve was generated using the “magic formula” of Refs. 16, 17, and 114, although other mathematical curve fitting techniques such as polynomials could have been used. As an example, the normalized lateral force, \bar{F} , as a function of the normalized slip angle, $\bar{\alpha}$, is represented by the “magic formula” as follows:

$$\bar{F} = D' \sin \theta \quad (14.5)$$

$$\theta = C' \arctan(B' \phi) \quad (14.6)$$

$$\phi = (1 - E')\bar{\alpha} + (E'/B') \arctan(B' \bar{\alpha}) \quad (14.7)$$

The parameters for the solid curve in Figure 14.1 are $B' = 0.714$, $C' = 1.40$, $D' = 1.00$, and $E' = -0.20$.

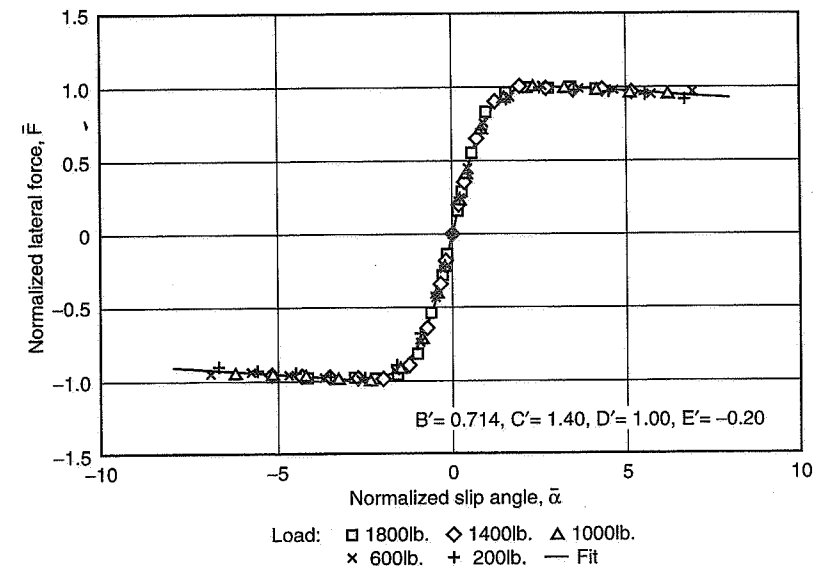


Figure 14.1 Normalized lateral force, 0° camber.

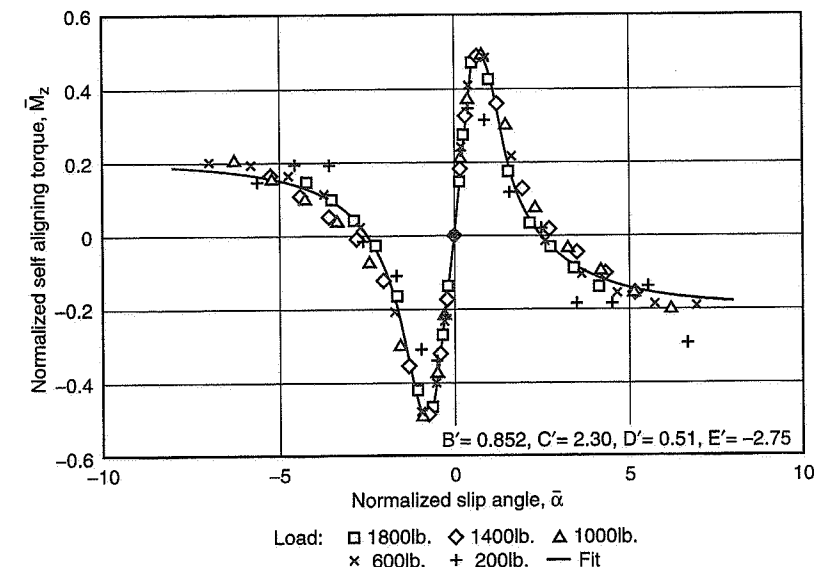


Figure 14.2 Normalized self-aligning torque, 0° camber.

Camber Angle and Load

When camber angle, γ , is varied at zero slip angle, one defines a normalized camber angle, $\bar{\gamma}$, as

$$\bar{\gamma} = \frac{G \sin \gamma}{\mu_y Z} \quad (14.8)$$

where G is the camber stiffness or ratio of camber thrust to camber angle.

Now \bar{F} , \bar{M}_z , and \bar{M}_x are functions of the normalized camber angle, $\bar{\gamma}$. Figure 14.3 shows normalized camber thrust vs. normalized camber angle for all five loads using the square symbol. Data points fall close to the line $\bar{F} = \bar{\gamma}$. (Data exaggerated by scales used in plot.)

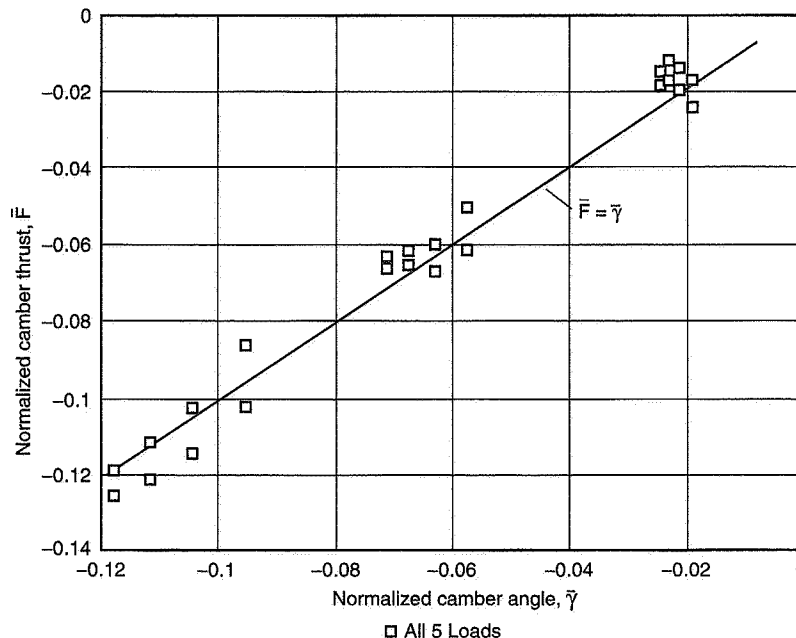


Figure 14.3 Normalized camber thrust, 0° slip angle.

Slip Ratio and Load

For the case of pure traction or braking, but zero slip and camber angles, one defines a normalized longitudinal force, \bar{F}_x , as

$$\bar{F}_x = \frac{F_x}{\mu_x Z} \quad (14.9)$$

and a normalized slip ratio, \bar{S} , as

$$\bar{S} = \frac{k_x S}{\mu_x Z} \quad (14.10)$$

where F_x is the traction or braking force
 k_x is the initial slope of longitudinal force with slip ratio
 μ_x is the longitudinal friction coefficient
 S is the SAE definition of the slip ratio, given by

$$S = \frac{\Omega R_0 - V \cos \alpha}{V \cos \alpha} \quad (14.11)$$

where Ω is the wheel angular velocity (radians per second)
 V is the forward speed of the axle
 R_0 is the rolling radius for free rolling at zero slip angle

For zero slip angle, Eq. (14.11) becomes

$$S = \frac{\Omega R_0}{V} - 1 \quad (14.12)$$

Included in the above definitions is the fact that friction coefficients may differ in the lateral and longitudinal directions.

Figure 14.4 shows data points for the same P195/70R-14 tire for \bar{F}_x as a function of \bar{S} , for five widely varying loads. Again, the points fall close to a single curve which, in fact, represents the same exact equation used to fit the nondimensional plot of lateral force vs. slip angle. This suggests that, once the data are made dimensionless, "one curve fits all." That is, the same mathematical fit can be used for normalized plots of \bar{F} vs. $\bar{\alpha}$, \bar{F} vs. $\bar{\gamma}$, and \bar{F}_x vs. \bar{S} . As described later in this chapter, this same fit applies to combined slip and camber angles and to the resultant normalized force when both lateral and longitudinal forces occur simultaneously, as for braking or traction in a turn. Thus, there appears to be a universal curve fit to the normalized data (for one tire and inflation pressure) that applies to several different forms of slip or combinations thereof.

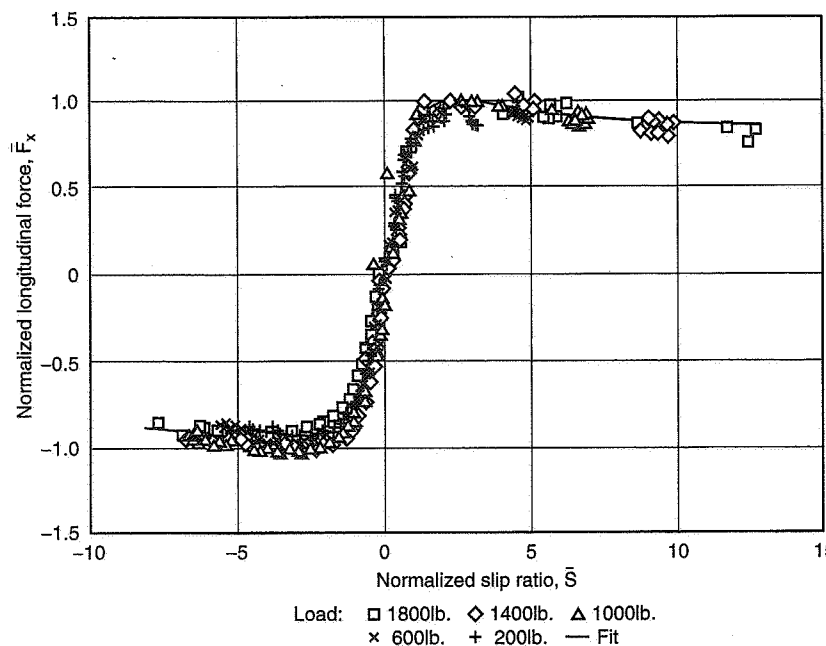


Figure 14.4 Normalized longitudinal force, 0° slip angle.

14.3 Combined Slip Characteristics

Slip and Camber Angles

When slip and camber angles occur simultaneously, we define a new combined slip/camber angle, $\bar{\beta}$, for positive camber angles:

$$\bar{\beta} = \frac{\bar{\alpha}}{1 - \bar{\gamma} \operatorname{sgn} \alpha} \quad (14.13)$$

where $\operatorname{sgn} \alpha$ means the algebraic sign of the slip angle, α . In addition, we introduce a new dimensionless lateral force, FN , again for positive camber angles ($\bar{\gamma} > 0$):

$$FN = \frac{\bar{F} - \bar{\gamma}}{1 - \bar{\gamma} \operatorname{sgn} \alpha} \quad (14.14)$$

FN reduces to \bar{F} of Eq. (14.1) for zero camber angle ($\bar{\gamma} = 0$). Now FN is a function of $\bar{\beta}$, independent of load. When the slip angle is zero, $\bar{\beta}$ is zero, FN is zero and Eq. (14.14)

reduces to $\bar{F} = \bar{\gamma}$, as indicated by the straight line in Figure 14.3. Before calculating and plotting normalized lateral force for combined slip and camber angles, we make use of the following relations for a perfect tire without conicity and ply steer effects:

$$F_y(\alpha, \gamma) \equiv -F_y(-\alpha, -\gamma)$$

$$F_y(-\alpha, \gamma) \equiv -F_y(\alpha, -\gamma)$$

That is, in the absence of conicity and ply steer, positive slip and camber angles yield the same lateral force as for the corresponding negative angles, except for a change of sign.

Figure 14.5 is a plot of the revised definition of dimensionless lateral force, FN , vs. normalized combined slip/camber angle, $\bar{\beta}$, for four different camber angles (0° , -2° , -6° , and -10°) at a load of 1800 lb. Figure 14.6 is a similar plot, but for five different loads and a camber angle of -6° . In both cases the data points fall close to a single (solid) curve, which is the same curve as shown in Figures 14.1 and 14.4.

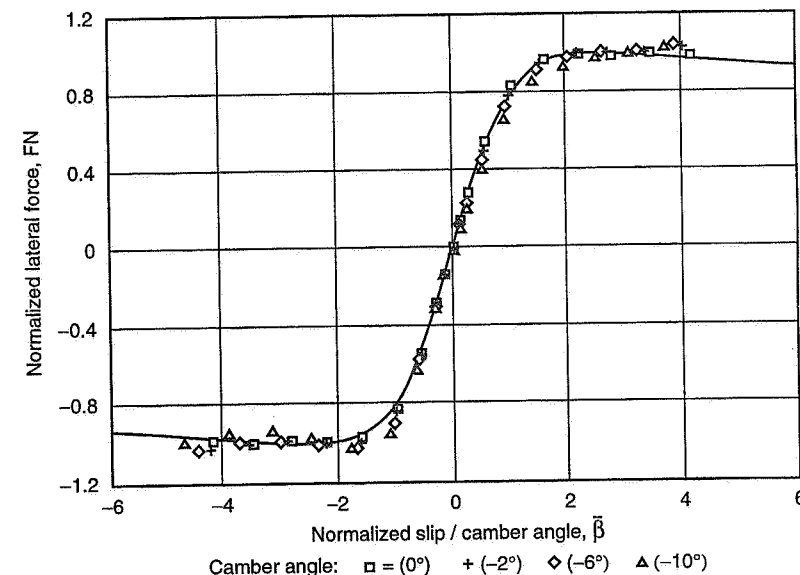


Figure 14.5 Normalized lateral force at 1800 lb. load.

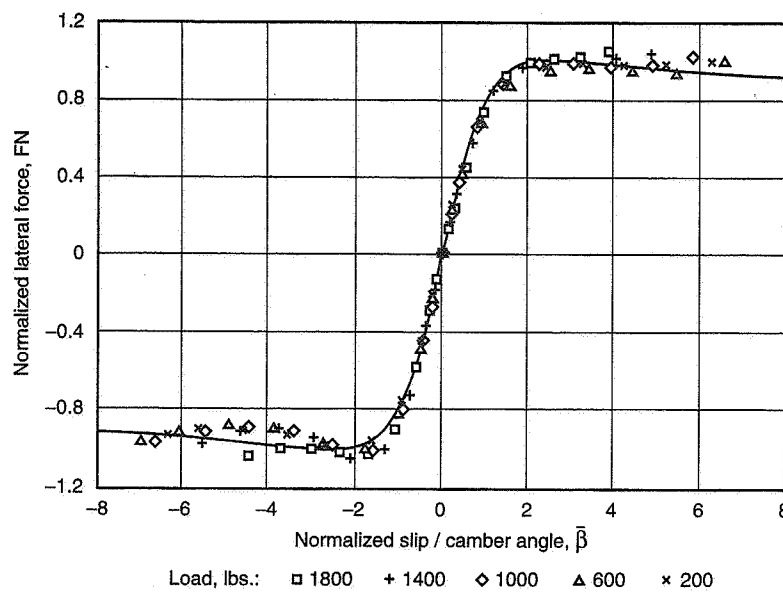


Figure 14.6 Normalized lateral force at -6° camber.

Slip Ratio and Slip Angle

When traction or braking occur in a turn, the tire develops a slip angle due to turning and a slip ratio caused by the longitudinal force. Hence we need a combined normalized slip variable:

$$k = \sqrt{S^2 + \bar{\alpha}^2} \quad (14.15)$$

and a normalized "resultant" force:

$$R = \sqrt{\bar{F}^2 + \bar{F}_x^2} \quad (14.16)$$

which is found to be a function of k : $R = R(k)$, independent of load.

These definitions are sufficient to make plots of R vs. k , but would be useful only if we could calculate \bar{F} and \bar{F}_x once we have R . To do so we need another relationship obtained from analysis of measured data:

$$\bar{F}S = \eta(k)\bar{F}_x \tan \alpha \quad (14.17)$$

The multiplier $\eta(k)$ is necessary to make Eq. (14.17) hold for both small and large slip angles and slip ratios. The $\eta(k)$ function is of the form:

$$\eta(k) = \begin{cases} \frac{1}{2}[1 + \eta_0] - \frac{1}{2}[1 - \eta_0] \cos(\frac{k}{2}) & |k| \leq 2\pi \\ 1 & |k| > 2\pi \end{cases} \quad (14.18)$$

For small k (i.e., small slip angle and small slip ratio), η is equal to η_0 , whereas for large k , η is 1.

η_0 is determined from the cornering stiffness, C , longitudinal stiffness, k_x , and lateral and longitudinal friction coefficients:

$$\eta_0 = \frac{C\mu_x}{k_x\mu_y} \quad (14.19)$$

Substitution of η_0 from Eq. (14.19) into (14.17), for small k , using the definitions from Eqs.(14.1) and (14.9) and rearranging, shows that:

$$\frac{F_y}{C \tan \alpha} = \frac{F_x}{k_x S}$$

Now, for small slip angles, $F_y = C \tan \alpha$, and for small slip ratios, $F_x = k_x S$. Hence both sides of the above equation are equal to 1 for small slip angles and small slip ratios.

Using Eq. (14.17) along with (14.16), one can separate the nondimensional lateral and longitudinal forces as follows:

$$\bar{F} = \eta(k)R(k) \left[\frac{\tan \alpha}{\sqrt{S^2 + \eta^2 \tan^2 \alpha}} \right] \quad (14.20)$$

$$\bar{F}_x = R(k) \left[\frac{S}{\sqrt{S^2 + \eta^2 \tan^2 \alpha}} \right] \quad (14.21)$$

In Figure 14.7 we have plotted R vs. k for slip angles varying from 1° to 28° , for a single load of 1000 lb. Again, the data points fall close to the solid curve calculated according to Eqs. (14.5) through (14.7) and with the same parameters B' , C' , D' , and E' as used for the normalized lateral force vs. normalized slip angle (Figure 14.1), or normalized combined slip/camber angle (Figure 14.5). Although not shown, the same result, i.e., fitting of the data with the same curve, occurred for other loads.

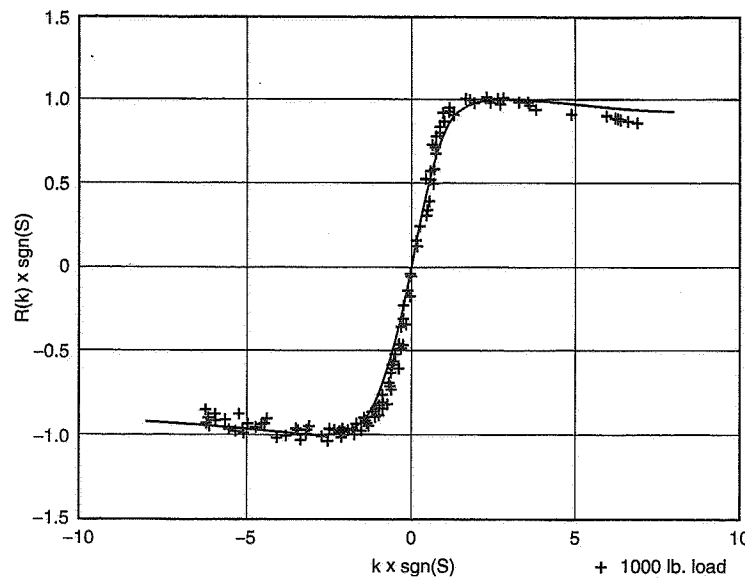


Figure 14.7 Normalized resultant force vs. normalized slip variable.

Once one has obtained a mathematical fit $R(k)$ as indicated, one can reexpand or reconstruct values of lateral and longitudinal force using Eqs. (14.20) and (14.21). This was done and the results plotted in Figure 14.8 for a load of 1000 lb. Raw data points are also plotted for comparison for slip angles of 1° , 2° , and 4° . Similar plotted comparisons are presented in Figure 14.9 for higher slip angles. These comparisons indicate that fitting of the normalized curves for multiple loads and combined cornering and traction/braking faithfully reproduce the original data while providing a compact yet relatively simple way to represent a volume of data.

14.4 Summary of Nondimensionalization of Tire Force/Moment Data

An extensive test program was run on a group of P195/70R-14 tires, including combined effects of slip angle, camber angle and load; slip angle, traction/braking and load. Data from these tests were “normalized” by methods derived from semi-empirical theories attributed to several different authors. The resulting nondimensional graphs indicate that data at different loads can be plotted so as to fall on top of each other. This is referred to as *data compression* because points at different loads nearly compress to a single curve.

In addition, it was found that slip angle and camber angle could be combined into one normalized combined angle and used as the independent variable for the functional

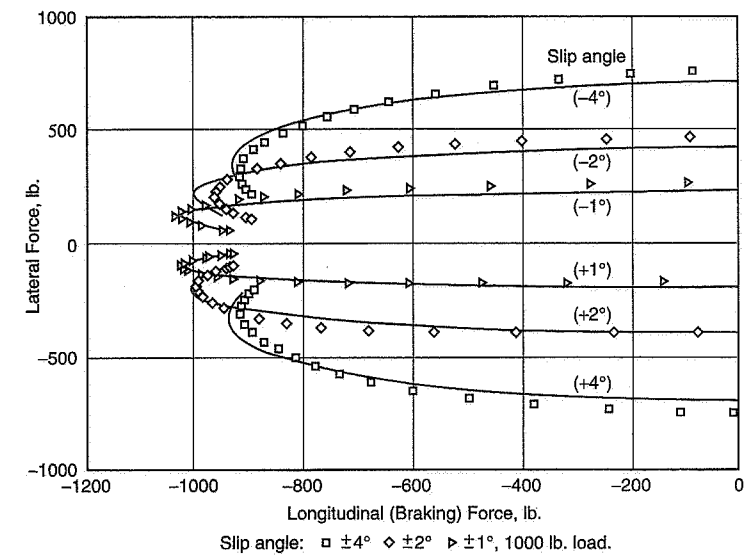


Figure 14.8 Lateral force vs. braking force, constant slip angles.

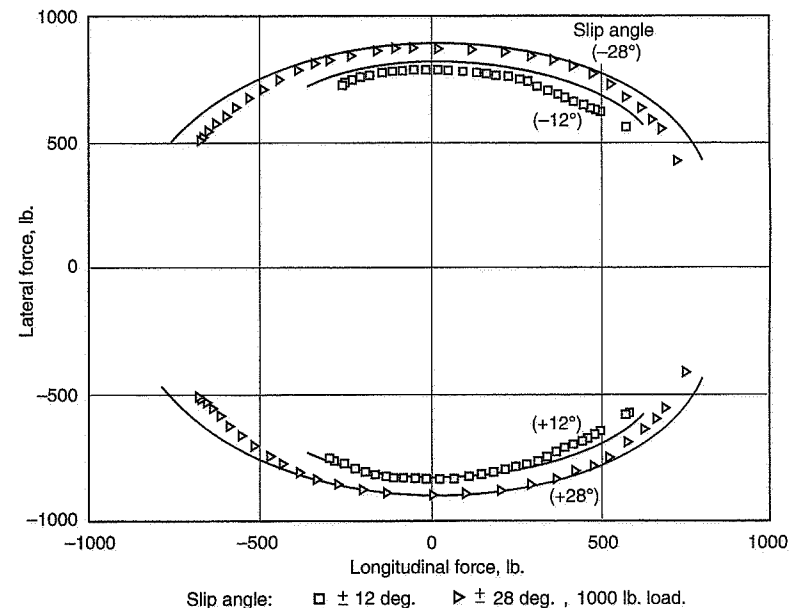


Figure 14.9 Lateral vs. longitudinal force, constant slip angles.

dependence of normalized lateral force that includes camber thrust. The single, normalized curve thus obtained is universal in the sense that it applies for one tire and inflation pressure, over the range of vertical loads, to cases of pure slip angle, pure camber angle, or combinations thereof.

A concurrence of several theories on combined lateral and longitudinal forces led to development of an approach with normalized resultant force as a function of a normalized resultant slip parameter. This function is universal in the sense that it is independent of load and applies equally well to pure slip angle (free rolling), pure traction/braking (zero slip angle), or combinations thereof. Once this function is defined, lateral and longitudinal forces can be obtained knowing slip ratio and slip angle. Essentially, by proper normalization of the data, one need determine only one normalized force function that applies to combinations of slip/camber angle vs. load and slip angle / slip ratio vs. load.

If tire data nondimensionalization and the resulting compression of data is found to be universally valid after further testing of race tires, then a major reduction in test duration can be achieved. Included with such tests are measurements to find the necessary slopes and friction ratios. Such a test program would consist of the following:

- Measurements, at small slip angle, at several loads, to obtain cornering stiffness, pneumatic trail, and overturning trail.
- Measurements at small camber angles, but at zero slip angle, to obtain camber stiffness, camber pneumatic trail, and camber overturning trail (several loads).
- Measurements at one or two high slip angles, at zero camber angle, and several loads to obtain lateral friction coefficients.
- Measurements with zero camber and slip angles, but with small slip ratios to obtain the longitudinal stiffness (slope of longitudinal force with slip ratio). Also, measurements with higher slip ratios to obtain longitudinal friction coefficient at several loads.
- Measurement of the complete cornering curve with slip angle at one intermediate load, zero camber angle, and free rolling.

The burden of effort is then placed on data reduction to determine slopes, normalize the data, fit the normalized data with mathematical functions, and then "reexpand" the forces and moments for varying load, slip angle, slip ratio, and camber angle.

In conclusion, a major problem with the use of vehicle computer models is the difficulty of obtaining consistent and believable tire data. Force/moment data must cover the full range of load, slip angle, camber, and traction/braking. Test facilities for measuring force/moment data suitable for race application are few and even those have operational limits. The nondimensional approach attempts to make up for the deficiencies of experimental data. Of particular importance to racing is the ability to adjust the data for other

friction coefficients in a fundamentally correct manner. The nondimensional approach provides a simple mechanism for varying friction coefficient. Furthermore, it rests on a substantial theoretical base.

Applied Aerodynamics

"I do not say that the theoretician gives all the answers that the designer wants, or that the designer always applies the theories correctly; but at least they [should] recognize each other's merits and short comings."

Dr. Theodore von Karman



Introduction

Chapter 3, Aerodynamic Fundamentals, surveys some aerodynamic fundamentals and testing techniques. In the present chapter a more specific examination is made of those aerodynamic factors and devices which are used to improve the performance of race cars.

It has been noted that racing is "all about maintaining the highest possible acceleration in the appropriate direction." Thus one should accelerate as fast as possible out of a corner and continue to accelerate to the braking point for the next corner or until maximum speed is reached. Braking should occur at maximum deceleration and cornering at maximum combined longitudinal and lateral acceleration. In short, to the extent practical, operation should be near or on the "g-g" diagram boundary. This can occur only if appropriate stability and control are also available.

All of the aerodynamic force and moment components affect the above requirements:

- Aerodynamic lift at the front and rear tracks (or downforce) has a prominent effect in increasing the size of the "g-g" diagram and on the directional balance of the car.

- Aerodynamic drag is a major determinant of forward acceleration and braking deceleration at the higher speeds; also of maximum speed.
- Aerodynamic side force is important for cornering in certain classes of racing and along with the yawing, rolling, and pitching moments affects directional stability and control.

Of the above, the provision of aerodynamic downforce and its distribution⁵³ has had the most sweeping effect on race car performance and understandably so for it directly affects (1) max cornering (limit) acceleration, (2) max traction and max braking, and (3) balance at max cornering.

For these reasons it is given priority in the following discussion. Some aspects of aero drag are then reviewed, along with flow control devices, internal airflow, flat plate aerodynamics, aerodynamics of certain configuration details, and finally, the use of aerodynamics in balancing out the vehicle.

15.1 Historical Note on Aerodynamic (Lift) Downforce

An upward aerodynamic lift force on the front of the car was noted by Daimler-Benz during record-breaking runs on the German Autobahn in the period 1936-39. For these speed trials, Daimler had developed an all-enclosed streamlined body which was installed on their current GP chassis (Ref. 84). At speeds in excess of 200 mph both Caracciola and Lang observed that the front end appeared to rise while steering sensitivity reduced. On one run in the vicinity of 250 mph, Caracciola reported a complete loss of steering, and roadside observers had the impression that the front wheels were off the ground.

In the post-WWII era, aerodynamic lift was noted (and could be measured by recording vertical wheel movements relative to the body) on both the front and rear of fully enclosed sports sedans and on Can-Am cars. This led to the development of front dams and "ducktails" or spoilers on the rear deck. These devices were aimed at reducing or controlling the lift and as such performed a useful function in many applications. They fall far short of the concept of intentionally using aerodynamics to generate high negative lift or downforce.

It took the innovative genius of Frank Winchell and his Chevrolet / Chaparral associates to recognize how beneficial the addition of substantial downforce on the wheels would be when it was achieved with only a very small increase in total vehicle weight.

⁵³ One can either think in terms of lift (downforce) at front and rear tracks or a resultant lift located at the mid-wheelbase/mid-track/ground point which is specified as the "resolving center" (axis system origin) in SAE J1594 (Ref. 2). In the latter case, the pitching moment also must be specified.

The Chevrolet / Chaparral approach was to mount a large wing over the rear wheels to increase the vertical load on the rear wheels during cornering. This first appeared on the Chaparral Can-Am Model 2E in 1966. The development continued through Models 2F and 2G (1968). The rear wing was supplemented by a "spoiler" mounted in the nose cone (Model 2G) (see Ref. 162).

The key features of the configuration were (1) high location of the wing in relatively "clean" air, (2) driver control of the angle of attack of the wing, and (3) aerodynamic downforce applied directly into the rear wheel support hubs (without loading the sprung mass and deflecting the suspension). Two wing angle of attack positions were employed, namely, a horizontal trimmed or "zero" position for minimum drag and a -12° nose-down position for maximum downforce (and also for maximum drag). With the front duct open a small additional downforce was obtained on the front of the car (which was reacted through the chassis). Since the Chaparral utilized an automatic transmission, left-foot braking was used. An additional pedal was provided for the driver's left foot; when this was held down, the wing was kept in the "zero" position (by hydraulic actuation). Whenever the driver engaged in left-foot braking the wing automatically went to the full nose-down (max downforce) position and the front duct opened.

By 1968 wings appeared in other forms of racing, notably Grand Prix, where a high strut-mounted wing on the rear was combined with a smaller wing mounted on the nose. The following year high-mounted wings were banned in F.1 by the FIA for "safety" reasons (structural failures). Thus began a period, yet to end, in which more and more regulations have been placed on the use of devices and design for enhanced aerodynamic downforce (Ref. 106). At the same time constructors, well aware of the performance potential of downforce, have come up with a succession of innovations. The use of adjustable surfaces, putting the downforce directly into the wheels, the location and size of fixed surfaces, etc., have all been subjected to legislation.

In 1970, Chevrolet / Chaparral pioneered another means of obtaining downforce. This scheme consisted of reducing the air pressure under the car (so-called *vacuum-traction*) by powered suction fans and peripheral sealing skirts around the bottom of the chassis. The Chaparral 2J "Sucker car" resulted. Although this machine ran in only a few races and was finally banned, it developed over $1.7g$ on a low-speed skid pad and established some record laps in Can-Am practice. It demonstrated the great virtues of a small pressure reduction over the large bottom area of a race car. Another approach to vacuum-traction was the Brabham F.1 Fan Car which also was banned.

The next major step occurred in 1977 when Lotus introduced a full "ground-effects" car, the Lotus 78 F.1 machine. By a proper shaping of the bottom of the car and the employment of side pods to increase the area and side skirts, a very large negative lift was achieved. Front and rear wings were still employed for small additional downforce and trimming. This pioneering development was accomplished by Peter Wright (Ref. 168), then Head of Research, Team Lotus. It set the stage for the remarkable increases in aerodynamic downforce that followed.

By 1982, maximum cornering accelerations had increased to over 3.5g with negative lift forces nearly twice the weight of the vehicle. Average circuit speeds increased by 15-20%. This sort of performance was not attained without problems, as recounted in Ref. 168. The suspension had to be stiffened to support the weight and to maintain the skirts in contact with the ground (to control porpoising). Suspension frequencies in heave, pitch, and roll increased to the 300-900 cycles/minute range, making the cars very rough on the drivers and requiring smooth circuits.

Elaborate attempts to improve the ride while maintaining the high downforce led to the Lotus 88 F.1 car with two separate suspension systems (banned shortly after introduction) and finally to fully active suspension via electrohydraulics with computer control.

Current F.1 regulations (1993) require a flat bottom back to the rear axle, and no skirts, but permit front and rear wings (limited in size and location). Indianapolis regulations are less stringent, permitting bottom shaping, front and rear wings (again with size and location limits), and a minimum height of any part of the side pods of 1.5 inches above the bottom of the tub. Designers of Indianapolis cars are finding ways of achieving large downforce from the bottom of the cars even under these regulations.

In the following sections we examine in more detail the several ways of controlling aerodynamic lift and generating aerodynamic downforce.

15.2 Spoilers and Dams

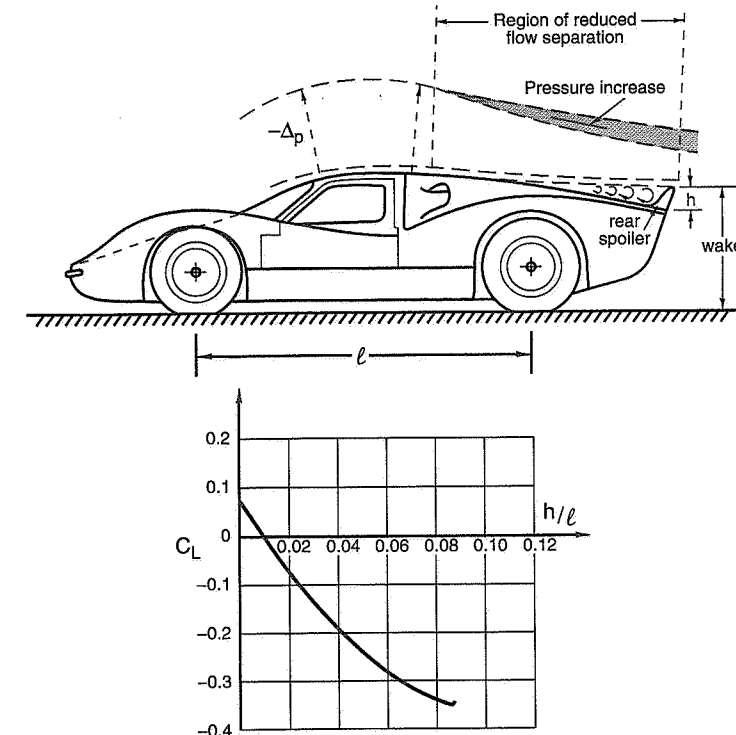
Considerable experimental data on rear spoilers and front dams exists in the nonproprietary literature. In presenting some of this data, it must be emphasized that it is very much "vehicle configuration" dependent. Thus a rear spoiler on one car may be more or less effective on another car shape. This is generally true in connection with aerodynamic devices, i.e., their effectiveness is a function of the flow field into which they are introduced. Specific wind tunnel or full-scale tests are the only ways to determine the quantitative aerodynamic forces and moments except in cases where the device (say a wing) is mounted in the remote flow field. In some cases, even the qualitative effect may not be obvious or monotonic (i.e., total drag vs. spoiler height) and wind tunnel tests are required.

Spoilers

Figure 15.1 shows the effect of a rear spoiler on an enclosed G.T. car (from Ref. 143). The lift coefficient, C_L , is based on the frontal area of the car (as per SAE, Ref. 2). The effectiveness of the device increases with its height. When the height of the spoiler is $0.02 \times$ wheelbase, ℓ , it produces a negative lift coefficient equal to the positive coefficient before the device was installed (for a 95" wheelbase, this spoiler would be approximately 2" high). A typical spoiler for such a car might be 5" high, or $h/\ell = 5/95 = 0.052$,

which gives a $C_L = -0.25$. If the frontal area of this car is 16 ft^2 , the negative aerodynamic lift (or downforce) at 140 mph comes out to be

$$L = qAC_L = 50.1 \times 16 \times (-0.25) = 200 \text{ lb.}$$



Effect of rear spoiler on typical G.T. racing car.

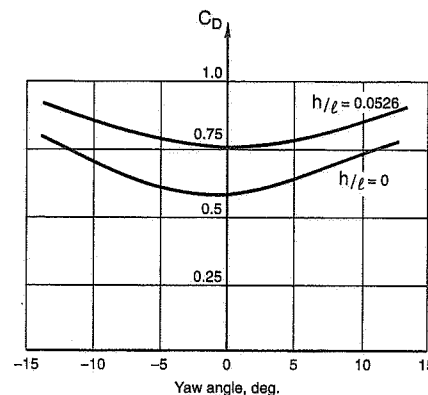
Figure 15.1 Rear spoiler on G.T. car (Ref. 143).

This spoiler works as follows: On a car of this shape the airflow over the rear deck is generally smooth and produces a negative pressure in this area. The spoiler produces a separation of the flow which increases the pressure, thus reducing the negative pressure and hence the lift at any yaw angle (see lower part of Figure 15.2). According to the report, the centroid of the pressure increase is approximately at the rear axle (front end lift is unaffected).

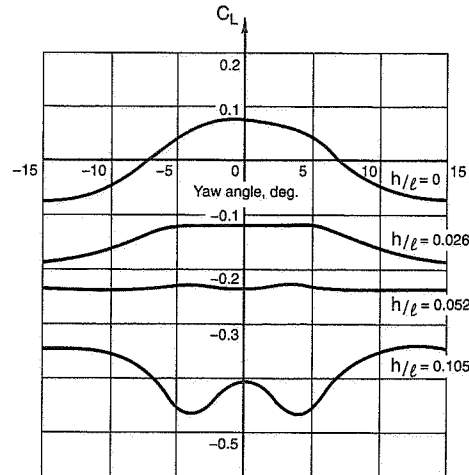
The addition of the spoiler adds some drag (see upper part of Figure 15.2), thus at 140 mph,

$$\Delta D = 50.1 \times 16 \times 0.16 = 128 \text{ lb.}$$

$$\Delta h_p = (128 \times 140) / 375 = 48$$



The effect of the rear spoiler on the total drag of G.T. car model.



Lift coefficient versus yaw angle for different rear spoiler heights (G.T. model)

Figure 15.2 Rear spoiler G.T. car, effect of yaw angle (Ref. 143).

A rough check on this spoiler drag can be made by assuming its frontal area is $0.4' \times 4.5' = 1.8 \text{ ft}^2$. If the spoiler drag coefficient is taken as 1.0 (about 0.8 of a flat plate coefficient), the drag at 140 mph is

$$\Delta D = 50.1 \times 1.8 \times 1.0 = 90 \text{ lb.}$$

This check is fortuitous since the spoiler also affects the drag of the car body. The drag change on the roof is a decrease while the spoiler adds drag by a reduction in base pressure (pressure on the rear end of the body). Both the lift and the drag of this spoiler vary with vehicle yaw angle as shown in Figure 15.2.

On a notchback sedan, a spoiler on the rear deck lid not only can give rear downforce but can also reduce the drag. There is an optimum spoiler height for the drag reduction. Figure 15.3, from Schenkel's work at General Motors (Ref. 140), illustrates these relationships.

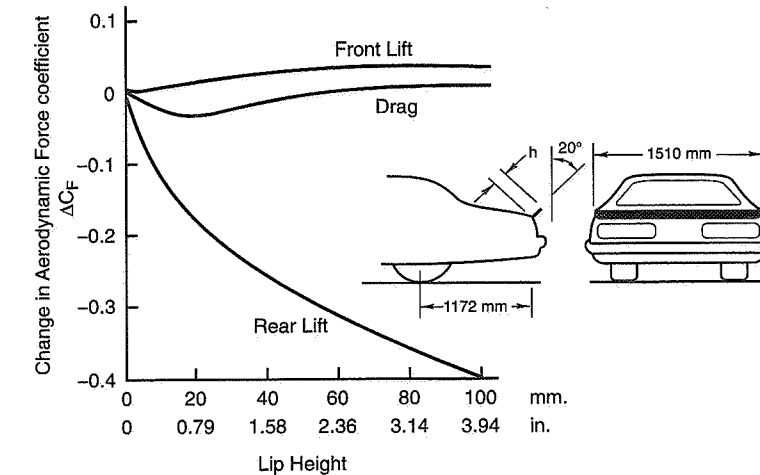


Figure 15.3 Effect of rear deck lip height on a notchback sedan (Ref. 140).

The minimum drag occurs at a spoiler height of less than an inch. At a spoiler height of approximately 2 inches there is little change in drag over no spoiler and a substantial lift reduction, $\Delta C_L \approx -0.3$, with a slight increase in front lift. Measured pressures and flow studies indicate that the spoiler (lip) decreases the downwash (reduces the streamline curvature), which increases the static pressure upstream to about the middle of the roof. The increase in pressure on the rear deck and back light area account for reduction in both lift and drag.

Dams

The term *dam* usually refers to a spoiler located under the nose of the car to reduce both drag and lift, and to increase radiator cooling airflow.

Although front spoilers (dams) may have been tried earlier, they were used by Chevrolet / Chaparral in 1962-64. To quote from Ref. 162, "Through the instrumentation, it soon became obvious that the front spoiler actually reduced air drag—no matter what the shape of the nose, whether with a vertical plate, or the more stylish 'whiskers'; if airflow under the car was prevented, air drag was reduced."

Detailed investigations since then by Volkswagen, Porsche, Chrysler, General Motors, etc., indicate that the effectiveness of a front dam is related to the shape of the nose of the car, as might be expected.

Ref. 86, by Marcell and Romberg of Chrysler, explores the effect of several sizes and locations of a front spoiler and two different nose shapes on the Charger Daytona, a 200-mph Grand National Stock Car. A spoiler tends to inhibit the flow underneath the car and route it over and around the nose. Since the "upper surface of the extended nose was more favorable from a drag standpoint," it was used for the experiments on spoiler size and locations.

Figure 15.4 depicts the results of the front under-nose spoiler on both the "drag" (the force along the horizontal axis of the car) and the lift. The spoiler (dam) was located at three different longitudinal locations. A NASCAR regulation at that time required a minimum ground clearance of 6.5" which meant that the spoiler chord varied with the longitudinal location. It can be seen that the drag was markedly reduced by all spoilers over a yaw angle range of about $\pm 10^\circ$. The lift also was reduced and actually became negative for the forwardmost (and largest chord) spoiler.

Since air dams can affect airflow into the cooling radiator, as well as overall front-end lift and drag, they must be designed on the basis of wind tunnel tests or full-scale development.

As a final example of controlling front and rear lift, Figure 15.5 shows the effectiveness of a front air dam plus a rear spoiler on the Porsche 911 Carrera (from Ref. 63).

15.3 Wings (Airfoils)

Chevrolet / Chaparral G.S. 2G (Example)

As noted earlier this was one of the first race cars (Can-Am) to employ a wing for the express purpose of adding downforce to the rear tires. At the end of the 1967 season this car was extensively tested at Midland, Texas, for engineering documentation (unpublished

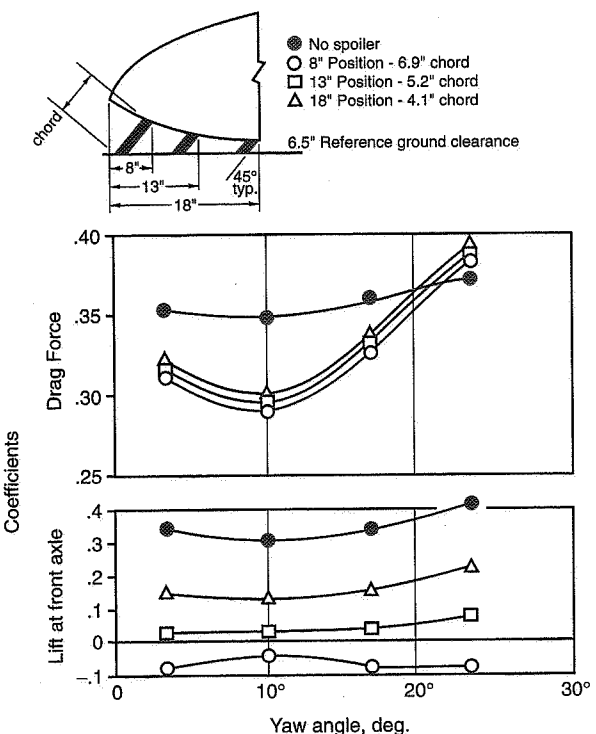


Figure 15.4 Front spoiler position—aerodynamics of Charger Daytona front end (Ref. 86).

memorandum). In this section, we propose to analyze the wing effectiveness and, by comparison to measured data on the vehicle, show how the measured forces came about. Figure 15.6 shows the Chaparral G.S. 2G with rear wing in the "spoiled" position, namely 12° nose down for maximum downforce and drag. Some pertinent data on this car and the wing are in Table 15.1.

The airfoil used on this rear wing was very close to NACA 0008 (or 0009). Data on this airfoil are available in the well-known airfoil reference volume by Abbott and von Doenhoff (Ref. 14). Figure 15.7 (from this reference) gives airfoil dimensions and also shows the velocity and pressure distribution for zero angle of attack.

Now, for our estimate, assume the vehicle is traveling at 100 mph. This is convenient as the Midland documentation was performed at this speed. At 100 mph, the Reynolds Number of the wing (based on chord length) is

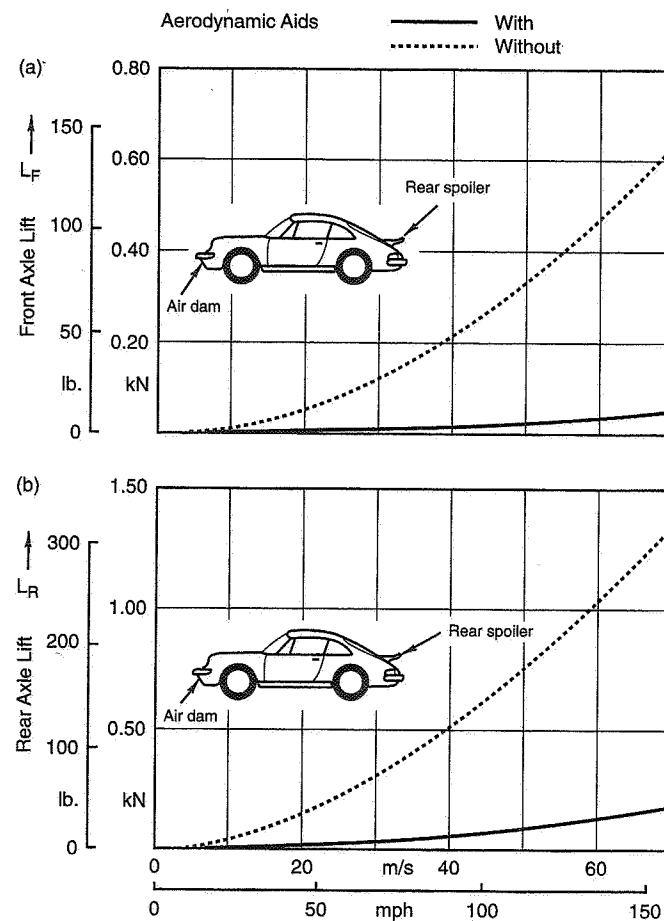


Figure 15.5 Front and rear axle lift vs. speed and aerodynamic aids (Ref. 63).

$$RN = 9230 \times 2.17 \times 100 = 2,002,910 \text{ (say 2 million)}$$

Some section lift data is given in Ref. 14, Chapter 8, on various airfoils tested by NACA. The closest airfoil tested to the section used on the Chaparral is NACA 0009 at a RN of 3 million. Since lift curve slopes are largely independent of RN in this range, these data should be satisfactory and are given in Figure 15.8.

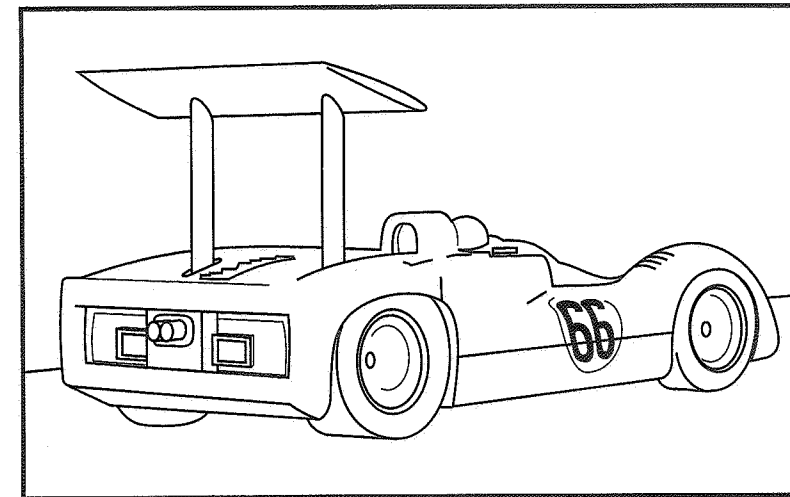


Figure 15.6 Chaparral G.S. 2G with high-mounted, two-position wing.

Table 15.1 Weight, Dimension, and Wing Data, G.S. 2G

G.W. = 1950 lb. (as tested)

a = 4.95 ft.

b = 2.55 ft.

ℓ = 7.50 ft. (wheelbase)

CG = 66% of wheelbase, aft

Front weight = 662 lb.

Rear weight = 1288 lb.

Wing

Rectangular

Chord = 26" = 2.17 ft.

Span = 72" = 6.0 ft.

Area = 13 ft.²

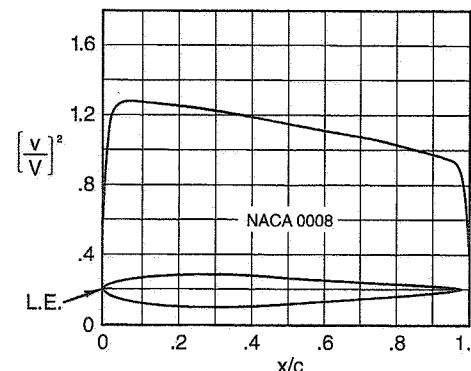
Aspect Ratio = 6.0 / 2.17 = 2.77

Airfoil section - symmetrical

Max. Thickness = 2"

Thickness Ratio = 2/26 (8%)

Location Max Thickness = 6" aft of L.E. = 6/26 (~23% aft)



c = Chord
 x = Distance along chord from L.E.
 v = Local velocity along airfoil surface
 (for zero angle of attack.)
 V = Velocity of remote stream = V_∞

The pressure distribution at zero angle of attack is given by:

$$\frac{\Delta p}{1/2 \rho V_\infty^2} = \frac{\Delta p}{q_\infty} = 1 - \left[\frac{v}{V_\infty} \right]^2$$

Figure 15.7 NACA 0008 airfoil data (Ref. 14).

The section lift coefficient, C_L , corresponds to a wing of infinite span or aspect ratio, i.e., two-dimensional flow. It is necessary to correct this slope for the aspect ratio of the Chaparral wing. This correction is based on the following formula derived from three-dimensional flow airfoil theory:

$$\left(\frac{dC_L}{d\alpha} \right)_{\text{for AR of interest}} = \frac{\left(\frac{dC_L}{d\alpha} \right)_{AR=\infty}}{1 + \frac{\left(\frac{dC_L}{d\alpha} \right)_{AR=\infty}}{\pi AR_{(\text{of interest})}}}$$

where all the slopes are in coefficient/radian.

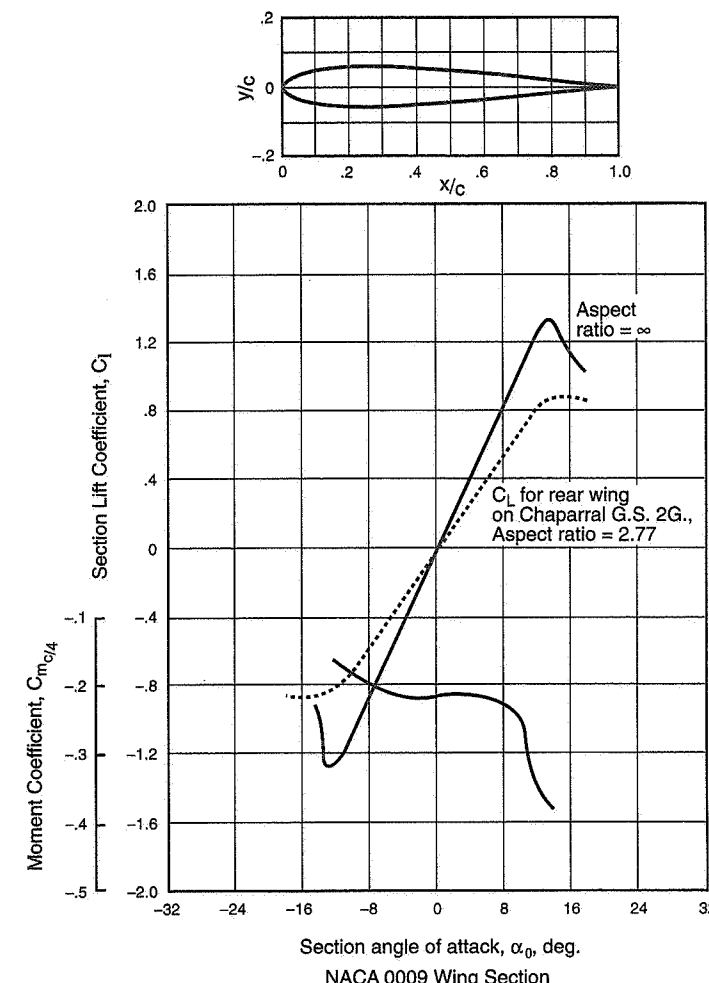


Figure 15.8 Airfoil characteristics corrected to Chaparral wing aspect ratio (Ref. 14).

Note: Assumed section characteristics same for 0009 as for 0008.

From Figure 15.8:

$$\left(\frac{dC_L}{d\alpha} \right)_{AR=\infty} = \frac{1.08}{10} \times 57.3 = 6.19 \text{ (1/rad)}$$

$$\left(\frac{dC_L}{d\alpha} \right)_{AR=2.77} = \frac{6.19}{1 + \frac{6.19}{3.14 \times 2.77}} = 3.62 \text{ (1/rad)} = 0.063 \text{ (1/deg.)}$$

The curve for the Chaparral wing, AR = 2.77, is drawn as the dotted line in Figure 15.8. It is assumed that the lift curve peaks at between 12°-14°, as it does for the two-dimensional wing section. The Chaparral wing has a quite low AR and the above formula can be viewed only as approximate, but satisfactory for these estimates.

Now assume that the Chaparral wing is operating in reasonably "clean" air, so that in its "spoiled" position of 12° nose down it is, in fact, at -12° angle of attack. From Figure 15.8, the corresponding lift coefficient is -0.8 (which is very near the peak of the curve).

At 100 mph, the basic downforce due to negative lift from this wing is

$$\begin{aligned} \text{Aero Lift (Down) Force} &= -C_L q A = -0.8 \times (V^2/391) \times 13 \text{ ft.}^2 \\ &= -0.8 \times 25.6 \times 13 \\ &= -266 \text{ lb., which went directly into the wheel hubs} \end{aligned}$$

Now there are **two** other sources of vertical force on the rear wheels from aerodynamic effects which must be considered:

1. The wing drag results in a moment that alters the loads at the front and rear wheels.
2. Any aerodynamic pressure change on the rear body which reaches the wheels through the suspension.

The documentation tests at Midland enable us to estimate the magnitude of the above effects.

Figure 15.9 gives the results of coastdown tests in which the total drag of the car was measured using accelerometer data for the "trimmed" and "spoiled" wing positions. Since the effect of opening or closing the front duct was small, we can assume that the difference in drag between "trimmed" and "spoiled" is entirely due to the change in angle of attack of the wing. Thus at a given speed, tire rolling resistance, wing strut drag, etc., can be taken as constant.

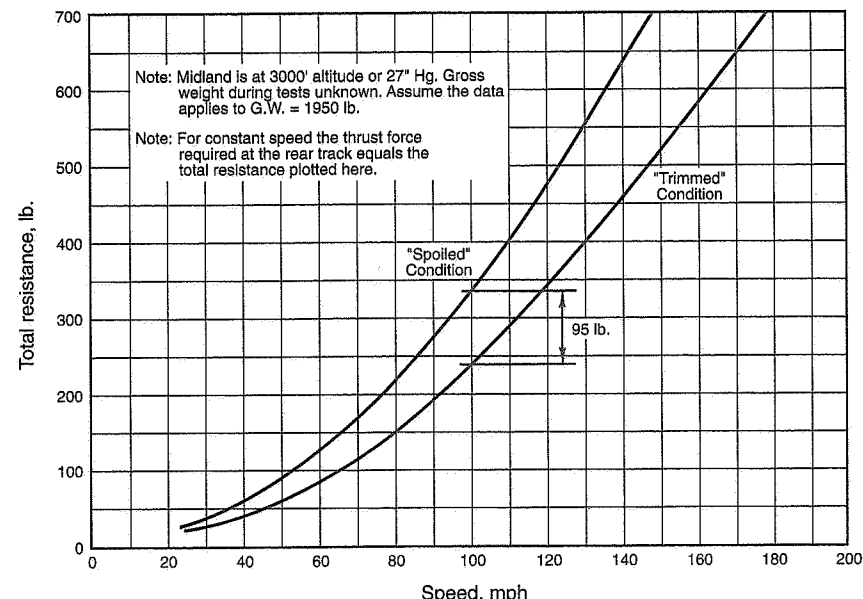


Figure 15.9 G.S. 2G total resistance from coastdown tests at Midland.

At 100 mph, the additional aero drag due to rotating the wing down is

$$330 - 235 = 95 \text{ lb. aft}$$

This drag force must be reacted by additional vertical force at the rear wheels, a decrease in vertical force at the front wheels, and by increased tractive force at the rear wheels. Referring to Figure 15.10 for wing drag effects only:

$$\begin{aligned} \Delta N_F &= -D_h / l = (-95)(4.75)/7.5 = -60 \text{ lb. decreased load on front} \\ \Delta N_R &= + D_h / l = + 60 \text{ lb. increased load on rear} \\ T &= +95 \text{ lb., increased tractive force on rear} \end{aligned}$$

Figure 15.11 depicts the results of pressure measurements on the body surface of the Chaparral at Midland. Measurements were made with the wing in the "trimmed" and "spoiled" positions. It will be noticed that on the top of the aft body there is a lower pressure (upward pointing pressure vectors) with the wing "spoiled" than with the wing "trimmed." In both cases the pressure on the deck is below atmospheric but more so with the wing at -12°. Even though we assumed the wing was in free air, the "upwash" from the wing creates an interference effect on the body in the nature of a reduced pres-

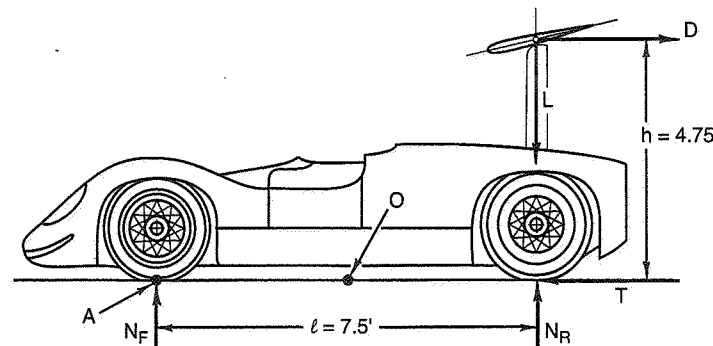


Figure 15.10 Changes in wheel load due to wing drag.

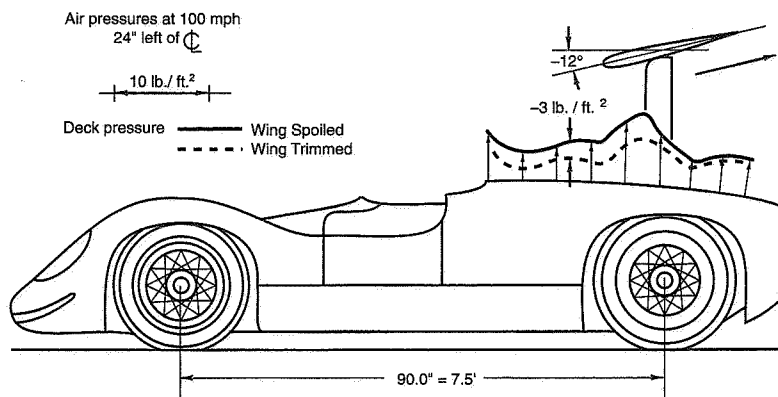


Figure 15.11 G.S. 2G full-scale pressure measurements, unpublished.

sure. The average pressure reduction when the wing is "spoiled" is about 3 lb./ft^2 using the pressure scale in Figure 15.11. The area of the deck on which this average pressure acts is

$$(50'' \times 70'') / 144 = 24.3 \text{ ft}^2$$

The upward force on the body, which is transmitted through the suspension to the wheels is

$$3 \times 24.3 = +72.9 \text{ lb. upward}$$

We are now in a position to sum up the vertical force components at the rear wheels due to aero effects:

Wing aero down lift:	266 lb. down
Wing aero drag:	60 lb. down
Pressure change on rear deck:	<u>73 lb. up</u>
Net downforce on rear wheels, wing 12° down:	253 lb. down

The downforce on the front wheels due to aero effects (at 100 mph) from Figure 15.12 is 57 lb. Since the rear wing (spoiled) decreased the load on the front track, we can figure backwards to calculate the aero downforce from the "wing" in the front duct. This is $60 + 57 = 117$ lb., a worthwhile contribution to the total aero downforce.

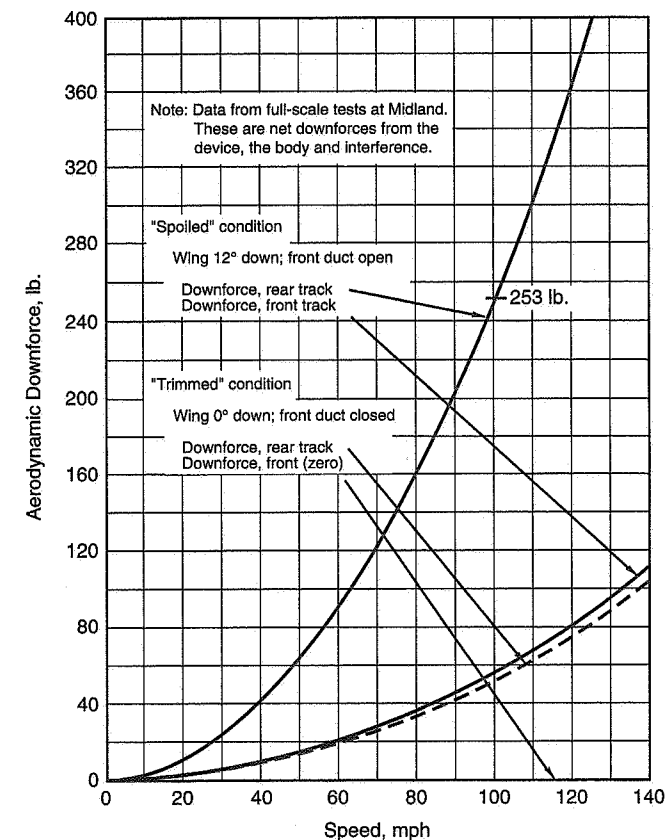


Figure 15.12 G.S. 2G aerodynamic downforce.

Performance Benefits from the Chaparral Wing

Based on the Midland documentation tests, it is instructive to examine the benefits of the wing.

No benefit was obtained from the wing on acceleration. The wheels can be spun only briefly below 20 mph with wide-open throttle (WOT) and at this speed no appreciable aerodynamic effects were present. To minimize aero drag effects, WOT acceleration was accomplished with the wing trimmed. Figure 15.13 shows the results of the acceleration runs.

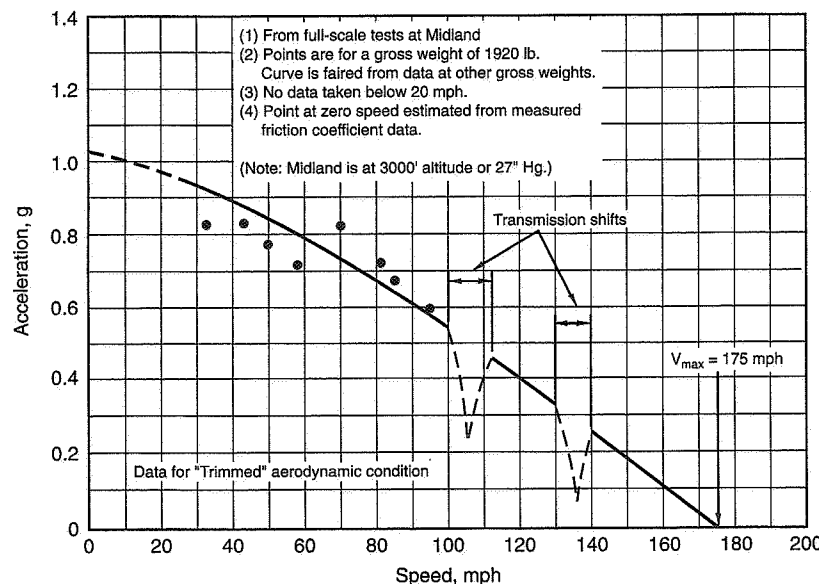


Figure 15.13 Acceleration, G.S. 2G WOT.

The deceleration was calculated (Figure 15.14) using the aerodynamic downforce and drag data given previously (Figures 15.9 and 15.11), wing in spoiled position and a fixed 55% front brake ratio. Engine braking effects were neglected. If the brake ratio were varied to achieve an optimum at each speed, a deceleration of 2.4g could be attained at 140 mph and 2.9g at 170 mph. All of these are based on a measured tire/road friction coefficient of 1.3. The benefits of aerodynamic downforce and drag are apparent.

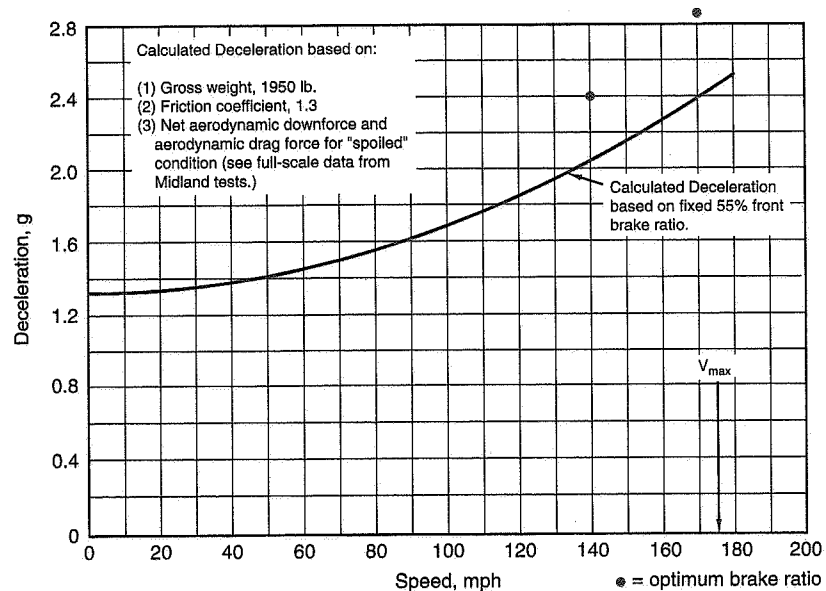


Figure 15.14 Deceleration, G.S. 2G.

Cornering Comparison

The effectiveness of the wing in steady-state cornering will now be examined.

The Chaparral is a high-powered rear-wheel-drive car. On such machines, experience indicates that a large part of the lateral load transfer distribution (LLTD) should be taken on the front pair of wheels, thus maximizing the tractive ability of the rear (driving) wheels. This was particularly desirable on G.S. 2G because an open differential was used to save horsepower. A large amount of lateral load transfer on the rear would facilitate spin-up of the lightly loaded wheel. A general rule is that at max cornering the load on the inside front wheel should be close to zero. The MMM analysis of Chapter 8 for Figures 8.12-8.13 and 8.17 assumed 80% of the LLTD was taken on front. This resulted in inside front wheel lift at 0.7-0.8g depending on the operating condition. When LLTD on front was reduced to 50%, wheel lift-off occurred at 1.2g, near max lateral for road load power at 100 mph trimmed (Figure 8.16).

For the present calculation assume that 45% LLTD on front will give wheel lift-off, or close to it, near max cornering for the two operating conditions of interest. In this situation, the vehicle is operating as a three-wheeler, with 55% of the total LLT taken on the rear. This permits calculation of the vertical load on each rear wheel and, of course, the

vertical load on the outside front wheel when the static loads and aerodynamic forces are known.

In order to perform the calculations, the aerodynamic downforces given in Figure 15.12 are necessary and also data on the lateral forces of the front and rear tires. A special rotating arm test rig, developed by Chevrolet and located at Midland, enabled the measurement of the lateral forces on the actual race tires for various loads and slip angles. These data are presented in Figures 15.15 and 15.16 for front and rear tire, respectively. The calculation for the *trimmed* condition follows.

Chaparral G.S. 2G

Aero Trimmed Condition

100 mph, 1.35g, RH Turn

Front Tire Performance

- 45% of LLTD taken on front track. From earlier MMM runs, this should result in lift-off of inside (RH) wheel at 1.35g.
- Load on outside (LH) front wheel:
Static load on front track (now on LH wheel) 662 lb.
Aero downforce on front track (see Figure 15.12) 0 Front duct closed
Load on LH front wheel 662 lb.
- For yaw-moment equilibrium, the lateral force required by LH front wheel is:
 $(G.W.)(b/\ell)(\text{Lat. Accel.}) = (1950)(2.55/7.5)(1.35) = 895 \text{ lb.}$
- From Figure 15.15 for a load of 662 lb. and a lateral force of 895 lb., $\alpha_F = 9^\circ$
The front tire is close to the peak of the lateral force curve.

Rear Tire Performance

- Total LLT = $(G.W.)(H)(\text{Lat. Accel.})$, where H = vertical height of CG = 1.25 ft.
 $= (1950)(1.25)(1.35) = 3291 \text{ lb.-ft.}$
- 55% of Total LLT is taken on the rear track = $(0.55)(3291) = 1810 \text{ lb.-ft.}$
- $\Delta L(\text{rear}) = \text{LLT Rear} / \text{Rear track} = 1810/4.33 = 418 \text{ lb.}$
- $\Delta L(\text{Rear})_{\text{Left}} = +418 \text{ lb.}$
- $\Delta L(\text{Rear})_{\text{Right}} = -418 \text{ lb.}$
- Aero downforce on rear track at 100 mph (see Figure 15.12)
 $= 54 \text{ lb. down or } 27 \text{ lb./wheel}$
- Load LH Rear Wheel = $644 + 418 + 27 = 1089 \text{ lb.}$
- Load RH Rear Wheel = $644 - 418 + 27 = 253 \text{ lb.}$

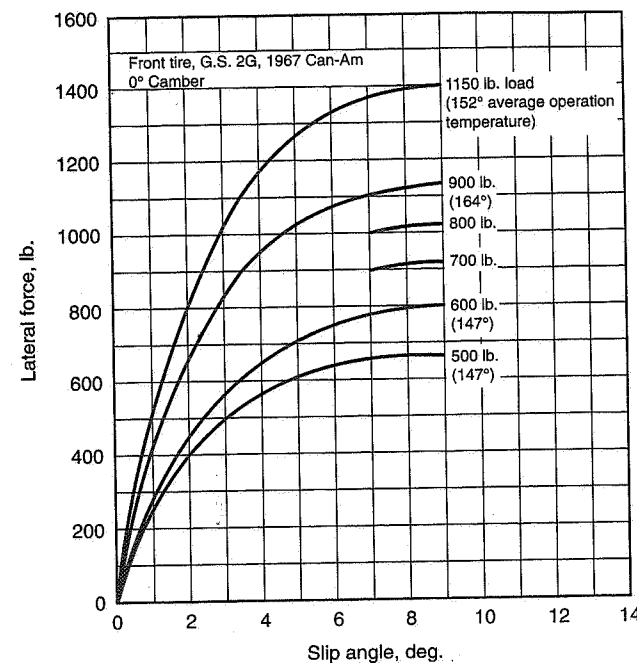


Figure 15.15 Firestone 10.50 × 16, 10" rim, 30 psi.

- For yaw moment equilibrium, the total lateral force required by rear track is $(0.66)(1950)(1.35) = 1738 \text{ lb.}$
- Assume the two rear wheels are at same slip angle (α_R). From Figure 15.16 for the tire loads above, $\alpha_R = 7^\circ$, giving tire lateral forces of

$$\begin{array}{ll} \text{LH Wheel} & 1380 \text{ lb.} \\ \text{RH Wheel} & \underline{368 \text{ lb.}} \\ & 1748 \text{ lb.} \end{array}$$

which is very close to giving yaw moment equilibrium. $7^\circ \alpha_R$ is also close to the peak.

The same calculations were performed for aero "spoiled" condition, 100 mph, 1.35g, RH turn, with the following results:

$$\begin{aligned} \alpha_F &= 8^\circ \text{ (on the peak)} \\ \alpha_R &= 6.5^\circ \text{ (close to peak)} \end{aligned}$$

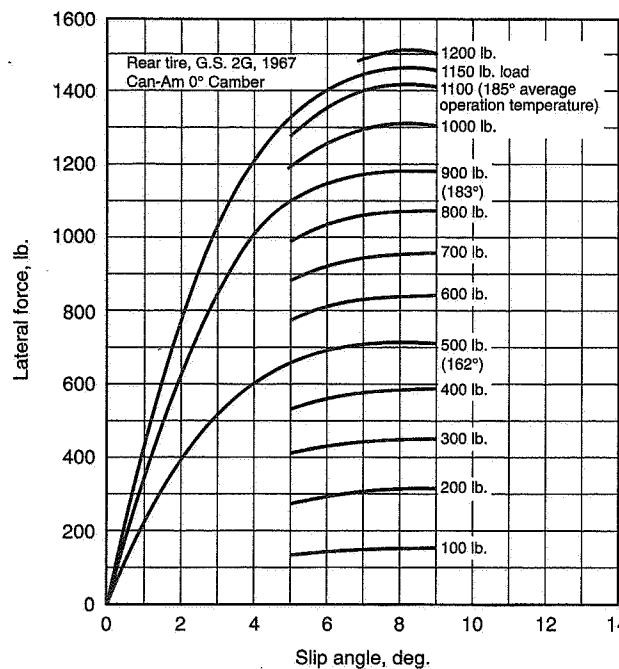


Figure 15.16 Firestone 6.00/13.50 × 15, 13" rim, 30 psi.

Chaparral G.S. 2G
140 mph, 1.35g, RH Turn

The following results were obtained:

$$\text{Aero Trimmed: } \alpha_F = 9^\circ$$

$$\alpha_R = 5.5^\circ$$

$$\text{Aero "Spoiled": } \alpha_F = 5^\circ \quad \text{Front duct open.}$$

$$\alpha_R = 3.5^\circ$$

Summary

When the wing is moved to the "spoiled" (down) position, the tractive force must be increased to counteract the increased aero drag. This limits the available lateral force via the friction circle. The increased down load tends to decrease the rear slip angle for a given lateral acceleration turn.

When the speed is increased the aero drag is also increased and must be counteracted by increased thrust, again affecting the available lateral force and slip angle.

If there were no change in drag force, a car that was balanced out at low speed would be balanced out at higher speeds as the aero downforce on the front and rear would increase at the same rate. With the change in drag force that actually occurs (from any cause) the rate of increase of downforce must be greater at the rear than at the front. Without tire data for combined slip angle, slip ratio and load, an accurate calculation is not possible. However, since the drag (and thrust) force and wing downforce all increase as velocity squared, it seems possible that with an appropriate sizing of front and rear wings, a car can remain balanced over a wide speed range, and Chaparral believes they accomplished this.

Downforce obtained from the bottom of the car may not be so well specified in terms of location and magnitude.

15.4 Legislated Wings

From 1969 to date (1994) wings of **limited size mounted on the sprung mass and non-adjustable en route** have been permitted in F.1, Indy, and other open wheel race cars. Since 1977, beginning with the Lotus 78 F.1, these cars have also achieved downforce (ground effect) by proper shaping of the bottom of the car, with (and later without) side skirts. In the present section attention is specifically directed to the **limited wings**, recognizing that there can be favorable reactions between these wings and the under-bottom ground effect (to be discussed later).

When wing sizes, dimensions, and maximum height and fore/aft location are subjected to legislation, designers are forced to find ways of maximizing aerodynamic downforce within the restrictions. This has led to specialized airfoil shapes, use of end plates, slatted and slotted airfoils, flaps, low drag mountings, etc., and a cleaning up of the body ahead of the rear wing to place the wing in smoother airflow with higher total pressure ($H = p + q$).

An early result of the legislation (circa 1969) was the Lotus F.1 car in which the rear "wing" formed an integral part of the body (see Figure 15.17). The center part of this wing acted as a deflector only and the low aspect ratio and lack of end plates resulted in a device of very low lift effectiveness. The unfaired protruding engine reduced the so-called "tail effectiveness" (an aircraft term which is the ratio of the total head at the tail to the total head free stream) to perhaps 50%. By the next year (1970) designers were using separate rear wings with end plates, located further aft and frequently with high-lift devices to increase downforce.

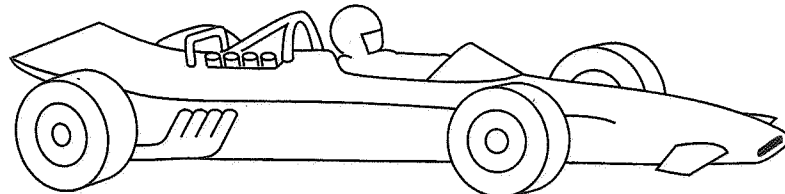


Figure 15.17 Negative-lift wing integrated with the body shape.

High-Lift Devices

The use of a leading edge slat and slots to extend the lift curve to higher angles of attack and hence more lift goes back to Handley Page's and G. Lachmann's work in the 1920s (see Ref. 165). Handley Page actually tested the seven-slotted wing shown in Figure 15.18 which gave a section lift coefficient of approximately 3.5 at a 25° angle of attack.

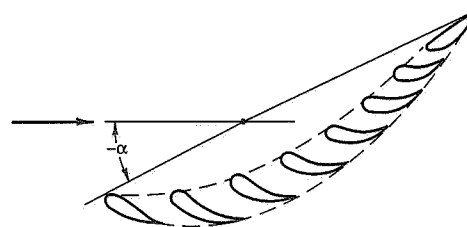


Figure 15.18 Multiple slotted airfoil (Ref. 165).

Interest in plain trailing-edge flaps (where the rear part of the airfoil is hinged and bent down (for aircraft)) occurred even earlier (circa 1913), later followed by the split flap and various forms of slotted flaps and leading-edge flaps. Modern commercial aircraft utilize various combinations of slat-slot-flap technology.

In Ref. 14, Chapter 8 is devoted to high-lift devices such as plain and slotted flaps, nose slats, leading-edge flaps, slotted airfoils, and various combinations. Ref. 61 contains chapters on trailing-edge wing flaps and leading-edge high-lift devices.

Figure 15.20 (based in part on Figure 95 of Ref. 61) is presented to clarify various high-lift concepts. Briefly, these devices work as follows:

- Flaps on the trailing edge effectively camber (increase the curvature of) the airfoil by moving the rear stagnation point down and increasing the circulation. They tend to move the entire lift curve (C_L vs. α) up parallel to itself. A slat on

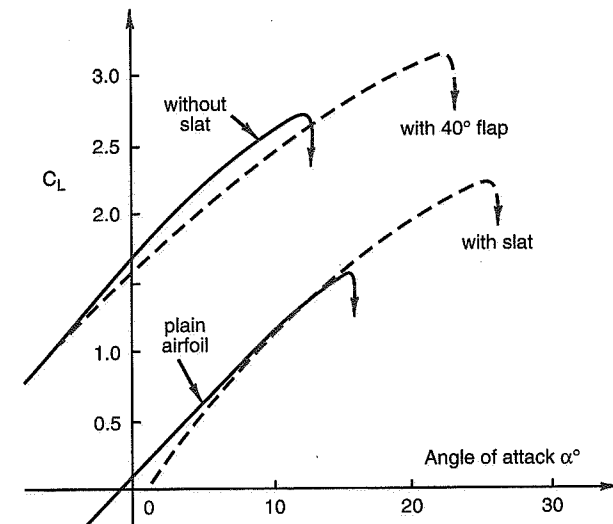
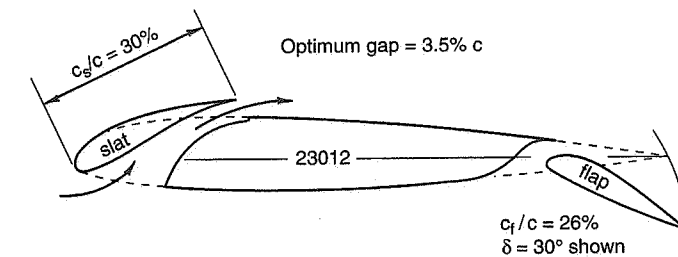


Figure 15.19 Effect of flaps and slats on airfoil lift characteristics (Ref. 61).

the L.E. helps to direct the air over the top of the L.E. at high α 's, hence delaying L.E. stalling. The associated slot utilizes the high pressure from the bottom of the wing to speed up the air and energize the boundary layer on the top of the wing, thus again delaying the stall; see Figure 15.19 (from Ref. 61, pp. 6-3).

- Slats and slots tend to extend the lift curve to higher α 's. Leading-edge flaps camber the airfoil and increase its lift at a given angle of attack.

The other characteristic common to F.1 and CART wings is the use of end plates. End plates increase the effective aspect ratio, as indicated in Figure 15.21 from Ref. 61. The important variable is the height of the end plate to the span of the wing (h/b). The side view shape of the end plate is less important but it should include the full chord of the wing. The effective aspect ratio is defined as $A_i = A + \Delta A$, or $A_i/A = 1 + \Delta A/A$. The

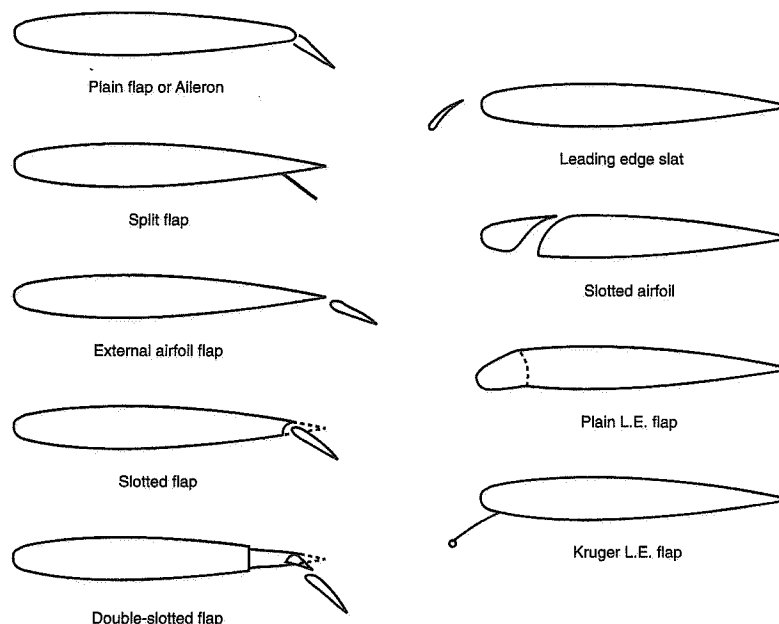


Figure 15.20 High-lift devices (Ref. 61).

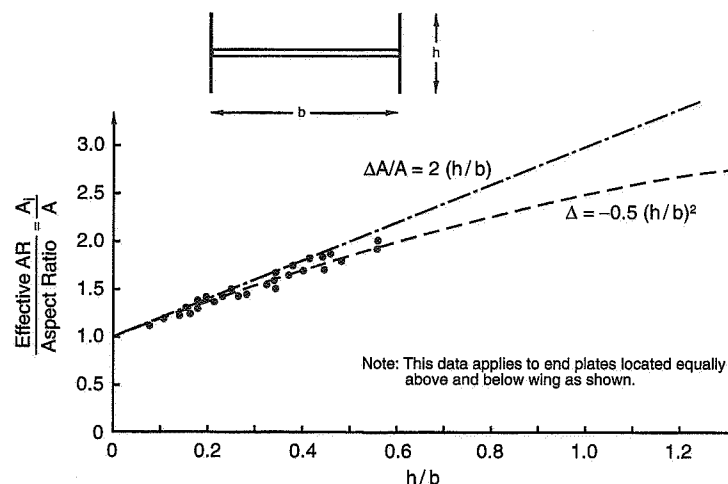


Figure 15.21 Effective aspect ratio of wings as a function of end plate height ratio (Ref. 61).

experimental data slope can be approximated up to $h/b = 0.5$ by $\Delta A/A = 2(h/b)$. For higher values of h/b , $\Delta A/A$ must be reduced, as shown.

Wing Aerodynamics—Open-Wheel Race Car (CART, Predecessor Indy Car)

Three significant papers have appeared in the open literature on the aerodynamics of open-wheel (CART type) race cars by Joseph Katz, formerly with NASA Ames and currently with San Diego State University, Dept. of Aerospace Engineering and Engineering Mechanics (Refs. 75, 76, and 77). With the permission of the SAE Publications Group, some abstracts and figures from these papers are given below with particular reference to rear-wing performance. Katz's work on underbody aerodynamics will be discussed later.

In Ref. 75, Katz develops a flow field model of an open-wheel race car configuration based on a potential-flow code plus experimental information on separation locations. Reference should be made to the paper for details of this model—suffice it to state here that once this model is available for the body and wheels of the vehicle, it is used for calculating the lift and drag performance of downforce wings with unseparated flows. As with any model its validity depends on the assumptions upon which it is based and to the extent it has been checked against experiments. The use of models based on potential flow theory for a device as complicated as a race car must be viewed with some caution.

Figure 15.22 shows the changes to the vehicle's lift and drag due to a rear wing at various angles of attack. The wing has a slotted flap at 60° which delays separation of the flow over the flap. For this figure it is assumed that no interference exists between the wing and the vehicle body. The coefficients ΔC_L and ΔC_D are based on the vehicle reference cross-sectional area (frontal area) of 15.82 ft^2 . The effect of end plates is also shown.

Based on the available flapped airfoil data, it is estimated that the stall would take place around $-35^\circ \alpha$, with a $\Delta C_L \approx 0.92$ for the wing with end plates. At 100 mph the maximum downforce due to the wing is

$$\Delta L = -\Delta C_L q A = 0.92 \times 25.6 \times 15.82 = -373 \text{ lb.}$$

or about 40% of the static load on the rear wheels.

The drag increment under the same conditions is

$$\Delta D = \Delta C_D q A = 0.42 \times 25.6 \times 15.82 = 170 \text{ lb.}$$

or $\Delta h_{hp} = (170 \times 100)/375 = 45.3$, or around 10% of the installed engine power.

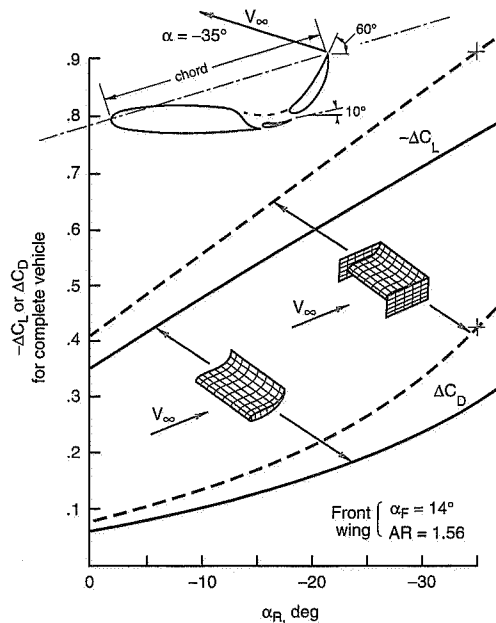


Figure 15.22 Rear wing effect on vehicle lift and drag (Ref. 75).

The end plates improve the wing's downforce by 22% and increase the wing's drag by 50%. The bottom line is that the downforce improvement doesn't come for free.

Figure 15.23 shows the actual effect of the vehicle body on the spanwise load distribution of the wing, when legislation limited the height of the wing to 1 meter (3.28 ft.) above the ground.

h is the vertical distance from the bottom of the wing down to the nearest point on the car—a distance which typically can be 25% of chord ($h/c = 0.25$). $h/c = \infty$ refers to the free stream case. A considerable loss in negative lift occurs near the car body. This figure also illustrates the advantage of end plates.

Figures 15.24 (a) and (b) are comparable to Figures 15.22 and 15.23 but are for a typical front wing. This front wing (no end plates) is effective in producing downforce because it is working in clean air and ground effect is favorable. With sweepback of the L.E., the loading increases toward the wing tip. Available airfoil data suggest local stall of this

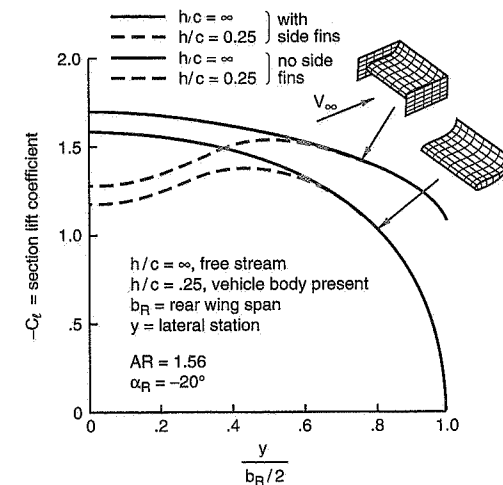


Figure 15.23 Spanwise load distribution of the rear wing (Ref. 75).

configuration at a ΔC_L of about -0.4 , based on vehicle reference area of 15.82 ft^2 . At 100 mph the downforce due to the front wing is

$$\Delta L = -0.4 \times 25.6 \times 15.82 = -161 \text{ lb.}$$

or about 22% of the static load on the front wheels.

The drag penalty under the same condition is

$$\Delta D = -0.12 \times 25.6 \times 15.82 = -49 \text{ lb.}$$

Ref. 76 is a more detailed study of desirable rear wing geometries under the (1989) CART regulations. Briefly, these regulations limited the wing chord to 28 inches. The "highest point on the wing should be lower than 36 inches above the chassis underbody." These requirements dictate "a highly cambered airfoil section of a low aspect ratio."

The study was initiated with a two-dimensional numerical analysis of a series of slotted and flapped airfoils that fit into the 28-in. chord and 10-in. height requirements. Figure 15.25(a) shows the six configurations analyzed. The analysis yielded pressure distributions of the individual elements of the airfoils, and hence the lift of each element. The results are summarized in Figure 15.25(b). These coefficients are based on the reference

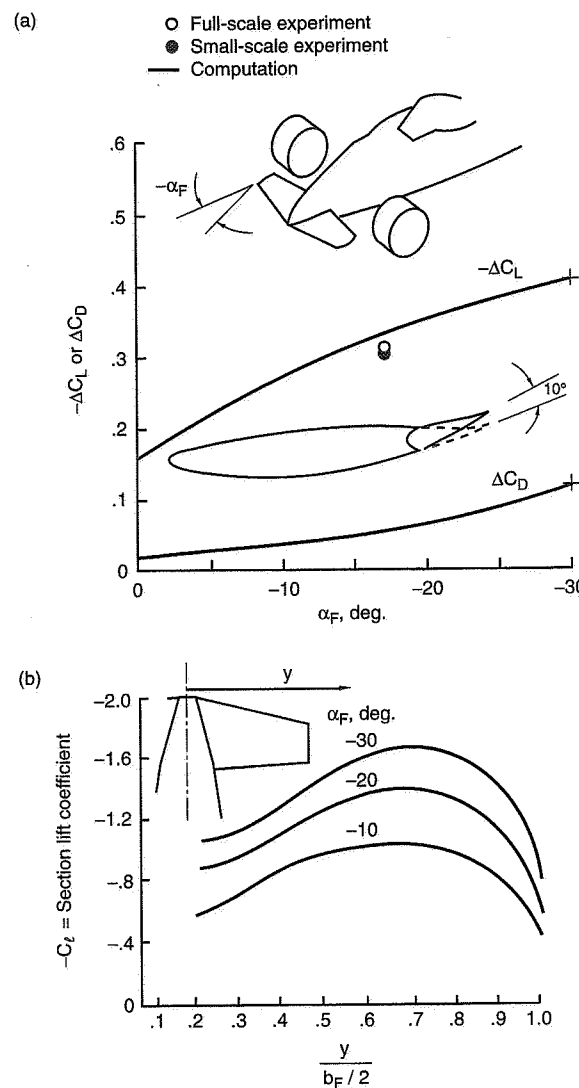


Figure 15.24 Front wing data (Ref. 75).

chord of the baseline airfoil (see Figure 15.25(a)). It is interesting to note that the section lift coefficients are comparable in magnitude to that obtained with the Handley Page multiple-slotted wing in the early 1920s (see Figure 15.18).

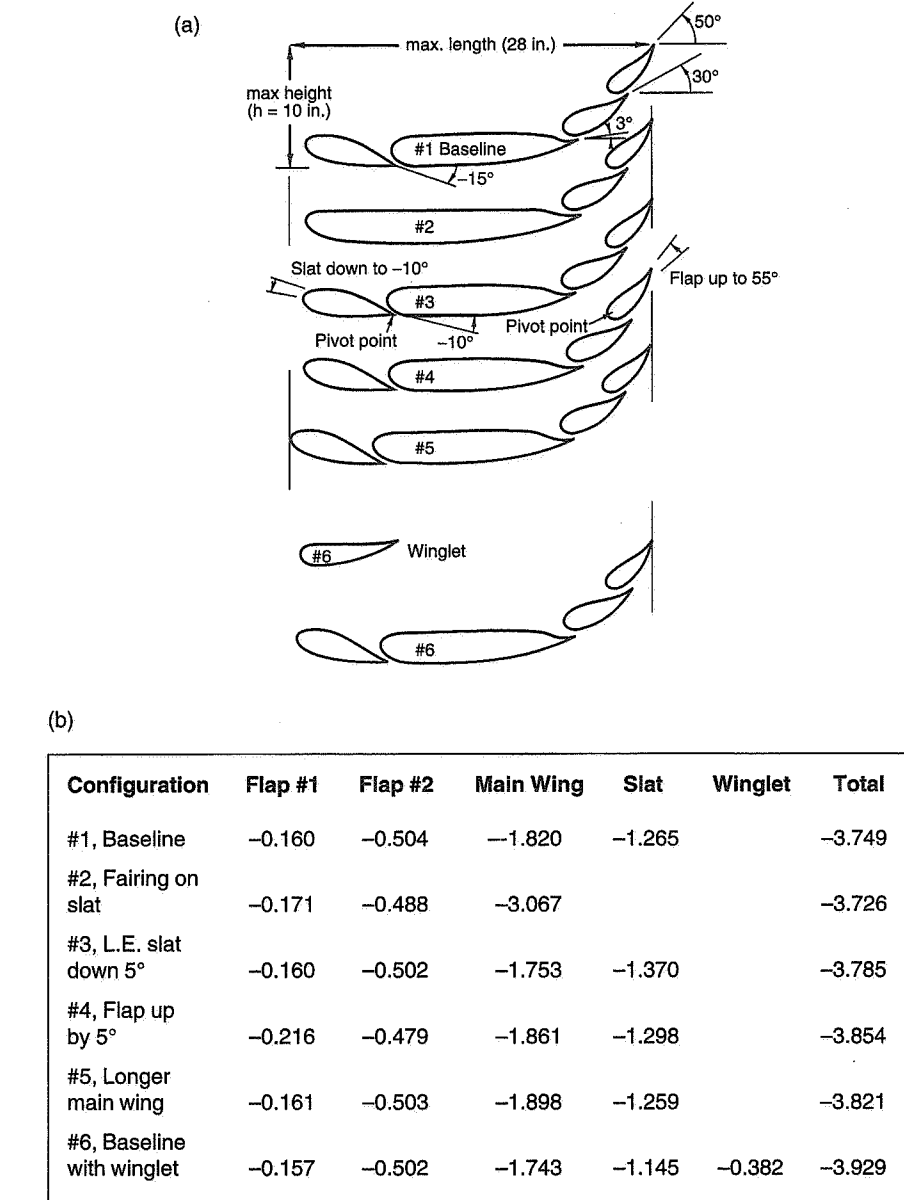


Figure 15.25 Two-dimensional airfoil shapes and computed lift coefficients (Ref. 76).

Katz then proceeds to perform three-dimensional calculations for practical rear wing configurations (falling within the CART requirements). These are summarized in Figures 15.26 (a) and (b). The conclusion is drawn that a practical CART rear wing should give a lift coefficient of about -2.2 at around zero angle of attack. Note: Side fin is a small 90° flap pointed outward.

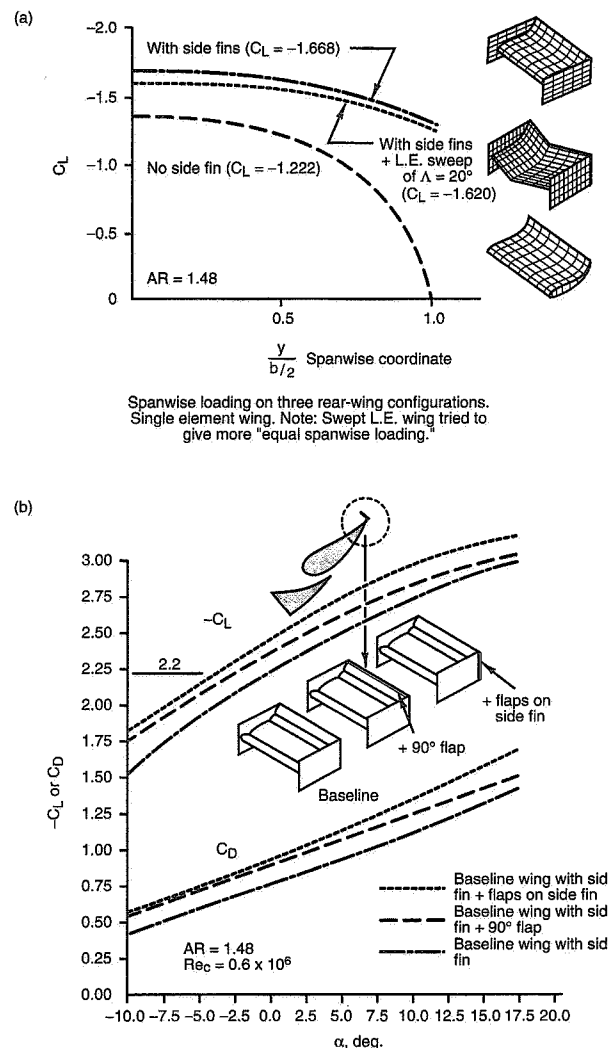


Figure 15.26 Modeling of three-dimensional airfoil shapes (Ref. 76).

In Ref. 76 there is a comparison of a three-dimensional analysis of the baseline wing with side fins and experimental measurements. This validation gives confidence in the results of Figure 15.26. The wings shown in Figure 15.26(b) are typical CART rear wing configurations for road racing.

In conclusion, it should be noted that considerable variations in wings will continue to appear depending on racing formulas, the particular event, the vehicle configuration, designer preference, etc.

15.5 Ground Effects

As noted earlier, increasing downforce by a reduction of pressure under the car had been demonstrated by the Chaparral 2J "Sucker Car" in the mid-1970s. It had recorded 1.7g⁵⁴ on a low-speed skid pad by comparison to 1.3, the best achieved by other cars on the same pad. The pressure reduction can be estimated as follows:

$$\text{Lat. Force} = \mu(W_0 + \Delta L)$$

$$\text{"g"} = \text{Lat. Force}/W_0 = \mu(1 + \Delta L/W_0)$$

where μ = effective friction coefficient (vehicle)
 W_0 = vehicle static weight
 ΔL = downforce due to pressure reduction under the car

For the 2J: $\mu = 1.3$ (measured at Midland)
 W_0 = estimated at 2500 lb.

For a "g" of 1.7, the ΔL comes out to be 770 lb.

If the effective bottom area was 50 ft.², the pressure change was $770/50 = 15.4 \text{ lb./ft.}^2 = 0.11 \text{ lb./in.}^2$ or about 1/100th of an atmosphere. At the skid pad speed of 50 mph, this corresponds to a $C_p = \Delta p/q = 15.4/6.4 = 2.4$, a very respectable figure.

The Chaparral 2J was provided with rigid perimeter skirts (of Lexan®) connected to the suspension by a cable and lever system to maintain a very small ground clearance. The pressure reduction was accomplished by an auxiliary engine-operated pump, thus the lowered pressure tended to be independent of speed, unlike modern ground-effects cars.

It remained for Lotus to demonstrate that pressure reduction of this and higher magnitudes could be obtained by appropriate shaping of the car's bottom and flexible side skirts. The Lotus research was accomplished in the Imperial College (London) wind tunnel under the direction of Peter Wright (Ref. 168) and led to the first true "ground-effects"

⁵⁴ This may still be a record for slow speed skid pad testing.

car, the Lotus 78. Figure 15.27 illustrates the remarkable progress that was made in ground effects on Grand Prix cars prior to the banning of sliding skirts in 1981. Part of the improvement is due to the wings; the C_L due to the tires is not included.

In Figure 15.27 the lift coefficient is based on *frontal area* (typical automotive practice) and, alternatively, *plan area* (corresponding to aircraft practice). These are defined in more detail in Ref. 168.

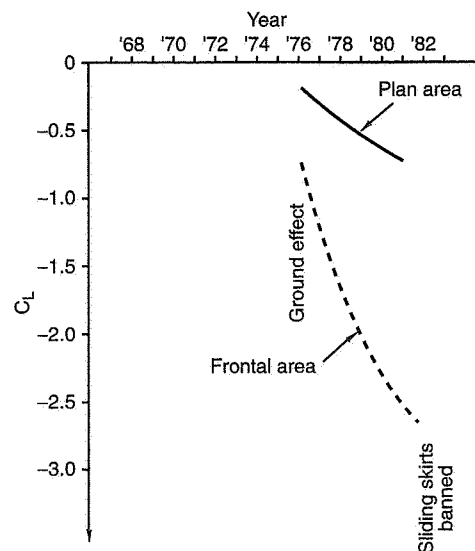


Figure 15.27 Historical development of negative lift (Ref. 168).

The next section starts with a general discussion of how ground effect works, followed by more specific information from the open literature.

Nature of Ground Effects

In Ref. 155, Stollery and Burns examine the forces on bodies operating close to the ground. Simple theory suggests that a two-dimensional symmetrical airfoil at zero angle of attack should develop a negative lift when near the ground. In this condition, the air velocity between the airfoil and the ground is increased and the local pressure decreased. A symmetrical section, three-dimensional, low aspect ratio shape (21% thick, 0.365 AR) was tested at various heights above the "ground" and for a range of angles of attack. The body shape and the lift results are shown in Figure 15.28. At zero α , the negative lift in-

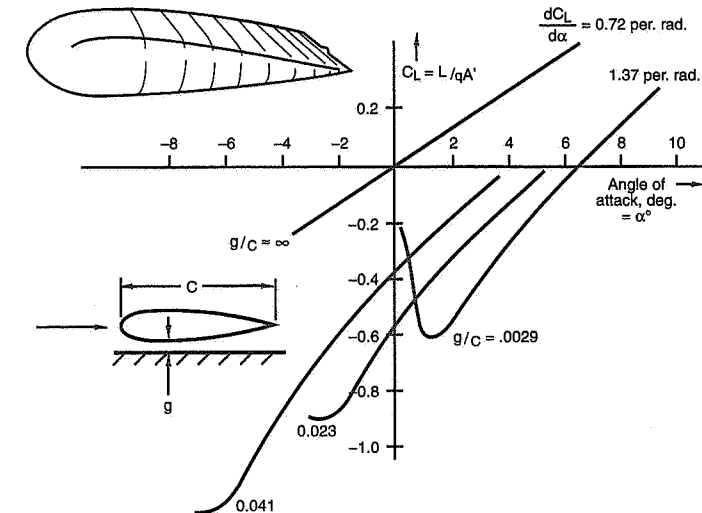


Figure 15.28 C_L vs. incidence, symmetrical nose, effect of ground (Ref. 155).

creases with proximity to the ground until it is very close. At ground contact one would expect a positive lift.

The Lotus ground-effect results are closely related to those described above. To quote Peter Wright from Ref. 168, "The main chassis/body unit of the car can be 'compared' to an inverted 41.4 ft.² plan area wing of aspect ratio 0.5 mounted on a fuselage and working in ground effect at a ground clearance to chord ratio of about 0.04. The tips of the wing have end-plates which extend to the ground. The simulation is complicated by the wheels ... in general the presence of wheels reduces maximum lift by over 30%."

The Lotus objective was to achieve the highest downforce at the best L/D ratio. Figure 15.29 indicates some results. Assuming the area of 41.4 ft.² (a chord length of 8.8 ft. and a "span" of 4.7 ft.) for the ground effect, the ground clearance comes out about 4 inches based on the clearance/chord ratio of 0.04. This gives a $C_L = -0.5$ based on plan area or a downforce at 100 mph of

$$-0.5 \times 25.6 \times 41.4 = -530 \text{ lb.}$$

At max speed of 180 mph, the downforce is

$$-0.5 \times 82.9 \times 41.4 = -1716 \text{ lb.}$$

or roughly the weight of the car. The ground effect increases as the square of the speed.

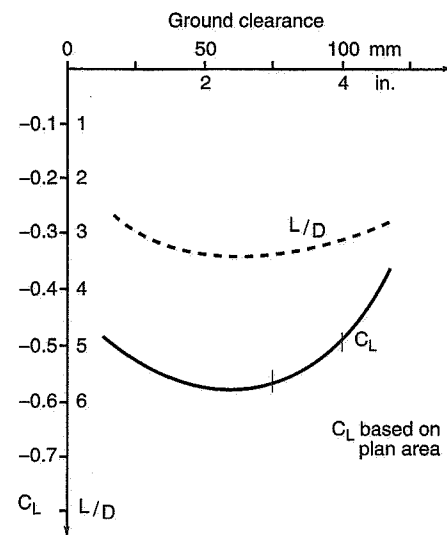


Figure 15.29 Lotus ground-effects wind tunnel results (Ref. 168).

This aerodynamic downforce may be reduced on an actual car by lift from the upper body surface and from the wheels.

In a personal communication, Peter Wright indicates that if the mass flow under the car was known, the application of Bernoulli's equation would largely account for the measured downforce. The following calculation is based on this assumption.

Figure 15.30 depicts the chassis of a simple ground-effects vehicle with side skirts, moving over the ground at speed V_∞ . For simplicity assume V_1 , the velocity of the air relative to the vehicle at section 1, is equal to V_∞ . Also assume that the Stagnation Point, A, is unknown and hence the cross-sectional area, A_1 , of the oncoming air at section 1. The static pressure at this section is $p_1 = p_\infty$. Assume incompressible flow and neglect effects of any boundary layer on the bottom of the car and any base pressure/diffuser effects. Also assume the skirts seal perfectly, hence vortices due to seal leakage are absent.

The *Law of Continuity* says that the mass flow across sect. 1 and across sect. 2 are equal:

$$\rho A_1 V_1 = \rho A_2 V_2 \quad \text{or} \quad V_2 = V_1 (A_1/A_2)$$

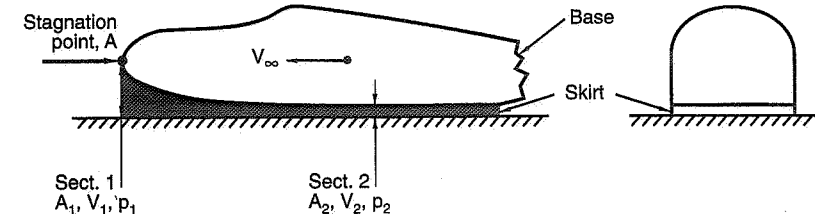


Figure 15.30 Simple ground-effects vehicle.

Bernoulli's equation says

$$p_\infty + \frac{1}{2} \rho V_\infty^2 = p_2 + \frac{1}{2} \rho V_2^2$$

$$\Delta p = p_2 - p_\infty = \frac{1}{2} \rho V_\infty^2 - \frac{1}{2} \rho V_2^2$$

or

$$\frac{\Delta p}{\frac{1}{2} \rho V_\infty^2} = 1 - \left(\frac{V_2}{V_\infty} \right)^2 = C_p$$

Working backwards from the Lotus downforce at 100 mph,

Downforce = $\Delta p \times \text{Bottom area}$

$$-530 = \Delta p \times 41.4$$

$$\Delta p = -12.8 \text{ lb./ft.}^2$$

$$C_p = \Delta p / q_\infty = -12.8 / 25.6 = -0.5$$

$$C_p = 1 - (V_2/V_\infty)^2 = 1 - (A_1/A_2)^2 = -0.5$$

$$A_1/A_2 = 1.22 = V_2/V_1$$

Thus a 22% increase in velocity under the car due to area ratio A_1/A_2 accounts for the downforce.

In an actual case, the prediction of downforce is not possible unless $\rho A V_1$ (mass flow) or the stagnation point is known.

Wright pointed out that they ultimately achieved a $C_p = -3.0$ (based on frontal area) or -0.77 (based on plan area). At 100 mph,

$$\Delta p = -0.77 \times 25.6 = -19.71 \text{ lb./ft.}^2$$

Downforce from the bottom of the car = $-19.71 \times 41.4 = -816 \text{ lb.}$

At 180 mph, the downforce would be -2643 lb. $A_1/A_2 = V_2/V_1 = 1.33.$

It appears safe to conclude that, to a first order, race car ground effects can be explained by Bernoulli's equation for incompressible flow. The car's underbody and the road act as a venturi. The net downforce on the car will be modified by contributions from the upper body (lift), wheels/tires (lift), and wings (downforce).

Ground Plane Simulation

Because of their convenience and test costs, small-sized, relatively low-speed wind tunnels have been extensively used for race car aerodynamic research and development. A perennial problem is that of ground plane simulation. A survey of the literature indicates that most model tests for ground effects have utilized a moving ground plane (power-driven belt) to achieve a zero relative velocity between the air and the "ground." This avoids a boundary layer on the tunnel floor and corresponds to the real world.

Early comparative tests with and without a moving ground plane were made at several facilities. The general conclusion was that results were qualitatively similar but appear quantitatively better with the moving ground plane (see Refs. 155, 49, and 50, for example). The use of a moving ground plane becomes more desirable for cars (models) with low ground clearance. More recent tests specifically aimed at evaluating the ground simulation problem (Refs. 138, 20, and 30) take the position that for low ground clearance race cars, a moving ground plane should be used.

Max Schenkel of the General Motors Wind Tunnel staff points out, however, that there are other ways of removing the boundary layer on the tunnel floor such as suction or blowing. GM uses a two-inch step in front of the test section and suction as appropriate. A boundary layer survey confirms the effectiveness of this arrangement. Porsche, in their tunnel, use distributed suction to locally remove the boundary layer as it builds up. In large, full-scale tunnels it is very difficult if not impossible to use a belt. It is not only difficult to keep the belt flat but the belt also interferes with the standard force measurement system located under the floor.

Another problem of using a belt is that the tires are in contact with the belt to simulate road conditions. Because tire lift loading is through the tire, not through the balance, tire aerodynamic lift cannot be measured in the balance. Lift forces on the sprung mass and overall drag forces can be measured with a sting or overhead balance, which is normally used with a belt.

Far too little comparison between tunnel and road measurements exist. It seems best to conclude that different solutions to this boundary layer problem will be used depending on the tunnel size, tunnel performance, vehicles/models to be tested, balance facilities, and other considerations.

Other Aspects of Ground Effects

Although the Bernoulli/venturi effect may be primary, there are a variety of other factors which contribute to the development of underbody force from Formula 1, CART (Indy), and other classes of race cars. Some of these are:

1. The amount of sealing from side skirts when used.
2. The boundary layer buildup on the bottom of the car which effectively changes the ground clearance distribution.
3. Upsweep of the rear bottom of the car to create a diffuser section.
4. The base pressure (pressure in the wake near the rear on the car).
5. The effect of the rear wing on the base pressure.
6. The development of longitudinal vortices due to leakage at the side seals.
7. Use of rear bottom channel configurations, and longitudinal vortices along the inside edges of these channels.
8. Airflow off the front and rear tires tends to divert airflow laterally into the underbody region diluting the suction effect.
9. The specific treatment of the car bottom in the vicinity of the rear wheels.
10. Three-dimensional flow over the entire car, which affects bottom flow conditions.
11. Flow interaction between a low-mounted front wing and underbody flow.
12. Treatment of engine/radiator cooling airflow, and so forth.

Since the banning of skirts in the early 1980s, the major advance in ground-effects technology has been the achievement of high downforce without skirts. This has been made possible by utilizing combinations of the above factors. Some technical information is available on this progress in the open literature and is discussed in the next section.

15.6 Ground Effects Without Skirts

Some Fundamental Studies

The effect of a large (20°) upsweep of the rear underbody of a bluff idealized vehicle shape has been investigated by A.R. George (Ref. 49) with the body near a fixed ground plane. These tests were performed at quite a low Reynolds Number. Figure 15.31 presents the lift and drag results for the basic body, body plus wheels, and with the addition of a rough underbody ahead of the upsweep. The coefficients are based on frontal area. At zero pitch angle on the basic body a negative lift coefficient of about -0.95 was measured. However, when the body was pitched nose down -10° (increasing the effective upsweep of the rear relative to the road), a negative lift coefficient of about -2.3 was obtained with or without the wheels. If one thinks of the region between the upsweep and the road as a "diffuser," then one would expect separation at the angle involved and hardly an increase in downforce. The actual increase in downforce was traced to the creation of two vortices (see Figure 15.32) whose induced flow eliminated separation on the upswept rear underbody, plus the effect of the negative angle of attack of the top of the body. The flow is bent upward effectively producing a cambered shape to the body (concave upward) or, equivalently, adding an up flap. The effect of the vortices is so strong that even with the rough forebody the flow remains attached (Figure 15.33).

This suggests the use of an upswept section of the rear underbody of a race car, provided flow control devices (such as bound vortices, vortex generators, etc.) are used to control separation. It is interesting to note that drag reductions also may be obtained.

In this same reference (49), George shows a comparison of testing on a fixed ground plane and a moving belt (Figure 15.34). He notes that there are a variety of reasons "why the flow around a body may be influenced by the speed of the ground." More fundamentally, how is the boundary layer on a stationary belt changed by belt movement and how do these boundary layer changes affect the flow around the body? Do they result in changes in circulation on the body, affect flow separation, or even result in a change in basic flow pattern?

For very low ground clearances the moving ground plane appears desirable but more research is needed to establish the definitive conditions, according to George.

In a later investigation (Ref. 50), George and Donis explore two types of ground-effects vehicles, the so-called *plenum* and *venturi* types. The venturi type has side skirts (not necessarily sealed to the ground) and is of interest in connection with current formula cars in which skirts **contacting** the ground are not permitted. Figure 15.35 shows the basic venturi model and numerous modifications tested. The forepart of the underbody was smooth and horizontal but the aft section had an adjustable diffuser with angles of 5° , 10° , and 15° to the horizontal. Adjustable height side skirts were provided and the model was tested with various skirt-to-ground clearances.

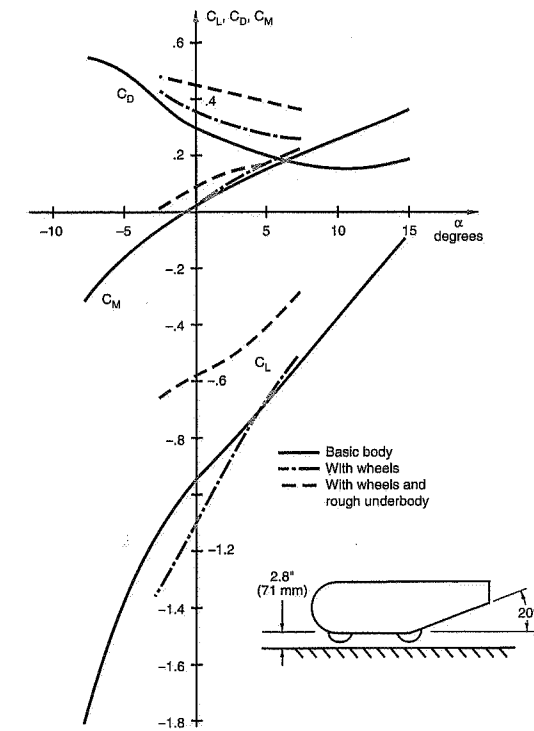


Figure 15.31 Lift, drag, and pitching moment near fixed ground board (Ref. 49).

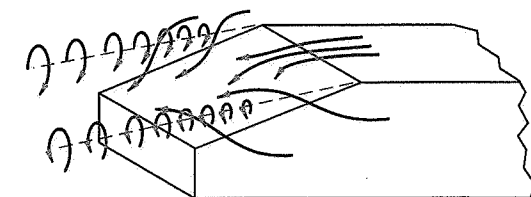


Figure 15.32 Sketches of flow with lee side vortices (Ref. 49).

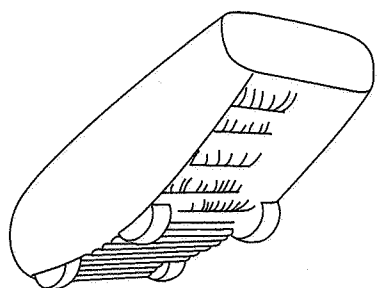


Figure 15.33 Body with wheels and rough underbody (Ref. 49).

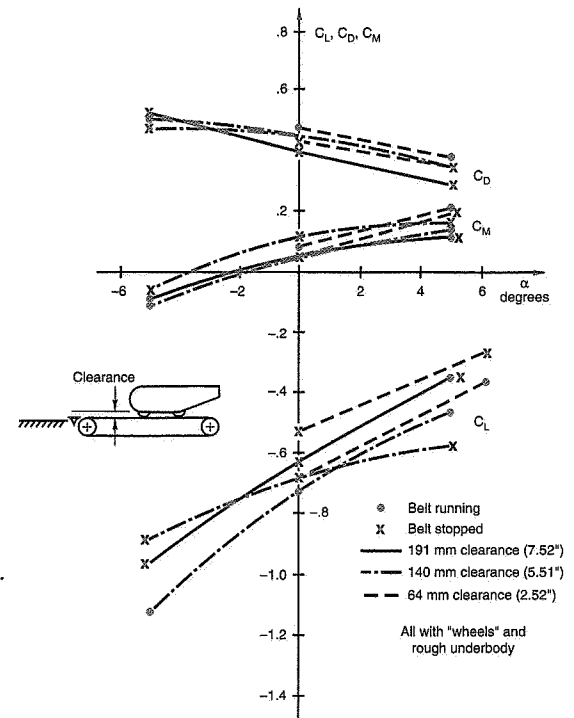


Figure 15.34 Tests with and without moving belt (Ref. 49).

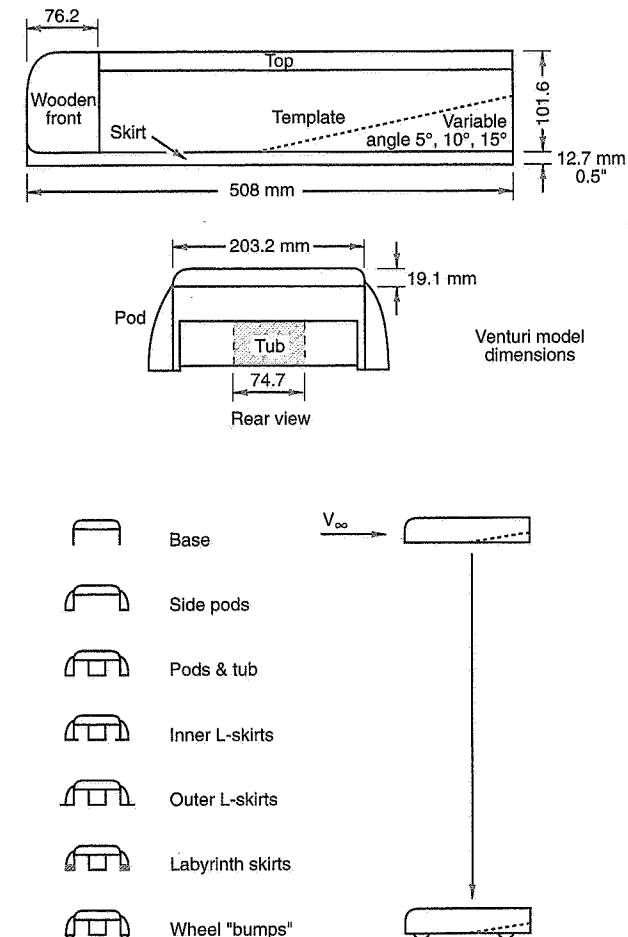


Figure 15.35 Venturi test configurations (Ref. 50).

The most significant flow feature was the development of longitudinal vortices along the inside of the skirt, when clearance between the skirt and the ground was present. The strength of these vortices depended on the transverse flow (in turn dependent on the skirt height above the ground). These vortices controlled the flow in the diffuser so that the larger diffuser angles could be used without flow separation. This resulted in lower pressures and larger downforces. Figure 15.36 illustrates the nature of the longitudinal vortices.

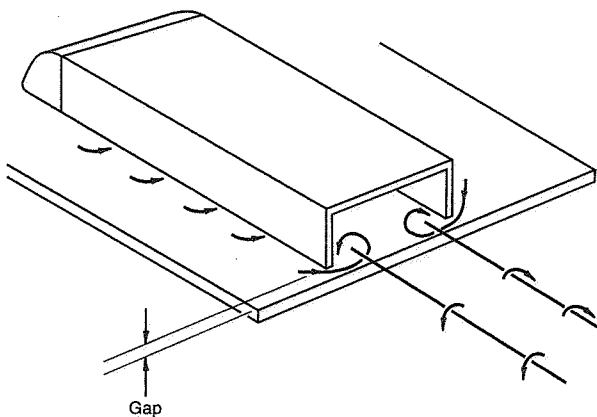


Figure 15.36 Flow with vortex formation under venturi model (Ref. 50).

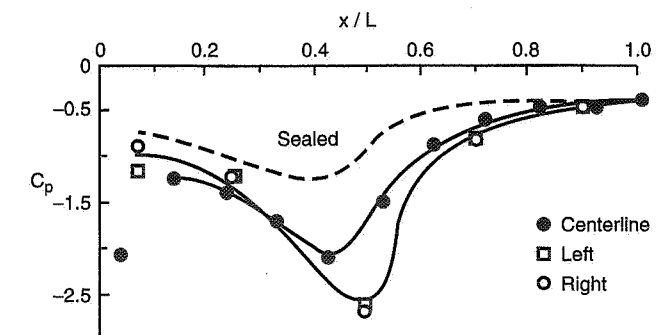
Figure 15.37 shows the increase in negative pressure coefficient along the length of the model when the 15° diffuser angle is used with nearly half an inch of clearance between the model skirt and the ground.

When “wheel-shaped” bumps were added to the side pods, the downforce was greatly reduced. It was postulated that they had interfered with the vortex formation. This result confirms experience on open-wheel race cars—that attention must be given to the three-dimensional flow around the rear wheels for optimum underbody and rear wing downforce performance.

Ref. 50 is well worth pursuing in more detail.

Race Car Applications

Two recent contributions by Katz illustrate the use of the underbody flow research described above to obtain downforce without a skirt to the ground. Figure 15.38, from Ref.



Static pressure distribution for 15° upsweep,
9.5 mm clearance at skirts and 22.2 mm
clearance under venturi.

Figure 15.37 Static pressure distribution (Ref. 50).

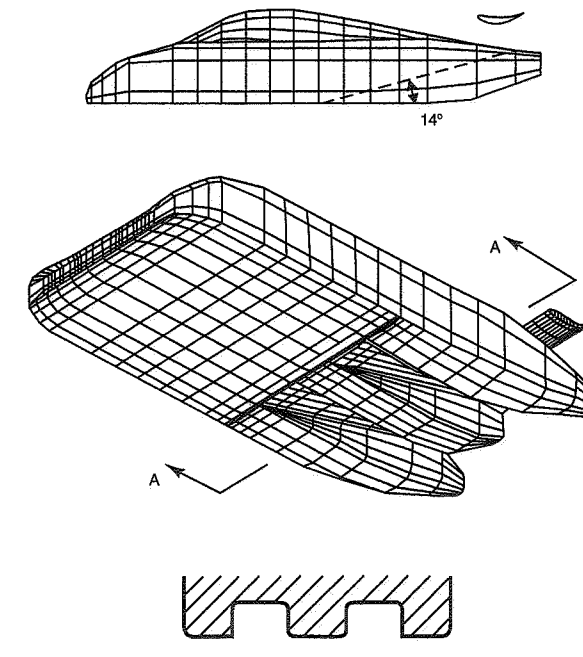


Figure 15.38 View of the underbody channels (Ref. 77).

77, is the model of an enclosed prototype race car with upswept underbody channels (model was tested without wheels).

Using flow visualization techniques it was found that two counter-rotating vortices exist in each channel (see Figure 15.39) and that the flow in the channels remains attached. The strength of these vortices depend on the lateral flow which is probably influenced by the presence of the wheels.

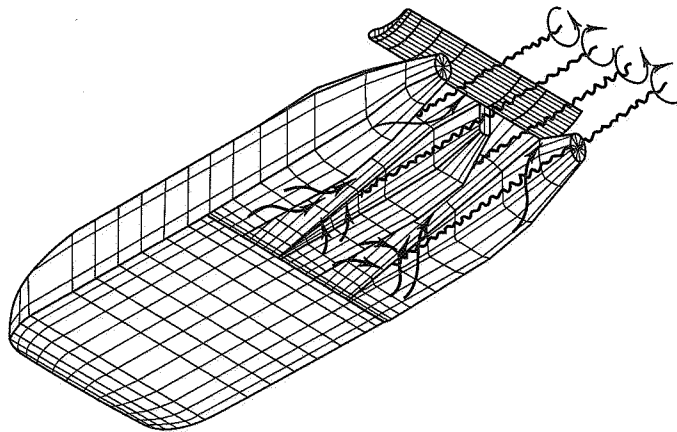


Figure 15.39 Vortices inside the underbody channels (Ref. 77).

Figure 15.40 shows a very high suction peak at the beginning of the channels for the model without the rear wing. The addition of the rear wing enhanced the suction in the channels over their full length. This was confirmed by Peter Wright's experience that a wing can reduce the base pressure by communicating forward. The Katz investigation suggested an optimum position for the wing L.E. slightly ahead of the channel exits and vertically close to the body (if the flow is clean in that location).

It should be pointed out that the rear wheels can have a large effect on the maximum pressure coefficient, $C_p \text{ max}$. Thus if the test of Figure 15.40 was repeated with wheels installed, the pressure peaks might be substantially reduced even with an enclosed body. With open-wheeled cars the effect of the wheels is much greater (see Figure 15.41).

Ref. 76 presents calculations and measurements for an open-wheel racing car model with twin underbody channels (diffusers) beginning ahead of the midpoint of the car and extending aft at an angle of 7°. Figure 15.41 gives pressure distributions along the

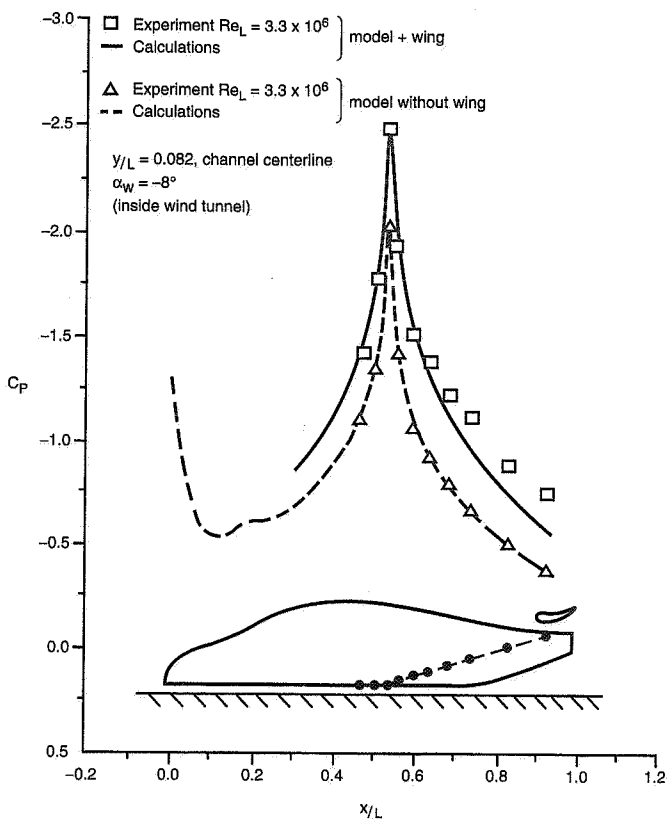


Figure 15.40 Effect of rear wing (Ref. 77).

vehicle centerline and in the center of one of the channels. There is a substantial suction peak slightly aft of the beginning of the channel. With the rear wing the suction is increased, the effect being largest near the rear of the car.

Figure 15.42, from Ref. 160, illustrates the use of rear bottom channels on F.1 (March chassis) and some other aerodynamic features.

The treatment of the body in the vicinity of the rear wheels on open-wheeled cars is still under debate. Figure 15.43 illustrates the use of flared side strakes, in this case on the Penske PC-18.

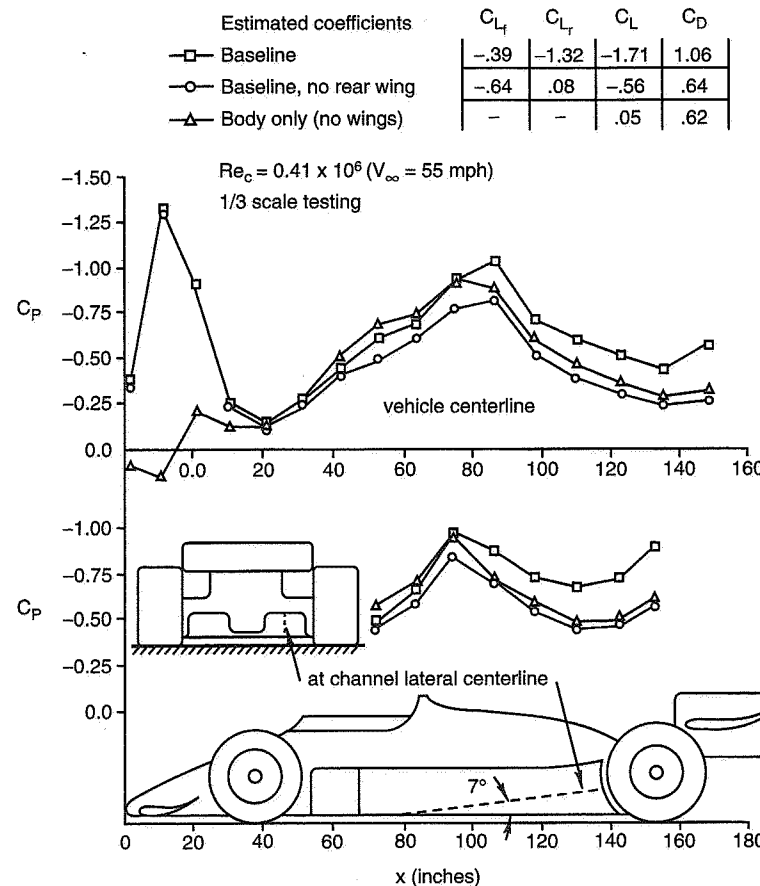


Figure 15.41 Effect of wings on underbody pressure distribution, CART car (Ref. 76).

15.7 Drag

In accordance with SAE J1594 (Ref. 2), *drag* (D) is defined as the aerodynamic force acting along the x-axis, but positive rearward ($F_x = -D$). The axis system is the conventional stability axis system fixed in the car (i.e., yaws with the car) and the x-axis is normally horizontal, positive forward, and the "resolving center" or origin is located mid-wheelbase, mid-track, and at ground level.

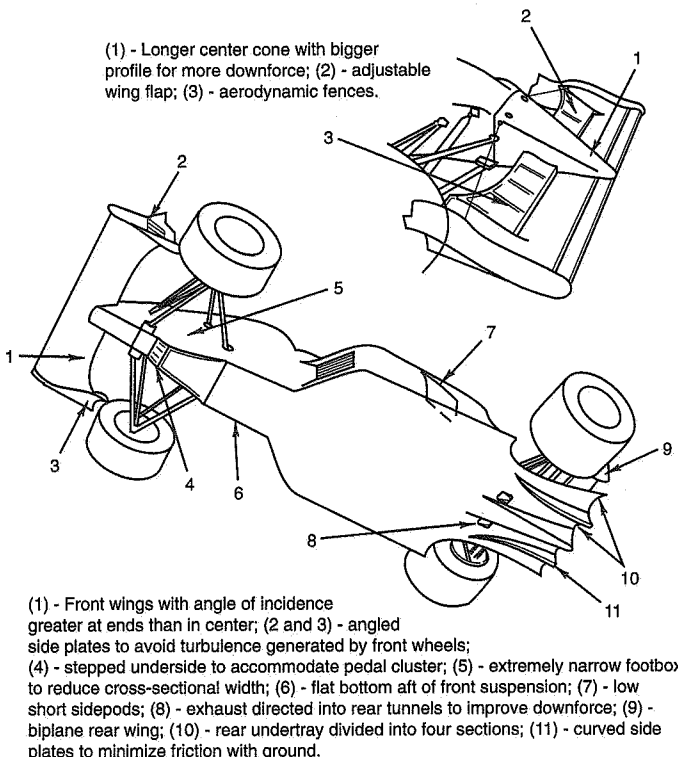


Figure 15.42 March F.1 aero features (Ref. 160).

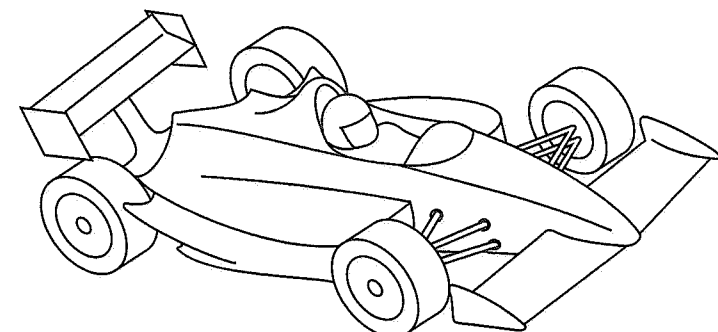


Figure 15.43 Penske PC-18.

The aerodynamic drag coefficient is defined as

$$C_D = \frac{D}{q_{\infty} A}$$

where $q_{\infty} = (1/2)\rho V_{\infty}^2$

A = Vehicle area projection in x-direction (frontal area)

For a given vehicle configuration and operating condition there is a single resultant aerodynamic drag force with an effective center of pressure above the ground; when this force is moved to the axis origin at ground level, a pitching moment results about the y-axis which is reacted by changes in vertical forces at the front and rear wheels.

The resultant drag force is made up of several components which arise from different effects and do not necessarily follow the same physical laws. Ways of classifying drag components are reviewed in the following sections.

Fundamental Drag Mechanisms

The most fundamental approach to drag classification is in terms of *flow types*. To get to the flow types of practical significance in creating race car aerodynamic drag, we will start with some idealizations.

As noted in Chapter 3, Aerodynamic Fundamentals, air particles can react on each other to produce normal (or pressure) forces and tangential (or shear) forces. The pressure forces in the smooth flow about a body (say an airfoil) can be computed by Bernoulli's equation, except in regions of separated flow. The shear forces are due to the viscosity of the fluid and occur in the thin boundary layer next to the body.

Consider a smooth two-dimensional (infinite span) body (Figure 15.44). The local pressure forces (vectors) act normal to the surface. If there were no boundary layer or separation (ideal fluid), the resultant of all the pressure force components in the drag direction would be zero and the flow would close in at the rear, with a rear stagnation point at "A." In actual fact, there is a boundary layer which on a very smooth surface starts out laminar and then transitions to a turbulent boundary layer which is thicker and more stable. The shear forces in these layers extract energy from the flow and slow it down, particularly toward the rear of the body. This interacts with the pressure recovery on the surface such that "separation" may occur, as shown in Figure 15.44 (separation phenomenon is discussed in more detail in Chapter 3). Separation results in stalled, turbulent flow in the aft wake and low pressure which acts on the base and rear part of the body. An integration of all of the local pressure force components in the x-direction will result in a *pressure drag* (also referred to as shape or form drag). An integration of all of

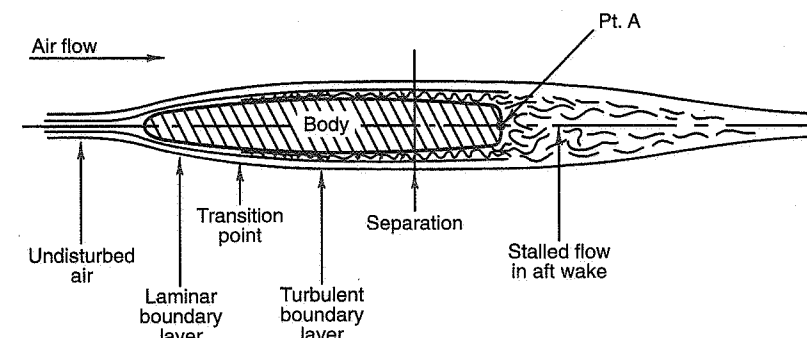


Figure 15.44 Types of airflow in boundary layer, two-dimensional flow.

the local shear forces on the body will result in a *skin friction drag*. Thus we have identified two fundamental types of drag mechanisms and their associated flows.

In addition to pressure and skin friction drag, the term *induced drag* frequently appears in the literature along with some misconceptions. Refs. 63, 31, and 65 clarify the nature of induced drag and the following discussion is indebted to them.

The term *induced drag* comes from aircraft use and is properly associated with airfoils of high aspect ratio (span/chord ratio). The three-dimensional flow about such wings under conditions of lift results in two major vortex structures at the wing tips (see Figure 15.45). These vortices induce downwash velocity components in the sheet of air behind the wing (creating a downwash angle). When the "lift" vector is oriented 90° to the average local flow, it has a drag component relative to the remote flow to which lift is normally referenced. The induced drag turns out to be a simple function of the lift.

On short, bluff, three-dimensional automobile and race car shapes, vortex structures reminiscent of those of a wing are common (see Figure 15.46, from Ref. 65), but they are intermixed with the two-dimensional flow and their drag bears no universal relationship to the lift. Also it must be remembered that the ground plane prohibits downwash, although upwash is still possible. The term *vortex drag* seems more suitable than induced drag. The vortices are generated at the expense of power through changes in pressure and skin friction drag.

Although it is convenient to sometimes think in terms of vortex drag and also drag due to the turbulent wake, Carr (in Ref. 31) makes the point that there are "just two components [of drag], pressure drag and skin friction" and that vortex and wake drags are merely alternative ways of looking at drag. A pressure survey on the wake which encompasses all of the momentum losses yields the total drag.

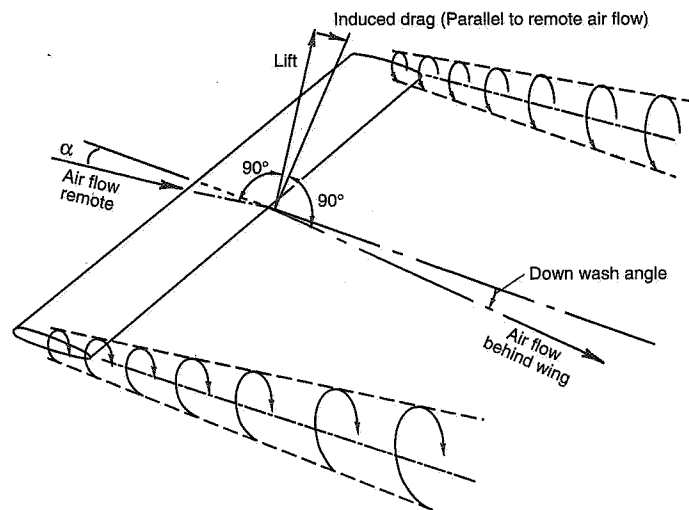


Figure 15.45 Induced drag, three-dimensional wing.

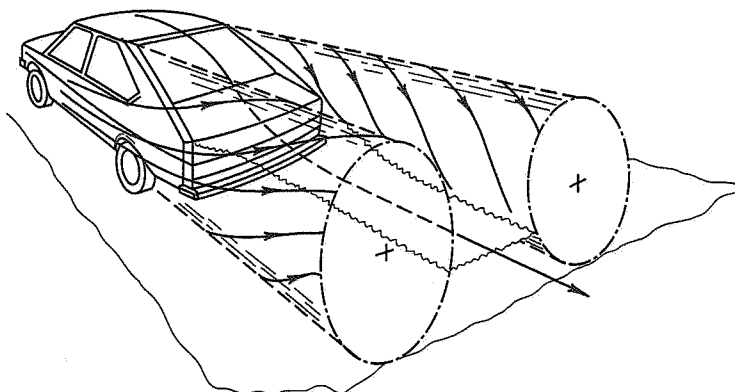


Figure 15.46 Idealized flow field around a fastback car, schematic (Ref. 65).

Race Car Drag Components

With the exception of extraordinarily clean research vehicles and land speed record-breakers, skin friction drag *per se* is a minor part of the aerodynamic drag of race cars. Even in those cases where it is a measurable component, in all likelihood it is associated with a turbulent, as opposed to a laminar boundary layer (see Figure 15.44). **Form or pressure drag, and associated separation(s), is the major drag mechanism in race cars.** Vortex flows may also produce a significant drag but may have compensating effects as already noted in controlling flow into underbody ducts for producing downforce on unskirted cars.

An alternative way of classifying drag components is in terms of the different parts of the car producing the drag. This leads to such breakdowns as:

1. Drag due to basic external shape
2. Drag due to wheels and wheel wells
3. Drag due to external flow control devices
4. Drag due to internal flow (for cooling and ventilation)
5. Drag due to less than perfect shape (roughness, external mirrors, handles, recesses, etc.)
6. Interference drag

In the next section some overall vehicle drag levels are discussed.

Complete-Vehicle Drag Levels

Drag comparisons are normally made on a drag coefficient basis since C_D is nondimensional, i.e., the drag per unit of dynamic pressure in the airstream and per cross-sectional area.

Figure 15.47, from Ref. 26, shows an idealized minimum drag body shape that might be used as a starting point for a practical car body. This was developed by Volkswagen and has a $C_D = 0.06$ in free stream (no ground plane). Figure 15.48 is a comparable shape developed by Professor A. Morelli, Turin Technical University (Ref. 97). This shape has a $C_D \approx 0.05$.

Progressing to a complete vehicle, the reduced-scale wind tunnel model of the Goldenrod land speed record car (wheel driven) had a C_D of 0.12 as measured in the GALCIT wind tunnel with no internal flow (Ref. 80) (Figure 15.49). At that time, this was the lowest drag coefficient that had been realized on a race car.

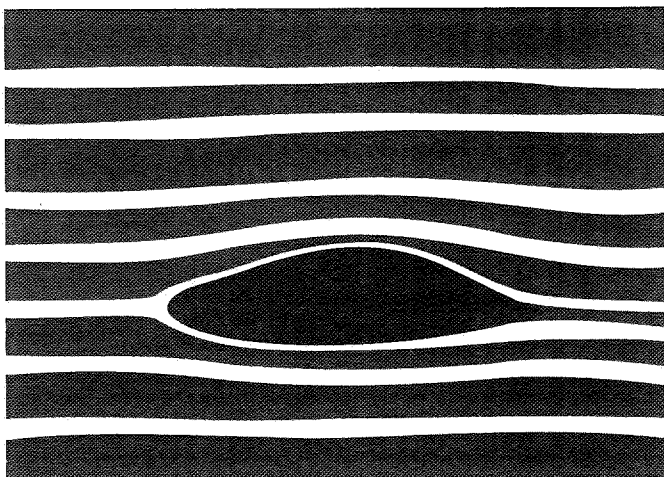


Figure 15.47 VW basic aerodynamic flow body (Ref. 26).

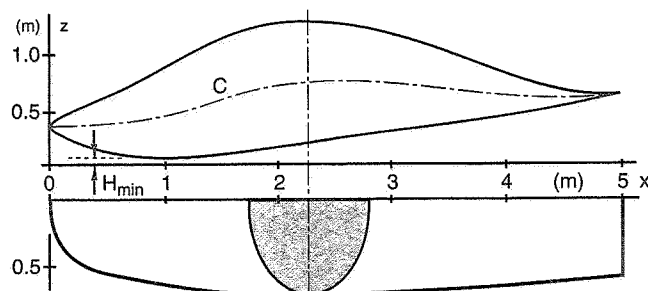


Figure 15.48 Morelli basic body shape (Ref. 97).

On the high end of the drag scale for race cars are the open-wheeled formula machines (F.1, Indy, etc.) and a few open cockpit enclosed-wheel sports and CanAm cars. Metz (Ref. 90) quotes Indy car drag coefficients⁵⁵ in the range of 0.8-1.0 for the 1985-87 period. Simanaitis (Ref. 146) reports on full-scale wind tunnel tests of a March 83C (1983) machine, which in CART form (for road racing with large aero downforce⁵⁶) has a C_D of

⁵⁵ All coefficients based on cross-sectional or frontal area.

⁵⁶ For low-speed tracks where downforce is so desirable and vehicles are not power limited, C_D 's may be over 1.0 (CART). The C_D is very dependent on the downforce, C_L .

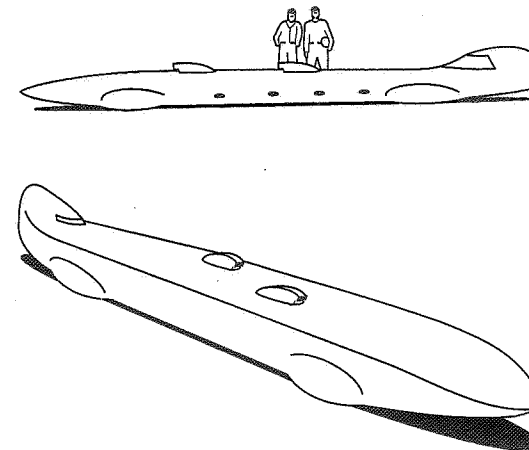


Figure 15.49 Goldenrod land speed record car (Ref. 80).

0.86 and in Indy set-up (compromised for downforce and drag) has a $C_D = 0.64$. A more complete analysis of open-wheeled cars in these categories appears to be that of Ref. 75. A drag comparison was made between small-scale wind tunnel tests and theoretical drag calculations based on a "simplified panel model," utilizing experimental data on separation lines and full-scale tests. The results are summarized in Figure 15.50. A C_D of 0.91 was determined (by computation) for the complete car with front and rear wings. Full-scale coastdown tests on the Chaparral G.S. 2G, 1967 CanAm car with high wing (see Section 15.3) gave $C_D = 1.00$ for rear wing in the high drag position and $C_D = 0.70$ for wing in trimmed position. It is difficult to talk about drag levels for cars with aerodynamic surfaces. The drag is heavily related to the aerodynamic configuration and the amount of downforce.

Examples of enclosed-wheel sports-racing category cars give drag coefficients ranging from $C_D = 0.32$ for Porsche 911 Group B to $C_D = 0.57$ for Porsche 917/30 CanAm (Ref. 63). The drag of the 917 depends on C_L or wing settings. Data for more recent cars was not available for this survey. For comparison, conventional passenger cars (1989 period) generally fall in the 0.3-0.4 range. Advanced aerodynamic concept cars have been produced which give C_D 's as low as 0.15, achieved by Ford Probe IV (1983) illustrated in Figure 15.51 (Ref. 137). The figure indicates the areas of the body which were given special aerodynamic consideration.

It is interesting to compare progress in automobile aerodynamic drag reduction with aircraft drag levels. If the drag coefficient of the Douglas DC-3 (pre-WWII) is computed based on frontal area and known performance it comes out 0.12. A similar exercise for a modern jet transport (say Boeing 747) yields around 0.08 at some reasonable cruise con-

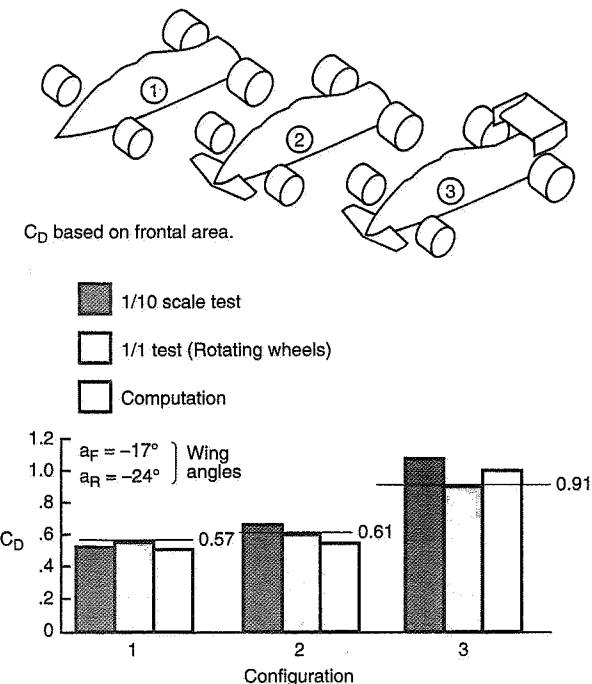


Figure 15.50 Comparison of computed drag forces with experimental values (Ref. 75).

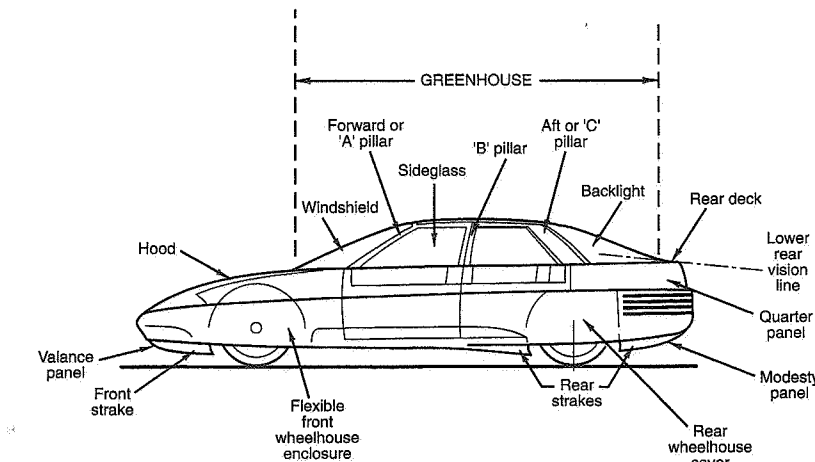


Figure 15.51 Probe IV body surface nomenclature (Ref. 137).

dition. The automobile is handicapped by the presence of the ground, its low altitude operation, its length/"diameter" ratio and its nonretractable wheels. It derives forces from both the ground and the air (a hybrid machine) and pays a price for the associated design compromises. On the other hand, aircraft are fully air supported and pay a price in induced drag associated with lift.

Drag Improvement and Estimation

When the class of racing, the circuit, and other factors suggest priority for aerodynamic drag reduction of an existing car, then initial effort should be directed toward locating and eliminating areas of separated flow and in wake reduction. Tuft studies on the full-scale vehicle, as discussed in Chapter 3, are a logical starting point. Separated flow is the result of such factors as:

1. Body contours with excessive diffuser angles
2. Too small radii in areas where flow direction is not known or can change in operation (nose, radiator air entry, etc.)
3. Sharp edges creating vortices, usually associated with surface roughness from mirrors and other attachments
4. Surface roughness
5. Improper treatment of entry, exit, and control of internal airflow for the engine, and for cooling of engine, brakes, transmission, driver, etc.
6. Wheel well and underbody treatment
7. Interface between local flows

Once the separated areas are known from tuft observation or photos, modifications to local body shape may be obvious. These can be accomplished for experimental purposes by resorting to old race-plane practice which used balsa wood, modeling clay, fabric/dope, etc. A little imagination is invaluable at this stage—the idea is to get the air past the car with as little disturbance and change in direction as possible. Since drag depends on frontal area as well as shape, every attempt should be made to minimize or at least not add frontal area.

In cases where separation cannot be cured by the simple means above, special flow control devices may be necessary. These are discussed in the next section and later with the problem of internal airflow and its control.

Extensive studies of the components of passenger car drag exist in the literature (Refs. 31, 45, and 64). Chapter 4, Section 4.3 of Ref. 63 is an excellent analysis of aerodynamic drag of passenger cars, much of which is applicable to some race car classes.

The estimation of race car drag is occasionally required in the design stage where the general vehicle configuration is known. As with aircraft this can be accomplished by three methods:

1. Wind tunnel measurements on the specific car model. The validity will depend on the model detail, the RN, and various wind tunnel correction factors.
2. A guess at the overall drag coefficient and a calculated frontal area.
3. An estimate based on the addition of the drag coefficients of the vehicle components plus interference effects between them.

Even with such relatively simple and idealized shapes as used in aircraft, method 3 above is not easy and an experienced guess (method 2) may give as good an answer. However, if you're going to be competitive, you have to use method 1.

15.8 Flow Control Devices

Flow control devices are used to (1) effect desirable changes in the aerodynamic forces and moments on the car and (2) control internal airflow for engine air consumption, cooling of engine, brakes, transmission, and ventilation for the driver. Some of the devices influence the boundary layer; others affect the remote (potential) flow. There are a large number of these devices, mostly from aeronautical sources. They have been applied and adapted to the race car as the need has arisen.

In the present section an attempt is made to categorize and discuss devices which have been used in racing. Flow control is an area where ingenuity and invention plays a large part; new devices may be anticipated as new problems arise.

Categorization

Various parts and components of race cars create aerodynamic forces and moments. One function of flow control devices is to modify these forces and moments in a desirable direction by changes in flow conditions. In this respect, a flow control device is acting as a catalyst by creating force effects large in relation to those experienced by the device itself. There are a number of ways of influencing flow conditions. If the influence takes place outside the boundary layer, one may expect simultaneous changes in pressure, velocity (both speed and direction), and vorticity or flow rotation. If the influence acts within the boundary layer, changes in the character of the flow may occur and separations and wake will be affected, which in turn can produce substantial force effects.

The other function of flow control devices (as mentioned earlier) is to facilitate the entrance, passage, and exit of internal airflow. Here again, one may expect simultaneous changes in several flow variables such as velocity, pressure, etc.

In practice it is common to think of flow control devices in terms of their primary function such as a change in flow direction, pressure, or speed. In trying to group the devices into various categories it will be convenient to adopt this scheme while realizing its shortcomings.

Devices for Directing or Containing the Flow

This category includes Dams, Fences, Vanes, Skirts, Brushes, Spoilers.

Spoilers and dams have been discussed in Section 15.2. Skirts and brushes were used with the Chaparral 2J "Sucker car" (rigid polycarbonate) and with the early ground-effects cars, where they were both rigid/slidable and flexible (brush-like); these are discussed in Section 15.5. They are mainly for prohibiting air from the outside from flowing into the low-pressure area under the bottom of the car so that the Bernoulli effect can be maintained.

Fences and vanes are common in aircraft practice where they are used to locally guide the flow. They are usually made of flat or curved plate. Figure 15.52 shows a fence on the upper surface of a wing to prohibit local spanwise flow. Because it is nearly aligned with the oncoming flow, its drag contribution is small.

The angled side plates by the front wheels of the March F.1 car (Figure 15.42)) are in the nature of guide vanes since they extend beyond the front wing end plates. It is also becoming common to use curved guide vanes in front of the rear wheels on open-wheel cars to direct the air toward the top of the rear wheels for drag reduction and downforce. Such an installation is shown on the Penske PC-18 (Figure 15.43). Guide vanes are also

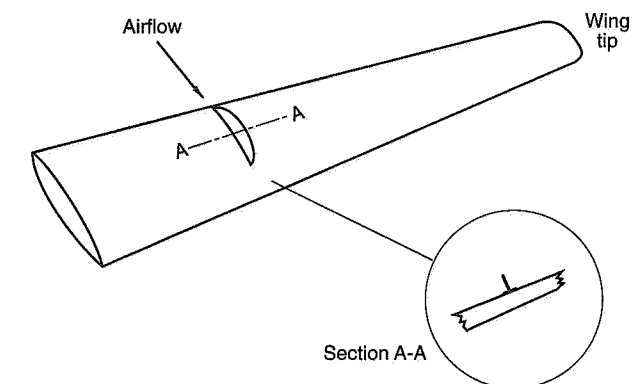


Figure 15.52 Fence on wing to prohibit spanwise flow.

used in engine air ducts to facilitate turning the air. A sketch of such an arrangement is shown in Figure 15.53. The function in this case is exactly similar to the turning vanes in a wind tunnel, as shown in the same sketch. Vanes also are used to direct air to the brakes, transmission, etc., either as part of ducting or separately.

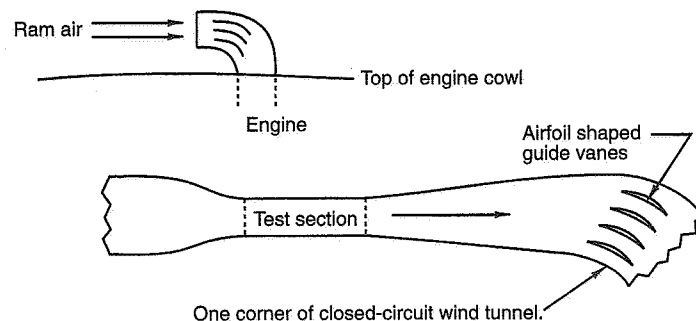


Figure 15.53 Guide vanes.

Figure 15.54 shows a fence on the side of the nose of a CanAm McLaren, designed to make the shovel nose more effective for downforce.

The above devices basically affect the flow outside the boundary layer; they are not intended to create useful vorticity.

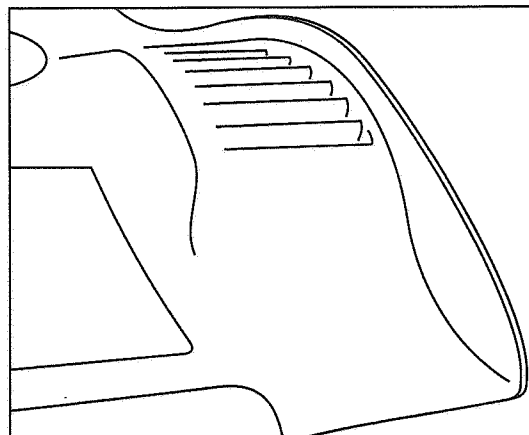


Figure 15.54 Fence on McLaren CanAm car (side of nose).

Devices for Creating Useful Vortices

This category includes Ledges, Edges, Cusps, Lips.

A vortex—a rotating body of air—induces velocities at some distance from its core axis of rotation. The induced velocities may usefully affect the flow. Also, a vortex has a lowered pressure in its core. The classical example of the former is the downwash behind a lifting wing due to the induced velocities from the large tip vortices, as was sketched in Figure 15.45. When vortices arise along the sides of cars (Figure 15.46), they also give rise to induced downflow effects.

Ledges, edges, etc., tend to create vortices because a real flow cannot turn around a sharp edge. Turning around a zero radius implies an infinite angular acceleration; the attempt to do so imparts angular momentum to the fluid. The sharp edges of the rear underbody channels of the configuration shown in Figure 15.39 create longitudinal vortices which draw air in from the outside and funnel it down the channels.

Vortex structures may occur *along* or *across* a vehicle. Some will form and detach in a periodic fashion while others may remain as “attached, trapped, or bound” vortices. With the proper slope to a fastback rear end, a horizontal lateral vortex may form and travel with the vehicle. This vortex can assist the flow in curving down over the rear of the car and reducing the wake size. Such a vortex is shown at “B” in Figure 15.55, from Ref. 63. This vortex structure tended to reduce the vehicle drag—had a favorable effect on the wake size. It is also noted that another vortex “A” is created which rotates in the opposite direction.

It has been proposed that by introducing a cusp at the rear top of a vehicle, a trapped vortex could be created for inducing a reduced wake (see Figure 15.56). For more information on the use of trapped vortices for automobile flow control, see Ref. 36.

The “vortex generator” is one of the more widely used and effective flow control devices. Its primary function is to energize the air in the boundary layer to delay separation. These devices may be seen in critical flow areas on the top surface of the wing on a number of commercial aircraft. They appear as small wing-like objects installed perpendicular to the wing surface at an angle of attack and usually in pairs. Any number of pairs may be distributed along the surface in the spanwise direction. Figure 15.57 illustrates the concept. Originally vortex generators had airfoil-like cross sections; small flat plates appear to perform almost as well. The simple explanation of their operation is as follows: Each vortex generator set at an angle of attack has a tip vortex, the core of which is roughly parallel to the surface on which the device is mounted. The vortex tends to mix the air in the boundary layer with the high-velocity free-stream air, as indicated in the figure. This process energizes the sluggish boundary layer air and delays the separation (which might otherwise occur in the pressure recovery area). Undoubtedly, the actual process is more complex.

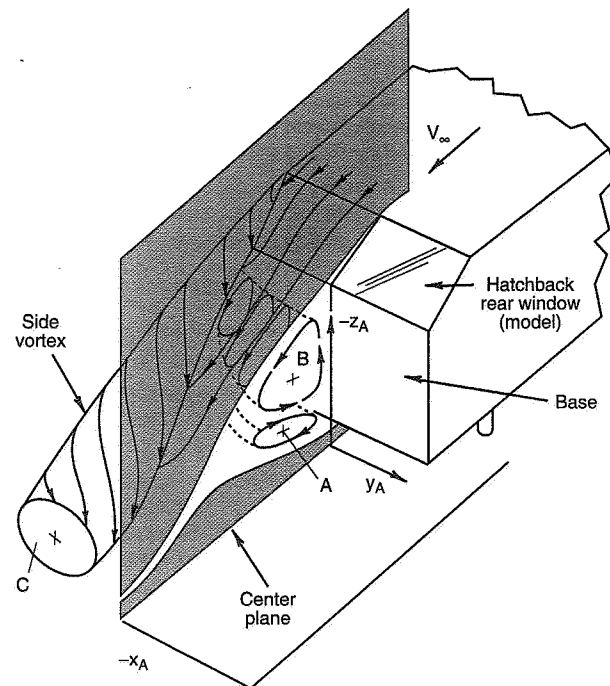


Figure 15.55 Vortex structure on rear of a car (Ref. 63).

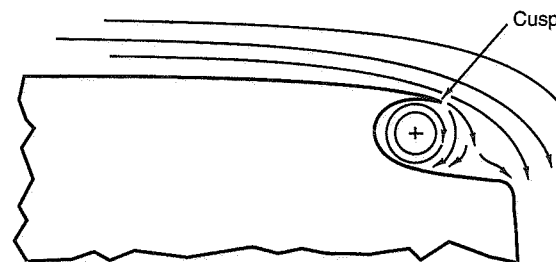


Figure 15.56 Trapped vortex produced by cusp on rear body top (see also Ref. 36).

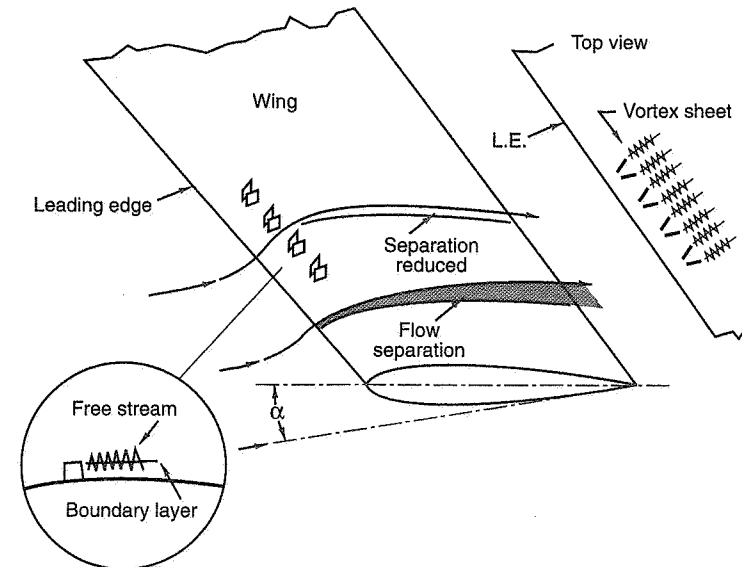


Figure 15.57 Vortex generator.

The beauty of the device is its simplicity and the fact that it can be used in almost any location of incipient separation. Any number of units may be installed. A typical size for race car use could be 1-1/4 to 2 inches high and a 1/2 to 3/4 inch chord. Vortex generators have a drag penalty and are most effective when used to cure a flow problem.

Devices for Creating Pressure Changes

This category includes Perforations, Vents, Bleeds, Scoops, Seals.

Figure 15.54 shows a series of rectangular-shaped vents in the front wheel housing top. A low-pressure area exists on the top of the wheel arch compared to the pressure in the wheel well itself. Together these two result in substantial front-end lift. By venting the air from inside to outside, this lift can be reduced. Similar pressure differences on other parts of the body (for example, on the hood) may indicate the same treatment.

Scoops for engine air are common. By extending them out into free stream, ram air can be utilized. This enables the passage of more air at a higher pressure. It is particularly effective when supercharging that works on a pressure ratio is employed. A typical ram air scoop is sketched in Figure 15.53.

Seals and bleeds can be utilized to adjust pressure levels.

Plain flaps have occasionally been used for air brakes or for adjustable doors on radiator ducting. Flutter or vibration of these flaps or doors can occur due to disturbed aerodynamic flow conditions. An effective countermeasure is to perforate the element which reduces the scale of the disturbing flow elements.

Pressure (and velocity) changes may also be accomplished by diffusers and contractors. Consider the radiator ducting of Figure 15.58. If efficiency in terms of losses in the air side of a radiator cooling system are important (and space and package permits), this arrangement could be used. This will be discussed at more length in Section 15.9. Suffice it to say here that the entrance diffuser efficiently (and reversibly) slows the air down before the radiator and the contractor behind the radiator speeds it up for re-entry into the external airstream. Diffusers and contractors may be used for other ducting requirements.

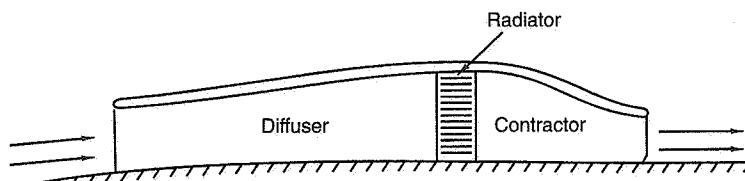


Figure 15.58 Use of diffuser and contractor in radiator air duct.

Devices Associated with Airfoils

This category includes Slats/Slots, Flaps, End Plates, Cuffs, Fillets, Trips.

Slats/slots and flaps were discussed under High-lift Devices in Section 15.4. A variety of these devices exist for both leading and trailing edges of wings. Reference has also been made to end plates (see Figure 15.21) as a means for effectively increasing the aspect ratio of a "legislated wing."

Figure 15.59, from Ref. 149, illustrates a device which has been variously called a "Gurney Lip," an "Indy Angle Iron," or a "Wicker Bill." This device is a very small, 90° plain flap installed at the trailing edge of an airfoil. In automotive use where airfoils are used for downforce, the installation is on the top T.E. As with any flap it has a decreased pressure behind it which tends to reduce T.E. separation on the airfoil to which it is attached. It is used to make fine adjustments in downforce.

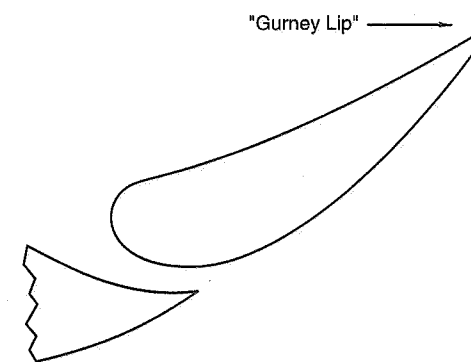


Figure 15.59 Gurney Lip installed on slotted T.E. flap (Ref. 149).

A type of slot recently introduced to aeronautical practice (Ref. 39) consists of a narrow vertical cut in the leading edge of a wing, called the *Rao slot* after its inventor, Dr. D.M. Rao of Vigyan Research Associates, Hampton, VA. Figure 15.60 illustrates an actual installation on the Questair Venture prototype aircraft (see above reference). When the wing is at a substantial angle of attack the "high-pressure airflow from the bottom of the wing shoots up through the slot, creating ... a tail of turbulent air streaming back over the top of the wing." The effect is that of creating an invisible flow fence against spanwise flow on the wing in this area. The air jet created is characterized as a "high-pressure vortex." Its effectiveness has been established through actual experience. This is an example of flow control innovation resulting from a specific need.

Figure 15.60 also illustrates a Cuff installation near the end of the wing. A cuff is an addition to an existing airfoil (usually on the leading edge) that modifies the airfoil shape and its local angle of attack. An additional benefit from the installation shown came from the sharp inboard end cutoff of the cuff. This apparently gave rise to a "trailing vortex" over the top of the wing which acted like a fence to reduce spanwise flow.

Fillets are installed at the juncture between two surfaces to improve the accommodation of the respective airflows, minimize separation, and reduce so-called interference drag. They originated at wing-fuselage junctions and were particularly useful with thick airfoils. Many modern aircraft with thin wings have very small fillets or none at all. Figure 15.61 illustrates a typical fillet installation. Race car applications include juncture of suspension links and body, juncture between radiator side pods and body, etc.

Trips are small devices (projections) attached to a surface to cause a laminar boundary layer to become turbulent. They are frequently used in wind tunnel work with small models to initiate formation of a turbulent B.L. for correlation with full-scale conditions.

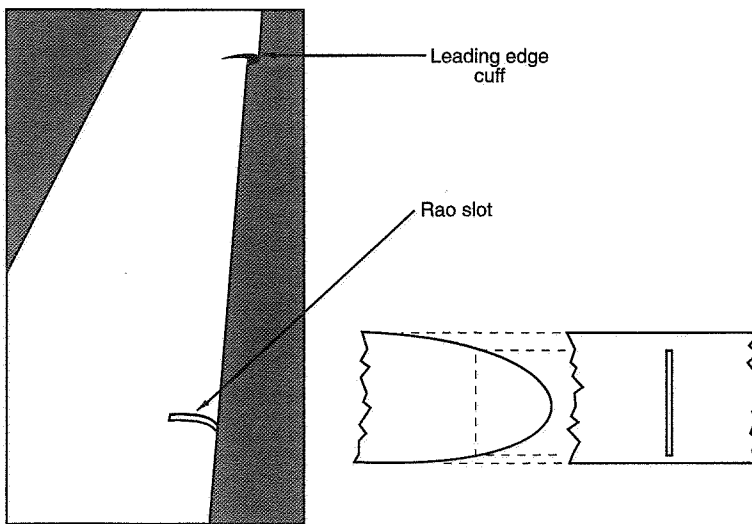


Figure 15.60 Rao slot and L.E. cuff (Ref. 39).

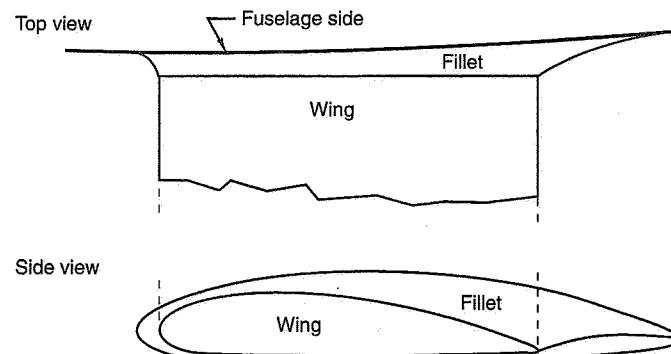


Figure 15.61 Fillet at wing/fuselage juncture.

Transition "strips" consist of attaching carborundum grit to the model surface to perform the same function. These are described in some detail in Ref. 119 (Chapter 7) by Pope and Harper. Trips are rarely used on full-scale race cars.

Active Flow Control Devices

Research indicates that blowing air into the boundary layer or boundary layer removal by suction can be extremely effective in eliminating separation, delaying stall, increasing circulation, and generally augmenting lift on airfoils. Remarkable performance gains have been achieved in the wind tunnel and on research aircraft. Large airflow volume may be required and the technology is more likely to become practical with jet rather than piston-engine aircraft. Ref. 83, edited by G. V. Lachmann, is an impressive summary of the state of the art. This type of control can be applied directly to the upper surface of the base airfoil or to L.E. or multiple T.E. slotted flaps.

A Renault F.1 car emitted engine exhaust tangential to a diffuser surface on the bottom of the car. March also attempted active flow control on their 1985-86 Indy car. Both were eventually outlawed.

Ref. 36 describes suction/blowing to create trapped vortices at locations where they may favorably influence the flow.

15.9 Internal Airflow

A number of internal systems in the race car require air, namely, engine "carburation," engine cooling (including oil cooling), brakes, transmission, general ventilation, etc. Air flowing along, through, or around surfaces and obstacles within the car creates drag just as it does on the external surfaces of the vehicle. It is important to meet the internal systems air requirements as efficiently as possible.

Ideally, the amount of air taken into the vehicle should be a minimum, just that required to meet the air requirements. Since the requirements are a function of the operating condition, an approach to the ideal requires adjustments to the air inlets and/or outlets or a controllable adjunct such as an electric fan. Aircraft use automatically controlled cowl flaps on radial engines and oil coolers. The conventional passenger car supplements the normal flow through the radiator with an electric fan for low speed, high temperatures. Such levels of sophistication are very seldom seen in race cars with a more restricted performance range, at least in a given race. Also, race regulations may prohibit adjustable aerodynamic devices. It is common to tape over the radiator air entrance if ambient air conditions so justify; in NASCAR, it is usual to tape over all cooling air entrances for qualifying—internal airflow produces a noticeable drag.

Other generalizations are that the air should be fully controlled, if possible, from its entry into the vehicle until it exits back into the airstream. The passage of the air should give maximum pressure recovery and avoid irreversible losses associated with separation.

There are three types of air entrances commonly used in racing. The first is the straight-through ram air entry as used with a nose radiator (for example) or the side ducted radia-

tors on open-wheel cars. A second means for getting air into the car is by scoops, for example, the high-mounted units for engine air. A scoop is used when it is necessary to turn the airflow (see Figure 15.53). A third type of entry is the flush duct or NACA submerged inlet.

An excellent practical treatment of these various types of air entrances, their use and design for racing, is given by Carroll Smith (Ref. 149). Ref. 63 contains both specific race car information and a comprehensive discussion of the design of engine cooling systems which covers more than just the aerodynamics. A very useful reference is Ref. 106 which presents a simple procedure for sizing radiator air entrance and exit ducts. Other significant references are 166 and 62, the latter having an entire chapter on the drag of internal systems. The present discussion is indebted to this last reference.

Ram Air Ducted Radiator

Consider an idealization of a ram air ducted radiator system (related to the side radiator ducted installation in current F.1 cars). Such an arrangement is shown in Figure 15.62. This illustrates a number of desirable features:

1. The entrance cone has well-rounded leading edges. This reduces the possibility of separation in the duct when it is at a modest yaw/pitch angle.
2. The long diffuser with a small diffuser angle (5°) theoretically enables the flow to slow down and build up pressure before the radiator without separation (i.e., in an efficient, reversible manner governed by Bernoulli's equation). The design could bring the velocity down to a level compatible with the radiator core heat transfer characteristics.
3. The radiator fits tightly in the duct. All of the incoming air must go through the radiator.
4. The contraction section aft of the radiator speeds up the air to near free-stream velocity, so it can be ejected with minimum loss. This process is assisted by the heat energy added to the air by the radiator—aircraft may actually generate a bit of thrust.

In actual practice, the ideal outlined above cannot be realized. In the first place, there is seldom, if ever, the space to package a long diffuser section. Further, long diffusers have boundary layer buildup that can lead to separation, except under the most ideal conditions. This decreases the size of the column of air as it approaches the radiator. Fortunately experience indicates that fairly short diffusers can be tolerated by appropriate shaping to avoid separation.

On the contractor or nozzle side, packaging can again be a limitation. About all that can be done in many instances is to avoid blocking the flow and provide as much contraction as possible in the air exit.

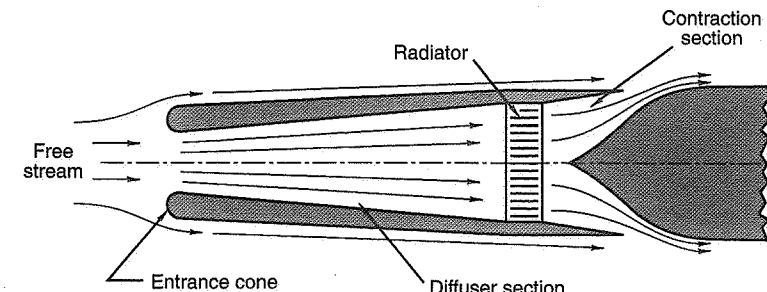


Figure 15.62 Ideal ram air ducted radiator.

The legislation against movable shutters and flaps severely limits the design. If the system is optimum for low speed, there may be excessive flow at high speed.

The rational design of an engine cooling system is a complex task and has been accomplished by the automotive industry only in recent years. Ref. 166 (1985) points out that historically front-end cooling openings were determined as "a certain percentage of the total radiator core area." Such a procedure is hardly adequate for modern cars where excessive aerodynamic drag is unacceptable.

In Ref. 106, a simple procedure is outlined for determining the inlet and outlet areas for a radiator duct for achieving appropriate cooling and low drag. Since this approach is instructive, a summary is given below:

Three parameters are defined which "closely relate" to the cooling performance of a radiator, namely,

1. Matrix (core) pressure drop coefficient,

$$K_P = \Delta P / (1/2)\rho V_F^2$$

where ΔP is the static pressure drop, front-to-rear (across) the radiator
 V_F is the velocity of air at the radiator face

Thus, $(1/2)\rho V_F^2$ is the dynamic pressure (kinetic energy) at the face.

2. Velocity ratio

$$R_V = V_F / V_0$$

where V_F is defined above
 V_0 is the free stream velocity

3. Drag coefficient of the radiator,

$$C_D = \text{Drag of radiator} / ((1/2)\rho V_0^2 A)$$

where A is the radiator face area.

In general, a large K_p (pressure drop across the radiator) and a large R_V (velocity ratio) produce the best cooling performance.

A simple cooling system model (of constant thickness perpendicular to the page) is next introduced as shown in Figure 15.63. In this model various inlet and outlet areas are created by rotating the duct elements around points (1) and (2). The size of the inlet (S_I) and outlet (S_O) ducts are given as fractions of the radiator height (S), or in tests by the areas in percent of the radiator size.

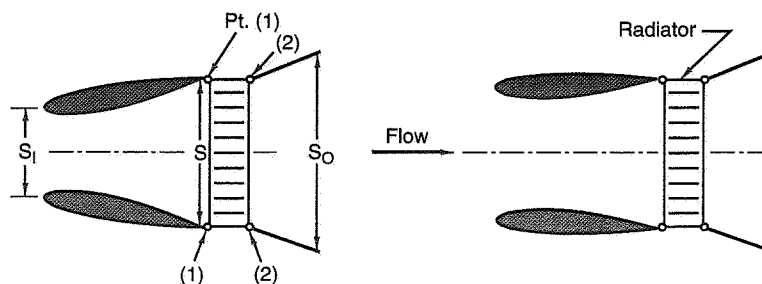


Figure 15.63 Simple cooling system model (Ref. 106).

A series of radiator cores with various numbers of tubes and fins (matrix) were tested. The denser the projected frontal area of these matrices, the higher the drag coefficient (as defined earlier) of the radiator—a result to be expected.

Another test showed an interesting relationship between the pressure drop across the radiator, K_p , the velocity ratio, R_V , and the size of the radiator. For a small pressure drop (low-density radiator, $K_p = 1.2$), inlet duct area larger than 80% of the radiator area produces no additional airflow. For high pressure drop ($K_p = 2.8$), the maximum airflow was obtained with an inlet duct area of 67% of the radiator area.

Care must be taken to avoid a duct configuration with a converging inlet; backflow and vortices can occur on the inside of the entrance duct and separation on the outside. Thus it is not true that increasing the size of the entrance duct face will increase the volume of air through the radiator.

As regards the outlet duct, an increase in size will increase the velocity ratio, R_V , up to a point, after which only an increase in drag will occur.

Based on the above investigations the following approach is suggested in a duct development for the greatest R_V (for cooling) and the least drag. To quote Muto, "start with an outlet area 1.2 times the radiator face area and gradually increase the intake size (while measuring R_V). Find the intake area where no further increase in R_V occurs. Using this area, measure R_V for different outlet areas until R_V is maximum." This development procedure requires only the measurement of two velocities by instrumentation techniques discussed in Chapter 3. It is likely that the optimum configuration will appear close to that of the left side of Figure 15.63.

Air Entrance Scoops

Figure 15.64, from Ref. 149, is a suggested design of a scoop/air box configuration for ram air to the engine. It has the following attributes:

1. The edges have adequate radii for minimizing separation even at substantial yaw angles.
2. The size of the entrance is designed to be sufficient for low-speed operation when ram is negligible.
3. It gradually expands in two dimensions to convert velocity to pressure. It is claimed that the shape shown does this while avoiding separation and producing uniform pressure at the various cylinder stacks.

For further details, see Ref. 149.

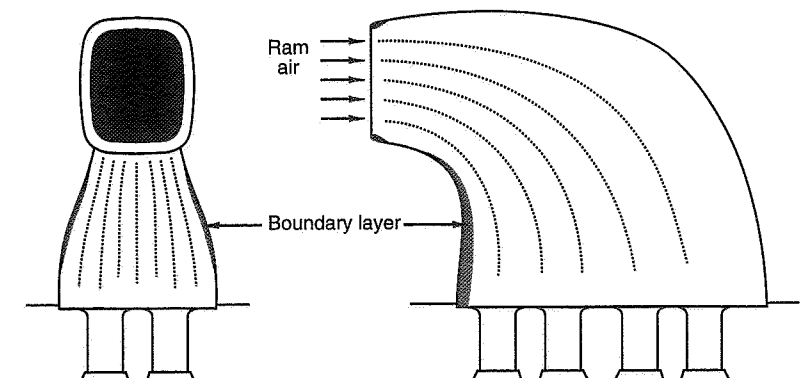


Figure 15.64 Efficient diffuser/plenum (Ref. 149).

NACA Submerged Inlet Duct

This type of inlet duct has seen extensive use on aircraft and race cars. It is described in some detail in Refs. 149 and 23. Figure 15.65 is from the latter. The upper part of the figure shows a typical installation and the lower part supplies the necessary dimensions. If the duct is made in accordance to the dimensions and ramp angle shown, it should work well, if, as Carroll Smith points out, it is “located in a shallow boundary layer and parallel to the local flow.” The best locations are usually ahead of the maximum cross section of the body, not in the pressure recovery area.

The simple theory of the NACA duct is that flow over the sharp edges on the two sides creates longitudinal vortices; these induce outside air to flow down into the ramp area. This suggests that the edges of the sides of the duct must be sharp and practice bears this out. The lip at the rear edge of the duct should be rounded. In general NACA ducts add little drag.

15.10 Flat Plate Aerodynamics

The use of flat plates to enhance lateral force and rolling moment in small oval / short track racing is common. Figure 15.66 illustrates the use of *sideboards*, in (a) as large end plates to a high-mounted wing and in (b) as a high-mounted large rectangular surface. This section presents some data on forces generated by flat surfaces.

Flat Plates Normal to Airstream

Consider first the case of a flat surface perpendicular to the flow (normal flow). Ref. 62 discusses this situation and points out that with sharp edges there is no way the flow can follow around the edge and produce a boundary layer in the rear. Thus the flow is stalled and completely turbulent. Figure 15.67 is a plot of the plate drag coefficient versus Reynolds Number based on length of one side for square plates and diameter for circular plates.

For most practical cases, the RN is in excess of 10^3 (1000) where the drag coefficient is constant at 1.17. For example, a 1-ft. square plate has a RN = $9230 \times 1 \times 100 = 923,000$ (or 9.23×10^5) at 100 mph. For years the aircraft industry used 1.28 as the drag coefficient of a large flat plate at high RN, so some variation in test results exists.

The aspect ratio of rectangular plates affects the normal drag coefficient. If h is the “height” of the plate and b its “width,” the aspect ratio can be defined as h/b . If the drag coefficient is 1.18 for a square plate ($h/b = 1$), it tends to increase as h/b decreases, as shown in Figure 15.68, from Ref. 62.

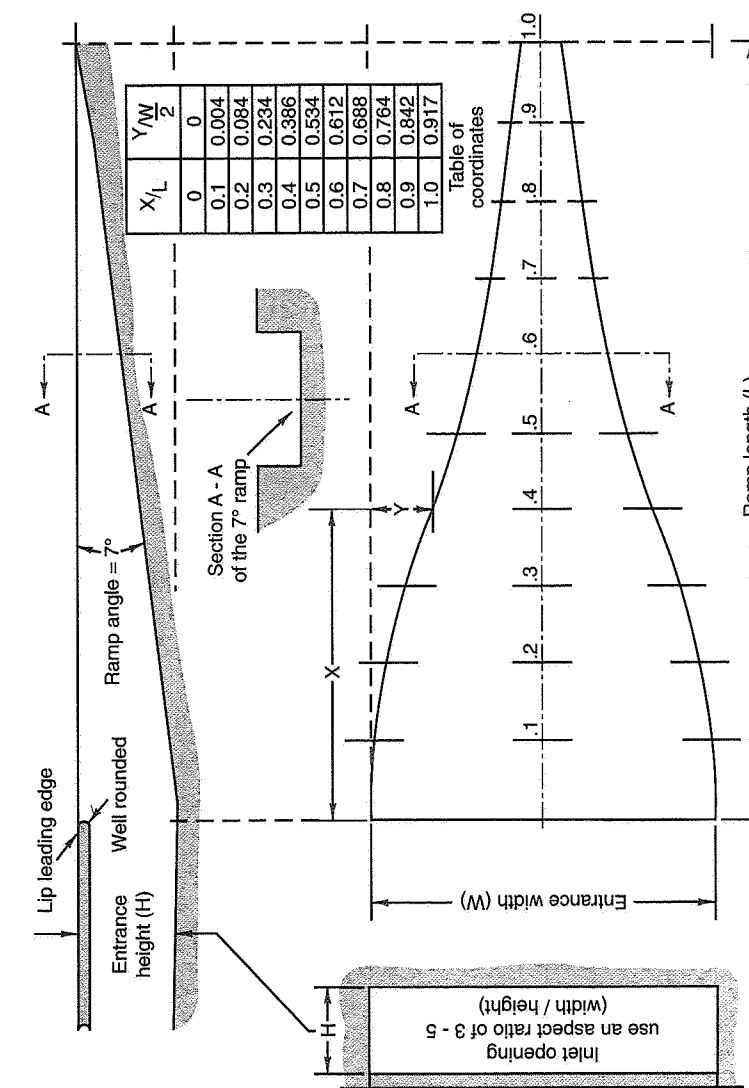


Figure 15.65 NACA inlet duct (Ref. 23).

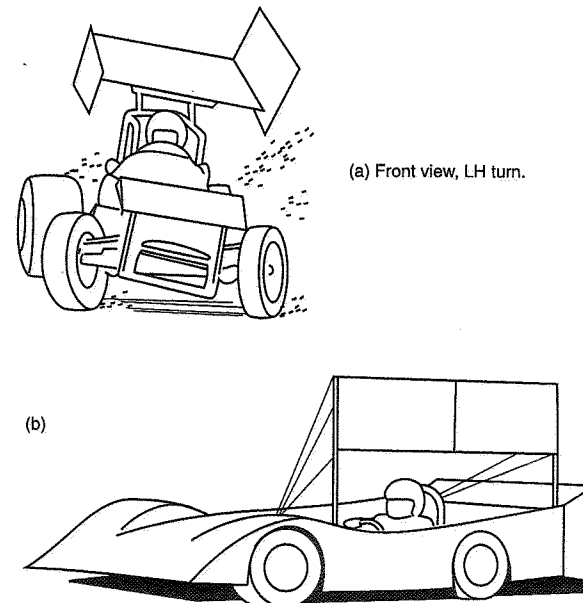


Figure 15.66 Large sideboards.

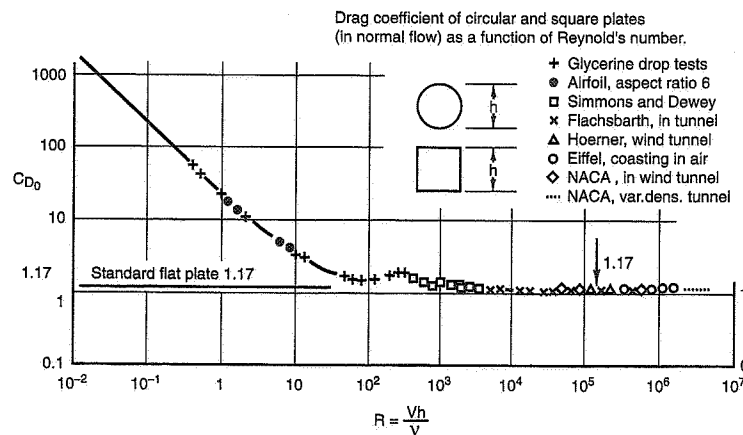


Figure 15.67 Flat plate drag (Ref. 62).

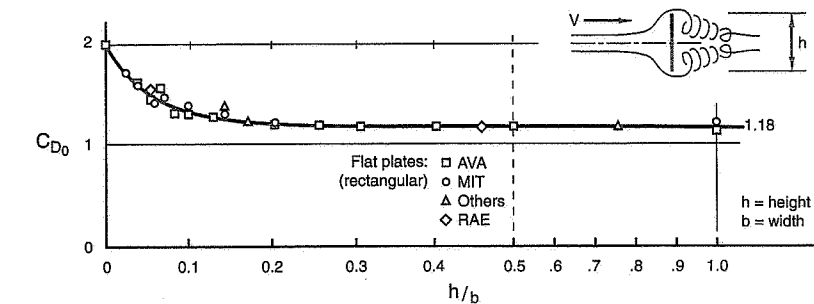


Figure 15.68 Drag coefficients of rectangular flat plate (Ref. 62).

Flat Plates at Angle to the Airstream

Figure 15.69 presents the lift and drag coefficients for a small rectangular flat plate as a function of angle of attack. The plate tested had an aspect ratio (length/width) of 6, with the longer side perpendicular to the wind direction (like a wing). The results are believed to apply closely to larger plates of the same proportions. This data came from Ref. 71.

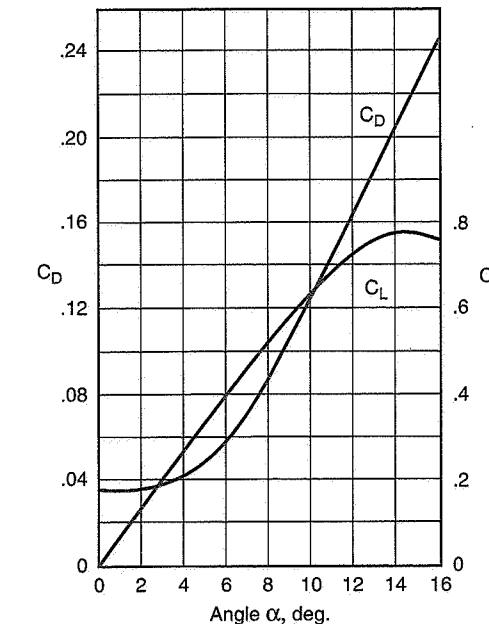
Figure 15.69 C_L and C_D for a flat plate, $AR = 6$ (Ref. 71).

Figure 15.70, from Ref. 62, presents normal force coefficient data for square and circular flat plates for angles of attack up to 90° . The square plate data is also valid for rectangular plates up to AR = 5. It is pointed out in the reference that above about $40^\circ \alpha$, the C_{normal} is constant which implies that the plate is completely stalled and turbulent on the downwind side. In this case, the lift and drag coefficients can be calculated from the normal (resultant force coefficient), as follows:

$$C_D = C_{\text{normal}} \times \sin \alpha$$

$$C_L = C_{\text{normal}} \times \cos \alpha$$

as sketched in Figure 15.71.

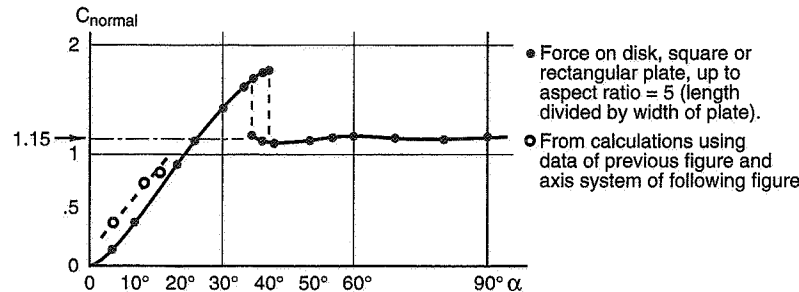


Figure 15.70 Normal force coefficient of square or circular plates (Ref. 62).

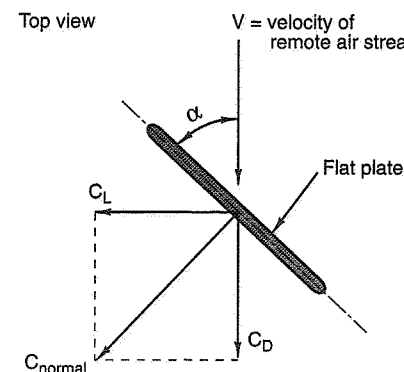


Figure 15.71 Flat plate axes.

It is of interest to check the data in Figures 15.69 and 15.70 against each other in the 0 - $16^\circ \alpha$ range. Make the check at 6° , 12° , and $16^\circ \alpha$, as done in Table 15.2.

Table 15.2 Flat Plate Drag By Two Different Methods

α°	From Figure 15.69		$\sqrt{C_L^2 + C_D^2}$		From Figure 15.70	
	C_L	C_D	C_L^2	C_D^2	$= C_{\text{normal}}$	C_{normal}
6°	0.380	0.058	0.144	0.003	0.383	0.19
12°	0.730	0.161	0.533	0.026	0.748	0.50
16°	0.765	0.247	0.585	0.061	0.804	0.70

The C_{normal} as calculated from data in Figure 15.69 is plotted in Figure 15.70 as "o". It appears to have the same slope but a small offset. This is difficult to account for without more detail on the models tested and procedures. Part of the difference in the peak values is due to different aspect ratio. For α 's less than 40° , it is suggested that C_L and C_D be obtained from Figure 15.69.

For α 's over 40° , C_L and C_D can be calculated from Figure 15.70 using the sine and cosine relationship given previously with $C_{\text{normal}} = 1.15$. The following example is presented:

A short track car with large end plates / sideboard is traveling at 100 mph. The sideboard is 5 ft. long by 3 ft. high (15 ft.² area) and the relative wind angle (angle of attack) is 42° .

$$C_D = 1.15 \sin \alpha = 1.15 \times 0.669 = 0.769$$

$$C_L = 1.15 \cos \alpha = 1.15 \times 0.743 = 0.854$$

$$D = C_D q A = 0.769 \times 25.6 \times 15 = 295 \text{ lb.}$$

$$L = C_L q A = 0.854 \times 25.6 \times 15 = 328 \text{ lb.}$$

The resultant normal force on the end plate is

$$N = 1.15 \times 25.6 \times 15 = 442 \text{ lb.}$$

or

$$= \sqrt{295^2 + 328^2} = 442 \text{ lb.}$$

15.11 Miscellaneous

Surface Roughness and Protuberances

In Ref. 78 the question of drag due to surface roughness is addressed. Figure 15.72 (from this reference) gives the "permissible roughness" in terms of the size of a small particle on the surface (grain size).

For example, at 200 mph the diameter of a surface particle can be 0.6 mils (0.00006 inch) without affecting the boundary layer enough to increase the surface friction drag. The curve in Figure 15.72 can be approximated by the following equation:

$$\text{Permissible grain diameter (inches)} = 0.126/\text{mph}$$

Using this equation several points (indicated by *) have been spotted in the figure.

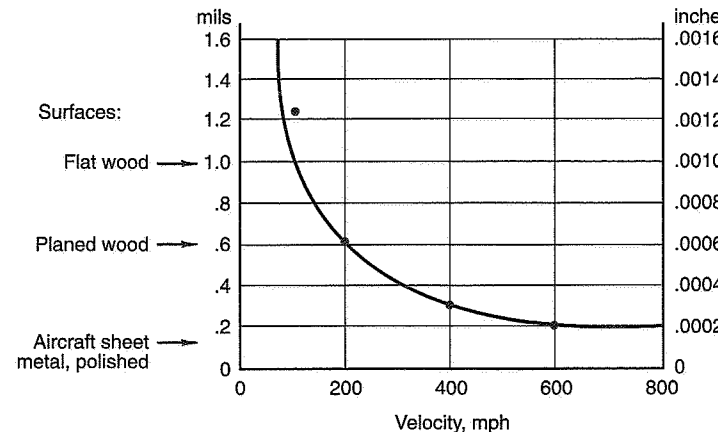


Figure 15.72 Permissible grain diameter to maintain min. surface drag (Ref. 78).

Ref. 78 notes that "show" paint on an automobile gives a surface smoothness on the order of 0.020 to 0.040 mils (0.00002 to 0.00004 inch). With this surface finish no amount of improvement will reduce the surface drag of automobiles operating at any speed. This is an exceptionally smooth surface obtained by sanding and polishing. Production paint has a grain size of 0.001 inch which is about at the limit line at 100 mph. Poorly applied paint at 0.008 inch and unpainted metal sheet at 0.002 inch can be improved upon.

Figure 15.73 (also from Ref. 78) gives some relative surface drag figures for (a) fasteners, (b) strips, and (c) surface gaps.

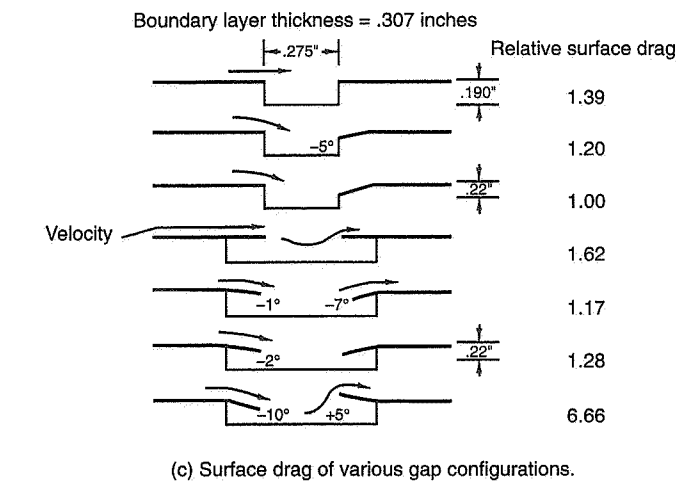
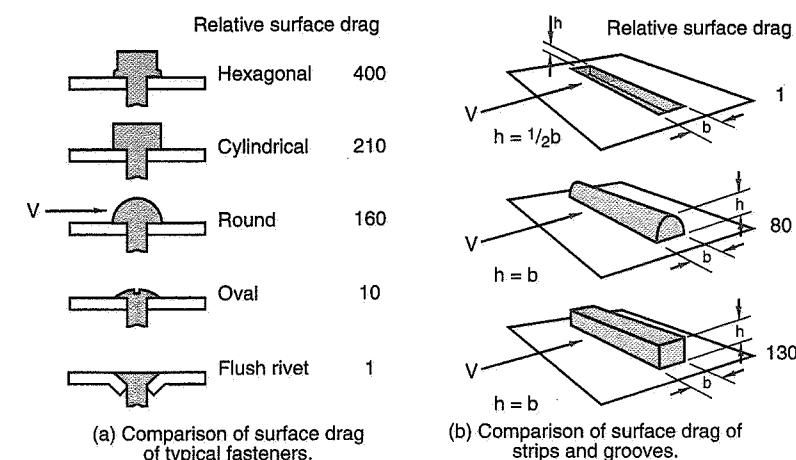


Figure 15.73 Relative drag of protuberances and gaps (Ref. 78).

Exposed Wheels

A number of investigators have studied flow conditions around exposed wheels (such as F.1 and Indy) and the associated pressures, velocities, and forces. Three significant references are those by Morelli (98, 1969), Fackrell and Harvey (44, 1973), and Cogotti (34, 1983).

Figure 15.74, from Ref. 34, illustrates (a) the wake pattern about a free stationary wheel, (b) a free rotating wheel, and finally, (c) a rotating wheel in the presence of the ground. The first two figures are supported by experimental observations, while the final figure is deduced from observations and vortex theory of lifting bodies.

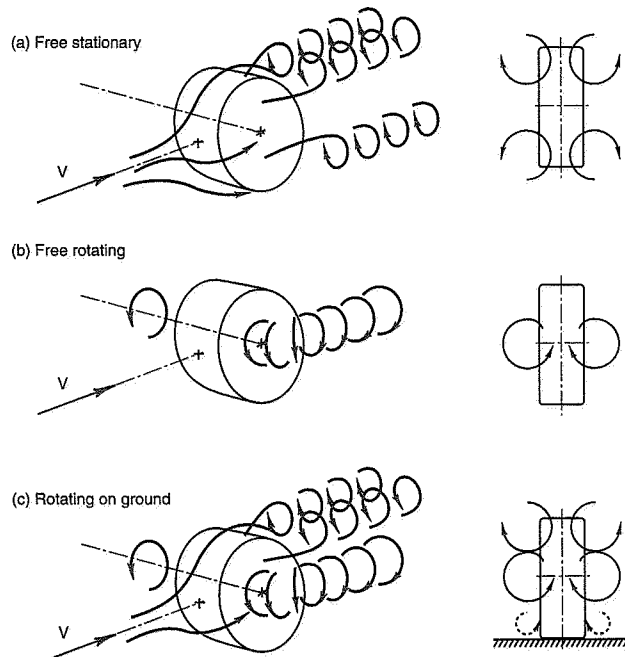


Figure 15.74 Wake patterns—isolated wheel (Ref. 34).

Figure 15.75 shows the pressure distribution (measured on the floor of the wind tunnel beneath the wheel) for different positions of the wheel relative to the ground. In Figure 15.75 the pressure coefficient, C_p , is

$$C_p = \frac{p - p_0}{q}$$

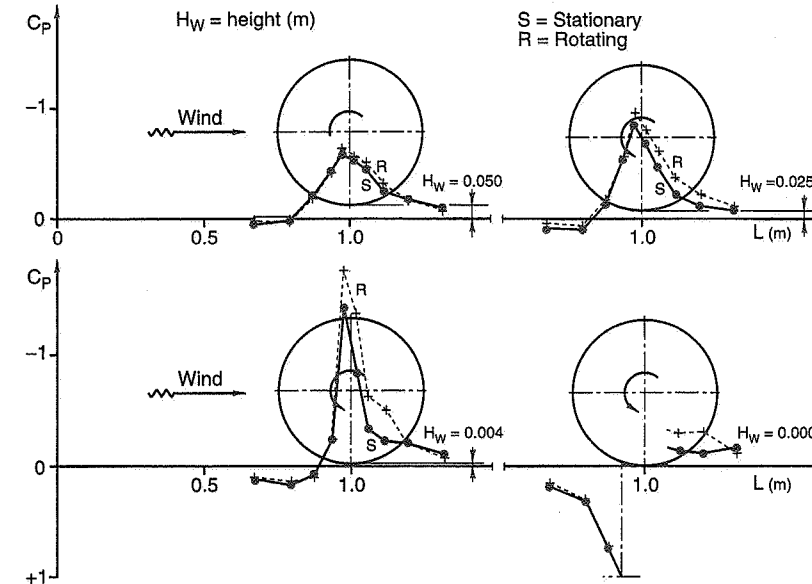


Figure 15.75 Pressure distributions beneath wheel (Ref. 34)

where p_0 is the pressure in the remote stream
 $q = (1/2)\rho V_0^2$, as usual

The interesting conclusion from these figures is that a negative pressure (below p_0) exists on the ground for all cases in which the wheel is not touching the ground. This negative pressure increases as the wheel approaches the ground (as Bernoulli's equation would predict). Once the wheel touches the ground and the gap is closed, a positive pressure and hence wheel lift occurs. The better the sealing the higher the lift.

It is known that the drag of circular cylinders, spheres, etc., is highly dependent on the Reynolds Number and this is also the case for an automobile wheel. The drag of any of these devices can change markedly in the transition range of 1×10^5 to 1×10^6 RN. The Cogotti paper suggests that for reliable drag measurements, wind tunnel tests should be performed at no smaller than 1×10^6 RN.

Tests (Ref. 34) on a full-sized 145SR-10 Cinturato Pirelli tire gave the results shown in Table 15.3 (in all cases the tire was on the ground, either stationary or rotating). These coefficients are based on wheel frontal area. They are higher than the coefficients for conventional passenger cars. The actual drags depend on the frontal areas, of course.

Table 15.3 Rotating Wheel Drag (Ref. 34)

Standard Rim		Rim Fairied on Both Sides, nearly flat caps	
Rotating	Stationary	Rotating	Stationary
C_{DW}	0.579	0.593	0.488
C_{LW}	0.180	0.272	0.178
			0.544
			0.296

Ref. 34 also gives drag, lift, lateral force, and the three moment coefficients as a function of yaw angle. These are summarized for 10° and 20° of yaw in Table 15.4.

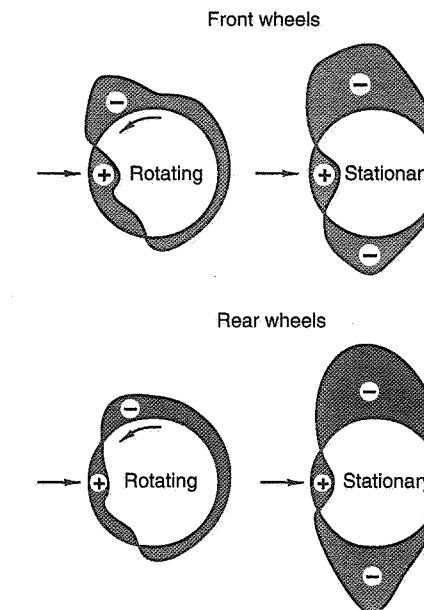
Table 15.4 Wheel Aero Forces and Moments (Ref. 34)

Yaw angle	10°	20°
<u>Coefficient</u>		
C_{DW}	+0.570	+0.545
C_{LW}	+0.425	+0.475
C_{YW}	+0.800	+1.490
C_{MW} (pitching)	-0.790	-0.730
$C_{\ell W}$ (rolling)	-0.720	-1.330
C_{NW} (yawing)	-0.630	-1.200

Wind tunnel testing of rotating wheels is more in the nature of research than routine measurement. As Metz points out in Ref. 90, an approximation to rotating wheels with zero ground clearance can be made with stationary (no rotation) wheels at small ground clearance. Small ground clearance is taken as less than 5% of the wheel diameter. Figure 15.76 shows pressure distributions for these two conditions (from Ref. 153), which exhibit a qualitative degree of similarity for the two conditions.

15.12 Aerodynamics and Balance

Aerodynamic downforce is used to increase the size of the "g-g" maneuvering diagram. The distribution of this downforce between the front and rear tracks affects the directional balance of the car in limit cornering and the fore and aft balance under acceleration and braking. In addition to the downforce from body and underbody shaping, most modern race cars have auxiliary aerodynamic devices front, rear, or both that can be used to



Negative and positive pressure regions are indicated by (−, +).

Figure 15.76 Pressure distributions around front and rear wheels (Ref. 153).

control the distribution and hence balance of the car. These devices, such as wings, spoilers, dams, etc., can be statically adjusted. In general, race regulations do not permit adjustment of these devices en route (although in the post-WWII period Mercedes used a movable air brake which also added down load to the rear wheels, at LeMans and elsewhere).

This final aerodynamic section addresses the use of these auxiliary devices for:

- Achieving balance
- Maximizing the total downforce under various operating conditions

The discussion generally assumes adjustable wings on the front and rear such as on Formula cars.

General Considerations

Balancing the car out to achieve the lowest lap times on a given circuit is a difficult task in the racing environment. Discussion with three engineers⁵⁷ whose experience covers Grand Prix, Cart/Indy, GT, Sports, and Grand National cars suggests some guidelines:

1. Do as much analysis as possible prior to track testing:

Hopefully some wind tunnel data are available on front and rear lift and drag or total lift, pitching moment, and drag. On low ground clearance formula cars the aerodynamics is a function of ride height and pitch attitude, particularly for front wings. Data at different wing/flap settings are necessary.

Full-scale tunnel data are generally best but useful data can be obtained on 3/8 scale models in a moving belt tunnel at the highest possible RN.

Calculate the "mechanical" balance of the car using available tire data and then add in different amounts of aero at several speeds to get a feel for balance changes.

2. At the track obtain driver comments from low- and high-speed corners to separate out "mechanical" and aero effects.

To balance the car, build up the aero downforce on the limiting end. For example, if the car is "plowing/pushing" at high speed use more front wing.

3. Work the "mechanical" and "aero" adjustments together to achieve low- and high-speed balance; avoid combinations in which mechanical and aero are bucking each other (creating drag on high-speed circuits).
4. It may not be possible to achieve optimal balance for all corners and operating conditions around a circuit. Seek best circuit performance at the expense of lowered performance on one or more corners.

Approach

The state of the art of race car analysis is such that given sufficient car, tire (including load sensitivity), and aero data, and a detailed layout of the circuit, a reasonable estimate of front/rear wing angles for good circuit performance can be made. This requires utilization of the better circuit models and MRA Moment Method or some other analytical tools. The real problem is one of acquiring the data and the time involved in establishing data sets for the different operating conditions. Thus, as suggested above, the successful teams use a combination of analysis, track testing, and experience. Teams differ considerably in their detailed approach.

⁵⁷ Charles Matthews, Terry Satchell, and Peter Wright. We have already covered Chaparral experience in this chapter and under Frank Winchell's section in Chapter 13 (Historical).

One approach is as follows:

- Make a best estimate of the (largest) rear wing setting possible, from previous analysis or experience.
- Use track tests and driver comments to achieve an initial circuit balance by front wing adjustment.
- Check lap times and maximum speed.
- Repeat with different rear wing setting(s).

The settings for minimum lap time and max speed may be different. Once a first-order approximation to desirable settings has been achieved, proceed to improve performance on different parts of the circuit. Some questions for the driver include:

- Is the control response of the car acceptable around the whole circuit?
- Is there a good compromise between mechanical oversteer/neutral behavior on slow corners and aero understeer on fast corners? It may be practical to use rear bias braking to improve turn-in on slow corners and compensate with aero for high-speed corners.

Front wing effectiveness is sensitive to front ride height and attitude; changes in front static ride height and bump stops may be used to control turn-in. Ride height changes of as small as 1 mm are reported as significant on F.1. The number of adjustments and combinations available for fine tuning the balance are only limited by the imagination.

Simplified Analysis of Cornering with Aero Downforce

When very high aero downforce was obtained with skirted large underbottom cars, it was reported⁵⁸ that on high-speed bends the lateral tire cornering forces (due to aerodynamic down load) increased faster with speed than the centripetal force. This implied that the speed on the bend was limited only by drag/power, the driver's ability to withstand the lateral acceleration, or the capability of the tires to function effectively under such high downforces. The present section examines this possibility in the context of a simple car in steady-state cornering on different radii at various road-load speeds.

The car can be thought of as a nonpitching, nonrolling vehicle with constant ride height (on the bump stops) and neutral steer with equal distribution of static load and aerodynamic downforce front and rear. In effect, it is a "point mass" subjected to centrifugal force, tire lateral forces, and aerodynamic downforces. Since ride height and pitch attitude are fixed, the effective angle of attack and lift coefficient are constant throughout

⁵⁸ During the early 1980s very large negative lift was achieved on F.1 cars (see Ref. 168 for data on these cars).

the analysis. The resultant aerodynamic downforce is from front and rear wings and bottom, but is centered at the mass center (CG). The assumption is made that the vehicle speed is not limited by power or traction.

The following car characteristics are assumed:

$$W = 1500 \text{ lb., all up weight}$$

$$C_L = -0.75, \text{ overall aero downforce coefficient based on a plan area, } A, \text{ of } 70 \text{ ft.}^2$$

This C_L represents a maximum value obtained on F.1 cars in the 1981 period (see Figure 9 of Ref. 168). The plan area is typical of F.1 cars of that time.

The maximum lateral force from the tires is the lateral friction coefficient times the total of the static load and aerodynamic downforce. The tires are "load sensitive" and the lateral friction coefficient varies with total load on the tires. Figure 15.77 is a plot of the lateral friction coefficient, μ_{lat} , against load for the Goodyear F.1 front tire ($25.0 \times 9.0 - 13$) and the Indy Car rear tire ($27.0 \times 14.5 - 15$) as given in Chapter 2, Figures 2.46 and 2.45, respectively. The slopes of these curves show the fall-off (or "roll-off") of the coefficients with load, the *load sensitivity* in $\mu/\text{lb.}$ of load. For our calculation assume the solid curve (lying between the F.1 and Indy data) with a slope of $0.00064 \mu/\text{lb.}$ load sensitivity. This line extended to zero load gives a $\mu_0 = 2.25$. It is also assumed that at some high load the load sensitivity ceases and the tire produces a sensibly constant coefficient regardless of load. This has arbitrarily been chosen as a coefficient of 1.1 at 1800 lb. load (see solid curve). In real tires the transition would take place more gradually. Unfortunately, little data is available on load sensitivity at high loads.

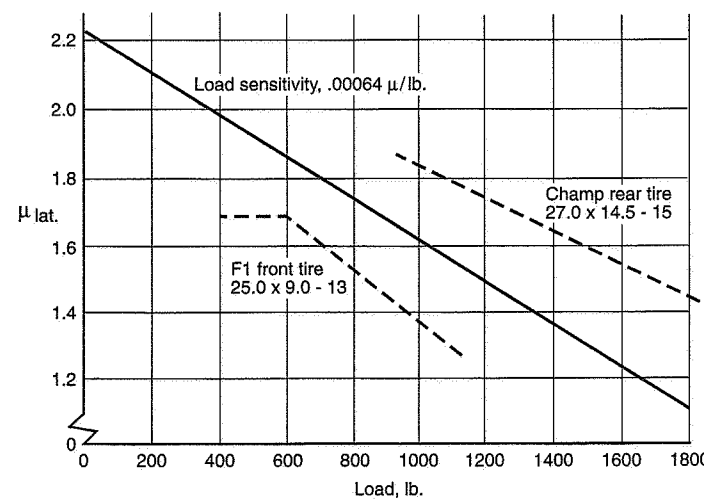


Figure 15.77 Tire load sensitivity.

It is now possible to plot curves of centrifugal force for various radii and speeds, and also car lateral tire force, F_Y , for the various speeds. The lateral tire force is independent of path radius:

$$CF = \left(\frac{W}{g} \right) \left(\frac{V^2}{R} \right) = \left(\frac{1500}{32.2} \right) \left(\frac{2.15 V_{\text{mph}}^2}{R} \right) = 100.15 \left(\frac{V_{\text{mph}}^2}{R} \right)$$

where R = path radius, ft.

The total tire lateral force is

$$F_Y = [\mu_0 - (\text{Load Sen.})(L/4)] L$$

where $L = W + \text{aero downforce}$

$$\text{Aero downforce} = C_L A q = (-0.75)(70) \left(\frac{V_{\text{mph}}^2}{391} \right) = -0.134 V_{\text{mph}}^2$$

Figure 15.78 is a plot of CF and F_Y . The centrifugal forces (CF) are the solid curves for various path radii from 250 ft. to 2500 ft. The tire F_Y (dashed curves) is plotted for three cases:

1. In the first case the load sensitivity of $0.00064 \mu/\text{lb.}$ applies at all speeds. At about 275 mph the aero downforce is some 10,134 lb. (2909 lb. total load/tire).
2. For the second case, the load sensitivity of $0.00064 \mu/\text{lb.}$ applies up to a speed of about 205 mph, an aero downforce of some 5631 lb. (1783 lb. total load/tire). Above 205 mph a constant coefficient, $\mu_{LAT} = 1.1$, is used.
3. There is no tire load sensitivity effect due to aero downforce in the third case, $\mu_{LAT} = 2.01$ (constant). The coefficient is reduced from 2.25 (at zero tire load) by the static load effect only.

An examination of Figure 15.78 will indicate that at any intersection of a tire lateral force curve with a centrifugal force curve ($F_Y = CF$, the condition for a steady turn), the slope of the CF vs. V curve is steeper than that of the F_Y vs. V curve. Thus, based on the assumptions of this analysis, it is not possible to take the particular radius at a still higher speed. If the tire load sensitivity is curtailed (Case 2) or removed (Case 3), one can more closely approach the unlimited speed condition on a given radius (assuming no power limitation). A scale of cornering acceleration in "g's" is given beside the force scale, indicating the high levels to which the driver is exposed. For example, on a 500-ft. radius at 200 mph (the peak for Case 1), some 5.2g is possible.

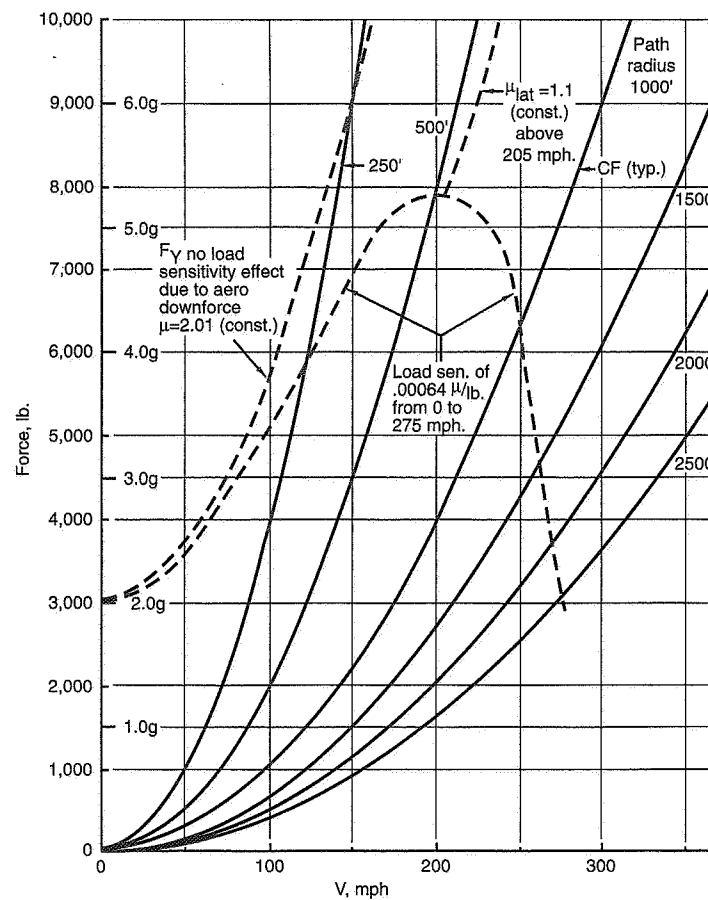
Figure 15.78 F_Y and CF vs. V .

Figure 15.79 presents the equilibrium conditions of 15.78, i.e., a plot of the intersection points of F_Y and CF for the three cases considered. If any of these cases resulted in a vertical curve at a particular radius, it would imply that this radius could be taken at any speed.

The general conclusion from this brief analysis for a simplified car is that the **tire load sensitivity** is an extremely important determinant of race car cornering performance—particularly with high aerodynamic downforce. Reduction in the load sensitivity via tire design is highly desirable.

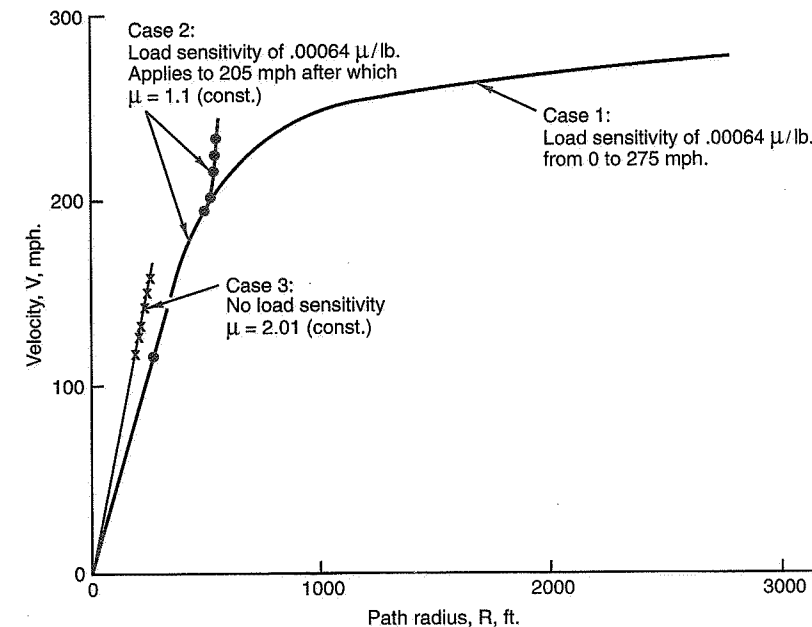


Figure 15.79 Velocity vs. path radius.

Ride and Roll Rates

"Figuring the suspension of a car is almost entirely a matter of making useful approximations. It is not an exact science. But neither is it a blind application of rule-of-thumb principles."

Maurice Olley
Notes on Suspension, 1961



Introduction

Calculating ride and roll rates from measured suspension properties is the subject of this chapter. First some definitions are made. A fairly complete example is worked with only a few assumptions—this might be used for a new car or track. A simplified example which uses more assumptions is also worked. This may be the most practical to use once there is some experience with a particular car. Regardless of what technique is used, calculation of ride and roll rates is an essential part of understanding race car set-up.

The ride and roll rates for a car (or for an end of a car) directly relate a change in wheel loading to a change in body position. A ride rate relates a change in the tire normal force at the ground for an individual corner of a car to a pure vertical change in body position. A roll rate refers to the moment produced by a differential change in tire normal force (side-to-side) as the body is rolled about its roll axis. Ride rate for a wheel at an indi-

Dave Segal, MRA, wrote this chapter except for the second example at the end, which was contributed by Terry Satchell.

vidual corner of a car is given in terms of pounds of tire normal force (or wheel load) at the ground per inch of vertical body motion or ride travel. Roll rate for a pair of wheels at one end of the car is given in terms of pound-feet of roll torque per degree of body roll angle or axle rotation relative to the body; the roll rate of the whole vehicle can also be expressed in these terms, pounds-feet per degree.

Ride and roll rates have a significant effect on cornering performance because they directly affect the distribution of tire normal forces and consequently tire lateral forces available at each corner. Unfortunately, the car designer or chassis tuner does not have direct control over the ride and roll rates of a car but only individual suspension elements—linkages, springs, and anti-roll bars. This chapter addresses the problem of relating the individual suspension components to the ride and roll rates for the car—more specifically to determine ride spring rates and anti-roll bar (or z-bar) rates at the springs that give satisfactory ride and roll rates. After the spring rates are specified, the springs can be designed (within the limitations of various spring design formulas) using Chapter 21.

Chapter 18 describes calculations that can be used to determine wheel loads for the full range of operating conditions. These wheel loads include the effects of fuel burn-off, aerodynamic download, banked turns, etc., and depend on the ride and roll rates. Unfortunately, the choice of ride and roll rates depends on the wheel loads—a typical design problem. It is necessary to start somewhere and then continue to iterate until a reasonable solution is found. By making some assumptions we can start the process of choosing suspension springs.

This chapter has little to say about ride (comfort) in the passenger car sense. Soft ride is generally incompatible with the stiff springs that are required to control body motion in roll and pitch under the high lateral and longitudinal accelerations found in race cars. For those cars that operate on bankings (or with high aero download) the problem extends to heave (pure vertical motion of the body) as well. Good ride in the passenger car sense also dictates the relationship between front and rear natural frequency which is usually incompatible with roll stiffness requirements.

16.1 Definitions

Rates

Before proceeding further it is helpful to define the various suspension rates that are commonly referred to.

1. **Spring Rate**—force per unit displacement for a suspension spring alone. For coil springs this is measured axially along the centerline. For torsion bar springs it is measured at the attachment arm. For leaf springs, measured at the axle seat. The

spring rate may be linear (force increases proportionally with displacement) or nonlinear (increasing or decreasing rate with increasing displacement). Units are typically pounds/inch, as described in Chapter 21.

2. **Wheel Center Rate**—vertical force per unit vertical displacement at the location along the spindle corresponding to the wheel centerline, measured relative to the chassis. This rate is generally lower than the corresponding spring rate due to the *installation ratio*. In other words, the wheel spindle vertical travel is usually larger than the corresponding displacement of the spring.

Wheel center rate is equivalent to the axle vertical rate for (left-right symmetric) solid axle suspensions. For leaf spring axles the wheel center rate may be nearly equal to the spring rate. For trailing arm installations where the spring is located further from the pivot than the tire center the wheel center rate will be higher than the spring rate.

3. **Tire Rate**—vertical force per unit vertical displacement of the tire at its operating load. This can be a large part of the total suspension spring on cars with stiff springing, designed for banked tracks or high aero downforce.
4. **Ride Rate**—vertical force per unit vertical displacement of the tire ground contact reference point relative to the chassis. This is equal to the wheel center rate modified by the tire vertical rate. For an infinitely stiff tire, the ride rate and wheel center rates would be equal. For a real tire (with finite vertical stiffness) the ride rate is always less than the wheel center rate.
5. **Roll Rate**—moment (torque) resisting body roll per degree of body roll. The term can be applied to either an individual axle or to a complete car. This resistance to body roll is provided by the ride rates, axle track width, and anti-roll bar (or z-bar).

6. Assumptions in the above definitions include:

- 0° camber and no camber change with ride
- No tire lateral distortion

Both of these can modify the actual ride and roll rates but are too complex to be treated here.

Expressing Ride and Roll Rates

The suspension spring rates can be described in several ways:

- Undamped natural frequency of the body in ride.
- Static wheel deflection in inches (one g vertical) for ride and in degrees per g (one g lateral) for roll. These can be thought of as in./g and deg./g.
- Wheel spring rate/load (in lb./in. or lb.-ft./deg.).

The first two are directly related by the chart in Figure 16.1 through the equation given in the chart.

More common descriptions of ride and roll rates used by race teams include:

- Wheel center rates
- Suspension spring rates
- Physical dimensions of the actual springs and anti-roll bars

These methods work as long as other factors remain constant. As soon as the load, installation ratio, aerodynamic characteristics, etc., change from one vehicle (or configuration) to another, wheel spring rate information alone will not suffice to choose springs for the new configuration.

16.2 First Example with More Complete Calculations

Approach

Ride—One can start with a desired frequency or with a maximum wheel travel / maximum load. Either one determines how hard/soft the ride/handling will be. Generally it is desirable to have the suspension as soft as practical in light of packaging, aerodynamic down load, banked turn loads, roll stiffness (and roll stiffness distribution). The undamped ride frequency for a given configuration (the frequency of the body moving up and down on the springs) can be determined from Figure 16.1, once the static deflection has been estimated. Ride frequencies for sports cars typically run from 70-90 cycles per minute. Older Indy type cars without ground effects run 95-120 cpm. With ground effects the frequencies can become very high—several hundred cpm. Passenger cars, by comparison, can be very low—30-50 cpm.

Wheel travels for several classes of vehicles are typically:

Off-road trucks ± 12 in.

Passenger cars ± 4 in.

Sports cars and small formula cars ± 2 to ± 4 in.

Indy type cars (ground effects) ± 0.5 in. (or less)

Roll—The stiffness in roll is conveniently expressed in normalized form as degrees of roll per unit lateral acceleration (deg./g). This is called the *roll gradient*. Table 16.1, prepared for the g*Analyst® “Operating Instructions” (Ref. 91) gives some typical values.

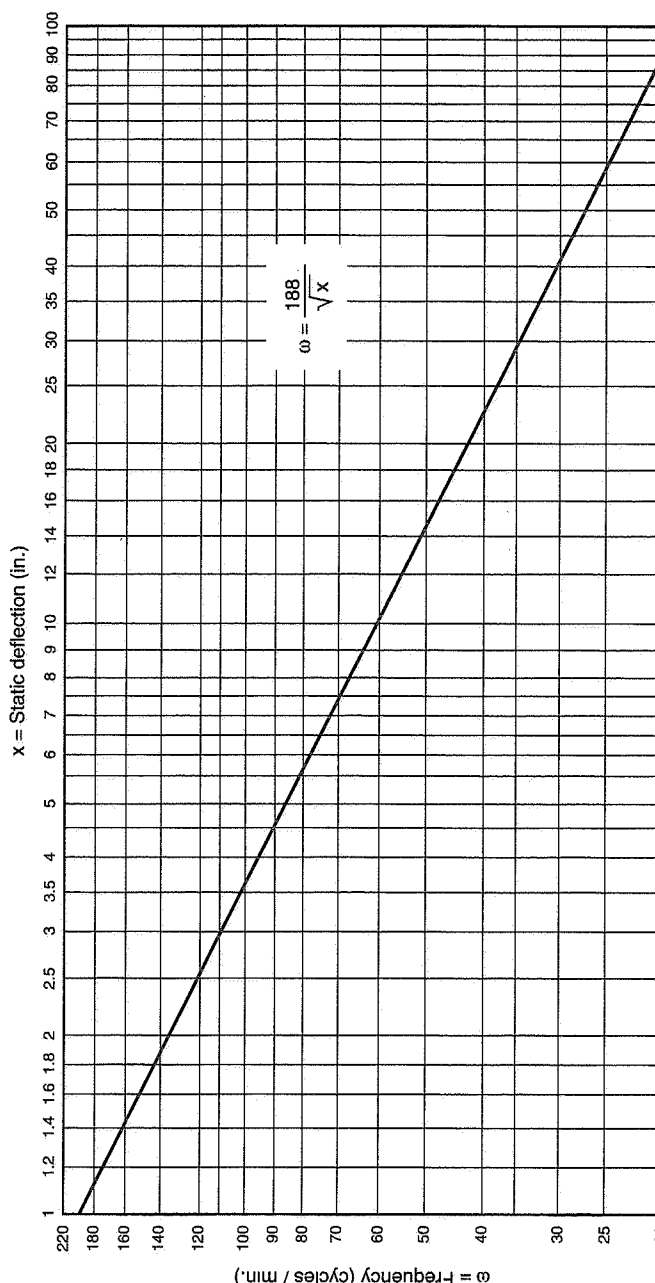


Figure 16.1 Ride natural frequency vs. static wheel deflection.

Table 16.1 Typical Roll Gradients, Based on Ref. 91

Very Soft—Economy and basic family transportation, both domestic and import, pre-1975.	8.5 deg./g
Soft—Basic family transportation, domestic and import, after 1975.	7.5
Semi-Soft—Contemporary middle-market sedans, domestic and import.	7.0
Semi-Firm—Imported sport sedans.	6.0
Firm—Domestic sport sedans.	5.0
Very Firm—High-performance domestic, such as Camaro Z-28 and Firebird Trans Am.	4.2
Extremely Firm—Contemporary very-high-performance sports, such as Corvette, and street cars extensively modified to increase roll stiffness.	3.0
Hard—Racing cars only.	1.5
Active Suspension—Servo-controlled roll stiffness. Roll-in, zero-roll, and roll-out all possible.	—

Ride Rate Specification / Independent Suspension

The problem the designer faces is to establish ride rate requirements for the particular car in question. Ultimately ride rate requirements are based on the wheel loading experienced by the car and the wheel travel allowed in a particular racing situation. Chapter 18 describes calculations that can be made to determine wheel loadings for a full range of operational conditions. These wheel loads include the effects of aerodynamic down-force, banked turns, grade, etc. Unfortunately, the wheel loadings themselves depend on the distribution of ride and roll rates, resulting in a typical design problem. It becomes necessary to make an initial estimate and continue to iterate until a reasonable solution to the problem is found.

To describe this design procedure, the following example is worked. First, some data is assumed for the vehicle. This set of assumptions is used to calculate wheel loads and the result is used to calculate new ride rates and roll rates. This data is compared with the desired combination and found (not surprisingly) to be off by a bit. Changes are made in the assumptions and the process is repeated until the desired result is achieved. This may

sound tedious and it is! Unfortunately, this problem does not have a “closed form” solution so an iterative process is the only reasonable way to narrow in on a solution.

In the following example we establish ride rates for a car that is traveling at 100 mph on a 600-ft. radius turn that is banked at 10°. Further we assume that the car is left-right symmetric and independently suspended. For simplicity, assume that the aerodynamic lift and rolling moment coefficients are zero and that driving torque and longitudinal acceleration are also zero. We will also use the simplified load calculation equations from Chapter 18.

The basic car is described by the following information:

Weights:

$$W_1 = 1020 \text{ lb.}$$

$$W_3 = 680 \text{ lb.}$$

$$W_2 = 1020 \text{ lb.}$$

$$W_4 = 680 \text{ lb.}$$

$$W_F = 2040 \text{ lb.}$$

$$W_R = 1360 \text{ lb.}$$

$$W_T = 3400 \text{ lb.}$$

Dimensions:

$$t_F = 5 \text{ ft.}$$

$$h = 1.5 \text{ ft. (CG height)}$$

$$t_R = 5 \text{ ft.}$$

$$H = 1.1 \text{ ft. (CG to Roll Axis)}$$

$$\ell = 9.5 \text{ ft.}$$

The cornering condition is a left-hand turn where:

$$\alpha = -10 \text{ deg. (roadway bank angle)}$$

$$R = -600 \text{ ft. (radius of the vehicle path, measured horizontally)}$$

$$V = 100 \text{ mph} = 146.7 \text{ ft./sec.}$$

We assume the following information:

Roll axis heights above ground:

$$z_{RF} = 0.25 \text{ ft.}$$

$$z_{RR} = 0.625 \text{ ft.}$$

Zero drive torque and longitudinal acceleration:

$$T_D = 0.0$$

$$A_X = 0.0$$

Finally, we assume the following roll rates:

$$K_{\phi F} = 70,000 \text{ lb.-ft./rad.} = 1222 \text{ lb.-ft./deg.}$$

$$K_{\phi R} = 50,000 \text{ lb.-ft./rad.} = 873 \text{ lb.-ft./deg.}$$

Note that because we don't yet know what the ride rates are, we also don't know the roll rates (as they are dependent on one another). We therefore have to assume roll rate values to start with. Also, because roll center locations can change with ride height and roll angle, we start with values at the static design positions.

First calculate the CG position. See Chapter 18 for a more complete treatment.

$$b = \frac{W_F \ell}{W_T} = \frac{2040 \times 9.5}{3400} = 5.7 \text{ ft.}$$

$$a = \ell - b = 9.5 - 5.7 = 3.8 \text{ ft.}$$

Since we have a symmetric car, y'' is zero.

Next, the lateral acceleration values relative to the earth and the banked turn are calculated. Again see Chapter 18 for a complete treatment.

$$A_\alpha = \frac{V^2}{Rg} = \frac{146.7^2}{-600 \times 32.2} = -1.11 \text{ g's}$$

$$A_Y = A_\alpha \cos \alpha - \sin \alpha = (-1.11 \times \cos(-10)) - \sin(-10) \\ = -1.09 + 0.17 = -0.92 \text{ g's}$$

where A_α = Horizontal lateral acceleration

A_Y = Lateral acceleration in car axis system

The effective weight of the car due to the banking is

$$W' = W (A_\alpha \sin \alpha + \cos \alpha) = 3400 (-1.11 \sin(-10) + \cos(-10)) \\ = 3400 \times 1.1776 = 4004 \text{ lb.}$$

And the effective front and rear axle weights are

$$W'_F = \frac{W'b}{\ell} = 4004 \left(\frac{5.7}{9.5} \right) = 2402 \text{ lb.}$$

$$W'_R = \frac{W'a}{\ell} = 4004 \left(\frac{3.8}{9.5} \right) = 1602 \text{ lb.}$$

The roll gradient is

$$\frac{\phi}{A_Y} = \frac{-W \times H}{K_{\phi F} + K_{\phi R}} = \frac{-3400 \times 1.1}{70,000 + 50,000} \\ = -0.03117 \text{ rad./g or } -1.786 \text{ deg./g}$$

where ϕ = body roll angle.

Then the front and rear lateral load (weight) transfers due to the lateral acceleration are

$$W_F = A_Y \times \frac{W}{t_F} \times \left(\frac{H \times K_{\phi F}}{K_{\phi F} + K_{\phi R}} + \frac{b}{\ell} \times Z_{RF} \right)$$

$$W_F = -0.92 \times \frac{3400}{5} \times \left(\frac{1.1 \times 70,000}{120,000} + \frac{5.7}{9.5} \times 0.25 \right)$$

$$W_F = -0.92 \times 680 \times (0.642 + 0.15) = -495 \text{ lb.}$$

$$W_R = A_Y \times \frac{W}{t_R} \times \left(\frac{H \times K_{\phi R}}{K_{\phi F} + K_{\phi R}} + \frac{a}{\ell} \times Z_{RR} \right)$$

$$W_R = -0.92 \times \frac{3400}{5} \times \left(\frac{1.1 \times 50,000}{120,000} + \frac{3.8}{9.5} \times 0.625 \right)$$

$$W_R = -0.92 \times 680 \times (0.458 + 0.25) = -443 \text{ lb.}$$

The magnitude of $A_\alpha \cos \alpha$ is greater than the magnitude of $\sin \alpha$ so the outside wheel load increases (the vehicle is above the "neutral speed" for this turn). Therefore the individual wheel (tire) loads are:

Front outside: $W_{FO} = 2402/2 + 495 = 1696 \text{ lb.}$

Front inside: $W_{FI} = 2402/2 - 495 = 706 \text{ lb.}$

Rear outside: $W_{RO} = 1602/2 + 443 = 1244 \text{ lb.}$

Rear inside: $W_{RI} = 1602/2 - 443 = 358 \text{ lb.}$

And the change from the static loads measured on level ground are:

Front outside: $W_{FO} = 1696 - 1020 = +678 \text{ lb.}$

Front inside: $W_{FI} = 706 - 1020 = -314 \text{ lb.}$

Rear outside: $W_{RO} = 1244 - 680 = +564 \text{ lb.}$

Rear inside: $W_{RI} = 358 - 680 = -322 \text{ lb.}$

The next step is to choose ride rates that are compatible with these wheel loads, that is, rates stiff enough so that the outside suspensions do not bottom or contact the bump stops. If, for example, you have 3.5 in. of jounce travel available, then you might wish to use 2.5 in. to accommodate the weight increase allowing 1 in. for additional travel due to acceleration, braking, and localized bumps on the track. The important point is to avoid

bottoming the suspensions as this will cause a sudden change in wheel loading and upset the balance of the car. Depending on the type of car and circuit, bump rubbers or nonlinear rising rate springing also may be used. Here we present the simple case of linear springs with no bump stop contact.

The allowed jounce travel that we are dealing with at this point could be one of two choices:

- The effective chassis to ground travel (total ride travel).
- The allowed travel before contacting the bump stops (the travel between the chassis and wheel center).

If the tire spring is infinitely stiff the calculations reflect both—the bump stop travel and chassis to ground travel are the same. If, for example, the wheel center rate and tire rate are the same then the bump stop travel is 1/2 the ride travel. If one has a vehicle with adequate ground clearance then concern is with striking the bump stop (destabilizing). If ground clearance is small, concern may be with bottoming out the car; this situation most commonly occurs with aerodynamic ground effects and on bankings.

Using the first case above (total ride travel) we continue with the example. The front and rear suspension ride rates required are the load changes divided by the allowed ride travel (2.5 in.).

$$K_{RF} = 678/2.5 = 271.2 \text{ lb./in.}$$

$$K_{RR} = 564/2.5 = 225.6 \text{ lb./in.}$$

Assuming side-to-side symmetry, ride frequencies can be calculated:

$$\omega_F = \frac{1}{2\pi} \sqrt{\frac{K_{RF} \times 12 \times 32.2}{W_2}} = \frac{1}{2\pi} \sqrt{\frac{271.2 \times 12 \times 32.2}{1020}} = 1.61 \text{ Hz}$$

or

$$\omega_F = 1.61 \text{ Hz} \times 60 = 96.6 \text{ cpm}$$

$$\omega_R = \frac{1}{2\pi} \sqrt{\frac{K_{RR} \times 12 \times 32.2}{W_4}} = \frac{1}{2\pi} \sqrt{\frac{225.6 \times 12 \times 32.2}{680}} = 1.80 \text{ Hz}$$

or

$$\omega_R = 1.80 \text{ Hz} \times 60 = 108.1 \text{ cpm}$$

Note that the "12" in the above formulas converts ride rate values from lb./in. to lb./ft. for consistency with other units and the 32.2 is "g" units in ft/sec.².

From experience, we know that on most rear-drive race cars the front natural frequency is higher than the rear, based on front roll stiffness requirements. At this point, we note that ω_R cannot be less than 108 cpm without using up the 2.5 in. of bump travel—this cannot be decreased. Thus, ω_F will be increased to 115 cpm for the following first pass through the calculation.

To increase ω_F we square the ratio of the natural frequencies:

$$\frac{\omega_{F\text{new}}}{\omega_{F\text{old}}} = \left(\frac{115}{96.6} \right)^2 = 1.19^2 = 1.417$$

to find the ratio of new to old suspension rates. The new ride rate is

$$271.2 \times 1.417 = 384.4 \text{ lb./in.}$$

To check, the new ω_F with this new K_{RF} is

$$\omega_F = \frac{1}{2\pi} \sqrt{\frac{384.4 \times 12 \times 32.2}{1020}} = 1.921 \text{ Hz} \text{ or } 1.921 \times 60 = 115.2 \text{ cpm}$$

With a first pass at the ride rates completed, we can now calculate the roll rates resulting from these ride rates and compare them with those assumed at the start of this example. Assuming left and right side ride rates are the same, these calculations are

$$K_{\phi F} = \frac{12 \times K_{RF} \times t_F^2}{2} = \frac{12 \times 384.4 \times 5^2}{2} = 57,660 \text{ lb.-ft./rad.}$$

$$K_{\phi R} = \frac{12 \times K_{RR} \times t_R^2}{2} = \frac{12 \times 225.6 \times 5^2}{2} = 33,840 \text{ lb.-ft./rad}$$

Note that if the left and right side ride rates are not the same, the roll rate calculation is

$$K_\phi = \frac{12 \times t^2 \times K_L \times K_R}{(K_L + K_R)}$$

where the subscripts "L" and "R" indicate the left and right side values, respectively.

These calculated roll rates are considerably lower than those assumed at the start of the example, even with the increase in front natural frequency. If anti-roll bar installation is possible, the differences can be made up by selection of a suitable bar.

For the sake of example, assume that a rear anti-roll bar cannot be fitted to the car but a front bar can, to bring the total front roll rate to the assumed 70,000 lb.-ft./rad. value. As with the spring sizes, the actual choice of bar diameter and length is treated later.

The roll gradient is then:

$$\frac{\phi}{A_Y} = \frac{-W \times H}{K_{\phi F} + K_{\phi R}} = \frac{-3400 \times 1.1}{70,000 + 33,840} = -0.036 \text{ rad./g} \text{ or } -2.06 \text{ deg./g}$$

and the revised front and rear weight transfers are (assuming that the roll center heights do not change):

$$W_F = -0.92 \times \frac{3400}{5} \times \left(\frac{1.1 \times 70,000}{70,000 + 33,840} + \frac{5.7}{9.5} \times 0.25 \right) \\ = -0.92 \times 680 \times (0.742 + 0.15) = -558 \text{ lb.}$$

$$W_R = -0.92 \times \frac{3400}{5} \times \left(\frac{1.1 \times 33,840}{70,000 + 33,840} + \frac{3.8}{9.5} \times 0.625 \right) \\ = -0.92 \times 680 \times (0.355 + 0.25) = -378 \text{ lb.}$$

The outside wheel loads are:

$$\begin{aligned} \text{Front outside: } W_{FO} &= 2402/2 + 558 = 1759 \text{ lb.} \\ \text{Rear outside: } W_{RO} &= 1602/2 + 378 = 1179 \text{ lb.} \end{aligned}$$

The changes from static loads are:

$$\begin{aligned} \text{Front outside: } W_{FO} &= 1759 - 1020 = +739 \text{ lb.} \\ \text{Rear outside: } W_{RO} &= 1179 - 680 = +499 \text{ lb.} \end{aligned}$$

The corresponding wheel ride displacements are:

$$\begin{aligned} \delta_F &= 739/384.4 = 1.92 \text{ in.} & \text{Note: } \delta \text{ here indicates a wheel position} \\ \delta_R &= 499/225.6 = 2.21 \text{ in.} & \text{instead of steer angle.} \end{aligned}$$

The difference between the front roll rate of 57,660 and the desired 70,000 (that is, 12,340 lb.-ft./rad.) will be made up by the front anti-roll bar.

We no longer need to change ride rates. We do need to properly size an anti-roll bar. For this example, we have reached a compromise for ride and roll rates. This compro-

mise results in nearly the desired wheel travel in this cornering situation. Obviously, individual cases can require more iterations and more trade-off compromises.

IMPORTANT—We have not made any evaluation of over/understeer characteristics of the car. Over/understeer is primarily a function of tire operating conditions and is changed by changing front and rear roll rates, roll center heights, aerodynamic lift coefficients, etc.

Given the desired ride and roll rates, the next section continues the analysis by adding in the effect of tire vertical spring rate to arrive at wheel center rate.

Transferring Ride/Roll Rates to Wheel Center Rates

Rates for an Independent Suspension

The overall ride rate for a suspension can be thought of as a series combination of two springs, one acting between the chassis and the wheel center, the other acting between the wheel center and the ground. The first represents what we call the wheel center rate; the second is the vertical tire rate.

Having developed our required ride/roll rates in the previous section, we must now relate those rates to the wheel center rates. The general formula and notation for linear springs in series is treated in Chapter 21. The total rate, S, is given by

$$S = \frac{S_1 S_2}{S_1 + S_2}$$

In this case, the total rate (made up of the tire and wheel center rates) and one of the two parts (tire rate) are known. The following formula has been solved for the wheel center rate:

$$K_W = \frac{K_R K_T}{K_T - K_R}$$

where K_W = wheel center rate, lb./in.

K_R = ride rate, lb./in.

K_T = tire vertical rate, lb./in.

Continuing our example and assuming a tire vertical rate of 2000 lb./in., the resulting front and rear wheel center rates are

$$K_{WF} = \frac{384.4 \times 2000}{2000 - 384.4} = 476 \text{ lb./in.}$$

$$K_{WR} = \frac{225.6 \times 2000}{2000 - 225.6} = 254 \text{ lb./in.}$$

As is seen, the wheel center rate is higher (stiffer) than the ride rate when a tire rate is included in the calculation.

With the front wheel center rate known, we can now estimate the additional roll rate that must be provided by the anti-roll bar. This is calculated as follows:

$$K_{\phi A} = \frac{K_{\phi DES} \times (12 \times K_T \times t^2/2)}{[12 \times K_T \times (t^2/2) - K_{\phi DES}]} - 12 \times K_W \times t^2/2$$

where $K_{\phi A}$ = additional roll rate needed, lb.-ft./rad.

$K_{\phi DES}$ = desired total roll rate, lb.-ft./rad.

K_W = wheel center rate, lb./in.

t = track, ft.

K_T = tire rate, lb./in.

For our sample front suspension, we had a desired total roll rate of 70,000 lb.-ft./rad. but had only 57,660 lb.-ft./rad. provided by the front ride rates acting in roll. Therefore the additional roll rate required (referred to the wheel centers) is

$$K_{\phi A} = \frac{70,000 \times (12 \times 2000 \times 5^2/2)}{[12 \times 2000 \times (5^2/2) - 70,000]} - 12 \times 476 \times 5^2/2$$

$$= 91,304 - 71,400 = 19,904 \text{ lb.-ft./rad.}, 4168 \text{ lb.-in./deg.}$$

Knowing these values, we can now refer our wheel center rates to actual suspension component rate, that is, springs and anti-roll bars.

Rates for an Axle Suspension

For a solid axle suspension the calculation of ride and roll rates is somewhat more complicated because the springs are not effectively positioned at the outboard track locations. Because they are inboard of the track, the springs are effectively softer in roll than the

same ride rates would be for a comparable independent suspension. It is therefore necessary to decouple the axle springs in the ride and roll modes and to work directly with spring rates (effective at the axle location) rather than ride rates to solve the problem.

As in the previous section the vertical axle rate (for each side) is found by removing the tire rate from the axle ride rate.

$$K_W = \frac{K_R K_T}{K_T - K_R}$$

where K_W = vertical axle rate, lb./in.

K_R = ride rate, lb./in.

K_T = tire rate, lb./in.

The vertical axle rate is the installed spring rate for a leaf spring suspended axle, but may not necessarily be the spring rate for other types of axle suspensions (see the next section on installation ratios).

The roll rate due to the vertical axle rate can then be calculated by the following equation:

$$K_\phi = \frac{12 (K_T \times T_R^2/2) \times 12 (K_W \times T_S^2/2)}{12 (K_T \times T_R^2/2) + 12 (K_W \times T_S^2/2)}$$

where K_ϕ = roll rate, lb.-ft./rad.

K_T = tire rate, lb./in.

K_W = vertical axle rate, lb./in.

T_R = track, ft.

T_S = spring track, ft.

If an anti-roll bar is included, the equation becomes:

$$K_\phi = \frac{(R_{aux} + 12 \times K_W \times T_S^2/2) \times (12 \times K_T \times T_R^2/2)}{(R_{aux} + 12 \times K_T \times T_R^2/2) + (12 \times K_W \times T_S^2/2)}$$

where R_{aux} = roll rate of the anti-roll bar, lb.-ft./rad. of body roll.

We should note that a leaf spring axle typically has a roll rate that is 30-50% greater than provided by the leaf springs vertical rate due to lateral and torsional deflection of the leaves. In this case we can use (assuming a 40% increase):

$$R_{aux} = 0.4 \times 12 \times K_W \times T_S^2 / 2$$

in the above equation.

If we modify our previous example so that we have a Hotchkiss rear axle (leaf spring, live axle) with a spring track of 3.5 ft. and the same rear ride rates of 225.6 lb./in., then the vertical axle rate (at each side) is as before:

$$K_{WR} = \frac{225.6 \times 2000}{2000 - 225.6} = 254 \text{ lb./in.}$$

And the roll rate is calculated from:

$$R_{aux} = 0.4 \times 12 \times 254 \times 3.5^2 / 2 = 7468 \text{ lb.-ft./rad.}$$

$$K_{\phi R} = \frac{\left[7468 + (12 \times 254 \times 3.5^2 / 2) \right] \times (12 \times 2000 \times 5^2 / 2)}{\left[7468 + (12 \times 254 \times 3.5^2 / 2) \right] + (12 \times 2000 \times 5^2 / 2)} = 24,042 \text{ lb.-ft./rad.}$$

Note that this is a substantial decrease in roll rate from that for the comparable independent rear suspension case as a result of moving the springs inboard of the wheel centers.

The roll gradient is then:

$$\frac{\phi}{A_Y} = \frac{-W \times H}{K_{\phi F} + K_{\phi R}} = \frac{-3400 \times 1.1}{70,000 + 24,042} = 0.0398 \text{ rad./g or } 2.23 \text{ deg./g}$$

And the revised front and rear weight transfers are (assuming that the roll center heights do not change):

$$W_F = -0.92 \times \frac{3400}{5} \times \left(\frac{1.1 \times 70,000}{70,000 + 24,042} + \frac{5.7}{9.5} \times 0.25 \right)$$

$$= -0.92 \times 680 \times (0.819 + 0.15) = -606 \text{ lb.}$$

$$W_R = -0.92 \times \frac{3400}{5} \times \left(\frac{1.1 \times 24,042}{70,000 + 24,042} + \frac{3.8}{9.5} \times 0.625 \right)$$

$$= -0.92 \times 680 \times (0.281 + 0.25) = -332 \text{ lb.}$$

The outside wheel loads are:

$$\begin{aligned} \text{Front outside: } W_{FO} &= 2402/2 + 606 = 1807 \text{ lb.} \\ \text{Rear outside: } W_{RO} &= 1602/2 + 332 = 1133 \text{ lb.} \end{aligned}$$

The changes from static loads are:

$$\begin{aligned} \text{Front outside: } W_{FO} &= 1807 - 1020 = +787 \text{ lb.} \\ \text{Rear outside: } W_{RO} &= 1133 - 680 = +453 \text{ lb.} \end{aligned}$$

16.3 Installation Ratios

To this point we have been dealing with the rates (either ride or roll) that are effective at the ground or the wheel center. These rates ultimately determine the steady-state turning performance of a car through their influence on wheel loads. The next step is to determine spring and anti-roll bar characteristics needed to give us the desired ride and roll rates. In order to accomplish this step, we introduce the concept of *installation ratio*.

The installation ratio is a geometric concept that relates the change in length (or angle) of a force-producing device (e.g., a spring, shock absorber, or anti-roll bar) to a change in vertical wheel center movement. It is really the inverse of mechanical advantage and can be illustrated by the sketch of a simple trailing arm suspension shown in Figure 16.2.

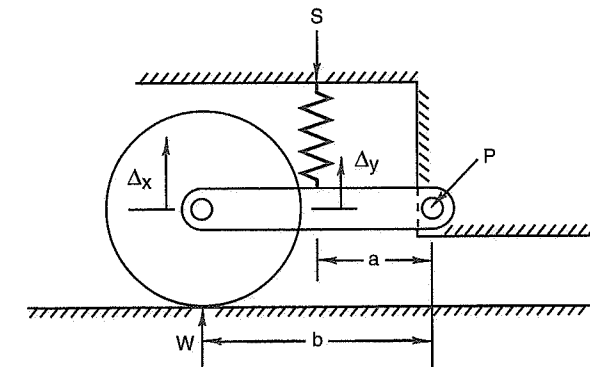


Figure 16.2 Installation ratio for a simple suspension.

As seen in the figure, a trailing arm is pivoted on the chassis at point P. The spring acts at a distance "a" along the arm from the pivot. The wheel center is at a distance "b" from the pivot. Due to the different dimensions "a" and "b," as the wheel moves vertically an amount Δ_x , the spring compresses an amount Δ_y . The installation ratio is defined as the

rate of change of spring compression with wheel movement, or $\Delta y/\Delta x$. If "b" is twice "a" the Δy is half Δx and the force at the wheel center, W , is half the force at the spring, S (the installation ratio times the spring force). Because the installation ratio reduces both the force and displacement of the spring, it must be squared to relate wheel center rate to spring rate.

The installation ratio is commonly used by itself to relate a suspension wheel center rate to a spring rate. If the change in spring compression is always the same for a unit change in wheel center position, i.e., the installation ratio is always constant, that is all we need to know. However, it is common for automobile suspensions to have an installation ratio that varies with wheel center position.

If the linkage ratio is not constant, we need to know how it varies in order to relate the rates to one another. A detailed analysis of the problem yields the formula:

$$K_w = F_s \left(\frac{\Delta IR}{\Delta \delta} \right) + K_s (IR)^2$$

where K_w = wheel rate, lb./in.

F_s = spring force, lb.

K_s = spring rate, lb./in.

IR = installation ratio

$\Delta IR/\Delta \delta$ = change of installation ratio with wheel displacement

The first term in the above formula is called the *geometric rate*. As is seen in the formula, if the change of installation ratio with wheel displacement is zero, then the wheel rate is related to the spring rate only by the installation ratio squared with no geometric rate term, or

$$K_w = K_s (IR)^2$$

For race cars that are stiffly sprung this is usually a sufficiently accurate approximation to "ballpark" spring rates for initial set-up even though the installation ratio may vary. However, one should be aware that as ride rates or ride frequencies decrease, the error in using this approximation can become very significant.

As an example, Figure 16.3 shows the installation ratio as a function of wheel ride position for a typical double wishbone suspension. As is seen, the installation ratio changes considerably, especially as the suspension goes into jounce. We can find the change of installation ratio from this figure and then calculate the true wheel rate and its component parts (that is, the geometric rate and the installation ratio squared times the spring rate) for various spring rates. Table 16.2 summarizes these calculations for three spring rates. The geometric rate for this suspension is negative and nearly constant for all three spring rates. For the soft spring rate it is nearly equal in magnitude to the total wheel rate.

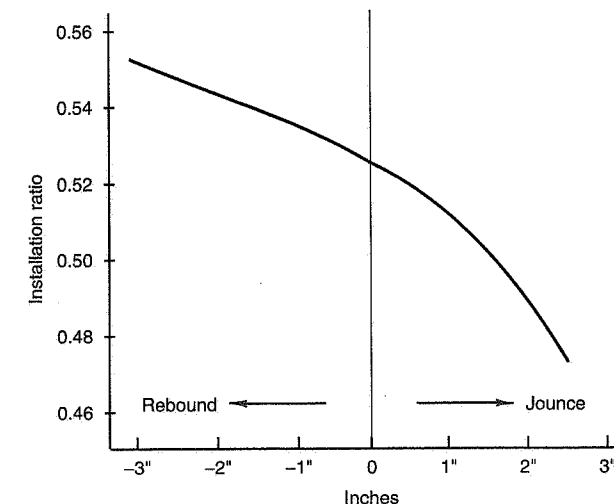


Figure 16.3 Installation ratio as a function of ride travel.

This example illustrates that for softly sprung suspensions, neglecting to consider the geometric rate term can lead to large errors in the true wheel rate. The effect is much less significant for stiff suspensions than for soft ones.

In general, if the slope of the installation ratio is negative (as in Figure 16.3, IR decreases as jounce increases), the geometric rate term will result in decrease in wheel rate from the installation ratio squared times spring rate term. If it is positive (increases with increasing jounce), it will increase the wheel rate—so-called "rising-rate" spring installations have this characteristic, which is somewhat similar to using progressive bump rubbers.

Table 16.2 Effect of Installation Ratio with Different Spring Rates

Spring Rate	Geometric Rate	Spring Rate times Installation Ratio Squared	Wheel Rate
200	-23.48	53.87	30.39
600	-24.74	161.62	136.88
1200	-26.62	323.23	296.61
(all rates are lb./in.)			

Finding the Installation Ratio for Linear Springs

The installation ratio for any given suspension can be found by several methods:

- Drafting layout
- Direct measurement
- Computer analysis.

Drafting layout is a traditional method at the suspension design stage and can be used with existing suspensions if accurate measurements of pivot point locations, suspension arm lengths, spring mount locations, etc., can be made. The process involves drawing the complete suspension system at various equally spaced ride heights and measuring the spring length at each ride height. The change in spring length divided by the change in ride height is the installation ratio. This is tabulated against the average ride height for each change (that is, if the ride height changes from 1.0 to 1.5 in., the average is 1.25 in.). Finally, a graph similar to that shown in Figure 16.3 can be drawn showing how the installation ratio changes with ride position.

The *direct measurement* method is similar to the drafting layout method except that it involves physical measurements on an actual suspension. This can be best accomplished by removing the spring and blocking up the chassis enough to allow full range of suspension motion. Then, from the static ride height position, accurate measurements must be made of the spindle height change (at the wheel centerline) and the spring length change (distance between the upper and lower spring mounts along the spring centerline). A tabulation and plot can then be produced as described above.

We should note that both of these procedures can be used for either independent or axle suspensions. However, for axle suspensions the entire axle must be moved vertically in ride relative to the car. Any change in axle roll angle will result in large errors.

The disadvantage of these two procedures is that they are generally not accurate enough to give the *geometric rate* with a great deal of precision. For a softly sprung suspension, the uncertainty in the true geometric rate can amount to a considerable error in the calculated wheel rate. Nevertheless they are accurate enough to indicate whether the geometric rate will subtract from or add to the spring-rate times installation-ratio-squared term by indicating the slope of the installation ratio vs. ride height.

The third method mentioned above, that of *computer analysis*, is most accurate but of course requires a suitable computer program. It also requires accurate dimensions of the suspension components as the output from any computer program is only as good as the input. In the past, suitable suspension analysis programs were usually custom-made for manufacturers and large-scale race teams and were generally not available to the racing community. Now this software is available from a number of sources, for example, the

SAE (1993-94) offers a Professional Development Seminar in the use of one such program named SKAT.

Installation Ratio for Torsional Springs

Generally the same comments hold true for torsional springs as for linear springs. In fact, if the torsion bar rate is available in terms of force vs. linear displacement of the end of the torsion bar lever arm, the analysis is the same as for linear springs with the effective spring length change being the change in vertical position of the torsion bar lever attachment point to the suspension. However, if only the torsion bar rate alone (in units of lb.-in./deg.) is known, we can get the effective installation ratio of the lever arm and its attachment point directly from measurement. This involves measurement of the lever arm angle change for incremental changes in ride height and is accomplished with an inclinometer in a manner similar to that for linear springs. Be sure to measure the lever arm angle in a plane perpendicular to the axis of the torsion bar.

Given the torsion bar rate, the wheel rate can be approximated as:

$$K_w = \frac{K_b I_b^2}{57.3}$$

where K_w = approximate effective wheel rate, lb./in.
 K_b = torsion bar rate, lb.-in./deg.
 I_b = torsion bar installation ratio, deg./in.

Installation Ratio for Anti-Roll Bars

For conventional anti-roll bars as applied to an independent suspension, the overall installation ratio, in terms of degrees (or radians) of bar twist per degree of chassis roll is needed to determine the contribution of the anti-roll bar rate to the total roll rate of the car. This requires knowledge of:

- The anti-roll bar lever arm length, measured between the centerline of the bar and the point of attachment to a suspension member.
- The installation ratio between the suspension member point of attachment and the wheel center.

The contribution of the anti-roll bar to the total roll rate is:

$$K_{\phi B} = K_{\theta B} I_B^2 \left(\frac{T^2}{L^2} \right)$$

where $K_{\phi B}$ = contribution of the anti-roll bar rate to the total car roll rate, lb.-ft./deg.
 $K_{\theta B}$ = anti-roll bar angular (twist) rate, lb.-ft./deg.
 L = anti-roll bar lever arm, ft.
 I_B = linear installation ratio of the anti-roll bar, inches of bar attachment point movement per inch of wheel center movement, in./in.
 T = track width, ft.

The same formula can be used for conventional anti-roll bars applied to a solid axle except that the linear installation ratio (I_B) must be determined with roll (not ride) movement of the axle. Some axle installations have inherent roll stiffness; it may be necessary to actually test the entire assembly to determine the axle roll rate.

16.4 Finishing the First Example Case

From earlier in this chapter, our desired front wheel rate was 475 lb./in. Assuming that the installation ratio of the front springs is as shown in Figure 16.3, we can calculate the spring rate required as:

$$K_s = \frac{K_w}{IR^2} = \frac{475}{0.525^2} = 1723 \text{ lb./in.}$$

Note that we are neglecting the geometric rate; for this installation ratio it is negative and it would be appropriate to increase this spring rate by about 10%.

Also, the additional front roll rate to be provided by the anti-roll bar was 19,900 lb.-ft./rad. or 347.3 lb.-ft./deg. Assuming a lever arm length of 9 in. (0.75 ft.) and a linear installation ratio of 0.3 in./in., our anti-roll bar rate must be

$$K_{\theta B} = \frac{K_{\phi B} L^2}{I_b^2 T^2} = \frac{347.3 (0.75^2)}{(0.3^2)(5^2)} = 86.8 \text{ lb.-ft./deg.}$$

or $4975 \text{ lb.-ft./rad.}$

From these values we can then calculate the physical characteristics of the springs and anti-roll bars that are needed based on the information given in Chapter 21.

As a final note, we emphasize that all of the above calculations are for an "ideal" car, that is, one that has a totally rigid chassis (especially in torsion), that is totally free of friction, and that has no compliance in pivots, mounts, etc. While this "ideal" car can never be achieved, the idealized calculation illustrates how various suspension elements work together. This technique can be used to give a first estimate of spring and anti-roll bar sizes to set up a new race car.

16.5 Second Example with Simplified Calculations

Approach

If, through experience, you know the basic characteristics that you want to achieve for a particular car type, a simpler set of calculations can usually get you very close to the spring and anti-roll (stabilizer) bar rates that work well with the car. In this section a set of calculations is given for a racing sports sedan. This particular class of car has a minimum weight of 2325 lb. with a legal maximum of 52% rear weight (without driver and fuel). As rear tires are allowed to be larger than fronts the basic weight distribution should be 1116 lb. front and 1209 lb. rear, right on the 52% point.

Assuming 25 gallons of fuel is required for a 100-mile race, a fuel weight distribution of -23% front and 123% rear (the fuel tank is behind the rear axle), and a driver weight of 160 lb. and 68.4% on the rear we can calculate the weights front and rear with driver plus half tank of fuel as in Table 16.3.

Table 16.3 Data for Simplified Example

Symbol	Front	Rear	Total	%Front
Basic car weight (lb.)	1116	1209	2325	48.0
Driver (lb.)	51	109	160	31.9
Half fuel (77.5 lb.)	-17.5	95		
Total weight (lb.)	W_F, W_R	1149.5	1413	2562.5
Unsprung weight (lb.)	W_{UF}, W_{UR}	-170	-250	
Sprung weight (lb.)	W_{SF}, W_{SR}	979.5	1163	2142.5
CG height (in.)	h			15
Wheelbase (in.)	ℓ			103

Ride Analysis

If we know that a front ride frequency (ω_F) of 1.9 Hz and a rear ride frequency (ω_R) of 1.7 Hz will work well on this car, we can calculate the spring rates required.

For the front, the ride rate is

$$K_{RF} = \frac{4\pi^2 \omega_F^2 (W_{SF}/2)}{386.4} = \frac{4(9.87)(1.9^2)(979.5/2)}{386.4} = 181 \text{ lb./in.}$$

Given a tire rate (K_T) of 2000 lb./in., the wheel center rate is

$$K_{WF} = \frac{K_{RF} K_T}{K_T - K_{RF}} = \frac{181(2000)}{2000 - 181} = 199 \text{ lb./in.}$$

Finally, a front spring installation ratio or linkage ratio (LR_F) of 0.728, the front spring rate is

$$K_{SF} = \frac{K_{WF}}{LR_F^2} = \frac{199}{0.728^2} = 375 \text{ lb./in.}$$

Similarly, for a rear ride frequency (ω_R) of 1.7 Hz, we can calculate the rear spring rate required:

$$K_{RR} = \frac{4\pi^2 \omega_R^2 (W_{SR}/2)}{386.4} = \frac{4(9.87)(1.7^2)(1163/2)}{386.4} = 172 \text{ lb./in.}$$

Given a tire rate (K_T) of 2000 lb./in., the wheel center rate is

$$K_{WR} = \frac{K_{RR} K_T}{K_T - K_{RR}} = \frac{172(2000)}{2000 - 172} = 188 \text{ lb./in.}$$

Finally, applying a rear spring installation ratio (LR_R) of 0.9615, the rear spring rate is

$$K_{SR} = \frac{K_{WR}}{LR_R^2} = \frac{188}{0.9615^2} = 203 \text{ lb./in.}$$

Roll Analysis

Once we have completed the ride analysis, we can do the roll analysis in order to calculate our anti-roll bar requirements. This requires additional information about the car which is summarized in Table 16.4.

Sprung mass CG height:

$$h_S = \frac{W_T h - W_{UF} RL_F - W_{UR} RL_R}{W_S}$$

$$= \frac{2562.5(15) - 170(11.25) - 250(12.75)}{2142.5} = 15.56 \text{ in.}$$

Table 16.4 Additional Data for Simplified Example—Roll Properties

	Symbols	Front	Rear
Roll center heights (in.)	Z_F, Z_R	3.1	6.8
Tire static loaded radius (SLR, in.)	RL_F, RL_R	11.25	12.75
Track (in.)	T_F, T_R	65.58	64.50
Spring linkage ratio	LR_F, LR_R	0.728	0.9615
Stabilizer bar linkage ratio	LB_F, LB_R	0.691	1.00
Rear spring track (in.)	T_S	—	47.1

Sprung mass weight distribution:

$$a_S = \frac{W_{SF}}{W_S} = \frac{979.5}{2142.5} = 45.7\% \text{ front}$$

Rolling moment lever arm:

$$h_{RM} = h_S - [Z_F + (Z_R - Z_F)(1 - a_S)]$$

$$= 15.56 - [3.1 + (6.8 - 3.1)(1 - 0.457)] = 10.45 \text{ in.}$$

Rolling moment per g lateral acceleration:

$$\frac{M_\phi}{A_y} = \frac{h_{RM} W_S}{12} = \frac{10.45(2142.5)}{12} = 1866 \text{ lb.-ft./g}$$

If, from our experience, we know that a roll gradient of 1.6 deg./g is desirable for this car, then we can calculate the roll rate required:

$$K_\phi = \frac{M_\phi / A_y}{RG} = \frac{1866}{1.6} = 1166 \text{ lb.-ft./deg.}$$

At this point we know the total roll rate we want for the car and must now determine how much must be provided by the stabilizer bars at the front and rear. First we calculate the available roll rate from the springs alone:

Front spring roll rate (independent suspension):

$$K_{\phi SF} = \frac{K_{RF} T_F^2}{1375} = \frac{181(65.58^2)}{1375} = 566 \text{ lb.-ft./deg.}$$

Rear spring roll rate (live axle):

$$K_{\phi SR} = \frac{(K_{WR} \times T_S^2)(K_T \times T_R^2)}{1375(K_{WR} T_S^2 + K_T T_R^2)}$$

$$= \frac{(188 \times 47.1^2)(2000 \times 64.5^2)}{1375[188(47.1^2) + 2000(64.5^2)]} = 289 \text{ lb.-ft./deg.}$$

The total available roll rate from the springs is

$$K_{\phi S} = 566 + 289 = 855 \text{ lb.-ft./deg.}$$

Therefore the stabilizer bars must provide:

$$K_{\phi B} = 1166 - 855 = 311 \text{ lb.-ft./deg.}$$

It is now necessary to size the front and rear bars. In order to do this we must know what lateral load transfer distribution to use. Again, based on experience with this specific racing sedan, we start with a front load transfer distribution of 5% more than the weight distribution. In this case we choose a front load transfer distribution of 49.85%.

The total load transfer is

$$\frac{TLT}{A_y} = \frac{W_T h}{T_{ave}}$$

where T_{ave} is the average front and rear track, $(T_F + T_R)/2$

$$TLT/A_y = (2562.5)(15)/65 = 591 \text{ lb./g}$$

Therefore we want a front load transfer (FLT) of $0.4985 \times 591 = 295 \text{ lb./g}$.

Calculation of front roll stiffness ($K_{\phi F}$) required:

$$\frac{FLT}{A_y} = \frac{12(K_{\phi F})\phi}{T_F} + \frac{W_{SF}Z_F}{T_F} + \frac{W_{UF}RL_F}{T_F}$$

$$295 = \frac{12(K_{\phi F})1.6}{65.58} + \frac{979.5(3.1)}{65.58} + \frac{170(11.25)}{65.58}$$

$$295 = 0.2928 K_{\phi F} + 46.3 + 29.2$$

or

$$K_{\phi F} = (295 - 46.3 - 29.2)/0.2928 = 750 \text{ lb.-ft./deg.}$$

The front roll stiffness must therefore be 750 lb.-ft./deg. Since the springs provide 566 lb.-ft./deg., the front stabilizer bar must provide $(750 - 566) = 184 \text{ lb.-ft./deg.}$. The rear bar must provide the difference between the total, front and that given by the rear springs:

$$K_{\phi BR} = K_{\phi} - K_F - K_{\phi SR} = (1166 - 750 - 289) = 127 \text{ lb.-ft./deg.}$$

Because the linkage ratio for the rear bar is 1.0, the bar itself must be sized to produce 127 lb.-ft./deg. However, for the front bar, the linkage ratio is 0.691. Therefore the bar itself must produce:

$$K_{bF} = 184/(0.691^2) = 385 \text{ lb.-ft./deg. of body roll}$$

It should be noted that in order to use this calculation method you must know what characteristics work best for the particular type of car you are dealing with. In other words, a good deal of experience is necessary. Some general characteristics that have proven successful for road circuit cars are summarized in Table 16.5.

Table 16.5 Suggested Numbers for Simplified Method

Ride Frequencies	
Non-aero sedans	1.6-2.0 Hz (with front higher)
Aero cars	3.0-5.0 Hz (with front higher)
Roll Gains	
Sedans	1.0-1.8 deg./g
Aero cars	0.25-0.5 deg./g
TLLTD's	
To insure initial understeer, calculate the Total Lateral Load Transfer Distribution (TLLTD) to be 5% more than the weight distribution at the front.	

Suspension Geometry

“Form follows function.”

Louis Sullivan



Introduction

Designing suspension systems for production or racing cars requires technical knowledge in several disciplines. This chapter will cover only one of those disciplines—the study of suspension kinematics or “geometry.” This chapter does not cover the effects of compliance or deflections of structural components under load; these effects are discussed in Chapter 23.

When we talk about suspension geometry it means the broad subject of how the unsprung mass of a vehicle is connected to the sprung mass. These connections not only dictate the path of relative motion, **they also control the forces that are transmitted between them.**

Any particular geometry must be designed to meet the needs of the particular vehicle for which it is to be applied. There is no single best geometry.

17.1 Degrees of Freedom and Motion Path

For an independent suspension, be it front or rear, the assemblage of control arms is intended to control the wheel motion relative to the car body in a single prescribed path. That path may have camber gain, caster change, and toe change as prescribed by the designer but it still follows only one path as it moves up and down. In engineering terms we could say that the wheel has a *fixed path* of motion relative to the car body. It is not allowed to move fore and aft or laterally relative to this path. The knuckle is not allowed to rotate other than as determined by this fixed path (of course the wheel is allowed to roll around the spindle axis!). The suspension linkages are expected to position the knuckle (wheel) very accurately in all directions while allowing it to move up and down against the spring and shock. In front suspensions we do have a steer rotation degree of freedom but only when it is demanded from the steering system.

For any body moving in space relative to another body, its motion can be completely defined by three components of linear motion and three components of rotational motion (see Figure 17.1). A single body is said to have six degrees of freedom of motion in a three-dimensional world. We said above that any independent suspension allows only one path of motion of the knuckle relative to the body. Another way to say the same thing is that the suspension provides five degrees of restraint (D.O.R.), i.e., it severely limits motion in five directions. In the real world, the mechanical components that supply the restraints are not "perfect" in the sense of restraining the motion to a particular degree of freedom. Therefore, the study of independent suspension geometries is to determine how to restrain the knuckle to limited motion in five directions.

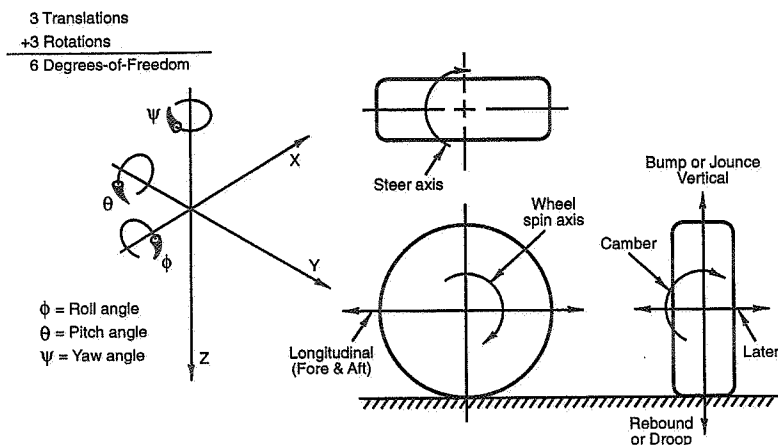


Figure 17.1 Degrees of freedom and suspension motion definitions (Ref. 1).

If the only components you could use to design a suspension geometry were straight links with rod ends (spherical joints) on each end, the required restraints can be provided with five of them. In other words to obtain five degrees of restraint requires exactly five tension-compression links.

To relate this concept to more familiar hardware, we need to understand how typical suspension components provide their restraining function. Looking at Figure 17.2 you can see that an A-arm is really equivalent to two straight links with their outer ends coming together at the ball joint. A MacPherson Strut is kinematically a "slider" mechanism which is equal to an A-arm that is infinitely long at right angles to the slider travel.

4 D.O.R. Requires 4 Links / 5 D.O.R. Requires 5 Links

Simple Tension - Compression Links



A-Arm = 2 Links



MacPherson Strut = 2 Links;
Slider = A-Arm of Infinite Length



Figure 17.2 Kinematics—all independent suspensions have five links.

Now, with this in mind, we can look at most independent suspensions and come up with a count of five links in every case (see Figure 17.3). The standard racing double wishbone suspension has two A-arms plus a tie rod. Thus, two links for each A-arm and one link for the tie rod adds up to five. A MacPherson Strut suspension has two for the strut, two for the lower A-arm, and the tie rod makes five. There are some suspensions that are less obvious because they have fewer links, but what they are usually doing is introducing a bending requirement to achieve restraint of motion. An example of this is a semi-trailing arm rear suspension. There is one arm that does the job of five links, but in order to do it, it must be strong in bending and torsion in the three directions of rotation.

For solid axle (or beam type) rear (and occasionally front) axles, the two wheels are tied together, so motion of one affects the other (see Figure 17.4). When two wheels are tied together, they have two different motions relative to the body; they can go up and down together (parallel bump motion) or they can move in opposite directions one up and one down (roll motion). In kinematic terms the axle has two degrees of freedom of motion relative to the body. There is a total of six degrees of motion in space; we must restrain four when we design a beam-type rear suspension. This can be accomplished with a linkage having just four tension-compression links.

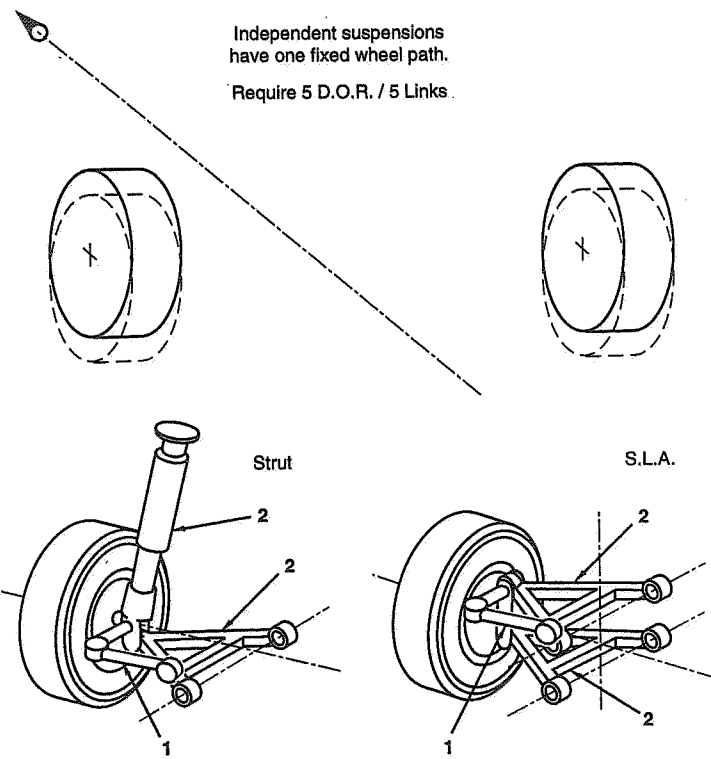


Figure 17.3 Kinematics—*independent wheel motion*.

17.2 Instant Center Defined

Throughout the rest of this chapter the term *instant center* (IC) will be used in describing and determining several common suspension parameters. To help achieve clarity in these discussions some comments about what is an instant center, are in order. The word “instant” means at that particular position of the linkage. “Center” refers to a projected imaginary point that is effectively the pivot point of the linkage at that instant. Figure 17.5 suggests how two short links can be replaced with one longer one. As the linkage is moved,⁵⁹ the center moves, so proper geometric design not only establishes all the instant centers in their desired positions at ride height, but also controls how fast and in what direction they move with suspension travel.

⁵⁹ For small motions of the links (in the “linear” range) the instant center remains nearly fixed. Since the system is really nonlinear for normal wheel motions the ICs move.

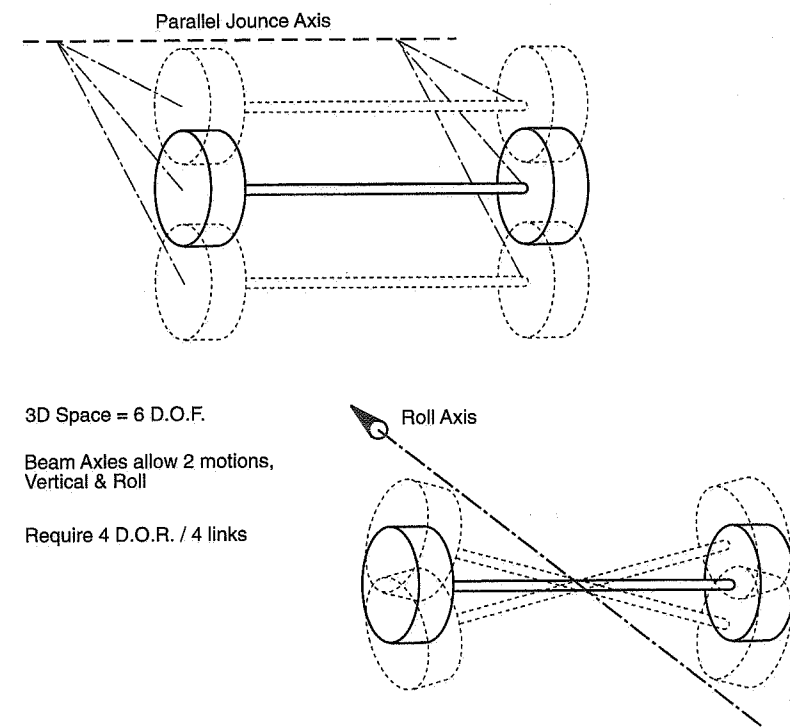


Figure 17.4 Kinematics—*axle suspensions have four links*.

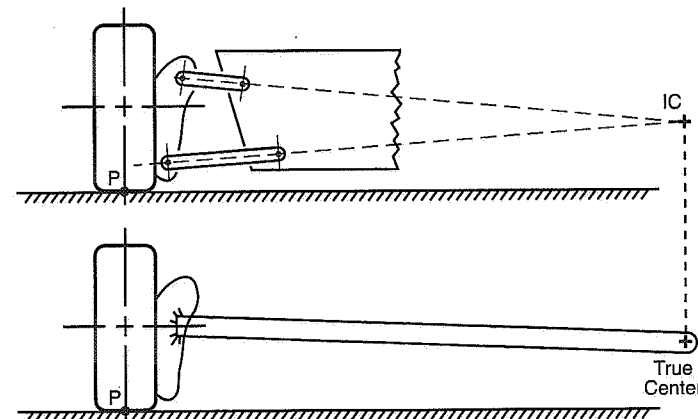


Figure 17.5 Instant center concept.

Instant centers come from the study of kinematics in two dimensions (in a plane). They are a convenient graphic aid in establishing motion relationships between two bodies. In suspension design it is convenient to break down this three-dimensional problem into two, two-dimensional problems. We talk about the front view and the side view geometry. What we are doing is cutting vertical planes (90° to the ground) through the wheel center, one parallel to the centerline of the car, and the other at a right angle to the vehicle centerline. We then project all the suspension points onto these planes.

When we connect a line between the ball joint and the control arm bushing and project it across the plane both for the upper and lower control arms they will usually intersect at some point. This intersection is an instantaneous linkage center. If you do the projection in the front view the instant center defines the camber change rate, part of the roll center information, scrub motion, and data needed to determine the steer characteristics. If you are working with the side view, the instant center will define the wheel fore and aft path, anti-lift and anti-dive/squat information, and caster change rate. As with any three-dimensional object, three orthogonal views are possible; because the third view (top view) is approximately along the single (ride) degree of freedom it contains little useful information about the path of the wheel.

Instant Axis

In true three-dimensional space, instant centers are replaced by instant axes. If we take the instant centers defined in the side view and the rear view and connect them together we get a line. This line can be thought of as the *instant axis* of motion of the knuckle relative to the body (see Figure 17.6).

Independent suspensions have one instant axis of motion because they have five restraints; of course, this instant axis moves with changes in ride height. Rear axles have two instant axes, one for parallel bump and one for roll; these also may move with changes in ride height. So whenever we are studying a particular suspension system we need to establish the instant centers and/or the instant axes. The remainder of this chapter will be devoted to the determination of these axes for many common types of front and rear suspensions, with additional comments in regard to their adjustability to meet the needs of race cars.

17.3 Independent Suspensions

For all independent suspensions there are the two instant centers (which change with bump and droop) that establish the properties of that particular design. The side view instant center controls force and motion factors predominantly related to fore and aft accelerations, while the front view instant (or swing) center controls force and motion factors due to lateral accelerations.

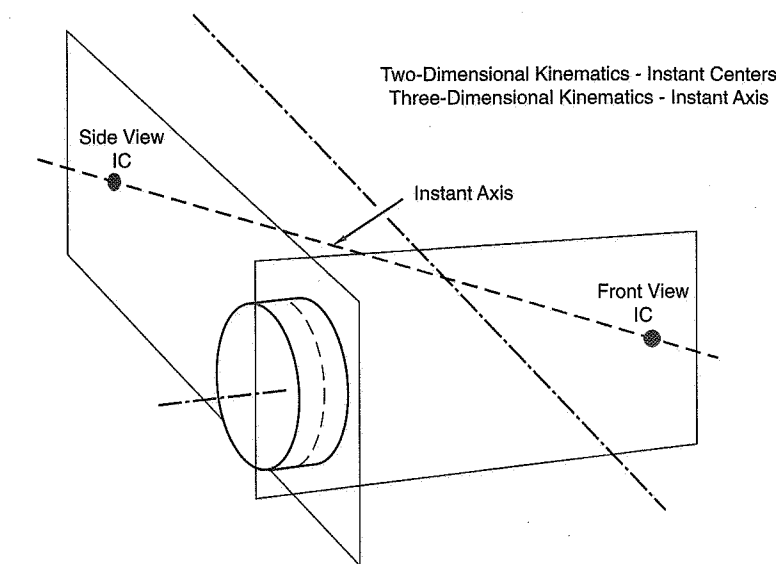


Figure 17.6 Kinematics—instant axis concept.

Front View Swing Arm Geometry

The front view swing arm (fvsa) instant center location controls the roll center height (RCH), the camber change rate, and tire lateral scrub. The IC can be located inboard of the wheel or outboard of the wheel. It can be above ground level or below ground. The location is up to the designers' performance requirements.

Roll Center Height

The roll center height is found by projecting a line from the center of the tire-ground contact patch through the front view instant center as shown in Figure 17.7(a). This is repeated for each side of the car. Where these two lines intersect is the roll center of the sprung mass of the car, relative to the ground. It is not necessarily at the centerline of the car, especially with asymmetric suspension geometry (Figure 17.7(b)) or once the car assumes a roll angle in a turn. It is obvious that the roll center location is controlled by the instant center heights above or below ground, the distance away from the tire that the instant center is placed, and whether the instant center is inboard or outboard of the tire contact patch.

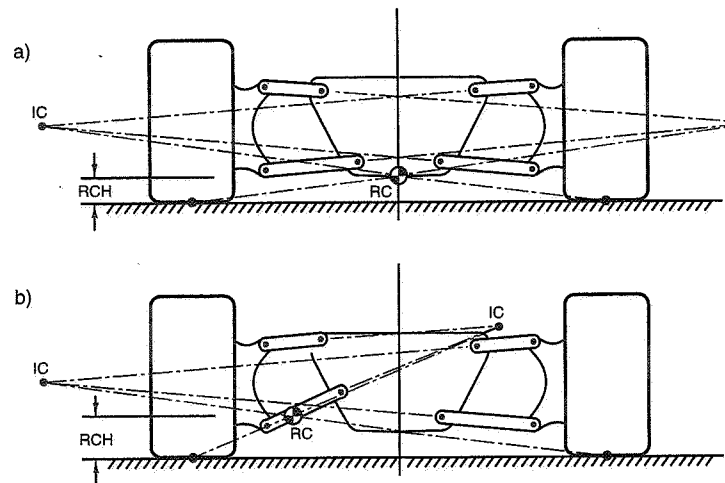


Figure 17.7 Roll center construction.

Now that you know how to find the roll center, what does it mean?

The roll center establishes the *force coupling* point between the unsprung and sprung masses. When a car corners, the centrifugal force at the center of gravity is reacted by the tires. The lateral force at the CG can be translated to the roll center if the appropriate force and moment (about the roll center) are shown. The higher the roll center the smaller the rolling moment about the roll center (which must be resisted by the springs); the lower the roll center the larger the rolling moment. You will also notice that with higher roll centers the lateral force acting at the roll center is higher off the ground. This lateral force \times the distance to the ground can be called the *nonrolling overturning moment*. So roll center heights are trading off the relative effects of the rolling and nonrolling moments. (See Chapter 18 for another explanation of these effects.)

The above part is simple and straightforward. There is, however, another factor in establishing the desired roll center height, and this is the horizontal-vertical coupling effect. If the roll center is above ground level the lateral force from the tire generates a moment about the instant center (IC). This moment pushes the wheel down and lifts the sprung mass; it is called *jacking* (see Figure 17.8(a)). If the roll center is below the ground level (possible with SLA suspension) then the force will push the sprung mass down. In either case the sprung mass will have a vertical deflection due to a lateral force! This is most apparent on older cars with swing axle rear suspensions such as the Formula Vee. An alternate way to analyze this situation is shown in Figure 17.8(b). Here the total force at the contact patch is drawn to its reaction point at the instant center and the lateral and vertical components are indicated; the vertical component in the case shown will lift the sprung mass.

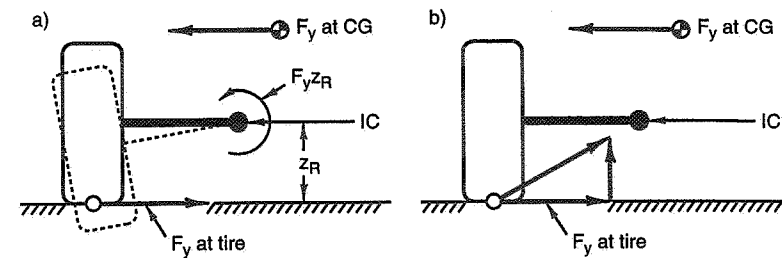


Figure 17.8 Jacking effect with a high roll center.

Camber Change Rate

While the roll center is a function of the fvsa length and height, the camber change rate is only a function of fvsa length (see Figure 17.9). If you replace the control arms of the suspension with a single link that ran from the knuckle to the instant center, the amount of camber change that was achieved per inch of ride travel would be camber change ($\text{deg./in.} = \arctan(1/\text{fvsa length})$). Note: This is different from the static camber setting or alignment.

Rate of Change of the Front View Swing Arm

As stated earlier in the definition of swing arms and instant centers the word "instant" means "at that position of suspension travel." Remember that instant centers move with wheel ride travel. How fast they move is a function of the absolute and relative lengths

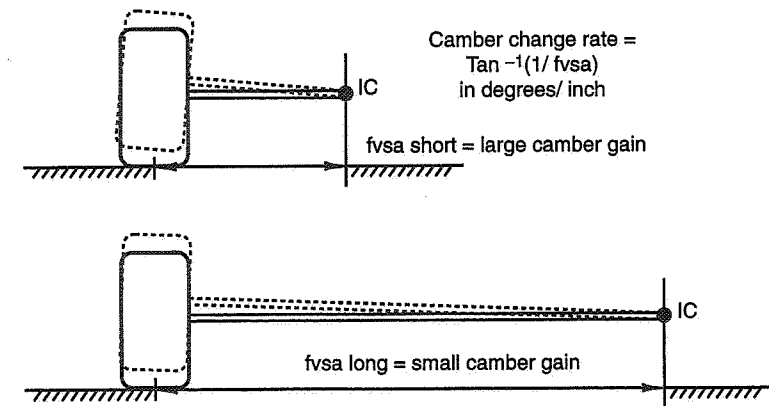


Figure 17.9 Camber change.

of the control arms in the front and side views. A camber curve can be made to have more or less camber change with wheel travel by altering the length of the upper control arm even though it is aimed at the same instant center at ride height. What this does is keep the same swing arm length at ride height but it shortens or lengthens faster or slower with wheel travel.

Scrub

Another front view variable is tire scrub. This is the lateral motion relative to the ground that results from vertical motion of the wheels (see Figure 17.10). Scrub occurs in every suspension system. The amount of scrub is a function of the absolute and relative lengths of the control arms and the position of the front view instant center relative to ground. When the front view instant center is at any position other than ground level, scrub is increased. If it is above ground and inboard, the tire will move outward as it rises; if it is below ground level and inboard, the tire will move inward with jounce travel. The amount that it moves is a function of the swing arm length and the absolute height from ground.

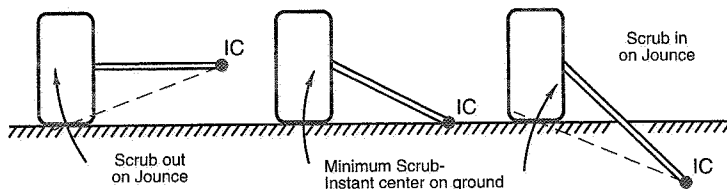


Figure 17.10 Scrub is a function of IC height.

On a rough road the wheel path is not a straight line if there is scrub (see Figure 17.11). Significant amounts of scrub introduce lateral velocity components at the tire which, when added to the forward velocity, change the tire slip angles. This in turn will laterally disturb the car. The same slip angles will also add viscous damping to the ride motion.

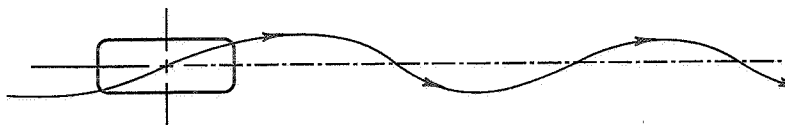


Figure 17.11 Wheel path on rough road with a large amount of scrub.

Side View Swing Arm Geometry

The side view swing arm (svsa) controls motions and forces in the fore and aft direction. Typical suspension parameters are anti-dive, anti-lift, anti-squat, and wheel path. The position of the svsa, ahead (or behind) and above (or below) the wheel center, are all possible solutions for front and rear independent suspensions. Typically, the instant center is behind and above the wheel center on front suspensions, and it is ahead and above on most rear suspensions.

“Anti” Features

The “anti” effect in suspensions is a term that actually describes the longitudinal to vertical force coupling between the sprung and unsprung masses. It results purely from the angle or slope of the side view swing arm.

Suspension “anti’s” do not change the steady-state load transfer at the tire patch. The total longitudinal load transfer under steady acceleration or braking is a function of the wheelbase (ℓ), CG height (h), and braking force (weight) \times (a_x/g) , as shown in the car freebody (Figure 17.12(a)). The actual change in wheel load, ΔLoad , is given by

$$\Delta\text{Load} \times \ell = W \times \frac{a_x}{g} \times h$$

$$\Delta\text{Load} = W \times \frac{a_x}{g} \times \frac{h}{\ell}$$

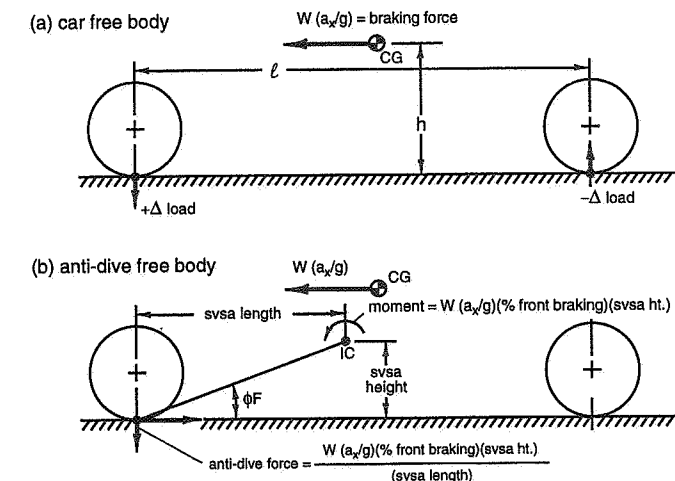


Figure 17.12 Derivation of braking anti features with outboard brakes.

The amount of suspension anti does, however, change the amount of load going through the springs and the pitch attitude of the car. Figure 17.12(b) shows a second freebody diagram for a car with the more common **outboard brakes** that describes the opposing forces from anti-dive and anti-lift geometry. The % brake distribution (or brake balance) determines the actual force as a fraction of the total longitudinal force; the % anti-dive on the front is given by

$$\begin{aligned}\% \text{ anti-dive front} &= \frac{m(a_x/g)(\% \text{ front braking})(svsa - \text{height}/svsa - \text{length})}{m \times (a_x/g) \times (h/e)} \\ &= (\% \text{ front braking})(\tan \phi_F)(e/h)\end{aligned}$$

For rear anti-lift calculation, substitute $\tan \phi_R$ and % rear braking.

Figures 17.13, 17.14, and 17.15 show the appropriate angle to use to calculate percentage anti for other cases. If a suspension has 100% anti, all the longitudinal load transfer is carried by the control arms and none by the suspension springs, so the suspension does not deflect when braking or accelerating. If a suspension has 0% anti, then all the load transfer is reacted by the springs and the suspension will deflect proportional to the wheel rate, none of the transferred load is carried by the suspension arms; 0% anti occurs when θ or ϕ in the figures equals zero.

The way that drive and brake torque is reacted by a particular suspension design alters the way in which you calculate the amount of anti present in the suspension. If the control arms react torque, either from the brakes or from drive torque, the anti's are calculated by the instant center location relative to the tire/ground contact point. If the suspension does not react drive/brake torque, but only the forward or rearward force (e.g., inboard brakes), then the anti's are figured from the instant center location relative

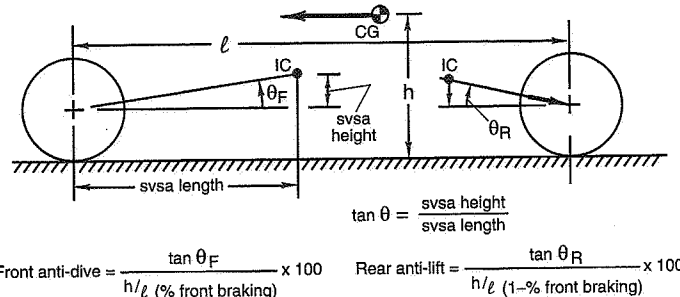


Figure 17.13 Braking anti features with inboard brakes.

$$F_{A-L} = F_{\text{Thrust}} \times \tan \theta$$

$$\% \text{ Anti-squat} = \frac{\tan \theta}{h/e} \times 100$$

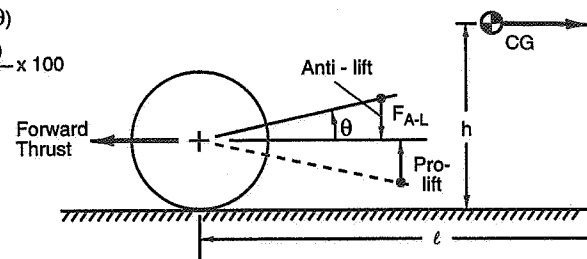


Figure 17.14 Front-wheel-drive anti-lift (or pro-lift).

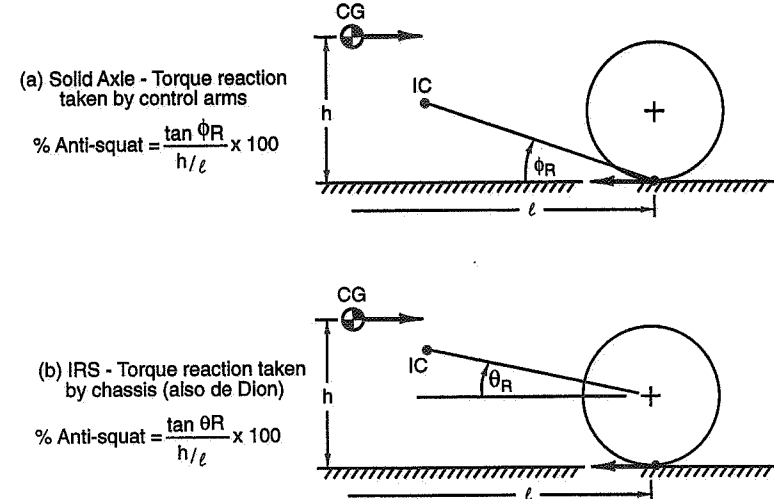


Figure 17.15 Rear anti-squat, (a) solid axle and (b) independent rear suspension.

- Anti-dive geometry in front suspensions reduces the bump deflection under forward braking (see Figures 17.12 and 17.13).
- Anti-lift in front suspensions only occurs with front-wheel drive and it reduces the suspension droop (droop is defined in Figure 17.1) deflection under forward acceleration (see Figure 17.14).
- Anti-lift in rear suspensions reduces droop travel in forward braking; the outboard brake case is shown in Figure 17.12. See Figure 17.13 for the inboard brake case.
- Anti-squat in rear suspensions reduces the bump travel during forward acceleration on rear-wheel-drive cars only (see Figure 17.15).

In each of the types indicated above, the anti feature was assumed to be positive and therefore always working in such a way that the pitch deflections of the whole car would be reduced. It is possible to have the geometry arranged in such a way that the longitudinal forces actually increase suspension deflections. This is called *pro-dive*, *squat*, or *lift*. Generally this is undesirable and is to be avoided for racing applications.

The anti-x features can develop a vertical force only when a longitudinal force is available. Therefore it is impossible to have any anti-lift on the front suspension of a rear-wheel-drive car. Likewise, there is no help from the side view geometry for rear squat of a front-wheel-drive car.

In addition to the actual location of the side view instant center at design height, we must be aware of how it moves with suspension ride travel. The length and angle of the svsa changes, and we must watch closely how much and in what direction the anti features change. For example, if you design in 30% front anti-dive but find that it falls to 0% with 0.75 inch of bump travel, you probably shouldn't have bothered with it in the first place.

Wheel Path

The path of the wheel center relative to the sprung mass in the side view is totally controlled (for "perfect" kinematics, no compliances) by the position of the instant center.

- If the IC is rearward and above wheel center height or forward and below, the wheel will move forward as it rises.
- If the instant center is behind and below wheel center or ahead and above, the wheel will move rearward as it rises.

The amount of curvature that the wheel center path has as the wheel rises or falls is totally a function of the swing arm length. The wheel path is not generally a concern in a race car, but on production cars the wheel center path affects the isolation capability when hitting impact bumps. The situation is similar to scrub but rotated 90°.

Caster Change Rate

Just like camber in the front view, caster changes in side view purely as a function of the length of the side view swing arm. There is very little reason to intentionally have caster change with suspension travel. What results is generally accepted as a function of some other parameter establishing the length of the swing arm. One result of caster change with suspension travel is that the bump-steer curve is more difficult to make linear throughout the total range of travel. For more information on bump-steer, see Chapter 19 on steering geometry.

17.4 Beam Type Axle Suspensions

As stated in the discussion on degrees of freedom and motion path, suspensions made with axles where the two wheels are tied together (by a tube, beam, or other rigid structure) have two motion paths relative to the body—parallel jounce and roll (see Figure 17.4). The parallel jounce axis is seen as a line in the rear view and as an instant center in the side view. The roll axis is seen in the side view as a line and in the rear view as an instant center of rotation. These two axes are what control the characteristics of this type of suspension.

Side View Swing Arm Geometry

The side view swing arm instant center of a beam type axle suspension controls the fore and aft forces and motions between the axle and the body. Typical parameters that are controlled by the side view instant centers are anti-lift, anti-squat, and the path the wheel follows relative to the body of the car. The components that control the side view geometry also take the driving and braking torque reactions, and the designer must comprehend these loads, which can be substantial.

Anti features for solid axles are similar to those discussed earlier for independent suspensions and include:

- Anti-squat (see Figure 17.15).
- Anti-lift (see Figures 17.12 and 17.13).
- Wheel path—As with independent suspensions the location of the side view instant center controls the motion of the wheel center. The length of the side view swing arm controls the wheel path arc; the height of the instant center controls the fore-aft to vertical motion ratio.

In general, the length of the side view swing arm should not be shorter than about 60 in. This is to minimize the possibility of power hop or brake hop becoming a problem. The rate of change of the swing arm length with suspension travel can create dynamic problems as well, so it should be made as long as practical, utilizing long control arms to slow down the rate of change of swing arm length.

Roll Axis Geometry

The roll axis concept is a bit different than the front view instant centers used in determining independent suspension geometry. With a beam axle we are concerned with the motion of the whole axle in roll, not just one wheel.

The roll axis for an axle is normally viewed in the side view so that it appears as a line. This line controls roll steer and roll center height. Solid axles have lateral-force to vertical-force coupling, similar to the “jacking” effect that occurs on an independent suspension, but it cannot be determined as simply as is conventionally done with independents (by looking at the roll center height).

The roll axis is found by determining the two lateral restraint points and connecting them with a line. Usually the geometry is viewed in the plan view to determine the forward and rearward lateral restraint centers of the roll axis. For example, the point where a Panhard bar crosses the centerline of the vehicle is a lateral restraint point. Plan view convergence points, of pairs of control arms that are basically in the same plane, become lateral restraint points.

A conventional four bar link rear suspension was common to many rear-wheel-drive American cars of the 1960s and 1970s and this design is shown in Figure 17.35. The roll axis of these suspensions is found by a double projection—first projecting the two lower control arms to a point in the plan view and then projecting that point back into the side view. The same is done with the upper control arm pair. The two points are then connected by a line in the side view. The slope of this line indicates the roll steer; the height of the line at the wheel center is the roll center height. There are many types of beam axle geometries and more will be discussed later. The determination of the roll axis is the key to understanding beam type rear suspensions.

Axle Roll Steer

The slope of the roll axis (rise/run = the tangent of the angle) is the roll steer value in percent, if you multiply by 100. If the roll axis tilts down to the front of the vehicle when viewed from the side then the suspension has roll understeer, for a rear suspension. If it tilts up to the front then the suspension has roll oversteer geometry. Another way to visualize what is happening is to realize that as the axle rolls relative to the body, the wheels move on a path that is at right angles to the roll axis. With roll understeer the wheel going into bump moves forward and the wheel drooping moves rearward. Because the wheels are connected by a rigid beam the forward motion in bump and rearward motion in droop means that the whole axle is steering relative to the centerline of the body.

Axle-Suspension Roll Center Height

The point where the instant-roll-axis of an axle suspension intersects the transverse-vertical-plane passing through the wheel centers is the location of the roll center. As with an independent suspension, this roll center is a theoretical point where a lateral force can be applied without a rolling moment being generated on the sprung mass.

With independent suspensions the roll center height is a direct measure of the lateral-vertical force coupling between the sprung and unsprung masses. With beam axles this is no longer true. The vertical-lateral force coupling is a function of the type and design of the lateral restraint elements.

As an aside, a lateral force applied at the roll center will, however, roll the unsprung mass (axle) on the tires unless the point of force application is at ground level; this “axle roll” does not occur with independent suspensions.

Lateral Restraint

There are numerous types of lateral restraint elements, some of which are shown in Figure 17.16. A pair of arms running at an angle so as to converge in the plan view is a lateral restraint device. An A-arm can be used, a track bar or Panhard bar, a Watt's linkage, a Jacob's ladder, and a pin sliding in a slot all qualify as lateral restraint devices. As the axle moves up and down relative to the body (or vice versa) it is desirable that it move on a straight vertical path. The A-arm, the pair of links, the Watt's linkage, and the sliding pin all provide linear motion. The Panhard bar is a link of finite length and therefore its end travels on a curved arc relative to its opposite end; the radius of curvature is the actual length of the bar. The longer the bar the closer it approximates linear motion. The sliding pin is not recommended as it may suffer lateral free-play and/or friction, unless it is cleverly designed. For simplicity, we have shown Panhard bars (track bars) in many of the following figures; in most cases, the Panhard bar could be replaced with a Watt's link or other lateral restraint.

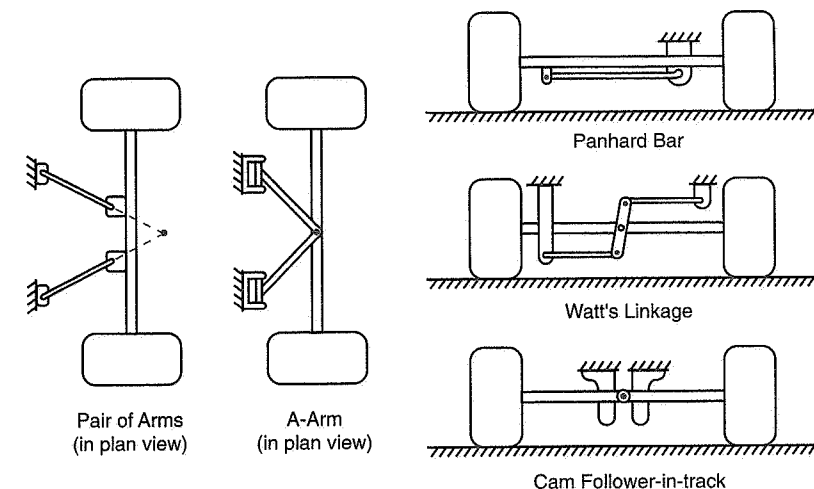


Figure 17.16 Lateral restraint devices.

Besides providing linear motion the restraint device must provide lateral force reactions between the sprung and unsprung masses. In so doing it is most desirable that the forces are transmitted only in a purely lateral sense, with no vertical component. For example, if a Panhard bar (track bar) is utilized, the slope of the bar in the rear view dictates the force coupling. If it is horizontal the coupling is zero. If it is sloped the coupling will either lift the sprung mass or pull it down depending on the direction of cornering and the slope of the bar. Some considerations in the design of a track bar include whether it is normally in tension or compression. For circle track racing, always turning left means that the bar should be attached to the body on the right side and to the axle on the left assuring that it is always in tension when cornering.

The pair of arms, the A-arm, and the sliding pin tend to have very low vertical-lateral coupling. The Panhard bar and the Watts linkage will always have some, but with attention to detail it can be minimized. This coupling effect must be controlled as much as possible because it tends to vary with the ride height and roll angle positions of the suspension. By keeping the angle small, the changes will be small and the effect minimized.

17.5 Front Suspensions

Introduction

Many types of front suspensions have been used over the years. They include various beam type axles with steering via kingpins at each end of the axle, the parallel trailing arm type such as the VW, the Morgan sliding pillar type, and the Chevrolet Dubonnet. In recent history, passenger car designs have come down to basically two types: the MacPherson Strut and the SLA (Short-Long-Arm).

This chapter will deal only with the last two mentioned as these make up the majority of front suspensions that will be encountered. The other types suffer from either high bending loads, poor geometry, high friction, or a combination of these problems. The best way to discuss each type is to go through the design process step by step. For each step a decision has to be made that is often a compromise. By discussing these decisions, hopefully a feeling for the limitations of the design will develop.

Front Suspension Design Issues—General

The first task in designing a front suspension of any type is to establish the packaging parameters that are fixed, or absolutely cannot be changed for whatever reason (see Figure 17.17). These should be listed so that they are not overlooked. The next task is to package the wheel, tire, brakes, and bearings. This is done in car position, so the track width has to be known. If it is not yet established, it should be made as wide as practical. This sounds evasive, but there are trade-offs in everything, even things as simple as choosing the track width. For example, what do the rules allow? What is the predominant race

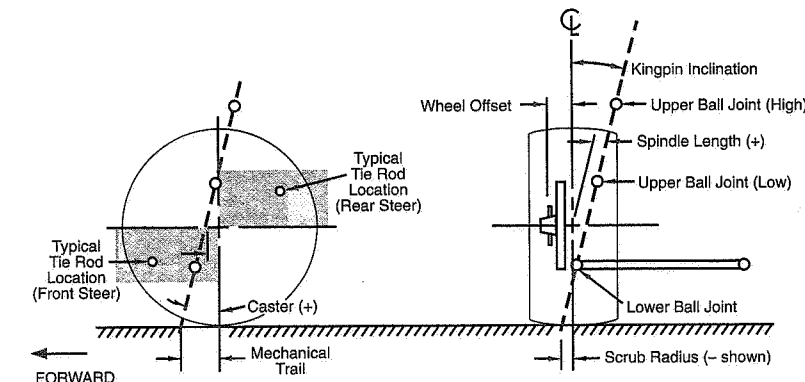


Figure 17.17 Front suspension packaging.

track type on which the car will run? Is top speed, thus low frontal area important? Are slow-speed tight street circuits of concern? All these issues can affect the decision on the basic track width!

Tire size and rim diameter and width must be settled. The specific wheel manufacturer needs to be known and a cross section of the wheel is desirable for optimizing the use of that wheel. Tire sizes are usually limited by the sanctioning body rules. In general, use all the tire they will let you get away with. Another point is to always design for the latest sizes being developed by the suppliers; this guarantees that the latest compounds and constructions will fit your car. Remember, the tire is the single most important chassis component on the car.

The wheel offset is worked out in conjunction with fitting the brake caliper to clear the inside surface of the wheel. Once the caliper is located, this automatically locates the brake rotor. With the rotor location comes the absolute farthest outboard location for the lower ball joint. Wheel bearings need to be looked at soon, as ideally they should be located such that the tire center is between the two rows of balls or rollers (to minimize loads on the bearings).

Now that the lower ball joint cross car boundary (lateral position) has been set, the height of the lower ball joint comes next. In production cars it must be above a 5-in. wash rack clearance requirement, but on race cars it should be made as low as possible for structural reasons. Usually there is no rule but some practical considerations such as deflated tire ground clearance might be in order. If it is totally inside the wheel all it has to do is clear the wheel and the brake rotor under all travel and load conditions.

The decision about the kingpin angle in the front view is the next order of business. The issues here become scrub radius, spindle length, and kingpin angle. They are interrelated

and a compromise is needed. If you want a certain scrub radius you now have two points established, i.e., the lower ball joint and the ground contact point of the kingpin (set by the scrub radius)—the kingpin angle becomes fixed automatically. If you want a certain kingpin angle then the scrub radius will not necessarily be what you want. Basically, on rear-wheel-drive cars push the lower ball joint out as far as possible and run a fairly low kingpin angle, less than 8° , and accept the scrub radius that results. If you are dealing with a front-wheel-drive car you **must** minimize the spindle length and have a negative scrub radius. This may result in a kingpin angle as high as 16° , but you will have to accept it or find another clever way around it.

Kingpin angle affects the performance of the car when the wheels are steered. One concept that should be understood is that the more the kingpin angle the more the car is lifted when it is steered. This is one source of steering returnability, the weight of the car returns the steering to center. The amount the car is lifted is also a function of the spindle length where a longer spindle means more lift.

The camber of the wheels when steered is a function of the kingpin angle and the caster angle. With no kingpin angle (and no caster angle) there is no camber change with steer lock. As kingpin is added (but still no caster) the wheel will “lose” camber with steer lock, or in other words it will change in a direction giving positive camber on the outside wheel.⁶⁰ As caster is added this modifies the effect of kingpin. With positive caster and no kingpin angle, the wheel gains negative camber on the outside wheel and positive camber on the inside wheel. Thus caster can add favorable camber angle to the effects of kingpin angle. In other words, the reason that low kingpin angles are desirable is that kingpin angle subtracts from the negative camber gain due to caster on the outside wheel.

The decision on a rack location depends on several packaging factors such as engine location and orientation, front-wheel drive vs. rear-wheel drive, whether it is to be high- or low-mounted, etc. In addition there are performance reasons for choosing the rack location. First we must assume that every structure is a spring and should be treated as such. As an example the rack mounting stiffness versus the upper or lower control arm mounting stiffness to the chassis will not necessarily be the same. Therefore, when a cornering force is applied, any difference in the lateral displacement of the ball joints in relation to the tie rod outer pivot will cause a steer angle. To assure stability it is better to have lateral force deflection toe-out (lateral force understeer) rather than toe-in. We can assure that this happens by the proper location of the rack. If a high-mounted rack is required it must be behind wheel center and if it is low-mounted then it must be ahead of wheel center as shown by the shaded areas in Figure 17.17.

Structural requirements for the suspension design must always be considered when packaging each element of the total system. Control arms that have one leg straight across from the ball joint are superior in system stiffness to arms that are splayed. Establishing

linkage ratios for the spring, shock, and stabilizer bar as close to 1:1 as possible will provide more direct load paths thus improving system stiffness while providing a lighter overall design.

Front Suspension Design Issues—SLA

The Short-Long Arm (SLA) suspension is the choice of designers without question for its ability to meet desired performance objectives with minimum compromise.

The design starts with the basic package as described above. The details of the track width, the wheel size, the tire, the brakes, etc., bring about the location available for the lower ball joint. The upper ball joint is located either via kingpin angle requirements or by scrub radius requirements. There is a little more freedom with the SLA that is not available to the strut design and that is the choice of a short knuckle or a tall knuckle.

The *short knuckle* means the upper ball joint is located basically within the diameter of the wheel. With high offset and large-diameter wheels the kingpin angle can be kept small (while achieving small spindle lengths and scrub radius) by tucking the upper ball joint into the wheel.

To reduce the loads on the control arms and other suspension components, it is desirable to have a long kingpin length, that is, separate the upper and lower ball joints as much as possible. Depending on details of the installation, the short knuckle may yield less than optimum kingpin length. The other alternative is the *tall knuckle* where the upper ball joint is above the tire. In the tall knuckle design the ball joints naturally have a very large span and thus reduce reaction loads. This option also allows reasonable kingpin angles while achieving desired spindle length and scrub radius. Another advantage for the tall knuckle is that build errors will result in smaller geometry errors than with short knuckle designs. Some negatives to the tall knuckle, of course, are the added structural requirements of the knuckle, and the limitation of never changing tire size or width without widening the track and increasing the spindle length and scrub radius after the design is completed.

With the upper and lower ball joint locations established, the tie rod outer point should also be set per the requirements established in Chapter 19 on steering geometry.

Front View Geometry

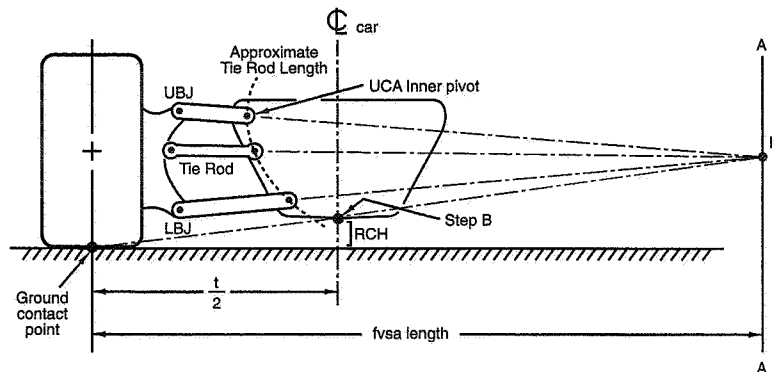
The front view geometry can now start. The front view swing arm instant center is uniquely determined by the desired roll center height and roll camber (see Figure 17.18). The desired roll camber sets the front view swing arm length (location of line A-A) as follows:

⁶⁰ That is, the wheel further from the turn center.

$$fvsa = (t/2)/(1 - \text{roll camber})$$

where t = track width

Roll camber = $\frac{\text{wheel camber angle}}{\text{chassis roll angle}}$ (with both measured relative to the road)



Step A—Establish front view swing arm length (line A-A')

Step B—Establish roll center location and project from ground contact point through RC to line A-A', establishing IC

Step C—Project lines from outer ball joints to IC

Step D—Choose control arm lengths to get inner pivot locations

Step E—Connect tie rod outer pivot to IC

Step F—Establish tie rod length.

Figure 17.18 SLA front view geometry.

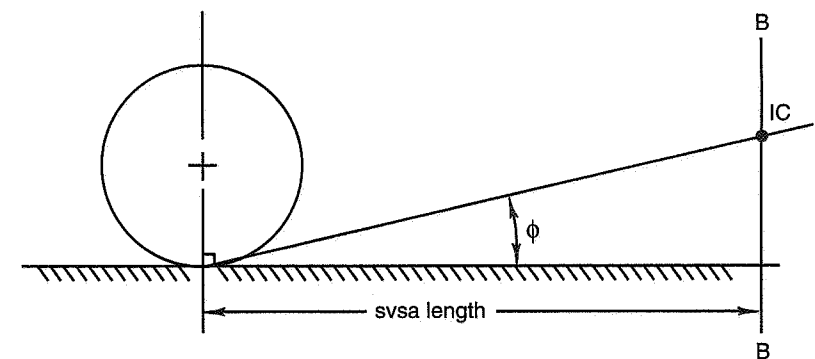
The front view instant center height is set by projecting a line from the tire center ground contact patch through the desired roll center height. The instant center must lie on this line. Now we can project lines from both ball joints to the instant center. These become the centerlines of the upper and lower control arm planes as projected into the vertical plane through the wheel center. Packaging requirements will establish the length of the lower control arm but it should be made as long as possible. The length of the upper control arm in relation to the lower arm adjusts the shape of the camber curve. If they are the same length the camber versus wheel travel curve will be a straight line. If the upper is longer than the lower, the curve will be convex with its curvature toward positive camber. If the upper is shorter than the lower, the curve will be concave toward negative camber. As the upper is made progressively shorter, the curvature increases. The ideal curve has progressive negative camber in bump with much less camber change

in droop. Some designers try to get the camber to go positive in droop and progressively negative in bump.

To finish the front view geometry, the tie rod and rack location should be roughed in. This is done by projecting a line through the tie rod outer point (established in Chapter 19 on steering) and the front view instant center. The correct tie rod length is then established for a linear ride toe curve. This length will be modified after the side view geometry is completed, but doing it now is a good idea to help plan a realistic rack location.

Side View Geometry

The side view geometry comes next in this design process. Remember that when we are dealing with the “side view geometry” we are looking at the side of the car but the point of interest that we are creating, i.e., the “instant center” is in the **plane of the wheel**. The desired instant center is established first. This is a result of calculating the desired anti features, the minimum side view swing arm length that is acceptable, and whether the wheel path must be receding in bump or not. Figure 17.19 is a graphic illustration of how this is done. Sometimes the desired parameters will conflict. For example, with front-wheel drive, anti-lift and a receding wheel in bump are incompatible. Another common compromise occurs when a high value of anti-dive is desired along with a large amount of wheel recession in bump. This usually yields a side view swing arm length that is too short to be practical. So the factors that are controlled by the side view instant center location have to be carefully assessed before the final point is chosen.



Step A—Angle ϕ establishes anti-dive

Step B—svsa length gives line B-B'

Side view IC is the intersection of steps A and B.

Figure 17.19 SLA side view geometry.

Once the instant centers are established, how does the designer guarantee that the geometry will actually provide the correct front view and side view instant centers? This is the next subject in the design process.

SLA Control Arm Inner Pivot Axis Construction

Two rules of descriptive geometry are used to coordinate the front view and side view. They are 1) three points determine a plane, and 2) the intersection of two planes forms a straight line. For the SLA and other suspensions the layout procedures will be given. Projection techniques of descriptive geometry are used to determine the A-frame planes such that their intersection forms the desired instant axis. No further theory of descriptive geometry is given here.

The front view upper and lower control arms that have been developed so far are really only a line in the transverse plane of the wheel at this stage of the design. We have not determined the actual positions for the front and rear inner pivots of these arms. We do know that whatever we do in the side view, we do not want to lose what we developed in the front view. The next step then is to extend the control arm lines in the front view outboard until they intersect the longitudinal plane of the wheel. Looking now in the side view, straight lines are drawn from these new control arm extension points to the predetermined side view instant center. In Figure 17.20 we will follow this procedure for clarity. For an actual layout, full-size drawing is necessary to maintain accuracy.

In front view, the upper control arm inner pivot is point #1, the upper ball joint is point #2, and the extension into the longitudinal plane is point #3. For the lower control arm the corresponding points are #11, #12, and #13. These six points are transferred to the side view. Two lines in the side view from the side view instant center should be extended through and beyond points #3 and #13. Next we choose an arbitrary point in the side view on the line between the IC and point #3 that is a few inches ahead of point #3 and number it point #4. Repeat this procedure for the lower arm creating point #14. Next we project these points into the front view so that both the side view and the front view contain points #1 through #4 and #11 through #14.

To maintain the desired geometry all upper arm points (#1 through #4) must be in a single plane, and all lower arm points (#11 through #14) must be in a single plane. As long as we always project straight lines through two points in a plane and establish new points on these lines, the new points will remain in the plane. Next we project a line from point #4 through point #2. This is done in both views and the line is extended in the front view at least as far inboard as point #1. Repeat for the lower arm using point #14 through #12 inboard at least to point #11.

For almost all suspension designs it is acceptable and even desirable to have the inner pivots of the control arms parallel to the centerline of the car. Therefore the next step will be to draw a vertical line through point #1 in the front view; this line is the front pro-

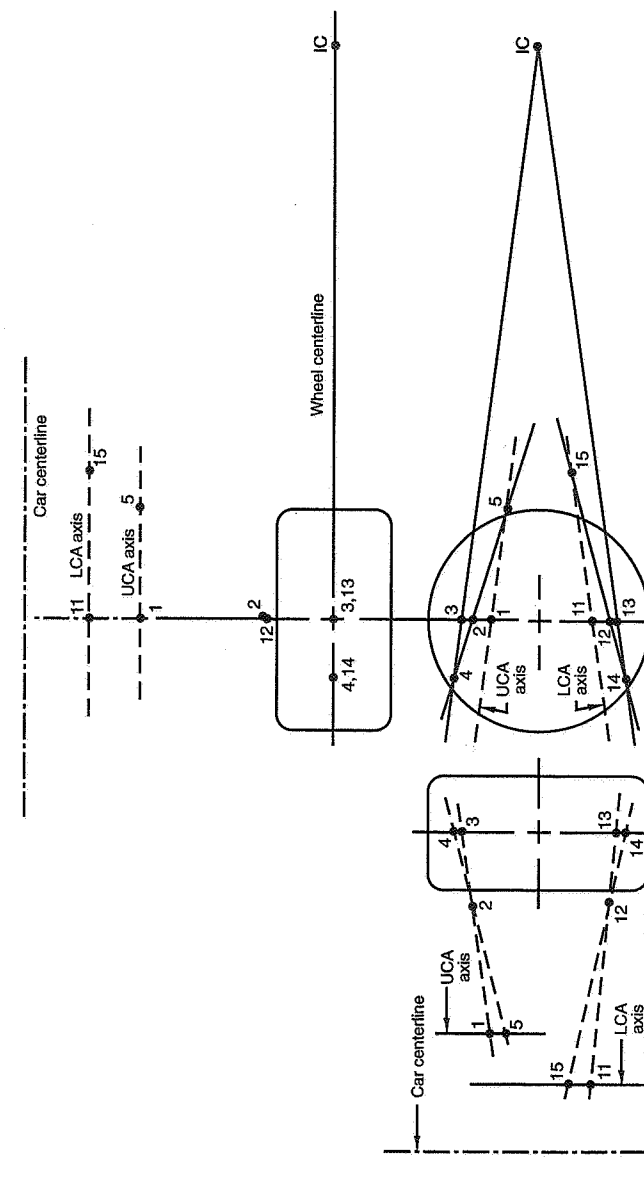


Figure 17.20 SLA control arm inner-pivot-axis layout.

jection of the upper control arm (uca) axis. Identify point #5 on this vertical line as the extension of a line from points #4 through point #2. Repeat for the lower control arm (lca) via a vertical line through point #11, finding point #15 from #14 through #12. Next project points #5 and #15 into the side view. Draw a line between #5 and #1 and between #15 and #11 (shown dashed in the side view). The control arm inner pivots must lie on these lines. They can be spread wider or narrower than the points but they must fall on the lines.

Referring back to Figure 17.6 we can now redraw it as Figure 17.21 to show that the uca and lca define two planes that intersect and form the instant axis for the suspension. It is left to the reader to extend the construction to include the desired caster (side view) angle of the steering (kingpin) axis.

The design is now complete except for fine-tuning the tie rod to obtain a linear ride-toe plot (ride steer).

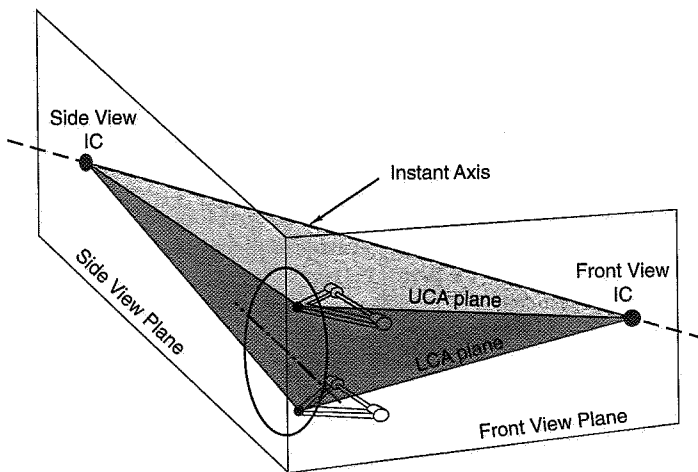


Figure 17.21 Choice of instant axis determines the control arm planes.

Front Suspension Design—MacPherson Struts

A MacPherson strut suspension can be thought of as a special case of an SLA. Instead of an upper control arm there is a strut, and, as described in the first section on kinematics, the strut is a slider or an infinitely long upper control arm. This long upper arm yields a camber curve that loses rather than gains negative camber in bump. This is one of the major compromises of the strut-type suspension, especially for performance applications.

To continue with the design process we start as we did with the SLA in establishing the wheel and tire sizes and locations, the brake caliper and rotor, and finally the lower ball joint cross car limit and height limits (refer to Figure 17.22). The upper strut to body mounting point is the next item established. It is the point about which the strut can rotate in all directions, but is fixed from translating in any direction. On passenger cars this is normally a rubber isolator mount. On race cars it is usually a monoball (spherical) type mounting.

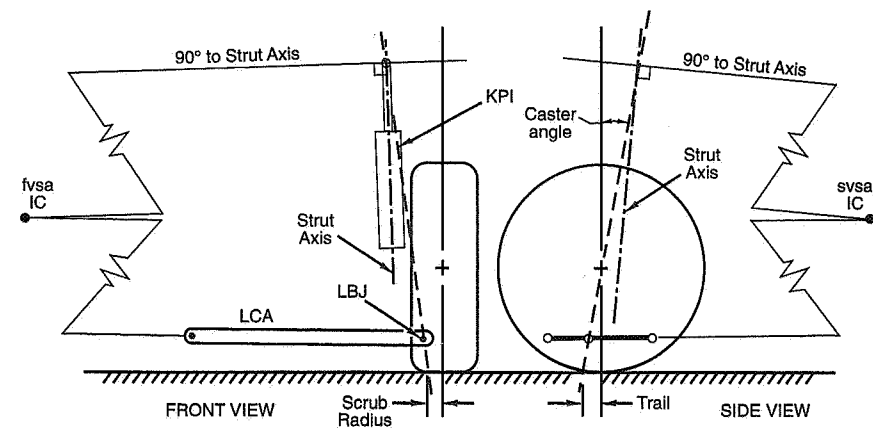


Figure 17.22 MacPherson strut layout.

The upper strut mounting point lies on the kingpin axis by definition. We choose a kingpin angle per the earlier discussion. Its position, heightwise, is a function of the particular strut that is being used, whether the spring is mounted on the strut or not, and how much wheel travel is to be allowed. An important point to make is that the axis of the strut is not necessarily coincident with the kingpin axis! The kingpin is the steering axis while the strut stroking axis dictates other suspension parameters to be discussed next.

A lower control arm is established by placing the ball joint as one point in the front view and aiming the other point at the desired instant center. The length of the arm is established by other packaging constraints, but in general it is best if it is long. Next the strut orientation in the front view is adjusted so that its centerline is 90° to a line from the instant center to the upper strut body mounting point. Depending on the hardware used and the packaging constraints this may be very easy, but often there is an incompatibility of component locations and desired geometry.

You will find that only certain realistic combinations of roll center heights and swing arm lengths will fit. This means that often a strut-type suspension has compromised geometry because it is a strut!

The steering tie rod outer point is chosen for reasons affecting Ackermann and other steering geometry issues. Once this is established the inner point height is located such that a line from the outer point through the inner point passes through the front view instant center. The length of the tie rod is then chosen to give a linear ride-toe curve. (See Chapter 19 on steering.)

With the front view completed we move to the side view. Again the first thing that must be established is the parameters that are affected by the side view instant center location. From the first part of this chapter we know these are the anti-dive, anti-lift, caster change, and wheel path. The establishment of these parameters uniquely defines the length and height of the instant center. Using the same procedure as described for the SLA, the lower control arm plane is projected into the longitudinal wheel plane giving a line in the side view that extends through the desired instant center. Next a line from the instant center to the strut body mounting point is drawn. The strut is now adjusted so that a plane 90° to the strut axis intersects the wheel plane, forming a line through the instant center. See Figure 17.22 for a further explanation of this concept.

One feature that makes struts hard to design is that you always have to work with a plane 90° to the strut slider axis in both views. Because of this, when you tilt the axis in one view it changes the tilt in the other view. So when you have done the front view and then gone to the side view you must go back to the front view again because it is no longer correct. These steps are repeated a few times before the final solution is confirmed. Even with a computer program to help, you still need to check both views and recheck them after any minor adjustment to the strut axis.

When the instant axis is finally established the bump steer can be finalized. The tie rod point chosen earlier while first working in the front view was to establish initial potential locations for the rack with respect to the overall package. The bump steer is best done by a computer program. The theory of how to get proper bump steer is covered in Chapter 19.

A few other points that should be checked during the design process are strut travel to wheel travel ratio, spring to wheel travel ratio, and spring centerline axis location to minimize strut bending loads. If the spring acts on the lower control arm, the strut bending moment will be equal to the vertical load on the wheel times the horizontal distance from the lower ball joint to the wheel center. When the spring is mounted on the strut, the centerline of the spring is projected downward to intersect with the lower control arm axis. If this intersection occurs in line with the wheel center there will be no bending loads in the strut (see Figure 17.23). This should be checked in both the front view and the side view. As the intersection deviates from ideal the bending loads grow. Bending loads create friction and friction is an absolute enemy of suspension function.

Ref. 169 discusses the problem of strut bending loads (and resultant friction) and the problem of packaging the spring at the correct angle (Figure 17.23) when wide tires are used. The reference discusses a novel spring used in a number of new production cars—in its free length state, the axis of this “side load spring” is bent (or curved) in the front

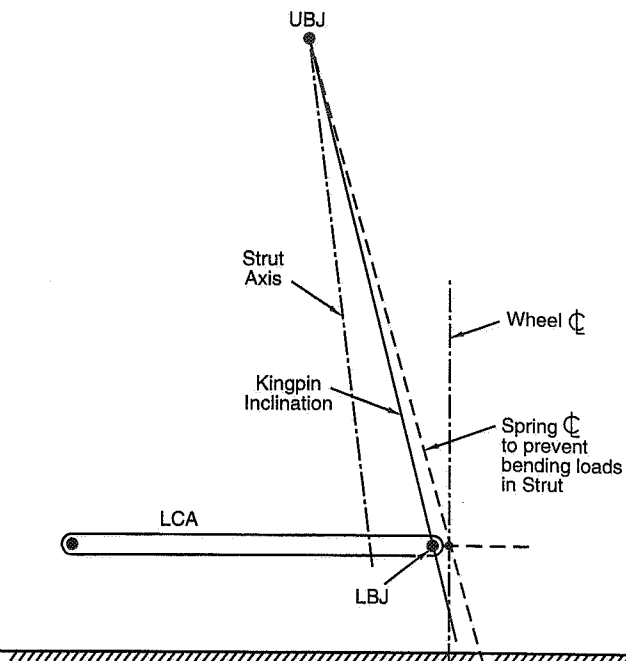


Figure 17.23 MacPherson strut spring location to minimize bending.

view. When this spring is compressed, the spring force is offset from the spring axis; this is equivalent to tilting the spring but reduces the spring/tire clearance problem. Springs of this sort introduce some new problems for the suspension tuner. First, they must be installed correctly (in top view rotation) or the offset force will be in the wrong direction—special spring perches must be used. Second, if springs are changed on a car originally fitted with side load springs, the replacement springs should be of the same type to avoid excessive strut friction. Alternatively, smaller coil diameter can be used and the spring perch moved outboard to achieve the correct geometry.

Summary—Front Suspensions

After the instant centers are set to achieve the desired geometry, clearance checks of the hardware interacting in all possible combinations of wheel travel and steer must be made. If there are interferences, either the hardware must be changed or the geometry must be redone to fit the hardware.

With a thorough understanding of this step-by-step design process it should now be possible to analyze the geometry of any front suspension that presents itself. Assuming one knows where to locate the instant centers (hence, instant axis), it is possible to use these procedures to determine locations of the suspension components.

17.6 Independent Rear Suspensions

Introduction

Rear suspensions can be broken into three basic categories: independents, beam axles, and twist axles. Previous sections contained discussions about independents and beam-type axles in a general sense. This section will concentrate on discussing several specific independent rear suspensions and how to analyze and design them. In these discussions, detailed comments with regard to the application and performance limitations will be made. The following sections will discuss beam and twist axle rear suspensions.

Three basic categories of independents are relevant: trailing arms, MacPherson struts, and SLAs.

Trailing Arm Types

Pure Trailing Arm

This suspension is a very simple hinge mechanism shown in Figure 17.24. The wheel is attached to the trailing end of an arm that pivots relative to the sprung mass by two bushings. The axis of the bushings is perpendicular to the centerline of the car and parallel to the ground forming the "instant axis" of the suspension. The side view instant center is at the bushing axis while the front view instant center is at infinity. The geometry that results from this mechanism is very simple and quite limiting. In the front view the roll center is on the ground and there is no camber change with wheel travel. In the side view the instant center height is the only variable available, while the length is fixed. This means there is some adjustment to the anti-lift and the wheel path in bump. There is no toe change at all so the roll steer is zero. Cornering forces will cause bushing and arm deflections that produce toe-out, which is an oversteer effect. In terms of the number of links used there is only one, the arm. This puts heavy structural requirements on this arm which must be strong in bending in all directions to resist braking torque, camber torque, and steer direction torques.

Semi-trailing Arm

This is similar to the pure trailing arm, the only difference is that the bushing axis (and "instant axis") now can run at an angle in all three views, as shown in Figure 17.25. The plan view angle means that the bushing axis will intersect the front view plane at a point

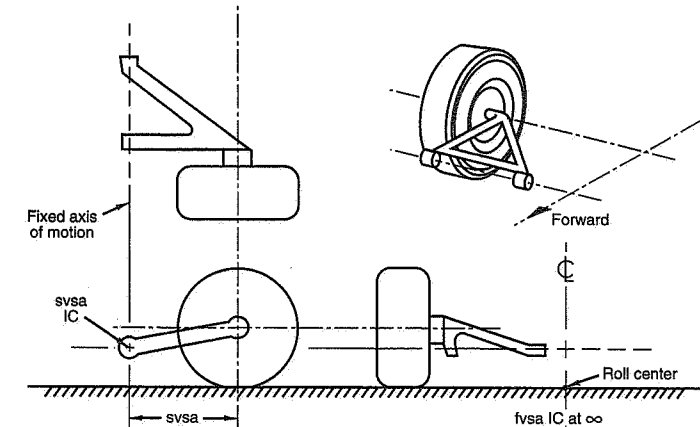


Figure 17.24 Trailing arm rear suspension.

inboard of the wheel, thus establishing the front view instant center. This instant center is fixed relative to the car and therefore the camber change is constant with wheel travel. The roll center is found by conventional means and can either be above or below ground level. With the instant axis angled in plan view the toe curve will never be a straight

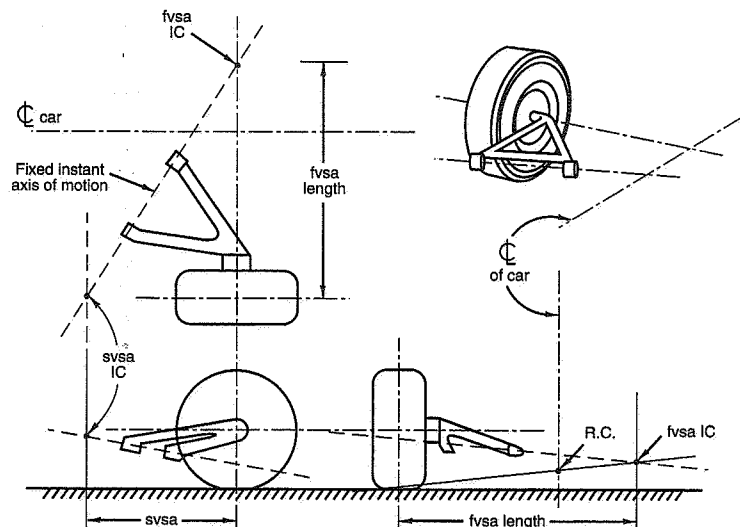


Figure 17.25 Semi-trailing arm rear suspension.

line; it will typically toe-in, both in bump and droop. The amount of toe change is a function of the plan view angle of the bushing pivot (instant) axis. Geometrically this suspension has two basic faults: the camber change is a straight line and the toe change is a curved line. We generally desire exactly the opposite in a good suspension!

Swing Axles

The swing axle rear suspension is a form of semi-trailing arm that has a large plan view angle instant axis (see Figure 17.26). The axis passes through the inner pivot joint of the half shaft, therefore only one universal joint is required. The resulting geometry has a very high roll center, large camber change, and severe toe-in with wheel travel. In the days when this suspension was invented the low cost and simplicity were very attractive while the negative consequences on the vehicle dynamics were poorly understood.

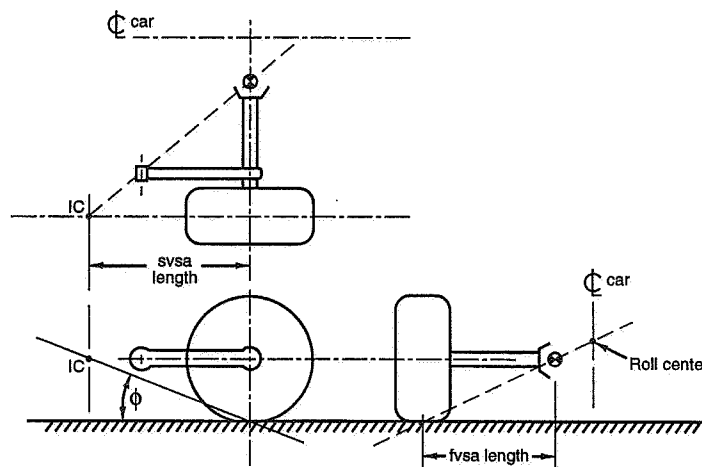


Figure 17.26 Swing axle rear suspension.

This suspension has large jacking forces resulting from its high roll center. Cornering forces raise the back of the car, and because of the large camber change with wheel travel, the outside loaded tire goes toward positive camber, further reducing the cornering power of the rear of the car—an oversteer effect to say the least. The jacking up of the rear also increases the weight transfer because it raises the vehicle center of gravity, thus further reducing cornering capability.

This suspension was first improved upon by Mercedes with their "low pivot" swing axle design. The lowering of the roll center brought dramatic improvements even though the

camber and toe relationships were not significantly altered. The development of the "semi-trailing arm" suspension discussed above was the next evolution away from the swing axle. The semi-trailing arm suspension (and low pivot swing arm) is quite a bit more expensive than the swing axle because half shafts must have provisions to change length with suspension travel. The evolution of these first independent suspensions parallel the evolutionary understanding of vehicle dynamics.

Pre-84 Corvette Type

As a further evolution of the basic swing axle suspension, the Corvette IRS used up to the 1984 redesign is an interesting example as shown in Figure 17.27. The semi-trailing arm concept is still there with the front view swing arm further lengthened by using two links, the fixed-length half shaft and the lower "camber link" as it is called. The side view swing center is still controlled by the single trailing arm that is rigidly part of the knuckle. This arrangement still has the toe versus wheel travel characteristics of the semi-trailing arm, i.e., toe-in with both bump and droop. The major improvement is the significant lengthening of the front view swing arm which slows down the camber change with ride travel.

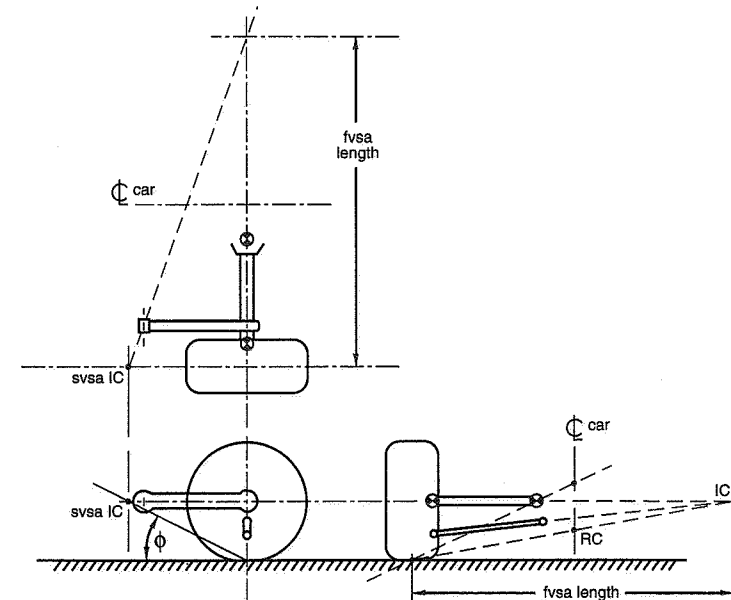


Figure 17.27 Pre-84 Corvette rear suspension.

Instant Axis Concept

All independent suspensions have an instant axis. The discussion above on trailing arm suspensions represent the simplest forms which have the actual bushing axis forming all (or part) of the instant axis. With these types the axis does not change with suspension travel.

The following sections will be describing more complicated designs but the concept is always the same. The instant axis is determined from the front view instant center and the side view instant center. All the suspension parameters are then determined from the instant centers, plus the toe curve must be optimized. All of the following designs will have changing instant axes with wheel travel.

MacPherson Strut Rear Suspensions

In the section on front suspensions a detailed method for achieving certain static design factors with struts was covered. That particular type of strut suspension had an A-arm and tie rod to form the kinematic system. That is very typical and actually the only realistic way to design strut front suspensions. With rear suspensions many more options exist because large steer angles and a specific kingpin and scrub radius, etc., are not absolutely required for proper function. The following designs are representative of several variations of struts done in the rear of a car.

Reversed A-arm and Trailing Link Strut

As the name implies, the kinematics involve an A-arm with the point of the "A" at the inboard attachment to the chassis and the two legs attaching to the knuckle. A trailing link runs longitudinally from the chassis to the A-arm or to the knuckle (see Figure 17.28(a)). The toe is controlled by the A-arm and its single point attachment to the chassis. This results in a toe curve very similar to semi-trailing arm suspensions where it will toe-in with both bump and droop travel. This design has good camber stiffness and fore-aft stiffness with a minimum number of chassis attachments spread over a wide base. The ability to obtain desired values for roll camber, roll center height, and anti properties are quite free within the general limitations of basic strut suspensions as discussed earlier. Another negative feature is that if rubber bushings are utilized at the trailing link pivots, toe-out will occur whenever a rearward load is applied to the tire such as braking or hitting a bump. The side view instant center will move with wheel travel because of the trailing link, thus changing the anti features with wheel travel.

A-arm and Toe Link Strut

There are two potential versions of this rear suspension, one being exactly like a typical front suspension but with a fixed toe link to a chassis grounded pivot. In terms of gen-

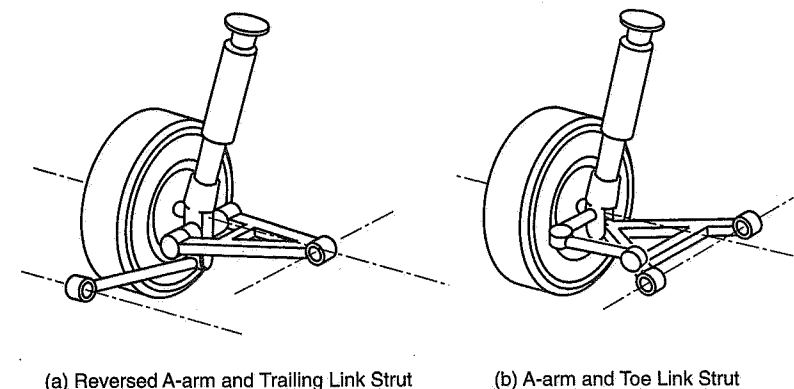


Figure 17.28 Rear strut suspensions—I.

eral geometry this type of design is very flexible with good control over the side view geometry, excellent toe control capability, and only the standard strut limitations in the front view. The rate of change of side view geometry is very controllable.

The second version of this type of strut has the toe link attaching back to the control arm rather than the chassis. This second type is shown in Figure 17.28(b). This design eliminates one attachment at the chassis. It is possible to obtain favorable toe control with this system, and all other geometry requirements can be met similar to the first basic version. One of the reasons this suspension is used is that the ride steer curve is less sensitive to build variations than with the standard toe link attached to the chassis.

H-arm Strut

An H-shaped arm having two bushings at each end will kinematically perform the jobs of three links (see Figure 17.29(a)) similar to the A-arm and toe link. There are limitations, however, when links are combined into structural members. In this case the axis of the inner bushing pivots must be perpendicular to the axis of motion of the strut at all times or bending of the strut will occur. With this limitation comes some side view geometry limits that cause long side view swing arms and very low values of anti-lift. It is unavoidable with this type of design. Roll steer is obtained by having the two bushings at the knuckle end of the arm out of plane. In other words if you think of the inner two bushings and one of the outer bushings representing three points that determine a plane, the fourth bushing intentionally does not lie in that plane. As the control arm pivots about the two inner bushings the two outer bushings start out at different heights, and therefore as they rise in their arcs the amount that they move inboard is different. By controlling this difference in inboard motion the amount of toe change with wheel travel can be controlled.

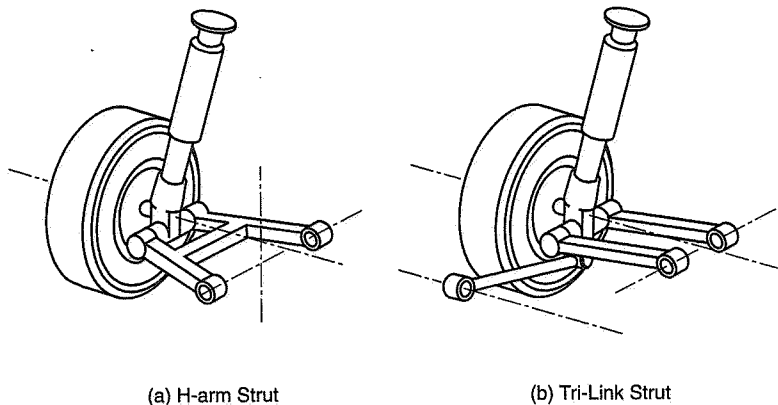


Figure 17.29 Rear strut suspensions—II

One negative factor of this design is that any flex in the arm or distortion of the bushings due to braking loads or bump loads causes side loading on the strut. With strut side load comes friction or resistance to axial motion. The suspension cannot isolate and perform all of its other functions properly when friction is present. This suspension has been thought of as a lower-cost version of the A-arm and toe-link. It almost is, but not quite because of this potential for causing friction.

Tri-Link Strut

A strut suspension with three individual tension-compression links is known as the tri-link strut (see Figure 17.29(b)). Along with the strut, the two lateral links control the toe and front view geometry while the single trailing link controls the side view. The two lateral links are usually not equal in length, a requirement for a linear toe curve. This type of suspension has good freedom for decoupling parameters without causing friction. The rate of change of side view geometry is a function of the length chosen for the trailing link. The front view geometry is as controllable as any strut. An advantage this suspension has for production cars is in the area of enhanced isolation. By installing soft bushings in the trailing link, which allows the wheel to move rearward while negotiating bumps, harshness is taken out without causing toe changes or upsetting the handling. The two lateral links act as a parallelogram and thus do not cause steer with longitudinal wheel motions.

SLA Rear Suspensions

SLA stands for short-long arm which is a generic name for a family of suspensions that have upper and lower control arms with the upper arm shorter than the lower. These

arms can be A-arms or individual links. This family of suspensions is generally regarded as the most flexible in achieving desired overall geometric parameters with the least amount of compromise. The detailed design method was described previously. Some variations of the common theme of the SLA are described below.

Double A-arm and Toe Link

This is the most common form of front suspension and can be used as a rear suspension very easily. The toe link is grounded to the chassis (instead of attaching to a rack) as shown in Figure 17.30(b). If a front suspension were to be used as the rear suspension this style is easy to adapt with one important consideration. The left front components should be installed as the right rear corner and the right front as the left rear. The reason these are “turned around” is that geometric toe considerations for front suspensions are exactly opposite of what is required for a rear suspension to give roll understeer.

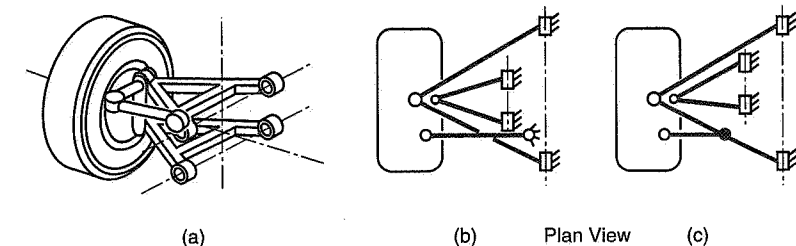


Figure 17.30 SLA rear suspension—double A-arm and toe link.

A minor variation of this design is the case where the toe link does not attach to the chassis; rather it is attached to either the upper or the lower control arm (shown to the lower arm in Figure 17.18(c)). This can be contemplated only when the toe link outer pivot is very close to the same height as the ball joint. This is called "an ungrounded" toe link. The ride toe characteristics are not always obvious on this type, especially when there is significant caster change present. For best results a computer simulation should be used.

Upper A-arm with Three Links

Sometimes a lower A-arm is not practical for packaging reasons. An equivalent suspension geometry using three individual straight links in place of a lower A-arm and a toe link along with an upper A-arm can provide very good geometry. The links can be arranged basically in two configurations (see Figure 17.31(a) and (b)), a trailing link and two lateral links, or two nontrailing basically lateral/diagonal links and another lateral link acting as a toe link. The trailing link arrangement will have more of a problem get-

ting the toe curve to be linear, and will have other parameters controlled by the side view swing arm that will change with ride travel. This may not be desirable. When the two lateral diagonal links are used, a virtual center (point "A" in Figure 17.31(b)) is created farther outboard in the wheel than a ball joint can physically be located. This feature can be an advantage in achieving a negative scrub radius and/or a short spindle length.

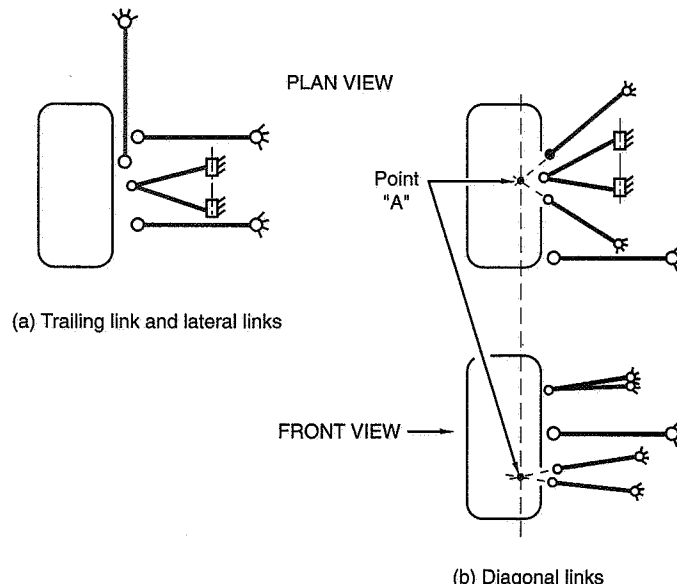


Figure 17.31 SLA suspensions—upper A-arm with three links.

Lower A-arm and Three Links

A system basically opposite of that described above is also a viable suspension in the SLA family. In this case the upper arm is formed by two of the links. Again a virtual center may be created to achieve a particular feature that is unobtainable with a ball jointed A-arm. The use of one link trailing and the other straight lateral is also possible but not generally recommended.

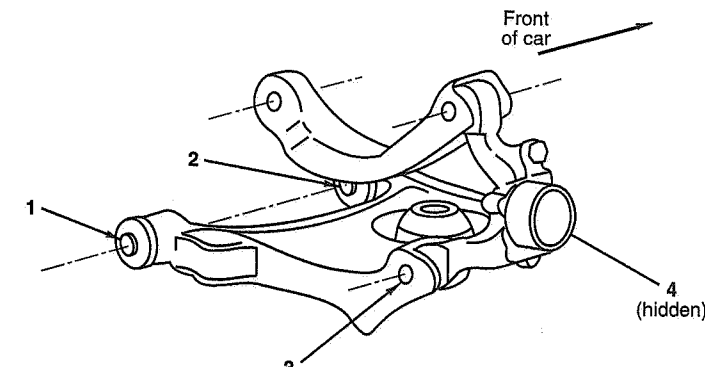
H-arm and A-arm

An H-arm functions as three links in this example and is similar to the A-arm with an ungrounded toe link (see Figure 17.30(c)). It can be used either as an upper arm or a lower arm in a rear suspension. When it is used, the inner pivot axis of the H-arm must be par-

allel to the inner pivot axis of the A-arm or else binding will occur with suspension travel due to the attempt to rotate the knuckle (caster change) thus twisting the H-arm. This means the side view swing arm instant center must be at infinity, thus making it difficult to obtain high values for anti features. This is a limiting factor for the use of H-arms in general. A potential cost advantage of the H-arm is that it requires only two chassis reaction points instead of three to perform its controlling functions.

H-arm Lower and Camber Link

The use of an H-type lower arm and a single lateral upper link is a special case where the H-arm is being asked to perform the function of four links instead of just three. It accomplishes this by reacting all braking loads as a torsional input. Reactions to all wheel center inputs in the longitudinal direction end up putting the H-arm in torsion over its length. The structural requirements of the arm become quite different in this case. The single upper link acts only in the front view and contributes to the determination of the front view instant center. The side view geometry is controlled totally by the H-arm inner pivot axis. It is determined in the same manner as the semi-trailing arm. A version of this rear suspension is used in the 1989 Thunderbird (see Figure 17.32).



H-Arm has four rubber bushings.

Figure 17.32 Thunderbird rear suspension—H-arm and camber link.

Five-link

A system utilizing five individual links can make a very satisfactory suspension. The placement and orientation is similar to the three-link and A-arm mentioned above with the A-arm now formed by two links; two variations are shown in Figures 17.33 and

17.34. The kinematics are very flexible with this type of design where the issue is to get the front view kinematics desired without compromising the side view geometry. Another major reason for doing a five-link is to obtain a short spindle length and a small negative scrub radius. This is done by aiming the links to virtual centers instead of having to package physical ball joints at the desired centers.

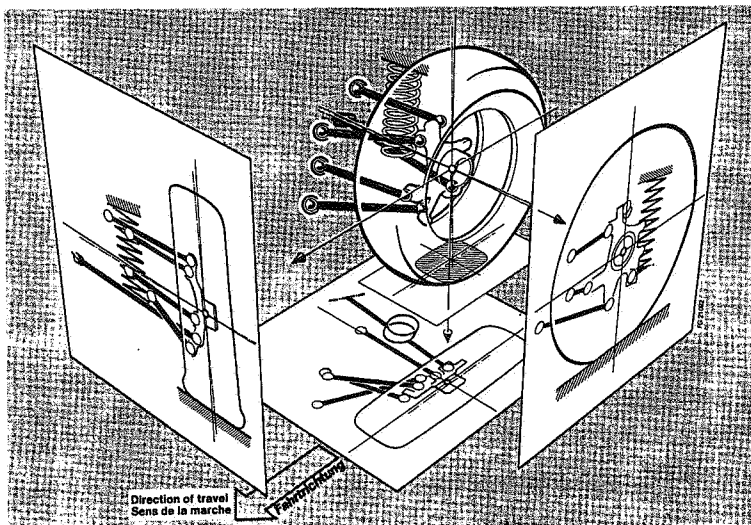


Figure 17.33 SLA suspensions—five-link Mercedes type.

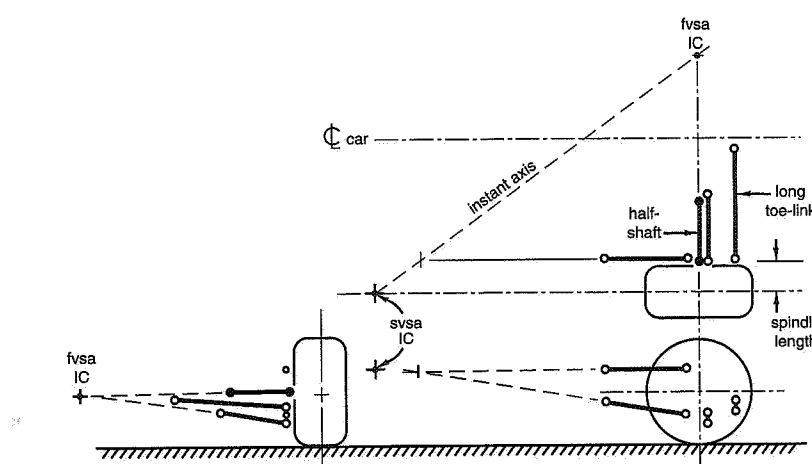


Figure 17.34 SLA suspensions—five-link Corvette type.

A caution in using this design is that the lateral diagonal pairing of upper and lower links to simulate A-arms is preferred to pure lateral and pure trailing links to form the arms. This is because the rate of change of the side view geometry is generally too high with the trailing arm concept. Also a trailing arm must be packaged inboard of the wheel edge which results in a spindle length at least as large as half the tire section width. See Figure 17.34 for an explanation of this concept. Examples that demonstrate the differences between the trailing arm and the lateral diagonal style are the '84 Corvette versus the Mercedes 190 five-link. The Corvette uses the half shaft and the camber link in the front view along with the two trailing links in the side view to form the upper and lower arms. A tie rod is the fifth link.

17.7 Beam Axe Rear Suspensions

As mentioned earlier in the general section on beam-type axles there are five basic kinematic properties that need to be controlled by the suspension links. The wheel path, anti-lift, and anti-squat are controlled by the side view instant center. The roll center height and roll steer are controlled by the roll axis. All loads that occur between the sprung and unsprung masses are reacted by the suspension links. The fore and aft loads such as braking and acceleration are coupled through the side view instant center and the lateral loads are coupled through the roll axis. So the basis for understanding any beam axle rear suspension is to understand how the instant centers and roll axis are defined. This will be covered for some typical rear suspension types that are commonly used.

Four Bar Links

The very first section of this chapter discussed degrees of freedom and motion path and it was shown that a beam axle suspension has two motion paths, therefore, the motion can be controlled by four links. There are various ways to arrange those four links to achieve a workable suspension. The list below includes some of the most popular.

Basic Four Bar Link

Figure 17.35 is representative of this style of geometry. The side view instant center is determined by projecting or extending a line through the ends of both the upper and lower arms until they intersect. Normally the intersection will occur 100 in. or so ahead of the wheel center and will have a height somewhere between ground level and the wheel center. This part of the analysis is simple and straightforward and can be done in one view of the design.

The roll axis determination is a little more complicated because it involves looking at things in both the side view and the plan (or top) view. The roll axis is a line connecting the two lateral restraint points. These lateral restraint points were discussed in the gen-

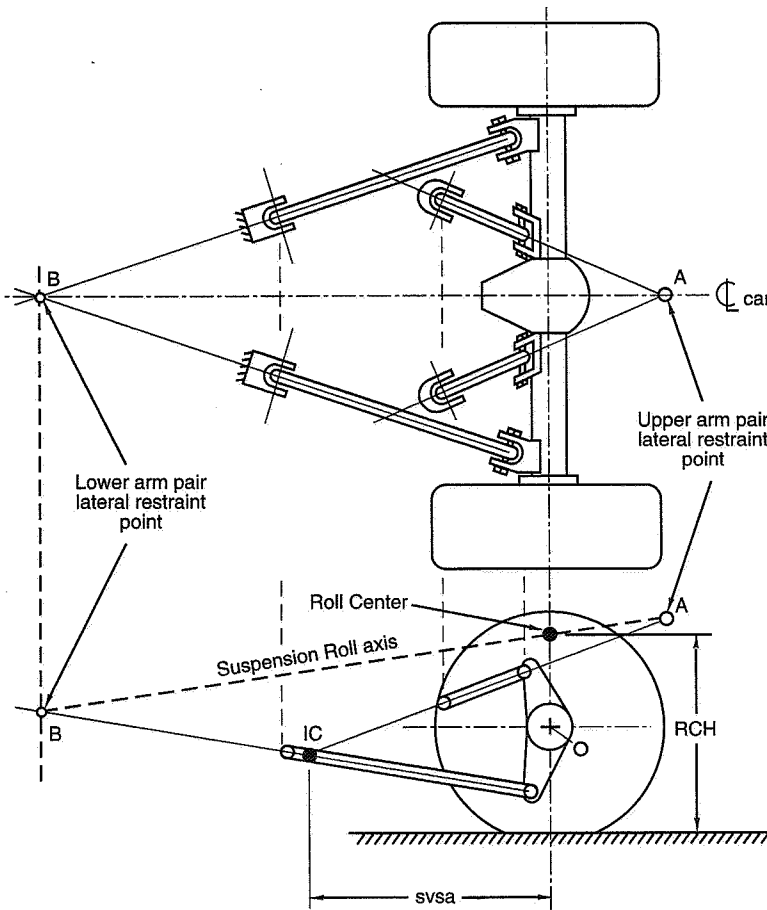


Figure 17.35 Basic four bar link axle suspension.

eral section on beam axles. For the basic four bar link the pair of upper control arms are angled in the plan view and therefore have an intersecting point which is a lateral restraint point, marked as "A" in the figure. This point is found in the plan view and then projected into the side view. The same is done for the lower pair of control arms, marked as "B." Now we connect the two lateral restraint points in the side view and we have the roll axis. The roll center height is simply the point where the roll axis crosses a vertical transverse plane through the wheel centers. The amount of roll steer is the slope of the roll axis in the side view.

You will note that in the plan view the upper and lower arm intersection points lie on the centerline of the car. This is because the right and left sides of the suspension are exactly the same. If they were not the same you would still use the same procedures to understand the geometry, but you might end up with a roll axis off center or one that angles in the plan view. This may or may not be desirable depending on the kind of performance that is needed.

When designing a four bar link rear suspension the side view geometry is adjusted by raising or lowering the pivots of the links relative to each other to get them to aim toward the desired instant center. The absolute and relative lengths of the upper and lower arms in the side view affect the rate of change of the side view instant center as well as how the axle housing rotates with wheel travel. This rotation is important to maintaining control over the propshaft joint angles. The change in pinion shaft angle with wheel travel is similar to camber change in the front view of an SLA suspension. The arm lengths and the ratio of their lengths control this.

Another design consideration is the vertical span between the upper and lower arms at the axle end. For a given torque output of the engine, the loads in the arms are lower if this vertical span is large. The cross car location of the arm reactions at the axle affects the amount of bending moment applied to the axle beam structure under acceleration and braking. Other than the springs and shocks the arms are the only connection between the axle and the rest of the car.

In the plan view we can alter the roll axis by changing the splay angle of the arms. Making the upper arm pair intersect farther away from the axle center will make the roll axis become more parallel to the ground in the side view, thus reducing roll understeer. It can be seen that changing the splay angle in the plan view does not change the side view instant center. This is an important feature to understand—that the four bar link has good separation and flexibility to achieve desired geometric parameters.

Parallel Lower Arm Four Bar Link

A special case of four bar link rear suspension is similar to the first one above except the lower arms are parallel to the centerline of the car. The side view geometry is not changed by this positioning; however, the roll axis determination is affected. The lower arm pair intersects at infinity thus there is no obvious lateral restraint point for this pair of arms. The roll axis is found in the side view by running a line through the upper arm pair lateral restraint point, "A," to the lower arm lateral restraint point which is at infinity. What this means is that the roll axis will run parallel to the side view angle of the lower control arm and pass through the upper arm restraint point (see Figure 17.36). The use of this type of suspension may satisfy some packaging requirements for lower arm positioning but in general it will not be as good as the standard four bar type geometry. The main problem is that the roll steer is equal to the slope of the lower arm in the side view. To assure that the suspension has roll understeer the arm must slope downward to

the front of the car. The side view instant center is by definition along a line projecting from the lower arm. To maintain roll understeer the side view instant center will be quite low and could even be below ground level. There is an interdependence of these parameters between the side view geometry and the roll axis geometry that just does not exist with the regular four bar link system.

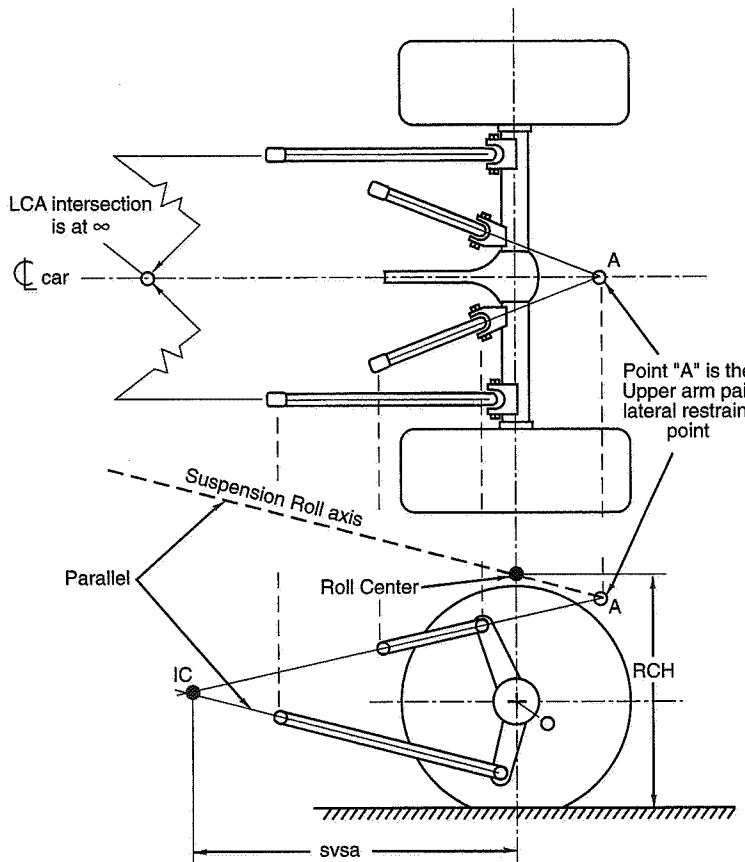


Figure 17.36 Parallel lower arm four bar link.

A-arm and Links

Another variation of the four bar link is the A-arm lower and two link upper system (Figure 17.37). The lower A-arm can be thought of as two links that come together at a common point, usually at the centerline of car beneath the axle center, so it really is a four

bar link system. The roll center is at the point of the "A" and will be quite low (under the axle housing). The roll axis will, by definition, pass through the point of the "A" of the lower arm. The slope of the roll axis is determined by the location of the other lateral restraint point. If the upper pair of arms is arranged to be parallel to the centerline of the car then the restraint point is at infinity and thus the roll axis slope is the same as the upper arm slope. The roll steer will be equal to the slope of the arm and will change with ride height as a function of the length of the arm.

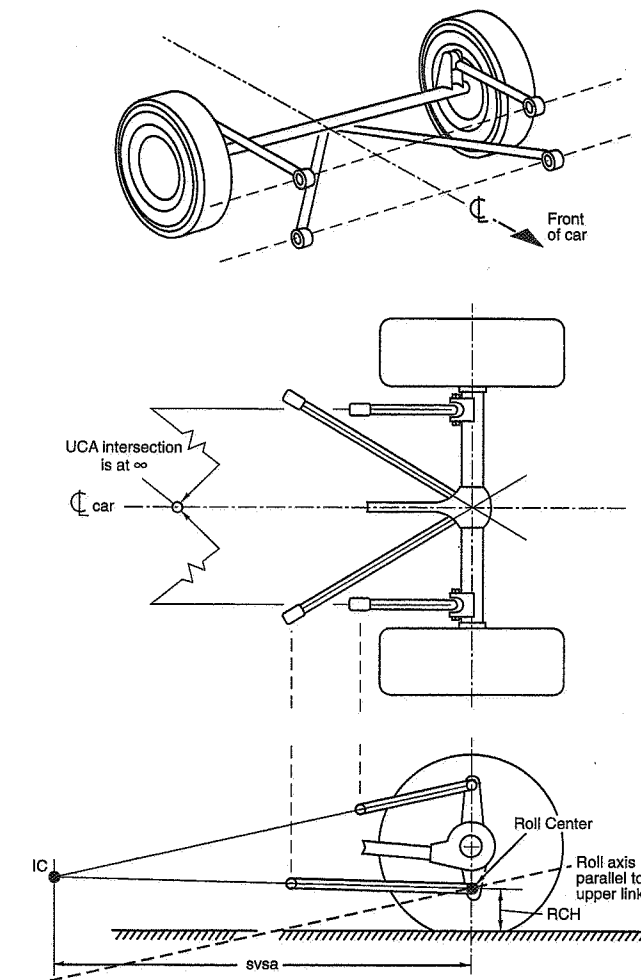


Figure 17.37 A-arm and links axle suspension.

If the upper pair of arms converges to a point ahead of the axle the roll axis will now project from this point through the point of the A-arm. If the convergence is far in front of the axle the roll axis will tend to slope downward to the front, giving roll understeer. If the convergence point is closer to the axle centerline, roll oversteer slopes will result.

The side view geometry is found in the standard manner by finding the instant center of the upper and lower arms in the side view. This is no different than any of the four bar link type rear suspensions.

Generally the upper arms attach to the axle at wide points just inboard of the tires. The lower point attaches to the axle under its center. Because of this offset between the upper and the lower reaction points, driving torque and braking torque will induce bending of the axle in the plan view.

There have been A-arm and link suspensions used where the A-arm is on the top and the lowers are individual links. The analysis of this variation follows the same rules. The roll center for this suspension will be quite high.

Three-link and Track Bar

This suspension, normally known as a three-link suspension, shown in Figure 17.38, really has four links. The track bar must be counted as one along with the other three. The point is to understand that it takes a minimum of four links to control the geometry properly; how they are arranged can be very different.

In this design the side view is evaluated the same as all of the four link suspensions. The intersection of the projection of the lower arms and the projection of the upper arm forms the side view instant center. The torque reactions are taken by the single upper arm and the pair of lower arms similar to the other four bar link designs, except the loads in the single upper arm are higher for the same inputs.

The roll axis determination is made by finding the lateral restraint points. We know the track bar provides lateral restraint so the point where its centerline crosses the centerline of the car ("A") is one of them. The other restraint point is determined from the lower control arms. The single upper arm cannot provide any restraint to lateral loads so it is not used in this determination. If the lower arms converge in the plan view, as shown in Figure 17.38, the intersection point ("B") is projected into the side view and now a line can be drawn between that point and the track bar point to produce the roll axis. Again the roll center is where the roll axis intersects a vertical plane through the wheel center.

The lower arms may run parallel to each other and the centerline of the car. If this is the case then they intersect at infinity. The roll axis would run through the track bar point parallel to the lower arms in the side view. The roll center would be where the roll axis crosses a vertical line through the wheel center.

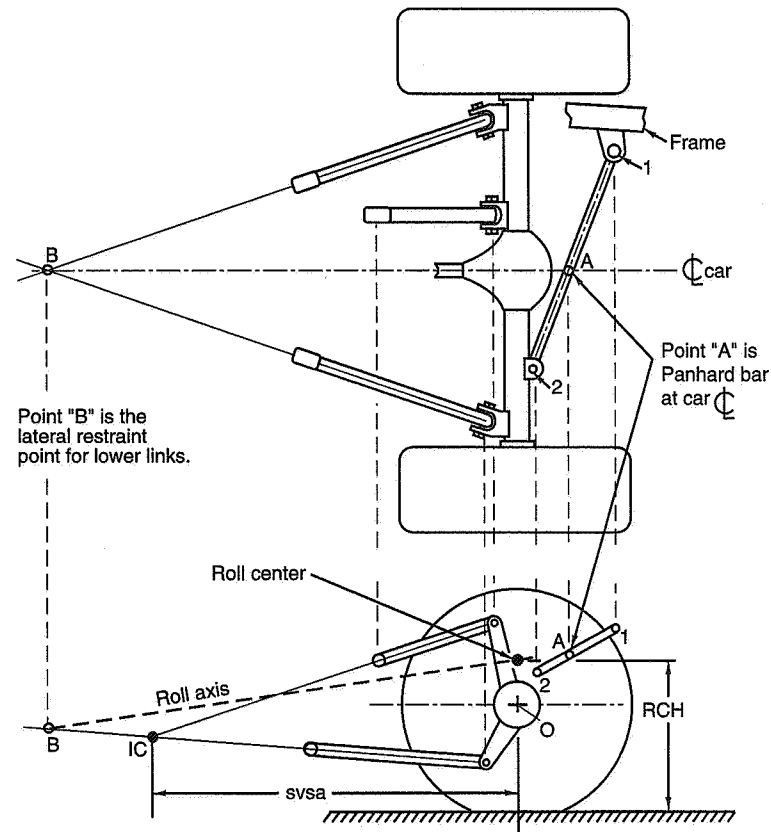


Figure 17.38 Three-link and track bar (Panhard bar).

Functionally the three-link and track bar is quite good. It is used extensively in short track racing and is often found on road-racing sedans.

The third link or upper link is often mounted in the center of the axle. Another option is to mount it off to the right-hand side of the center. It can be shown that if the offset distance is in the correct proportion to the axle ratio being used, the load on the tires will remain equal under acceleration and the sprung mass will not roll. Under braking there would be a slight tendency to roll to the right, however.

Torque Tube and Torque Arm Suspensions

As the name implies these suspensions have a device to react torque other than through the control arms. These types are not used on passenger cars today but they remain in some racing series. There are a couple of variations of a similar theme here that will be explained. In general they do not have four tension-compression links controlling all motions. This means that some elements are providing the control by working in bending rather than just pure tension and compression.

Torque Tube

This suspension, shown in Figure 17.39, has no control arms. One structural tube runs from the axle to some point near the back of the transmission. It is rigidly attached to the axle and pivotally mounted to the transmission or frame. There is also a lateral restraint device, typically a Panhard bar. The side view instant center is the forward pivot of the torque tube. The roll axis is defined by the track bar at centerline of car and the forward pivot of the torque tube. That is all there is to it.

Structurally there is triangulation from the outer ends of the axle to the front of the torque tube, so the whole axle is one structure with the torque tube, and it attaches to the car at only two places. The springs and shocks are done in a conventional manner. Typically the propshaft ran down the center of the torque tube and the front pivot was either at or very close to the front universal joint. With this design the rear u-joint angle was fixed at all wheel positions and the front joint angle varied as a function of wheel travel and torque arm length. There is no plunge required of the propshaft with wheel travel when the front u-joint and the torque tube mount are at a common point. Wheel torque reactions, both braking and driving, are reacted by bending loads in the torque tube and end up as a vertical force at the forward tube pivot.

Functionally the side view instant center can be in an acceptable location and it does not change with wheel travel at all. Therefore the anti features do not change with wheel travel. As long as the track bar is above the forward torque tube pivot, roll understeer will be assured.

NASCAR Stock Car Rear Axles

The favored rear suspension for NASCAR is a slight variation of the one described above and is shown in Figure 17.40. Instead of the torque tube, there are two I-beam arms running diagonally from the axle to near the center of the tunnel at the transmission tail shaft. The arms are not pivoted at the axle, rather they are rigidly attached with U-bolt clamps, thus they take the torque reactions. At the front of the beams/arms are the pivots. The point of arm to chassis attachment is just either side of the tunnel for propshaft clearance. They are nearly convergent to a common point but not quite. With the long

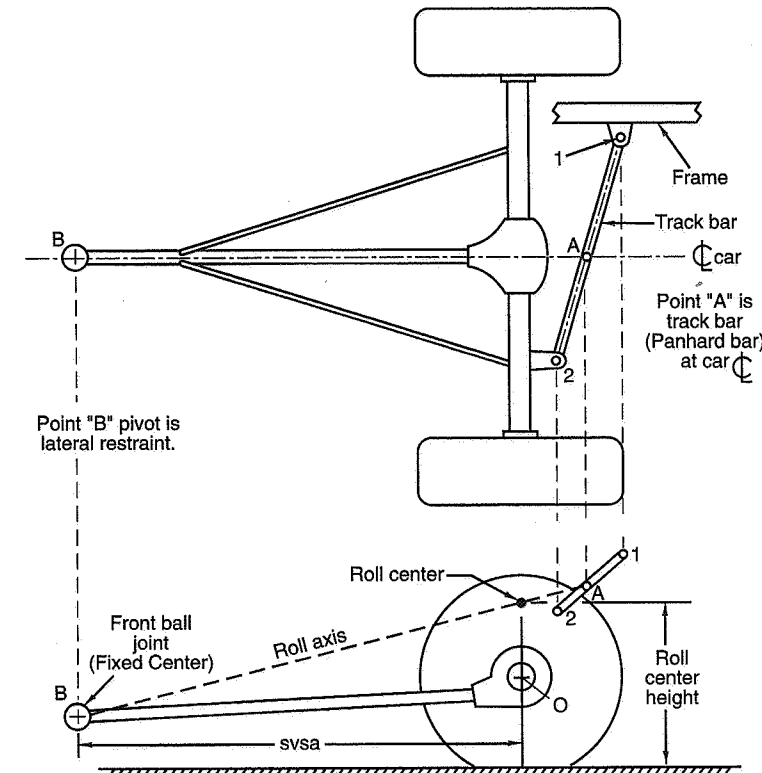


Figure 17.39 Torque tube rear axle.

arms that are torsionally flexible as I-beams are, and the front pivots almost on vehicle centerline, the system acts almost exactly like the torque tube as described above. Theoretically, for this suspension to roll, the axle tube has to twist a little, but the I-beam arms take most of the twist instead of the axle as they are torsionally weaker.

The function of this type of suspension is exactly like the torque tube. The side view instant center is at the pivot of the torque arms. The roll axis is the line between the pivot axis and the point where the track bar crosses vehicle centerline.

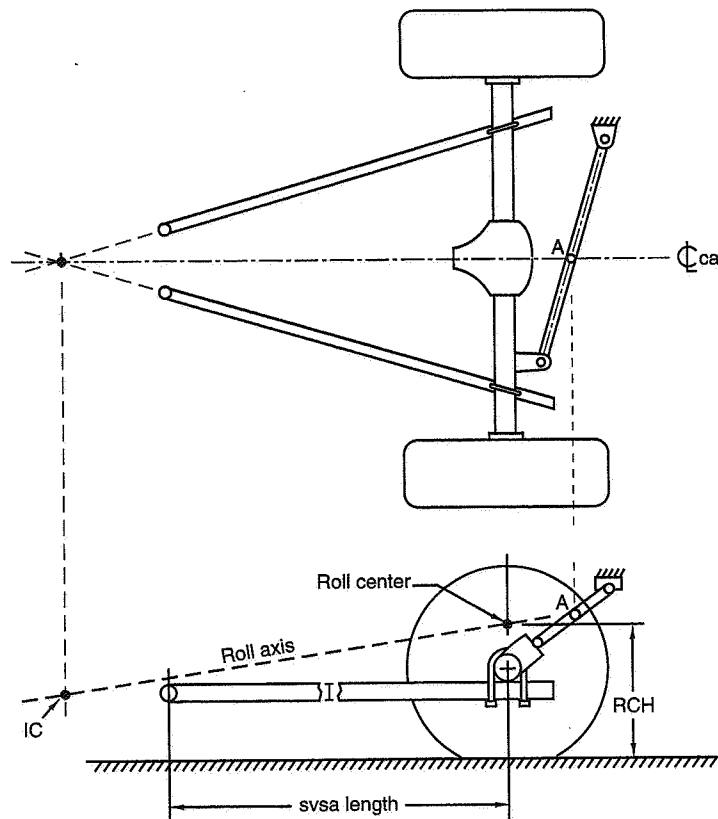


Figure 17.40 "NASCAR" type rear axle.

Torque Arm Suspensions

There are other styles of suspensions using an arm in bending to react torque. The General Motors F-car line (Firebird and Camaro) has one such example, shown in Figure 17.41, which is also similar to the Type 35 Bugatti of 1924. Here the system is very much like the three-link and track bar except instead of the third link upper arm there is a torque reaction beam rigidly attached to the axle housing and extending forward to the transmission end housing. The torque beam is mounted in rubber and is free to slide fore and aft but is not allowed to move up and down or side to side. There are two lower control arms and a Panhard bar to complete the kinematic control.

The kinematics are a bit unique for this case in that the side view instant center is not obvious. First a line is extended through the lower control arm pivots forward past the

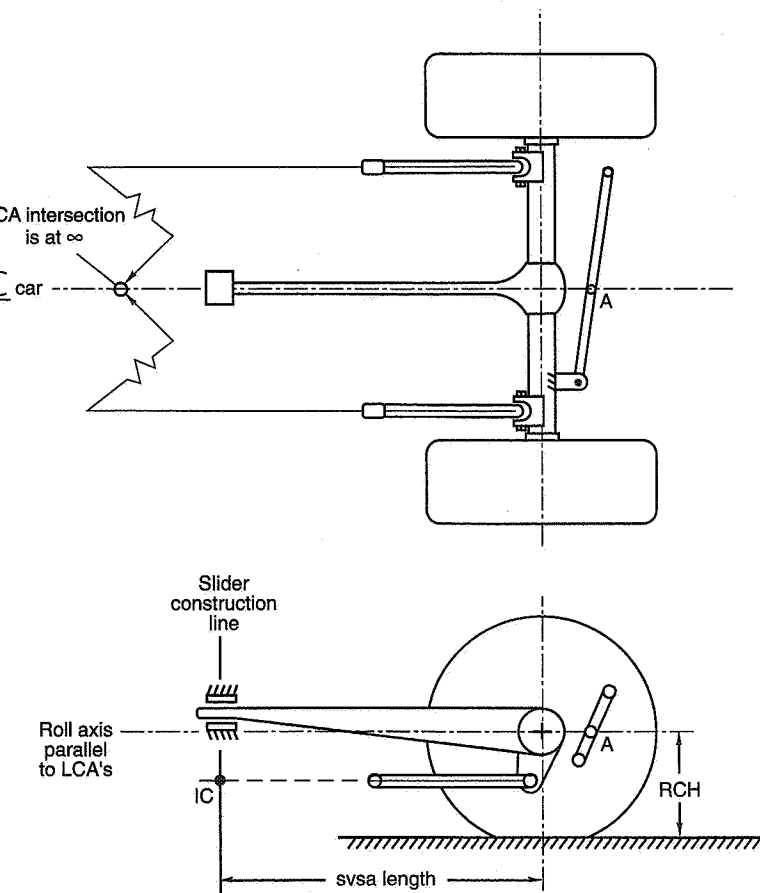


Figure 17.41 Torque arm rear axle suspension.

transmission area. Next a line is drawn perpendicular to the front end of the torque beam where it is attached at its rubber slider joint. This is basically a vertical line. Where this vertical line crosses the line of the lower control arms is the side view instant center. The roll axis is determined like the three-link design. If the lower arms are parallel to each other and centerline of car then they converge at infinity. The roll axis then runs parallel to the lower control arms in side view and goes through the Panhard bar point on centerline of car. If the arms converge in plan view, the convergence point is projected to the side view and connected with the Panhard bar point, and this establishes the roll axis.

This suspension has a fixed length side view swing arm that is borderline acceptable. Power hop and/or brake hop can occur with this type of suspension. The amount of anti-squat obtainable is limited because the height of the side view instant center can never realistically be raised even as high as the crank centerline. Thirty percent is about the maximum obtainable. To assure roll understeer, the lower control arms must angle down towards the front. This also means that the side view swing arm instant center height will be low.

Decoupled Rear Suspensions

There are some suspensions that do not exactly fit into the categories above but they are worthy of mention. The basics still apply in terms of understanding the kinematics. These suspensions were invented to decouple or disassociate some features from others.

Decoupled Torque and Braking Reactions

The suspension shown in Figure 17.42 is sometimes called a *compound* and has the following features.

1. The upper and lower longitudinal control arms are in pairs and are attached to a structure that is free to rotate around the axle tube. This is sometimes called a "bird cage."
2. The arms can either be arranged parallel above and below the axle with both arms ahead of the axle or they can be arranged with one ahead and one behind, like a Watt's linkage, as shown in Figure 17.42.
3. The primary lateral restraint device is either a Panhard bar (as shown) or a Watt's linkage.
4. Because the control arms do not react any torque (the "bird cage" is free to rotate), another means to react driving torque must be provided. This is done with a torque beam attached to the middle of the axle housing and running forward anywhere from 30 to 60 in. The torque beam is then connected to the chassis through a coil over shock system. This is sometimes called a fifth coil system.
5. Brake calipers are mounted with rotationally free brackets to the axle tube as well and these brackets are then connected to the frame with their own control links.

With all these components it is possible to change one of the primary kinematic features without changing any others. This is not possible with the other suspensions we have studied. This is called *decoupling* the design.

An example of the decoupling is the anti-squat. The side view instant center can easily be at infinity with parallel arms. Normally this would mean very low to no anti-squat

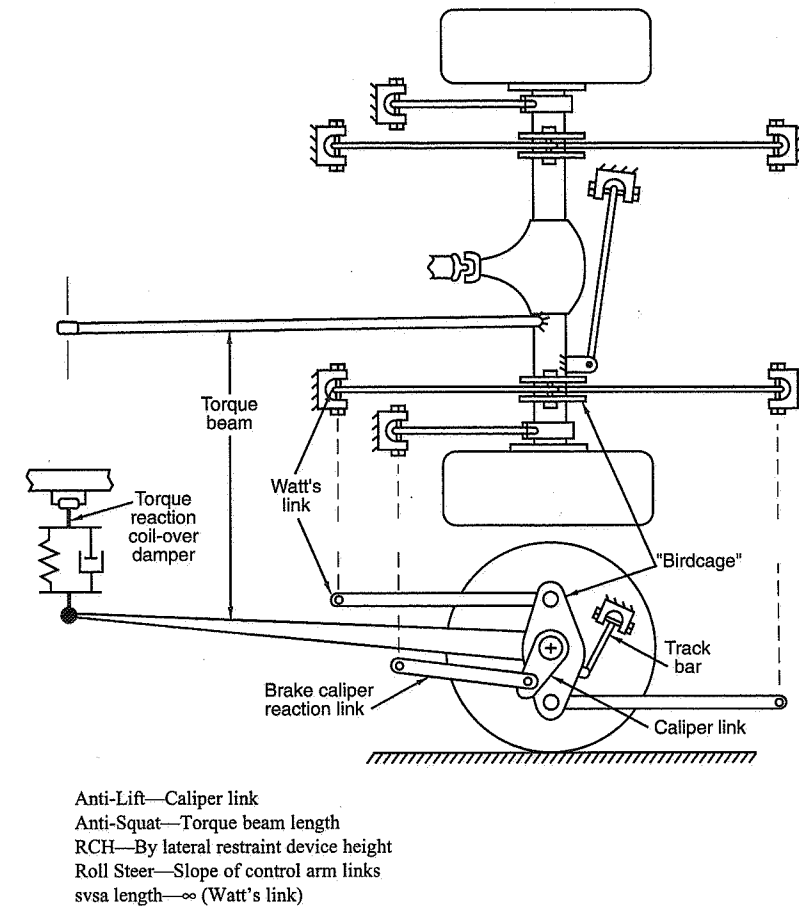


Figure 17.42 Decoupled rear axle suspension.

capability. But the torque reaction is taken by the torque beam and therefore the anti-squat is a function only of the length of the arm relative to the tire radius; anti-squat can be increased by shortening the beam. The spring and shock connection to the chassis is provided to cushion the power-on / power-off torque spikes, even though large values of anti-squat are used.

Roll steer is tunable by adjusting the angle of the control arms in the side view. This does not change the anti-squat as it would in a conventional system.

The braking anti-lift is a function only of the angle in side view of the control link that connects the brake caliper reaction to the frame. This can be adjusted absolutely independent of any other parameter.

This suspension is not widely used, probably because it is not well understood. It can be very useful to be able to adjust all of these parameters independently. But if a racer knows what combination of parameters will work best on his car at his tracks, then one of the other types may offer these solutions at a lower cost and complexity.

de Dion Rear Suspension

A de Dion rear suspension is shown in Figure 17.43. The purpose of this design is to decouple the mass of the driving gears from the unsprung weight. An independent-rear-suspension-type differential is mounted to the chassis and uses half shafts like an independent. The two wheel carriers are tied together by a stiff beam like all beam-type axles; however, in this case the structure must be bent around the differential. Usually it's made from a large-diameter bent tube. There are packaging considerations to leave room for this tube to move up and down as the wheels travel.

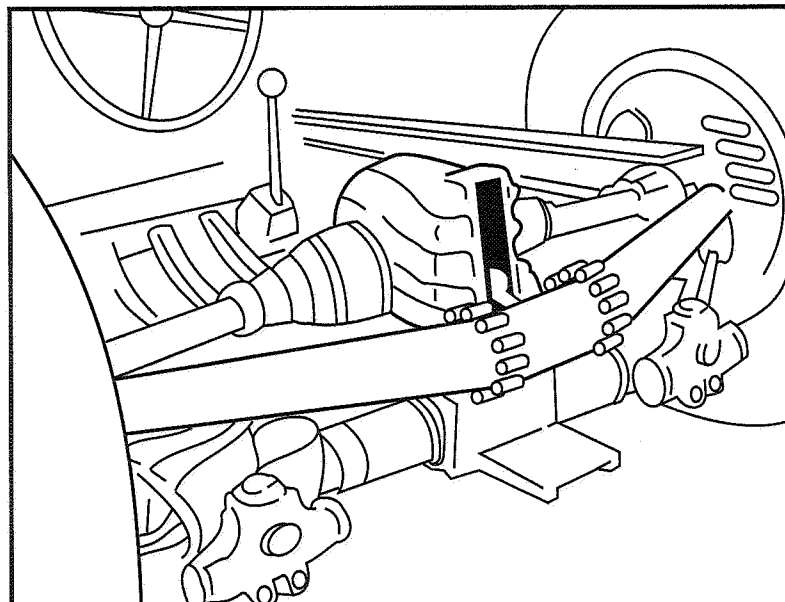


Figure 17.43 Mercedes W125 de Dion rear axle suspension (Ref. 29).

Kinematically the tube can be controlled by any of the systems already discussed. There is no drive torque reaction requirement, however, because the differential is mounted to the chassis. Usually a form of four bar link is utilized. Anti-squat values are calculated like an independent suspension. The slope to the side view instant center comes from the wheel center rather than the ground contact patch.

The advantages of the de Dion are that the unsprung mass is much lower resulting in better road holding on rough roads (like independent suspension). It is a beam-type axle so the tires always remain square to the road, thus no camber compromise exists (unlike independent suspension). This gives it supposed advantages over both the independent and the conventional beam axle.

Hotchkiss Axle

One of the oldest types of beam axle rear suspensions is shown in Figure 17.44. It is simply an axle with a pair of longitudinal leaf springs. The springs perform not only the springing function but also locate the axle laterally and react acceleration and braking torques. One problem with these suspensions is that the kinematics are not very precisely controlled. Instead of links with exact centers of rotation, the leaf spring controls the wheel center path via its flexibility. The exact side view instant center depends on how the axle is loaded at that particular instant.

Functionally these suspensions are quite rugged. The lateral restraint performance is subject to attention to detail. For example, the shackle design must be very stiff in lateral bending. The amount of arch the spring has at a given loading condition will affect its ability to resist lateral loads with minimum deflections.

Kinematically the side view swing arm instant center is found by some very complicated mathematics or by using some simple rules of thumb and coming up with a close approximation as shown in the figure. The roll steer and the roll center height are found by determining the forward and rearward lateral restraint points. These are usually the front spring eye bushing height and the top shackle bushing height as shown in the figure.

Leaf spring rear suspensions have very little use on modern racing cars.

17.8 Twist Axle Rear Suspensions

This family of rear suspensions is a fairly recent development and they all are used on front-wheel-drive cars. The only time one would be on a racing car is in a showroom stock-type class. The reason they are called twist axles is that in order for the car to roll, the axle beam has to twist. The kinematics of this type of suspension still provides all the control parameters that other suspensions have except for anti-squat because there is no rear drive torque to react.

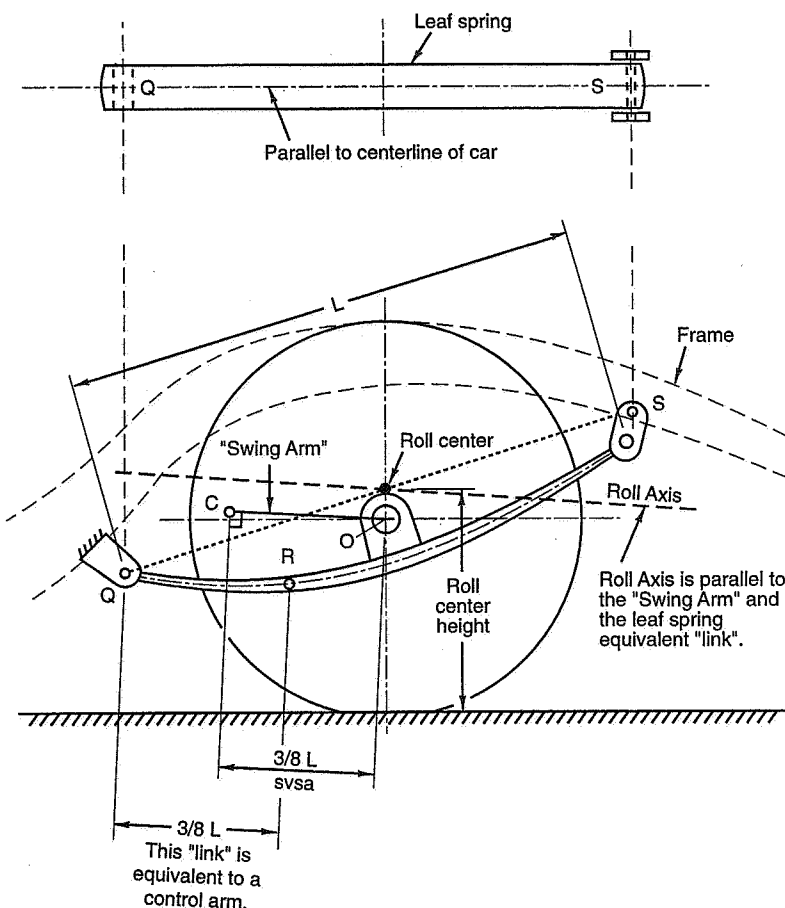


Figure 17.44 Hotchkiss rear axle (leaf springs).

There are three basic types of twist axles; these are shown in Figure 17.45. The main difference is in the fore-aft location of the cross beam.

- The first type (a) has the beam at the bushing center. This suspension is very much like the pure trailing arm independent.
- The next type (b) has the cross beam partway between the bushings and the wheel center. In parallel jounce the bushings are the instant axis and it acts like a simple hinge. In roll, however, the axle has properties like a semi-trailing arm suspension. The instant axis is a line through the crossbeam twist center at the centerline of car and the bushing. This axis runs diagonally in plan view.

- The third type (c) has the crossbeam at the wheel centers. This design requires a Panhard bar to control lateral forces and deflections. For further details on the design of these types of suspensions refer to SAE Paper No. 810420 (Ref. 139).

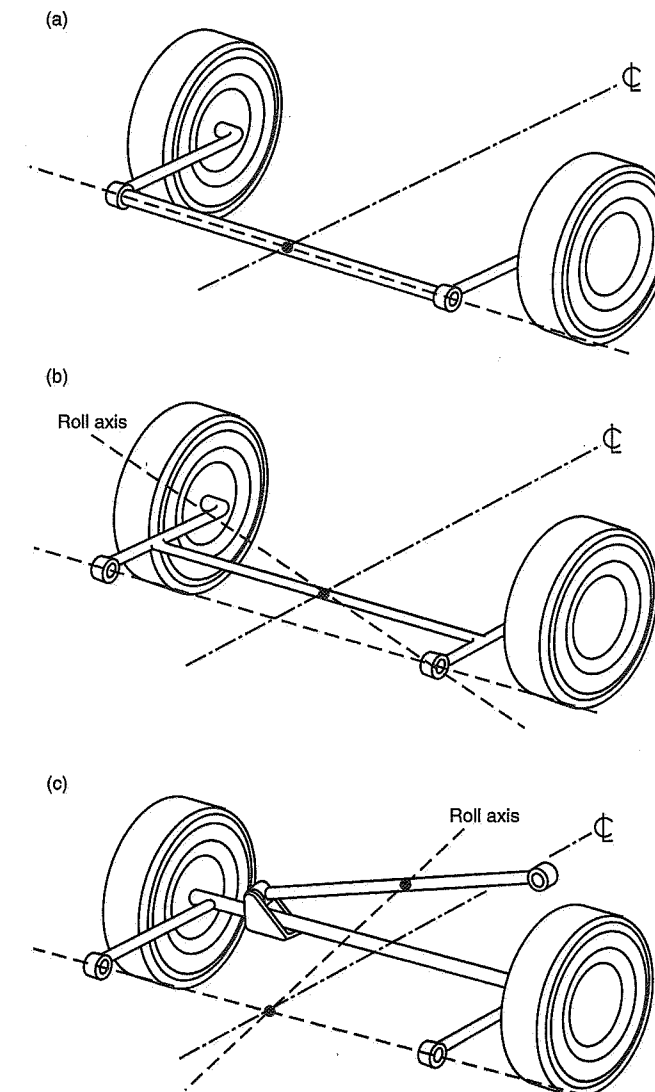


Figure 17.45 Twist axle types.

Wheel Loads

"Remember the car is balanced on only four tires. All they do is press the road with a force equal to the load carried on each wheel."

Pat Bedard
from Expert Driving



Introduction

This chapter shows how to calculate the loads at each wheel given basic car data and operating conditions. The loads at each wheel are extremely important in determining a car's maximum steady-state cornering capability. Some insight into the how the wheel loads are developed can be valuable in setting up a vehicle for maximum performance.

18.1 Assumptions Used in this Chapter

In a real car, the wheel loads are constantly changing. In order to demonstrate how wheel loads can be calculated, a number of operational and simplifying assumptions are made.

First, we are dealing only with **steady-state operating conditions**—that is, smooth roadway, constant speed cornering, constant longitudinal acceleration, constant grade, etc.

This chapter was written by Dave Segal, MRA.

The vehicle is also in steady-state—all of the variables discussed are in equilibrium in these solutions. Transient behavior of the vehicle and sprung and unsprung mass dynamics (ride/roadholding) are ignored.

Second, we assume that all of the basic car data used in the calculations (roll rates, spring rates, etc.) are linear, and that basic dimensional data (front and rear track, wheelbase, CG height, etc.) are **constant**. If any of these data items change (most do change to some extent) then the closed form solutions presented here are not completely accurate. The closed form solutions are valid in practice when reasonable data is available. If large nonlinearities and dimensional changes are present then it will be necessary to go to iterative procedures (and a computer program is probably required).

Third, the assumption of linearity implies that the principle of **superposition** is valid. This principle states that the total of a series of effects considered concurrently is identical to the sum of the individual effects considered individually. Therefore, in the material that follows, we can numerically add the changes in wheel loads due to lateral load transfer, longitudinal load transfer, aerodynamics, etc., to produce loads that are valid for combined operational conditions.

Finally, as discussed later, all calculations presented are based on the assumption that the chassis of the car under consideration is **rigid**. If the chassis is flexible, particularly in torsion (twisting), the calculations will not be completely accurate. It is well recognized that a torsionally stiff chassis is needed for most of the traditional chassis adjustments to be effective. A reasonably stiff chassis forms the starting point for the calculations described in this chapter.

18.2 Center of Gravity Location

The location of the center-of-gravity (CG) of a race car is one of the most fundamental determinants of performance because tire cornering force capability is very dependent on the vertical (or normal) load applied to the tire. Most chassis changes that are made in an attempt to tune the handling performance of race cars have, in one way or another, an effect on wheel loads. This may be either through CG position changes or changes that affect the weight transfer distribution during cornering.

The first step in calculating the individual wheel loads in steady-state cornering, accelerating, or braking conditions is to determine the CG location. This section describes procedures and calculations for finding the CG location.

Total Vehicle Horizontal (*x* and *y*) Location of the CG

The general case will be assumed, in which the front and rear tracks are not necessarily equal and the CG is not necessarily on the longitudinal centerline. For this calculation,

the centerline of the car is defined as a line connecting the center of the front and rear tracks.

Test Conditions—The starting point is to settle the vehicle at ride height on a level surface. Then, roll the vehicle carefully (use ramps) onto four individual scales that have been leveled.

Data Required—First, record the individual wheel weights. At the same time record the loading condition: with or without driver, the amount of fuel, etc. Measure the front and rear track (tread) width (taken between the centerline of the tires); measure the wheelbase (average left and right sides if they are not equal). All dimensions must be in the same units (i.e., feet).

Figure 18.1 shows the various dimensions and their variable names. The total vehicle weight is the sum of the four individual wheel weights measured on level ground beneath each tire:

$$W_1 + W_2 + W_3 + W_4 = W = \text{Total Vehicle Weight}$$

The first calculation step is to take moments about the rear axle:

$$b = \frac{W_F \times \ell}{W}$$

and

$$a = \ell - b$$

This establishes the fore-and-aft location of the CG.

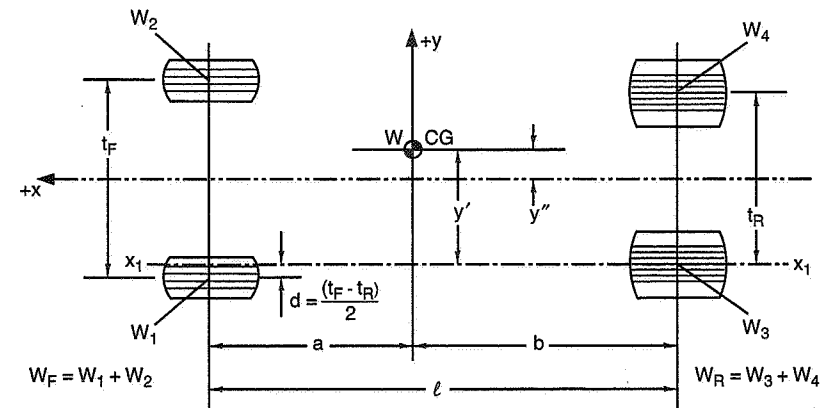


Figure 18.1 Horizontal location of total vehicle center of gravity.

Next take moments about the x_1-x_1 axis (a line parallel to the centerline of the car through the center of the left rear tire):

$$y' = \frac{W_2}{W} (t_F - d) - \frac{W_1}{W} (d) + \frac{W_4 t_R}{W}$$

This can then be solved for y'' (since $y'' = y' - (t_R/2)$) to give the lateral shift of the CG (if any) from the x axis (centerline):

$$y'' = \frac{W_2}{W} (t_F - d) - \frac{W_1}{W} (d) + \frac{W_4 t_R}{W} - \frac{t_R}{2}$$

Note that y'' as shown in the figure represents a positive value. A negative value represents a lateral shift of the CG to the left as is generally the case for oval track cars.

These equations apply to the general case. If $t_F = t_R = t$, the expression reduces to

$$y'' = \frac{W_2 + W_4}{W} t - \frac{t}{2}$$

Finally, if the front and rear tracks are equal and the CG is on the centerline (in the x-z plane) then $W_2 + W_4 = W/2$, and no lateral offset exists.

Total Vehicle Vertical Location of the CG

One method of determining the height of the CG is to jack the rear axle up so that the front to rear wheel centerlines are at an angle, θ , with the horizontal. The various dimensions of interest are shown in Figure 18.2.

Test Conditions—for this test the suspension motion must be locked up. A standard way to do this is to replace the shock absorbers with rigid links that will keep the car at ride height (for example, weld up an old set of shocks). The front wheels are chocked on scales and the rear axle is raised as shown in the sketch. **CAUTION**—The front wheel chocks are the only thing that keeps the car from rolling—THEY MUST BE SECURE to keep the car from falling off the scales. The method of raising the rear axle must not pull horizontally on the car; several methods can be used:

- Overhead hoist—keep the cables vertical.
- Four post lift—the rear wheels must roll freely on horizontal ramps.
- Trailer—load the car halfway on and level the trailer ramps.

Any load that could shift must be secured; fuel tank(s) should be empty (or full, vents closed!).

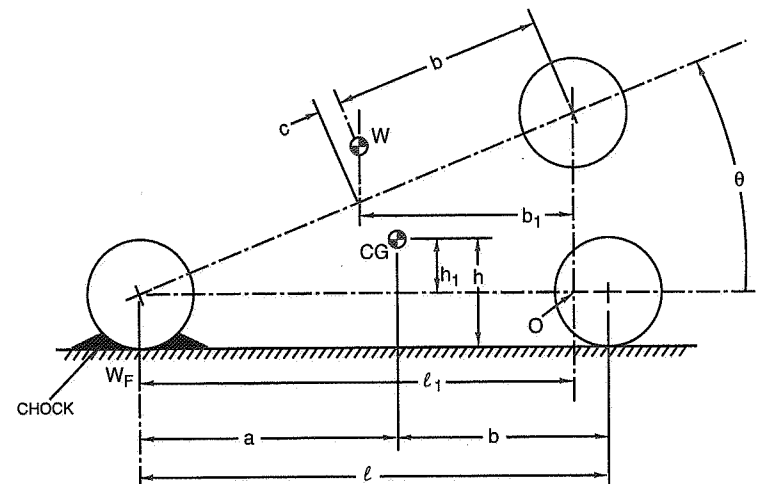


Figure 18.2 Vertical location of the center of gravity.

Data required:

W	total weight of vehicle, lb.
W_F	weight of front wheels with rear elevated, lb.
b	horizontal distance from rear axle to CG, ft.
ℓ	wheelbase, ft.
R_{LF}	loaded radius of front wheels (axle height above ground, ft.)
R_{LR}	loaded radius of rear wheels (axle height above ground, ft.)
$\tan\theta, \cos\theta$	tangent and cosine of the angle to which the vehicle is raised

The trigonometric steps are as follows:

$$\ell_1 = \ell \cos \theta$$

and, taking moments about the point, O,

$$W_F \ell_1 = W b_1$$

from which

$$b_1 = (W_F/W) \ell \cos \theta$$

Also,

$$\frac{b_1}{b + c} = \cos \theta$$

from which

$$c = \left(\frac{W_F}{W} \ell \right) - b$$

Using $c/h_1 = \tan\theta$, the final expression is

$$h_1 = \frac{W_F \ell - Wb}{W \tan \theta}$$

Note that h_1 is the height of the center of gravity above the line connecting the wheel centers which are at height R_L . If the R_L is the same front and rear the CG height above the ground is

$$h = R_L + h_1$$

If R_L is different front and rear, the height of the line connecting front and rear wheel centers at the CG location must be found by

$$R_{LCG} = R_{LF} \left(\frac{b}{\ell} \right) + R_{LR} \left(\frac{a}{\ell} \right)$$

If R_L is different front and rear the CG height is

$$h = R_{LCG} + h_1$$

For example:

$$W = 2000 \text{ lb.}$$

$$W_F = 1301 \text{ lb., measured at } \theta = 0.2025 \text{ rad.}$$

$$b = 5 \text{ ft.}$$

$$\theta = 0.2025 \text{ rad. (11.6°)}$$

$$\ell = 8 \text{ ft.}$$

$$R_{LF} = 0.9 \text{ ft. (front wheel)}$$

$$R_{LR} = 1 \text{ ft.}$$

$$h_1 = \frac{1301(8) - 2000(5)}{2000(0.2053)} = 1.0 \text{ ft.}$$

$$R_{LCG} = 0.9(5/8) + 1(3/8) = 0.9375 \text{ ft.}$$

$$h = \text{CG height} = 1 + 0.9375 = 1.9375 \text{ ft.}$$

The above method is applicable even if $t_F \neq t_R$ and/or the CG is not in the x-z plane (centered left-right between the wheels). However, if the CG is appreciably shifted out of the x-z plane the rear axle must remain horizontal when jacked up.

Another form of the expression for h_1 , above, is

$$h_1 = \frac{\Delta W_F \ell}{W \tan \theta}$$

where ΔW_F is the change in W_F from $\theta = 0$ to the test value.

Because the CG is often close to the height of the wheel centers (R_{LF} and R_{LR}), the change in load as the car is jacked is small. To get the best results from this test it is best to take data at several angles and average them.

Sprung Mass CG Location

For some of the calculations later in this chapter it is necessary to know where the sprung mass (chassis and body) center of gravity is located. We already know where the total center of gravity is located from the previous calculations; the sprung mass CG location can be calculated if we also know the weights of the unsprung masses. Unsprung mass includes wheels, tires, knuckles, brakes (outboard), and approximately 1/2 of all the connecting components—links, half shafts, springs, dampers. For a solid axle, the whole axle assembly is unsprung.

Figure 18.3 shows a plan view of a car in the most general case. The total vehicle CG, W , is located longitudinally by a and b and laterally by y' and y'' . The individual unsprung weights are located at the center of each wheel. The weight of the sprung mass is simply the total vehicle weight minus the unsprung weight:

$$W_S = W - W_{U1} - W_{U2} - W_{U3} - W_{U4} = \text{Sprung Weight}$$

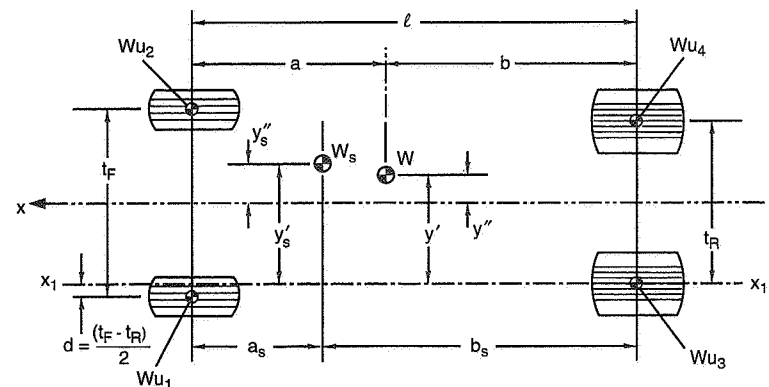


Figure 18.3 Lateral and longitudinal sprung mass CG location.

The total front and rear unsprung weights are

$$\begin{aligned} W_{UF} &= W_{U1} + W_{U2} = \text{Front Unsprung Weight} \\ W_{UR} &= W_{U3} + W_{U4} = \text{Rear Unsprung Weight} \end{aligned}$$

The longitudinal location of the sprung mass CG is found by taking moments about the rear axle:

$$b_s = \frac{W_b - W_{UF}\ell}{W_s}$$

and

$$a_s = \ell - b_s$$

The lateral location of the sprung mass center of gravity is found by taking moments about the x_1 - x_1 axis:

$$y'_s = \frac{W}{W_s} y' - \frac{W_{U4}}{W_s} t_R - \frac{W_{U2}}{W_s} (t_F - d) + \frac{W_{U1}}{W_s} d$$

and

$$y''_s = y'_s - \frac{t_R}{2}$$

If the front unsprung weights are the same either side ($W_{U1} = W_{U2} = W_{UF}/2$) and the rear unsprung weights are also the same either side ($W_{U3} = W_{U4} = W_{UR}/2$), then the equation for the lateral position reduces to

$$y'_s = \frac{W}{W_s} y' - \frac{W_{UR}}{2W_s} t_R - \frac{W_{UF}}{2W_s} t_F + \frac{W_{UF}}{W_s} d$$

Furthermore, if the front and rear tracks are equal ($t_F = t_R = t$ and $d = 0$), the expression becomes

$$y'_s = \frac{W}{W_s} y' - \frac{W_{UR}}{2W_s} t - \frac{W_{UF}}{2W_s} t$$

The sprung mass CG height is found by viewing the x - z plane as shown in Figure 18.4. Data required are the total vehicle CG height, h , and the front and rear unsprung weights, W_{UF} and W_{UR} (total for both sides), and their heights above the ground (a good first approximation is the wheel center height). The sprung mass center of gravity height, h_s , is found by taking moments about the ground:

$$h_s = \frac{W}{W_s} h - \frac{W_{UF}}{W_s} R_{LF} - \frac{W_{UR}}{W_s} R_{LR}$$

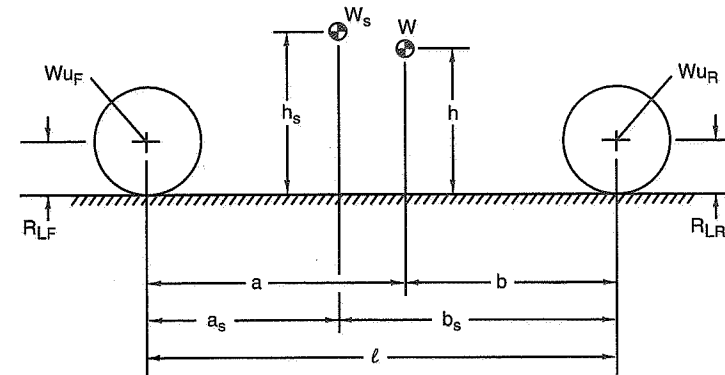


Figure 18.4 Sprung mass center of gravity height.

18.3 Chassis Stiffness

Before proceeding further in discussing and calculating wheel loading under various driving conditions, it is important to recognize that all simple calculations are based on the assumption that the chassis of the car is rigid, that is, it does not bend or twist under any driving condition.

Stiffness is resistance to bending or flexing; torsional stiffness is resistance to twisting. A performance vehicle must have adequate chassis torsional stiffness around the x -axis. Think of the chassis as a large spring connecting the front and rear suspensions: if the chassis torsional spring is weak, attempts to control the lateral load transfer distribution (and "balance" the car's handling by resisting more of the rolling moment on one track than the other) will be confusing at best and impossible at worst. This is because a flexible chassis adds another spring to an already complex system. Predictable handling can best be achieved if the chassis is stiff enough to be safely ignored, as it will be for all of the calculations in the following sections in this chapter.

Further arguments for a torsionally stiff chassis are

- It is not practical to dampen structural twisting in the chassis with current technology.
- A chassis that flexes may be prone to fatigue, and further "softening" with use, eventually resulting in failure (and possibly an accident).
- Suspension compliances may be increased or decreased by bending or twisting of the chassis.

Measuring Chassis Torsional Stiffness

Torsional stiffness may be measured in a number of different ways. One method that is documented in Ref. 118 and shown in Figure 18.5 will be summarized here.

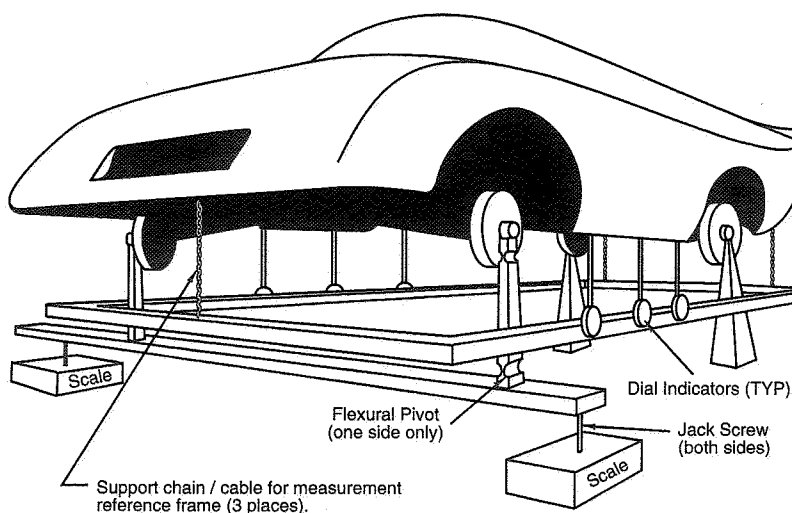


Figure 18.5 Chassis assembly set up for torsional stiffness testing (Ref. 118).

Reactions (loads) front and rear are taken directly below the axle locations. The front end is supported on knife edges at the outer ends of the lower A frames, and the front springs are blocked out or replaced by rigid struts. The knife edges are mounted on screw jacks which in turn rest on two scales. The rear end is supported on knife edges that are firmly supported off the floor or surface plate. In the case of rear leaf spring suspension, the springs are replaced by rigid beams mounted to the spring attachments; for coil spring rear suspension, the knife edges are located at the upper spring perches.

A series of dial indicators are mounted on a rigid frame under the vehicle. These are located in left-right pairs at points of interest along the sides of the vehicle. The rigid frame is hung from the vehicle at three points, one between the front wheels and the other two in the plane of the rear axle. The chassis is ballasted to keep all four knife edges in contact as it is twisted.

Torque is applied to the chassis by raising or lowering one screw jack. The scale readings before and after the torque is applied are noted and the applied torque is half the scale reading difference times the distance between the front knife edges. If the distance

is in ft. and the scale readings are in lb., the torque will be in lb.-ft. In order to minimize hysteresis, the test commences with zero torque (scale readings equal), then one jack is raised until the maximum torque is applied. Then the process is reversed until maximum torque is applied in the reverse direction and finally back to zero.

After the vehicle has settled, the dial indicators are zeroed and the chassis is again cycled in torque to perhaps ± 500 lb.-ft. (for a sedan, less for a lighter vehicle) with readings noted. A plot is made like Figure 18.6. To convert from indicator readings to degrees, use the proportionality 1 in. in 57.3 in. = 1° . For example, if the indicators show a difference of 0.050 in. and this pair of indicators is located 45 in. apart, the amount of twist at this station is $(0.050/45) \times 57.3 = 0.064^\circ$. A plot of torsional deflection along the length of the chassis is shown in Figure 18.6.

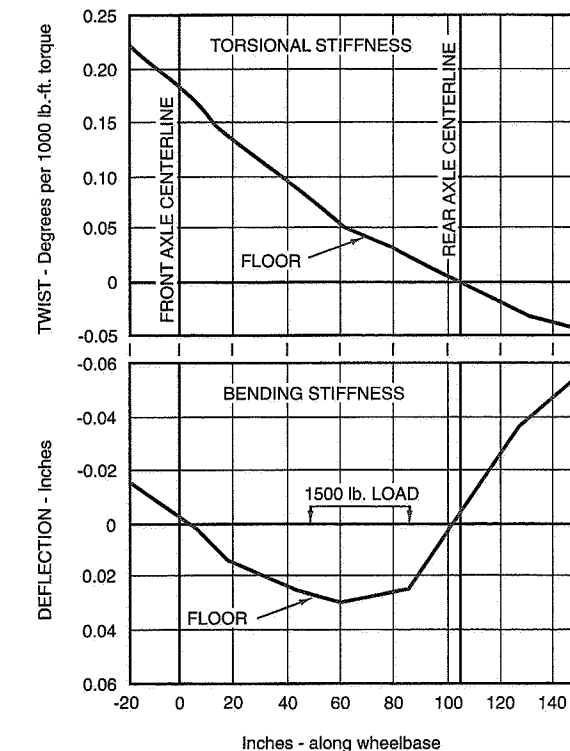


Figure 18.6 Bending and torsional stiffness plotted along the length of the chassis (Ref. 118).

How Torsionally Stiff?

How stiff is stiff enough? Typical unibody sedans are in the range of 4000 to 10,000 lb.-ft./deg. Current small formula cars may be 3000 lb.-ft./deg. and current composite (very stiffly sprung) Formula One cars have been quoted at 12,000 lb.-ft./deg. and up. Note that the numbers quoted may be for the bare chassis or tub, without the deflection of the suspension links or the various brackets (etc.) required to attach the suspension to the car; measurements on only part of the system can be misleading. It doesn't hurt to be too stiff (unless the vehicle is made overweight in the quest for stiffness), but modifying the chassis stiffness will change the set-up—different springs, anti-roll bar settings, etc., may be required.

Again, the reason for torsional stiffness is to provide a rigid platform for the suspension, to allow the lateral loads to be distributed front to rear in proportion to the roll stiffnesses of the suspension. Compare the front and rear roll stiffness (calculated in Chapter 16) to the chassis torsional stiffness—the chassis must resist approximately the difference between the front and rear roll rates. Then think about the amount of stagger or wedge it takes to change the handling and the actual load change seen by the tires.

Design for High Torsional Stiffness

The type of construction and the actual design determine the torsional stiffness that can be expected from a chassis. Probably the stiffest chassis currently made are composite stressed skin (or "monocoque"). Other types that are less efficient (less torsional stiffness for the same weight) are:

- Aluminum and steel stressed skin as seen in many purpose-built racing cars and in most modern passenger cars ("unit body" construction).
- Space frames built of tubing as seen in many production-based cars where the structure doubles as the roll cage. It is important that the tubes are arranged to form triangles with the major loads applied at the intersections of tubes, otherwise the structure will work in bending which is much less efficient than tension/compression.
- Ladder frames as used in many older design cars are perhaps the weakest. This type of frame has two "frame rails" connected at various points by crossmembers to carry the engine, suspension, and body.

Probably the easiest technique for quickly getting a feel for torsional stiffness is to build a model of the proposed design. The model can be made of wood, welding rod, etc. Twisting the model chassis will reveal any areas that are especially weak in torsion. At the same time, areas that are especially stiff may be redesigned to save weight.

Increasing Torsional Stiffness

Some methods of increasing torsional stiffness include:

- Add diagonals in the roll cage. This is the thing to do if the vehicle is already built and found to be too flexible. Diagonals work best if they connect to major load points such as suspension/spring mounts.
- Remember that the engine can function as part of the chassis provided that the loads are not so high that the block is distorted. Some engines are designed especially for this purpose; the Cosworth DFV F.1 engine is the standard example.
- If tubes must be used in bending (as opposed to tension-compression in a triangulated space frame), plate reinforcements may be used at the joints to pass load more effectively from one tube to another (see Figure 18.7 which is taken from Ref. 164).
- Add additional crossmembers to the chassis. For production-based cars the front engine bay can often be improved in this way by the addition of a member connecting the tops of the spring mounts with the fire wall (a "K" member).

Stiffness measurements will help pinpoint any especially weak areas of the chassis.

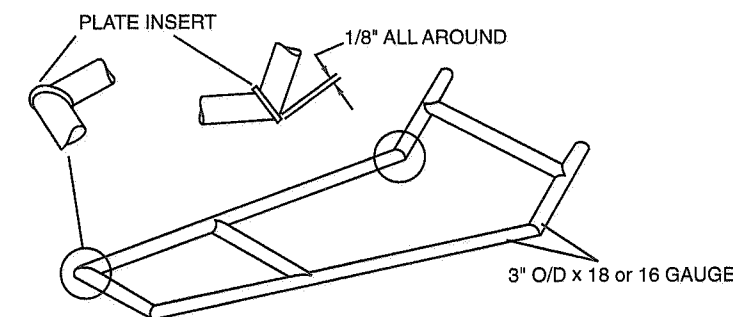


Figure 18.7 Stiffening up tubing joints in bending (Ref. 164).

Bending Stiffness

Chassis bending stiffness is generally not as important as torsional stiffness. There are two reasons for this. First, static chassis bending will not significantly affect wheel loads or their distribution. Second, and more significantly, Platt (Ref. 118) has shown that a chassis that has good torsional stiffness also has adequate bending stiffness. If care is taken to insure adequate torsional stiffness, bending is not likely to cause a problem. A plot of a bending stiffness test is shown in Figure 18.6.

18.4 Lateral Load Transfer

When cornering in a steady turn, load is transferred from the inside pair of wheels to the outside pair of wheels because the car center of gravity is above the ground. This section shows how to calculate the total load transfer due to cornering and, more importantly, the distribution of load transfer at the front and rear axles.

Total Lateral Load Transfer

When a car is in a steady-state turn an inertial reaction force called *centrifugal force* is developed which opposes the lateral acceleration produced by tire cornering forces. If we compress the car to a single axle, a right-hand turn situation results as illustrated in Figure 18.8. The cornering force produced by the tires, $S_L + S_R$, results in a lateral acceleration, a_y (in units of ft./sec.²) or A_Y (in "g" units, that is, $A_Y = a_y/32.2$). The inertial reaction or centrifugal force is WA_Y (with sign opposite to a_y).

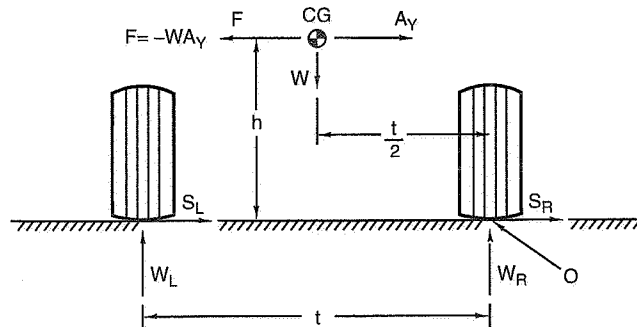


Figure 18.8 Total lateral load transfer.

Taking moments about O (the right side of the tire track), we have

$$W_L t = W \left(\frac{t}{2} \right) + WA_Y h$$

or

$$W_L = \frac{W}{2} + \frac{WA_Y h}{t}$$

Since the initial weight on the left-hand side of a symmetric car is $W/2$, the weight transfer due to cornering is $W_L - W/2$:

$$\Delta W = W_L - \frac{W}{2} = \frac{WA_Y h}{t}$$

where ΔW is the increase in left side load and decrease in right side load due to cornering.

Expressed as a fraction of total weight this becomes

$$LLT = A_Y h / t$$

where LLT = total lateral load transfer as a fraction of total weight

h = height of CG, ft.

t = track or tread width, ft.

A_Y = lateral acceleration, g's

This represents the total load transferred and does not attempt to calculate how the load is distributed on the four wheels. For example, a vehicle is cornering at 1.2g, the CG height is 1.5 ft. (18 in.) and the track is 5.42 ft. (65 in.), $1.5/5.42 \times 1.2 = 0.33$.

If the car was balanced left-right to start with, the inside right wheels now have $0.5 - 0.33 = 0.17$ (or 17%) of the total weight on them. The outside wheels have $0.5 + 0.33 = 0.83$ or 83% of the total weight of the vehicle on them.

If the car has 60% of the weight on the right-hand wheels to start with, the inside wheels now have $0.60 - 0.33 = 0.27$ (27%) of the total weight while the outside wheels carry $0.4 + 0.33 = 0.73$ or 73% of the total weight.

If the weight is biased to the left and we are cornering to the left (A_Y is negative), the inside and outside wheels are reversed but the percentages remain the same.

Distribution of Total Lateral Load Transfer

The information in this section applies only to steady turns, no consideration is given to combined lateral and longitudinal accelerations or other dynamic situations (i.e., power on/off, braking, or rough roads). Total lateral load transfer distribution (TLLTD) is sometimes erroneously called "roll couple distribution." The problem is that roll couple distribution is only part of the mechanism that controls the distribution of loads in a steady turn.

As seen previously, load is transferred from the inside track to the outside track when cornering because of the height of the CG. The distribution of this load transfer between

the front and rear tracks is one of the major ways to influence under/oversteer and limit behavior (push/spin). There are two mechanisms and their effects add:

- Through the springs in proportion to relative front and rear roll stiffnesses. Calculation of roll spring rates from ride rates and anti-roll bar rates is covered in Chapter 16.
- Direct application of loads, from the tires, to the chassis through the suspension members as determined by the heights of the front and rear roll centers. Roll center height (RCH) is covered in Chapter 17.

This section describes a technique for calculating the loads on the four wheels in a steady turn once the contributions of the RCH and the roll stiffnesses are known.

First, some definitions are important. These are given in Ref. 1 and repeated here:

- Roll Center—That point in the transverse vertical plane through any pair of wheel centers and equidistant from them, at which lateral forces may be applied to the sprung mass without producing an angular (roll) displacement of the sprung mass.
- Neutral Roll Axis—The line joining the front and rear roll centers.
- Roll Rate or Roll Stiffness—The change in the restoring couple exerted by the suspension at either pair of wheels on the sprung mass of the vehicle per unit change in roll angle of the sprung mass **about a horizontal axis**. Roll rate of the complete vehicle is the sum of the separate roll rates of all vehicle suspensions.

The major assumptions that will be made in this section are:

- A horizontal lateral (transverse) load applied anywhere along the neutral roll axis (NRA) produces no roll of the sprung mass.
- The front and rear roll rates are measured independently.
- Tire deflection rates are included in the front and rear roll rate values.
- Solid axle roll relative to the ground will not enter into the calculations.
- The vehicle CG and roll centers are located on the centerline of the car.

The approach taken here will be to treat the car as a three mass system consisting of the sprung mass (the chassis and body) and the front and rear unsprung masses (wheels, brakes, hubs, axles, and half of the mass of A-frames, springs, and shock absorbers). Figure 18.9 shows the geometry involved. As the figure suggests, the mathematics involved is straightforward but somewhat complex. For this discussion we will not go through it in its entirety but, instead, give the step-by-step rationale and the outcome along the way.

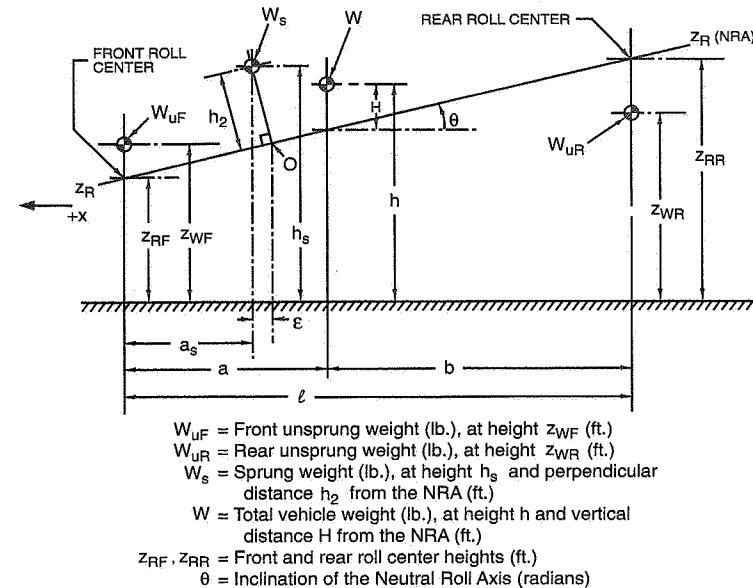


Figure 18.9 Lateral load transfer geometry.

In the first step we look forward along the NRA and note that the lateral acceleration, A_Y , produces a force, $F_s = -W_s A_Y$, and, in turn, a moment about O of magnitude

$$M_s = -W_s h_2 (A_Y - \phi)$$

where ϕ = the roll angle of the chassis.

The roll term is a gravity component which is included for completeness but can be neglected for small roll angles. Note that if A_Y is positive (a RH turn), the moment, M_s , on the sprung mass is negative and produces a negative roll angle, that is, the car rolls to the outside of the turn.

The effect of force, F_s , at height, h_s , is the same as a force, F_s , at the origin, O, on the NRA and a moment, M_s (above). The force, F_s , can be split into front and rear components (in proportion to the sprung weight on each axle) which will produce load transfers at the axles independent of the roll rates. The moment, M_s , produces a roll angle, ϕ , measured in a plane perpendicular to the NRA whose magnitude will depend on the sum of front and rear roll rates (or roll stiffnesses), K_F and K_R (in lb.-ft./rad.); for small θ these rates—which are defined in Ref. 1 as being around a horizontal axis—can be assumed to be around the NRA.

We next equate M_s to the roll stiffness moment and get

$$\frac{\phi}{A_Y} = \frac{-W_s h_2}{K_F + K_R - W_s h_2} = K_\phi$$

which gives us the **roll sensitivity** to lateral acceleration in radians per "g."

Next, the moment, M_s , is split fore and aft according to their individual roll stiffnesses and the previously apportioned F_s (fore and aft) are all combined to produce individual load transfers at each axle (including the inertial reactions of W_{uF} and W_{uR}).

Using all of the above we finally arrive at lateral load transfer equations for the front and rear axles that are expressed as sensitivities (or gains) to A_Y .

$$\frac{\Delta W_F}{A_Y} = \frac{W_s}{t_F} \left[\frac{h_2 K_F'}{K_F + K_R - W_s h_2} + \frac{\ell - a_s}{\ell} z_{RF} \right] + \frac{W_{uF}}{t_F} z_{WF}$$

where $K_F' = K_F - (\ell - a_s) W_s h_2 / \ell$

for the front axle, and a similar expression for the rear axle:

$$\frac{\Delta W_R}{A_Y} = \frac{W_s}{t_R} \left[\frac{h_2 K_R'}{K_F + K_R - W_s h_2} + \frac{a_s}{\ell} z_{RR} \right] + \frac{W_{uR}}{t_R} z_{WR}$$

where $K_R' = K_R - a_s W_s h_2 / \ell$

The units of these expressions are pounds of load change per "g" of lateral acceleration—increased load on the outside or decreased load on the inside.

It is obvious that the above expressions are cumbersome and they require a rather detailed knowledge of a car's geometry. These equations can be simplified if one uses the total vehicle CG and its height above the NRA (H in Figure 18.9). This implies a single mass system and the following replacements are made in the equations:

$$\begin{aligned} W_{uF} &\approx W_{uR} \approx 0 \\ W_s &\approx W \\ a_s &\approx a \\ h_2 &\approx H \\ h_s &\approx h \\ K_F' &\approx K_F \\ K_R' &\approx K_R \end{aligned}$$

Also, the gravity term associated with roll angle, ϕ , can be neglected.

If these assumptions are made the above equations reduce to

$$\frac{\phi}{A_Y} = \frac{-WH}{K_F + K_R} = K_\phi$$

$$\frac{\Delta W_F}{A_Y} = \frac{W}{t_F} \left[\frac{HK_F}{K_F + K_R} + \frac{b}{\ell} z_{RF} \right]$$

$$\frac{\Delta W_R}{A_Y} = \frac{W}{t_R} \left[\frac{HK_R}{K_F + K_R} + \frac{a}{\ell} z_{RR} \right]$$

In order to see what effect the above simplifications have on the original ΔW expressions we will calculate an example with both sets of equations.

The car data are:

$$\begin{array}{lll} \ell = 9.5 \text{ ft.} & a = 4.56 \text{ ft.} & b = 4.94 \text{ ft.} \\ h_s = 1.583 \text{ ft.} & h_2 = 1.16 \text{ ft.} & H = 1.069 \text{ ft.} \\ h = 1.5 \text{ ft.} & & \end{array}$$

$$\begin{array}{ll} z_{RF} = 0.25 \text{ ft.} & z_{RR} = 0.625 \text{ ft.} \\ z_{WF} = 1 \text{ ft.} & z_{WR} = 1 \text{ ft.} \end{array}$$

$$\begin{array}{ll} W = 3500 \text{ lb.} & W_s = 3000 \text{ lb.} \\ W_{uF} = 200 \text{ lb.} & W_{uR} = 300 \text{ lb.} \end{array}$$

$$K_F = 67,600 \text{ lb.-ft./rad.} = 1180 \text{ lb.-ft./deg.} \quad K_R = 36,100 \text{ lb.-ft./rad.} = 630 \text{ lb.-ft./deg.}$$

$$\begin{array}{ll} a_s = 4.37 \text{ ft.} & \\ t_F = t_R = 5.0 \text{ ft.} & \end{array}$$

Note that while roll rates are traditionally expressed in units of lb.-ft./deg., they must be converted to units of lb.-ft./rad. for use in these formulae by multiplying by 57.3 deg./rad.

The results of the calculations are:

	<u>Full Formula</u>	<u>Simplified</u>	<u>Difference</u>
$\Delta W_F/A_Y$	590.8 lb./g	579.3 lb./g	-11.5 (-2.0 %)
$\Delta W_R/A_Y$	483.4 lb./g	470.7 lb./g	-12.7 (-2.7 %)

At both the front and rear axles the simplified formula gives answers that are lower than given by the full formula.

There are two parameters, given in Ref. 1, that are related to lateral load transfer. They are:

$$\text{Front Roll Rate Distribution} = K_F / (K_F + K_R)$$

$$\text{Rear Roll Rate Distribution} = K_R / (K_F + K_R)$$

and

$$\text{Front Total Lateral Load Transfer Distribution} = \Delta W_F / (\Delta W_F + \Delta W_R)$$

$$\text{Rear Total Lateral Load Transfer Distribution} = \Delta W_R / (\Delta W_F + \Delta W_R)$$

In the above example:

$$\text{Roll Rate Distribution} = 65\% \text{ front and } 35\% \text{ rear}$$

$$\text{Lateral Load Transfer Distribution} = 55\% \text{ front and } 45\% \text{ rear}$$

Finally, the calculated roll sensitivity, K_ϕ , in the above example is

$$K_\phi = \frac{-W_s h_2}{K_F + K_R - W_s h_2} = -0.035 \text{ rad/g} = -2.0^\circ/\text{g}$$

18.5 Longitudinal Weight Transfer

When a car is under positive acceleration, a_x (driving traction, measured in ft./sec.²), or negative acceleration, $-a_x$ (braking traction), an inertial reaction force is developed that is similar to the centrifugal force in a turn. In a turn that force is WA_Y ; under longitudinal acceleration the force, F , is WA_X (with sign opposite to a_x), where A_X is a_x expressed in "g" units; that is, $A_X = a_x / 32.2$.

Figure 18.10 shows the case for driving traction.

Taking moments about O (the front tire contact patch location), we have

$$\Delta W_X \ell = hWA_X$$

and

$$\Delta W_X = \frac{h}{\ell} WA_X, \text{ lb.}$$

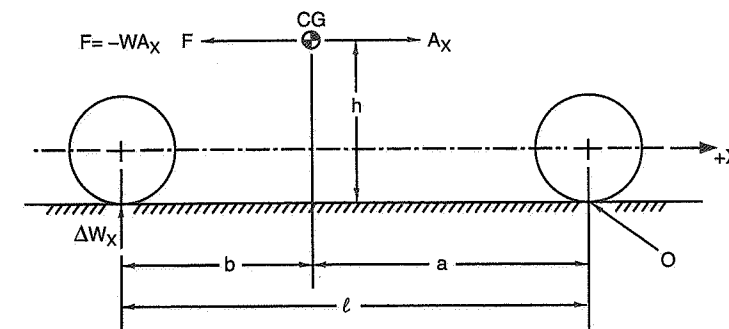


Figure 18.10 Longitudinal weight transfer—driving.

where ΔW_X is the increase in rear axle downward load (and the corresponding upward increase in the road reaction on the axle) or the corresponding decrease in front axle load.

For negative accelerations (braking), ΔW_X is given by the same expression but the front axle load is increased.

In some suspension designs there is a significant change in ride height with longitudinal acceleration so it is necessary to make sure that the correct dynamic CG height, h , is used. This ride height change is due to suspension geometry effects and ride/pitch effects that are variously called *anti-dive*, *anti-lift*, and *anti-squat*. These effects are treated in Chapter 17.

18.6 The Effects of Banking

In the previous sections we developed expressions for the calculation of longitudinal and lateral load transfer for operation on a horizontal surface. In this section we will look into the effects of operation on a banked (or superelevated) road, where the road surface forms a piece of a cone. The discussion will be limited to steady-state cornering, that is, without longitudinal acceleration. In other words, we will be dealing with lateral load transfer but not longitudinal load transfer. In addition the CG is assumed to be on the centerline of the car.

In Figure 18.11, we have a car cornering at speed V and radius R , measured in a horizontal plane passing through the CG, on a banked road with bank angle α .

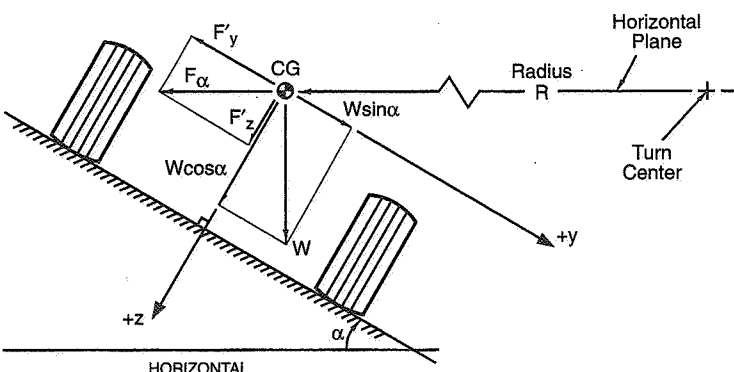


Figure 18.11 Banked RH turn, looking forward.

The centrifugal force, F_α , is no different than that for a car cornering on a horizontal surface and is equal to WA_α , where

$$A_\alpha = V^2/Rg$$

Resolving this force along the y and z axes we have

$$F'_y = -F_\alpha \cos \alpha \text{ and } F'_z = F_\alpha \sin \alpha$$

If we similarly resolve the gravitational force, W, along y and z and add the components to F'_y and F'_z we have

$$F_y = -F_\alpha \cos \alpha + W \sin \alpha \text{ (along the y axis)}^{61}$$

$$F_z = F_\alpha \sin \alpha + W \cos \alpha \text{ (along the z axis)}$$

Since $F_\alpha = WA_\alpha$ these expressions become

$$F_y = W(-A_\alpha \cos \alpha + \sin \alpha) \quad (18.1)$$

$$F_z = W(A_\alpha \sin \alpha + \cos \alpha) \quad (18.2)$$

⁶¹ The negative sign on the first term is consistent with the terminology used in Chapter 5, a positive side force is along +y.

If $\alpha = 0$ but $A_\alpha \neq 0$ (turning in a horizontal plane), these reduce to ($\cos \alpha = 1$ and $\sin \alpha = 0$):

$$F_y = -WA_\alpha \text{ (like } -WA_Y \text{ for the horizontal plane case)}$$

and

$$F_z = W, \text{ as expected.}$$

From Eq. (18.2) it is seen that the effect of banking is to change the "weight" component of tire loads. If the changed weight is called W' then

$$W' = W(A_\alpha \sin \alpha + \cos \alpha) \quad (18.3)$$

Note that if $A_\alpha \sin \alpha$ is very small and $\alpha > 0$, W' will be less than W , since $\cos \alpha$ is always less than 1.0. For example if $A_\alpha = 0$ (car is stationary), $W' < W$. On the other hand, if $A_\alpha \sin \alpha$ is large, W' will be greater than W .

Finally, the "new" front and rear weight distributions are

$$W'_F = W' \frac{b}{\ell}$$

and

$$W'_R = W' \frac{a}{\ell}$$

Note that these "weight" changes are symmetrical left and right and do not result in lateral load transfer.

The force, F_y , of Eq. (18.1) does produce lateral load transfer and has to be added to the "weight" changes just discussed above. However, it is important to recognize that in this section we are using a single-mass approach, comparable to the simplified approach of the Lateral Load Transfer Distribution section, and not the more exact three-mass approach. If one goes through the same procedures as in the previous section one finds that the resulting expressions for lateral load transfer are similar to the simplified case of the previous section. The equations are

$$\Delta W_F = (A_\alpha \cos \alpha - \sin \alpha) \left(\frac{W}{t_F} \right) \times \left[\frac{HK_F}{K_F + K_R} + \frac{b}{\ell} z_{RF} \right] \quad (18.4)$$

and

$$\Delta W_R = (A_\alpha \cos \alpha - \sin \alpha) \left(\frac{W}{t_R} \right) \times \left[\frac{HK_R}{K_F + K_R} + \frac{a}{\ell} z_{RR} \right] \quad (18.5)$$

where ΔW_F and ΔW_R are in pounds and are positive for an increase in load on the outside wheels.

The difference between these expressions and the previous ones is that the gravity component is independent of A_α and prevents writing the expressions in the $\Delta W/A_\alpha$ form. Also, note that if $\alpha = 0$ these expressions reduce to the previous ones (i.e., A_α becomes A_Y).

The values for ΔW given by Eqs. (18.4) and (18.5) represent an increase in load on the outside tire only if $A_\alpha \cos \alpha > \sin \alpha$, that is, the centrifugal force component is greater than the gravity component. Two examples will illustrate this and the calculation of total loads at the four wheels. For each example the following data apply:

$$\begin{aligned} W &= 3500 \text{ lb.} & a &= 4.56 \text{ ft.} \\ K_F &= 67,600 \text{ lb.-ft./rad.} & b &= 4.94 \text{ ft.} \\ K_R &= 36,100 \text{ lb.-ft./rad.} & \ell &= 9.5 \text{ ft.} \\ H &= 1.069 \text{ ft.} \\ Z_{RF} &= 0.25 \text{ ft.} & t_F &= 5 \text{ ft.} \\ Z_{RR} &= 0.625 \text{ ft.} & t_R &= 5 \text{ ft.} \\ R &= 1000 \text{ ft.} & \alpha &= 22^\circ \end{aligned}$$

Example 1: (above neutral speed, car wants to slide up the bank)

$$\text{Vehicle speed } V = 130 \text{ mph} = 190.7 \text{ ft./sec.}$$

$$A_\alpha = \frac{V^2}{Rg} = \frac{190.7^2}{1000(32.2)} = 1.129g$$

$$A_\alpha \cos \alpha = 1.129 \cos 22^\circ = 1.047$$

$$\sin \alpha = \sin 22^\circ = 0.375$$

Since $A_\alpha \cos \alpha$ is greater than $\sin \alpha$, the outside load increases.

The effective "weight" due to the bank angle and speed is

$$W' = W(A_\alpha \sin \alpha + \cos \alpha) = 3500 (1.129 \sin 22^\circ + \cos 22^\circ) = 4725.4 \text{ lb.}$$

And the effective front and rear axle weights are

$$W'_F = W' \frac{b}{\ell} = 4725.4 \frac{4.94}{9.5} = 2457 \text{ lb.}$$

$$W'_R = W' \frac{a}{\ell} = 4725.4 \frac{4.56}{9.5} = 2268 \text{ lb.}$$

The front lateral load transfer is

$$\Delta W_F = (1.129 \cos 22^\circ - \sin 22^\circ) \left[\frac{3500}{5} \right] \left[\frac{1.069(67,600)}{67,600 + 36,100} + \frac{4.94}{9.5} (0.25) \right]$$

$$\Delta W_F = (0.672)(700)(0.8269) = 389 \text{ lb.}$$

And for the rear,

$$\Delta W_R = (1.129 \cos 22^\circ - \sin 22^\circ) \left[\frac{3500}{5} \right] \left[\frac{1.069(36,100)}{67,600 + 36,100} + \frac{4.56}{9.5} (0.625) \right]$$

$$\Delta W_R = (0.672)(700)(0.6721) = 316.2 \text{ lb.}$$

Finally, the individual tire loads are:

$$\begin{aligned} \text{Front outside: } & W_{FO} = 2457/2 + 389 = 1617.5 \text{ lb.} \\ \text{Front inside: } & W_{FI} = 2457/2 - 389 = 839.5 \text{ lb.} \\ \text{Rear outside: } & W_{RO} = 2268/2 + 316 = 1450.0 \text{ lb.} \\ \text{Rear inside: } & W_{RI} = 2268/2 - 316 = 818.0 \text{ lb.} \end{aligned}$$

Example 2: (below neutral speed, car wants to slide down the bank)

Using the same car and track data as in Example 1 except that the speed is 60 mph (88 ft./sec.), we have:

$$A_\alpha = \frac{V^2}{Rg} = \frac{88^2}{1000(32.2)} = 0.2405g$$

$$A_\alpha \cos \alpha = 0.2405 \cos 22^\circ = 0.223$$

$$\sin \alpha = \sin 22^\circ = 0.375$$

Since $A_\alpha \cos \alpha$ is less than $\sin \alpha$, the inside load increases (and the car is said to be traveling at less than "neutral speed").

The effective "weight" due to the bank angle and speed is

$$W' = W(A_\alpha \sin \alpha + \cos \alpha) = 3500 (0.2405 \sin 22^\circ + \cos 22^\circ) = 3560.5 \text{ lb.}$$

And the effective front and rear axle weights are

$$W'_F = W' \frac{b}{\ell} = 3560.5 \frac{4.94}{9.5} = 1851.5 \text{ lb.}$$

$$W'_R = W' \frac{a}{\ell} = 3560.5 \frac{4.56}{9.5} = 1709.0 \text{ lb.}$$

The front lateral load transfer is

$$\Delta W_F = (0.2405 \cos 22^\circ - \sin 22^\circ) \left[\frac{3500}{5} \right] \left[\frac{1.069(67,600)}{67,600 + 36,100} + \frac{4.94}{9.5} (0.25) \right]$$

$$\Delta W_F = (-0.1516)(700)(0.8269) = -87.7 \text{ lb.}$$

And for the rear,

$$\Delta W_R = (0.2405 \cos 22^\circ - \sin 22^\circ) \left[\frac{3500}{5} \right] \left[\frac{1.069(36,100)}{67,600 + 36,100} + \frac{4.56}{9.5} (0.625) \right]$$

$$\Delta W_R = (-0.1516)(700)(0.6721) = -71.3 \text{ lb.}$$

Finally, the individual tire loads are:

$$\text{Front outside: } W_{FO} = 1851.5/2 - 87.7 = 838 \text{ lb.}$$

$$\text{Front inside: } W_{FI} = 1851.5/2 + 87.7 = 1013 \text{ lb.}$$

$$\text{Rear outside: } W_{RO} = 1709.0/2 - 71.3 = 783 \text{ lb.}$$

$$\text{Rear inside: } W_{RI} = 1709.0/2 + 71.3 = 926 \text{ lb.}$$

18.7 Other Terrain Effects

Just as banking has an effect on the normal loads seen by each tire, other terrain effects also can alter the total tire loading and load distribution. In this section we show how to modify tire loading conditions due to grades, dips, and crests.

Grade

The effects of grade modify both the total normal load (perpendicular to the ground) and its fore and aft distribution. As seen in Figure 18.12, the total vehicle weight vector remains the same regardless of grade; that is, it points toward the center of the earth. However, the vector component perpendicular to the ground depends on the grade angle, θ . This results in a reduction of total normal force $W_F + W_R$. The grade angle also results

in a component of weight parallel to the ground which, as in the case of accelerating or braking on flat ground, results in a longitudinal weight transfer. The effects of grade and longitudinal acceleration can be combined in finding the changes in front and rear loads due to both.

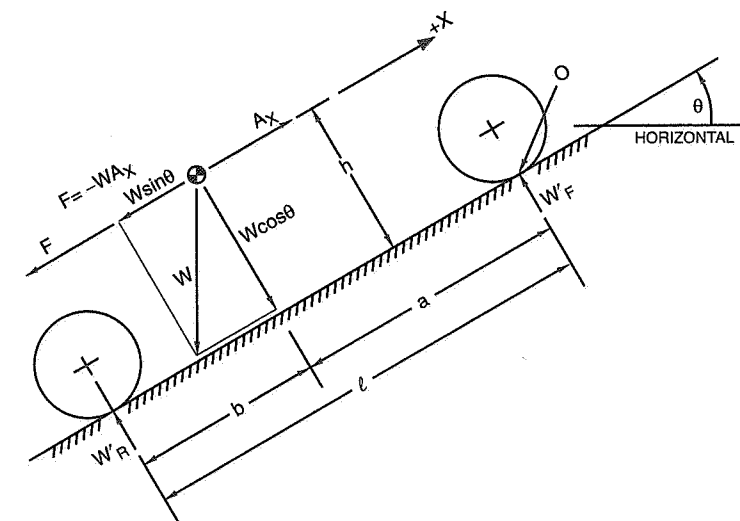


Figure 18.12 Effect of grade.

In Figure 18.12, a positive grade ($+\theta$, uphill) is shown with the car accelerating at $+A_X$ (in g's). The total vehicle weight vector has a component $W \cos \theta$ perpendicular to the ground and a component $W \sin \theta$ parallel to the ground. The acceleration results in an inertial reaction force, F , whose magnitude is $W A_X$ and sense opposite to A_X (that is, $F = -W A_X$). The force components parallel to the ground are additive.

Summing the forces perpendicular to the grade we have

$$W'_F + W'_R = W \cos \theta \quad (18.6)$$

and taking moments about O produces

$$\sum M_O = W'_R \ell - (W A_X + W \sin \theta) h - W \cos \theta a = 0$$

or

$$W'_R = W \left(\frac{a}{\ell} \right) \cos \theta + W \left(\frac{h}{\ell} \right) (A_X + \sin \theta) \quad (18.7)$$

Substituting into (18.6) we find

$$W'_F = W \cos \theta \left(1 - \frac{a}{\ell}\right) - W \left(\frac{h}{\ell}\right)(A_X + \sin \theta)$$

or

$$W'_F = W \left(\frac{b}{\ell}\right) \cos \theta - W \left(\frac{h}{\ell}\right)(A_X + \sin \theta)$$

On flat ground with $V = 0$ or $V = \text{constant}$ ($A_X = 0$) and neglecting aero lift, the front and rear axle weights reduce to

$$W_F = W \left(\frac{b}{\ell}\right) \text{ and } W_R = W \left(\frac{a}{\ell}\right)$$

Therefore, the change in axle loading due to grade and longitudinal acceleration is

$$\Delta W_F = W'_F - W_F = W \left(\frac{b}{\ell}\right)(\cos \theta - 1) - W \left(\frac{h}{\ell}\right)(A_X + \sin \theta)$$

$$\Delta W_R = W'_R - W_R = W \left(\frac{a}{\ell}\right)(\cos \theta - 1) + W \left(\frac{h}{\ell}\right)(A_X + \sin \theta)$$

As an example, assume a car is accelerating up a hill at $A_X = +0.2g$ with a grade angle of $+10^\circ$. Further let:

$$\ell = 9.5 \text{ ft.} \quad a = 4.56 \text{ ft.} \quad b = 4.94 \text{ ft.} \quad h = 1.5 \text{ ft.} \quad W = 3500 \text{ lb.}$$

$$\Delta W_F = 3500 \left(\frac{4.94}{9.5}\right)(\cos 10^\circ - 1) - 3500 \left(\frac{1.5}{9.5}\right)(+0.2 + \sin 10^\circ)$$

$$\Delta W_F = 3500(0.52)(0.9848 - 1) - 3500(0.1579)(0.2 + 0.1736) = -27.7 - 206.5 = -234.2 \text{ lb.}$$

$$\Delta W_R = 3500 \left(\frac{4.56}{9.5}\right)(\cos 10^\circ - 1) + 3500 \left(\frac{1.5}{9.5}\right)(+0.2 + \sin 10^\circ)$$

$$\Delta W_R = 3500(0.48)(0.9848 - 1) + 3500(0.1579)(0.2 + 0.1736) = -25.5 + 206.5 = +181.0 \text{ lb.}$$

Note that the above holds equally for downgrades and braking conditions with sign changes for θ and A_X .

Crests

Wheel loads are also modified when cresting a hill. This is because a car cresting a hill is traversing a vertical curve of radius R and therefore develops a centrifugal force in the same manner as in cornering. The magnitude of this force is WV^2/Rg and, for cresting, reduces the wheel loadings.

The general crest case is shown in Figure 18.13. For this case we have a car traveling at speed V (in ft./sec.) traversing a hill crest of radius R . The car is not yet at the top of the hill but is at an angle θ from the top. Note that this is essentially the same as the flat grade case looked at previously. The only differences are:

- The centrifugal force, WV^2/Rg , reduces wheel loading.
- Differences in road curvature between the front and rear axles result in slightly different directions of axle normal forces from the angle θ .

This latter effect can be ignored for typical vertical curve radii.

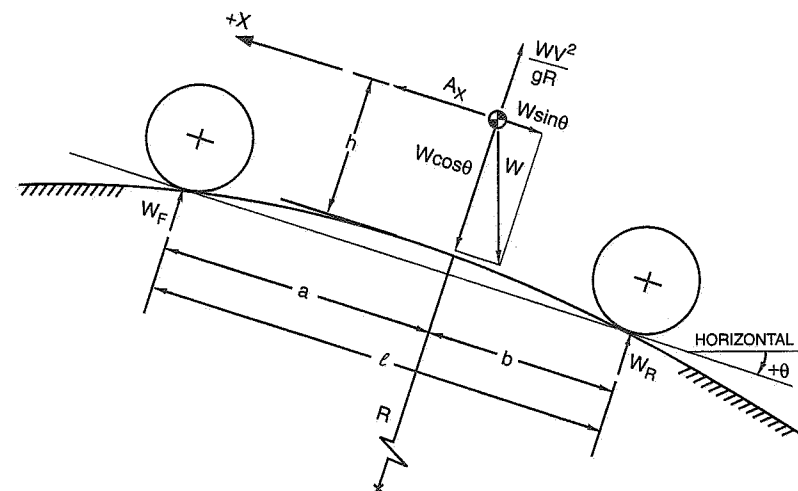


Figure 18.13 Effect of crests.

Applying a similar analysis procedure as used for the flat grade case we find that the changes in axle loadings are

$$\Delta W_F = W \left(\frac{b}{\ell} \right) \left(\cos \theta - \frac{V^2}{Rg} - 1 \right) - W \left(\frac{h}{\ell} \right) (A_X + \sin \theta)$$

$$\Delta W_R = W \left(\frac{a}{\ell} \right) \left(\cos \theta - \frac{V^2}{Rg} - 1 \right) + W \left(\frac{h}{\ell} \right) (A_X + \sin \theta)$$

As before, A_X can be either positive (accelerating) or negative (braking) and θ can be positive (uphill—before the crest) or negative (downhill—after passing the crest).

Dips

Traversing a dip in the road is the same situation as traversing a crest except that the centrifugal acceleration acts to increase axle loadings.

The axle load change equations become

$$\Delta W_F = W \left(\frac{b}{\ell} \right) \left(\cos \theta + \frac{V^2}{Rg} - 1 \right) - W \left(\frac{h}{\ell} \right) (A_X + \sin \theta)$$

$$\Delta W_R = W \left(\frac{a}{\ell} \right) \left(\cos \theta + \frac{V^2}{Rg} - 1 \right) + W \left(\frac{h}{\ell} \right) (A_X + \sin \theta)$$

Note, however, that in this case, a positive θ (nose uphill) occurs after the dip.

18.8 Aerodynamic Loads

A discussion of aerodynamics as related to race cars is contained in Chapters 3 and 15. In this section we will summarize the effects that aerodynamic forces have on wheel loads.

By SAE convention the aerodynamic axis system for automobiles is located in the ground plane equidistant from the four tires (that is, at the half wheelbase, half track position). With this axis system, only the aerodynamic pitch and roll moments and overall lift affect wheel loads. These are calculated from:

Lift:	$L = C_L q A$	(lb.)
Pitching Moment:	$PM = C_{PM} q A \ell$	(lb.-ft.)
Rolling Moment:	$RM = C_{RM} q A \ell$	(lb.-ft.)

where q = dynamic pressure (lb./ft.²)
 A = reference frontal area (ft.²)
 ℓ = wheelbase (ft.)
 C_L = lift coefficient
 C_{PM} = pitch moment coefficient
 C_{RM} = roll moment coefficient

In racing applications overall lift and pitching moment are usually combined into separate front and rear lift acting at the respective axle locations and are calculated from:

Front lift:	$LF = C_{LF} q A$	(lb.)
Rear lift:	$LR = C_{LR} q A$	(lb.)

where C_{LF} = front lift coefficient
 C_{LR} = rear lift coefficient

If overall lift and pitching moment coefficients are available instead of the front and rear lift coefficients, the conversion is as follows:

$$C_{LF} = 1/2 C_L + C_{PM}$$

$$C_{LR} = 1/2 C_L - C_{PM}$$

Given the front and rear aerodynamic lift forces, the changes in wheel loads on the left and right sides are simply the negative of 1/2 the force (negative because lift reduces wheel loading).

A positive aerodynamic rolling moment increases loads on the right side and decreases loads on the left. The rolling moment is distributed to the front and rear axles in proportion to the roll stiffness. Therefore the total aerodynamic load changes for each wheel are calculated as:

$$\Delta W_1 = -\frac{LF}{2} - \frac{K_F}{K_F + K_R} \left(\frac{RM}{t_F} \right) \quad (\text{lb.})$$

$$\Delta W_2 = -\frac{LF}{2} + \frac{K_F}{K_F + K_R} \left(\frac{RM}{t_F} \right) \quad (\text{lb.})$$

$$\Delta W_3 = -\frac{LR}{2} - \frac{K_R}{K_F + K_R} \left(\frac{RM}{t_R} \right) \quad (\text{lb.})$$

$$\Delta W_4 = -\frac{LR}{2} + \frac{K_R}{K_F + K_R} \left(\frac{RM}{t_R} \right) \quad (\text{lb.})$$

where the subscripts 1, 2, 3, 4 refer to the left front, right front, left rear, and right rear wheels, respectively.

As an example, consider the following car data:

$$A = 20 \text{ ft.}^2 \quad t_F = 5 \text{ ft.} \quad t_R = 5 \text{ ft.} \quad \ell = 9.5 \text{ ft.}$$

$$K_F = 67,600 \text{ lb.-ft./rad.} \quad K_R = 36,100 \text{ lb.-ft./rad.}$$

$$C_{LF} = 0.120 \quad C_{LR} = 0.090 \quad C_{RM} = 0.035$$

At 100 mph, the dynamic pressure (q) is

$$q = \frac{1}{2} \rho V^2 = \frac{1}{2} (0.00237) \left(100 \times \frac{88}{60} \right)^2 = 25.5 \text{ lb./ft.}^2$$

where ρ is the air mass density in slugs/ ft.^3

The aerodynamic forces are

$$LF = (0.120)(25.5)(20) = 61.2 \text{ lb.}$$

$$LR = (0.090)(25.5)(20) = 45.9 \text{ lb.}$$

And the rolling moment is

$$RM = (0.035)(25.5)(20)(9.5) = 169.6 \text{ lb.-ft.}$$

Note that the sign of the rolling moment is dependent on the direction of the apparent wind relative to the car. By convention the relative wind angle is positive if it is coming from the left front of the car. This would normally be the case when a car is cornering to the right, in still air, with a sideslip angle. If the apparent wind is coming from the right front of the car, the sign of the rolling moment must be reversed.

Finally the changes in wheel loading can be calculated:

$$\Delta W_1 = -\frac{61.2}{2} - \frac{67,600}{67,600 + 36,100} \left(\frac{169.6}{5} \right) = -52.7 \text{ lb.}$$

$$\Delta W_2 = -\frac{61.2}{2} + \frac{67,600}{67,600 + 36,100} \left(\frac{169.6}{5} \right) = -8.5 \text{ lb.}$$

$$\Delta W_3 = -\frac{45.9}{2} - \frac{36,100}{67,600 + 36,100} \left(\frac{169.6}{5} \right) = -34.8 \text{ lb.}$$

$$\Delta W_4 = -\frac{45.9}{2} + \frac{36,100}{67,600 + 36,100} \left(\frac{169.6}{5} \right) = -11.1 \text{ lb.}$$

18.9 Engine Torque Reaction

Conventional front-engine, rear-wheel-drive cars with live rear axles are subject to wheel load changes due to drive torque. This is most apparent when accelerating hard in a low gear. With a conventional counterclockwise-turning driveshaft (as viewed from the rear), no special torque reaction members in the suspension and an open differential, the right rear tire spins first.

The problem occurs because the driveshaft torque must be reacted by a change in rear axle wheel loads with the left rear increasing and the right rear decreasing. However, solving for the changes in wheel load is compounded by the fact that the driveshaft torque must also be reacted by the chassis through the engine mounts. This requires that a moment reacting the driveshaft torque be produced at the front of the car due to chassis roll.

Assuming that only pure roll of the rear axle and chassis takes place, a solution for the load changes resulting from driveshaft torque can be found by knowing the roll stiffnesses of the front suspension, the rear axle on its tires, and the rear springs.

Figure 18.14 illustrates the conventional live rear axle suspension and chassis. A driveshaft torque, T_D , is applied to the differential case.

The rotational stiffness of the rear axle due to the tires is

$$K_T = 12k_T (t_R)^2/2 \quad (\text{lb.-ft./rad.})$$

And the moment produced is

$$M_T = -K_T \phi_A$$

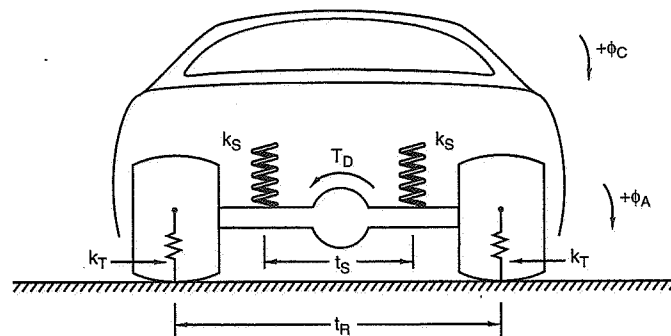


Figure 18.14 Conventional live rear axle (rear view).

where k_T = the tire vertical spring rate, lb./in.

t_R = the rear track, ft.

ϕ_A = rear axle roll angle (relative to ground) positive right side down, rad.
12 = a conversion of k_T and (and k_S below) to units of lb./ft.

The moment produced on the rear axle due to the springs and rear stabilizer bar is

$$M_S = [k_R + 12k_S(t_S)^2/2](\phi_C - \phi_A) = K_S(\phi_C - \phi_A)$$

where k_R = the rear stabilizer bar rate in lb.-ft./rad. of axle roll

k_S = the rear spring rate, lb./in.

t_S = the rear spring track, ft.

ϕ_C = the chassis roll angle, positive right side down, rad.

There also exists a restoring moment in the chassis due to the front roll rate. This is

$$M_F = -K_F\phi_C$$

where K_F = the total front roll rate in lb.-ft./rad.

Under steady-state conditions, the application of a driveshaft torque results in a negative torque applied to the axle and an equal but opposite torque applied to the chassis through the motor mounts. The net moment on the rear axle must sum to zero:

$$\sum M_A = -K_T\phi_A + K_S(\phi_C - \phi_A) - T_D = 0 \quad (18.8)$$

Similarly the net moment on the chassis must sum to zero:

$$\sum M_C = -K_F\phi_C - K_S(\phi_C - \phi_A) + T_D = 0 \quad (18.9)$$

Solving (18.8) for ϕ_A :

$$\phi_A = \frac{-T_D + K_S\phi_C}{K_T + K_S} \quad (18.10)$$

Substituting (18.10) into (18.9) we solve for ϕ_C :

$$\phi_C = \frac{+T_D}{K_F + K_S + \left(\frac{K_F K_S}{K_T} \right)} \quad (18.11)$$

The increase in the right front wheel load is

$$\Delta W_2 = K_F\phi_C / t_F \quad (18.12)$$

with a corresponding decrease in the left front.

The increase in the left rear wheel load is

$$\Delta W_3 = -K_T\phi_A / t_R \quad (18.13)$$

with a corresponding decrease in the right rear.

Example: $K_F = 67,600$ lb.-ft./rad. (total front roll rate)

$k_S = 300$ lb./in.

$k_T = 1500$ lb./in.

$t_S = 4$ ft.

$t_R = 5$ ft.

$t_F = 5$ ft.

$k_R = 7000$ lb.-ft./rad. (rear anti-roll bar rate)

$T_D = +300$ lb.-ft.

$$K_T = 12(1500)(5^2/2) = 225,000 \text{ lb.-ft./rad.}$$

$$K_S = 7000 + 12(300)(4^2/2) = 35,800 \text{ lb.-ft./rad.}$$

$$\begin{aligned} \phi_C &= \frac{300}{67,600 + 35,800 + \left(\frac{67,600 \times 35,800}{225,000} \right)} \\ &= 0.00263 \text{ rad.} = 0.151^\circ \text{ of chassis roll} \end{aligned}$$

$$\phi_A = \frac{-300 + 35,800(0.00263)}{225,000 + 35,800}$$

$$= -0.00079 \text{ rad.} = -0.0452^\circ \text{ of axle roll}$$

$$\Delta W_2 = 67,600(0.00263)/5 = 35.6 \text{ lb.}$$

$$\Delta W_1 = -35.6 \text{ lb.}$$

$$\Delta W_3 = -225,000(-0.00079)/5 = 35.6 \text{ lb.}$$

$$\Delta W_4 = -35.6 \text{ lb.}$$

Note that the driveshaft torque produces a diagonal jacking effect of significant magnitude. Also, this load transfer does not occur with an independent rear suspension because the differential is fixed to the chassis and the engine torque is reacted through the chassis, not the rear springs.

Some conventional live axles have a torque tube or arm used to take all or some of the driveshaft torque back to the chassis. If this is the case, then the effect of drive torque, T_D , should be reduced by the amount taken out by the chassis in the above example.

18.10 Asymmetrical Effects

On a closed race course, a car always turns 360° more per lap one way than the other. This is most apparent on oval tracks where completing one lap requires 360° of left turning and no right turning. Even on road courses (generally lapped clockwise), a car turns 360° to the right more than the left in completing a lap. Because of this it is often advantageous to bias a car's cornering capability in the direction most frequently turned.

One way of achieving a cornering bias is to make the car asymmetric. Commonly used asymmetries (particularly on oval track cars) include:

- Static CG offset (from centerline)
- Weight jacking (or wedge)
- Stabilizer bar preload
- Tire and tire pressure differences
- Tire stagger (diameter differences)
- Ride—camber characteristics

The reason that asymmetries affect cornering performance relates directly to basic tire characteristics. With the exception of camber, all of the above items affect static wheel loadings. In turn, wheel loadings while cornering are modified. As was shown in Chapter 7, the tire side force as a function of load for a pair of wheels on an axle is maximized when the wheels are loaded equally. Conversely, the greater the tire loading difference, the less maximum side force available.

A static CG offset toward the inside of a turn compensates for the normal lateral weight transfer occurring in a turn and therefore increases maximum side force available. The tire loads will be more equal left and right after weight transfer occurs than if the CG were on the centerline.

Weight jacking, roll bar preload and stagger changes all affect wheel load distribution but do not affect the CG position. They all result in a weight increase on one diagonal (e.g., right front, left rear) and a corresponding decrease on the opposite diagonal. As such, they change the maximum side force distribution front to rear. They are therefore trim change parameters that affect over/understeer.

For example, if a left-turning car is loose at the limit (rear axle limits the maximum lateral force), increasing the static weight on the RF wheel will result in a greater load difference at the front axle while cornering and thus a decreased maximum side force potential for the front track. At the same time, the LR load is increased which results in a decrease in load difference at the rear axle and a corresponding increase in maximum side force capability for the rear track. Both of these changes are in the direction of push and the car becomes tighter while cornering. This example will hold true for small changes in load on cars that are "well behaved," that is, cars which do not exhibit large changes in other areas as a result of the jacking.

In the remainder of this section we will show how to calculate wheel loads for the most general situation—an offset CG car cornering on a banked track while undergoing longitudinal acceleration.

Longitudinal Load Transfer

The expression for longitudinal load transfer given in Section 18.5 gives the axle load transferred, in pounds, for a given longitudinal acceleration, A_x . The axle load transferred is not dependent on the lateral acceleration of the CG. However, if the CG is offset by an amount y'' , the wheels on the side of the offset will take a greater proportion of the weight transfer than the opposite side.

To account for the CG offset, it can be shown that the axle load transfer need only be multiplied by a coefficient, C_x , to obtain the load transferred to an individual wheel on an axle.

First, define the offset ratio as

$$\gamma = \frac{y''}{t/2}$$

which is the proportion of the offset ratio with respect to the half track, front or rear, whichever applies. The CG offset, y'' , is positive to the right (see Figure 18.3). The various C_X coefficients are then:

$$C_{X1} = \frac{1}{2}(1 - \gamma_F) \quad C_{X2} = \frac{1}{2}(1 + \gamma_F)$$

$$C_{X3} = \frac{1}{2}(1 - \gamma_R) \quad C_{X4} = \frac{1}{2}(1 + \gamma_R)$$

The longitudinal load transfer for each wheel is then:

$$\Delta W_1 = -C_{X1}(W)\left(\frac{h}{\ell}\right)A_X \quad \Delta W_2 = -C_{X2}(W)\left(\frac{h}{\ell}\right)A_X$$

$$\Delta W_3 = +C_{X3}(W)\left(\frac{h}{\ell}\right)A_X \quad \Delta W_4 = +C_{X4}(W)\left(\frac{h}{\ell}\right)A_X$$

where A_X is positive for acceleration and negative for braking.

Lateral Load Transfer

In this section we will make use of the analysis of the distribution of total load transfer of Sections 18.4 and 18.6 but extend both to the case where a CG offset exists. Figure 18.15 illustrates a cross section of a car through the CG while cornering on a banked turn. In the figure, note that the CG is offset to the right an amount y'' (positive) and that the height of the CG above the roll center axis is H .

By applying analysis procedures similar to those shown previously, the car roll angle while cornering can be shown to be

$$\phi = \frac{-WA_YH + (W' - W)y''}{K_F + K_R - WA_Yy'' - W'H}$$

where $A_Y = (A_\alpha \cos \alpha - \sin \alpha)$, g's

$W' = W(A_\alpha \sin \alpha + \cos \alpha)$, lb.

$A_\alpha = V^2/Rg$, g's

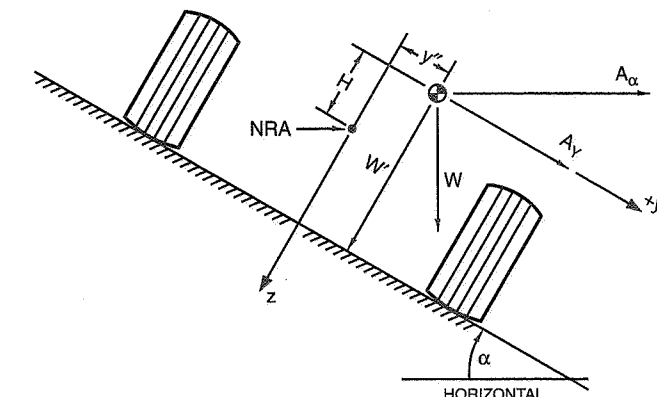


Figure 18.15 Offset CG car on banked RH turn.

Other symbols are as defined previously.

The weight transfer from right to left wheels for the front axle is

$$\Delta W_F = \frac{K_F[W A_Y H - (W' - W)y'']}{t_F(K_F + K_R - W A_Y y'' - W'H)} + W A_Y \left(\frac{b}{\ell} \right) \left(\frac{Z_{RF}}{t_F} \right)$$

where a positive value indicates an increase in left wheel load.

And for the rear,

$$\Delta W_R = \frac{K_R[W A_Y H - (W' - W)y'']}{t_R(K_F + K_R - W A_Y y'' - W'H)} + W A_Y \left(\frac{a}{\ell} \right) \left(\frac{Z_{RR}}{t_R} \right)$$

We have yet to determine the effective static weight on each wheel resulting from the banking. In Section 18.6 it is shown that for a car with the CG on the centerline, the effective front to rear weight distribution is the same as on flat ground. This is also true for left to right weight distribution ignoring any load transfers. We can use the same C_X coefficients as calculated above to find the effective wheel loads.

$$W_1 = C_{X1}(W') \left(\frac{b}{\ell} \right) \quad W_2 = C_{X2}(W') \left(\frac{b}{\ell} \right)$$

$$W_3 = C_{X3}(W') \left(\frac{a}{\ell} \right) \quad W_4 = C_{X4}(W') \left(\frac{a}{\ell} \right)$$

18.11 Summary Example

For a final summary example, we will calculate the wheel loads on a car with a negative CG offset (to the left) while cornering to the left on a banked turn. The car is also accelerating, has a live rear axle, and is subject to aerodynamic forces.

Most of the basic vehicle parameters are those used in previous examples and are in the following list:

Flat ground wheel weights:

$$\begin{aligned} W_1 &= 1092 \text{ lb.} \\ W_3 &= 1008 \text{ lb.} \end{aligned}$$

$$\begin{aligned} W_2 &= 728 \text{ lb.} \\ W_4 &= 672 \text{ lb.} \end{aligned}$$

$$\begin{aligned} W_F &= 1820 \text{ lb.} \\ W_R &= 1680 \text{ lb.} \end{aligned}$$

$$t_F = 5 \text{ ft.}$$

$$h = 1.5 \text{ ft.}$$

$$K_F = 67,600 \text{ lb.-ft./rad.}$$

$$t_R = 5 \text{ ft.}$$

$$H = 1.069 \text{ ft.}$$

$$K_R = 36,100 \text{ lb.-ft./rad.}$$

$$\ell = 9.5 \text{ ft.}$$

$$Z_{RF} = 0.25 \text{ ft.}$$

$$\alpha = -22^\circ$$

$$R = -500 \text{ ft.}$$

$$Z_{RR} = 0.625 \text{ ft.}$$

$$V = 100 \text{ mph} = 146.7 \text{ ft./sec.}$$

Note that the sign of α and R reflect a left-hand turn.

$$T_D = 350 \text{ lb.-ft}$$

$$A_X = +0.1g$$

CG Location

First calculate basic CG location parameters:

$$b = 1820(9.5)/3500 = 4.94 \text{ ft.}$$

$$a = 9.5 - 4.94 = 4.56 \text{ ft.}$$

$$y = [(728 + 672)/3500] 5 - (5/2) = -0.5 \text{ ft.}$$

Weight Transfer due to Forward Acceleration

Weight transfer due to A_X is:

$$\gamma_F = \frac{-0.5}{2.5} = -0.2$$

$$\gamma_R = \frac{-0.5}{2.5} = -0.2$$

$$C_{X1} = \frac{1}{2}(1 + 0.2) = 0.6$$

$$C_{X2} = \frac{1}{2}(1 - 0.2) = 0.4$$

$$C_{X3} = \frac{1}{2}(1 + 0.2) = 0.6$$

$$C_{X4} = \frac{1}{2}(1 - 0.2) = 0.4$$

$$\Delta W_1 = -0.6(3500)\left(\frac{1.5}{9.5}\right)0.1 = -33.2 \text{ lb.}$$

$$\Delta W_2 = -0.4(3500)\left(\frac{1.5}{9.5}\right)0.1 = -22.1 \text{ lb.}$$

$$\Delta W_3 = +0.6(3500)\left(\frac{1.5}{9.5}\right)0.1 = +33.2 \text{ lb.}$$

$$\Delta W_4 = +0.4(3500)\left(\frac{1.5}{9.5}\right)0.1 = +22.1 \text{ lb.}$$

Drive Axle Torque Reaction

Weight transfer due to drive torque is calculated as follows, where

$$t_S = 4 \text{ ft. (spring track)}$$

$$k_R = 7000 \text{ lb.-ft./rad.}$$

$$k_S = 300 \text{ lb./in.}$$

$$k_T = 1500 \text{ lb./in.}$$

$$K_T = 12(1500)(5^2/2) = 225,000 \text{ lb.-ft./rad.}$$

$$K_S = 7000 + 12(300)(4^2/2) = 35,800 \text{ lb.-ft./rad.}$$

$$\phi_C = \frac{350}{67,600 + 35,800 + \left(67,600 \times \frac{35,800}{225,000}\right)} = 0.003066 \text{ rad.}$$

$$\phi_A = \frac{-350 + 35,800(0.003066)}{225,000 + 35,800} = -0.000921 \text{ rad.}$$

$$\Delta W_2 = 67,600(0.003066)/5 = +41.4 \text{ lb.}$$

$$\Delta W_1 = -41.4 \text{ lb.}$$

$$\Delta W_3 = -225,000(-0.000921)/5 = +41.4 \text{ lb.}$$

$$\Delta W_4 = -41.4 \text{ lb.}$$

Aerodynamic Load Changes

Using the load changes from the example in Section 18.8, noting, however, that we are now cornering to the left, the load changes are:

$$\begin{aligned}\Delta W_1 &= -8.5 \text{ lb.} & \Delta W_2 &= -52.7 \text{ lb.} \\ \Delta W_3 &= -11.1 \text{ lb.} & \Delta W_4 &= -34.8 \text{ lb.}\end{aligned}$$

The left and right values from the previous example have been swapped due to the change in roll moment sign.

Lateral Weight Transfer

The lateral weight transfer calculation proceeds as follows:

$$A_\alpha = \frac{146.7^2}{-500 \times 32.2} = -1.34g$$

$$A_Y = -1.34 \cos(-22^\circ) - \sin(-22^\circ) = -0.868$$

$$W' = 3500 [-1.34 \sin(-22^\circ) + \cos(-22^\circ)] = 5002 \text{ lb.}$$

$$\Delta W_F = \frac{67,600[3500(-0.868)(1.069) - (5002 - 3500)(-0.5)]}{5[67,600 + 36,100 - 3500(-0.868)(-0.5) - 5002(1.069)]} + \frac{3500(-0.868)(4.94)(0.25)}{9.5(5)}$$

$$\Delta W_F = \frac{67,600(-2496.6)}{5(96833.9)} - \frac{319.8(4.94)(0.25)}{5} = -348.6 - 79.0 = -427.6 \text{ lb.}$$

$$\Delta W_R = \frac{36,100(-2496.6)}{5(96833.9)} - \frac{319.8(4.56)(0.625)}{5} = -186.2 - 182.3 = -368.5 \text{ lb.}$$

Where the negative signs indicate weight transfer from left to right. Therefore the individual wheel load changes are

$$\begin{aligned}\Delta W_1 &= -427.6 \text{ lb.} & \Delta W_2 &= +427.6 \text{ lb.} \\ \Delta W_3 &= -368.5 \text{ lb.} & \Delta W_4 &= +368.5 \text{ lb.}\end{aligned}$$

Effective Wheel Loads due to Banking

The effective load on each wheel (exclusive of any of the above load changes) due to the banking is:

$$\Delta W_1 = C_{X1}(W') \left(\frac{b}{\ell} \right) = 0.6(5002) \left(\frac{4.94}{9.5} \right) = 1560.6 \text{ lb.}$$

$$\Delta W_2 = C_{X2}(W') \left(\frac{b}{\ell} \right) = 0.4(5002) \left(\frac{4.94}{9.5} \right) = 1040.4 \text{ lb.}$$

$$\Delta W_3 = C_{X3}(W') \left(\frac{a}{\ell} \right) = 0.6(5002) \left(\frac{4.56}{9.5} \right) = 1440.6 \text{ lb.}$$

$$\Delta W_4 = C_{X4}(W') \left(\frac{a}{\ell} \right) = 0.4(5002) \left(\frac{4.56}{9.5} \right) = 960.4 \text{ lb.}$$

Total Wheel Loads

The total load on each wheel is obtained by summing all of the above calculated effects. This assumes that superposition works in this case, as explained at the beginning of this chapter. The final results for this example are shown in Table 18.1.

Table 18.1 Wheel Load Summary

Effect	Wheel Location			
	1	2	3	4
Effective load due to banking	1560.6	1040.4	1440.6	960.4
Longitudinal load transfer	-33.2	-22.1	+33.2	+22.1
Drive torque load transfer	-41.4	+41.4	+41.4	-41.4
Aero load changes	-8.5	-52.7	-11.1	-34.8
Lateral load transfer	-427.6	+427.6	-368.5	+368.5
Total wheel loads	1049.9	1434.6	1135.6	1274.8

CHAPTER 19

Steering Systems

"It was undoubtedly those shattering bumps that caused our downfall. It began when Zborowski said: 'Steering's gone again.'"

*Motor Racing
by S.C.H. Davis
Grand Prix, Lyon, 1924*



Introduction

This chapter begins with a discussion of steering geometry—caster angle, trail, kingpin inclination, and scrub radius. The next section discusses Ackermann geometry followed by steering racks and gears. Ride steer (bump steer) and roll steer are closely related to each other; without compliance they would be the same. Finally, wheel alignment is discussed. This chapter is tied to Chapter 17 on Suspension Geometry—when designing a new chassis, steering and suspension geometry considerations are high priorities.

19.1 Steering Geometry

The kingpin in a solid front axle is the steering pivot. In modern independent suspensions, introduced by Maurice Olley at Cadillac in 1932, the kingpin is replaced by two (or more) ball joints that define the steering axis. This axis is not vertical or centered on

Much of the material in this section resulted from detailed conversations with Terry Satchell, Penske Racing, formerly Pontiac and C-P-C Engineering.

the tire contact patch for a number of reasons. See Figure 19.1 to clarify how kingpin location is measured.

- In front view, the angle is called *kingpin inclination* and the offset of the steering axis from the center of the tire print measured along the ground is called *scrub* (or *scrub radius*). The distance from the kingpin axis to the wheel center plane, measured horizontally at axle height, is the *spindle length*.
- In side view the kingpin angle is called *caster angle*; if the kingpin axis does not pass through the wheel center then *side view kingpin offset* is present, as in most motorcycle front ends. The distance measured on the ground from the steering axis to the center of the tire print is the *trail* (called *caster offset* in Ref. 1).

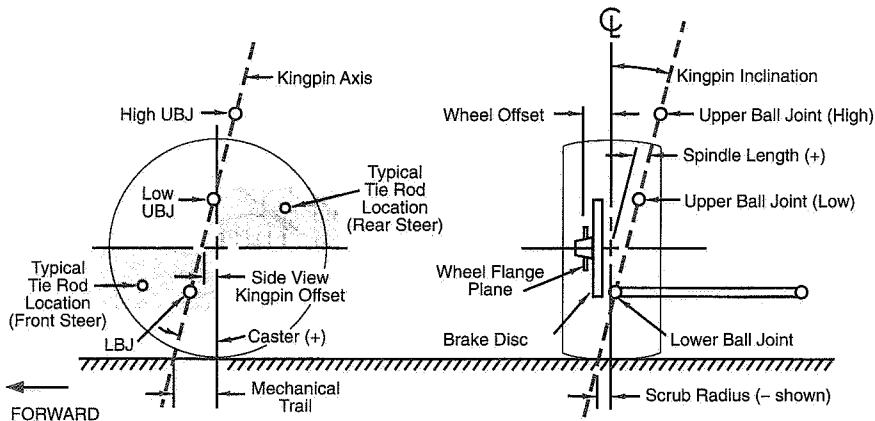


Figure 19.1 Kingpin geometry.

Kingpin Front View Geometry

As mentioned in Chapter 17, kingpin inclination, spindle length, and scrub are usually a compromise between packaging and performance requirements. Some factors to consider include:

- With a positive spindle length (virtually every car is positive as shown in Figure 19.1) the car will be raised up as the wheels are steered away from center.
- The more the kingpin inclination is tilted from vertical the more the car will be raised when the front wheels are steered. This effect always raises the car, regardless of which direction the wheel is steered, unless the kingpin inclination is true vertical. The effect is symmetric side to side only if there is no caster angle. See the following section on Caster Angle.

For a given kingpin inclination, a longer positive spindle length will increase the amount of lift with steer.

- The effect of kingpin inclination and spindle length in raising the front end, by itself, is to aid centering of the steering at low speed. At high speed any trail will probably swamp out the effect that rise and fall have on centering.
- Kingpin inclination affects the steer-camber characteristics. When a wheel is steered, it will lean out at the top, toward positive camber, if the kingpin is inclined in the normal direction (toward the center of the car at the upper end). Positive camber results for both left- and right-hand steer. The amount of this effect is small, but significant if the track includes tight turns.
- When a wheel is rolling over a bumpy road, the rolling radius is constantly changing, resulting in changes of wheel rotation speed. This gives rise to longitudinal forces at the wheel center. The reaction of these forces will introduce kickback into the steering in proportion to the spindle length. If the spindle length is zero then there will be no kick from this source. Design changes made in the last model of the GM "P" car (Fiero) shortened the spindle length and this resulted in less wheel kickback on rough roads when compared to early model "P" cars.
- The scrub radius shown in Figure 19.1 is negative, as used on front-wheel-drive cars (see below). Driving or braking forces (at the ground) introduce steer torques proportional to the scrub radius. If the driving or braking force is different on left and right wheels then there will be a net steering torque felt by the driver (assuming that the steering gear has good enough reverse efficiency). The only time that this is not true is with zero scrub (centerpoint steering) because there is no moment arm for the drive (or brake) forces to generate torque about the kingpin.

With very wide tires the tire forces often are not centered in the wheel center plane due to slight changes in camber, road surface irregularities, tire nonuniformity (conicity), or other asymmetric effects. These asymmetries can cause steering kickback regardless of the front view geometry. Packaging requirements often conflict with centerpoint steering and many race cars operate more or less okay on smooth tracks with large amounts of scrub.

- For front drive, a negative scrub radius has two strong stabilizing effects:
First, fixed steering wheel—if one drive wheel loses traction, the opposing wheel will toe-out an amount determined by the steer compliance in the system. This will tend to steer the car in a straight line, even though the tractive force is not equal side-to-side and the unequal tractive force is applying a yaw moment to the vehicle.

Second, with good reverse efficiency the driver's hands never truly fix the steering wheel. In this case the steering wheel may be turned by the effect of uneven

longitudinal tractive forces, increasing the stabilizing effect of the negative scrub radius.

Under braking the same is true. Negative scrub radius tends to keep the car traveling straight even when the braking force is not equal on the left and right side front tires (due to differences in the roadway or the brakes).

Caster Angle and Trail

With mechanical trail, shown in Figure 19.1, the tire print follows behind the steering axis in side view. Perhaps the simplest example is on an office chair caster—with any distance of travel, the wheel aligns itself behind the pivot. More trail means that the tire side force has a larger moment arm to act on the kingpin axis. This produces more self-centering effect and is the primary source of self-centering moment about the kingpin axis at speed. Some considerations for choosing the caster angle and trail are:

1. More trail will give higher steering force. With all cars, less trail will lower the steering force. In some cases, manual steering can be used on heavy sedans (instead of power steering) if the trail is reduced to almost zero.
2. Caster angle, like kingpin inclination, causes the wheel to rise and fall with steer. Unlike kingpin inclination, the effect is opposite from side to side. With symmetric geometry (including equal positive caster on left and right wheels), the effect of left steer is to roll the car to the right, causing a diagonal weight shift. In this case, more load will be carried on the LF-RR diagonal, an oversteer effect in a left-hand turn.

The diagonal weight shift will be larger if stiffer springing is used because this is a geometric effect. The distance each wheel rises (or falls) is constant but the weight jacking and chassis roll angle are functions of the front and rear roll stiffness. This diagonal load change can be measured with the car on scales and alignment (Weaver) plates.

Keep in mind that the front wheels are not steered very much in actual racing, except on the very tightest hairpin turns. For example, on a 100-ft. radius (a 40-50 mph turn), a 10-ft. wheelbase neutral steer car needs only about 0.1 rad. (5.7°) of steer at the front wheels (with a 16:1 steering ratio this is about 90° at the steering wheel).

For cars that turn in one direction only, caster stagger (differences in left and right caster) is used to cause the car to pull to one side due to the car seeking the lowest ride height. Caster stagger will also affect the diagonal weight jacking effect mentioned above.

If the caster is opposite (positive on one side and negative the same number of degrees on the other side) then the front of the car will only rise and fall with steer, no diagonal weight jacking will occur.

3. Caster angle affects steer-camber but, unlike kingpin inclination, the effect is favorable. With positive caster angle the outside wheel will camber in a negative direction (top of the wheel toward the center of the car) while the inside wheel cambers in a positive direction, again leaning into the turn.

In skid recovery, “opposite lock” (steer out of the turn) is used and in this case the steer-camber resulting from caster angle is in the “wrong” direction for increased front tire grip. Conveniently, this condition results from very low lateral force at the rear so large amounts of front grip are not needed.

4. As discussed in Chapter 2, tires have *pneumatic trail* which effectively adds to (and at high slip angles subtracts from) the mechanical trail. This tire effect is nonlinear with lateral force and affects steering torque and driver feel. In particular, the fact that pneumatic trail approaches zero as the tire reaches the limit will result in lowering the self-centering torque and can be a signal to the driver that the tire is near breakaway.

The pneumatic trail “breakaway signal” will be swamped out by mechanical trail if the mechanical trail is large compared to the pneumatic trail.

5. Sometimes the trail is measured in a direction perpendicular to the steering axis (rather than horizontal as shown in Figure 19.1) because this more accurately describes the lever (moment) arm that connects the tire lateral forces to the kingpin.

Tie Rod Location

Note that in Figure 19.1 a shaded area is shown for the steering tie rod location. Camber compliance under lateral force is unavoidable and if the tie rod is located as noted, the effect on the steering will be in the understeer (steer out of the turn) direction. If the suspension and/or rack are mounted on some sort of flexible subframe, the situation becomes much more complex than can be covered here.

19.2 Ackermann Steering Geometry

As the front wheels of a vehicle are steered away from the straight-ahead position, the design of the steering linkage will determine if the wheels stay parallel or if one wheel steers more than the other. This difference in steer angles on the left and right wheels should not be confused with toe-in or toe-out which are static adjustments and add to (or subtract from) Ackermann geometric effects.

For low lateral acceleration usage (street cars) it is common to use Ackermann geometry. As seen on the left of Figure 19.2, this geometry ensures that all the wheels roll freely with no slip angles because the wheels are steered to track a common turn center. Note that at low speed all wheels are on a significantly different radius, the inside front

wheel must steer more than the outer front wheel. A reasonable approximation to this geometry may be made as shown in Figure 19.3.

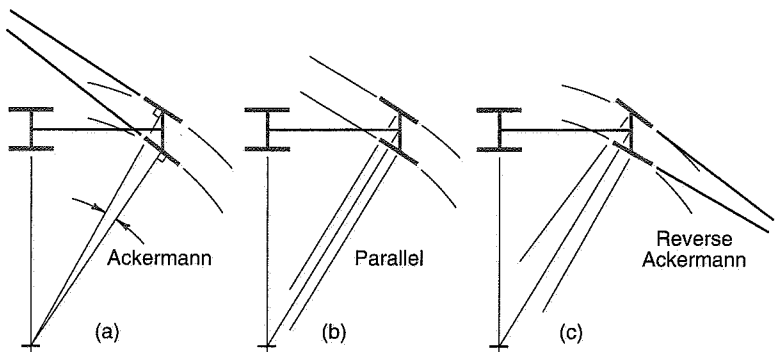


Figure 19.2 Ackermann steering geometry.

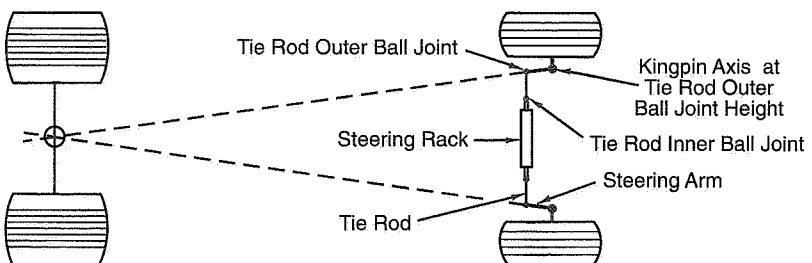


Figure 19.3 Ackermann geometry, with steering rack behind the axle line.

According to Ref. 99, Rudolf Ackermann patented the double pivot steering system in 1817⁶² and, in 1878, Charles Jeantaud added the concept mentioned above to eliminate wheel scrubbing when cornering. Another reason for Ackermann geometry, mentioned by Maurice Olley, was to keep carriage wheels from upsetting smooth gravel driveways.

High lateral accelerations change the picture considerably. Now the tires all operate at significant slip angles and the loads on the inside track are much less than on the outside

⁶² As opposed to cart and wagon steering where the axle is pivoted on a turntable located at the centerline of the vehicle.

track. Looking back to the tire performance curves, it is seen that less slip angle is required at lighter loads to reach the peak of the cornering force curve. If the car has low-speed geometry (Ackermann), the inside front tire is forced to a higher slip angle than required for maximum side force. Dragging the inside tire along at high slip angles (above the peak lateral force) raises the tire temperature and slows the car down due to slip angle (induced) drag. For racing, it is common to use parallel steering or even reverse Ackermann as shown on the center and right side of Figure 19.2.

It is possible to calculate the correct amount of reverse Ackermann if the tire properties and loads are known. In most cases the resulting geometry is found to be too extreme because the car must also be driven (or pushed) at low speeds, for example in the pits.

Another point to remember is that most turns in racing have a fairly large radius and the Ackermann effect is very small. In fact, unless the steering system and suspension are very stiff, compliance (deflection) under cornering loads may steer the wheels more than any Ackermann (or reverse Ackermann) built into the geometry.

The simplest construction that generates Ackermann geometry is shown in Figure 19.3 for "rear steer." Here, the rack (cross link or relay rod in steering box systems) is located behind the front axle and lines starting at the kingpin axis, extended through the outer tie rod ends, intersect in the center of the rear axle. The angularity of the steering knuckle will cause the inner wheel to steer more than the outer (toe-out on turning) and a good approximation of "perfect Ackermann" will be achieved.

The second way to design-in differences between inner and outer steer angles is by moving the rack (or cross link) forward or backward so that it is no longer on a line directly connecting the two outer tie rod ball joints. This is shown in Figure 19.4. With "rear steer," as shown in the figure, moving the rack forward will tend more toward parallel

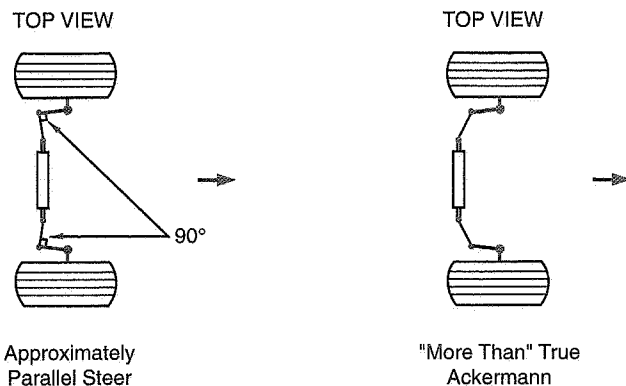


Figure 19.4 Modified steer geometry—moving steering rack forward and backward.

steer (and eventually reverse Ackermann), and moving it toward the rear of the car will increase the toe-out on turning.

A third way to generate toe with steering is simply to make the steering arms different lengths. A shorter steering arm (as measured from the kingpin axis to the outer tie rod end) will be steered through a larger angle than one with a longer knuckle. Of course this effect is asymmetric and applies only to cars turning in one direction—oval track cars.

Recommendation

With the conflicting requirements mentioned above, the authors feel that parallel steer or a bit of reverse Ackermann is a reasonable compromise. With parallel steer, the car will be somewhat difficult to push through the pits because the front wheels will be fighting each other. At racing speeds, on large-radius turns, the front wheels are steered very little, thus any Ackermann effects will not have a large effect on the individual wheel slip angles, relative to a reference steer angle, measured at the centerline of the car.

19.3 Steering Gears

The steering rack or steering box translates rotary motion of the steering wheel to linear motion at the tie rods. In turn, the tie rods translate this linear motion back to rotary motion about the kingpin axis (steering axis) resulting in steer of the front wheels.

The first thing that should be obvious is that there are a lot of connections in the steering system. All of these connections are a source of compliance (bending or deflecting) or lost motion (looseness or slop), any of which will make the steering imprecise—the driver will not know exactly in which direction the front wheels are aimed. The steering system components must all be tight and mounted securely for both safety and control.

Steering Ratio

The overall steering ratio is defined as degrees of steering wheel angle divided by corresponding front wheel angle. For race cars it varies from over 20:1 (slow) for Superspeedway cars to less than 10:1 (very fast) for Formula One cars on tight street circuits. Of course, the ultimate in fast steering is the go-kart with nearly 1:1. Common values in road racing are 16:1 to 18:1. With Ackermann (or reverse Ackermann) geometry, the steering ratio will be different side to side. Depending on the linkage configuration the steering may be nonlinear, that is, the ratio may vary with wheel angle.

Steer-steer test

A straightforward way to measure the overall steering ratio is to set the front end on alignment tables (Weaver plates) with a steering scale. A circular protractor is mounted (centered) on the steering wheel and a suitable pointer is attached so that the steering wheel angle can be measured. This test is called *steer-steer* and should be performed with the car at known load and ride height. The steering wheel is turned to the right in even intervals, perhaps 45°, 90°, etc., and the steer angles of both front wheels are noted. The test continues by rotating the steering wheel back to center, stopping at each angle, and checking the front wheel steer angles again to look for any slop (or hysteresis). Continue past center, steering to the left, and finally return to center.

Data and a plot of the results of this test are shown in Figure 19.5. From the plot, the average slope of the data points is called the *overall steering ratio*. Note that the data plots make loops; this is called *hysteresis* and means that there is some compliance and/or lost motion in this steering system. Also note that the plot is not straight; this nonlinear characteristic indicates that the linkage is not “perfect,” common in many steering systems. For racing, it is appropriate to take data points only in the range of steering wheel angles that are normally used. Steering ratio data near full lock will reflect performance only during low speed maneuvers.

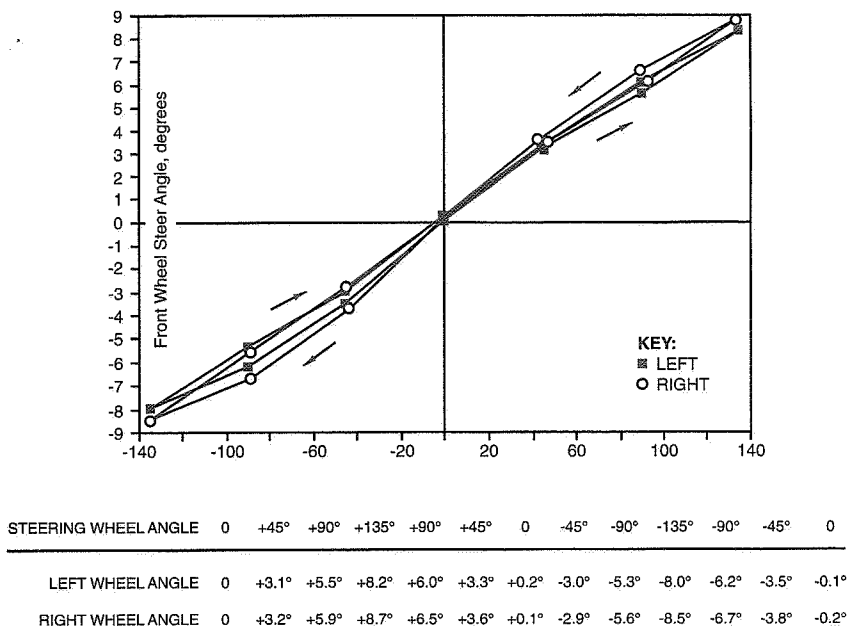


Figure 19.5 Steering ratio test.

Steering ratio partially determines the steering effort that is required for a manual steering system in conjunction with the kingpin geometry (trail and scrub). Higher (20:1) ratios will require less effort than lower (quicker) ratios. When interpreting driver comments, be aware that a quick steering ratio can often be confused with a fast vehicle transient response time, as discussed in the chapters on vehicle dynamics.

Steering ratio can be calculated as described in the following sections.

Rack-and-Pinion Steering Box Ratio

Rack-and-pinion gearsets convert rotary motion at the steering wheel to linear motion at the inner tie rod ball joint. The steering ratio is calculated using the rack *c-factor* and the steering arm length (as measured from the outer ball joint to the kingpin axis).

$$\text{c-factor} = \text{travel (in.)}/360^\circ \text{ pinion rotation}$$

Often, a steering rack will be described as a "1-7/8-inch rack" or a "2-inch rack"; this dimension is the amount the rack moves for one rotation of the steering wheel—the c-factor.

Once the c-factor is known for the rack, the steering ratio can be calculated approximately by

$$\text{Steer ratio} = \sin^{-1}(\text{c-factor}/\text{steering arm length})/360$$

where dimensions are in in.

angles are in deg.

\sin^{-1} is the same as "the angle with sin of," or arcsin

The approximation will be good as long as the angularity in the system is minimal, that is, the tie rod is nearly perpendicular to the steering arm in top and front view. For designs with high angularity, a layout is required to determine the steering ratio.

Recirculating Ball Steering Box Ratio

Recirculating ball gearsets (and also the higher-friction equivalent, worm and sector) are still used in many cars. If the box ratio is unknown, it may be easiest to measure the Pitman arm motion (with a dial indicator) for 360° of steering wheel rotation and then use this dimension (inches) as the c-factor in the rack-and-pinion equation above.

If the steering gearbox ratio is known, then the following formula may be used to approximate the steering ratio:

$$\text{Steer ratio} = \text{box ratio} \times (\text{Pitman arm length} / \text{steering arm length})$$

where all the ratios are "—to-1" as in 10-to-1
all lengths are in inches

Recirculating ball (and worm and sector) steering systems have additional linkage (compared to the rack-and-pinion system), typically a Pitman arm, cross link (relay rod), and idler arm. Because of this, angularity is much more likely to upset these simple ratio calculations. A layout may be required to design-in a desired ratio.

Reverse Efficiency

Reverse efficiency refers to the ability of the steering mechanism to pass road inputs back to the driver for feedback. Depending on the application, more or less feedback may be desirable.

Rack-and-pinion and also recirculating ball steering gears have high efficiency—most of the torque about the kingpin will appear in the steering wheel. This is desirable for smooth surface race tracks where the aligning torque signals will help the driver determine the approach of front tire breakaway.

Worm and sector steering gears do not have the ball-bearing screw that recirculating ball units have and thus they have more friction. The amount of friction is, of course, a function of the wear, adjustment, and lubrication of the unit. This type of steering system has poor (low) reverse efficiency—torques about the kingpin cannot drive the worm (steering wheel) through the sector gear. For many off-road vehicles this may be desirable to reduce driver fatigue.

Steering dampers offer another solution to the rough road situation. The steering damper is designed to offer low resistance to motion at low velocities but much higher resistance at higher velocities. This assumes that driver control happens at lower frequencies while road noise is higher frequency; the steering damper acts like a filter reducing the steering kickback.

Steering dampers reduce driver feel if there is too much damping at low velocities. The damper can mask the aligning torque (centering) feel and make limit driving more difficult, especially skid recovery. This effect is worse on low-coefficient surfaces where the aligning torque signal to the driver is weak to begin with. Steering dampers are **not recommended** unless absolutely necessary to cure a problem.

Steering dampers are also fitted to vehicles with solid front axles. In this case, the damper is to prevent (or reduce) shimmy and/or tramp caused by gyroscopic (or other) coupling between axle motions (especially axle roll on one wheel bump) and the steering system. Solid axles can have very complex dynamic motions depending on the type of axle location, brake reaction, drive reaction (FWD and 4WD), and steering geometry.

The compromises involved in producing a front suspension with good ride and handling caused the general move to independent front suspension for most vehicles.

Power Steering

Power steering is now used in many heavy, stock-based race cars such as in NASCAR, Trans-Am and GTO. The stated reason is usually to reduce driver effort and a power box (rack) will certainly have this effect.

The problem with power steering is that the units are usually modified production parts which have a built-in nonlinear characteristic. The force gain is approximately linear around center, as controlled by a spring (usually a torsion bar), and once the spring is deflected significantly the gain increases dramatically. This nonlinearity cannot be a good thing as far as driver feedback from the front wheels is concerned.

Another way to lower the driver steering effort is to design the steering geometry with very little kingpin and caster angle, a minimum of scrub radius, and a small amount of trail. With this geometry, even a very heavy car can be steered without the use of power assist, and all the associated weight and complexity. With small values of trail it is important that the suspension and steering system have very little compliance so that the geometry does not vary from design.

As an aside, production cars without power steering are often designed to lower the steering effort, some examples include:

1. Large scrub radii may be used so that at low speed (parking) the wheels can “roll around” the kingpin axis. This dramatically lowers the steering effort when compared to scrubbing the tire with centerpoint steering. Of course, steering while standing still with the brakes locked will be very difficult because the tires must be scrubbed around the kingpin axis! As mentioned earlier, large scrub radii (and spindle length) are not recommended for racing purposes because of the effects on steering kickback.
2. Negative (or zero) trail is sometimes used to counter the effect of tire pneumatic trail. Of course, at high lateral accelerations the tire pneumatic trail is generally near zero anyway.
3. Centrifugal caster refers to designing the knuckle so that its center of mass is ahead of the kingpin axis. In some cases weights are actually added to the knuckle ahead of the kingpin line. When this is done, the centrifugal force in a turn tends to steer the front wheels outward—an understeer effect. This might be done to counter the effect of negative trail, as mentioned above.

For racing, any additional unsprung weight (on the knuckle) will reduce road holding and is not advisable. Arranging the steering gear ahead of the kingpin

(front steer) adds centrifugal caster, as does moving the brake calipers to the front side of the disk.

4. Check the installation and set-up requirements carefully for the power steering box; they often require that a certain position in the box travel be lined up with straight-ahead road and steering wheel position.

19.4 Ride and Roll Steer

In general, steer that results from wheel ride (bump) motion and body roll (and pitch) motion is undesirable. With most types of steering and suspension systems some steer with ride travel is inevitable. The reason to run zero bump steer is very simple: If the wheel steers when it runs over a bump or when the car rolls in a turn, the car will travel on a path that the driver did not select.

Ride steer measurement can be made in a number of ways. Figure 19.6, taken from Ref. 150, shows a simple and accurate measurement rig that uses two dial indicators on a stand and a flat plate attached to the spindle. With the spring removed, the suspension is moved through its normal ride travel (by a jack) and the difference in the dial indicator readings gives the steer change.

This measurement will be in units of inches-of-steer per inch-of-wheel-ride travel for a known span between the dial indicators. The data are plotted as shown in Figures 19.7, 19.8, and 19.9 to describe the ride steer characteristics of a particular set-up. To compare ride steer from car to car it is useful to convert the readings to degrees-of-steer per inch of ride travel. This may be done easily using radian measure and the small angle assumption ($\tan \theta = \theta$, in radian measure). An angle of 1 inch in ~ 57 inches is very nearly 1° ; this linearity assumption is within 4% at 20° , but quickly loses accuracy at larger angles. If the span of the dial indicators is made to $57/4 = 14.25$ in., then a 1/4-in. difference in the dial indicator readings is 1° .

Sign convention—It is easiest to classify the various ride and roll steers as toe-in or toe-out as a function of ride travel, as done in the figures. A more general way to think about these steer effects is in terms of understeer or oversteer effects. If the effect steers the front wheel out of the turn, it reduces the lateral force and is said to be understeer. On the rear, the opposite is true—if a wheel is steered toward the turn center, the effect is understeer. Steer effects opposite to these are called oversteer.

Ride and roll steer are a function of the suspension geometry and the steering system geometry. As discussed in Chapter 17, every suspension has an instant axis of motion. If the tie rod is not aimed at the instant axis then steer will occur with ride because the steering and suspension are moving about different centers. If the tie rod is not the correct length for its location then it will not continue to point at the instant axis when the suspension is traveled in ride. Thus, choice of tie rod location and length are both important.

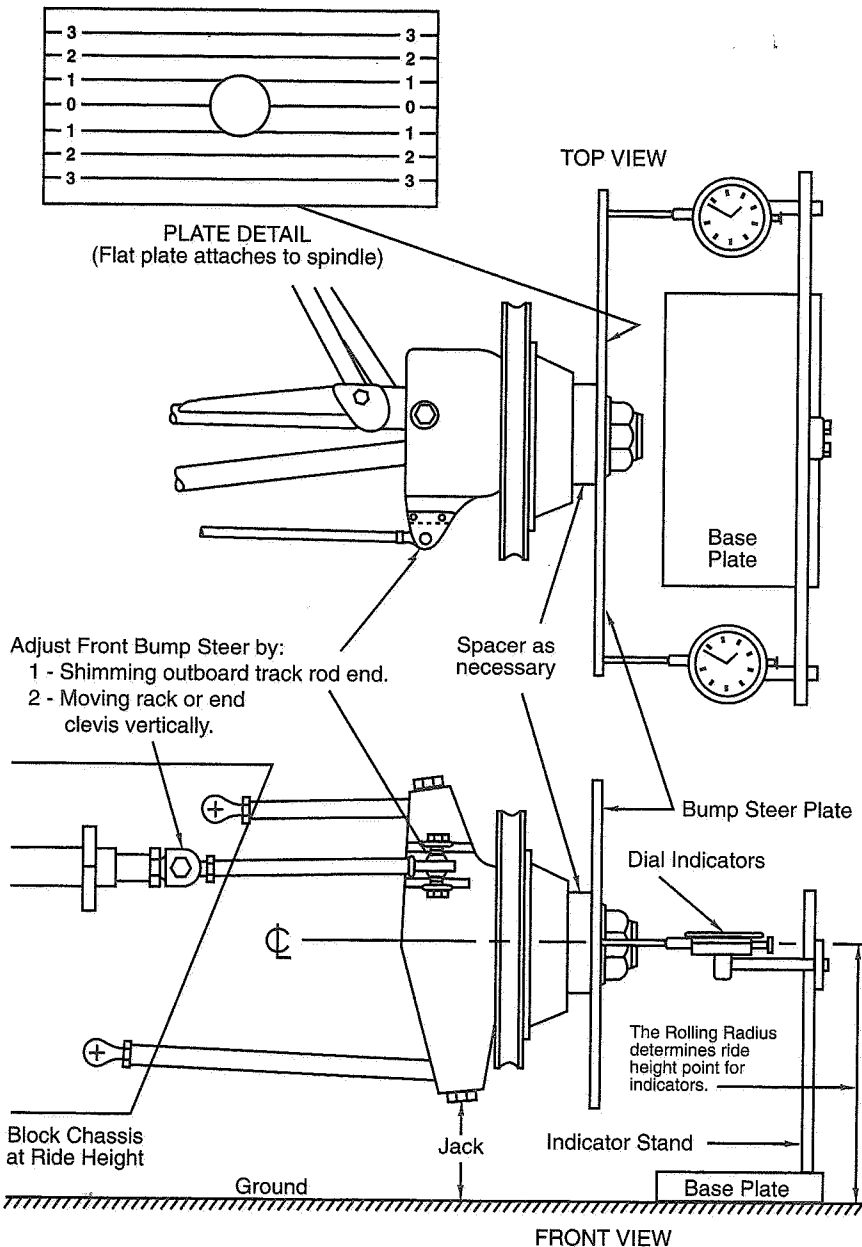


Figure 19.6 Ride steer equipment (Ref. 150).

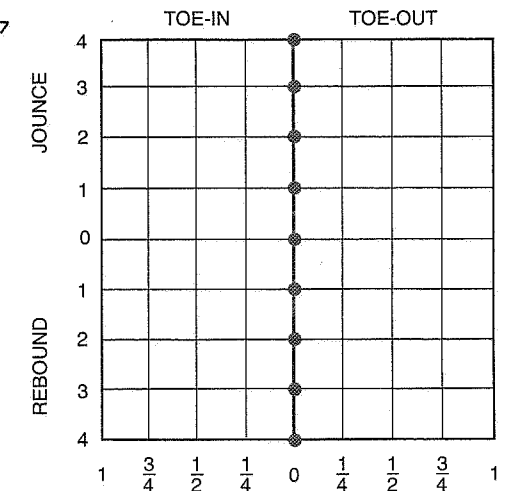
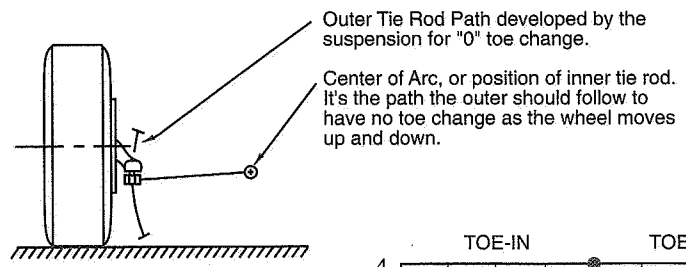
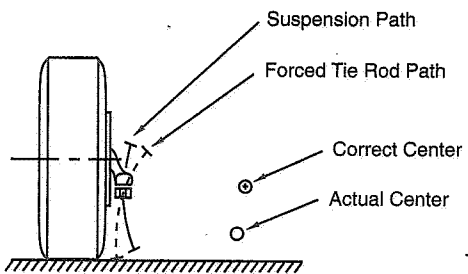


Figure 19.7 Zero ride steer—generally most desirable.

If the tie rod height and angle are adjustable it is usually possible to tune most of the ride steer out of a suspension. Figures 19.7, 19.8, and 19.9 show various cases and the general direction of the solution.

Curved ride steer plots, as shown in Figure 19.9, are to be avoided because they result in a net change in toe with ride. Another problem with curved ride steer plots is that the steer effect changes from understeer to oversteer depending on the wheel ride position. If the ride steer plot is curved as shown in this figure, another possible solution (with SLA suspension) is to raise both ends of the tie rod, to move it closer to the shorter, upper A-frame. Once this is done, the tie rod angle will also have to be adjusted.

A linear, but sloped, ride steer plot, as shown in Figure 19.8, may be used to add roll understeer to a suspension; this may help driver feel and may also compensate (somewhat) for undesirable compliance effects, as discussed in the next paragraph.



If the inner tie rod is too low, or the outer tie rod is too high as pictured above, the wheel will toe-out in jounce and toe-in in rebound. To correct for this condition, the outer should be lowered.

The slope of the line indicates the height error existing at the inner or outer tie rod end. This curve shows a correct length but a too high outer (or a too low inner).

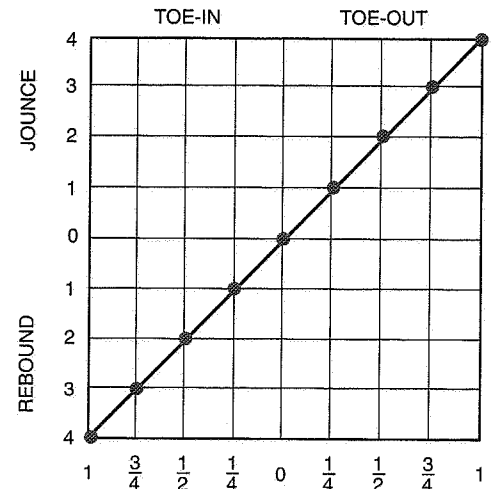


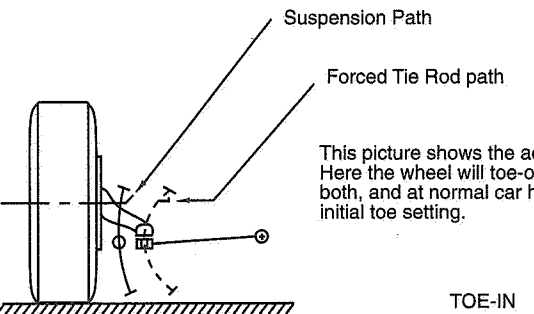
Figure 19.8 Linear ride steer—tie rod length correct, height incorrect.

Solid Front Axle

Solid front axles are typically steered with worm and sector or recirculating ball steering boxes mounted to the chassis. A solid axle has two motion paths—ride and roll, as discussed in Chapter 17. This makes it impossible to choose a location for a single steer link that will minimize both ride and roll steer because there are two instant axes of axle motion (approximately perpendicular). Solid axles can be made to have zero ride and roll steer if the steering box is mounted on the axle, as is done for some commercial vehicles; this increases the unsprung weight and will hurt road-holding performance.

Compliance Effects

Ride steer and roll steer are similar for an unloaded suspension. With the suspension loaded with lateral (and longitudinal) forces, compliance effects will cause differences between ride steer and roll steer for the following reasons:



This picture shows the actual tie rod to be too short. Here the wheel will toe-out in jounce and rebound both, and at normal car height will pass through the initial toe setting.

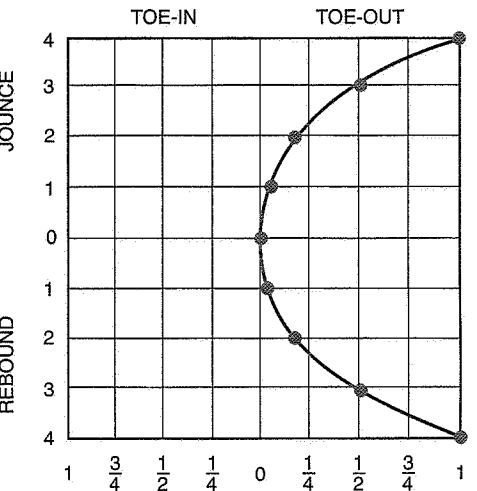


Figure 19.9 Nonlinear ride steer—tie rod length incorrect.

- With both wheels moving together (over a bump in the road), the suspension components are loaded to either compress or stretch the steering rack.
- In roll, the wheels move in opposite directions (one up and the other down) and the steering rack has a side force trying to move it to either the left or right.

The steering rack attachment and the suspension link attachments will determine how much compliance steer there is in each case. Another place where compliance can occur is in the cross link on cars with recirculating ball steering boxes—often these links are not straight for packaging reasons: A bent link in compression or tension will change length much more easily than a straight link.

In many cases, the compliance steer due to lateral force is much greater than any geometric steer (ride, roll, Ackermann effect, etc.) that is measured in the shop with or without

the springs removed. Careful attention to suspension and steering attachment points to the chassis can minimize compliances. In most cases this will be all that can be done. These effects can be measured on a suspension parameter measuring machine such as the Chevrolet Vehicle Handling Facility (VHF), or by careful application of a lateral force at the tire print.

19.5 Alignment

The alignment of the car describes the static settings for toe and camber at each wheel.

Toe—The toe settings can be referenced across the car, as measured by a tape measure front and back of the tire. The problem with this simple measurement is that it will not tell if the rear suspension is set at an angle, causing the car to crab. More accurate toe measurements can be made by referencing to the car centerline. An easy way to do this is to prepare two removable crossmembers that pin to the chassis front and rear. Strings tied to the ends of these crossmembers are run outside the wheels parallel to the chassis centerline. With this set-up, individual wheel toe is measured to the strings. The measurement may be converted to degrees, so that cars with different measuring spans can be compared using the small angle assumption (since 1 rad. = 57.3° , 1 in. in 57.3 in. is 1° —conveniently, most cars have a track width of about 57 in.).

The amount of static toe on the front will depend on other suspension parameters such as Ackermann (or reverse Ackermann) steering geometry, ride and roll steer, compliance steer (front or rear steer rack location), and camber (both static and dynamic with ride and roll motion). Minimum static toe is desirable to reduce rolling resistance and unnecessary tire heating/wear that will be caused by the tires working against each other.

Alignment changes can be used to overcome deficiencies in the car. A simple example—rear toe-out (independent suspension) can be used to improve turn-in. As the car turns in, load is added to the outside wheel and the effect is in an oversteer direction.

Camber—Camber angle to the road surface is one of the fundamental variables that determine tire performance, along with load, slip angle, pressure, temperature, etc. The static camber angle is used in conjunction with the camber compensation of the suspension geometry to position the tire at the optimum camber angle while turning.

Camber also works like steer: When a tire is cambered it tends to pull the car in the same direction in which the top of the tire is leaning. A simple way to think about this is camber-steer force equivalence. For many radial tires, 1.0° of camber produces about the same lateral force as 0.1° of steer (10:1). For bias-ply tires the effect is more pronounced:

1.0° of camber is equivalent to about 0.2° of steer (5:1). From this simple rule of thumb, it can be seen that static negative camber will require toe-out to keep the wheels from fighting each other.

CHAPTER 20

Driving and Braking

"Bolt it up and let it happen."

Anon.



Introduction

As is obvious by now, this book is primarily concerned with the turning behavior of vehicles. This chapter concentrates on the mechanical components involved with longitudinal acceleration (and deceleration). Certainly driving and braking are a very important part of the "g-g" diagram. The chapter starts with a discussion of the merits of different drive types—front-, rear-, and four-wheel drive, goes into detail on drive axle differentials, and concludes with some basic information on brakes.

20.1 Merits of Front-, Rear-, and Four-Wheel Drive

Front-, rear-, and four-wheel drive have all been used on successful racing cars at different times and under different rules and operating conditions. This section gives a historical overview of each drive type and reasons favoring its use under certain conditions. The material is general; a detailed technical look at this subject is for another book.

This chapter starts with some historical information that was originally written by Bill Close, MRA, in a white paper called "Front Drive Performance Applications," for Chevrolet Race Shop (now GM Motorsports Technology). Some of the interpretation of differential operation came from discussions with Terry Satchell.

Front-Wheel Drive

The current popularity of front-wheel drive in passenger cars might suggest that this drive concept is a relatively new one. This is hardly the case. Some historians point to the Cugnot steam carriage of 1770 as the first application of the front-drive system.

Walter Christie appears as the front-drive pioneer (circa 1904-09). His race cars were powered by huge engines in various configurations with powers approaching 100 bhp. The slow-turning engines were located transversely such that the drive was taken directly off the two ends of the crankshaft through a flywheel/clutch and universal joint to each wheel. The clutches performed the differential function. The machines were used for record attempts in dirt track racing and in several road races. One of the machines is responsible for the term "plow" which is so frequently used to describe the limit understeer of FWD competition cars. Barney Oldfield driving a Christie in a dirt track competition literally "plowed" two wide ruts in the track as he accelerated out of a turn! Recommended reading for those interested in early FWD is Ref. 53.

A number of front-drive Millers competed at Indy in the period 1924-34 including two wins with 151 cu. in. engines and one with a 220 cu. in. engine of about 200 bhp (1934). The cars were reported to have strong dropped throttle oversteer, and for this reason were consistently more successful on the high-banked board tracks at steady high speeds.

In 1947-50 the Blue Crown Specials with 270 bhp Offy engines achieved three firsts and three seconds at Indy. These cars ran on hi-test aviation gasoline reducing pit stops when compared to alcohol-burning cars. They were light, reliable machines with some 65% of the weight on the front wheels. Since then no front-drive car has won Indianapolis, nor have any appeared in the first three places since 1950. The famous FWD Novi which appeared in 1946 was reported to produce over 500 bhp. Although it was extremely fast and established lap records, it suffered from tire wear, fuel consumption and handling problems. One fatal accident with this machine was apparently due to limit understeer.

The Saab FWD appeared in 1955, the first automotive product of the Swedish aircraft firm. It was to become popular for winter driving under low-coefficient conditions and performed extremely well in long-distance rallying with such drivers as Erik Carlsson using his hand brake technique for corner entry. Following the Saab, the English Mini has been very successful in rallying and also in small displacement sedan racing.

From this brief history of front-wheel-drive race cars the following conclusions may be drawn:

1. Front drive has been most successful in the lower power/weight range and in situations in which superior directional stability on low coefficients is important. There has never been a successful front-drive Grand Prix car nor a competitive Indianapolis car of more than 300 hp.

2. In straight-line acceleration, the load on the front wheels is reduced by the longitudinal load transfer. This leads to the use of forward static weight bias to control wheel spin at the lower speeds in the lower gears. The situation is aggravated in higher-powered, lighter vehicles and may require 60-70% (or more) of the static weight on the front wheels. A limited-slip differential may be desirable to control the lightly loaded wheel under combined cornering/acceleration (turn exit) but this may induce undesirable steering forces and generally interfere with control feedback to the driver. Some success is now found with the viscous type of limited slip.
3. Forward weight bias combined with tractive effort on the front tends to induce excessive understeer in the linear range, plow at the limit (in steady-state), and reduced max lateral. This is due to tire load sensitivity and friction circle effects and is most noticeable on acceleration out of turns. The understeer/plow may be reduced by stickier tires on the front and by taking some of the lateral load transfer on the rear. The amount of LLTD on the rear is limited by lift of the inside rear wheel.
4. The forward weight bias is basically unfavorable to maximum braking because of tire load sensitivity losses due to unequal front and rear loading. The situation is improved if larger tires are used on front. Proportionally more rear brake (or even lockup of the rear tires) is one technique which has been used to get the tail out for promoting "turn-in" and rear slip angle for cornering. It has been used in various forms such as the so-called "hand-brake turn" (popular in rallying) and "trail braking" where the left foot is used for braking and the right foot remains on the throttle to keep the front wheels from locking up.
5. Trim changes occur frequently in circuit racing, for example, if balked by another competitor in a turn. Dropped throttle transfers load forward, increases the inward lateral force on the front wheels, and increases the size of the tire circle diagram on front. A destabilizing moment is created with a magnitude depending on the amount of engine motoring torque (note that with an automatic transmission, motoring torque at the wheels may be very small). If the vehicle is stable it will retrim without control action at a higher lateral acceleration. If near the limit it may spin out if not caught by control action. As Reid Railton pointed out, when a front drive is loose and near incipient spin the best treatment may be to ease on the throttle and transfer load aft, but "the relief is only temporary." Driving a high-powered front drive at the limit requires more judgment and experience, as the Novi history demonstrates.

In summary, it is more difficult to achieve a neutral vehicle over the operating range with front-wheel drive than with rear- or four-wheel drive. The compromises required to achieve a balance of handling and performance over a circuit are critical. The situation becomes progressively more difficult as power is increased.

FWD cars have appeared with a variety of engine/transmission arrangements, for example:

1. Longitudinal engine, behind differential
2. Longitudinal engine, in front of differential
3. Longitudinal engine, above differential
4. Transverse engine, above transmission
5. Transverse engine, in line with transmission

The choice of any one type over another probably is a question of packaging and possibly weight distribution.

Rear-Wheel Drive

Rear-wheel drive is by far the most successful in racing. The combination of front-wheel steering and rear-wheel drive gives the driver control over both ends of the vehicle, by "steering with the throttle."

When compared with the front-wheel drive above, the rear drive is more compromised for control rather than stability.

With respect to high power, large tires can be fitted to a rear drive more easily (packaging FWD includes wheel clearance at steering lock).

With dropped throttle trim change, the reaction to more front load is always destabilizing. With RWD the removal of road-load driving thrust increases the lateral force potential of the rear tires and is a stabilizing effect, opposing the destabilizing moment.

RWD cars are available with a variety of engine/transmission arrangements, for example:

1. Front-mounted longitudinal engine in unit with transmission and driveshaft to the rear
2. Mid-mounted longitudinal engine, otherwise as above
3. Forward-mounted longitudinal engine with engine-speed propshaft to rear-mounted transaxle
4. Mid/rear transverse engine with unit-mounted transaxle
5. Mid-mounted longitudinal engine in unit with transaxle
6. Rear-mounted longitudinal engine in unit with transaxle

Four-Wheel Drive

Four-wheel-drive race vehicles have had the most success off-road and on low-coefficient surfaces, especially with very high power. A recent example is the domination of stage rallying and Pikes Peak by 4WD turbocharged cars.

On paved surfaces, 4WD has been less successful and some probable reasons are:

1. At all but the lowest speeds, modern race tires have been able to develop enough grip to eliminate wheel spin. In dragsters, 4WD was common for a brief period before the development of cars with rear weight bias (resulting in little tractive contribution from the front tires).
2. 4WD adds a weight penalty and weight is extremely important, both for the obvious reason of power-to-weight ratio for acceleration and also tire load sensitivity.
3. With fixed torque split (near 50% each end) 4WD, the car attitude cannot be changed easily with the throttle. This calls for special driving technique. Some 4WD Grand Prix cars have been built with variable torque split center differentials. In these cars the driver's tendency is to reduce the front wheel percentage as much as possible, at which point the traction advantages of 4WD become questionable, even at low speed.

4WD cars have been built with front, mid and rear engines and a wide variety of transmission and final drives. The most successful seem to have been symmetrical front to rear in terms of weight distribution, suspension type, tires, etc.

The choice of differential type(s) greatly influences the handling of 4WDs. For racing applications it has often been found that locking out the center differential gives the best results. Front differentials are limited to open or possibly the viscous limited-slip types to avoid steering problems. Rear differentials are often limited-slip types.

20.2 Differentials

This section begins with a brief discussion of the utility of differentials. It continues with mechanical and operational descriptions of several common types that are used in racing including:

- Open differential
- Locked (spool)
- Various limited-slip units including:
 - Torsen®
 - Dana Trak-Loc (Corvette)

- Salisbury type
- Viscous differentials
- Electronic traction control (and variants)

Finally, interaction of the differential with other aspects of race car set-up are discussed.

The modern differential was invented in 1827 by Pecquer (Ref. 99) and was first used on steam traction engines for the same reason that it is still used—cornering with the drive wheels mounted on a single shaft (spool) requires tire slip, especially on tight turns. Another solution to the problem, used on some pioneer autos, was one-wheel drive. The very-low-power GM SunRaycer solar-electric race car is a successful modern example of one-wheel drive; eliminating the differential in this car saved weight and reduced drive-line complexity.

Some reasons for fitting a differential are to lower the power required when turning, reduce the turning circle for given steer angle, and to permit smooth low-speed operation. The geometry of low-speed turning is shown in Figure 20.1, and a first approximation to the amount of tire slip induced (for a locked axle) is given by the ratio of the outside wheel turning radius to the inside wheel turn radius or approximated by the ratio of the track width to the corner radius:

$$V_{\text{diff}} = \frac{R_O - R_I}{R_I} = \frac{R_O}{R_I} - 1$$

or it may be approximated as

$$V_{\text{diff}} = \frac{t}{R_{\text{ave}}}$$

where V_{diff} = Difference in apparent road velocity, outside wheel / inside wheel

R_O = Turn radius, outside wheel

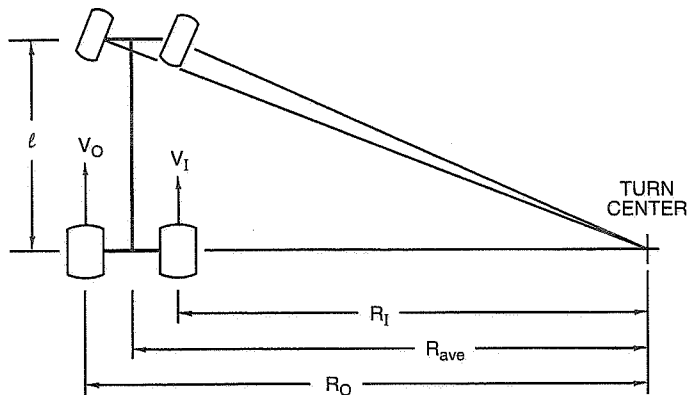
R_I = Turn radius, inside wheel

t = Axle track width (or tread width)

R_{ave} = Turn radius, measured to the center of the axle

For a turn with 30-ft. radius and a track width of 5 ft., the speed difference is $32.5 / 27.5 - 1 = 0.18$, which might be split up 9% each side with a locked axle. This is well into the sliding/squealing range for most tires.

The open differential gear cleverly allows the sum of the outside and inside wheel rotational velocities to equal a constant while allowing one wheel to speed up and the other to slow down. Of course, another result of the differential mechanism is that torque is split equally between the two sides and if one wheel loses traction the total drive force available will be just twice the force available from the tire with the least grip. The



Low-Speed Turning - Circumference of turning circle is proportional to radius, thus V_O and V_I are proportional to R_O and R_I .

Figure 20.1 Differential wheel speed, low-speed turning.

simple solution is to lock both wheels together, but of course then the low-speed turning problem returns.

All of the mechanical differentials that are currently available fall somewhere along the range from locked axle to open differential. Over the years, many limited-slip designs have been tried to provide a compromise between the low-speed turning / low drag and the high torque / wheel slip operating conditions. There is no magic in differential design; mechanical devices appear to be limited to combinations of these two basic axle types. With the addition of electronic control and computation, there is now a range of new devices that can sense and react to additional variables beyond what is practical with a purely mechanical device. These promise better performance, with the usual trade-off of more complexity.

Open Differential

The operation of the open differential is shown schematically in Figure 20.2, next to cutaways of typical bevel and spur gear units. The schematic view is from above and the link represents the differential gear (spider gear) that connects the ring gear carrier (input torque) to the two side gears. Rotation of the link is analogous to spider gear rotation.

Note that these diagrams show torque as force-vector-length. The pivots have no friction (for this simple example) and the torque split must be even, both in case (a) and in (b) where the lever is rotated due to differences in output velocity.

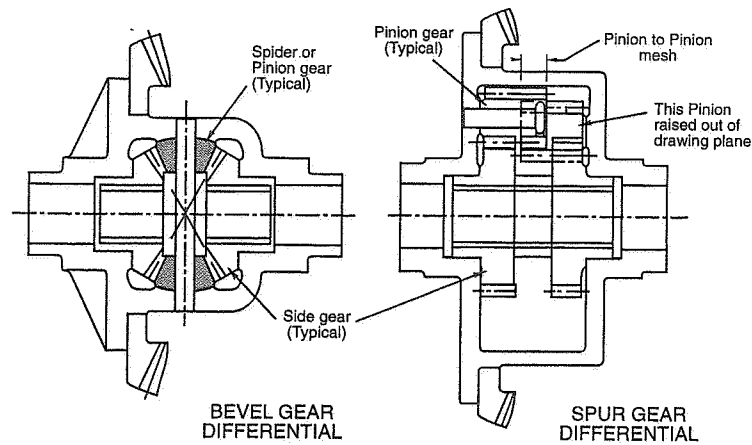


Figure 20.2 Open differentials and lever analogy to differential gear action (Ref. 99).

The wheel output torques for an open differential are shown by Figure 20.3 which plots:

$$\Delta RPM = RPM_{\text{left wheel}} - RPM_{\text{right wheel}} \quad \text{on the x-axis}$$

and

$$\Delta Torque = \text{torque}_{\text{right}} - \text{torque}_{\text{left}} \quad \text{on the y-axis}$$

In a real open differential there is stick-slip (Coulomb friction) in all the gear meshes and bearings and a small amount of hydraulic damping (proportional to velocity or velocity squared) due to oil churning. This is shown in Figure 20.3 which shows a small step in Δ Torque at the point of fast-slow wheel reversal (due to the friction), and a very gradual increase in Δ Torque with increase in Δ RPM. The result of the friction is to slightly "lock" the two output shafts to each other. This gives a small offset and slope to the theoretically even torque split. The wheel that gets more torque is always the slower wheel.

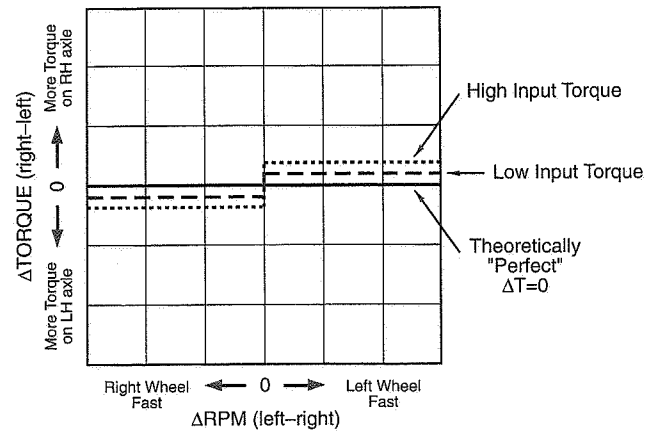


Figure 20.3 Open differential characteristics.

Note that in Figure 20.3 there are two curves for high and low engine input torque. The difference between these two curves depends on the design of the differential; an increase in friction may occur with an increase in torque. One possible mechanism for this effect is distortion of the differential case with high torque, resulting in binding of the bearings.

As mentioned in the introduction to this section, the disadvantage of open differentials is that with high power and/or low traction, the drive force at the road is limited by the tire with less traction. For low-speed operation in snow/mud, a simple solution is to partially apply the parking brake (assuming that the parking brake is on the drive axle!). This increases input torque and more total driving force will be delivered to the ground.

Another solution to the lack of traction with an open differential is to partially lock the two axles by increasing internal friction, perhaps by preloading some of the journal bearings (typically the spider gears). Now the slow wheel receives more torque and the fast wheel less torque. Referring back to Figure 20.3, extra friction will increase the size of the step in torque at the fast-slow wheel reversal point. This increase in friction will generate excess heat when the wheel speeds differ (in cornering) and some means of cooling may be required for heavy-duty usage.

In racing, various tricks have been used to good advantage when open differentials are mandated. Of course, the tech inspectors have caught on and will check that the wheels counter-rotate freely with the drive wheels jacked off the ground.

The open differential, with or without some added friction, is likely to be with us for many more years. Its strengths are in situations where rolling resistance is important (high-speed turning) and high torque / low gear / wheel spin are not problems.

Open differentials probably have the least effect on handling of any of the various types because they cannot contribute yaw moments (from left-right thrust imbalance) to the vehicle under any circumstances, either power-on or power-off. In situations where traction is broken, the inside wheel acts as a "safety valve" when it spins up. Under these circumstances, the outside wheel maintains some lateral force capability.

Open Differential with Uneven Torque Split

Referring back to the simple lever diagram of Figure 20.2, if T_{in} is moved upward, as the left side of Figure 20.4, T_1 at the top will be greater than T_2 at the bottom. In this case the two output torques will vary by the inverse of the ratio of the lever lengths.

Conventional bevel gearset differentials require that the spider gears rotate between side gears of equal size and this precludes the unequal lever arm design. There are, however,

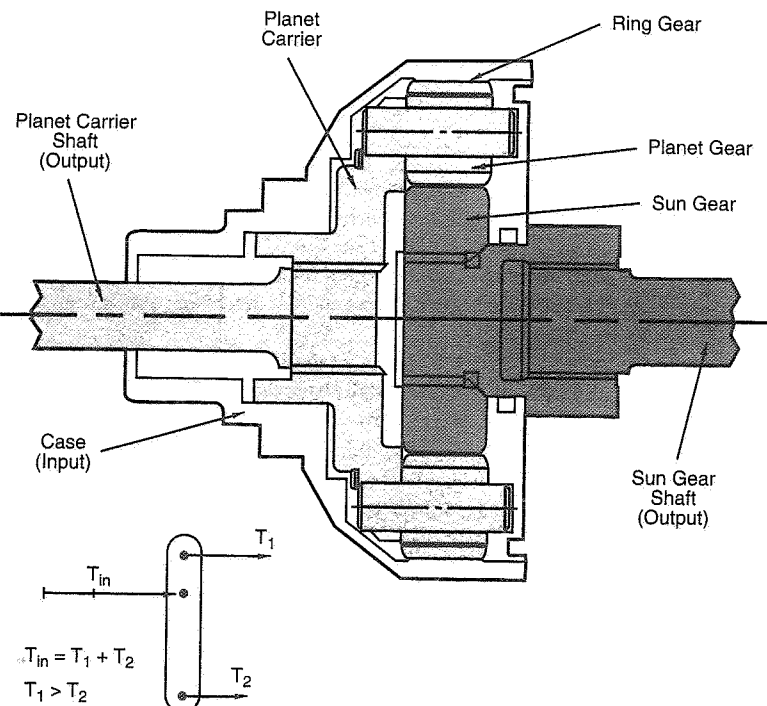


Figure 20.4 Planetary, unequal torque differential.

many other configurations of gears that give differential action. For example, planetary gearset differentials as shown in Figure 20.4 allow the two output "lever" lengths to be unequal. This is the basis for the uneven torque split differentials that may be found in the center location of four-wheel-drive cars.

Locked Axle (Spool)

A plot of locked axle behavior is shown in Figure 20.5. There is no uncertainty in rpm when both sides are locked together. The torque split to the two wheels is determined by a variety of tire-related factors such as radius of turn (of whole vehicle), revs/mile (circumference of tires), load, and lateral force / friction circle effects. Tire traction characteristics are nonlinear (similar to the lateral force characteristics discussed in Chapter 2) and it is very difficult to determine the torque split at any given operating condition.

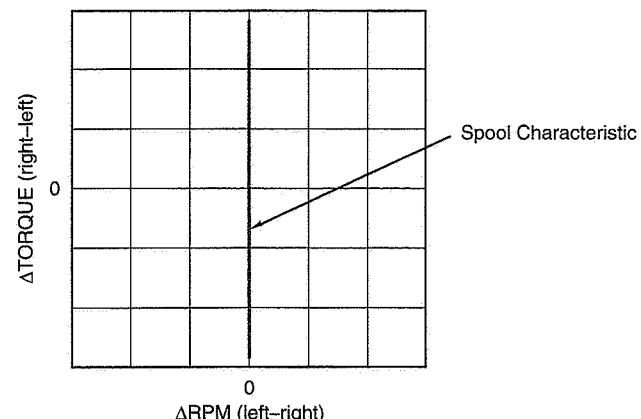


Figure 20.5 Locked axle characteristic (spool).

Locked axles are very desirable where traction is poor—low speed / low gear / poor surface operation. The tractive force that the whole axle can deliver is approximately the sum of the grip available at each tire.

Locked axles add a stabilizing yawing moment (tends toward push or understeer). Any attempt to turn the vehicle tries to slow one tire while trying to speed up the other; the resulting moment on the axle is counter to the direction of turn. Unfortunately, the effect decreases with high-speed / large-radius turns. See Chapter 5 for a description of the various moments acting on a car in a turn, including the yaw damping moment.

This stabilizing yaw moment comes with a rolling resistance penalty: tight turning scrubs the tires and uses power. Anyone who has pushed cars in the pits knows how much harder it is to push a car with a spool around turns.

A locked rear axle has a substantial effect on handling and balance, especially at lower speeds where wheel spin is possible. If a car has a spool substituted for an open differential, it typically becomes more understeer in the linear and transitional lateral acceleration ranges of tire performance. This will require more front tire lateral force capability to achieve the same balance. Conversely, a car that is loose may be improved by a spool in the linear and transitional ranges of tire performance.

However, at the limit of tire performance, under very high power, the spool will cause both wheels to spin simultaneously and cornering capability will be lost. If the drive axle is on the rear, the vehicle will lose most of the stabilizing moment from the rear and get loose (spin) very quickly.

If turning is in only one direction, tire stagger (circumference difference left-right) can be used to lower the average rolling drag by “splitting the difference” between equal rpm across the axle while straight-running and while turning. Note that with a load difference (inside to outside wheel), the actual measured static tire circumference probably cannot be directly related to the true revolutions per mile that the tire experiences at speed under power. This explains why stagger numbers are often bigger than simple rolling-distance calculations explain.

Limited-Slip Differentials

In general, limited-slip differentials attempt to compromise between the two extremes of open differential and locked axle. We place devices using mechanical friction in this category.

Dana Trac-Loc®

This limited-slip unit is standard equipment on the Chevrolet Corvette. It is shown in Figure 20.6. Clutch packs made of hardened steel plates running in a special lubricant lock the two output shafts together under certain operating conditions. The load on the clutch packs determine the torque bias. Clutch pack load is generated in two ways. First, preload on the clutch packs is provided by Belleville spring washers which are chosen to provide the static breakout torque required at zero input torque. Second, the spider gear / side gear mesh has been carefully designed to add load to the clutch packs as input torque is increased—the gear teeth are specially wedge-shaped for this purpose. There are other variations of this design that use coil springs to provide the preload torque.

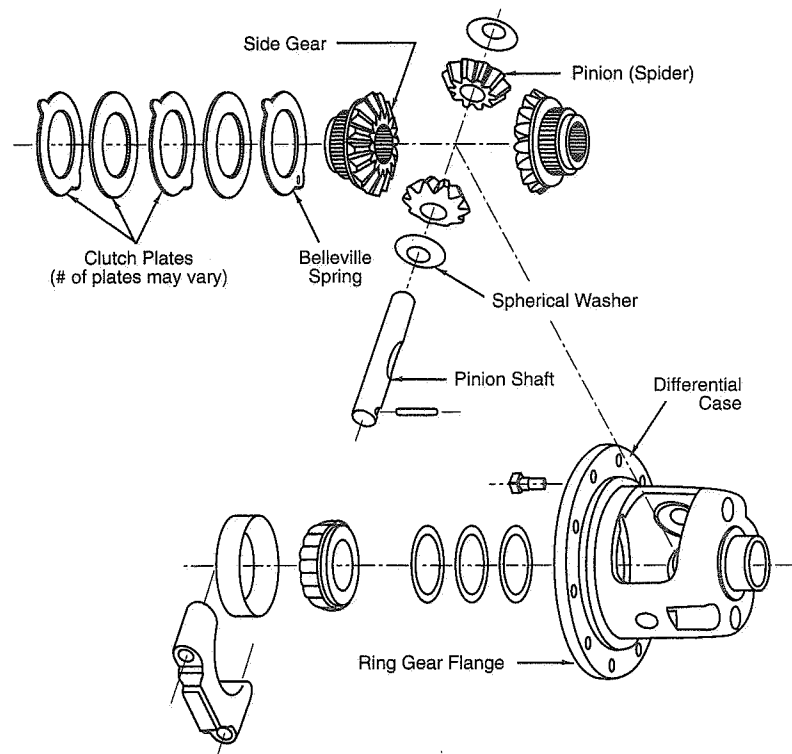


Figure 20.6 Dana Trac-Loc® limited-slip differential.

Changes in the preload are made by changing the spring washer. Changes to the torque-sensitive slope are a function of the gear pressure angles which makes tuning all but impossible (except by the manufacturer).

The operating characteristics of clutch pack limited-slip differentials are commonly shown in two types of plots, given in Figure 20.7. A good analysis of this general type (clutch pack), along with a discussion of lubrication requirements, is given in Ref. 56 from Oldsmobile.

Salisbury Axle

Another variant of limited slip, also originally designed by the Dana Corp., is the so-called Salisbury axle, shown in Figure 20.8. Like the Trac-Loc, clutch packs are used to

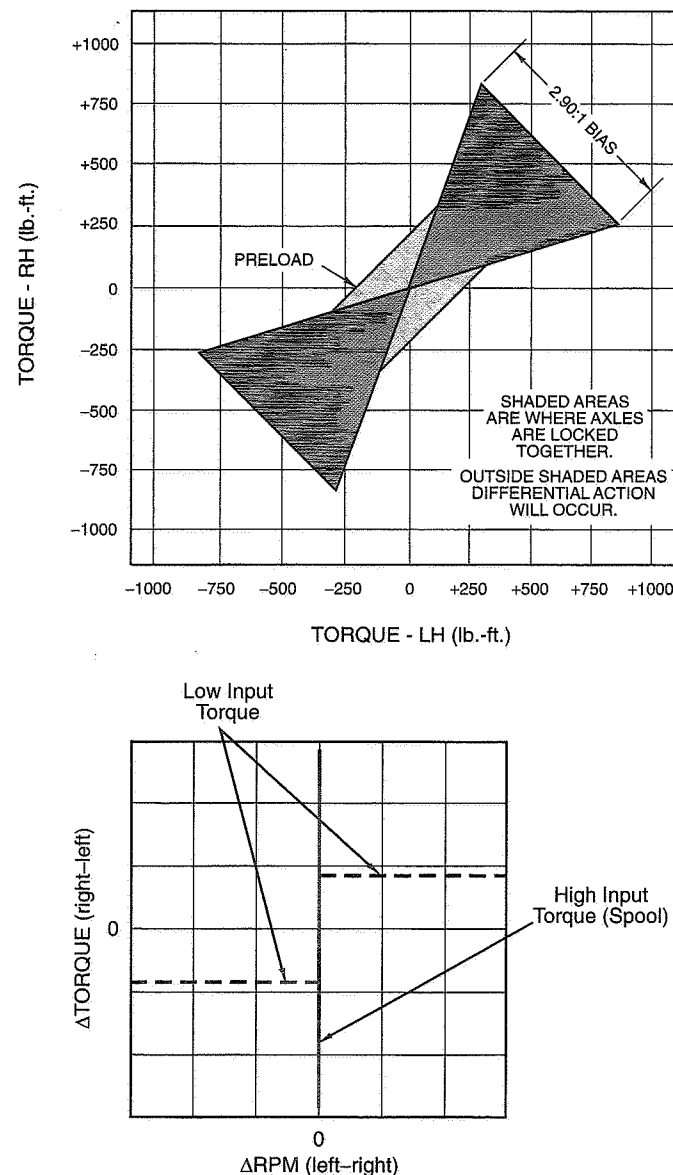


Figure 20.7 Dana Trac-Loc® characteristics.

progressively lock the two output shafts together. Here the spider gear axles rest against wedges which are spread by input torque. The wedges are numbered "5" in Figure 20.8 and the wedge angle is shown as α . With this design the bias ratio can be varied between driving and engine braking. Many other variants of this basic type have been used over the years with different types of springs used for preload and different configurations of clutch plates.

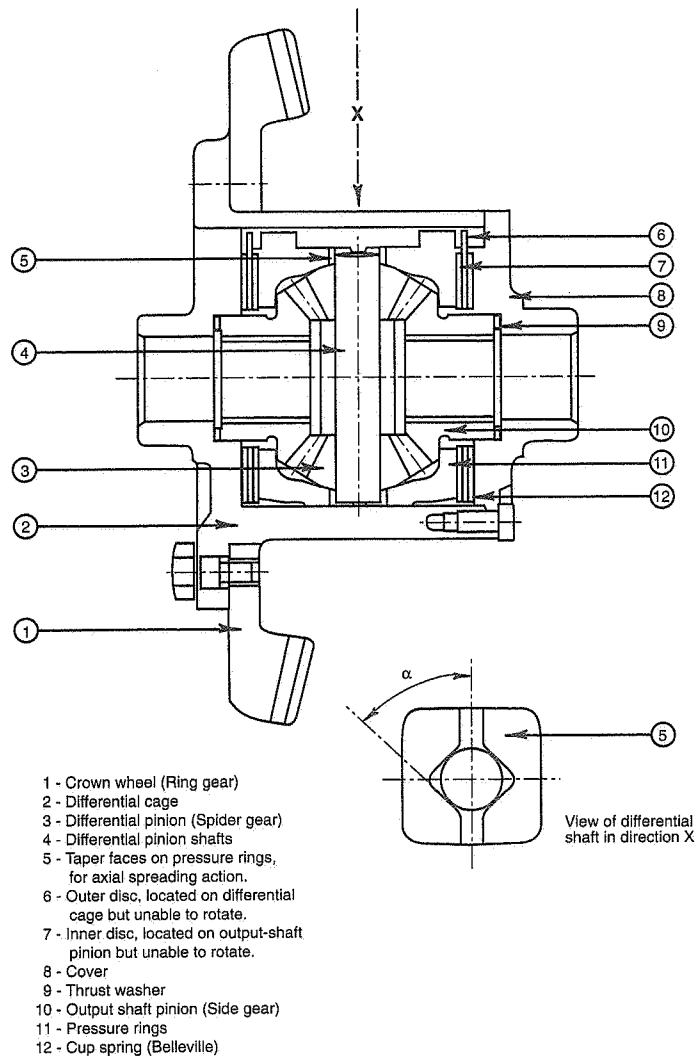


Figure 20.8 Salisbury axle (from ZF).

Tuning is perhaps easiest with this unit as preload is changed with spring changes and the bias ratio can be changed relatively easily by varying the wedge angles.

Torsen® and Torsen II® Differentials

The original Torsen® differential (Figure 20.9) uses high-helix angle INVEX™ gears combined with spur gears to substitute for the side and spider gears in a conventional open differential. The configuration might better be compared with the spur gear differential shown in Figure 20.2, but with the spurs turned 90°.

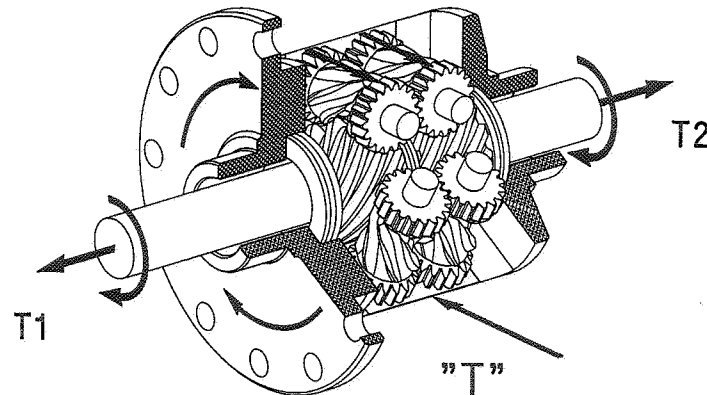


Figure 20.9 Torsen® all-gear limited-slip differential.
(Courtesy Zexel-Gleason USA, Inc.)

The name Torsen is derived from the words “torque sensing” which can be described as a change in the operating characteristics as a function of input torque. The Torsen offers a characteristic that is somewhat different from clutch pack units.

Under low input torque the differential gears are lightly loaded and, in fact, with the tires off the ground they spin freely like an open differential (in opposite directions, assuming the input shaft is locked). With increasing torque, the gear meshes are “loaded-up” and at some combination of differential speed and input torque the two output shafts are locked together like a spool. The major friction elements in the Torsen are the gear meshes.

The Torsen characteristic is similar to the other limited-slip types, but note that the bias ratio (torque on high-torque-wheel divided by torque on low-torque-wheel) can be controlled over a wide range. Bias ratio can vary from a high of 6:1 or 7:1 to a low of about

2.5:1. Tuning of the bias ratio is by selection of gear angles, gear surface treatments, and types of bearings (plain, roller, etc.) used in the unit and can be performed only by the manufacturer.

The high bias ratio and low friction at low load means that under power the original Torsen performs very much like a spool. At low input torque, such as on corner entry, it differentiates nearly freely like an open.

The newer Torsen II design (gear arrangement shown in Figure 20.10) reduces friction (and thus torque bias ratio) by placing all the gears on parallel shafts. This design operates like the original Torsen but the bias ratio can be tuned over a range of about 1.8:1 to 3:1.

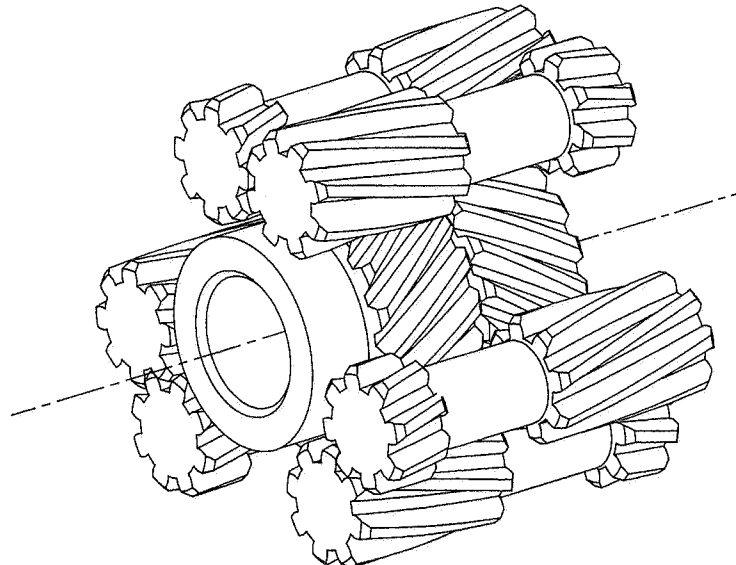


Figure 20.10 Torsen II® all-gear limited-slip differential.
(Courtesy Zexel-Gleason USA, Inc.)

Overrunning Clutch Types

In these units, such as the Weismann and the Detroit Locker, power is transmitted to the slower rotating axle (with drive torque applied) while the faster axle “overruns”; the reverse happens on overrun. Thus on corner exit, power is added to the lightly loaded in-

side wheel until its rpm increases to that of the outside wheel. At this point the two wheels are locked together as with a spool.

Depending on the power required mid-turn, the outside wheel may be unpowered and will generate maximum cornering force. With the car in "one-wheel drive" there will be no drag caused by this type of differential in cornering. Driving these types of differentials can be tricky as the characteristic changes quickly from free to locked. The relative speed of lockup in the Detroit Locker can be adjusted somewhat by changing a preload adjustment.

Viscous Differential

The viscous differential, shown in Figure 20.11, takes advantage of the characteristics of a special high-viscosity fluid. The two output shafts are connected to each other with a standard open differential and also through a multi-plate "clutch" with no mechanical contact (but very tight clearances). As can be seen on the top of Figure 20.12, the torque across the unit is a function of output shaft speed difference. As with all limited slips, the torque bias is toward the slow wheel.

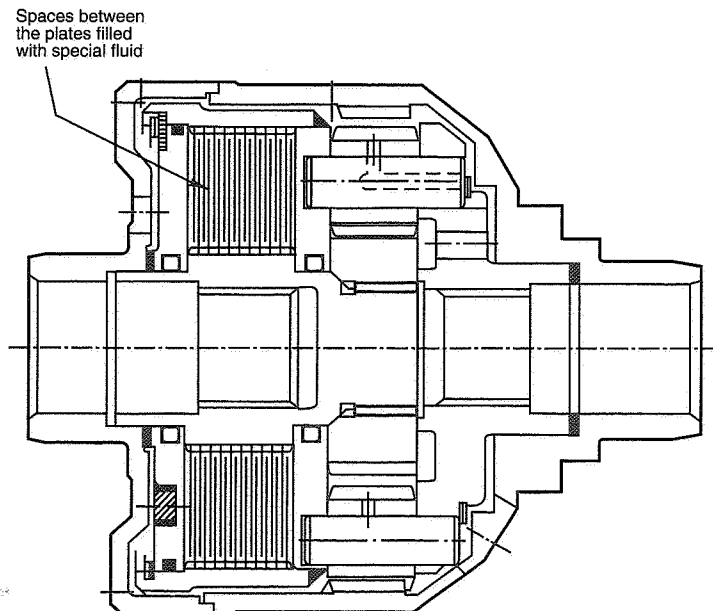


Figure 20.11 Ferguson Formula viscous differential with planetary differential for 4WD center-box use.

While typical lubricating oils thin out with increasing temperature, the special fluid used in viscous differentials increases viscosity above some temperature. As the "clutch" plates slide relative to each other, the special fluid heats up and the two output shafts are progressively locked together once the temperature exceeds approximately 100°C. This is plotted by the manufacturer on the bottom of Figure 20.12 and is called the "hump" curve.

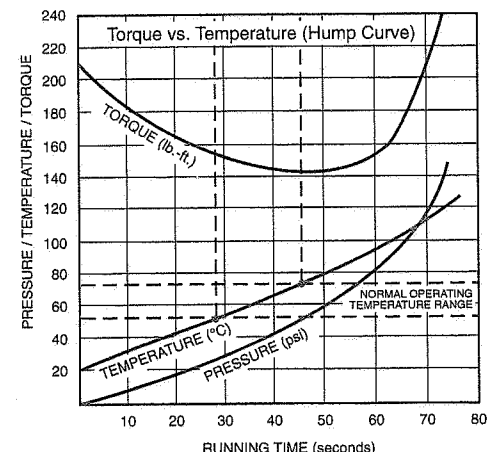
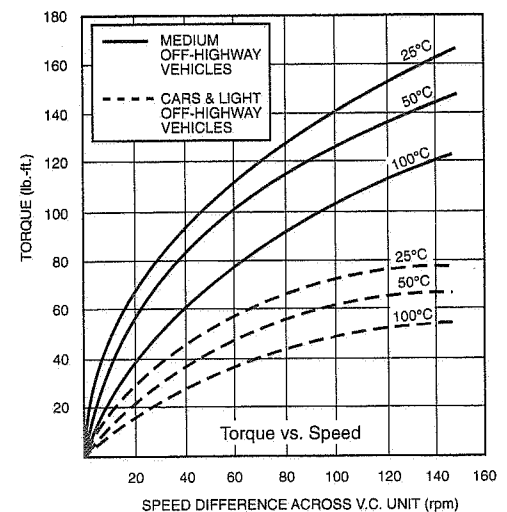


Figure 20.12 Ferguson Formula viscous differential characteristics.

Small differences in speed, as in cornering, are not enough to lock the unit and it acts like a standard open differential. Only wheel spin generates enough heat to lock the unit up, and even this takes some time to occur.

Viscous differentials have seen use as the center differential in some full-time four-wheel-drive systems and also have been used on front- and rear-wheel-drive cars.

Application to racing is relatively new and little data are available. Because the viscous differential has a time lag in its response to wheel spin, it may not be appropriate for situations where wheel spin happens only briefly. Because it is basically an open differential (until it is heated), the viscous differential should have little effect on handling. The locking effect is gradual and this also indicates that the driver will not be surprised by the action of this unit.

Traction Control and Other Electronic Improvements

As noted above, mechanical and viscous limited-slip differentials can sense input torque and/or output shaft speed differences. With electronic (computer) control, it becomes possible to sense output shaft speed and react quickly to single (or both) wheel spin. As of this writing, traction control is beginning to be offered as a production option on higher-priced cars. On sensing wheel spin-up, typical control strategy is to first apply the vehicle brake to slow the spinning wheel and then to pull-off the throttle so as not to overheat the brake.

When added to an anti-lock brake system, traction control often requires only a small amount of additional hardware and some extra computer software. In production, on a car already fitted with anti-lock, traction control may be cheaper than a limited-slip differential and possibly more effective.

Other sensors may be added to increase the "smartness" of the algorithm. For example, steer angle, speed, and (possibly) yaw rate can be used to make a calculation of the differential wheel speeds expected at any given time. When compared to the measured wheel speeds, the computer can determine if a wheel is truly spinning or not.

With a sophisticated system, traction control may offer the best solution yet to the differential problem, especially as related to handling. In normal cornering, the brakes are not in use and the open differential has its usual benign effects on handling. Under high power, wheel spin is stopped "as it happens" and in high-speed cornering there is no extra rolling resistance.

With appropriate sensing and control, the understeer moment created by a spool may even be partially simulated by traction control in response to the beginning of a spin.

20.3 Brake Systems

The braking system is one of the main component systems on a vehicle and its proper operation is important to the safety and performance of competition cars. The brake system may be broken down into four basic areas:

1. Suitable mechanical components—disk, caliper, pads, etc.
2. Hydraulic system
3. Adequate cooling
4. Brake distribution (adjustable)

Components

The first decision is the choice of manual or power boost. The manual brake system is generally more responsive at the price of higher pedal effort. Chevrolet power boost units (and possibly other brands) may be modified by removal of the noise attenuator (filter) packing around the pushrod opening to improve the response time of the diaphragm during pedal application.

The master cylinder reservoir must be located such that "g" forces cannot uncover the feed holes which would allow air into the master cylinder. The reservoir capacity must be adequate to fill all of the caliper pistons with the pads "worn-out" (bottomed). Check this whenever caliper or master cylinder type is changed.

The master cylinder pushrod must be adjusted so that the piston fully returns when the pedal is released. This allows the master cylinder to refill from the reservoir between brake applications. Before the system is filled, the master cylinder also can be checked for full stroke without pedal bottoming. In dual master cylinder systems fitted with a balance bar, check that no binding occurs that would tend to vary the brake balance.

If possible, flexible brake lines should be replaced with metal braided hose to minimize volume change due to hose expansion. Hose expansion is one possible cause of a soft or low pedal. All rigid lines must be steel with properly double-flared ends. Brake line routing should avoid loops that will trap air and make bleeding difficult. Brake lines should be routed away from exhaust systems and other hot areas.

Another cause of soft pedal is caliper flex which is visible on many of the newer, light-weight production calipers. While aluminum calipers will reduce unsprung weight, steel (or iron) calipers of the same design will be stiffer. To aid smooth brake modulation, check that the calipers work freely (especially if they are the single piston type). It is useful to polish the forward edge of the opening in the caliper housing and the leading edge of the brake shoes to a smooth finish and apply a minimum amount of a lubricant

such as Molycote to reduce the friction between the pad and caliper housing during brake application (keep lubricant off of the disks).

Brake pads are available in many styles and materials. Probably some experimentation will be necessary to find the correct combination unless your racing class has already "standardized" on a particular type. New pads typically need to be bedded in. This involves bringing them up to operating temperature in the hopes of causing any gas components in the bonding agents to leave. In at least one case that the authors are aware of, gas (or liquid) that evolved from new brake pads adhered to the brake disks and interfered with proper braking until it was removed.

Brake disk rotors must be machined to run true on the wheel bearings. Any runout will knock the pads back and cause a low pedal, not to mention steering vibration (on front).

Hydraulics

The second part of the brake system is the bleeding of the hydraulic system. It is essential that all of the air be removed from the system in order to maintain a firm pedal. First, use clean, new brake fluid. Brake fluid will absorb moisture from the air which will reduce the fluid boiling point. Due to the extreme braking temperatures encountered in competition, use DOT-approved 550° boiling point fluid. Regular fluid changes to avoid possible vapor lock under high temperature are recommended because of the above-mentioned affinity of glycol-based hydraulic fluid for water. Care should be taken when pouring the fluid into the master cylinder to prevent the formation of small bubbles which can become trapped in the system.

Silicone fluid should be used only if the system in question has silicone-compatible seals, silicone-based fluid should **not** be mixed with glycol-based fluid.

The bleed screws on the calipers must be at the extreme top of the caliper, otherwise the bleeding process will not remove all of the air. When calipers are changed for a new type it is very easy to overlook the location of the bleed screw. If the bleed screw is on the bottom of the caliper, often a switch from left to right will solve the problem, otherwise the caliper may need to be removed and rotated to raise the bleed screw to the top. In this case, the pads must be spaced apart by a shim of approximately the disk thickness during the bleeding process; the calipers can be reattached once they are bled.

When bleeding, either by pressure bleed system or by manual stroking of the pedal, tap the caliper housings with a small rubber hammer to free any lodged air bubbles that may get caught in the calipers. Use sufficient fluid to purge the system and ensure complete elimination of air bubbles.

Ventilation

Adequate ventilation for the rotors and calipers must be provided. Air must be ducted directly to the eye of the rotor and, optionally, air blast may be directed at the caliper if fluid boiling (spongy pedal) is a problem. As the front brakes do most of the work, cooling them is most important; rear cooling may also be necessary depending on the application.

Brake cooling air should be taken from a high-pressure location, for example, the front of an air dam (chin spoiler). To be effective, ducting should use 3-in. minimum diameter hose unless the duct is very short.

Brake Distribution

Proper brake balance is extremely important. First, the vehicle will not achieve the maximum braking deceleration unless all four tires are brought to the friction peak simultaneously. Second, improper brake balance will cause one end or the other to lock up first and this end of the car will lose cornering traction on corner entry. Proper brake balance is a function of the loads on the wheels, which is in turn a function of the deceleration.

There are two common ways to adjust the brake balance. The first type is most appropriate for systems that use a production-type dual piston master cylinder. This amounts to fitting a brake pressure regulator in line with whichever end of the car tends to lock up first. The other method is to use a dual master cylinder set-up with an adjustable balance beam splitting the pedal force between the two cylinders.

In either case, the brakes should be initially adjusted to bias them toward front lockup. After the driver is familiar with this characteristic, the brakes can be progressively biased toward the rear until rear lockup (leading to a spin) is approached. Take note of the direction of adjustment for your particular system. A common mistake when making small adjustments is to adjust in the wrong direction!

Estimates of proper brake balance can be made. First, a maximum deceleration must be assumed to calculate the approximate wheel loads during braking. For vehicles that will race on wet as well as dry surfaces, the calculations must be made twice to find the range of adjustment required.

$$W_{1 \text{ braked}} = W_1 + W(a/g)(h/\ell)$$

where $W_{1 \text{ braked}}$ = weight on front axle during a stop of (a/g) deceleration
 W_1 = weight on front axle with no braking but with any aero effects (download, drag) at the speed of interest
 W = gross weight of vehicle
 a/g = deceleration of the vehicle in "g" units; values can range from over 3.0g for high speed with aero download to about 0.1g for ice
 h = height of the vehicle center of gravity above ground
 ℓ = wheelbase, measured in the same units as h

The load on the rear track is given by

$$W_{2 \text{ braked}} = W_2 - W(a/g)(h/\ell)$$

where $W_{2 \text{ braked}}$ = weight on rear axle during a stop of (a/g) deceleration.

A quick look at these equations shows that at very low decelerations (when a/g is small) the weight on the wheels is nearly the same as the weight distribution. For high g decelerations the second term becomes significant. To minimize the second term effect, a low CG and long wheelbase are necessary.

Next, tire data for braking coefficient of friction is necessary. Tire braking coefficient (μ) decreases with increasing load (similar to cornering performance). Because of this "load sensitivity," the maximum μ will likely be higher on the rear axle (lightly loaded). This will probably be true even if the same design tire is used front and rear. Tire data will usually be difficult to estimate unless manufacturers' data are available. Some idea can be had by looking at the tire data for cornering given in Chapter 2.

Once the available μ at the operating load is known (or estimated), the braking force, $F = W_{\text{braked}} \times \mu_{\text{effective}}$ can be calculated. The braking force for straight-line braking will be split approximately evenly left and right so the weight and braking force on each tire will be half the total for its axle. To generate this force at the wheel, the following formula may be used to calculate the required brake line pressure:

$$p = \frac{F_x \times (R_\ell/r)}{A_c \times \mu_{\text{pad}}}$$

where p = Brake line pressure, lb./in.²
 F_x = Required longitudinal force from a wheel, lb.
 R_ℓ/r = Loaded radius of the tire / brake caliper radius
 A_c = Total caliper piston area, in.² (sum of all the pistons' areas)
 μ_{pad} = Coefficient of friction of brake pad (typical range = 0.3 to 0.45)

To generate this pressure, there will be a certain pedal force, as increased by pedal ratio, applied to the area of the master cylinder piston. Assuming that the system is not boosted, a master cylinder area is known, and there is a desired pedal force, the following formula will allow calculation of the pedal ratio for single master cylinder systems. If a dual cylinder system is used, the balance bar ratio must also be taken into effect.

$$R_{\text{pedal}} = p \times \frac{A_{\text{master}}}{F_{\text{foot}}}$$

where R_{pedal} = Distance (foot to pedal pivot) / distance (pushrod to pedal pivot); this number will be greater than 1

A_{master} = Area of master cylinder, in.²

F_{foot} = Pedal force, lb.; use a scale under your driver's foot to estimate the desired pedal force; a typical number for street cars is 40 lb. for a 1g stop

Once this calculation is made, check that the pedal ratio chosen will allow the master cylinder to travel through its full stroke. It may be necessary to cycle through the calculations several times for a new design to balance the various piston areas and to achieve a reasonable pedal force. In the above calculations, it was assumed that there is no loss in the hydraulic system, which is nearly true.

Anti-lock Brakes

The most recent advance in brake systems involves the addition of wheel speed sensors, a computer, and a mechanism for lowering brake line pressure. Current anti-lock brake systems (ABS) cycle the brakes between "near free-rolling" and "near lockup" while attempting to maintain the tire near the friction peak on a variety of surfaces.

Current ABSs use the wheel speed signal for two purposes. First, with the wheel free-rolling, the wheel speed defines the vehicle speed. Second, with the brakes applied, the wheel speed determines the percent slip. The latter is maintained near the best slip ratio for the particular tire, often about 10%. Thus the brakes must cycle-off for a small time to update the computer as to the actual vehicle speed. As the computer algorithms are improved, the "off" time is reduced and performance is still further improved.

In the future, vehicles may be fitted with an additional road speed sensor independent of any wheel speed. With this extra information, the ABS computer can be programmed to hold the tire at the correct slip ratio for best braking whenever maximum braking is commanded.

For paved circuit racing, a skilled driver with a well-balanced brake system is still the most common set-up. There are two reasons for this: Anti-lock does not increase the stopping power of the brakes for straight-line braking, and often the driver uses a slightly

biased brake system to modify the handling during turn in. For any type of competition where the various wheels will be on different coefficients, or where braking must be done with one or more wheels off the ground, ABS may be an advantage. A four-wheel ABS system effectively adds an additional left-right brake balance to the standard front-rear balance and braking performance should be improved.

CHAPTER 21

Suspension Springs

"A spring is a spring is a spring."

Larry Rathgeb
Manager (ret.)
Stock Car Programs
Chrysler Corporation



Introduction

In this chapter we will discuss ways to calculate (approximately) certain properties of suspension system springs. We will concentrate on spring rate and maximum stress but also touch on problems associated with usage, i.e., fatigue. The types of springs covered will include torsion springs, coil springs, and leaf springs.

The material covered is insufficient for detailed design engineering calculations—for that the reader will have to go to the literature, especially the referenced SAE design handbooks and spring manufacturers' handbooks.

21.1 Torsion Springs

In a torsion spring the elastic properties of a long thin "bar" in torsion (twist) is used to produce a rectilinear spring rate that is comparable to that of a coil spring. The spring

With the exception of "Leaf Spring Installation," the material in this chapter was written by Fred Dell'Amico, MRA.

load or force is usually converted to torque around the centerline of the "bar" by means of a lever arm at one or both (anti-roll bar) ends. Figure 21.1 gives the basic geometry of a torsion spring.

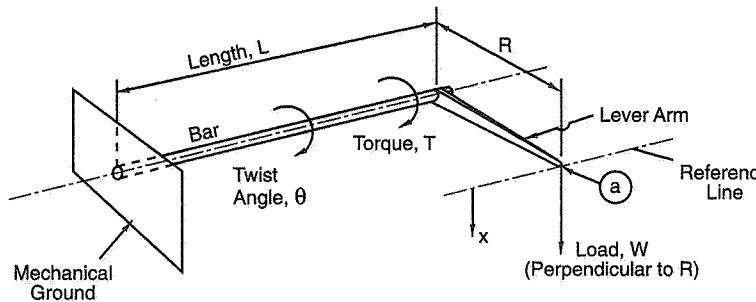


Figure 21.1 Basic geometry of a torsion spring.

In practice the load is not always perpendicular to R throughout the entire twist angle excursion. Thus, in precise engineering design calculations, twist angle correction factors are introduced (see Ref. 7, for example).

The torsion bar itself may have any number of different cross sections, ranging from the most widely used circular bar to an oval bar or a rectangular bar. In these notes we will focus on the circular bar and the square bar. The configuration of the lever arm, R, is not important insofar as stress, spring rate, etc., are concerned; its only function is to convert W into a torque (WR) around the centerline of the bar. If the wheel load is applied directly at point "a" the spring rate is also the wheel rate.

Maximum Stress

When an external torque is applied to a torsion bar the resisting moment developed can be expressed as a function of the bar's cross-sectional geometry and the maximum shear stress, f , developed in the bar. If we call the resisting moment M , we can find expressions for different bar cross sections in any good engineering handbook (for example, Ref. 19). The resisting moment for a circular and a square bar are:

$$\text{Circular bar: } M = \pi d^3 f / 16, \text{ lb.-in.} \quad (21.1)$$

$$\text{Square bar: } M = d^3 f / 4.8, \text{ lb.-in.} \quad (21.2)$$

Since resisting moment, M , is equal to the applied moment, WR (ignoring friction torque), we can express maximum shear stress as:

$$\text{Circular bar: } f = 16WR/\pi d^3, \text{ psi (in. and lb. units)} \quad (21.3)$$

$$\text{Square bar: } f = 4.8WR/d^3, \text{ psi} \quad (21.4)$$

In Eqs. (21.3) and (21.4) we can see that the maximum stress is directly proportional to the applied torque, WR , and inversely proportional to the fundamental dimension, d ; it is not a function of bar length, L (which enters into the determination of twist angle and spring rate).

To make a direct comparison between the circular and the square bar we can focus on the maximum stress per unit applied torque.

Using the above equations we have

$$f/WR = k$$

$$\text{Circular bar: } k = 16/\pi d^3, \text{ psi/lb.-in.} \quad (21.5)$$

$$\text{Square bar: } k = 4.8/d^3, \text{ psi/lb.-in.}$$

Figure 21.2 is a plot of k vs. bar area, with equal d 's keyed in. The plots show that for **equal cross-sectional area** (and therefore equal weight for the same length, L), the circular section has a lower k . The difference is most pronounced at low equal area but diminishes as equal area increases. For example, at 1.5 in.² equal area the circular bar has a k that is approximately 28% lower than that of the square bar. We shall hold off on declaring this feature a significant advantage until we have examined spring rates.

Spring Rate for Torsion Bar

The rectilinear spring rate, S , of a torsion bar / lever arm installation is the load per unit rectilinear deflection at the end of the lever arm. In Figure 21.1 this is

$$S = W/X = W/R\theta, \text{ lb./in.} \quad (21.6)$$

This expression is accurate only if θ is small; for large excursions in θ (which generally correspond to a deviation from the perpendicular between W and R) one has to resort to the more exact methods of Ref. 7, for example.

The twist angle, θ , is given in engineering handbooks for different cross-sectional configurations. For example, the expressions for θ for circular and square bars are:

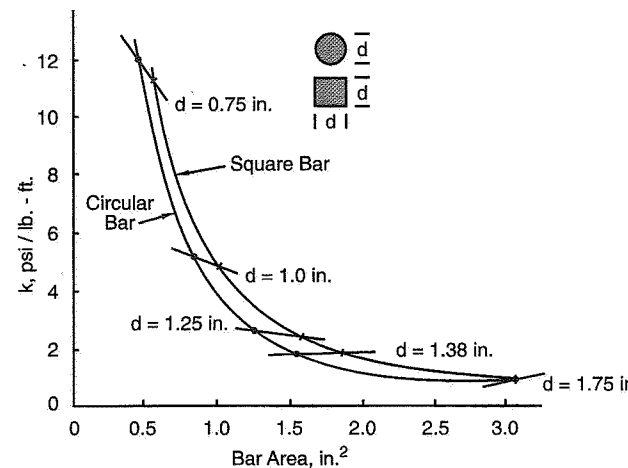


Figure 21.2 Maximum stress per unit applied torque, k , vs. bar area.

$$\text{Circular: } \theta = 32TL/\pi d^4G, \text{ rad.} \quad (21.7)$$

$$\text{Square: } \theta = 7.11TL/d^4G, \text{ rad.} \quad (21.8)$$

where T = applied torque, WR

G = Shear modulus of the material, psi

To convert rad. to deg., multiply by 57.3

The equations show that for a given G , θ increases with applied torque, T , and with bar length, L . If the θ expressions are put into Eq. (21.6) the spring rates become:

$$\text{Circular: } S = (0.098)d^4G/R^2L, \text{ lb./in.} \quad (21.9)$$

$$\text{Square: } S = (0.141)d^4G/R^2L, \text{ lb./in.} \quad (21.10)$$

We can compare the two bars by dividing the first equation by the second; using subscripts c (circular bar) and s (square bar) we have, for the same material, G , and the same R^2L .

$$S_c/S_s = 0.695(d_c^4/d_s^4) \quad (21.11)$$

If we apply the equal area criterion used in the previous section we have

$$\pi d_c^2/4 = d_s^2$$

and

$$d_c^2/d_s^2 = 4/\pi = 1.273$$

from which

$$d_c^4/d_s^4 = 1.273^2 = 1.621$$

When this result is substituted into Eq. (21.11) we have

$$S_c = 0.695(1.621) S_s = 1.127 S_s \quad (21.12)$$

In other words, for the same area (the diameter of the circle is 1.127 times the side of the square), and for the same G/R^2L , the circular bar has a 13% stiffer spring rate. This fact, together with the previous conclusion that the circular bar has a lower k (stress per unit applied torque), says that there is no particular advantage of the square bar over the circular bar unless the square bar has certain installation advantages such as simpler or lighter mechanical grounding hardware (end fastening) or lever arm hardware.

Shear Modulus and Stress Levels

The shear modulus of different steels varies little from one to another. Ref. 19 gives the following data:

Type of material	Shear Modulus, psi
Cold Rolled Steel	11.5×10^6
Stainless Steel (18-8)	10.6×10^6
Carbon, heat-treated	$11.0-11.9 \times 10^6$
Titanium	$5.8-6.2 \times 10^6$

For use in design and stress calculations Ref. 7 recommends a value of 11.0×10^6 psi. Of course there are other material properties that enter into consideration for torsion bar springs, e.g., hardenability and machineability. For such considerations see Ref. 7, for example.

Typical maximum operating stress levels for torsion bar springs are given in Table 21.1 (which is table 2.2 from Ref. 7). The unit for stress in the table is the megaPascal (MPa); multiply by 145 to get psi. The range for passenger cars and trucks is approximately 800-900 MPa, or 116,000-130,000 psi.

Table 21.1 Operating Stress Levels—Round Torsion Bars (from Ref. 7)

Class No.	Operating Shear Stress, Max (MPa)	Load Direction		SAE Steel (Typical)		Typical Application
		Single Only	Reverse	Shot Peened	Preset	
1250	1250	10 Max	Yes	—	Yes	T20811 (MOD)
1200	1200	10 Max	Yes	—	Yes	
1150	1150	10 Max	Yes	—	Yes	H4340 (ESR) ^b H4350 (ESR) ^b
1100	1100	10 Max	Yes	—	Yes	
1000	1000	10 Max	Yes	—	Yes	H43400 H51600 H61500 H15621
900	900	2-4	Yes	—	Yes	H43400 H51600 H61500 H15621
800	800	2-4	Yes	—	Yes	H43400 H51600 H61500 H15621
700	700	2-4	—	Permissible	As required	G10650 to G10900
550	550	2 Max	—	Permissible	As required	G51600 G61500
550S ^a	550	2 Max	—	Permissible	As required	G10450 to G10900

^a Torsion bars in class 550S are normally produced from shallow hardening carbon steel grades; they cannot be expected to have the depth of hardenability which can be achieved with alloy steels.

^b (ESR) = Electro Slag Remelt.

psi = MPa/0.00689

Sample Calculations

For some sample calculations we will use a neutral steer car in which:

$$W_T = 1500 \text{ lb. (total weight)}$$

$$\ell = 8 \text{ ft. (wheelbase)}$$

$$a = 5.6 \text{ ft. (CG to front axle)}$$

$$b = 2.4 \text{ ft. (CG to rear axle)}$$

The calculations are for round torsion bar springs at the front suspensions.

- Front wheel weight = $W = (1/2)(b/\ell)(W_T) = (1/2)(2.4/8.0)(1500) = 225 \text{ lb.}$
- We will select the wheel spring rate on the basis of a desired undamped natural frequency of 2 Hz:

$$\omega = \sqrt{K/m} = 2\pi(2) = 12.56 \text{ rad./sec.}$$

Squaring both sides, we have

$$K = 12.56^2(225)/32.2(12) = 91.9 \text{ lb./in.}$$

- Using this spring rate and Eq. (21.9) we have

$$S = 0.098d^4G/R^2L = 91.9 \text{ lb./in.}$$

Using a G of $11 \times 10^6 \text{ psi}$ this becomes

$$R^2L/d^4 = 0.098(11 \times 10^6) / 91.9 = 11,730 \quad (\text{a})$$

- Using Eq. (21.3) and setting the maximum stress at 100,000 psi we have

$$100,000 = 16WR/\pi d^3 = 16(225)R/\pi d^3$$

or

$$R/\pi d^3 = 27.78 \quad (\text{b})$$

Eqs. (a) and (b) can now be used to determine the required d , R , and L . In this example we will arbitrarily select an $R = 5 \text{ in.}$ Then from (b),

$$d^3 = 5/\pi(27.78) = 0.0573$$

and

$$d = 0.386 \text{ in. diameter}$$

Putting this d and R (5 in.) into (a),

$$L = 11730(0.386)^4/25 = 10.41 \text{ in. length}$$

The above calculations illustrate an approach that can be used in evaluating an existing installation. If the wheel load, W , remains substantially perpendicular to the lever arm, R , and the excursion in θ is small, the results will be fairly accurate.

21.2 Coil Springs

Coil springs utilize the elastic properties of a wire in torsion to produce a rectilinear spring rate; they are the most widely used spring type in independent suspensions for automobiles and they are also used in solid axle suspensions. The most common shape is the helix in which the mean diameter of the coil is constant; variations range from tapered coils (in which the mean diameter varies) to coils with varying wire diameter. Coil springs can be designed for use in compression or extension. In these notes we will confine our attention to the helical coil spring, used in compression, with constant-diameter round wire. Figure 21.3, taken from Ref. 6, gives the nomenclature for the helical coil spring and typical ends that are used for compression springs.

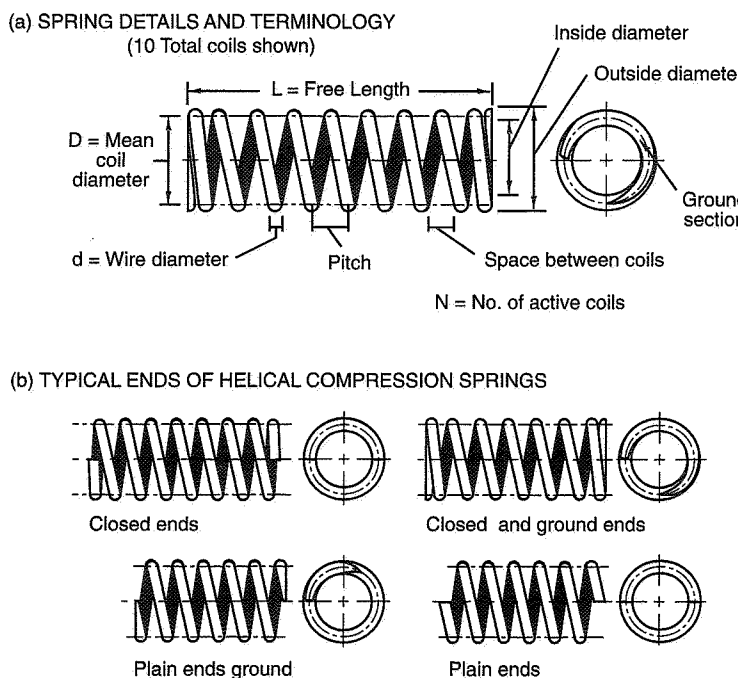


Figure 21.3 Helical coil compression springs (Ref. 6).

The important parameters shown in Figure 21.3(a) are:

Free length (base length) of unloaded spring = L , in.

Wire diameter, d , in.

Mean diameter, D , in.

Number of active coils, N (an active coil sweeps one full circle)

Figure 21.3(b) shows the different end treatments that determine the number of active coils. According to Ref. 6 a spring with closed ends or closed and ground ends has one inactive coil at each end, springs with plain ends "are considered to have virtually no inactive end coils unless they are fitted with specially shaped spring seats," and springs with plain ends **ground** are considered to have "about 1/2 inactive coil at each end." The parameter N figures importantly in the determination of spring rate, but from the above it is clear that there is some uncertainty in assigning a value to N ; the reader should keep this uncertainty in mind when calculating spring rates.

Maximum Stress

The maximum shear, f , in a coil spring with load, W , is given by

$$f = 8DW/\pi d^3 = 2.55 DW/d^3 \quad (21.13)$$

If we compare this with the stress equation for a torsion spring (round wire, Eq. (21.3)) we find that for the same load, W , and the same stress, f ,

$$D = 1.99 (d_c/d_t)^3 R \quad (21.14)$$

where c and t stand for coil and torsion bar, respectively.

For example, if d_c/d_t , the wire size ratio of the coil to the torsion bar, is 1/2 then Eq. (21.14) becomes

$$D = 2.0 (0.5)^3 R$$

$$D = 0.25R$$

In other words, the mean diameter, D , of the coil spring is one fourth of the lever arm, R .

The maximum stress given by Eq. (21.13) is designated the "*uncorrected*" stress; it does not take into account stresses caused by the curvature of the wire into a coil and other factors. A multiplying factor, called the Wahl factor, **must be used** to increase the result found in the right-hand side of Eq. (21.13). This factor (given in Refs. 6 and 10) is a nonlinear (and inverse) function of the ratio of mean diameter to wire diameter. For

example, if D/d is 5 the factor is 1.3, but if D/d is 12 the factor is about 1.1 (still, a 10% correction). The larger the D/d the smaller the correction factor. If this correction factor is not used and the spring is designed close to the material limits, it will probably yield (sag) in service.

Spring Rate

The spring rate (pounds of load per unit deflection) is given by

$$S = Gd^4/8D^3N = W/X, \text{ lb./in.} \quad (21.15)$$

As noted earlier, any uncertainty in the number of active coils, N , will affect the determination of S .

Shear Modulus and Stress Levels

Since the principal stresses in coil springs are shear stresses, as is the case for torsion bar springs, the shear modulus recommendations in the previous section apply. This means that for all practical purposes a value of 11.0×10^6 psi will serve most needs.

Recommended maximum shear stress levels for coil springs is given in Ref. 5 (Table 5.1) as a percentage of minimum tensile strength. For three broad categories of steel these are given in Table 21.2.

Table 21.2 Recommended Maximum Stress Levels for Coil Springs

Steel	% of Tensile Strength
Oil Tempered Alloy Steel	50-55
Oil Tempered Carbon Steel	45-50
Hard Drawn Carbon Steel	42-45

For precise work one should determine accurately the grade of steel used and apply the percentages in Table 21.2 and the Wahl factor to arrive at a recommended stress level. In fact, Ref. 6 tabulates the minimum tensile strength for several different steel designations which, incidentally, decreases as wire diameter increases. For rough calculations we can take the minimum tensile strengths given in Ref. 10 and apply the above percentages. This is done in Table 21.3.

Table 21.3 Maximum (Uncorrected) Stress Levels for Coil Springs

Steel Type (Ref. 11)	Minimum Tensile Strength	% (from Table 21.2)	Recommended Max. Stress Level
Hard drawn			
0.250 in. dia.	182,000 psi	42%	76,400 psi
0.500 in. dia.	156,000 psi	42%	65,500 psi
Oil tempered			
0.250 in. dia.	180,000 psi	50%	90,000 psi
0.500 in. dia.	165,000 psi	50%	82,500 psi

Comparing these with the recommended stress levels for torsion bar springs given in the previous section, it is seen that they are considerably lower. When the Wahl factor is applied they are lowered further. All of this points to the need for the user to take advantage of the expertise of the manufacturer in selecting springs.

Material Treatment

There are a number of material treatments to which commercially available springs can be subjected. These include heat-treatment/hardening, hot or cold forming, shot peening and presetting,⁶³ to cite a few. The value of these treatments to the user is best left to discussions with the spring manufacturer.

Installed Spring Rate

If a coil spring is loaded along its centerline, the computation of deflection is straightforward: $X = W/S$ or the load divided by the spring rate. In testing springs for rate, Ref. 6 recommends that the rate be defined over the deflection range of $\pm 25\text{mm}$ ($\pm 1\text{ in.}$) about the design load length (or height). This implies that a spring may not be precisely linear over a larger range; and for race car use it is advisable to measure the spring rate over the active length range. A nonlinear rate implies that fundamental quantities like the roll rate may change as the suspension travels in ride.

⁶³ Presetting, also known as scrapping or cold setting, involves stressing the spring beyond its elastic limit, for example, by loading it at or near its closed length. The result is a shorter free length but the beneficial effect is a better stress distribution in the coils (see Ref. 6).

21.3 Coil Springs in Series and Parallel

There are a number of ways in which springs can be used in different installations to produce a composite rate. Two of the most common combinations are springs in *series* and in *parallel*.

Two Springs in Series

Two coil springs, with rates S_1 and S_2 , are said to be in series if their centerlines coincide, as in Figure 21.4.

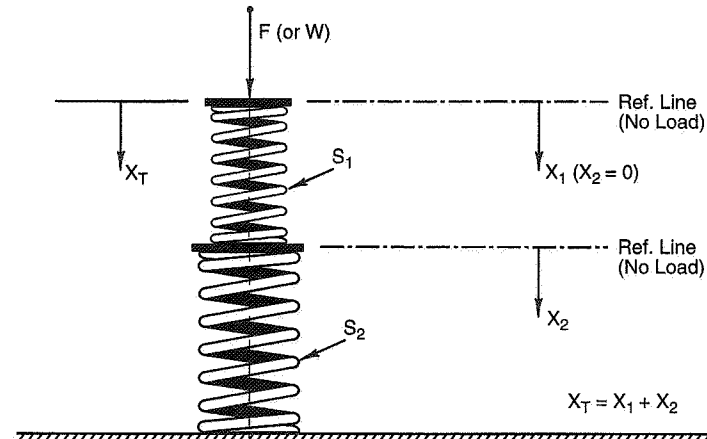


Figure 21.4 Springs in series.

By considering the deflections of each of the springs under the load, F , and adding them, it can be shown that the composite spring rate, S , is

$$S = S_1 S_2 / (S_1 + S_2), \text{ lb./in.} \quad (21.16)$$

This is analogous in electronics to the resistance of two resistors in parallel and, as in that case, the combined S is always smaller than the lower of the two S 's.

If, in the above case, neither spring bottoms out (is not forced to its closed length) over the operating range of X_T , the composite rate is given by Eq. (21.16) and is linear (provided that S_1 and S_2 are linear). On the other hand, if either S_1 or S_2 bottoms out, the composite rate then becomes that of the other spring. Although this behavior can be

shown analytically it is really more easily seen by going to the spring load-deflection plots, as in Figure 21.5.

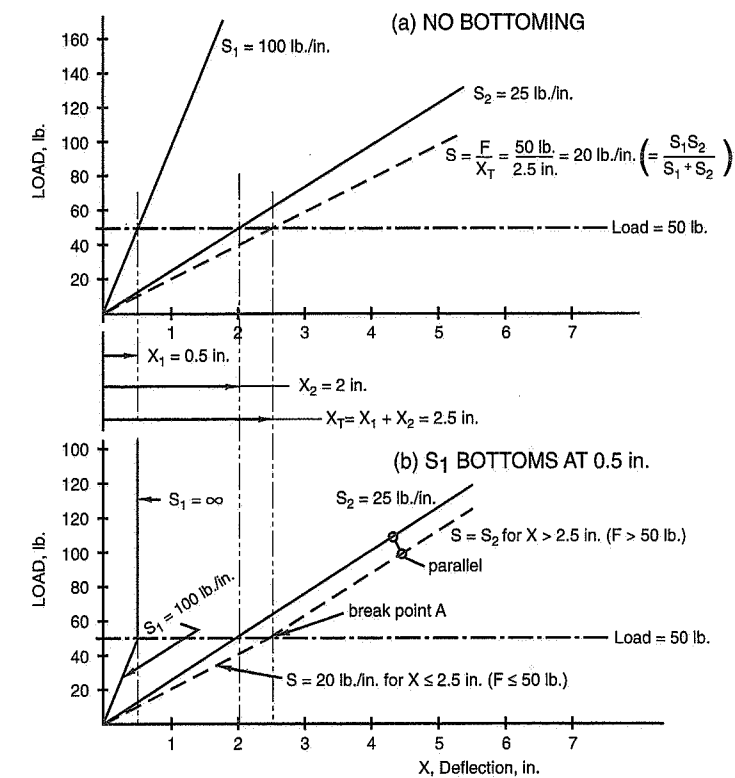


Figure 21.5 Two springs in series, (a) no bottoming and (b) one bottoming.

In part (a), in which no bottoming occurs, the composite spring rate (for any load—in this case 50 lb.) is obtained graphically from the plots as 20 lb./in., which is the answer that Eq. (21.16) gives. In part (b) the stiffer (upper) spring, S_1 , bottoms out at $X_1 = 0.5$ in. of deflection (at 50 lb.). At that point the total deflection, $X_T (= X_1 + X_2)$, is 2.5 in., and from that point onward the combination has an S equal to S_2 .

The above illustration is particular, i.e., specific rates are used. In the more general case the following procedure can be used to find the composite rate. Referring to Figure 21.6, the steps are:

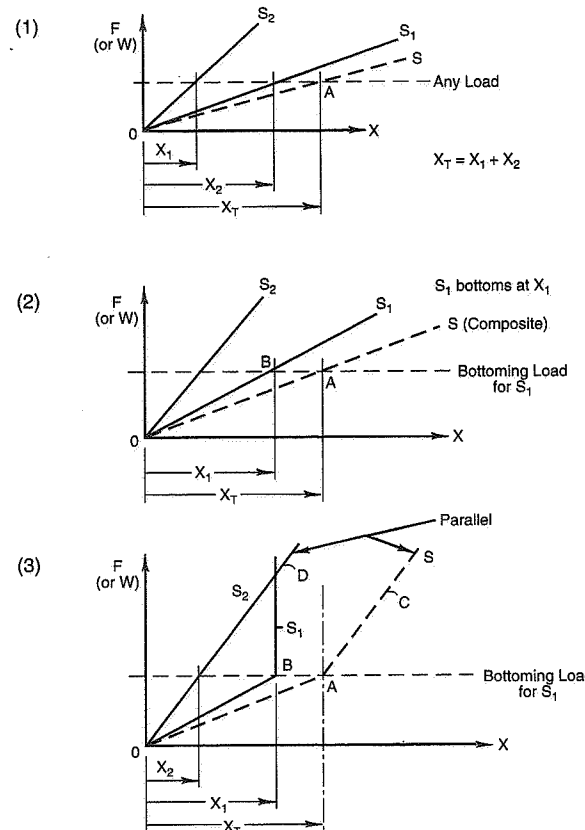


Figure 21.6 Springs in series—general case.

- Assuming that S_1 and S_2 are linear, draw in the straight lines for S_1 and S_2 . In this case the top spring, S_1 , is the softer of the two. Draw in any load line within the operating range of the deflections involved. Where $X_T (= X_1 + X_2)$ intersects the load line, at A, determines the composite rate, S . Notice that S is lower than S_1 or S_2 .
- If the top spring, S_1 , bottoms at a given load (and X_1), draw in the bottoming load line and the corresponding X_1 ; they intersect at B. As before the point A is the intersection of the load line and the X_T line (as in 1 above).
- The composite rate beyond point A is now S_2 . Therefore line AC is parallel to OD. The composite rate is softer than either spring up to the bottoming deflection X_T ; beyond that it has the stiffer rate of S_2 .

The above procedure applies equally well no matter which spring is the softer or which bottoms out.

Multiple Springs in Series

If multiple springs are connected in series the inverse of the total rate is given by the sum of the inverses of the individual spring rates as follows:

$$1/K_T = 1/K_1 + 1/K_2 + 1/K_3 \dots$$

If one spring bottoms out, its term is dropped ($1/\infty = 0$) when the calculation is taken past the load at which it bottoms.

This formula may be useful when a spring is grounded to a soft (flexible) mounting location. In this case, the installed spring rate can be much lower than the rate of the spring alone. This often occurs when torsion bars are mounted to flexible structure or if a rubber isolator is used at the end of a coil spring.

Two Springs in Parallel

Springs are said to be in parallel if they always share a load. Figure 21.7 shows a solid axle installation in which $S_1 = S_2$.

Coil springs in parallel are analogous to electrical resistors in series (where the total resistance is the sum of the resistors in series). In this case the composite rate, S , is

$$S = S_1 + S_2, \text{ lb./in.} \quad (21.17)$$

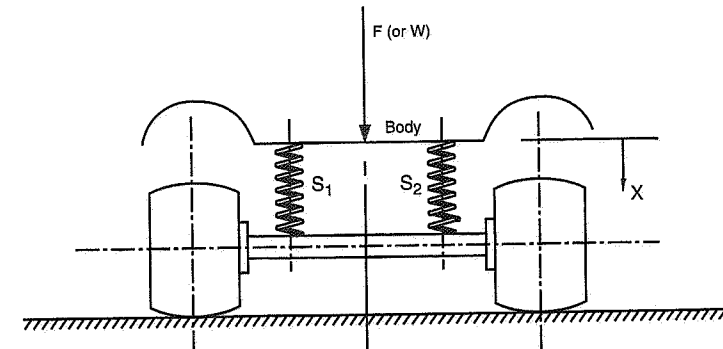


Figure 21.7 Springs in parallel.

If in Figure 21.7 the load is centered and $S_1 = S_2$, the deflection is

$$X = F/S = F/(S_1 + S_2), \text{ in.} \quad (21.18)$$

The equation shows the deflection, X , is less than it would be if F were applied along the centerline of either spring. If the load, F , is not centered then one has to calculate the left-right load distribution. If S_1 still equals S_2 the deflections will be different and the body will tilt and can be restored to the upright condition only by changing S_1 and S_2 so that their deflections are equal. Finally, if S_1 and S_2 represent composites of springs in series, the methods of the previous paragraphs have to be applied first. Then Eq. (21.18) can be used, keeping in mind that S_1 and S_2 are composites and are piece-wise linear; they have breakpoints at A in Figure 21.6.

21.4 Coil Spring Calculations

Assume that we wish to design a coil spring at the wheel of a front wishbone suspension with the same rate as the torsion bar spring of the previous section. The rate in that case was 91.9 lb./in. The relationship between wheel rate and spring rate in a wishbone suspension is covered in Chapter 16. For our purposes we will assume the required spring rate is four times the wheel rate, or 368 lb./in. Using Eq. (21.15), we have (with $G = 11.0 \times 10^6$ psi)

$$S = Gd^4/8D^3N = 368 = 11 \times 10^6 d^4/8D^3N$$

or

$$d^4/D^3N = 267.6 \times 10^{-6} \quad (a)$$

The maximum uncorrected stress will be set at 70,000 psi so that Eq. (21.13) becomes

$$f = 2.55DW/d^3 = 70,000$$

from which

$$D/d^3 = 70,000 / (2.55 \times \text{static load}) \quad (b)$$

The static spring load in a wishbone suspension is given by (see Chapter 16 for more detail)

$$F_S = W/IR$$

where IR = Installation Ratio.

In this expression the assumed factor of 4 (above) between the spring rate and wheel rate corresponds to an IR = 1/2, so that the spring static load is twice the wheel load. Putting this in (b) we have

$$D/d^3 = 70,000 / [2.55 (2 \times 225)] = 61.0 \quad (c)$$

At this point it becomes a matter of trial and error; one picks a wire size, d , and calculates D from (c) then puts d and D into (a) to find N . This is done below for several different wire sizes:

Wire Size, <u>d, in.</u>	Mean Coil Diameter, D , in.	Number of Coils, N
0.30	1.65	6.7
0.375	3.22	2.2
0.50	7.63	0.5

From such an exercise the trade-offs become clear: Is D too small, risking a "column" or "buckling" effect (see Ref. 6)? Is N so small that it is unrealistic (as in $d = 0.50$, above)? What are the space limitations? And so on. One thing is clear, however: both D and N are very strong functions of wire size, d . The final choice will probably be determined by the availability of wire sizes and space limitations. The latter will influence coil pitch as will static load deflection requirements—topics which we have not been able to cover in these notes.

Progressive Rate Coil Springs

It is possible to produce coil springs that increase in rate as they are compressed. This is accomplished by varying the number of active coils. As the spring is compressed some of the coils "bottom out" and the rate increases. The analysis of this type of spring is too complicated for this text but is available in Ref. 133.

Measuring Spring Rate

Spring rate can be measured with any type of load test equipment that is capable of compressing the spring and recording load and deflection. A common brand in test labs is "Tinius-Olsen." A typical spring test records the spring load for every 1/2 in. of deflection from fully open to coil bottoming (if the spring can be fully closed without overstressing). The results of a spring rate test are shown in Figure 21.8.

21.5 Leaf Springs

The design of leaf springs is considerably more complex than the design of torsion bar or coil springs. This results primarily from the fact that the number of design variables is larger. Leaf width and thickness may vary, the leaves may be tapered in thickness and/or in width along their length, the end constraints may vary, being fixed by spring eyes or shackled, the load carried may be symmetrically applied or off-center, etc. Thus, while the basic theory of operation is often simple enough, the variable parameters will usually require the application of "correction" factors.

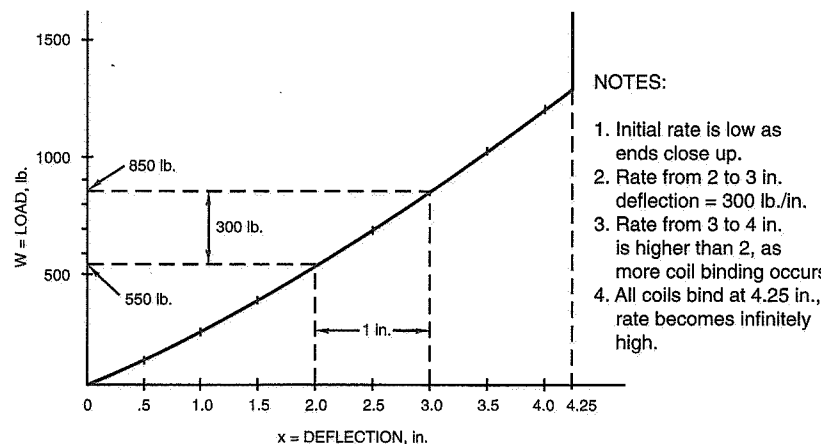


Figure 21.8 Coil spring rate test.

Ref. 5 will give the reader some idea of the complexities involved which make it very difficult to provide a "textbook" approach in these notes. We will, however, give the "uncorrected" fundamental stress and spring rate formulae for three elementary spring types; for additional information, Refs. 5 and 12 are recommended.

Single Leaf Cantilever Spring

The cantilever spring provides the theoretical basis for many leaf spring types. For this spring, shown in Figure 21.9(a),

$$\text{Bending Stress} = f = 6\ell F/bt^2, \text{ psi} \quad (21.19)$$

$$\text{Spring Rate} = S = F/X = Ebt^3/4\ell^3 \quad (21.20)$$

where E is Young's modulus, in psi

Other dimensions are as shown in Figure 21.9(a)

Single Leaf Parabolic Spring

This spring behaves like two back-to-back cantilevers, hence the bending stress formula is the same as the cantilever, as shown in Figure 21.9(b):

$$f = 6\ell F/bt^2, \text{ psi} \quad (21.19a)$$

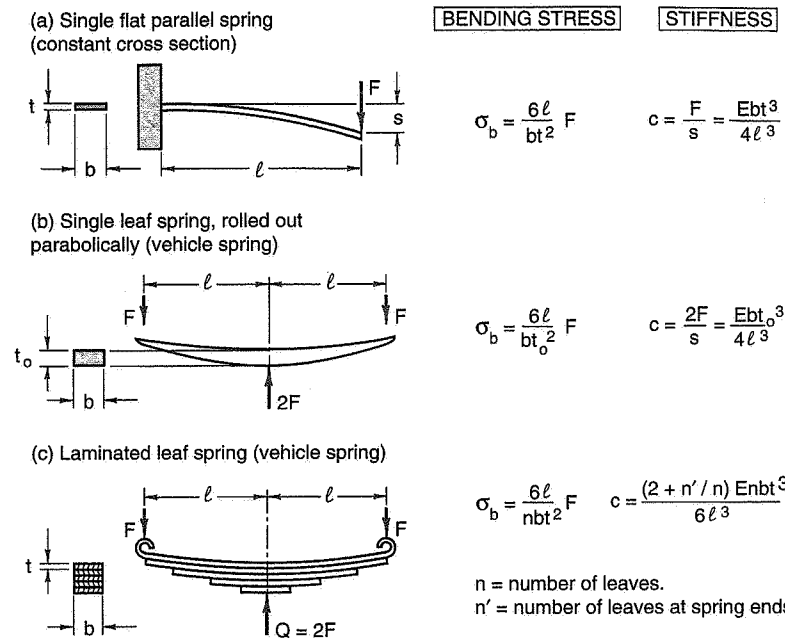


Figure 21.9 Leaf springs (Ref. 12).

The spring rate expression is also the same but it is based on the center load, $2F$. Thus

$$S = 2F/X = Ebt_0^3/4\ell^3 \quad (21.20a)$$

Laminated Leaf Spring

The laminated spring with n identical leaves (thickness and width) behaves like n single leaf springs that share the load, except for interleaf friction, discussed in a subsequent section.

For the "tapered" laminated spring, shown in Figure 21.9(c),

$$\text{Bending Stress} = f = 6\ell F/nbt^2, \text{ psi} \quad (21.21)$$

$$\text{Spring Rate} = 2F/X = \frac{[2 + (n'/n)]Enbt^3}{6\ell^3}, \text{ lb./in.} \quad (21.22)$$

where n' = number of leaves at spring ends.

As can be seen in Eq. (21.21), the bending stress is $1/n'$ times the stress for the single leaf.

Young's Modulus and Stress Levels

For all non-stainless spring steels, Young's Modulus is the familiar 30×10^6 psi. As for recommended stress levels one should note that the bending elastic limit varies widely for spring steels. For this reason one should accurately identify the steel used and use as low a stress as is practical. For example, Ref. 5 indicates that the range used in passenger cars is from about 90,000 to 110,000 psi; the reference also states that for "properly heat-treated alloy steel the minimum yield stress is generally accepted as 1200 mega-Pascals" (about 175,000 psi).

Sample Calculation

As in the torsion bar calculations, we will use the neutral steer car of Chapter 5 and select a single leaf parabolic spring for each rear wheel:

- Rear wheel weight = $W = (1/2)(aW_T/\ell) = (1/2)(5.6/8)(1500) = 525$ lb.
- Using the same undamped natural frequency as before, we have

$$\omega = \sqrt{K/m} = 12.56 \text{ rad./sec.}$$

from which the required spring rate is 214 lb./in. Putting this rate into Eq. (21.20a) we have

$$S = 2F/X = 214 \text{ lb./in.} = Ebt_0^3/4\ell^3 \quad (a)$$

Using a leaf width of 2 in. and $E = 30 \times 10^6$ psi we have

$$t_0^3/\ell^3 = 214(4)/30 \times 10^6(2) = 14.27 \times 10^{-6} \quad (b)$$

Using Eq. (21.19a) and a maximum stress of 90,000 psi we have

$$F = 6\ell F/2t^2 = 90,000 = (6\ell/2t^2)(525/2) \quad (c)$$

and

$$\ell/t_0^2 = 114.3 \quad (d)$$

Eqs. (b) and (d) are two simultaneous equations and can be solved for t and ℓ .

Using (b) first we find that

$$\ell = \sqrt[3]{70,100} (t_0) = 41.23 t_0 \quad (e)$$

Putting this in (d) we have $t_0 = 0.36$ in. If this t_0 is put back into (d) we get $\ell = 14.8$ in. As is the case with other spring types one has to go through an iterative procedure to make the spring parameters meet other requirements (space, static load position, etc.).

21.6 Leaf Spring Installation Considerations

The basic spring rate of a leaf spring is measured with one end of the spring unconstrained, that is, the spring is free to change length as it is deflected. Leaf spring installation in a vehicle may have a large effect on the actual spring rate that is realized in any given situation.

Shackled Ends

When the spring shackle is at some angle other than at right angles to a line between the spring eyes, the spring rate is modified when compared to the bare spring. The two cases shown in Figure 21.10 have the chassis "over-slung" (shackle goes up to the chassis mount). The descriptions also hold if the installation is "under-slung" (shackle below the spring) with the shackle in the dotted line position. The load on the spring is F and is shown split approximately in two at the ends, $F/2$. The angle, θ , is the shackle angle.

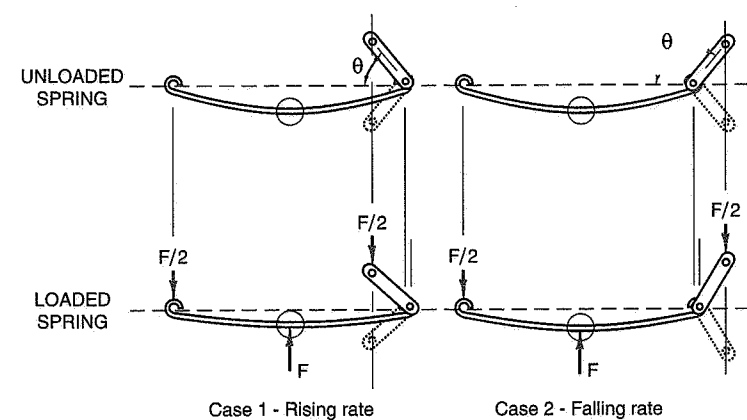


Figure 21.10 Shackle angle effect on spring rate.

Case 1—Chassis mounts closer together than spring length

When the spring is concave upward (as shown) and the shackle is angled (toward the nonshackled end of the leaf spring, θ less than 90°), the installation has a “rising rate.” That is, the spring rate increases as the spring is deflected in bump, assuming that the spring stays “concave upward” as shown in the figure (does not reverse curve).

Case 2—Chassis mounts further apart than spring length

Again with the spring concave upward but with the shackle angled away from the non-shackled end of the leaf spring (θ greater than 90°), the installation has a “falling rate.” That is, the spring rate starts out higher than the bare spring and decreases as the spring is deflected in bump. This continues until the shackle is at right angles to a line between the spring eyes. At this point the installation is converted to Case 1 above. This again assumes that the spring remains concave upward at all times.

If the spring arch is reversed (concave downward), Cases 1 and 2 must be reversed as the distance between the spring eyes is now decreasing as the spring is loaded.

The result of shackle angle is that a linear rate leaf spring is acting as a nonlinear spring. With nonlinear springing, other parameters of the vehicle will change with ride height. For example, if the spring is concave upward and the shackle is angled as in Case 1, the roll rate will increase when the car is on a banked turn (as the suspension travels in ride and the ride rate increases).

With all the possible combinations of direction of spring arch and shackle angle/length, a wide variety of variable rate curves can be produced, if desired. If the shackle length is changed (by a series of holes) to control diagonal weight jacking, it is likely that different variable rate curves will result; this is probably undesirable.

Linear Spring Rate

A linear spring rate may be obtained from a leaf spring in several ways:

1. Shackles may be used if the spring is nearly flat (not arched) in the normal range of travel and if the shackle angle is always near perpendicular to the spring. An arched spring changes length (and shackle angle) much more with deflection than a flat spring.
2. *Rollers or sliders* may be used in place of shackles to allow for the length change with ride motion. No freeplay during normal operation is permissible if the spring is also serving a location function for an axle. If a weight jacker is desired, the roller/slider assembly should be moved relative to the frame rails.

Interleaf Friction

Carriages and early automobiles relied on interleaf friction for damping, often having no other shock absorber. The damping produced is of the Coulomb or stick-slip type and is not appropriate for race cars where smooth changes in tire load are desired. If a multileaf spring is used, lubrication or anti-friction materials may be used to reduce this effect. Another solution is to change the design to a single leaf type. An approximate tapered leaf (triangular) stiffness can be achieved by tapering in either plan view or thickness or both.

Installations

The example shown in Figure 21.10 is for a longitudinal spring locating a solid axle (Hotchkiss), and common race car practice has the springs operating with a minimum of arch (for lateral stiffness) and near horizontal (to reduce roll steer).

If other means are used to locate the axle (longitudinal links, lateral link—Panhard Rod, traction snubbers, etc.), their effect on spring rate must also be considered. In general, if the spring is deflected by the additional device, the spring rate and friction will probably increase.

These examples are also applicable to transverse leaf springs with shackled ends (with the appropriate changes in spring curvature and force direction). Note that if a transverse leaf spring locates the axle through shackles at both ends, the shackles must be short and relatively horizontal. If not, the axle will be very poorly located laterally and may require that one shackle be locked-up for tolerable steering.

21.7 Fatigue

When springs are subjected to cyclical loading and, as a result, cyclical stresses above the static load stress level, it is generally accepted that they have limited life, i.e., that failure is likely to occur after an estimated total number of cycles. Failure may be attributed to any number of causes, including surface imperfections (cracks, seams, pits), corrosion, improper heat treatment, or decarburization.

Fatigue life is usually determined by accelerated life tests in the laboratory and generally involves the use of sophisticated statistical techniques. It is beyond the scope of these notes to go into such matters.

For engineering purposes the statistical data are reduced to relatively simple plots; Figure 21.11 (Figure 8.1 of Ref. 5) is an example of such a plot. An initial stress, usually the static load stress, is entered (vertical line) and an expected maximum stress also entered (horizontal line); their intersection is then read from the “cycles” to failure lines (keep in

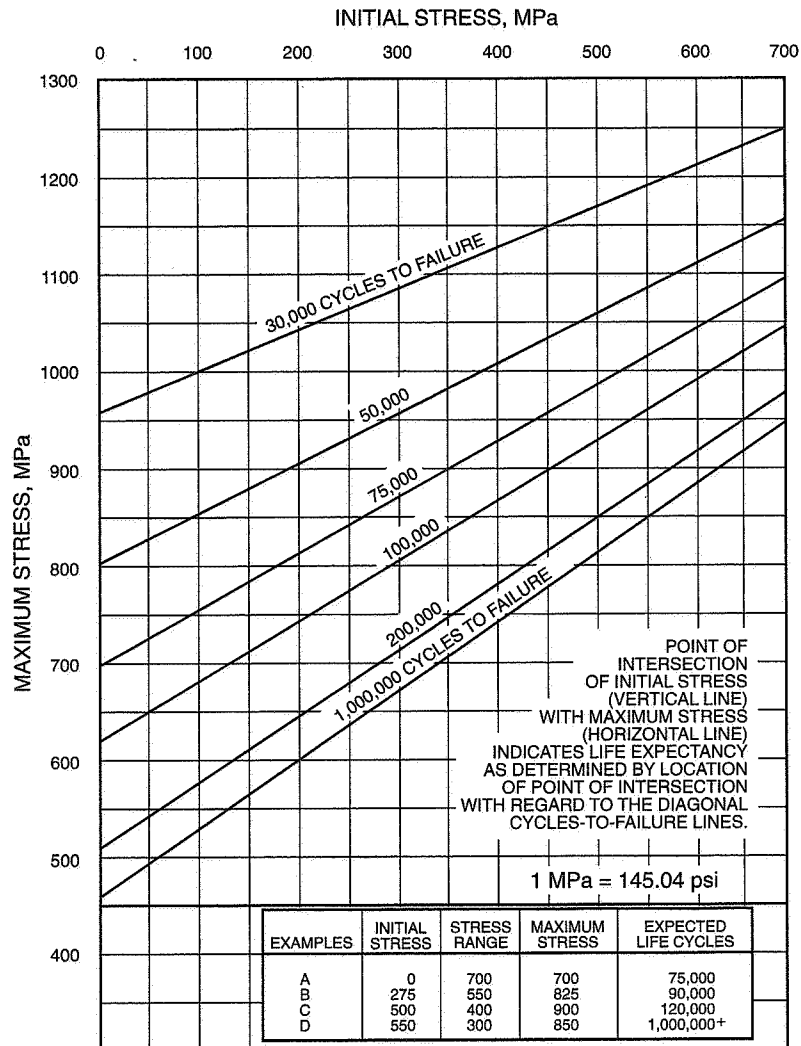


Figure 21.11 Estimating fatigue life of steel leaf springs (preset / not shot peened) (Ref. 5).

mind that $\text{MPa} \times 145 = \text{psi}$). Figure 21.11 is for leaf springs; similar data for coil and torsion bar springs are given in Refs. 6 and 7.

Figure 21.11 and other types of fatigue or life-cycle data show that for a given initial stress level long life is associated with low maximum stress. Note also that it is the ratio of maximum stress to initial stress that is important. For example, if the maximum stress is 700 MPa (101,500 psi), a higher initial stress produces a longer life (i.e., the stress "swing" is lower).

In the absence of accurate life-cycle data for the particular steel involved, its treatments, and the type of spring into which it is shaped, one is well advised to be conservative by using stress levels well below limiting values.

Dampers (Shock Absorbers)

"Sometimes I think that I would have enjoyed racing more in the days of the friction shock. Since you couldn't do anything much to them or with them, I would have spent a lot less time being confused."

Carroll Smith
Tune to Win, 1978



Introduction

The use of springs to permit vertical movement of the wheels relative to the chassis on rough roads goes back to horse-drawn vehicles. This method for improving ride was adopted early in the history of the automobile. The damper was later introduced between the sprung and unsprung masses to suppress oscillation and control the motion of the sprung mass due to longitudinal and lateral acceleration.

According to Ref. 147, the first "primitive" shock absorbers (dampers) were installed on the 1902 Mors and the 1906 French Grand Prix Renault. The damping forces were generated by moving a vane or piston in a fluid. An early form of rebound control, the

The section on Damping Fundamentals was prepared by ride expert Tony Best of Anthony Best Dynamics Ltd., Bradford on Avon, England.

Gabriel Spring Snubber appeared in the early 1920s and at about the same time the Hartford Friction Damper was introduced. These were followed in the mid-1920s by the cam and lever type of hydraulic unit (initially one-way and later two-way acting), the Houdaille Rotary Vane being a typical example. In the early 1930s Monroe introduced the direct-acting telescopic hydraulic shock absorber (derived from aircraft practice). This type of unit, based on the resistance due to forcing oil through orifices, has become the most popular damping device.

A large number of improvements and design variations in the direct-acting telescopic dampers have occurred since their introduction. These include extensive seal development, additional valving to enable control at various levels of piston velocity, adjustable orifice sizes and blow-off valve springs, and the addition of gas pressure to accommodate the displaced volume of the piston rod and oil aeration. Bump and rebound control are generally different and various schemes have been provided for their adjustment either statically or on the road. Stroke sensitive as well as velocity sensitive valving can be provided. The damper can also be used for load leveling (trim). One arrangement utilizes the damper piston as a pump to draw or return fluid to a reservoir whenever an off-trim condition exists. This operation depends on incidental motion of the damper during the travel of the vehicle. A more rapid scheme is based on changing the pressure in a gas-filled damper by an auxiliary pressure source.

One unique spring/damper combination which has reached high volume production was developed by Dr. Alex Moulton in England. In the Hydrolastic implementation, it was first used on the original B.M.C. Mini, circa 1959. A later version, the Hydragas, has been used on B.M.C. Austin products. Hydragas is currently original equipment on the 1990 Rover Metro (Refs. 51, 100, 101, 102, and 103). In these self-contained units, a water-based fluid is forced through bleed holes at low velocity supplemented by rubber flap valves which open progressively at higher velocities. The valving also permits different rates for bump and rebound damping.

Starting in about 1985, dramatic advances in the application of electronic control to dampers has taken place as the result of intense competition to improve the ride quality of the conventional passenger car. One incentive is the desire to approach active car ride with simpler and more cost-effective systems of the adaptive and semi-active types. In these systems the damper adjustments are changed dynamically as a function of a wide variety of sensed variables such as body attitude, angular velocity (yaw rate), acceleration, disturbance frequencies, brake and steering inputs, etc. The control algorithms (strategy) vary from relatively simple to highly complex.

All of the damper developments mentioned above have or will likely be utilized in the future in racing cars. Many of them were, in fact, inspired by racing. As elaborate electronic adaptive and semi-active systems become more common in passenger cars, one can imagine their acceptance in various classes of racing; they have already been used in Grand Prix.

22.1 Approach

A central problem faced by the race car designer and race engineer is one of damper choice, sizing, and tuning to the chassis, tires, circuit, and driver characteristics. In the past the choice of damper (shock absorber) has been largely determined by reputation and availability, ease of adjustment, packaging requirements, and specific features such as gas filled to minimize aeration under hard usage. Setting up the shock has been largely a process of trial and error following a few simple procedures suggested by the damper manufacturer or from experience. Since the damper acts on both sprung and unsprung masses (thus both ride and handling), some compromise is usually involved, with priority (in racing) toward handling.

The judgment (measure) of a given damper setting has been largely a subjective one by the driver supplemented by lap and interval times. Certain drivers are more adept at this process than others and can converge to race settings more rapidly; this has led to the belief that damper tuning is a "black art." With the increasing use of instrumentation in nearly all classes of racing, one can envision the development of more rational procedures.

This chapter will discuss certain aspects of the application of conventional shock absorbers to race cars. Adaptive, semi-, and fully active systems are beyond the scope of this book although reference may be made to them to illustrate a point or for those who wish to explore the technical literature. This chapter begins with some notes on the technical literature and a summary of background theory.

Since there are some important differences in the application of dampers to race cars with (1) modest and with (2) very large aerodynamic downforces, they will be treated separately in later sections.

We have been generously assisted in the preparation of this chapter by a number of individuals and teams, notably Lotus and Penske.

22.2 Technical Literature

Up to about 1955, technical details of dampers and their installation are largely lacking in the open technical literature. The classical analysis of automobile suspensions by Rowell and Guest (Refs. 134 and 54) which appeared in the 1922-25 period, regards the automobile as a mass supported on undamped springs. No references to dampers appear in the Automobile Engineer's Reference Book, 1956 (Ref. 99), although other components of the automobile and its suspension are covered in detail. However, in the Chrysler Institute Graduate School lecture notes for 1950-51, a purely descriptive chapter on shock absorbers is included. This covers most of the damping devices up to that period and concludes with a discussion of the Oriflow direct-acting unit adopted by Chrysler for

1951 models. Damper development up to this time had been proceeding on a proprietary and trade secret basis at the component manufacturers.

An excellent primer on direct-acting dampers aimed at "the nature of the component itself so that its versatility can be fully appreciated and its limitations..." was presented by Jackson of Delco Products at the SAE in 1959 (Ref. 67). He points out that the advent of the independent suspension with lowered ride frequency resulted in a change in emphasis in ride development. Having softened the ride, the behavior and "control of the unsprung masses became the problem," thus moving into the areas of steering and road-holding. The paper itself focuses on the damper detailed design plus performance in terms of force versus velocity for various orifices and blow-off valve characteristics.

The mathematical treatment of mechanical vibrating systems was well known before its application to automobile suspensions. Prior to 1945, the SAE had established a Ride Comfort Research Committee (which later became the Vehicle Dynamics Committee) that published the linear treatment of simple, undamped harmonic motion, i.e., the behavior of a mass on a spring. By 1965, this committee published Ref. 68 which covers free and forced vibration with both Coulomb and viscous damping, the force transmission into the body, and human response to vibration. Much of the material stems from Janeway's earlier work, for example, Ref. 69. As with most of the early suspension analyses, these references concentrate on ride as opposed to road-holding. In fact, the conclusion is reached (Ref. 69) that "dampers absorb energy but transmit shock, and therefore the amount of control should be kept to the minimum conditions."

An early presentation of ride theory in book form appears in Ref. 154 by Steeds. This covers the basic mathematics of undamped and damped motion with both Coulomb and viscous damping and forced oscillations. This theory is then applied to various approximations to a real suspension plus a brief discussion of the roll mode. Again the emphasis is on ride.

A significant survey paper by Julien, 1960 (Ref. 74), covers a variety of suspension problems that impact damper design. He points out the well-recognized fact that, for a constant rate spring, the static deflection (hence trim height and natural frequency) changes with load. With softer suspensions, trim change becomes a major problem. Of the various spring and independent trim compensation devices, the incorporation of load leveling into the shock absorber was to become one of the most popular. He recognizes the compromise in ride and road-holding, noting that wheel damping forces are transmitted to the body and suggests that independent dynamic dampers for the wheels may be desirable. Finally, he makes a strong appeal "for development in dampers to match progress ... in springing technology."

In Ref. 96 a one corner suspension model is used to complete the frequency response from DC to beyond wheel hop. Body acceleration is taken as the measure of ride and dynamic load between the tire and road as a criterion for road-holding. Influences of vehicle mass, spring rate, and damping constant are studied. For any practical level of

damping for racing, road-holding at wheel hop frequency is improved but ride suffers. This work is also reviewed in Ref. 60.

Another early investigation of both ride and road-holding is that of Bruns and Fiala, 1967 (Ref. 24). Starting with a random road representation (power spectral density and probability distribution) and using analog computation (including suspension nonlinearities), they develop time histories of the displacements of the car body, the road wheel, and the seat in relation to the random road excitation displacement. They also calculate the associated time histories of the load in the wheel, the spring, and the damper. Various spectral densities (amplitude of the road roughness as a function of wavelength) of typical roads are used and nonlinear representations of the suspension, including dry friction, and the gas-filled hydraulic damper. Various measures of ride and road-holding are developed. The rms (root mean square) of K^{64} (the human sensation for mechanical vibration) is used as a ride criterion, while the rms of the wheel load is the measure for road-holding. This measure for road-holding is one valid criterion for analyzing shock settings for racing.

A brief discussion of choice of damper characteristics is given in Ref. 51, Chapter 3 (by Richard Hodkin). He points out that in practical dampers some friction exists, due to piston movement and seal—also inertia and hysteresis in the valves. Thus dampers seldom develop forces strictly proportional to velocity. He notes that the work done by the damper per cycle is measured by the area under the force-velocity curve. The bump setting of the damper is generally low to minimize the forces put into the body, whereas the rebound setting is larger and accounts for more of the damper work. This is the case when optimum ride is sought but he suggests that for road-holding, bump and rebound settings may be closer together.

Ref. 158 by Thompson somewhat parallels the work of Bruns and Fiala (Ref. 24). Computer studies (digital and analog) with particular inputs and random road roughness are used. Linear dampers with different bump and rebound slopes are simulated. The calculations are effectively for one end of the vehicle. One general conclusion is that the damper rates for optimum ride and for road-holding are quite different, the latter being much harder. This is, of course, well known from practice. The analytical approach offers the opportunity to explore a variety of design variables with numerical results.

Ref. 58 reviews various leveling means for vehicles with soft suspensions and loading changes. The conclusion is drawn that air shock leveling has the largest number of advantages. In this device a conventional hydraulic damper is provided with an auxiliary air chamber that changes the spring force (and thus suspension trim position) of the damper when pressurized. Auxiliary air supply and some form of height sensor are required. Ref. 59 details a Monroe Air-Spring Shock Absorber leveling unit that has an

⁶⁴ K could be chosen as the vertical acceleration of the seat.

integrated sensing system and electronic control. This unit supplements the suspension springs while providing damping and leveling.

A basic examination of damper requirements has been performed by a research group in Nissan's Vehicle Research Laboratory and reported in Ref. 48. The authors present measured data on the spring and damper forces for four conditions related to handling, ride, harshness, and road noise typical of passenger car operation. Since the damping force requirements are different for the four operating conditions, they can plot the range of piston velocity for each condition and also the range of piston stroke. Piston velocities on a rough road and over a large bump were found to be about the same but little damping is required on the single bump (for reduced harshness), while substantial damping is required on a rough road (for road-holding). Since a single bump involves only a small piston stroke while rough road stroke is much greater, a stroke-sensitive damping feature can be used to reduce harshness. While this referenced paper is not directly related to racing, the general approach taken is well worth studying. Some of the test results for optimum rough road damping are presented later in Section 22.4.

As a further effort to optimize damper performance, another group at Nissan performed a linear analysis to estimate the ideal damping ratio for various operating conditions (see Ref. 156). The measure used for road-holding is the root-mean-square average of the unsprung mass ride motion relative to the road. This should be minimized—if the unsprung mass followed the road contour exactly, the average displacement would be 0. A relationship for optimum damping coefficient for road-holding is developed in terms of the ratios of (Sprung + Unsprung mass)/(Unsprung mass) and (Suspension Spring Stiffness)/(Vertical Tire Rate). In a later section of this chapter, calculations for an oval track Indy car are presented based on this paper.

Donald Bastow, in Ref. 18, devotes a complete chapter to dampers with performance curves (force vs. velocity) for various types and a discussion of their pros and cons. He describes a monotube gas/oil emulsion damper (no floating piston) which is compact and obviously avoids problems of leakage across a floating piston. Reference is made to a dual tube Woodhead damper under development which depends on emulsion damping and offers lighter weight and other advantages.

In the period 1985-90, electronically controlled dampers have become popular as the key element in semi-active suspensions. While these are not discussed here, a selected list of references is given under Ref. No. 170.

22.3 Damping Fundamentals

In this section a review of basic damper design and characteristics is presented. It is given in the context of passenger car usage since that is where most damper technology has been developed. Applicability to racing is discussed in the following sections. The

symbols in this section relating to the spring-mass-damper system are somewhat different from those used in Section 6.2.

Basic Ideas

In a damped spring and mass system such as shown in Figure 22.1, there are three forces which govern the dynamic behavior:

1. The *inertial force* is due to accelerating the mass which is a function of the mass and the acceleration.
2. The *damping force* is a function of the velocity across the damper and the damping coefficient. The damping coefficient is expressed in terms of force/unit velocity.
3. The *spring force* is a function of the displacement of the spring and the spring rate. The spring rate is expressed in terms of force/unit displacement.

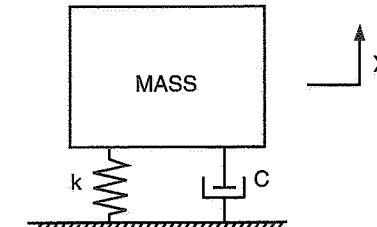


Figure 22.1 Damped spring and mass system.

These three forces can be expressed mathematically as follows:

$$\text{Inertia force} = m \left(\frac{d^2x}{dt^2} \right)$$

$$\text{Damping force} = C \left(\frac{dx}{dt} \right)$$

$$\text{Spring force} = k(x)$$

where m = mass

C = damping coefficient

k = spring rate

x = position or displacement (see Figure 22.1)

$\frac{dx}{dt} = \dot{x}$ = velocity (1st derivative of position)

$\frac{d^2x}{dt^2} = \ddot{x}$ = acceleration (2nd derivative)

m , C and k define two other important parameters. One is the resonant frequency of the system:

$$\omega_n = \frac{1}{2\pi} \sqrt{\frac{k}{m}} \text{ (Hz)}$$

The other is a "critical level" of the damping coefficient. If the mass is given a step displacement then the damping level that allows that mass to return to steady-state position most quickly with no overshoot is the *critical damping*.

Figure 22.2 shows the time history behavior to a step input for twelve levels of damping.

The damping coefficient for critical damping can be expressed mathematically:

$$C_{\text{crit}} = 2\sqrt{km}$$

The relation of the damping coefficient C to the coefficient at critical damping, i.e., the ratio of C/C_{crit} is fundamental to the choice of damping in all damped spring and mass systems. This ratio is called the *damping ratio*, usually given the symbol ζ .

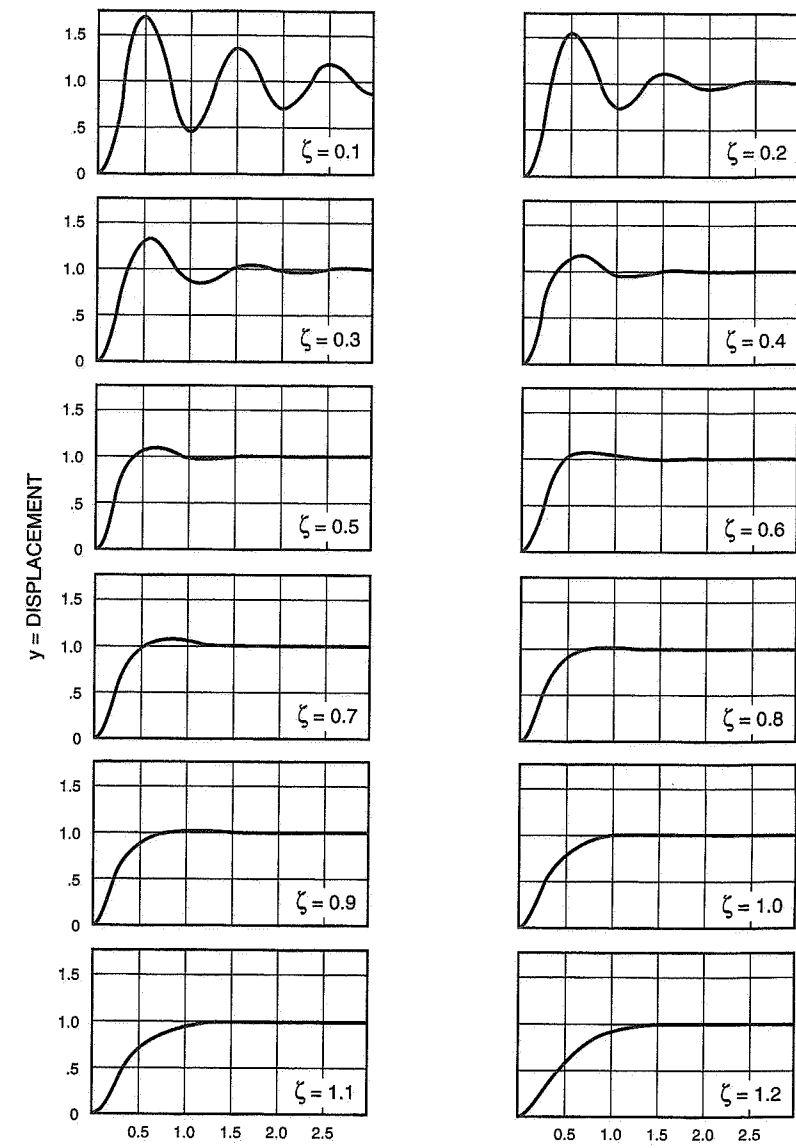
In an automobile, a suspension is used to reduce the discomfort induced by unevenness in the highway. A measure of discomfort is the vertical acceleration that the passenger is subjected to while sitting in the vehicle.

Highways have an unevenness where the vertical amplitude of a bump is roughly related to its wavelength. Large vertical amplitudes are associated with long-wavelength bumps and small vertical amplitudes are associated with short-wavelength bumps. An automobile traveling along a highway will receive inputs from these bumps which appear in the frequency domain such that the large-amplitude long-wavelength bumps are at low frequency and the small-amplitude short-wavelength bumps are at high frequency.

We can therefore approximate a road to a mixture of sine wave inputs such that their amplitudes reduce with increasing frequency. This is idealized as an input that has constant peak velocity at all frequencies.

A constant velocity input applied to the system shown in Figure 22.3, modeling one corner of the automobile, produces vertical acceleration levels on the body shown in Figure 22.4, when values typical of automobile practice are used for the constants. To the first order the higher the acceleration level the more the discomfort.

As the damping is increased, i.e., the C/C_{crit} goes from 0.15 to 0.5, the peak at about 1 Hz is reduced, but the vertical acceleration above 2 Hz is increased. A compromise is thus inevitable in choosing damping levels.



$$x = \frac{t}{t_n} = \frac{\text{Time}}{\text{Period of Undamped Natural Frequency}}$$

Figure 22.2 Time histories showing different levels of damping ratio, $\zeta = 0.1$ to 1.2.

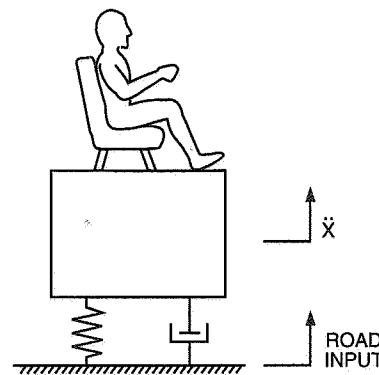


Figure 22.3 Simple "one corner" ride model.

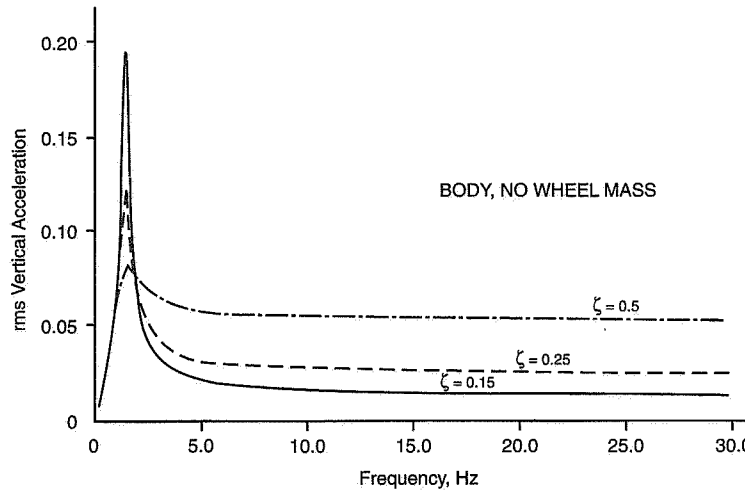


Figure 22.4 Vertical accelerations on simple "one corner" ride model.

An automobile is slightly more complicated than our Figure 22.3 model since the tire also has its own vertical flexibility, or spring rate, supporting the unsprung mass. The behavior of this mass also has to be considered (see Figure 22.5).

Figure 22.6 shows the effect of the unsprung mass resonance on the body acceleration giving a secondary peak in the acceleration trace at about 11 Hz. Figure 22.7 shows the

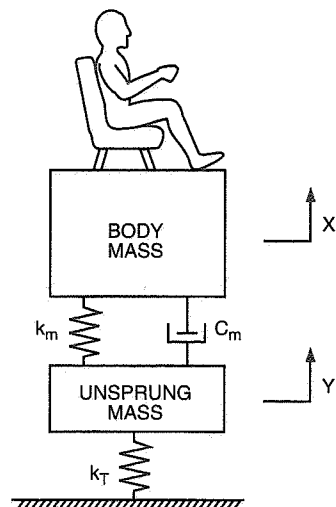


Figure 22.5 "One corner" ride model including unsprung mass and tire spring.

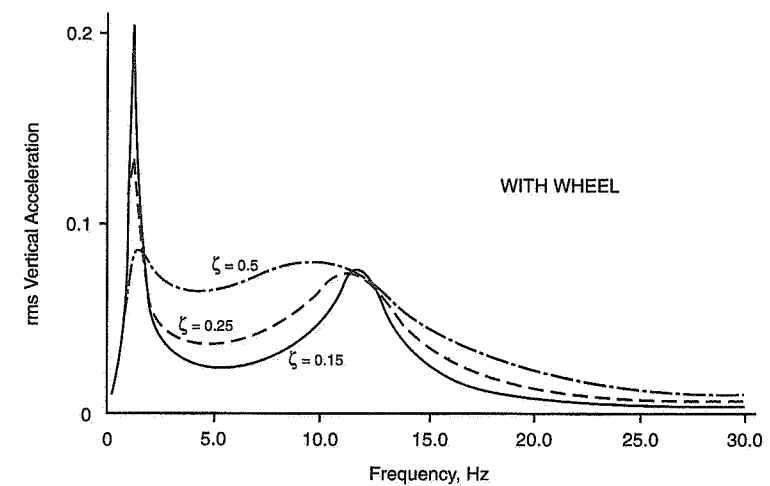


Figure 22.6 Vertical accelerations on "one corner" ride model of Figure 22.5.

transmissibility of the unsprung mass. This is the ratio of the amplitude of the wheel to the amplitude of the road wave. As the damping is increased, this transmissibility is reduced.

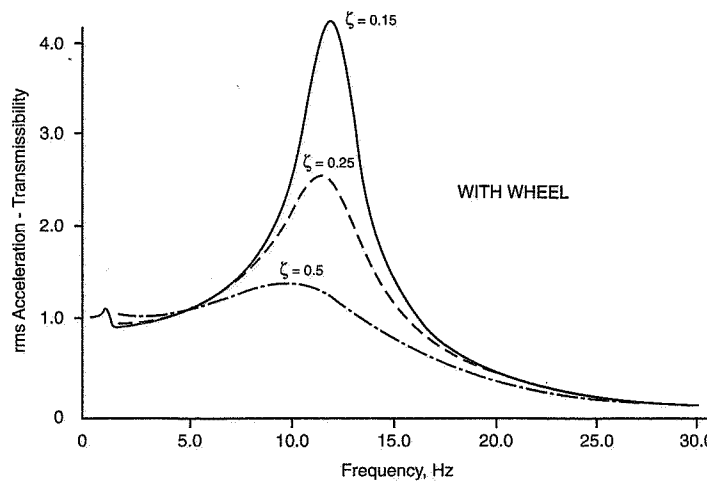


Figure 22.7 Transmissibility of unsprung mass.

It is another task of the damper to control the resonance of the unsprung mass. As a general guide a transmissibility over about 2.5 will tend to permit significant wheel hop and adversely affect the vehicle handling.

We can improve the mathematical model of our car a little further by adding the seat flexibility shown in Figure 22.8. The acceleration levels on the passenger are shown in Figure 22.9.

As the damping ratio is increased from 0.15 to 0.5, the height of the main ride peak (at about 1 Hz) is reduced but the acceleration level over the rest of the frequency range is increased, giving reduced comfort.

To give an indication of the overall comfort level, we can calculate the mean acceleration of the curves in Figure 22.9; results are shown in Figure 22.10. This shows that the lower the critical damping the greater the comfort.

However, Figure 22.11 (which is similar to Figure 22.7) shows how reducing the damping ratio from 0.5 to 0.15 considerably increases the wheel resonance transmissibility. An acceptable compromise is to limit the unsprung mass transmissibility to 2.5, implying a damping ratio of about 0.25.

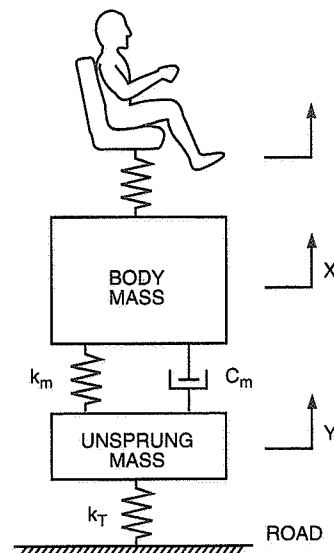


Figure 22.8 Ride model including seat flexibility.

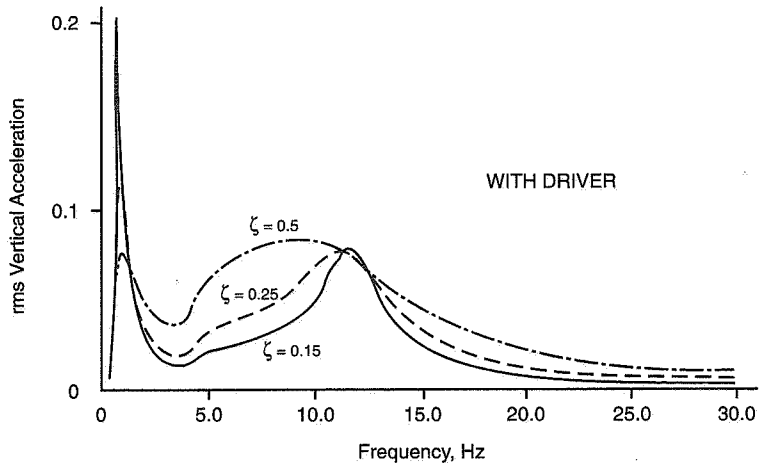


Figure 22.9 Passenger acceleration, including seat flexibility.

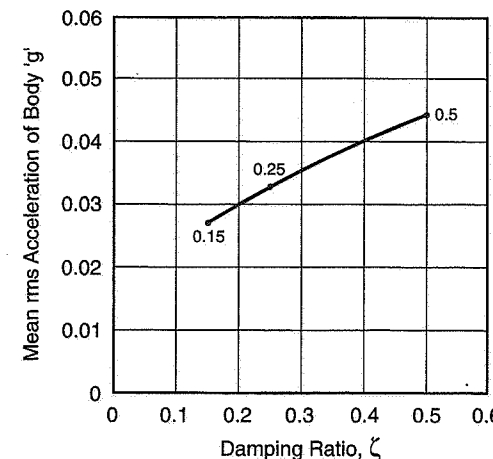


Figure 22.10 Passenger acceleration vs. damping ratio, ζ .

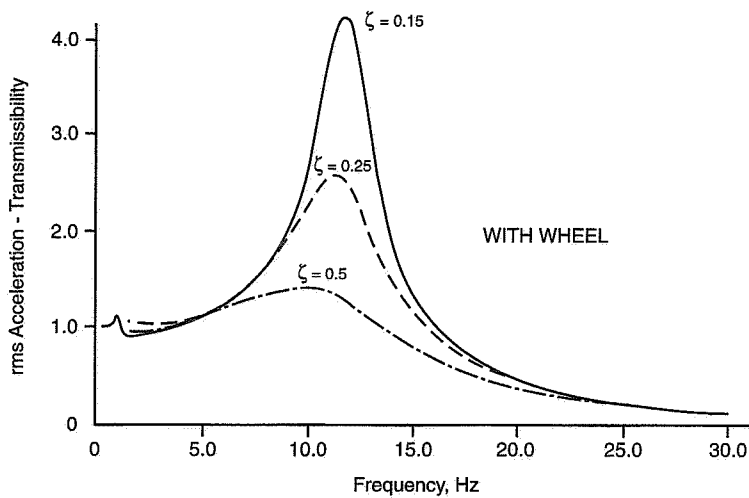


Figure 22.11 Figure 22.10, with wheel transmissibility.

Mode Centers

Up to this point we have simplified the system by assuming the automobile has only one main spring and one wheel. As soon as we consider the more realistic model of an automobile with a wheel at each end, we should consider the dynamic behavior of one end relative to the other.

In general a lightly damped vehicle will exhibit two modes of vibration: a "pitchy" bounce and a "bouncy" pitch, each with its own center of oscillation and frequency. The "pitchy" bounce has its center of oscillation outside the wheelbase and the "bouncy" pitch has its center of oscillation within the wheelbase.

Taking the example shown in the upper part of Figure 22.12, the front wheel will hit the bump first and begin moving at 84 cpm whereas the rear wheel will start moving a little later and move at 68 cpm. The comparative behavior is shown in Figure 22.13 and will tend to give a pitchy ride. These frequency and mode positions are controlled by the static deflection (mass/stiffness) at each end.

The upper part of Figure 22.12 shows a static deflection (referenced to the unloaded height) of 5 in. at the front and 7.5 in. at the rear. By softening the front springs and stiffening the rear springs we can give a front static deflection of 7.5 in. and a rear one of

WHEEL RATE		STATIC DEFLECTION		$\frac{K^2}{ab} = 0.8$	PITCH
FRONT lb/in	REAR lb/in	FRONT inches	REAR inches		
100	66	5	7.5		
				68 C.P.M.	PITCH
66	100	7.5	5		
				84 C.P.M.	PITCH

Figure 22.12 Conventional suspension pitch and bounce centers.

5 in. Hence the rear of the automobile will move faster than the front and tend to catch up, with the relative behavior as shown in Figure 22.14. This gives the "flat" ride.

The dynamics of a vehicle can be modeled on a computer and run on a typical road where the input to the rear wheel is delayed according to the speed. The third graph in Figure 22.15 shows how the soft-front/stiff-rear car exhibits less than half the pitch angle displacement, giving the flat ride.

To obtain the flat ride in a lightly damped vehicle it is important to have the static deflection at the front greater than the static deflection at the rear. With heavily damped vehicles, where the main ride resonance is well suppressed, this requirement is less important (race cars, for example).

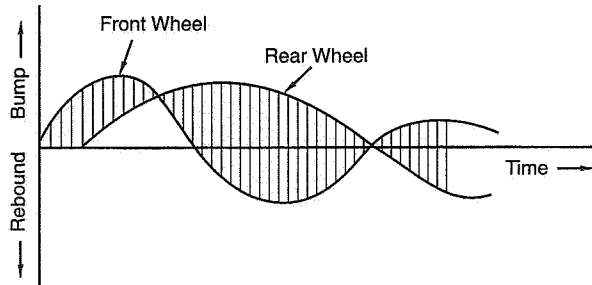


Figure 22.13 Time history of Figure 22.12 (upper part).

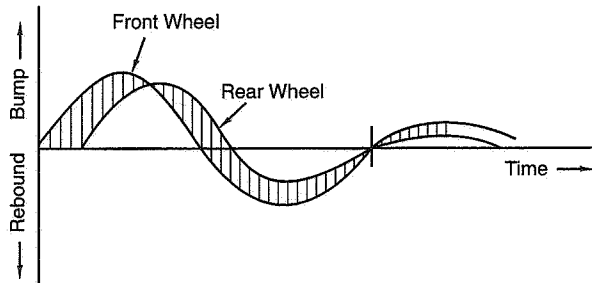


Figure 22.14 Time history of Figure 22.12 (lower part).

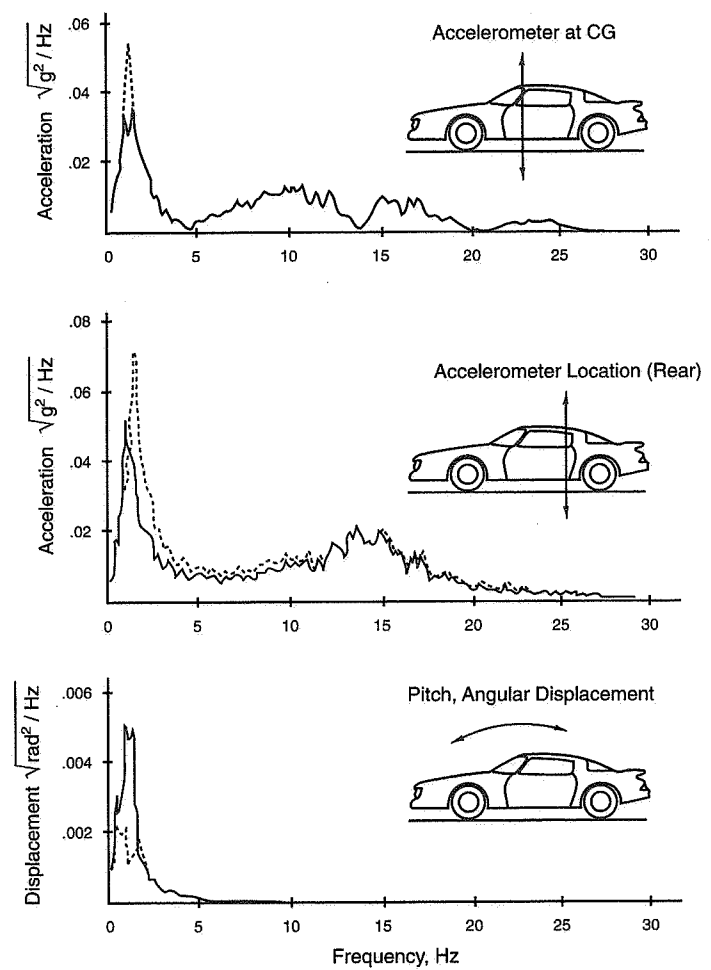


Figure 22.15 Ride comparison in frequency domain.

Effects of Damper End Rubbers

Flexibility in series with the damper (Figure 22.16), often called a "relaxation spring," has only a small effect on the mean rms acceleration of the body (comfort level) (see upper part of Figure 22.17), but a significant effect on the wheel transmissibility (see lower

part of Figure 22.17). Figure 22.17 shows mean values over the range 0-30 Hz, based on the detailed response curves shown in the damper relaxation spring plots (Figures 22.27, 22.28, and 22.29). As flexibility is introduced with a given damping ratio, the wheel transmissibility is increased and wheel control is eventually lost. Some of the drop in damping can be recovered by increasing the damping ratio, but the comfort level is then reduced. In practice, the best use of damper end rubbers is with nonlinear rates, with significant flexibility occurring over only very small deflections (say 1/10 in.); the rubbers stiffen up on larger deflections. This allows the benefits of lower transmissibility at high-frequency small-amplitude inputs (above 20 Hz), while maintaining control over the wheel at larger amplitudes.

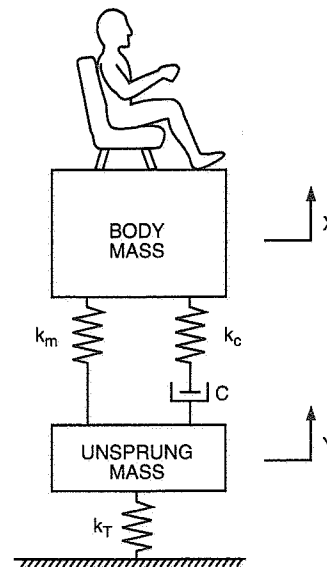


Figure 22.16 Ride model including damper end rubber isolators.

Damper Characteristics

The characteristics of the damper itself will now be considered in more detail by considering the acceleration the damper imparts to the vehicle when its ends have a relative velocity of V in./sec. Using the expressions given earlier for the damping ratio and resonant frequency, equations given in a later section (Body Acceleration due to Damper Velocity) show that this acceleration is given by

$$g_d = 4\pi \times (\text{damping ratio}) \times \omega_n \times V/g$$

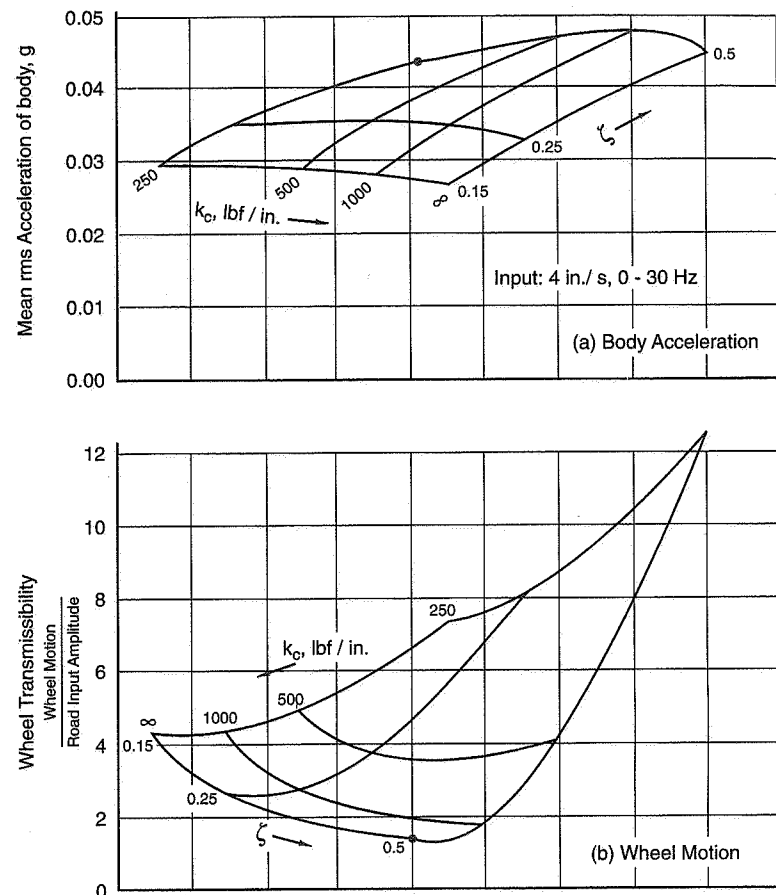


Figure 22.17 Effects of damper relaxation spring, k_C (carpet plot).

where g_d is the body acceleration due to damper in g's
 ω_n is the resonant frequency
 $g = 386.4 \text{ in./sec.}^2$ (acceleration of gravity)

Using the best compromise value of 0.25 for the damping ratio (for ride and handling of passenger cars),

$$g_d / \omega_n = \pi V/g = 0.0081 \times V$$

Figure 22.18 shows this relationship graphically.

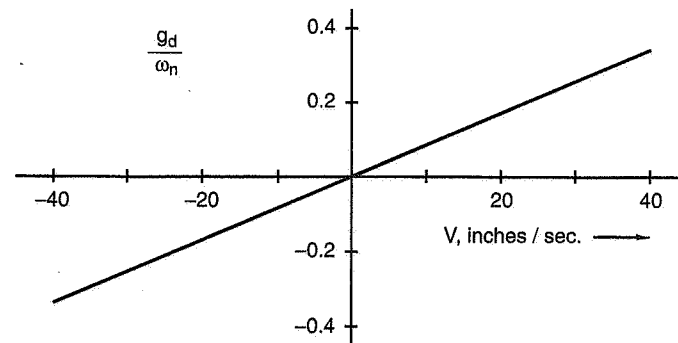


Figure 22.18 Simple damper characteristics.

As an example of the use of the equation, suppose we have a vehicle whose resonant frequency is 1.2 Hz. Then, if the velocity across the damper at an instant is 20 in./sec., the body acceleration will be

$$g_d = 0.0081 \times V \times \omega_n = 0.0081 \times 20 \times 1.2 = 0.194g$$

In practice, this simple relationship is modified by several factors. Measurements on vehicles have shown that wheel velocities in the upward (bump) direction are generally considerably higher than in the downward (rebound) direction by a factor of about two. The damper is manufactured to have a corresponding asymmetry, with the coefficient in rebound being about twice that in bump, thereby keeping forces on the vehicle symmetric. The result is shown in Figure 22.19, where the slopes have been chosen to have an average value the same as the slope of Figure 22.18.

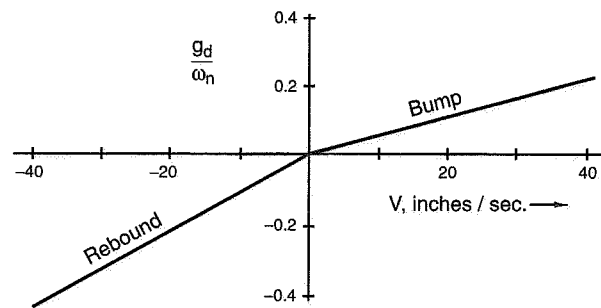


Figure 22.19 Damper characteristic showing bump-rebound force ratio.

Other departures from Figure 22.18 are due to hardware factors. Hydraulic dampers use the pressure required to force oil through an orifice to generate the damping force, and this results in a parabolic rather than straight-line characteristic. As a consequence, g_d values become very high at high V . To counteract this, a blow-off valve can be incorporated to bypass some of the flow at high velocities. The resulting characteristic with a "knee" proves to be uncomfortable. Another departure from the idealized relationship of Figure 22.18 is a small "deadband" around the origin due to the unavoidable presence of some "dry" friction (stiction) in the suspension linkage. While this is detrimental to the ride qualities, it can improve the vehicle handling by introducing what is effectively a very high damping coefficient at the very low velocities occurring during maneuvers such as braking and cornering. Figure 22.20 illustrates the parabolic characteristic, the dry friction deadband, and the "knee."

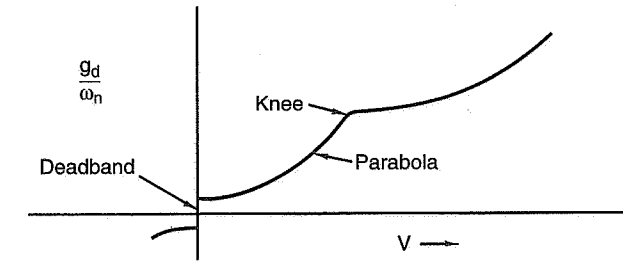


Figure 22.20 Damper characteristic including orifice effects and "dry" friction.

Damper characteristics are often plotted with the rebound curve reflected, so that it lies in the same quadrant as the bump curve. This is shown in Figure 22.21. Dampers with this idealized characteristic subject passengers to very high accelerations during the relatively infrequent motions involving very high velocities; it is therefore desirable to incorporate some "roll-off" from the straight line at high velocities, at some small expense to the control of wheel hop. Figure 22.22 shows a damper characteristic with roll-off.

Dampers for sports cars, in which more emphasis is placed on handling and less on comfort, have similar characteristics but values of g_d / ω_n are up to two times greater than for saloons.

Effects of Leverage

Dampers are of necessity connected to the unsprung mass somewhat inboard of the wheel center. The wheel velocity thus exceeds the damper velocity by a factor of N , say. Then, for a given wheel velocity, V , the damper generates a force of CV/N . The effect of the lever ratio on the forces is to reduce the force acting on the wheel by a further factor

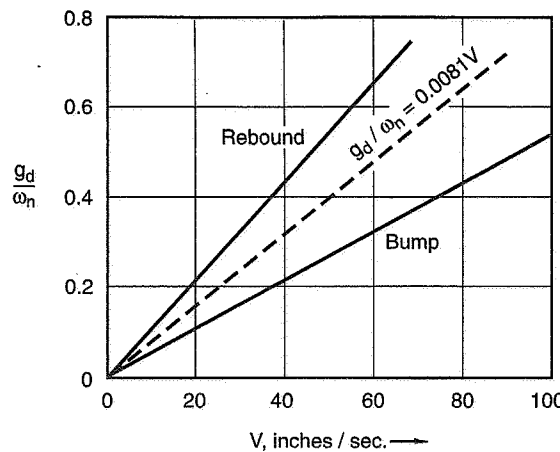


Figure 22.21 Bump and rebound both plotted in the first quadrant.

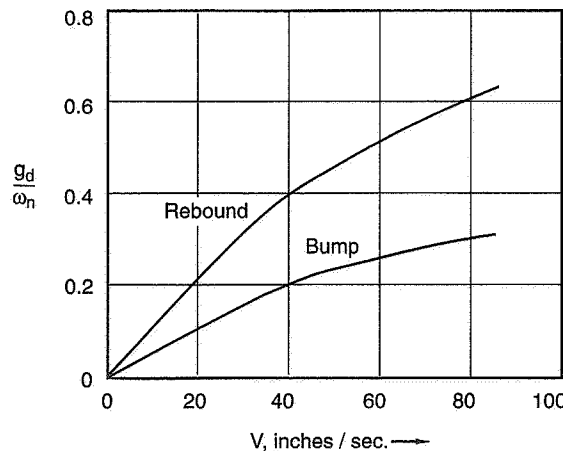


Figure 22.22 Damper characteristic with high velocity roll-off.

of N, to CV/N^2 . Therefore, to provide a given damping coefficient at the wheel, the actual damper must have a coefficient N^2 times as big.

Damper Construction

The majority of dampers today are of the telescopic type. As these operate, the length of piston rod within the oil-filled damping cylinder varies, and three different approaches are used to accommodate the resulting change in volume. The dual tube design uses a valve in the base of the damper to let oil through into the outer chamber (Figure 22.23(a)). One form of monotube damper uses an emulsion of gas and oil as the working fluid, with the gas compressing as more piston rod comes within the working cylinder (Figure 22.23(b)). An alternative monotube design uses a floating piston with pressurized gas below it which becomes further compressed as the damper is compressed (Figure 22.23(c)). Both the monotube types exhibit a static force tending to extend the damper, which is due to the pressure within the working cylinder.

In Figure 22.23, different types of bump rubbers are shown on the piston rods. While these have nothing to do with the damping performance as such, the piston rod provides a convenient location. The "rising rate" (nonlinear spring) provided by the bump stop is often critical to overall race car performance, especially on rough surfaces. Bump rubbers are available in different sizes and shapes, and may also be cut down to provide a wide variety of different rate curves. When a bump rubber is used, the combined spring rate with the main spring may be calculated using the springs-in-parallel calculation in Chapter 21.

Measurement of Damper Characteristics

In the past it has not been practical to use constant velocity tests to measure the damper properties. The conventional damper tester couples one end of the unit to the throw on a crankshaft and a technique using "carding" loops is used. The damper is subjected to a series of sinusoidal motions all with the same amplitude but at increasing frequencies. A load cell is fitted to measure the damper force. In modern systems, the force-displacement data are usually captured by a high-speed data acquisition and analysis system such as the Anthony Best Dynamics "CARDS" equipment. A graph is plotted of the force generated against displacement; each test results in a single loop. A typical series of loops is shown in Figure 22.24. The damper being tested was of the gas-filled type, and the associated preload has caused the zero offset on the force axis. For a particular loop corresponding to sinusoidal motion at frequency, f, the peak velocity (at zero displacement) is given by

$$V = 2\pi \times \omega \times \text{amplitude}$$

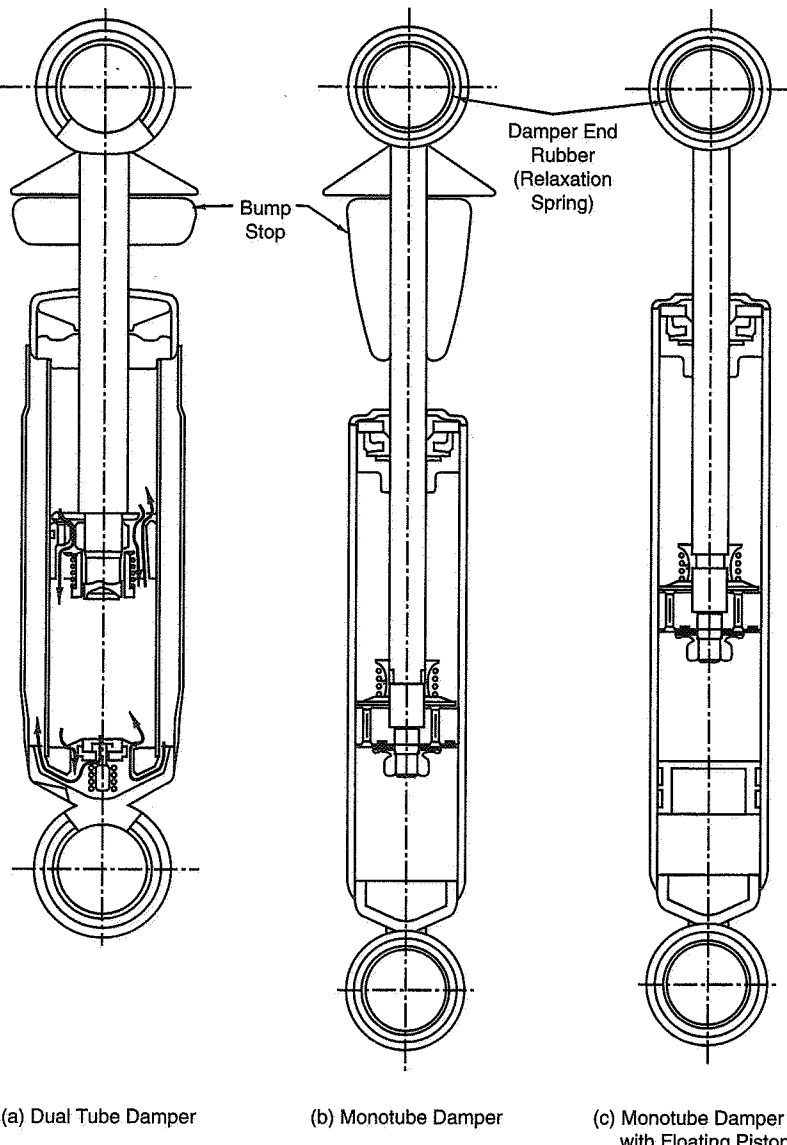


Figure 22.23 Damper constructions.

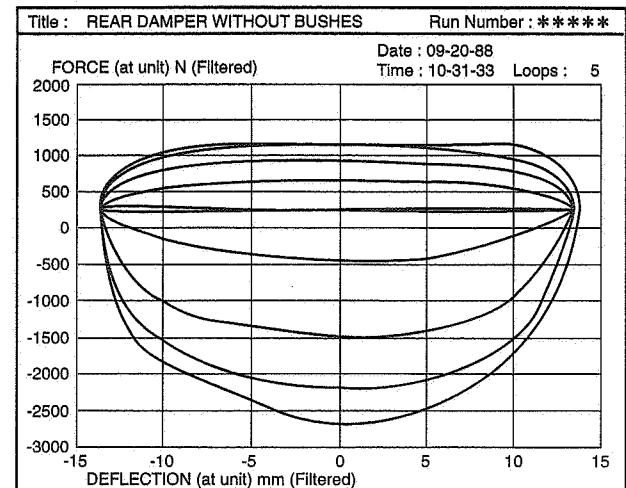


Figure 22.24 Damper characteristic, force vs. deflection, classical measurement.

And the corresponding bounce and rebound forces can be read from the plot (see Figure 22.25). In this way, the complete damper characteristic shown in Figure 22.26 can be built up.

Recently, the classic crankshaft test rig has been replaced by an electrohydraulic servo cylinder on some test machines. Cylinder position can be slaved to a variable-frequency constant-amplitude triangle wave. This test set-up generates constant velocities for es-

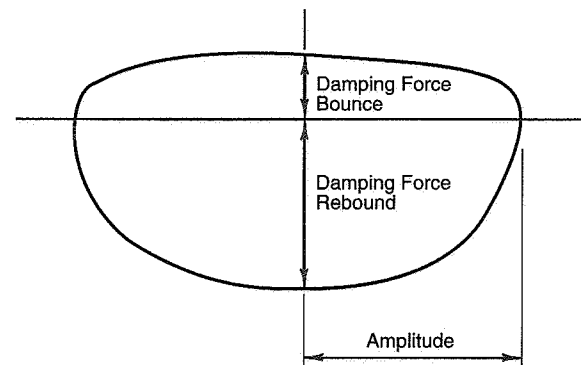


Figure 22.25 Damper characteristic, single loop of the classical measurement.

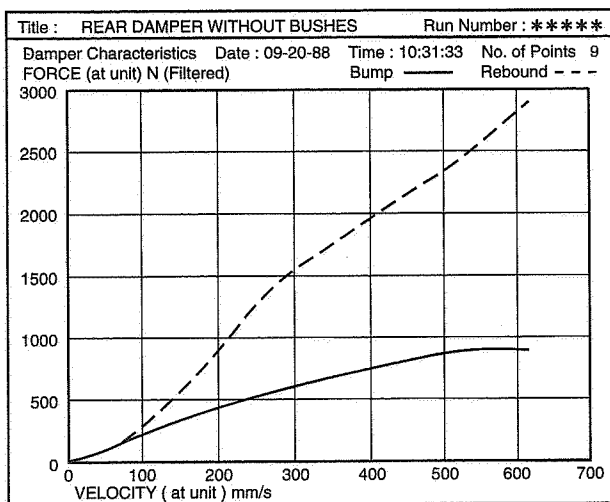


Figure 22.26 Damper characteristic, replotted against velocity.

sentially all of the chosen stroke, allowing data at each chosen velocity to be taken directly.

Damper Relaxation Spring—Plots

Detailed graphs for the effects of a damper relaxation spring (damper end rubber, see page 797) are given in Figures 22.27, 22.28, and 22.29.

Body Acceleration due to Damper Velocity

A derivation of body acceleration due to damper velocity (damper shaft speed) follows.

Consider a damper at an instant when one end has a velocity, V , relative to the other. The force generated, F , is given by

$$F = C \times V$$

From the definition of the damping ratio, ζ ,

$$C = \zeta \times C_{\text{crit}}$$

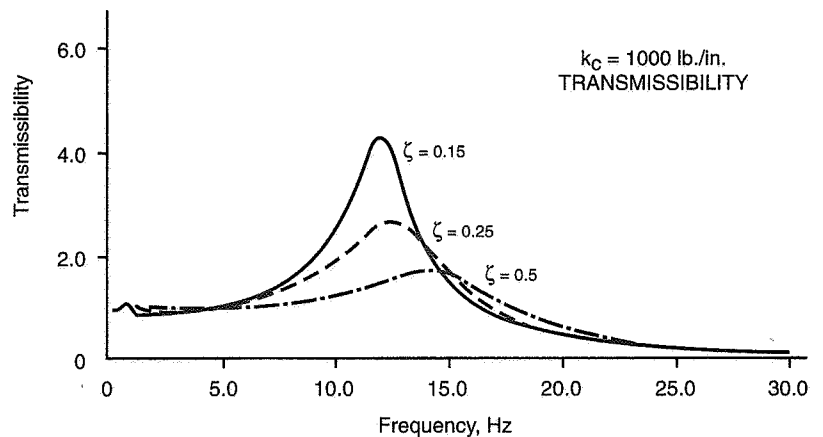
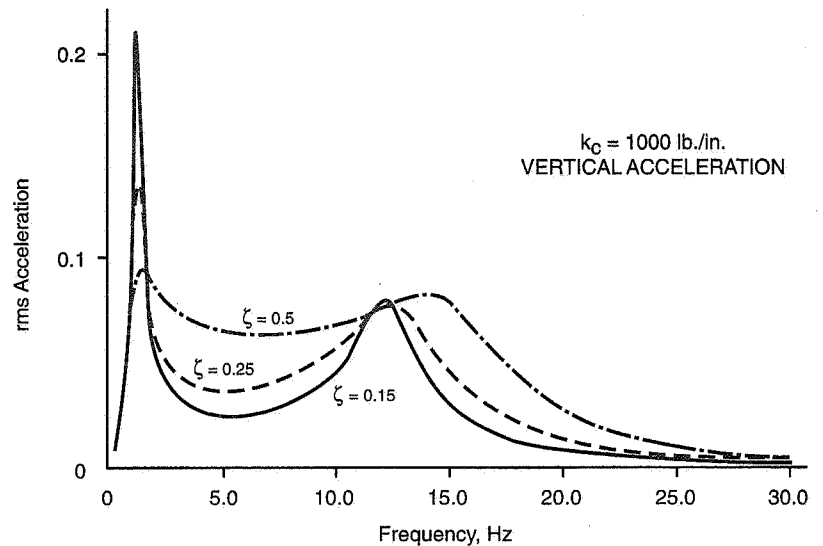


Figure 22.27 Effects of damper relaxation spring, 1000 lb./in.

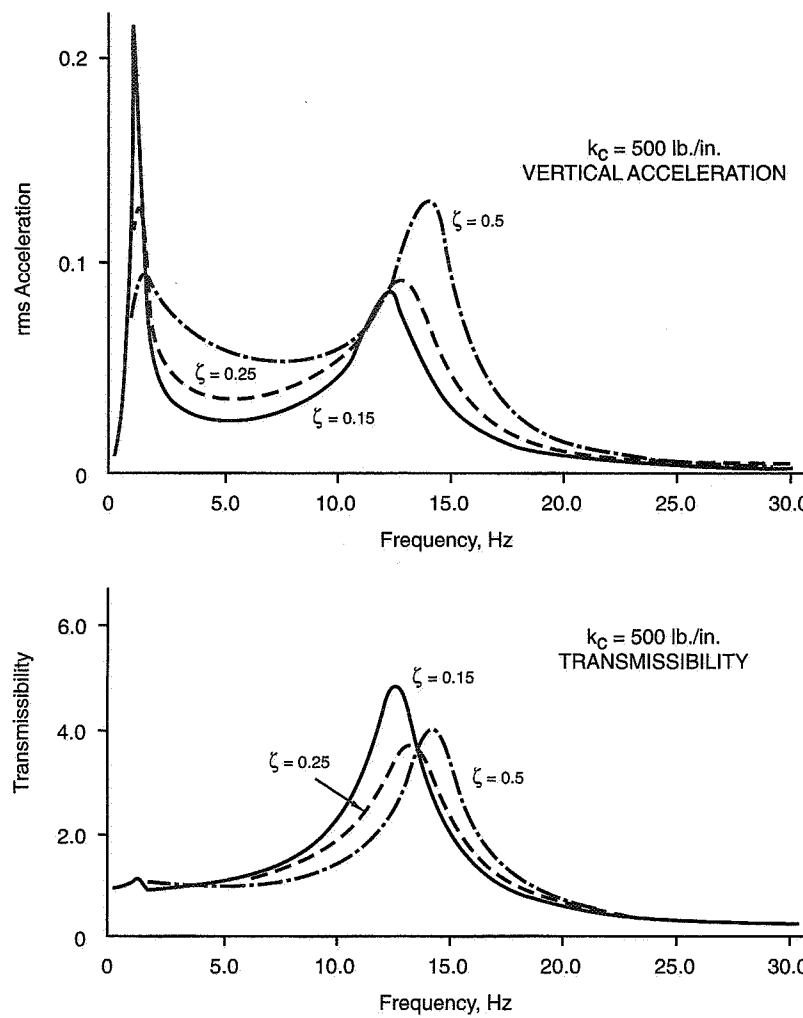


Figure 22.28 Effects of damper relaxation spring, 500 lb./in.

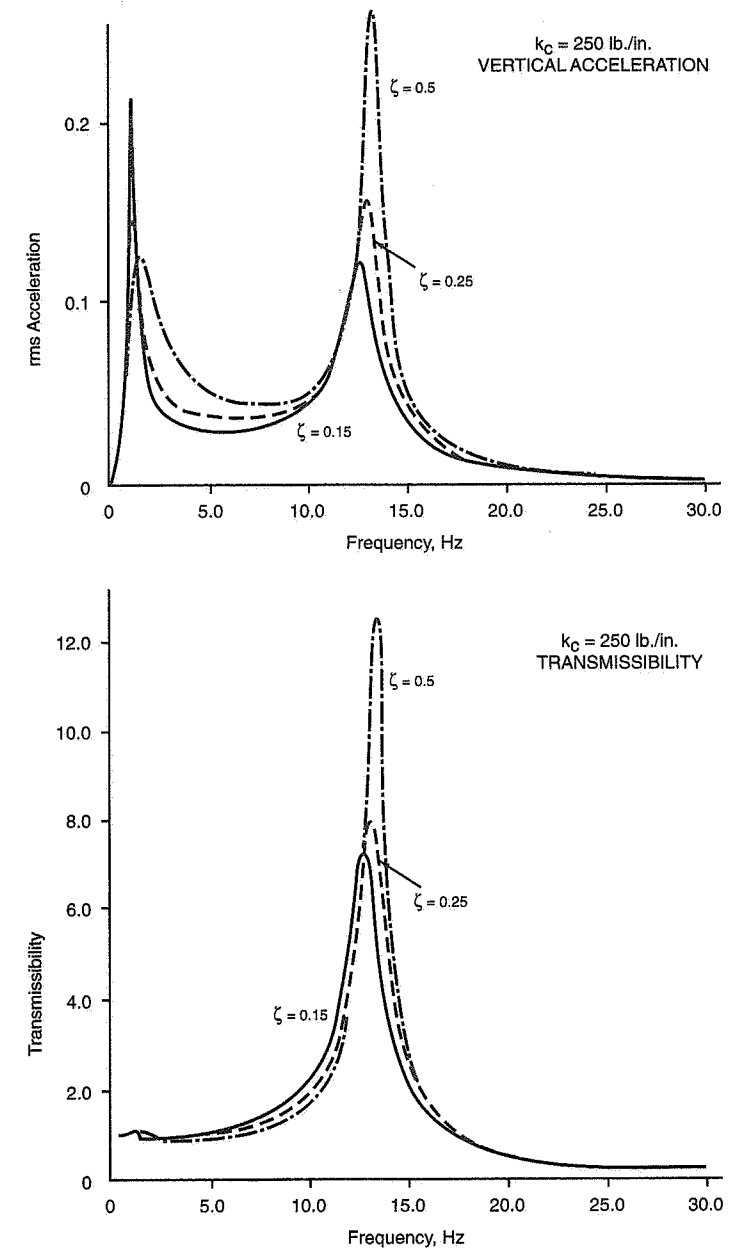


Figure 22.29 Effects of damper relaxation spring, 250 lb./in.

So,

$$F = \zeta \times C_{\text{crit}} \times V = \zeta \times 2\sqrt{km} \times V$$

The vehicle acceleration is this force divided by the mass:

$$\text{Acceleration} = \frac{\zeta \times 2\sqrt{km} \times V}{m} = 4\pi\zeta \times \omega_n \times V$$

Expressed in g units:

$$g_d = 4\pi\zeta \times \omega_n \times V/g$$

For further information on the material of this section, see Refs. 102, 103, and 22.

22.4 Racing Application

On the passenger car, dampers are biased toward good ride as measured by rms acceleration at, say, the driver's seat. An average or mean rms acceleration over the road input frequency range is used because stiffer dampers reduce body resonance (or float) which occurs at 1-2 Hz, but increase harshness (force transmission from the unsprung mass into the body) over most of the higher frequency range. A damping ratio (percent critical damping) of 0.25 for the body gives several overshoots at resonance (which is acceptable because there is relatively little low frequency content in highways) but markedly reduced harshness. This same level of damping (shock setting) gives about 25% critical damping of the unsprung mass, which has proven acceptable for softly sprung passenger cars. These numbers may vary for different manufacturers and for U.S., European, and Japanese practice, but the philosophy of compromise between float and harshness is universal.

For the racing car, the damping must be considerably higher. For accurate vehicle control, particularly at higher speeds, float is unacceptable on race and sports cars. Also, higher damping is necessary for road-holding/control of the unsprung mass motion. The predictable result is better low-frequency ride (less wallowing) but more high-frequency harshness. Race cars are compromised toward road-holding at the expense of ride. If damping is too high, dampers tend to control the suspension motion and overpower the spring rates.

The Ride/Handling Compromise

The "transmissibility" of the unsprung mass has been defined as the ratio of the vertical wheel motion to the vertical amplitude of the road. If X_0 is the height of the road (referenced to some zero height) and X_1 is the wheel motion, the transmissibility is given by X_1/X_0 . If this ratio is 1.0 the excursion of the wheel matches the road and the force be-

tween the wheel and the road is theoretically the static load. If the ratio is large, the unsprung mass is transmitting forces into the body while the force between the wheel and the road is reduced. Thus one measure of road-holding is the transmissibility of the unsprung mass, as defined here. Some average measure is required over the input frequency (track roughness) of interest.

A related way of assessing road-holding is that of Ref. 156. The "evaluation criterion" for road-holding performance is the load fluctuation rate, R , defined as

$$R = \frac{k_1}{(m_1 + m_2)g} \times \bar{\sigma}$$

where k_1 = vertical tire spring rate

m_1 = unsprung mass

m_2 = sprung mass

g = gravitational constant

$\bar{\sigma}$ = root-mean-square of $X_0 - X_1$

This definition of R is based on a quarter-car model (i.e., one wheel suspension) linear analysis.

In this same reference, a measure of a mean vertical acceleration of the body taking into account human susceptibility to acceleration is developed, denoted as P . Relationships for ride, P , and road-holding, R , as functions of damping ratio are then developed. Figure 22.30 shows the optimum damping ratios, ζ , for ride and road-holding using data for a compact passenger car. (The results are presented nondimensionally by normalizing with the minimum values of P and R , respectively.)

As expected, the optimum damping ratio for road-holding is higher, about 0.45 for this vehicle, and 0.15 for ride. It is interesting to note that for this vehicle there is a rather broad optimum range for road-holding while there is little range for optimum ride.

Some further insight into the ride/handling compromise and optimum damping for road-holding can be obtained from the analyses of Ref. 48. In this paper, road-holding is defined in terms of tire-ground contact rate and load fluctuation rate, defined as shown in Figure 22.31.

The values of tire-ground contact rate and load fluctuation rate were developed from a simulation of a car and its suspension and data on road surface inputs.

Figures 22.32 and 22.33 are calculations for a smooth road and for a rough road (typical), respectively. For a smooth road, tire-ground contact rate is 100% (Figure 22.32) and the load fluctuation rate is approximately zero. As noted in the paper, "ground contact per-

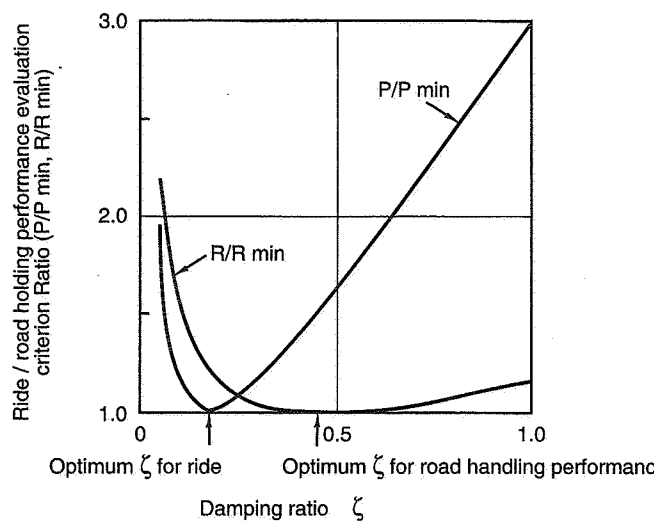


Figure 22.30 DR vs. ride and road-holding performance, compact passenger car.

Tire-Ground Contact Rate is the distance traveled with the wheel in contact with the road ($T - \sum T_i$) as a percentage of the total distance traveled.

Load Fluctuation Rate is the rms of the wheel load change/wheel load.

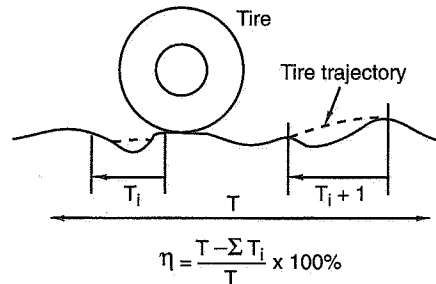


Figure 22.31 Definitions of tire-ground contact and load fluctuation rates.

formance is thus secure at any damper setting." The desirable setting is determined by ride—in this case a compromise between front and rear body acceleration.

For the rough road case, which is probably more typical of high-speed race operation on many circuits, the tire-ground contact rate only approximates 100% at a high damping coefficient. The load fluctuation rate reaches a minimum at approximately the same high damping coefficient (note the scale changes between Figures 22.32 and 22.33). On these

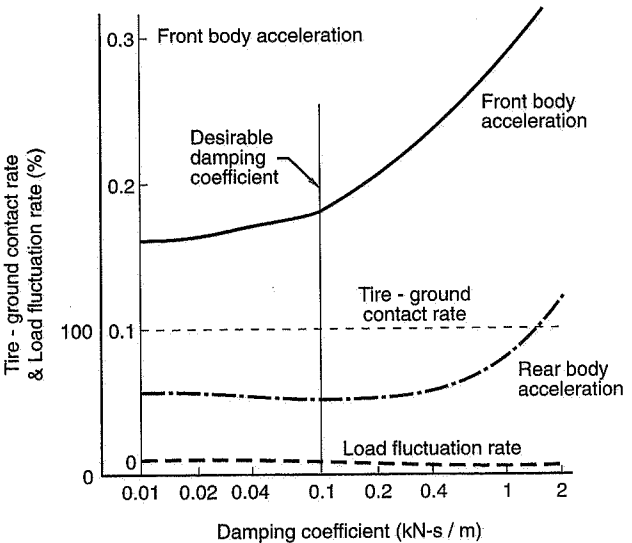


Figure 22.32 Load fluctuation and body acceleration, smooth road.

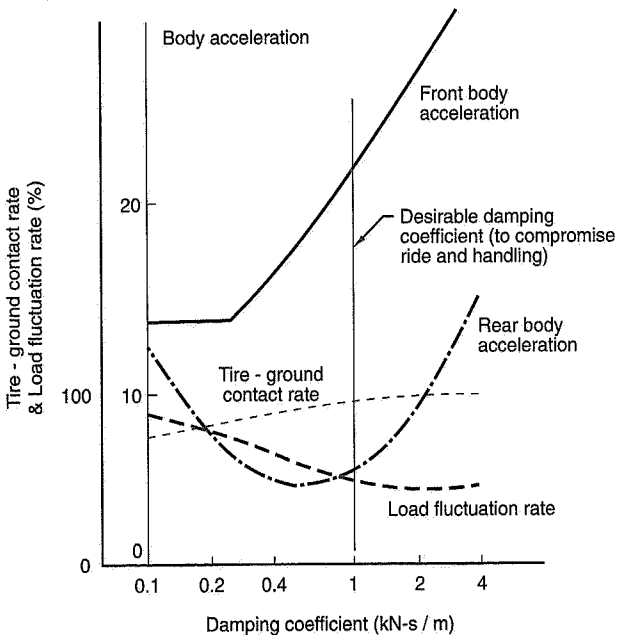


Figure 22.33 Load fluctuation and body acceleration, rough road.

figures, the damping coefficient is given in kN/m/s, which can be converted to lb./in./sec. by multiplying by 5.7. Thus 2 kN/m/s in Figure 22.33, desirable for rough road-holding, corresponds to 11.4 lb./in./sec. This rate is very low compared to what modern racing shocks can be set up to produce (which can be over 100 lb./in./sec.) because race cars use much stiffer springs. The value of this analysis is that it shows the considerable difference rough surfaces demand of the damper for road-holding compared to that for a smooth surface.

Steering Activity

It is well known that rough roads affect the steering activity required to follow a desired path. One would expect that the level of suspension damping would affect the level of steering activity. This matter has been explored in Ref. 130 by Rill of Daimler-Benz. The analysis is based on a comprehensive nonlinear vehicle model that is used to simulate a constant-radius, steady-state skid pad test with three different surfaces varying from very smooth to very rough. Curves of tire lateral force loss with load variation (due to road roughness) are developed from tire data as shown in Figure 22.34, where subscript, N, refers to values corresponding to static load conditions. The next step in this analysis is to calculate the conventional skid pad curve for a variety of road conditions, assuming that speed on the circle is increased very slowly (essentially steady-state). In all cases, he sets the condition that the steering activity of the model controller keeps the vehicle on the circle.

Figure 22.35 compares the skid pad curve for an ideal surface with the results for his good (average) roadway for a baseline vehicle with "standard" dampers. The effect of changing damper characteristics is shown in Figure 22.36. The steering activity with the

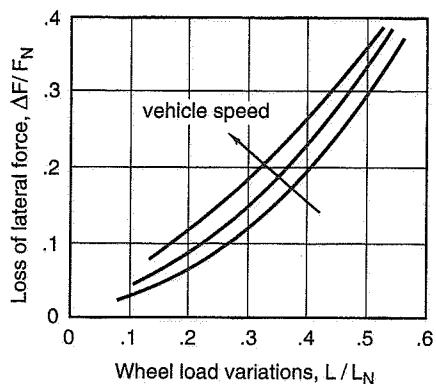


Figure 22.34 Loss of lateral force due to wheel load fluctuation.

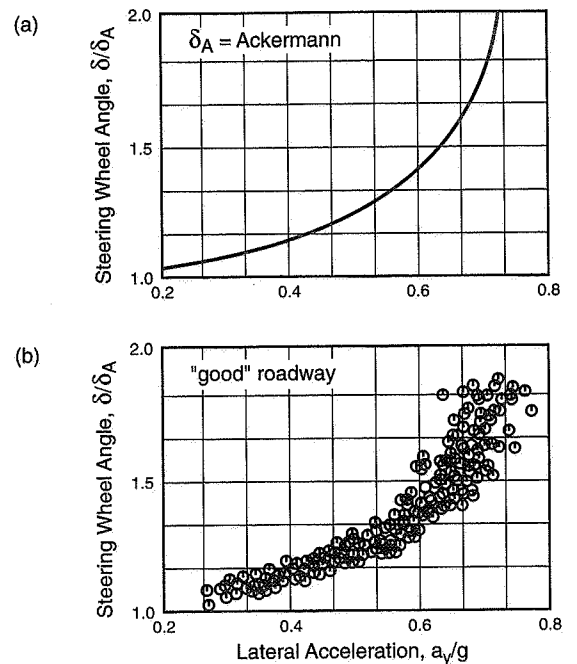


Figure 22.35 Steady-state cornering on smooth and good (average) road surface.

reduced dampers has increased appreciably from that of Figure 22.35(b). The "driver" is confronted with more workload to maintain the given path.

Figure 22.37 shows the steering activity on a "poor roadway" with standard dampers. In this situation the workload is obviously very high, as the driver augments the stability which changes from instant to instant due to the lateral tire force variation associated with the rapidly changing wheel loads. Through the "efforts" of the model (perfect) driver the vehicle does follow the intended circle and the illusion is created that the steady-state stability as measured by the slopes on Figure 22.35(a) exists. This kind of situation was aptly referred to as "controlled stability" by Prof. Otto Koppen (MIT Aero Dept., c. 1930) before the term "augmentation" had come into use.

Transient Maneuvering

In addition to controlling the unsprung mass on rough surfaces (as discussed under Ride/Handling Compromise), the damper comes into play on turn entry and exit—the transient phases of cornering. During these phases the vehicle has a rolling velocity which creates

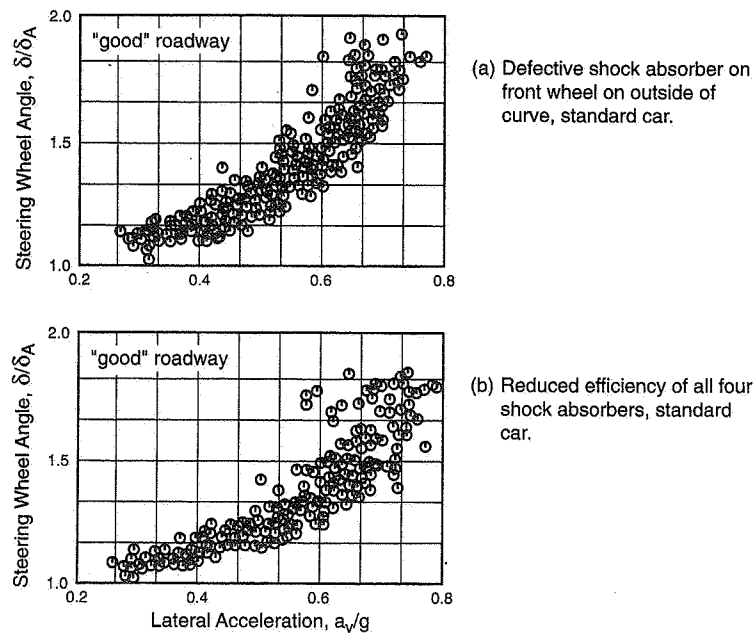


Figure 22.36 Steady-state cornering with damper degradation.

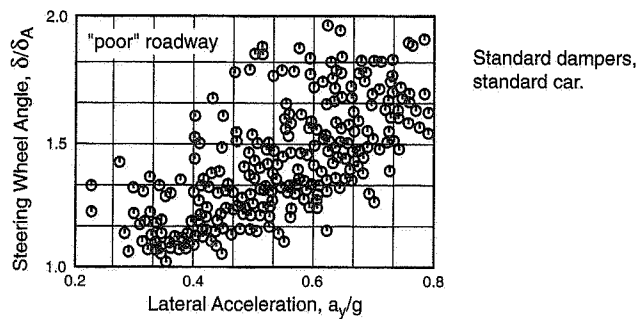


Figure 22.37 Steady-state cornering on uneven roadways.

damper velocity and force. A similar situation exists with pitch due to acceleration or braking. Roll and pitch occur simultaneously in racing as the driver works around the “g-g” diagram. The effect of the dampers is to change the loads (and load distribution) on the wheels during transients. These load changes in turn result in changes in the lateral tire forces, changing the directional stability and control, particularly near the limit of adhesion.

The subject of transient wheel loads is one which has yet to be fully explored. Certainly the resultant wheel load is the sum of contributions from springs, anti-roll bars, dampers, suspension anti-roll and pitch, friction in suspension components, etc., as well as the static weight distribution and the load transfer from horizontal and vertical accelerations. How these different load components come on during the transient and the relative magnitudes must have a prominent effect on “turn-in” or turn recovery.

With sufficient instrumentation much can be learned about transient wheel loads but it is certainly not an easy task in the vibration, etc., environment of the race car. The alternative is an analytical one using a vehicle dynamics computer model such as MRA Vehicle Dynamics Simulation (VDS) discussed at the end of Chapter 6. All of the suspension elements are represented in this model in nonlinear form. One example of this type of calculation is given below.

The maneuver considered is a ramp input of left-turn steer of 33° at the steering wheel. A ramp time of 0.1 sec. is used (the time from 0° to 33° of steer). After steady-state turning is reached and held for a few seconds, the steering is removed. The maneuver is performed at 70 mph, drive torque is just enough to maintain speed. The calculation is set up such that the lateral weight transfer at the front suspension is artificially minimized and the lateral force and yawing moment from the front is maintained essentially constant. The calculations and results presented are for the rear suspension. For the particular comparison shown here, the rear roll center height is zero (on the ground) so there are no jacking or “anti-roll” effects. The curves show the contributions to the left and right rear wheel loads due to the suspension spring, damper, anti-roll bar, and suspension friction (in this case, almost unnoticeable). The numbers used for the vehicle and tires were for a hypothetical high-performance car.

Figure 22.38 presents the time histories of the load components of the left and right rear wheels for the case of the “standard dampers.” Figure 22.39 shows the results when the damper constant is effectively doubled.

Referring to Figure 22.38, one can observe how the damper contributes an increased force on the right wheel during turn entry and a substantial reduction in wheel load during turn exit where the damper is in rebound. The rebound damper constant is higher than the bump setting. The relative magnitudes of the damper, spring, and anti-roll bar are clearly shown. The left wheel is unloaded by all components during this maneuver, the maximum value of the damper in rebound equals that of the anti-roll bar (in the tran-

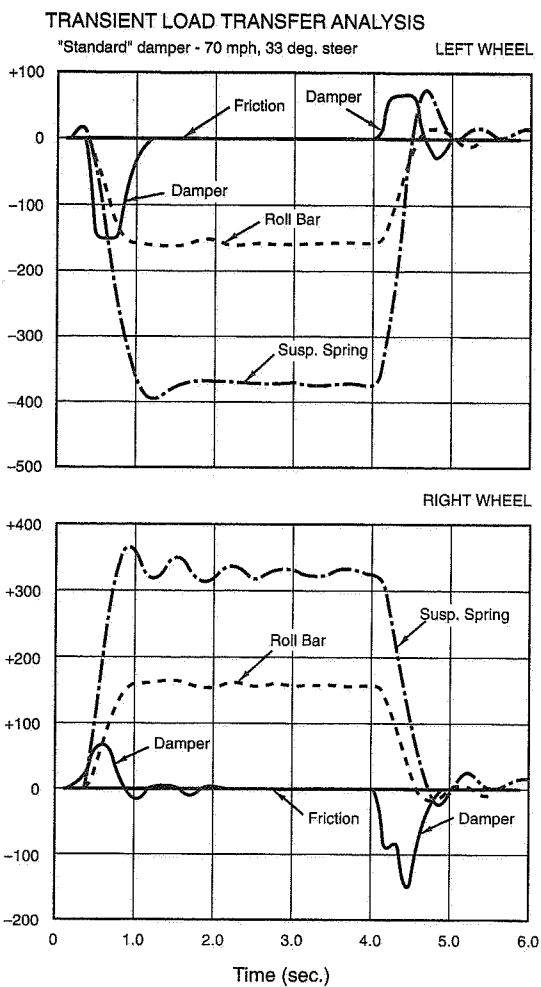


Figure 22.38 Transient maneuver with standard damper.

sient phase). The damper force which depends on the velocity tends to come on before the spring elements in the suspension which depend on displacement.

Figure 22.39 for the larger damper indicates a much more prominent effect from this component. The larger damper slows down the onset of the spring forces (suspension spring and anti-roll bar). The rebound damper force on the right wheel during turn exit is

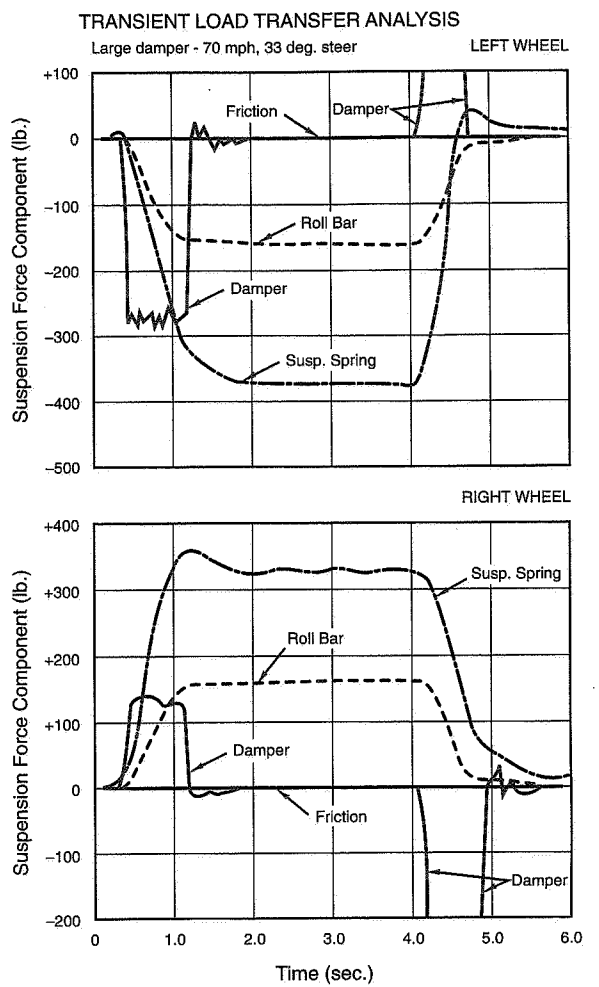


Figure 22.39 Transient maneuver with twice standard damper.

very large (off the scale). The duration of the damper effect is longer with the stiffer unit.

Further discussion on racing application of dampers is given in the next two sections. The next applies to race cars with modest aerodynamic downforce and the last section applies to vehicles with large aerodynamic downforce.

22.5 Race Cars with Modest Aerodynamic Downforce

The material in this section applies to race cars which do not realize a large part of their aerodynamic downforce from the underbody (especially flat bottoms); in other words, cars where the aerodynamic lift is not critically affected by changes in ride height, roll, and pitch. This includes most classes of sports cars, sedans, and short track cars, but excludes Grand Prix, Indy Car, CanAm, and Group 6 (LeMans-type endurance sports cars).

Of the several racing damper models available, KONI (of Holland) has proven to be a very popular manufacturer. They are adjustable in both bump and rebound, come in the necessary range, and are tough and reliable. The KONI organization has extensive experience in racing, provides direct assistance at race tracks, and publishes instructions for adjusting or tuning their product.

A generation of racers including Carroll Smith (Refs. 148, 149, and 150) have relied heavily on KONI's published instructions for damper adjustment at the track. Smith also covers other related information and "hints" on sizing, installation, cooling, testing, and interpreting test results in his books, which we recommend. The KONI instructions are reproduced below:

Bump Damping Bump damping controls the unsprung weight of the vehicle. It controls the upward movement of the suspension as when hitting a bump on the track. It should not be used to control the downward movement of the vehicle when it encounters dips. Also, it should not be used to control either roll or bottoming.

Depending on the vehicle, the ideal bump setting can occur at any point within the adjustment range. This setting will be reached when "side-hop" or "walking" in a bumpy turn is minimal and the ride is not unduly harsh. At any point other than this ideal setting, EITHER the "side-hopping" will be more pronounced OR the ride will be unduly harsh.

Adjusting The Bump Control

Step 1—Set all four dampers on minimum bump and minimum rebound settings.

Step 2—Drive one or more laps to get the feel of the car. NOTE: when driving the car during the bump adjustment phase, disregard body lean or roll and concentrate *solely* on how the car feels over bumps. Also, try to notice if the car "walks" or "side-hops" on a rough turn.

Step 3—Increase bump adjustment three clicks on all four dampers. Drive the car one or two laps. Repeat step 3 until a point is reached where the car starts to feel hard over bumpy surfaces.

Step 4—Back off bump adjustment two clicks. The bump control is now set. NOTE: The back off point will probably be reached sooner on one end of the vehicle than the other. If this occurs, keep increasing the bump on the soft end until it, too, feels hard. Then back it off two clicks. The bump control is now set.

Rebound Damping Once you have found what you feel to be the best bump setting on all four wheels, you are ready to proceed with adjusting the rebound.

The rebound damping controls the transitional roll (lean) as when entering a turn. It does NOT limit the total amount of roll; it does limit how fast this total roll angle is achieved. How much the vehicle actually leans is determined by other things such as spring rate, sway bars, roll center heights, etc.

It should be noted that too much rebound on either end of the vehicle will cause an INITIAL loss of lateral acceleration (cornering power) at that end which will cause the vehicle to oversteer or understeer excessively when entering a turn. Too much rebound in relation to bump will cause a condition known as "jacking down." This is a condition where, after hitting a bump and compressing the spring, the damper does not allow the spring to return to a neutral position (ride height) before the next bump is encountered. This repeats with each subsequent bump until the car is actually lowered onto the bump stops. Contact with the bump stops causes a drastic increase in roll stiffness. If this condition occurs on the front the car will understeer; if it occurs on the rear, the car will oversteer.

Adjusting Rebound Control

Step 1—With rebound control set on full soft and the bump set from your testing, drive the car one or two laps, paying attention to how the car rolls WHEN ENTERING A TURN.

Step 2—Increase rebound damping three sweeps (1/4 turn) on all four corners and drive the car one or two laps.

Step 3—Repeat Step 2 until the car enters the turns smoothly (no drastic attitude changes) and without leaning excessively. Any increase in rebound stiffness beyond this point is unnecessary and may in fact be detrimental. EXCEPTION—It may be desirable to have a car that assumes an oversteering or understeering attitude when entering a turn. This preference, of course, will vary from one driver to another depending on individual driving style.

Bump Stops Since racing dampers are usually required to limit the travel of the suspension, all KONI racing dampers come supplied with a specially-designed cellular polyurethane bump stop. This provides safe and controlled bottoming of the suspension as well as preventing internal damage within the damper from metal-to-metal contact. [Author note: A diagram of the force characteristics of these bump stops is available from KONI.] Between races it is good practice to inspect the bump rubbers. If they show signs of deterioration, they should be replaced.

All too often we have seen racers using the bump rubbers solely as a suspension travel indicator. This is unfortunate since the information derived from this practice is virtually useless when compared to the realistic benefits, in the form of increased cornering power, which are obtained from the correct use of the bump rubber combined with the proper spring rate. [See KONI Graph A reproduced here as Figure 22.40.] A good way to check if the proper spring rate and bump rubber have been chosen would be to place the bump rubber against the damper body, and, if after one hard lap of driving the bump rubber is not pushed up all the way, it is an indication that either the spring rate is too high or the static shock length, ride height, etc., is incorrect.

Properly designed bump stops add a progressive rate spring in parallel to the primary suspension spring. The characteristics of bump stops can be varied widely.

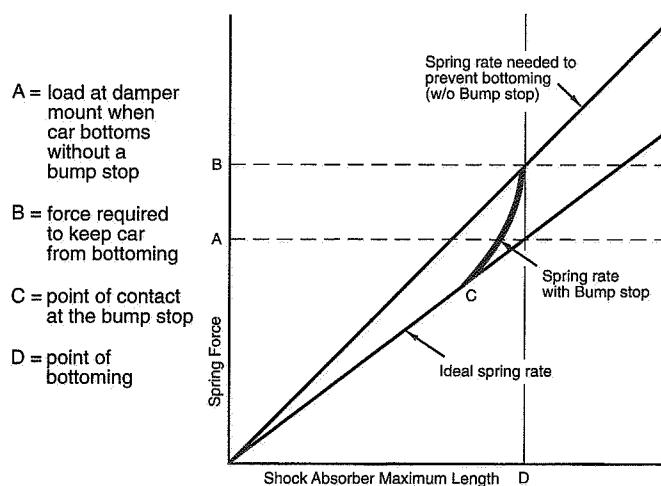


Figure 22.40 KONI "Graph A."

Ref. 120 discusses the mono-tube Bilstein shock which has a pressurized gas (nitrogen) chamber for maintaining pressure on the oil. This tends to minimize oil foaming, cavitation, and fade. The damping effect still takes place in the oil. Because it is single tube, this damper tends to operate cooler than twin-tube types. The Bilstein will operate equally well in any attitude which is helpful in packaging, particularly when connected to the suspension by a linkage. The elimination of any foaming insures that the unit gives "uninterrupted damping for even the smallest wheel deflections." Mono-tube dampers are also lighter than twin-tube units.

There are other so called gas dampers in which the pressurized gas acts directly on the oil—in this case the damping fluid rapidly becomes an emulsion of oil and gas with use.

Whatever make of damper one uses, it is desirable to obtain the manufacturers literature and consult with the technical representatives of the manufacturer.

22.6 Race Cars with Aerodynamics Critically Affected by Ride Height and Pitch

Formula 1, Indy Car, CanAm, and LeMans-type sports cars may be characterized by the large amount of aerodynamic downforce developed from flat or specially shaped underbodies operating at low ground clearance. Although the more successful teams are reluctant to divulge definitive data on the performance of their underbottom configurations, a few facts are common knowledge. Thus the aerodynamic downforce is **critically dependent** on the pitch attitude relative to the ground and the ride height, particularly on front. Much of the aerodynamic development of these machines is done in wind tunnels with moving ground planes, where the details of the flow may be measured. As one Grand Prix group reports, a very small change in attitude or angle of attack relative to ground can "transform the aerodynamics" of the underbottom. The larger the bottom and downforce, the more critical the situation becomes.

Current Suspensions

From the standpoint of developing and maintaining the largest amount of aerodynamic downforce, it would seem desirable to have the car infinitely stiff in pitch, heave, and roll. For a perfectly smooth circuit this suggests no suspension at all; however, circuits are never ideally smooth and some wheel travel is necessary to realize the highest level of adhesion between the tire and the ground and to damp out the tire spring (which is nearly undamped). The suspension also provides the means for tuning the handling to best compromise the several phases of cornering. With modern sticky tire compounds, tire temperatures and durability must be considered. Finally, all of these conditions must be met at different weights as fuel is burned.

The net result of the above requirements is that all of these machines are stiffly sprung. Furthermore, on-board suspension adjustments, as well as those which can be made rapidly in the pits, may be provided for controlling handling and tire durability during a race.

One current G.P. car appears to have a static deflection of the sprung mass of 0.18 in. at the front and 0.21 in. at the rear. This translates to an undamped natural frequency of the body of about 440 cpm and 400 cpm rear, which is three to four times that of comparable machines without large aerodynamic downforce. The undamped natural frequency of the unsprung mass (wheel hop) approaches 1450 cpm front and 1660 cpm rear. When the tire spring rates are added in (in series with the suspension springs) then the ride rate that the driver feels is reduced to a livable point. To quote Tony Rudd, (retired) Executive Chairman of Team Lotus (former head of BRM), "everything is like the 1960s except now we work in millimeters instead of inches."

Indy Cars are generally less stiffly sprung than Grand Prix (on equivalent road courses) but the tire vertical spring rates may be higher.

Damping Levels

In addition to stiff suspensions, Grand Prix, Indy, etc., cars are characterized by very heavy damping. In general, a stiffer suspension requires heavier damping to achieve a desired percent critical for road-holding on anything but the smoothest surface. Additional damping is also required to reduce attitude changes, to control the aerodynamic downforce in transient conditions.

Some simple linear calculations are presented next based on the methods of SAE Paper No. 851652 (Ref. 156) reviewed earlier. In these calculations, ride criteria are expressed as a function of vertical acceleration of the body and road-holding as a function of wheel-load variation. The roll and pitch criteria say that the dynamic roll and pitch angles shall be less than the steady-state values.

The characteristics for an Indy Car oval track car are summarized in Table 22.1. This is, of course, estimated but believed to be typical.

The optimum damping ratios, in percent critical, based on the criteria cited above for a **nonaerodynamic downforce version** of this car are given in Table 22.2. The calculations were performed for some variations in the front and rear spring rates. It will be noted that the optimum criteria are all met with damping ratios (percent critical) of 0.71 or less. Note that these optimum damping ratios are a function of the spring and tire rates and sprung and unsprung masses.

Table 22.3 gives the damping ratios associated with ride, roll, and pitch based on the actual damper rates assumed for the oval track Indy car (of Table 22.1) with **aerodynamic**

Table 22.1 Indy Oval Track Car—Baseline Configuration

Item	Symbol	Units	Whole Car	2 Corners		1 Corner	
				Front	Rear	Front	Rear
Gross Weight	W	lb.	1600				
Wheelbase	ℓ	ft.	9.0				
CG Location			60% Aft.				
	a	ft.	5.4				
	b	ft.	3.6				
Unsprung Wt.		lb.	260	120	140	60	70
Unsprung Mass	m_1	slugs		3.73	4.35	1.86	2.17
Sprung Wt.		lb.	1340	536	804	268	402
Sprung Mass	m_2	slugs		16.65	24.97	8.33	12.49
Tire Rate	k_1	lb./ft.				36,000	36,000
Spring Rate	k_2	lb./ft.		38,400	50,000	19,200	25,000
Damper Const.	C_2	lb.-sec./ft.		1500	1670	750*	835*
Track	T	ft.		6	5.66		
Roll Stiffness	K	ft.-lb./rad.		691,200†	800,890†		
Roll Inertia	I_R	lb.-ft.-sec. ²		13.7			
Pitch Inertia	I_p	lb.-ft.-sec. ²		252.5			

*Aver. of Bump & Reb'd, i.e.,

C_2 Bump F 620 C_2 Reb F 880

C_2 Bump R 720 C_2 Reb R 950

Assume CG is at pitch center.

† $K = k_2 T^2 / 2$

downforce. Both the spring and damper rates have been raised and lowered in the calculations to ensure that they cover the ranges in practice.

The calculations confirm that this vehicle and, in general, race cars with underbody downforce are overdamped in the sense that the damping levels are well in excess of critical, particularly in pitch and roll. Referring to Figure 22.41, the time to reach steady-state for the overdamped case can be made much longer than for the critically damped case. If the response variable is pitch or roll angle, it can be slowed down with heavy damping to the point where it may never reach steady-state in typical racing transient braking/acceleration or cornering situations. The dampers appear as a powerful means

Table 22.2 Non-Aerodynamic Version of Indy Oval Track Car

Condition	Optimum Damping Ratio, Fraction Critical			
	Ride	Roll	Pitch	Road Holding
1. Baseline Config.	Front: 0.400 Rear: 0.450	0.710	0.710	Front: 0.376 Rear: 0.417
6. Front Springs Up 50%	Front: 0.495 Rear: 0.450	0.710	0.710	Front: 0.447 Rear: 0.417
7. Front Springs Dn 50%	Front: 0.286 Rear: 0.450	0.710	0.710	Front: 0.360 Rear: 0.417
8. Rear Springs Up 50%	Front: 0.400 Rear: 0.553	0.710	0.710	Front: 0.376 Rear: 0.512
9. Rear Springs Dn 50%	Front: 0.400 Rear: 0.319	0.710	0.710	Front: 0.376 Rear: 0.344

Table 22.3 Indy Oval Track Car Damping Ratios

Condition	Damping Ratio, Fraction Critical			
	Ride F.	Ride R.	Roll	Pitch
1. Baseline Config.	0.938	0.747	5.944	2.188
2. Max. Damping on Front	1.938	0.747	9.129	3.750
3. Min. Damping on Front	0.219	0.747	3.655	1.066
4. Max. Damping on Rear	0.938	1.387	8.477	2.809
5. Min. Damping on Rear	0.938	0.157	3.606	1.616
6. Front Springs Up 50%	0.766	0.747	5.356	1.907
7. Front Springs Dn 50%	1.326	0.747	6.781	2.647
8. Rear Springs Up 50%	0.938	0.610	5.278	2.012
9. Rear Springs Dn 50%	0.938	1.057	6.949	2.421

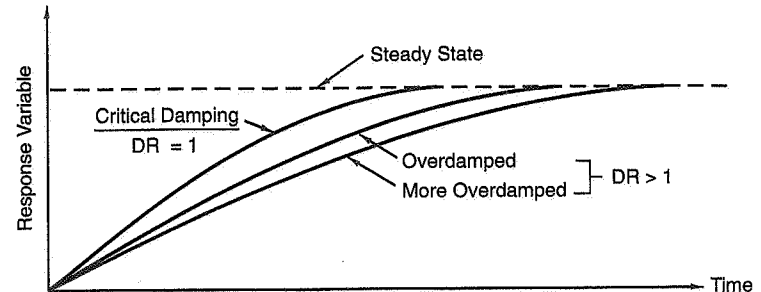


Figure 22.41 Transient response as a function of damping ratio, DR.

for controlling vehicle attitude for maintenance of aerodynamic downforce in transient maneuvers.

Damping levels used on these cars depend greatly on the circuit. For smooth circuits, they may be well above critical; for bumpy street circuits they may be less than critical, and near critical for smooth road circuits.

Limit Handling

In addition to controlling attitude of the vehicle body referenced to ground, it is necessary to control the load changes at the wheels. Using the springs to tune the cornering behavior assumes some movement of the sprung mass relative to the unsprung. When this movement is small, when anti-roll bar size becomes excessive, or when the problem appears to be involved in the transient phases of cornering, damper adjustments are added to the list of tools available to work with.

The use of dampers for chassis tuning assumes the presence of a relative velocity between the sprung and unsprung masses—a transient condition. Drivers often claim that damper changes are effective throughout a turn; this indicates that either a bumpy track keeps the dampers “working” through the corner or that the dampers are stiff enough that the car never reaches a true steady-state cornering condition.

A recent trend is cockpit-adjustable dampers (along with cockpit-adjustable anti-roll bars that have been in use for some time). Stiffening or softening of one end of the car relative to the other can sometimes help a pushing or spinning condition. As with the use of asymmetrical springing, asymmetrical damping is often used on oval track cars. Dampers are frequently revalved (as required) in practice.

Dampers will increase transient load in a similar fashion to the way anti-roll bars generally work. Adding damping (bump and/or rebound) on the front tends toward push while additional rear damping tends toward spin. Because the dampers are so important to total grip (load fluctuation) and sprung mass stability (with ground-effect aero), caution must be used when balancing the car with the dampers—too much or too little damping will heavily compromise these other areas.

Future Trends

From current experience as described above, for cars with underbody downforce, a few generalizations and possible future trends emerge. Two items are critical:

1. Body attitude control (pitch, roll and ride height)
2. Transient handling characteristics

The tendency to provide most of the body control by a very stiff suspension appears to be giving way to an increasing use of dampers. This follows from a recognition of the importance of transient behavior and the associated advantages of giving the suspension some movement in these very high-performance vehicles. We have seen that heavy damping can slow down the body motions over time periods similar to race car maneuvers.

Giving the suspension some movement facilitates development of satisfactory handling and improved driver ride. For handling, controlling the wheel loads and the onset of wheel loads in transients is important. Since the wheel velocities are in a different range from those for body control, the dampers can play a major part in load control.

As a result of active and semi-active suspension developments by Lotus and others, there is an increasing sense of what can be done with dampers with various control systems. The fully active systems developed by Lotus and used successfully in Grand Prix illustrate certain desirable characteristics that may find their way into passenger cars. In particular, damping is provided separately for the sprung and unsprung masses because acceleration on each is sensed separately and damping forces can be referenced to inertial space (called "sky-hook" damping). The unsprung masses on the active car can effectively be reduced to nearly zero because power can be added to the suspension through the actuator. The result is a vehicle in which ride and handling can be optimized separately. The ride and road-holding of active suspension cars must be experienced to be fully appreciated.

Notes on Dampers

Bilstein, KONI, Penske, and others produce gas-pressurized dampers. This is widely accepted as the best current design for reasons of temperature stability, fade and cavitation resistance, and sensitivity to small movements in the transition from bump to rebound and vice versa (positive valve operation).

The amount of pressure varies from manufacturer to manufacturer and also for different types of races. For example, KONI use 400 psi (nitrogen) for Indy which results in about 90 pounds of preload on the piston. Penske tends to use less, say 250 psi, under comparable circumstances. For smaller cars even less may be used. These gas pressures, frequently referred to as "nose pressures," act as an initial spring rate which is a significant performance parameter in itself.

It is interesting to note that on these high aerodynamic downforce cars the contribution of the damper to the control of the body is so important that one damper designer thinks of the damper as "a hydraulic/pneumatic body control" device.

Tire size and construction has a large influence on choice of damper stiffness. F.1 tires are relatively softer (vertically) than Indy tires and 50-60% of the bump energy may go into the tire. Damper shaft travel on F.1 cars is quite small, 0.5-0.7 in., hence the stiff damper settings. On Indy Cars the tires are smaller with harder sidewalls. Most of the energy goes into the dampers and travel can be an inch or more.

It is becoming common to present damper characteristics as plots of damping force (lb.) vs. shaft speed (in./sec.), for the various valve settings. Figures 22.42 and 22.43 present damper characteristics for Penske oval track and road race units in this format. The curves are labeled with the spring washer adjustment thickness. The road course dampers have an external adjustment feature (double adjustment), and the amount of external adjustment is shown by the shaded area, modifying each major (spring washer) adjustment.

Racing engineers often think in terms of ranges of damper speed, either two or three ranges. The lowest range, say 0-5 in./sec., is used for body control. The 5-10 and 10-15 in./sec. ranges are for unsprung control. Above 15 in./sec. is generally seen only on large bumps or in off-road racing. For lower-performance race cars (sedans, etc.), damper speeds in excess of 10 in./sec. are seldom seen.

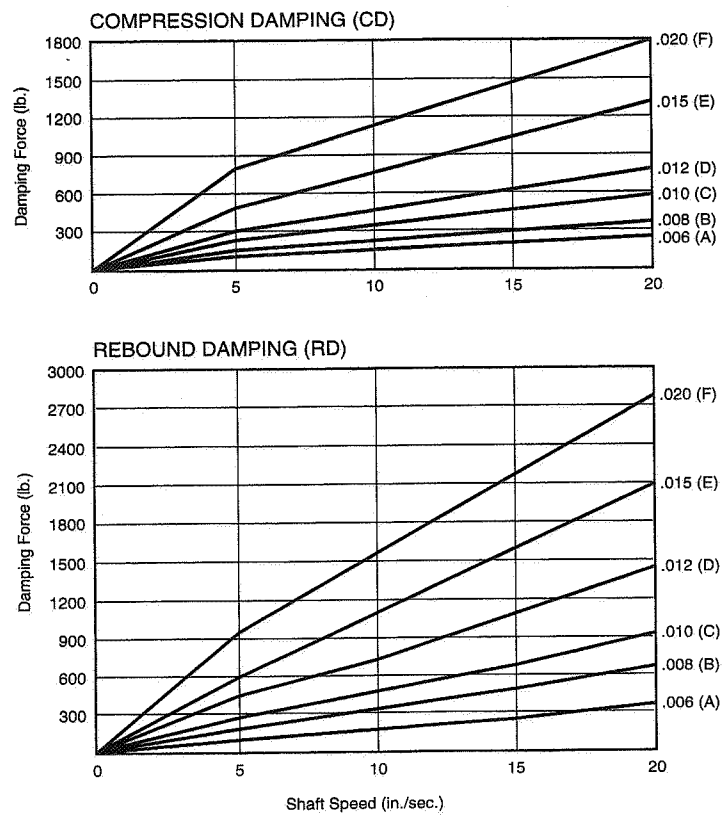


Figure 22.42 Penske oval track dampers.

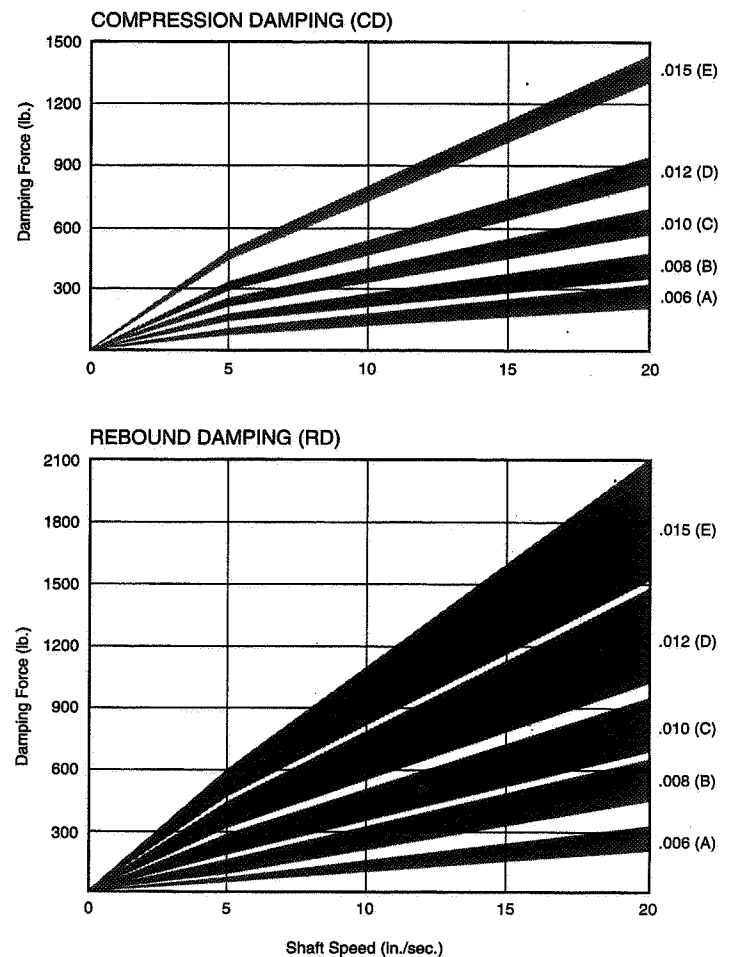


Figure 22.43 Penske road course dampers.

Compliances

"In the final analysis, every engineering material is rubber."

Sir Henry Royce
Rolls-Royce



Introduction

Compliance is the inverse of stiffness, that is, a compliant part will deflect under load. Sir Henry's advice cannot be ignored—every part that is under load will deflect and this can modify geometric (unloaded) relationships significantly. In the case of suspensions for passenger cars compliance is necessary to achieve good ride. Compliance is introduced in several ways:

- Elastomeric (rubber) suspension pivots
- Rubber mounted crossmembers (or cradles)
- Rubber mounted steering racks and other steering joints
- Hard parts that deflect under load—these can include suspension links, steering links, and the chassis mounts for suspension and steering

In passenger cars the compliant portions of the suspension are carefully chosen to give an appropriate balance between noise/vibration/harshness and handling. The compliances have a large effect on linear range understeer; rubber bushing stiffnesses are chosen to control the amount of linear range (below 0.3-0.4g lateral acceleration) understeer.

For racing applications, compliance generally causes problems. When the tires are flexibly connected to the chassis it is difficult to control the steer and camber at the tires.

Compliance effects are often classified in terms of the applied force component. The standard compliances are due to:

- Lateral force, from cornering, side wind, banked road.
- Longitudinal force, from driving force and braking force.
- Aligning torque—Tire aligning torque measures the longitudinal offset of the effective tire force from the center of the print. This torque varies with lateral and longitudinal tire force.
- Overturning moment—Tire overturning moment is similar to aligning torque but it is a measure of the lateral offset of the effective tire force from the center of the tire print. This effect is often ignored when the tires are held near perpendicular to the road.

Compliances are also classified by the effect on the wheel position relative to the chassis. The effects of interest for racing are:

- Steer compliance—The specified force affects the steer angle of the road wheel.
- Camber—The specified force affects the camber (or inclination angle) of the wheel.

Understeer and Oversteer Effects

It is customary to think of the signs of the compliance terms as *understeer* or *oversteer*.

Consider a car on a skidpad at modest lateral acceleration. If the speed is fixed then the only variable is the steering wheel angle required to track the circle. The addition of an understeer compliance to a car on a skid pad will cause the car to travel on a larger circle. An oversteer effect will cause the car to run on a smaller circle.

If the steering wheel is adjusted to follow the same circle before and after the change in compliance is made, the steering angle change divided by the lateral acceleration is the magnitude of the effect in "degrees per g," where front wheel or steering wheel angle is specified. For example:

1. A car is instrumented with a protractor on the steering wheel and a pointer mounted so that steering wheel angle can be read by the driver in steady turns. In "baseline" condition the car is found to require 78° of steering wheel angle to follow the circle at a fixed speed which results in a lateral acceleration of $0.4g$.

2. The front steering rack rubber mounts are stiffened.
3. A test shows that following the circle at the same speed now requires 72° of steering wheel angle.
4. The change is in the oversteer direction and the amount is $78^\circ - 72^\circ = 6^\circ$ divided by 0.4, the lateral acceleration at which the test was run. The change is 15° per g at the steering wheel.
5. If it is desired to measure the effect independent of the steering ratio this can be divided out. If the steering ratio is 20° steering wheel = 1° front wheel, then the effect of the rack mount change was $15/20 = 0.75^\circ/g$ at the front wheels.

In general, effects that steer the tire away from the turn center are understeer on the front and oversteer on the rear.

Each of the compliance terms (or effects) is discussed separately below.

Lateral Force Compliance Steer—Front

Lateral force compliance steer is a measure of the steer due to a lateral force applied at the center of the tire contact patch. This can be either US or OS. It is a function of the relative stiffnesses of the various parts that pass the lateral force through to the chassis and the loads that those parts see.

The suspension links and the steering system share the lateral force on the front (unless there is zero caster angle and offset). If the steering system is "softer" or "stiffer" than the suspension (with all the various different leverage effects taken into account) then the location of the steering gear (ahead of or behind the front axle line) will change the direction of the compliance from OS to US or vice versa.

If the steering and suspension links are made stiff enough then the compliance steer due to lateral force will be low and there will be little difference in compliance steer between "front" and "rear" locations for the steering system. This is not to say that "front" or "rear" steering gear locations are interchangeable—often the steering gear location determines the amount of Ackermann or reverse-Ackermann in the steering linkage.

Lateral Force Compliance Steer—Rear

The various different types of rear suspension all deflect somewhat under lateral force. The detail design determines the direction of the effect. For example, trailing arm rear suspension will often have an OS effect. Some cars have controlled amounts of compliance-rear-steer built in to influence steady-state and/or transient response.

Lateral Force Compliance Camber—Front

Tire lateral force acts at the ground, below all of the suspension components. This always results in the top of the tire leaning away from the turn center (camber in the positive direction on the outside wheel). For this reason it is common to see some static negative camber used such that under cornering the tire deflects to the desired camber angle to the road. Camber due to ride travel and vehicle roll also must be accounted for at the same time.

In most cases, if the tire leans out of the turn (positive camber on the outside wheel) then tire lateral force capability is reduced. This says that lateral force compliance camber on the front is always an understeer effect.

Lateral Force Compliance Camber—Rear

The rear tire also can be expected to lose lateral force capability if it cambers positively on the outside tire. This says that lateral force compliance camber on the rear will be an oversteer effect.

Longitudinal Force Compliance Effects

The front and rear wheels can be expected to steer and camber with braking forces (and driving forces for driven axles). The relative stiffnesses of the various links that connect the wheel to the chassis and also the front view steering offset at the ground (for steering axles) determine the sense (US or OS) and amount of these effects.

Aligning Torque Compliance Steer

This is almost always an understeer effect on the front axle and an oversteer effect on the rear axle. This is because the tire aligning torque (and usually the geometric trail) is trying to "straighten out" the wheels. At maximum lateral force the tire aligning torque drops to low values and may reverse in sign. If the mechanical trail is small the kingpin torque may reverse sign. In this case the effect would reverse from US to OS (front) and OS to US (rear). An interesting note: With some older cars with a minimum of caster/trail it is possible to have the steering torque reverse in very tight turns (where the trail/caster is reduced by steer angle) and the steering actually will go "hard over"—the car will stay in the turn hands off of the steering wheel.

The tire aligning torque is largest in the mid-range of tire lateral force performance and this is where the AT compliance steer has its largest effect. If the steering box or rack is flexibly mounted to the chassis, the understeer effect on the front can be very large.

Measuring Compliance Effects

As well as full-scale tests (as described in the example previously) there are indoor test machines that can measure compliance effects. The first comprehensive machine built for this purpose is the Chevrolet Vehicle Handling Facility. A car is clamped rigidly on the machine and pads are moved under the tire patches to apply loads to the suspension. Changes in wheel steer angle and camber are measured relative to the applied load.

Figure 23.1 is taken from Ref. 109. It shows the VHF applying a lateral force to a rear suspension. Figure 23.2 (from the same paper) shows the data obtained from this lateral force compliance test.

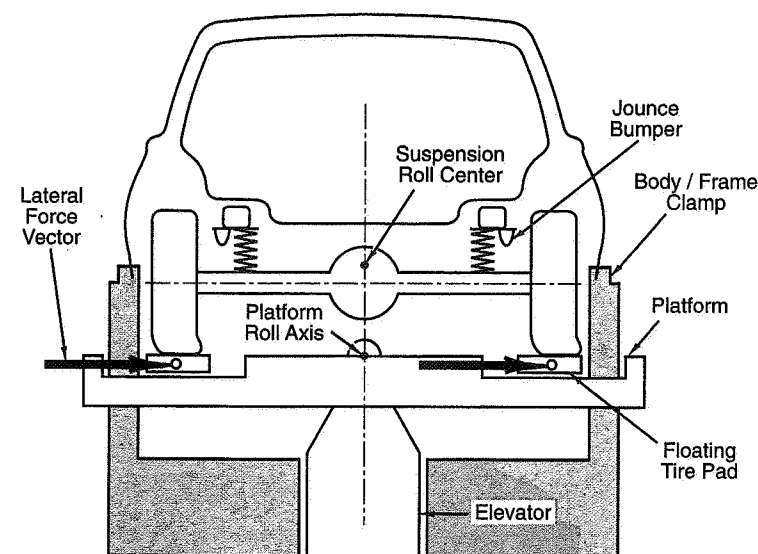


Figure 23.1 Lateral force application (Ref. 109).

Discussion

Compliance effects are often ignored in race car design because they are difficult to calculate and measure. If the suspension components and the points to which they are attached are made very rigid, this oversight may not be a source of difficulties.

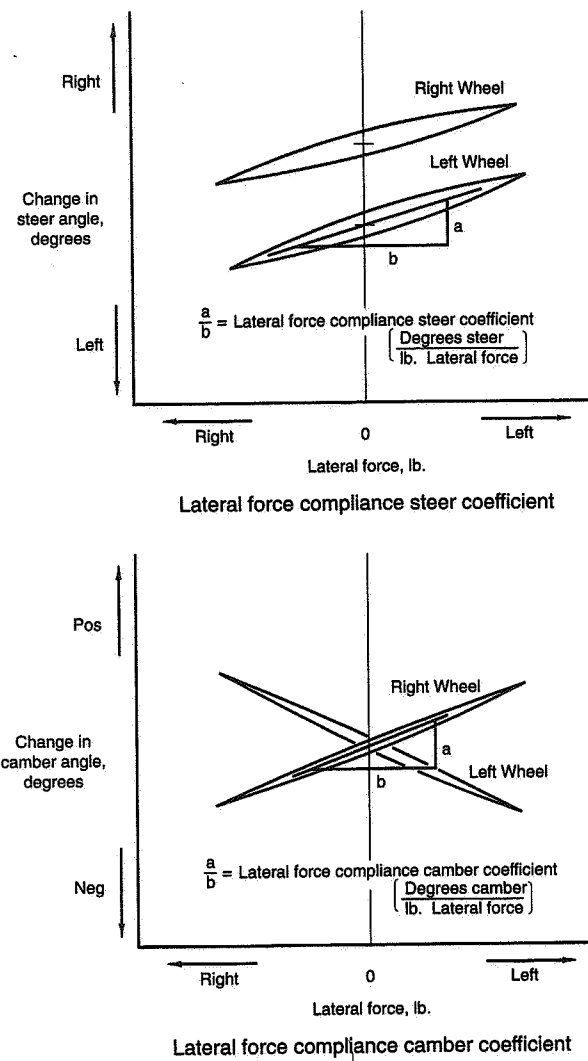


Figure 23.2 Lateral force compliance test data (Ref. 109).

Often parts that look rigid are actually not very rigid under the high loads that exist in suspension components. The result is that the actual steer and camber angles of the wheels are unknown and this can be a source of unexplained behavior.

It is often tempting to "design in" compliances to give certain effects. For example, lateral force compliance understeer on the front may be used to reduce the effect of the increase in lateral force that occurs when the outside front wheel hits a bump. Another example, longitudinal force deflection rearward when a wheel hits a bump, will soften the ride on rough roads.

Fully understanding compliant suspension mounting requires a great deal of engineering effort. Passenger car suspensions are first modeled with special-purpose computer programs and then tested in the lab and on the proving ground. For most racing applications it is advisable to try to avoid suspension compliance effects to as great a degree as possible.

References

1. "Vehicle Dynamics Terminology" SAE J670e, Society of Automotive Engineers, Inc., Warrendale, PA, July 1976.
2. "Vehicle Aerodynamics Terminology," SAE J1594, Society of Automotive Engineers, Inc., Warrendale, PA, June 1987.
3. "Proposed Passenger Car and Light Truck Directional Control Response Test Procedures," SAE XJ266, Society of Automotive Engineers, Inc., Warrendale, PA, 1985.
4. "Laboratory Testing Machines for Measuring the Steady State Force and Moment Properties of Passenger Car Tires," SAE J1106, and "Laboratory Testing Machines and Procedures for Measuring the Steady State Force and Moment Properties of Passenger Car Tires," SAE J1107, Society of Automotive Engineers, Inc., Warrendale, PA, September 1975.
5. Manual on Design and Application of Leaf Springs, SAE HS-788, Society of Automotive Engineers, Inc., Warrendale, PA, April 1980.
6. Manual on Design and Application of Helical and Spiral Springs, SAE HS-795, Society of Automotive Engineers, Inc., Warrendale, PA, April 1990.
7. Manual on Design and Manufacture of Torsion Bar Springs, SAE HS-796, Society of Automotive Engineers, Inc., Warrendale, PA, July 1990.
(Refs. 5, 6, and 7 are available in one volume as SAE AE-11.)
8. "Road vehicles—Steady state circular test procedure," ISO 4138-1982(E), International Organization for Standardization, 1982.
9. "Road vehicles—Lateral transient response test methods," ISO 7401-1988, International Organization for Standardization, 1988.
10. Handbook of Mechanical Spring Design, Associated Spring Corporation, Bristol, CT, 1964.
11. "Guide to Design With Versatile Steel Wire," American Iron and Steel Institute.
12. Automotive Handbook, Robert Bosch GmbH, distributed by Society of Automotive Engineers, Warrendale, PA, 1994.
13. "Chaparral G. S. Documentation Tests," Chevrolet File, February 26, 1968, revised April 15, 1968.
14. Abbott, Ira H., and Albert E. von Doenhoff, Theory of Wing Sections, McGraw-Hill Book Co., New York, 1949.

15. Anderson, John D., Fundamentals of Aerodynamics, 2nd Ed., McGraw-Hill Book Co., New York, 1991.
16. Bakker, E., L. Nyborg, and H.B. Pacejka, "Tire Modeling for Use in Vehicle Studies," SAE Paper No. 870421, Society of Automotive Engineers, Warrendale, PA, 1987.
17. Bakker, E., H.B. Pacejka, and L. Lidner, "A New Tire Model with an Application in Vehicle Dynamics Studies," SAE Paper No. 890087, Society of Automotive Engineers, Warrendale, PA, 1989.
18. Bastow, Donald, Car Suspension and Handling, 2nd Ed., Pentech Press Ltd., London, 1987.
19. Baumeister and Marks, Standard Handbook for Mechanical Engineers, 7th Ed., 1967.
20. Bearman, P W., D. De Beer, E. Hamidy, and J.K. Harvey, "The Effect of a Moving Floor on Wind Tunnel Simulation," SAE Paper No. 880245, Society of Automotive Engineers, Warrendale, PA, 1988.
21. Bedard, Patrick, Expert Driving, Valentine Research Inc., Cincinnati, OH, 1987, see also Ref. 91.
22. Best, A., "Vehicle Ride—Stages in Comprehension," *Phys. Technol.*, Vol. 15, 1984.
23. Bingelis, Antoni, "Installing a Submerged Inlet Ventilation System," *Sport Aviation*, December 1981.
24. Bruns, H.J., and E.J.H. Fiala, "Road Roughness and Passenger Comfort," ASME Publication, 67-Tran-15, 1967. Also, Automotive Technology Series, Volume 1, Iliffe Books Ltd., London, 1968.
25. Bryan, G.H., Stability in Aviation, MacMillan & Co., London, 1911.
26. Buchheim, R., "Aerodynamics at Volkswagen," VW Press Introduction, 1982.
27. Bundorf, R.T., "The Effect of Vehicle Design Parameters on Characteristic Speed and Understeer," SAE Paper No. 670078, Society of Automotive Engineers, Warrendale, PA, 1967.
28. Bundorf, R.T., R.L. Leffert, "The Cornering Compliance Concept for Description of Directional Control Properties," General Motors Engineering Publication No. 2771, 1967, 1973. Also, SAE Paper No. 760713, Society of Automotive Engineers, Warrendale, PA, 1976.
29. Campbell, Colin, New Directions in Suspension Design, Robert Bentley, Inc., Cambridge, MA, 1981.
30. Carr, G.W., "A Comparison of the Ground-Plane-Suction and Moving Belt Ground-Representation Techniques," SAE Paper No. 880249, Society of Automotive Engineers, Warrendale, PA, 1988.
31. Carr, G.W., Potential for Aerodynamic Drag Reduction in Car Design, Proceedings of the International Association for Vehicle Design, Special Publication SP3, 1983.
32. Chiesa, A., and L. Rinonapoli, "Vehicle Stability Studied with a Nonlinear Seven Degree Model," SAE Paper No. 670476, Society of Automotive Engineers, Warrendale, PA, 1967.
33. Clark, Samuel K., ed., Mechanics of Pneumatic Tires, DOT HS 805 952, U.S. Department of Transportation - NHTSA, Washington, D.C., 1981.
34. Cogotti, A., "Aerodynamic Characteristics of Car Wheels," Impact of Aerodynamics on Vehicle Design, Proceedings of the International Association of Vehicle Design, SP3, 1983.
35. Cornell Aeronautical Laboratory Staff, "A Proposal for Further Experimental and Analytical Investigation of Static Directional Stability and Control of Automobiles (Appendix C)," CAL Proposal No. 3398, November 1972.
36. Cornish, J.J. III, "Trapped Vortex Flow Control for Automobiles," Proceedings of the Second AIAA Symposium on Aerodynamics of Sports and Competition Automobiles, ed. Bernard Pershing, Vol. 16, AIAA Lecture Series, American Institute of Aeronautics and Astronautics, Los Angeles, CA, May 1984. (Also distributed by Motorbooks International, Minneapolis, MN.)
37. Cooper, George E., and Robert P. Harper, Jr., "The Use of Pilot Rating in the Evaluation of Aircraft Handling Qualities," NASA Report TN D-5153, Ames Research Center, 1970.
38. Costin, Michael, and David Phipps, Racing and Sports Car Chassis Design, 2nd Ed., Robert Bentley, Inc., Cambridge, MA, 1965.
39. Cox, Jack, "New Venture, EAA World Part Two," *Sport Aviation*, November 1988.
40. Dell'Amico, Fred, "Steady-State Stability of the Automobile—An Approach Based on a Method of Tethered Vehicle Testing Using a Yaw Constraint," Technical report prepared for General Motors Engineering Staff by Cornell Aeronautical Laboratory, Inc., CAL No. YC-3004-K-1, 1971.
41. Donahue, Mark, and Paul van Valkenburgh, The Unfair Advantage, Dodd, Mead & Co., 1975.
42. Dugoff, H., P. Fancher, and L. Segel, "An Analysis of Tire Traction Properties and Their Influence on Vehicle Dynamic Performance," SAE Paper No. 700377, Society of Automotive Engineers, Warrendale, PA, 1970.
43. Etkin, B., Dynamics of Flight, Wiley and Sons, 1959.
44. Fackrell, J.E., and J.K. Harvey, "The Flow Field and Pressure Distribution of an Isolated Road Wheel," Paper 10, Advances in Road Vehicle Aerodynamics, BHRA Fluid Engineering, England, 1973.

45. Flegl, H., and V. Bez, "Aerodynamics—Conflict or Compliance in Vehicle Layout?" Proceedings of the International Association for Vehicle Design, Special Publication SP3, 1983.
46. Fonda, A.G., Tire Tests and Interpretation of Experimental Data, Institute of Mechanical Engineers, London, 1956.
47. Fonda, A.G., "Pneumatic Trail as an Index of Tire Behavior, Avon Ltd., Tire Data," FDM 2272, Cornell Aeronautical Laboratory, August 1957.
48. Fukushima, N., K. Hidaka, and K. Iwata, "Optimum Characteristics of Automotive Shock Absorbers under Various Driving Conditions and Road Surfaces," *JSAE Review*, March 1983.
49. George, A.R., "Aerodynamic Effects of Shape, Camber, Pitch and Ground Proximity on Idealized Ground-Vehicle Bodies," *Journal of Fluids Engineering*, Vol. 103, December 1981.
50. George, A.R., and J.E. Donis, "Flow Patterns, Pressures and Forces on the Underside of Idealized Ground Effect Vehicles," Aerodynamics of Transportation - II, Fluids Engineering Division, ASME, FEO - VOL. 7, pp 69-79, November 1983.
51. Giles, J.G. (Ed.), Steering, Suspension and Tyres, Iliffe Books Ltd., London, 1968.
52. Gough, V.E., "Tire-To-Ground Contact Stresses," *WEAR*, Vol. 2, No. 2., November 1958, presented to Stress Analysis Group Conference on Contact Stresses, London, May 1958.
53. Grayson, Stan, "The Front-Wheel-Drives of John Walter Christie, Inventor" *Automobile Quarterly*, Vol. 14, No. 8.
54. Guest, J.J., "The Main Free Vibrations of an Autocar," *Proceedings, Institute of Automobile Engineering*, Vol. 20, 1925-6, also 1925 "Engineer," Vol. 120.
55. Gusakov, I., "Measuring Rolling Resistance of Tires in the Laboratory," Presented at the International Rubber Conference, Kiev, October 1978.
56. Haas, Ronald H., and R.C. Manwaring, "Development of a Limited Slip Differential," SAE Paper No. 710610, Society of Automotive Engineers, Warrendale, PA, 1971.
57. Hall, J., and D.E. Davis, "What Makes Cars Handle?" *Car and Driver*, 1967.
58. Hegel, R., "Vehicle Attitude Control Methods," SAE Paper No. 730166, Society of Automotive Engineers, Warrendale, PA, 1973.
59. Hegel, R., M.R. Bethell, and R.L. Sorenson, "Electronic Sensing for Vehicle Height Control," SAE Paper No. 770396, Society of Automotive Engineers, Warrendale, PA, 1977.
60. Hodkin, D., and B.D.A. Phillips, "Ride Evaluation—Art or Science?" *Advances in Automobile Engineering*, ed. G.H. Tidbury, The MacMillan Co., New York, 1963.
61. Hoerner, Dr.Ing. S.F., Fluid-Dynamic Lift, Hoerner Fluid Dynamics, Albuquerque, NM, 1975.
62. Hoerner, Dr.Ing. S.F., Fluid-Dynamic Drag, Hoerner Fluid Dynamics, Albuquerque, NM, 1965.
63. Hucho, W.H., ed., Aerodynamics of Road Vehicles, Cambridge University Press, 1986, available in the U.S. through the Society of Automotive Engineers, Warrendale, PA.
64. Hucho, W.H., "Designing Cars for Low Drag—State of the Art and Future Potential," Proceedings of the International Association for Vehicle Design, Special Publication SP3, 1983.
65. Hucho, W.H., "The Aerodynamic Drag of Cars, Current Understanding, Unresolved Problems and Future Prospects," Aerodynamic Drag Mechanisms of Bluff Bodies and Road Vehicles, Proceedings of Symposium at General Motors Research Laboratories, Plenum Press, New York, 1978.
66. Irving, F.G., An Introduction to the Longitudinal Static Stability of Low-Speed Aircraft, Pergamon Press, 1966.
67. Jackson, G.W., "Fundamentals of the Direct Acting Shock Absorber," SAE Paper No. 590089, Society of Automotive Engineers, Warrendale, PA, 1959.
68. Janeway, R.N., W. LeFevre, W.C. Oswald, and J. Versace, "Ride and Vibration Data Manual," SAE J6a, Society of Automotive Engineers, Warrendale, PA, 1965.
69. Janeway, R.N., "Problems in Shock and Vibration Control," *Industrial Mathematics*, Vol. 5., Detroit, MI, 1955.
70. Janssen, L.J., and W.H. Hucho, "Aerodynamische Formoptimierung der Typen VW-Golf und VW-Scirocco," Kolloquium ueber Industrie-aerodynamik, Aachen, Part 3, pp. 46-69, 1974.
71. Jones, Bradley, Elements of Practical Aerodynamics, 3rd Ed., John Wiley & Sons, Inc., New York, 1942.
72. Joy and Hartley, "Tyre Characteristics as Applicable to Vehicle Stability Problems," Proceedings, Institute of Mechanical Engineering, Automotive Division, London, 1953-54.
73. Joy, Hartley, and Turner, "Tyres for High Performance Cars," SAE Preprint #549, Summer 1955.
74. Julien, M.A., "Present State of Problems Related to Suspensions, Shock Absorption and Road Performance," (translated from French), FISITA paper C-1, 1960.
75. Katz, Joseph, "Aerodynamic Model for Wing-Generated Down Force on Open Wheel-Racing-Car Configurations," SAE Paper No. 860218, Society of Automotive Engineers, Warrendale, PA, 1986.

76. Katz, Joseph, and Lee Dykstra, "Study of an Open-Wheel-Racing-Car's Rear Wing Aerodynamics," SAE Paper No. 890600, Society of Automotive Engineers, Warrendale, PA, 1989.
77. Katz, Joseph, "Integration of Computational Methods into Automotive Wind Tunnel Testing," SAE Paper No. 890601, Society of Automotive Engineers, Warrendale, PA, 1989.
78. Kelly, Kent, and Harry Holcombe, "Aerodynamics for Body Engineers," SAE Paper No. 640050, Society of Automotive Engineers, Warrendale, PA, 1963.
79. Koenig-Fachsenfeld, F.R., Aerodynamik Des Kraftfahrzeugs, Umschau Verlag Frankfurt, 1951.
80. Korff, W. H., "The Aerodynamic Design of the Goldenrod to Increase Stability, Traction and Speed," SAE Paper No. 660390, Society of Automotive Engineers, Warrendale, PA, 1966.
81. Korzybski, A., Science and Sanity, 4th Ed., The Institute of General Semantics, Lakeville, CT, 1958.
82. Kroll, C.V., and R.D. Roland, Jr., "A Preview-Predictor Model of Driver Behavior in Emergency Situations," Cornell Aeronautical Laboratory Report VJ-2251-V-6, Buffalo, NY, August 1970.
83. Lachmann, G.V., ed., Boundary Layer and Flow Control—Its Principles and Application, 2 volumes, Pergamon Press Inc., New York, 1961.
84. Ludvigsen, Karl, The Mercedes-Benz Racing Cars, Bond/Parkhurst Books, Newport Beach, CA, 1971.
85. Maeda, Teruo, and Hitoshi Uemura, "A Development of Vehicle Dynamics by Means of a Digital Computer," SAE Paper No. 690233, Society of Automotive Engineers, Warrendale, PA, 1969.
86. Marcell, R.P., and G.F. Romberg, "The Aerodynamic Development of the Charger Daytona for Stock Car Competition," SAE Paper No. 700036, Society of Automotive Engineers, Warrendale, PA, 1970.
87. McHenry, Raymond R., "Analysis of Spring Installations for Low-Frequency Suspension of Vehicles," *Industrial Mechanics*, Vol. 10, Part 1, The Industrial Mathematics Society, Detroit, MI, 1960.
88. McHenry, Raymond E., "Research in Automobile Dynamics—A Computer Simulation of General Three-Dimensional Motions," SAE Paper No. 710361, Society of Automotive Engineers, Warrendale, PA, 1971.
89. Meriam, J.L., Statics and Dynamics, John Wiley & Sons, New York, 1969.
90. Metz, D., "Aerodynamic Properties of Indy Cars," SAE Paper No. 870726, Society of Automotive Engineers, Warrendale, PA, 1987.
91. Milliken, D.L., gAnalyst® Learning Guide, Appendix 1, also gAnalyst® Operating Instructions, Valentine Research Inc, Cincinnati, OH, October 1986.
92. Milliken, W.F., Jr., et al., Research in Automobile Stability and Control and in Tire Performance, collection of papers, The Institute of Mechanical Engineers, London, 1956.
93. Milliken, W.F., Jr., Fred Dell'Amico, and Roy S. Rice, "The Static Directional Stability and Control of the Automobile," SAE Paper No. 760712, Society of Automotive Engineers, Warrendale, PA, 1976.
94. Milliken, W.F., Jr., and Roy S. Rice, "Moment Method," IME paper C113/83, The Institute of Mechanical Engineers, London, 1983.
95. Mitchell, Bill, "Beyond Round & Black, Part I - Part VII," series of articles in *Sports Car* magazine, March 1985 to January 1986.
96. Mitschke, M., "Influences of Road and Vehicle Dimensions on the Amplitude of Body Motion and Dynamic Wheel Loads," SAE Preprint, International Congress, 1961.
97. Morelli, Alberto, "Aerodynamic Basic Bodies Suitable for Automobile Applications," Proceedings of the International Association for Vehicle Design, Special Publication SP3, 1983.
98. Morelli, Alberto, "Aerodynamic Actions of an Automobile Wheel," Paper 5, Proceedings of the First Symposium on Road Vehicle Aerodynamics, The City University, London, 1969.
99. Molloy, E., and G.H. Lanchester, Automobile Engineer's Reference Book, 1st Ed., George Newnes Ltd., London, 1956.
100. Moulton, A.E., and P.W. Turner, "Rubber Springs for Vehicle Suspension," Proceedings, Institute of Mechanical Engineers, Automobile Division, London, December 1956.
101. Moulton, A.E., "Rubber Suspension for Four and Two Wheel Vehicles," Proceedings, Society of Automobile Engineers, Japan, 1964.
102. Moulton, A.E., and A. Best, "From Hydrolastic to Hydragas Suspension," IME Proceedings, Vol. 193, No. 9, London, 1979.
103. Moulton, A.E., and A. Best, "Hydragas Suspension," SAE Paper No. 790374, Society of Automotive Engineers, Warrendale, PA, 1979.
104. Moss, Stirling, and Doug Nye, Stirling Moss, My Cars, My Career, Patrick Stephens Ltd., England, 1987.
105. Moss, Stirling, and Lawrence Pomeroy, Design and Behaviour of the Racing Car, William Kimber, London, 1963.
106. Muto, Shinri, Automobile Aerodynamics, pp. 86-87, San'ei Shobo, 4-18-16-6F, Japan, June 1985.

107. Nakatsuka, Takeshi, and Katsuji Takanami, "Cornering Ability Analysis Based on Vehicle Dynamics System," Isuzu Motors Ltd., Report, circa 1970.
108. Nakatsuka, Takeshi, Katsuji Takanami, and Yoshito Kawamura, "Analysis of Car Performance in the Circuit Race," Isuzu Motors Ltd., Report, circa 1970.
109. Nedley, A.L., and W.J. Wilson, "A New Laboratory Facility for Measuring Vehicle Parameters Affecting Understeer and Brake Steer," SAE Paper No. 720473, Society of Automotive Engineers, Warrendale, PA, 1972.
110. Niles, Alfred S., and Joseph S. Newell, Airplane Structures, John Wiley & Sons, Inc., New York, 1938.
111. Nordeen, Donald L., "Vehicle Directional Control Equations for an Inclined Roll Axis," General Motors Proving Ground Report A-2165, July 1969.
112. Olley, M., "National Influences on American Passenger Car Design," Proceeding of the Institution of Automobile Engineers, Vol. 32, England, 1937-38.
113. Pacejka, H.B., "Tyre Characteristics and Vehicle Dynamics," Technische Hogeschool, Delft, 1986.
114. Pacejka, H.B., and R.S. Sharp, "Shear Force Development by Pneumatic Tyres in Steady State Conditions: A Review of Modeling Aspects," Vehicle System Dynamics, Vol. 20, pp. 121-176, 1991.
115. Perkins, C.D., and R.E. Hage, Airplane Performance, Stability and Control, Wiley and Sons, 1949.
116. Pershing, Bernard, ed., The Aerodynamics of Sports and Competition Vehicles, American Institute of Aeronautics and Astronautics, Los Angeles, CA, 1969.
117. Pershing, Bernard, ed., Second Symposium—The Aerodynamics of Sports and Competition Vehicles, American Institute of Aeronautics and Astronautics, Los Angeles, CA, 1975.
118. Platt, Maurice, "The Structure of the Automobile," Crompton - Lanchester Lectures, The Private Car, The Institute of Mechanical Engineers, Automobile Division, London, 1960.
119. Pope, Alan, and John J. Harper, Low Speed Wind Tunnel Testing, John Wiley & Sons, Inc., London, 1966.
120. Puhn, Fred, How to Make Your Car Handle, H. P. Books, Los Angeles, CA, 1981.
121. Radt, H.S., and W.F. Milliken, Jr., "Motions of Skidding Automobiles," SAE Paper No. 600133, Society of Automotive Engineers, Warrendale, PA, 1960.
122. Radt, H.S., and H.B. Pacejka, "Analysis of the Steady-State Turning Behavior of an Automobile," presented at Symposium on Control of Vehicles, Institute of Mechanical Engineers, London, 1963.

123. Radt, H.S., and W.F. Milliken, Jr., "The Application of Stability Derivatives to Vehicle Handling," technical report, Milliken Research Associates, Inc., January 1992.
124. Radt, H.S., and D.A. Glemming, "Normalization of Tire Force and Moment Data," *Tire Science and Technology*, TSTCA, Vol. 21, No. 2, pp. 91-119, April-June, 1993.
125. Rauscher, Manfred, Introduction to Aeronautical Dynamics, John Wiley & Sons Inc., New York, 1953.
126. Rice, R.S., "Measuring Car-Driver Interaction with the g-g Diagram," SAE Paper No. 730018, Society of Automotive Engineers, Warrendale, PA, 1973.
127. Rice, R.S., "Goodyear Orientation Program in Automotive Vehicle Dynamics—Lecture #4, Two-Degree of Freedom Car Transient Dynamics," Cornell Aeronautical Laboratory, Inc., 1972.
128. Rice, Roy S., and D.A. Alianello, "A Driver Characterizing Function—The g-g Diagram," Cornell Aeronautical Laboratory Report No. VJ-2882-K, June 1970.
129. Riede, P.M., R.L. Leffert, W.A. Cobb, "Typical Vehicle Parameters for Dynamic Studies Revised for the 1980's," SAE Paper No. 840561. Society of Automotive Engineers, Warrendale, PA, 1984.
130. Rill, G., "Steady-State Cornering on Uneven Roadways," SAE Paper No. 860575, Society of Automotive Engineers, Warrendale, PA, 1986.
131. Roland, R. Douglas, Jr., "A Nonlinear Analysis of Automobile Dynamics," Cornell Aeronautical Laboratory Report VJ-2633-K-2, Buffalo, NY, February 1969, and revised version, CAL Report VJ-2633-K-2-R, June 1971.
132. Roland, R. Douglas, Jr., and Carl F. Thelin, "Computer Simulation of Watkins Glen Grand Prix Circuit Performance," Calspan Report No. ZL-5002-K-1, August 1971.
133. Roller, Albert E., "Design and Calculation of Progressive Compression Springs," *Industrial Mechanics*, Vol. 10, Part 1, The Industrial Mathematics Society, Detroit, MI, 1960.
134. Rowell, H.S., "Principle of Vehicle Suspension," Proceedings, Institute of Automobile Engineering, Vol. 17, Part 2, 1922-3.
135. Rudd, Tony, It Was Fun, Patrick Stephens (part of Haynes Publishing Group), England, 1993.
136. Sakai, H., "The Dynamic Properties of Tires," Bulletin, JSOE No. 3, p.70-71, 1971, also, *International Journal of Vehicle Design*, Vol. 2, No. 1, 1981, and Vol. 3, No.3, 1982.

137. Santer, R.M., and Mark E. Gleason, "The Aerodynamic Development of the Probe IV Advanced Concept Vehicle," SAE Paper No. 831000, Society of Automotive Engineers, Warrendale, PA, 1983.
138. Sardou, Max, "The Sensitivity of Wind-Tunnel Data to a High-Speed Moving Ground for Different Types of Road Vehicles," SAE Paper No. 880246, Society of Automotive Engineers, Warrendale, PA, 1988.
139. Satchell, Terry L., "The Design of Trailing Twist Axles," SAE Paper No. 810420, Society of Automotive Engineers, Warrendale, PA, 1981.
140. Schenkel, Franz K., "The Origins of Drag and Lift Reductions on Automobiles with Front and Rear Spoilers," SAE Paper No. 770389, Society of Automotive Engineers, Warrendale, PA, 1977.
141. Schuring, D.J., K.D. Bird, J.F. Martin, "Tire Energy Consumption and Vehicle Fuel Savings," presented before the Tire Mechanics Session of the Akron Rubber Group, 1974.
142. Scibor-Rylski, A.J., Road Vehicle Aerodynamics, Halstead Press, div. of John Wiley & Sons, New York, 1975.
143. Scibor-Rylski, A.J., "Negative Lift Devices on Racing Cars," Paper 19, Proceedings of the First Symposium on Road Vehicle Aerodynamics held in The City University, London, November 6-7, 1969.
144. Segel, Leonard, "Theoretical Prediction and Experimental Substantiation of the Response of the Automobile to Steering Control," The Institute of Mechanical Engineers, London, 1956.
145. Segel, Leonard, "Keynote Address: Some Reflections on Early Efforts to Investigate the Directional Stability and Control of the Motor Car," Transportation Systems, ASME Publication AMD, Vol. 108, 1990.
146. Simanaitis, Dennis J., "Putting the CART Before the Wind," Road and Track, June 1984.
147. Simanaitis, Dennis J., "Shock Absorbers," Automotive Engineering, Society of Automotive Engineers, Warrendale, PA, November 1976.
148. Smith, Carroll, Engineer to Win, Motorbooks International, Osceola, WI, 1984.
149. Smith, Carroll, Tune to Win, Aero Publishers Inc., Fallbrook, CA, 1978.
150. Smith, Carroll, Prepare to Win, Aero Publishers Inc., Fallbrook, CA, 1975.
151. Sovran, G., T. Morel, and W.T. Mason, Jr., eds., Aerodynamic Drag Mechanisms of Bluff Bodies and Road Vehicles, Symposium at General Motors Research Laboratories, September 1976. Proceedings published by Plenum Press, New York-London, 1978.
152. Staniforth, Allan, High Speed Low Cost, Patrick Stephens (part of Haynes Publishing Group), London, 1969.
153. Stapleford, W.R., and G.W. Carr, "Aerodynamic Characteristics of Exposed Rotating Wheels," MIRA Report No. 1970/2, 1969.
154. Steeds, W., Mechanics of Road Vehicles, Iliffe and Sons, Ltd., London, 1960.
155. Stollery, J.L., and W.K. Burns, "Forces on Bodies in the Presence of the Ground," The Proceedings of the First Symposium on Road Vehicle Aerodynamics, held at The City University, London, 1969.
156. Sugawara, F., et al., "Electronically Controlled Shock Absorber System Used as a Road Sensor which Utilizes Supersonic Waves," SAE Paper No. 851652, Society of Automotive Engineers, Warrendale, PA, 1985.
157. Terry, Len, and Alan Baker, Racing Car Design and Development, Robert Bentley, Inc., Cambridge, MA, 1973.
158. Thompson, A.G., "Optimum Damping in a Randomly Excited Non-Linear Suspension," Proceedings of the Institute of Mechanical Engineers, Automobile Division, London, 1969-70.
159. Van Eldik Thieme, H.C.A., and H.B. Pacejka, The Tire as a Vehicle Component, Delft University of Technology, Delft, The Netherlands, 1971.
160. Van Valkenburgh, Paul, "Some Technicalities from 1988," Road and Track, April 1989.
161. Van Valkenburgh, Paul, "What's It Really Like Out There?" Road and Track, October 1983.
162. Van Valkenburgh, Paul, Chevrolet = Racing...?, Walter R. Haessner and Associates, Inc., Newfoundland, NJ, 1972.
163. von Karman, Theodore, Aerodynamics, McGraw-Hill, New York, 1963.
164. Ward, Jeff, and John Pitchers, eds., Design for Competition, 3rd Ed., The 750 Motor Club, England, 1966.
165. Warner, Edward P., Airplane Design—Aerodynamics, 1st Ed., McGraw-Hill, 1927.
166. Williams, Jack, "An Automotive Front-End Design Approach for Improved Aerodynamics and Cooling," SAE Paper No. 850281, Society of Automotive Engineers, Warrendale, PA, 1985.
167. Wright, P.G., "Speed Graphic," Road and Track, June 1984.
168. Wright, P.G., "The Influence of Aerodynamics on the Design of Formula One Racing Cars," International Journal of Vehicle Design, Vol. 3, No. 4, p. 383, 1982.
169. Wünsche, Thomas, Karl-Heinz Muhr, et al., "Side Load Springs as a Solution to Minimize Adverse Side Loads Acting on the McPherson Strut," SAE Paper No. 940862, Society of Automotive Engineers, Warrendale, PA, 1994.

170. The following references all relate to shock absorbers / dampers.
- Advanced Suspensions, Proceedings of the Institute of Mechanical Engineers (IME), London, 1988.
- Adachi, M., *et al.*, "A State Adaptive Control Algorithm for Vehicle Suspensions," SAE Paper No. 881769, Society of Automotive Engineers, Warrendale, PA, 1988.
- Akatsu, Y., *et al.*, "An Active Suspension Employing an Electrohydraulic Pressure Control System," SAE Paper No. 905123, Society of Automotive Engineers, Warrendale, PA, 1990.
- Barak, P., and D. Hrovat, "Application of the LQG approach to design of an automotive suspension for three-dimensional vehicle models," IME C421/88, London, 1988.
- Carbonaro, O., "Hydrafive Suspension Electronic Control System. Control Technology and Philosophy," SAE Paper No. 905101, Society of Automotive Engineers, Warrendale, PA, 1990.
- Crolla, D.A., and A.M.A. Aboul Nour, "Theoretical comparisons of various active suspension systems in terms of performance and power requirements," IME C420/88, London, 1988.
- Daver, R., *et al.*, "Analysis of the Procedures of Active Control of Vehicle Suspensions and of Their Strength," SAE Paper No. 905126, Society of Automotive Engineers, Warrendale, PA, 1990.
- Decker, H., *et al.*, "A Modular Concept for Suspension Control," SAE Paper No. 905124, Society of Automotive Engineers, Warrendale, PA, 1990.
- Decker, H., *et al.*, "A practical approach towards advanced semi-active suspension systems," IME C430/88, London, 1988.
- Decker, H., W. Schramm, and M.R. Bethell, "An Optimized Approach to Suspension Control," SAE Paper No. 900661, Society of Automotive Engineers, Warrendale, PA, 1990.
- Doi, S., *et al.*, "An experimental study of optimal vibration adjustment using adaptive control methods," IME C433/88, London, 1988.
- Foag, W., "A practical control concept for passenger car active suspensions with preview," IME C424/88, London, 1988.
- Guy, Y., *et al.*, "A Solenoid-Actuated Pilot Valve in a Semi-Active Damping System," SAE Paper No. 881139, Society of Automotive Engineers, Warrendale, PA, 1988.
- Hagele, K.H., *et al.*, "Continuously Adjustable Shock Absorbers for Rapid-Acting Ride Control Systems (RCS)," SAE Paper No. 905125, Society of Automotive Engineers, Warrendale, PA, 1990.
- Hennecke, D., *et al.*, "EDCIII—The New Variable Damper System for BMW's Top Models—A Further Development of our Adaptive, Frequency-Dependent Damper Control," SAE Paper No. 900662, Society of Automotive Engineers, Warrendale, PA, 1990.
- Hennecke, D., *et al.*, "Further Market-Oriented Development of Adaptive Damper Force Control," SAE Paper No. 905143, Society of Automotive Engineers, Warrendale, PA, 1990.
- Hennecke, D., and F.J. Ziegelmeyer, "Frequency dependent variable suspension damping—theoretical background and practical success," IME C431/88, London, 1988.
- Hine, P.J., and P.T. Pearce, "A practical intelligent damping system," IME C436/88, London, 1988.
- Konishi, J., *et al.*, "Development of Electronically Controlled Air Suspension System," SAE Paper No. 881770, Society of Automotive Engineers, Warrendale, PA, 1988.
- Lemme, C.D., and F.J. Furrer, "Hydraulically Controlled Adjustable Dampers," SAE Paper No. 900660, Society of Automotive Engineers, Warrendale, PA, 1990.
- Lizell, M., "Semi-active damping," IME C429/88, London, 1988.
- Mastinu, G., "Passive automobile suspension parameter adaptation," IME C425/88, London, 1988.
- Meller, T., and F. Fruhauf, "Variable damping—philosophy and experiences of a preferred system," IME C432/88, London, 1988.
- Michelberger, P., *et al.*, "Design of Active Suspension System for Road Vehicles: An Eigenstructure Assignment Approach," SAE Paper No. 905146, Society of Automotive Engineers, Warrendale, PA, 1990.
- Miller, L.R., and C.M. Nobles, "The Design and Development of a Semi-active Suspension for a Military Tank," SAE Paper No. 881133, Society of Automotive Engineers, Warrendale, PA, 1988.
- Miller, L.R., "The effect of hardware limitations on an on/off semi-active suspension," IME C422/88, London, 1988.
- Mizuguchi, M., T. Suda, *et al.*, "Chassis Electronic Control Systems for the Mitsubishi 1984 Galant," SAE Paper No. 840258, Society of Automotive Engineers, Warrendale, PA, 1984.
- Parker, G.A., "A novel valve for semi-active vehicle suspension systems," IME C427/88, London, 1988.
- Reuter, R.J., "Speed Dependent Damping for the 1989 Cadillac Allante," SAE Paper No. 890178, Society of Automotive Engineers, Warrendale, PA, 1989.

Shim, J.S., *et al.*, "Effect of a Semi-actively Controlled Suspension Unit on the Vehicle Dynamic Characteristics," SAE Paper No. 905040, Society of Automotive Engineers, Warrendale, PA, 1990.

Soltis, M.W., "1987 Thunderbird Turbo Coupe Programmed Ride Control (PRC) Suspension," SAE Paper No. 870540, Society of Automotive Engineers, Warrendale, PA, 1987.

Tanahashi, H., *et al.*, "Toyota Electronic Modulated Air Suspension for the 1986 Soarer," SAE Paper No. 870541, Society of Automotive Engineers, Warrendale, PA, 1987.

Yokoya, Y., K. Asami, *et al.*, "Toyota Electronic Modulated Suspension (TEMS) System for the 1983 Soarer," SAE Paper No. 840341, Society of Automotive Engineers, Warrendale, PA, 1984.

Index

- Abbott, Ira H.
 NACA airfoil data, 497, 500
- Acceleration, elements of
 cornering, acceleration vectors in, 5–7
 lateral acceleration, 6–8
 longitudinal acceleration, 7–9
 typical G-G measurements (Grand Prix car), 9–11
 in Vehicle Axis System, 117–118
 See also G-G diagrams; Lateral acceleration;
 MRA Moment Method (MMM); Pair analysis; Stability and control (steady-state, transient)
- Ackermann steering. *See under* Steering systems
- Active suspension system (Lotus), 469–470
- Aerodynamics, applied
 introduction, 83–84, 489–490
 aerodynamic axis system (SAE), 109–110
 balancing the race-car
 introduction/general considerations, 570–572
 approach, 572–573
 cornering with aero downforce (simplified analysis), 573–577
 boundary layers
 boundary-layer flow control, 555
 and surface drag of grooves and gaps, 567
 in two-dimensional airflow, 539
 in wind tunnels, 526
 See also drag, flow/flow control (below)
- Chaparral - historical notes
 Chaparral Can-Am Model 2E, 490
 Chaparral 2J "Sucker car," 491
 early experiences (FERD 1, MERD V8), 455–456
 front treatment, 456
 rear treatment, 457
 rear wing: glory and grief, 457
 Riverside dam, 455
- cornering
 with aero downforce (simplified analysis), 573–577
 cornering comparison (Chaparral G.S. 2G), 507–511
 tire load sensitivity, importance of, 576
- dams
 defined, 496
 effects of (Charger Daytona), 496, 497
 effects of (Porsche 911 Carrera), 496, 498
- downforce, aerodynamic
 calculated (100 mph, Chaparral G.S. 2G), 502
 and G-G boundary, 11, 350
 and high-speed braking, 396
 and high-speed steady-state cornering, 396–397
 measured vs. speed (Chaparral G.S. 2G), 505
 moment-method N-A_V charts (Chaparral Gs 2G), 320, 324–326
 performance benefits from (Chaparral G.S. 2G), 506–507
 and pressure coefficient (example), 108
 rear spoiler (typical GT car), 493
 and tire behavior, 15
 and vortex formation, 528–530, 534–535
 See also ground effects (below)
- drag, aerodynamic
 vs. boundary layer thickness (grooves and gaps), 567
 defined, 536
 drag coefficients: transport aircraft vs. cars, 543, 545
 drag forces: theoretical vs. measured, 543–544
 drag reduction, factors for, 545–546
 of enclosed-wheel sports-racing cars, 543–544
 flat plate drag (table), 565
 fundamental mechanisms of, 538–539
 and high-speed braking/acceleration, 396–397
 induced drag, 539, 540
 Indy car drag coefficients (typical), 542
 vs. lip height (rear spoiler, notchback car), 495
 Morelli basic body shape, 541–542
 pressure drag (a.k.a. shape drag, for drag), 536
 race car drag components, 541

Aerodynamics, applied (*continued*)
 drag, aerodynamic (*continued*)
 of rear spoiler (GT and notchback cars), 494–495
 rear wing lift/drag vs. angle of attack, 515–516, 517
 skin friction drag, 539
 of strips, grooves and fasteners, 567
 of surface (paint) roughness, 565–567
 total vehicle drag (coastdown, Chaparral G.S. 2G), 502–503
 vortex drag, 539, 540
 wind-tunnel tests of (March 83C), 542–543
 wing drag and wheel load changes (Chaparral G.S. 2G), 503–504
 vs. yaw angle (front spoiler, Charger Daytona), 497
See also boundary layers, flow/flow control, vortices, wheels
 flat plate aerodynamics
 flat plate drag (table), 565
 plates at an angle to airstream, 563–565
 plates normal to airstream, 560, 562–563
 sideboards, 560, 562
 flow/flow control - external
 boundary-layer flow control, 555
 cuffs, 553–554
 directing/containing flow, devices for, 547–548
 fillets, 553–554
 flow control devices, categorization of, 546–547
 Gurney lip, 552–553
 Morelli basic body shape, 541–542
 pressure changes, devices for creating, 551–552
 Rao slots, 553–554
 strips, 553–554
 underbody vortex formation, 528–530, 532, 534–535
 useful vortices, devices for creating, 549–551
 vortex drag, 539
 VW basic aerodynamic flow body, 541, 542
 flow/flow control - internal
 introduction, 555–556
 air entrance scoops, 559
 NACA submerged inlet duct, 560, 561
 ram air ducted radiator, 556–559

force-moment coefficients, 110–111
 ground effects
 and Bernoulli's equation, 524–526
 Chaparral 2J, calculations for, 521
 effect of rear wings on, 534–536
 frontal area vs. plan area, 522
 ground plane simulation, 526–527
 historical note, 521–522
 Indianapolis vs. F.1 regulations, 492
 Lotus 77 F.1 machine, 491, 492
 Lotus wind tunnel tests, 523–524
 March F.1 aero features, 537
 other aspects of, 527
 Penske PC-18 general configuration, 537
 and pitch/roll motion limitations, 245–246
 race car applications, 532–536, 537
 tests of symmetrical bodies, 245–246
 underbodies without skirts, 528–536
 venturi model, 528, 531–532
 vortex formation, 528–530, 532, 534–535
 lift, aerodynamic
 Daimler-Benz experience (ca. 1936–39), 490
 front lift vs. lip height (rear spoiler, notchback car), 495
 front lift vs. speed (air dam and rear spoiler, Porsche 911), 498
 front lift vs. yaw angle (front spoiler, Charger Daytona), 497
 lift coefficient vs. yaw angle (rear spoiler, GT car), 494
 rear lift vs. lip height (rear spoiler, notchback car), 495
 rear lift vs. speed (air dam and rear spoiler, Porsche 911), 498
 Lotus developments
 Lotus 77 F.1 machine, 491, 492
 Lotus 78 F.1 machine, 521–522
 Lotus 88 F.1 machine, 492
 Lotus F.1 machine (ca. 1969), 511–512
 side skirts
 banning of, 492, 522, 527
 and Chaparral 2J, 491
 downforce without, 527
 ground effects without, 528–536
 and Lotus 78 F.1, 491
 sealing from, 527
 spoilers, rear
 action of, 493

Aerodynamics, applied (*continued*)
 spoilers, rear (*continued*)
 drag effects (GT car), 494
 effect of (GT car), 492–493
 effect of (notchback car), 495
 lift coefficient vs. yaw angle (GT car), 494
 wheels, exposed
 aero forces and moments for (Pirelli), 570
 drag coefficients for (Pirelli), 569–570
 pressure distribution beneath wheel, 568–569
 wake patterns (isolated wheel), 568
 wind tunnels
 book : *Low Speed Wind Tunnel Testing* (Ref. 119), 554
 boundary layer control in, 526
 flat belts, difficulty in using, 526
 ground plane simulation in, 526–527
 Lotus tests in, 523–524
 race car configuration with underbody channels, 532–535
 test of rough, upswept, underbody, 528–530
 test results: moving-belt vs. fixed ground plane, 528, 530
 tests of March 83C, 542–543
 venturi test configuration, 528, 531–532
 wings - Chaparral G.S. 2G example
 airfoil data (original, corrected), 500–502
 configuration (pictorial), 499
 cornering comparison, 507–511
 downforce, calculated (100 mph), 502
 downforce, measured (vs. speed), 505
 performance benefits, 506–507
 Reynolds number for, 497–498
 total vehicle drag (trimmed, untrimmed wing), 502–503
 vehicle parameters (table), 499
 wings - general
 airfoil flow-control devices (slots, flaps, etc.), 552–554
 banning of, 457, 791
 cuffs, 553–554
 effects on underbody aerodynamics, 534–536
 end plates (and aspect ratio), 513–515
 Gurney lip, 552–553
 high-lift devices (airfoils, slots, flaps), 512–514
 Indianapolis vs. F.1 regulations, 492
 legislated wings, 511

multiple-slotted airfoils, 512
 Rao slots, 553–554
 rear wing lift/drag vs. angle of attack, 515–516
 spanwise load distribution, rear wing, 516–517
 two-dimensional airfoil shapes and lift coefficients, 517–519
 yaw
 effect of downforce on N-A_y chart (Chaparral Gs 2G), 324–326
 yaw angle vs. lift coefficient (rear spoiler, GT car), 494
See also Aerodynamics, basic; MMM (MRA Moment Method)
 Aerodynamics, basic
 aerodynamic axis system (SAE), 109–110
 air, particle interaction in, 84–85
 Bernoulli's equation
 basic assumptions, 87–88
 terms in, discussion of, 90–95
 boundary layer airflow
 and computer modeling, 101
 disturbed wakes from, 98–99
 pressure recovery in, 97–98
 tangential, shear, gradients in, 84–85, 97
 thickening and turbulence in, 97–99, 102
 and wind tunnel testing, 102
See also flow/flow control
 Boyle's, Charles' Laws, 86
 density
 discussion, 85–86
 vs. pressure and temperature, 86
 flow separation
 around typical hatchback, 98, 99
 and computer modeling, 101
 favorable effects from, 101
 and pressure recovery, 97–98
 at sharp edge, 100
 turbulence, drag, in, 85
 in wind tunnel diffuser, 100
 flow visualization, wind tunnel
 lampblack and kerosene, 106
 smoke tunnels, 105–106
 streamlines, VW Rabbit, 100
 tufting, 104–105
 force-moment coefficients, 110–111
 free stream airflow
 particle interactions in, 84
See also stream tubes (below)
 lift, generation of by an airfoil, 96

See also stream tubes (below)
 lift, generation of
 by an airfoil, 96
 pressure coefficient C_p , 107–108
 pressure distribution
 around an airfoil, 95–97
 stagnation point, 94
 pressure measurement
 dynamic pressure, 92–93
 pressure/velocity (pitot tube), 95
 stagnation pressure, 94
 static pressure, 90–92
 stop pressure, 92–93
 total pressure, 93–94
 Reynolds Number
 and viscosity, 87
 and wind tunnel testing, 103–104
 stream tubes
 and Bernoulli's equation, 90
 described, 88–89
 energy in, 89–90
 viscosity
 discussion, 86–87
 kinematic, absolute, viscosity, 87
 and Reynolds number, 87
 wind tunnel testing
 boundary layer considerations in, 102
 flow similarity problems in, 102
 ground effects in, 102
 and Reynolds number, 103–104
 scaling problems in, 101–102
See also Aerodynamics, applied
 Aligning torque. *See under* Tire behavior
 Anderson, John D.
 comments on nondimensional coefficients, 473
 “anti” features (in SVSA geometry). *See under* Suspension geometry
 Anti-lock braking systems, 753–754
 Anti-pitch characteristics
 pitch and bounce centers, geometry of, 795–796
 and secondary chassis set-up, 403–404
 and straight line acceleration, 395
 Anti-roll bars, 281
See also Ride and roll rates; Wheel loads
 Anti-squat, 395–396, 404, 617–619
 Apparent wheelbase, 245. *See also* Stability and control, transient
 Axis systems
 Aero, 109; tire, 61, 62; vehicle, 113–116

Bastow, Donald
 book: *Car Suspension and Handling* (Ref. 18), 786
 Bedard, Pat
 comment on tire forces, 665
 Best, Anthony
 acknowledgement re authorship, 781
 Anthony Best Dynamics, Ltd., 781
 CARDS equipment (damper measurement), 803
 Bethell, M.R.
 paper on Monroe electronic air-spring dampers (Ref. 59), 785–786
 Bicycle (2DF) model
 elementary automobile, defined, 126–128
See also Stability and control, steady-state
 Bidwell, Joe
 basic research, willingness to publish, 429
 early career at GM, 432–433
 and GM vehicle dynamics studies
 aerodynamics research and CAL thruster, 436
 analytical models and Bundorf Compliance Concept, 437–438
 development of experimental techniques, 438
 early directional control, comments on, 432–433
 ride simulator, construction of, 434
 tire testing, development of, 445–447, 453
 “Unicontrol” steering system, 436
 and variable response vehicle, 437
 variable stability vehicle (with CAL), 437, 438–439
 Vehicle Dynamics Terminology (J670) (with CAL), 433
 head, GM Engineering Mechanics Department, 429, 432
 moves to GM Engineering Staff, 439
 photo of, 432, 470
 and precursor to IVHS technology, 436
 prior Schilling work, comment on, 433
 SAE Technical Committees, comment on, 433–434
 Bierley, Bob
 and GM human factors group, 434–435
 Bilstein dampers, 823, 829
 Bird, King
 at CAL Vehicle Research, 439, 465
 and Calspan Tire Research Facility (TIRF), 461–462
 paper on Calspan Tire Research Facility, 461

photo of, 461
 Blue Crown Specials (FWD Indy cars), 730
 Boyle's Law, 86
 Braking systems
 anti-lock
 and paved-circuit racing, 753–754
 sensors in, 753
 4WD ABS system and brake balance, 754
 balance
 alternative designs for, 751
 analysis of, 751–753
 combined braking and cornering, 393
 and high-speed braking, 396
 importance of, 751
 initial adjustment of, 751
 pedal force and travel, 753
 pedal ratio, choice of, 753
 tire data for, 752
 in 4WD ABS system, 754
 basic components of, 749
 design considerations
 brake disc rotors, 750
 brake lines: materials and routing, 749
 brake pads, 750
 caliper flex, 749–750
 manual or power boost, 749
 master cylinders, 749
 hydraulics
 bleeding the system, 750
 brake fluid, discussion of, 750
 silicone vs. glycol-based fluid, incompatibility of, 750
 ventilation of, 751
See also Braking/tractive force; Chassis setup
 Braking/tractive force
 braking force
 and CG location, 391
 and Chaparral GS 2G (MRA Moment Method), 324
 discussion, 35
 and tire print characteristics, 36
 and vehicle performance limitations, 346
 and vehicle thrust, drag, 63–66
 and resultant tire force, 44–46
 vs. slip angle, slip ratio (Sakai data), 41–42, 44
 vs. slip ratio (TIRF data), 37–39
 slip ratio, definitions of, 39–41
 and suspension “anti” features, 617–620
 tire/rim size
 effect on cornering, 394

effect on steering-wheel kickback, 400
 effect on straight-line braking, 391
 tractive force
 discussion, 33–35
 and print characteristics, 34
 vehicle performance limitations, 346
 vehicle thrust, drag, 63–66
 wheel spin
 and CG position, 395, 401
 and differential type, 395
See also Aerodynamics, applied; Friction circles; G-G diagrams; Tire behavior; Stability and control (steady-state, transient); Wheel loads
 Breakaway. *See under* Tire behavior
 Broulhet, George
 paper on tire slip angle (1925), 418
 and tire slip angle concept, 418–419
 Bruns, H.J.
 paper on passenger comfort (Ref. 24), 785
 Bull, A.W.
 paper on tire behavior, 420
 Bull, Giff (CAL)
 and variable stability airplane course, 441
 Bump steer
 in dropped throttle turns, 397
 and high cornering stiffness tires, 406, 407
 on poor roads, 398–399
 with small scrub radius, 398
 and steering arm changes, 400
See also Steering systems, under ride steer
 Bundorf, R.T.
 paper on CAL/GM Variable Stability Automobile, 439
 paper on characteristic steer and understeer (Ref. 27)
 paper on cornering compliance (Ref. 28)
 Bundorf cornering compliance
 derivation of, 172, 227–228
 discussion of (Bidwell), 437–438
 and Olley view of understeer, 419
 and tangent speed, 176–177
 and understeer gradient, 172–173
See also Bundorf/Leffert paper on cornering compliance (Ref. 28)
 Burnett, Bill
 and Olleyism, 420
 Burns, W.K.
 paper on ground effect theory (Ref. 155), 522–523

CAL (Cornell Aeronautical Laboratory)
changed atmosphere at, 439
GM research program at
hydrogen peroxide rocket thruster, 436
instrumentation for force measurements,
425–426
Junkers Aircraft tire model, 424
Leonard Segel appointed Project Manager,
422
step steer, instrumentation for, 425
summary of accomplishments, 427
tire data for (Hedekel, U.S. Rubber), 423–
424
tread wear, effects of, 426
validation of quasi-static tire model, 424
variable stability vehicle, 437, 438–439
vehicle equations of motion, 424–425
IME papers, presentation of (Milliken, et al.,
1956), 430–431
six-component test rig (photo), 428
Transportation Division formed (1963), 439
Vehicle Dynamics Department (WFM, Mgr.),
429
and Watkins Glen, Lime Rock, analyses, 340,
341
W.F. Milliken service at, 414–415
Calspan TIRF facility
accomplishments of, 463
description, 22–24
development of (King Bird), 461–462
slip ratio, (definition for, 39, 40–41
sponsorship of, 462–463
test data
braking/tractive force vs. slip ratio, 37–39
camber vs. load sensitivity, 54
camber vs. side, lateral, force, 49, 50–53
lateral force vs. slip angle, 24–27

Camber
aligning torque from
introduction, 47
camber vs. steer angle, 69–70
camber angle vs. camber thrust (normalized,
various loads), 478
camber force/thrust, 46
camber stiffness, 46–47
in chassis secondary set-up, 405–406
defined (SAE), 46
effect of (in axle pair analysis), 290
inclination angle (SAE), 46, 63
vs. lateral force
constant load, 50–53

lateral force compliance camber (front,
rear), 836
for motorcycle tires, 47
peak lateral force, 48–50
variable load, 54
negative, 50
optimization of, 50–54
print distortion from, 46, 47
roll-off, 48
slip/camber ratio vs. lateral force (normalized,
various loads), 479–480
in steady-state cornering, 394
tire data, typical, 50–53
See also Steering systems; Suspension
geometry
Carlsson, Erik, and Saab FWD rallying, 730
Carr, G.W.
on drag components (Ref. 31), 539
Caster. *See under* Steering systems
CG (center of gravity)
and braking force, 391
and chassis set-up
braking and cornering, 393, 394, 398
dropped throttle in a turn, 397
in secondary set-up, 401–402
steering kickback, 402
straight line acceleration, 395
straight line braking, 391
in Corvair controversy, 441
and ride and roll rates (IS), 586
in rough road behavior cornering (US), 401
static CG height (axle pair analysis curves),
291
and steering system kickback, 402
in wheel load calculations, 666–671, 704
and wheel spin, 395, 401
Chaparral
See Aerodynamics, applied; Chevrolet-
Chaparral racing; MRA Moment
Method
Chapman, Colin
and aerodynamic downforce, 468–469
and RERD race cars, 448
Characteristic speed, 181–185
Charles' Law, 86
Charmichael, Tom
and Maypole test, 296
Chassis set-up
compliance: caveats and challenges, 387–388
objectives and procedure, 388–389
primary set-up, performance factors in
acceleration out of a corner, 395

braking and cornering, 393, 396, 398
dropped throttle, 397–398
poor road behavior, 398–399
steady-state cornering, 394, 396–397
steering kickback, 400
steering wheel force and ratio, 399–400
straight line acceleration, 395–396, 397
straight-line braking, 391, 393, 396
tables and discussion, 389–391, 392
roll center location, effects of
on acceleration out of a corner (FWD),
403
braking and cornering, 393
on lateral load transfer, 403
on rough road behavior, 403
and secondary set-up, 403
and steady-state cornering, 394, 403
on tuck-in, 403
roll stiffness distribution
and acceleration out of a corner, 395
in braking and cornering, 393–394
in secondary chassis set-up, 410–411
secondary set-up, variables in
anti-pitch geometry, 403–404
camber, 405–406
differentials, 407–408
moving the CG, 401–402
moving the roll center, 403
ride spring rate, 409–410
ride/roll steer characteristics, 406–407
roll stiffness and distribution, 410–411
set-up items (table, discussion), 401, 402
steering axis geometry, 404–405
tires and rims, 409
track width, 408–409
See also Aerodynamics, applied; Pair
analysis; Ride and roll rates; Suspension
geometry
Chassis stiffness, torsional and bending, 673–677
Chevrolet. *See* Chevrolet-Chaparral racing;
Corvair, controversy over
Chevrolet-Chaparral racing, 442
and aerodynamic downforce. *See* Aerody-
namics, applied
background and introduction, 442–444
Can-Am Model 2E, historical note on, 491
Chaparral 2J "Sucker" car, historical note on,
491
MERD Chevy V8 monocoque, 449
MERD Corvette, genesis of, 448
on-board instrumentation, 450–452
skid pad testing, 452–453

summary of program results, 449–450
suspension geometry, 455
tire testing, 453
torsional stiffness, importance of, 454–455
transient dynamics, Chevrolet interest in,
441–442
See also Aerodynamics, applied; MMM
(MRA Moment Method)
Christie, Walter, and FWD race cars, 730
Close, Bill
and Air Force tire tester, 428–429
photo of, 470
 C_N-A_Y diagrams. *See under* MMM (MRA
Moment Method)
Cogotti, A.
flow and forces around exposed wheels (Ref.
34), 568–570
Cole, Ed
and Chevrolet R&D, 421
Collier, George (Grandpa Throttlebottom)
drifting, comment on, 231
Collier, Miles
comment on limit driving, 336
Compliance
aligning torque compliance steer, 836
in chassis set-up, 387–388
choice of (passenger cars), 833
classification of (applied force, wheel
position), 834
defined, 833
disadvantages of (in racing cars), 834
lateral force compliance camber, 836, 838
lateral force compliance steer, 835, 838
longitudinal force compliance effects, 836
measuring compliance effects, 837
and ride/roll steer, 724–726
sources of, 833
summary and discussion, 837, 839
US/OS effects, introduction and example,
834–835
See also Bundorf cornering compliance
Conicity, tire, 57
Constrained testing
D'Alembert's principle in, 295
at GM
checkerboard test (Ken Stoner), 421
Chevrolet/Chaparral testing, 452–453
constrained linear test (railcar, Chevrolet),
296–297, 299
in Corvair investigation, 444–447
1G/100mph skid pad, 447
Maypole test, 296

simulated roadability test (Chevrolet, 1963), 296, 298
 skid pad development (1937), 420, 421
 history of, 296–299
 MIRA (England) tethered testing, 297, 299
 MTS Flat-Trac Roadway Simulator, 300–301
 skid pad, force diagram for, 298
 three-wire system, principles of, 295–296
See also MMM (MRA Moment Method)
 Cooling systems, engine, 556–559
 Cornering, dynamics of. *See* Acceleration; Aerodynamics, applied; Lateral force; Stability and control (steady-state, transient); Tire behavior
 Corvair, controversy over
 Corvair exonerated, 449
 Moss gives testimony, 449
 skid pad and tire testing at GM, 444–447
 Winchell demonstrates CG position *vs.* car dynamics, 441
 Winchell designated “expert witness” for defense, 443–444
 Corvette
 Corvette five-link rear suspension, 646
 pre-84 Corvette-type IRS swing axle, 639
 Coulomb friction
 in open differentials, 736–737
 Course angle, 118
 Crane, Henry
 and K² Rig, 417
 Cranfield College of Aeronautics, 468
 Critical speed, 177–181
 Currie, Malcolm
 and Watkins Glen analysis, 341
 Cyrus, W., photo of, 470

D'Alembert's principle
 in constrained testing, 295
 and lateral load transfer (LLT), 281

Dampers
 introduction and historical note, 731–732
 in active suspension systems (Lotus), 469–470
 body acceleration
 and damper velocity, 806, 810
 and load fluctuation rate (smooth, rough, roads), 811–814
 in “one corner” ride model, 790–794, 898
 and passenger acceleration, 793–794
 vs. relaxation spring, 799, 807–809
 body attitude

control of, 823, 828
See also mode centers, below
 bump damping
 asymmetry in (bump-rebound), 800, 802
 bump control adjustment (KONI), 820–821
 bump stops (KONI), 822
 damping force *vs.* shaft speed (Penske), 830–831
 discussion of (KONI), 820
 damper characteristics
 asymmetry in (bump-rebound), 800, 802
 body acceleration due to damper velocity (\dot{g}_d), 798–799
 deadband (orifice effects and dry friction), 801
 discussion of, 785
 force *vs.* deflection (carding loops), 803, 805
 force *vs.* velocity, 806
 high velocity rolloff, 802
 simple, 798–800
 velocity. *See* damper velocity (below)
See also relaxation spring (below)
 damper construction
 bump rubbers, 803–804, 822
 direct-acting telescopic, improvements in, 782
 end rubbers, 797–798, 799, 806–809
 monotube, dual-tube, 803–804
 pressurized gas, 823, 829
 damper velocity
 and body acceleration, 806, 810
 shaft speed *vs.* damping force, 829–831
 velocity plot, 806
 damping coefficient, 787–788
 damping fundamentals
 bump amplitude *vs.* wavelength, 789
 critical damping, damping coefficient for, 788
 damping force, 787
 damping ratio, defined, 788
 displacement *vs.* damping ratio (step input), 789
 inertial force, 787
 resonant frequency, system, 788
 spring force, 787
 damping ratio
 and critical damping, 788
 defined, 788
 vs. displacement, time histories of, 789
 ideal, discussion of, 786

Dampers (continued)
 damping ratio (continued)
 optimum (Indy car), 824, 826
 optimum (road-holding), 811
 vs. transient response (Indy car), 825, 827
 electronically controlled, 786, 828
 end rubbers. *See* relaxation springs (below)
 future trends, 828
 jacking down, 821
 and lateral acceleration (steady-state cornering), 814–816
 leverage, effects of, 801, 803
 limit handling, 827–828
 load fluctuation rate, 810–814
 mode centers
 pitch and bounce centers, geometry of, 795–796
 ride comparison (in frequency domain), 797
 passenger car applications, 810–812
 and primary set-up
 dropped-throttle behavior, 398
 poor road behavior, 399
 racing car applications (general discussion), 810
 racing car applications (critical aerodynamic downforce)
 baseline configuration, Indy car, 825
 current suspensions, 823–824
 damping levels, 824
 discussion, 823
 Indy *vs.* Grand Prix cars, 824
 optimum damping ratio, Indy car, 824, 826
 transient response *vs.* damping ratio, 825, 827
 racing car applications (modest aerodynamic downforce)
 KONI dampers, 820–822
 other gas dampers, 823
 rebound damping
 asymmetry in (bump-rebound), 800, 802
 damping force *vs.* shaft speed (Penske), 830–831
 discussion of (KONI), 821
 rebound control adjustment (KONI), 821
 relaxation spring
 description and model, 797–798
 and transmissibility, 799, 807–809
 and vertical acceleration, 799, 807–809
 the ride/handling compromise, 810–814
 road holding, evaluation criteria for, 811
 shaft speed. *See* damper velocity (above)
 “sky-hook” damping, 828
 and spring-mass-damper system, 240–241.
See also body acceleration (above)
 and suspensions (Indy and GP cars), 823–827, 851–854
 technical literature on, 783–786, 851–854
 testing of, 803, 805
 CARDS equipment (crankshaft test rig), 803
 electrohydraulic servo system, 805–806
 tire-ground contact rate, 811–813
 tires, influence of, 823, 829
 and transient wheel loads
 introduction, 817
 with standard damper, 817–818
 transient handling (future trends), 828
 with twice standard damper, 818–819
 transmissibility
 defined, 790–791
 effects of (carpet plot), 799
 vs. frequency (various k_c and damping ratios), 792, 794, 807–809
 and passenger acceleration (simple ride model), 794
 unsprung mass, effects of
 body/passenger acceleration (simple model, no seat), 791
 and load fluctuation rate/road-holding ability, 810–814
 passenger acceleration (simple model, with seat), 793–794
See also transmissibility (above)
 Damping, tire. *See* Stability and control, steady-state; Tire behavior
 Dana Trac-Loc differential, 740–741, 742
 Davis, David E.
(Car & Driver) article (Ref. 57), 441
 Davis, S.C.H.
 on Grand Prix steering failure, 709
 de Levaud, Sensaud
 and early IFS research, 418
 deDion rear axle, 660–661
 DeFusco, Ernie
 photo of, 470
 Dell'Amico, Fred
 and application of static concepts, 206
 at CAL Vehicle Research, 439
 and constrained testing research, 465–466
 and MMM (MRA Moment Method), 293
 and path curvature stiffness, 201
 photo of, 464
 and unbalanced force-moment equations, 206

Derivative notation. *See under* Stability and control, steady-state
 Detroit Locker (differential), 745–746
 Diagonal weight jacking, 281–282
Differentials
 basic types, 733–734
 and chassis set-up (secondary), 407–408
 design limitations of, mechanical, 735
 geometry of low-speed turn, 734, 735
 invention of (1827), 734
 limited slip
 acceleration out of a corner, 395, 407
 Dana Trac-Loc, 740–741
 dropped throttle performance, 398, 408
 rough road traction/cornering (FWD, RWD), 408
 Salisbury axle, 741–744
 in secondary chassis set-up, 407–408
 and steering kickback, 400
 and straight line acceleration, 396
 Torsen differentials, 741–742
locking
 acceleration out of a corner, 395, 407
 applications of, 739
 cornering capability of, 740
 dropped throttle performance, 398, 408
 effects on handling/balance, 740
 locked spool characteristics, 739
 and rough road traction/cornering (FWD, RWD), 408
 stabilizing effects of, 739–740
 and straight line acceleration, 396
 and tire stagger, 740
 and wheel spin, 395
open
 acceleration out of a corner, 395, 407
 action during a turn, 734–735
 bevel and spur gear units, arrangement of, 736
 disadvantages of, 407–408, 737
 dropped throttle performance, 398, 408
 handling effects of, 738
 operation and lever analogy, 735–736
 partial (friction) locking of, 737
 performance characteristics of, 737
 stick-slip (Coulomb friction) in, 736–737
 with uneven torque split, 738–739
overrunning clutch types, 745–746
solid axle
 vs. IFS (in chassis set-up), 407
 straight line acceleration, 396

traction control and electronic improvements, 748
 viscous differential, 746–748
DK-4 vehicle dynamics model (Chevrolet), 273, 460–461
Donahue, Mark
 comments
 on full “g-g” diagram cornering technique, 364
 on handling an “unsorted” sedan, 387
Donis, J.E.
 studies on ground effects (Ref. 50), 528–533
Downforce. *See* Aerodynamics, applied
Drag, aerodynamic. *See* Aerodynamics, applied
Drag, induced (tire). *See under* Tire behavior
Drive types
 four-wheel drive
 differential types, choice of, 733
 paved surface disadvantages of, 733
 race vehicle experience with, 733
 front-wheel drive, 730
 effect on vehicle handling/performance, 730–731
 engine/transmission arrangements, typical, 732
 historical note (FWD competition cars), 730
 one-wheel drive, 734
 rear-wheel drive
 control advantages of, 732
 dropped-throttle stabilizing effect of, 732
 engine/transmission arrangements, typical, 732
 packaging (tire size) advantages of, 732
See also Chassis tuning; Braking systems;
 Differentials
Driver performance
 dampers and steering activity, 814–816
 driver “willingness” (and “g-g” diagrams), 348
 driver-induced oscillation, 271–272
 driver-vehicle relationship
 control: the driver’s contribution, 374, 375
 generalized block diagram and discussion, 124–125
 response augmentation, driver, 375, 376
 Roy Rice comment on, 345
 Stirling Moss comments on, 219, 374
 and vehicle motion behavior, 374–375
 friction circle cornering example, 60–61

and “g-g” diagrams. *See under* “g-g” diagrams
 race-driving techniques (and MMM diagram), 312–313
 spin recovery (RWD), 267, 269–272
 and understeer, 229
See also Stability and control, transient
Durometer readings (Goodyear racing tires), 81
Dye, Ed
 photo of, 470
Dykstra, Lee
 paper on CART car wing aerodynamics (Ref. 76), 515

Elastic distortion, tire, 20
Elementary automobile, 126–127. *See also* Damping; Stability and control, steady-state
Equations of motion. *See under* Stability and control, steady-state

Fackrell, J.E.
 flow around exposed wheels (Ref. 44), 568
Ferguson Formula (viscous differential), 746–748
Fiala, E.J.H.
 paper on passenger comfort (Ref. 24), 785
Firestone tires, tests of (on Chaparral G.S. 2G), 508–510
Fisher, L.P.
 comment on Olley research expense, 418
Fitch, John
 and Watkins Glen, Lime Rock, analyses, 340
Fonda, Albert G.
 and Air Force tire tester, 429
 Corvette “g-g” diagram (1958), 361–362
 early friction circles (Avon data), 359–361
 paper on pneumatic trail vs. tire behavior (Ref. 47), 359, 361
 photo of, 470
 and tire-as-damper analogy, 185
Footprint. *See* Print
Force-moment analysis. *See* MMM (MRA Moment Method)
Four-wheel drive. *See under* Drive types
Fraction Load Transfer (FLT). *See under* Pair analysis
Friction, coefficient of, 26
Friction circles
 introduction and description, 57–59
 cornering example (monocycle), 60–61

and “g-g” diagram, 60, 61, 346–347
 typical plots
 passenger car tire (Sakai), 58
 racing tire performance, 59
 and vehicle performance limitations, 346
Front-wheel drive. *See under* Drive types
Fuchs, Henry
 member of Olley Cadillac Group (1934–39), 419
Fukushima, N.
 paper on shock absorbers vs. driving conditions (Ref. 48), 786

gAnalyst®, 357, 359
George, A.R.
 studies on ground effects (Ref. 50), 528–533
“g-g” diagrams
 introduction, 8–11
 conceptual development, 345–348
 Corvette “g-g” diagram (Fonda, 1958), 361–362
 driver performance comparison, 348–349
 and driver “willingness,” 348
 early friction circles (Fonda, Avon data), 359–361
 effect of speed (measured race-car, Belle Isle), 356–359
 full “g-g” diagram cornering technique (Donahue comment on), 364
 and gAnalyst®, 357, 359
g-force, defined, 8
Isuzu Motors “g-g” diagrams (ca. 1970), 364–366
 measured race-car performance (Wright, Team Lotus), 354–357, 360
 measurements on Grand Prix car, 10
 Mercedes race car circuit analysis (Moss comment on), 340
 and task performance quantification, 348
 and vehicle capability
 calculated “g-g” boundaries (Segal), 350, 352–354
 experimental vs. analytical evaluation, 350–351
 trim change sensitivity, 354
See also Aerodynamics, applied
GM (General Motors)
 aerodynamics research at (Bidwell), 436
 Bidwell heads Engineering Mechanics Department, 429

constrained testing at
 checkerboard test (Ken Stoner), 421
Chevrolet/Chaparral testing, 452–453
constrained linear test (railcar, Chevrolet),
 296–297, 299
in Corvair investigation, 444–447
1G/100mph skid pad, 447
Maypole test (1950), 296, 298
simulated roadability test (Chevrolet,
 1963), 296, 298
Corvair. *See* Corvair, controversy over
development of experimental techniques
(Bidwell), 438
flat bed tire tester, development of, 435
human factors group at, 434–435
IFS, Olley pioneering work on, 418
K² Rig (Olley design), 417–418
Olley group at Cadillac, accomplishments of,
 418–420
racing activities, halting of, 444, 448–449
research group activities (1934–39), 418
research program at CAL. *See under* CAL
(Cornell Aeronautical Laboratory)
ride simulator, construction of, 434
Schilling awards research contract to CAL/
WFM (1935), 415
skid pad testing at, 420, 421
SLA suspension problems at (1935), 415
stability and control tests (Lotus, go-kart), 447
step steering research (with Bob Schilling), 421
tire testing facilities, 445–447
“Unicontrol” steering system, 436
Variable Response Vehicle, 437, 439
Variable Stability Automobile, 439
Winchell appointed VP Engineering, 439
See also Chevrolet-Chaparral racing
Goodyear tires, tests of
 aligning torque vs. slip angle, 76–80
cornering stiffness, 81–82
Eagle GT-S
 aligning torque vs. slip angle, 30
 lateral force vs. load, 29
 lateral force vs. slip angle, 25–27
 rim force vs. trail, 33
Eagle P225/70 R15
 lateral force vs. camber (constant load),
 53–54
 peak lateral force vs. camber (variable
 load), 49
 peak side force vs. camber (variable load),
 49

Eagle P225/50 VR15
 in MMM sports car tests, 328–332
lateral force vs. slip angle, 76–80
rubber durometer readings (typical racing
tires), 81
Gough, Eric, 20
Gough testing
 Gough testing machine, 20–22
 typical data, high slip angle, 22, 23
Grandpaw Throttlebottom (George Collier)
 drifting, comment on, 231
Granville, “Granny”
 aircraft speed, comment on, 83
Grylls, Harry (Rolls-Royce)
 understeer vs. English country roads, com-
 ment on, 279
Guest, J.J.
 paper: *The Main Free Vibrations of an
Autocar* (1925, Ref. 54), 783
Gurney lip, 552–553

Hall, Jim
 (*Car & Driver*) article (Ref. 57), 441
photo of, 440
and Rattlesnake Raceway, 442
variable stability airplane course (CAL), 441
Harper, John J.
 on trips and transition strips (Ref. 119), 553–
 554
Harvey, J.K.
 flow around exposed wheels (Ref. 44), 568
Heading angle, 118
Hegel, R.
 paper on air shock leveling (Ref. 58), 785
 paper on Monroe electronic air-spring
 dampers (Ref. 59), 785–786
Herman, Bob
 single-lane traffic flow analysis, 435
Hidaka, K.
 paper on shock absorbers vs. driving condi-
 tions (Ref. 48), 786
Hodkin, David
 and MIRA (England) tethered testing, 297
Hodkin, Richard
 and damper characteristics (in Ref. 51), 785
Hucho, W.H.
 Porsche 911 Carrera aerodynamic data, 496,
 498
Hunt, O.E.
 and IFS implementation, 418

HVOSM (Highway Vehicle-Object Simulation
Model), 273, 460

IME (Institution of Mechanical Engineers)
 presentation of CAL papers (Milliken, et.al.,
 1956), 430–431

Inclination angle
 vs. camber angle, 46, 63
 defined (SAE), 46, 62
 See also Camber

Induced drag. *See under* Tire behavior

Inertia coefficients, 241–242

Installation ratio, suspension springs, 595–600

ISO standards/specifications
 7401–1988 *Road Vehicles - Lateral Transient
Response Test Methods*, 260–261
 Technical Committee/Subcommittee TC22/
 SC9, 210

Isuzu Motors Ltd.
 “g-g” diagrams from (ca. 1970), 364–366

Iwata, K.
 paper on shock absorbers vs. driving condi-
 tions (Ref. 48), 786

Jacking
 diagonal weight jacking, 281–282
 jacking down (from rebound damping), 821
 jacking forces (in rear-suspension swing
 axles), 638
 and roll center height, 614–615

Jackson, G.W.
 paper on direct acting shock absorber (Ref.
 67), 784

Janeway, R.N.
 ride and vibration data manual (Ref. 68), 784
 text on shock and vibration control (Ref. 69),
 784

JARI (Japan Automobile Research Institute). *See*
 Sakai

Jounce
 and installation ratio, 596–597
 jounce travel and ride rates, 587–588

J-turn test (SAE), 301–302

Julien, M.A.
 paper on suspension problems (Ref. 74), 784

Junkers Aircraft
 tire model, structural, 424

Kamm, W., photo of, 470

Katz, Joseph

modeling of three-dimensional airfoil shapes,
 520–521

papers on automotive aerodynamics (Refs.
 75–77), 515

Kettering, Charles “Boss”
 and IFS implementation, 418

Kickback, steering. *See under* Steering systems

Kidd, Ed
 at CAL Transportation Division, 439

Kingpins. *See* Steering systems; Suspension
 geometry

Knudsen, Bill
 and IFS implementation, 418

Kohr, Bob
 and GM vehicle dynamics research, 433
 and vehicle dynamics models, 434, 437

KONI dampers, 820–822, 829

Koppen, Otto
 on controlled stability, 815

Kunkel, Dennis
 and MMM (MRA Moment Method) develop-
 ment, 293
 papers on MMM testing of DK-4 and MX-1
 vehicles, 466

Lachmann, G.
 use of slots and slats (ca. 1927), 512

Lap Time Simulation, 3–4, 340–343, 356–359,
 364–366

Lateral acceleration
 and C_N-A_Y diagrams (MRA Moment
 Method)
 building the diagram, 301–302
 Chaparral GS-2G tests, 319–326
 example: RH turn, RL power, 304–306
 example: sports car chassis tuning, 327–
 332
 force-moment diagram for, 303–304
 typical four-quadrant MMM diagram,
 307–308

and dampers, 814–816
 vs. driving thrust (2DF), 221–223
expressed as g force, 8

vs. Fraction Load Transfer (FLT)
 Ackerman steer, 285–286
 motorcycle tire (reverse Ackermann
 steer), 290, 292

and lateral velocity, 7

response times (from steering inputs), 261–
 264

and ride rate design example, 586–587

and ride/roll steer, 397, 407
 vs. roll angle (MRA Moment Method), 329
 vs. steer angle δ (steady-state cornering)
 neutral steer, 132–133
 oversteer, 141–142
 understeer, 139
 skid pad test, typical, 383–384
 vs. tire slip angle α (steady-state cornering)
 neutral steer, 130–134
 oversteer, 140–143
 understeer, 135–140
 vector representation of, 5–7, 9
 vs. vehicle slip angle β (NS), 221–223
 vs. yaw velocity (VDS test correlation), 274, 276
See also “g-g” diagrams; MRA Moment Method (MMM); Pair analysis, steady-state; Tire behavior; Stability and control (steady-state, transient)

Lateral force
 vs. camber, 50–54
 derivative notation for, 149–150
 lateral force compliance camber (front, rear), 836
 load sensitivity, tire, 27–28
 vs. load (various slip angles, Eagle GT-S), 28, 29
 mechanism of (in elastic range), 17
 nondimensional, 475
 normalized curves for
 vs. normalized slip variable, 483–484
 vs. normalized slip/camber angle (various camber angles), 480–482
 vs. normalized tire slip angle (various loads), 475–477
 vs. tire slip angle (Eagle GT-S), 26–27
 orientation of, geometric (SAE), 15
 resultant force
 derivation of, 482–483
 vs. normalized slip variable, 483–484
 vs. resultant slip velocity (Sakai), 44–46
 speed independence (in elastic range), 22
 and steady-state cornering (NS car), 130–132
 tire print characteristics (Gough test data), 22–23
 vs. tire slip angle α
 introduction and discussion, 19–20
 at constant load (Eagle GT-S, TIRF data), 24–25
 at constant/variable slip ratios (Sakai), 41–43

in 2DF bicycle model, 148–149
 model tires, MRA Moment Method, 302–306
 normalized curves for, 26–27, 475–477
 for racing tire, 314
 steady-state cornering, neutral steer, 129–131
 steady-state cornering, oversteer, 140–142
 steady-state cornering, understeer, 135–138
 various loads (Goodyear data), 76–80
 various loads (Goodyear GT-S, TIRF data), 25–29
See also normalized curves for (above)

vs. tractive forces
 analysis of, general, 63–66
 braking force (various slip angles), 484–485
 longitudinal force (various slip angles), 484–485
 racing car, steady-state turn, 221–223
 vs. vehicle slip angle β
 model tires, MRA Moment Method, 305–306
 vs. wheel load variations, 814
See also Friction circle; MMM (MRA Moment Method); Stability and control (steady-state, transient); Tire behavior

Lateral load transfer (LLT). *See* Pair analysis, steady-state; Ride and roll rates; Wheel loads

Lateral velocity
 and lateral acceleration, 7
 tire (2DF model), 146–148

Ledwinka, Hans
 and early IFS research, 418

LeFevre, W.
 ride and vibration data manual (Ref. 68), 784

Leffert, R.L.
 paper on cornering compliance (Ref. 28)

Limit behavior. *See under* MMM (MRA Moment Method)

Limited-slip differentials, 740–745

Lind-Walker
 paper on neutral steer concept, 421–422

Load transfer. *See* Pair analysis; Stability and control, transient; Wheel loads

Longitudinal force, normalized
 vs. normalized slip ratio, 479–480

Lotus, active suspension system, 469–470

Lotus 88: double suspension and banning, 468
 Lotus 78 F.1 ground-effect cars, 491
Team Lotus
 in-car instrumentation system for, 468
 Peter Wright Research Director, 468
LTS (Lap Time Simulation), 343

MacPherson struts. *See under* Suspension geometry

Magic formula (for nondimensionalization), 476

Marcell, G.P.
 paper on front spoiler shapes (Ref. 86), 496, 497

Matthews, Charles
 balancing the car (aero and mechanical forces), 572

Mays, Raymond
 diligence, comment on, 373

McHenry, Raymond
 background and experience, 459–560
 and HVOSM, 273, 277, 560
 McHenry model (and spiral jump), 272–273, 458
 receives medal, award, 460

Metz, D.
 Indy car drag coefficients (Ref. 90), 542
 wind tunnel tire tests (Ref. 90), 570

Miller FWD Indy cars, 730

Milliken, Douglas
 and MRA Moment Method development, 293
 and VDS model development, 276

Milliken, Peter
 and Pathopt, 341

Milliken, William F.
 and Air Force tire tester, 428
 and application of static concepts, 206
 attends variable stability airplane course at CAL, 441
 attends Winchell handling dynamics seminar, 441
 becomes consultant to Chevrolet, 441
 contract with GM, 415
 force-moment concept, original proposal at CAL, 293
 IME papers, presentation of (1956), 430–431
 Manager of CAL Vehicle Dynamics Department, 429
 meeting with Winchell, 439–440
 paper on directional stability and control, 466
 photo of, 440, 470
 service at CAL, 414–415

and Type 35 Bugatti, 414
 and Watkins Glen analysis, 341
 Winchell appreciation of, 443

MIRA (England)
 Olley advice to, 421
 tethered testing at, 297, 299

Mitchell, Bill
 and Chaparral 2 body profile, 454
 and Monza XP777, 447–448
 personality and philosophy, 454

Mitschke, M.
 paper on suspension model dynamics (Ref. 96), 784–785

MMM (MRA Moment Method)
 approach, 294
 description, general, 294
 original force-moment concept proposal, 293, 463–464
example: Chaparral GS 2G
 introduction and run list, 319–320
 “aero configuration” of, 320
 baseline diagram (40 mph, RL, trimmed), 320–322
 condition #2: (100 mph, RL, trimmed), 322–323
 condition #3: (100 mph, 0.66g, trimmed), 323–324
 condition #4: (1.0g braking, trimmed), 324
 condition #5: (change in LLT, trimmed), 325
 condition #6: (aero downforce), 325–326
example: sports car chassis tuning
 vehicle description and parameters, 327–328
 baseline configuration, 328–329
 roll angle vs. lateral acceleration, 329
 first N-A_Y diagram (manual plot, at CAL), 465
 genesis of
 in CAL memo (1952), 293
 in DK-4 model, 274, 461

lap time analysis
 introduction and discussion, 340–341
 Formula 1 performance envelope (c. 1971), 342
 Formula 1 performance profile (Watkins Glen), 342
LTS (Lap Time Simulation), 343
 Pathopt (Path Optimizer), 341
 RCSIM (Race Circuit Simulation), 341

limit behavior
 introduction, 313
 aircraft analogy for, 315–316
 final under/oversteer, 314–315
 force-moment envelopes (limit characteristics), 318–319
 idealized cornering force curve, 316
 stability and control, 313–315
 trim at the limit, 315
 under/oversteer, conceptual discussion, 313–315

limit behavior (sports car example)
 baseline rescaled, 334–335
 friction circle, 338–339
 vehicle changes and summary of results, 335–337

moment method diagrams (C_N - A_Y)
 building the diagram, 301–302
 Chaparral GS-2G tests, 319–326
 example: RH turn, RL power, 304–306
 example: sports car chassis tuning, 327–332
 force-moment diagram for, 303–304
 four-quadrant diagram, typical, 307–308
 maneuvering on the diagram, 309, 312–313
 steady-state, defined, 308–309
 summary of MMM diagrams, 310–311

post-processing: sports car example
 friction circle, baseline, 333–334
 stability index, 330, 331
 steer angle response, 329, 331
 steering sensitivity (GM), 330, 332
 trimmed sideslip, 330, 331
 understeer gradient, 330, 332
 test results: importance and scope, 301, 465–466

See also Constrained testing; “g-g” diagram

Model tire. *See* Tire behavior

Moments
 force-moment analysis. *See* MMM (MRA Moment Method)
 force-moment coefficients (aerodynamic), 110–111
 rolling, nonrolling, 614
 in Vehicle Axis System (SAE), 119
 yawing moment. *See under* Yaw
See also Stability and control (steady-state, transient); Steering systems; Suspension geometry; Trail

Monkhouse, George
 on Nuvolari racing, 231

Monza XP777
 Jim Musser project engineer, 447
 Larry Shinoda body design, 447

Morelli, Alfredo
 flow around exposed wheels (Ref. 98), 568
 Morelli basic body shape, 541–542

Mortimer, Rudy
 and GM human factors group, 434–435

Moss, Stirling
 comment on Mercedes race car circuit analysis, 340
 comments on race driving, 219, 315, 374
 gives testimony re Corvair, 449

Motorcycle tires
 and camber, 47
 FLT vs. A_Y (reverse Ackermann steer), 290, 292

Moulton, Alex
 and Hydrolastic/Hydragas dampers, 782

Moyer, Ralph
 skid resistance measurements (ca. 1934), 419

MRA (Milliken Research Associates)
 Lap Time Simulation (LTS) program, 3–4
 Vehicle dynamics, steady-state (Vehicle Dynamic Simulation), 274–276
See also MMM (MRA Moment Method)

MTS Flat-Trac Roadway Simulator, 300–301

Musser, Jim
 Monza XP777 project engineer, 447
 photo of, 440
 stability tests at Waterford, 447

Muto, Shinri
 radiator duct analysis (Ref. 106), 557–558, 559

Muzey, Cliff
 and Air Force tire tester, 428–429

NACA airfoil data, 497, 500

Nader, Ralph, 444

Neutral steer. *See under* Stability and control, steady-state

NHTSA (National Highway Traffic Safety Administration)
 safety proposals of, 435

Nissan
 Vehicle Research Laboratory
 damper requirements examination (Ref. 48), 786
 damping ratio vs. operating conditions (Ref. 156), 786

Nordeen, Don
 and GM flat bed tire tester, 435

and vehicle dynamics models, 437
 Novi FWD Indy car, 730
 Nuttall, Cliff
 photo of, 470
 Nuvolari, comment on, 231

Oldfield, Barney
 and plow (in FWD Christie car), 730

Olley, Maurice
 boyhood and early years, 416
 comments
 on aircraft vs. automotive design approach, 123
 on automotive design, 367
 on IFS and tire tests, 13
 on piecemeal car design, 422
 on suspensions, 579
 definitions
 over/understeer, 167–169
 slip angle steers, 168–171, 227
 at GM
 activities at Cadillac, 417–418
 first independent front suspension, 418
 K² Rig (Olley design), 417–418
 “million dollar” test cars, 418
 Olley group (1934–39), 419
 Olley group (1952), 415
 “Olleyisms,” 420–421
 skid pad testing, 420
 SLA suspension, camber effect of, 419
 step steer research, 421
 and independent suspensions, 709
 papers
Independent Wheel Suspension... (1934), 418
Road Manners of the Modern Car (1946), 421
Suspension and Handling (1937), 419–420
 photo of, 416
 at Rolls-Royce, 417
 WFM appreciation of, 422
 Winchell appreciation of, 443

Olson, Paul
 and GM human factors group, 434–435

On-board instrumentation
 Chevrolet-Chaparral, 450–452

Oswald, W.C.
 ride and vibration data manual (Ref. 68), 784

Oversteer, *See under* Stability and control, steady-state; *See also* MMM (MRA Moment Method)

Page, Handley
 use of slots and slats (ca. 1927), 512, 518

Pair analysis, steady-state
 introduction, 279–280
 axle pair analysis curves
 camber, effect of, 290
 drive torque, effect of, 291
 roll rate and center height, effect of, 290
 static CG height, effect of, 291
 static toe, effect of, 291

Fraction Load Transfer (FLT)
 defined, 284
 vs. lateral acceleration (cornering coefficient), 285–286
 vs. lateral acceleration (motorcycle tire, reverse Ackermann steer), 290, 292
 lateral force potential diagram, 285
 and lateral load transfer, 285
 and MRA program for axle pair analysis, 287–291

lateral acceleration
 vs. FLT and Ackermann steer (cornering coefficient curve), 285–286
 vs. FLT and reverse Ackermann steer (motorcycle tire), 290, 292

lateral force potential diagram, 285–286

lateral load transfer (LLT)
 discussion, 289–291
 and FLT, 285
 and ride spring rates, 409
 and track width, 408
 and vehicle performance, 346

MRA computer program for
 introduction and development, 287–288
 example: sports car calculations, 288–291

procedure for calculating, 283–286

track performance, factors affecting
 anti-roll bars, 281
 cambers, 282
 diagonal weight jacking, 281–282
 engine torque reaction, 282
 geometric steers, 282
 load transfer (lateral, longitudinal), 280
 roll couple distribution, 281
 shock absorbers, 283
 slip ratio, longitudinal, 282–283

stagger, 282
 static wheel loads, 280
 suspension springs, 283
 wedge, 281–282
 Z-bars, 281

Past, remembering the (Santayana), 439

Pathopt (Path Optimizer), 341

Penske, Roger
 and aluminum Chevy block, 448
 and Cooper F1 MERD, 448

Penske dampers, 829, 830–831

Pirelli
 exposed wheels
 aero forces and moments for, 570
 drag coefficients for, 569–570

Platt, Maurice
 appraisal of Olley IFS work, 421
 and early IFS research, 418
 heads Chevrolet R&D section, 421

Plow
 and FWD limit understeer, 730

Ply steer, tire, 57

Pope, Alan
 on trips and transition strips (Ref. 119), 553–554

Pressure, tire
 and aligning torque, 55
 and cornering stiffness, 54–55
 ride, effect on, 55
 and tire drag, 55
 and tire temperature, 56

Pressure measurement, air. *See under Aerodynamics*, basic

Pretz, Phil
 and Olleyism, 420

print. *See under Tire behavior*

Race car design
 introduction: resources vs. expectations, 367–368
 constraints, defined, 368
 design objectives, 368–369
 design process
 approach, 369–370
 preliminary design, 370–371
 setting up: the difficult problem, 372
 specific design areas, 372
 stress analysis and reliability, 372
 wind tunnel testing, 371

Racing
 race circuit, speed/distance simulation of, 3–4

technical objective of, 3

Radt, Hugo S.
 paper on skidding, 266
 and SVDM development, 272

Rao, D.M.
 Rao slots, 553–554

Rasmussen, Dick
 and development of experimental techniques (GM), 438

Rathgeb, Larry
 comment on springs, 755

RCSIM (Race Circuit Simulation), 341, 343

Rear-wheel drive. *See under Drive types*

Resultant force
 derivation of, 482–483
 vs. normalized slip variable, 483–484
 vs. resultant slip velocity (Sakai), 44–46
See also Lateral force

Resultant force (tire)
 vs. resultant slip velocity (Sakai), 44–46

Rice, Roy S.
 and application of static concepts, 206
 comments
 on driver performance, 345
 on friction circles, 346, 348
 Moment Method, accolade for, 293
 and MMM (MRA Moment Method), 465–467
 photo of, 464

Ride and roll rates
 introduction and definitions, 579–581
 anti-roll bars
 action of, 281
 installation ratio for, 599–600
 and low lateral acceleration, 410
 roll bar rate, additional, 592
 roll bar rate, intrinsic, 600
 and turn stability, 410

design example (independent suspension)
 anti-roll bar rate, additional, 592
 anti-roll bar rate, intrinsic, 600
 CG calculation, 586
 jounce travel, 587–588
 lateral acceleration, 586
 lateral load transfer, 587, 590
 ride frequencies, 588–589
 ride rates, 588
 roll gradient, calculated, 586, 590
 roll gradient, defined, 582
 roll gradient, typical values of (table), 584
 roll rates, 585, 589
 US/OS, caution regarding, 591
 wheel loads, 587, 590

wheel ride displacements, 590
See also Wheel loads

design example (simplified)
 description and assumptions, 601, 603
 ride rate, 601
 road circuit cars, general characteristics for, 605
 roll stiffness, 603–605
 rolling moment, 603
 spring rates, 602
 sprung mass analysis, 602–603
 total load transfer, 604
 wheel center rate, 602

design example (solid axle)
 difficulties in calculating, 592–593
 lateral load transfer, 594
 roll gradient, 594
 roll rate, 593–594
 vertical axle rate, 593
 wheel loads, 595

geometric rate
 defined, 596
 and installation ratio, 596

installation ratio
 for anti-roll bars, 599–600
 defined, 595
 and geometric rate, 596, 597
 for linear springs, 598–599
 vs. ride travel (double wishbone), 595–596
 for torsional springs, 599
 and wheel rate, 581, 596–597

jounce
 and installation ratio, 596–597
 jounce travel and ride rates, 587–588

ride frequency
 vs. static wheel deflection, 583
 undamped: various vehicle classes, 582

ride quality (sports vs. race cars), 580

ride rate
 defined, 581
 and rough road behavior, 399
 and secondary chassis set-up, 409–410
See also design examples (above)

roll rate, 581
 defined, 581
 establishing: need for iteration, 584
 methods of expressing, 581–582

roll stiffness
 normalized expression for, 582
 and secondary chassis set-up, 410–411
 typical values (from g-Analyst®), 584

SKAT program (for linear spring IR), 598–599

spring rate
 defined, 580–581
 methods of describing, 581–582

tire rate, defined, 581, 591–594

wheel center rate
 additional, from anti-roll bar, 592
 calculated, 591–592
 defined, 581, 591
 vs. installation ratio, 581
 vs. spring rate and IR (table), 597

wheel deflection
 vs. undamped natural frequency, 582

wheel travel
 various vehicle classes, 582

Z-bars, action of, 281
See also Roll; Wheel loads

Ride steer. *See under Steering systems*

Rim force, steering wheel
See Steering systems; Trail

Roland, R. Douglas
 and DK-4 advanced vehicle dynamics model, 273, 460

and MMM (MRA Moment Method) development, 293, 465

photo of, 464
 and Watkins Glen analysis, 341

Roll center
 force definition, 680
 kinematic definition, 613–614

Roll steer. *See under Steering systems, ride steer*

Rolling resistance. *See under Tire behavior*

Rollings, “Coach”
 race start, comment on, 113

Rolls-Royce, Maurice Olley at, 417

Romberg, G.F.
 paper on front spoiler shapes (Ref. 86), 496, 497

Rose, Mauri
 stability tests at Waterford, 447

Rough road behavior
 and bump steer, 398–399

cornering
 and roll understeer, 407
 and spring rate, 410
 and track width, 409

dampers, effect of, 399

and ride height, 399

and ride rate, 399

and roll stiffness, 411

spring rates, importance of, 410

tracking
and track width, 408
and understeer, 401
traction and differential type, 408
and trail, 398
Rough road behavior cornering
cornering
US configuration: CG set forward, 401
Rowell, H.S.
seminal paper: *Principles of Vehicle Suspension* (1922, Ref. 134), 783
Royce, Sir Henry
comment on engineering materials, 833
Rudd, Tony
metric dampers, comment on, 824
torsional stiffness, comment on, 373

Saab FWD (1955), 730
SAE standards/specifications
J1594 (*Vehicle Aerodynamics Terminology*)
aerodynamic axis system, 109–110
downforce (negative lift) in, 15
sign conventions (vs. tire axis system), 119–121
J670e (*Vehicle Dynamics Technology*)
development of (Joe Bidwell, et al.), 433
slip ratio, defined, 37, 39, 40–41
slip ratio (SAE vs. Sakai conventions), 41
slip velocity, longitudinal (defined), 36–37
tire axis system, 15, 61–63
XJ266 (*Proposed Passenger Car and Light Truck Directional Response Test Procedures*)
and Moment Method testing, 301–302
SAE Technical Committees
Joe Bidwell comment on, 433–434
Ride Comfort Research Committee, 434, 784
Vehicle Dynamics Committee, 434, 784
Sakai (JARI)
Friction circle, passenger car tire, 55–56
slip ratio
defined, 40
vs. lateral force (various slip angles), 42, 43
vs. resultant force, slip velocity, 44–46
SAE vs. Sakai conventions, 41
vs. tractive/braking force (various slip angles), 41–42, 44
Salisbury axle (Dana), 741, 742–743
Santayana, George, 439
Satchell, Terry

balancing the car (aero and mechanical forces), 572
Schenkel, Max
and wind-tunnel boundary layer control, 526
Schilling, Bob
accolade for Olley IFS development, 418
and directional control equations, 433
and GM step steering research, 421
paper on handling factors, 421
photo of, 432
supports research contract with CAL and WFM (1935), 415
Scrub radius
and bump steer, 398
as function of instant center (IC) height, 616
and high-speed stability, 405
and kingpin inclination angle, 398, 710–711
negative, in FWD, 398, 400, 404, 711–712
and parking-lot-speed steering force, 399–400, 720
and power steering, 720
and rough-road tracking, 400, 616
and steering kickback, 400, 405
and steering wheel rim force, 400, 405
See also Chassis set-up; Steering geometry
Segal, Dave
and HVOSM, DK-4, models, 461
and MRA Moment Method development, 293, 461, 467
and RCSIM-2, 3432
and VDS model development, 276
Segel, Leonard
and CAL's GM research program, 423–427.
See also CAL (Cornell Aeronautical Laboratory)
paper on CAL/GM Variable Stability Automobile, 439
photo of, 423, 470
and publication of GM basic research, 429–430
Set-up. See Chassis set-up
Sharp, Hap
and Chevrolet-Chaparral racing, 442
photo of, 440
WFM appreciation of, 442
Shinoda, Larry
Monza XP777 body design, 447
Shock absorbers
See Dampers
Side force, tire. See Lateral force, tire
Sideslip angle. See Slip angle, vehicle (β)
Sign conventions

in vehicle axis systems, 119–120
Simanaitis, Dennis J.
and drag coefficient tests, 542–543
SKAT program (for linear spring IR), 598–599
Skid. See Steering systems; Tire behavior (breakaway)
Skid pad testing. See Constrained testing
Slip angle, tire (α)
vs. aligning torque
effect of camber, 46–47
Goodyear test data, 76–80
normalized curves for (various loads), 474–477
and pneumatic trail, 28–30
vs. braking/tractive force (Sakai), 41–42, 44
Broulheit, George, papers by, 418–419
and cornering stiffness
Goodyear data, 81
for model tires (MRA Moment Method), 302–304
defined, 17–18
and Gough testing, 22, 23
vs. lateral acceleration (steady-state cornering)
neutral steer car, 130–134
oversteer car, 140–143
understeer car, 135–140
vs. lateral force
introduction and discussion, 19–20
at constant load (Eagle GT-S, TIRF data), 24–25
constant/variable slip ratios (Sakai), 41–43
in 2DF bicycle model, 148–149
model tires, MMM (MRA Moment Method), 302–306
normalized curves for, 26–27, 475–477
for racing tire, 314
steady-state cornering, NS car, 129–131
steady-state cornering, OS car, 140–142
steady-state cornering, US car, 135–138
various loads (Goodyear data), 76–82
various loads (Goodyear GT-S, TIRF data), 25–29
and model tire behavior, 17–18
vs. resultant force, slip velocity (Sakai), 44–46
slip angle steers (Olley definitions), 168–171, 227
slip/camber angle
defined, 480
vs. normalized lateral thrust, 480–481
vs. steer angle δ
steady turn, 266–267

step steer input, 267–268
and tire drag, 64–66
and Vehicle Axis System, 119–120
walking analogy to, 18–19
and yaw moment equilibrium, 130–131
See also Friction circle; MMM (MRA Moment Method); Stability and control (steady-state, transient)
Slip angle, vehicle (β)
and control response, 155
defined, 118, 131
front- vs. rear-wheel driving force
steady turn, 266–267
step steer input, 267–268
geometry of (2DF model), 127, 131
vs. lateral acceleration, 221–223
spin recovery, rear-wheel driving force, 267, 269–272
vs. steering angle δ
oversteer car, 140–142
understeer car, 136–137
vs. tire slip angle α .
for model tires (MRA Moment Method), 303–305
Slip ratio
vs. braking/tractive force
Sakai test data, 41–42, 44
TIRF test data, 37–39
conventions for (SAE vs. Sakai), 41
defined, 39–41, 479
and longitudinal slip velocity, 36–37
normalized
defined, 479
vs. normalized longitudinal force (various loads), 479–480
vs. resultant force, slip velocity (Sakai), 44–46
servo measuring systems for, 37, 39
and tire instability (spin-up, lock), 37
See also Friction circle
Slip velocity
longitudinal
SAE definition for, 36–37
and slip ratio, 37
resultant
vs. resultant force, slip ratio (Sakai), 44–46
Smith, Carroll
on air entrances (Ref. 149), 556
comment on friction dampers, 781
and KONI dampers (Refs. 148–150), 820
Sorenson, R.L.
paper on air-spring dampers (Ref. 59), 785–786

Speeds, significant. *See under Stability and control, steady-state*
 Spin recovery
 rear-wheel driving force, 267, 269–272
 See also Stability and control, transient
 Spiral jump (McHenry model), 272–273, 458
 Spring-mass-damper system. *See Dampers;*
 Stability and control, transient
 Spring selection. *See Ride and roll rates*
 Springs, automotive. *See Suspension springs*
 Sprung mass, 115, 671
 Stability and control, steady-state
 acceleration, components of (in vehicle axis system), 117–118
 Ackermann steering angle
 Ackermann speed, 174
 vs. Ackermann steering (classic), 129
 and characteristic speed, 181–182
 and critical speed, 181
 described, 128–129
 in neutral steer, 158–159
 steering angle gradient, 164, 211–212
 automotive vs. aircraft practice, 206, 228
 Bundorf cornering compliance
 derivation of, 172, 227–228
 discussion of (Bidwell), 437–438
 and Olley view of understeer, 419
 and tangent speed, 176–177
 and understeer gradient, 172–173
 control
 control moment components (table), 183
 and static stability (discussion), 191–192
 cornering dynamics (2DF, NS), 130–133
 cornering geometry (2DF model), 128–129
 damping, tire
 damping analogy, 184–186
 damping center, 187–188
 damping-in-sideslip, 188–189
 damping-in-yaw, 189–190
 and generalized yaw moment, 190–191
 and static margin, 188
 tire damper side force (2DF model), 187
 derivative notation
 and equations of motion, 149–150
 physical significance of, 151–153
 and track effects (front, rear), 173
 driver-vehicle relationship, 124–125
 elementary automobile, defined, 126–127
 equations of motion
 introduction, 144
 derivative notation for, 150
 terminology and symbols for (table), 145

See also lateral force, yawing moment (below)
 general conclusions on steady-state, 224
 geometric steer
 cornering geometry, 128–129
 discussion of, 143
 lateral acceleration
 vs. driving thrust, 221–223
 vs. slip angle α (NS), 130–134
 vs. slip angle α (OS), 140–143
 vs. slip angle α (US), 135–140
 vs. steer angle δ (NS), 131–132
 vs. steer angle δ (OS), 141–143
 vs. steer angle δ (US), 139
 vs. vehicle slip angle β (NS), 221–223
 lateral force
 derivative notation for, 149–150, 152–153
 vs. steer angle δ (US), 136–139
 vs. vehicle slip angle β , 148–149
 lateral velocity
 of front, rear, tires, 147–148
 for steady turn, 146
 in transient maneuver, 146–147
 vector geometry of, 127
 neutral steer, 130–132
 Ackermann relationship, 158–159
 applied side force, response to, 157–158
 applied yawing moment, response to, 158
 control response characteristics, 157
 cornering dynamics of (constant δ), 130–132
 and critical speed, 178
 defined, 132, 168
 neutral steer point (2DF model), 164–166
 Olley definitions, 168, 169, 227
 stability index (variation with V), 208
 steady-state cornering: definitions and constraints, 129
 steer behavior, summary of, 159–160
 on tilted road, 133–134
 vehicle slip angle, 131
 See also lateral acceleration (above)
 oversteer
 conceptual discussion of, 313–315
 cornering dynamics of, 140–141
 and critical speed, 178–181, 226–227
 defined, 140, 142, 164, 168
 Olley definitions, 168, 169, 227
 oversteer “spring,” 151–152
 path curvature, yawing velocity, response, 162–163
 stability factor K, 161–164

Stability and control, steady-state (*continued*)
 oversteer (*continued*)
 stability index (variation with V), 209–210
 on tilted road, 143, 168
 See also lateral acceleration (above)
 parallel steer, 129
 path curvature
 general curvature response, 160–161
 and induced slip angles, 201–202
 path radius vs. thrust, 220–223
 and stability factor K, 161–164
 stiffness, steady-state, 201–202
 stiffness and yaw damping, 202–204
 position control vs. force control, 126–127
 pull, 57
 response, nonlinear
 vs. driving thrust, 221–223
 introduction, 215, 217–219
 and steer angle, 215, 217–218
 and tire forces, 221–223
 and understeer gradient, 215, 217
 response, steady-state
 Ackermann gradient angle in, 211–212
 to applied side force, 155–156
 to applied yawing moment, 156–157
 constant radius/variable speed tests, 211–213
 constant speed/variable radius tests, 211–213
 control response characteristics, 154–155
 sports, passenger, cars (typical), 214
 speeds, significant
 Ackermann speed, 174
 characteristic speed, 181–183, 184–185
 critical speed, 177–181, 184–185
 tangent speed, 174–177
 stability balance and vehicle performance, 346
 stability factor K
 and critical/characteristic speeds, 184–185
 derivation of, 162, 225–226
 and path curvature response (US/OS), 162–164
 and static margin, 170–171
 and yawing velocity response (US/OS), 162–164
 stability index
 derivation of, 204–205, 228
 variation with velocity, 208–210
 static margin
 and cornering stiffness (Dell’Amico), 206–207
 derivation of, 166–167, 225
 See also lateral acceleration (above)
 understeer gradient
 and Bundorf cornering compliance, 172–173

and stability factor K, 170–171
 and [tire] damping center, 188
 static stability
 and control (discussion), 191–192
 vs. direction of travel, 198
 front- vs. rear-wheel blowout, 199
 and neutral steer, 194–195, 198
 and oversteer, 197–198
 vs. slip angle disturbance, 198–199
 and trim, 192–194, 197
 and understeer, 195–197, 198
 steering sensitivity
 of Grand Prix car, 215, 216, 218–219
 linear sensitivity, derivation of, 214–215
 vs. speed, 215, 216
 steers, slip angle
 and Olley definitions, 168–171, 227
 trim, 192–194, 197
 turns, three phases of, 127–128
 unbalanced forces
 acceleration components, transient, 146–147
 derivative notation for, 149–150
 lateral tire force, total, 149
 tire velocities: front, rear, 147–148
 tire yawing moment, 149
 understeer
 and characteristic speed, 181–183, 184–185, 226
 conceptual discussion of, 313–315
 constant radius test data for, 139–140
 and cornering compliance, 173
 cornering dynamics of, 136–137
 and critical speed, 178
 defined, 137, 164, 168
 Olley definitions, 168, 169, 227
 path curvature, yawing velocity, response, 162–163
 stability factor K, 161–164
 stability index (variation with V), 208–209
 on tilted road, 143, 168
 turn radius and Ackermann angle, 137–138
 understeer and the driver (discussion), 229
 understeer budget (passenger car), 173
 understeer gradient. *See below*
 understeer “spring,” 151–152
 See also lateral acceleration (above)

defined (SAE), 214
 and MMM post-processing (high-performance sports car), 330, 332
 and stability factor K, 211
 and steering sensitivity, 214–217, 224–225
 summary and discussion of, 224–225
 understeer budget (passenger car), 173
 vehicle slip angle β
 and control response, 155
 vs. driving thrust, 221–223
 induced, by path angle curvature, 201–202
 neutral-steer (2DF model), 131
 slip angle steers (and Olley definitions), 168–171, 227
 yaw damping, 202–204
 yawing moment (2DF model)
 coefficient notation for, 228
 derivative notation for, 149–152
 in 2DF bicycle model, 149
 moment of inertia (about z axis), 145
 untrimmed (and tire damping), 190–191
 yawing velocity response (US/OS models)
 and control inputs, 183–184
 derivation, 161
 and stability factor K, 162–164
 yaw-balanced, steady-state turns, 221
See also Aligning torque; MMM (MRA Moment Method); Pair analysis; Tire behavior; Lateral force

Stability and control, transient
 introduction, 231–233
 advanced dynamics models
 the Chevrolet DK-4 model, 273
 the McHenry model, 272–273
 the MRA Moment (MMM) method, 273
 use of (discussion), 276–277
 Vehicle Dynamics Simulation (VDS), 274–276

dynamic stability - 2DF model
 damping coefficients, 241–242
 geometry to inertia ratio, 244
 inertia coefficients, 241
 lateral and yaw damping, 245
 spring coefficients, 241
 stability factor K and transient dynamics, 244–245
 total cornering factor, 243–244
 US/OS factor and yaw natural frequency, 242–243
 wheelbase: apparent vs. true (and KV²), 245

early analytical approach
 driving thrust: effect on steady turn, 265–266
 driving thrust: effect on step steer response, 267–268
 spin recovery, 267, 269–271
 SVDM (Simplified Vehicle Dynamics Model), 272
 lateral acceleration
 response times (from steering inputs), 261–264
 vs. time (lane change, VDS correlation), 274, 276
 roll velocity vs. time (lane change, VDS correlation), 274–275
 sideslip angle
 and ramp steer input, 261–262
 and spin recovery, 267, 269–271
 and step steer response, 267–268
 single-DF analysis
 downforce, ground effect, 245–246
 spring-mass-damper system
 introduction, 233–235
 chassis natural frequency, 239–240
 coupled vs. uncoupled systems: cautionary note, 241
 critical damping, 237
 damped natural frequency vs. damping coefficient, 251
 damped torsional pendulum, 250–251
 damping ratio, 236–238, 788–789
 dynamics of, 236
 quarter-car example, 238–241
 rotational vs. rectilinear dynamics (table), 238
 sprung/unsprung mass, shock absorber for, 240–241
 sprung/unsprung mass (SAE axis system), 115–116
 statics of, 235–236
 suspension system example, 238–241
 undamped natural frequency, 236
 under/overdamping, 237
 wheel natural frequency, 240
See also Dampers

stability derivative concept, notes on, 260

step responses (2DF)
 example: Formula 1 car, 257–259
 example: small FWD car, 256–257
 moment of inertia, rotational, expression for, 250–251
 step response charts, 251–255

step/ramp steer input, transient responses to
 driver-induced oscillation, 262–263
 free control responses, 264–265
 ISO 7401 test procedure, 260–261
 response, peak response, 261–262
 transient responses, 262–264

yaw velocity
 and driver-induced oscillation, 271–272
 and spin recovery, 267, 269–272
 and step steer response, 267–268
 vs. time (lane change, VDS correlation), 274, 276

yawing moment
 equation, definitions, of motion (1DF model), 247–248
 index of stability for (1DF model), 248–249
 oscillatory response (1DF model), 249
 response to steer angle (1DF model), 247–248
 yaw natural frequency and US/OS factor (2DF model), 242–243

Stagger, 282

Steeds, W.
Paper: *Mechanics of Road Vehicles* (1960), 784

Steering. *See* Steering angle; Steering systems, Trail

Steering angle δ
 vs. lateral acceleration
 neutral steer car, 131–133
 oversteer car, 141–142
 skid pad test, 383–384
 understeer car, 139
 vs. roll velocity (VDS correlation), 274–275
 and spin recovery, rear-wheel driving force, 267, 269–271
 vs. tire slip angle α
 driving thrust, effect of, 266
 model tires, constant α (MMM), 303–306
 vs. vehicle slip angle β
 model tires, constant β (MMM), 302–304
 oversteer car, 140–142
 understeer car, 136–137

See also MMM (MRA Moment Method); Stability and control, steady-state; Steering systems

Steering systems
 Ackermann steering geometry
 Ackermann speed, 174
 and characteristic speed, 181–182
 and critical speed, 181

described, 128–129, 713–716
 and FLT (cornering coefficient), 285–286
 at high lateral acceleration, 714–715
 at low lateral acceleration (street cars), 713–714
 “more than” true Ackermann, 715–716
 in neutral steer, 158–159
 reverse, and FLT (motorcycle tire), 290, 292
 reverse, and secondary chassis set-up, 404
 and steering angle gradient, 164, 211–212
 and steering rack location (rear steer), 714, 715
 and steering ratio, 716
 with unequal steering arms, 716

alignment
 camber, 726–727
 toe, 726

caster (and mechanical trail)
 and breakaway, skid recovery, 713
 and caster stagger, 712
 geometry of, 710
 and steer camber, 713
 steering force, effect on, 712
 weight shifting and weight jacking, 712
 wheel rise/fall (with steer), 712

compliance steer
 and Ackermann steer, 835
 and aligning torque, 836
 lateral force, coefficient of, 838
 lateral force (front, rear), 835

driver steering effort, lowering
 centrifugal caster, 720–721
 large scrub radii, 720
 negative trail, 720

kickback, steering
 and CG location, 402
 and kingpin spindle length, 711
 and limited-slip differential, 400
 and scrub radius, 400, 405
 and tire/rim size, 400, 710

kingpins
 and front-end raising, 710–711
 geometry of, 710

inclination angle, defined, 46, 710
 inclination angle vs. camber angle, 46, 63
 kingpin axis vs. MacPherson strut axis, 46, 63

offset and scrub radius, 400
 and scrub radius, 398, 710, 711
 spindle length and steering kickback, 711
 and steer-camber characteristics, 710

and steering force, 399, 402
See also caster (above); Suspension geometry
 power steering
 installation and set-up requirements for, 721
 power steering, nonlinearity of, 720
 ride steer
 and bump steer, relationship of, 399
 compliance effects in, 724–726
 curved plots, problems with, 723
 defined, 398–399
 and dropped throttle turns, 397
 and lateral acceleration, 397, 407
 linear: geometry and plot, 724
 measurement of, 721–722
 nonlinear: geometry and plot, 725
 origins of: effect of tie rods, 721, 723
 and rough road behavior, 398–399
 sign conventions for: US/OS, 721
 and solid front axles, 724
 zero: geometry and plot, 723
 scrub radius
 and bump steer, 398
 as function of instant center (IC) height, 616
 and high-speed stability, 405
 and kingpin inclination angle, 398, 710–711
 negative, in FWD, 398, 400, 404, 711–712
 and parking-lot-speed steering force, 399–400, 720
 and power steering, 720
 and rough-road tracking, 400, 616
 and steering kickback, 400, 405
 and steering wheel rim force, 400, 405
 steer torque
 and breakaway [skid] warning, 31–32; 713
 steering dampers, 719–720
 steering gears
 introduction, 716
 rack-and-pinion ratio, 718
 recirculating ball ratio, 718–719
 reverse efficiency of, 719
 steering, hysteresis in, 717
 steering ratio, 716–718
 worm-and-sector, 719
 steering sensitivity
 and MMM post-processing (high-performance sports car), 330, 332
 steering wheel rim force

and breakaway [skid] warning, 32–33, 713
 and tire/rim size, 400
 tie rod location, 713
 tire axis system (SAE), 61–63
See also Camber; Steering angle δ ; Suspension geometry
 Stick-slip
 in open differentials, 736–737
 Stollery, J.L.
 paper on ground effect theory (Ref. 155), 522–523
 Stoner, Ken
 checkerboard test, 421, 433
 skid pad and steering tests, 433
 Sugawara, F.
 paper on electronically controlled shock absorbers (Ref. 156), 786
 Sullivan, Louis
 “form follows function,” 607
 Suspension geometry
 introduction, 607
 A-arm struts
 reversed, and trailing link, 640, 641
 and toe link, 640–641
 “Anti” features (in SVSA geometry)
 calculation of (drive/brake torque reaction), 618
 effect on longitudinal load transfer, 617, 618
 when “anti” doesn’t work: FWD vs. RWD, 620
 Anti-dive features (SVSA geometry)
 anti-squat (IRS), 619
 anti-squat (solid axle), 619
 and bump deflection, 619
 and inboard brakes, 618
 and outboard brakes, 617–618
 Anti-lift features (SVSA geometry)
 anti/pro lift (IFS), 619
 and outboard brakes, 618
 and suspension droop, 619
 basic concepts
 beam axles, kinematics of, 609, 611
 degrees of freedom (D.O.F.), 608
 degrees of restraint (D.O.R.), 608
 independent suspensions, kinematics of, 609, 610
 instant axis, 612, 613
 instant center (IC), 610–612
 motion path (of knuckle), 608
 tension-compression links vs. D.O.R., 609–611

Suspension geometry (*continued*)
 beam axles
 “anti” features for, 619, 621
 axle roll steer, 622
 axle-suspension roll center height, 622–623
 in four-bar linkage suspension, 622, 648
 lateral restraints in, 623–624
 lateral/vertical force coupling in, 622, 623, 624
 parallel jounce and roll in, 622
 roll center location, defined, 622
 SVSA instant center of, 621
 wheel loads on acceleration, 407
 camber
 camber change rate and fvsa, 615
 in front suspensions - general design issues, 626
 caster
 caster change rate and SVSA, 620
 in front suspensions - general design issues, 626
 deDion rear axle, 660–661
 front suspensions - general design issues
 introduction, 624–625
 camber and caster in, 626
 kingpin angle, 625–626
 lower ball joint height, 625
 packaging, geometry of, 625
 rack location, 626
 structural requirements, 626–627
 tire/rim size, 625
 wheel offset, 625
See also front suspension - MacPherson strut
 front suspensions - MacPherson strut
 anti- features and side view, 634
 design iterations: front vs. side views, 634
 functional description of, 632
 installation, need for care in, 635
 as kinematic slider mechanism, 609
 layout of, 633
 lower control arm line (ball joint placement), 633
 MacPherson strut axis vs. kingpin axis, 633
 steering tie rod outer point, choice of, 634
 strut axis vs. kingpin axis, 633
 strut bending loads, 634–635
 wheel/strut travel, 634
 front suspensions - SLA
 camber curve, shape of, 628–629

control arm inner pivot axis, construction of, 630–632
 control arm planes *vs.* instant axis, 632
 front view geometry, design procedure for, 627–628
 instant center height, 628
 kingpin length *vs.* tall/short knuckle, 627
 rod and rack location, 629
 side view geometry, design procedure for, 629–630
 summary, 635–636
 tall/short knuckles, selection criteria for, 627
 upper/lower ball joint location, 627
See also front suspensions - MacPherson struts
 front view swing arm (FVSA) geometry
 and camber change rate, 615
 construction (geometry) of, 614
 and force coupling (sprung/unsprung masses), 614
 horizontal-vertical coupling effect, 614
 instant center location, 613
 and jacking, 614–615
 rate of change of, 615–616
 roll center height, 613–614
 and rolling/nonrolling moments, 614
 and tire scrub, 616
 Hotchkiss axle, 661
 independent suspensions, general
 instant centers in, 612
See also front suspensions, rear suspensions
 instant axis concept
 in independent front suspensions, 612
 in independent rear suspensions, 640
 instant center concept, 610–612
 jacking forces
 in swing-axle IRS, 638
 kingpins
 kingpin angle, 625–626
 kingpin length *vs.* tall/short knuckle (SLA), 627
 MacPherson strut axis *vs.* kingpin axis, 633
 MacPherson struts. *See* front suspensions - MacPherson strut; rear suspensions - MacPherson strut
 Panhard bar
 in beam axles, 623
 in three-link rear suspensions, 652–653

rear suspensions - beam axle
 A-arm and links, 650–652
 basic four-bar link, 647–649
 parallel lower arm four-bar link, 649–650
 three-link and track bar (Panhard bar), 652–653
 rear suspensions - decoupled
 “bird cage,” 658–659
 characteristics and layout, 658–659
 “compound,” 658–660
 decoupling described, 658
 deDion rear axle, 660–661
 example: anti-squat/anti-lift, 658–660
 Hotchkiss axle, 661
 rear suspensions - MacPherson strut
 A-arm and toe link strut, 640–641
 H-arm strut, 641–642
 in independent rear suspensions, 640–642
 instant axis concept, 640
 MacPherson strut axis vs. kingpin axis, 633
 reversed A-arm and trailing link strut, 640, 641
 tri-link strut, 642
 rear suspensions - SLA
 caution regarding of change, 647
 Corvette five-link suspension, 646, 647
 double A-arm and toe link, 643
 five link, 645–646
 H-arm and A-arm, 644–645
 H-arm lower and camber link, 645
 lower A-arm with three links, 644
 Mercedes five-link rear suspension, 646, 647
 Thunderbird H-arm rear suspension, 645
 upper A-arm with three links, 643–644
 rear suspensions - torque arm, 656–658
 rear suspensions - torque tube
 discussion and geometry, 654, 655
 NASCAR stock car rear axles, 654–656
 rear suspensions - trailing-arm
 introduction, 636
 jacking forces (in swing axles), 638
 pre-84 Corvette type (swing axle), 639
 pure trailing arm, 636, 637
 semi-trailing arm, 636–638
 swing axles, 638–639
 rear suspensions - twist axle
 introduction, 661
 basic types of, 662–663
 ride height, and rough road behavior, 399
 scrub, as function of IC height, 616

and rough-road wheel path, 616
 side view swing arm (svsa) geometry
 “anti” features in. *See* Anti- features, above
 caster change rate, 620
 wheel path in, 620
 solid axles. *See* beam axles (above)
 toe links
 and A-arm MacPherson strut suspensions, 640–641
 and double A-arm SLA suspensions, 643
 ungrounded, 643
 torque tubes, 654–656
 tri-link struts, 642
 Watt’s linkage (in beam axles), 623
 Suspension springs
 coil springs
 geometry and terminology for, 762–763
 helical compression springs, end treatments of, 762–763
 installed spring rate, 765
 material treatments of, 765
 maximum stress in, 763–764
 multiple springs in series, 769
 presetting of (scrapping, cold setting), 765
 progressive rate coil springs, 771
 shear modulus and stress levels, 764–765
 spring rate, 764
 spring rate, measuring, 771, 772
 two springs in parallel, 769–780
 two springs in series, 766–769
 typical calculations: front wishbone, 770–771
 Wahl factor, 763, 764
 leaf springs
 introduction, 771–772
 fatigue, 777–779
 installation considerations, 775–777
 interleaf friction, 777
 laminated, 773–774
 linear spring rates, 776
 sample calculation: NS car, single parabolic springs, 774–775
 single leaf cantilever, 772
 single leaf parabolic, 772–773
 Young’s modulus and stress levels, 774
 spring coefficients, 241–242
 torsion springs
 introduction and basic geometry, 755–756
 maximum stress of, 756–757
 operating stress levels for, 759–760
 sample calculations for, 761–762
 shear modulus for, 759

spring rate for, 757–759
See also Dampers; Stability and control, transient (spring-mass-damper systems)
 Suspension system, active. *See under* Dampers
 SVDM (Simplified Vehicle Dynamics Model), 272
 Symbol conventions, vehicle and tire axes, 121
 Task performance analysis, 435
 Temperature, tire
 components of, 55–56
 speed/temperature effects, 56
 and tread compound, 56
 Testing and development
 CAL six-component test rig (photo), 428
 desirable vehicle characteristics
 chassis adjustability, trend toward, 376
 checklist of, 375
 maneuverability, 376
 tire design, criteria for, 376
 development, general notes on, 381–383
 driver-vehicle relationship
 control: the driver’s contribution, 374, 375
 response augmentation, driver, 375, 376
 Stirling Moss comment on, 374
 vehicle motion behavior, 374–375
 fundamentals of testing
 checklist, 376–377
 passenger vs. race cars, 377
 Gough testing machine, 20–22
 laboratory testing
 chassis subsystems: criteria for testing, 377–378
 quantitative vs. subjective data, 377
 skid pad testing, circular
 caveats and uncontrolled variables in, 385
 main uses of, 383
 for race car development, 385
 SAE recommended practice for, 383
 test data, typical, 383–385
 and understeer budget, 383
 test methodology
 accelerometer gain and offset, 380
 aero testing, full-scale, 381
 definition of terms, 378–379
 good data, principles for obtaining, 380
 track test program planning, 378
See also Aerodynamics, applied; Calspan TIRF facility; Sakai (JARI) Thelin, C.F., and Watkins Glen analysis, 341
 Thompson, A.G.
 paper on optimum damping (Ref. 158), 785
 Thrust, vehicle
 and lateral, longitudinal, forces, 63–65
 Tire axis system (SAE), 15, 61–63
 Tire behavior
 related terms:
 Braking/tractive force
 Calspan TIRF facility
 Camber
 Chassis set-up
 Friction circles
 “g-g” diagrams
 Lateral acceleration
 Lateral force
 MMM (MRA Moment Method)
 Pair analysis
 Slip angle, tire (α)
 Stability and control (steady-state, transient)
 Tire data treatment
 Trail
 introduction to, 13–14
 aligning torque
 aligning torque compliance steer, 836
 and breakaway, 28, 31–32, 713
 camber vs. slip angle, effect of, 47, 69–70
 defined, 28
 geometry of, 70
 normalized, 475–477
 and print distortion, 28
 self-aligning torque vs. slip angle (normalized), 477
 sign reversal of, 30
 vs. slip angle and load, 29–30, 76–80
 and steer angle stability, 69
 and steering wheel rim force, 32, 33, 400
 and tire pressure, 55
See also Trail
 breakaway
 aligning torque at, 30, 31–32
 and high slip angle, 18
 and mechanical trail swamp-out, 713
 transitional zone, 28, 314–317
See also Friction circle; “g-g” diagrams
 conicity, 57, 476
 cornering, tire forces in
 on banked road, 20
 discussion of, 19–20
 force curve, idealized, 317
 force curves for model tires, 302
 total cornering factor, 243–244

Tire behavior (*continued*)
 cornering, tire forces in (*continued*)
See also Chassis set-up; "g-g" diagrams; MMM (MRA Moment Method); Stability and control (steady-state, transient)
 cornering stiffness
 defined, 25, 54
 and high negative camber, 290–292
 and motorcycle tires, 47
 nibbling, 409
 and slip angle (Goodyear data), 81
 and static margin (Dell'Amico), 206–207
 and steering kickback, 400, 409
 and steering wheel force and ratio, 400
 and tire load (Goodyear data), 82
 and tire pressure, 54–55
 tread wear, effect of, 426
See also MMM (MRA Moment Method); Pair analysis
 damping, tire
 damping analogy, 184–186
 damping center, 187–188
 damping-in-sideslip, 188–189
 damping-in-yaw, 189–190
 and generalized yaw moment, 190–191
 and static margin, 188
 tire damper side force (2DF model), 187
 effect on chassis set-up
 steering kickback, 400, 409
 steering wheel force and ratio, 400
 and elastic [tire] distortion, 20
 induced drag
 and Ackermann steering (at high speeds), 715
 discussion, 66
 example: four-wheel computer simulation, 68–69
 geometry and dynamics of (bicycle model), 67
 horsepower to overcome (example), 69
 vs. tire pressure, 55
 model tire
 described, 16
 Junkers Aircraft model, 424
 lateral distortion pattern, 18. *See also* print (below)
 lateral force, introduction to, 15, 17
 rolling (vs. slip angle), 18
 static lateral deflection and sliding, 16–17
 walking analogy (to tire slip), 18–19
 nibbling, 409

overturning moment, 70–71, 476
 ply steer, 57, 476
 print
 basic description of, 14–15
 braking, print characteristics for, 35–36
 camber distortion of, 46, 47
 distortion and aligning torque, 28
 driving, print characteristics for, 34–35
 Gough testing, 20–22, 23
 lateral distortion pattern, 18
 and lateral slippage (low slip angles), 20, 22
 rolling resistance
 geometry of, 65
 net, expression for, 64–65, 74
 net (normalized curves for), 65–66
 vs. tire pressure, 55
 rolling resistance moment
 and driving-wheel tractive force, 72–73
 free-rolling tire, 71–72
 torque about wheel spin axis, 74–75
 variation with load, speed, 74
 slip, lateral
 at low slip angles, 20
 occurrence at back of print, 22
See also Slip angle α
 speed effects, 56
 spinning, 37. *See also* Braking/tractive force; Differentials
 temperature
 components of, 55–56
 speed/temperature effects, 56
 and tread compound, 56
 test methods/facilities
 advanced test facilities at GM, 445–447, 453
 CAL and Air Force tire tester, 429
 GM flat bed tire tester, 435
 Gough machines, 20–22, 23
See also Calspan TIRF facility
 tire axis system (SAE), 15, 61–63
 tire forces, basic
 braking/tractive force (Sakai), 63–66
 induced tire drag (bicycle model), 67–69
 lateral force, 63
 measured force (F_x), 64
 net rolling resistance, 64, 65
 normal force (load), 63
 test data (typical), 66
 total thrust (or drag), 64–65
 tractive/lateral forces (SAE axis system), 63–66

vs. vehicle response, 221–223
 tire moments, basic
 aligning moment (M_z), 69–70
 overturning moment, 70–71
 rolling resistance moment, 71–74
 rolling resistance torque, 73
 tire-as-damper analogy, 185–190
 tire/rim size, effects of
 in chassis secondary set-up, 400
 steering kickback, 400, 409
 steering wheel force and ratio, 400
 and vehicle response, 221–223
 Tire data treatment
 introduction to, 473–474
 nondimensionalization of
 camber angle vs. camber thrust (normalized, various loads), 478
 and conicity/plysteer, 476
 "magic formula" for, 476
 objectives of, 474–475
 overturning moment, 476
 self-aligning torque, 475, 476
 slip angle α vs. lateral force (normalized, various loads), 475–477
 slip angle α vs. self-aligning torque (normalized, various loads), 475–477
 slip/camber angle vs. lateral force (normalized, various loads), 480–482
 summary and discussion, 484, 486–487
 normalized force, derivation of, 482–483
 normalized slip variable, derivation of, 482–483
 test program for, proposed, 486
 TIRF research facility. *See* Calspan TIRF facility
 Torque, input
 and net rolling resistance, 64, 66
 Torsen differentials, 744–745
 Torsion bars
 action of, 281
See Ride and roll rates (anti-roll bars); Suspension springs; Wheel loads
 Track width
 and rough road cornering, 409
 and secondary chassis set-up, 408–409
 Traction control systems, 748
 Tractive force. *See* Braking/tractive force
 Trail
 and driver performance, 31–32
 mechanical
 and breakaway warning, 31–32, 713
 and caster angle (geometry of), 30–31, 712–713
 and kingpin offset, 30, 410
 and steering forces (chassis set-up), 399
 overturning
 and normalized overturning moment, 476
 pneumatic
 and aligning torque, 28, 31–32, 69–70
 and breakaway, 31–32, 713
 and normalized aligning torque, 476
 and print asymmetry, 28
 and rough road performance, 395
 and skid warning, 32
 steer torque (mechanical vs. pneumatic), 31, 713
 and steering wheel rim force, 32–33, 713
 and rough road behavior, 398
 and tire data treatment, 476
See also Camber; Steering systems; Suspension geometry
 Transitional zone (radial vs. bias ply), 28
 Transmissibility. *See* Dampers
 Tread compounds
 Durometer readings, racing tires (Goodyear data), 81
 and lateral friction coefficient, 27
 temperature sensitivity of, 56
 and tire temperature, 56
 Trim
 at the limit, 315
 stable vs. unstable, 315
 and static stability, 192–194, 197
 trim change sensitivity and "g-g" diagrams, 354
 "trimmed in lateral force," 304
 trimmed sideslip (high-performance sports car), 330, 331
 Tuck-in
 dropped throttle, 403
 Tuning. *See* Chassis set-up
 Two-degree-of-freedom (2DF) model
 vector geometry of, 127
 Understeer, *See* Stability and control, steady-state; MMM (MRA Moment Method)
 Understeer gradient
 and Bundorf cornering compliance, 172–173
 defined (SAE), 214
 and skid pad testing, 383
 and stability factor K, 211
 and steering sensitivity, 214–217, 224–225
 summary and discussion of, 224–225
 understeer budget (passenger car), 173

Unsprung mass, 115, 671
See also Dampers; Stability and control, transient

Valentine, Dick
 and dynamic vehicle response analysis, 434

Valentine, Mike
 and g-Analyst®, 359

Van House, Bob
 and GM flat bed tire tester, 435

Van Valkenburgh, Paul
 comment on front spoilers (Ref. 162), 496

Vectors
 acceleration, 5–8, 9
 addition of, 8, 9
 velocity, 4–5
See also Vehicle axis systems; Stability and control (steady-state, transient)

Vehicle axis systems
 introduction, 113–114
 aerodynamic axis system (SAE), 109–110
 angle vectors in, 118–119
 earth-fixed axis system, 114
 forces and moments in, 117–119
 historical background of, 114–115
 path analysis in, 117–118
 SAE nomenclature for, 116
 sign conventions in, 119–120
 slip angle, discussion of, 119–120
 sprung/unsprung masses in (SAE), 115–116
See also Tire axis system

Velocity
 lateral, 7
 vectors, race car, 4–5
See also MRA Moment Method (MMM); Stability and control (steady-state, transient); Vehicle axis systems

Versace, J.
 ride and vibration data manual (Ref. 68), 784

Viscous differentials, 746–748

von Doenhoff, Albert E.
 NACA airfoil data, 497, 500

Vortices. *See under* Aerodynamics, applied

Walking analogy (tire slip), 18–19

Watkins Glen
 computer analysis of, 341
 Formula 1 performance profile, 342

Weaver plates, 717

Wedge, 281–282

Weismann differential, 745

Wheel loads
 aerodynamic loads
 introduction and definition of terms, 694–695
 example: 100-mph car, 696–697
 lift coefficients, 695
 wheel load changes, 695–696

assumptions used, 665–666

asymmetrical effects (oval tracks)
 introduction, 700
 and banked turns, 703
 cornering bias, means of achieving, 700
 discussion of, 701
 lateral load transfer, 702–703
 longitudinal load transfer, 701–702

banking, effects of
 examples: initial conditions for, 688
 example 1: above neutral speed, 688–689
 example 2: below neutral speed, 689–690
 geometry and analysis of, 685–687
 lateral load transfer, 687–688
 weight distribution, 687

CG, location of
 horizontal, 666–668
 spring mass, 671–673
 vertical, 668–671

chassis stiffness
 bending stiffness, 675, 677
 how stiff is stiff enough?, 676
 importance of, 673
 torsional stiffness, methods for increasing, 677

torsional stiffness: set-up and measurement of, 674–675

torsional stiffness, structures for, 676

crests, effects of
 introduction, 693
 axle loads, 694
 geometry of, 693

dips, effects of, 694

engine torque reaction
 introduction, 697
 example, 699–700
 geometry and derivation of terms, 697–699

jacking effect, 700

grades, effects of
 introduction, 690–691
 axle loads, 692

example: accelerating uphill, 692
 geometry and analysis of, 691–692

lateral load transfer, distribution of
 the car as a three-mass system, 680–681
 definitions and assumptions, 680
 LLT geometry and analysis, 681–683
 mechanisms of load transfer, 679–680
 roll rate distribution, defined, 684
 total LLT distribution, defined, 684
See also Pair analysis, steady-state; Ride and roll rates

lateral load transfer, total
 geometry and analysis, 678–679
 total LLT distribution, defined, 684
 typical calculation, 679
See also lateral load transfer, distribution of (above)

longitudinal weight transfer
 geometry and analysis, 684–685

summary example (all influences)
 aerodynamic load changes, 706
 CG location, 704
 effective wheel loads (due to banking), 707
 lateral weight transfer, 706–707
 total wheel loads, 707
 vehicle parameters, 704
 weight transfer (drive axle torque reaction), 705–706
 weight transfer (due to forward acceleration), 704–705
 wheel load summary (table), 708

Wheel spin. *See under* Braking/tractive force

Wheelbase angle. *See* Steering systems (Ackermann steering geometry)

Wheelbase stretcher, 245. *See also* Stability and control, transient

Whitcomb, Dave
 neutral steer relationship, 159
 and path curvature stiffness, 202
 photo of, 429, 470

Williams, David
 develops Lotus in-car instrumentation, 468–469
 photo of, 467
 suggests active suspension system (Lotus), 469

Winchell, Frank
 appointed VP Engineering (GM), 439
 and Bill Milliken
 approves first MRA Moment Method effort, 293, 463–464
 attends variable stability airplane course at CAL, 441–442

makes handling dynamics presentation to WFM, 441
 meets, argues with, WFM, 439–440
 WFM appreciation of, 440–441
 designated “expert witness” for Corvair defense, 443–444
 and GM racing ban, 448–449
 and Penske aluminum Chevy block, 448
 photo of, 440
See also Chevrolet-Chaparral racing

Wind tunnel testing. *See under* Aerodynamics, applied

Wings. *See under* Aerodynamics, applied

Wolf, Bob
 at CAL Transportation Division, 439

Wright, Peter
 background and early experience, 468
 balancing the car (aero and mechanical forces), 572
 basic research on aerodynamic downforce, 468
 and Lotus 78 F.1 ground-effect cars, 491, 521–522, 523–524
 measured race-car performance data (Team Lotus), 354–357, 360
 photo of, 467
 race-car driving, comment on, 3
 Research Director, Team Lotus, 468

Yaw

damping
 and Ackermann steer angle, 202–203
 damping-in-yaw (tire), 189–190
 lateral, and yaw (DFN NS car), 245
 and path curvature stiffness, 202–204

yaw natural frequency
 and US/OS factor, 242–243

yaw velocity
 and driver-induced oscillation, 271–272
 vs. slip angle α , 266
 and spin recovery, 267, 269–272
 spin recovery, rear-wheel driving force, 267, 269–272
 steady turn vs. driving force, 266–267
 step steer input vs. driving force, 267–268
 and step steer response, 267–268

VDS test correlation of, 274–275

yawing moment
 angular acceleration and $C_N \cdot A_Y$ diagram, 309
 applied, NS response to, 158

applied, steady-state response to (2DF), 156–157
coefficient notation for (2DF), 228
and damped torsional pendulum, 250–251
derivative notation for (2DF), 149–150
derivatives, physical significance of, 151–152
in 2DF bicycle model, 149
equilibrium and tire slip angle (α), 130–131
generalized, and tire damping, 190–191
index of stability for (1DF), 248–249
and lateral tire force, 149
and locked-spool transmissions, 739–740
moment of inertia, z-axis (2DF), 145
neutral steer response to, 158
oscillatory response (1DF), 249
response to steer angle (1DF), 247–248
vs. slip angle α (model tires, MRA Moment Method), 302–306

steady-state response to, 156–157
untrimmed, and tire damping (2DF), 190–191
yaw natural frequency and US/OS factor (2DF), 242–243
yaw-balanced, steady-state turns, 221
yawing motion
equation and definitions of (1DF), 247–248
yawing velocity response
control inputs (US/OS), 183–184
derivation of (US/OS), 161
and path curvature (OS), 162–163
and stability factor K (US/OS), 162–164
understeer (2DF), 162–163
yaw-balanced, steady-state turns (US/OS), 221

Z-bars. *See* Ride and roll rates; Wheel loads

Comments Requested!

Every attempt has been made to check the accuracy of this text. But, in the course of proofreading we have learned that there will always be “another error.” The authors welcome reader feedback on any aspect of the book, be it:

- Conceptual arrangement and contents
- Details of the equations (always a difficult typesetting problem)
- Accuracy of credits
- Choice of references
- Typographical errors

or any other improvement. Please send a marked-up copy of the relevant page(s) to:

SAE
Product Manager, General Publications Division
400 Commonwealth Drive
Warrendale, PA 15096-0001

with a note to forward it to the authors.

The authors may also be contacted by e-mail. Please use the link on the MRA website, <www.millikenresearch.com>.

Comments and corrections will be acknowledged by the authors, and, if possible, added to future printings with reference to the contributor.

List of Symbols

1DF	Single-degree-of-freedom system
2DF	Two-degree-of-freedom system
3DF	Three-degree-of-freedom system
4WD	Four-wheel drive
A	Area
A_x	Longitudinal acceleration (g)= a_x/g
A_y	Lateral acceleration (g)= a_y/g
AR	Aspect ratio (of a wing)
B.L.	Boundary layer (of a wing)
C	Damping constant or coefficient
C	Vehicle cornering stiffness
CF	Centrifugal force
CG	Vehicle center of gravity
C_a	Tire cornering stiffness
C_F, C_R	Cornering stiffness for bicycle model front and rear tires
C_γ	Tire inclination stiffness
C_ϕ	Tire camber stiffness
C_0	Control moment gain
C_X	Longitudinal force coefficient
C_Y	Lateral force coefficient
C_N	Yawing moment coefficient = N/W
C_L	Aerodynamic lift coefficient
C_D	Aerodynamic drag coefficient
C_S	Aerodynamic side force coefficient
C_{PM}, C_M	Aerodynamic pitching moment coefficient
C_{YM}	Aerodynamic yawing moment coefficient
C_{RM}	Aerodynamic rolling moment coefficient
C_p	Aerodynamic pressure coefficient
D	Aerodynamic drag or tire drag
D_F, D_R	Bundorf cornering compliance
DR	Damping ratio
D.T.	Dropped throttle
F	Force
F_B	Tire braking force
F_R	Tire net rolling resistance
F_T	Tire tractive force
F_x, F_y, F_z	Forces on the vehicle axes
F_x, F_y, F_z	Forces on the tire axes
FLT	Fraction load transfer
FT	Full throttle
FWD	Front-wheel drive
G	Overall steering ratio (δ_{SW}/δ)
G.W.	Gross (total) weight
H	Total head pressure, aerodynamic
H	Height of total CG above roll axis
H_s	Height of sprung mass CG above roll axis
Hz	Hertz (cycles per second)
I	Moment of inertia
IC	Instant center (suspension linkage)
IR	Installation ratio (suspension spring)
I_Z	Moment of inertia about Z axis, commonly called polar moment of inertia
K	Stability factor
K', K_R	Spring constant (lb./in., lb./ft.)
K_F, K_R	Axle roll stiffness or $K_{\phi F}, K_{\phi R}$
KE	Kinetic energy
L	Aerodynamic lift
L	Surface length (as in RN)
L.E.	Leading edge (of a wing)
L.F.	Lateral force
LLTD	Lateral load transfer distribution
M	Moment
M_x	Tire overturning moment
M_y	Tire rolling resistance moment
M_z	Tire aligning torque
N	Yawing moment
NRA	Neutral roll axis
NS	Neutral steer
NSP	Neutral steer point
O	Origin of axis system
OS	Oversteer
P	Point
PC	Path curvature
P.E.	Potential energy
PM	Aerodynamic pitching moment
R	Tire undeflected radius
R_0	Tire rolling radius, 0° slip angle
R_e	Tire effective rolling radius (rev./mile)
R_ℓ	Tire loaded radius
R	Turn radius or resultant
RC	Roll center location
RCH	Roll center height
RWD	Rear-wheel drive
RL	Road load
RM	Aerodynamic rolling moment
RN	Reynolds Number
S	Distance or aero side force
S	Spring rate
SI	Stability index
SLA	Short long arm suspension
SM	Static margin
SR, S	Tire slip ratio
T	Absolute temperature or torque

List of Symbols

T	Thrust	rms	root-mean-square average
T_{in}	Wheel input drive torque	rpm	Revolutions per minute
T.E.	Trailing edge (of a wing)	svsa	Side view swing arm (length)
UG	Understeer gradient	t	Thickness (aerodynamic boundary layer)
UO	Understeer/oversteer	t	Temperature or time
US	Understeer	t	Track (tread width)
V	Velocity, damper velocity	u	Velocity along x in xyz system
V_{Char}	Characteristic speed	ubj	Upper ball joint location
V_{Crit}	Critical speed	uca	Upper control arm
V_t	Tangent speed	v	Lateral velocity component in xyz system
V_∞	Velocity of remote airstream	x,y,z	SAE vehicle and tire axes systems
W	Weight (force)	z_{RF}, z_{RR}	Front and rear roll center height
W_F, W_R	Lateral load transfer	z_{WF}, z_{WR}	Unsprung CG heights
W_s	Weight of sprung mass	Δ	Small change in
W_u	Weight of unsprung mass	Σ	The sum of
WOT	Wide open throttle	Ω	Angular velocity
X, Y, Z	SAE earth fixed axis system	α	Tire slip angle or aero angle-of-attack
X, Y, Z	Forces in vehicle axis system	α	Angular acceleration
YM	Aerodynamic yawing moment	β	Vehicle slip angle at CG
a	Distance CG to front axle or track	δ	Front wheel steer angle
a	Acceleration in ft./sec. ² units	δ_{Acker}	Ackermann steer angle at front wheel
b	Distance CG to rear axle or track	δ_{SW}	Steering wheel steer angle
c	Circumference of circle or wing chord	$\dot{\delta}_{SW}$	Rate of change of steering wheel angle
cpm	Cycles per minute	ε	Small distance
d	Distance	ϕ	Angle
f	Force or friction force	ϕ	Camber angle or body roll angle
f	Function	γ	Tire inclination angle
ft.-lb.	Foot-pounds (Work)	η	Coefficient or factor
fvsa	Front view swing arm (length)	μ	Coefficient of friction
g	Acceleration due to gravity, ft./sec. ² units	μ	Coefficient of absolute air viscosity
h	Height of vehicle CG	ν	Kinematic air viscosity
h	Roll center height, also z_{RF}, z_{RR}	π	3.14159...
h_e	Effective CG height, pair analysis	θ	Angle
hp	Horsepower (550 ft.-lb./sec.)	ρ	Air mass density
k	Understeer gradient, also UG	τ	Time constant
k	Radius of gyration	ω	Angular velocity
k	Spring rate (lb./in.)	ω_n	Damped natural frequency
lb.-ft.	Pounds-foot (Torque)	ψ	Undamped natural frequency
ℓ	Length or wheelbase (a+b)	ζ	Heading angle
lbj	Lower ball joint location	Subscripts:	Damping ratio
lca	Lower control arm	1 or F	Front axle location
m	Mass	2 or R	Rear axle location
mph	Miles per hour	LF, RF, LR, RR	Individual wheel positions
p	Point	∞	Ambient conditions
p	Aerodynamic static pressure		
psi	Pounds per square inch, pressure		
q	Aerodynamic dynamic pressure		
r	Yaw rate or radius of circle		